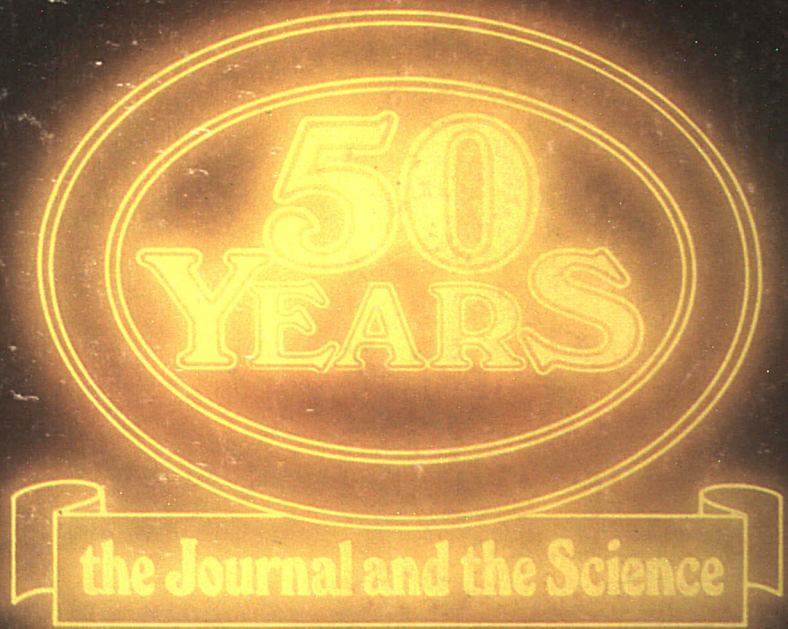
NOVEMBER 1978

analytical chemistry

ANCHAM



NANOpure™



Measurably Superior

Since its introduction, NANOpure has become the most popular reagent grade water system available. And for good reason. NANOpure delivers the Type I water quality you need, with the convenience, economy and reliability you demand.

Now we've made NANOpure even better with some subtle but significant improvements. Check these important features, then write for complete information.

☐ ***New and unique temperature-compensated digital purity meter provides instant and accurate verification of outlet purity.***

☐ ***New quieter pump eliminates traditional noise problems—you can install NANOpure right at the point of use.***

☐ ***NANOpure offers twice the flow rate of other systems—up to 3 liters/min. of CAP/NCCLS/ASTM Type I water on demand.***

☐ ***NANOpure cartridges have more than twice the total capacity of the other popular brand. The result is fewer cartridge replacements and substantially lower operating costs.***

☐ ***NANOpure and NANOpure cartridges are available off-the-shelf from leading laboratory supply distributors.***

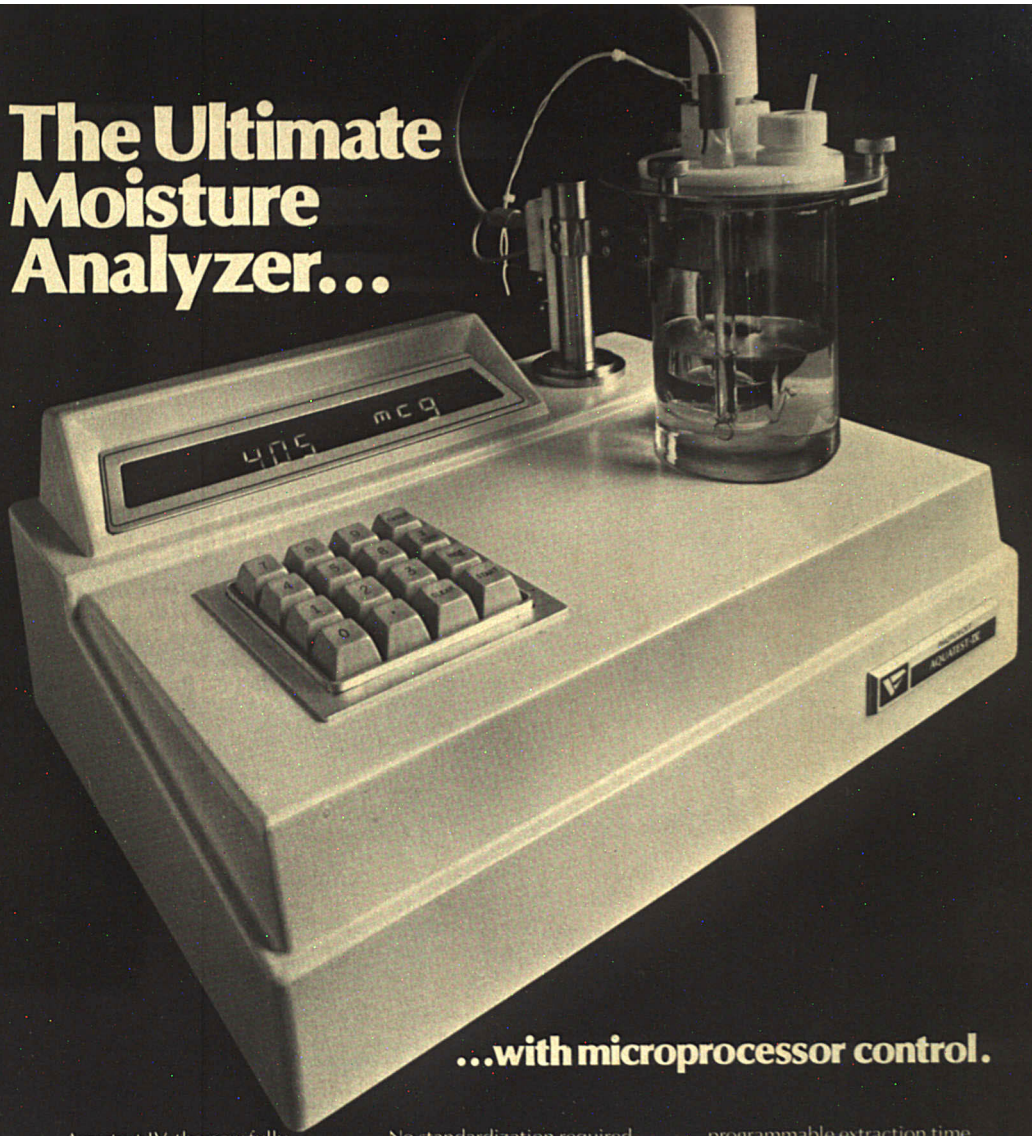
Send for a copy of the Barnstead Guide to Reagent Grade Water and inquire about our unique, no obligation water analysis service. Find out why no other laboratory water system measures up to the new NANOpure.

Barnstead Company, Division of Sybron Corp.
225 Rivermoor Street, Boston, MA 02132
(617) 327-1600

SYBRON | Barnstead

CIRCLE 24 ON READER SERVICE CARD

The Ultimate Moisture Analyzer...



...with microprocessor control.

Aquatest IV, the new fully automated Karl Fischer titrator with digital readout, displays water content without calculations in ppm, percentages or micrograms.

No standardization required.

Aquatest IV automatically corrects for interfering reactions.

And has automatic blank correction when extracting, plus programmable extraction time.

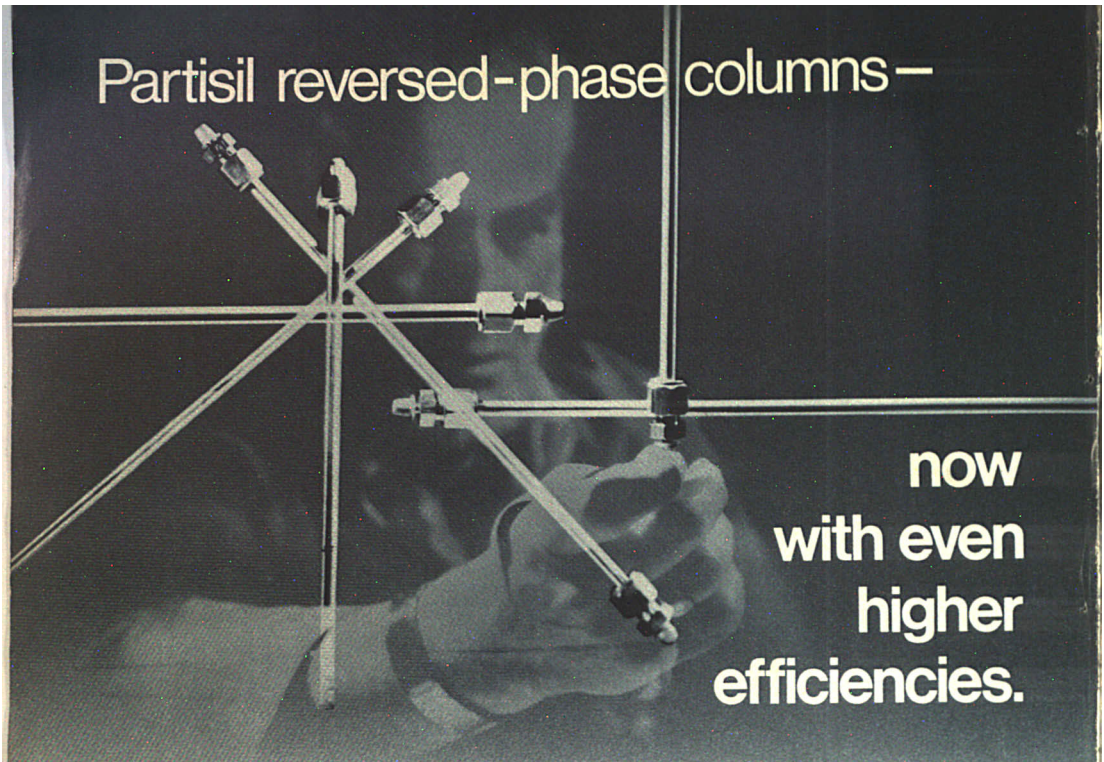
For a free demonstration in your lab, call toll-free (800) 221-5182. In New York State, call collect (212) 989-0484.

After you lift a finger, you don't have to lift a finger.

Photovolt Corporation
1115 BROADWAY, NEW YORK, N.Y. 10010

CIRCLE 172 ON READER SERVICE CARD

Partisil reversed-phase columns—



now with even higher efficiencies.

The state of the art, redefined.

We invite your attention to the following:

Column	Plates/ Meter	Carbon Load	Coverage
Partisil-5 ODS (C_{18})	45,000	10%	98+
Partisil-10 ODS-2 (C_{18})	25,000	15%	75
Partisil-10 ODS (C_{18})	15,000	5%	50

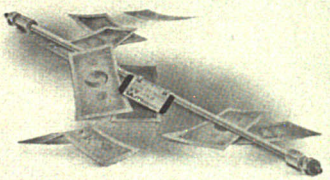
And those are *minimum guaranteed efficiencies.*

You will never receive a Whatman Partisil ODS column with fewer plates.

These new efficiencies, an improvement of up to 50%, are the result of a year-long effort: new, tight, particle size distribution control; major modification of our "ramjet" packing methods; fully computerized quality assurance . . . and some media chemistry we're not quite ready to discuss.

Partisil reversed-phase columns. Surely the state of the art in R-P HPLC.

TRADE-UP TO PARTISIL ODS NOW AND SAVE $25.



If you're in the market for a C_{18} reversed-phase column we'll allow you $25.00 for your used microparticle column (any packing, any brand), if you'll ship it to us, toward your next Partisil ODS analytical column*. For details write or call **Whatman Inc.** ▪ 9 Bridewell Place, Clifton, New Jersey 07014 ▪ Tel: 201-777-4825.

*Expiration date of this offer is 31 January 1979. Valid in U.S.A. only

CIRCLE 232 ON READER SERVICE CARD

Whatman

Volume 50, No. 13, November 1978
ANCHAM
50(13) 1165A–1282A/1729–1952 (1978)
ISSN 0003–2700

© Copyright 1978
by the American Chemical Society

Permission of the American Chemical Society is granted for libraries and other users to make reprographic copies for use beyond that permitted by Sections 107 or 108 of the U.S. Copyright Law, provided that, for all articles bearing an article code, the copying organization pay the stated per-copy fee through the Copyright Clearance Center, Inc. For further information, write to Office of the Director, Books and Journals Division, ACS, 1155 16th St., N.W., Washington, D.C. 20036.

Published monthly with review issue added in April and Laboratory Guide in August by the American Chemical Society, from 20th and Northampton Sts., Easton, Pa. 18042. Executive and Editorial headquarters, American Chemical Society, 1155 16th St. N.W., Washington, D.C. 20036 (202) 872-4600. Second class postage paid at Washington, D.C., and at additional mailing offices.

1978 Subscription prices—including surface postage

	1 yr	2 yr	3 yr
MEMBERS:			
Domestic	$10.00	$18.00	$25.00
Foreign	19.00	36.00	52.00
NONMEMBERS—PERSONAL:			
Domestic	14.00	26.00	38.00
Foreign	23.00	44.00	65.00
INSTITUTIONAL:			
Domestic	14.00	26.00	38.00
Canada	23.00	44.00	65.00
Other foreign	29.00	54.00	77.00

Airmail and air freight rates are available from Membership & Subscription Services, ACS, P.O. 3337, Columbus, Ohio 43210 (614) 421-7230.

New and renewal subscriptions should be sent with payment to the Office of the Controller at the ACS Washington address.

Subscription service inquiries and changes of address (include both old and new addresses with ZIP code and *recent mailing label*) should be directed to the ACS Columbus address noted above. Please allow six weeks for change of address to become effective.

Claims for missing numbers will not be allowed if loss was due to failure of notice of change of address to be received in the time specified; if claim is dated (a) North America: more than 90 days beyond issue date, (b) all other foreign: more than one year beyond issue date; or if the reason given is "missing from files".

Microfiche subscriptions are available at the same prices but are mailed first class domestic and airmail foreign. Inquiries and payments to Microform Program, ACS Washington address.

Single issues, current year, $3.00 except review issue and Labguide, $4.00; **back issues and volumes; microfilm editions** from volume 1 to present: *write or call* Special Issues Sales, ACS Washington address (202) 872-4365.

Advertising Management: Centcom, Ltd., 25 Sylvan Road South, Westport, Conn. 06880 (203) 226-7131

analytical chemistry

CONTENTS

50TH ANNIVERSARY SYMPOSIUM **1189 A**

INSTRUMENTATION

Dallas L. Rabenstein of the University of Alberta discusses resolution enhancement with multiple-pulsed techniques in pulsed Fourier transform NMR spectroscopy **1265 A**

REGULATIONS

Methodology development and rigorous analyses are called for by new EPA regulations **1229 A**

NEWS

Preliminary information on the 1979 Pittsburgh Conference is presented. Leslie S. Ettre, J. Calvin Giddings, and R.P.W. Scott win the M. S. Tswett Chromatography Medals **1213 A**

BOOKS

Books on NMR applications, mass spectrometry, thermal analysis, TLC, and an ACS audio course on NMR spectra interpretation are reviewed by Howard Hill, S. P. Markey, Joseph Jordan, V. W. Rodwell, and Anthony Foris **1249 A**

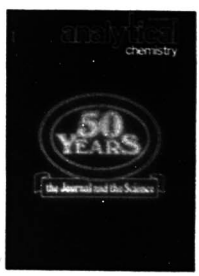
EDITORS' COLUMN

The 10th Annual Report of the National Science Board provides an opportunity to look closely at the current status of federally funded basic research in the U.S. **1261 A**

EDITORIAL

The beginnings of ANALYTICAL CHEMISTRY and the groundwork for the evolution of the JOURNAL's present format are presented **1729**

Technical Contents/Briefs	**1168 A**
Reader Survey	**1182 A**
Letters	**1186 A**
Meetings	**1218 A**
Short Courses	**1220 A**
New Products	**1236 A**
Chemicals	**1239 A**
Manufacturers' Literature	**1243 A**
Advertising Index	**1280 A**
Author Index	**IBC**
Future Articles	**IBC**



Our cover commemorates the golden anniversary of ANALYTICAL CHEMISTRY

หอสมุด กรมวิทยาศาสตร์ -3 พ.ค. 2522

Briefs

Effect of Heating Rates in Graphite Furnace Atomic Absorption Spectrometry 1730

The increase in peak absorbance with heating rate is correlated with the activation energy of the rate-determining step in the atomization process of seven elements.

D. C. Gregoire, C. L. Chakrabarti,* and P. C. Bertels, Metal Ions Group, Department of Chemistry, Carleton University, Ottawa, Ontario, Canada K1S 5B6 *Anal. Chem., 50 (1978)*

Design and Construction of a Time Multiplex Multiple Slit Multielement Flame Atomic Absorption Spectrometer 1737

The system presently allows the simultaneous determination of any four of ten possible elements.

Eric D. Salin and J. D. Ingle, Jr.,* Department of Chemistry, Oregon State University, Corvalllis, Ore. 97331 *Anal. Chem., 50 (1978)*

Performance of a Time Multiplex Multiple Slit Multielement Flame Atomic Absorption Spectrometer 1745

Detection limits, sensitivity, noise characteristics, and calibration curves are presented.

Eric D. Salin and J. D. Ingle, Jr.,* Department of Chemistry, Oregon State University, Corvallis, Ore. 97331 *Anal. Chem., 50 (1978)*

Preparation and Characterization of Thin Metal Films for Exploding-Conductor Excitation 1752

Thin films of Al and Ag are suitable for vaporization and excitation of micro solution and powder samples deposited on the film surface.

D. V. Duchane and R. D. Sacks,* Department of Chemistry, University of Michigan, Ann Arbor, Mich. 48109 *Anal. Chem., 50 (1978)*

Parametric Investigation of Exploding Thin-Film Excitation 1757

The control of emission line-to-background intensity ratios through manipulation of gas pressure, explosion energy, capacitor voltage, and film thickness.

R. D. Sacks* and D. V. Duchane, Department of Chemistry, University of Michigan, Ann Arbor, Mich. 48109 *Anal. Chem., 50 (1978)*

Atomic Emission Determination of Selected Trace Elements in Micro Samples with Exploding Thin-Film Excitation 1765

Analytical curves and reproducibility data are presented for Mn, Sn, Cd, Pb, and Pd, both with and without an internal reference technique.

D. V. Duchane and R. D. Sacks,* Department of Chemistry, University of Michigan, Ann Arbor, Mich. 48109 *Anal. Chem., 50 (1978)*

Nebulizer for Analysis of High Salt Content Samples with Inductively Coupled Plasma Emission Spectrometry 1769

The nebulizer is free from clogging associated with most conventional nebulizers.

Ronald F. Suddendorf and Kenneth W. Boyer,* Division of Chemistry and Physics, U.S. Food and Drug Administration, Washington, D.C. 20204 *Anal. Chem., 50 (1978)*

Intensified Diode Array Detector for Molecular Fluorescence and Chemiluminescence Measurements 1772

Spectra for the fluorescence of quinine sulfate and vitamins A, B_1, and B_2, and chemiluminescence of pyrogallol and lucigenin are recorded from 197 to 823 nm.

Mary Andrieu Ryan, Robert J. Miller, and J. D. Ingle, Jr.,* Department of Chemistry, Oregon State University, Corvallis, Ore. 97331 *Anal. Chem., 50 (1978)*

Quantitative Measurement of Ethylene Incorporation into Propylene Copolymers by Carbon-13 Nuclear Magnetic Resonance and Infrared Spectrometry 1777

The infrared absorbance at 732 cm^{-1} is sensitive to the ethylene incorporation to determine the wt % ethylene to within 0.1–0.2% at the 95% confidence level.

John R. Paxson* and James C. Randall, Phillips Petroleum Company, Research and Development, Bartlesville, Okla. 74004 *Anal. Chem., 50 (1978)*

Electron Capture Negative Ion Chemical Ionization Mass Spectrometry 1781

Detection of amphetamine, dopamine, and Δ^9-tetrahydrocannabinol at the 10^{-18} M level is reported.

Donald F. Hunt* and Frank W. Crow, Department of Chemistry, University of Virginia, Charlottesville, Va. 22901 *Anal. Chem., 50 (1978)*

Plasma Chromatography of Benzene with Mass Identified Mobility Spectra 1784

The temperature dependence of the observed mobility spectra is explained in terms of the theoretical mobility equation.

S. H. Kim, K. R. Betty, and F. W. Karasek,* Guelph–Waterloo Centre for Graduate Work in Chemistry, Department of Chemistry, University of Waterloo, Ontario N2L 3G1 *Anal. Chem., 50 (1978)*

Solvent Extraction–Spectrophotometric Determination of Boron with 2,4-Dinitro-1,8-naphthalenediol and Brilliant Green 1788

About 0.5 ppb of boron in an aqueous solution can be determined.

Kiyoaki Kuwada, Shoji Motomizu, Kyoji Tôei,* Department of Chemistry, Faculty of Science, Okayama University, Tsushimanaka, Okayama-shi, Japan *Anal. Chem., 50 (1978)*

* Corresponding author.

ORION's new "BOD electrode".

Measure dissolved oxygen with your pH meter.



a complete O_2 measuring system

Using any pH meter as the readout, the ORION 97-08 oxygen electrode greatly simplifies the routine measurement of dissolved oxygen and particularly the measurement of biological oxygen demand. Incorporated into one small package is an O_2 sensor, a thermocompensator, electronic circuits, and operating controls.

pH meter readout

The miniaturized circuits built into this electrode change the electrical output of the O_2 sensing element into a signal that can be "read" by your present analog or digital pH meter (eliminating the expense of a dedicated oxygen meter). This conversion makes sense because typical dissolved oxygen concentrations of water happen to fall into the range 0 to 14 ppm, making the pH scale of your meter well suited for reading oxygen levels.

fast, simple standardization

Standardization is made extraordinarily simple by the independent controls on the electrode that let you use room air as your standard rather than the air-saturated water used with conventional electrodes.

simplified BOD measurements

The electrode comes with an accessory overflow funnel that simplifies the measurement of oxygen in BOD bottles. The funnel is inserted into the bottle before measurement to provide a reservoir for the water displaced by the electrode. The funnel prevents sample spillage and allows you to make oxygen measurements in the same BOD bottle before and after incubation. The neck of the overflow funnel extends down into the bottle and incorporates a captive magnetic stirring bar that provides the sample agitation necessary for accurate results (no retrieving stirring bars from your sample bottles!).

fool-proof maintenance

The sensor portion of the electrode employs a replaceable membrane/electrolyte module that eliminates the cutting and mounting of membranes as well as the electrolyte refills necessary with most oxygen electrodes.

The ORION model 97-08 oxygen electrode makes O_2 measurement as simple as pH measurement. This electrode is available from most leading laboratory supply distributors.

ORION RESEARCH

380 Putnam Ave. Cambridge, MA 02139 (800) 225-1480

CIRCLE 156 ON READER SERVICE CARD

Briefs

Spectrophotometric Determination of Trace Sulfate in Water 1793

A sensitivity of 1 ppm and precision of ±4% are achieved with a 100-μL aliquot.

Purnendu K. Dasgupta, Lionel G. Hanley Jr., and Philip W. West,* Environmental Sciences Institute, Chemistry Department, Louisiana State University, Baton Rouge, La. 70803 *Anal. Chem., 50 (1978)*

AC-Coupled Inverse Raman Spectrometry 1796

Induced absorption down to 0.005% is measured, giving better detection limits than CARS and no nonresonant background.

Michael D. Morris,* David J. Wallan, G. Patrick Ritz, and Jeanne P. Haushalter, Department of Chemistry, University of Michigan, Ann Arbor, Mich. 48109 *Anal. Chem., 50 (1978)*

Computer-Controlled Dual Wavelength Spectrophotometer 1799

A wavelength modulation precision of better than $\pm 2.5 \times 10^{-4}$ nm is achieved.

K. L. Ratzlaff, School of Chemical Sciences, University of Illinois, Urbana, Ill. 61801, and **F. S. Chuang, D. F. S. Natusch, and K. R. O'Keefe,*** Department of Chemistry, Colorado State University, Fort Collins, Colo. 80523 *Anal. Chem., 50 (1978)*

Resolution and Instrument Line Shape Effects on Spectral Compensation with Fourier Transform Infrared Spectrometers 1804

Boxcar truncation is found preferable to triangular apodization for special subtraction of weak bands; compensation of stronger bands depends on the band half-width and resolution.

Robert J. Anderson, Department of Chemistry, Ithaca College, Ithaca, N.Y. 14850, and **Peter R. Griffiths,*** Department of Chemistry, Ohio University, Athens, Ohio 45701 *Anal. Chem., 50 (1978)*

Speed of Analysis in Open Tubular Columns Gas Chromatography 1812

Narrow bore capillary columns permit a large decrease in analysis time and high efficiencies without marked reduction in sensitivity.

Georges Guiochon, Laboratoire Chimie Analytique Physique, Route de Saclay, 91128 Palaiseau, Cedex France *Anal. Chem., 50 (1978)*

Determination of Nitrogen Compound Distribution in Petroleum by Gas Chromatography with a Thermionic Detector 1822

The method is sensitive to low ppm concentrations of N, and has an accuracy of about 7 to 8% relative.

D. Kendall Albert, Standard Oil Company (Indiana), Amoco Research Center, Naperville, Ill. 60540 *Anal. Chem., 50 (1978)*

Cubic Spline Interpolation for the Calculation of Retention Indices in Temperature-Programmed Gas–Liquid Chromatography 1829

The method described is used when the indices serve as input for statistical analyses and identification procedures.

Wolfgang A. Halang,* Rolph Langlais, and Ernst Kugler, Coca-Cola GmbH, Research & Development Department, Kaninenbergstr. 66, 4300 Essen 1, West Germany *Anal. Chem., 50 (1978)*

Comparison of Thin-Layer and Column Chromatography for Separation of Sedimentary Hydrocarbons 1833

The two techniques may be used interchangeably for purification of sedimentary hydrocarbon extracts.

Juanita N. Gearing* and Patrick J. Gearing, Marine Ecosystems Research Laboratory, Graduate School of Oceanography, University of Rhode Island, Kingston, R.I. 02881, and **Thomas F. Lytle and Julia S. Lytle,** Gulf Coast Research Laboratory, P.O. Drawer AG, Ocean Springs, Miss. 39564 *Anal. Chem., 50 (1978)*

Determination of Volatile Halogenated Hydrocarbons in Water with XAD-4 Resin 1836

The degree of adsorption is studied with two series-connected columns, and the chloroethenes are found to be more strongly adsorbed than the haloalkanes.

Lars Renberg, Special Analytical Laboratory, National Swedish Environment Protection Board, Wallenberg Laboratory, University of Stockholm, S-106 91 Stockholm *Anal. Chem., 50 (1978)*

Solid Sorbent for Sampling Acrolein in Air 1839

Activated 13X molecular sieves are suitable for sampling acrolein in air, providing quantitative trapping and recovery and stability in storage.

Avram Gold,* C. E. Dubé, and R. B. Perni, Department of Environment Health Sciences, Harvard School of Public Health, 665 Huntington Avenue, Boston, Mass. 02115 *Anal. Chem., 50 (1978)*

Comparison of Porous Copolymers and Related Adsorbents for the Stripping of Low Molecular Weight Compounds from a Flowing Air Stream 1842

Adsorption isotherms and the effects of particle size, column length and reuse, flow rate, coelution of water and of organic compounds are determined.

Robert Sydor and Donald J. Pietrzyk,* Chemistry Department, The University of Iowa, Iowa City, Iowa 52242 *Anal. Chem., 50 (1978)*

Determination of Sub-nanogram per Gram Quantities of Light Hydrocarbons (C_2–C_9) in Rock Samples by Hydrogen Stripping in the Flow System of a Capillary Gas Chromatograph 1848

The lowest detectable quantity is about 10^{-11} g butane, representing 0.01 ppb for the maximum weight of 1 g.

Rainer G. Schaefer,* Bernd Weiner, and Detlev Leythaeuser, Kernforschungsanlage Jülich GmbH, Programmgruppe für Erdöl and Organische Geochemie, Postfach 1913, D-5170 Jülich 1, Federal Republic of Germany *Anal. Chem., 50 (1978)*



The voyage has value beyond the cargo.

There's got to be more to it than the conveyance of goods for dollars. That's why we've chosen this ship, shown in a glorious moment of passage, to communicate our feelings as we celebrate our 78 years as a company.

We want to thank those who have given our venture purpose as well as reward. We'd like them to join us in the thought that commerce need not be dull.

There are still challenges which require the skilled coordination of minds and hands. To this requisite ability is added the confidence that our craft was well designed and soundly built, and continues stoutly manned and competently handled. Arthur H. Thomas Company, Vine Street at Third, Philadelphia, PA 19106.

ARTHUR H. THOMAS COMPANY

CIRCLE 200 ON READER SERVICE CARD

NEW

Tape Recordings on

TOXIC SUBSTANCES CONTROL

☐ **Toxic Substances Control Act**

Implementation of the Toxic Substances Control Act poses many problems and offers some opportunities. The role of Government, industry and universities is discussed.
5 Speakers

☐ **Methods for Risk Assessment**

Risks and hazards posed to society by chemicals, radiation, and other toxic materials are discussed by scientists and Government spokesmen. **5 Speakers**

☐ **Monitoring Toxic Substances**

Dr. Bruce Ames and scientists from ERDA and MIT discuss hazards and detection of carcinogens, mutagens, and other toxic substances found in industrial environments.
4 Speakers

☐ **Biological Effects of Pollutants**

Experts examine the effects of environmental pollutants on health. Long-term/low-level studies, and controlled studies in humans are discussed. **5 Speakers**

☐ **Chemical Carcinogens**

An in-depth look at the problem of hazardous substances in the environment. Experts from N.I.O.S.H., EPA, and the National Cancer Institute discuss the what, why, how, and management of this growing national problem.
5 Speakers

Prices: $19.95 per title (Postpaid)

cassettes only
price includes printed copies of slides used

SPECIAL—$49.95 Any Three Titles (Postpaid)

ORDER FROM:
American Chemical Society
1155 Sixteenth Street, N.W.
Washington, D.C. 20036
Dept. AP

Name _____

Address _____

City _____ State _____ Zip _____

(Allow 4 to 6 weeks for delivery)

Briefs

Oscillating Slit Mechanism for the Determination of Hydrogen Isotope Ratios in a Microwave Induced Plasma 1903

The hydrogen and deuterium atomic emissions are measured alternately by a monochromator with an oscillating exit slit mechanism.

Frederick P. Schwarz,* Walter Braun, and Stanley P. Wasik, National Bureau of Standards, Washington, D.C. 20234
Anal. Chem., 50 (1978)

Diffuse Reflectance Measurements by Infrared Fourier Transform Spectrometry 1906

An optical system for diffuse reflectance infrared spectrometry is described.

Michael P. Fuller and Peter R. Griffiths,* Department of Chemistry, Ohio University, Athens, Ohio 45701
Anal. Chem., 50 (1978)

Separation of Alkylphenols by Normal-Phase and Reversed-Phase High-Performance Liquid Chromatography 1911

Empirical correlation factors are developed which relate log k' values for alkylphenols, the naphthols, and two phenylphenols to structural features.

J. F. Schabron and R. J. Hurtubise,* Department of Chemistry, University of Wyoming, Laramie, Wyo. 82071, and **H. F. Silver,** Mineral Engineering Department, University of Wyoming, Laramie, Wyo. 82071
Anal. Chem., 50 (1978)

Polarographic Behavior of Benzylpenicillenic Acid 1917

The direct current and differential pulse polarography of the sulfhydryl group of benzylpenicillenic acid in the absence and presence of Triton X-100 is investigated.

Mohammed Jemal and Adelbert M. Knevel,* Department of Medicinal Chemistry and Pharmacognosy, School of Pharmacy and Pharmacal Sciences, Purdue University, West Lafayette, Ind. 47907
Anal. Chem., 50 (1978)

Buffers for the Physiological pH Range: Thermodynamic Constants of 3-(*N*-Morpholino)-propanesulfonic Acid from 5 to 50 °C 1922

The pK_2 values for the dissociation of the NH^+ charge center of the ampholyte molecule are determined with hydrogen and silver–silver bromide electrodes.

Munessar Sankar and Roger G. Bates,* Department of Chemistry, University of Florida, Gainesville, Fla. 32611
Anal. Chem., 50 (1978)

Instrumental Approach to Potentiometric Stripping Analysis of Some Heavy Metals 1924

A battery-operated potentiostat and a x-t recorder are the major instrumentation used in the determination of Bi, Cu, Tl, Cd, Pb, and Zn.

Daniel Jagner, Department of Analytical Chemistry, University of Gothenburg, Fack, S-402 20 Göteborg (Sweden)
Anal. Chem., 50 (1978)

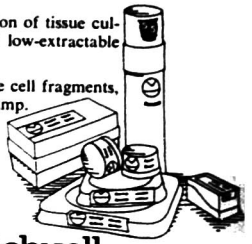
The Antlia™ hand pump puts pressure on the liquid, not on you.

You've seen this little drama in your lab: you homogenize some tissue into liquid, put it into a standard syringe, then try to separate the plasma from the debris by running it through a membrane. Only it takes more muscle than you have to drive down the plunger to push the solution through the debris-clogged membrane . . . and then, to add to your problems, the syringe starts to leak.

S&S puts an end to all this with the S&S Antlia system — because its unique hand pump can build and sustain pressures as high as 75 psi — far more than can be developed by a standard syringe. It's designed to separate out the soluble fractions from homogenized cells without impossible effort, without leaking, without clogging. And that's why, in the fields of immunochemistry and immunology, it's the most-used device of its kind.

For greatest efficiency in using the Antlia system for this application, we recommend S&S BA85 membrane filters (0.45μm). The Antlia is used for any number of other applications as well, e.g., cold-sterilization of tissue culture media where we recommend low-extractable BA83/1 (0.2μm).

To remove the effort, as well as the cell fragments, use the Antlia pneumatic hand pump. For complete information on the Antlia system and S&S membranes, ask Schleicher & Schuell, Inc., Keene, New Hampshire 03431; (603) 352-3810.

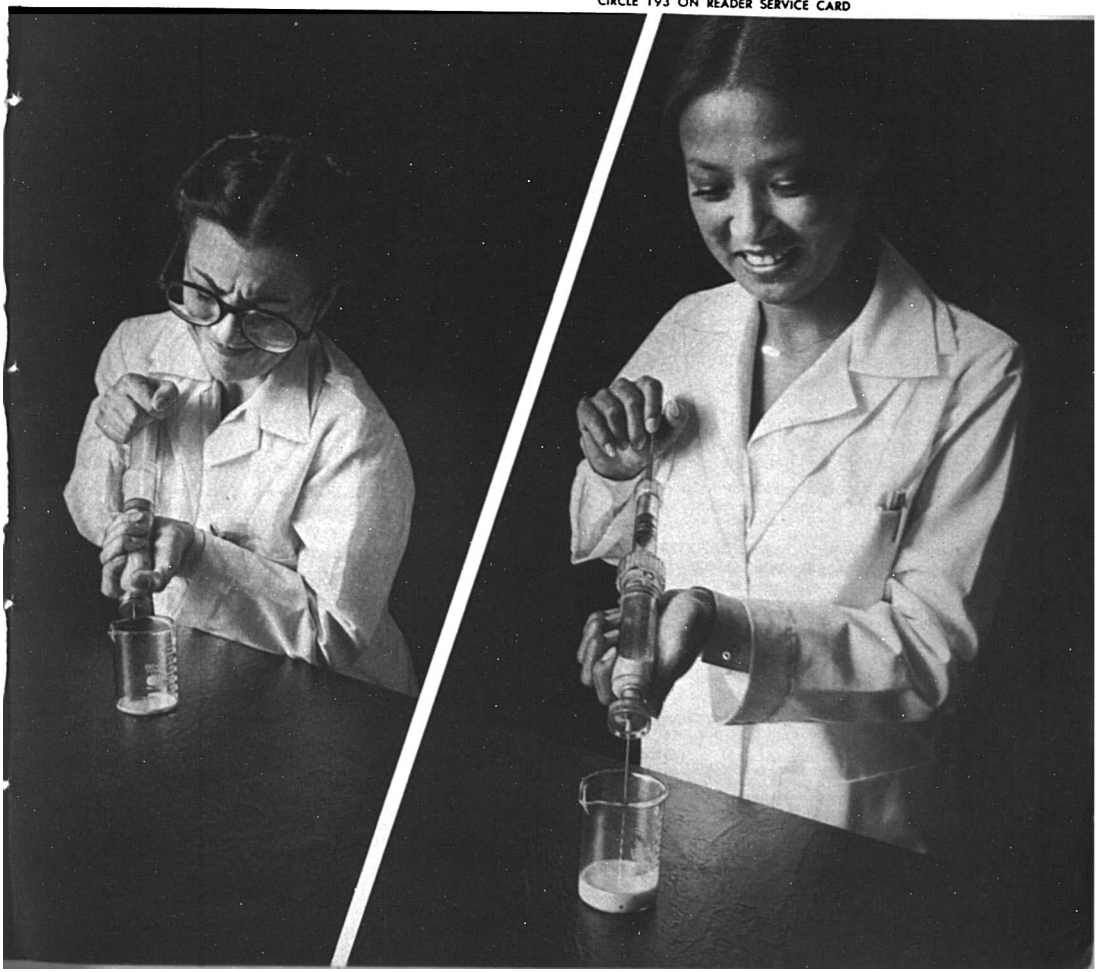


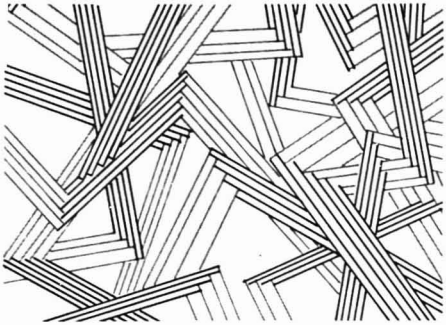
Schleicher & Schuell

Schleicher & Schuell, Inc.
Keene, New Hampshire 03431

Schleicher & Schüll GmbH, D-3354, Dassel, West Germany
Schleicher & Schüll AG, 8714, Feldbach ZH, Switzerland

CIRCLE 193 ON READER SERVICE CARD





Copolymers, Polyblends, and Composites

Advances in Chemistry Series No. 142

Norbert A. J. Platzer, *Editor*

A symposium sponsored by the Division of Industrial and Engineering Chemistry, and co-sponsored by the Division of Polymer Chemistry, the Division of Organic Coatings and Plastics Chemistry, and the Division of Cellulose, Wood, and Fiber Chemistry of the American Chemical Society.

This timely collection of thirty-eight papers is comprehensive and unique in its coverage of the latest research results on copolymers, polyblends, and composites which are used to toughen brittle polymers with active fillers, and to strengthen or stiffen plastics with fibers or minerals.

Specific topics include:

- determination of MWD in homopolymers; liquid-liquid phase transition phenomena
- grafting kinetics of ABS; rubber-modified polymers; block copolymers; laminating resins; vinylene carbonate
- polymerization and copolymerization behavior; covulcanization of elastomer blends

482 pages (June 1975) $34.50 clothbound (ISBN 0-8412-0214-1).

SIS/American Chemical Society
1155 16th St., N.W./Wash., D.C. 20036

Please send _____ copies of *No. 142 Copolymers, Polyblends, and Composites* at $34.50 per book.

☐ Check enclosed for $ _____ ☐ Bill me.
Postpaid in U.S. and Canada, plus 40 cents elsewhere.

Name

Address

City State Zip

Briefs

Capacitive Integration to Produce High Precision Isotope Ratio Measurements on Methyl Chloride and Methyl Bromide Samples 1930

The RSD of measured ratios for methyl chloride is 13 parts in 10^6 while that for methyl bromide is 7 parts in 10^6.

John F. Willey and James W. Taylor,* Department of Chemistry, University of Wisconsin, Madison, Wis. 53706
Anal. Chem., 50 (1978)

Correspondence

High-Resolution Nulcear Magnetic Resonance Spectrometry in Thermotropic Nematic Liquid Crystals with Negative Diamagnetic Anisotropy 1934

Ludwig Pohl* and Rudolf Eidenschink, E. Merck, Darmstadt, Germany *Anal. Chem., 50 (1978)*

Thermal Effects upon Spatial Mode Structure of a Linear Flashlamp-Pumped Dye Laser 1936

John R. FitzPatrick and Edward H. Piepmeier,* Department of Chemistry, Oregon State University, Corvallis, Ore. 97331
Anal. Chem., 50 (1978)

Exchange of Comments on Interferometric Concentration Determination of Dextran after Gel Chromatography 1937

F. El-Hosseiny* and R. D. Gilbert, Fiber Sciences Department Weyerhaeuser Company, 3400-13th Avenue SW, Seattle, Wash. 98134, and **Lars Hagel,** Pharmacia Fine Chemicals AB, Box 175, S-751 04 Uppsala, Sweden *Anal. Chem., 50 (1978)*

Aids for Analytical Chemists

Programmable-Gain or Auto-Gain Amplifier 1938

K. R. O'Keefe, Department of Chemistry, Colorado State University, Fort Collins, Colo. 80523 *Anal. Chem., 50 (1978)*

Highly Regulated Power Supply for Hydrogen or Deuterium Arc Lamps Used in Ultraviolet Spectrometry 1941

Ronald E. Edstrom, Department of Biochemistry, The Medical School, University of Minnesota, Minneapolis, Minn. 55455
Anal. Chem., 50 (1978)

BASIC READERS: 1978

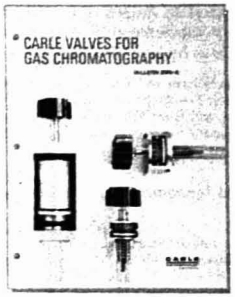
Free Technical Literature from Carle Instruments



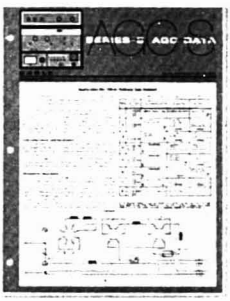
Automated Series-S AGCs put a price on the answer
Series-S Analytical Gas Chromatographs are each application engineered for a specific analysis. Each utilizes Carle's unique column sequencing techniques to produce fast, sensitive, and complete analyses—automatically. Brochure contains complete technical information and a table detailing components separated in each application.
CIRCLE 40



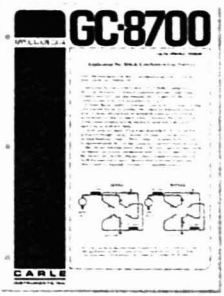
New Generation Basic™ Gas Chromatographs
Here's the GC that puts a price on the answer at a cost everyone can afford. The new BGCs are now factory dedicated to perform specific analyses, and many models include built-in gas sampling and switching valves. An 8-page full color brochure describes the technical features of both TCD and FID models.
CIRCLE 41



Carle "Lifetime" Valves for Gas Chromatography
All Carle valves now carry a lifetime warranty, and this revised 1978 bulletin has 10 pages of technical details on the rotary shear seal technology which makes it possible. The different features offered on Carle valves are explained, enabling selection of the one best suited to your needs. A companion piece to Carle's "Imagineering" applications booklet (below).
CIRCLE 42



Series-S AGC Data Sheets
The automated, multi-column multi-valve techniques which have put the Series-S AGC at the leading edge of GC technology are described in these highly informative application data sheets. 20 different applications are covered and include chromatograms and system flow diagrams. Send for sample data sheet plus list of others available.
CIRCLE 43



Application Data Sheets for Basic™ Gas Chromatographs
Each new generation BGC is application engineered to perform a specific analysis. Carle has prepared data sheets detailing how each of the 15 different analyses are accomplished. Included with the description is a chromatogram and GC flow diagram. Send for sample data sheet plus list of others available.
CIRCLE 44



Imagineering with Carle GC Valves
A 70 page how-to-do-it manual, filled with application material available from no other source. Contains 36 individual applications described and diagrammed for easy installation, including gas sampling, sampling liquids and liquefied gas, multi-column switching, backflush, series/bypass, detector selection, fraction selection and heartcut, stream selection, multi-function and multi-valve combinations.
CIRCLE 45

For quick action in obtaining Carle's 1978 Basic Readers, call Carle Instruments direct at 714-761-9000.

CARLE
INSTRUMENTS, INC.
A Hach Company

1200 Knollwood Circle
Anaheim, CA 92801

Briefs

Carboxylate Anions from Fatty Acids by Esterification with *p*-Nitrobenzyl Bromide for Analysis of Fatty Acid Mixtures by Negative Ion Mass Spectrometry 1943

Yukio Hirata and Tsugio Takeuchi, School of Materials Science, Toyohashi University of Technology, Toyohashi 440, Japan, and **Kozo Matsumoto,*** Department of Synthetic Chemistry, Faculty of Engineering, Nagoya University, Nagoya 464, Japan
Anal. Chem., 50 (1978)

Rapid Transferring Device for Immiscible Liquids 1944

Harvey A. Schwertner, Department of Pathology, The University of Texas Health Science Center at San Antonio, 7703 Floyd Curl Drive, San Antonio, Tex. 78284
Anal. Chem., 50 (1978)

Automatic Gravimetric Titration System 1945

Roger Guevremont and Byron Kratochvil,* Department of Chemistry, University of Alberta, Edomonton, Alberta T6G 2G2, Canada
Anal. Chem., 50 (1978)

Trace Determination of Subnanogram Amounts of Acrylonitrile in Complex Matrices by Gas Chromatography with a Nitrogen-Selective Detector 1948

R. S. Marano,* S. P. Levine, and T. M. Harvey, Ford Motor Company, Technical Sciences Department, Engineering & Research, Scientific Research Staff—Research, Dearborn, Mich. 48121
Anal. Chem., 50 (1978)

Pepperbush Powder, a New Standard Reference Material 1950

Kensaku Okamoto,* Yuko Yamamoto, and Keiichiro Fuwa, National Institute for Environmental Studies, P.O. Yatabe, Ibaraki, 300-21, Japan
Anal. Chem., 50 (1978)

Metal Dendrites for Lithium Cationization in Mass Spectrometry 1951

Tim L. Youngless, Maurice M. Bursey,* and Carl E. Rechsteiner, Jr., William Rand Kenan, Jr.-Laboratories of Chemistry, The University of North Carolina, Chapel Hill, N.C. 27514
Anal. Chem., 50 (1978)

CONSERVE GAS — SAVE $$$ WITH GAS MISER™

Helium or other carrier gas costs for GC can be reduced considerably with the Gas Miser from Matheson. Gas Miser enables gas chromatographers to maintain a reduced carrier gas flow when their GCs are on standby. The Gas Miser pays for itself in less than a year.



Matheson recommends that gas chromatographs be set on standby when not in use. Until now, this entailed spending valuable time adjusting the pressure regulators and needle valves – only to readjust them when the system was put back into use. Gas Miser does the job of reducing the gas flow with the flick of a switch. Full gas flow is restored just as easily.

Construction is of copper and brass. Gas Miser is sold with a 100 psig gauge. Instructions for set up are included with every instrument.

CIRCLE 138 ON READER SERVICE CARD

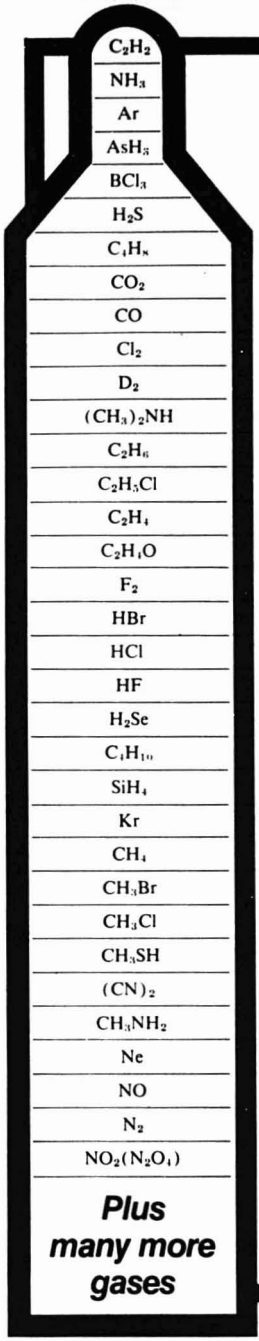
MATHESON PROVIDES PRECISE RADIOACTIVE GAS MIXTURES

Matheson can now supply most any combination of radioactive gases with Krypton-85, Carbon-14 and Tritium. Radioactive gas mixtures are available from Matheson prepared to either of two accuracies. Certified Standards, with a radioassay accurate to ± 10%, are the common analyzed calibration mixtures used in industry today. Where maximum accuracy is desired, Primary Standards are available with a radioassay to ± 5% and a mass spectrometer scan for impurities of the component gases.

Using radioactive gases for tracing can provide accurate, inexpensive information where chemical tracers cannot be used. Applications for radioactive gas mixtures in biochemistry include testing properties of materials, labeling compounds and tracing biochemical reactions.

Matheson is the only supplier of radioactive gas mixtures that provides a radioassay at no extra charge. The company states that this service ensures that the radioactive component gas has precisely the activity required. Matheson also provides a written certification for NRC (Nuclear Regulatory Commission) inventory records. **Matheson, P.O. Box E, Lyndhurst, NJ 07071.**

CIRCLE 139 ON READER SERVICE CARD



Only Matheson has a full range of gases...and the delivery systems to control them

Matheson supplies more than 90 gases in a large variety of purities...enough to meet every requirement.

Some of these gases present real storage and handling problems. Matheson experience provides its customers with delivery systems specially designed for the safe use of these gases in lab or plant.

Matheson can stock these gases...all of them...at 13 different plants in the U.S., Canada and Europe. These are Matheson owned plants, and they are dedicated to Specialty Gases... our only business.

When you need gases, come to Matheson. We supply more gases in more sizes with more technology for their proper use than does any other specialty gas supplier. Fifty years of service to the scientific community makes us the first in specialty gases.

Matheson
Lyndhurst, N.J. 07071

East Rutherford, N.J. 07073/Morrow, Georgia 30260/La Porte, Texas 77571
Gloucester, Massachusetts 01930/Joliet, Illinois 60434/Gonzales, Louisiana 70737
Cucamonga, California 91730/Newark, California 94560/Bridgeport, N.J. 08014
Dorhey, Maryland 21227/Whitby, Ontario, Canada L1N 5R9
Edmonton, Alberta, Canada T5B 4K6/B2431 Oevel, Belgium
6056 Heusenstamm, West Germany

CIRCLE 140 ON READER SERVICE CARD

From Technicon, innovators of the most advanced systems for automated chemical analysis ..... providing acknowledged benefits

Automated Colorimetric Analysis
Automated Ion Selective Electrode Analysis
Automated UV Spectrophotometric Analysis
Automated Thermometric Analysis
Automated Infrared Reflectance Analysis
Automated Fluorometric Analysis
Automated Flame Photometric Analysis
Automated Sample Preparation for GC

With these, Technicon Industrial Systems, the pioneer and a pacesetter in automated analytical chemistry, offers improved profits and productivity in laboratory analysis and on-line in the plant.

- ☐ Faster Analytical Response
- ☐ Improved Precision and Accuracy
- ☐ Greater Sample Handling Capacity

which afford

- ☐ Tighter Tolerance Control
- ☐ Higher Product Yield
- ☐ Lower Raw Material Costs

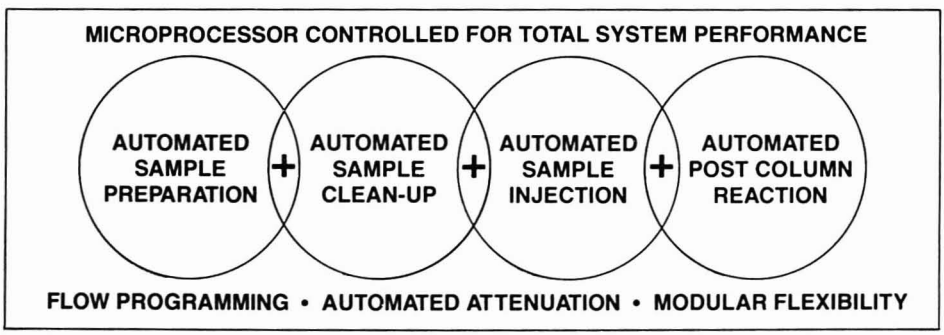
Plus,

- ☐ Dramatically Reduced Technician Time and Involvement

Technicon FAST-LC™

FULLY AUTOMATED SAMPLE TREATMENT

Continuous-flow technology combined with HPLC..



FAST•LC is the only full capability, totally automated LC system with functions ranging from automation of existing UV detection HPLC assays to automation of sample pre-treatment to automation of post-column derivatization, with no intermediate manual steps!

FAST•LC is an advanced technology for expanding the capabilities of HPLC and meeting the growing workload of analytical laboratories. It is uniquely designed for the laboratory that *must*:

▷ Increase productivity and slash manual costs in HPLC work.
▷ Obtain the sensitivity and specificity furnished by post-column derivatization.
▷ Have the precise results provided by completely automated HPLC assays.



FAST•LC delivers acknowledged benefits
PLUS!

- ○ Expanded detection capability that permits many new substances to be analyzed, using post-column derivatization in conjunction with UV, fluorometry, colorimetry and ISE.
- ○ Automated handling of both solid and liquid samples.
- ○ Automated attenuation for superior quantitation in multi-component samples.
- ○ Flow programming solvent delivery, to maximize sample analysis rates.

..a revolutionary new dimension in analytical chemistry!

Just as the Technicon AutoAnalyzer automated manual wet chemistry, now Technicon FAST•LC *truly* automates HPLC.

PLUS!

If your laboratory already possesses HPLC equipment, you can update it to a modern research system simply by adding the needed Technicon FAST•LC components!

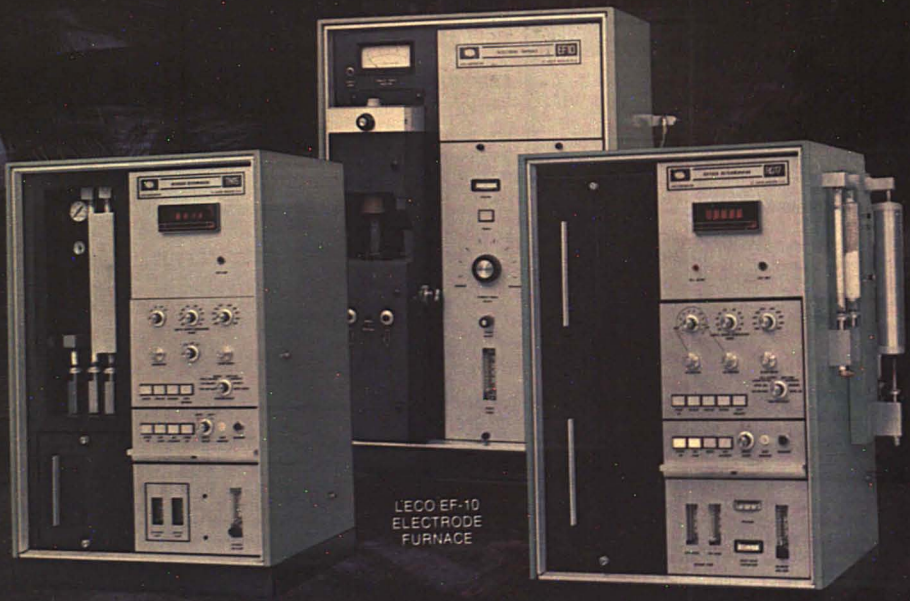
For the complete story on how FAST•LC can benefit you, telephone toll-free 800-431-1970, ext. 2486, or write Dept. KX072.

Technicon Industrial Systems
Tarrytown, New York 10591

TM

CIRCLE 204 ON READER SERVICE CARD

LECO® is No.1 in analyses of gases in metals



LECO TN-15
NITROGEN DETERMINATOR

LECO EF-10
ELECTRODE
FURNACE

LECO RO-17
OXYGEN DETERMINATOR



LECO® Gas Determinators for the Rapid and Accurate Determination of Nitrogen, Oxygen, and Hydrogen in Metals.

LECO® offers a complete line of instruments for determining oxygen, nitrogen and hydrogen in ferrous and non-ferrous metals, and other inorganic materials. These instruments are ideal for both laboratory and production control applications and are available with data output interfaces for remote printout and computer compatibility.

Contact LECO Today!

LECO CORPORATION 3000 Lakeview Ave. St. Joseph, MI 49085, U.S.A. Phone: (616) 983-5531

LECO®

CIRCLE 133 ON READER SERVICE CARD

Letters

GLP's and Regulations

Sir: I really enjoyed Mr. Horwitz' article entitled "Good Laboratory Practices in Analytical Chemistry," which appeared in the May 1978 issue. I discussed the article with my students in my analytical chemistry course at the University of Zulia. My main purpose in doing this was to emphasize the needs and responsibilities of analytical chemists in our jobs. This is a necessary and valid idea to inculcate in new generations of chemists.

Also, I have the opportunity, by using the illustrations, to lecture about safety (mainly on the need to wear eye protectors like goggles). I feel in our country we do not have enough safety rules for academic laboratory work. We are struggling to elaborate and apply these rules to guarantee safety in the chemistry lab. Our people still don't understand why safety glasses must be worn, why mouth pipetting must be avoided, or why chemicals must not be inhaled, touched, or tasted, regardless of what chemicals one is working with.

I suggest you publish some articles on this topic, which I'm sure would be welcome in many countries around the world.

Romer A. Romero
Safety Committee Chairman
Department of Chemistry
University of Zulia
Maracaibo, Venezuela

Reply: We plan to have an article on laboratory safety early in 1979.

Sir: In reference to your editorial on GLP's, analytical chemists might participate in the decision-making process if they knew what the decisions were about and how to participate. Few will have access to the document. I suggest that you publish it in sections because it is too long for one issue of ANALYTICAL CHEMISTRY. Comment upon the sections by someone familiar with FDA thinking would be helpful in revealing the meaning of the bureaucrateese and the location of potential booby traps.

Part of GLP's is already in GMP's (good manufacturing practices), and some of it will undoubtedly be included in future G?P's. Who is next? The clinical chemists? That will be an interesting encounter for the FDA lawyers who concoct the regulations.

Progressive chemistry departments will establish at least one course to teach chemists to read and understand regulations. They will learn, what is to them, the peculiar thought process of lawyers and of other qualitative people who dominate government. These people seem to think that proceeding according to regulations and doing the paper work are all that are necessary to achieve correct results.

My suggestions are: print the GLP's in sections, solicit comment on each section, print section and comments together, and pay particular attention to comments from within the FDA concerning unstated nonscientific aspects of the document.

Voluminous comments have been made and should be available to you. Should you decide to use existing material, it should be selected very carefully by an experienced analyst (not a journalist) with the unofficial assistance from someone from FDA. The reasons the GLP's were written are worth publishing. It is time that analysts become aware of the politics of regulations and the part analysts had in causing them to be written. A bit of the real world would not be out of place in ANALYTICAL CHEMISTRY.

Frederick Kavanagh
231 Blue Ridge Road
Indianapolis, Ind. 46208

Reply: An ad hoc committee was appointed by the Analytical Chemistry Division of the American Chemical Society in September at Miami Beach to contribute material for publication in the REGULATIONS section of the JOURNAL. Robert A. Libby of Procter & Gamble is chairman of this committee, which also includes Donald T. Sawyer, University of California, Riverside; William T. Donaldson, EPA; and Warren Crummett, Dow Chemical Co. This committee will be addressing some of the problems you raise in your letter. See Dec. REGULATIONS.

The JOURNAL itself cannot spare the space for publication of the GLP's or other regulations as they are published. Our pages are urgently needed for publication of original research contributions. Many libraries subscribe to the *Federal Register*. Subscriptions to the *Federal Register*, which is published daily, Monday–Friday, are available, postage free for $5.00 per month or $50 per year, payable in advance. Individual copies are 75¢ for each group of bound pages. Send check or money order payable to the Superintendent of Documents, U.S. Government Printing Office, Washington, D.C. 20402.

Free workshops on how to use the *Federal Register* will be held in Nov. and Dec.; see For Your Information, page 1221 A, this issue.

Typo Noted

Sir: We have recently noticed a typographical error in the "Side by Side Drinking Water Analysis Handbook" (published by Hach Chemical Co., Ames, Iowa, copyright 1977) that could cause serious injury. On page 31 of this manual, under Arsenic determination, Note E recommends the replacement of the zinc slurry with a sodium borohydride solution. The procedure for preparing this solution as written recommends a 25% sodium borohydride solution instead of a 2.5% solution. The use of the 25% solution results in extremely vigorous generation of hydrogen accompanied by large pressure buildup.

Because this manual may be used by water quality labs as a quick reference for lab technicians, we felt it advisable to notify others of this potential safety hazard.

William G. Leseman
City of Tallahassee Water Quality Lab
City Hall
Tallahassee, Fla. 32304

Contributions from readers are invited for the LETTERS section. Topics should preferably be of broad interest to readers and/or may be comments on material published in the A-pages. See Prof. Laitinen's editorial, page 1281, August 1977.

Trace Element Analysis: How to be sure that those traces are really in the sample... and not in the acid.

"...in each step of trace analysis the risk of contaminating the sample is real."*

J.T. Baker—the company that sells more laboratory acids for all uses than anyone else—has several acid product lines specifically designed for trace analysis. These can assure that you're not unknowingly adding contaminants and that you're actually measuring your sample... *and not the contaminants in your reagents.*



ULTREX® Acids
These acids represent the ultimate in purity and product definition commerically available... J.T. Baker is the world's largest supplier of such ultrahigh purity acids. For the lowest blanks, for maximum product definition (actual lot analysis on each certificate), for assurance that your work will not be compromised or jeopardized by impurities or uncertainties, no other acids can even begin to match ULTREX acids.

'Baker Analyzed'® Reagent Acids (BAR)
These acids—and all the other acids discussed here—are the only ones commercially available with the *actual lot analysis* on every container label. More than that: 'Baker Analyzed' Reagent acids are routinely subjected to more tests than required to meet ACS purity standards. BAR acids are ideal for demanding trace analysis and, as with all Baker acids intended for trace analysis, only your sample is an "unknown." *Currently available:* acetic, hydrochloric, hydrofluoric, nitric, perchloric, and sulfuric acids.

Baker Specialty Acids
- Sulfuric acid for the Babcock Milk Test (meets Food Chemical Codex specifications).
- Low-mercury acids: with mercury controlled to less than 5 ppb, they are especially suitable for mercury determinations. *Available:* sulfuric, perchloric, and nitric acids. Note that these specialty acids are also 'Baker Analyzed' Reagents and meet the same stringent specifications previously discussed for this grade.

A note about Baker acid containers
Baker offers a wide choice of safe and appropriate-to-the product containers. For example, our acids are always in *clear* glass, never brown. (Brown bottles leach impurities into the acid and hide discoloration and particulate matter.) Clear glass bottles with protective plastic coating are also available.

For more information
Check with your local Baker distributor (there are 120 stocking locations) or write or call J.T. Baker, Phillipsburg, New Jersey 08865, phone 201/859-2151 or use coupon below.

In the final analysis... the professional chooses J.T. Baker

J.T.Baker® CHEMICALS

J.T. Baker Chemical Company
Phillipsburg, New Jersey 08865

* "Tracing the Elements," A.J. Barnard, Jr. and R.W. Dudley, *Industrial Research*, March 1973.

CIRCLE 18 ON READER SERVICE CARD

J.T. Baker Chemical Co.
Phillipsburg, N.J. 08865 • 201/859-2151

I'm interested in learning more about your acids for trace analysis:
- ☐ ULTREX® Ultrapure acids
- ☐ 'Baker Analyzed'® Reagent acids
- ☐ Sulfuric acid for the Babcock Milk Test
- ☐ Low-mercury acids.

Name_____
Title_____
Department_____
Organization_____
Address_____
_____ Zip
Telephone_____ (Area Code) _____ (Ext.)

Announcing:

Finnigan Series 1020 Automated GC/MS

Now the power of GC/MS analysis is within reach of every laboratory.



- Significantly lower initial cost
- Simplified, automated operation
- Fast sample throughput
- Highest qualitative and quantitative performance
- Reduced maintenance and operating costs

The need for a GC/MS system suitable for routine, simplified, general purpose analyses has led to the Finnigan 1020. A number of design innovations, based on our years of experience in GC/MS and in data system technology, make the Finnigan 1020 suitable for modern laboratories which need the performance of GC/MS analysis but which have been reluctant to use it.

A powerful set of data acquisition, data processing and system control software is included with the instrument. The operator need not be an instrument expert however, because of the 1020's unique method of automatic program selection. Maximum analysis throughput is achieved because the system can acquire and process data simultaneously; that is, perform both foreground and background computer operation.

Data collected on the disc cartridge can be further processed on any Incos data system such as that incorporated in the Finnigan 4000 Series. This capability makes the Series 1020 an ideal workhorse partner for the 4000 in laboratories already equipped with the more comprehensive Finnigan instrument.

If your laboratory requires the power of GC/MS analysis, let Finnigan—the GC/MS people—show you how the 1020 Series can meet your needs more easily and inexpensively than ever before. It'll pay for itself many times over.

finnigan
Instruments
A DIVISION OF FINNIGAN CORPORATION
845 WEST MAUDE AVENUE
SUNNYVALE, CALIFORNIA 94086
(408) 732-0940

CIRCLE 73 ON READER SERVICE CARD



50th Anniversary Symposium of ANALYTICAL CHEMISTRY in honor of Lawrence T. Hallett, editor from 1955–1965

On September 13, 1978, at Miami Beach, Fla., ANALYTICAL CHEMISTRY celebrated its 50th volume year with a symposium chaired by Herbert A. Laitinen, current editor of the JOURNAL. The presentations will be published in the November and December issues

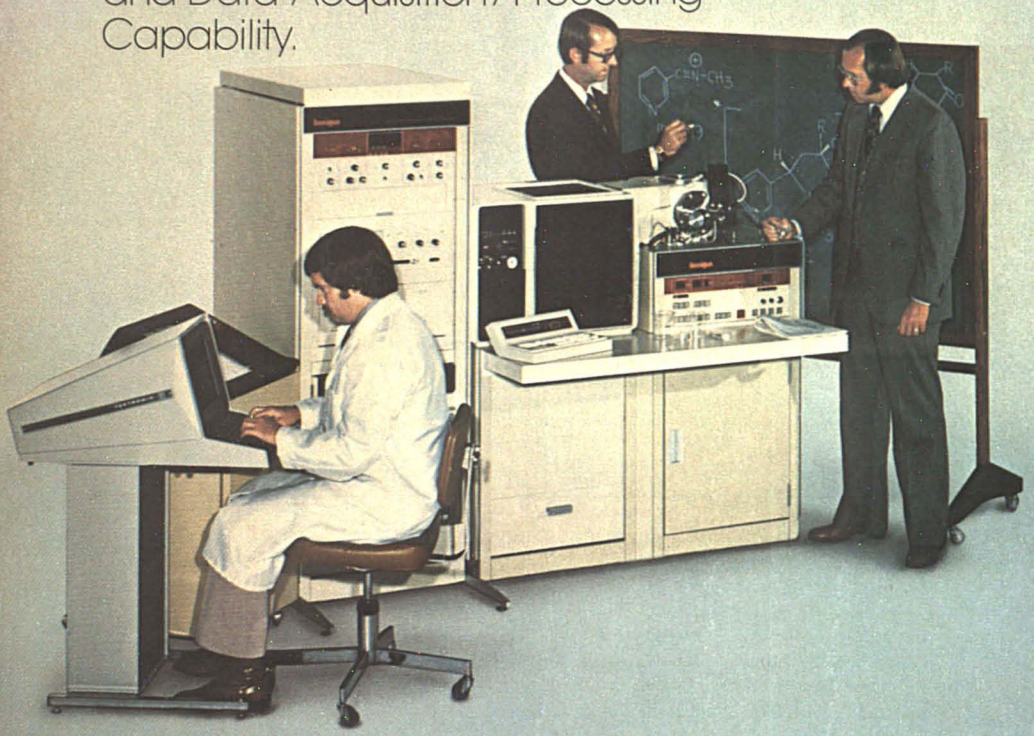
Editorial: Our Golden Anniversary—I. The Formative Years	1729
Edward Hart, The Man Behind the JOURNAL G. Earl Peace, Jr., Lafayette College	1194 A
L. T. Hallett, The Early Years Sidney Siggia, University of Massachusetts	1199 A
Analytical Chemistry: The JOURNAL and the Science, the 1930's Vernon A. Stenger, The Dow Chemical Co.	1201 A
Analytical Chemistry: The JOURNAL and the Science, the 1940's H. A. Laitinen, University of Florida	1205 A
Editorial: Our Golden Anniversary—II. Scientific Maturation	Dec. issue
Analytical Chemistry: The JOURNAL and the Science, the 1950's L. B. Rogers, University of Georgia	Dec. issue
Analytical Chemistry: The JOURNAL and the Science, the 1960's J. D. Winefordner, University of Florida	Dec. issue
Analytical Chemistry: The JOURNAL and the Science, the 1970's and Beyond Bruce R. Kowalski, University of Washington	Dec. issue
Some Concluding Remarks I. M. Kolthoff, University of Minnesota	Dec. issue
End of Symposium	
Analytical People: Faces Behind the Type Josephine M. Petruzzi, ANALYTICAL CHEMISTRY	Dec. issue

The symposium presentations and the additional material listed above will be available to interested persons as a combined reprint early in 1979. For copies at $1.00 each to cover postage and handling, write to ANALYTICAL CHEMISTRY, 1155 16th St., N.W., Washington, D.C. 20036

Presenting:

Finnigan 4023 Automated GC/MS

Unmatched GC/MS Performance and Data Acquisition/Processing Capability.



Finnigan's 4023 Automated GC/MS system is the most advanced of the 4000 Series instruments which have made Finnigan the recognized leader in the GC/MS field.

The 4023 provides the finest GC/MS performance available by any criterion, whether sensitivity, spectral quality, reliability, selectivity, or adaptability to special applications.

This GC/MS performance is coupled with a data acquisition/processing capability unequalled for speed, sophistication, choices in output formatting, and capability for chaining commands for individualized automation procedures.

Recent innovations include liquid chromatograph interfacing (LC/MS) and combined positive ion/negative ion mass spectrometry (PPINICI).

Finnigan users with previous Series 4000 GC/MS systems can update their present equipment by incorporating these and all other Finnigan advances. Finnigan's policy of maintaining adaptability of advances in the art to existing Finnigan equipment gives you the assurance you need that the system you acquire today will meet your needs for years to come.

Inquire today how Finnigan—the GC/MS people—can keep you at the forefront of research in your field.

finnigan
Instruments
A DIVISION OF FINNIGAN CORPORATION
845 WEST MAUDE AVENUE
SUNNYVALE, CALIFORNIA 94086
(408) 732-0940

CIRCLE 74 ON READER SERVICE CARD



G. Earl Peace, Jr., a native Virginian, received his BS degree in chemistry from Lafayette College in 1966. He earned his MS and PhD degrees in 1968 and 1971 from the University of Illinois at Urbana-Champaign. He then returned to Lafayette College where he is now associate professor of chemistry. In 1976 Dr. Peace was appointed to the Citizens Advisory Council to the Pennsylvania Department of Environmental Resources by Gov. Milton Shapp.



Sidney Siggia received his BS degree from Queens College in New York in 1942 and his MS and PhD degrees in 1943 and 1944 from Polytechnical Institute of Brooklyn. After working in analytical research and managerial positions at both General Aniline and Film and Olin Mathieson, he was appointed professor of chemistry at the University of Massachusetts in 1966. Professor Siggia is an inspired and gifted teacher who specializes in organic analysis and has published over 100 papers in this field in addition to six books and numerous chapters in textbooks. He has served in various advisory capacities and leadership roles including membership on ANALYTICAL CHEMISTRY's Advisory Board (1961–63). He received the Anachem Award (1969), the ACS Analytical Chemistry Award (1975), and the Kolthoff Award in Analytical Chemistry (1975).



Vernon A. Stenger, after studying chemical engineering at the University of Denver, turned to analytical chemistry under I. M. Kolthoff at the University of Minnesota and received his PhD in 1933. Subsequently, he has been employed in the Analytical Laboratories of the Dow Chemical Co., most recently as a consultant. Coauthor of parts of Kolthoff's "Volumetric Analysis", he has also contributed various papers and reviews on applied analysis and is a coinventor of instrumental methods for the carbon content and oxygen demand of water. He is a member and past chairman of the ACS Committee on Reagent Chemicals. Dr. Stenger served on ANALYTICAL CHEMISTRY's Advisory Board (1953–6) and in 1970 received the Anachem Award.



Herbert A. Laitinen, editor of ANALYTICAL CHEMISTRY, received his PhD in 1940 at the University of Minnesota where he worked under Prof. I. M. Kolthoff on electroanalytical chemistry with stationary and rotating microelectrodes. In 1940 he joined the University of Illinois where he became full professor and remained until 1974 when he accepted his present position as Graduate Research Professor at the University of Florida in Gainesville. His research interests are in electroanalytical chemistry, with emphasis on surface chemistry, molten salt chemistry, and environmental chemistry. In 1953 and 1962 he was awarded Guggenheim fellowships for study in Europe. Dr. Laitinen received the ACS Award in Analytical Chemistry in 1961, the 1964 Minnesota Outstanding Alumni Award, and the SOCMA Award in Environmental Chemistry in 1975. He has numerous publications, including several books, to his credit. Most recently, he coedited with Galen Ewing the multiauthored "A History of Analytical Chemistry."



Lockhart B. Rogers, Graham Perdue Professor of Chemistry at the University of Georgia, earned his PhD at Princeton University in 1942. He taught at Stanford University, directed long-range analytical research at Oak Ridge, and taught at MIT and Purdue University before moving to Georgia in 1974. His main research interests have been in chromatography and more specifically in absorbents, optimizing separations in gas and liquid chromatography and in interfacing chromatography and computers. Dr. Rogers has been active in scientific organizations and has served in advisory capacities for various programs including ANALYTICAL CHEMISTRY (1961–63). He has numerous publications and has been especially effective in motivating and inspiring other scientists by his own dynamic and overriding interest in many subjects. Dr. Rogers won the ACS Award in Analytical Chemistry in 1974.



James D. Winefordner received his BS, MS, and PhD degrees from the University of Illinois in 1954, 1955, and 1958. He joined the University of Florida as an assistant professor in 1959 and is now Graduate Research Professor and chairman of the analytical division of the department of chemistry. His research interests include atomic and molecular emission, absorption and fluorescence in flames and hot gases, molecular fluorescence and phosphorescence of species in the condensed phase, and the development of liquid chromatography detectors and spectroscopic instrumentation. He serves and/or has served in various advisory capacities including ANALYTICAL CHEMISTRY's Advisory Board (1969–71). He received the 1971 Sigma Xi University of Florida Research Award, the 1968 Meggers Award, the 1973 Pittsburgh Society of Spectroscopy Award, the 1973 ACS Award in Analytical Chemistry, and the 1978 Analytical Division Chemical Instrumentation Award.



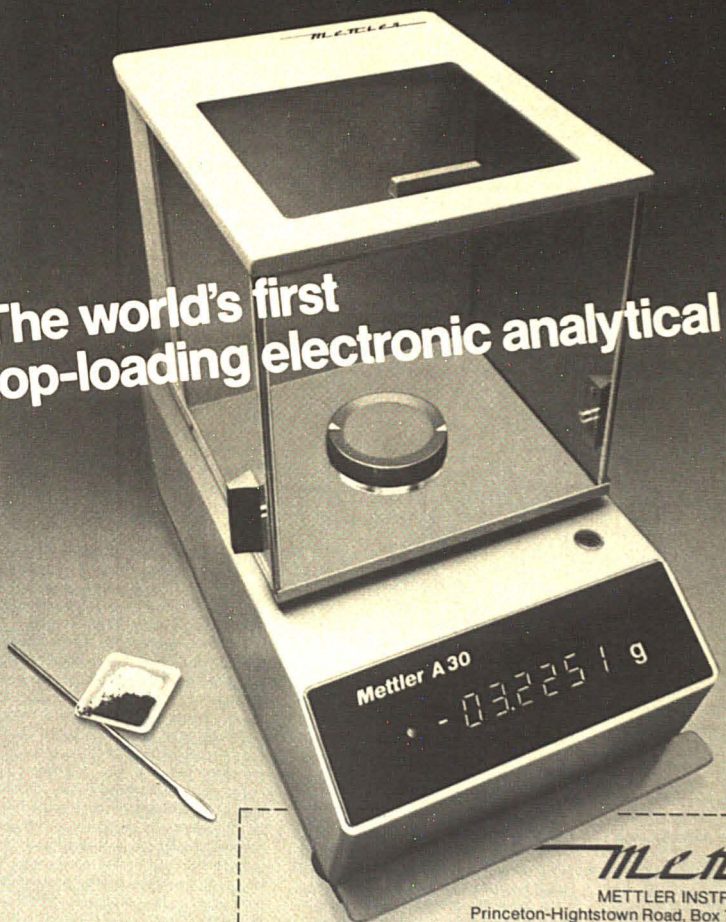
Bruce R. Kowalski is an associate professor of chemistry at the University of Washington. In 1969 he received his PhD from the University of Washington and joined the Shell Development Co. in Emeryville, Calif. After spending one year at the Lawrence Livermore Laboratory, he became an assistant professor of chemistry at Colorado State University in 1972. He then moved to Seattle where he has been since December 1973. As an analytical chemist and cofounder of the Chemometrics Society, his research interests focus on improving the analytical measurement process and obtaining more useful chemical information from analytical measurements by using advanced mathematical and statistical methods.



Izaak M. Kolthoff, professor emeritus at the University of Minnesota, was born in Holland and received his PhD from the University of Utrecht in 1918. He came to this country in 1927 as professor and chief of the division of analytical chemistry at the University of Minnesota where he remained until his appointment as professor emeritus in 1962. Professor Kolthoff has received numerous honors and awards and has served in leadership capacities in many national and international scientific organizations. His research interests have been in analytical and physical chemistry with main topics of research in potentiometry, conductivity, polarography, and the theory and applications of acid-base equilibria, titrations, and precipitation phenomena. Professor Kolthoff is the author or coauthor of nine books and some 900 publications and is coeditor of the multivolume "Treatise on Analytical Chemistry." I. M. Kolthoff is fortunate in being able to watch his educational grandchildren pursue outstanding careers in research and teaching.

Mettler's new A30 analytical balance, readable to 0.1 mg, is as fast and as simple to use as any Mettler electronic top loader. ☐ A touch of the control bar performs all necessary operations—on, off, tare. Place the sample on the weighing pan and read the result. No weights to dial, no hanging pan to oscillate. Just simplicity, speed and convenience. ☐ For weighing in materials, place container on pan, press control bar to tare and begin weighing. For checkweighing, the reference weight is tared into the balance memory. When objects to be compared are placed on the pan, the A30 indicates deviations with the correct plus or minus sign on the readout panel. ☐ Weighing range is 0 to 30 g. The tare range (by subtraction) is also 0 to 30 g. Additional tare, up to 30 g, is possible by removing tare discs located under the weighing pan. ☐ The A30, in addition to the usual two sliding doors found on analyticals, has a top entry door as an extra convenience. Standard equipment also includes an automatic stability detector and attachments for below-balance weighings. BCD output is optional as is a conversion kit for determining densities of solids. ☐ For a demonstration of this new top-loading analytical, or for additional information, mail the coupon.

The world's first top-loading electronic analytical balance.



Mettler

METTLER INSTRUMENT CORPORATION
Princeton-Hightstown Road, Box 71, Hightstown, NJ 08520.

☐ I would like a demonstration of the new A30. ☐ Please send me more information.

NAME _____ TITLE _____

COMPANY _____

ADDRESS _____

CITY _____ STATE _____ ZIP _____



Edward Hart, the man behind the Journal

G. Earl Peace, Jr.
Department of Chemistry
Lafayette College
Easton, Pa. 18042

The *Journal of Analytical Chemistry* first appeared in January 1887, edited and published quarterly by Edward Hart, PhD, head of the Chemistry Department at Lafayette College. In many respects, Dr. Hart was uniquely suited to undertake this timely endeavor, but his major strengths were his limitless energy and enthusiasm, his ability to carry any task through to fruition, and, first and foremost, his love for chemistry.

Edward Hart was largely self-taught when he was invited to study with Professor Thomas M. Drown at the University of Pennsylvania in 1872. When Dr. Drown went to Lafayette College as professor of analytical chemistry in 1874, Hart went with him as assistant in chemistry. In 1876 Hart was awarded one of 10 fellowships to Johns Hopkins University, despite the fact that he had no college degree. He studied with Dr. Ira Remsen and received his PhD degree in 1878, the same year that his first book, "Handbook of Volumetric Analysis", was published.

Soon after returning to Lafayette College, Dr. Hart resolved to improve his financial situation by taking advantage of the shortage of pure reagents for analyses. In 1881 Hart and John T. Baker, one of his graduates, began a company for the manufacture of pure hydrochloric, nitric and sulfuric acids, and ammonia. The first sales were to Lafayette College, and delivery was by wheelbarrow. In 1885 Hart developed and patented the ceresin bottle for use in the sale of hydrofluoric acid, a bottle that was used continually until it was displaced by polyethylene in 1950. The partners incorporated into the Baker and Adamson Chemical Co. in 1890 (George P. Adamson, a 1884 graduate of Dr. Hart's, was added as a business partner). Hart's name was omitted because Lafayette College preferred that the business activities of its staff remain unpublicized.

With the future of the new company apparently secure due to the income from the ceresin bottle patent, Dr. Hart left the day-to-day operation to his partners and continued his association primarily as a consultant. He now, however, sought another outlet for his energies.

The need for a publication that could make available newly devised analytical methods was widely recognized by 1887. Until recently the majority of analyses had been performed by professors at colleges and universities, with the remainder being performed by individual analysts in business for themselves. By the middle of the 1880's, however, most of the larger industries, particularly the iron and steel industry, had come to recognize the importance of analyses that were both accurate and rapid so that necessary changes in production processes could be made as quickly as possible. This requirement led to widespread revisions of existing methods and an unparalleled rush to develop new methods and devices that would meet these needs. Dr. Hart decided to begin such a publication. The journal, to a large extent, served to disseminate these new advancements, as evidenced by the titles of articles found in volume I:

- "Titanium Carbide in Pig Iron"
- "Nitrogen in Commercial Fertilizers"
- "Manganese in Steel"
- "Sulphur in Iron"
- "Rapid Method for the Determination of Phosphorus"

These early volumes also contained many articles of general interest reflective of the far-reaching applications of analytical research:

- "Progress in Chemical Methods of Sanitary Water Analysis"
- "Refractive Index of Oils"
- "A Short Scheme for Qualitative Analysis"
- "The Melting Point of Fats"

The latter two articles are works that found acceptance for many years. The former describes the basic separation scheme for the metal cations used with only minor revisions in high school and college laboratories today. The latter describes a method used for many years to differentiate pure butter from "an adulterated article". Another example of an article describing a technique of unknown origin used today is "A Reliable Method for Cracking Glass Tubes" in volume I.

Dr. Hart considered it critical to make these developments available to other workers in the field as quickly as possible. Because of difficulties in getting the first few issues out on time, he finally resolved to also become his own printer. He persuaded one of his students, Eugene C. Foster, who had had some experience, to become the foreman of this printing operation upon his graduation in June 1887. A one-story structure was built on the site of the barn that had only recently housed the faculty cow (a fringe bene-

0003-2700/78/A350-1194$01.00/0
© 1978 American Chemical Society

fit that yielded liquid assets). The first issue to come from this venture was the August 1887 volume. All printing operations were carried out on this site until 1895.

A good deal of the research of that time was concerned with refining the atomic weight scale, as shown by the following articles:

"Recalculation of the Atomic Weights"
"The Proper Standard for Atomic Weights"
"Table on Atomic Weights"

The author of this latter article, Professor F. W. Clarke, regularly contributed reviews of atomic weight determinations and became one of the recognized authorities on this subject.

There was also considerable interest in analytical methods applied to toxicology and forensic chemistry. Some of the papers on these subjects include:

"Opium Analysis"
"Detection of Chloral Hydrate in Toxicological Investigations"
"The Chemistry of Tyrotoxicon and Its Action Upon Lower Animals"
"A Recent Poison Case"

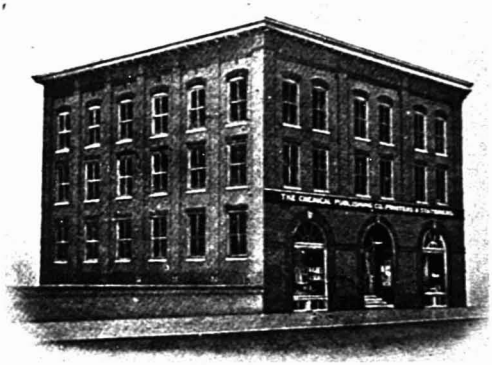
As editor, Dr. Hart imposed on the contributors his own strongly opinionated views on style and content developed through the writing of his several textbooks. This philosophy of writing and teaching is best described by the following quotation of Dr. Hart, "How intelligent men can put treatises into the hands of beginners, *beginners*, understand me, passes my comprehension. . . . They persist in thinking that what is clearly perceptible to them after years of intensive training also must be perceptible to men who have had no training." (*1*)

In 1891, with the fifth volume, the title of the journal was changed to *Journal of Analytical and Applied Chemistry*, although the basic format and types of articles appearing remained unchanged. This volume did, however, mark the first appearance of articles on electrochemical methods of analysis:

"The Electrolytic Assay of Copper"
"The Electrolytic Determination of Mercury"
"The Electrolytic Determination of Gold"
"The Electrolytic Method Applied to Rhodium"

The latter three articles were all written by Professor Edgar F. Smith of the University of Pennsylvania, who would later publish a manual of electrochemical methods of analysis. These articles served to heighten interest in this fledgling field, as demonstrated by the dramatic increase in papers on methods and instrumentation over the next few years.

One of the more perplexing problems of that period appears to have been "solved" by the final report of the Committee on Spelling and Pronunciation of Chemical Terms of the American Association for the Advancement of Science (of which Dr. Hart was a member), which is found in volume VI.



The Chemical Publishing Co., predecessor to Mack Printing Co.

In volume VII, A. H. Welles, at the request of Dr. Hart, began to write a feature article entitled "Patents of Interest to Chemists", which appeared regularly thereafter. Volume VII also contains the first analysis of errors leading to different results from different laboratories, "Discrepancies in Chemical Work by Different Workers", by C. B. Dudley. In this straightforward work, Dudley sets forth, in print, the four most common sources of error, three of them determinate and one indeterminate, and berates his colleagues for not noticing or speaking out about them previously.

In 1893 Dr. Hart was asked by Dr. H. W. Wiley, chief of the Bureau of Chemistry in the U.S. Department of Agriculture and newly elected president of the American Chemical Society, to become editor of the *Journal of the American Chemical Society*. Unable to edit both this journal and his own, Hart chose to consolidate his own journal with that of the Society. He felt that the major reason for his selection as editor was to add to the membership through the subscription list of his own journal, which was now a paying investment. This, in fact, is precisely what happened. Treasurer's reports to the General Meetings of the Society in 1892 and 1893 reflect a doubling of income due to subscriptions, from $44.36 in 1892 to $80.75 in 1893.

The *Journal of the American Chemical Society* then adopted a style and format identical to that of Hart's own journal, with the exception that it was published monthly. One rather drastic change which Hart instituted was to discontinue publishing the entire list of Society members as part of the annual Proceedings, and to substitute in its place a listing of newly elected members to the Society and honorary members. Each month's edition ended with the article on patents of interest and a review of new books. In August of 1894, Dr. Hart reported at the Ninth General Meeting of the Society that the journal had approximately 875 paid subscriptions and that the issues had been enlarged to 72 pages and would soon be enlarged further. The major problem he faced as editor was the financial inability to process all of the material submitted for publication. He also predicted that the membership of the Society would exceed one thousand before the end of the year.

The printing operation begun by Dr. Hart in 1887 had continued to grow and was moved to a larger location in 1895. At its present location, Mack Printing Co., formerly the Chemical Publishing Co., continues to print all of the journals of the Society.

Dr. Hart resigned as editor in 1901 after nine years, but continued as as-


P-250
500 g
(1.1 lb)
Certified A.C.S.
Potassium
Hydroxide
Pellets
FISHER SCIENTIFIC CO
Chemical Manufacturing D
Fair Lawn, New Jersey
FIRST AID — ANTIDOTE
give emetics. Give wa
large amounts of diluted
lemon, or orange (wice Fo
milk or whites of
with water. Apply ar
tion if not breathin
warm and quiet.
S-271
500 g
(1.1 lb)
Certified A.C.S.
Sodium
Chloride
For laboratory and
manufacturing use
only, not for drug, food,
or household use.
LOT
FISHER SCIENTIFIC COMPA
Chemical Manufacturing Divisio
Fair Lawn, New Jersey 07410
Made in U.S.A.

Reagents don't do you any good until they're on your shelf.

Nobody gets them there faster than Fisher.

Fisher delivers **the goods**. Whether your reagent needs are in routine testing or purest research. Our product range is spectacular. From high-pressure liquid chromatography and ppb pesticide trace analysis . . . to histology, electronics, and in vitro diagnostics. We develop new reagents. We manufacture them. We test them scrupulously. And we deliver them — dependably. Some **20,000** different chemicals and chemical specialties in all. Shipped to you from strategically located warehouses coast to coast. Your order is monitored every step of the way by one of the most sophisticated computers the lab supply industry has ever seen. (It's one reason Fisher will shortly be the first American reagent-maker to be 100% metric.) Thinking reagents? **Reach for the label.**

Fisher Scientific Company

CIRCLE 79 ON READER SERVICE CARD

The 1979 Fisher Chemical Index
will soon be off the press.
For your copy, circle reader-service card.



Fractomette® Alpha 200

Liquid Fraction Collector

RELIABLE: New single motor drive offers greater reliability than more complex mechanisms. Solid-state circuitry is designed for cold room use. Unit is overflow protected and includes a patented liquid detecting shutdown device.

VERSATILE: Push-button control of time, drop count or volume collection. An exclusive lift off collection platform provides unloading and cleaning convenience.

COMPACT: No other 200 tube collector is so compact. Occupies less than 1½ square feet of bench space; will fit in an ordinary household refrigerator.

COMPATIBLE: System compatible with metering pumps, column monitors, recorders and other accessories. Support rod lattice facilitates mounting.

Yes, there are many reasons for you to select the Alpha 200 when your applications require a liquid fraction collector. In fact, no other fraction collector offers *all* the *features* available in the Buchler Fractomette Alpha 200. Write for details.

Buchler Instruments, Inc.

1327 Sixteenth St., Fort Lee, N.J. 07024 U.S.A. (201) 224-3333

made in U.S.A., sales and service worldwide.

CIRCLE 27 ON READER SERVICE CARD

sociate editor for some time. The Proceedings of the Twenty-Fifth General Meeting of the American Chemical Society include the following statement by Albert C. Hale, secretary, "The Society is thus called upon to lose one of its most faithful and successful workers, one who has contributed largely to bring it into the front rank of the scientific bodies of the world, and who has seen its journal in his own hands attain so great an eminence as that which it now occupies."



THE

Journal of Analytical Chemistry

EASTON, PA.

PUBLISHED BY THE EDITORS.

Edward Hart died on June 6, 1931, leaving behind a legacy of accomplishments that survive to the present day. A poem written by Dr. Hart entitled "The Hobo" provides a complete antithesis to the personality of this dynamic and indefatigable man (2):

I think some evil molecules,
Must in my system lurk.
I really am not lazy,
I just don't like to work.

Acknowledgment

The author gratefully acknowledges the assistance of Ronald W. Wynkoop of Phillipsburg, N.J., who made available his collection of historical photographs.

References

(1) Edward Hart, *Chem. Age*, **30** (9), 405 (1922).
(2) Eugene C. Bingham, *Ind. Eng. Chem.*, **15** (9), 975 (1923).



L.T. Hallett, the early years

Sidney Siggia
University of Massachusetts
Amherst, Mass. 01003

I am pleased to have this opportunity to describe the early years of L. T. Hallett's participation in the field of analytical chemistry. I regret not being able to be there in person but am sure that John Crum will make a good reading of this paper.

I first met Larry in 1942. He was staffing an analytical research and service group for General Aniline & Film, a confiscated German firm. These were war years, and manpower was scarce. However, with his quiet zeal for the subject, Larry was able to put together a first rate group.

I might relate a short story of how I happened to join GAF. Larry was on a recruiting trip and stopped at Brooklyn Polytechnic Institute where I was a first year graduate student. I had seen the notice of Hallett's visit, but it made no impression on me since it was too early for me to think about jobs. In fact, *none* of the graduate students signed up for interviews. Dr. Raymond Kirk, the head of the Chemistry Department, wanted to make a positive impression on this visiting dignitary and "drafted" all the grad students to get interviewed. So, I got interviewed. The job that Hallett described was just what I was looking for, and I seemed to suit Hallett. So it came to pass that I wound up at GAF.

Hallett's technical contributions were in the field of micro-organic elemental analysis. He advanced the state of the art with the use of movable furnaces for carbon–hydrogen analysis. He also promoted the use of high-temperature combustion and the use of pure oxygen instead of air.

The first people Hallett hired were the service staff comprised of about six technicians. The first PhD was Frank Hamm, a microscopist who at first did most of the qualitative work and later did basic research, particularly in the photographic aspects of the company business.

I was hired to carry on the development of quantitative analytical research and to troubleshoot the various processes with which the company had to deal. Shortly after I arrived, a third PhD, Clark (Pete) Gould, was hired to carry on the qualitative analytical work.

Larry was very progressive in his philosophy, and instruments were acquired as fast as they appeared on the market. When I arrived on the scene in 1944, the lab already had a Beckman DU and some filter photometers, a polarograph, a single beam IR, X-ray diffraction equipment and a fully equipped microscopy lab. Kurt Snowden was hired to handle our Instrument Lab. Larry foresaw the potential in instrumental methods and hired Dr. Ralph Müller as consultant to lead us into new instrumental directions. Dr. Fernwood Mitchell was hired to work with Müller. This team created an automated potentiometric titrator that plotted a curve as titrant was added. This was achieved in the late 1940's and early 1950's, before the instrument companies had produced any such instruments.

Under Larry's direction an automatic liquid chromatograph was created with a refractometer detector—this was in the early 1950's. It took almost 20 years for the field to catch up.

Dr. Hans Stolten, one of Ralph Müller's students, was hired to expand our instrumental service and research facilities. The Analytical Department under Hallett's leadership grew from zero in 1942 to a vibrant group of 40 people at its peak in 1950.

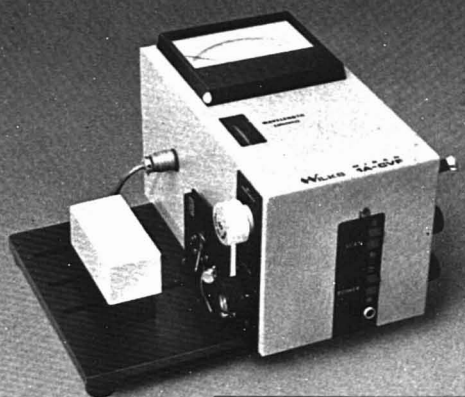
Hallett was also progressive in his handling of people. We were encouraged to develop new ideas and new methods. Many papers issued from that laboratory. That analytical lab at GAF was recognized within the company for its effectiveness, and was recognized outside the company for its leadership in the analytical field.

Hallett's missionary attitude toward analytical chemistry made him a natural to get involved with the ACS analytical JOURNAL, then called INDUSTRIAL AND ENGINEERING CHEMISTRY, ANALYTICAL EDITION. Larry was first the associate editor with Walter Murphy as editor. He spent part of his time with the JOURNAL into 1955 when GAF suffered severe setbacks and Hallett's fine group was curtailed along with the rest of the Central Research Lab. Since Hallett could not perform in the manner he felt necessary, he left. Walter Murphy had left I&EC (ANAL. ED.) shortly before, and Hallett was named to fill the void.

Hallett always emphasized quality in his work and extended this emphasis to his efforts with the JOURNAL. He was a firm believer in the "review-by-peers" system as one means to ensure quality. His esteem for Ralph Müller led to the famous column INSTRUMENTATION authored by Müller and continued today under multiauthorship. The "A" pages contained many other feature articles meant to stimulate thought and discussion and

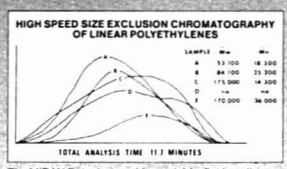
0003-2700/78/A350-1199$01.00/0
© 1978 American Chemical Society

Now, get highest LC specificity without sensitivity to flow or temperature.



The MIRAN® LC Detector is a truly universal liquid chromatography detector which employs infrared techniques but requires *no* knowledge of infrared analysis.

More important, the Detector gives the chromatographer a specificity unequalled by other LC detectors such as Ultraviolet and Refractive Index systems. And, it is insensitive to changes in flow or temperature.



The MIRAN Detector provides a stable, flat baseline with excellent signal-to-noise characteristics even at 145°C as shown above. Accurate molecular weight distribution is thus routinely achievable.

You get all this in an instrument which not only is easy to operate but will analyze an extremely broad spectrum of components in Size Exclusion Chromatography, Interactive Chromatography or Gradient Elution studies.

Put the specificity of the MIRAN Detector to work in your liquid chromatography applications. Send for our new MIRAN LC Detector brochure or contact us for a demonstration: Foxboro/Wilks, Inc., P.O. Box 449, South Norwalk, CT 06856. Telephone (203) 853-1616.

WILKS
Foxboro Analytical

CIRCLE 78 ON READER SERVICE CARD

also act as a news periodical for the analytical chemistry community.

In the late 1930's and early 1940's Larry published the first review article; the subject was microchemistry. The article was very well received, and requests for reprints poured in.

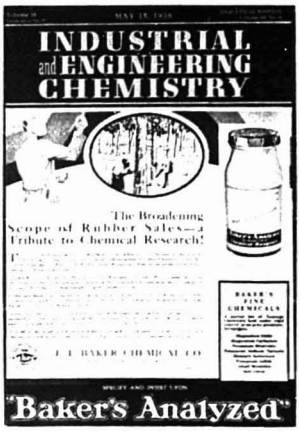
Hallett promoted the sale of advertising to keep the cost of the JOURNAL low. This was so effective that ANALYTICAL CHEMISTRY has always been "in the black". Hallett also promoted the use of artful, interesting covers that have made the JOURNAL stand out among other technical journals.

He had a flair for organization. This characteristic surfaced in the way he ran his laboratory at GAF and proved to be his most valuable asset when he became editor of ANALYTICAL CHEMISTRY. He crystallized the various components of the JOURNAL into a coordinated, viable, attractive unit. The prestige gained by the JOURNAL increased the prestige of the discipline of analytical chemistry during times when the discipline was under pressure from the "pure" sciences.

I will never forget the exciting times at GAF: the time the acetylene chemicals plant exploded, the strange case of the calculator that mysteriously exploded one night, and the many "crises". I learned a great deal from working with that staff.

Hallett did a good job of ensuring the perpetuation of a quality JOURNAL by his selection of a top flight staff. Herb Laitinen took over the editorship upon Larry's retirement. John Crum, Virginia Stewart, and Josephine Petruzzi who were all on Hallett's staff, each in turn, took over the managing editorship.

Presented by John K. Crum.



Analytical Chemistry: the Journal and the science, the 1930's

Vernon A. Stenger
Analytical Laboratories
The Dow Chemical Co.
Midland, Mich. 48640

In this symposium we celebrate the 50th publication year of ANALYTICAL CHEMISTRY and are also pleased to honor one of its former editors, Lawrence T. Hallett. Dr. Hallett has the unique distinction of being the only former editor who survived his term of office to enjoy retirement. He served conscientiously from 1944 to 1966, through the positions of associate editor, science editor, and finally in full charge as editor. Later speakers will tell of the progress of the JOURNAL through those years.

Perhaps one measure of a man who held a responsible position is the caliber of those who preceded or succeeded him in office. It was my privilege to have joined ACS in 1929 and to have known all four of the editors; thus from personal knowledge I can testify that they have all been men of character, intelligence, friendliness, and tremendous capacity for work. Moreover, all have been strongly motivated toward the advancement of chemistry, and especially analytical chemistry, as a science and profession. Each has made unique contributions to the JOURNAL, and it is a pleasure to express gratitude to all, particularly to Dr. Hallett and Prof. Laitinen who are still with us.

Our present JOURNAL owes its beginnings to Harrison E. Howe (Figure 1), who became editor of the *Journal of Industrial and Engineering Chemistry* in 1921. Dr. Howe was born in Georgetown, Ky., in 1881. At the age of 20 he graduated from Earlham College, Indiana, with a BS degree and began graduate work at the University of Michigan. However, he apparently had some financial problems and left school to work in a sugar factory at Croswell, Mich. In 1904 he joined the Bausch and Lomb Optical Co. as a chemist in Rochester, N.Y. There he remained for 12 years, meanwhile earning a master's degree at the University of Rochester. Shortly before the United States entered World War I, he became assistant to the president of A. D. Little, Inc., a consulting firm, and served as a consultant to the Nitrate Division of U.S. Army Ordnance. After the war he worked with the National Research Council raising funds for construction of the Marine Biological Laboratory at Woods Hole, Mass., and for the publication of International Critical Tables, until his appointment as editor (*1*, *2*).

In those days the most highly regarded publication of the American Chemical Society, especially among academic chemists, was its monthly *Journal*. Most Society members subscribed to that and to *Chemical Abstracts*, which appeared semimonthly in fairly small editions. Chemical engineers and chemists in industry were likely to take the *Journal of Industrial and Engineering Chemistry*, also issued monthly by the Society, or *Chemical and Metallurgical Engineering*, published by the McGraw-Hill Co., N.Y. *JI&EC* served also as a general news medium for the chemical profession, though the ACS *Journal* published all official proceedings of the Society up until 1938. The *Journal of Physical Chemistry*, then edited and published privately by Prof. W. D. Bancroft of Cornell University, handled many of the U.S. articles in its field.

In 1923, with the Society's consent, Dr. Howe split the *Journal of Industrial and Engineering Chemistry* into two parts, one retaining articles on applied chemistry and the other taking over the news-reporting functions. The *News Edition* appeared twice a month, whereas the original magazine, which soon became known popularly as the *Industrial Edition*, continued as a monthly. This change was quite successful in providing faster news coverage, more text pages for research papers, and greater advertising revenue. Its success probably furnished the impetus for Howe's next move, the 1929 regrouping of analytical papers from *Industrial and Engineering Chemistry* into a new quarterly designated as the ANALYTICAL EDITION.

The timing may have been a little unfortunate; 1929 is remembered as the year of the stock market crash,



Figure 1. Harrison E. Howe

0003-2700/78/A350-1201$01.00/0
© 1978 American Chemical Society

หอสมุด กรมวิทยาศาสตร

which preceded the great depression of 1930–34. Nevertheless, the ANALYTICAL EDITION survived; pertinent data about its growth are shown in Figures 2 and 3. There is small doubt that survival during the difficult early years depended upon exceptional efforts by Dr. Howe and his staff. Subscription rates were kept low, starting with $1.50 per year for ANAL. ED. alone in 1929 and rising only to $2.50 in 1939. Meanwhile, the bargain price for a combined annual subscription to all three editions dropped from $7.50 to $6.00.

One way in which Dr. Howe promoted his journals as well as the professions of industrial and analytical chemistry was by speaking to local ACS sections. To emphasize the newer developments of chemistry in industry, he carried a large valise packed with appropriate samples. His demonstrations and easy speaking manner made him a popular lecturer, and his "magic bag" became almost a trademark. He also enjoyed getting laughs by relating some of his editorial experiences. I recall his telling of a woman who occasionally visited his office in the old Mills Building to discuss world problems. Once when he smiled at one of her comments, she suddenly leaned over and inquired, "Say, is them your own teeth?"

It is perhaps only natural that most of the papers that appeared in the early ANALYTICAL EDITIONS were of the type that previously would have been printed in *I&EC* rather than in *JACS*. Superficially the pages seem overloaded with descriptions of modifications in laboratory apparatus, as well as minor improvements of known analytical procedures. For younger chemists today the need that then existed for such papers may not be apparent. It should be realized that the applied analytical chemistry of that period depended mainly upon hand operations. Although the basic scientific theory relating to solubility products, electrolytic dissociation, pH, etc., was being taught and utilized, there was really no substitute for human labor in carrying out determinations. If any way could be found to simplify a procedure, improve accuracy, or eliminate an interference, it was well worth publishing. Similarly, if labor and time could be saved by employing a test of some physical property to replace a complicated analysis, or to yield useful results when one did not even know what analysis might be needed, then a successful new physical or empirical method surely deserved publication.

Under such conditions it is not surprising that most of the authors of ANAL. ED. papers during its first decade were chemists either in industry or in institutions concerned with applied chemistry. Generally, each of such persons submitted relatively few papers. On the other hand, the highly prolific contributors of that period were professors in educational institutions having strong graduate programs in analytical chemistry. The data of Table I, considered along with the research interests of the men listed, are instructive with regard to their views of where to publish. G. Frederick Smith (Illinois) was a born gadgeteer and also oriented toward applied chemistry; therefore, it was logical that most of his papers went to ANAL. ED. However, his more general or fundamental studies were often directed to *JACS*, whereas many others, such as those dealing with perchloric acid uses, appeared in *J. Chem. Ed.*, specialized publications, or in British or German journals.

Hobart Willard (Michigan) saw nearly half of his papers between 1929 and 1939 published in ANAL. ED., but most of the rest went to *JACS* and the remaining few to journals specializing in electrochemistry. So far as the importance of the papers was concerned, it is difficult to distinguish between those that appeared in the various journals. Since Willard, as well as Smith, had numerous industrial contacts, he may have been inclined toward sending the more industrially applicable methods to ANAL. ED. Although during the same period most of the manuscripts of I. M. Kolthoff (Minnesota) were given to *JACS*, *J. Phys. Chem.*, and foreign journals, he still sent enough to ANAL. ED. to put his name in our list. In order for us to guess at what may have led to the selection of a particular medium for publication, it is interesting to consider the papers that Prof. Kolthoff coauthored with Ernest Sandell (who in his own right later established an international reputation in inorganic trace analysis). Coprecipitation studies usually went to *J. Phys. Chem.* To *JACS* were given two papers on exchange adsorption, one discussing its effect on the solubility of ionic precipitates and the other dealing with calcium oxalate monohydrate purity. A third paper covered the microdetermination of iodine by a chronometric method involving catalysis of the ceric ion-arsenite reaction. An extension of the latter appeared later in *Mikrochim. Acta*. The articles sent to ANAL. ED. were mostly on titrimetric methods; three presented oxidation-reduction titrations of metals, and one was a

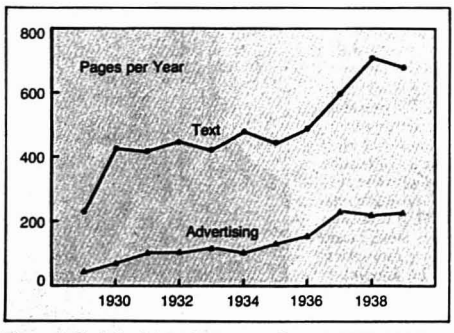


Figure 2. Statistical data, ANALYTICAL EDITION, 1929–1939

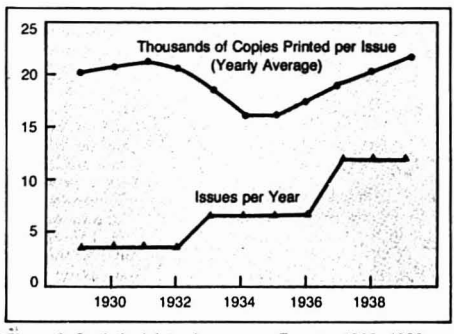


Figure 3. Statistical data, ANALYTICAL EDITION, 1929–1939

study of the acid-base titration of sulfuric acid with barium hydroxide. However, there was also a paper on calcium oxalate monohydrate as a weighing form. It appears that methods likely to find prompt applicability went to ANAL. ED., but those seeming more unique or mainly of theoretical interest were given to other journals.

Beginning in 1929, Earle Caley of Princeton University published more of his papers in ANAL. ED. than in any other single journal, but they did not seem to be his best ones. Most were on apparatus notes or applications of methods described elsewhere. His work on the detection and determination of alkali metals, as well as on the use of hydriodic acid for reducing insoluble compounds like barium sulfate and stannic oxide, usually appeared in *JACS*. Toward the end of the decade, his interest turned toward the analysis of ancient metal coins and statuary, and that work was submitted to museum publications.

Melvin G. Mellon of Purdue distributed his work among a variety of journals. Several of his earlier papers on color appeared in *J. Phys. Chem.*, but after he and H. W. Swank had obtained and modified a recording spectrophotometer from the General Electric Co., his students performed careful studies on a number of spectrophotometric determinations; most of those reports appeared in ANAL. ED. However, his classical 1938 paper with W. B. Fortune on the color ranges of acid-base indicators was published in *JACS*.

The one man on our list who published only in the ANALYTICAL EDITION between 1929 and 1939 was Fred E. Beamish of the University of Toronto. His first three papers dealt with micro combustions for elemental analysis, but all of the rest were concerned with assay methods for the platinum metals and gold.

Others who contributed frequently to ANAL. ED. were: Beverly Clarke of the Bell Telephone Laboratories, 12 papers mainly on microanalysis; E. B. Sandell of Minnesota, 11 papers already mentioned; W. R. Kirner of the Carnegie Institute of Technology, 10 papers on microanalysis; and J. H. Bruun of the Sun Oil Co., with the same number on fractional distillation. Seven other men representing both industry and universities authored 9 papers each. One of these was Union Carbide's Thomas R. Cunningham, an expert in the analysis of ferrous alloys.

Several well-known teachers of the period can be singled out for having offered very few of their papers to ANAL. ED. G. P. Baxter of Harvard published most of his atomic weight work in *JACS*, and his name appeared in ANAL. ED. only in connection with reports of the ACS Committee on Analytical Reagents. Though W. T. Hall of MIT was nearing the end of his career, he had two papers in ANAL. ED. during the decade. N. H. Furman of Princeton was represented by five papers but had a vastly greater number in *JACS*, including most of his work on redox titrations with ceric solutions.

Dr. Howe went to considerable effort to obtain papers presenting the state-of-the-art or science in analytical chemistry. It was probably no accident that the first article in volume 1 was "Quantitative Analysis with the Spectrograph", by C. C. Nitchie of the New Jersey Zinc Co. Volume 2 contained the reviews given at an ACS symposium on analytical chemistry, including "Modern Trends" (Willard), "Microscopical Methods" (C. W. Mason, Cornell), "Applications of the Photo-Electric Cell" (H. M. Partridge, NYU), "Potentiometric Titrations" (Furman), "Conductometric Titrations" (Kolthoff), and "Electrode Potentials" (S. Popoff, Iowa). In 1936 Howe published a review he had especially requested from F. Feigl of Vienna, "Organic Reagents in Inorganic Analysis"; submitted in German, it was translated by Harvey Diehl (then at Michigan). 1938 saw publication of a definitive article, "Chemical Analysis by X-ray Diffraction", by Hanawalt, Rinn, and Frevel, with extensive tables of powder diffraction data. The following year a lengthy paper on photo-electric methods in analytical chemistry, by Ralph H. Müller of NYU, was featured on page 1. During the early years Müller and coworkers contributed half a dozen papers, two of which described an electronic recording balance and a cathode ray-tube polarograph.

Another long paper offered in 1938 was a review on the ultracentrifuge by The Svedberg of Uppsala, Sweden. Svedberg had won the 1926 Nobel prize in chemistry for his ultracentrifuge studies. It is interesting to note that two other men who later won Nobel prizes also had papers in ANAL. ED. during its first 10 years. One was R. B. Woodward. While at MIT he published with W. T. Hall on the behavior of barium in qualitative analysis, and with R. L. Emerson on a pressure regulator for vacuum distillations. Apparently he considered it no disgrace to publish a paper on apparatus. The other eventual prize winner was Selman Waksman, who with K. R. Stevens in 1930 described a system for the proximate chemical analysis of plant materials. There was no lack of quality among authors who contributed to ANAL. ED. Of the 33 men who have won ACS Fisher Awards so far, 14 had papers published therein prior to 1940. Two of the winners were Herbert Laitinen and James Lingane, who collaborated in devising a cell and dropping electrode for polarography. Another gadget!

At the beginning, a single advisory board served for all three editions. In 1936, however, Dr. Howe appointed separate boards for each. Those appointed for ANAL. ED. were B. L. Clarke, T. R. Cunningham, N. H. Furman, I. M. Kolthoff, G.E.F. Lundell, and H. H. Willard. All of these except Dr. Lundell have been mentioned previously. He was a man eminently respected, whose friendship was highly valued by everyone privileged to work with him at the National Bureau of Standards, in ACS, or with the ASTM. Although only one of his papers appeared in ANAL. ED., that one

Table I. Leading Contributors to the ANALYTICAL EDITION, 1929–1939

Author	Papers published				
	Anal. Ed.	*JACS*	*J. Phys. Chem.*	Other U.S.	Foreign
G. Frederick Smith	26	9	0	16	7
H. H. Willard	19	22	0	4	0
I. M. Kolthoff	16	76	32	10	41
E. R. Caley	16	13	0	8	1
M. G. Mellon	14	1	5	11	1
F. E. Beamish	13	0	0	0	0

free LC News

Pharmaceuticals

Analysis of Pharmaceutical Products



Quality control, drug metabolism studies, preparative separations, and drug stability studies are important separation and quantitation tasks that can be effectively completed by LC.

CIRCLE 239 ON READER SERVICE CARD

Obtaining Kilos of Pure Compounds

Pharmaceutical chemists use preparative LC to purify enantiomer intermediates. Only 5% of the time previously required by open column chromatography was needed.



CIRCLE 240 ON READER SERVICE CARD

Finished Product Assays for Cosmetics and Toiletries



Kolmar Laboratories uses LC to improve speed, accuracy and specificity in finished product assays of cosmetics and toiletries.

CIRCLE 241 ON READER SERVICE CARD

Waters

The Liquid Chromatography People

Waters Associates, Inc.

Maple Street, Milford, MA 01757

(617) 478-2000

was a classic: "The Chemical Analysis of Things as They Are" (*3*). Much of his own research had been done prior to 1929, and most of his later papers appeared in the *Bureau of Standards Journal of Research*, which started in 1928.

Dr. Edward Wichers, who had also worked for many years at the Bureau, recalls that Lundell while serving on the advisory board had expressed concern that too many of the articles being accepted did not deal with analytical *chemistry*. The preface of Lundell's book "Applied Inorganic Analysis" (with W. F. Hillebrand, 1929) contained the statement, "After all is said and done a good analyst is primarily a chemist who can quantitatively manufacture pure chemicals." One wonders what he would think today, when most separations are chromatographic, most detection and determination methods are physical, and authors have difficulty in getting a paper past ANALYTICAL CHEMISTRY's reviewers if it has much to do with simple chemistry!

While Lundell's statement does accurately reflect the situation at that time, he was also alert to progress in new directions. I remember hearing him speak around 1936 of the friendly competition between spectroscopists and chemists to see who could determine the lowest trace concentrations of elements in rocks, ores, metals, or plant residues. Diphenylthiocarbazone had just opened new possibilities for trace analysis, and other new reagents were being introduced. In our laboratories the situation was not so much competition as collaboration. As either group made progress, it helped to confirm what the other group had already attained and to stimulate further efforts. We chemists often worked hard to analyze mixtures that the spectroscopists could use as standards.

To summarize the state of analytical chemistry during 1929–39, titrimetry was approaching its peak, with adequate indicators, a variety of useful reagents, the glass electrode, and many potentiometric methods. Yet to become popular were functional group analyses and the widely applicable Karl Fischer reagent. Classical gravimetry was on a high plateau, with improved understanding of coprecipitation phenomena and extensive usage of micromethods, but it would gradually lose out to faster procedures. Colorimetry, having seen great advances in reagents, was being replaced by filter photometry and simple spectrophotometry, though the latter would not attain full utility until the improvement of instrumentation. Heyrovsky's polarograph was attracting attention. The known forms of chromatography, mainly liquid-solid, were rudimentary. Emission spectrography had reached a high plane, but awaited development of the direct reader. Radiochemistry was only in its infancy. Except for vacuum tube apparatus, the bulk of the electronic revolution was still to come.

ANAL. ED. adequately reflected current progress in all of those fields. Where it may have failed, and indeed where most practicing and teaching chemists failed, was in not recognizing the developments that were being started by physicists. One of these was mass spectroscopy, which with improved apparatus was beginning to be used for atomic weight determination and the identification of isotopes. The work was being reported in physical journals, which were seldom studied by analytical chemists. Similarly, work with infrared radiation was published in optical journals.

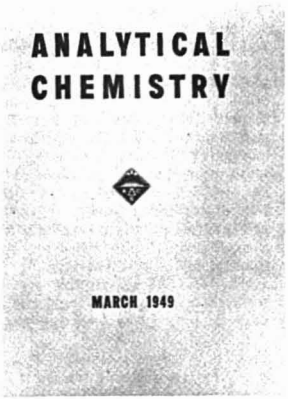
To this writer it seems that the main contributions of analytical chemists of those days lay in using whatever means they had to learn as much as possible about all kinds of materials. In doing so, they and their contemporary engineers and scientists were able to bring about vast improvements in the properties of alloys, cement, and rubber. They learned about both beneficial and harmful effects of many inorganic elements and compounds in foods and water. Chemical process control was greatly improved. Knowledge of natural substances, including petroleum, fats, proteins, wood, etc., was increased even under great difficulties. The ANALYTICAL EDITION played its part in promulgating information about new procedures, apparatus, and results as they became available. Even had it not fared so well in later years, its first editor could justifiably take pride in what was accomplished at the beginning.

In closing I would like again to pay tribute to all the editors, Howe, Murphy, Hallett, and Laitinen, and to their loyal staff members.

References

(1) F. J. Van Antwerpen, *Science*, **97**, 182 (1943).
(2) M. T. Bogart, *Chem. Eng. News*, **21**, 678 (1943).
(3) G.E.F. Lundell, *Ind. Eng. Chem., Anal. Ed.*, **5**, 221 (1933).

50 YEARS



Analytical Chemistry: the Journal and the science, the 1940's

Herbert A. Laitinen
Department of Chemistry
University of Florida
Gainesville, Fla. 32611

The 1940's represent a decade during which dramatic changes occurred, both in the science of analytical chemistry and its primary American publication. At the beginning of the period, Europe was already embroiled in World War II, and the conflict was soon to involve the USA, USSR, Japan, and many other areas. As a consequence, many technical and scientific developments were stimulated, but the dissemination of scientific information was greatly impeded, both by secrecy restrictions and the disruption of traditional channels of international scientific communication.

At the beginning of the 1940's, the ANALYTICAL EDITION of INDUSTRIAL AND ENGINEERING CHEMISTRY was still edited by Harrison E. Howe, the editor of the parent journal. The six-man analytical Advisory Board that had been appointed in 1935 remained unchanged through 1942, even though the initial appointments had been made for terms of 1, 2, and 3 years to permit rotation. The members were: Beverly L. Clarke (then at Bell Telephone Laboratories and later at Merck), T. R. Cunningham (Union Carbide), N. H. Furman (Princeton University), I. M. Kolthoff (University of Minnesota), G.E.F. Lundell (National Bureau of Standards), and H. H. Willard (University of Michigan).

In 1940 there were perhaps a dozen USA universities that were acknowledged centers for academic research and PhD training in analytical chemistry. These included Cal Tech (E. H. Swift), Harvard (G. P. Baxter), the University of Illinois (G. F. Smith, G. L. Clark), Iowa State (H. Diehl), the University of Michigan (H. H. Willard), the University of Minnesota (I. M. Kolthoff), Ohio State University (C. W. Foulk), Princeton University (N. H. Furman), Purdue University (M. G. Mellon), the University of Virginia (John H. Yoe), and the University of Wisconsin (V. W. Meloche). A few other places and individuals could be cited, notably Ralph Holcombe Müller, professor of chemistry at New York University. In the field of instrumentation Müller was a pioneer destined to play a leading role in the evolution of the JOURNAL.

To picture the state of the JOURNAL at the beginning of the 1940's, let us look at some typical titles of research papers in the January 1940 issue of the ANALYTICAL EDITION of INDUSTRIAL AND ENGINEERING CHEMISTRY:

"Low Temperature Set as Measure of State of Vulcanization"
"Identification of Commonly Used Waxes in Admixture"
"Computing Titration Blanks"
"Dynamic Fatigue Life of Rubber"
"Potentiometric Determination of Exchangeable Hydrogen in Unsaturated Oils"
"Qualitative Spectrographic Analysis in Arc, with Graphite Electrodes"

A separate microchemistry section carried several papers including a combustion method for sulfur in organic compounds, an apparatus for qualitative semimicro analysis, and a small silver reductor for microdetermination of iron.

These papers, however, would give an incorrect impression of research in analytical chemistry at that time. Many fundamental papers were appearing in other journals, as illustrated by the following papers in the January 1940 issue of the *Journal of the American Chemical Society*.

"Analytical Procedures Employing Karl Fischer Reagent II. The Determination of Alcoholic Hydroxyl", W. M. Bryant, J. Mitchell, Jr., and Donald Milt on Smith

"The Extraction of Ferric Iron from Hydrochloric Acid Solutions by Dichloroethyl Ether and the Formula of the Iron Compound in the Ether", Joseph Axelrod and Ernest H. Swift

"An Investigation of the Exchange between a Metal and Ions in Solution by Using Radioactive Indicators", B. V. Rollin

"The Determination of Organic Peroxide", H. A. Liebhafsky and W. H. Sharkey

"Amperometric Titrations II. The Titration of Nickel with Dimethylglyoxime Using the Dropping Mercury Electrode as Indicator Electrode", I. M. Kolthoff and A. Langer. This single issue carried papers by four authors later destined to win the Fisher Award in Analytical Chemistry. In addition, several other papers had a substantial analytical component.

Perhaps the most prolific analytical research chemist of that day (or any day!) was I. M. Kolthoff, who published 15 papers in 1940. Of these, only 1 appeared in the ANALYTICAL EDITION, 9 appeared in *J. Am. Chem. Soc.*, 2 in *J. Phys. Chem.*, and 3 in non-ACS journals. During the 5-year period, 1940–44, he published 11 papers in the ANALYTICAL EDITION, 35 in *JACS*, 8 in *J. Phys. Chem.*, and 5

0003-2700/78/A350-1205$01.00/0
© 1978 American Chemical Society

in other journals. Of the 11 analytical papers, 4 were on chemical methods and 7 on polarography and amperometric titrations.

Perhaps the first significant step toward modernization of the JOURNAL was taken by Harrison E. Howe, who commissioned a series of 3 articles by Ralph H. Müller (Figure 1). The first of these, "Photoelectric Methods in Analytical Chemistry", appeared in the January 1939 issue, followed by two entire issues in October 1940 and October 1941 devoted respectively to "American Apparatus, Instruments, and Instrumentation" and "Instrumental Methods of Chemical Analysis".

Howe died in 1942, and late in that year Walter J. Murphy (1899–1959), Figure 2, succeeded him as editor of *Chemical and Engineering News* and of the two editions (*Industrial* and ANALYTICAL) of INDUSTRIAL AND ENGINEERING CHEMISTRY. Murphy had a background in chemistry, but since 1930 his career had been centered around publishing. In 1939 he had become editor and general manager of *Chemical Industries*, which later became *Chemical Week*, published by McGraw-Hill. When Walter Murphy joined the ACS staff, he was confronted by a group of scientists who planned to approach the ACS Council to make the ANALYTICAL EDITION of I&EC a publication of the ACS Division of Analytical Chemistry and Microchemistry and to authorize the Division to appoint its editor. Murphy rejected the plan but offered to withdraw as editor if tangible improvements were not evident within 1 or 2 years.

In 1943 Murphy appointed M. G. Mellon and R. H. Müller to replace N. H. Furman and I. M. Kolthoff on the ANALYTICAL EDITION Advisory Board. Recognizing the need for an analytical chemist in the editorial function, he appointed Lawrence T. Hallett (Figure 3) as associate editor in 1944.

Hallett was well recognized as an analytical and microchemist. He had received his PhD at the University of Wisconsin in 1928, and after a brief period in teaching, held several industrial positions. The two most notable were at Eastman Kodak (1933–43) where he was in charge of quantitative microanalysis, and at General Aniline and Film where he was head of the analytical section of the central research laboratories (1943–49) and the corporate coordinator of analytical and testing (1949–56). In 1938 when the ACS Division of Microchemistry was established, he served as its first secretary and as its chairman in 1939. In 1940 the Division of Microchemistry merged with the Analytical Section of the Division of Physical and Inorganic Chemistry to form the Division of Analytical Chemistry in 1949. This evolution is described here to emphasize the fact that Dr. Hallett's background in microchemistry was important to his acceptance by a large segment of the analytical community of the early 1940's as an editor of the analytical JOURNAL.

Hallett also had a good background in instrumentation. He engaged Ralph



Figure 1. Ralph H. Müller

H. Müller as instrumentation consultant at General Aniline and Film and proceeded to build a strong instrumental analysis group beginning in 1943. Among others, he recruited Sidney Siggia, now at the University of Massachusetts.

Murphy and Hallett constituted a powerful editorial team, combining Murphy's organizational and business talents with Hallett's scientific background. Both recognized the fact that many wartime analytical developments would be destined to revolutionize the instrumentation industry. In an editorial published in December 1950, Walter J. Murphy discussed the rotation of Advisory Board members and spoke of two retiring members, R. H. Müller and M. G. Mellon, as being "members of the original Advisory Board which your editor activated when he was appointed to his present post in 1943. Prior to that date the Advisory Board met only infrequently, if at all". He then described meetings of the "original board" in 1943–45 when the evolution of a new publication completely divorced from INDUSTRIAL AND ENGINEERING CHEMISTRY was discussed. In listing the "original board" members, no mention was made of Furman or Kolthoff, who had served from 1935 to 1942. Kolthoff later had no recollection that the Advisory Board had ever met prior to Murphy's editorship.

Beginning in 1947, the Advisory Board was enlarged to 9 members, in 1949 to 12 members, and in 1954 to its present size of 15 members. Rotation of membership began in 1948 and continues today, with 3-year terms.

When the directions of the new JOURNAL were set forth, the decision was made to emphasize instrumentation. Beginning in January 1946, Ralph H. Müller contributed a monthly feature "Instrumentation in Analysis", which continued through 1968. An editorial comment stated, "The war stimulated greatly the development and use of instrumental methods of chemical analysis and unquestionably this trend will continue to grow in the future. There has been a long-felt need among analytical chemists for a timely, unbiased, and authoritative discussion and interpretation of new developments in the field of instrumentation".

The INSTRUMENTATION articles called to the attention of analytical chemists recent developments in measurement science, as well as commercial instruments, and were undoubtedly influential both in teaching and research. In March 1948 Müller remarked, "One wonders how our universities can continue in the thousand year old belief that they are the fountainhead of new knowledge. Current practice in modern analysis is far ahead, and there is excellent evidence that the gap cannot be closed by one or two well planned courses tacked on to an outmoded curriculum". Among the topics he discussed during this period in addition to descriptions of commercial instruments were servomechanisms (March 1946), automatic analysis (May 1946), microwave absorption (June 1946), supersonics (June 1946), trigger and gate circuits (September 1946), computers (October 1946), the thermistor (April 1947), electronic counting (June 1947), thermal conductivity cell for gas analysis (May 1948), the transistor (September 1948), cybernetics (January 1949), flame ionization detectors (June 1949), and cathode ray tubes (July

1949). Many of these subjects were covered well ahead of their analytical applications.

The policy of combining a "magazine" section with the journal section in ANALYTICAL CHEMISTRY was a natural outgrowth of the recognition that the readers of the new JOURNAL would be influential in the purchase of analytical instruments as well as being scientifically involved in their development. For its success, this policy required that technical material be interwoven with advertising matter in the magazine section without compromising the scientific integrity of the journal section. Hallett recognized that an editorial staff with a background in chemistry was essential to such an operation, and gradually built up in the Washington editorial office a team of BS or MS chemists, often with industrial experience, to originate and edit technical A-page feature articles as well as to help with processing the traditional peer review of research articles.



Figure 2. Walter J. Murphy

The postwar era of the late 1940's was revolutionary for both the JOURNAL and the science. Wartime developments in instrumentation were ready for commercial development, and ANALYTICAL CHEMISTRY proved to be an ideal advertising medium. By taking advantage of advertising revenues, it was possible to keep a low subscription cost, which in turn stimulated a large readership, without which advertising clientele could not be attracted. To this day, ANALYTICAL CHEMISTRY is essentially unique in representing a primary research journal which is combined with a magazine in a symbiotic relationship.

Undoubtedly, the new format of the JOURNAL stimulated a broadening of the definition of the field. In 1943 [IND. ENG. CHEM., ANAL. ED., **15**, 477 (1943)] the "fundamental purpose" of the ANALYTICAL EDITION was stated to be: (1) to publish fundamental chemistry of analysis and analysis methods, and (2) to publish applied analytical methods. Although by today's standards these were indeed modest goals, they represented a distinct advance over the initial policy published in January 1935, which included the statement, "Articles dealing with the fundamental or theoretical considerations of no immediate application to chemical analysis belong more properly in the *Journal of the American Chemical Society*".

By 1946 [IND. ENG. CHEM., ANAL. ED., **18**, 218 (1946)] the types of papers considered most suitable were described as follows (paraphrased for brevity): (1) Papers presenting an improved or new procedure for the analysis or testing of some element compound or property. The tools may be chemical or physical, and the procedures may deal with organic, inorganic, physical, or biological chemistry. The physical chemistry, in many cases, may approach pure physics. (2) Review papers, either invited or submitted. (3) Papers on the evolution of analytical results or the statistical treatment or interpretation of analytical and test data. (4) Papers dealing with principles and theory of analytical chemistry, which do not necessarily include experimental work. (5) General papers on the college training of personnel, and dealing with training programs, organization, and operation of analytical laboratories. (6) Papers discussing floor plans and layout of physical equipment. (7) Papers describing the application and development of instruments designed for analysis.

The increasing importance of the field of instrumentation was pointed out in the same 1946 article on the scope, with specific mention of the new monthly series by Ralph H. Müller, beginning in January of that year. An example of the new editorial attitude was the appearance of an article by L. G. Longsworth, "Optical Methods in Electrophoresis" [IND. ENG. CHEM., ANAL. ED., **18**, 219 (1946)]. It described in detail a schlieren instrument for electrophoretic analysis of proteins. The nearest approach to an analytical procedure in this paper was the description of precise measurements of refractive index differences in aqueous solutions. Another article in the same issue was entitled "Application of Platinum Resistance Thermometry to Some Industrial Physicochemical Problems" by Daniel R. Stull of the Dow Chemical Co. Automatic recording of temperature-time curves was applied to determining the purity of organic compounds.

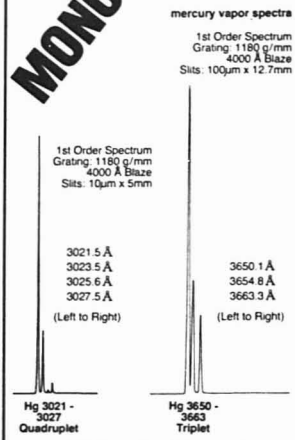
Another article in the same issue by John Mandel, then of Columbia University, dealt with statistical analysis of replicated measurements for increasing precision. Still noticeably lacking during that period were papers dealing with the theory of chemical methods. Work of this type was going on, but it still was being published in nonanalytical journals. For example, I. M. Kolthoff published a series of 45 papers between 1934 and 1954 on the aging of precipitates and coprecipitation, but not one of these papers appeared in the ANALYTICAL EDITION or its successor.



Figure 3. Lawrence T. Hallett

In January 1949 the First Annual Review of Analytical Chemistry included 29 articles entitled "Fundamental Analysis" and in the following month 11 articles on "Applications of Analytical Developments". These reviews, dealing with fundamentals and applications in alternate years, continue to the present day in the form of special issues. Surely they have influenced the type of research papers being submitted to ANALYTICAL CHEMISTRY, because they have covered a wide array of physical as well as chemical methods. Even so, the emphasis was on applications rather than fundamentals, and experiment rather than theory. Paging through the De-

HIGH RESOLUTION MONOCHROMATOR



UNDER $2,000



MODEL MP-1018B CZERNY-TURNER MONOCHORMATOR for UV, Visible, and Near-Infrared. 1180 groves/mm standard. Wavelength readout directly in angstroms. Variable slit width readout in microns. Six switch-selectable scanning speeds; bidirectional. Computer compatible. *Brochure available.*

PACIFIC PRECISION INSTRUMENTS
Formerly McKee Pedersen Instruments
1040 Shary Court
Concord, California 94518
(415) 827-9010

CIRCLE 173 ON READER SERVICE CARD

cember 1949 issue of ANALYTICAL CHEMISTRY, one finds 36 research articles, 15 "Notes on analytical procedures", and one lengthy report on recommended specifications of microchemical apparatus. Of the 36 full articles, the vast majority involved instrumental methods, but only a half dozen or so could be stated to involve a fundamental study.

The decade of the 1940's witnessed the establishment of several other analytical journals in the immediate postwar era of 1946–7. These included the broad-based journals *Analytica Chimica Acta* and *Zhur. Anal. Khim.*, as well as the specialized journals *Applied Spectroscopy* and *Spectrochimica Acta*. After the backlog of wartime research had been assimilated, publications remained in a stable configuration for the remainder of the decade, to undergo proliferation and expansion again as research generally moved into its long-term growth pattern.

Textbooks were slower than journals to respond to postwar changes. Although a book by W. N. Lacey had appeared under the title "Instrumental Methods of Analysis" as early as 1924, the teaching of comprehensive undergraduate and graduate courses involving spectrochemical, electrochemical, and other instrumental methods did not become commonplace until after the appearance of the pioneering text of the same title by Willard, Merritt, and Dean in 1948. This text was closely tied to commercial instruments, and only briefly covered fundamental principles, but it greatly influenced the modernization of undergraduate curricula.

During the late 1940's, ANALYTICAL CHEMISTRY took an active part in the professional activities of the ACS Division of Analytical Chemistry and took editorial positions on matters of professional interest generally. In an editorial in March 1947 entitled "The Profession of Analytical Chemist", several recommendations were made including "insistence upon a sharp distinct line of demarcation in title between the professional chemist and the laboratory technician", the development of "ideal curricula" in analytical chemistry at the undergraduate and graduate levels, including the field of instrumentation, "the establishment of at least one award for outstanding work in the field of analytical chemistry. In addition, several awards for postgraduate students are highly desirable", and "consideration of ways and means of educating industry and particularly top-flight management on the true importance of analytical chemistry and analytical chemists".

In June 1947 excerpts were published of several letters in response to this editorial. These letters, although not identified as to source, represent an interesting cross section of attitudes among industrial and academic analytical chemists of that time. In October 1947 the establishment of the Fisher Award in Analytical Chemistry was announced and traced directly to the March editorial. In November and December 1947 and January 1948, there appeared a series of short articles written by industrial and academic chemists under the general title, "What Is Analysis? What Is the Role of the Analyst?"

In January 1948 under the title "Official at Last", the formal adoption of the name ANALYTICAL CHEMISTRY, which had been in informal use for the previous year, was announced.

In April 1948 another editorial urged industrial sponsorship of postgraduate fellowships and endowed chairs of analytical chemistry. In May 1948 the first Summer Symposium on Analytical Chemistry was announced under the topic "Nucleonics and Analytical Chemistry". This series, cosponsored by the Division and the JOURNAL, continues to this day.

In October 1948, again as a direct result of the March 1947 editorial, the Merck Fellowship in Analytical Chemistry was announced. This nationally competitive fellowship was continued for 9 years, 1949–57 inclusive, and formed the pattern for the Division fellowships that were established in 1966.

In April 1949 in an editorial entitled "The Scope of Analytical Chemistry", a special plea was made for authors to submit fundamental articles. The worldwide scope of its coverage was also emphasized.

As the decade drew to a close, a gradual expansion of PhD-granting programs in analytical chemistry, a new awareness of fundamental research in this field as opposed to the empirical development or improvement of analytical methods, and the emergence of research in instrumentation as opposed to instrumental analysis, especially in industry, were taking place. All of these trends were to continue and accelerate later, but the beginnings were already evident in the late 1940's. Other articles in this symposium will cover developments in subsequent decades.

INTRODUCING I-DARSS

Unparalleled sensitivity for rapid UV, VIS, near-IR spectroscopy.

Tracor Northern's new Intensified Diode Array Rapid Scan Spectrometer system combines the most recent advances in image intensification, fiber optics, and detector array development to provide the highest sensitivity, widest dynamic range, and lowest noise of any optical spectroscopy system available. I-DARSS enables you to perform previously impossible low-level spectral measurements, even of rapidly changing phenomena such as encountered in pulsed laser measurements. *Consider these features:*

Simultaneous detection in up to 1024 channels. I-DARSS simultaneously acquires information for all wavelengths imaged.

Single photoelectron detection. Maximum sensitivity is up to 4 times greater than needed to detect single photoelectrons.

Broad spectral coverage. Advanced UV scintillator-extended ERMA response for the highest quantum efficiency available from 200-900 nm.

Detector resolution of up to 25 line pairs/mm. Your application's resolution requirements can be met by interfacing the detector to the spectrometer of your choice, with twice the simultaneous spectral coverage of any other system.

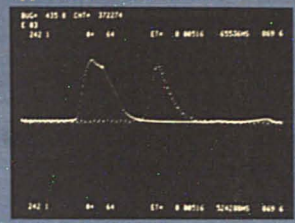
Dynamic range > 4000:1. Thermoelectric cooling of the detector provides low noise and extended signal integration.

Versatile signal averaging capability. Detector exposure times and repetitive scans are adjustable over a wide range, giving you the highest S/N for your application.

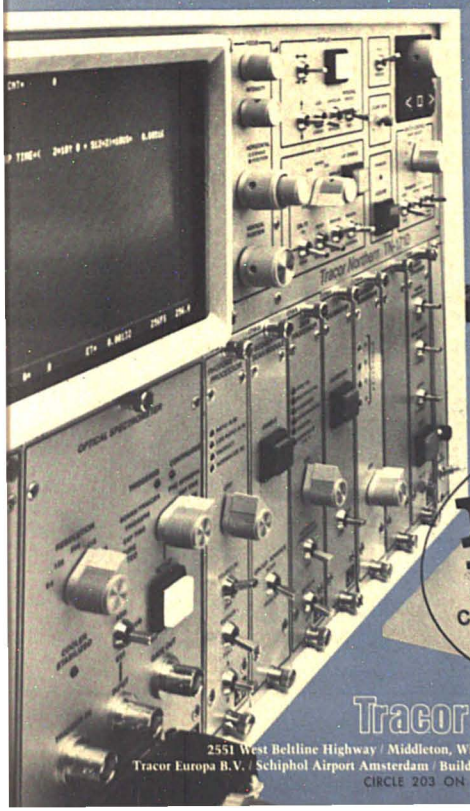
Modular, microcomputer-based TN-1710 signal analyzer provides convenient firmware control of data acquisition, processing, and display. Accessories include floppy disk for mass storage of spectra and operating programs.

I-DARSS has the sensitivity to meet your spectral measurement needs with the highest speed and the lowest noise. Some applications are luminescence, fluorescence, and Raman spectroscopy, and chemical kinetics measurement.

Contact us for assistance in applying I-DARSS to your application or for a demonstration.



5-millisecond molecular fluorescence spectrum. Spectra can be expanded and overlapped for comparison. In addition to spectral data, all measurement parameters are displayed.



Modular TN-1710 microcomputer-based signal analyzer

TN-1223 Intensified DARSS detector

TN-1150 Holographic grating spectrograph

I·R 100 COMPETITION WINNER

Cited by Industrial Research/Development magazine for developing one of the 100 most significant technical products of the year

1978

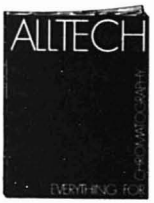
Tracor Northern

2551 West Beltline Highway / Middleton, Wisconsin 53562 / (608) 831-6511 / TWX—910-280-2521
Tracor Europa B.V. / Schiphol Airport Amsterdam / Building 106, The Netherlands / Telephone (020) 41 1865 / Telex 13695

CIRCLE 203 ON READER SERVICE CARD

WHEN YOU THINK OF CHROMATOGRAPHY.....
.....THINK OF ALLTECH ASSOCIATES

- *We have over 6000 different supplies and accessories that will help you do your work easier, faster and better.*
- *We stock these products in 4 geographical locations so that we may serve your needs quickly. We're as close as your telephone.*
- *We have the technology and the people to help you with any of the chromatographic problems you may encounter.*



WRITE FOR YOUR FREE COPY OF OUR NEW 160 PAGE CATALOG

WRITE:

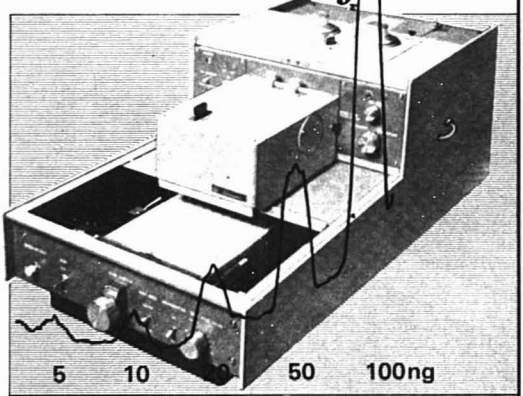
ALLTECH ASSOCIATES

202 CAMPUS DRIVE • ARLINGTON HEIGHTS, ILLINOIS 60004 • 312-392-2670

CIRCLE 6 ON READER SERVICE CARD

Announcing a New Generation of TLC and Gel Scanner

Award Winning CS-910 Offers Excellent Capabilities!



What's new about CS-910?

It is the first scanner to combine the quantitative accuracy of TLC densitometry with the high resolution of gel scanning.

1. •DUAL-WAVELENGTH METHOD eliminates baseline fluctuations caused by local irregularities in thin-layers or gels.
2. •ZIG-ZAG SCANNING TECHNIQUE eliminates errors caused by the irregular shape of the developed spots.
3. •Unique WORKING CURVE LINEARIZER provides excellent linearity over a wide density range—eliminates errors resulting from different size spots.
4. •Built-in BACKGROUND CORRECTOR minimizes the effects of contamination on TLC plates.
5. Extremely sensitive FLUOROMETRY MODE permits precise quantitation of ultra-micro content samples.
6. TRANSMISSION OR REFLECTION METHOD can be easily selected.

Contact us today for detailed information on the new CS-910 scanner, Spectrophotometers, Spectrofluorophotometers or Gas Chromatographs.

•U.S. PATENT 4,013,364 and 3,994,587

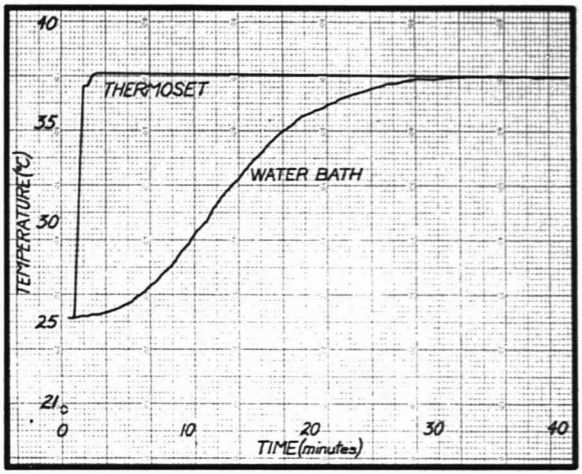
SHIMADZU SCIENTIFIC INSTRUMENTS, INC.
9147 Red Branch Road, Columbia, Md. 21045, U.S.A.
Phone:(301) 596-6978, (301) 997-1227 Telex No.:23087959

SHIMADZU (EUROPA) GmbH
4000 Düsseldorf 1, Postfach 2706, Georg-Glockstr. 14 F.R. Germany
Phone (0211) 4570290 Telex No.:08584119

SHIMADZU SEISAKUSHO LTD.
1, Nishinokyo-Kuwabaracho, Nakagyo-ku, Kyoto 604, Japan
Cable Add.: SHIMADZU KYOTO Overseas Telex No.:05422-166

CIRCLE 195 ON READER SERVICE CARD

Comparison of 25 - 37°C equilibration time of ThermoSet (70 secs) with waterbath system(30 mins). Measurements made in the cuvette show true sample temperature. (Both systems were pre-equilibrated at 25°C.)



Gilford's new ThermoSet™... for those who've always wished they could take repeatable temperature control for granted.

If you're engaged in temperature-dependent studies like enzyme rates, you've probably long wished for sample temperature control you could take for granted. The "set-it-and-forget-it" kind of device that eliminates careful periodic scrutiny of a thermometer and avoids constant temperature correction...the kind of device that's safe as well as repeatable, convenient as well as accurate.

Such a device is Gilford's new ThermoSet™, an all-electronic system which automatically regulates sample temperature anywhere you set it between 0 and 100°C...independent of ambient conditions.

Easy-To-Use Small-Volume Cuvettes

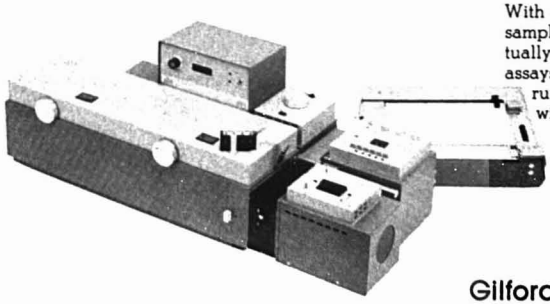
ThermoSet accommodates up to four individual cuvettes (of three varieties) for greater flexibility and productivity. They're easy to fill and to empty, easy to handle. And minimum volumes are only 250 µl.

Faster Results

You get answers sooner because of convenient sample handling plus rapid setup and faster sample temperature equilibration. Just dial in the temperature (you can set it to a tenth of a degree); seconds later --instead of minutes -- you will read the stabilized temperature to 0.01°C from ThermoSet's L.E.D. readout. And the final results of your assays will be just that much faster.

Repeatability Along With Accuracy

With ambient-independent electronic regulation of sample temperature to within 0.05°C, ThermoSet virtually eliminates temperature as a variable in your assays. Each result will be more accurate, and if you run it again, the same temperature characteristics will be assured.



gilford INSTRUMENT
Oberlin, Ohio 44074
(216) 774-1041 Telex: 98-0456
Paris (Evry 91), France
Düsseldorf, W. Germany
Teddington, Middx., England

CIRCLE 86 ON READER SERVICE CARD

Gilford Research Spectrophotometers: every job easier, every result more accurate.

THE DU PONT LC COLUMN

New bimodal SEC revolutionizes analysis of polymer molecular weight distribution.

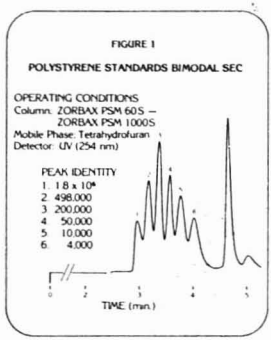
Innovative technology developed by DuPont now enables you to analyze polymeric systems having extremely wide molecular weight ranges with unprecedented speed and precision. Just a single pair of our new bimodal high-performance size exclusion columns does the job.

Covering the molecular weight range of 10^2 to about 4 x 10^6, the bimodal technique is the most significant development in molecular weight distribution analysis since DuPont introduced high-performance, high-temperature size exclusion chromatography two years ago.

The bimodal technique removes the guesswork in tailoring resins for specific properties, selecting optimum reaction conditions, comparing resin batches against standards, evaluating alterations in process formulations and solving many other polymer production and processing problems.

New Zorbax* PSM packings are keys.

DuPont has developed two all-new packings with pore sizes of approximately 60 and 1000 Angstrom. These sizes were carefully matched to polymer analysis requirements. Coupling two Zorbax PSM columns gives you an SEC system with an exceptionally wide linear range of calibration, as shown

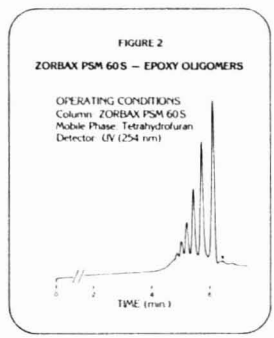


in Figure 1. The uncertainty in matching multiple columns for the right molecular weight range has been eliminated.

These silica-based packings are produced by the patented Zorbax technology, which has become a recognized standard for chromatography. Their high performance results from their rigid, stable nature coupled with close control of pore structure.

Zorbax PSM 60 and PSM 1000 columns are both available in a chemically bonded silanized form for organic solvents and in untreated form for aqueous applications. The silanized form eliminates adsorption without creating undesirable partition effects.

In addition, Zorbax PSM 60 columns give extremely high resolution when used alone for materials under 1000 in molecular weight. Figure 2 shows an excellent separation of the well-known epoxy oligomers.



Get our new bimodal bulletin.

This bulletin, latest in our series of LC Column Reports, gives details on the bimodal technique, with examples. Drop a note to: DuPont Instruments, Room 36736, Wilmington, DE 19898.

Free technical aid from Du Pont's long polymer experience.

As a company whose extensive involvement in polymer chemistry has led to a host of innovative products, DuPont has amassed unique experience in analytical methods for characterizing polymers. Write to us about your problem, or contact our staff by calling, toll free, 800-441-7458 (in Delaware, 772-5273).

*Trademark for DuPont's liquid chromatography columns & packing

Liquid Chromatography Columns
Scientific & Process Instruments Division

DUPONT

CIRCLE 50 ON READER SERVICE CARD

Pittsburgh Conference

March 5–9, 1979

The 1979 Pittsburgh Conference on Analytical Chemistry and Applied Spectroscopy will be held at the Cleveland Convention Center, Cleveland, Ohio, March 5–9, 1979. This year's conference theme will be "Continued Growth in Analytical Chemistry and Applied Spectroscopy Through Expanded Communication." The conference will be highlighted by 15 planned symposia and five award presentations. Early information on the conference provides the following titles of these symposia: **Liquid Chromatography for Environmental Regulatory Requirements, Practical Applications of Glass Capillary Columns in Gas Chromatography, Problems and Solutions in Capillary Gas Chromatography, Applications of Ion Chromatography, Photoacoustic Spectroscopy, Laboratory Systems Management, Microprocessors in Action, New Surface Techniques, Trace Analysis in Characterization of Materials, Environmental Analysis of Water and Sediment, The Use of ICAP Emission for Environmental Analysis, Symposium on Biomedical Aspects, New Analytical Techniques on the Horizon, Fourier Transform/Computer Dispersive Groups,** and **New Surface Analysis Instrumentation.**

The awards symposia include the Spectroscopy Society of Pittsburgh Award, Society for Analytical Chemists of Pittsburgh Award, Hasler Award, Dal Nogare Award, and the Coblentz Award. Only two of these five awards were available at press time. John S. Waugh, Noyes Professor of Chemistry at MIT, will receive the 1979 Spectroscopy Society of Pittsburgh Award. Dr. Waugh will be cited for his many valuable contributions toward the development of NMR instrumentation and the mathematical treatment of nuclear spin systems. His developments include techniques for obtaining high resolution NMR spectra of solids, multiple-pulse techniques for proton and ^{19}F NMR in solids, and the cross-polarization technique for obtaining ^{13}C solid state spectra. He is currently the editor of the Academic Press series entitled "Advances in Magnetic Resonance," and is a Fellow of the American Academy of Arts and Sciences and of the American Physical Society.

The awardee of the 1979 Maurice F. Hasler Award is Professor John H. Beynon of the Dept. of Chemistry of Wales, Swansea, Glamorgan. The Hasler Award, given by Applied Research Laboratories and administered by the Spectroscopy Society of Pittsburgh, is awarded biennially to an outstanding scientist in the areas of instrumentation and analytical techniques.

Program chairman for the 1979 meeting is S. David Cifrulak, Calgon Corp., P.O. Box 1346, Pittsburgh, Pa. 15230. The publicity chairman is Charles J. Belle, Ferro Corp., 7500 E. Pleasant Valley, Independence, Ohio 44131. For exhibition space, contact: Allen J. Sharkins, ALCOA Laboratories, Alcoa Center, Pa. 15069.

Chromatography Awards

The M. S. Tswett Chromatography Medals were awarded to Leslie S. Ettre, J. Calvin Giddings, and R.P.W. Scott at the 13th International Symposium on Advances in Chromatography held in St. Louis, Mo., October 16–19, 1978.

Leslie S. Ettre, senior staff scientist at Perkin-Elmer Corp., is cited for his involvement in gas chromatography since 1957. His activities cover a wide variety of fields including trace analysis, studies on detector response,



Lawrence T. Hallett, former editor of ANALYTICAL CHEMISTRY (left), and wife Alice Hallett are shown with current editor Herbert A. Laitinen at the Analytical Division reception and dinner in Miami Beach, Fla., Sept. 12. With David Hercules, chairman of the Division, as host the Division paid tribute to ANALYTICAL CHEMISTRY's 50th anniversary with a gala affair attended by more than 90 people



Leslie S. Ettre

the retention index system, and particularly open tubular capillary columns. In the latter field, noteworthy contributions include the introduction of support-coated open tubular columns and the investigation of their properties. Dr. Ettre has lectured widely and has been active in the organization of several international symposia in chromatography. He has served as the chairman of the anniversary symposium on chromatography at the 164th National ACS Meeting in New York, the symposium on selective chromatography detectors at the 172nd National ACS Meeting in San Francisco, and cochairman of the summer symposium in analytical chemistry of the ACS Analytical Division in 1973. He is one of the editors of *Chromatographia* and serves on the editorial advisory board of the *Journal of Chromatographic Science.* Dr. Ettre is author and coauthor of approximately 100 scientific and technical papers and a number of books of which the best known are "Open Tubular Columns in Gas Chromatography" (1965), "Practice of Gas Chromatography" (1967), "Ancillary Techniques of Gas Chromatography" (1969), and "Open Tubular Columns—An Introduction" (1973).



J. Calvin Giddings

J. Calvin Giddings, author of more than 180 scientific papers, is cited for his wide-ranging research interests. His early studies on flame theory, quantum mechanics, and chemical kinetics soon yielded to his interests in chromatography and related methods. His interest in chromatography dates from his graduate years at the University of Utah. His work in this area has shed light on nearly every chromatographic process, including nonequilibrium, diffusion, eddy diffusion, pressure changes, flow in paper and thin-layer chromatography, preparative scale and programmed-temperature GC, exclusion chromatography, electrophoresis and the generation of nongaussian zones. He has worked extensively with the optimization of chromatography and has developed new high-pressure chromatographic systems and the one-phase system called field-flow fractionation.

Dr. Giddings, coeditor of 16 volumes of "Advances in Chromatography," has written a book "Dynamics of Chromatography" (1965) and a textbook "Chemistry, Man and Environmental Change" (1973), which reflects his long standing interest in the environment. He is also the recipient of the ACS Award in Chromatography and Electrophoresis, the Utah Award of the local section of the Society, and the ROMCOE Award for Outstanding Environmental Achievement in Education.

Raymond Peter William Scott, director of the Physical Chemistry Department at Hoffmann-La Roche, Inc., in Nutley, N.J., started his activities in gas chromatography practically at the inception of the technique. He pioneered the development of high resolution columns and high sensitivity detectors, and presented fundamental discussions on the relationship between the theory and practice of the technique. Joining the early chromatographers who became involved in the development of modern HPLC, Dr. Scott pioneered many of the achievements that today are utilized routinely by many analytical laboratories.

Dr. Scott is author and coauthor of over 100 scientific papers that largely involve the theory and practice of both gas and liquid chromatography. He edited the proceedings on gas chromatography (1960 Edinburgh symposium) and is the author of two books, "Contemporary Liquid Chromatography" and "Liquid Chromatography Detectors." Dr. Scott was a founding member of the Gas Chromatography Discussion Group and exhibited his high-speed columns at the Royal Society Tercentenary Exhibition in 1961. He received the ACS Award in Chromatography in 1977 and is a fellow of the Royal Institute of Chemistry.



Raymond P. W. Scott

Perkin-Elmer Receives Tswett Medal

A special Tswett Commemorative Medal was awarded to the Perkin-Elmer Corp. by the Soviet Union Scientific Council for Chromatography at a symposium dedicated to the discovery of chromatography in 1903 by the Russian botanist, M. S. Tswett. Perkin-Elmer's involvement in chromatography started in 1955 with the first highly successful commercial gas chromatograph, the Model 154. The company and its scientists and engineers pioneered in a number of important developments such as open tubular columns and improved detectors, and helped in solving the problems of many industrial laboratories.

NRC Postdoctoral Research Programs in 1979

Applications are now being accepted for the NRC Research Associateship Programs for 1979. These programs provide scientists and engineers with opportunities for postdoctoral research on problems in the fields of

The Bausch & Lomb Blue Line of SPECTRONIC® Spectrophotometers.

You're looking at the finest family of single beam spectrophotometers in the world.

The Blue Line.

These four great Bausch & Lomb instruments give you sampling versatility that can't be matched.

They give you longer wave-length ranges, a choice of narrow spectral slit widths, and a variety of sample handling techniques.

They give you speed and accuracy with features such as automatic 0%T, direct concentration readouts, optional flow cells, and automation systems.

They even give you updateability, because they're designed to grow as you grow. The more demanding you are, the more capable they can become.

The Blue Line—the SPECTRONIC 70, 88, 710, and the famous SPECTRONIC 100—is the best, not just because of Bausch & Lomb's proven reputation for the finest performing instrumentation.

And not just because the Blue Line is supported by a nationwide network of product support specialists.

But because you can get research quality from any one of the Blue Line at a routine instrument price.

Call your nearest Bausch & Lomb representative, or one of our dealers—Fisher Scientific or VWR Scientific. Or call us at (716) 385-1000, ext. 325.

We'll show you that getting into a blue-blooded family need not be expensive.

One very blue-blooded family.

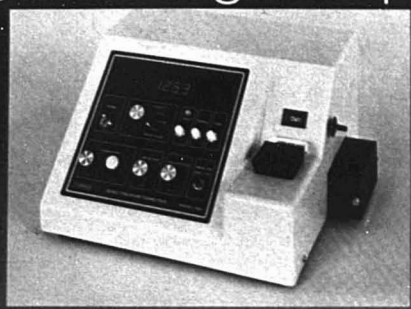


BAUSCH & LOMB

ANALYTICAL SYSTEMS DIVISION
ROCHESTER, NEW YORK 14625

CIRCLE 31 ON READER SERVICE CARD

The Turner Spectrophotometer NEW with digital display.



Continuing a tradition of excellent performance at a sensible price.

The new Turner Spectrophotometer combines all of the features that have put our popular spectrophotometers in a price/performance class by themselves. The Model 380 goes a step further by offering you the convenience of a bright, easy to read digital display of linear absorbance, concentration values or transmittance. There's also a special provision for easy entry of constants for kinetic enzyme assays.

The high performance features of the Model 380 include narrow, 9 nanometer bandwidth; low (0.5%) stray light; ±2 nanometer wavelength accuracy; wide standard operating range (320-710 nanometers); excellent linearity (up to 1.7 absorbance) even at 340 nanometers.

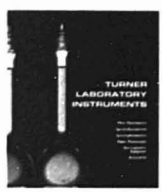
A wide variety of accessories that expand the versatility of our established Models 330 and 350 Spectrophotometers may also be used with the Model 380. These include the Turner **Enzyme Calculator/Printer** shown here and the Instafill® accessory for micro-flow work. At $1725, the Model 380 is priced within the budget of every laboratory. So are the accessories. For example, the **Printer** is $1420. The **Enzyme Calculator/Printer,** $2150. No one else offers comparable instrumentation for so little.

Your inquiry will bring more details, a copy of our popular Spectrophotometer checkout guide, and our 1978 catalog! Contact Turner Associates, Division of American Sterilizer Co., 2524 Pulgas Avenue, Palo Alto, CA 94303.
Phone (415) 324-0077.

Turn to

TURNER

. . . today



Free new catalog

CIRCLE 205 ON READER SERVICE CARD

chemistry, mathematics, physics, space sciences, atmospheric and earth sciences, engineering, and life sciences. Awardees conduct research on problems of their choice in selected Federal research laboratories at approximately 65 geographic locations in the U.S. Appointments are made on a competitive basis and are open to recent recipients of the doctorate and, in some cases, to senior investigators. Some programs are open to non-U.S. citizens.

Approximately 250 new awards will be made in 1979. The basic stipend (subject to income tax) will be $18 000 for recent recipients of the doctorate. Higher stipends are awarded to senior investigators. The awards include relocation grants and funds for limited professional travel during tenure. Applications must be postmarked by January 15, 1979. Results will be announced in the spring.

Application forms and detailed information about specific opportunities for research are available from the Associateship Office, JH 608-D3, National Research Council, 2101 Constitution Ave., N.W., Washington, D.C. 20418 (202-389-6554).

Academic Investigator Award in Toxicology

The Academic Investigator Award in Toxicology will provide support for a period of up to three years in an amount not to exceed $90 000 direct costs. The goal of the program is to provide a mechanism by which toxicological research experience can be gained by scientists not now working in the field, so that they may undertake subsequent research projects in environmental toxicology. Receipt dates for applications are Feb. 1, 1979, and June 1, 1979. For application forms and further information, contact: Christopher Schonwalder, Program Director, Research Manpower Development Section, National Institute of Environmental Health Sciences, P.O. Box 12233, Research Triangle Park, N.C. 27709, or call 919-755-4022.

Sharing of Scientific Equipment

While informal equipment sharing prevails among university researchers, NSF is encouraging increased sharing of scientific research equipment on campuses to reduce requests for equipment purchase support in proposals to NSF. A General Accounting Office report, "Minimum Requirements Are Needed for Colleges and Universities to Justify Research

at home in your lab



For more than thirty-five centuries all the glass made was "soft." Then Corning originated the hard, borosilicate glass used in PYREX® ware for your lab and your home.

Corning uses the same glass in the popular UN-CANDLE®.

Corning also originated the hexagonal base on cylinders to prevent rolling, the glass shoulder that protects pouring lips, the LIFETIME RED® panels that enhance readability, the Teflon® dripless cylinder, and class A precision borosilicate cylinders.

PYREX®, UN-CANDLE® and LIFETIME RED® are registered trademarks of Corning Glass Works. TEFLON® is a registered trademark of the E.I. duPont deNemours & Co. (Inc.)

PYREX®

ONLY FROM CORNING

PYREX CORNING

TOTAL VALUE

We try diligently to see that you get the total of Corning's many capabilities in every product we make.
We know that's how we earn your trust and retain your business.
We know you would never settle for less than **Total Value** from Corning.

Free Catalog. If you don't own the 42nd Edition of the Corning catalog of total value labware, clip this coupon to your letterhead for a free copy.

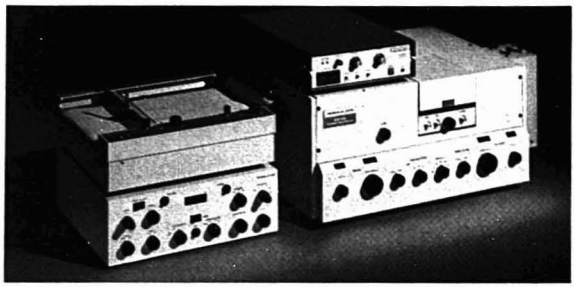
Free "At Home" cup. You'll get this special PYREX® "At Home in the Lab" cup with the catalog – for cup only, use the reader service card in this magazine.

CORNING
Science Products Division
Building 21-5
Corning Glass Works, Corning, N.Y. 14830

CORNING PYREX

CIRCLE 34 ON READER SERVICE CARD

HOW WE MADE THE BEST IN FLUORESCENCE BETTER.



INTRODUCING THE MPF-44B.

For years, no other research grade fluorescence instrument could touch our Model MPF-44A in performance, operating convenience, or dollar value.

That's why the new MPF-44B is so important. In addition to its predecessor's proven advantages, it brings to you benefits that are the product of our long-time experience.

New optics and electronics. The 150W xenon lamp is ozone-free, hermetically sealed in a special ceramic housing. For optimum efficiency, it's easy to focus. For better performance, both monochromators have a new high-efficiency grating which results in a significant improvement in sensitivity.

The 3½-digit display gives you instantaneous readings of fluorescence intensity, dynode voltage or concentration readout. Integration circuitry permits high-precision intensity measurement by averaging readings accumulated over selected time periods. And there's an X-Y recorder interface with a built-in time drive and X-coordinate expansion capability.

The new DCSU-2. This advanced differential corrected spectra unit is a microprocessor accessory with many capabilities. Besides corrected and differential spectra, it gives you automatic polarization and anisotropy spectra or calculations, plus first and second derivative spectra.

More accessories. You can add more than 20 other accessories to the MPF-44B to widen its range. You can convert it to an LC detector, select TLC, low temperature luminescence (phosphorescence), polarization, and solid sampling, for example. All the MPF-44A accessories will work on the MPF-44B.

Compare and decide. Send for our literature on the MPF-44B and compare it with any other fluorescence spectrophotometer, feature by feature. If you have any questions about a specific application, call us now at (203) 762-6095. Or write Perkin-Elmer Corp., MS-12, Main Ave., Norwalk, CT 06856.

PERKIN-ELMER

Expanding the world of analytical chemistry.

CIRCLE 167 ON READER SERVICE CARD

News

Equipment Purchases," identifies procedures used by certain universities when requesting equipment funds in research proposals. It also describes NSF's and NIH's policies and procedures regarding funds for equipment. The report (Stock #HRD-78-52) is available from GAO, 441 G St., N.W., Washington D.C. 20548.

Synchrotron Radiation Facility at Cornell

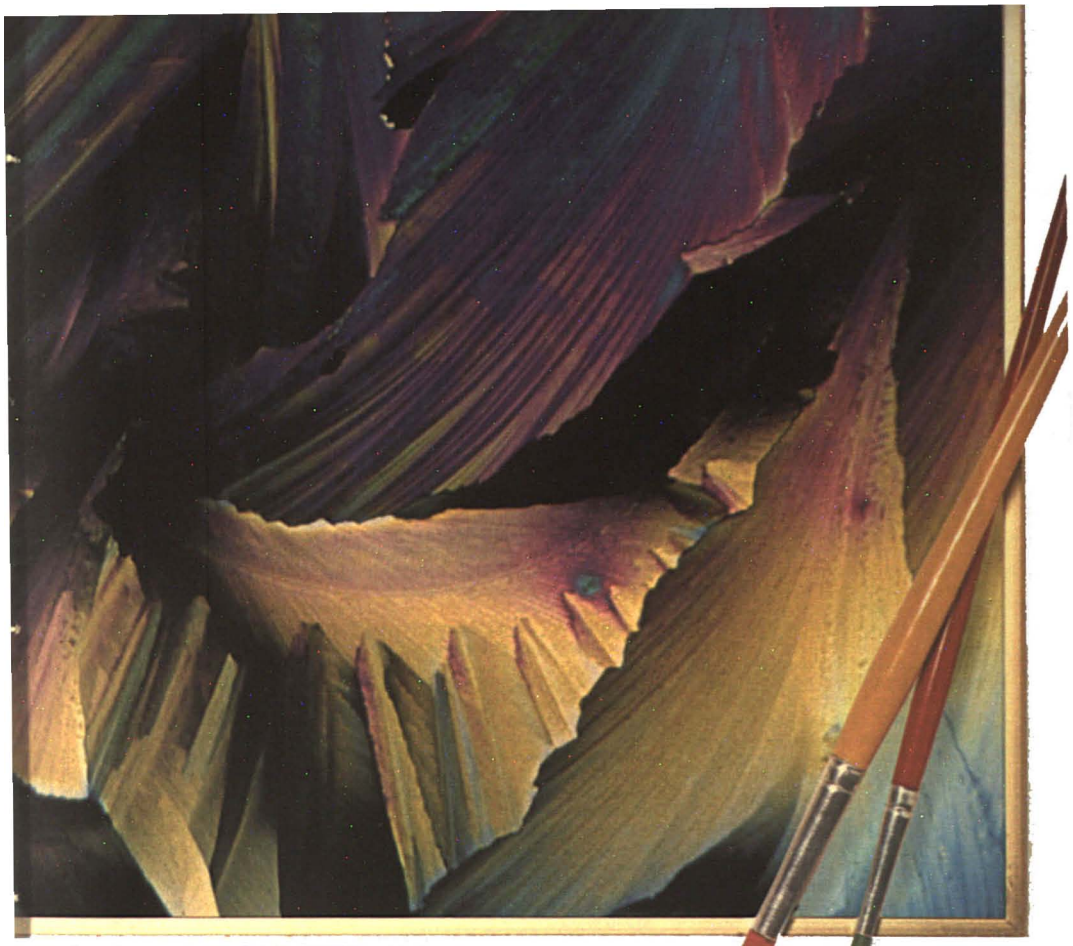
An intense source of X-rays with energies much higher than can be produced by any other existing or planned facility in the nation will soon be available to researchers probing the basic properties of matter. The National Science Foundation has approved a grant of $1 million over the next three years for construction at Cornell University of a radiation laboratory known as the Cornell High Energy Synchrotron Source. The radiation lab and the Cornell Electron Storage Ring, a high-energy particle accelerator being built at Cornell's Wilson Laboratory, will be available to researchers nationwide. The Electron Storage Ring is expected to begin operation by spring 1979, and the radiation lab should begin providing X-rays to users by summer 1979. Boris W. Batterman, professor of applied and engineering physics, is director of the facility, and Neil W. Ashcroft, professor of physics, is associate director.

Detecting Ancient Human Settlements

Dr. Robert C. Eidt, a University of Wisconsin-Milwaukee geographer, has developed a technique for testing evidence of ancient human activity. Phosphate is the key chemical in the test. The rate and manner by which phosphate becomes fixed in the soil provide evidence of human activities such as harvesting, livestock husbandry, irrigation, plowing, and other modifications of the terrain. First, colorimetry is used to indicate color traits and proportions of phosphate. More exact analyses are made in the laboratory.

Meetings

- **Symposium on Oil Shale Sampling, Analysis, and Quality Assurance.** Nov. 6–10. Denver Hilton Hotel, Denver, Colo. *Contact: Robert Pressey, Program Chairman, Denver Research Institute, University of Denver, Denver, Colo. 80208. 303-753-2911*



Photomicrograph by John Delly, McCrone Research Institute

FOR THE CREATIVE CHEMIST:

EASTMAN REAGENTS FOR PROTEIN CHEMISTRY.

This dramatic photomicrograph of EASTMAN Organic Chemical 192, p-Nitrophenol, taken by John Delly of McCrone Research Institute, demonstrates what can happen when you use your imagination and EASTMAN Organic Chemicals.

Start with our products for protein and polypeptide synthesis and analysis, and let your creativity emerge in practical, everyday applications. You can rely on their purity and consistent quality. Eastman amino acids; coupling , blocking , deblocking , protein-modifying, sequenation , visualization , and gas-liquid chromatography reagents; polymeric supports; and thin-layer chromatography products are available only through your EASTMAN Organic Chemicals dealer.

See your dealer for our many other chemicals for electrophoresis: liquid scintillation counting; and dyes, stains, and indicators. Your dealer can give you fast, reliable service, and a colorful free reminder that chemistry is creative.

For complete details on our products for protein chemistry, send for our free technical literature, JJ-8. Write Eastman Organic Chemicals, Eastman Kodak Company, Dept. 412L, Rochester, N.Y. 14650.

Take a close look at EASTMAN Organic Chemicals. Dealers handling EASTMAN Organic Chemicals: American Scientific & Chemical, Bio Clinical Laboratories, Brand-Nu Laboratories, Inc., Bryant Laboratory, Inc., Custom Chemical Laboratories, Inc., Fisher Scientific, GAC Laboratories, Inc., Labproducts, Inc., Midland Scientific, Inc., North-Strong, Inc., Preiser Scientific, Sargent-Welch, Scientific Products, Scientific & Industrial Sales & Service, Inc., VWR Scientific Inc., Ward's Natural Science Establishment, Inc.

- **AAMI/FDA Conference on Medical Device Regulations.** Nov. 14–15. Hyatt Regency, Washington, D.C. *Contact: Renee L. Pietrangelo, Association for the Advancement of Medical Instrumentation, 1901 N. Fort Myer Dr., Suite 602, Arlington, Va. 22209. 703-525-4890*
- **Clinical and Environmental Applications of Quantitative Thin-Layer Chromatography.** Jan. 15–17, 1979. Philadelphia, Pa. *Contact: H. M. Stahr, Iowa State University of Science and Technology, Ames, Iowa 50011. 515-294-1950*
- **2nd European Conference on Surface Science.** Mar. 26–29, 1979. Cambridge, England. Topics include: synchrotron studies and EXAFS, surface kinetics and adsorption, ion and molecular beam effects, semiconductor and polymer surfaces. *Contact: The Conference Chairman, 2nd European Conference on Surface Science, c/o Birches Industrial Estate, East Grinstead, Sussex, England. Page 1114 A, Oct.*
- **International Symposium on Occupational Radiation Exposure in Nuclear Fuel Cycle Facilities.** June 18–22, 1979. Los Angeles, Calif. *Contact: John H. Kane, Special Assistant for Conferences, Office for Technical Information, Dept. of Energy, Washington, D.C. 20545*
- **Combined 37th Annual Meeting of the Electron Microscopy Society of America and 13th Annual Meeting of the Microbeam Analysis Society.** Aug. 13–17, 1979. San Antonio, Tex. *Contact: Dale Newbury, Chairman, MAS Program Committee, NBS, Bldg. 222, Room A121, Washington, D.C. 20234. 301-921-2875*

Short Courses

ACS Courses. For more information, contact: Department of Educational Activities, American Chemical Society, 1155 Sixteenth St., N.W., Washington, D.C. 20036. 202-872-4508

Interpretation of Mass Spectra
Boston. Nov. 3–4. Don C. DeJongh. $220, ACS members; $260, nonmembers

Statistics for Experimental Design
Boston. Nov. 3–4. John Hromi. $215, ACS members; $255, nonmembers

Chemical Carcinogenesis
Chicago. Nov. 16–17. Irving Selikoff. $265, ACS members; $310, nonmembers

Creative Problem Solving
Chicago. Nov. 16–17. Moshe F. Rubinstein. $215, ACS members; $255, nonmembers

Toxicology for Chemists
San Francisco. Nov. 28–30. Frederick Sperling and Morris Joselow. $485, ACS members; $555, nonmembers

Gas Chromatography–Mass Spectrometry
San Francisco. Nov. 29–30. J. Throck Watson and O. David Sparkman. $265, ACS members; $310, nonmembers

Interpretation of NMR Spectra
San Francisco. Nov. 29–Dec. 1. LeRoy F. Johnson and Roy H. Bible, Jr. $280, ACS members; $330, nonmembers

Microprocessors and Minicomputers—Interfacing and Applications
Blacksburg, Va. Dec. 10–15. Raymond E. Dessy and the Chemistry Department Instrument and Design Group from VPI&SU. $455, ACS members; $515, nonmembers

Liquid Chromatography, Theory and Practice
Blacksburg, Va. Dec. 11–14. Harold McNair. $450, ACS members; $510, nonmembers

Stack Stampling & Ambient Air Monitoring
Sheraton Motor Inn, East Brunswick, N.J. Nov. 8–10. $425. *Contact:* Mary Sobin, Dept. NR, Center for Professional Advancement, P.O. Box H, East Brunswick, N.J. 08816. 201-249-1400

Introduction to Gas Chromatography
Donaldson Brown Center for Continuing Education, VPI&SU, Blacksburg, Va. Nov. 9–11. H. M. McNair and D. T. Stafford. $250. *Contact:* Linda Leffel, Center for Continuing Education, VPI&SU, Blacksburg, Va. 24061. 703-961-5241

Liquid Chromatography—Instrumentation and Application
University of Wisconsin-Madison, Wisconsin Center, Madison. Nov. 20–21. $260. *Contact:* James E. Nicholls, Dept. of Engineering, University of Wisconsin-Extension, 432 N. Lake St., Madison, Wis. 53706. 608-262-2061

Chemical Derivatization for Chromatography and Mass Spectrometry
Cincinnati. Nov. 27–29. M. Quilliam. $375. *Contact:* Ann Woolley, Finnigan Institute, 11750 Chesterdale Rd., Bldg. #5, Cincinnati, Ohio 45246. 513-772-5500

Digital Electronics and Microcomputer Interfacing Basics
Sheraton Red Lion Inn, Blacksburg, Va. Nov. 27–29. P. R. Rony, D. G. Larsen, C. A. Titus, and P. E. Field. $245. *Contact:* Linda Leffel, Center for Continuing Education, VPI&SU, Blacksburg, Va. 24061. 703-961-5241

Industrial Toxicology
Houston, Tex. Nov. 29–Dec. 1. $475. *Contact:* Mary Sobin, Dept. NR, Center for Professional Advancement, P.O. Box H, East Brunswick, N.J. 08816. 201-249-1400

Microcomputer, Instrument, and Analog Converter Interfacing and Programming
Sheraton Red Lion Inn, Blacksburg, Va. Nov. 30–Dec. 2. P. R. Rony, D. G. Larsen, C. A. Titus, and P. E. Field. $245. *Contact:* Linda Leffel, Center for Continuing Education, VPI&SU, Blacksburg, Va. 24061. 703-961-5241

Forensic and Clinical Toxicology
Cincinnati. Dec. 11–15. B. Finkle, T. Jennison, and M. Peat. $625. *Contact:* Ann Woolley, Finnigan Institute, 11750 Chesterdale Rd., Bldg. #5, Cincinnati, Ohio 45246. 513-772-5500

Electronics for Automation, Instrumentation, and Signal Conditioning
Donaldson Brown Center for Continuing Education, VPI&SU, Blacksburg, Va. Dec. 18–21. P. R. Rony, D. G. Larsen, C. A. Titus, and P. E. Field. $295. *Contact:* Linda Leffel, Center for Continuing Education, VPI&SU, Blacksburg, Va. 24061. 703-961-5241

Gas Chromatography
Villanova University, Villanova, Pa. Jan. 3–5. Sponsored by the Chromatography Forum of the Delaware Valley. *Contact:* Robert L. Grob, Chemistry Dept., Villanova University, Villanova, Pa. 19085

Pharmaceutical Quality Assurance & Control
Sheraton Motor Inn, East Brunswick, N.J. Jan. 8–12. $655. *Contact:* Mary Sobin, Dept. NR, Center for Professional Advancement, P.O. Box H, East Brunswick, N.J. 08816. 201-249-1400

Hazardous Materials
Sheraton Motor Inn, East Brunswick, N.J. Jan. 22–24. $435. *Contact:* Mary Sobin, Dept. NR, Center for Professional Advancement, P.O. Box H, East Brunswick, N.J. 08816. 201-249-1400

Basic Interpretation of Mass Spectra
San Francisco. Jan. 22–26. D. DeJongh and G. Ouchi. $400. *Contact:* Ann Woolley, Finnigan Institute, 11750 Chesterdale Rd., Bldg. #5, Cincinnati, Ohio 45246. 513-772-5500

Interpretation of Mass Spectra: Applications
San Francisco. Jan. 29–30. $250. *Contact:* Ann Woolley, Finnigan Institute, 11750 Chesterdale Rd., Bldg. #5, Cincinnati, Ohio 45246. 513-772-5500

Testing for Drugs in Race Horses
Cincinnati. Jan. 29–Feb. 1. G. Maylin and J. Henion. $500. *Contact:* Ann Woolley, Finnigan Institute, 11750 Chesterdale Rd., Bldg. #5, Cincinnati, Ohio 45246. 513-772-5500

For Your Information

For any person who uses the ***Federal Register*** **and the Code of Federal Regulations,** free Friday workshops will be held on Nov. 3 and 17 and Dec. 1 and 15 from 9 to 11:30 a.m. at the Office of the Federal Register, Rm. 9409, 1100 L St., N.W., Washington, D.C. For reservations, call Mike Smith, Workshop Coordinator, at 202-523-5235.

The first edition of the **"Directory of Canadian Environmental Experts"** is now available. Its two parts are: an alphabetical listing of the name and affiliation of the researchers, and the title of their research projects. The second part is a computer-produced subject index arranged alphabetically by terms appearing in the titles. Copies are available at $15 each from: Information Exchange Centre, CISTI, National Research Council of Canada, Ottawa, Canada K1A 0S2.

Beckman Instruments, Inc., has completed the acquisition of Altex Scientific Inc., a Berkeley, Calif.-based manufacturer of high-performance liquid chromatography systems. Altex will continue to operate in Berkeley under its present management as a wholly owned subsidiary of Beckman.

The June 1978 issue of ***Chromatography Newsletters,*** available from Perkin-Elmer, features articles on advanced technology applications in LC and GC. The titles in this recent issue (order #CHN-11) are: Improved Analysis of Alpha-Olefins, Evaluation of an Electrochemical LC Detector, Determination of Dipropylacetic Acid by Liquid Chromatography with Pre-Column Labelling and Ultraviolet Detection, LC Performance of the Model 650-10 Fluorescence Detector, Concentration and GC Determination of Organic Compounds from Air and Water, Analysis of Chlorinated Hydrocarbons by High-Performance Gas Chromatography, and Evaluation of New Internal Standards for the Analysis of Carbamazepine and Procainamide by Liquid Chromatography. Call or write: Perkin-Elmer Corp., Instrument Division, Main Ave., Mail Station 12, Norwalk, Conn. 06856 (203-762-6853).

The Buhrke Co. announces the availability of some **used scientific equipment.** Call or write: The Buhrke Co., 2180 Sand Hill Rd., Suite 160, Menlo Park, Calif. 94025 (415-854-5689).

Mallinckrodt's Science Products Division has established **a toll-free telephone service** to provide direct customer access to the company's technical and sales management team. The toll-free number to call is 800-325-7840.

An Infrared Bulletin #66 entitled **"A Collection of Reference Spectra for Flame Retardant Reagents"** gives spectra for over 30 commercially available flame retardant chemicals. Some of these reagents, which are added to plastics, fabrics, and many other materials, contain brominated phosphates. Others are highly halogenated hydrocarbons or diphenyl ethers. Details on five sampling methods are given. For a free copy, ask for order #IRB-66 by calling or writing: Perkin-Elmer Corp., Instrument Division, Main Ave., Mail Station 12, Norwalk, Conn. 06856 (203-762-6853).

Tracor Inc., an analytical instrument detector service company, **has agreed to purchase Searle Analytic** in Des Plaines, Ill., a division of G. D. Searle & Co. Tracor is purchasing all assets related to Searle Analytic's two major product lines of Beta and Gamma counting instruments. The purchase is expected to be effective Sept. 30, 1978.

Why there's no better acid than a Corco acid.



All Corco acids are certified reagent grade acids. We've been specialists in reagent grade acids since 1953. And we've built our reputation on meeting the requirements and specifications of our customers, ACS and ASTM.

Corco can provide reagent grade hydrochloric, nitric, sulfuric acids and sodium hydroxide — plus acetic, fuming nitric, fuming sulfuric, hydrofluoric, perchloric and phosphoric acids. Also bases, standard solutions, solvents and specialty chemicals.

When you require the highest purity, you can rely on Corco to deliver. From pints to tank trucks. Write, call or circle the number for more information.

CORCO

CORCO CHEMICAL CORPORATION
Manufacturers of
Reagent & Electronic Chemicals
Tyburn Road & Cedar Lane • Fairless Hills, Pa. 19030
(215) 295-5006

CIRCLE 33 ON READER SERVICE CARD

Progress in Analytical Atomic Spectroscopy, Vol. 1, Nos. 1–2, 1978, initiates a new journal devoted to publication of comprehensive review articles in atomic spectroscopy. The broad scope of the journal includes atomic absorption spectroscopy; optical emission spectroscopy with excitation by arc, spark, and other spark sources specially by high-temperature plasma; atomic fluorescence spectroscopy; and X-ray and electron beam techniques. The entire first issue is dedicated to a 199-page article on recent advances in electrothermal atomization in graphite furnace atomic absorption spectrometry written by R. E. Sturgeon and C. L. Chakrabarti, who is also editor-in-chief of the journal. The first issue is published in the conventional typeset format, but later issues will be printed from author-furnished camera-ready typewritten text. The review articles will be solicited and contributed. The Forthcoming Events column will be a regular feature, and book reviews will also be included from time to time. The journal in one volume of four parts per year is available at $52 from Pergamon Press Inc., Maxwell House, Fairview Park, Elmsford, N.Y. 10523, or Pergamon Press Ltd., Headington Hill Hall, Oxford OX3 0BW, England.

Pacific Photometric Instruments, manufacturer of light measuring instrumentation, **has been acquired by H.C.P. Industries,** a California-based manufacturer of technical ceramics. The former company will operate as the Pacific Precision Instruments division of H.C.P. Industries, according to John Hueckel, the appointed division manager. Operations have been moved to larger facilities at 1040 Shary Court, Concord, Calif., 20 miles east of San Francisco.

The **Inter-Society Color Council announces** the first two in a series of ***ISCC Technical Reports.*** Report 78-1 is entitled "A Comparison of Several Proposed Methods for Evaluating Daylight Simulators in the Ultraviolet Range," written by David H. Alman and Franc Grum. Price is $2.50 for ISCC members and $5.00 for nonmembers and libraries. Report 78-2, "Guide to Material Standards and Their Use in Color Measurement," is written by Ellen C. Carter and Fred W. Billmeyer, Jr. Price is $5.00 for ISCC members and $10 for nonmembers and libraries. These reports may be ordered from Dr. Fred W. Billmeyer, Jr., ISCC Secretary, Rensselaer Polytechnic Institute, Troy, N.Y. 12181.

Results of a study on benzene emissions and control costs for selected segments of the chemical industry **conducted by the Foster D. Snell Division of Booz, Allen & Hamilton** show actual emissions to be only 40% of those estimated in earlier studies. Nearly two thirds of all benzene emissions come from benzene-consuming processes, primarily vent sources. The remaining third are from benzene production, primarily storage tanks. Loading and fugitive benzene emissions account for only 3% of the total. Control of only process vents and storage tanks could achieve a 95% emission reduction under a total strategy for only 67% of the capital cost required for the removal of all emissions. The 244-page report is available for $9.50 by ordering PB283781/AS from the National Technical Information Service, 5285 Port Royal Rd., Springfield, Va. 22161.



Circle #35 for brochure.
Circle #36 for technical representative to call.



Pennies per Element.

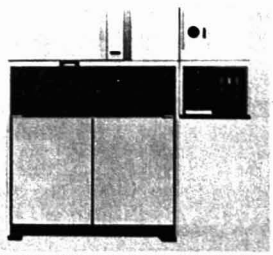


No-nonsense Plasma AtomComp™ 965 from Jarrell-Ash breaks price barrier in multi-element analysis.

At last: a plasma spectrometer for the modest budget. For the lab that wants the sensitivity of AA with the unique **simultaneous** capability of plasma.

Model 965. All our years of experience in computer-controlled direct-reading plasma emission spectrometers have gone into this new basic model. Only Jarrell-Ash could bring you **true plasma** instrumentation — with a price tag this low. Only Jarrell-Ash could bring you simultaneous analyses at a literal cost of pennies per element.

You can choose a 965 Plasma AtomComp to suit **your** specific needs: 20 channels, 30, you name it. You get high-speed DECwriter input/output system and dual floppy-disc storage as standard features. And a comprehensive selection of options. Like automated sample-introduction system.



Spectrum-shifter. "N+1" channel.

Thought you couldn't **afford** plasma? Think again. Send for literature on the 965 Plasma AtomComp today.

Jarrell-Ash Division
Fisher Scientific Company

590 Lincoln Street
Waltham, Massachusetts 02154
Phone (617) 890-4300

CIRCLE 108 ON READER SERVICE CARD

A computer-aided analytical laboratory is in full operation at Warner Laboratories, Inc., in Cresson, Pa. The computer interacts with the sample testing from the receipt of samples to final preparation of analysis reports. Although Warner Laboratories provide a variety of services for sampling and testing fuels, potable waters and plant effluent streams, stack emissions and construction materials, the main activity in terms of sample numbers is in the analysis of fuels, principally coals. Tests cover moisture, heating value, elemental analysis of ash, forms of sulfur, trace elements, and various specialized determinations.

The National Science Foundation has established a 15 single-spaced typewritten page limit for the project description portion of research proposals. The change is made in view of an increase in length of research proposals sent to NSF over the years. A statement of the new policy appears in the new edition of "Grants for Scientific Research" (NSF 78-41A) and is effective immediately. Reviewers of NSF basic research proposals were informed of the policy change through information forms sent October 1.

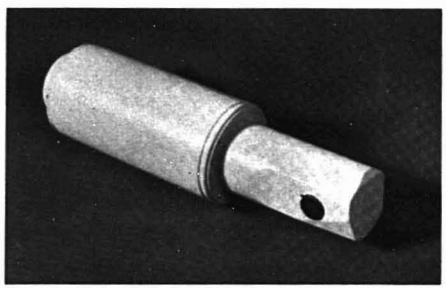
UTI has acquired the mass spectrometer products and patents of Analog Technology Corp., Irwindale, Calif. UTI's headquarters are located at 325 North Mathilda Ave., Sunnyvale, Calif.

Cramer Electronics, Inc., has announced a course schedule for Cramer University on microcomputer systems. The seminars, to be held at various locations in the southern California area, are offered in conjunction with four other manufacturers: Analogic, Motorola, RCA, and Texas Instruments. The seminar courses are: TI-9900 and Analogic Data Acquisition Systems, Motorola M6800, and RCA COSMAC. Course outlines and schedules can be obtained by calling 617-969-7700, ext. 586.

The **EPA's Air Pollution Training Institute,** located at Research Triangle Park, N.C., **conducts** a broad spectrum of **air pollution courses** ranging from orientation level courses for personnel with little or no experience to highly technical courses to meet the needs of the more experienced air pollution control personnel. There is a new schedule available for October 1, 1978–Sept. 30, 1979, which lists all courses offered and provides descriptions for each. For a copy of this schedule, write: Registrar, Air Pollution Training Institute, USEPA, MD-20, Research Triangle Park, N.C. 27711.

Some of the **papers** that were **presented at** the **Proceedings of the Tenth Annual Symposium on Advanced Analytical Concepts for the Clinical Laboratory** held on March 16–17, 1978, at Oak Ridge, Tenn., **are published** in a single issue of *Clinical Chemistry,* Vol. 24, No. 8. The papers are grouped into either advanced concepts, analytical systems, or future trends in advanced analytical concepts. Some of the analytical techniques used are HPLC, dual-column cation-exchange chromatography, thin-layer chromatography, immobilized enzymes and substrates, and calorimetry.

Machlett's New Dual-Target Spectroscopy Tubes



Improved direct replacement for GE/DIANO EA-75

- **DTS — 75A for Air-Helium Spectrometer**
- **DTS — 75V for Vacuum Spectrometer**

Increased cooling has been designed into the anode structure of these beryllium window x-ray tubes that are rated for operation up to 75 kVp.

Tungsten and chromium targets are standard. Other combinations can be provided on special order.

The standard 0.010" (0.25 mm) Be window can be replaced with 0.005" (0.125 mm) for long wavelength radiation on special order.

For data sheets, prices and deliveries contact:

Product Manager, Industrial X-ray
The Machlett Laboratories, Inc.
1063 Hope Street
Stamford, Conn. 06907
Tel: 203-348-7511 TWX: 710-474-1744

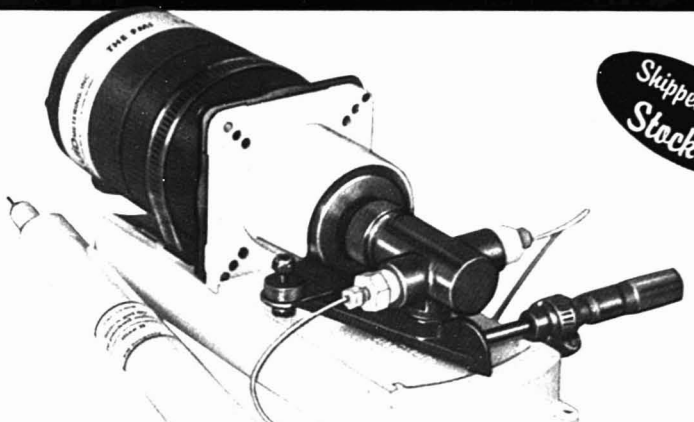
MACHLETT **The Machlett Laboratories, Incorporated**

A Raytheon Company

CIRCLE 179 ON READER SERVICE CARD

Improved!

Solvent Delivery Pumps for Liquid Chromatography



Shipped from Stock!!!

REDUCE ANALYSIS TIME 15 TO 20 FOLD OVER HYDROSTATIC PRESSURE METHODS!

- *FULL FLOW RANGE FROM 0 TO 1164 ML/HOUR.*
- *ACCURATE AT PRESSURES TO 100 P.S.I.G.*
- *REPEAT YOUR FLOW SETTINGS TO WITHIN 0.1%.*
- *DRIFT-FREE ACCURACY FOR LONG RUNS.*
- *REVERSIBLE WHILE RUNNING FOR QUICK COLUMN BACK FLUSH AND REGENERATION.*
- *SOLVENTS ONLY CONTACT HARD ALUMINA CERAMIC AND T.F.E.*
- *ABRASION-RESISTANT CERAMIC PISTON AND CYLINDER LINER.*
- *QUIET SYNCHRONOUS STEPPER MOTOR DRIVE.*
- *SMALL: ONLY 10.7" X 5" X 3.2" WIDE AND 8 POUNDS LIGHT.*
- *INEXPENSIVE:*

#RPSY-1CSC F.M.I. LAB PUMP	*$450.00*
#R428 MICROMETER KIT	*$ 40.00*
#R479 ¼-28 T.F.E. PORT ADAPTERS	*NO CHARGE*
COMPLETE F.O.B. PRICE	*$490.00*

NOTE: FOR EXPLOSION-PROOF DRIVE, SPECIFY RPSYX-1CSC, R428, AND R479 *ONLY $630.00*

FMI FLUID METERING, INC.

P.O. BOX 507, OYSTER BAY, N.Y. 11771 • (516) 922-6050

CIRCLE 76 ON READER SERVICE CARD

The Nobe

The Nobel Prizes that gave birth to an idea

One part of every LKB instrument is over 30 years old: our experience in biochemical separation techniques.

30 years ago the Nobel Prize winners Prof. The Svedberg and Prof. Arne Tiselius instilled into the new company the need for high quality in scientific instruments. Their cooperation and encouragement developed into close contacts with scientists worldwide. As a result, LKB is today in the forefront of ideas in biochemistry, and can present to the scientist the right equipment and techniques at the right time.



Using LKB equipment guarantees nobody a Nobel Prize, but it does lay a sure and certain basis for careful experiments and accurate results.

Complete and versatile equipment means access to a wide variety of methods

At LKB research and development of the instrument go hand in hand with research and development of the technique, so that the one is ideally suited to the other. Often, LKB instruments are developed with several techniques in mind. This allows the scientist to change methods easily without changing equipment, or to experiment within one method.

LKB supplies equipment necessary for growing and disintegration of microorganisms through to the final characterisation of a purified substance. Probably the most important techniques in biochemistry are those involving separation and analysis, and there we have our greatest experience.

LKB helps science advance, and serves the scientist

For science to advance, knowledge must be shared. At LKB knowledge comes from our experience and research and from our many worldwide contacts. We share our knowledge in several ways: in the quality of our instruments, as Workshops and Seminars, literature such as *Acta Ampholinae*, Application Notes and SCIENCE TOOLS.

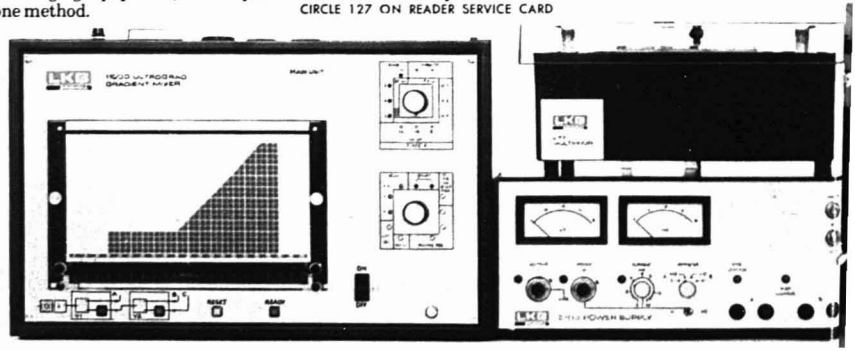


Electrophoresis

This technique laid the basis of LKBs entry into biochemical separations, and prepared the way for further developments. In developing reliable equipment we were greatly helped and encouraged by Arne Tiselius, whose important work on electrophoresis was rewarded by a Nobel Prize in 1948.

LKB provides the basic equipment needed for an electrophoretic system, analytical or preparative, column or thin layer: equipment such as power supplies with constant power, voltage and current; Multiphor for thin layer electrophoresis and immunoelectrophoresis; and Uniphor® for column electrophoresis.

CIRCLE 127 ON READER SERVICE CARD



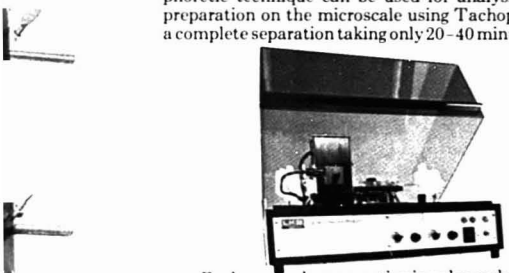
Prize Kit

Electrofocusing

LKB has led the world in electrofocusing since we introduced it in 1966. Our breakthrough then was with Ampholine® carrier ampholytes and electrofocusing columns. The recent introduction of Multiphor, the ready-to-use Ampholine® PAG-plates, and the PEGG kit for preparative electrofocusing in granulated gel has extended even further the scope of this very efficient, high resolution, technique. CIRCLE 128 ON READER SERVICE CARD

Isotachophoresis

Kohlrausch's theory of 1897 was turned into simple practice when LKB introduced Tachophor in 1974. This latest and most advanced electrophoretic technique can be used for analysis or preparation on the microscale using Tachophor, a complete separation taking only 20 - 40 minutes.



For large-scale preparation in polyacrylamide gel, Uniphor should be used.
CIRCLE 129 ON READER SERVICE CARD

Gel filtration

The lagging development of gel filtration media has been given a new impulse by the introduction of LKB Ultrogel®. This new medium, a copolymer of polyacrylamide and agarose, gives better resolution and high flow rates. Ultrogel is becoming the gel of choice, especially in the difficult area of serum protein fractionation.

All the equipment you need for gel filtration - columns, Uvicord® UV monitors, Perpex Pumps, UltroRac® and RediRac fraction collectors - is made by LKB. CIRCLE 130 ON READER SERVICE CARD

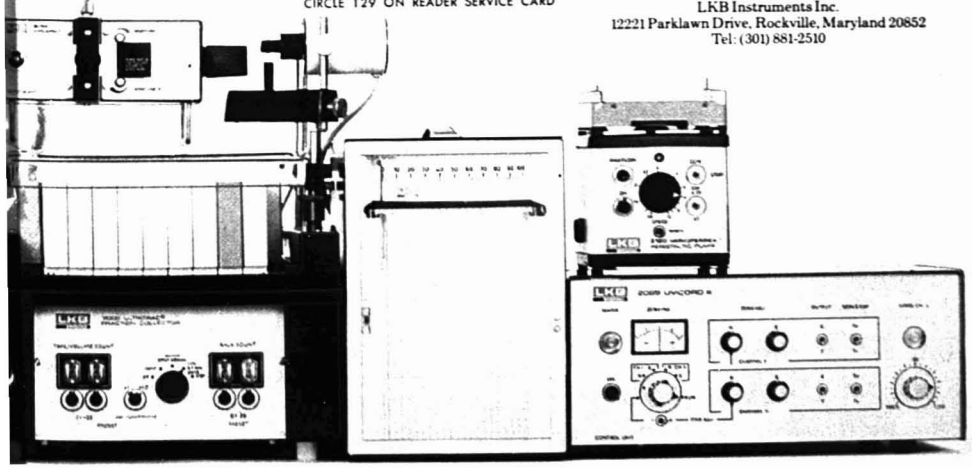
Ion exchange, affinity and adsorption chromatography

The "adapted gradient technique", using LKB Ultrograd® gradient mixer, gives much improved resolution over ordinary gradient elution. You dictate the shape of the gradient simply by cutting it out on chart paper. Ultrograd produces controlled and reproducible gradients, and to scale-up for preparative work you simply increase the flow rate. CIRCLE 131 ON READER SERVICE CARD

This summary of LKB equipment is necessarily short. Our new 58-page colour booklet "LKB Systems and Methods for Biochemical Research" illustrates all LKB equipment and describes in some detail the methods for which they are used. Our colour poster "Preparative Separation Principles in Biochemistry" is a worldwide attraction: like the booklet you can get a free copy by contacting us. CIRCLE 132 ON READER SERVICE CARD

LKB

LKB Instruments Inc.
12221 Parklawn Drive, Rockville, Maryland 20852
Tel: (301) 881-2510



Bio-Rad backs you up.

With the industry's most comprehensive (160 pages) catalog on materials, equipment and systems for **chromatography, electrophoresis, membrane filtration** and **immunochemistry.**
And: **A great catalog on the best HPLC columns in the business.**

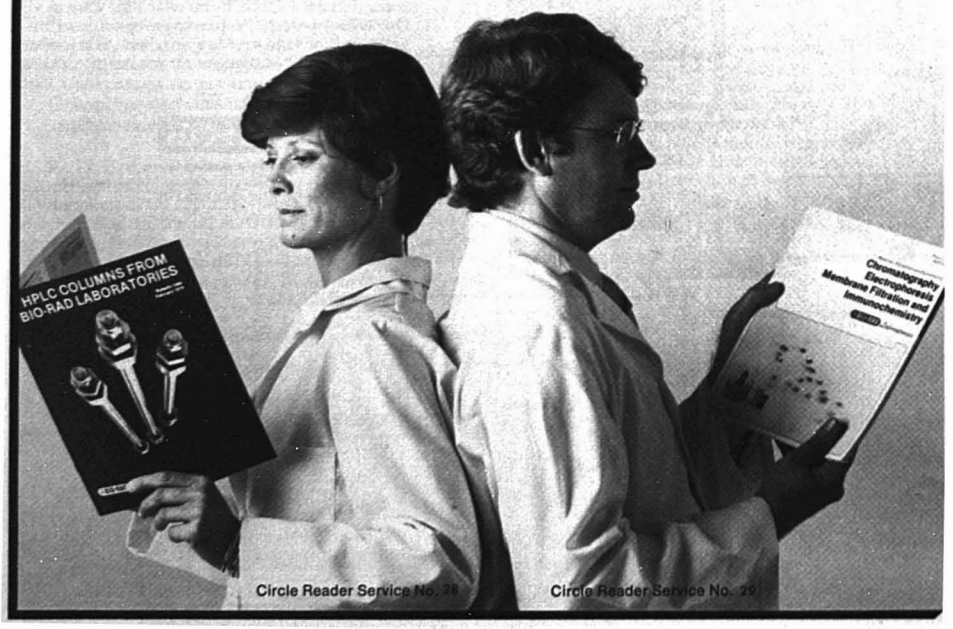
Price List D is crammed with applications data, product specifications, performance data, numerous useful illustrations and complete ordering information.

Bulletin 1056 tells you what to look for in HPLC columns and why we're able to **guarantee** the specified performance of our HPLC columns. And since the column is the least expensive part of your liquid chromatography system, why not use the best? Bio-Rad columns.

Both the catalog and the HPLC bulletin are **free.** Call, write or circle the number below for your copy.

BIO-RAD *Laboratories*
2200 Wright Avenue • Richmond, CA 94804
Phone (415) 234-4130

Also in: Rockville Centre, N.Y.; Mississauga, Ontario; London; Milan; Munich; Sao Paulo; Vienna.



Circle Reader Service No. 28 Circle Reader Service No. 29

R. A. Libby[1] and F. E. Freeberg
The Procter & Gamble Co.
Cincinnati, Ohio 45247

Methodology Development and Rigorous Analyses Are Called for by New EPA Regulations

A series of regulations and guidelines covering testing standards for environmental and human safety testing is being drafted by the Environmental Protection Agency (EPA). These regulations and guidelines will apply to pesticides, selected existing chemicals currently being marketed, and to all new chemicals. Because of the broad scope of the substances regulated, these rules will apply across the entire chemical industry, and thus affect a great many, if not all, industrial analytical facilities.

Although the materials being regulated cover a broad range of chemicals and are regulated by different organizational units within the EPA, the Agency has decided to make all regulations and guidelines as consistent as the laws will permit. Therefore, the testing standards proposed to regulate pesticides, for example, will be the same as those proposed for chemicals. These standards include record keeping, facility operation and personnel requirements, detailed specific test methods for environmental and toxicological testing, and detailed analytical characterization requirements.

In addition to being internally consistent, the EPA intends to make their standards as consistent as possible with testing requirements issued by other Federal regulatory bodies. To accomplish this, an Interagency Regulatory Liaison Group has been established to review the regulations being proposed by other regulatory agencies including the Food and Drug Administration (FDA) and the Consumer Product Safety Commission (CPSC). Because of this interagency regulatory activity, we can expect that many of the testing standards being developed by the EPA will be adopted across other regulatory agencies resulting in the development of generic procedures. This desire for consistency in regulations is attractive to many. However, to specify detailed tests and how they are to be conducted for such a wide variety of chemicals risks the elimination of professional scientific judgment regarding the selection of the most meaningful and appropriate tests. Since the Agency's methods and procedures will be designed to cover the most serious and critical cases, this could result in excessive and inappropriate effort for noncritical cases and result in wasteful use of scarce scientific resources.

To demonstrate the impact the various regulatory activities of the EPA will have on analytical chemists, we will now discuss in some detail regulations and guidelines proposed or being drafted.

Pesticide Testing Guidelines

The pesticide testing guidelines proposed by the EPA in the *Federal Register* on July 10 and August 22, 1978, under the Federal Insecticide, Fungicide and Rodenticide Act (FIFRA for short) describe the chemistry requirements as well as safety and environmental tests necessary to supply data required for Federal approval and marketing of pesticides. A "pesticide" covered by these rules ranges from an agricultural insecticide to a household antibacterial product such as liquid bleach. One disadvantage of generic guidelines is that all materials get the same treatment. In FIFRA the chemical requirements seek establishment of limits not only for the pesticide active chemical and all intentionally added inert ingredients, *but each impurity, each reaction product, and each degradation product that is known or theorized to be present in a formulation down to ppm levels.* Similarly, rigorous analyses are required for materials undergoing safety testing. These guidelines illustrate the broad, discretionary power the EPA has in requesting analytical data. Further, the applicant must certify and maintain all these product limits under penalty of regulatory action. In practice, the only way for a manufacturer to ensure that a finished product meets these certified limits, particularly for ppm level impurities, is by development of analytical methods for finished product assay. Since most commercial chemicals and products can contain many chemical species at ppm levels, an exhaustive analytical methods development program would be required, especially for trace level methods. Some have suggested a more viable approach could be to focus effort against those materials that are present at a level having a likely adverse affect on health or the environment. Such an approach would more efficiently utilize the nation's already limited analytical resources.

Testing Standards for Existing Chemicals and New Chemicals

Probably the most broadly applicable rules being drafted by the EPA are those involved with implementation of the new Toxic Substances Control Act (TSCA). Under Section 4 and 5 of the legislation, the EPA is empowered to issue regulations and guidelines covering testing standards needed to establish that a chemical does not present an unreasonable risk to the environment or to human health. Currently, the Agency is in the final stages of drafting what tests should be run and detailed step-by-step methods for running them. TSCA regulations will contain General Quality Assurance Procedures (QAP) that are to be adopted by all laboratories involved in safety testing required by the EPA, including associated analytical laboratories. These QAP's are the EPA's version of the FDA's proposed Good Laboratory Practices (GLP) regulations (*1*). As in the GLP's, these regulations describe in detail the personnel qualifications, record keeping requirements, data handling proce-

[1] Chairman, Ad Hoc Committee on Regulatory Affairs, Analytical Division, American Chemical Society.

0003-2700/78/A350-1229$01.00/0
© 1978 American Chemical Society

dures, laboratory operations, facility design, and the establishment of a quality assurance unit as a distinct organizational entity. Since regulations such as GLP's and QAP's describe laboratory operating procedures that must be followed when conducting safety studies, it is most important that all agencies work hard at adopting common procedures if we are to avoid multiple procedures in the same laboratory.

The toxicity testing for TSCA regulations will involve considerable analytical effort in the safety test protocols prescribed by toxicologists. For example, a two-year chronic feeding study specifies repeated analyses for the test substance in animal fluids and tissues. This will require exhaustive analytical method development of trace levels in complex biological matrixes because chronic testing precludes the use of radiolabeled materials. We must be certain that the analytical chemists and the toxicologists have the opportunity to use their collective scientific judgment in designing the appropriate toxicity tests.

Conclusions

New regulations and guidelines being developed by the EPA will have a considerable impact on the field of analytical chemistry. Although one can understand the desire on the Agency's part to have all data developed under standard methods, it may not be appropriate or scientifically feasible to develop standard safety procedures that are applicable to all chemicals. As stated by the ACS (2) in a statement to the Senate subcommittee during the drafting stages of TSCA, "Testing requirements should be reasonable and should be determined for each specific case." It was further stated that it is "unwise to utilize scientific resources and manpower for conducting extensive tests that scientific judgment indicates would have little chance of providing significant data" (2).

Finally, although the EPA has obtained the help of professional toxicologists during the drafting of these testing standards, it appears that *input from analytical chemists has been much less.* Analytical chemistry as a discipline is greatly impacted by both FIFRA and TSCA. Yet as a group, analytical chemists have not been active enough in the regulatory formation process. Representatives of the EPA working on regulations have stated on numerous occasions that *input from all fields is needed and would be welcomed.* It is only throug direct involvement of analytical experts, as well as other scientists, that regulations can be developed that will both meet Agency objectives and yet be scientifically sound and practical. Analytical chemists cannot afford to stand aside and let others debate and determine how their science is to be conducted.

Comments on FIFRA guidelines can be sent to:

Federal Register Section
Technical Services Division (WH-569)
Office of Pesticide Programs, EPA
Room 401, East Tower
401 M Street, S.W.
Washington, D.C. 20460

For more information on testing standards being considered under TSCA, contact:

Office of Toxic Substances (WH-557)
EPA
401 M Street, S.W.
Washington, D.C. 20460

References

(1) R. A. Libby, *Anal. Chem.*, **50**, 975A (1978).
(2) Official Public Policy Statements and Communications, ACS, VII, p 24 (ACS 75-003) (1976).



ECHIDNA
Tachyglossus Aculeatus.

SGE capillary columns make your chromatograms much more pointed.

Packed columns are alright in their place. But if you want greater resolution and faster analysis times, then you should consider high performance capillary columns. Not only will you improve the accuracy of your analysis but the time saved will effectively reduce your costs.

SGE produces glass SCOT and WCOT columns, in a range of versatile and refined phases. WCOT columns provide the ultimate in separation (up to 200,000 Neff), but SCOT columns (up to 50,000 Neff), with their high sample loading and simplicity of GC operation are an excellent compromise between packed and WCOT columns.

All columns are deactivated and supplied with a test chromatogram indicating a guaranteed performance. Apart from hydrocarbon, petroleum and essential oils analyses, consider these applications:— Amino acids, PCB's, chlorinated insecticides, steroids, trace component analysis.

Of course, there is more to capillary column chromatography than simply ordering a column. SGE can supply virtually every component you'll need to successfully upgrade your GC, and with the minimum of downtime.

Why not write for our "Glass Capillary Columns & Accessories" catalogue.

Scientific Glass Engineering Pty. Ltd.

Head Office
Scientific Glass Engineering Pty. Ltd.,
111 Arden St., North Melbourne, 3051
Australia.
Tel: (03) 329 6633

European Office
Scientific Glass Engineering (U.K.) Ltd.,
657 North Circular Road, London NW2 7AY.
Great Britain
Tel: 01-452 6244

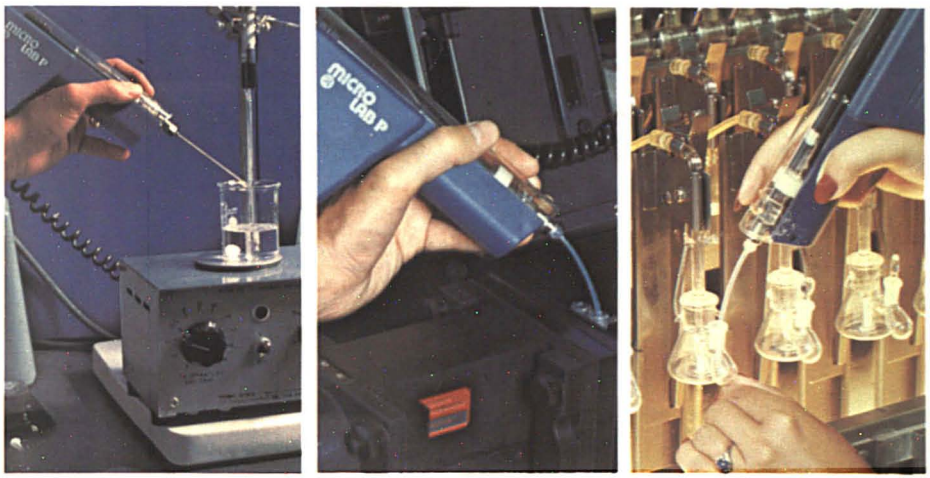
U.S.A Office
Scientific Glass Engineering Inc.,
2800 Longhorn Blvd., Suite 104
Austin, Texas. 78758 U.S.A
Tel: (512) 837 7190

SGE
*Trademarks of S.G.E.

CIRCLE 190 ON READER SERVICE CARD

MICROLAB® P

THE FIRST PROGRAMMABLE MICROPROCESSOR PIPETTE



SAVES TIME + REAGENTS = MONEY

The MICROLAB®P combines the accuracy and precision of the Hamilton Microliter® gastight syringe, with computer logic and precise mechanical accuracy.

The Microprocessor controls and monitors all dispensing and diluting functions. The operator has complete control over all procedures, thereby producing accurate, reliable, repeatable results.

Cost savings are ensured by the reduction of technologist's time and the accuracy and precision offered by the MICROLAB® P, a time and money saver.



ONLY FROM

HAMILTON

For more information about MICROLAB® P, its functions and programs, give us a call or drop a line

HAMILTON COMPANY
Post Office Box 10030
Reno, Nevada 89510
Telephone (702) 786-7077
Telex 354-467

CIRCLE 98 ON READER SERVICE CARD

The smallest balances with the largest selection.

Sartorius 1200 MP. Protected from obscolescence with micro processors.

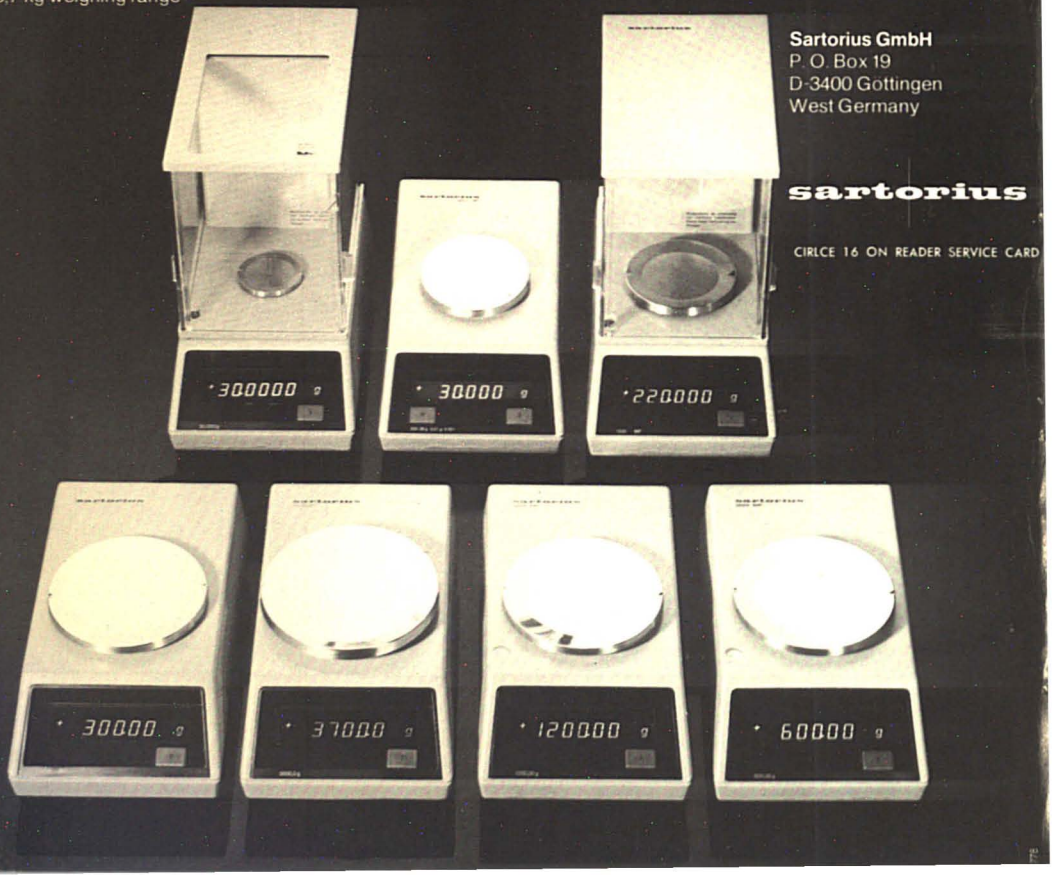
The only line of electronic top-loaders offering...

...all in one housing: an analytical balance with 0,1 mg readability as well as a precision balance with 3,7 kg weighing range –

...micro processors as standard equipment –

...integration into commercial data processing systems plus connections to a wide variety of economical accessories for the solution of weighing problems.

Find out more about this line of future orientated miniature balances by requesting our 1978 catalog.

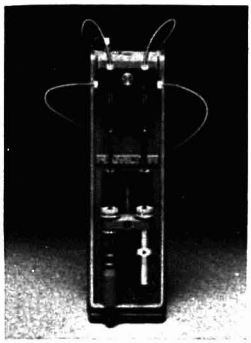


Sartorius GmbH
P. O. Box 19
D-3400 Gottingen
West Germany

sartorius

CIRLCE 16 ON READER SERVICE CARD

NEW! PRECISION LIQUID DISPENSERS



Single and Dual Channel Dispensers

Now you can solve almost all of your liquid dispensing problems with Hamilton's new and improved, low-cost Precision Liquid Dispensers (PLD). Designed for industrial R&D, quality control, and filling operations, with accuracy and precision where strict tolerances are required.

Check these features:

- ☐ New, improved valve system
- ☐ Longer valve life saves downtime
- ☐ Easy cleaning and changing
- ☐ Simple, trouble-free operation
- ☐ Weight-balanced, rugged construction
- ☐ Operates in any position or environment
- ☐ Pneumatic (non-electric) operation
- ☐ Ideal for operations where oxygen or flammables are present, or in most extremes of temperature or viscosity
- ☐ Under standard conditions, precision is ± 05%, accuracy is ± 1%

If you have a liquid dispensing problem, call the experts. We'll send out a trained sales engineer or put you in touch with one of our dealers. Write for literature to John Nadolny, Hamilton Company, P.O. Box 10030, Reno, Nevada 89510, or call (702) 786-7077.

HAMILTON

CIRCLE 95 ON READER SERVICE CARD

NOVEMBER 1978

VALID THROUGH MARCH 1979

ADVERTISED PRODUCTS:

7	8	9	10	11	12	13	14	15	16	17
18	19	20	21	22	23	24	25	26	27	28
29	30	31	32	33	34	35	36	37	38	39
40	41	42	43	44	45	46	47	48	49	50
51	52	53	54	55	56	57	58	59	60	61
62	63	64	65	66	67	68	69	70	71	72
73	74	75	76	77	78	79	80	81	82	83
84	85	86	87	88	89	90	91	92	93	94
95	96	97	98	99	100	101	102	103	104	105
106	107	108	109	110	111	112	113	114	115	116
117	118	119	120	121	122	123	124	125	126	127
128	129	130	131	132	133	134	135	136	137	138
139	140	141	142	143	144	145	146	147	148	149
150	151	152	153	154	155	156	157	158	159	160
161	162	163	164	165	166	167	168	169	170	171
172	173	174	175	176	177	178	179	180	181	182
183	184	185	186	187	188	189	190	191	192	193
194	195	196	197	198	199	200	201	202	203	204
205	206	207	208	209	210	211	212	213	214	215
216	217	218	219	220	221	222	223	224	225	226
227	228	229	230	231	232	233	234	235	236	237
238	239	240	241	242	243	244	245	246	247	248
249	250	251	252	253	254	255	256	257	258	259

NEW PRODUCTS:

401	402	403	404	405	406	407	408	409	410	411
412	413	414	415	416	417	418	419	420	421	422
423	424	425	426	427	428	429	430	431	432	433
434	435	436	437	438	439	440	441	442	443	444
445	446	447	448	449	450	451	452	453	454	455
456	457	458	459	460	461	462	463	464	465	466
467	468	469	470	471	472	473	474	475	476	477
478	479	480	481	482	483	484	485	486	487	488
489	490	491	492	493	494	495				

READER SURVEY:

301	302	303	304	305	306	307	308	309	310	311
312	313	314	315	316	317	318	319	320	321	322
323	324	325	326	327	328	329	330	331	332	333
334	335	336	337	338	339	340	341	342	343	344
345	346	347	348	349	350	351				

TO VALIDATE THIS CARD, PLEASE CHECK ONE ENTRY FOR EACH CATEGORY BELOW:

Intensity of product need:
- ☐ 1. Have salesman call
- ☐ 2. Need within 6 mos.
- ☐ 3. Future project

Primary field of work:
- ☐ A. Energy
- ☐ B. Environmental
- ☐ C. Medical/Biological
- ☐ D. Drug/Cosmetic
- ☐ E. Forensic/Narcotic
- ☐ F. Textile/Fiber
- ☐ G. Metals
- ☐ H. Pulp/Paper/Wood
- ☐ I. Soaps/Cleaners
- ☐ J. Paint/Coating/Ink
- ☐ K. Electrical/Electronic
- ☐ L. Instrument Dev./Des
- ☐ M. Plastic/Polymer/Rub
- ☐ N. Agricultural/Food
- ☐ O. Inorganic Chemicals
- ☐ P. Organic Chemicals

Primary area of employment:

INDUSTRIAL
- ☐ A. Research/Development
- ☐ B. Quality/Process Control

MEDICAL/HOSPITAL
- ☐ C. Research/Development
- ☐ D. Clinical/Diagnostic

GOVERNMENT
- ☐ E. Research/Development
- ☐ F. Regulate/Investigate

COLLEGE/UNIVERSITY
- ☐ G. Research/Development
- ☐ H. Teaching

INDEPENDENT/CONSULTING
- ☐ I. Research/Development
- ☐ J. Analysis/Testing

This copy of Analytical is:
- ☐ 1. Personally addressed to me in my name.
- ☐ 2. Addressed to other person or to my firm.

NAME: _____

TITLE: _____

FIRM: _____

STREET: _____

CITY: _____

STATE: _____ ZIP: _____

PHONE: (___) _____ - _____

FLAME and ATOMIC ABSORPTION STANDARDS

SPEX has the SOLUTIONS for your problems . . .

prepared from Spex HiPure chemicals
assayed volumetrically or gravimetrically
certified as to metal concentration
67 elements in 9 matrices and customized standards
for atomic absorption, x-ray fluorescence,
and Inductively Coupled Plasma spectroscopy

SPEX INDUSTRIES, INC. • BOX 798, METUCHEN, N.J. 08840 • ☎ 201-549-7144

CIRCLE 191 ON READER SERVICE CARD

FIRST CLASS
Permit #27346
Philadelphia, PA

BUSINESS REPLY MAIL

NO POSTAGE NECESSARY IF MAILED IN THE UNITED STATES

POSTAGE WILL BE PAID BY:

analytical chemistry

P.O. BOX #7826
PHILADELPHIA, PA 19101

FIRST CLASS
Permit #27346
Philadelphia, PA

BUSINESS REPLY MAIL

NO POSTAGE NECESSARY IF MAILED IN THE UNITED STATES

POSTAGE WILL BE PAID BY:

analytical chemistry

P.O. BOX #7826
PHILADELPHIA, PA 19101

YOUR "READER SURVEY" VIEWS ARE VITAL

Analytical Chemistry occasionally presents a Reader Survey section that provides you with an opportunity to indicate your interests and activities. Your answers help us in planning editorial material that will be useful to you in your work.

To express your Reader Survey views, simply circle your answers on one of these adjacent reply cards and drop it in the mail. No postage is required.

NOVEMBER 1978 VALID THROUGH MARCH 1979

ADVERTISED PRODUCTS:										
1	2	3	4	5	6	7	8	9	10	11
12	13	14	15	16	17	18	19	20	21	22
23	24	25	26	27	28	29	30	31	32	33
34	35	36	37	38	39	40	41	42	43	44
45	46	47	48	49	50	51	52	53	54	55
56	57	58	59	60	61	62	63	64	65	66
67	68	69	70	71	72	73	74	75	76	77
78	79	80	81	82	83	84	85	86	87	88
89	90	91	92	93	94	95	96	97	98	99
100	101	102	103	104	105	106	107	108	109	110
111	112	113	114	115	116	117	118	119	120	121
122	123	124	125	126	127	128	129	130	131	132
133	134	135	136	137	138	139	140	141	142	143
144	145	146	147	148	149	150	151	152	153	154
155	156	157	158	159	160	161	162	163	164	165
166	167	168	169	170	171	172	173	174	175	176
177	178	179	180	181	182	183	184	185	186	187
188	189	190	191	192	193	194	195	196	197	198
199	200	201	202	203	204	205	206	207	208	209
210	211	212	213	214	215	216	217	218	219	220
221	222	223	224	225	226	227	228	229	230	231
232	233	234	235	236	237	238	239	240	241	242
243	244	245	246	247	248	249	250	251	252	253
254	255	256	257	258	259					

NEW PRODUCTS:										
401	402	403	404	405	406	407	408	409	410	411
412	413	414	415	416	417	418	419	420	421	422
423	424	425	426	427	428	429	430	431	432	433
434	435	436	437	438	439	440	441	442	443	444
445	446	447	448	449	450	451	452	453	454	455
456	457	458	459	460	461	462	463	464	465	466
467	468	469	470	471	472	473	474	475	476	477
478	479	480	481	482	483	484	485	486	487	488
489	490	491	492	493	494	495				

READER SURVEY:										
301	302	303	304	305	306	307	308	309	310	311
312	313	314	315	316	317	318	319	320	321	322
323	324	325	326	327	328	329	330	331	332	333
334	335	336	337	338	339	340	341	342	343	344
345	346	347	348	349	350	351				

TO VALIDATE THIS CARD, PLEASE CHECK ONE ENTRY FOR EACH CATEGORY BELOW:

Intensity of product need:
- ☐ 1. Have salesman call
- ☐ 2. Need within 6 mos.
- ☐ 3. Future project

Primary field of work:
- ☐ A. Energy
- ☐ B. Environmental
- ☐ C. Medical/Biological
- ☐ D. Drug/Cosmetic
- ☐ E. Forensic/Narcotic
- ☐ F. Textile/Fiber
- ☐ G. Metals
- ☐ H. Pulp/Paper/Wood
- ☐ I. Soaps/Cleaners
- ☐ J. Paint/Coating/Ink
- ☐ K. Electrical/Electronic
- ☐ L. Instrument Dev./Des
- ☐ M. Plastic/Polymer/Rub
- ☐ N. Agricultural/Food
- ☐ O. Inorganic Chemicals
- ☐ P. Organic Chemicals

Primary area of employment:
INDUSTRIAL
- ☐ A. Research/Development
- ☐ B. Quality/Process Control

MEDICAL/HOSPITAL
- ☐ C. Research/Development
- ☐ D. Clinical/Diagnostic

GOVERNMENT
- ☐ E. Research/Development
- ☐ F. Regulate/Investigate

COLLEGE/UNIVERSITY
- ☐ G. Research/Development
- ☐ H. Teaching

INDEPENDENT/CONSULTING
- ☐ I. Research/Development
- ☐ J. Analysis/Testing

This copy of Analytical is:
- ☐ 1. Personally addressed to me in my name.
- ☐ 2. Addressed to other person or to my firm.

NAME: _____

TITLE: _____

FIRM: _____

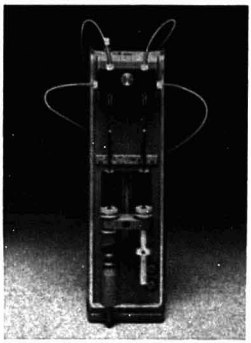
STREET: _____

CITY: _____

STATE: _____ ZIP: _____

PHONE: (___ ___ ___) ___ ___ ___ - ___ ___ ___ ___

NEW! PRECISION LIQUID DISPENSERS



Single and Dual Channel Dispensers

Now you can solve almost all of your liquid dispensing problems with Hamilton's new and improved, low-cost Precision Liquid Dispensers (PLD). Designed for industrial R&D, quality control, and filling operations, with accuracy and precision where strict tolerances are required.

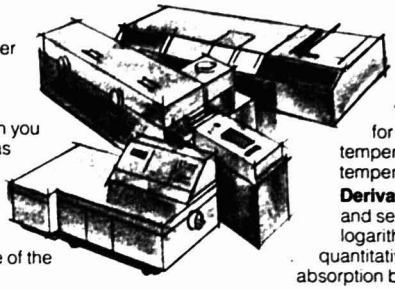
Check these features:
- ☐ New, improved valve system.
- ☐ Longer valve life saves downtime.
- ☐ Easy cleaning and changing.
- ☐ Simple, trouble-free operation.
- ☐ Weight-balanced, rugged construction.
- ☐ Operates in any position or environment.
- ☐ Pneumatic (non-electric) operation.
- ☐ Ideal for operations where oxygen or flammables are present, or in most extremes of temperature or viscosity.
- ☐ Under standard conditions, precision is ±.05%, accuracy is ±1%.

If you have a liquid dispensing problem, call the experts. We'll send out a trained sales engineer or put you in touch with one of our dealers. Write for literature to John Nadolny, Hamilton Company, P.O. Box 10030, Reno, Nevada 89510, or call (702) 786-7077.

HAMILTON

CIRCLE 95 ON READER SERVICE CARD

Don't settle for an ordinary UV-Vis spectrophotometer...



The most expensive mistake you'll ever make selecting a UV-Vis spectrophotometer could be spending too little. Especially in these days of budget squeeze and grant combination when you have to consider long range as well as short range needs.

For just a few dollars more than you would pay for an average spectrophotometer you can have the high optical and photometric performance of the versatile Varian Cary 219.

The 219 is by far the most sensitive and reproducible double-beam spectrophotometer ever offered in this price range. Performance features that give you extra capability include the following:

Kinetics System—a five-sample, five-reference automatically timed sample changer.

Routine Sampling System—an automatic sipper which can heat or cool 500 microliters of sample to 20°, 25°, 30°, 32°, and 37°C in less than fifteen seconds. It's also available in an unthermostatted version.

Wavelength Programmer—unparalleled positioning of selectable wavelengths.

Temperature Readout—for absorbance versus temperature curves and precise temperature monitoring in the cell.

Derivative/Log A—calibrated first and second derivative and the logarithm of absorbance for those quantitative analyses of overlapping absorption bands.

20-cm Gel Scanner—for use on polyacrylamide disc gels and autoradiographs.

Smart Printer—microprocessor-based to give sample or cell number and absorbance versus wavelength, or absorbance versus time, as hard copy data.

Stirrer Accessory—capable of stirring five sample and five reference cells simultaneously.

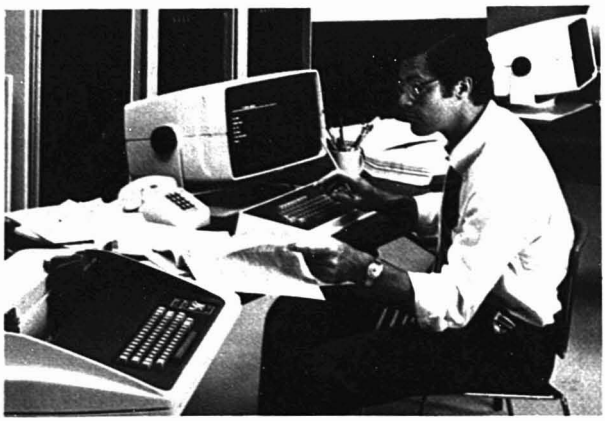
For all the facts on how you can get a lot more spectrophotometer for just a few more dollars, circle Reader Service Number **224. Circle 225 if you'd like our** technical rep to call.

when a versatile Varian Cary 219 is within your budget.



varian

New Products



The Eclipse S/250 minicomputer has high computational speed and I/O capabilities. It is targeted at broad range of real-time, computational and communications applications. An optional integral array processor handles signal processing, transform, and matrix calculations. Features include main memory expansion to 1 megabyte and I/O transfer rates up to 10 megabytes/s. Data General Corp. **401**

Temperature Calibration Standard

The YSI Model 60 gallium temperature standard at 29.770 °C provides an International Practical Temperature Scale (IPTS) fixed reference point for establishing calibration curves in small thermistor and thermocouple probes. The Model 60 automatically maintains a gallium-filled cell in a temperature-controlled environment that prolongs pure gallium's melt plateau of 29.770 °C for 6–8 h. Yellow Springs Instrument Co., Inc. **407**

Ionization Detector

Model 05 multiphoton interaction detector is a gas-flow proportional counter/ionization detector used in laser spectrometry to determine multiphoton interaction wavelengths of sample traces. The detector incorporates a pulse amplifier with a sensitivity of 1.5×10^{13} V/coulomb, a 1000 to 1 gain adjustment, and an output pulse with a 0.4-μs rise and a 3-μs fall. Price is $1000. J. E. Manson Co. **411**

Microsampler for AA

The Model AS-3 automatically injects either 50- or 100-μL samples directly into the flame AA spectrometer's nebulizer. Preselection of 1–10 analyses/sample for up to 30 samples is possible. An analysis cycle, including a two-step wash, is completed in 15 s. Perkin-Elmer Corp. **414**

Centrifugal Filtering System

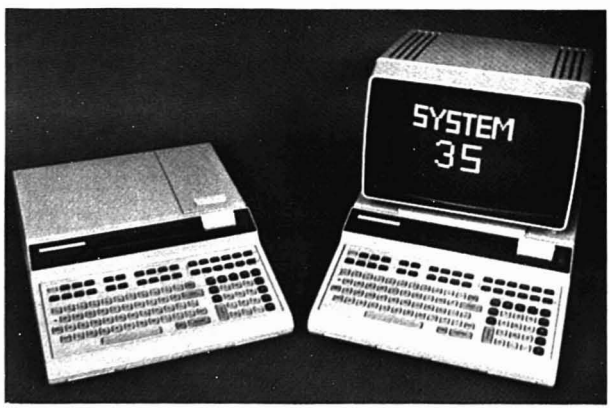
The Filtermatic accelerates separations of laboratory scale suspensions, emulsions, and high-speed filtration of solvents. Speeds of up to 6000 rpm are achieved. Any grade of filter paper can be used with the nonvacuum filtering system. Applications include enzyme separation, coal preparations, slurry analysis, and field sample separations. Technilab Instruments, Inc. **412**

Mass Spectrometer

The MS25Q mass spectrometer is used for the analysis of gases, vapors, and oils. It combines a hexapole system with a temperature-regulated source of 0.1% and scan rates down to 1000 s/decade. Resolving power better than 2500 (10% valley) is provided for accurate quantitation of the *m/e* 28 multiplet. Kratos Inc. **409**

Flow Injection Analyzer

The AMFIA Mark-Chem. II provides unsegmented flow analysis in excess of 150 tests/h and eliminates pulsation in the jet stream. It features colorimetric and fluorometric detection, computer readout, autosampler for 40 samples, and picomole sensitivity. Accuracy is better than 1%. Mark Instrument Co. **408**



The HP9835 A & B models are midrange desktop computers that feature a larger memory capacity and assembly language capability with enhanced basic. Both models feature a read/write capacity of up to 256 bytes, unified mass storage, a tape cartridge directory read/write memory, and a bad memory error detect system. Price for Model A is $9900, and Model B is $8700. Hewlett-Packard Co. **403**

For more information on listed items, circle the appropriate numbers on one of our Readers' Service Cards

INTRODUCING
the Varian 5000 family of liquid chromatographs



It makes LC responsive and simple

The Varian 5000 Series is a family of powerful microcomputer-CRT-based liquid chromatographs that make LC easy for anyone.

It makes tough separations seem simple. The helpful CRT continuously displays *all* instrument conditions. Tells you everything you need to know, right now. Responds to you. Helps you build programs. Prompts and leads you. Makes LC easier than ever before.

It comes with full support. With your Model 5000 you receive a commitment from Varian to provide strong, continuing support — training, service and applications assistance — that will assure successful solution of your liquid chromatography problems.

Price/performance. There are six basic models in the 5000 Series: from simple isocratic to completely automatic gradient systems. Each is designed to offer unbeatable price/performance; to provide a new level of LC capability at system prices lower than most LC components.

Upward expandability. 5000 Series chromatographs are upward expandable and offer many options. You can configure a 5000 that is exactly right for your laboratory. Later, as your needs change, you can add whatever new capability you require.

For full details on a 5000 that may be exactly right for you, circle Reader Service Number 222.

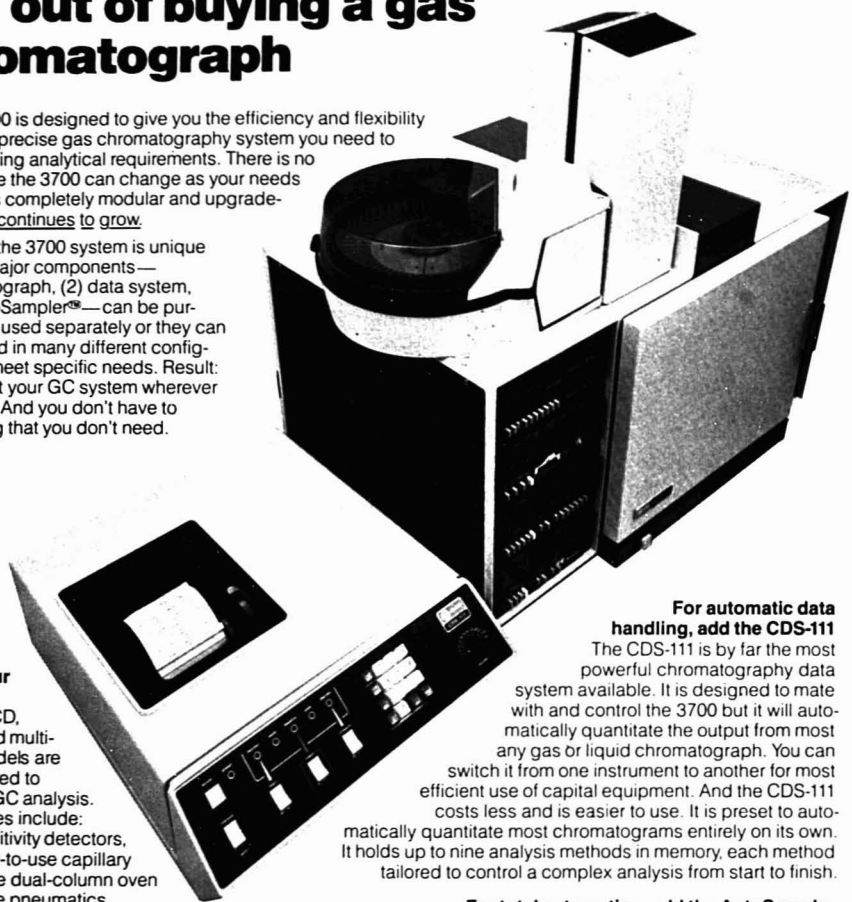
To have a Varian representative contact you, circle Reader Service Number 223.

varian

How Varian's 3700 series takes the risk out of buying a gas chromatograph

Varian's 3700 is designed to give you the efficiency and flexibility to build the precise gas chromatography system you need to meet changing analytical requirements. There is no risk because the 3700 can change as your needs change. It is completely modular and upgradeable, and it continues to grow.

In addition, the 3700 system is unique in that the major components—(1) chromatograph, (2) data system, and (3) AutoSampler®—can be purchased and used separately or they can be combined in many different configurations to meet specific needs. Result: You can start your GC system wherever you want to. And you don't have to buy anything that you don't need.



Choose a 3700 for your application
TCD, FID, ECD, FPD, TSD and multi-detector models are offered tailored to handle any GC analysis. Major features include: highest sensitivity detectors, the first easy-to-use capillary system, large dual-column oven and separate pneumatics compartment for versatility and convenience. You can begin with a basic dual-column unit and add capability as you need it. Or you can start right now with the world's most powerful and fully automatic GC system by combining the 3700 with the CDS-111 data system and the 8000 AutoSampler.

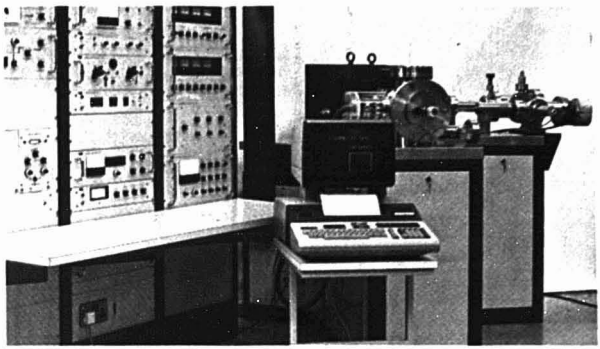
For automatic data handling, add the CDS-111
The CDS-111 is by far the most powerful chromatography data system available. It is designed to mate with and control the 3700 but it will automatically quantitate the output from most any gas or liquid chromatograph. You can switch it from one instrument to another for most efficient use of capital equipment. And the CDS-111 costs less and is easier to use. It is preset to automatically quantitate most chromatograms entirely on its own. It holds up to nine analysis methods in memory, each method tailored to control a complex analysis from start to finish.

For total automation, add the AutoSampler
The reliable, proven Model 8000 AutoSampler obtains injection reproducibility that sets the standard for automatic gas chromatography. Sample cross contamination is virtually eliminated. It will handle up to 60 samples in a single unattended run. Model 8000 can be used with any gas chromatograph. Or it can be microproccesor controlled by the CDS-111 in a completely automatic fail-safe system with the Model 3700 Gas Chromatograph.

Let us help you select a gas chromatography system that will meet your changing analytical needs.

varian

For detailed information circle the indicated **Reader Service Numbers:** **226** CDS-111 Chromatography Data System, **227** Model 8000 AutoSampler, **228** Model 3700 Gas Chromatographs, **229** Model 3711 Automatic Gas Chromatographs, **230** Have a representative call.



The Isomass 54E is an automatic mass spectrometer for isotope analysis by use of the thermal ionization technique. The spectrometer is controlled by a HP9845 computer with VDU, 64KV, two cassette drives, and printer. It is used for Rb/Sr, U, Pb, Pu, Li, B, and rare earth element isotopic analysis. Abundance sensitivity is less than 1 ppm and an absolute sensitivity of 500 atoms to give one ion. Micromass, VG-Isotopes Limited, Ion Path, Road 3, Winsford, Cheshire, CW7 3BX, United Kingdom **402**

Gradient Programmer

Model GP-1 gradient programmer can be used with HPLC pumping systems that provide a constant solvent flow. The GP-1 operates on the low-pressure side of a single reciprocating pumping system. It performs any gradient profile including concave, convex, and linear. Glenco Scientific, Inc. **410**

Water Analyzer

Model 2010 is a multiwater analyzer that measures 35 different tests including Al, ammonia, Ba, Cl free and total, chloride, chromate, color, Cu, dissolved O, hex chrome, Fe, Mn, Ni, nitrate, pH, phenol, silica, sulfate, sulfide, turbidity, and alkalinity. Each test has its own meter scale. The analyzer also has solid state circuitry and precalibrated direct readout. Kernco Instrument Co., Inc. **413**

Water Analyses for Organics

The OWA-Series GC/MS systems are designed to handle all organics-in-water analyses. With preprogrammed parameters built into the data system, a large number of samples can be accommodated. Each OWA system contains a processor-controlled gas chromatograph with capillary and packed column injectors and respective GC/MS interfaces, a liquid sample concentrator, a vacuum system, a quadrupole mass analyzer, minicomputer with 32 K memory, graphics display terminal, 10-megabyte disc drive, and a high-speed printer/plotter. The instrument meets or exceeds specificity and sensitivity requirements set by EPA. The water analyzer will be commercially available in February 1979. Finnigan Instruments **415**

Chemicals

Liquid Enzyme Reagents

The liquid-Stat UV reagents are based on a proprietary method in which labile enzyme components are chemically locked into a polymeric matrix. Users combine coenzyme and substrate as needed. The reagents are available in 100- and 225-mL ready-to-use packages for the UV assay of SGOT, SGPT, LDH-L, and HBDH. Beckman Instruments, Inc. **420**

TLC Kit

The TLC chromatofilm kit contains all components for spotting and developing plates. The components include applicator, test dye, silica gel, drying racks, spotting template, reagent sprayer, and a developing tank. Scientific Manufacturing Industries **421**

HMA Chemistry Products

The HMA-1600 analyzer is packaged in multiple test kits. Fifteen HMA chemistries are available: cholesterol, total protein, albumin, uric acid, total bilirubin, inorganic phosphorus, calcium, creatinine, urea nitrogen, glucose, alkaline phosphatase, LDH, SGOT, SGPT, and CPK. Many of the reactions are read in the UV range. Hycel, Inc. **423**

Varian announces training courses in gas chromatography

Schedule for November, December, January and February:

Basic Gas Chromatography

Nov. 29-Dec. 1, '78, Chicago, IL
Jan. 17-19, '79, Palo Alto, CA
Lecture & lab, 3 days, $225
Lecture only, 2 days, $155

Chromatography Data System

Dec. 4 & 5, '78, Chicago, IL
Lecture & lab, 1 day, $95

Automatic Gas Chromatography*

Dec. 6-8, '78, Chicago, IL
Jan. 24-26, '79, Palo Alto, CA
Lecture & lab, 3 days, $200

Gas Analysis by Gas Chromatography

Jan. 22-23, '79, Palo Alto, CA
Lecture & lab, 2 days, $225

Glass Capillary Gas Chromatography

Feb. 13-14, '79, Denver, CO
Lecture & lab, 2 days, $225

To enroll in courses, please contact the Varian Instrument Division Training Department, 2700 Mitchell Drive, Walnut Creek, CA 94598; Telephone (415) 939-2400, ext. 225

**One tuition-free course per Model 37111 purchase.*

varian

CIRCLE 231 ON READER SERVICE CARD

ad ad ad ad ad ad ad

New releases from Mercury Communications:

Getting Your Share of the R&D Funds — $37.50

. . . a complete guide to U.S. government R&D funding sources that tells you:

- **Where the R&D funds are, and**
- **How to get your share of them.**

In view of the government's increased interest in R&D activities, the timing of this new book from Mercury is extremely appropriate. Written by the authors of *How to Create a Winning Proposal, Getting Your Share of the R&D Funds* offers a wealth of valuable information to R&D firms seeking contracts, grants, awards and project funding.

Fully indexed for easy reference, "Getting Your Share" provides a comprehensive survey of the U.S. government R&D market. It includes in-depth coverage of both military and civilian agency funding activities — with a complete breakdown of the R&D funding sources, what types of projects they fund, where they are located, who to contact, and how to sell your project to them.

Excellent guidelines are given on preparing and submitting government R&D proposals and grant applications. The book also provides current patent information, and explains how to protect your inventions or ideas from unauthorized use or disclosure.

Info-Sources Directory — $44.50

Mercury's *Info-Sources Directory* contains a complete listing of the prime sources of scientific and high-technology information currently available in the U.S., including all of the major government data banks. The sources are detailed by areas of specialization — with descriptions of the information, documents, services, and technical assistance available from each one.

Info-Sources Directory is a critical desk-top reference for scientists, engineers, researchers, project managers — anyone who requires quick and easy access to state-of-the-art information in a given field. The book also provides the most current information available on government-sponsored assistance programs. Other topics include:

- **Where to get reports** on on-going government-sponsored research and engineering projects
- **How to gain access** to the NASA and DOE data banks
- **Who to contact** for a listing of government-patented inventions available for sale or licensing
- **Where to get free assistance** developing and marketing new high-technology products

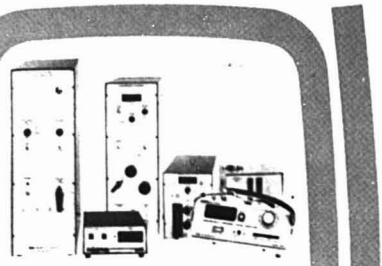
Info-Sources Directory also features prime sources of English-language translations of scientific and technical information from around the world.

Ordering information:

Copies of these publications are available prepaid from Mercury Communications Corp. Prices include shipment inside the U.S. Foreign orders, please add $3.00 postage and handling per title. In Calif. add 6% sales tax. Payment must accompany all orders. Master Charge and VISA orders accepted. Please state card no. and exp. date. C.O.D. orders call 408/425-8444.

Mercury Communications
730 Mission St., Suite 400
Santa Cruz, CA 95060

CIRCLE 142 ON READER SERVICE CARD



TSI Makes Generators for

PARTICLE RESEARCH

TSI's particle generators are used in basic research, toxicology, inhalation studies, medical research, light scattering studies, calibration of impactors, cyclones and optical instruments in a 0.01 - 40 μm range. For instance, TSI offers the **Model 3050** for generating extremely uniform particle size. **Model 3076** for ultrafine droplets with constant output . . . the automatic, fluidized bed **Model 3400** for complete dispersion of powder or dust. Or the **Model 3071** Electrostatic Classifier for generating uniform particle size in the 0.01 to 0.3 μm range.

For more information about TSI's family of particle research instruments, contact:

TSI Incorporated
P.O. Box 3394
St. Paul, MN 55165 USA
612/483-0900 Telex 297-482

tsi®

CIRCLE 202 ON READER SERVICE CARD

ELEMENTAL AND SURFACE ANALYSES BY SPARK SOURCE & ESCA*

Comprehensive elemental analyses of solid and liquid industrial and environmental samples by Spark Source Mass Spectrometry (SSMS). Up to 70 elements determined simultaneously to sub-ppm levels. Isotope dilution SSMS is also available for high precision work.

Surface chemical analysis using ESCA—X-Ray Photoelectron Spectroscopy.* Depth profiling by ion etching, and VUV analysis of gases and solids are also available.

Current clients include: chemical manufacturers, coating operations, catalyst developers, thin-film manufacturers, specialty metals producers, semi-conductor manufacturers, and the U.S. Environmental Protection Agency.

For consultation: regarding your specific problem or project, contact Dr. Arthur S. Werner, Manager, Analytical Laboratory. (617) 275-9000.

GCA

GCA CORPORATION
Technology Division
Burlington Road
Bedford, Mass. 01730
(617) 275-9000

CIRCLE 88 ON READER SERVICE CARD

YOU DO MORE THAN JUST pH MEASUREMENTS.



SO DO OUR pH METERS.

We offer a complete line of pH meters that are not only reliable and easy to operate. They're also flexible. In fact, we make pH meters that are convertible to titration systems for pH, pX or mV. We're one of the few companies that do.

And we offer you a number of special features. For example, our PHM 64 has adjustable ISO pH control. This creates a close match between the pH meter and electrode for increased accuracy. This precise research pH meter also features a 5-digit display and calibrated electrode sensitivity (slope) control.

And all of our pH meters, from the low-priced battery-operated PHM 29 to the ultra-sophisticated PHM 64, feature solid-state electronics. This means virtually drift-free performance.

In addition, we offer a full line of electrodes, including combined pH, metallic and reference. We also bring you a complete choice of various ion selective electrodes.

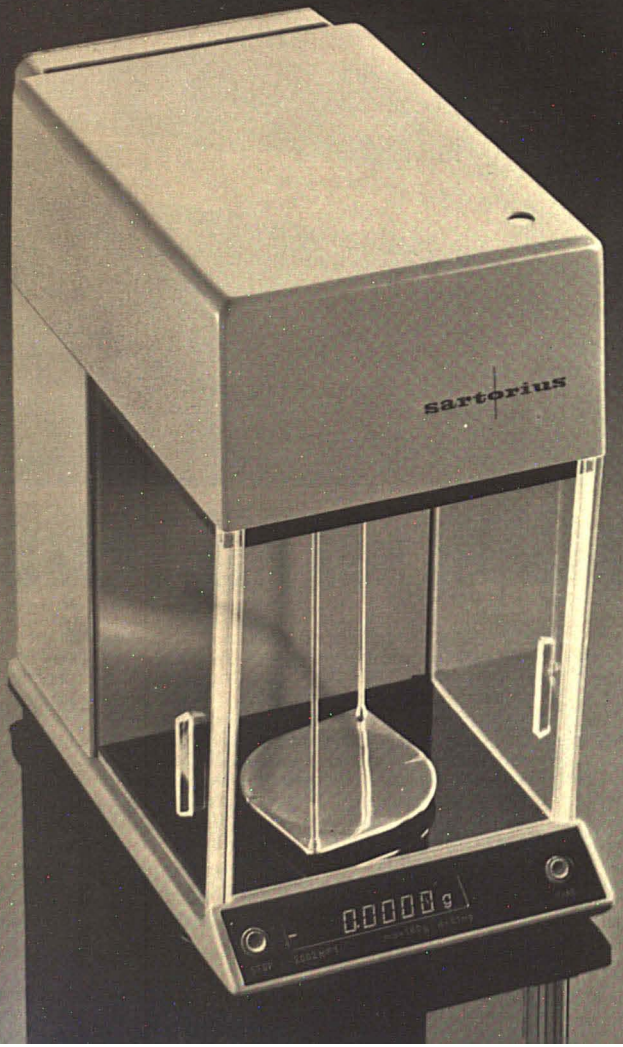
Radiometer pH meters are modern, compact and backed up by 40 years of experience.

For more information, contact your local representative or Radiometer A/S, Emprunej 72, DK-2400 Copenhagen NV, Denmark. In the United States, contact The London Company, 811 Sharon Drive, Cleveland, OH 44145.

RADIOMETER COPENHAGEN

Circle #125 for Information.
Circle #126 for Demonstration.

0,1 mg instant readability. Electronic analytical balances Sartorius 2000 MP.



Analytical weighing simplified down to the touch of a finger – for zero point adjustment or taring. Load the balance pan and read off the weight without waiting – a spectacular contrast to the awkward procedure of conventional weighing.

For your convenience: large 16 g electronic measuring range – total range 160 g. Fully automatic weight compensation with models 2002 MP1 and 2003 MP1 (manual application on one model only – 2001 MP2). The entire line features micro processors for custom-programming and connection to data systems of your choice.

Caught your interest? Write for more specific documentation to

Sartorius-Werke GmbH
P.O. Box 19
D-3400 Göttingen/West Germany

CIRCLE 188 ON READER SERVICE CARD

LC through the UV.



A BRAND NEW, VARIABLE WAVELENGTH LC-UV DETECTOR THAT EXTENDS THE LIMITS OF YOUR ANALYSIS.

This new detector from Pye Unicam has been designed specifically for liquid chromatography. Based on and incorporating many of the best design qualities of the proven LC3-UV, the new detector offers many advanced features.

The wavelength range permits the detection of an extremely wide variety of compounds. Even those not normally considered as UV absorbers can usually be detected in the far UV, around 200nm.

The addition of a visible range accessory extends the upper limits giving the detector a total range of 190 to 600nm.

Unique reference compensated optics combine many of the benefits of single and double beam instruments and, with the low noise and drift characteristics, enable the chromatographer to make full use of the high performance capability.

Coated optics, minimised warm-up time, switchable active filter and lockable wavelength control are just some of the many other features of this new easy-to-use instrument.

The LC-UV Detector is just part of a new range of chromatography instruments from Pye Unicam. A range that offers the customer a complete capability in both liquid and gas chromatography.

Turn the page for more information on the new LC-UV Detector from Pye Unicam.

PHILIPS

Pye Unicam

A SCIENTIFIC INSTRUMENT COMPANY OF PHILIPS

The LC-UV Detector

1 Reference compensated system
Reliable high sensitivity measurements can be made due to the low noise and drift characteristics of the detector. These characteristics are achieved by using a unique reference compensated system. Light emerging from the monochromator is divided by a beam splitter, a small percentage being reflected onto a reference photocell. The output of this reference photocell is amplified and used to electrically compensate for intensity changes in the arc of the deuterium lamp.

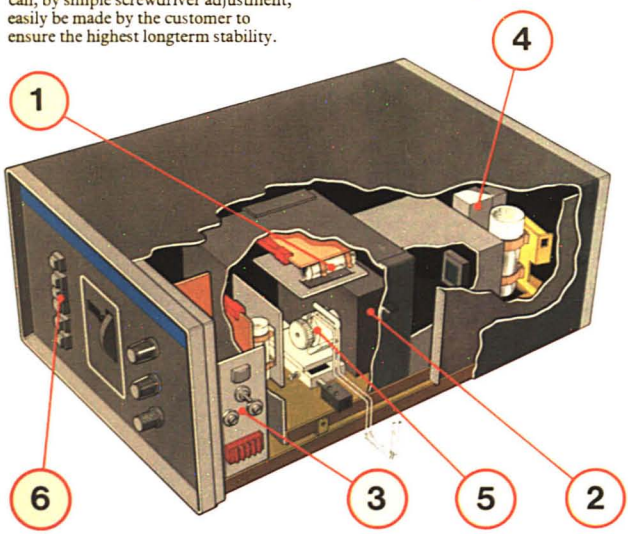
2 Coated optics
Optical components are coated with a thin layer of silica ensuring that their high standard of performance is maintained for year after year.

3 Dark current compensation
Compensation for photocell dark current can, by simple screwdriver adjustment, easily be made by the customer to ensure the highest longterm stability.

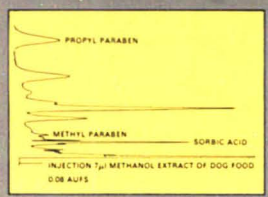
4 Standby Heater
This low-power heater can be left on when the lamp is not in use, thus maintaining the electronics at a constant temperature and reducing instrument warm-up time.

5 Flow cell
Designed for high performance this low volume temperature equilibrated flow cell is simplicity itself to dismantle for cleaning and to reassemble. Adjustment for maximum energy throughput is achieved by a single screwdriver operation with readout on to the recorder.

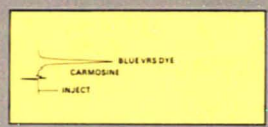
6 Switchable Filter
Baseline noise can be minimised by means of an active filter which can operate with a time constant of 0.5, 1 or 2 seconds, selected by a push-button control on the front panel.



The wavelength range of the LC-UV detector allows an extremely wide variety of compounds to be detected, including those in the far UV around 200nm. Detector sensitivity can be maximised by choosing the optimum wavelength for a particular analysis or selectivity increased by using a wavelength at which interfering impurities do not absorb.
The visible range accessory can be added to the detector in order to extend the wavelength range to 600nm thus catering for such important application areas as the analysis of food and dyestuffs.



Dog food analysis – 200nm
Careful selection of detector wavelength allows the analysis of sorbic acid together with methyl and propyl paraben in a complex food extract.
Column: Partisil-10 ODS
Mobile Phase: Water Acetonitrile Perchloric Acid 89.7 10 0.3



Mixture of Dyestuffs – 600nm
At 600nm Blue VRS dye can be readily analysed in the presence of Carmosine.
Column: Partisil-10 ODS
Mobile phase: Methanol 0.1 M potassium dihydrogen phosphate, 0.1 M disodium hydrogen phosphate + 0.01 M tetrabutyl ammonium hydroxide 50 50.

The LC-UV Detector is just part of Pye Unicam's complete capability in LC – a capability that includes complete systems, modules, columns and accessories. For further information contact Pye Unicam or use the Reader Reply Service No.170

Pye Unicam Ltd
York Street Cambridge CB1 2PX England
Telephone (0223) 58866 · Telex 817331

Printed in England by Lund Humphries 9/78
7042·05·2895·11

Manufacturers' Literature

HPLC Applications Briefs. The application of HPLC to LC separations is detailed in six briefs labeled A through F. They describe the analysis of: catecholamines by native fluorescence (A), catecholamines in brain tissue by corrected fluorescence excitation scanning (B), tryptophan in serum by corrected fluorescence excitation scanning (C), benzo(α)pyrene by fluorescence (D), serotonin by fluorescence (E), and amino acids and peptides by absorption at 200 nm (F). 1 p each. Schoeffel Instrument **427**

Basics of Filtration and Separation. Various types of filter media and systems, principles of membrane separation, ultrafiltration, reverse osmosis, and microfiltration principles are covered. 70 pp. Nuclepore Corp. **428**

Mass Flow Meters. Models A50A and A100A, representing $\frac{1}{2}$- and 1-in.-diameter flow sensors, respectively, are described in a schematic bulletin. 4 pp. Micro Motion, Inc. **434**

LC Detector. A brochure entitled Wilks Miran LC Detector contains information on the operation, applications, and results of using the Wilks Miran LC detector to monitor functional groups. 4 pp. Foxboro Co. **430**

Computer-Controlled Spectrometer. A bulletin describes the company's Model 750 AtomComp spectrometer system. The spectrometer is used for simultaneous multielement analyses. 18 pp. Fisher Scientific Co., Jarrell-Ash Division **431**

Centrifugal Chemistry Analyzer. Applications of the IL Multistat III microcentrifugal analyzer are detailed. The analyzer includes a computer, programmed cassette tapes, disposable 20-place rotor, and precision loader. 5 pp. Instrumentation Laboratory Inc. **432**

Superconducting Susceptometer. A technical bulletin on Variable Temperature Superconducting Susceptometer Systems describes the Model VTS susceptometer. High resolution measurements can be made over a temperature range of 4.5–400 K and magnetic fields of 0–5 Tesla. 19 pp. S.H.E. Corp. **433**

For more information on listed items, circle the appropriate numbers on one of our Readers' Service Cards

Intermediate Chemicals. A brochure, called Du Pont Idea Intermediates, provides molecular structures, outlines characteristics, and gives typical end uses for 28 chemicals. 18 pp. Du Pont Co. **429**

Gas Analyzer. The Superspec 600 is detailed in a brochure which describes applications, features, specifications, and data system options. Any gas is monitored in a process stream situation with sensitivity of 5 ppm. 12 pp. CVC Products, Inc. **435**

Catalogs

Inorganic and Organic Reagents. Features HPLC reagents, Ultrex, Photrex, Baker Resi-Analyzed, and Baker Analyzed reagents. Ordering information and price list are given. 128 pp. J. T. Baker Chemical Co. **459**

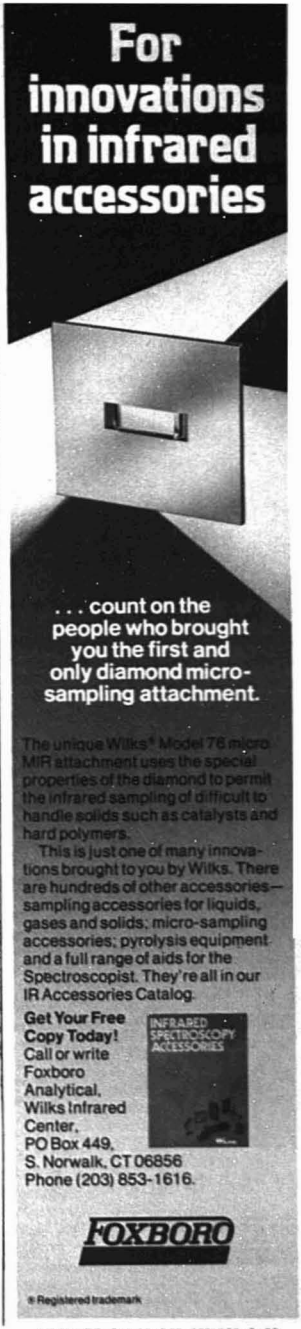
Liquid Chromatography. Contains Adjusta-Chroma recycling columns, systems II, standard systems, accessories, and a feature on the Michel-Miller high-performance, low-pressure liquid chromatography system. 24 pp. Ace Glass Inc. **440**

Balances. A wide variety of weighing and auxiliary systems manufactured by the company. Depicts several peripheral systems and electronic microbalances also. 20 pp. Mettler Instrument Corp. **441**

Corrosion Monitoring Instruments. Featured are the data acquisition system, the potentiodyne analyzer, portable field instruments, industrial automatics, corrosion systems, probes, and electrodes. 6 pp. Petrolite Corp. **442**

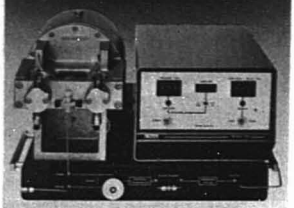
pH Electrodes. Single glass, reference, or combination designs can be customized for membrane shape, composition, temperature range, length, and diameter requirements. Connectors are available. Ingold Electrodes, Inc. **443**

Radiation Monitors. The equipment described in the catalog entitled Health Physics Equipment includes: portable rate meters and probes; portable dose-rate meters; air and particulate monitors; hand, clothing, and goot monitors; installed monitors; lab and field counting instruments; and radiation dosimetry and calibration systems. 8 pp. Nuclear Enterprises Ltd., Bath Rd., Beenham, Reading, RG7 5PR, England **444**



CIRCLE 77 ON READER SERVICE CARD

Accepted as the best HPLC pump today!





Constant flow assured by pressure/flow feedback under all conditions



Electronic pulse correction



Up to 10,000 psi at 10 ml/min

The Altex 100A Liquid Chromatography Solvent Metering System is designed to get the very highest performance from today's small particle packings.

Electronic circuitry eliminates pulses at all pressures and flow rates, assuring high-speed analytical separations without detector baseline fluctuations. Preparative separations to 28 ml/min are possible with the optional pump head.

The Altex 100A is in use today in most leading LC laboratories. Try it!

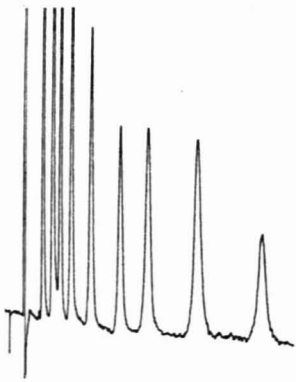
Circle Reader Service No. 7

ALTEX

ALTEX SCIENTIFIC INC. 1780 Fourth St.
Berkeley, California 94710 (415) 527-5900
Telex: 33-5403

Proven! The best selling HPLC pump today.





The Altex Model 110A HPLC Metering Pump gives you all this:

- Electronic pulse compensation
- Gradient and flow programming
- Digital flow rate selection
- 6000 psi (420 bar)
- 0.1 to 10 ml/min
- Upper/lower pressure limits
- Solvent compressibility adjustment
- Low cost

Those are *some* of the reasons the 110A is the best selling HPLC Pump today. See and evaluate it before you buy anything else. It's all the pump you need at half the cost!

Circle Reader Service No. 8

ALTEX

ALTEX SCIENTIFIC INC. 1780 Fourth St.
Berkeley, California 94710 (415) 527-5900
Telex: 33-5403

Get this HPLC literature



A. New, Totally-Programmable Automated Liquid Chromatographs
Complete brochure describes these new systems based on the concept of "distributed intelligence."
Circle Reader Service No. 9

B. "CHROMATOGRAM" keeps you up to the minute on all phases of the science
Published regularly, the ALTEX "CHROMATOGRAM" gives details of the latest applications and provides useful tips on how to obtain the optimum results from your equipment.
Circle Reader Service No. 10

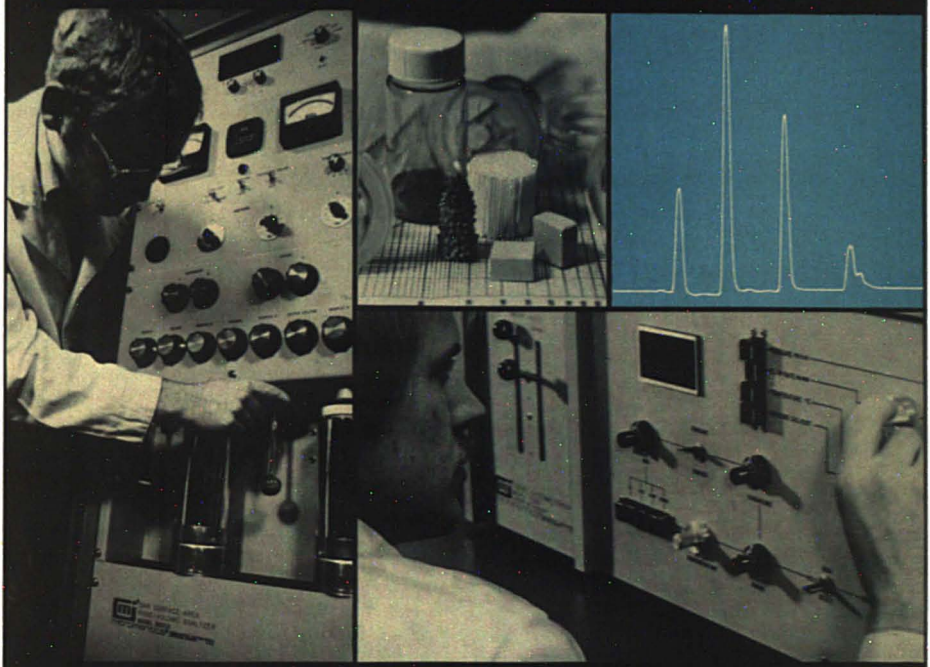
C. Complete High Performance Liquid Chromatography Catalog
32 pages describing the latest modular pumping systems, detectors, valves and accessories for all types of liquid chromatography.
Circle Reader Service No. 11

D. Innovation in Column Technology
Brochure gives details of the latest pre-packed columns for reverse-phase, ion pair, adsorption, ion-exchange and size exclusion chromatography.
Circle Reader Service No. 12

ALTEX

ALTEX SCIENTIFIC INC. 1780 Fourth St.
Berkeley, California 94710 (415) 527-5900
Telex: 33-5403

micromeritics



A Proven Leader Worldwide in Particle Technology and Liquid Chromatography

THE RECOGNIZED WORLD LEADER IN CHARACTERIZING MATERIALS: Automatic **Particle Size** analyzers, fast **B.E.T. Surface Area** analyzers; manual and automatic **Adsorption-Desorption Isotherms, Surface Area, Pore Structure** and **Chemisorption** studies; single and multi-chamber porosimeters for **Pore Volume** and **Pore Size** analysis; manual and automatic helium pycnometers to measure **Absolute Volume** for **True Density** determinations; and a versatile analyzer for **Electrophoretic Mobility** and **Zeta Potential** determination. We also have an outstanding **Materials Analysis Laboratory** for physical properties measurements.

INTEGRATED SYSTEMS FOR SUPERIOR PERFORMANCE HPLC: Liquid Chromatographs—gradient and isocratic; **Automatic Injectors**—manual and microprocessor controlled; **Detectors**—UV, RI and UV-Vis variable wavelength; **Columns**—a full line, pre-packed with high efficiency/resolution; Microparticulate **Column-Packers** for analytical and preparative columns; and a complete line of **Accessories.**

For additional information, contact Micromeritics Instrument Corporation, 5680 Goshen Springs Road, Norcross, Georgia 30093. Phone (404) 448-8282. Telex: 70-7450.

micromeritics® instrument corporation

CIRCLE 135 ON READER SERVICE CARD



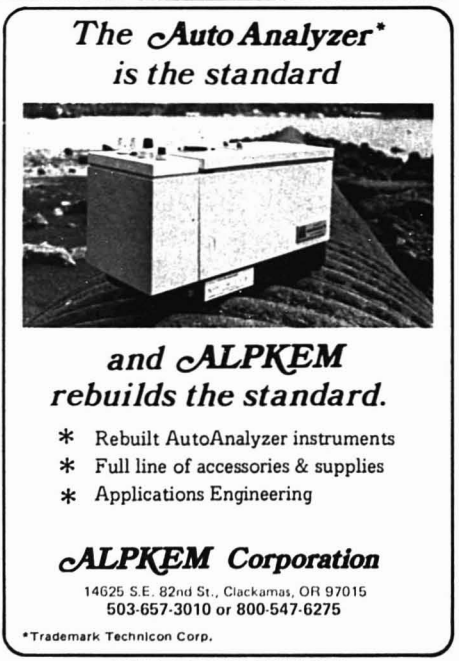
CIRCLE 197 ON READER SERVICE CARD



CIRCLE 233 ON READER SERVICE CARD



CIRCLE 14 ON READER SERVICE CARD



CIRCLE 1 ON READER SERVICE CARD

As at 8 ppb, Hg at 1/2 ppb, Sn at 5 ppb

Now...detect and measure concentrations like these in 30 to 60 seconds per measurement

Baird's Atomic Absorption Spectrophotometer and its accessory equipment can provide unprecedented sensitivity in the detection of many trace elements. Yet the cost of this advanced instrument is substantially less than that of comparable equipment in the field.

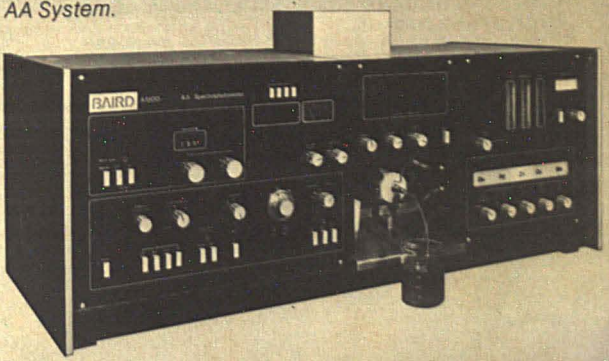
Available for both premixed flame and flameless sample atomization, the Baird AA System is extremely flexible — can be used in emission and fluorescence, as well as absorption, modes.

Automatic Data Handling



Teamed with a sophisticated programmable calculator, the Baird AA System can provide a wide range of automated analyses. Utilizing Baird-supplied software, it provides automatic, high-speed printout of direct concentration readings in both flame absorption and emission modes. Calibration and curve correction functions are performed automatically, and calibration curves can be printed out and curve fit computed.

Send for complete data on the versatile, economical Baird AA System.



BAIRD

BAIRD CORPORATION
ANALYTICAL INSTRUMENTS DIVISION
125 MIDDLESEX TURNPIKE
BEDFORD, MASSACHUSETTS 01730
TEL: (617)276-6355 — TELEX:923491
(Formerly BAIRD-ATOMIC)

CIRCLE 30 ON READER SERVICE CARD



WE HAVE THE SOLUTIONS BEFORE YOU HAVE THE PROBLEMS.

Making specialty and rare gases is a lot tougher than using them. That may be tough for us, but it's good for you.

It's tough because our experts, like Frank Kramer, have to make sure every cylinder or other container of our pure gases and gas mixtures are exactly what we certify them to be. And we have to make sure they'll perform exactly as you expect them to perform.

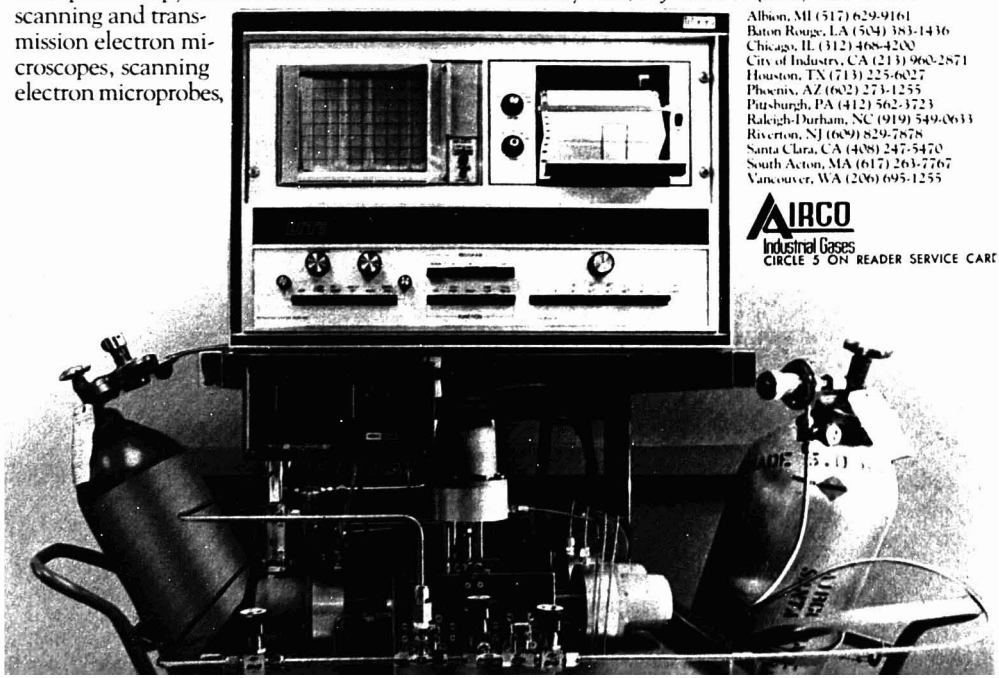
We have to make sure there are no trace heavy-metals in your electronics gases. We have to know your NO calibration gases are not polluted with excess NO_2. And we want you to know that you will not get 0.12-ppm hydrocarbons in your 0.10 certified zero air.

To do that, we use the same kind of instrumentation in our specialty gas production plants that you do in your facilities. Mass, emission, x-ray, infra-red and atomic absorption spectroscopy, flame ionization detectors, scanning and transmission electron microscopes, scanning electron microprobes, x-ray fluorescence and, of course, gas chromatographs. (We regard the gas chromatograph as a piece of production equipment, and we probably have more GC experience than most of our customers combined.)

In addition, we often set up the same equipment in the same application environment that you do just to make sure everything you're doing will work without a hitch.

All of which is good for you because—whatever you're doing with your specialty gases and equipment—Airco people like Frank Kramer have probably done it before. Hundreds of times over.

We're happy to share our knowledge, experience and facilities—and even Frank—with you any time you like. Simply call or write our Specialty Gases and Equipment Dept., Airco Industrial Gases, 575 Mountain Ave., Murray Hill, NJ 07974. (201) 464-8100.



Albion, MI (517) 629-9161
Baton Rouge, LA (504) 383-1436
Chicago, IL (312) 468-4200
City of Industry, CA (213) 960-2871
Houston, TX (713) 225-6027
Phoenix, AZ (602) 273-1255
Pittsburgh, PA (412) 562-3723
Raleigh-Durham, NC (919) 549-0633
Riverton, NJ (609) 829-7878
Santa Clara, CA (408) 247-5470
South Acton, MA (617) 263-7767
Vancouver, WA (206) 695-1255

AIRCO
Industrial Gases

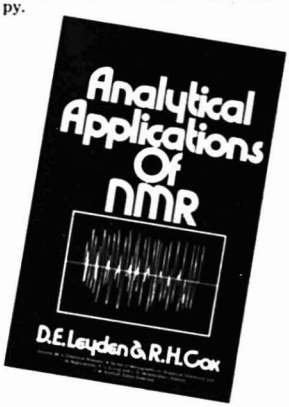
CIRCLE 5 ON READER SERVICE CARD

NMR Applications

Analytical Applications of NMR. D. E. Leyden and R. H. Cox. ix + 456 pages. John Wiley & Sons, Inc., 605 Third Ave., New York, N.Y. 10016. 1977. $27.50

Reviewed by Howard Hill, Varian Associates, 611 Hansen Way, Palo Alto, Calif. 94303

The authors have aspired to provide a practical text as an introduction to a wide range of analytical applications of NMR and have succeeded admirably. They have selected applications of both proton and carbon-13 spectroscopy.



The theory of NMR is presented in a fairly standard way with an emphasis on the physical interpretation of the phenomenon and the practical usefulness of the parameters. The experimental aspects are covered in a separate chapter with perhaps a little too much emphasis on CW techniques. This is probably a reflection of the time at which the book was written (the latest reference in this chapter was published in 1974).

Two chapters are devoted to the basic methods of analysis of chemical structure using proton and carbon-13 NMR. Analysis of proton spectra is covered in enough detail to solve many practical problems, and other experimental aids to interpretation, such as double-resonance techniques and the use of shift reagents, are described briefly. Factors influencing carbon-13 chemical shifts are described at some length, and there is an additional brief but comprehensive review of the experimental techniques used for assigning carbon-13 spectra.

Almost half the book is devoted to examples of applications. One chapter covers applications of quantitative measurements. There is a good range of applications, but the discussion of experimental techniques for quantitative measurement is limited to CW and non-Fourier transform pulse methods. The final chapter of the book covers a wide variety of analytical applications. Throughout, there is an emphasis on problems of practical interest, and many of the examples are taken from industry-related applications.

In addition to the references cited in each chapter, an extensive list of books and other articles covering specific topics is included as an appendix. This is a well-organized collection of references, which should make it an extremely useful bibliography.

The last references quoted in the book were published in 1975, but the authors have made an attempt in several places to indicate sources of recurring reviews to allow the reader to locate more current references.

Quantitative Mass Spectrometry. Brian J. Millard. x + 171 pages. Heyden & Son Inc., 247 South 41st St., Philadelphia, Pa. 19104. 1977. $15

Reviewed by Sanford P. Markey, Dept. of Health, Education & Welfare, NIH, Bldg. 10-2D46, Bethesda, Md. 20014

This concise 170-page volume is intended to fill the gap in the existing mass spectrometric texts regarding the techniques employed by a growing number of biomedical and environmental scientists quantitating organic compounds by use of mass spectrometry. After two chapters on instrumentation, the bulk of the text is devoted to a presentation of sources of error, treatment of calibration data, and quantitation by selected ion monitoring from various inlet systems. The chapters on instrumentation include background material on ionization, metastables, types of ion sources, and other miscellaneous topics which would have been better omitted than included in a cursory fashion. The choice and priority of topics are unclear—for example, why should there be more discussion of metastable ions than of quadrupole analyzers (one paragraph), and why is there no description of total ion current measurement, although the term is frequently used in the text?

Unfortunately, there is no task-oriented division of topics. This is confusing, not only to the novice who might wish for an example of "how to do it," but also for the specialist trying to find a discussion of specific topics such as methods of checking accuracy or the method of standard additions. In the text layout, the discussion on handling of data precedes chapters on sample introduction.

More troubling is the fact that the author has chosen to present several topics from a very personal perspective as a gas chromatograph–mass spectrometer user, rather than reviewing the literature in quantitative methodology, separation science, and other fields that impinge on the development of mass spectrometry as a quantitative tool. For example, he suggests that there are specific adsorption sites in a gas chromatographic column that can completely distinguish between nondeuterated and octadeuterated methyl arachidonate, as opposed to the generally accepted notion of modest isotopic fractionation effects. Much is made of these specific sites in a discussion on the relative merits of various types of internal standards, and the entire subject is clouded by puzzling data from the author's laboratory. This example of the treatment of a minor topic is mirrored in several other areas, with the result that it is often difficult to discriminate between the author's opinions and fact.

The physical format and printing quality of the book are good. Figures are clearly drawn, but the mass spectral figures employed as examples do not always contain reference chemical structures. Because many of the examples are drugs, the structures are not generally known to many scientists. Units of pressure are not standardized in the text—atm, mm, and torr are used.

The text is certain to have the author's desired effect of stimulating "a more questioning approach to the whole concept of quantitative determinations by mass spectrometry." Consequently, it can be recommended with some reservations to mass spectroscopists. However, it would not be a suitable text for teaching students or introducing other scientists to quantitative mass spectrometry.

SUB MICRON
PARTICLE SIZE ANALYSIS
DOWN TO 0.01 MICRON
IT'S SIMPLE WITH A JOYCE-LOEBL
DISC CENTRIFUGE 3

Benefit from the wealth of experience established in our application's laboratory in analysing a wide spectrum of particulate materials. The results are summarised in a free booklet 'APPLICATION REPORTS' covering the following major end-user groups:

* Polymer Emulsions
* Inks and Pigments
* Titanium Dioxide
* Magnetic Iron Oxide
* Carbon Black
* And many others

For your copy circle the reader enquiry card or write to



JOYCE-LOEBL
Marquisway, Team Valley
Gateshead NW11 0QW
England

JOYCE LOEBL

Vickers Instruments Inc.
100A Commerce Way
Woburn
Massachusetts 01801
U.S.A.

CIRCLE 109 ON READER SERVICE CARD

SPAIN
an on-going process you must know about.



In the International Chemical Exhibition.

A professional, industrial and commercial Rendez-vous holding two important meetings.

First Mediterranean Congress on Chemical Engineering and the International Congress on Analytical Techniques in Environmental Chemistry

Exhibits include:
- Analytical Instrumentation.
- Research and development; production processes.
- Control and Regulation, equipment goods.
- Industrial installations. Related industries.
- Raw materials, semi-finished and finished products.



21/30 November
BARCELONA

EXPOQUIMIA
Spanish Technology for world wide service

CIRCLE 189 ON READER SERVICE CARD

Books

Differential Thermal Analysis. M. I. Pope and M. D. Judd. vii + 197 pages. Heyden & Son, Inc., 247 South 41st St., Philadelphia, Pa. 19104. 1977. $18

Reviewed by Joseph Jordan, Dept. of Chemistry, The Pennsylvania State University, 152 Davey Laboratory, University Park, Pa. 16802

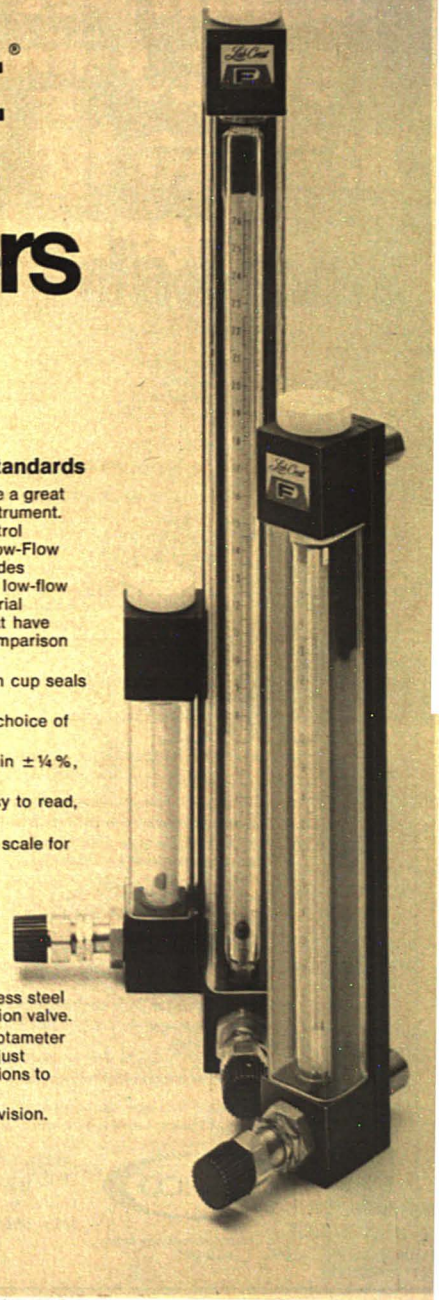
This reviewer has become exasperated by the tendency, encountered all too often in recent scientific monographs, that the contents are not at all what a reader would normally expect from the title and preface. The book by Pope and Judd is refreshingly different. It "delivers" *exactly* what the subtitle promises, viz., "a guide to the technique (of DTA) and its applications." The authors have focused the write-up on the objective set forth in the preface, i.e., "to show the engineer, scientist, or technologist, how differential thermal analysis can be used to solve problems encountered in his own particular field of work." Indeed, discrete chapters are devoted to numerous and diverse fields of application, including phase diagrams; thermal decomposition; chemical reactions involving solids; purity specifications; determination of material adsorbed on the surface; catalytic activity; liquid crystals; ferroelectric transitions; polymers, coals, petroleum, and fibers; explosives and propellants; hydraulic cements; glass and ceramics; coordination compounds; space studies; and reaction kinetics. Thus, the salient feature of this monograph is breadth of coverage.

On the other hand, this book is definitely a "user's manual" (rather than a scholarly treatise). As such, it is well written: Tidbits of history, e.g., the story on the discovery of DTA by Le-Chatelier in 1887, make "good reading." The presentation is lucid and down-to-earth, but is somewhat shallow and overly empirical. The authors have evidently catered to an audience which lacks a sophisticated understanding—in depth—of thermodynamics and kinetics. Even so, readers may resent, as an insult to their intelligence, the dismally elementary cookbook approach which transpires, e.g., from the following typical passage on page 37:

The calibration constant, K, can readily be obtained from the equation (Total peak area) = K × (known enthalpy change). Experimental enthalpy changes can then be calculated as follows. Experimental enthalpy change = Experimental peak area/K.

In view of this situation, this book may appeal primarily to an audience of technicians. The authors seem to have recognized this, by including in

Lab-Crest® Low-Flow Rotameters



The New Performance Leader . . . By All Standards

Now you can get all the features and options that make a great low-flow rotameter, combined in one and the same instrument. Built by the industry's most experienced team of control engineers and glass craftsmen, the new Lab-Crest Low-Flow Rotameter features a unique precision valve that provides linear control throughout the range of flows . . . a new low-flow tube with ⅛-inch float that operates reliably in industrial environments . . . plus all the time-tested features that have made Fischer & Porter rotameters the standard of comparison since the birth of the industry:

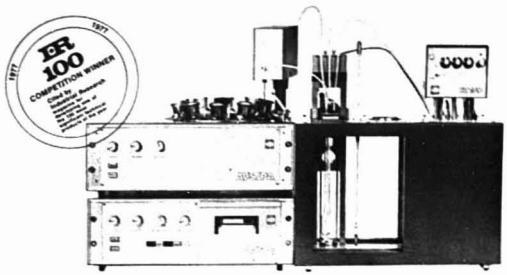
- **Convenience.** Quick-release metering tubes with Viton cup seals are easily interchanged without tools.
- **Rangeability.** Eight interchangeable tubes provide a choice of flow ranges from 50 cc/min to 148 SCFH (air).
- **Accuracy.** Instantaneous readings are repeatable within ±¼%, a direct result of F&P's unsurpassed experience.
- **Visibility.** Ceramic scale with white background is easy to read, permanently fused into the borosilicate glass surface.
- **Versatility.** Choice of meter bodies with 3, 6 or 10-inch scale for in-line or panel-mounting . . . or with tripod mount.
- **Controllability.** Precision sixteen-turn valve with interchangeable stems and sleeves provides linear control at all flow rates, as well as positive shut-off; low-cost valve also available for less sensitive applications.
- **Corrosion Resistance.** Standard aluminum end fittings are also available with interchangeable brass or stainless steel inserts; stainless steel standard on models with precision valve.

More than ever, it makes sense to call us for all your rotameter needs, whether you are looking for OEM quantities or just one of a kind. We have the right type and the right options to meet your requirements exactly.

Call (215) 674-6000 and ask for Lab-Crest Scientific Division. Fischer & Porter Company, County Line Road, Warminster, Pa. 18974.

LAB-CREST SCIENTIFIC
A DIVISION OF FISCHER & PORTER

CIRCLE 75 ON READER SERVICE CARD



Save Lab Time

Automatic Viscosity Measuring Systems — AVS — Automates Capillary Viscosity Measurements.
System AVS/PA with 10 sample capacity employs one capillary viscometer and performs selected test programs of testing single or repeat measurements, discharge, rinsing and sample change automatically.
AVS/G base unit in conjunction with AVS/PA provides a seven digit tape print out with a 0.01 sec resolution.
Efflux time is measured opto-electronically resulting in accuracy of measurement of 0.1%. Covers measuring range of 0.3 to 30.000 cSt at temperatures up to +150°C.
AVS systems for single and serial measurement also available.

Send for descriptive color brochure now.

SCHOTT

JENA™ GLAS JENA™ GLASWERK SCHOTT & GEN. INC

11 East 26th Street • New York, New York 10010 • (212) 679-8535

CIRCLE 192 ON READER SERVICE CARD

Glenco 3400 & 3500 Series Liquid Chromatography Columns

THE CHROMATOGRAPHERS' CHOICE





- Diameters from 6mm to 150mm ID - all available in standard lengths (15cm to 150cm) "off the shelf."
- Operating pressures to 150 psi.
- Borosilicate glass construction with polypropylene threaded collars and end plates.
- Aqueous and organic solvent systems available. Entire system autoclavable.
- Upper end plates with center inlet port and a side vent port which can be used to bleed air and to layer on sample with a long needle or tubing.
- Lower end plates with packing support of (10 micron) mesh cloth suspended over a woven grid and retained with snap ring.
- 1/8" or 1/16" Teflon Multifit connectors on each end plate for easy connection with polyethylene or teflon tubing.

Send today for our complete 60 page catalog of columns, fittings, valves, plungers, and accessories.

GLENCO®

Liquid Chromatography Specialists since 1962

Glenco Scientific Inc.
2802 White Oak
Houston, Texas 77007
(713) 861-9123

CIRCLE 89 ON READER SERVICE CARD

Books

their preface the following caveat: "... a detailed mathematical approach has deliberately been avoided.... Any further information can generally be obtained from the references cited." Two to 35 references are indeed listed at the end of each of the 23 chapters. Scientists and engineers knowledgeable in chemistry would be well advised to consult these, rather than rely solely on the contents of the book.

Interpretation of NMR Spectra. LeRoy Johnson and R. Bible. 117-page manual + 8 audiotape cassettes (5.9 hours). Dept. of Educational Activities, American Chemical Society, 1155 16th St., N.W., Washington, D.C. 20036. 1978. $175. Additional manuals: 1–9 copies, $9.50 each; 10–49 copies, $7.50 each; 50 or more, $7.00 each

Reviewed by Anthony Foris, E. I. du Pont de Nemours & Co., Chem., Dyes and Pigments Dept., Jackson Laboratory, Wilmington, Del. 19898

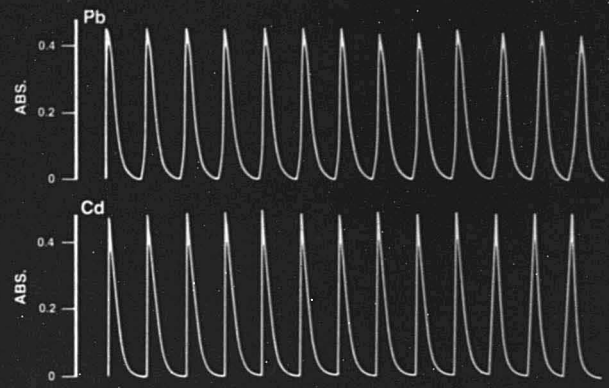
This ACS audio course, taught by two eminently qualified practitioners of NMR, provides an excellent introduction to the theory and practice of one of the most powerful techniques in modern analytical chemistry.

The course is composed of eight audio cassettes (total playing time about 5.9 hours) and a 117-page manual. The topics discussed include elementary NMR theory; the chemical shift; spin-spin coupling; the use of the integration curve; interpretation of first and second order spectra; nonequivalence due to hindered rotation, molecular geometry, and configurational isomerism; line-broadening effects; solvent effects; exchange of labile protons; variable temperature studies; numerical analysis of second order spectra, etc. The manual also contains a chart of chemical shifts, a table of shielding constants for aliphatic methylene groups, and an especially usefui compilation of proton-proton coupling constants. Also included are answers to the problem sets and an outline of the various sections of the manual and of the tapes.

The audio presentation is generally quite good. The information content is, by necessity, fairly high, and the pace is occasionally a little too fast. The student may find, therefore, that listening beyond the 20–30-min period (the average duration of each side of a tape) will exceed his attention span. However, the great advantage of an audio course is that the student can proceed at his or her own speed.

Emphasis throughout the course is on the practical aspects, and theory is kept at an absolute minimum. Each new concept is introduced with the

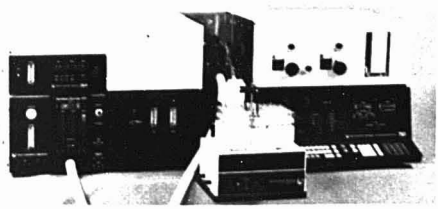
You may be looking at the most impressive atomic absorption data ever produced.



Simultaneous Determination of Trace Cd and Pb with IL751 AA, IL555 CTF Atomizer and FASTAC Autosampler.

The analysis: Simultaneous trace concentrations of cadmium and lead. Precision: 1.00% for lead, 0.52% for cadmium. Elapsed time for 10 pairs of readings: 8 minutes.

The equipment: The IL751 dual-channel double-beam Atomic Absorption Spectrophotometer, the



new IL555B CTF (Controlled-Temperature Furnace) Atomizer, and the new IL254 FASTAC™ Flame/Furnace Autosampler, all from Instrumentation Laboratory.

There's more where that came from. FASTAC's 95-place sample table produced 85 more peak pairs just like those above. That's 150 furnace determinations per hour. Remember, a year ago 30 hourly analyses represented the impossible dream.

Twenty-five successful labs can't be wrong. Dual-channel analysis might be great, but is it real? To check, we surveyed 28 U.S. users of the new IL751. Twenty-five were actually doing two-channel analysis with highly varied samples. Everybody who had tried it had succeeded. No careful element pairing was needed. Interested? Please request *Report 100*.

Keeping up with the jet set. That's the induction-coupled plasma jet set. A plasma direct reader can turn out a lot of samples. But so can the IL751 with FASTAC. An article in *Canadian Research* describes lube oil analysis for six elements at a rate of 540 determinations per hour. That's moving. Write for *Report 99*.

The atomic absorption leader has a new name. It's. . .

Instrumentation Laboratory Inc.
Analytical Instrument Division
Jonspin Road
Wilmington, MA 01887

CIRCLE 105 ON READER SERVICE CARD

help of simple and clear diagrams and well-chosen "real" spectra. At the end of each session, problems are assigned, the solutions of which require the use of information learned during the previous sessions. At the beginning of each successive session, the solutions to the previously assigned problems are discussed in detail. All in all, close to 90 spectra of gradually increasing complexity are discussed during the sessions. If the beginner conscientiously works through all of them, at the end of the course he should be ready to tackle structural problems on his own. Most logical questions are anticipated, and there are relatively few trivial errors and inconsistencies between the audio and the written parts of the course. Most of these should cause no real difficulty for the attentive listener.

The course is, by design, restricted to structural determination by proton NMR. It does not cover NMR of other nuclei, instrumentation, or quantitative analysis. As an introductory course, it fulfills its purpose admirably and is highly recommended to students and teachers, technicians, chemists, and managers alike—in short, to all those who wish to learn the basics of NMR spectrometry.

Practice of Thin Layer Chromatography. J. C. Touchstone and M. F. Dobbins. xxiii + 383 pages. Wiley-Interscience, 605 Third Ave., New York, N.Y. 10016. 1978. $19.95

Reviewed by Victor W. Rodwell, Dept. of Biochemistry, Purdue University, Lafayette, Ind. 47907

This new treatment of the popular and ubiquitous topic of TLC echoes the lecturing style of the senior author, Joe Touchstone—a practical, down-to-earth approach and readily comprehended style. Although theory is not neglected, this is primarily a practical rather than a theory-oriented book. Most major aspects of modern TLC technique are discussed. Valuable features include a glossary of TLC terminology, extensive discussion of layer preparation and the virtues of commercially prepared layers, development and visualization techniques, and a list of TLC equipment suppliers. Of even greater value are the excellent discussions of quantitation, solvent selection, sample application, and the use of TLC in combination with other separatory and/or analytical techniques (e.g., column and gas chromatography, MS and IR spectroscopy). It is unfortunate that HPTLC (high-performance TLC), a promising new technique, is not discussed, probably because of its recent introduction.

This book represents a worthwhile purchase for teachers of analytical chemistry or separations science, and for both new and relatively experienced users of TLC techniques. It is highly recommended as a readable overview of TLC in 1978.

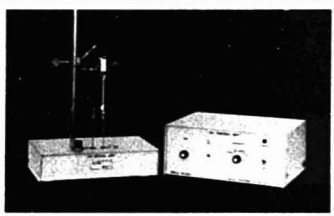
New Books

Tables of Standard Electrode Potentials. G. Milazzo and S. Caroli. xvi + 419 pages. John Wiley and Sons, Inc., 605 Third Ave., New York, N.Y. 10016. 1978. $39.95

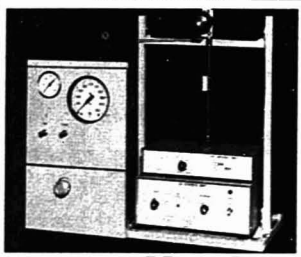
A complete compilation of standard electrode potentials is the aim in presenting these tables. The tables collect all data published and abstracted in *Chemical Abstracts* from 1945 to the

NEW! from GOW-MAC

a teaching LC good enough for QC



Model No. 80-500



a QC LC good enough for research

Model No. 80-600

and both priced good enough for anybody

Both LC units employ rugged, modular GOW-MAC design for reliable operation. The basic Model 80-500 offers pulseless solvent delivery with a constant pressure pump (300 ml capacity to 1000 psi), a modular design for uniform manual injections, column holder, complete with 20 micron Silica Gel column, and reliable 254 nm, low volume (8 μl) UV detector. Only $1750.

The high-performance Model 80-600 offers a continuous solvent delivery system with constant volume, variable flow-rates from 0.5 $cm^3 min^{-1}$ – 5 $cm^3 min^{-1}$ with a low dead volume damping system. Pressures go to 3000 psi. For highly reproducible injections, a six-port rotary valve, modularly designed into column and detector system.

The 80-600 has a 10 micron Silica Gel column and a 254 nm, low volume (8 μl) UV detector. $3245.

Other detectors, columns and accessories are available. In addition, each unit shipped comes with a useful book, Elementary Theory of Liquid Chromatography with Bibliography and Experiments. For further information, inquire.

GOW MAC

GOW-MAC INSTRUMENT CO.
P.O. Box 32, Bound Brook, NJ 08805
Telephone: 201/560-0600
Shannon Free Airport, Co. Clare, Ireland
Telephone: 61632 Telex: 6254

CIRCLE 87 ON READER SERVICE CARD

Everything You've Wanted in a Spectrophotometer. And Much More.



Introducing the Model 100-80 Computer Controlled Double Beam Ratio Recording Spectrophotometer

Not just a spectrophotometer but a spectrophotometric system with unsurpassed performance and flexibility. The overall concept of the Model 100-80 is to provide the analyst with the utmost flexibility in wavelength scanning and greatly expand the capability and methods of collecting, processing and reporting quantitative data at fixed wavelengths.

The Model 100-80 also provides a level of automation, data acquisition, data processing, data presentation and operating functions never before available in a spectrophotometer.

Just a few of the many standard features:

- Wavelength scanning
- Repetitive scanning — superimposed or stacked
- Derivative — first and second scanning and fixed λ
- Time scan
- Wavelength programming
- Auto printing
- Enzyme — complete program Δ Abs. and log of Δ Abs.

And all this at a reasonable price, too! Seeing is believing. Contact us for demonstration or free literature. NSI Hitachi Scientific Instruments, 450 E. Middlefield Road, Mountain View, CA 94043, (415) 969-1100

NSI HITACHI
SCIENTIFIC INSTRUMENTS

Circle #150 for literature.
Circle #151 for demonstration.

end of 1973. An appendix contains some new data abstracted from the end of 1973 to the end of 1975 in *Chemical Abstracts, Analytical Abstracts,* and *Electroanalytical Abstracts.* The most important sources of electrode potential values are original papers. The tables are arranged by element in the order of the periodic table. For each element an extended table contains the following information: electrochemically conducting phase, intermediate species, solution composition, solvent, temperature, pressure, measuring method, comparison electrode, liquid junction, electrode reaction, standard value, uncertainty, temperature coefficient, notes, references, and electrode reference number.

Mössbauer Effect Data Index Covering the 1976 Literature. J. G. Stevens and V. E. Stevens, Eds. x + 357 pages. Plenum Publishing Corp., 227 West 17th St., New York, N.Y. 10011. 1978. $95

The data are compiled by computer programming, and references are included on the Mössbauer effect in chemistry, physics, biology, geology, metallurgy, and mineralogy. A summary sheet on the parent decay and nuclear level schemes for each isotope precedes the Mössbauer data and references. "Selected values" from a critical review of published results are listed for the experimental results. A reference list for analysis, instrumentation, review, and theory is also given.

Toxic Substances Control II. Marshall Lee Miller, Ed. viii + 256 pages. Government Institutes, Inc., 4733 Bethesda Ave., N.W., Washington, D.C. 20014. 1978. $25

The papers provided in this book are the results of the proceedings of the second annual Toxic Substances Control Conference, held in Washington, D.C., December 8–9, 1977. EPA regulatory developments, OSHA's proposed National Cancer Policy, identification and classification of toxic substances, practical industrial concerns, and disposal of toxic substances are just a few of the many issues presented.

The Analytical Chemistry of Synthetic Dyes. K. Venkataraman, Ed. xxiv + 591 pages. John Wiley & Sons, Inc., 605 Third Ave., New York, N.Y. 10016. 1977. $42.50

This comprehensive survey begins with a classification of dyes for analytical purposes, describes all of the important methods for the analysis of dyes, and gives examples of structure determination. The various uses of chromatography, NMR, and MS to separate and identify synthetic dyes are detailed in six of the 20 chapters. The 23 authors are specialists on the topics they have covered.

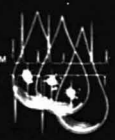
Continuing Series

Advances in Magnetic Resonance, Vol. 9. John S. Waugh, Ed. x + 427 pages. Academic Press Inc., 111 Fifth Ave., New York, N.Y. 10003. 1978. $44

The four articles (eight contributors) included in this volume are temperature-dependent splitting constants in the ESR spectra of organic free radicals; magnetic resonance induced by electrons: studies of the simplest atomic and molecular systems; intramolecular dipolar relaxation in multispin systems; and NMR studies of molecules oriented in thermotropic liquid crystals.

The symbol of excellence since 1959

Distilled in Glass™



Residue-Free Solvents from Burdick & Jackson

Purified to the exacting requirements of gas chromatography, liquid chromatography and spectrophotometric analysis.

Acetone	Iso-hexanes
Acetonitrile	Methanol
Benzene	2-Methoxyethanol
Butanol-1	Methylene Chloride
Butanol-2	Methyl Ethyl Ketone
n-Butyl Acetate	Methyl Isoamyl Ketone
Butyl Chloride	Methyl Isobutyl Ketone
Carbon Tetrachloride	N-Methylpyrrolidone
Chlorobenzene	Nonane
Chloroform	Pentane
Cyclohexane	Petroleum Ether, 30-60°
Cyclopentane	beta-Phenethylamine
o-Dichlorobenzene	Propanol-1
Dimethyl Acetamide	Propanol-2
Dimethyl Formamide	Propylene Carbonate
Dimethyl Sulfoxide	Pyridine
Dioxane	Tetrahydrofuran
2-Ethoxyethanol	Tetramethyl Urea
Ethyl Acetate	Toluene
Ethylene Dichloride	Trichloroethylene
Ethyl Ether	1,1,2-Trichloro-1,2,2-Trifluoroethane
Heptane, 98-99°	2,2,4-Trimethylpentane, 99-100°
Hexadecane	o-Xylene
Hexane, 68-69°	
Isobutyl Alcohol	

Ask for Bulletin BJ-25/U.S. Agencies use F.S.S.

BURDICK & JACKSON LABORATORIES, INC.

1953 South Harvey Street, Muskegon, Michigan U.S.A. 49442 (616) 726-3171

CIRCLE 25 ON READER SERVICE CARD

X-ray analytical equipment is a big investment. Don't you deserve a look at the best investment?

Whether it be spectrometers or diffractometers, Siemens analytical x-ray units are the best investment.

Siemens SRS 200 is a sequential spectrometer that uses x-ray fluorescence methods to non-destructively analyze solid, powder, and liquid samples for all elements from fluorine to uranium. Sample changers are available to accommodate up to 80 specimens. That's flexibility.

For process control applications demanding speed and accuracy, the MRS 400 spectrometer provides up to 28 simultaneous analyses in less than one minute. That's speed.

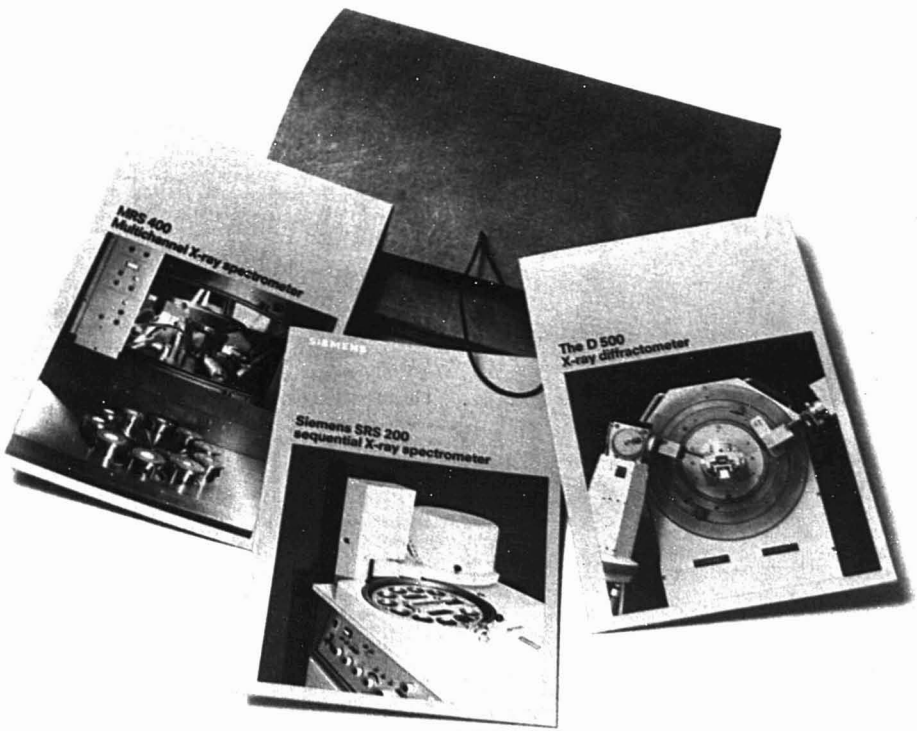
Siemens D 500 diffractometer provides for material examination; including structure and layer determination, texture and stress measurement, and phase analysis.

The D 500 is available with 1, 30, or 80 specimen magazines, with sample rotation capabilities... perfect for the routine analysis of a large number of samples.

All three units are designed and built to be either automatic or manual. So when you invest in an automatic unit, you get an automatic unit, not just a retrofitted manual instrument.

For more information on your best x-ray analytical investment and a free x-ray periodic table chart, write or call: Mr. Pedro Arredondo, Siemens Corporation, Measurement Systems Division, 2 Pin Oak Lane, Cherry Hill, New Jersey 08034. Telephone: (609) 424-9210.

SIEMENS



CIRCLE 194 ON READER SERVICE CARD

1979-80 PIERCE HANDBOOK-CATALOG

FREE! FOR JUST ASKING



CONTENTS INCLUDE:

- Clinical Reagents
- Laboratory Aids
- Gas Chromatography Accessories
- Thin Layer Chromatography
- Liquid Chromatography
- Derivatization Procedures
- Amino Acid Analysis
- Sequence Determination
- Protein Modification
- Peptide Synthesis
- Controlled Pore Glass
- Many Unique New Products

Pierce Eurochemie B.V.,Netherlands ● Pierce & Warriner United Kingdom ● Lab Supply Pierce N.Z. New Zealand

PIERCE CHEMICAL COMPANY
Box 117, Rockford, Illinois 61105

CIRCLE 174 ON READER SERVICE CARD

The LC Detection System with a mind... ...not a mind of its own.



Now—using a Schoeffel variable wavelength absorption detector, you can stop the flow in your LC system and scan the spectrum for positive identification of an eluted fraction. Without having to worry about baseline variations. Without spending valuable time correcting for solvent and background absorbance.

Because of the mind: Schoeffel's MM 700 Memory Module makes absorbance profiling ('fingerprinting') a snap. Solvent and background absorbance are *automatically* removed from sample analysis. For fast, simple, more accurate qualitative determinations. Also useful in gradient elutions.

Best of all, the MM 700 is used with Schoeffel's UV-VIS absorption detector —the SF 770 Spectroflow Monitor— with motorized wavelength drive. An industry standard since its introduction in 1973. Write for our brand new literature—or phone us for a demonstration.

U.S.A.: 24 Booker Street, Westwood, New Jersey 07675
(201) 664-7263, Telex 134356
EUROPE: 2351 Trappenkamp, Celsiusstrasse 5, W. Germany
(04323) 2021, Telex 299660

KRATOS Inc.
SCHOEFFEL INSTRUMENT DIVISION

CIRCLE 198 ON READER SERVICE CARD

Sixth Annual ACS Chemistry and Public Affairs Fellowship to begin in the Fall of 1979

Interact with the Legislative and Executive Branches of the Government

The objectives of the fellowship program are:

- To provide an opportunity for scientists to gain firsthand knowledge of the operations of the legislative and executive branches of the federal government,
- To make available to the government an increasing amount of scientific and technical expertise, and
- To broaden the perspective of both the scientific and governmental communities regarding the value of such scientific-governmental interaction.

Applications should be submitted by January 19, 1979 to the:

Department of Chemistry and Public Affairs
American Chemical Society
1155—16th St., N.W.
Washington, D.C. 20036

Applications consist of a letter of intent, resume, and two letters of reference. The letter of intent should include a description of the applicant's experience in public-oriented projects in which scientific or technical knowledge was used as a basis for interaction and a statement that tells why they have applied for the Fellowship and what they hope to accomplish as a Chemistry and Public Affairs Fellow. The resume should describe the candidate's education and professional experience and include other pertinent personal information and the names of the two references. Letters of reference should be solicited from people who can discuss not only the candidate's competence but also the applicant's experience in public-oriented projects. Arrangements should be made to send the letters of reference directly to ACS.

For further information call (202) 872-4383.



"Sure, our SEM showed us what a surface *looked* like," Bob told us recently, "but we ran into surface problems in our contract analysis business that called for chemical analysis, too. That's why we started looking at Secondary Ion Mass Spectrometry technology—the SIMS.

"It didn't take long to decide on 3M's system. We were really impressed by its sensitivity, its resolution area, and its wide area imaging capabilities . . . which enabled us to provide our clients with more comprehensive surface data than ever before. But the question was settled when we realized 3M is the only company that offers a fully compatible SIMS attachment system for our equipment."

Bob's story is short and simple, and it has a happy ending. Yours can, too.

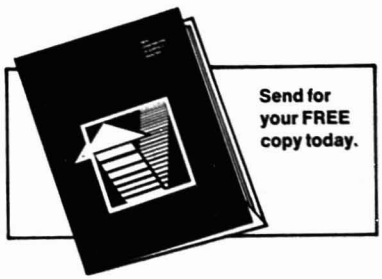
Like Bob, you can choose from 3M's line of modular components (which we'll install) to expand the capabilities of the SEM you're now using.

You can't do better. And we'll prove it.

We'll match 3M's SIMS system against any competitor . . . assume total "turn-key" responsibility . . . and hand it over ready to run. But that's for later.

Right now, we just want you to have the facts. You can get them quickly and easily by writing to the address below.

Just say, "Send me New Dimensions in Surface Analysis." We'll handle the rest.



Analytical Systems
New Business Ventures Division/3M
Building 53-3S 3M Center
Saint Paul, Minnesota 55101
612/778-4009

3M

CIRCLE 148 ON READER SERVICE CARD

CHN+O/S 1106 Elemental Analyzer

the truly automatic and reliable alternative for the solution of your microanalysis problems!

If the doubters want proof, then here it is.

Automation
50 CHN + 50 O or S determinations in 24 hours, *fully unattended*

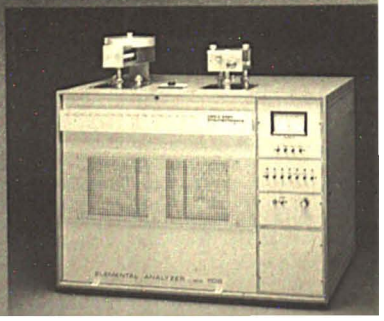
Accuracy
better than ± 0.3%

Reproducibility
better than ± 0.2%

Low cost per analysis
Less than 50 U.S. cents including labour



For further information in Europe and USA please contact our local Subsidiary or Distributor.



GRUPPO MONTEDISON
CARLO ERBA

CARLO ERBA STRUMENTAZIONE
P.O. BOX 4342 I - 20100 MILANO

CIRCLE 32 ON READER SERVICE CARD

Editors' Column

Federally Supported Basic Research

Participants in the nation's basic research—whether one's participation is through scientific investigation or appropriation of necessary funds and formulation of governmental policies—are provided with an opportunity to look closely at the current status of federally funded basic research in the U.S. The recently released 405-page study entitled **"Basic Research in the Mission Agencies: Agency Perspectives on the Conduct and Support of Basic Research,"** prepared for submission to the President, and through him to Congress, is the 10th Annual Report of the National Science Board (NSB).

In preparing the report, NSB solicited information from 14 mission agencies and two other entities of the Federal Government. Each agency was asked to submit its own report in the format required by the Board for inclusion in the study. The general format provides for the definition of the agency mission, the agency definition of basic research and what it perceives as the role of basic research, examples of basic research, current and future research emphasis, and organization and management of research activities. These data are presented in Part I. Part II consists of the Board's analysis of trends and problems in basic research. The analysis is derived from data obtained directly from the mission agencies and also from statistical data collected regularly by the National Science Foundation. Finally, a comparative analysis of the mission agencies and the historical trends of their support of basic research is collected in Part III.

The Board was very careful not to take an advocacy role although it is naturally concerned with the adequacy of basic research support. The greatest difficulty in preparing the survey, however, was drawing a sharp distinction between basic and applied research. When the distinction is imposed for the compilation of statistical data, the division is often an arbitrary one. Thus, what one agency classifies as basic research may be applied research to another. For example, at the National Oceanic and Atmospheric Administration (NOAA), its support of fundamental research on atmospheric processes is reported as applied research because the subject is directly related to NOAA's mission in weather forecasting. On the other hand, when NSF supports the same research, it is reported as basic. Numerous other examples can be found throughout the report. In addition, the statistical classification may reflect the national priority of the time. Therefore, the research classified as basic by an agency at one time may be reported as applied at another time by the same agency.

Given these limitations, however, it is still possible to draw some general conclusions. All funding agencies conclude that federally funded basic research continues to make significant contributions to the solution of national problems. To this end, various examples of payoffs from investments in basic research are cited. Nonetheless, Federal support of basic research has steadily declined in constant dollar amounts over the last 10 years. In current dollars, Federal basic research obligations have grown by an annual average rate of 4.3% in the period from 1968 to 1976, but in constant dollars have actually declined by 1.8% annually. In spite of the efforts to reverse the trend in recent years, the estimated total obligations for 1978 are still 5% lower in constant dollars than the obligations for 1968. In relation to other types of research, the basic research share of Federal R&D obligations has remained fairly constant, ranging between 11 and 12%.

A close examination of the data over the past decade also reveals significant shifts in the support among the fields of science, which are divided into eight categories: life sciences, psychology, physical sciences, environmental sciences, mathematics and computer sciences, engineering, social sciences, and other. Of these, the life and physical science fields have received the greatest share of the total Federal support for basic research through the past decade. In 1977 the life sciences share was 37%, or $1 007 million of the total $2 755 million, and physical sciences approximately 29% or $806 million. However, the relative growth in current dollars for the two fields from 1968 to 1977 was 73.9% for the life sciences and 34.6% for the physical sciences. The field registering the greatest growth rate in the same period was environmental sciences with 98% gain, and the field with the greatest rate of decline was psychology with a 3.6% decline. A further breakdown of the physical sciences support shows that the support of chemistry as a separate discipline grew from $119 million in 1968 to $203 million in 1977, an increase of 70.6%. This increase is much

VWR

CHEMICAL REAGENTS

YOUR NEW CHOICE for REAGENT GRADE CHEMICALS



Acids
Salts
Solvents

- Meet or exceed A.C.S. standards for purity
- Convenient packaging for maximum safety in handling and storage
- Priced to fit your laboratory budget

VWR CHEMICALS— WE'RE DELIVERING

VWR Scientific Inc.
subsidiary of Univar
P.O. Box 3200, San Francisco, CA 94119

CIRCLE 220 ON READER SERVICE CARD

Automatic Sizing Analyzer Plotter



HIAC Model PA-520 ASAP
Automatic Sizing Analyzer Plotter

Measures particle size/volume (weight) distributions with pushbutton simplicity—delivers X-Y plots in 40 seconds!

Just put in the sample, insert a chart and press a button. In less than a minute ASAP measures particle size and computes, in its microprocessor, particle size and volume (weight) distributions. 11" x 17" X-Y plots are automatically delivered in your choice of any or all of six different modes of data presentation, cumulative or differential.

NON-ELECTROLYTIC HIAC® PRINCIPLE/ You don't have to use electrically conductive carrier fluids. You can use water, alcohol, oil, solvents—almost any liquid—even viscous fluids, with HIAC accessories. Standard sensors cover from 1 micron through 1000 microns!

HIGH RESOLUTION PRECISION/ ASAP can analyze up to one million particles per sample, with an accuracy traceable to NBS certified materials. Wide-range sensors analyze broad size distributions quickly, easily.

DIVERSE APPLICATIONS/ Include powdered materials of all kinds—pigments, pharmaceuticals, metals, abrasives, ceramics, sediments, fillers, cement, ash, toners, food products. Liquid applications include emulsions, synthetic fibers, resins, agricultural chemicals, catalysts. Research and Development or Quality Control, ASAP can analyze your material quickly, accurately and easily.

GET A FREE DEMONSTRATION—ASAP!
In your lab on your material—
or send a sample for free analysis
in our Applications Laboratory.

PACIFIC SCIENTIFIC™ HIAC HIAC INSTRUMENTS DIVISION
P.O. Box 3007, 4719 Brooks St., Montclair, Calif. 91763 Phone: (714) 621-3965
CIRCLE 168 ON READER SERVICE CARD

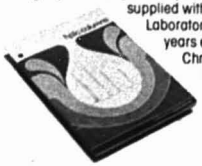
Editors' Column

larger than that for physics, which grew at a more modest rate of 18.2%. However, the physics share of the total physical sciences support remains greater than any other discipline; i.e., in 1977 the support for physics was $416 million as opposed to $203 million for chemistry.

Other notable aspects of the report are some of the concerns expressed by the funding agencies. Limited funding was viewed as one of the major barriers to the conduct of basic research. However, the emphasis was not so much on the amount of money as on fluctuations and uncertainties in the levels of funding. The situation is perhaps best illustrated by the NIH response in which the scientist of bygone days working alone with homemade equipment is contrasted with the way biomedical research is currently conducted. Biomedical science today requires a range of technical support services, complex equipment, often collaboration between a number of scientists, and frequently a great deal of time. All of this is expensive and when funding becomes unpredictable, the problem is compounded. Another major area of concern to the mission agencies is the legislative expansion of agency responsibilities without a corresponding increase in funding. This unintentionally can lead to reductions in basic research funding in order to meet operational or other requirements. For example, NBS notes that a large number of tasks have been mandated by Congress in 15 laws passed since 1965, frequently with no funds appropriated to implement them. Similarly, the U.S. Geological Survey lists 13 pieces of legislation in the last nine years that have increased its responsibilities without providing increased resources with which to meet them. Other frequently cited barriers to basic research include shifts from basic to applied research, from long- to short-term projects, and from high- to low-risk projects.

The general trends and problems noted above are probably not surprising to those experienced in Federal grantsmanship. For these the most useful aspect of the report is the detailed compilation of priority and gap areas in each individual agency. This compilation is an indispensable guide to a scientist seeking Federal support, particularly in deciding to which agency to submit a specific grant proposal and also in identifying fruitful areas of research to pursue. Copies (price $5.75, stock number 038-000-00365-8) can be ordered from the Superintendent of Documents, U.S. Government Printing Office, Washington, D.C. 20402. *Barbara Cassatt*

Now you can get pre-tested High Performance Liquid Chromatography Columns in three styles: Standard – five lengths from 5 to 50 cm and IDs from 2.1 to 20 mm . . . with more than 100 different packings. Economy – because of volume, these columns are offered at low cost for immediate delivery; and Custom-made – any packing, connection, length (to 100 cm) and ID (to 25 mm) to your specification. All pre-tested and supplied with test chromogram, report, and sample. Chrompack Laboratories are dedicated to manufacturing columns, with eight years experience in HPLC columns. Write for free catalog to Chrompack, P.O. Box 3, Middelburg, The Netherlands, or in the U.S. to P.O. Box 4131, Whittier, CA 90607.



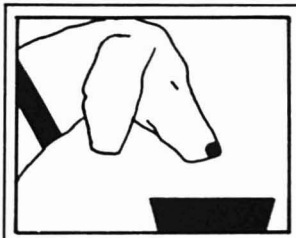
Free Catalog

Pre-Tested HPLC Columns



Chrompack U.S.A. Inc.

CIRCLE 38 ON READER SERVICE CARD



Flavor Chemistry of Animal Foods

ACS Symposium Series No. 67

Roger W. Bullard, *Editor*
U.S. Fish and Wildlife Service

A symposium sponsored by the Division of Agricultural and Food Chemistry of the American Chemical Society.

The recent revolution in animal foods has produced high quality, more palatable foods for domestic pets and food-producing animals. Now research is also being directed toward meeting the needs of threatened wildlife species as well as toward controlling their destruction of human food supplies.

Since animals cannot directly appraise food or food additives, there are many unique problems in animal flavor research that require the cooperation from specialists in many different fields. This volume covers the problems and recent advances in this field. Many domestic and non-domestic animals are discussed by specialists in organic and analytical chemistry, biochemistry, behavior, biology, nutrition, and physiology.

CONTENTS

Animal Flavor Research • Food Preference Behavior • Methodology of Behavioral Testing • Chemical Fractions from Estrus Urine • Bacterial Action and Chemical Signalling • Taste and Smell • Carnivore Taste Systems • Diets for Food-Producing Animals • Palatable Foods for Domestic Pets • Repellents to Protect Crops

175 pages (1978) clothbound $19.00
LC 77-27295 ISBN 0-8412-0404-7

SIS/American Chemical Society
1155 16th St., N.W./Wash., D.C. 20036

Please send _____ copies of *SS 67 Flavor Chemistry of Animal Foods* at $19.00 per copy.

☐ Check enclosed for $_____. ☐ Bill me.
Postpaid in U.S. and Canada, plus 75 cents elsewhere.

Name _____

Address _____

City _____ State _____ Zip _____

VWR

CHEMICAL REAGENTS

YOUR ASSURANCE OF

PURITY
QUALITY
VALUE



Acids
Salts
Solvents

- Large inventories stocked at key distribution centers
- Prompt delivery anywhere in the United States
- 24 sales/service offices nationwide

VWR CHEMICALS – WE'RE DELIVERING

VWR Scientific Inc.
subsidiary of Univar
P.O. Box 3200, San Francisco, CA 94119

CIRCLE 221 ON READER SERVICE CARD



ChromAR® HPLC Solvents
The High Performance Winners.

High-performance racing cars are a different breed from standard automobiles. So are Mallinckrodt's ChromAR HPLC solvents in comparison to others.

Mallinckrodt's Science Products Division was first to recognize that high-performance, high-pressure liquid chromatography requires specially processed solvents. Now, we offer an extensive array of ChromAR solvents to provide the wide selection of characteristics you need in your HPLC applications . . . with the uniform performance you have the right to expect:

- ChromAR solvents are rigidly controlled for low levels of water, free acid, evaporative residue, UV absorbance. Fluorescence levels are typical of those for quality reagent solvents.
- They meet a 99% GLC assay or better (and we publish the limits for all impurities).
- Filtration through a 1-micron filter helps protect against damage to high-pressure pumps and columns.
- Each ChromAR solvent is specially processed. For example, our THF and ether are both packaged under nitrogen in specially-treated light-proof containers to eliminate peroxide formation **without** adding any optically-active stabilizers. ChromAR HPLC Chloroform contains no stabilizer affecting polarity or absorbtion.
- All ChromAR solvents are guaranteed for their intended use . . . and they're available at low prices you'll find pleasing to your budget.

ChromAR solvents are conveniently available from any of the more than 300 Mallinckrodt distributors. Contact Mallinckrodt Science Products Division today for more information and the name of the distributor nearest you.

Call the: Mallinckrodt® Hot Line

(800) 325-7840

When you need something special

Mallinckrodt, Inc./Science Products Division
P.O. Box 5840/St. Louis, Missouri 63134

CIRCLE 143 ON READER SERVICE CARD

Resolution Enhancement with Multiple-Pulsed Techniques in Pulsed Fourier Transform Nuclear Magnetic Resonance Spectroscopy

Dallas L. Rabenstein
Department of Chemistry
University of Alberta
Edmonton, Alta., Canada

High resolution nuclear magnetic resonance spectroscopy is now usually performed in the pulsed Fourier transform mode (*1, 2*). A high-power radio frequency pulse of short duration is applied to the sample and causes a transient response, the free induction decay, in the time domain. The free induction decay (FID) is sampled and stored in a data acquisition system. Fourier transformation of the free induction decay gives the familiar frequency domain spectrum.

The experiment as described uses a one-pulse sequence, that is, a single radio frequency pulse is applied, followed by the acquisition of the FID. If the signal-to-noise ratio is low, signal averaging is done by repetitive application of the one-pulse sequence, with coaddition of the individual FID's. State-of-the-art NMR spectrometers also have the capability of doing experiments in which a series of rf pulses is applied to the sample prior to acquisition of the FID, generally for the purpose of measuring spin-lattice (T_1) and spin-spin (T_2) relaxation times. This article describes how these multiple-pulse techniques can also be used to enhance resolution. Two general approaches will be described. One is based on the "sorting" of resonances according to differences in their T_1's and/or T_2's, and the other is based on spin-spin coupling modulation (J modulation) of resonance intensity in the spin-echo multiple-pulse experiment.

One-Pulse Sequence

It is convenient to begin with the one-pulse sequence. Figure 1A, a representation of the one-pulse sequence, shows the pulse followed by the FID. M_t is the magnitude of the signal from the nuclear magnetization at time t.

The origin and shape of the FID can be accounted for in terms of the behavior of the nuclear magnetization in a rotating 3-axis coordinate system (frame 1 of Figure 2A). The spectrometer magnetic field H_0 is applied along the z axis, and the x' and y' axes rotate around the z axis at the carrier frequency of the spectrometer (which usually is near the Larmor frequency of the nuclei). Because the two possible orientations of the individual nuclear magnetic moments for spin one-half nuclei are of slightly different energy and because nuclei in each of these orientations are randomly distributed around the direction of H_0, the ensemble of nuclei in the sample gives rise to a residual magnetization, M_0, which is colinear with and in the direction of H_0. From this point the NMR experiment will be discussed in terms of the behavior of this residual magnetization.

Magnetization along the y' axis is detected by the spectrometer to give the NMR signal. At equilibrium, this is zero. Application of an rf pulse along x' rotates M_0 about the x' axis through an angle α given by Equation 1:

$$\alpha = \gamma H_1 t_w \qquad (1)$$

where γ is the magnetogyric ratio of the nucleus being investigated, H_1 the intensity of the rf pulse, and t_w the length of the pulse (generally in the range of microseconds). With the appropriate combination of H_1 and t_w, M_0 is rotated through 90° and becomes colinear with the y' axis, giving rise to a signal.

This is a nonequilibrium condition, and the system returns to equilibrium by two relaxation processes. The magnetization in the $x'y'$ plane relaxes by spin-spin relaxation according to

$$M_t^{x'y'} = M_0 e^{-t/T_2} \qquad (2)$$

where t is the time following the 90° pulse, while the magnetization returns to equilibrium along the z axis by spin-lattice relaxation according to

$$M_t^z = M_0 (1 - e^{-t/T_1}) \qquad (3)$$

As the magnetization returns to equilibrium, the magnitude of the signal

0003-2700/78/A350-1265$01.00/0
© 1978 American Chemical Society

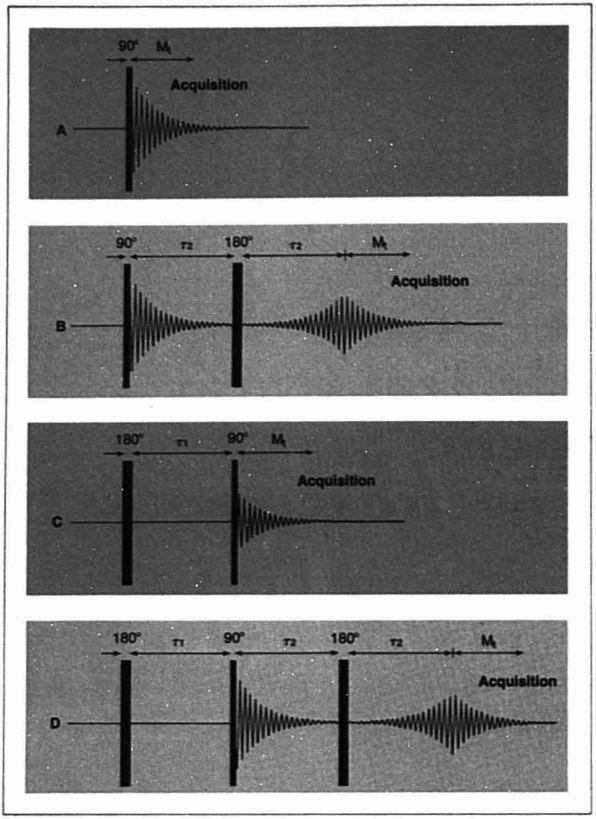


Figure 1. Representations of (A) one-pulse sequence, (B) spin-echo sequence, (C) inversion-recovery sequence, and (D) inversion-recovery-spin-echo (IRSE) sequence

decreases. At the same time the component of the magnetization along y' is modulated at a frequency equal to the difference between the Larmor frequency and the spectrometer carrier frequency. This gives rise to frequency modulation of the signal as shown in Figure 1. The FID's in Figure 1 are those for a single resonance frequency; the FID for a sample having more than one resonance is the sum of the individual FID's. Fourier transformation of the overall FID gives the frequency domain spectrum.

Spin-Echo Sequence

Generally, the major contribution to relaxation in the $x'y'$ plane is loss of phase coherence due to inhomogeneity in H_0; thus, the effective T_2, T_2', is a function of the natural T_2 and H_0 inhomogeneity. The spin-echo experiment was developed by Hahn for purposes of eliminating the effect of H_0 inhomogeneity on the measurement of T_2's (3).

The Hahn spin-echo sequence consists of a 90° pulse, a delay interval of length τ_2, a 180° pulse, and a second delay of length τ_2. The pulse sequence is represented by sequence B in Figure 1, and the behavior of the nuclear magnetization in the rotating coordinate system by sequence B in Figure 2. Following the 90° pulse, the magnetization in the $x'y'$ plane fans out due to loss of phase coherence from spin-spin relaxation and inhomogeneity in H_0. Inhomogeneity in H_0 contributes to the fanning out because nuclei in some parts of the sample precess more rapidly than the average while others precess more slowly. Following the 180° pulse, the individual vectors precess at the same rate as before so that those precessing more rapidly now catch up with the average, those precessing more slowly fall back to the average, and an echo results

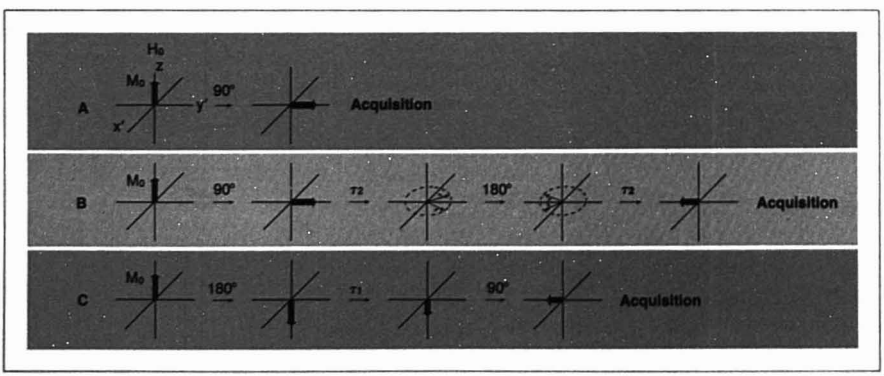


Figure 2. Behavior of nuclear magnetization during (A) one-pulse sequence, (B) spin-echo sequence, and (C) inversion-recovery sequence

The first is the world-famous Bausch & Lomb SPECTRONIC® 20 Spectrophotometer. For over twenty years, it's been a laboratory wonder, providing reliability, capability, and versatility. And it remains a favorite because it's economical.

The next four are some of the world's finest single beam instruments. We call them our Blue Line of SPECTRONIC Spectrophotometers. They give you versatility that can't be matched. And because there are four—the SPECTRONIC 70, 88, 100, and 710—you can choose from wide continuous wavelength ranges, spectral slit widths, readouts and readout modes, and a choice of sampling techniques to suit your applications perfectly.

To support our five wonders is a company with over 125 years of optical experience—Bausch & Lomb. We make more spectrophotometers than anyone else. We have manufacturing facilities in both the U.S. and Belgium, and dealer sales and service throughout the world.

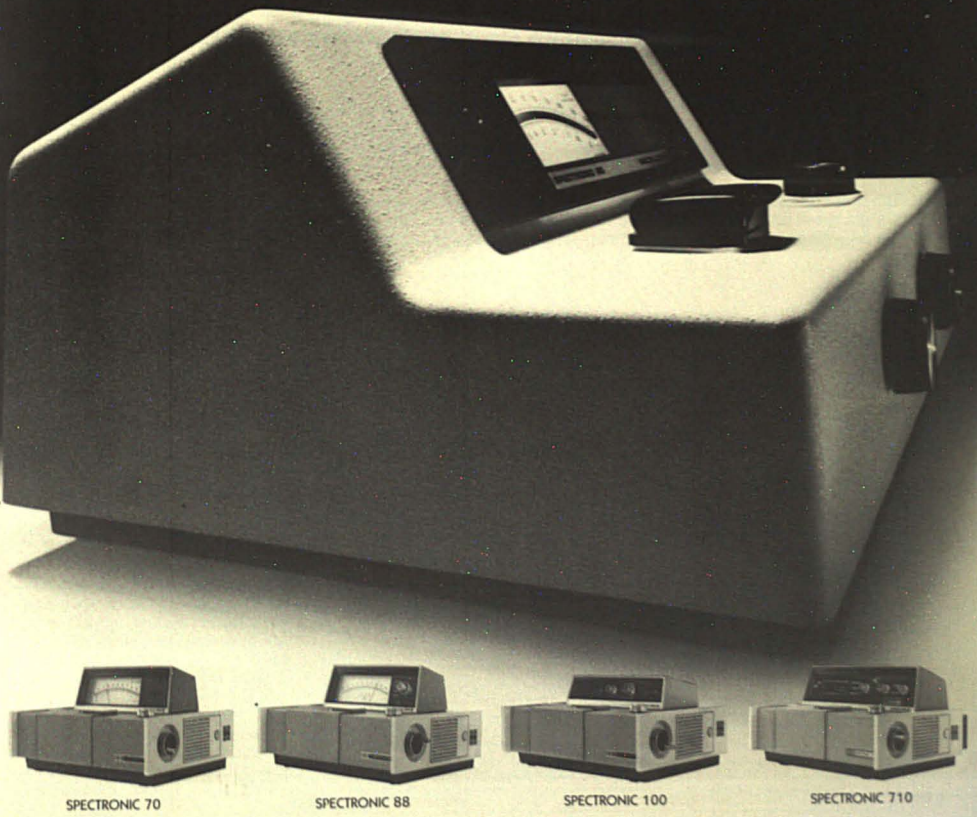
Contact your local Bausch & Lomb representative. Ask about the SPECTRONIC 20 or our Blue Line. You'll see why it's really no wonder the world keeps choosing Bausch & Lomb.

BAUSCH & LOMB

ANALYTICAL SYSTEMS DIVISION
INTERNATIONAL OPERATIONS, 820 LINDEN AVE.
ROCHESTER, NEW YORK 14625 U.S.A.

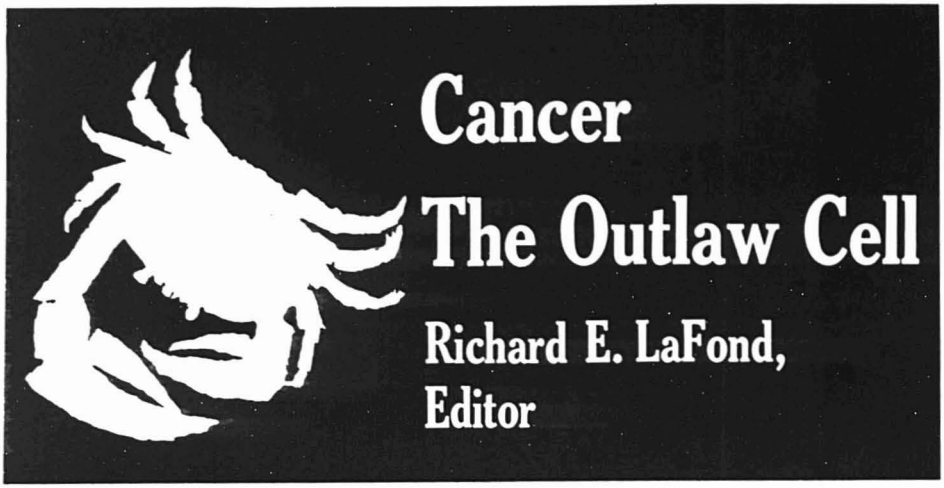
CIRCLE 19 ON READER SERVICE CARD

Five wonders of the world. By Bausch & Lomb.



SPECTRONIC 70 SPECTRONIC 88 SPECTRONIC 100 SPECTRONIC 710

European Headquarters: Bausch et Lomb France, Division Instruments, 7 rue des Chantiers, 78000 Versailles, France; Bausch & Lomb Belgium, N.V., Rochesterlaan 6, 8240 Gistel, Belgium; Bausch & Lomb GmbH, Analytical Systems Division, Munchener Strasse 72, 8043 Unterfohring, Germany



An estimated 390,000 Americans will die of cancer this year alone and one out of every four will develop some form of this dread disease within their lifetime.

Statistics such as these show the need for a book that will explain our current state of the art in cancer research using simple, straightforward, non-medical language. *Cancer — The Outlaw Cell* successfully fulfills this need by making the latest advances in cancer research available to the general public in a clear, non-technical style that can be read and understood by both the professional scientist and non-scientist.

Written by leading experts at the forefront of their specialties and profusely illustrated in color, this collection of articles covers the great strides that have been made in understanding the causes of cancer, how this disease is spread, cancer as a biochemical problem, and non-surgical modes of therapy.

CONTENTS

Cancer — An Overview, *Henry C. Pitot*
Tumor Growth and Spread, *Isaiah J. Fidler and Margaret L. Kripke*
Control of Cell Growth in Cancer, *Arthur B. Pardee and David S. Schneider*
Cancer as a Problem in Development, *Armin C. Braun*
Puzzling Role of Cell Surfaces, *David I. Meyer and Max M. Burger*
Cancer-Causing Chemicals, *Elizabeth K. Weisburger*
Cancer-Causing Radiation, *Robert L. Ullrich, J. Michael Holland and John B. Storer*
Cancer and Viruses, *Arnold J. Levine*
RNA Tumor Viruses, *Robert D. Cardiff*
Herpesviruses — A Link in the Cancer Chain, *Ariel C. Hollinshead and William A. Knaus*
Cancer and The Immune Response, *John L. Fahey*
Immunotherapy of Human Cancer, *Larry A. Schafer and Evan M. Hersh*
Radiation Therapy, *Diana F. Nelson and Philip Rubin*
Chemotherapy of Cancer, *Joseph H. Burchenal and Joan R. Burchenal*

192 pages (1978) clothbound $15.00
LC 78-2100 ISBN 0-8412-0405-5

192 pages (1978) paperback $8.50
LC 78-2100 ISBN 0-8412-0431-4

SIS/American Chemical Society/1155 16th St., N.W./Wash., D.C. 20036

Please send _____ copies of *Cancer—The Outlaw Cell.*

☐ cloth $15.00 (ACK 0405-5) ☐ paper $8.50 (ACK 0431-4) ☐ Check enclosed for $_____. ☐ Bill me.
Postpaid in U.S. and Canada, plus 75 cents elsewhere.

Name _____

Address _____

City _____ State _____ Zip _____

along the y' axis. The echo maximum is at time $2\tau_2$ after the 90° pulse. With this pulse sequence, effects due to H_0 inhomogeneity on T_2' are self-eliminating so that the net loss in magnetization at the echo maximum is due only to the natural spin-spin relaxation.

The second half of the echo is also a free induction decay and differs from that following the 90° pulse only in amplitude, due to the spin-spin relaxation which has occurred during the interval $2\tau_2$ (*4*). If the spectrum consists of a number of resonances that have different T_2's, the decrease in amplitude at the echo maximum will be different for the different resonances with a relative enhancement of signals from those resonances with the longer T_2's. For example, the magnetization at the echo maximum is 0.819 M_0, 0.368 M_0, 0.135 M_0, and 0.018 M_0 for T_2 values of $10\tau_2$, $2\tau_2$, τ_2, and $\tau_2/2$, respectively. If the T_2's of the different resonances are sufficiently different and τ_2 is properly chosen, the magnetization in the $x'y'$ plane from the resonances with the shorter T_2's will have relaxed to zero at time $2\tau_2$, so that only those resonances having the longer T_2's will be observed in the spectrum obtained by Fourier transformation of the second half of the echo (*5*).

Resolution enhancement by the Hahn spin-echo sequence is illustrated in Figure 3 by the proton NMR spectra for a solution containing bovine serum albumin (BSA) and *N*-methylglycine. The top spectrum was obtained with the one-pulse sequence. The broad, rather featureless peaks are due to the protons of the BSA with the *N*-methylglycine giving the two singlets superimposed at 2.84 and 3.72 ppm. The bottom spectrum was obtained from the second half of the echo in a Hahn spin-echo sequence with τ_2 = 0.060 s. The T_2's of the protein resonances are so short that by 0.120 s after the 90° pulse, their magnetization has decayed to zero in the $x'y'$ plane, leaving the spectrum for the *N*-methylglycine. The signal centered around 4.80 ppm is the residual signal from the HDO solvent, most of which has been eliminated by the presaturation technique (*6*).

Our recent work on human red blood cells provides another example of an application of the Hahn spin-echo sequence for resolution enhancement (*7*). Spectrum A in Figure 4 is the normal one-pulse spectrum and is due mainly to resonances from hemoglobin. Spectra B and C are spin-echo spectra obtained with τ_2's of 0.020 and 0.060 s, respectively. Because hemoglobin is a large molecule, the T_2's of most of its resonances are short. As Figure 4 shows, the hemoglobin signals disappear as τ_2 is increased

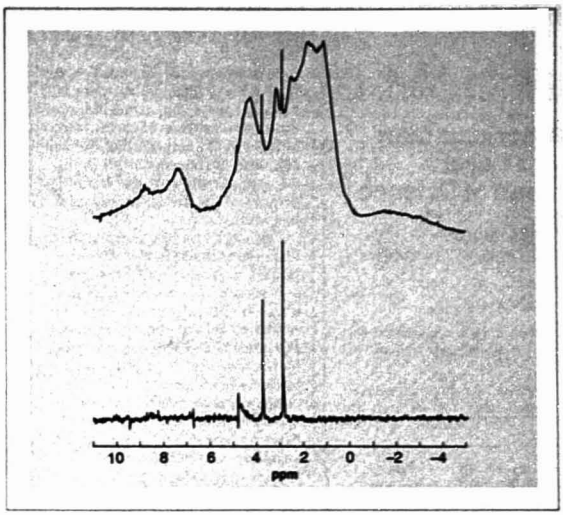


Figure 3. 100-MHz proton NMR spectra of D_2O solution containing 0.003 *M* bovine serum albumin and 0.003 *M N*-methylglycine

Top spectrum obtained with one-pulse sequence; bottom spectrum obtained with spin-echo sequence using τ_2 of 0.060 s

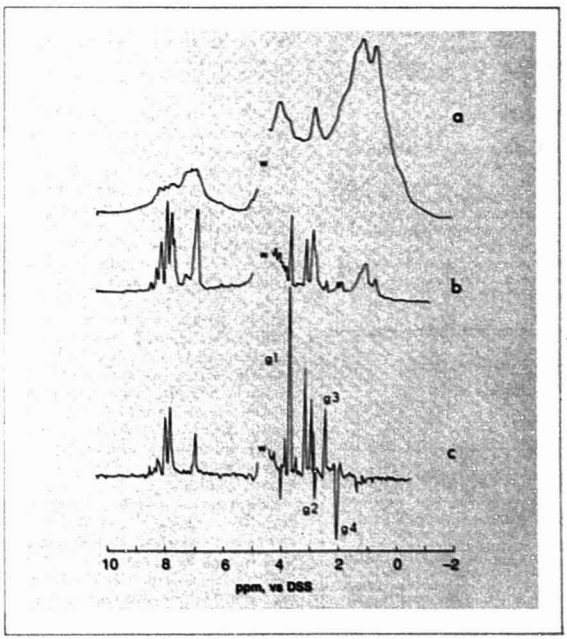


Figure 4. 270-MHz proton NMR spectra of human red blood cells washed with isotonic saline in D_2O (*7*)

Spectrum a, normal pulsed Fourier transform spectrum; b, spin-echo spectrum using τ_2 of 0.020 s; c, spin-echo spectrum with τ_2 = 0.060 s

Reprinted with permission from ref. 7. Copyright 1977 Federation of European Biochemical Society

American Men And Women of Science

Now Available — Volumes Organized by Subject

Now you can have . . .

- resource tools to help you find the best personnel prospects in a technical specialty.
- quick references for finding acknowledged professionals for lectures, for securing expert witness, and for consulting.
- ready access to your colleagues in hundreds of specific scientific areas.

CHEMISTRY

This new discipline directory contains biographical sketches of 29,689 currently active American and Canadian scientists. The alphabetically arranged listings are also drawn from the 13th edition of *American Men and Women of Science*, and each provides full biographical and professional information. Disciplinary and geographic indexes are furnished.
ISBN 0-8352-1011-1. $45.00

CONSULTANTS

This new directory makes it easy for you to locate scientists with consulting experience included in the 13th edition of *American Men and Women of Science*. 15,447 biographical sketches from the base volumes are arranged alphabetically, with full biographical and professional information for each. Disciplinary and geographic indexes are included.
ISBN 0-8352-1017-0. $35.00

SEND YOUR ORDER TO:
R.R. Bowker Dept. MM
P.O. Box 1807
Ann Arbor, Michigan 48106

Name_____

Address_____

City_____

State/Zip_____

SATISFACTION GUARANTEED! Individuals must pre-pay or include purchase order. Books in salable condition may be returned for any reason within 14 days of receipt for full refund. Prices are subject to change and slightly higher outside the U.S. and possessions. Outside Western Hemisphere: Order from Bowker, Erasmus House, Epping, Essex, England.

in the spin-echo experiment. At a τ_2 of 0.060 s, the majority of the spectrum consists of resonances from protons having relatively long T_2's, mainly protons of the smaller, more mobile components of the intracellular medium as well as those of certain structural units of the hemoglobin. For example, most of the resonances in the 6.5–9 ppm region are due to imidazole protons of the histidyl residues of hemoglobin.

Our work on red blood cells follows from our interest in glutathione (GSH), a tripeptide of the sequence γ-L-glutamyl-L-cysteinyl-glycine, which is naturally present in human red blood cells at the 2–3-m*M* level. For some time I have been intrigued by the idea that it might be possible to study GSH directly in red blood cells by proton NMR spectroscopy. As shown by spectrum A in Figure 4, however, the one-pulse spectrum is an envelope of overlapping resonances. Fortunately, GSH is among the small red cell molecules whose resonances can be resolved by the Hahn spin-echo sequence. Resonance g1 in spectrum C is due to the methylene protons of the glycine residue of GSH, resonance g2 those of the cysteinyl residue, and resonances g3 and g4 are due to those of the glutamyl residue.

With the Hahn spin-echo technique, it has been possible to study intracellular processes involving GSH directly (*7*). For example, one function of the GSH in the red cell is to protect the cellular membrane and components from oxidizing species such as hydroperoxides. In doing so, the sulfhydryl group of GSH is oxidized to the disulfide form (GSSG), with the oxidation catalyzed by glutathione peroxidase. When the GSH is oxidized, the chemical shift of resonance g2 changes. Using the specificity of the enzyme-catalyzed conversion of GSH to its oxidized form and the intensity of resonance g2, we have followed by NMR the selective titration of the intracellular GSH with *t*-butyl hydroperoxide. Then after complete conversion to GSSG, glucose was added, and the time course for the enzymatic conversion back to GSH was obtained while simultaneously obtaining the time course for the metabolism of glucose to lactic acid.

The Hahn sequence is the simplest of the spin-echo sequences. Others (for example, the Carr-Purcell and the Carr-Purcell-Meiboom-Gill sequences) use a series of 180° refocusing pulses (*1*). These sequences must be used when the magnitude of τ_2 in the Hahn sequence becomes so large that molecules have time to diffuse to different regions of H_0; thus, the effects of H_0 inhomogeneity on T_2^* are no longer reversible.

Resolution enhancement with the spin-echo sequence is based on selective loss of signals from resonances having the shorter T_2's. To some extent, similar effects can be achieved with the one-pulse sequence by using digital filtering (convolution) techniques (*8–10*) or by introducing a delay time between the end of the pulse and the start of data collection (*11*). These techniques take advantage of the differential rates of decay of signals in the FID due to differences in T_2's.

Inversion-Recovery Sequence

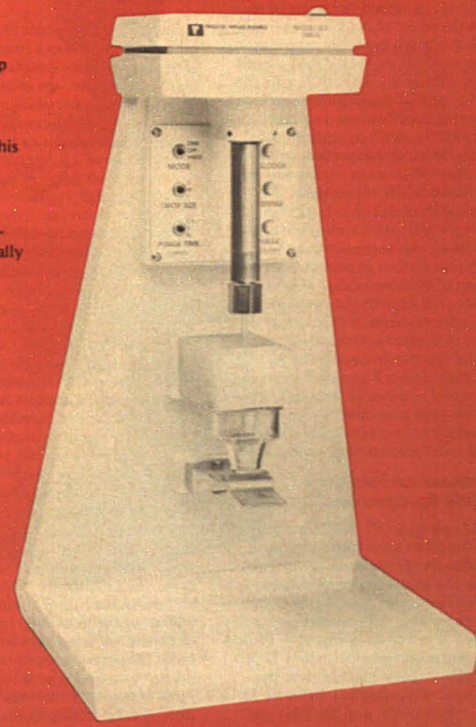
The inversion-recovery sequence is a standard sequence for measuring T_1 values, but it also can be used to enhance resolution by taking advantage of any differences in the T_1's of overlapping resonances. The inversion-recovery sequence (sequence C in Figure 1) consists of a 180° pulse followed by a time interval of length τ_1 and then a 90° pulse. The 180° pulse inverts the magnetization along the z axis (sequence C in Figure 2), so that immediately following the 180° pulse, the magnetization is of magnitude M_0 but in the negative z direction. As time passes, magnetization along the negative z axis decreases, passes through zero, and then grows toward its equilibrium value by spin-lattice relaxation. Application of the 90° pulse when the magnetization is in these three states results in a negative resonance, no resonance, and a positive resonance, respectively, in the frequency domain spectrum. The magnitude of the magnetization along the z axis at time τ_1 following the 180° pulse is given by $M_0(1 - 2\,e^{-\tau_1/T_1})$, according to which the magnetization for a given resonance passes through a null at $\tau_1 = 0.69\ T_1$. Thus, by careful choice of the time at which the 90° sampling pulse is applied, one can selectively null resonances in overlapping patterns on the basis of differences in their T_1's.

The selective elimination of the residual HDO peak in NMR spectra of D_2O solutions by applying the 90° pulse at $\tau_1 = 0.69\ T_{1,\mathrm{HDO}}$ was one of the first applications of the inversion-recovery sequence in this way (*12*). This technique, termed the water-eliminated-Fourier-transform (WEFT) technique, can be used to observe resonances under the HDO resonance if the T_1's of the HDO resonance and the resonance of interest are different, and to solve the dynamic range problem encountered in pulsed Fourier transform NMR of dilute solutions in D_2O. An inherent disadvantage in the latter application is that the magnetization for the resonances of interest is most likely less than M_0 at the time the 90° pulse is applied due to incomplete relaxation. Thus, the signal strength in the inversion-

Introducing The Model 303 Static Mercury Drop Electrode Module...

See what you've been missing!

- Higher Sensitivity
- Greater Convenience
- Lower Cost



• HIGHER SENSITIVITY

The name of the game! The new 303 Static Mercury Drop Electrode Module gets you down to concentration levels that you were probably only guessing at before. With the 303 electrode, baseline distortions at ppb concentrations are drastically lowered and drop sizes are much larger. This means you'll get improved detection limits for both differential pulse polarography and stripping voltammetry (using the same static drop).

Hang in there! You get higher sensitivity with the 303 because each mercury droplet, rather than growing continually as in the conventional approach, is caused to remain stationary at the optimum size over the course of each current measurement. This is a great way to overcome the baseline distortion caused by the differential capacitance curve.

And talk about simplicity! There's no assembly required of the operator. Simply fill the reservoir with mercury and start running your analyses. A single moving part within the 303 Module controls the extrusion of each mercury drop.

• GREATER CONVENIENCE

Simple switchover! Use the Model 303 for either polarography or stripping voltammetry. Convert from one mode to the other by flipping a single panel switch. No other adjustments are necessary since the same capillary serves both techniques. And you'll appreciate the additional controls for purge, purge times, drop size, drop extrusion and drop dislodge.

• LOWER COST

Now that's progress! The Model 303 costs less than the two previous electrode assemblies you needed for doing polarography and stripping voltammetry. The 303 Module includes the mercury electrode, reference and counter electrodes, purge tube, cell bottoms, electronics package and a sturdy support stand.

For more information, contact EG&G PRINCETON APPLIED RESEARCH, P. O. Box 2565, Princeton, NJ 08540; or phone 609/452-2111.

EG&G PRINCETON APPLIED RESEARCH

For additional information only Circle #169.

recovery experiment is less than that in the one-pulse experiment, and more signal averaging is required. Use of the inversion-recovery sequence to enhance resolution in protein NMR spectra has also been described (5).

Inversion-Recovery-Spin-Echo (IRSE) Sequence

The IRSE sequence is a combination of the inversion-recovery sequence and the spin-echo sequence. The sequence is 180°-τ_1-90°-τ_2-180°-τ_2-acquisition (sequence D in Figure 1). Following the first 180° pulse, which inverts M_0 along the z axis, the magnetization is allowed to relax back toward its equilibrium value for a time τ_1. The magnetization is then sampled by applying a 90° pulse, but acquisition of a FID is delayed for a period $2\tau_2$ to achieve resolution enhancement by the selective relaxation of those resonances having the shorter T_2's. As in the Hahn sequence, the 180° pulse separating the two time intervals of length τ_2 is a refocusing pulse to reverse the effect of H_0 inhomogeneity. With this pulse sequence, overlapping resonances can be sorted first according to differences in their T_1's by the 180°-τ_1 part of the sequence, and then according to differences in their T_2's by the 90°-τ_2-180°-τ_2 part of the sequence. With this sequence, we then have three resolution parameters in the pulsed NMR experiment: the chemical shift and spin-lattice and spin-spin relaxation times. We have been using this sequence to enhance resolution further in proton NMR studies of red blood cells. This sequence also permits the measurement of T_1's for resonances from small molecules in protein solutions, e.g., the T_1's for the two resonances of *N*-methylglycine in Figure 3, by variation of τ_1 while τ_2 is held constant. In this way, we have measured T_1 for the methylene protons of GSH in red blood cells (resonance g1 in Figure 4).

2-Dimensional Spin-Echo FT NMR Spectroscopy

2-D spin-echo FT NMR spectroscopy is based on spin-spin coupling modulation (*4*) of resonance intensities in the spin-echo experiment (*13, 14*). To illustrate, proton spin-echo spectra for alanylglycine are shown for a series of τ_2 values in Figure 5. Mutual coupling between CH_3 and CH protons of the alanyl residue gives the doublet and quartet at 1.54 and 4.12 ppm, respectively, and the CH_2 protons of the glycine residue give the AB pattern at 3.80 ppm. The lines in the individual patterns are phase modulated as τ_2 is varied, at frequencies determined by the nature of the multiplet patterns and the spin coupling constants. For example, the two components in a first-order doublet are phase modulated at a frequency of $J/2$, the outer two components of a first-order triplet are phase modulated at a frequency of J whereas the central component does not change phase, and the outer and inner two components of a first order quartet are phase modulated at frequencies of $3J/2$ and $J/2$, respectively. Modulation of the individual lines in second-order multiplet patterns is a more complex function of J.

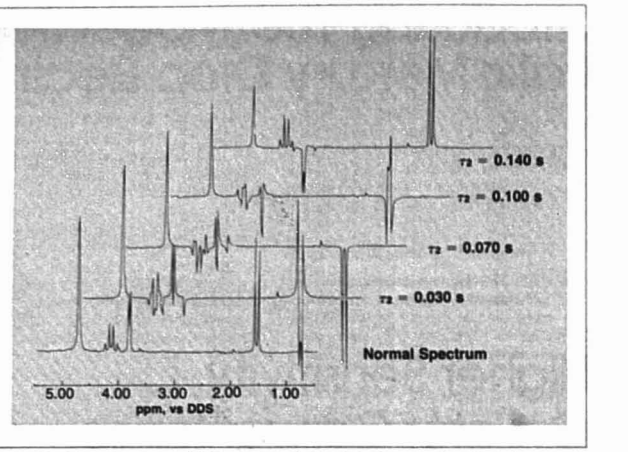


Figure 5. Spin-echo proton NMR spectra of alanylglycine as a function of τ_2

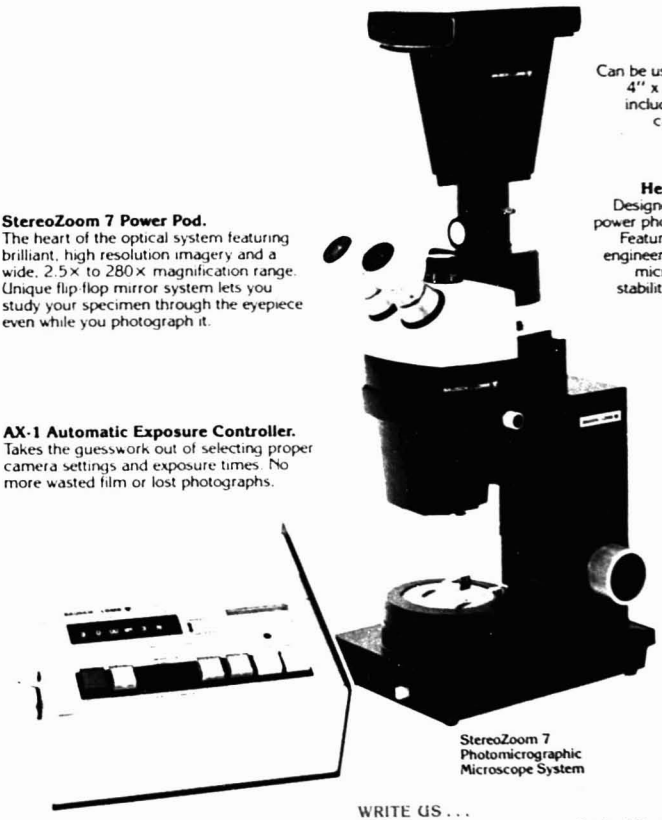
The phase modulation of resonance intensity is due to the fact that the spin states of protons coupled to the protons giving the multiplet pattern are different during the two delay periods. Consider, for example, the two lines of the methyl doublet in Figure 5. In this case, a doublet is observed because of the two possible orientations of the methine proton relative to H_0. Following the 90° pulse, the magnetization from each of the lines of the doublet is colinear with the y' axis. For convenience, assume the spectrometer carrier frequency to be equal to the frequency midway between the two lines so that, during the delay period immediately after the 90° pulse, the higher frequency component of the doublet is moving ahead of the carrier frequency while the lower frequency component falls behind. At time τ_2, a broadband 180° pulse is applied to reverse the orientation of the methyl protons. Because it is a broad band pulse, however, it simultaneously reverses the orientation of the methine proton. Thus, those methyl protons that were originally coupled to a methine proton of the orientation which gives rise to the faster rotating component of the doublet now are coupled to a proton of the opposite orientation. Thus, the magnetization from this component precesses more slowly during the second delay period and, consequently, does not refocus at time $2\tau_2$ as happens with fanning out due to H_0 inhomogeneity in sequence B, Figure 2. Likewise, the slower precessing component will be out of phase with the carrier frequency at time $2\tau_2$, giving rise to the phase modulation in Figure 5.

In 2-dimensional spin-echo FT NMR, FID's are obtained from spin-echo experiments at a series of closely spaced τ_2 values, and each is Fourier transformed to give spectra of the type shown in Figure 5. The data from the series of spin-echo spectra are then rearranged to give the amplitude as a function of τ_2 at particular frequencies over the chemical shift region of interest. The amplitude in the "echo interferogram" at a particular chemical shift is modulated at frequencies determined by the nature of the resonance patterns at that particular chemical shift. Thus, Fourier transformation of the echo interferogram separates overlapping resonances in the J dimension according to their modulation frequency.

To illustrate, Figure 6 shows the 1.5–2.1 ppm region of the 2-D proton NMR spectrum of α-santonin, a polycyclic lactone natural product. F_1 and F_2 represent the J dimension and the chemical shift dimension, respectively. Projection of the individual spectra onto the F_2 axis gives the conventional NMR spectrum, as shown by the top spectrum in Figure 7. Projection onto the F_1 axis gives rise to J spectra. The individual components of a given multiplet appear at frequencies in the F_1

THINK BAUSCH & LOMB

...when your research demands the total package of precision components for lifelike stereoscopic viewing and photomicrographic documentation.



Choice of Camera Attachments.
Can be used with 3¼" x 4¼" x 4" x 5" or 35mm formats, including almost every SLR camera available today.

Heavy-Duty "R" Stand.
Designed specifically for high power photomicrographic work. Features the same advanced engineering of the BALPLAN™ microscope stand for total stability and precise focusing action.

StereoZoom 7 Power Pod.
The heart of the optical system featuring brilliant, high resolution imagery and a wide, 2.5× to 280× magnification range. Unique flip-flop mirror system lets you study your specimen through the eyepiece even while you photograph it.

AX-1 Automatic Exposure Controller.
Takes the guesswork out of selecting proper camera settings and exposure times. No more wasted film or lost photographs.

StereoZoom 7
Photomicrographic
Microscope System

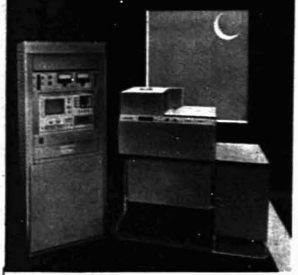
WRITE US . . .
and ask for a demonstration or complete information. Or call your nearest authorized Bausch & Lomb dealer. Consult the Yellow Pages under "Microscopes".

ROCHESTER, NEW YORK 14602 USA, 716-338-6000, TWX 510-253-6189, TELEX 97-8231, CABLE: BAUSCH & LOMB

BAUSCH & LOMB
Scientific Optical Products Division

CIRCLE 22 ON READER SERVICE CARD

This X-ray analyzer works all night alone



And tackles rush jobs the next day

Owning a SPECTRACE 440 is much like having two X-ray fluorescence analyzers. One, fully automatic, does routine tasks unattended while you sleep. Another is versatile, adaptable and always available to get urgent, non-routine tasks done on time.

SPECTRACE 440 makes energy-dispersive qualitative and quantitative analyses of all elements from Na to Pu. Handles samples from 1 mm in diameter to 1 foot high. Gives you a choice of three types of excitation: Bremsstrahlung, transmission target and secondary target. Excites up to 40 samples on a single tray—solids, liquids, powders or deposits on filter paper. Automatically indexes the sample tray and selects tube voltage, tube current, and the programmed transmission filters or secondary targets.

Sensitivity, repeatability and long-term stability are superb. So is long-term dependability. Some users have now run over 10,000 samples.

The compact SPECTRACE 440 is easy to install. Just plug into any ordinary AC outlet. No water cooling required.

Send for our 16-page well-illustrated brochure. Contact United Scientific Corporation, Nuclear Semiconductor Division, Dept. B, 1400 Stierlin Road, P.O. Box 1389, Mt. View, Calif., 94042. Phone: (415) 969-4646.

US UNITED SCIENTIFIC
NUCLEAR SEMICONDUCTOR DIVISION

CIRCLE 208 ON READER SERVICE CARD

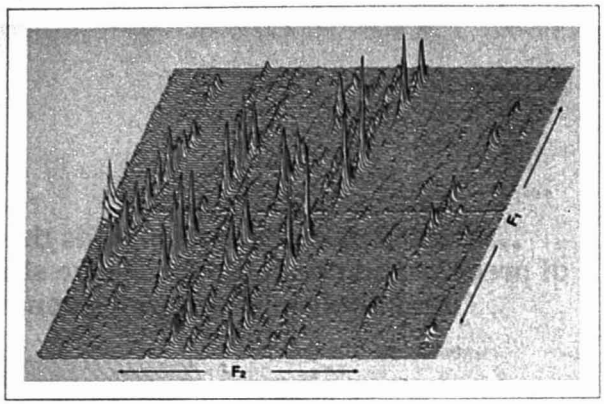


Figure 6. 1.5–2.1 ppm region of 2-D spin-echo FT NMR spectrum of α-santonin
F_1 and F_2 are J and chemical shift dimensions, respectively

and F_2 dimensions such that the individual lines of a given multiplet are overlapping for a projection at an angle of 45° relative to F_1 and F_2. For example, the bottom spectrum in Figure 7 is obtained from the projection of the intensities in Figure 6 onto an axis at an angle of 45° relative to F_1 and F_2. The important result is that single lines are obtained for the chemically shifted protons rather than the multiplet patterns in the normal spectrum.

Figure 8 shows the methyl region of the 2-D proton NMR spectrum of glycylvaline. The regular proton NMR

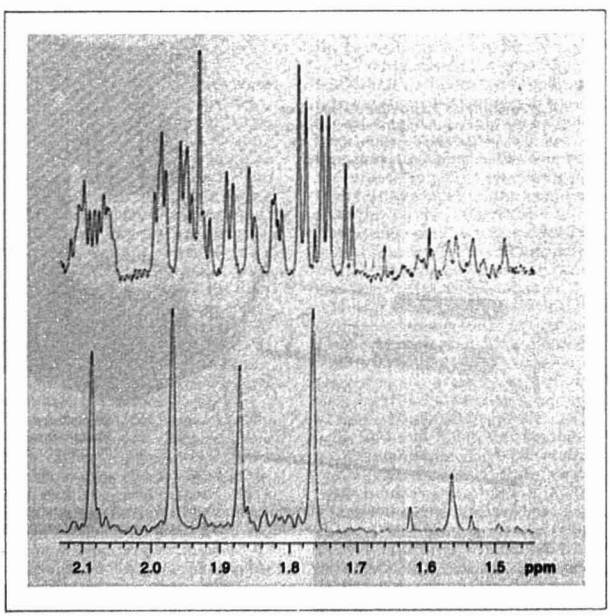


Figure 7. Spectra obtained by projection of 2-D spectrum of α-santonin onto chemical shift axis (top) and at angle of 45° relative to J and chemical shift axes (bottom)

WHICH SIM RECORD WOULD YOU BELIEVE?

The task . . . . . Identify and quantify—*unambiguously*—a vasodilator in plasma extract using SIM GC/MS. Concentration: 1 ppm

The problem . . . . Interfering compounds at the same nominal mass

The solution . . . . Increased Mass Spectrometer Resolution, with the KRATOS MS25S

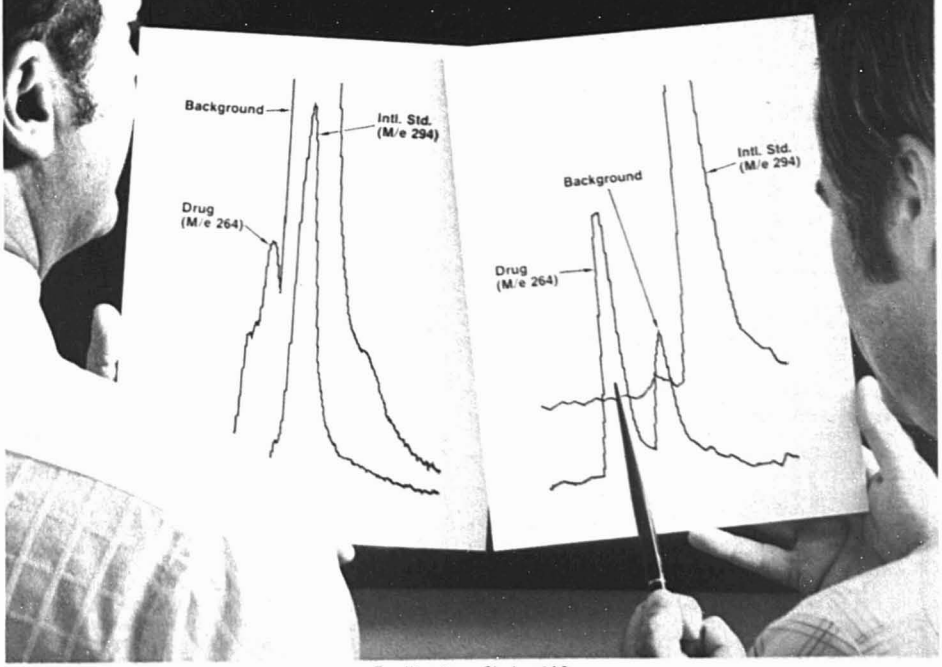
Note the tremendous improvement in specificity for the drug measurement by increasing resolution from 1200* (on the left) to 10,000* (on the right). The signal is totally resolved from background, giving credibility to the identification and quantification of the compound.

Tired of fighting your quadrupole for answers that are just out of reach? The KRATOS MS25S routinely delivers superior performance at a price you can afford. Let us show you how it can give you all the data you need.

*Half-height definition

KRATOS, INC.
8322 Clairemont Mesa Blvd.
San Diego, CA 92111
Telephone (714) 292-0925

KRATOS, LTD.
Barton Dock Road, Urmston
Manchester, England M31 2LD
Telephone 061-865-4466



For literature, Circle #116.
For salesman to call, Circle #117.

Read on...

...the Series 8000 Intelligent Recorders



The intelligent approach to data management.

Ideal for analytical instrumentation, process control, and as computer peripherals.

Features multichannel data acquisition, permanent, compact storage on magnetic disk, and microprocessor-based data processing, all for only $5450.

...Battery testing in development and manufacturing



Convenient and accurate data acquisition, processing and display.

With the Series 8000, multiple cell parameters are monitored simultaneously, data are conveniently stored for easy comparison of charge/discharge cycles, and amp-hr capacities are directly determined.

...Analytical Instrumentation



A better way to manage data.

For LC, TGA, IR, UV, Fluorescence, the intelligent recorder offers accurate qualitative and quantitative analysis, direct integration, differentiation, and baseline correction.

For your free copies of these new brochures, write:

Bascom-Turner Instruments

111 Chapel Street, Newton, MA 02158
800-225-3298,(In Mass.)617-965-2710

CIRCLE 17 ON READER SERVICE CARD

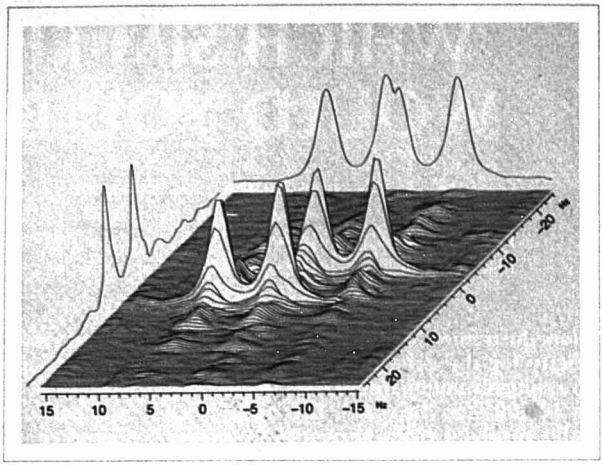


Figure 8. Methyl region of 2-D spin-echo FT NMR spectrum of glycylvaline, and spectra obtained by projection onto chemical shift axis (top) and at angle of 45° relative to J and chemical axes (side)

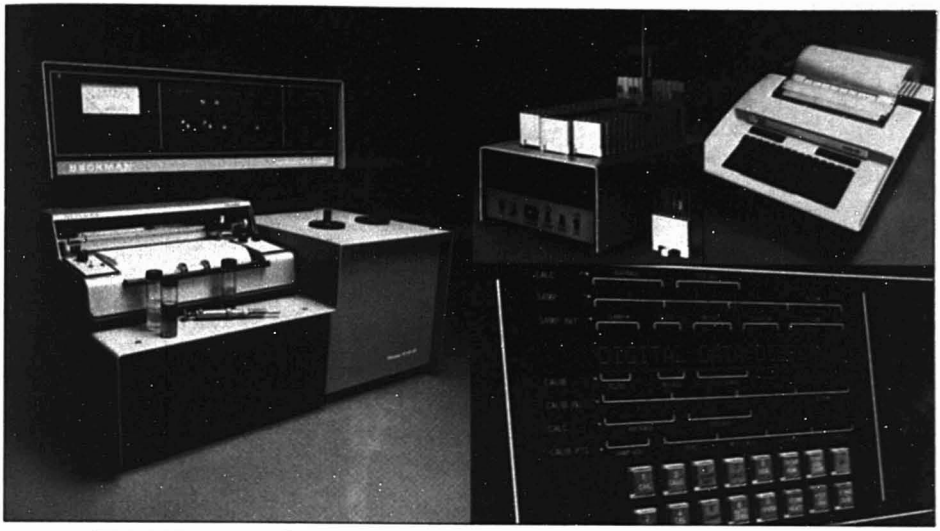
spectrum obtained by projection onto the chemical shift dimension is shown behind the 2-D spectrum, and the single line spectrum obtained from a 45° projection is shown to the left. The regular spectrum consists of two partially overlapping doublets, with the doublet structure due to coupling to the methine proton between the two methyl groups. The phase modulation in the spin-echo experiment is different for the two overlapping resonances; thus, they are resolved in the 2-D spectrum.

As discussed above, the two-dimensional NMR experiment is based on phase modulation due to different precessional frequencies during the two delay periods in the spin-echo sequence. In proton NMR the precessional frequencies are different because the broadband 180° pulse changes all the spin states of mutually coupled nuclei. In the usual ^{13}C spin-echo experiment using broadband proton decoupling, the precessional frequencies of the ^{13}C nuclei are the same during both delay periods. The necessary difference in precessional frequencies for 2-D spin-echo NMR can be achieved by several methods, including the "proton-flip" method, in which a broadband 180° pulse on the ^1H resonances is applied simultaneously with the 180° ^{13}C pulse but the ^1H decoupler is off during the two delay periods, and the "gated-decoupler" technique in which the broadband ^1H decoupler is on during only one of the two delay periods (*13, 15*). In both techniques the ^1H decoupler can be off or on during acquisition of the FID and give ^1H-coupled and ^1H-decoupled two-dimensional ^{13}C spectra, respectively. Overlapping lines in the normal ^1H-decoupled ^{13}C spectrum will be pulled apart in the two-dimensional spectrum according to differences in the nature of their ^1H-coupled multiplets.

Two-dimensional FT NMR spectroscopy is a recent development, and the reader is referred to the rather extensive paper by Freeman and coworkers (*13*).

Summary

A number of techniques based on multiple-pulse sequences are now available for resolution enhancement in NMR spectroscopy. Those based on differences in T_1's and T_2's take advantage of differences in the rates of relaxation processes, whereas the 2-D spin-echo FT NMR technique takes advantage of spin-spin coupling modulation of resonance intensities. These techniques are possible only in the pulsed FT mode of spectrometer operation. Most state-of-the-art spectrometers are equipped to do the multiple-pulse sequences, which give resolution enhancement based on differences in relaxation rates. However, the 2-D FT NMR experiment requires extensive computer memory for data acquisition and manipulation, and rather elaborate software which is now available from some of the instrument manufacturers. These resolution enhancement methods can be expected to extend considerably the range of applications of NMR spectroscopy; for example, they have provided us



BUY NOW. GROW LATER.

Beckman introduces microprocessor-controlled Total Organic Carbon Analyzer.

Here's the TOC Analyzer that meets your needs today and tomorrow.

Today. The 915-B provides 2-3 minute analysis in ranges of 0-1 ppm up to 0-4000 ppm with repeatability ±2% of full scale over 5 ppm; ±5% of full scale at 5 ppm and below. An integral microprocessor provides temperature control, over-temperature protection, temperature display and fast warm-up for the standard TC combustion furnace and the optional IC combustion furnace. Other features include high solids sample handling capacity, choice of IC removal methods and a simplified vertical sample injection system that reduces catalyst recharge time and frequency by up to 75%.

Tomorrow. Today's 915-B will grow with your needs, adding functional modules and a digital display for TOC and temperature readout. The microprocessor will be used for calibration, linearization, peak picking and averaging, scaling, auto-zero, channel correlation and service diagnostic checks.

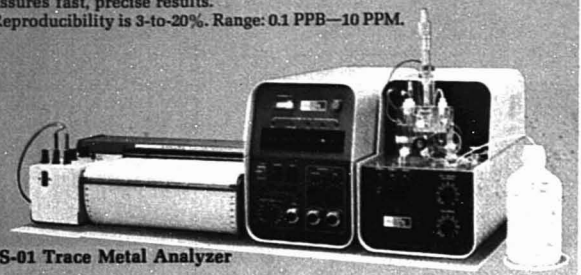
The Beckman 915-B is successor to the 915—field-proven for more than 15 years. It incorporates the same precision and dependability demonstrated by the 915 in more than 2,000 installations worldwide. It makes possible new standards of accuracy and speed in such applications as measurement of wastewater effluents, detection of heat exchanger leaks, monitoring of evaporative processes, analysis of potable water supplies, and determination of waste treatment efficiency. For further information contact Process Instruments Division, Beckman Instruments, Inc., 2500 N. Harbor Boulevard, Fullerton, CA 92634.

BECKMAN®

CIRCLE 13 ON READER SERVICE CARD

Reliable. Fast and Easy. MCI automatic analyzer.

Utilizes ASV method to simultaneously measure concentrations of 5 different trace heavy metals. Ultra-high sensitivity and automatic sample feed/discharge measuring cell assures fast, precise results.
Reproducibility is 3-to-20%. Range: 0.1 PPB—10 PPM.



AS-01 Trace Metal Analyzer

MITSUBISHI CHEMICAL INDUSTRIES LIMITED
Instruments Dept., Mitsubishi Bldg., 5-2, Marunouchi 2-chome, Chiyoda-ku, Tokyo, 100 Japan Telex: J24901 Cable Address: KASEICO TOKYO

CIRCLE 136 ON READER SERVICE CARD

At last— a disposable filter so good, it can sterilize air— so economical, you won't mind replacing it!



Balston's new Microfibre® Disposable Filter Unit gives you truly high efficiency filtration—to the sterile level in gases, and 98% retention of 0.3 micron particles in liquids—combined with the convenience of complete disposability. It's ideal for

- sterilizing air and other gases—autoclavable
- filtration of samples to analyzers
- complete removal of oil, dirt and water from air and gases to 125 psig
- filtration of small quantities of liquids with minimum hold-up and no cross-contamination

All this at a price of only about $4.00 each.
For more detailed information, use the Reader Service Card. For a FREE SAMPLE, write on your letterhead, describing your application. Address Dept. AC-17.



BALSTON, INC.
P.O. Box C, 703 Massachusetts Ave.
Lexington, Massachusetts 02173
(617) 861-7240 · (617) 862-7455
Telex 92-3481

CIRCLE 26 ON READER SERVICE CARD

with a small window through which we now can observe some of the processes that take place in red blood cells.

Acknowledgment

It is a pleasure to acknowledge numerous discussions about the techniques described in this article with Tom Nakashima and Glen Bigam. Some of the red blood cell work was done while on sabbatical leave at Oxford, and received considerable stimulation from a lecture given by R.J.P. Williams at a meeting of the Chemical Society. The spectra in Figures 6–8 were provided by Nicolet Technology Corp., Mountain View, Calif. 94041.

References

(1) T. C. Farrar and E. D. Becker, "Pulse and Fourier Transform NMR", Academic Press, New York, N.Y., 1971.
(2) D. Shaw, "Fourier Transform NMR Spectroscopy", Elsevier, New York, N.Y., 1976.
(3) E. L. Hahn, *Phys. Rev.*, **80**, 580 (1950).
(4) R. Freeman and H.D.W. Hill, in "Dynamic Nuclear Magnetic Resonance Spectroscopy", L. M. Jackman and F. A. Cotton, Ed., p 131, Academic Press, New York, N.Y., 1975.
(5) I. D. Campbell, C. M. Dobson, R.J.P. Williams, and P. E. Wright, *FEBS Lett.*, **57**, 96 (1975).
(6) D. Shaw, "Fourier Transform NMR Spectroscopy", p 196, Elsevier, New York, N.Y., 1976.
(7) F. F. Brown, I. D. Campbell, P. W. Kuchel, and D. L. Rabenstein, *FEBS Lett.*, **82**, 12 (1977).
(8) A. DeMarco and K. Wuthrich, *J. Magn. Reson.*, **24**, 201 (1976).
(9) I. D. Campbell, C. M. Dobson, R.J.P. Williams, and A. V. Xavier, *ibid.*, **11**, 172 (1973).
(10) M. Gassner, O. Jardetzky, and W. Conover, *ibid.*, **30**, 141 (1978).
(11) C.H.A. Seiter, G. W. Feigenson, S. I. Chan, and M.-C. Hsu, *J. Am. Chem. Soc.*, **94**, 2535 (1972).
(12) S. L. Pratt and B. D. Sykes, *J. Chem. Phys.*, **56**, 3182 (1972).
(13) G. Bodenhausen, R. Freeman, R. Niedermeyer, and D. L. Turner, *J. Magn. Reson.*, **26**, 133 (1977).
(14) W. P. Aue, E. Bartholdi, and R. R. Ernst, *J. Chem. Phys.*, **64**, 2229 (1976).
(15) L. Muller, A. Kumar, and R. R. Ernst, *J. Magn. Reson.*, **25**, 383 (1977).



Dallas L. Rabenstein is an associate professor of chemistry at the University of Alberta. His research interests include nuclear magnetic resonance spectroscopy, clinical applications of liquid chromatography, coordination chemistry, and the chemistry of heavy metal toxicology.

Other than headache, what are the symptoms of overexposure to mercury vapor?

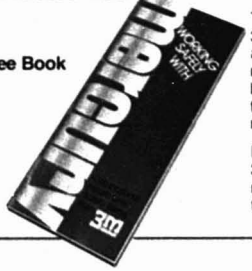


There's a better alternative than learning the answer by first-hand experience

If you work with mercury, chances are you know the answer. Chances are you have a full work safety program. But does everyone in the program know that fatigue, irritability and inflammation of the gums are some of the other symptoms of chronic poisoning? Would everyone know if they were overexposed?

An integrated plan of information and detection is obviously a better alternative than first-hand experience of symptoms. And 3M has an inexpensive plan applicable to every size laboratory whether it involves one person, 50 or more.

Free Book



Working Safely With Mercury is the informational phase of the plan. It's a free 20-page booklet written by 3M as an objective overview for those who work with mercury and those responsible for health and safety.

It's a concise presentation of the history, potential problems, methods of detection and protection, as well as current government recommendations for safe handling — even of small quantities.

The First Maintenance-free Mercury Vapor Monitor

Monitoring is a sure way to detect whether or not a person has been exposed to more than the government Threshold Limit Value (0.05 mg/m^3 in an 8 hour period).

The 3M Brand Mercury Vapor Monitor 3600 is the easy system. Nothing to assemble. No pumps. No maintenance. The lightweight badge-size monitor is simply clipped to the collar. Provides a precise measurement of personal exposure.

In comparison to a pump system, the 3600 is inexpensive enough so that monitors can be worn by everyone in the area of the mercury.



For analysis, you simply send the monitors to 3M. You'll receive a confidential report of Time Weighted Average concentrations for each monitor.

For your free copy of *Working Safely With Mercury* and detailed information about the maintenance-free 3600 monitor, write Occupational Health and Safety Products Division, 3M Company, P.O. Box 8327, Dept. H3 St. Paul, MN 55113.

Additional copies of *Working Safely With Mercury* are available upon written request.

ANOTHER STEP TOWARDS BETTER OCCUPATIONAL HEALTH AND SAFETY

3M

CIRCLE 149 ON READER SERVICE CARD

QUADREX INTRODUCES A SUPERB 10 METER GLASS CAPILLARY COLUMN FOR GAS CHROMATOGRAPHY

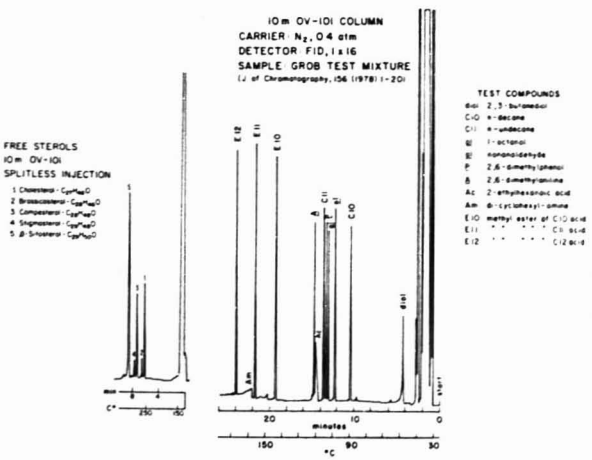
With recent advances in capillary column technology and instrumentation, there are very few reasons left for chromatographers to remain exclusively with packed columns

- These short capillary columns are guaranteed to yield 30,000 or more theoretical plates (3000 +plates/m at $k' > 3$–4—with test chromatogram)
- These short capillary columns are available with a wide variety of stationary phases (21 at latest count)
- These short capillary columns are relatively inexpensive ($105 to be exact!)
- These short capillary columns are an excellent compromise in providing speed of analysis, resolution, and sample capacity. They permit the very efficient elution of 'high boilers' at much lower temperatures in shorter periods of time when compared to packed columns. Note the rapid separation of 5 closely related sterols.
- These short capillary columns are subjected to a unique proprietory deactivation procedure which is considered to be the finest in the industry to date. Note the analysis of the New Grob Mixture on one of our ten meter columns.

The highest quality glass capillary columns are also available in 25, 50, 75, or 100 meter lengths. All columns have a coil diameter of ~12 cm, with an i.d. of 0.22–0.25 mm and an o.d. of 0.75–0.80 mm. All columns can be coated with the following stationary phases—SE 30, SE 52, OV-101, Squalane, Apiezon L, C-87 Hydrocarbon (Kovats), OV-17, Carbowax 20M, FFAP, Polyphenyl ether (OS-138), SP 2340, Silar 5C and 10C, Ethylene glycol adipate, Dexsil 300, 400, and 410, DC 550, UCON 1715, 5100 and 90,000.

Custom made columns upon request. We also carry a complete line of capillary column accessories.

Write for our very latest brochure.



QUADREX CORPORATION
P.O. Box 3881, Amity Station
New Haven, Conn. 06525 Telephone (203)-389-6620

CIRCLE 176 ON READER SERVICE CARD



Little things mean a lot in HPLC

Inlet filters. Rheodyne inlet filters can be connected between the sample injection valve and the column to protect the column from plugging. The 2 micron filter element prevents plugging caused by particles in the samples or by injection valve wear particles. Pressure rating of the filter assembly is 7000 psi (500 bar). Only type 316 stainless steel and PTFE contact the stream.

U.S. prices are $40 for the Model 7302 Column Inlet Filter and $20 for a package of 5 2$\mu$m filter elements and gaskets.

Pressure Relief Valve. Rheodyne's Model 7037 Pressure Relief Valve protects your equipment against damage from over-pressure. You can set it anywhere in the range of 2000 to 7000 psi (140 to 500 bar). U.S. price is only $250. So, when you consider the fact that you can blow a pressure gauge in less than 1 second, it's a real bargain.

Teflon Rotary Valves. Type 50 Rheodyne Valves are real workhorse accessories for your LC equipment.

Use them for sample injection, column switching, recycling, reagent switching, fraction collection, stream sampling and quantitive reagent injection. Available in four different versions, these valves are chemically inert with zero dead volume, operate at 300 psi. They are offered in 0.8 or 1.5 mm bore and in either manual or automatic versions.

U.S. price of 0.8 mm bore 3 and 4-way valves is $70. The 6-position and sample injection valves are priced at $85. Cost of 1.5 mm bore valves is $2 more.

Write for more data. For full information, please address Rheodyne, Inc., 2809 Tenth Street, Berkeley, CA 94710. Phone (415) 548-5374.

RHEODYNE
THE LC CONNECTION COMPANY

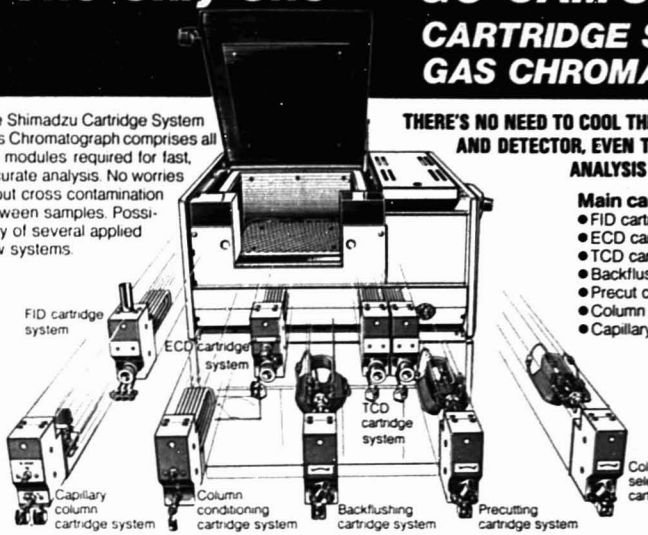
CIRCLE 178 ON READER SERVICE CARD

The Only One---- GC-6AM SERIES
CARTRIDGE SYSTEM GAS CHROMATOGRAPH*

The Shimadzu Cartridge System Gas Chromatograph comprises all the modules required for fast, accurate analysis. No worries about cross contamination between samples. Possibility of several applied flow systems.

THERE'S NO NEED TO COOL THE COLUMN, INJECTION PORT AND DETECTOR, EVEN TO CHANGE THE ENTIRE ANALYSIS SYSTEM!

Main cartridge systems are:
- FID cartridge system
- ECD cartridge system
- TCD cartridge system (factory installed)
- Backflush cartridge system
- Precut cartridge system
- Column conditioning cartridge system
- Capillary column cartridge system



*U.S. PATENT 4044593

SHIMADZU SCIENTIFIC INSTRUMENTS, INC. 9147 Red Branch Road, Columbia, Md. 21045 SHIMADZU

CIRCLE 196 ON READER SERVICE CARD

PHOTREX®
Spectrophotometric Solvents
(Where the proof of purity is right on the label.)

These J. T. Baker multi-purpose solvents are ideal in Quality Control and R&D for

- determination and identification of organic compounds
- inorganic analysis • trace element analysis

They provide extremely reliable performance in UV, visible and IR spectrophotometry. Also excellent for high-performance liquid chromatography (UV detector).

47 unsurpassed spectrophotometric solvents are available with detailed definition by UV absorbances and GC assay.

Every label carries the actual lot analysis featuring the GC assay, trace impurity analysis, IR "windows", and lot absorbance values at key wavelengths in the UV region.

The 'Baker Analyzed' Photrex label provides proof of purity and spectro suitability, as well as valuable reference data.

Write for free brochure

For Instrumental Analysis the professional chooses J. T. Baker

J. T. Baker Chemical Co.
Phillipsburg, N.J. 08865
201 859-5411

J.T.Baker CHEMICALS

CIRCLE 20 ON READER SERVICE CARD

What makes this Model 601 PPM Standard Reference Generator so Unique?



The 601 is unique.....because it is totally unlike any permeation device, and has none of the drawbacks. It needs no electricity, and is explosion-proof. It is portable for lab and field usage.

The 601 is unique.....because it automatically generates unlimited quantities of fresh, uniformly-blended, accurate calibration standard samples the instant they are needed, with unrestricted rangeability.

The 601 is unique.....because it accomplishes precision-blending of two or more gas streams to accurately obtain one or more streams of known composition, for determining analyzer accuracy, stability, and calibration.

The 601 is unique.....because it is easy to operate, flexible, and versatile. Get the total details on this unique Model 601 by calling **Dept. A, Applications Engineering, at 713/462-6116...or write HOUSTON ATLAS, INC., 9441 Baythorne Drive, Houston, TX. 77041.**

HOUSTON ATLAS, INC.

LABORATORY SERVICE CENTER

p-Aminoacetophenone • β-Amino-n-butyric Acid • Ammonium Reineckate
Barium Diphenylaminesulfonate • Benzanilide • Benzylidineaniline
2-Bromotoluene • Cetylpyridinium Bromide • α-Chloralose • Chloranil
Dihydroxyacetone • 2,3-Dimercaptosuccinic Acid • s-Diphenyl Urea
2,2'-Dipyridyl • Ethyl Lactate • Glucose-1-phosphate DiK & Na Salts
Glycolic Acid • HABA • p-Hydroxybenzonitrile • Methyl-n-propyl Ketone
Mucobromic Acid • Nadic Anhydride • Oxalacetic Acid • Oxamic Acid
Phenol Disulfonic Acid • Salicin • Sodium β-Naphthoquinone-4-sulfonate

Write for our Products List of over 3000 chemicals

Tel: 516-273-0900 TWX: 510-227-6230

EASTERN CHEMICAL BOX 2500 K
Division of GUARDIAN CHEMICAL CORP. HAUPPAUGE, N. Y. 11787

ANALYTICAL SERVICES
• Gas Analysis, GC, Org. Mass Spec, I.C.
• Industrial Hygiene, Pollution Tests
GOLLOB ANALYTICAL SERVICE
47 Industrial Rd.
Berkeley Heights, NJ
(201) 464 2331

CUPRIC SELENITE—$CuSeO_3 \cdot 2H_2O$
Kjeldahl Catalyst available from:
Laramie Chemical Co.
P.O. Box 3611
Laramie, Wyoming 82071
phone (307) 742-3100

LAB SAFETY
Send for 1978 Catalog
LAB SAFETY SUPPLY CO.
P.O.Box 1422, Janesville, WI 53545

SOLVENTS—Highest Purity
Call or write for prices.
Pollard & Co. Box 7131 Wilmington, DE 19803
Phone: 302-656-0060

Laboratory Service Center (Equipment, Materials, Services, Instruments for Leasing), Maximum space — 4 inches per advertisement. Column width, 2-3/16"; two-column width, 4-9/16". Artwork accepted. No combination of directory rates with ROP advertising. Rates based on number of inches used within 12 months from date of first insertion. Per inch: **1" — $63; 12" — $62; 24" — $60; 36" — $59; 48" — $58.**

CALL OR WRITE BARBARA AUFDERHEIDE

ANALYTICAL CHEMISTRY
25 Sylvan Road, So.
Westport, Ct. 06880
203-226-7131

INDEX TO ADVERTISERS IN THIS ISSUE

CIRCLE INQUIRY NO.	ADVERTISERS	PAGE NO.
5	* Airco Industrial Gases (Hammond Farrell Inc.)	1248A
6	* Alltech Associates (Chromad)	1210A
1	* Alpkem Corporation (Alpkem Advertising Company)	1246A
7–12	* Altex Scientific Inc. (Oliver Smith Advertising, Inc.)	1244A
30	Baird Corporation (Buck & Berglund, Inc.)	1247A
18, 20	J. T. Baker Chemical Co. (Naimark & Barba, Inc.)	1187A, 1279A
26	Balston, Inc. (Levy Advertising Associates, Inc.)	1276A
24	Barnstead (Marketing Dimensions, Inc.)	IFC
17	Bascom-Turner Instruments (Franklin Advertising Associates, Inc.)	1274A
22	* Bausch & Lomb (Wolff Associates, Inc.)	1271A
31	Bausch & Lomb (Blair Advertising Inc.)	1215A
19	** Bausch & Lomb International (Blair Advertising Inc.)	1266B
13	* Beckman Instrument, Inc. (N. W. Ayer ABH International)	1275A
28, 29	* Bio-Rad (Fred Schott & Associates)	1228A
14	* Blue M Electric Company (South Suburban Advertising)	1246A
16, 23	* Brinkmann Instruments, Inc. (Blatt Advertising, Inc.)	OBC, 1232A
27	* Buchler Instruments (Jud Jaffe Advertising)	1198A
25	* Burdick & Jackson Laboratories, Inc. (Studio 5 Advertising)	1256A
40–45	* Carle Instruments (The Knollwood Advertising Group)	1177A
32	Carlo Erba Strumentazione (Publicitas S.p.A.)	1260A
35, 36	* Chromatix, Inc. (David R. McClurg)	1222A
38	Chrompack (Mealer & Emerson, Inc. Adv.)	1263A
33	Corco Chemical Corporation (Sit/Com)	1221A
34	Corning Glass Works (Winterkorn, Hammond and Lillis, Inc.)	1217A
50	* DuPont-Liquid Chromatography Columns (N W Ayer ABH International)	1212A
xxx	* Eastman Kodak Company (Rumrill-Hoyt, Inc.)	1219A
73, 74	* Finnigan Instruments (Robert Pease & Company Advertising)	1188A, 1190A
75	Fischer & Porter Company (Furlong Promotions, Inc.)	1251A
79	* Fisher Scientific Company (Tech Ad Associates)	1196A–1197A
76	Fluid Metering, Inc. (Arnold H. Nachman Associates)	1225A
77, 78	* Foxboro Analytical (Shepherd, Tibball, Galog Associates)	1200A 1243A
88	* GCA Technology (Kenyon & Eckhardt Advertising, Inc.)	1240A
86	* Gilford Instrument Laboratories, Inc. (Oberlin Industrial Advertising)	1211A
89	* Glenco Scientific (Boone Advertising, Inc.)	1252A

INDEX TO ADVERTISERS IN THIS ISSUE

CIRCLE INQUIRY NO.	ADVERTISERS	PAGE NO.
87	* **Gow-Mac Instrument Company** Kenyon Hoag Associates	1254A
95	* **Hamilton Company** Mealer & Emerson, Inc. Adv.	1233A, 1234A
98	* **Hamilton Company** MPR	1231A
96	* **Hewlett-Packard** Benn Associates, Inc.	1183A
xxx	**Houston Atlas, Inc.** Harold Siegel Consultants	1279A
105	**Instrumentation Laboratory** Aries Advertising Inc.	1253A
108, 110	* **Jarrell-Ash Div., Fisher Scientific Co.** Tech-Ad Associates	1182A, 1223A
109	**Joyce-Loebl** S.&.M.E. Winship	1250A
118	* **Kevex Corporation** Fred Schott & Associates	1173A
115	* **Kontes** Aitkin-Kynett Company, Inc.	1282A
116, 117	* **Kratos, Inc.** Mesa Copy	1273A
133	**LECO Corporation** LECOM	1184A–1185A
127–132	**LKB Instruments, Inc.** Jarman, Spitzer & Felix, Inc.	1226A–1227A
125–126	**The London Company** Brand Advertising Inc.	1241A
148	**3M Analytical Systems Division** D'Arcy, MacManus & Masius	1259A
149	**3M Occupational Health & Safety** Kamstra Communications	1277A
143	**Mallinckrodt** Goldberg & Brumbaugh, Inc.	1264A
138–140	* **Matheson** Kenyon Hoag Associates	1178A, 1179A
xxx	* **MC/B Manufacturing Chemists, Inc.** Northlich, Stolley, Inc.	1220B–1220C
142	**Mercury Communications Corp.**	1240A
xxx	* **Mettler** McKinney, Inc.	1193A
135	* **Micromeritics Instrument Corporation** Adgraphics	1245A
136	* **Mitsubishi Chemical Industries Ltd.** Global Advertising Co., Ltd.	1276A
150, 151	* **NSI-Hitachi Scientific Instruments** Kaneko-Murakami, Inc. Adv.	1255A
156	* **Orion Research, Inc.** OBC Advertising	1169A
173	**Pacific Precision Instruments** Bocek Associates	1208A
168	**Pacific Scientific** Allen, Dorsey & Hatfield, Inc.	1262A
167	* **Perkin-Elmer Corporation** Marquardt & Roche, Inc. Adv.	1218A
172	**Photovolt Corporation** Michel-Cather Inc.	1165A
174	* **Pierce Chemical Company** Pierce Ad Graphics	1258A
169	* **Princeton Applied Research Corporation** The Message Center	1269A
170	** **Pye Unicam Ltd.**	1242B–1242C
176	**Quadrex** J. Wethersbee Associates	1278A
179	**Raytheon Medical Electronics** James A. Ford Advertising	1224A
178	* **Rheodyne** Bonfield Associates, Inc.	1278A
188	**Sartorius Werke** Agentur Busche	1242A
193	* **Schleicher & Schuell, Inc.** Jarman, Spitzer & Felix, Inc.	1175A
198	* **Schoeffel Instrument** Mar-Bet Associates	1258A
192	**Schott & Gen., Inc. New York** Bloom-Zagoren, Inc. Adv.	1252A
190	* **Scientific Glass Engineering** Arden Advertising Agency	1230A
197	* **Sensorex** 10346 Agency	1246A
195, 196	**Shimadzu Seisakusho Ltd.** General Advertising Agency, Inc.	1210A, 1279A
194	* **Siemens** Hogan Gazzara Associates	1257A
189	**Spain Expoquimia** Publicitas S.A.	1250A
191	**SPEX Industries** Seymour Nussenbaum	1233A
204	**Technicon Industrial Systems** Mediad Inc.	1180A–1181A
200	**Arthur H. Thomas** McKinney, Inc.	1171A
203	* **Tracor Northern, Inc.** Aitchnew Energetics	1209A
202	**TSI Inc.** Visual-Media Inc.	1240A
205	**Turner Associates** Fred Schott & Associates	1216A
208	**United Scientific** Bonfield Associates	1272A
222–231	* **Varian** Moran, Lanig & Duncan Adv.	1235A, 1237A, 1238A, 1239A
220–221	**VWR Scientific, Inc.** Unigraphica	1261A, 1263A
239–241	* **Waters Associates** Marketing Dimensions, Inc.	1204A
232	* **Whatman, Inc.** J. S. Lanza & Associates	1166A
233	**C. N. Wood Manufacturing Company** Blavat Advertising, Inc.	1246A

* *See ad in ACS Laboratory Guide*

** *Company so marked has advertisement in Foreign Regional edition only.*

Advertising Management for the American Chemical Society Publications

CENTCOM, LTD.

Thomas N. J. Koerwer, President; James A. Byrne, Vice President; Clay S. Holden, Vice President; Benjamin W. Jones, Vice President; Robert L. Voepel, Vice President; C. Douglas Wallach, Vice President, 25 Sylvan Rd. South, Westport, Connecticut 08880 (Area Code 203) 226-7131

ADVERTISING SALES MANAGER
James A. Byrne

SALES REPRESENTATIVES

Atlanta, GA . . . Robert E. Kelchner, CENTCOM, Ltd. Telephone: 203-226-7131

Boston, MA . . . Don Davis, CENTCOM, LTD. Telephone 203-226-7131

Chicago . . . Thomas Hanley, CENTCOM, LTD., 540 Frontage Rd., Northfield, Ill. 60093. 312-441-6383.

Cleveland . . . James Pecoy, CENTCOM, LTD., 17 Church St., Berea, Ohio 44017, 216 234-1333.

Houston . . . Robert LaPointe, CENTCOM, LTD., 415-692-0949.

Denver . . . Clay S. Holden, CENTCOM LTD., 213-776-0552.

Los Angeles 90045 . . . Clay S. Holden, CENTCOM, LTD., Newton Pacific Center, 3142 Pacific Coast Highway, Suite 200, Torrance, CA 90505, 213-325-1903

New York 10017 . . . Don Davis, Richard L. Going, CENTCOM LTD., 60 East 42nd St., 212-972-9660

Philadelphia . . . Richard L. Going, CENTCOM LTD., GSB Building, Suite 510 1 Belmont Avenue Bala Cynwyd, Pa. 19004. Telephone: 215-667-9666

San Francisco, CA . . . Robert LaPointe, CENTCOM, LTD., Room 235, 1499 Bayshore Highway, Burlingame, CA 94010. Telephone: (415) 692-0949

Westport 06880 . . . Don Davis, CENTCOM, LTD., 25 Sylvan Rd. So., 203-226-7131.

Manchester, England . . . Jill E. Loney, Technomedia Ltd., 216, Longhurst Lane, Mellor, Stockport, SK6 5PW, Telephone: 061-427-5660

Reading, England . . . Malcolm Thiele, Technomedia Ltd., Wood Cottage, Shurlock Row, Reading, RG10 OQE. Telephone 073-581-302

Tokyo, Japan . . . Haruo Moribayashi, International Media Representatives Ltd., 2-29 Toranomon, 1-Chome Minato-ku Tokyo 105 Japan, Telephone: 502-0656

Verviers, Belgium . . . Andre Jamar, Etablissements Andre Jamar, 1 Rue Mallar, 4800 Verviers. Telephone (087) 22-53-85.

PRODUCTION DEPARTMENT

Production Director
Joseph P. Stenza

Advertising Production Assistant
Barbara Aufderheide



We're kind of a chromatographic hardware store... if you don't see it, ask us.

Over recent years, we've developed what is probably the broadest line of chromatographic apparatus and supplies available from one company.

Being candid about it, we didn't do it ourselves.

Many of the developments that we've added to our Chromaflex® line came from users—researchers and leaders in the field of chromatography. We paid attention to needs and worked with researchers to solve peculiar problems they had.

Then we had a new piece of apparatus to offer researchers with similar needs.

Some of these items were unique, such as the first separable column with removable fritted disc; the first all-glass ground TLC plates; the first conical bottom Microflex® storage tubes for valuable samples; and recently, the first practical disposable column.

What's meaningful to you now is that many of these firsts have grown into complete lines, and we no doubt have what you need in chromatographic apparatus ready for off-the-shelf delivery.

But unlike a hardware store, we carry only one brand—the Kontes crown—which says quality, no matter what you ask for from us.

Ask your Kontes salesman for our new Chromaflex® Catalog CA-3, or contact the home store.

® Trademark of Kontes Glass Company

KONTES
Vineland, N.J. 08360

Exclusive Distributors: **KONTES OF ILLINOIS**, Evanston, Illinois • **KONTES OF CALIFORNIA**, San Leandro, California
KONTES (U.K.) LTD., Carnforth, England

CIRCLE 115 ON READER SERVICE CARD

Use this card to receive 1979
your own monthly copy of

ANALYTICAL CHEMISTRY

Toll Free: New Orders: 800-638-2000/Md. only 301-949-1551

	U.S.	Canada**	Foreign**
ACS Members*	☐ $12.00	☐ $21.00	☐ $21.00
Nonmembers	☐ $16.00	☐ $25.00	☐ $33.00

☐ Bill me ☐ Bill Company ☐ Payment enclosed
(Make payable: American Chemical Society)

Name _____

Position _____

Your Employer _____

Address ☐ Home ☐ Business _____

City _____ State _____ ZIP _____

Employer's business ☐ Manufacturing ☐ Academic ☐ Government ☐ Other _____

If manufacturer, type of products produced _____

_____

*Subscriptions at ACS member rates are for personal use only.
**Payment must be made in U.S. Currency, by international money order, UNESCO coupons, U.S. bank draft; or through your book dealer.

Allow 60 days for your first copy to be put in the mail. 9998-G

Mail this postage-free card today

Use this card to receive 1979
your own monthly copy of

ANALYTICAL CHEMISTRY

Toll Free: New Orders: 800-638-2000/Md. only 301-949-1551

	U.S.	Canada**	Foreign**
ACS Members*	☐ $12.00	☐ $21.00	☐ $21.00
Nonmembers	☐ $16.00	☐ $25.00	☐ $33.00

☐ Bill me ☐ Bill Company ☐ Payment enclosed
(Make payable: American Chemical Society)

Name _____

Position _____

Your Employer _____

Address ☐ Home ☐ Business _____

City _____ State _____ ZIP _____

Employer's business ☐ Manufacturing ☐ Academic ☐ Government ☐ Other _____

If manufacturer, type of products produced _____

_____

*Subscriptions at ACS member rates are for personal use only.
**Payment must be made in U.S. Currency, by international money order, UNESCO coupons, U.S. bank draft, or through your book dealer.

Allow 60 days for your first copy to be put in the mail. 9998-G

Mail this postage-free card today



NO POSTAGE
NECESSARY
IF MAILED
IN THE
UNITED STATES

BUSINESS REPLY MAIL

FIRST CLASS PERMIT NO. 10094 WASHINGTON, D. C.

POSTAGE WILL BE PAID BY ADDRESSEE

AMERICAN CHEMICAL SOCIETY
Attn: Gayle Hebron
1155 Sixteenth Street, N.W.
Washington, D. C. 20036



NO POSTAGE
NECESSARY
IF MAILED
IN THE
UNITED STATES

BUSINESS REPLY MAIL

FIRST CLASS PERMIT NO. 10094 WASHINGTON, D. C.

POSTAGE WILL BE PAID BY ADDRESSEE

AMERICAN CHEMICAL SOCIETY
Attn: Gayle Hebron
1155 Sixteenth Street, N.W.
Washington, D. C. 20036

analytical
chemistry

Editor: **Herbert A. Laitinen**

EDITORIAL HEADQUARTERS
1155 Sixteenth St., N.W.
Washington, D.C. 20036
Phone: 202-872-4570 Teletype: 710-8220151

Managing Editor: Josephine M. Petruzzi
Associate Editor: Andrew A. Husovsky
Associate Editor, Easton: Elizabeth R. Rufe
Assistant Editors: Barbara Cassatt, Nancy J. Oddenino
Editorial Assistant: Andre D'Arcangelo
Production Manager: Leroy L. Corcoran
Art Director: John V. Sinnett
Designer: Alan Kahan

Advisory Board: Donald H. Anderson, Peter Carr, Velmer Fassel, David Firestone, Kurt F. J. Heinrich, Philip F. Kane, Barry L. Karger, J. Jack Kirkland, Lynn L. Lewis, Marvin Margoshes, Harry B. Mark, Jr., J. W. Mitchell, Harry L. Pardue, Garry A. Rechnitz, W. D. Shults

Instrumentation Advisory Panel: Gary D. Christian, Catherine Fenselau, Nathan Gochman, Gary M. Hieftje, Gary Horlick, Peter J. Kissinger, James N. Little, C. David Miller, Sidney L. Phillips.

Contributing Editor: Claude A. Lucchesi
Department of Chemistry, Northwestern University, Evanston, Ill. 60201

Published by the
AMERICAN CHEMICAL SOCIETY
1155 16th Street, N.W.
Washington, D.C. 20036

Books and Journals Division
Director: D. H. Michael Bowen
Editorial: Charles R. Bertsch
Magazine and Production: Bacil Guiley
Research and Development: Seldon W. Terrant
Circulation Development: Marion Gurfein

Manuscript requirements are published in the January 1978 issue, page 189. Manuscripts for publication (4 copies) should be submitted to ANALYTICAL CHEMISTRY at the ACS Washington address.

The American Chemical Society and its editors assume no responsibility for the statements and opinions advanced by contributors. Views expressed in the editorials are those of the editors and do not necessarily represent the official position of the American Chemical Society.

Our Golden Anniversary—
I. The Formative Years

The end of 1978 marks the fiftieth anniversary of the establishment of the *Analytical Edition* of *Industrial and Engineering Chemistry* as a separate publication. In this issue, we are publishing the first of a two-part series of papers presented at the Miami Beach ACS meeting under the title Analytical Chemistry, the Journal and the Science.

With one dramatic exception, the changes in the journal have been gradual and almost imperceptible from one issue to the next. The exception, of course, is the change of name, and even this occurred informally in 1947 before becoming official in 1948. Far deeper than merely a change in title, the new format represented the development of a basically different publication, a magazine *cum* journal, which retains a unique character to this day.

It is appropriate that the 50th Anniversary Symposium was held in honor of Laurence T. Hallett, who was the first person really trained as an analytical chemist to hold the editorship, and who did so much to mold the publication into its present form. A good deal of credit also goes to Walter J. Murphy, his predecessor, who in 1943 succeeded Harrison E. Howe as editor of the parent publication, *Industrial and Engineering Chemistry*. As a chemist who had turned journalist, Murphy recognized the enormous impact that war-time developments in instrumentation would be destined to exert on the field of analytical chemistry. He engaged Ralph H. Müller, then Professor of Chemistry at New York University, as a contributing editor in instrumentation, as well as Hallett, then at General Aniline and Film, as a part-time associate editor. Murphy and Hallett, together with academic and industrial advisers, soon began discussions that culminated in the establishment of *Analytical Chemistry* essentially in its present form.

It was recognized that appropriate advertising matter would not only be a welcome source of revenue, but would also serve a professional function in providing technical information about new commercial developments in instrumentation. The magazine section could provide popular and technical features not normally carried in a primary research journal. Hallett, from the first, insisted upon a strict segregation of research articles from magazine features. He broadened the mission of the research section to encourage fundamental as well as procedure-oriented articles. He built up an editorial staff with training and experience in analytical chemistry, and established a rigorous peer review procedure for contributed papers. The groundwork was thus laid by the late 1940's for an evolutionary process that continues to this day.



Effect of Heating Rates in Graphite Furnace Atomic Absorption Spectrometry

D. C. Gregoire, C. L. Chakrabarti,* and P. C. Bertels

Metal Ions Group, Department of Chemistry, Carleton University, Ottawa, Ontario, Canada K1S 5B6

The peak and integrated absorbances of Mo, V, Al, Ni, Cu, Zn, and Cd as a function of the rate of heating of the graphite tube in a modified HGA 2100 atomizer are reported. The increase in peak absorbance with heating rate is correlated with the activation energy of the rate-determining step in the atomization process. Integrated absorbances of relatively volatile elements decreased exponentially with increasing heating rates, whereas those of relatively involatile elements, such as Mo and V, increased exponentially with increasing heating rates. Characterization times (τ_1, τ_2, τ_1/τ_2) of the absorption pulse are discussed and their applicability to analysis of real samples is assessed.

In recent years, models for temporal signal profiles obtained using various types of electrothermal atomizers have been proposed (*1–15*). The instrumental parameters that affect the absorption signals obtained with various atomizers have been studied also (*9–11*). Among these are the drying, ashing, and atomization temperatures, atomizer design, the influence of different sheath gases on absorption signals, the rate of heating of the atomizer, and the response time of the measurement system.

Assuming, for the sake of simplicity, that analyte atoms are introduced into the analysis volume simply by the vaporization of analyte from the graphite surface (i.e., ignoring all other intermediate steps that may be involved in the atom formation), the rate of evaporation $R(t)$ of an analyte element as a function of the absolute temperature is given by

$$R(t) = Ae^{-E_v/RT} \tag{1}$$

where A is a pre-exponential factor and E_v is the heat of vaporization for the analyte element. Since the temperature of the graphite furnace increases rapidly during the atomization step, Equation 1 is modified as shown in Equation 2:

$$R(t) = Ae^{-E_v/R(T + \alpha t)} \tag{2}$$

where t is time in ms and α is the rate of heating of the graphite tube in K ms^{-1}.

This exponential dependence of the rate of vaporization of the analyte atoms from a graphite surface can be used to account for exponential rise in the peak absorbance with increasing heating rates.

L'vov's model (*16*) for electrothermal atomization in an isothermal graphite cuvette describes the temporal variation of an absorption signal profile. L'vov (*17*) and Katskov and L'vov (*18*) have shown that, for accelerated atomization, the variation of the atomic population within the analysis volume with time may be described by:

$$N_{t \le \tau_1'} = \frac{2N_o\tau_2'^2}{\tau_1'^2}\left(\frac{t}{\tau_2'} - 1 + e^{-t/\tau_2'}\right) \tag{3}$$

where N_t is the analyte atomic population at any instant of time t, N_o is the number of analyte atoms in the sample, τ_1' and τ_2' are atomization time and residence time, respectively.

L'vov's (*16*) model for electrothermal atomization in an isothermal graphite cuvette also predicts that provided the sample is completely atomized during the time of measurement, the integrated absorbance, Q_N', is proportional to the residence time, τ_2', of atoms in the analysis volume, and the total number of analyte atoms in the sample, N_o'.

$$Q_N' = N_o'\tau_2' \tag{4}$$

The primes on τ_1', τ_2', and Q_N' will be used for designating these parameters as they appear in L'vov's model (*14*), and they will be differentiated from their experimentally observed counterparts (i.e., the values obtained using commercial atomizers), which will be designated simply as τ_1, τ_2, and Q_N. Atomization time, τ_1', is defined as the time elapsed from the appearance time to the peak of the absorption pulse (*10, 11*). Residence time, τ_2', is defined as the time taken for any absorbance value in the decay part of the absorption pulse to decay to $1/e$ of its value provided that complete atomization has occurred before the initial point in the measurement (*10, 11*). However, with commercial graphite tube atomizers, the latter proviso is sometimes not fulfilled and the experimental τ_1' and τ_2' values are sometimes different from the theoretical τ_1 and τ_2 values, respectively (*10, 11*).

Equation 3 shows that the measured absorbance ($A \propto N_t$) should increase as the τ_1/τ_2 decreases. For constant τ_2, the absorbance should increase exponentially as τ_1 decreases. Since the peak of the absorbance–time profile (i.e., at $t = \tau_1$) is taken as the measure of the absorbance signal, the peak height should increase exponentially with α, the rate of heating of the atomizer, because τ_1 decreases exponentially with α (Table I).

Equation 4 shows that the integrated absorbance is entirely independent of the atomization time, τ_1', i.e., independent of the kinetics of atomization, and hence, is independent of the heating rate. Here the only requirements are complete atomization and maintenance of experimental conditions so that the length of time spent by the atoms in the analysis volume (i.e., residence time, τ_2') remains constant.

It has been reported (*10, 11*) that the above mentioned conditions are not fulfilled by commercial graphite tube atomizers; hence, Q_N (experimental integrated absorbance) may not be independent of the kinetics of atomization and the heating rate.

Based upon the L'vov's model (*16*), Sturgeon et al. proposed mechanisms of atom formation (*14*) and atom loss (*15*) in a commercial graphite tube atomizer. This paper is based upon the above model (*14, 15*) and reports the results of studies made on the effect of the heating rate on the peak and the integrated absorbances in a graphite tube atomizer.

Torsi, Tessari, et al. (*5–9*) developed a theoretical model and reported experimental results for the release of gaseous atoms at the electrothermal rod atomizer. The most important features of the model were the following: (i) the overall atomization process was assumed to be kinetically controlled by the atom transfer at the solid/gas interphase, the possibility of redeposition of atoms being ignored; (ii) in a preliminary

0003-2700/78/0350-1730$01.00/0 © 1978 American Chemical Society

simplified model (*5*), only the convective mechanism of transport was considered; whereas in a following more sophisticated treatment (*6*) the diffusive and convective mechanisms were both included in order to calculate the time-dependent number of atoms present in the volume of optical observation; (iii) reliance on thermodynamic data from the literature was a priori avoided and an effort was made (*7*) to obtain directly from the experimental data some information about the binding energy between the solid substrate and the atom to be released. The reported experimental result—nickel (*8*) and lead (*9*), both in hydrogen atmosphere—confirmed the validity of this model.

In the above model (*5–9*), the authors assumed that the analyte atoms are bound to the graphite surface with a monolayer distribution, and the gaseous phase behaves as an infinite sink for the evaporating atoms. It was further assumed that the linear velocity of the evaporating atoms was constant, and also that the diffusion coefficient of the released atoms was constant in time and position. Taking into account the depletion of the surface layer of atoms with time in the atomization step, a linear increase in the analytical sensitivity was predicted with increasing heating rates. Experimentally, these results were verified for 4.0×10^{-14} kg of chromium atomized at heating rates of up to 4.0 K ms^{-1}. Above this heating rate, the absorbance began to show progressively smaller increases with increasing heating rates.

The model developed by Torsi, Tessari, and co-workers (*5–9*) for the electrothermal rod atomizer is not applicable to the electrothermal graphite tube atomizer for at least four reasons. First, in the graphite tube atomizer, since the partial pressure of the analyte atomic vapor is not zero, the gaseous phase above the atomizer surface does not behave as an infinite sink for the evaporating atoms; also, the evaporation of atoms may not be an irreversible process because of the possibility of condensation of the analyte atoms in cooler parts of the graphite tube and their subsequent re-evaporation (*15*). Secondly, it will be shown in this paper that the residence time of the atoms in the graphite tube atomizer is not a constant and therefore the velocity of the atoms must be changing with time. Thirdly, in the graphite tube atomizer, diffusional mechanism of transport is predominant (*15*), whereas in the electrothermal rod atomizer (*5–9*), both the convective and the diffusional mechanism of transport play an important role. Fourthly, in the model developed for the electrothermal rod atomizer (*5–9*), the prompt establishment of equilibrium conditions at the interphase between solid and gas phase plays a central role in the overall atomization process, whereas in the model for the graphite tube atomizer (*14*, *15*) quasi-equilibrium conditions are assumed for the release process.

The effect of heating rates of an electrothermal atomizer on the absorbance of elements has been reported in the literature (*4*, *5*, *10*, *11*, *13*, *19–22*). The heating rate of a graphite tube or filament atomizer has been found to have a large effect on the absorbance of elements. Using a graphite tube atomizer, Johnson et al. (*19*) found that the shape of the germanium absorbance signal varied with the voltage applied to the atomizer unit. Above a certain minimum voltage, the absorption pulse increased in height and decreased in width as the input power was increased. A heating rate of 1.6 K ms^{-1} was observed at the maximum applied voltage, 11 V. These authors postulated that the germanium atomic vapor was formed by the gas phase dissociation of the volatile GeO species, and that high atomizer heating rates were necessary in order to reach rapidly a temperature at which the thermal decomposition of GeO(g) was thermodynamically favorable; the time to reach the above temperature must be much shorter than the time required for the GeO(g) to diffuse out of the graphite tube. This conclusion was supported by the fact that an open filament-type atomizer gave extremely low sensitivities for Ge since in these atomizers, the residence time of gas-phase species in the analysis volume was far less than in the enclosed, tube-type atomizer. A similar effect was observed by Donega and Burgess (*20*), who determined Si in an enclosed Ta boat atomizer. These authors also concluded that the rapid loss of gaseous SiO (which was supposed to be the precursor of the gas-phase Si atoms) below a minimum input power level accounted for the low sensitivity obtained at low atomizer heating rates.

Montasser and Crouch (*23*) pointed out that for those cases where the atomization process goes through an oxide formation step and voltilization of the oxide occurs at a temperature much lower than the atomization temperature, it is essential (in order to prevent sample loss) that the atomizer achieve the desired final temperature instantaneously.

Cresser and Mullins (*24*) have also stated that the rate at which any given molecular species leaves the atomizer (graphite filament) and the degree of atomization depend on the rate of increase of temperature at temperatures at which the analyte molecular species exhibits a significant vapor pressure.

Torsi and Tessari (*5*) have published a mathematical treatment of heating rates and its effect on the peak absorbance for Cr. Their model predicts (and they have experimentally verified the prediction using a carbon filament atomizer), that a linear relationship exists between the peak absorbance and the input power. These authors (*5*), however, have not observed this linear relationship above the heating rate of 4 K ms^{-1}.

Maessen and Posma (*21*) have reported the effect of the heating rate of the graphite tube for a Carbon Rod Atomizer-63 (CRA 63) on the peak separation between the analyte peak and the matrix peak. The present authors have plotted these results—absorbance vs. the square of the input voltage, V—for gold and cobalt in blood plasma and have found that the curves show an initial, approximately linear increase in the peak absorbance with increasing V^2 (i.e., the heating rate), followed by a slower increase in the absorbance with higher V^2 values.

Work done with a carbon filament atomizer by Johnson et al. (*4*) indicates that the peak height absorbance is a linear function of V^2 and, hence, is also a linear function of the filament heating rate. These authors (*4*) have observed a correlation between the temperature at which the atomic vapor becomes just detectable (i.e., the appearance temperature) and the heat of vaporization of the metal or the bond dissociation energy of the metal oxide, whichever is larger.

Posma et al. (*13*) have reported variation of peak height absorbance for copper with the heating rate of a CRA 63 for various time constants. These authors (*13*) have found that when recording undistorted signals, peak height absorbance increases up to a heating rate of about 0.850 K ms^{-1}, but when recording signals under optimum signal-to-noise ratio conditions, (e.g., a time constant of 0.3 s), the measurement system can follow the signal increase up to about 0.400 K ms^{-1}, whereafter the peak height absorbance remains constant. Using a very slow response system, i.e., a time constant of 3.0 s, these authors (*13*) have observed that peak height absorbance increases slowly up to 0.450 K ms^{-1}, after which it decreases slowly. They have obtained similar results with silver and cobalt.

The use of extremely high heating rates, up to 40 K ms^{-1}, with a capacitive discharge system, as a means of improving analytical sensitivity has been suggested by L'vov (*25*), and the present authors (*26*). Sturgeon and Chakrabarti (*22*) have reported that increased heating rates of the HGA 2100 graphite tube generally increase peak height absorbance;

however, few conclusions of general applicability to high heating rates can be drawn from the results presented.

In most of the studies discussed above, the power supply was so designed that any change in the rate of heating of the atomizer also resulted in a change in the maximum temperature of the atomizer. Since the maximum temperature of the atomizer affects the characteristics of the absorption pulse of elements (*10, 11*), the effect of the heating rate cannot be separated from the effect of the temperature attained. In order to achieve a complete separation of these two effects, the power supply needs to be so designed that the heating rate and the maximum temperature attainable must be independently controllable. Such independent control was provided by the power supply used in this study.

EXPERIMENTAL

Apparatus. The atomic absorption spectrophotometer used for this study has been described in earlier publications (*10, 11, 22, 27*) from this laboratory. The design of the graphite tube atomizer built in this laboratory, is similar to that of the Perkin-Elmer HGA 2100 (and, hence, the apparatus will be called a modified HGA 2100). It is fitted with large water-cooled chambers to prevent over-heating of the metal from the atomizer during long or high-temperature atomization cycles. Single-piece unit construction of the atomizer allows its use at power input levels of 15 V at 1000 A. The graphite cones and graphite tubes were those commerically available from the Perkin-Elmer Corporation for HGA 2100—the graphite tubes were pre-coated with pyrolytic graphite in the authors' laboratories.

A novel power supply used for this study was designed and fabricated in this laboratory so as to separate the maximum temperature attainable by the atomizer from its rate of heating (*22*). Unlike conventional graphite furnace power supplies, this has, in addition to the usual dry and ash stages, two high-temperature atomization stages. In addition, its power capabilities are much greater than the commercial units. A custom-wound transformer (Electrodesign Ltd., Ville Lasalle, Quebec, Canada) operating at 208 V provides 1000 A at 15 V to the atomizer. It has been demonstrated by numerous authors (*4, 5, 10, 11, 13, 19–22*) that the rate of rise of temperature of the atomizer is an important parameter in determining peak absorbance. With conventional atomization units, the highest rate of rise of temperature requires the maximum atomization setting, resulting in the maximum temperature of the atomizer being attained. The power supply described above allows maximum rate of heating of the atomizer for a short period of time with the first atomization stage while maintaining a controllable upper limit on the temperature with the second atomization stage. This flexibility allows use of a wider variety of heating regimes which may be used to achieve very rapid heating to a present temperature followed by isothermal conditions. This allows one to separate the effects of the heating rate from the effects of the temperature on the analytical parameters of an absorption pulse. There are two significant differences between this power supply and conventional graphite furnace power supplies: (1) The same (maximum) temperature can be attained with this power supply using different heating rates, whereas this can be achieved with conventional graphite furnace power supplies using only one particular heating rate; (2) temperatures > 3000 K can be attained with this power supply, whereas such temperatures cannot be attained with conventional graphite furnace power supplies using low heating rates (*27*).

All temperatures were measured with an automatic pyrometer, series 1100 (Ircon Inc., Niles, Ill.), which had been calibrated by the manufacturer, and the calibration checked in this laboratory by measurement with thermocouples and by the melting points of selected pure metals covering the entire range of temperatures studied. Perkin-Elmer and Varian Techtron single-element hollow cathode lamps were used as narrow-line sources. Aliquots of 5 μL of sample solution were delivered to the graphite tube by means of an Eppendorf pipet fitted with disposable plastic tips.

Reagents. All reagents used were of ACS reagent-grade purity. Stock solutions of 1000 μg/mL of each metal studied were prepared from pure metals dissolved in appropriate acids or bases with the exception of vanadium, which was prepared from vanadium pentoxide, and molybdenum, which was prepared from molybdenum trioxide. Immediately prior to use, each standard solution was diluted to the desired concentration with ultrapure water obtained directly from a Milli-Q water system (Millipore Corporation). Argon gas used to sheath and to purge internally the atomizer was of 99.95% purity and was supplied by Roncar Oxygen Company.

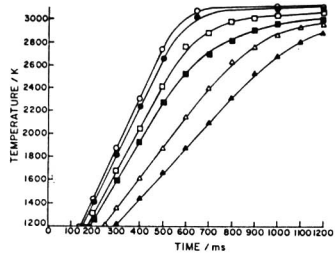


Figure 1. Temperature–time curves of the graphite tube heated at different heating rates. ○ 4.33 K ms^{-1}, ● 4.17 K ms^{-1}, □ 3.68 K ms^{-1}, ■ 3.40 K ms^{-1}, △ 2.60 K ms^{-1}, ▲ 2.17 K ms^{-1}

RESULTS AND DISCUSSION

Temperature–Time Characteristics of the Atomizer. The surface temperatures of the graphite tube as a function of time at different heating rates are presented in Figure 1. The curves in Figure 1 show an initial linear part during which the atomizer is heated to some temperature, followed by a short nonlinear part, the end of which marks the end of the first atomization stage and the beginning of the second atomization stage; and finally, a nearly horizontal part where the atomizer asymptotically approaches the preset maximum temperature. The maximum temperature marks the balance between the input power and the heat losses. The power supplied to the atomizer is partly dissipated by radiation, conduction, and convection, and is partly used in raising the temperature of the graphite tube atomizer. At low temperatures, and at the center of the inner surface of the graphite tube (where experimental surface temperatures are measured), heat losses arising from radiation, conduction, and convection should be small; hence, at low temperatures, the rate of heating (α) of the atomizer can be related to the input power by Equation 5:

$$\frac{dT}{dt} = \alpha = \frac{P}{mc} \tag{5}$$

where dT/dt is the rate of heating of the atomizer (K ms^{-1}), P is the power consumption of the atomizer (J·s^{-1}), m is the mass of the carbon tube (kg), and c is its specific heat capacity (J kg^{-1} K^{-1}). According to Equation 5, at low temperatures, a linear relationship exists between the input power and the initial rate of heating of the atomizer. This linear relationship has been experimentally confirmed by the present authors for the atomizer unit described above for the range of input power reported in this study.

Each curve in Figure 1 represents a different heating rate of the graphite tube surface. This heating rate is determined by the input power set on the first atomization stage and, therefore, one could reach any preset maximum temperature of the graphite tube surface at a rapid or slow heating rate. With the power supply described in this paper, heating rates of up to 4.33 K ms^{-1} were achieved. The fact that the rate of heating is variable and that the maximum temperature at each new rate of heating is the same, allowed the authors to study changes in the analytical parameters as a function of the heating rate at a nearly constant maximum temperature.

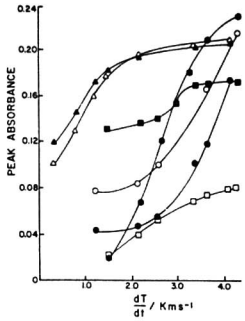


Figure 2. Peak absorbance as a function of graphite tube heating rates. ▲ Zn, △ Cd, ■ Cu, ○ Mo, ● V, • Al, □ Ni

Unless stated otherwise, a drying temperature of 370 K maintained for 30 s and an ashing temperature of 570 K maintained for 20 s were used. Maximum temperatures above 3200 K were impractical since at higher temperatures excessive scattering of the incident radiation occurs by the carbon ejected from the graphite tube surface, and the useful life of the graphite tube is greatly shortened.

Although the highest absorption signals were not obtained for some of the elements studied at this high maximum temperature, a constant maximum temperature was used to provide a basis for comparison of the elements studied. A high maximum temperature was necessary in order to ensure that low-volatility elements, such as Mo and V, were atomized. Sturgeon et al. (*11*) presented a good discussion of the peak and the integrated absorbances for a series of elements in a HGA 2100 as a function of the maximum temperature employed.

It is interesting to compare the performance of this modified HGA 2100 with the unmodified HGA 2100. The input power of the unmodified HGA 2100 determines the maximum temperature of the atomizer surface. Its power supply can give a maximum temperature of ~3000 K; its rate of heating, at the temperature setting of 2700 C is 1.23 K ms^{-1}. However, with the unmodified HGA 2100, when the power input (and, hence, the rate of heating) is altered, the maximum temperature is also altered. For example, power inputs giving maximum temperatures of 2370, 2770, and 2970 K give heating rates of 0.73, 1.06, and 1.23 K ms^{-1}, respectively. These heating rates agree with those reported by Sturgeon and Chakrabarti (*27*). This coupling of the maximum temperature attained and the heating rate in the case of the commercial atomizer makes it difficult to study the changes in the analytical parameters of an absorption signal caused solely by changes in the heating rate of the graphite tube.

The modified HGA 2100 provides linear heating curves over the entire absorption pulse of the elements studied with the exception of the less volatile metals, Mo and V. In the case of Mo and V, only a part of the decay region of the absorption pulse occurs during the final, nonlinear part of the heating curves.

Effect of Heating Rate on Peak Absorbance. Figure 2 presents peak absorbance as a function of the graphite tube heating rate from 0.33 to 4.33 K ms^{-1} for a number of elements atomized. The elements studied were chosen from each of the three groups referred to in this paper as the relatively volatile elements (Cd, Zn), medium-volatility elements (Cu, Al, Ni), and low-volatility elements (Mo, V). The relationship seen in Figure 2 between the peak absorbance and the rate of heating appears to be complex. Close examination, however, reveals that the curves are approximately sigmoid in shape. For relatively volatile elements (Cd and Zn) and for a medium-volatility element (Cu), the curves can be divided into three distinct regions. At low rates of heating, a rather slow increase in the peak absorbance occurs with increasing rates of heating. This is followed by a second region in which an exponential increase occurs in the peak absorbance with increasing heating rates. Finally, there is a third region where further increase in the heating rate produces little change in the peak absorbance. These results agree with those obtained by other workers (*13, 21*).

For the elements of medium and low volatility, only certain parts of the curves obtained for the relatively volatile elements are seen in Figure 2. For example, Al and Ni show an increase in the peak absorbance with the increasing heating rate, and then the peak absorbance of both show signs of levelling off at the highest rates of heating studied. Molybdenum and vanadium, however, still show an exponential increase in the peak absorbance at a heating rate of 4.17 K ms^{-1}. At still higher heating rates (i.e., >4.33 K ms^{-1} which are not attainable with the present equipment), it is expected that the peak absorbance of Mo and V would follow the trend observed with the other elements, i.e., with further increase in the heating rate, the increase in the peak absorbance would be progressively smaller and finally, the peak absorbance would level off.

Figure 2 also shows that in a series of elements, with decreasing volatility, the point of vertical inflection in the sigmoid-shaped curve is shifted to higher rates of heating. For example, Zn and Cd both have their inflection points at a heating rate of about 0.50 K ms^{-1}, whereas that of Al is shifted to 2.75 K ms^{-1}. The inflection points of Mo and V are not reached even at the highest rate of heating available with the present equipment. Mathematically, a point of vertical inflection is defined as the turning point in a curve the slope of which increases (or decreases), becomes infinity at the inflection point, and thereafter decreases (or increases). In Figure 2, as any point of vertical inflection is approached from the side of low heating rates, the slope of the curve increases, becomes infinity at the inflection point, and thereafter decreases. It would be instructive to find out why the peak absorbance initially increases with increasing heating rates up to the point of inflection and thereafter decreases with further increase in heating rates. The above phenomenon is interpreted as follows.

It has been shown by Sturgeon et al. (*14, 15*) that both the magnitude and the position of the peak of an absorption pulse are determined by the rates of formation and loss of atoms, the absorption maximum marking the point of balance between these rates (i.e., at the pulse maximum, the net rate of increase in the number of atoms is zero), and that an increase in the rate of loss both decreases the peak height and shifts the pulse maximum to an earlier point in time. Sturgeon et al. (*15*) demonstrated the above fact by means of an oscilloscopic trace showing the effect of an internal purge gas (i.e., forced convection) on the peak of absorption pulses from 4×10^{-13} kg Cu atomized in a HGA 2100; in the presence of the internal purge gas (i.e., forced convection) the peak decreased in magnitude and shifted to an earlier point in time. Since the peak of an absorption pulse marks the point of balance between the rates of formation and loss of atoms, an increase in the rate of loss decreases the peak height and shifts the peak to an earlier point in time. Like the convection in the above case, any increase in any other loss processes, viz., diffusion, forced expulsion due to expansion of the purge gas, formation of refractory compounds, may affect the peak of an absorption pulse both in magnitude and position in time. An increase in the pulse height and position can result from either an increase in the rate of atom formation and/or a

Table I. Effect of Heating Rates on Experimental Atomization Time, τ_1

dT/dt/ K ms^{-1}	τ_1/ms Mo	V	Al	Ni	Cu	Cd	Zn
4.33	450	180	140	320	180	120	90
4.17	500	200	160	340	195	120	90
3.68	650	210	200	400	212	130	95
3.40	750	230	250	490	230	140	100
2.60	1000	245	350	600	250	150	115
2.17	1400	300	410	780	275	160	125
1.47	2500	-	560	1160	-	200	160
1.23	-	-	-	-	-	270	220
0.79	-	-	-	-	-	360	290

Table II. Effect of Heating Rates on Experimental Residence Times, τ_2

dT/dt/ K ms^{-1}	τ_2/ms Mo	V	Al	Ni	Cu	Cd	Zn
4.33	900	360	125	460	135	80	70
4.17	950	390	130	470	150	80	70
3.68	1200	430	130	480	155	110	75
3.40	1250	440	150	480	170	140	90
2.60	1500	475	210	560	205	150	145
2.17	1750	500	245	600	270	165	160
1.47	-	-	-	-	-	230	175
1.23	-	-	-	-	-	260	180
0.79	-	-	-	-	-	430	250

Table III. Effect of Heating Rate on the Ratio of Experimental Atomization Time/Experimental Residence Time

dT/dt/ K ms^{-1}	τ_1/τ_2 ratio Mo	V	Al	Ni	Cu	Cd	Zn
4.33	0.50	0.50	1.12	0.69	1.33	1.50	1.29
4.17	0.53	0.51	1.23	0.72	1.30	1.50	1.29
3.68	0.54	0.49	1.54	0.83	1.37	1.18	1.27
3.40	0.60	0.52	1.67	1.02	1.35	1.00	1.11
2.60	0.67	0.52	1.67	1.07	1.22	1.00	0.79
2.17	0.80	0.60	1.67	1.30	1.02	0.97	0.78
1.47	-	-	-	-	-	0.87	0.91
1.23	-	-	-	-	-	1.04	1.22
0.79	-	-	-	-	-	0.84	1.16

decrease in the rate of atom loss.

For relatively volatile metals (Zn and Cd), at the heating rates used in this study the entire absorption pulse occurs in the period of time during which the temperature of both the atomic vapor and the diffusion medium is rapidly increasing; hence, the diffusion coefficient of the analyte species increases with time (i.e., with increasing temperature) causing an increased diffusional loss of the analyte atomic vapor (*15*, *22*). This is because the rate of diffusional loss increases according to $T^{1.5}$ (*28*), where T is the temperature of the gas phase in degrees Kelvin. The greater the heating rate, the greater is this diffusional loss, and the earlier the pulse peak occurs. With increasing heating rate, besides increased diffusional loss, there are also losses due to expulsion of the analyte species from the analysis volume by rapid expansion of the purge gas inside the graphite tube, and also due to convection—all of these factors contribute to the atom loss. Given a constant rate of atom loss, the peak absorbance should increase with increasing heating rate (i.e., decreasing τ_1' values), and as τ_1' becomes much smaller than τ_2', the peak absorbance reaches a limiting (maximum) value. However, for relatively volatile elements, increased atom loss with increasing heating rates makes τ_2' progressively smaller, decreases the peak height, and shifts the peak position to an earlier point in time. This is reflected in the inflection points occurring at lower heating rates for the relatively volatile elements than for the relatively involatile elements. For relatively involatile elements, increasing heating rates decreases τ_1' without a proportionate decrease in τ_2' with the result that the peak absorbance continues to increase with increasing heating rates and the inflection points are not reached even with the highest heating rate available with the power supply.

The practical significance of the above observations is that with the commercial, semi-enclosed graphite tube atomizers, high heating rates increase the peak height sensitivity of elements; the more involatile the element the greater, generally, is the increase in the peak height sensitivity—the greatest increase in the peak height sensitivity with increasing heating rates (up to a heating rate of at least 4.33 K ms^{-1} and probably, much higher heating rates) is found with relatively involatile elements. Heating rates higher than about 5 K ms^{-1} are best accomplished by capacitive discharge heating (*25*, *26*).

The above discussion based solely on the relative volatility of elements is valid only in the simple case in which the atom formation and loss reactions for an analyte element are not complicated by the formation of its intermediates of significantly different volatilities in the temperature range studied, and is generally valid for the above elements.

The experimental atomization time, τ_1, measured for the elements over the range of heating rates studied is presented in Table I. For each element studied, the experimental atomization time, τ_1, at first decreases rapidly with increasing heating rates and then decreases slowly at higher heating rates. The latter effect may be the results of the atom loss increasing at a faster rate (relative to the atom formation) as the rate of heating approaches the highest rate of heating available; the consequence of this being that the time to reach the peak absorbance (τ_1) does not decrease as rapidly as at lower rates of heating.

At high rates of heating, thermal gradient across the length of the graphite tube increases sharply and atom loss due to diffusion and convection across this thermal gradient toward the cold end-cap windows also increases. Furthermore, because of the rapid expansion of the purge gas inside the graphite tube, there is an increase in the loss due to mechanical expulsion of atoms through the sample injection port. At high rates of heating, there is probably also an increase in the loss by diffusion through the pyrolytic graphite tube walls although such loss is probably negligible at lower rates of heating (*15*).

The experimental residence time, τ_2, is presented in Table II. L'vov's model (*16*) predicts that a maximum in the pulse peak height occurs when the ratio $\tau_1'/\tau_2' << 1$. Therefore, as the peak absorbance increases, the experimental τ_1/τ_2 ratio is expected to decrease. The experimental τ_1/τ_2 ratios measured for each element over a range of heating rates are presented in Table III. As predicted, the ratio does in fact decrease in most cases with increasing heating rates. It is expected that the elements of relatively low volatility (Mo, V) would give higher experimental τ_1/τ_2 ratios than the elements of relatively high volatility (Cd, Zn). Examination of the horizontal rows in Table III shows that this is not realized in practice. This anomaly can be explained as follows. L'vov's model (*16*) assumes that atomization is complete at time = τ_1', and it further assumes that the decay of the absorption signal is independent of its growth, and the decay of the absorption signal is solely due to atom loss by diffusion alone. These assumptions are not valid with commercial atomizers. For elements of low volatility such as Mo and V, the experimental τ_1 values were smaller and τ_2 values were larger than the theoretical values (τ_1' and τ_2', respectively) of L'vov's model (*16*) because the atomization was not complete at time = τ_1 and continued beyond the point in time of the peak absorbance. This resulted in smaller experimental τ_1 values

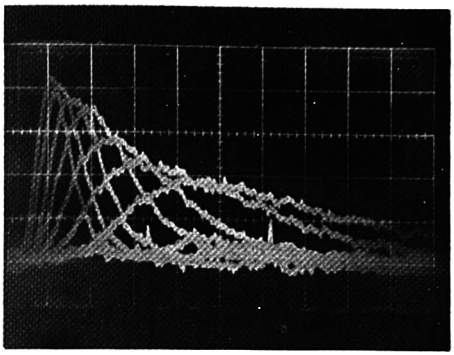


Figure 3. Oscilloscopic trace of 1.25×10^{-14} kg Cd atomized at different heating rates. Left to right: 3.40 K ms^{-1}, 2.17 K ms^{-1}, 1.47 K ms^{-1}, 1.23 K ms^{-1}, 0.79 K ms^{-1}, 0.33 K ms^{-1}, 0.20 K ms^{-1}. Horizontal scale: 200 ms/scale div. Vertical scale: 0.05 absorbance/scale div

Table IV. Effect of Heating Rate on Peak Temperature of 1.25×10^{-14} kg Cd

heating rate/K ms^{-1}	peak temperature/K
0.20	750
0.33	785
0.79	995
1.23	1120
1.47	1160
2.17	1240
3.40	1560

and larger experimental τ_2 values than the theoretical τ_1' and τ_2' values, respectively. Hence, for Mo and V, the experimental τ_1/τ_2 ratios were smaller than the theoretical τ_1'/τ_2' ratios.

Of particular interest is the change in the shape of the absorption pulse as a function of the rate of heating. Figure 3 is a photograph of a series of oscilloscopic traces for 1.25×10^{-14} kg of Cd atomized over a wide range of heating rates. As the heating rate of the graphite tube is increased, some interesting changes occur. The atomization time, τ_1, is greatly diminished (Table I) and the appearance time is also decreased. Also, increasing heating rates greatly shorten the pulse duration time. The appearance temperature is a constant (for any given element) and independent of the heating rate of the graphite tube. However, as can be seen from Table IV, the peak temperature (defined as the temperature corresponding to the peak of the absorption pulse) was found to be very dependent on the heating rate. As the heating rate was increased from 0.2 K ms^{-1} to 3.40 K ms^{-1}, the peak temperature of Cd increased from 750 K to 1560 K, respectively.

Sturgeon et al. (*14*) elucidated the mechanism of atom formation in a Perkin-Elmer Heated Graphite Atomizer Model 2100. The authors (*14*) used the absorbance values from the initial 200–300 ms portion of the transient absorption pulse during which the temperature of the gas phase was equal to that of the graphite surface (*27*), and constructed a plot of the log absorbance vs. the reciprocal of the absolute temperature. The slope of the straight line plot so obtained was identified with the activation energy, E_a, for the rate-determining step. The above paper (*14*) has established that mechanism of atom formation in many cases involves intermediate species formed by analytes.

In thermodynamic equilibrium, the population of analyte species having energy equal to or more than the activation

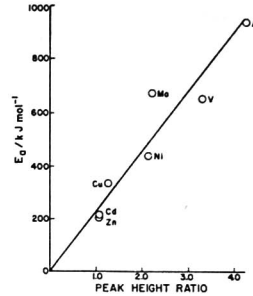


Figure 4. Correlation plot of the increase in peak height ratio as a function of the E_a of atomization.

Table V. Activation Energy, E_a, for Atomization[a]

element	temperature range/K	atomization mechanism	E_a/ kJ mol^{-1}
Cu	1270–1326	$Cu_{(s)} \rightarrow Cu_{(g)}$	320
	>1326	$Cu_{2(g)} \rightarrow 2Cu_{(g)}$	180
Cd	>720	$CdCl_{2(g)} \rightarrow Cd_{(g)} + 2Cl_{(g)}$	210
Zn	>1140	$ZnCl_{2(g)} \rightarrow Zn_{(g)} + 2Cl_{(g)}$	200
Al	2080–2237	No mechanism has been established	980
	>2237	No mechanism has been established	480
Ni	1590–1688	$Ni_{(s)} \rightarrow Ni_{(g)}$	410
	>1688	$Ni_{2(g)} \rightarrow 2Ni_{(g)}$	210
V	2200–2360	$VO_{(g)} \rightarrow V_{(g)} + O_{(g)}$	640
	>2360	$V_{(l)} \rightarrow V_{(g)}$	490
Mo	>2100	$Mo_{(s)} \rightarrow Mo_{(g)}$	690

[a] Taken from reference 14.

energy, E_a, for the rate-determining step, is governed by the Boltzmann factor, $e^{-E_a/RT}$ (this factor determines the number of activated complex, N). This number, N, can be written in terms of the Boltzmann distribution as

$$N = N_0' e^{-E_a/RT} \quad (6)$$

where E_a is the activation energy of the rate-determining step in the atom-releasing process; N is the number of analyte species having energy equal to or greater than E_a; N_0' is the number of analyte atoms in the sample, R is the universal gas constant, and T is the temperature in degrees Kelvin. The exponential term in Equation 6 indicates that the effect of a given change in the temperature, T, on the number of activated complex, N, will be greater, the larger the value of the activation energy, E_a. Since temperature is a linear function of the heating rate, at least during the initial part of the temperature–time curve (Figure 1), the latter can be substituted for the temperature in the above discussion. Thus, the greater the heating rate, the greater is the number of analyte species having energy equal to or greater than E_a. Also, for those elements which are relatively difficult to atomize, i.e., which have larger values for the activation energy, E_a, a given change in the heating rate will produce a greater change in the number of activated complex species, N, and hence in the analytical sensitivity than for those elements which are relatively easy to atomize, i.e., which have smaller values for the activation energy, E_a. This was experimentally observed, as is seen from Figure 4.

Figure 4 is a correlation plot of the activation energy, E_a, and the PEAK HEIGHT RATIO which is the ratio of the peak absorbance at the heating rate of 4.0 K ms^{-1} to that at

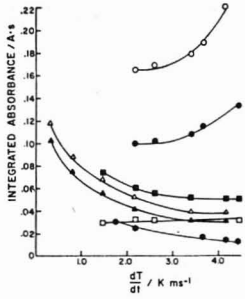


Figure 5. Integrated absorbance as a function of graphite tube heating rates. ○ Mo, ● V, □ Ni, ■ Cu, △ Cd, ▲ Zn, ● Al

the heating rate of 2.0 K ms^{-1}. The activation energy values taken from the paper by Sturgeon et al. (*14*) who used the same experimental setup are presented in Table V. Figure 4 shows that the higher the E_a value of the rate-determining step in the atom-releasing process, the greater the increase in the peak absorbance due to a given increase in the heating rate.

Effect of Heating Rates on Integrated Absorbance. Integrated absorbances of a number of metals as a function of the heating rate are presented in Figure 5. Three general trends emerge from examination of these curves. Copper, Al, Cd, and Zn show an exponential decrease in the integrated absorbance with increasing heating rates; Mo and V show an exponential increase in the integrated absorbance with increasing heating rates; the integrated absorbance of Ni is virtually independent of the heating rate over the range of the heating rates studied.

According to Equation 4, the integrated absorbance is directly proportional to the residence time, τ_2', of the atoms in the analysis volume; this equation to be valid, however, requires fulfillment of two conditions, viz., complete atomization of the analyte and a constant residence time. These conditions, however, are not always fulfilled in the case of commercial atomizers. For example, even for relatively volatile elements such as Zn and Cd where complete atomization is expected, the atomizer surface temperature is changing rapidly throughout the duration of the absorption pulse (*27*). A continuously changing thermal gradient across the longitudinal axis of the graphite tube surface greatly affects the residence time, τ_2', of the analyte atomic vapor in the analysis volume. Also, except for a 200–300 ms period from the beginning of the absorption pulse, the temperature of the vapor phase in a HGA 2100 graphite tube lags behind the graphite tube surface temperature; the magnitude of the lag continues to increase throughout most of the duration of the pulse and becomes constant only for a short period at the end of the absorption pulse (*27*). Thus, as the heating proceeds, the rapidly changing temperature and the large thermal gradient across the longitudinal axis of the graphite tube yield an analyte atom population, N_o, which is less than N_o', which is the number of analyte atoms present in the sample. Thus, the experimental values of the integrated absorbance, Q_N, are not constant and are less than the theoretical value, Q_N'. Furthermore, complete atomization of the analyte element sometimes did not occur, as was evidenced by Mo (2.5 ng) which even after prolonged atomization periods (8 s at 3000 K) still yielded a "memory effect" in subsequent blank firings of the graphite tube.

Although Equation 4 cannot be strictly applied to this case, the "memory" signal resulting from a typical quantity of Mo (1.0 ng), atomized under the experimental conditions used in this study, did not account for more than a few percent of the total signal, and, hence, such residual Mo does not alter the interpretation of the experimental results for Mo presented here.

For commercial graphite furnaces, Equation 4 should be modified as shown in Equation 7:

$$Q_N = N_o\tau_2 \tag{7}$$

where Q_N = experimental integrated absorbance, N_o = number of atoms in the analysis volume, and τ_2 = experimental residence time. Q_N will be a constant if both N_o and τ_2 or their product remains constant.

Using Equation 7, the curves in Figure 5 for Cu, Al, Cd, and Zn can be rationalized in terms of the number of analyte atoms N_o in the analysis volume and experimental residence time, τ_2. In Figure 2, if it is realized that the number of analyte atoms at the peak of the absorption pulse is given by N_o rather than the number of analyte atoms in the sample, N_o', as would be when $\tau_1' << \tau_2'$ as in L'vov's model (*16*) for an isothermal graphite cuvette, then the levelling of the peak absorbance of the above elements in Figure 2 can be interpreted as that the N_o for each element attains a nearly constant value at high heating rates, whereas the N_o value is lower and changing at low heating rates. Table II shows that the values of experimental residence time, τ_2, for the elements studied are smaller and constant or nearly constant (within the experimental uncertainty) at high rates, whereas they are larger and changing at low heating rates. It seems from Figure 5 that in the case of the elements studied, with increasing heating rates, the sharp decrease in τ_2 values more than cancels the rather small increase in the peak absorbance, the net result being a rather sharp decrease in Q_N values. In the case of Ni, the near-constancy of Q_N values as a function of heating rates is probably a result of fortuitous cancellation of a rather smaller increase in N_o by an equally smaller decrease in the τ_2 values with increasing heating rates. In the case of Mo and V, the increase in Q_N is due to the increase in N_o (see the peak absorbance in Figure 2) predominating over proportionately smaller decreases in τ_2 values at high heating rates.

Table II also shows that the experimental τ_2 values are not constant for any of the elements studied. Only for the easily-atomized elements (Cd and Zn) did the absorbance maximum mark the end of the atomization time; for the other elements, the absorbance maximum simply marked the point of balance between the rates of formation and loss of analyte atoms. Hence, the experimental τ_2 values of the elements except Cd and Zn contained contributions from the continuing atomization of the analyte beyond the point of the absorbance maximum, and the experimental τ_2 values were therefore greater than the theoretical τ_2' values. The less easily the elements are atomized, the greater will be the effect of this continuing atomization on the experimental τ_2 values and, hence, the effect will be greatest for Mo and much less for V, Ni, Al, and Cu.

CONCLUSIONS

The analytical sensitivities of the elements which are difficult to atomize experience the greatest enhancement from higher graphite tube heating rates than what are now commercially available. Instantaneous heating (heating rate up to 50 K ms^{-1}) by capacitive discharge offers attractive possibilities for enhancement of analytical sensitivities, and is now under study at the authors' laboratories.

LITERATURE CITED

(1) W. C. Campbell and J. M. Ottaway, *Talanta*, **21**, 837 (1974).
(2) J. Aggett and A. J. Sprott, *Anal. Chim. Acta.*, **72**, 49 (1974).
(3) C. W. Fuller, *Analyst (London)*, **99**, 739 (1974).
(4) D. J. Johnson, B. L. Sharp, T. S. West, and R. M. Dagnall, *Anal. Chem.*, **47**, 1234 (1975).
(5) G. Torsi and G. Tessari, *Anal. Chem.*, **45**, 1812 (1973).

(6) S. L. Paveri-Fontana, G. Tessari, and G. Torsi, *Anal. Chem.*, **46**, 1032 (1974).
(7) G. Torsi and G. Tessari, *Anal. Chem.*, **47**, 839 (1975).
(8) G. Torsi and G. Tessari, *Anal. Chem.*, **47**, 842 (1975).
(9) G. Torsi and G. Tessari, *Anal. Chem.*, **48**, 1318 (1976).
(10) R. E. Sturgeon, C. L. Chakrabarti, I. S. Maines, and P. C. Bertels, *Anal. Chem.*, **47**, 1240 (1975).
(11) R. E. Sturgeon, C. L. Chakrabarti, and P. C. Bertels, *Anal. Chem.*, **47**, 1250 (1975).
(12) Wim M. G. T. van den Broek and L. de Galan, *Anal. Chem.*, **49**, 2176 (1977).
(13) F. D. Posma, H. C. Smit, and A. F. Rooze, *Anal. Chem.*, **47**, 2087 (1975).
(14) R. E. Sturgeon, C. L. Chakrabarti, and C. H. Langford, *Anal. Chem.*, **48**, 1792 (1976).
(15) R. E. Sturgeon and C. L. Chakrabarti, *Anal. Chem.*, **49**, 1100 (1977).
(16) B. V. L'vov, "Atomic Absorption Spectrochemical Analysis", translated by J. H. Dixon, Adam Hilger Ltd., London, 1970.
(17) B. V. L'vov, *Pure Appl. Chem.*, **23**, 11 (1970).
(18) D. A. Katskov and B. V. L'vov, *Zh. Prikl. Spektrosk.*, **15**, 783 (1971).
(19) D. J. Johnson, T. S. West, and R. M. Dagnall, *Anal. Chim. Acta*, **67**, 79 (1973).
(20) H. M. Donega and T. E. Burgess, *Anal. Chem.*, **42**, 1521 (1970).
(21) F. J. M. J. Maessen and F. D. Posma, *Anal. Chem.*, **46**, 1439 (1974).
(22) R. E. Sturgeon and C. L. Chakrabarti, *Spectrochim. Acta, Part B*, **32**, 257 (1977).
(23) A. Montasser and S. R. Crouch, *Anal. Chem.*, **47**, 38 (1975).
(24) M. S. Cresser and C. E. Mullins, *Anal. Chim. Acta*, **68**, 377 (1974).
(25) B. V. L'vov, "Electrothermal Atomization—The Way Towards Absolute Analysis", presented as an invited paper at the 3rd FACSS meeting and the 6th International Conference on Atomic Spectroscopy, Philadelphia, Pa., November 15–19, 1976.
(26) D. C. Gregoire, C. L. Chakrabarti, and P. C. Bertels, unpublished results.
(27) R. E. Sturgeon and C. L. Chakrabarti, *Spectrochim. Acta, Part B*, **32**, 231 (1977).
(28) J. O. Hirschfelder, C. F. Crutiss, and R. B. Bird, "Molecular Theory of Gases and Liquids", J. Wiley and Sons, New York, N.Y., 1954, p 14.

RECEIVED for review January 20, 1978. Accepted August 2, 1978. The authors are grateful to the National Research Council of Canada for research grants supporting this research.

Design and Construction of a Time Multiplex Multiple Slit Multielement Flame Atomic Absorption Spectrometer

Eric D. Salin[1] and J. D. Ingle, Jr.*

Department of Chemistry, Oregon State University, Corvallis, Oregon 97331

A multielement spectrometer has been developed for the simultaneous determination of four elements by flame atomic absorption (AA). The spectrometer is based on a multiple exit slit monochromator and uses a mirrored funnel to direct light from the various exit slits to a single photomultiplier. A single element hollow cathode (HC) lamp is used for each element and the beams from these HCs are combined by beam splitters. HC lamp pulsing and data acquisition are implemented with a time multiplex approach. The HC lamp pulsing is controlled by simple digital circuitry which sequentially pulses each HC lamp and digitally integrates HC and background signals for each element at a 12.5 Hz rate for up to 240 cycles. The system presently allows the simultaneous determination of any four of ten possible elements. There are no moving parts during operation and the instrument requires little more hardware than necessary for a conventional single element AA.

Simultaneous multielement analysis can offer distinct advantages to the analyst. Sample size and analysis cost and throughput time can be reduced and, in addition, multiple wavelength systems may offer distinct advantages with respect to accuracy and precision when difficult matrix problems are encountered by the use of an internal standard or other compensation techniques.

A primary encumbrance to multielement AA has been the alignment of several sources such that the radiation from all of the sources is combined into a single beam to pass through the same portion of the flame. Gratings (*1*), fiber optics (*2*), beam splitters (*3–5*), and mirror arrangements (*6*) have been used for this purpose. Gratings and mirror arrangements require careful alignment and are not convenient for a rapid change of analytes. Fiber optics have not been especially successful as beam combiners (*2*).

Multielement hollow cathode (HC) lamps can be used for certain combinations of elements (*3, 4, 7, 8*). The significant difference in the intensity of resonance lines for different elements causes dynamic range problems when they are used with detectors with a limited dynamic range (e.g., multichannel semiconductor detectors) (*8*).

Multielement detection systems for AA have varied considerably. Direct readers have been used (*1, 2, 6, 7, 9, 10*) and moveable slit type readers for a limited number of elements have been developed (*7, 9*). In general, direct reader systems are relatively complex and expensive with low light collection efficiency. The fixed slit direct reader systems are inflexible to wavelength changes and the moveable slit direct reader systems are limited to a few elements.

Semiconductor multichannel detectors (Vidicons and linear diode arrays) have been successfully applied to multielement AA work (*4, 11–13*). These detectors offer great versatility in wavelength selection; however, compared to a photomultiplier tube (PMT), the dynamic range is much lower and the spectral responsivity (i.e., quantum efficiency) below 300 nm, where most AA work is done, is less (*14*). Also because of their limited size (e.g. 1 inch) and the need to maintain good resolution, only a relatively small wavelength range (e.g., 10–50 nm) can be covered. To reduce amplifier-readout noise to a low level, an intensifier stage must be added to multichannel detectors which can considerably increase the expense.

Echelle monochromator systems with banks of PMTs, multichannel detector, or image dissector photomultipliers seem to offer the potential for carrying out multielement AA with a continuum light source with background correction (*15–18*) though a limited amount of work appears to have been presented on actual multielement applications. An echelle monochromator has been used with HC lamps and a Vidicon for multielement AA (*19*).

A multislit AA spectrometer providing background correction using a rotating sector wheel and computer control (*3*) was constructed for the determination of three elements using a nonflame atomizer. This system is less expensive than

[1] Present address, Department of Chemistry, University of Alberta, Edmonton, Alberta, T6G 2G2, Canada.

0003-2700/78/0350-1737$01.00/0 © 1978 American Chemical Society

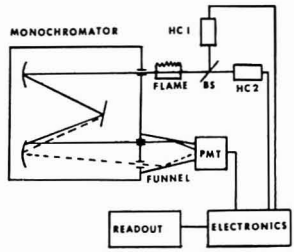


Figure 1. TMMS flame AA schematic

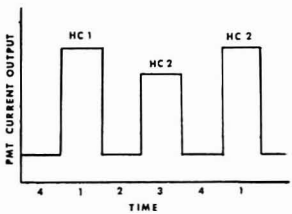


Figure 2. TMMS PMT output

a direct reader system, but requires computer control and is complex.

For multielement AA, resonance detection has been used (*20, 21*) and the use of resonance modulation has been suggested (*22*) but not yet been actively applied to multielement AA. Dawson (*23*) developed a rapid scan monochromator for multielement AA and AE analysis. The detection limits reported were relatively high because of the inherent low duty cycle of this approach. Most of the above detector systems would be considered expensive and require either a computer or extensive supplemental electronics.

It was felt that a less complicated and expensive multielement flame AA system could be developed that provided the demonstrated performance characteristics of single element AA instruments. The instrument developed is well suited to increase the sample throughput in laboratories in which a few elements or sets of elements are determined routinely for many similar well characterized samples. The system can be constructed as a modification of an existing single element AA system.

The multielement system described here is denoted the TMMS (Time Multiplex Multi Slit) AA system. It employs a multislit monochromator with an exit slit for each element and a single PMT detector. A separate hollow cathode lamp is used for each element being determined, and these are pulsed sequentially so as to differentiate their signals. During operation, there are no moving parts and computer control is not required.

INSTRUMENTATION

The design of a new multielement flame AA spectrometer is based on the use of a multiple slit monochromator with a single detector and a time multiplex (TM) mode of operation for the HC lamps and data acquisition which was previously used for multielement AF measurements (*24*). A "box car" type up–down integration technique previously described (*25*) is employed to process the signals. The general operation of the instrument is illustrated by Figures 1, 2, and 3 and the specific components used are specified in Table I. Much of the instrument is similar to a common single-element AA; however, the radiation from four lamps (one single element

Table I. Equipment List

electronics	
380 J electrometer amplifier used as current to voltage converter	Analog Devices
4705/01 1-MHz voltage to frequency converter	Teledyne Philbrick
ADD (Analog Digital Designer) modules EU 801-11 (Power Supply) EU 801-15 (Digital Readout) EU 800-KC (Crystal Clock Card)	Heath Company
regulated power supply (0-35V/5A) LA 50-03 BM (for digital circuits)	Lambda Corp.
HV regulated power supply model 71 (0-500 V, 200 mA) (for use with HCs)	Lambda Corp.
model 244 high voltage power supply (0–2225 V, for use with PMT)	Keithley Instruments
1P28 photomultiplier tube	RCA
current meter, 55064 (0-20 mA, dc)	Knight (Allied Radio)
rack mountable strut cage $4^1/_2 \times 19 \times 12$ in.	Vector
bread board/printed circuit board, 22-finger, $4^1/_2 \times 8^1/_2$ in.	E & L Instruments
optical components	
filters	Corion Corp.
lenses, 1 in., *f*/3 (quartz)	Essco
1-m triangular aluminum optical rail	Ealing
3.5-in. component carrier for above rail	Ealing
1.5-in. component carrier for above rail	Ealing
3-in. mountings	Ealing
entrance slits and slit assembly (7260)	Oriel
beam splitters, 1-in., polka dot (no. 01-101-232-00)	Varian
hollow cathode tubes	Westinghouse (Jarrell-Ash for Fe)
Hg pen lamp	Ultraviolet Products
grating, 600 grooves/mm, blaze angle 5°10′, $2^1/_2 \times 2^1/_2$ in, catalog number 35-53-06-010	Bausch & Lomb, Inc.
concave mirror, 18-in. focal length, 3-in. diameter	McKee-Pedersen
miscellaneous	
counter, gear driven G-567066 (used on monochromator drive)	Stewart Warner
photo plates, 2 × 2 × 0.04, high resolution, emulsion identification 106G-A15C4	Precision Photoglass Ind.
Shadowgraph	Nippon Kogaku (Nikon)
reduction camera, Mann type 1003	David W. Mann Co. (GCA Corp.)
vacuum evaporator	Mikros, Inc.
pressure regulators	Victor Corp.
flow meters, size #3	Gilmont
slot burner, 10 cm	Jarrell-Ash

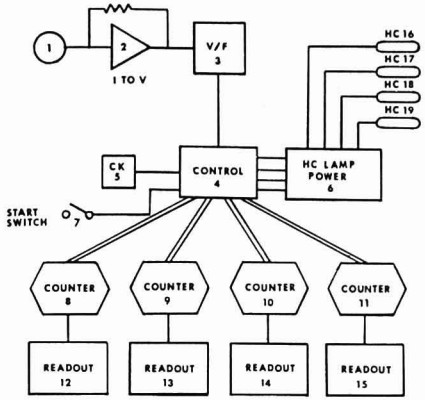


Figure 3. General electronic schematic. See text for identification of components

lamp for each element to be determined) is directed through the flame with the use of beam splitters. The normal single exit slit in the focal plane of the monochromator is replaced by a multiple slit array such that the appropriate resonance radiation line from each element's HC lamp passes through the appropriate exit slit. For this work, a slit array was made for the following elements with the wavelength in nm in parentheses: Cu (324.7), Mg (285.2), Pb (283.2), Mn (279.5), Au (267.0), Fe (248.3), Co (240.7), Ni (232.0), Cd (228.8), and Zn (213.9).

The signals for each element are distinguished with a TM approach. With a clock and central control circuit, each element's HC lamp is pulsed at the same frequency but only one is turned on at a time in a sequential manner. The duty cycle (% time that a given lamp is on) is considerably less than the typical 50%. The same clock and control circuit control the data acquisition and direct the photomultiplier signal to a separate data acquisition and readout channel for each element.

The data acquisition channels consist essentially of up-down counters. When a given lamp is pulsed on, the photomultiplier signal is integrated for a specified time. This integration is accomplished digitally by counting the number of pulses from the V/F converter for a given length of time. This integrated "lamp on" signal is proportional to the lamp signal and any signals from the PMT dark current or flame background emission. To correct for the nonlamp related portion of the signal, the PMT signal is integrated for the same time period after the lamp is turned off. This signal is subtracted from the first integrated signal. This is accomplished by subtracting the number of V/F pulses counted in the "lamp off" period from the counts accumulated during the "lamp-on" period. This integration addition-subtraction or up-down counting can be carried out separately for each lamp for any number of lamp pulses up to 240 or until overflow occurs.

For simplicity in the following discussion and Figures 1 and 2, a two-element (2 HC lamp) system will be considered although the final system is designed to determine four elements simultaneously with exactly the same principle. At time 1, HC lamp 1 is pulsed on (solid line Figure 1) for one clock period (typically 10 ms). The light from this HC hits the beam splitter (a semisilvered mirror). Approximately half is reflected and the other half is transmitted. The reflected portion goes down the optical path and through the flame where absorption can take place. This light is then focused on the entrance slit of the monochromator and passes through the system where resonance radiation is directed through its slit. The resonance radiation and any flame background emission over the spectral bandpass is then reflected down a mirrored funnel into a PMT. The current from the PMT is converted to a voltage and finally a frequency proportional to the voltage. After a brief delay (typically 0.7 ms), the signal is integrated (counted) for 9.3 ms. Time 2 then begins. HC 1 is turned off and, after the same brief delay, the background signal is integrated for 9.3 ms and the result is subtracted from the previously stored signal in counter 1. At time 3, HC lamp 2 is pulsed on for 10 ms and the same procedure is again initiated except that the resonance radiation (dotted line in Figure 1) is passed through another slit and the signal is integrated for 9.3 ms in counter 2. At time 4, after the delay, the background signal is integrated for 9.3 ms and subtracted from the result in counter 2. Another cycle will then begin after each 40 ms (in this example). Each complete cycle is called a lap and normally 10 or 100 laps are run. The 0.7-ms delays allow sufficient time for the HC signals to rise and fall to their equilibrium values.

More detailed discussion of the optical and electronic components is given below and complete details of construction and operation are available from the authors or reference 26.

Optical Components. The monochromator was constructed in this laboratory in a standard $f/8$ Czerny–Turner configuration with a linear reciprocal dispersion of 3.5 nm/mm. A 120-μm entrance slit was used to provide a spectral bandpass of 0.42 nm. A exit slot 2.0 by 8.4 cm was cut in the focal plane wall of the monochromator. The grating position can be adjusted manually by a sine bar assembly. A slit array holder assembly is mounted on the outside of the focal plane wall to hold the slit array in the proper position to intercept the spectrum passing through the exit slit slot.

The slit array holder assembly is pictured in Figure 4. The exact positioning of the slit array (the quartz slide on which the slits are etched) along the exit slit is not critical since the grating can be rotated to move the spectrum into position. It is important that the slit array rest in the focal plane, and this is ensured by machining the thickness of the slide holder carefully (0.001 in tolerance) and laying the etched side of the slit array on the slit array holder before gluing. Only the tilt of the slit holder needs to be adjusted with the 40 turn per inch adjustment screw so that the spectral images coincide exactly with the slits and are not tilted. This adjustment is needed only once for any given slit array/slit array holder combination. The entire assembly can then be removed and replaced with only minor adjustment of the grating.

Slit spacing were determined photographically. The resonance line slit images were recorded on standard Kodak Spectrum Analysis #1 photoplates which had been cut to approximately 2 × 3 inch size and placed in the focal plane by placing them emulsion side down on the surface of an unoccupied slit array holder. The distances were measured by a Nikon Shadowgraph, essentially a microscope with a micrometer traversing stage which is accurate to 2 μm. A separate calibration photographic plate was made for each element by exposing it first to the light from the appropriate hollow cathode tube and then the light from a Hg pen lamp. All measurements were referenced to the 254 nm Hg line.

The slit manufacturing technique is a hybrid of classical photographic and modern integrated circuit technology and can be broken down into the following steps: aluminum (Al) deposition, photoresist deposition, mask manufacture, mask photography, slide exposure and development. The slits are manufactured from quartz microscope slides which are coated

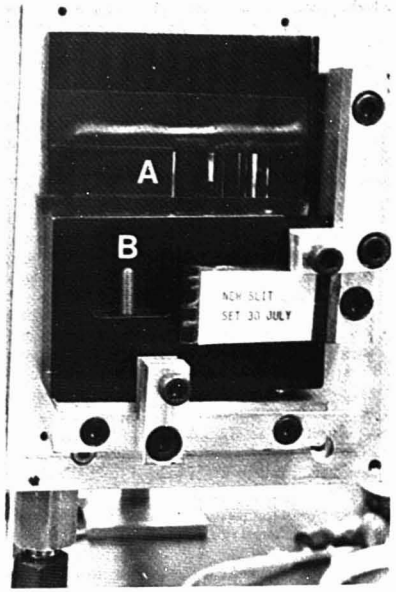


Figure 4. Slit array holder. (A) Masked slit array; (B) tilt adjustment

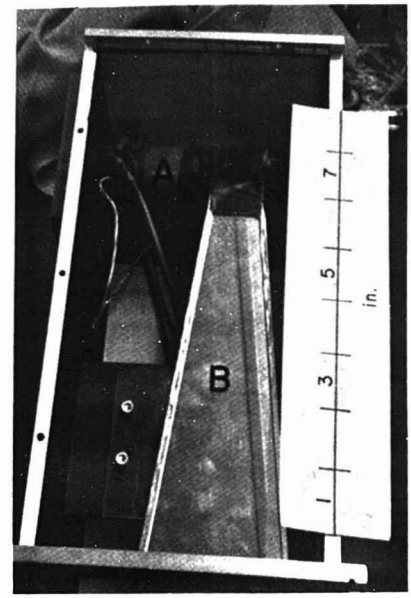


Figure 5. Photon funnel. (A) PMT; (B) mirrored photon funnel

with Al by vacuum deposition. Next the Al-coated slide is placed on a spinner assembly designed to hold a microscope slide and the surface is completely coated with AZ 1350 positive acting photoresist applied with a dropper. The slide is then brought up smoothly to about 1500 rpm and allowed to spin for about 5 s. The spinning is stopped and the slide is dried in an evacuated oven. It can then be stored (away from UV light and dust) for periods exceeding one month.

A mask is used in the exposure portion of the slit manufacturing process. The mask must pass UV light only in the locations where the slits are desired. After experimentation, it was concluded that the most convenient method of mask production would be through the utilization of photoreduction techniques. A mask exactly 20 times larger than the final mask is constructed on a milling machine using the data obtained during the slit spacing determination procedure (all measurements are scaled up by exactly a factor of 20). The 20X mask was machined from $^1/_8$-inch Plexiglas with a $^3/_{32}$-inch milling cutter to produce 2.4 mm × 25 cm slits with a positioning accuracy of 25 μm. After 20X reduction, the slits should be 120 μm wide and 12 mm high with a positioning accuracy of 1.3 μm. After milling, the 20X mask is painted flat black.

A photoreduction is made by placing the 20X mask on the transparent screen of a GCA photoreduction assembly. The camera carriage is carefully adjusted to produce the correct reduction by checking the size of the images through a traversing microscope mounted on the reduction assembly. A reversal of this plate is made by contact exposure (as with a contact printing) and this plate is the final mask. This mask is placed face downward on a photoresist covered slide which is placed with the aluminized face upward. The photoresist is exposed through the final mask with light from a high intensity quartz–halogen lamp and then developed. The aluminum surface that is exposed by developing is then removed by etching, leaving an aluminum coated slide with slits at the proper positions. The actual slit widths and interslit distances were determined on the Shadowgraph. The slits were then tested in the TMMS monochromator to determine the placement error. For unknown reasons, the manufacturing process produced slits narrower than the expected 120 μm. The average slit width was about 85 μm. This problem had not been encountered in preliminary runs and may be due to an incorrect exposure of one of the photographic plates. The placement data indicate that only the Mn slit is significantly misplaced. It is extremely fortunate that the primary Mn resonance line, 279.482 nm, is part of a triplet. The other two lines are 279.827 and 280.106 nm. The relative absorbances of these lines are 10, 8, and 5 (27), respectively, and the 0.42 nm bandpass of the TMMS system effectively mixes the radiation from the first two lines so that experimentally no difference in absorbance for the same solution could be detected when the grating was removed from the "aligned" position to the position providing the maximum Mn signal. None of the other slits was more than 25% out of alignment from a maximum signal.

Many light collection schemes were considered involving fiber optics and mirrors, but the unique photon funnel was finally chosen because it is inexpensive, compact, rugged, and easily designed. The purpose of the photon funnel is to direct all light exiting from any exit slit over a 2-inch region onto the 0.8 × 0.4 in. photocathode surface with minimal light loss. The light exits from each slit in a conical fashion as determined by the focusing mirror and slit position. The plane angle of the cones ranges from 8.0° to 9.5° so that the light could be spread over a 1.3-inch region 8 inches from the slit.

The photon funnel, PMT and funnel/PMT housing compartment are shown in Figure 5. The funnel is constructed from two trapazoidal and two rectangular pieces of a front surface mirror. The side-on 1P28 PMT is glued to the small end of the funnel and covered with black electrical tape to avoid light leaks. The dimensions of the funnel are critical

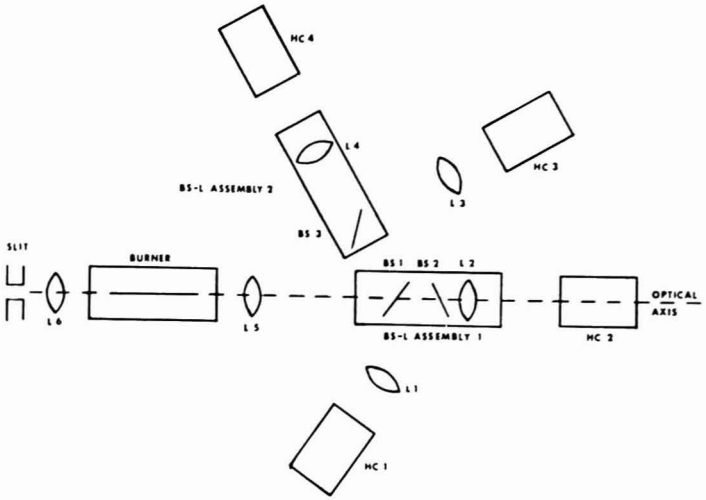


Figure 6. Arrangement of hollow cathode tubes, beam splitters, and lenses. (L) Lenses, (BS) beam splitters, (BS-L) assemblies, beam splitter and lens holder

and are determined by ray tracing techniques (26) to minimize the number of reflections (which was kept to 3 or less) and the dead zone for a given slit. The dead zone is the planar angle zone in which rays going through a given exit slit will go out the end of the funnel and miss the photocathode surface. The dead zone at no time exceeded 25% of the total plane angle. Provision is made for adjusting the position of the funnel along the optical axis plane parallel to the optical table so that the large end of the funnel can be butted against the slit array or moved up to a distance of 0.1 inch away from the slits so that individual slits can be masked (blocked). The efficiency was tested with a Hg pen lamp and a 254-nm filter so as to have essentially monochromatic 254-nm radiation. The slit array was removed and the monochromator grating was rotated so that the slit image moved across the exit slot. Over 75% of the exit slot range, the attenuation is less than 25% from the maximum signal. At the extremes of the exit slot, the worse attentuation is 55% of the maximum value. Calculations indicate that, with good aluminized mirrored surfaces, the maximum signal obtained in the middle of the exit slot range should be within 90% of that obtained with the PMT directly behind the exit slit because the dead zone is negligible and at most one reflection is suffered.

The lenses, beam splitters, and HC lamps are arranged as shown in Figures 6 and 7. Original alignment of the external optics is carried out in a straightforward manner with the use of a standard laboratory He–Ne laser. Conditions are arranged so that the beam travels from the center of the entrance mirror out through the center of the entrance slit (i.e., backwards through the system) and along the optical axis. The position of each beam splitter and lens is adjusted so that the laser beam strikes the center of the optical component and passes down the center axis of the HC holders.

When the slit array holder and the optics have been aligned as above, the grating must be moved to the correct position. This is accomplished by masking all the slits but the Mg slit, placing the Mg HC lamp in one of the HC holders, and initiating system operation with the flame off. A Mg 285.2-nm filter is used to remove unwanted lines, and the grating is moved to the position of maximum intensity throughput as indicated by the electronic readout. The Mg HC line (285.2 nm) is the reference line used for all operation. When it is correctly aligned, the grating is correctly aligned for all slits. The above operations need be carried out only when warranted by the insertion of a new slit array or other change and need not be carried out if the slit assembly is not changed.

Electronics. The following discussion will use Figure 3 in which each component has been numbered and labeled for ease of reference. A PMT [1] is used to transduce light into an electrical signal, in this case a current. The current is converted to a voltage by an operational amplifier [2] operated in the current-to-voltage (I–V) converter mode. If necessary it can be further amplified by an additional amplifier at this point. The voltage is then converted to a frequency which is proportional to that voltage by the voltage to frequency (V/F) converter [3]. The digital pulse train is then input into the control section [4] where it is directed at the correct time to the appropriate set of cascaded up-down counters [8], [9], [10], and [11]. Each set of counters has its own digital readout [12], [13], [14], and [15] which constantly displays the aggregate sum stored in the counters.

The control card is timed by an input from a crystal controlled clock [5]. This clock signal is used at all times to control the pulsing of the HC lamps through the HC lamp power assembly [6]; however, the control section will only allow data from the V/F to pass through into the counters after the start switch has been actuated. At this time it will reset itself, clear the counters, and begin pulsing the first HC and putting data into the corresponding counter. It will then proceed to pulse the other HCs and place the data accordingly for a set number of laps (cycles). At the end of data collection, the control section will continue to pulse the HCs until requested to begin again.

Two demultiplexers (7442) are used in the control circuit. Figure 8 contains a useful simplified schematic. One demultiplexer [11] controls the pulsing of the HCs while the other [9] controls the sequential channeling of the V/F pulse train to the appropriate up–down counter. Since both demultiplexers are controlled by the A, B, and C BCD coded outputs of the same decade counting unit (DCU, 74161) [10]

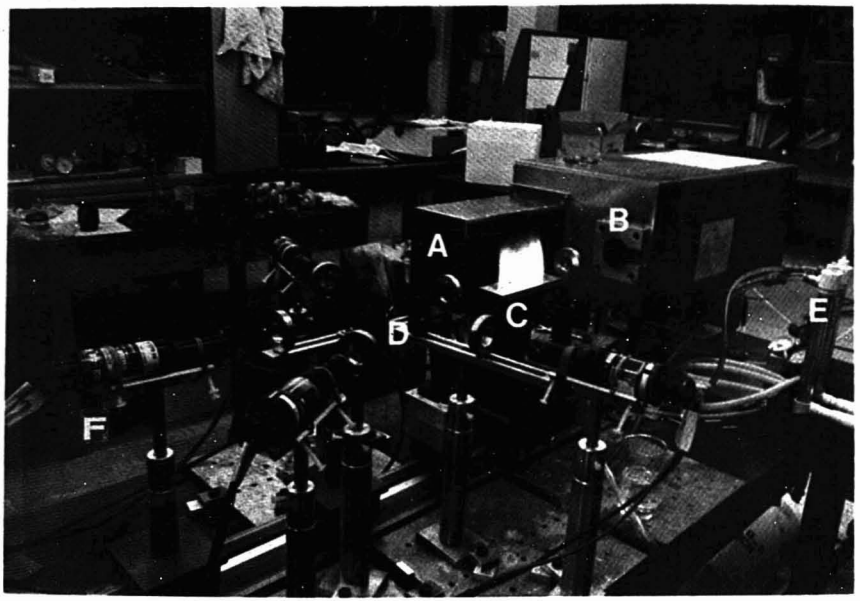


Figure 7. Photograph of instrument. (A) PMT housing, (B) entrance slit, (C) burner, (D) beam splitter, (E) flow meters, (F) hollow cathode lamp

the pulsing of the lamps and data acquisition are perfectly synchronized. The demultipliers are the heart of the system and all other components are used to control the rate of pulsing and data acquisition, to stop and start data acquisition and to provide delays.

The data acquisition is initiated with the start switch which triggers monostable [1] (74121) to produce a 0.7-s logic 1 pulse. This monostable acts as a momentary bounceless switch. When the output of monostable [1] returns to logic 0, monostable [2] (74121) is triggered to produce a 1-μs pulse. This pulse clears the lap counter, the demultiplexer counter, sets the output up–down counters to zero and resets the clock.

The demultiplexer counter [10] will trigger on the first clock pulse after the starting pulse, and the A output of that counter will go to logic 1. This will cause the D input, always a logic 0, of the lamp demultiplexer, to be input via the demultiplexer to inverter [15]. This in turn will turn on HC 1 for the period of the input clock frequency. The second 0 clock pulse after the starting pulse will cause the demultiplexer counter A output to go to 0 and the B output to 1. This will turn HC 1 off for one clock period. The 3rd and 4th transitions from the clock turn HC 2 on and off for one clock period. Similarly HC lamps 3 and 4 are turned on and off. The sequence is repeated continually until the start switch is activated again. This interrupts the cycle and restarts it again with HC 1.

The pulse train from the V/F converter is directed to the appropriate up and down inputs of the up–down counter through input *b* of gates [4] and [5], and input D of the signal demultiplexer. NAND gates [4] and [5] will pass the pulse train only if their *a* inputs are logic 1.

Input *a* of gate [4] is controlled by monostable [3] (74221) which is triggered by the starting pulse from monostable [2] or the clock pulse. Thus when monostable [3] is triggered, the output goes to logic 0 which blocks gate [4] until *a* returns to logic 1. This delay period was chosen to be about 0.7 ms to prevent data from being acquired during the rise and fall times of the signal from the HC lamp.

Input *a* of gate 5 is controlled in a somewhat different manner. The lap counter [7] (7493) receives one pulse from the C output of the demultiplexer counter and NAND gate [8] after every eight clock pulses (one lap). After a preselected number of laps (determined by ABCD outputs connected to NAND gate [6]) the output of gate 8 is driven to logic zero which blocks any more data acquisition via gate 5. Simultaneously one of the inputs to NAND [8] is driven to logic 0 thereby stopping the lap counter from further counting. The actual lap counter is 2 cascaded 4-bit binary counters and, hence, 1 to 240 laps may be chosen.

During the first clock period, when HC 1 is on, the logic output of the counter demultiplexer [10] causes the pulse train to be directed through the signal demultiplexer [9] to the up input of counter 1 (after the delay period). During the 2nd clock period, when lamp 1 is off, the pulse train will be directed to the down input of counter 1 after the delay period. This will be repeated sequentially for counters 2, 3, and 4. One complete sequence of collection from each of the HC lamps is called a "lap". The circuitry will continue to do laps until the lap counter blocks gate 7. At this time, the HC lamps will continue to be pulsed but data collection will be terminated.

Five 74192 up–down counters are cascaded together in the traditional manner (28) and mounted on a PC (Printed Circuit) board. There is one PC board for each of the four channels. The up–down inputs of the first counter on each card are connected to the signal demultiplexer output on the control card. When a pulse train is transmitted to the up channel, it will cause the counter to count up (add). When a pulse train is directed to the down channel it will result in down (subtraction) counting. The BCD outputs of each of the 4 up–down counters is connected to a separate digital display.

The control circuitry, counter PC cards, and HC pulsing circuits are all mounted in a rack mounted Vector strut cage.

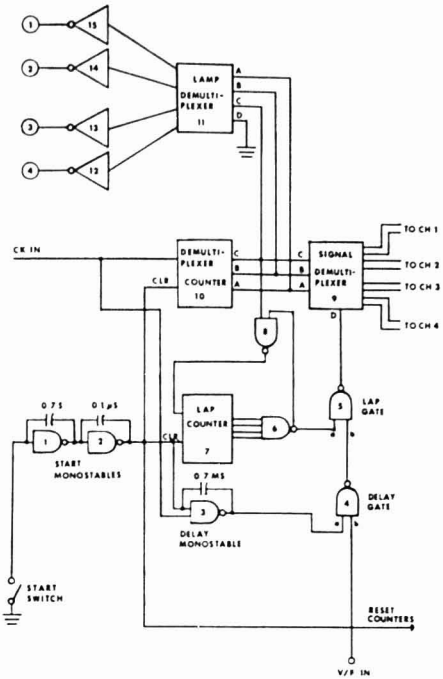


Figure 8. Simplified control electronics schematic. See text for identification of components

The control circuitry is mounted on a breadboard assembly affixed to a 22-finger edge connector PC board. This entire assembly and the DIALCO digits are powered by one 5-V power supply. The V/F counter and I-V converter are mounted in separate BUD boxes in standard configurations as specified by the manufacturer.

For the parameters used (i.e., 100-Hz clock rate, 100 laps, a delay time of 0.7 ms, and a 100 kHz/V V/F conversion factor), the relationship between the number of counts accumulated in a given counter (N) and the peak-to-peak voltage at the output of the I-V converter due to the HC lamp (E) is

$$N = 9.3 \times 10^4 E \quad (1)$$

The number of counts to be accumulated is limited by several factors. First, the maximum value of E into the V/F converter must be less than 10 V. Second, to prevent overflow on the readout, $N < 10^5$ counts. Hence for 100 laps, the maximum value of E from Equation 1 is 1.07 V.

There will be an uncertainty of ±1 count for each lap since the pulse train and integration time are not synchronized. Thus the relative readout digitization readout error (RDE) for n laps is given by

$$\mathrm{RDE} = n^{1/2}/N \quad (2)$$

and will be equal to 10^{-4} for 100 laps, if $N = 10^5$. To prevent readout limitations, it is critical that the relative noise always be greater than RDE.

Each of the 4 HC lamps is pulsed with a separate conventional simple circuit consisting of a power transistor (RCA SK311), a load power resistor (1–20 kΩ, 5 W), and the HC lamp in series with the power supply. Each lamp is pulsed sequentially by the outputs from inverters ([12]–[15], Figure 8) on the control circuit board which drive the base of the power transistor on, and hence the HC lamp, when the inverter output is high. Only one high voltage power supply is used, and it is possible to vary the currents through individual HC lamps by changing the load power resistors. The current through a given HC may be observed by inserting a current meter in place of a shorting bar that is in series with each HC lamp. More details are available from the authors.

OPERATION

Normal operating procedure is as follows. The slit array is masked (unused slits blocked with tape) so as to open only the four slits corresponding to the elements to be determined after it has been determined that the analysis of a particular combination of elements is feasible (29). The HC lamps are placed into the various HC holders and filters, if necessary because of spectral overlap problems, are placed between the HC lamps and the beam splitters (usually next to the lenses). The HC lamps are warmed for at least 5 min and longer if very good stability is required. During this time, the HC lamp positions are adjusted for maximum throughput. The I-V converter feedback resistance and PMT gain are adjusted for 100 laps so that the output of the I-V converter for the most intense HC lamp is about 1 V. The feedback capacitor is adjusted for a time constant of 0.1 ms to prevent distortion of the photocurrent signal. The flame is then turned on and operation proceeds in a conventional manner except that there are four readouts rather than one and the readout is in transmittance.

CONCLUSIONS

The TMMS system is similar to a single element flame AA because, like a single element AA, it requires only one PMT and power supply, a medium resolution monochromator and one HC power supply. The simple electronics, beam splitters and filters, photon funnel, and slit array required add relatively few components. It is considerably less expensive than other multielement systems which employ expensive direct readers or multichannel detectors. In contrast to a direct reader system, the exits slits can be very close together (e.g., the Pb and Mg slits are 540 μm apart on the multiple slit array). A computer is not necessary for operation, and the electronics and optics are simple and rugged with no moving parts during operation. All the signal processing is carried out in the digital domain. The system is almost as easy to operate as a single element AA unit. The conversion time to another set of four elements of the 10 elements for which a multislit array is constructed is about 20 min.

The dynamic range, detector noise characteristics, and detector responsivity below 300 nm of the PMT system are superior to both the Vidicon and diode array based multielement systems. The use of the TM mode of operation allows the individual HC lamp intensities to be adjusted so as to reduce differences in signal sizes, and it also minimizes spectral overlap problems because only one HC lamp is on at a given time. For the TMMS system, a separate single element HC and often a filter is required for every element, whereas in other multielement AA systems, multielement HC lamps or continuum sources may be employed.

The photon funnel is constructed to collect light over the 200- to 400-nm range, which is a wider spectral range than covered by most multichannel AA detector based systems. As for direct reader based systems, it would be time consuming to convert to other elements or lines for which slit positions have not been established or multislit arrays prepared. Here multichannel (Vidicon or diode array) detector based systems

have an advantage because any wavelength in the spectral range covered by the detector can be changed under software control. However, other multiple slit arrays with more slits could be constructed to make it possible to determine simultaneously any four of 27 elements with an air/C_2H_2 flame or of 24 elements with a N_2O/C_2H_2 flame.

The overflow problem that occurs for 100 laps, if the input to the V/F converter exceeds 1 volt, could easily be solved by adding an additional digit or two to the DIALCO digital readout and several more up–down counter chips to the counter PC boards.

The circuitry could be simply modified in one of several ways to reduce the dynamic problems (differences in HC intensities of different elements). Two V/F converters could be used which have conversion rates (Hz/V) differing by a factor of 10. The outputs of these V/Fs would both go to the present demultiplexing circuitry; however, the output of each would be gated and coordinated so that the less intense signals would be gated from the higher conversion rate V/F, and the more intense signals would be gated out of the lower conversion rate V/F. Another solution to the same problems is to use a switched gain amplifier and one V/F. The operator would set which gain would be applied to which HC signal.

A third solution to the dynamic range problem would be the addition of a log ratio circuit between the I-V and the V/F converters. This would provide a readout proportional to the logarithm, and hence the absorbance of the signals, and thus would eliminate a calculation step and reduce readout resolution limitations for weak lamps and high absorbances.

While a computer is not necessary with this system, it would be an asset in that it would minimize the operator time involved with data handling. An inexpensive computer could be directly interfaced to one of the counter PC boards. The BDC output up–down counter chips can be directly replaced with binary output up–down counters so that a BCD binary software conversion scheme would not be necessary. The computer could automatically control digitally either a switched gain amplifier or multiplex two V/F converters and would eliminate the need for the three other counter cards and all readouts. The computer could rapidly calculate absorbances, compare data with standards, and print out results. This would minimize the time spent by the operator doing tedious and time consuming data handling. Only a simple microprocessor is needed with a serial interface to a teletype and enough digital I/O ports to handle its limited functions.

It would probably be better to manufacture the slits from metal, rather than be etching Al from a quartz slide. This would eliminate the need for masking off large portions of unused space on the slide so as to eliminate the passage of unwanted light through the "pinholes" which seem to be a by-product of the multiple slit array production. Also this would eliminate reflection losses at the air/quartz interfaces (about 8%) of the slide and possibly reduce stray light.

The performance of the TMMS instrument is discussed in detail in another paper (*29*).

ACKNOWLEDGMENT

The authors thank Jimmey Hosch for the idea of the photon funnel design and J. Looney for equipment and information relating to the manufacture of the multiple slit array.

LITERATURE CITED

(1) R. Mavrodineau and R. C. Hughes, *Appl. Opt.*, **7**, 1281 (1968).
(2) R. A. G. Rawson, Rothamsted Experimental Station, Harpenden, Herts., England, unpublished work, 1973.
(3) E. Lundberg and G. Johansson, *Anal. Chem.*, **48**, 1922 (1976).
(4) K. W. Jackson, K. M. Aldous, and D. G. Mitchell, *Appl. Spectrosc.*, **28**, 569 (1974).
(5) F. Brech, *Proc. Colloq. Spectrosc. Int., 13th, Ottawa*, 1191 (1967).
(6) J. F. Alder, D. Alger, A. J. Samuel, and T. S. West, *Anal. Chim. Acta*, **87**, 301 (1976).
(7) L. R. P. Butler and A. Strasheim, *Spectrochim. Acta, Part B*, **21**, 1207 (1965).
(8) K. M. Aldous, D. G. Mitchell, K. W. Jackson, *Anal. Chem.*, **47**, 1034 (1975).
(9) R. Woodriff and D. Shrader, *Appl. Spectrosc.*, **27**, 181 (1973).
(10) L. C. J. Pickford and G. Rossi, *Analyst (London)*, **98**, 329 (1973).
(11) G. Horlick and E. Codding, *Appl. Spectrosc.*, **29**, 167 (1975).
(12) D. G. Mitchell, K. W. Jackson, and K. M. Aldous, *Anal. Chem.*, **45**, 1215A (1973).
(13) K. W. Jackson, K. M. Aldous, and D. G. Mitchell, *Spectrosc. Lett.*, **6**, 315 (1973).
(14) N. G. Howell and G. H. Morrison, *Anal. Chem.*, **49**, 106 (1977).
(15) A. T. Zander, T. C. O'Haver, and P. N. Keliher, *Anal. Chem.*, **49**, 838 (1977).
(16) A. T. Zander, T. C. O'Haver, and P. N. Keliher, *Anal. Chem.*, **48**, 1166 (1976).
(17) P. N. Keliher and C. C. Wohlers, *Anal. Chem.*, **48**, 140 (1976).
(18) W. Elliot, *Am. Lab.*, March, 67 (1970).
(19) H. L. Felkel, Jr., and H. L. Pardue, *Anal. Chem.*, **49**, 1112 (1977).
(20) A. Walsh, *Pure Appl. Chem.*, **23**, 1 (1970).
(21) J. V. Sullivan and A. Walsh, *Appl. Opt.*, **7**, 1271 (1968).
(22) R. L. Cochran and G. M. Hieftje, *Anal. Chem.*, **49**, 98 (1977).
(23) J. B. Dawson and D. J. Ellis, *Spectrochim. Acta, Part B*, **23**, 695 (1968).
(24) E. F. Palermo, A. Montaser, and S. R. Crouch, *Anal. Chem.*, **46**, 2154 (1974).
(25) R. W. Spillman and H. V. Malmstadt, *Anal. Chem.*, **48**, 303 (1976).
(26) E. D. Salin, Ph.D. Thesis, Oregon State University, Corvallis, Ore., 1978.
(27) M. L. Parsons, B. W. Smith, and G. E. Bentley, "Handbook of Spectroscopy", Plenum Press, New York, N.Y., 1975.
(28) R. L. Wilson and J. D. Ingle, Jr., *Anal. Chim. Acta*, **83**, 203 (1976).
(29) E. D. Salin and J. D. Ingle, Jr., *Anal. Chem.*, following paper in this issue.

RECEIVED for review April 10, 1978. Accepted July 31, 1978. Presented in part at the 1978 Pittsburgh Conference on Analytical Chemistry and Applied Spectroscopy, Cleveland, Ohio.

Performance of a Time Multiplex Multiple Slit Multielement Flame Atomic Absorption Spectrometer

Eric D. Salin[1] and J. D. Ingle, Jr.*

Department of Chemistry, Oregon State University, Corvallis, Oregon 97331

The performance characteristics of a new multielement flame atomic absorption (AA) spectrometer are presented. Compared to a conventional single element AA, the absolute light levels measured are considerably lower and additional spectral overlap problems arise. These differences do not significantly affect detection limits, sensitivities, precision, and calibration curves in most cases. Detection limits (in ppb) of 50 (Au), 8 (Cd), 40 (Co), 9 (Cu), 60 (Fe), 2 (Mg), 5 (Mn), 50 (Ni), 50 (Pb), and 20 (Zn) were obtained under favorable multielement conditions and are within a factor of two of detection limits obtained on a good quality commercial single element AA operating with comparable spectral bandpass and integration time. The relative measurement precision at moderate absorbances is typically 1% or better.

The design and construction of a new multielement flame atomic absorption (AA) spectrophotometer were described along with a review of other multielement AA spectrophotometers in a recent paper (*1*). This instrument is denoted a Time Multiplex Multiple Slit (TMMS) system. It is similar to a conventional single-element AA except that the light beams from four single element hollow cathode (HC) tubes are directed through the flame by the use of beam splitters and the exit slit is replaced by multiple exit slit array (one slit for each element). The light passing through all exit slits is directed to one photomultiplier tube (PMT). The HC lamps are pulsed on sequentially (one on at a time) with a 12.5% duty cycle at a 12.5-Hz rate. Data acquisition is synchronized with the lamp pulsing such that the lamp signal from each element's HC lamp is directed to a separate data acquisition–readout channel at the proper time. To signal average, typically 100 "laps" or 10-ms duration lamp pulses are averaged for each element. The system is configured to determine simultaneously any four of the following ten elements: Cu, Mg, Pb, Mn, Au, Fe, Co, Ni, Cd, and Zn. In this paper the performance characteristics of this instrument are critically examined.

EXPERIMENTAL

The TMMS instrument and its general operation have been previously described (*1*). For all flame AA measurements on the TMMS instrument, the burner air and C_2H_2 flow rates were 4.6 and 0.5 L/min, respectively, and the sample flow rate was 4.6 mL/min. The PMT bias voltage was adjusted to 600–800 V and R_f was 10^5–10^7 Ω. Solutions were prepared from reagent grade metal salts and distilled and deionized water.

The most common AA analysis lines were used in all cases except for Au and Pb. The Au 267.6 nm line provides an AA sensitivity and lamp intensity near those of the more common 242.8 nm line and avoids any possible overlaps with the Co 242.5 nm line and the Sn 242.1 nm line. The Pb 283.3 nm line was chosen as opposed to the normal 217.0 nm line because it is five times more intense and the AA sensitivity is within a factor of two of the 217.0 nm line. A Au slit was included on the mask because Au is a good internal standard element for correction of dilution, flow, and nebulization changes because of its low natural abundance (2).

RESULTS AND DISCUSSION

In order to appreciate the capabilities and limitations of this multielement AA system, it is best to compare its performance with a single element AA system. For this purpose we have utilized the Varian model AA-6. It represents a typical modern high quality AA. Bower (*3, 4*) has extensively studied the S/N characteristics of this AA-6 instrument and has determined the typical photocathodic currents for many elements. The photocathodic current is proportional to the absolute light intensity striking the photomultiplier detector and optical throughput of the instrument and is independent of the electronic and photomultiplier gain. The performance (e.g., AA sensitivity, light throughput, etc.) of the Varian AA-6 should be very similar to that of the TMMS used as a single element instrument (one slit, no beam splitters, 50% HC lamp duty cycle) because for both instruments the same HC lamps were used, the burner aspirators have similar design and solution and gas flow rates, the flame path lengths are the same (10 cm), and similar PMTs are employed. The external light collection optics are similar, *f*/3 lenses are used in both. The *f* number and linear reciprocal dispersion are 10 and 3.3 nm/mm and 8 and 3.5 nm/mm for the AA-6 and TMMS monochromators, respectively. Hence, the light collection efficiency of the AA-6 is slightly less but the resolution for a given slit width is better.

In this section, the two instruments are compared in terms of AA sensitivity, detection limits, calibration curves, S/N characteristics, and optical efficiency. Data are presented to indicate the typical performance of the TMMS instrument as a multielement AA and to what degree performance is degraded in the multielement mode. More specifically, the goal is to determine the effect of having more than one exit slit, pulsing lamps with less than a 50% duty cycle, using beam splitters to combine the be ms from a number of HC lamps, using the mirrored photon funnel to direct the light from all slits into one PMT, and the use of compromise flame conditions and spectral bandpass for all elements.

Because some of the design features are quite different from those of a single element AA, different problems will arise than those normally encountered in single element AA. The use of multiple exit slits allows more flame and concomitant background emission radiation to strike the PMT with a resultant increase in average background emission signal and noise. Also light from a given HC can pass through other than the desired slit and give rise to "stray light" problems. A smaller duty cycle means that all signals are averaged for only a small fraction of the total observation time. To keep the lamp signal per unit time the same, the lamp must be pulsed at higher currents which can cause loss of AA sensitivity. The use of beam splitters, filters, and the photon funnel will reduce the lamp signal reaching the PMT and make noises independent of the lamp signal (0% T noise) more important. Finally, lamp intensities must be adjusted to be within an

[1] Present address, Department of Chemistry, University of Alberta, Edmonton, Alberta, T6G 2G2, Canada.

0003-2700/78/0350-1745$01.00/0 © 1978 American Chemical Society

order of magnitude of each other for all elements and, hence, not optimal for all elements.

Excess Light. The term "excess light" refers to light from a given HC which travels through exit slits other than the desired exit slit through which the element's resonance radiation passes (resonance slit). It differs from the term "stray light" in that stray light is radiation that passes through the resonance slit from the correct HC lamp which is not resonance radiation. It can be light outside the spectral bandpass due to monochromator imperfections or light within the spectral bandpass from other lines produced by the HC. Excess light is unique to certain multiple slit or detector instruments while stray light is equally a problem in single element work. For direct reader or multichannel detector (e.g., Vidicon or diode array) based multielement AA systems, the effect of excess light is usually minimal since there is a separate detector or detector element for each element unlike for the TMMS design.

The problem of excess light is reduced by the use of a TM design since the electronic channel of a given element responds only to the radiation present when that element's HC is pulsed on, and not to radiation from other HC lamps. HC lamp cathodes may be made of a variety of elements, and these elements along with a filler gas will emit a variety of lines. These additional lines can cause either excess or stray light problems; however, the effect is the same. Since it is unabsorbed radiation, it will result in reduced AA sensitivities and result in a negative deviation of the calibration curve. The most obnoxious case arises when one of the other elements in the analyte cathode is one of the elements of interest in the analysis. In this case, a slit will be open which will pass the resonance radiation of the other element and, when the analyte HC is turned on, light from the HC may be absorbed by both elements since both resonance wavelengths are present in the spectrum of this HC. In most cases, the problem of excess light can be minimized by the appropriate choice of filters to place in front of each HC.

An excess light table (available from the authors) was prepared which indicates the relative signals due to the radiation from each of the ten single element HC lamps which passes through each of the ten exit slits. The values in the table were determined by directing the radiation from one HC at a time into the monochromator and sequentially measuring under identical conditions the lamp signal due to the light passing through each slit with the remaining slits covered. If a significant amount of excess light was measured for a particular HC lamp–slit combination, then a determination was made whether the excess light is resonant, nonresonant, or partially resonant. This was accomplished by measuring the absorbance with only the slit in question opened and only the HC lamp producing excess light turned on. For instance, radiation from the Zn HC lamp was found to pass through the Cu slit. The absorbance with a Cu standard solution aspirating and only the Cu slit open was the same with either the Zn or Cu HC lamp operating. Thus, in this case, the excess light is resonant. If the absorbance was less or zero with the Zn HC lamp on, then the excess light would be partially resonant or nonresonant, respectively.

The excess light data allow the user to quickly identify the excess light problems which might arise for the determination of a particular set of four elements. The data show that excess light problems are minimal for Au, Cu, Mg, and Pb and significant for one element for Mn (Cu(R) slit), and Cd (Cu slit). Significant excess light for many elements exists for Fe (Cu(PR), Mg, Pb, Mn, and Co slits), Co (Cu, Mg(PR), Mn, Au, Fe, Ni, and Cd slits), Ni (Cu, Mg(R), and Mn(PR) slits), and Zn (Cu(R), Pb(R), and Fe slits). Many elements suffer excess light problems with the Cu slit. The coding R (resonant) and PR (partially resonant) indicates whether the excess light going through that slit is absorbed by the corresponding element and to what degree.

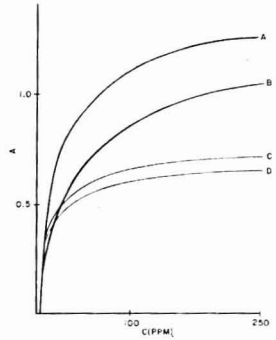


Figure 1. Calibration curves for Cd with excess light and different hollow cathode lamp currents. (A) Only Cd slit open; 2 mA; (B) only Cd slit open, 5 mA; (C) Cd and Cu slit open, 20% excess light; (D) theoretical curve with 20% excess light

Nonresonance excess light causes no interference in multielement work with the TMMS instrument; however it degrades performance by reducing sensitivity and causing more severe negative deviations because it is light that will not be absorbed by the analyte. The severity of the effect depends on the calibration curve of the element in the single element mode. If the total signal due to light passing through the other three slits in a particular application is less than 5% of the resonance line intensity signal, the loss in AA sensitivity is only 5% or less and the deviation from linearity at an absorbance of 0.5 is 9% or less.

The effect of excess light is illustrated in Figure 1 for Cd under various conditions. Comparison of absorbances taken under conditions A and C indicates the significant effect of excess light. The theoretical curve D was calculated from the simple stray light formula, $T' = f + (1 - f)T$, where T is the transmittance measured without excess light, T' is the transmittance with excess light, and f is the fraction of excess light. The agreement between curve D and the experimental points taken under condition C is good.

In multielement TMMS work, interferences will result when excess light is resonance or partial resonance radiation because the signal observed in one element's electronic channel will be affected by two elements. In the case of partial resonance, the effect will be less severe and insignificant if the fraction of excess light that is resonant is small (e.g., effect of Mn on Ni).

It might be possible to reduce the magnitude of excess light with a smaller spectral bandpass, or other HC lamps, or better alignment of slit positions on the multiple slit array. The above possibilities were not pursued because, in most cases, the excess light could be minimized by placing an interference filter in front of the appropriate HC which would pass the desired resonance line but (ideally) no light in regions where overlap existed with other slits.

Another excess light table was prepared with the use of the interference filters identified in Table I. All the significant excess light problems identified above were reduced to an acceptable level except for Co with the Ni and Cd slits. Hence most combinations of four out of the ten studied elements can be run simultaneously without significant problems from excess light.

The excess light values for a given element and HC can be determined with a conventional monochromator by measuring

Table I. Relative Hollow Cathode Lamp Intensities and Filter Data

HC	TMMS[a]	AA-6[a,b]	ratio 1, %[c]	filter wavelength, nm[d]	element wavelength, nm	filter transmittance, %[d]	ratio 2, %[a]
Au	4.0 (2)	—	—	—	267.6	—	—
Cd	4.9 (5)	51 (3)	5	225.0	228.8	17	0.85
Co	1.0 (5)	8.1 (5)	12	225.0	240.7	4	0.48
Cu	16 (4)	46 (3)	25	322.5	324.7	20	5.0
Fe	1.4 (5)	5.5 (5)	26	248.6	248.6	4	1.0
Mg	15 (2)	114 (3)	18	285.2	285.2	15	2.7
Mn	4.4 (3.5)	94 (5)	8	277.5	279.5	21	1.7
Ni	1.4 (5)	14 (5)	10	225.0	232.0	15	1.5
Pb	7.2 (2)	—	—	277.5	283.3	20	—
Zn	1.1 (3.5)	12.8 (5)	11	225.0	213.9	10 (13)[f]	1.4

[a] The actual rms cathodic currents may be obtained by multiplying normalized values by the conversion factor 8.6×10^{-14} A/normalized unit. Peak currents are 8 × rms current. In parentheses, the rms HC current used. The photocathodic current was obtained from $E = mR_f i$ as discussed in reference 3 where E is the measured p-p output voltage from the I-V converter, m is the photomultiplier gain, and R_f is the I-V converter feedback resistance. [b] From reference 3, spectral bandpass 0.2 nm for all elements except 0.5 nm for Mg and 0.1 for Co; no data reported in reference 3 at these wavelengths for Au and Pb. [c] The % ratio of the TMMS intensity without filters to the AA-6 intensity at the same HC lamp current (estimated for TMMS in some cases). [d] The wavelength of maximum transmittance of % maximum transmittance. [e] The % ratio of TMMS intensity with filter to AA-6 intensity at the same HC lamp current. [f] The wavelength of maximum transmittance of an interference filter may be changed to shorter wavelengths by rotating the filter. This was done in this case raising the throughput from 10 to 13%.

the light from a given HC that passes through the slit at wavelength settings for other elements. In this manner, the effect of lamp current and spectral bandpass as well as excess light problems for elements other than those tested here can be determined independently for any particular system. The AA-6 was used to check the excess light values obtained on the TMMS and good agreement was found in most cases.

Absolute Light Levels and Attenuation by Beamsplitters. The light levels in the TMMS system are compared to those of the AA-6 in terms of photocathodic currents in Table I. The photocathodic current is the product of the radiant power incident on the photocathode and the cathodic responsitivity in A/W. Since the cathodic surfaces of the PMTs on both instruments are similar, the photocathodic current gives a good indication of absolute light level. In Table I all the rms photocathodic currents ($^1/_8$ of the peak currents) for the TMMS were determined with the HC lamp in the number 2 HC position (see Figure 6 in reference 1) where the beam must pass through two beam splitters and, therefore, under conditions that would be used in multielement analysis. Values are also reported for the AA-6 with the same HC lamps. In both cases, rms HC operating currents are in parentheses. Values are normalized to 1.0 for Co at 5 mA. Co is the weakest HC lamp. The light throughputs compared to the AA-6 are shown to vary from 5 to 26% (ratio 1).

The use of two beam splitters and one addition lens was found experimentally to reduce the photocathodic lamp signal current for lamp position 2 to roughly 20% of the value without the additional optical components. This is close to the predicted value obtained from the measured optical efficiencies of the additional components. Table I shows (see Ratio 1 column) that the difference in photocathodic signal current between normal single element operation and TMMS multielement operation at the same HC lamp rms current is usually within a factor of 2 of that predicted. Differences from the exact predicted value (20%) are due to the attenuation by the photon funnel and the dependence of intensity of the positioning of the HC lamp along the optical axis. The optical efficiency for other HC lamp positions in within a factor of 40% of that obtained in position 2.

Light Loss Due to Filters. While filters do, in many cases, minimize excess light problems and make possible combinations of elements that would otherwise be impossible, it is important to realize that they always substantially attenuate the signal as shown in Table I. In some cases, the attenuation is rather drastic and can result in worse detection limits and reduction in the S/N in situations where the dominant noise is either independent of the signal or is signal shot noise. Unfortunately, for the weak intensity HC lamps Fe, Zn, and Co, the transmission losses are more severe because the filter is not well matched to the resonance wavelength. Comparison of the relative intensities with filters to the values obtained with a single element instrument (see column Ratio 2 in Table I) reveals that with filters the photocathodic signal current is reduced to 5 to 0.5% of the single element values.

Dynamic Range Problems. To obtain 0.1% resolution in the reference signal and not overflow the counters, the largest and smallest signals must not differ by more than a factor of 10. Under normal rms HC lamp current conditions, intensities among the lamps tested varied by over a factor of 15 and with filters by a factor of 10. Comparing relative signals for bright HCs without filters (e.g., Cu, Mg) to weakest HCs with filters (Co, Fe, Ni, Zn) gives a range up to about 400. Thus, depending on the choice of elements and the need for filters, serious dynamic range problems can exist. Unfortunately, the weakest HCs often require a filter because of excess light problems whereas the brighter lamps do not.

The dynamic range problem can be somewhat reduced by operating intense HC lamps at low currents and weak lamps at high currents. The intensity of intense lamps can be reduced with filters even if excess light problems are negligible. Reduction of light levels can cause S/N problems in some cases, and high operating HC currents reduce sensitivities and increase detection limits as discussed in the next sections.

Effect of Lamp Current on Sensitivity. The sensitivity or the slope of the calibration curve in AA depends on the line profile of the source radiation as well as other factors. The source line profile of HC lamps increases with HC current and, in general, reduces sensitivity (*2, 4*) and increases negative deviations. Figure 1 illustrates the effect of increasing the rms lamp current upon absorbance and thus sensitivity with the TMMS instrument for Cd. The effect of increasing lamp current (compare the data taken under conditions A and B) is similar to that produced by excess light (curve C), although, for this particular case, the effect is not as drastic but is quite significant. For most elements studied, except Zn, Mg, and Ni, the effect of higher currents is much less. Usually HC lamps are operated in the 50% duty cycle mode in which the HC is on 50% of the time and off 50% of the time. In the TM mode for four elements, the HC lamps must be operated

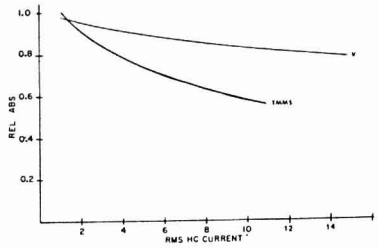


Figure 2. Relative absorbance vs. rms HC lamp current for Fe

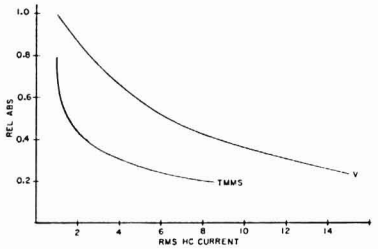


Figure 3. Relative absorbance vs. rms HC lamp current for Zn

at a smaller 12.5% duty cycle. If measurements are limited by signal shot noise or 0% T noise, it is necessary to increase the light level by a factor of four to maintain the same S/N as in the 50% duty cycle mode; thus, one must operate at higher peak currents. It is especially important that higher HC currents be used in situations where the intensities have been attenuated severely by the use of filters.

For all ten elements studied, the absorbance was determined using the same solution on both the Varian AA-6 and the TMMS instrument (one slit open) at different HC lamp currents. The concentrations were chosen so that the absorbance at low lamp currents was in or close to the linear region of the calibration curve (A = 0.2–0.4). Typical plots are shown in Figures 2 and 3 where the absorbances are normalized with the highest absorbance of either system being given the value of 1.0. For the same rms HC current, the peak HC current of the TMMS is 4 times higher than the AA-6 HC current, so different sensitivities might be expected.

Most elements exhibit the behavior shown for Fe in Figure 2. At a given rms lamp current, the sensitivity with the TMMS system is usually less but within 50% of the values obtained in the AA-6 and there is no more than a 50% loss in sensitivity in running at high HC currents (10–15 mA) as compared to normal operating currents (3–5 mA). The plots for Zn in Figure 3 show a worse case situation. For Cd, Zn, Ni, and Mg there is more than a 50% loss in sensitivity in running at higher rms currents and, for Zn and Mg, the relative absorbance is considerably less at a given rms current for the TMMS system. This is not a problem for Mg since the Mg, HC is intense and can be run at low currents but for Zn, higher rms currents are necessary to prevent S/N problems.

Calibration Curves, Sensitivity, and Detection Limits. To test the performance of the instrument in the multielement mode, each element was run simultaneously with three other elements' slits open. These combinations are tabulated in Table II. For most elements, two possible cases were studied. In case 1, three other elements were chosen such that excess light problems were minimal and no filter was required. These represent a favorable case. For case 2, the elements chosen

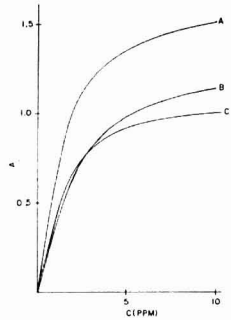


Figure 4. Calibration curves for the TMMS and Varian AA-6 for Mg. (A) Varian; (B) TMMS, case 1; (C) TMMS, case 2

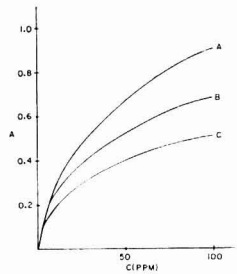


Figure 5. Calibration curves for the TMS and Varian AA-6 for Ni. (A) Varian; (B) TMMS, case 1; (C) TMMS, case 2

often resulted in a serious excess light problem such that a filter is required. The use of a filter often necessitates using a higher lamp current to maintain a good S/N (e.g., Co, Fe, Mn, Ni, Pb, and Zn) which often results in a loss of sensitivity and increased negative deviation in the calibration curve. In case 2, the other analyte elements often had resonance lines (slits) at longer wavelengths where background emission noise is much worse (see noise section). Because case 2 is always with a filter and often with a larger background emission noise, it can usually be considered an unfavorable case. Case 1 was not attempted for Co because serious excess light problems exist with almost all slits requiring the use of a filter for almost any combination. A case 2 for Au is not presented because a Au filter was not available.

The detection limits (DLs) and sensitivities reported in Table II were obtained when experimental runs were made with 100 laps, which corresponds to approximately 2-s observation time per element. These are compared in the table to DLs and sensitivities obtained on the Varian AA-6 under comparable conditions: a 0.42-nm spectral bandpass and 1-s integration time.

Calibration curves for all ten elements were obtained on the TMMS and Varian AA-6 instruments. Typical examples are shown in Figures 4 and 5. For most elements and cases, the calibration curves are similar to Figure 4 for Mg where at high absorbances there is slightly more negative deviation on the TMMS instrument due to excess light or operation at a higher peak HC current. In general the case 2 curve is lower than the case 1 curve because of the effect of a higher lamp current and/or a greater fraction of excess light. For Cu and Pb(1), the calibration curves were more linear on the TMMS instrument. The Ni calibration curves in Figure 5 illustrate

Table II. Instrumental Performance

element (wavelength, nm)	inst[a] (case)	slits open	RMS HC current	AA sens, ppb[b]	DL, ppb[c]	excess light, %[d]
Au	V		4.0	360	70	—
(267.6)	TMMS (1)	Au, Cu, Mn, Ni	3.2	310	50	6
Cd	V		3.0	31	9 (0.6)	—
(228.8)	TMMS (1)	Au, Cd, Pb, Zn	3.5	38	8	1
	TMMS (2)	Cd, Cu, Mn, Ni	3.5	33	20	0.4
Co	V		5.0	110	60 (7)	—
(240.7)	TMMS (2)	Au, Co, Fe, Zn	9.5	190	40	6
Cu	V		3.0	55	5 (3)	—
(324.8)	TMMS (1)	Cd, Cu, Ni, Zn	1.5	50	9	0.05
	TMMS (2)	ALL	2.5	52	7	0.04
Fe	V		5.0	120	50 (5)	—
(248.3)	TMMS (1)	Cd, Fe, Ni, Zn	2.7	100	60	3
	TMMS (2)	Fe, Mg, Mn, Pb	6.0	140	100	2
Mg	V		3.0	7	0.8 (0.3)	—
(285.2)	TMMS (1)	Co, Fe, Mg, Ni	1.5	11	2	0.02
	TMMS (2)	Cu, Mg, Mn, Pb	1.8	8.2	2	3
Mn	V		5.0	50	8 (3)	—
(279.5)	TMMS (1)	Co, Fe, Mn, Ni	4.0	34	5	3
	TMMS (2)	Cu, Mg, Mn, Pb	8.0	50	20	5
Ni	V		5.0	110	40 (8)	—
(232.0)	TMMS (1)	Co, Fe, Ni, Zn	4.0	100	50	3
	TMMS (2)	Cu, Mg, Mn, Ni	9.0	180	100	0.3
Pb	V		6.0	360	90	—
(283.3)	TMMS (1)	Cd, Pb, Ni, Zn	2.0	390	50	0.04
	TMMS (2)	Cu, Mg, Mn, Pb	4.0	410	100	2
Zn	V		5.0	16	20 (2)	—
(213.9)	TMMS (1)	Au, Cd, Ni, Zn	4.0	35	20	6
	TMMS (2)	Cu, Fe, Cd, Zn	6.5	60	40	7

[a] Inst (case): The instrument used (the case, see text). V: Varian AA-6. TMMS: Time Multiplex Multi Slit Instrument. [b] AA Sens: Atomic Absorption Sensitivity (concentration yielding 0.0043 absorbance). [c] DL: Detection Limit for 100 laps on TMMS or 1-s integration time with V (manufacturers DL in parentheses). DL is defined as the concentration yielding an absorbance twice the rms noise in the reference signal in absorbance units. [d] Ratio of signal due to radiation from the analyte HC lamp passing through the other open slits to the signal due to the analyte slit.

one of the three elements where there is considerably more negative deviation at lower absorbances with the TMMS instrument. Case 1 performance is worse because of excess light and case 2 performance is worse because of the use of a higher lamp current. Similar characteristics were observed for Co (2) and Zn (1) and Zn (2). Note that the differences in calibration curves would affect performance only significantly at higher absorbance or concentration levels.

Several general conclusions can be drawn from Table II.

(1) The sensitivities obtained with the TMMS for cases 1 and 2 are usually within a factor of 2 and sometimes better than those obtained on the AA-6 under similar conditions except for in the case 2 of Zn (factor of 4 worse).

(2) The sensitivity is usually better for case 1 than 2 where a significantly higher lamp current has been necessary in case 2 (e.g., Co, Fe, Mn, Ni, and Zn).

(3) The DLs for case 1 on the TMMS are comparable or within a factor of 2 of those determined on the Varian AA-6 except for Mg. DLs for case 2 are within a factor of 2 of the Varian AA-6 except for Mg, Mn, Ni, and Cd which are a factor of 2.5 worse.

Detection limits were also determined with 10 laps (0.8 total measurement time for four elements) and the detection limits were generally a factor of 2 to 3 worse than the 100-lap detection limits.

Noise Considerations. With sufficient readout resolution, noise is always obvious and limits the detection limit and precision at all concentrations, so the S/N characteristics of the system are important to consider. Because of the design of the TMMS instrument, the relative importance of different noise sources is expected to differ from a conventional single element AA. Table III lists the relative magnitude of noise in various signals and compares these to values previously obtained on the AA-6 (*3, 4*). All noises were determined by collecting sequentially 30 values of the measured voltage with 100 laps and compensating for drifts as previously described (*3, 4*).

The different noises measured are identified below in accordance with the terminology developed by Ingle and Bower (*3, 4*). σ'_{ot} is the standard deviation in the signal recorded with the HC lamp and flame off and is due to amplifier-readout noise and dark current noise from the PMT. σ_{ot} or the 0% T noise is the standard deviation in the signal recorded with the blank aspirating into the flame but with the HC lamps off. It is due to σ'_{ot} noise plus noise due to the flame background emission. In the table both of the above noises are presented as relative standard deviations (RSDs) by dividing by E_r (the reference signal). σ'_{rt} is the standard deviation in the signal measured with the HC lamp on (E'_r) but the flame off. The noise is due to σ'_{ot} noise plus shot noise and source flicker noise in the lamp signal. It is recorded relative to E'_r in Table III. σ_{rt} or the 100% T noise is the standard deviation in the total reference signal (E_{rt}) and is measured with the HC lamp on and the blank aspirating into the flame. It consists of σ'_{rt}, flame background emission noise and flame transmission noise (noise due to the fluctuating transmission properties of the flame). It is recorded relative to E_r in Table III. It is sometimes called the blank noise and is used to calculate the detection limit since the reference rms noise in absorbance units is equal to $0.43\ \sigma_{rt}/E_r$. The RSD in absorbance (σ_A/A) at moderate absorbances is calculated from measurements made with an analyte solution aspirating yielding an absorbance of 0.2–0.4 and is due to all the types of noise present in σ_{rt} measurement plus analyte emission noise and analyte absorption noise (noise due to fluctuations in the viewed neutral ground state population of the analyte). σ_A/A is compared to values obtained on the AA-6 as a comparable absorbance (*3, 4*). The shot noise in the reference lamp signal $(\sigma_r)_{q+s}$ is the fundamental noise due to the quantum nature of light and is calculated as previously described (*3, 4*). E_r

Table III. Relative noises on the TMMS and Varian AA-6[a]

element	$(\sigma_r)_{q+s}/E_r$		σ'_{rt}/E'_r		σ_{rt}/E_r		σ_{ot}/E_r		σ'_{ot}/E_r	σ_A/A		E_r, volts	$i_r \times 10^{13}$ A	
	TMMS	V	TMMS	V	TMMS	V	TMMS	V	TMMS	TMMS	V		TMMS	V
Au (1)	0.4	—	0.5	—	0.7	—	0.2	—	0.09	3	—	0.3	1.6	—
Cd (1)	0.5	0.3	0.4	0.5	1.1	2	0.3	0.3	0.15	3	12	0.2	0.9	36
Cd (2)	1.2	0.3	1.7	0.5	3	2	1.2	0.3	0.13	7	12	0.3	0.2	36
Co (2)	1.5	0.6	1	1.1	1.1	1.3	0.5	0.09	0.16	14	14	0.3	0.13	7
Cu (1)	0.2	0.3	0.7	0.5	0.9	0.5	0.1	0.07	0.07	3	8	0.9	5	40
Cu (2)	0.3	0.3	0.7	0.5	0.7	0.5	0.14	0.07	0.05	5	8	0.4	2.3	40
Fe (1)	0.8	0.7	0.9	1.5	3	1.7	0.2	0.3	0.06	5	7	0.7	0.4	5
Fe (2)	1.6	0.7	1.4	1.5	5	1.7	3	0.3	0.2	10	7	0.2	0.1	5
Mg (1)	0.14	0.18	0.5	0.4	0.7	0.5	0.09	0.3	0.6	3	8	0.6	12	98
Mg (2)	0.4	0.18	0.5	0.4	1.1	0.5	0.4	0.3	0.1	6	8	0.3	1.4	98
Mn (1)	0.2	0.2	0.5	0.4	0.8	0.6	0.2	0.07	0.3	3	8	0.2	10	80
Mn (2)	0.6	0.2	0.9	0.4	2	0.6	0.5	0.07	0.3	6	8	0.1	0.8	80
Ni (1)	0.7	0.5	0.5	1.5	2	1.8	0.6	0.1	0.3	5	9	0.09	0.5	9
Ni (2)	1.4	0.5	1.2	1.5	4	1.8	2	0.1	0.11	9	9	0.4	0.2	9
Pb (1)	0.4	—	0.5	—	0.7	—	0.2	—	0.11	7	—	0.2	1.3	—
Pb (2)	0.7	—	0.9	—	1.7	—	0.12	—	0.04	3	—	0.9	0.5	—
Zn (1)	0.5	0.6	1.2	0.9	3	3	1.6	0.1	0.14	8	13	0.2	1.1	7
Zn (2)	1.6	0.6	3	0.9	3	3	3	0.1	1.1	9	8	0.2	0.12	7

[a] All relative noises × 10^3, see text for identification of symbols.

is the peak voltage when the lamp is on and i_r is the rms reference photocathodic current.

All relative noises are compared to values obtained on the Varian AA-6 with about the same integration time or noise equivalent bandpass. With the TMMS instrument with 100 laps, both the lamp signal and the background are each integrated for 0.93 s. The AA-6 measurements are for 1.0-s integration time in which the lamp signal and background are viewed for 0.5 s each.

At the detection limit and for small absorbances, precision is normally limited in a conventional AA by lamp flicker noise and flame transmission flicker noise (*3, 4*). In Table III, these terms are all included in σ_{rt}/E_r. Comparison of the magnitude of σ_{rt}/E_r between the TMMS and Varian instruments indicates that usually they are within a factor of 2 (except for Mn (2)) and accounts for the detection limits being generally about the same. Since the rms photocathodic current (i_r) is a factor of 6 to 180 less on the TMMS instrument compared to the Varian but the actual integration time is eight times longer, the number of photons integrated is about the same to 20 times less than on the Varian. Thus, because of the square root nature of shot noise, the relative signal shot noise ($(\sigma_r)_{q+s}/E_r$) is generally about the same to a factor of four larger than on the Varian and essentially accounts for all the lamp noise (σ'_{rt}/E'_r) except for Cu (1), Cu (2), Mg (1), Mn (1), Zn (1), and Zn (2) where source flicker noise is obvious. However, on the Varian the signal shot noise is usually an insignificant part of the blank noise. Thus the signal shot noise becomes a more or the most significant part of the blank noise but is not increased to the point where it significantly degrades precision at low absorbances. Correspondingly, the source and flame transmission noise are less important on the TMMS instrument even though the relative magnitudes of these are the same. The lower photocathodic current also makes the 0% T noise (σ_{ot}) more important on the TMMS instrument and for case 2 for Fe, Ni, and Zn, σ_{ot} is a significant part of σ_{rt} but not to such an extent that it seriously degrades precision at low absorbances. For the elements tested here, $\sigma_{ot} \ll \sigma_{rt}$ on the Varian AA-6. For about half the cases σ_{rt}/E_r is greater by a factor of 2–3 than σ'_{rt}/E'_r because of flame transmission and flame background emission noise.

The magnitudes of σ_A/A with A = 0.2–0.4 are essentially identical on the TMMS and the AA-6. It has been shown (*3, 4*) that at moderate absorbances in single element work, noise from the HC lamp and background emission are usually negligible because analyte absorption noise is limiting. This also appears to be true here, so measurements are limited by the fluctuating nature of analyte atomization. Because σ_{ot}/E_r is larger on the TMMS instrument, the absorbance at which σ_{ot} becomes limiting may be less than for the Varian (typically at A = 1.0–1.5).

At high absorbances 0% T noise (σ_{ot}) will limit precision. Comparison of σ'_{ot}/E_r and σ_{ot}/E_r indicate that σ'_{ot}/E_r is smaller or about the same size. On the Varian, σ'_{ot}/E_r is typically 0.01–0.04 × 10^{-3} and, hence, much smaller and negligible compared to σ_{ot}/E_r. Thus in some cases on the TMMS instrument, amplifier-readout noise and dark current noise limit the precision of the 0% T signal but, in the majority of cases, background emission is limiting as on the Varian. The magnitude of σ'_{ot}/E_r could be reduced in many cases by adjusting the PMT voltage to adjust E_r closer to 1 V.

Usually σ_{ot}/E_r is greater than for the AA-6 indicating that background emission noises and, in some cases, amplifier-readout and dark current noise are a larger relative component of the total noise. First, the lamp intensities are lower than those in single element work because of the use of beam splitters and the need for filters. This is particularly apparent when comparing cases 1 and 2 for Fe, Mg, Ni, and Cd where the lamp signal is much smaller for case 2. Second, three more slits are open than in normal single element work. If the background radiation passing through all slits was equal, this would cause an increase in the total background light level of a factor of four. If background emission shot noise is dominant and the total observation time per element is the same as in single element work, the absolute noise would increase by a factor of $(4)^{1/2} = 2$. In fact the relative effect will be much greater in many cases with the TMMS system because of the signal attenuation and different amounts of background radiation passing through each slit.

A brief study of the background emission noise for two wavelength regions was carried out. It was expected that a bandhead around 300 nm (*2*) would cause a higher noise level through the slits in that region. To carry out the study, two sets of four slits each were selected. Region I consisted of the Cu, Mg, Pb, and Mn slits and ranged from 324.8 to 279.5 nm. Region II consisted of the Co, Cd, Ni, and Zn slits and ranged from 240.7 to 213.9 nm. The noise in both was measured under identical gain conditions and with 100 laps and the absolute noise was 8.4 larger in region I. Thus, if measurements are made for an element in region II with slits open in region I, the absolute and relative background emission

noise and σ_{ot} will be considerably larger than for single element work with the element.

An excellent example of the effect of flame background emission noise is the comparison of σ_{ot}/E_r in cases 1 and 2 of Fe. In case 2, a filter attenuates the signal by 96% and two of the case 2 slits are in region I. The data indicate that the relative background emission noise increases by about a factor of 10. The result is that the flame background emission noise rises from being a small fraction (0.07) to a large fraction (0.6) of the total blank noise, σ_{rt}.

At an absorbance of one, in normal single element work, analyte absorption noise is usually limiting and σ_A/A can be as low as 0.2%. To prevent signal shot noise from significantly reducing precision at $A = 1.0$, the rms photocathodic current (i_r) must be greater than about 0.03 pA. For Cd (2), Co (2), Fe (2), Ni (2), and Zn (2), i_r is slightly less than 0.03 pA but this has little affect on precision since 0% T noise is limiting at $A = 1$ for all these cases. To prevent 0% T noise from becoming limiting at $A = 1.0$, σ_{ot}/E_r should be less than 0.024%. For Cd (2), Co (2), Fe (2), Mn (2), Ni (1), Ni (2), Zn (1), and Zn (2), this is not true and would seriously degrade precision compared to normal single element work at $A = 1.0$ especially for Cd (2), Fe (2), Ni (2), Zn (1), and Zn (2).

The S/N could probably be increased by a factor of 2 or 3 by increasing the total data collection time to 80 s (1000 laps); however, for some HC lamps, drift is significant over this period so little improvement will result.

During the course of these experiments, the HC position had been established by adjusting its position along the optical axis to obtain 1:1 imaging. After the majority of the data was taken, the effect of HC position along the axis or throughput was investigated. By changing position on the axis, it was possible to increase the light throughput by a factor of 3 to 5 depending on the lamp by moving the HC lamp closer to its focusing lens. This was accomplished without a loss in AA sensitivity or increased negative deviation. The detection limit and noise data for Co (2) and Fe (2) were taken under these new conditions because they were the most light limited cases. Hence a 3–5 increase in i_r could be expected for all other elements and cases with the ensuing reduction in relative signal shot noise and 0% T noise.

CONCLUSIONS

The overall performance characteristics (Table II) demonstrate that the TMMS system is a viable flame AA multielement analysis system. Under favorable multielement conditions the DLs were roughly equivalent to those obtained on the Varian AA-6 with a comparable integration time and spectral bandpass for the following elements: Au, Cd, Co, Cu, Fe, Mn, Ni, Pb, and Zn. With unfavorable multielement conditions, all the DLs were within 2.5 of the AA-6. The DLs on the Varian were obtained under compromise spectral conditions. Probably many of the DLs on the Varian could be improved by a factor of 2–3 with longer integration times (e.g., 10 s) or a smaller spectral bandpass in some cases (Co, Fe, and Ni). In other cases (Au and Pb), another wavelength might lead to some improvement. At moderate current levels, the AA sensitivity is roughly equivalent for the TMMS and Varian systems except for Zn whose sensitivity is a factor of two poorer with the TMMS system. At higher current levels, the AA sensitivity of Co and Ni are degraded by a factor of two and the Zn AA sensitivity is four times poorer than on the AA-6. At low and moderate absorbances the precision is comparable to that obtained on the Varian.

As with any multielement AA system, the inherently small dynamic range of AA makes it difficult to analyze samples with a wide range of elemental concentrations. So, at the expense of time, dilutions might be necessary to bring absorbances of elements at high concentrations down to reasonable levels. Also, in some cases, other resonance lines could be employed.

The use of beam splitters and a 12.5% duty cycle reduces the absolute light levels available compared to single element work with a 50% duty cycle. This increases the relative amount of signal shot noise and 0% T noise (flame background emission noise). The average background emission noise is also higher than for single element work because the PMT views the flame background emission from more than one slit and hence spectral region. A higher HC peak current can be used to maintain the absolute intensity per unit time; however, this significantly reduces AA sensitivity in a few cases.

Excess light or radiation from one HC passing through another slit is a unique problem of the TMMS system which causes severe negative deviations, loss of AA sensitivity, and spectral interferences in some cases, and eventually affects the DLs of several elements. The use of filters successfully minimizes excess light and its deleterious effects. However the attenuation by the filters requires in some cases that the HC lamp current be raised to increase the light level to maintain the S/N which sometimes significantly decreases the AA sensitivity. Although the much lower light levels increase the relative signal shot noise and 0% T noise, the measurement precision is adversely affected only at higher absorbances for some elements.

Another disadvantage of the TMMS system is that background correction for molecular absorption with a H_2 lamp is not possible for four elements since the H_2 lamp continuum radiation would pass through all slits. Background correction is important for certain samples for elements with resonance lines near 200 nm. Background correction could be achieved for one or two elements by replacing one or two elements HC lamps with a H_2 HC lamp with a filter to restrict the continuum radiation to the desired slit.

There are certain improvements which could be made to the system to enhance its capabilities other than instrumental improvements previously discussed (*1*). Light intensities could be increased by the use of high transmission filters and higher output HC lamps. It is possible to purchase 25% transmission interference filters for all elements and this would significantly increase light intensities for Co, Fe and Zn. Filters better matched to the element's resonance wavelength could reduce excess light problems. For Co the relative amount of excess light from the Ni and Cd slits is worse with than without the filter because of a filter mismatch. The need for filters could be reduced with the use of HC lamps with purer cathodes (e.g., no Cu in Zn cathode). Higher light intensities would improve the detection limits for some elements by a factor of 2 and possibly 4 for Zn (2) and increase precision at high absorbances for some elements (Co, Cd, Fe, Mn, Ni, and Zn) where 0% T noise or signal shot noise is limiting. Under flame background noise limited conditions, the improvement in S/N would be directly proportional to the increase in intensity.

With more beam splitters, simultaneous analysis of more than four elements would be possible, however, with more beam splitters and the need for a smaller lamp duty cycle, lamp signals would be reduced and increase S/N problems. Also, resolution, or the maximum counts accumulated per lamp pulse would be decreased. Lamp intensities could be increased with ensuing problems with loss in sensitivity and more negative deviations and lamp stability problems. With more slits open, the average background emission noise and excess light problems would be increased. At some point, possibly 6–8 elements, the above limitations and the inherent limited dynamic range of AA would take the choice of a more expensive multielement system such as an ICP emission direct reader justifiable. Hence, as originally intended, the TMMS system is best suited for routine analysis of a few elements

in similar and well characterized samples where the elemental concentrations are above normal single element AA DLs.

LITERATURE CITED

(1) Eric D. Salin and J. D. Ingle, Jr., *Anal. Chem.*, preceding paper in this issue.
(2) W. J. Price, "Analytical Atomic Absorption Spectrometry", Heyden and Son, London, 1972, p 205.
(3) N. W. Bower and J. D. Ingle, Jr., *Anal. Chem.*, **49**, 574 (1977).
(4) N. W. Bower, Ph.D. Thesis, Oregon State University, Corvallis, Ore., 1978.
(5) Varian Techtron, "Hollow Cathode Lamp Data", 1973.

RECEIVED for review April 10, 1978. Accepted July 31, 1978. Presented in part at the 1978 Pittsburgh Conference on Analytical Chemistry and Applied Spectroscopy, Cleveland, Ohio.

Preparation and Characterization of Thin Metal Films for Exploding-Conductor Excitation

D. V. Duchane[1] and R. D. Sacks*

Department of Chemistry, University of Michigan, Ann Arbor, Michigan 48109

Thin films of Al and Ag were prepared which are suitable for vaporization and excitation of micro solution and powder samples deposited on the film surface. The advantages of thin films over wires and foils are discussed. The thin-film coating apparatus and capacitive discharge film exploding circuit are described. Films are prepared by vacuum thermal vaporization of the preweighed metal. Experimental values of film mass show reasonable agreement with prediction. Absorbance and resistance measurements are useful for film thickness and quality monitoring. Al films were exploded from glass, polyethylene, polypropylene, and Plexiglas substrates using a 180-J, 4-kV discharge. Only glass showed significant unvaporized film and sample residue after an explosion. Emission line intensities from test elements deposited on the Al film surface are lower with glass substrates than with the other materials. Relative standard deviations are smaller with polyethylene and polypropylene substrates.

A new class of high current density, transient electrical discharges is currently being evaluated as potential atomization cells and excitation sources for the determination of trace elements in micro solution and solid samples. These sources, which are based on the electrical explosion of low mass metallic conductors, possess some properties which may make them attractive in applications involving multielement determinations over a wide concentration range in samples of restricted size. Conventional furnace techniques, while often showing excellent sensitivity for micro samples, are frequently characterized by low precision, significant matrix effects, poor performance for refractory samples, and, with atomic absorption, a limited dynamic range and only single element capabilities.

Previous reports (*1*, *2*) presented preliminary studies of exploding wires for the determination of trace cations in large volume solution samples. Controlled potential electrodeposition, which was used to preconcentrate the analyte on the surface of a Ag wire, resulted in protracted analysis time, poor reproducibility, and applicability to only the relatively few elements with cations that can be easily reduced to the metals in aqueous media. However, some analytically attractive properties including a linear dynamic range of three to four decades, relatively good powers of detection, and minimal matrix effects provided the impetus to consider exploding-foil excitation for micro solution samples (*3*, *4*).

The flat surface of the foil permits the direct introduction of micro solution samples with straightforward pipetting techniques. This increases the potential application of exploding-conductor excitation to all elements usually determined by emission spectroscopy. While absolute detection limits in the low nanogram and picogram range, three to four decade concentration range, and minimal interelement effects are attractive features, relatively poor precision was obtained. Typical values ranged from ±15 to ±30% without an internal reference technique. While the use of a reference improved these values significantly, reference techniques often are impractical with micro samples and multielement procedures.

The studies reported here make the logical extension of exploding-conductor excitation sources to thin metal films. The greater uniformity of mass, texture, and geometry attainable with thin films compared to foils results in improved precision and obviates the need for an internal reference technique. In addition, the greatly reduced mass of thin films relative to wires or foils of comparable surface area results in a substantial reduction of continuum background radiation as well as line radiation from the exploding conductor itself. Finally, the use of a polymeric film substrate rather than glass, results in both improved analytical performance and greater convenience.

This report will consider the production, testing, and properties of thin metallic films useful for exploding-conductor excitation as well as considerations used in choosing a substrate. Companion reports present detailed parametric studies of exploding thin-film excitation and preliminary analytical results for 10-μL solution samples.

EXPERIMENTAL

Film Preparation. Thin films of Ag and Al were prepared by conventional vacuum deposition techniques. The thermal vaporization apparatus is shown in Figure 1. The bell-jar chamber is evacuated to a pressure of 5×10^{-5} Torr by an oil diffusion pump with a liquid nitrogen cold trap. The pressure was monitored with a cold cathode ionization gage. The charge of metal to be evaporated after weighing to ±0.1 mg is placed in a refractory metal heater, which is operated from a 2.5-kW, 16-V ac power supply. The heater element is clamped between two large Cu blocks, which serve as heat sinks as well as electrical contacts.

Up to 14 substrate blanks (5.1 cm × 1.3 cm) are coated simultaneously. A 12.7-cm square stainless steel plate, which is located 52 cm above the heater, is used to support the substrates and mask appropriate areas on their surface. All films used in

[1] Present address, Los Alamos Scientific Laboratory, P.O. Box 1663, Los Alamos, N.M. 87544.

0003-2700/78/0350-1752$01.00/0 © 1978 American Chemical Society

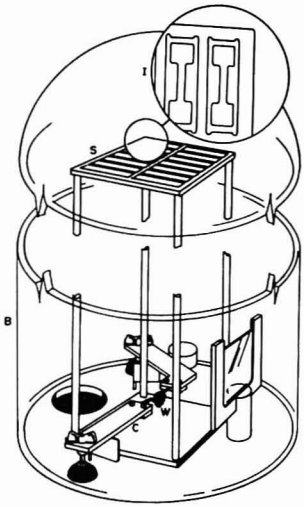


Figure 1. Thermal vaporization apparatus for preparing Al and Ag thin films. W, tungsten basket furnace; C, Cu connectors and heat sinks; B, bell jar; S, substrate support and mask; I, inset showing tensile bar film shape

this work had a tensile bar shape (see inset in Figure 1) with a 0.95-cm square area at each end for electrical contact and a 1.9-cm × 0.32-cm center region. Only this center strip is exploded.

Glass, high density polyethylene (HDPE), polypropylene (PP), and *Plexiglas* were used as substrate materials. Glass was cut from 1.0-mm thick microscope slides. Blanks of Plexiglas were machined from 1.2-mm thick stock. HDPE and PP blanks were cut on a paper cutter from 0.8-mm thick sheets (Cadillac Plastic Co., Detroit, Mich.). Substrate blanks were cleaned by soaking in reagent grade isopropyl alcohol for 24 h.

Film Monitoring. The resistance of each film was measured immediately after production using a digital multimeter. The resistance was measured along the narrow portion of the film. Absorbance measurements were made on a Joyce-Loebl MARK IIIB recording microdensitometer. Scans were made at several points across the short dimension of selected test films. The mass of Ag films was determined by coating two preweighed 5.1 cm × 7.6 cm glass microscope slides. The plated slides then were reweighed. The mass of 3.0 cm^2 Al films formed on HDPE blanks was determined by dissolving each film in 10 mL of 5 N HNO_3. The Al in 10-μL aliquots was determined using graphite furnace atomic absorption.

Film Cassette and Explosion Chamber. Films were exploded in a 12.1-cm i.d., 1.6-cm wall, 16-cm long cylindrical nylon chamber sealed on both ends with 1.27-cm thick Plexiglas disks. Two 3.8-cm diameter quartz windows are located 6.4 cm from the upper rim and on opposite sides of the cylinder. Electrical connection is made with two 2.2-cm diameter brass rods, which are sealed with O-rings and located normal to the viewing axis and 12.7 cm from the upper rim. A vacuum line connection is also provided in the chamber wall.

The film cassette is shown in Figure 2. A 2.5-cm thick Plexiglas block is used to insulate the contacts and provide a base for the rest of the device. The film substrate rests on a second Plexiglas block which contains a slightly relieved area to position reproducibly the substrate blanks. The electrical contact assemblies are made from brass plates, which are fastened with nylon screws to the lower Plexiglas block. Attached to each plate is a brass block machined to rest on the brass rods sealed in the chamber wall. Electrical contact with the film is made by two 1.25-cm diameter hemicylindrical carbon electrodes (Ultra Superior Purity Grade Carbon Rod Ultra Carbon Corp., Bay City, Mich.). Each

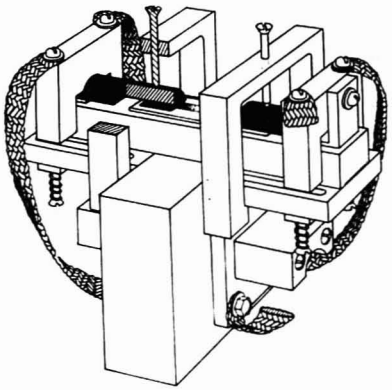


Figure 2. Thin film explosion cassette

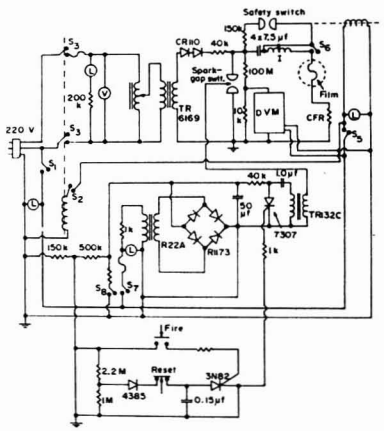


Figure 3. Explosion circuit and associated electronics

electrode is held in a two-piece brass bracket, as illustrated. The brackets are attached by spring-loaded screws to slotted brass tables. This allows the length of film exploded to be varied from 1.3 to 5.0 cm. A nylon screw in a U-shaped Plexiglas bracket allows the inner end of each carbon electrode to be tightened against the film surface, thus ensuring good electrical contact on the wide portion of the film. Electrical connection between the fixed lower portion and movable upper portion of each assembly is provided by a flexible cable.

Explosion Circuit and Associated Electronics. The capacitive discharge circuit and spark-gap trigger are shown in Figure 3. The charging circuit (top portion of Figure 3) consists of a high-voltage transformer TR6169, a CR110 rectifier stack, 40-kΩ charging resistor, and a bank of four 7.5-μF, 12-kV General Electric pyranol capacitors. The capacitors cannot be charged unless a metal film is in the circuit. The discharge circuit consists of the capacitor bank, a variable inductor I, the thin film, a current monitoring shunt CFR, and a three-electrode spark-gap switch. A digital voltmeter with a 1:10^4 resistive divider is used to measure charging voltage. The safety switch discharges the capacitors when the main power switch S_1 or charging switch S_2 is open.

The spark-gap switch is fired from the secondary of an EG and G TR132C high-voltage pulse transformer. A current pulse is delivered to the transformer primary by discharging a 1.0-μF capacitor through a 7307 silicon control rectifier. The capacitor

Table I. Surface Area, Mass, and Vaporization Energy for Al Wires, Foils, and Thin Films

form	dimensions	surface area, cm^2 (A)	mass, mg (B)	A/B	energy to vaporize, J
wire	0.008 cm diam. × 3.8 cm long	0.1	2.0	0.05	28
	0.008 cm diam. × 38 cm long	1.0	20	0.05	280
	0.025 cm diam. × 12.7 cm long	1.0	68	0.014	960
foil	2.5×10^{-3} cm × 0.25 cm × 0.4 cm	0.1	0.68	0.14	9.6
	2.5×10^{-3} cm × 0.25 cm × 4 cm	1.0	6.8	0.14	96
film	4.0×10^{-6} cm × 0.25 cm × 0.4 cm	0.1	0.0011	91	0.015
	4.0×10^{-6} cm × 0.25 cm × 4 cm	1.0	0.011	91	0.15

is charged to 400 V from an unregulated dc supply. The silicon control rectifier is fired on command by a push-button switch, which discharges a 0.15-μF capacitor charged to 30 V through a 3N82 silicon control switch. Construction details of the spark-gap switch and current shunt are found in Reference 1.

Optical Monitoring and Calibration. All spectra were recorded on Kodak SA1 plates with a 1.0-m Czerny Turner spectrometer (Jarrell-Ash Corp., Waltham, Mass) having a first-order reciprocal dispersion of 0.8 nm/mm and using a 35-μm entrance slit. Plate processing and calibration as well as absorbance to intensity conversion are discussed in Reference 5. A 5-cm diameter, 15-cm focal length quartz lens is used to image the explosion on the collimator of the spectrometer. The lens was positioned to view the entire plasma volume and to fill the aperture of the collimator.

Materials and Reagents. Silver as 100-mesh needles and Al as ~3-mm diameter lumps both of 99.999% minimum purity (Alfa Ventron, Beverly, Mass.), were evaporated from Ta boats and multifilament W baskets, respectively. Analyte solutions were prepared daily from 1000-ppm stock solutions of reagent-grade salts. A micropipet was used to place 10 μL of sample as five small drops on the narrow portion of each film. The solvent was evaporated with a heat lamp.

RESULTS AND DISCUSSION

Previous studies (*1–4*) with exploding wires and foils indicated that the intensity of continuum radiation as well as line radiation from the exploding conductor material increases with decreasing conductor mass until the mass is less than about 1 mg per 100 J of explosion energy. Further reduction in mass results in a corresponding reduction in intensity. Thus, very low conductor mass is attractive in obtaining higher analyte line-to-background intensity ratios for a fixed analyte concentration as well as fewer line interference problems from the conductor material.

Table I summarizes the surface area, mass, and vaporization energy for Al wires, foils, and thin films of dimensions similar to those used in this and previous studies (*1–3*). Large surface area is desirable for convenient sample introduction. The ratio of surface area to mass for thin films is about three orders of magnitude greater than for wires or foils. Only with thin films is the vaporization energy an insignificant fraction of the total energy consumed during the explosion (50–500 J). Thus changes in film and sample mass result in insignificant changes in the available excitation energy following vaporization.

Figure 4 shows microdensitometer traces of the spectra from a 6.1-mg Al foil, a 0.43-mg Al wire, and a 0.013-mg Al film. All explosions were conducted in dry air at 700 Torr with a 4-kV, 180-J discharge. The Al (I) resonance lines at 308.2 and 309.2 nm appear as strongly self-reversed regions in a very intense continuum for the wire and foil explosions. While the continuum intensity for the lower mass wire decreases more rapidly with increasing wavelength relative to the foil explosion, it is still unacceptably high even 10 nm from the resonance lines. In addition, wires of this size are very fragile and difficult to handle. With the low mass Al film, the resonance lines appear mainly in emission, and the continuum intensity falls off quite rapidly to acceptable values.

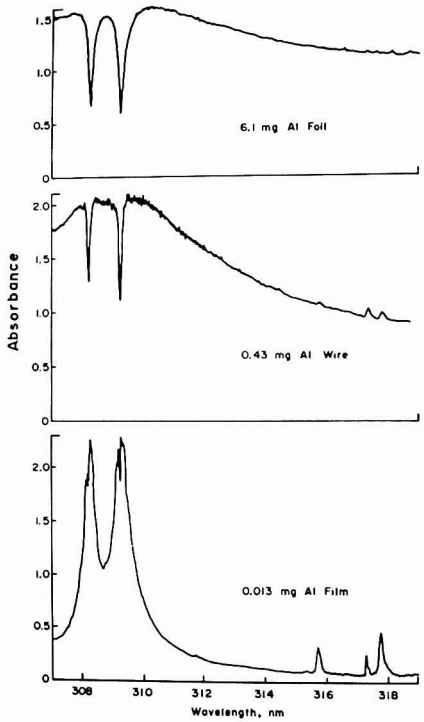


Figure 4. Microdensitometer traces of spectra obtained from an Al foil, wire, and thin film. All explosions were conducted in dry air at 700 Torr with a 4-kV, 180-J discharge

Film Preparation. Total vaporization of a weighed furnace charge was used to control film mass and batch-to-batch uniformity. This is considerably simpler and cheaper than monitoring film thickness during preparation. Preparation of Ag films is straightforward since the Ag does not react to a significant extent with the Ta boat furnace. Repeated heating and cooling of the boat, however, enbrittled the Ta,

Table II. Heating Cycles for Thin Film Production

Al[a]		Ag[b]		
time, s	current, A	time, s	current, A	observations
30	8	60	18	no visible effect
30	16	60	30	furnace glows dull red
25	30	60	45	melting occurs
25	150	90	80	rapid evaporation

[a] W basket #ME17 3x.025W, R. D. Mathis Co., Long Beach, Calif. [b] Ta boat #S13-.005Ta, R. D. Mathis Co., Long Beach, Calif.

and some breakage did occur. Evaporation of Al poses some problems since it reacts with all refractory metals forming low melting alloys (6). Because of the limited solubility of Al in W, a W filament furnace can be used if evaporation of the Al occurs rapidly after melting. Rapid evaporation also is useful in reducing the inclusion of residual gases in the films. No W was detected in Al films made by this method using an analytical technique sensitive to 0.03% W by weight (7). Some deterioration of the W basket occurred with each evaporation, and a new basket was used for every production run of 112 films.

It was found that rapid initial heating of the Al or Ag charge often resulted in spattering and loss of some metal. Thus, an initial low-current heating period to drive out included gases and melt the charge followed by rapid evaporation at high furnace current is most satisfactory. The heating cycles used in this work are shown in Table II.

Films prepared by this procedure were very uniform in appearance. Films prepared on glass and Plexiglas substrates appeared flawless and highly reflective. Very thin Ag films had a blue color in transmitted light. Films prepared on PP were less reflective and revealed numerous scratches and flaws in the substrate. Films on HDPE were quite dull because of the finely mottled substrate surface. Films on all substrates were very adherent and could be rubbed off only with some difficulty.

Film Monitoring. The actual mass of metal vaporized during an explosion is less significant than the reproducibility of the mass from shot to shot. Film-to-film mass variation will result in a corresponding variation in background intensity.

For an evaporant material of density ρ, a furnace charge of mass M will produce a film thickness t which is given by

$$t = \frac{m}{4\pi\rho R^2}$$

For a basket type furnace, which disperses metal vapor through 4π steradians, R is the distance from the furnace to the receiver surface. Any point on the surface of a sphere with the furnace at its center should receive the same vapor flux. For a boat furnace, which disperses metal vapor through 2π steradians, R is half the distance from the furnace to the receiver if the receiver is directly above the source. Here, any point on the surface of a sphere of radius R and tangent to both the furnace and receiver should receive the same vapor flux.

When a 0.5008-g charge of Ag was evaporated from a Ta boat, a 68-cm^2 receiver collected 4.9×10^{-3} g of metal as determined directly by weight difference. Assuming bulk density for the film, the mass calculated for a 2π evaporation source is 4.1×10^{-3} g. When 32.4 mg of Al was evaporated from a W basket and the Al in the film determined by graphite furnace atomic absorption, the film thickness, assuming bulk density, was found to be 360 Å ± 17%. The thickness calculated for a 4π evaporation source is 370 Å.

Table III. Absorbance Data for Silver Films

film thickness, Å[a]	no. of scans	no. of films	no. of evaporation runs	av. absorbance	rel. std. dev., %
13	5	1	1	0.35	1.6
27	5	1	1	0.35	1.7
58	5	1	1	0.35	2.7
120	5	1	1	0.39	3.1
230	5	1	1	1.09	1.0
290	5	1	1	1.51	1.2
350	5	1	1	1.98	0.6
58	20	4	1	0.25	4.3
120	20	4	1	0.40	2.8
230	20	4	1	1.06	3.4
230	40	8	2	1.10	4.1

[a] Computed values based on the evaporant mass and assuming a 2π source.

Table IV. Resistance Data for Silver Films

film thickness, Å[a]	no. of films	no. of evaporations	av. resistance, Ω	rel. std. dev., %
58	7	1	1279	77.3
120	8	1	50-70	*b*
170	8	1	7.5	15.0
230	7	1	5.6	7.6
290	7	1	3.2	5.4
350	8	1	3.1	5.4
230	15	2	5.5	6.3

[a] Computed values based on the evaporant mass and assuming a 2π source. [b] Several films showed no electrical continuity.

Absorbance and electrical resistance measurements were evaluated for routine film quality and reproducibility monitoring. Figure 5 shows typical plots of absorbance and resistance as functions of film thickness for Ag films. Thickness values were computed from the Ag charge mass assuming a 2π evaporation source. Little change in absorbance was observed for films less than 120 Å thick. This may result from the discontinuous, island-like structure of thin Ag films (8) as well as a change of film color in transmitted light. For films thicker than about 500 Å, the absorbance is too high for reliable measurement. Absorbance measurements were not practical for films on HDPE or PP because of the translucent nature of the materials.

Table III summarizes absorbance data for Ag films. Scans made at several points along a film indicate that thickness variations along the films are relatively insignificant. Thickness variations from film to film for a specific evaporation seldom exceeded ±4%, and more significantly, films produced at different times from about the same evaporant mass showed thickness variations which typically were no larger than those from a specific evaporation.

Table IV summarizes resistance data for Ag films. The very large standard deviations for films less than 150 Å thick probably result from their island-like structure. Often these films showed no electrical continuity. Resistance measurements were quite reliable for Ag films thicker than about 200 Å. Similar results were obtained for Al films except resistance measurements were somewhat more reliable with very thin films, and films thicker than about 275 Å were too optically thick for reliable absorbance measurements.

While absorbance measurements resulted in somewhat smaller relative standard deviations, the technique was too

Table V. Effect of Substrate on Analyte Line Intensities and Standard Deviations

emission line, nm	substrate	100 Torr rel. intensity	100 Torr rel. std. dev., %	700 Torr rel. intensity	700 Torr rel. std. dev., %
Mn(II) 294.9	glass	115	33	320	17
	HDPE	302	14	349	6
	Plexiglas	395	13	393	39
	PP	262	6	258	20
Sn(I) 326.2	glass	0.8	26	7.2	15
	HDPE	7.5	16	14.8	6
	Plexiglas	15.9	5	16.0	4
	PP	12.3	4	13.4	5
Cd(I) 346.6	glass	6.6	27	15.1	11
	HDPE	10.8	12	10.7	5
	Plexiglas	13.1	10	10.1	31
	PP	11.6	4	8.4	1

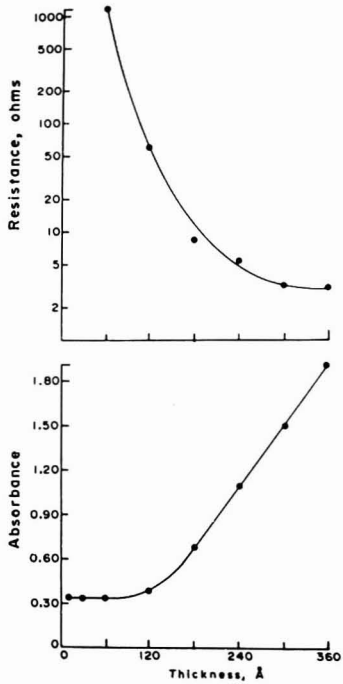


Figure 5. Absorbance and resistance vs. film thickness for Ag films prepared on glass substrates

time-consuming for the routine evaluation of every film as well as being unsuitable for thicker films and any films on PP or HDPE substrates. Resistance measurements were used for all further studies. Prior to its explosion, the resistance of each film was checked by connecting a meter across the terminals of the loaded cassette.

Explosion Reproducibility. To be useful as an excitation source for atomic emission determinations, the exploding thin-film plasma, which is produced by dielectric breakdown of the metal vapor or surrounding gas, must provide a reproducible excitation environment for samples vaporized with the films. The reproducibility of line and background intensities from the film material should provide good indication of the analytical utility of thin-film excitation. Intensity measurements were made on the Al(I) 305.0 nm and Al(II) 266.9 nm lines along with the background adjacent to these lines for five 400 Å thick (13 μg) Al films from the same evaporation. Each film was exploded from a HDPE substrate using a 4-kV, 180-J discharge. Dry air at 300 Torr was used for all explosions. The relative standard deviations for the line intensities are 7.3% and 5.2%, respectively, and the values for the background adjacent to the lines are 4.1% and 3.9%, respectively.

Substrate Material. Preliminary studies suggested that vaporization of the film and sample during an explosion was significantly affected by the substrate material. Figure 6 shows post-explosion substrate photographs for 400 Å (13 μg) Al films exploded in dry air at 100 and 700 Torr using a 5-kV, 185-J discharge. A 10-μL sample containing 10 ppm Cd, 10 ppm Sn, and 5 ppm Mn was applied to each film prior to its explosion. The dark area at the ends of each substrate is unvaporized Al, which was under the carbon electrodes. A very significant residue of apparently unvaporized Al and sample is observed for glass substrates at 100 Torr. The small spots on the residue correspond to the locations of the sample droplets. Inspection of the glass surface showed that extensive etching had occurred. The other substrate materials showed only a slight discoloration in the form of a brown residue. When the residue was wiped off, there was no evidence of substrate deterioration, and it was found that the substrates could be reused with no performance diminution. The amount of residue was slightly less with PP or Plexiglas substrates. The residue on glass at 700 Torr, while considerably less than at 100 Torr, is still significant as is etching of the glass. Virtually no residue is observed for the other substrate materials at 700 Torr.

Table V presents line intensity and relative standard deviation data for the four substrates at 700 and 100 Torr. Relative standard deviations are based on five explosions with each substrate material. While the analyte line intensities show relatively little dependence on substrate material at 700 Torr, the relative standard deviations are significantly better with the HDPE and PP substrates. In fact, the three values for HDPE approach the limits imposed by photometric measurements on photographic emulsions.

At 100 Torr, analyte line intensities are significantly lower with glass substrates relative to the other materials. This probably results from incomplete vaporization of the film and sample. The relative standard deviations with glass substrates also are larger at 100 Torr. Again this suggests incomplete vaporization. The relative standard deviations with PP and HDPE were all quite satisfactory at 100 Torr with the PP values approaching the photometric limit.

These results may be explained by the much lower resistivity of glass relative to the other materials. At room temperature, the resistivity of glass is about 9×10^9 Ω-cm and

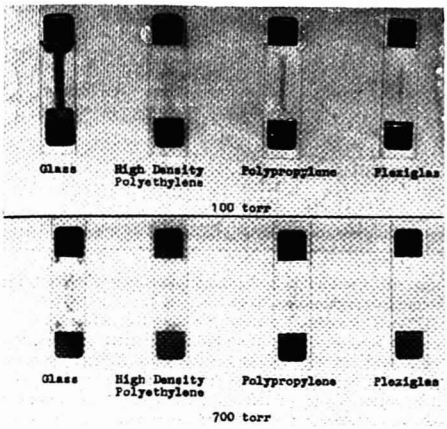


Figure 6. Post-explosion substrates showing effects of material and pressure on film vaporization for 400-Å films exploded in dry air at 5 kV and 185 J

that of HDPE is about 10^{16} Ω-cm. Further, the resistivity of glass decreases to as low as 1×10^4 Ω-cm as the glass is heated to near its annealing temperature (*9*). Thus, sufficient discharge current may be shunted through the glass, particularly near its surface where it is heated by ohmic dissipation in the film, to etch the surface and decrease the vaporization efficiency of the Al film and sample. This effect probably is more pronounced at 100 Torr because of the earlier transfer of discharge current from the solid or liquid film to the gas surrounding the expanding metal vapor cloud (*2*, *3*).

These results suggest the use of HDPE or PP as substrate materials for analytical applications. Not only are analyte line intensities larger and relative standard deviations smaller, but also the greater convenience of these materials, which are easily cut to size with a paper cutter and reused if desired, favor their use for routine determinations.

CONCLUSIONS

The preparation of thin metal films of sufficient quality and reproducibility for use as sample cells and excitation sources for quantitative emission spectroscopy is both straightforward and inexpensive. The materials cost for film preparation is very small, less than five cents per film, and even the relatively small system described here can produce over 250 films in eight hours. Since the PP and HDPE substrates can be cut with a paper cutter, their preparation is simple and rapid.

Excitation with thin films appears to be more reproducible than with metal foils. This may result from the greater uniformity of thin films together with more complete and more rapid vaporization of the film and sample. Finally, the larger surface area available with thin films of reasonable mass should permit the use of larger sample volume as well as simplify sample introduction.

LITERATURE CITED

(1) J. A. Holcombe and R. D. Sacks, *Spectrochim. Acta, Part B*, **28**, 451 (1973).
(2) R. D. Sacks and J. A. Holcombe, *Appl. Spectrosc.*, **28**, 518 (1974).
(3) C. S. Ling and R. D. Sacks, *Anal. Chem.*, **47**, 2074 (1975).
(4) C. S. Ling and R. D. Sacks, *Anal. Chem.*, **48**, 1500 (1976).
(5) J. A. Holcombe, D. W. Brinkman, and R. D. Sacks, *Anal. Chem.*, **47**, 441 (1975).
(6) L. Holland, "Vacuum Deposition of Thin Films", Wiley and Sons, New York, N.Y., 1958, pp 169–176.
(7) J. Strong, "Modern Physical Laboratory Practice", Blackie, London, 1944.
(8) R. L. Sennett and G. D. Scott, *J. Opt. Soc. Am.*, **40**, 203 (1950).
(9) G. W. Morey, "The Properties of Glass", Reinhold, New York N.Y., 1954, p 558.

RECEIVED for review June 13, 1978. Accepted August 7, 1978. Work supported by the National Science Foundation through grant number CHE76-11646 AO1.

Parametric Investigation of Exploding Thin-Film Excitation

R. D. Sacks* and D. V. Duchane[1]

Deparment of Chemistry, University of Michigan, Ann Arbor, Michigan 48109

The dependence of analysis line and Al thin film matrix emission line intensities as well as continuum background radiation intensity and analysis line-to-background ratios on experimental parameters has been investigated. These parameters include the film thickness, the pressure and composition of the plasma support gas, the total discharge energy at both constant charging voltage and constant capacitance, and the charging voltage at constant energy. Line intensities from analyte as well as film species increase with film thickness. Line-to-background ratios are greater in air than in Ar at all pressures. Precision is greater in air and at pressures greater than 100 Torr. Suggested analytical conditions employ 400-Å thick Al films exploded in dry air at 300 Torr by 180-J, 4-kV discharges. Two explosion mechanisms are discussed, a high current density mode at high energy and pressure and a diffuse mode at low energy and pressure.

[1]Present address, Los Alamos Scientific Laboratory, P.O. Box 1663, Los Alamos, N.M. 87544.

The radiative properties of wires and foils exploded by capacitive discharge largely can be controlled through manipulation of certain parameters including discharge energy, wire or foil mass, and surrounding gas pressure and composition (*1*, *2*). A change from 100 Torr Ar to 50 Torr He reduced detection limits by as much as an order of magnitude when exploding-foil excitation was used for the atomic emission determination of trace elements in 10-μL aqueous samples (*3*). A companion report (*4*) has shown that greater precision, more complete sample consumption, significantly lower background intensity, and greater convenience of film preparation and sample introduction may render exploding thin-film excitation more useful than wire or foil excitation for micro solution and solid samples.

Since exploding wires and foils have found many engineering as well as military applications, a considerable literature exists on their electrical and radiative properties (*5–8*). This provided a useful starting point in the development of analytical procedures and applications using these systems. Very little literature, however, is available for exploding thin

0003-2700/78/0350-1757$01.00/0 © 1978 American Chemical Society

films. This, coupled with significant differences in mass, surface area, and electrical resistance of films relative to wires and foils provided the impetus for a detailed investigation of their radiative properties. Such studies are needed in choosing experimental conditions for specific analytical problems and may provide insight into the vaporization, plasma formation, and current conduction processes responsible for the observed radiation patterns.

Unlike wires and foils, thin film mass is easily controlled during production and thus is a principal variable in this study. Experiments were conducted to relate empirically analysis line and film matrix line intensities, continuum background intensities, analysis line-to-background ratios and analytical precision to the film mass, the composition and pressure of the support gas, the total discharge energy at both fixed capacitance and fixed charging voltage, and the charging voltage at a fixed total discharge energy.

EXPERIMENTAL

Apparatus. The capacitive discharge circuit and its associated electronics, the explosion chamber, and the thin film production apparatus are described in a companion report (*4*). In all experiments the film was oriented perpendicular to both the optical axis and spectrograph slit. A 5-cm diameter, 15-cm focal length quartz lens was used to image the entire plasma volume onto the collimator mirror of a 1.0-m Czerny-Turner spectrograph (Jarrell-Ash Model 78-460) using a 35-μm entrance slit and having a first-order linear reciprocal dispersion of 0.8 nm/mm. Current waveforms from the capacitive discharge circuit were recorded on a Nicolet Model 1090A digital storage oscilloscope, which has a 2-MHz bandwidth and a sampling interval of 0.5 μs per point. All spectra were recorded on Kodak SA1 photographic plates. Photographic processing and calibration procedures are described in Reference 9.

Film Preparation. All films were prepared from 99.999% pure Al lumps (Alfa-Ventron, Beverly, Mass.). High density polyethylene was used as a substrate material. Substrate blanks were cleaned by soaking for 24 h in reagent grade isopropyl alcohol. Each film had a tensile bar shape with a 0.95-cm^2 region on each end for electrical contact and a 1.9 cm × 0.32 cm center region on which the sample solution was applied. Prior to its explosion, the resistance of each film was measured along its long dimension using a digital multimeter.

Sample Preparation. A 10-μL aqueous sample containing 200 ng each of Mn and Pd was applied to the film with a microsyringe as five small spots uniformly spaced along the narrow portion of the film. A heat lamp was used to evaporate the water leaving a solid, microcrystalline residue. Working solutions were prepared daily from 1000 μg/mL stock solutions of Mn as $Mn(NO_3)_2$ and Pd as $Pd(NO_3)_2$.

RESULTS AND DISCUSSION

Manganese and palladium were chosen as test elements because of their very different vaporization temperatures. The nitrate salts were selected because Al is somewhat resistant to attack by acidic nitrate solution. The Pd solution was quite acidic since it was prepared by dissolving Pd metal in HNO_3. Upon heating, $Mn(NO_3)_2$ decomposes to MnO_2, which volatilizes after further decomposition at about 2300 K (*10*). The $Pd(NO_3)_2$ is converted to $Pd(OH)_2$ and then to elemental Pd, which does not vaporize until a temperature of about 4250 K is attained (*11*). Aluminum metal vaporizes at about 2720 K (*12*). It should be noted that the thermochemistry of these materials may be somewhat altered with the extremely rapid heating and vaporization occurring with exploding thin-film excitation. Oscilloscopic monitoring of discharge current waveforms indicated that vaporization is complete and dielectric breakdown of the support gas occurs in less than 1.0 μs.

Table I summarizes information regarding the spectral lines monitored in this study. One neutral-atom and one ion line were selected for each test element as well as from the Al film material. Continuum background intensity was measured in a line free region near 323.0 nm.

Table I. Emission Lines Used in Parametric Study

species	wavelength, nm	excitation potential relative to species ground state, eV	ionization potential, eV
Al(I)	305.0	7.63	5.96
Al(II)	266.9	4.62	18.75
Mn(I)	322.8	5.93	7.40
Mn(II)	289.8	8.37	15.57
Pd(I)	340.4	4.44	8.30
Pd(II)	285.4	8.31	19.34

Film Thickness. To investigate the effect of film thickness on the intensity of continuum background and selected emission lines, 250, 400, and 550 Å thick Al films were exploded in dry air at various pressures using 180-J, 4-kV discharges. Visual examination of the substrates after the explosions revealed no noticeable differences as a function of film thickness. As was found in all parts of this study, residual Al remained on the substrates for explosions at pressures less than 300 Torr. However, this occurred for all film thicknesses.

Figure 1 shows the relative intensity of the continuum background, Al(I) line, and Al(II) line as functions of pressure for the three film thicknesses. Each point in this and in subsequent figures is based on an average of five explosions at the indicated condition. Error bars for estimates of standard deviations from the five measurements are indicated for representative points. The intensities, in general, decrease with decreasing pressure for all film thicknesses with the continuum intensity decreasing most significantly. It is noteworthy that the rate of decrease with pressure is greatest at higher pressure for the continuum radiation and greatest at lower pressure for both Al species. This is in contrast with previous studies with Al foils, which showed that the continuum radiation as well as that from Al species decreases with pressure more precipitously at lower pressure (*3*).

The Al(II) intensity is relatively pressure independent above about 300 Torr but does show indication of passing through a broad maximum at 500 Torr for the thicker films. The higher intensities from the Al species for the thicker films at nearly all pressures is easily explained by the greater available mass of Al. It is not clear, however, why the continuum intensity at all pressures is lowest for the 400-Å films. This suggests that the continuum radiation is not associated directly with the quantity of Al vapor produced.

Figure 2 shows similar plots for Mn(I) and Mn(II) lines. Again, a trend toward lower intensity at lower pressure is observed for both species. The rate of decrease with pressure is greater for the thicker films. Significantly these analyte intensities are greater with the thicker films in nearly all cases. This is surprising since unlike the Al, the Mn was present at constant concentration. Moreover, the range of intensity values for Mn(I) for the different film thicknesses is even greater than that observed for Al(I) at pressures greater than 100 Torr. These trends may be related to the stronger shock wave produced by the rapid vaporization of the more massive films (*13*). Very similar results were obtained for Pd(I) and Pd(II) lines.

Table II lists the line-to-background intensity ratios for these emission lines at several different pressures for the three film thicknesses. Note that for the Al(I) line, the line-to-background ratio consistently increases with increasing film thickness. For the Al(II) line, however, the behavior of the ratio is somewhat erratic. It peaks at the intermediate film thickness for the 700- and 300-Torr explosions but is lowest

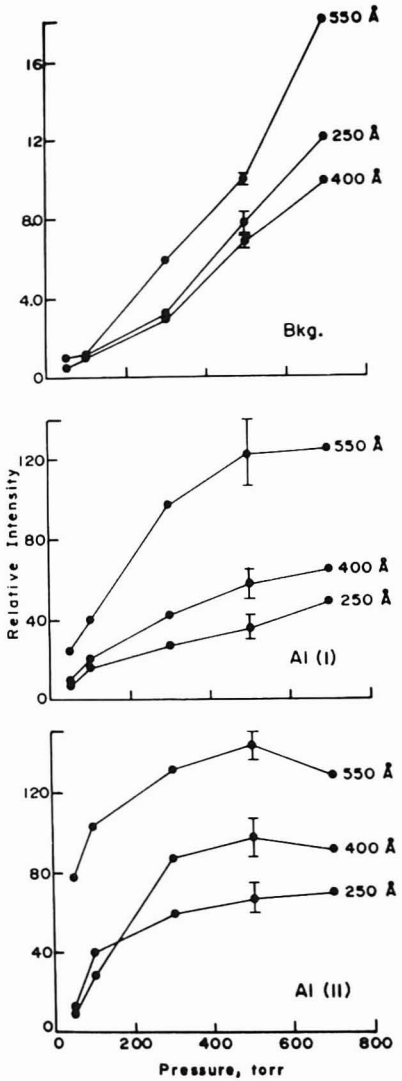


Figure 1. Plots of relative intensity of continuum background, the Al(I) line and the Al(II) line as functions of pressure for three film thicknesses and explosions conducted in air at 4 kV and 180 J

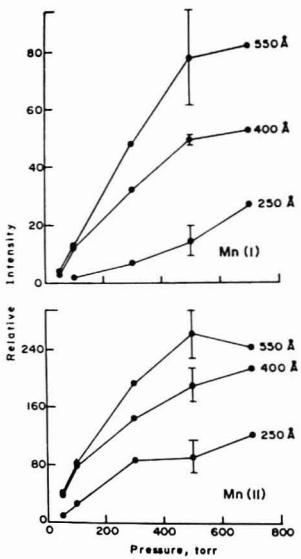


Figure 2. Plots of relative intensity of the Mn(I) and Mn(II) lines as functions of pressure for three film thicknesses and explosions conducted in air at 4 kV and 180 J

Table II. Line-to-Background Intensity Ratios of Emission Lines at Selected Pressures and Film Thicknesses

film thickness, Å	emission line, nm		pressure, Torr 700	300	100
250	Al(I)	305.0	40.3	84.1	141.8
	Al(II)	266.9	5.9	18.7	35.1
	Mn(I)	322.8	2.2	2.0	1.7
	Mn(II)	289.8	10.1	27.4	23.1
	Pd(I)	340.4	12.0	27.4	36.0
	Pd(II)	285.4	7.2	24.7	15.7
400	Al(I)	305.0	65.8	145.7	196.2
	Al(II)	266.9	9.4	30.2	27.5
	Mn(I)	322.8	13.7	18.9	19.0
	Mn(II)	289.8	34.7	70.6	87.7
	Pd(I)	340.4	56.0	111.4	139.6
	Pd(II)	285.4	15.9	35.0	54.1
550	Al(I)	305.0	69.4	165.2	349.6
	Al(II)	266.9	7.2	22.5	89.6
	Mn(I)	322.8	4.5	8.1	10.7
	Mn(II)	289.8	13.4	32.9	72.7
	Pd(I)	340.4	22.4	50.8	97.4
	Pd(II)	285.4	6.9	18.9	50.8

at the intermediate film thickness and highest for the thickest films at 100 Torr. Most significantly, the analyte lines all show the maximum line-to-background ratio at the intermediate thickness film for each of the pressures examined. For this reason, 400-Å thick Al films were used for all further aspects of this study.

Gas Pressure and Composition. Previous results for exploding wires (*1*) and foils (*3*) indicated that gas pressure and composition are the most important factors in determining analyte line-to-background ratios. Sacks and Holcombe (*14*) have shown that for exploding wires, a change in the plasma restrike mechanism from axial to peripheral occurs as the pressure is reduced to 200 Torr or less. This has broad analytical implications.

Explosions were conducted in Ar and dry air at pressures of 700, 500, 300, 100, and 50 Torr. At the two lowest pressures, a significant fraction of the film material often was left unvaporized. In earlier studies with Al foils (2), explosions were conducted successfully at pressures as low as 10 Torr. When explosions of Al films were attempted at 10 Torr, dielectric breakdown of the gas occurred so rapidly that film vaporization took place only in a small area near each carbon electrode. This may result from the much higher initial

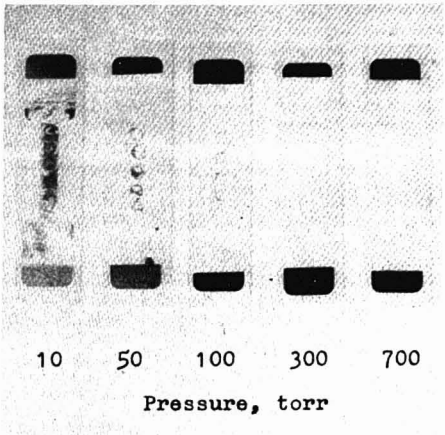


Figure 3. Post-explosion substrates showing effect of pressure on film vaporization for 400-Å films exploded in air at 4 kV and 180 J

resistance of Al films (~5.5 Ω) relative to Al foils (~0.017 Ω). Under such conditions, the explosions are of little analytical utility.

Figure 3 shows a photograph of several post-explosion substrates obtained at different pressures in dry air using 180-J, 4-kV discharges. There is no visible residue at 700 or 300 Torr. At 100 Torr, unvaporized material is observed only where the five sample droplets were applied to the film. It was not determined if this residue is unvaporized Al film or sample or both. At 50 Torr, the residue at the location of the sample droplets is more pronounced. At 10 Torr, much of the entire film remains unvaporized. The greater persistence of the residue at the sample droplet locations may result from an increase in electrical resistance in these areas due to attack of the film surface by the dilute HNO_3 used in preparing the analyte test solutions. While HNO_3 has a passivating action on the Al surface (*15*), even a relatively small corrosion depth would be significant with a 400-Å film. The more complete vaporization at higher pressure probably results from a longer period of metallic current conduction prior to dielectric breakdown of the surrounding gas together with greater ablation of the substrate surface in the higher density gas plasma after breakdown.

Studies of the effects of pressure on emission intensities were carried out at discharge energies of 180 J (22.5 μF at 4 kV) and 281 J (22.5 μF at 5 kV) in both air and Ar. Figure 4 shows results for continuum background, Al(I) and Al(II). The continuum intensity shows a nearly linear decrease with decreasing pressure in all four cases. The continuum is significantly more intense in Ar at both energies as well as being more intense at higher energy in both gases.

The decrease in continuum intensity with pressure may reflect a lower current density plasma resulting from reduced inertial confinement of the plasma at reduced pressure. The effect of discharge energy also may be explained in terms of current density, since the peak current in the first current half-cycle after vaporization increases from 7.9×10^3 A at 4 kV to 1.0×10^4 A at 5 kV. The greater continuum intensity in Ar relative to air is consistent with the more intense ion–electron recombination continuum in Ar reported for other plasma sources (*16*).

The Al(I) intensities are seen to decrease with decreasing pressure under all conditions of energy and atmospheric

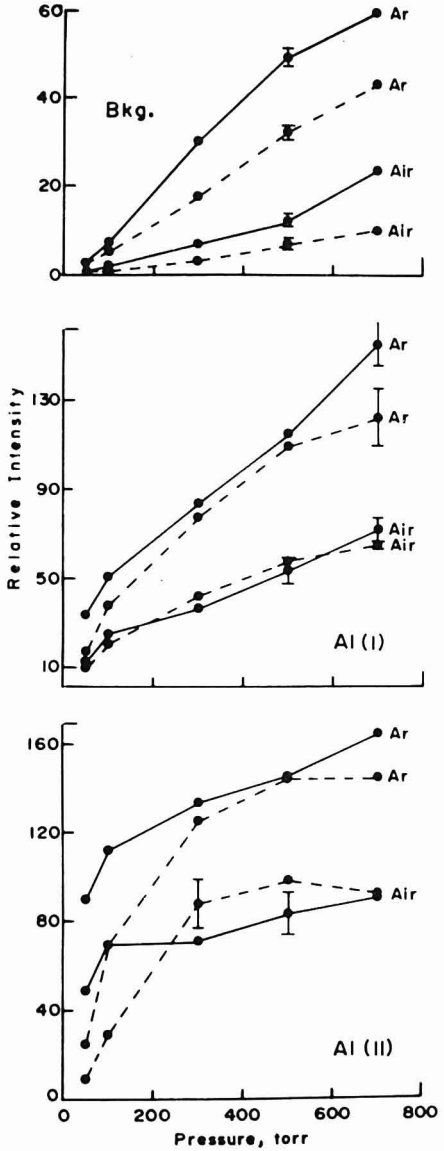


Figure 4. Plots of relative intensity of continuum background, the Al(I) line and the Al(II) line as functions of pressure for 400-Å Al films exploded in air and Ar at 180 (broken lines) and 281 (solid lines) J

composition. However, they are much less dependent on discharge energy than the continuum background intensities, particularly in dry air. Also, the rate of decrease of Al(I) intensity with decreasing pressure is seen to accelerate at pressures less than 100 Torr. This is even more apparent for Al(II), where the line intensities show only modest decreases

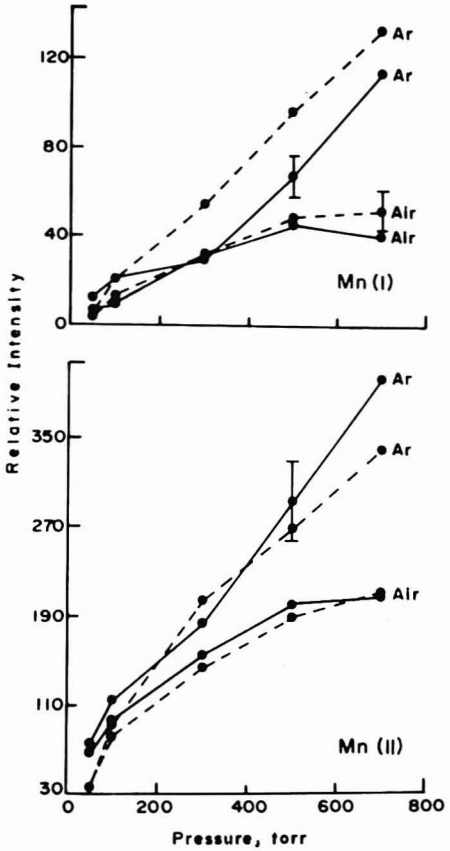


Figure 5. Plots of relative intensity of the Mn(I) and Mn(II) lines as functions of pressure for 400-Å Al films exploded in air and Ar at 180 (broken lines) and 281 (solid lines) J

until the pressure is reduced to less than 100 Torr for explosions at 281 J and modest or no decrease until the pressure is reduced to less than 300 Torr for explosions at 180 J. It is at pressures below 300 Torr that incomplete vaporization was found to occur. This suggests that, at pressures less than 300 Torr, the intensities of the Al emission lines may be limited by inefficient vaporization of the film material. A change in the plasma current conduction mechanism also may be involved as the pressure is reduced below 300 Torr.

Figure 5 shows similar plots for the Mn(I) and Mn(II) analyte lines. As for the Al lines, the Mn line intensities are relatively independent of discharge energy at all pressures in air and are relatively pressure independent in air at higher pressure. In Ar, however, the Mn(II) intensity is seen to increase more significantly with increasing pressure at high pressure relative to Al(II). Again, very similar results were obtained for Pd(I) and Pd(II) lines.

The qualitatively similar trend toward lower intensity at lower pressure for continuum background, lines from the Al film material and analyte lines is in contrast with previous results for wires (*14*) and foils (*3*) which indicated that analyte

Table III. Line-to-Background Intensity Ratios in Air and Ar at Several Pressures

emission line, nm		atmosphere	pressure, Torr 700	500	300	100	50
Al(I)	305.0	dry air	65.7	85.2	146	196	194
		argon	28.3	34.1	43.9	72.8	68.2
Al(II)	266.9	dry air	9.4	14.6	30.2	29.1	17.5
		argon	3.4	4.5	7.1	13.5	13.0
Mn(I)	322.8	dry air	5.3	7.3	11.0	15.6	7.6
		argon	3.1	3.0	3.1	3.9	2.2
Mn(II)	289.8	dry air	5.6	7.9	12.4	20.7	21.9
		argon	4.4	4.3	5.2	10.0	10.1
Pd(I)	340.4	dry air	26.5	32.5	57.1	113	144
		argon	12.8	12.4	18.3	28.6	29.7
Pd(II)	285.4	dry air	3.6	6.0	11.3	17.0	9.8
		argon	2.3	2.5	3.7	9.6	7.3

Table IV. Relative Standard Deviations (%) in Air and Ar at Several Pressures

emission line, nm		atmosphere	pressure, Torr 700	500	300	100	50
Al(I)	305.0	dry air	6	14	9	9	8
		argon	14	7	10	29	43
Al(II)	266.9	dry air	6	10	7	16	26
		argon	16	5	7	22	81
Mn(I)	322.8	dry air	20	4	10	29	27
		argon	21	25	33	48	50
Mn(II)	289.8	dry air	25	13	8	20	20
		argon	37	21	27	4	39
Pd(I)	340.4	dry air	7	9	7	8	5
		argon	35	7	17	8	32
Pd(II)	285.4	dry air	18	13	8	23	22
		argon	19	16	16	15	38

line intensities decrease with decreasing pressure to a point but then often increase as the pressure is reduced to 200 Torr and below. With wires and foils, differential vaporization, which favors an increased ratio of sample-to-matrix element concentration in the plasma at low pressure, was postulated. No such differential vaporization is apparent with thin films. In this respect, it should be noted that the wires and foils were on the order of 10^4 times more massive than the analyte material placed on them, while the thin film mass is only about 50 times greater than the 200 ng of sample element used in these studies. Thus, inefficient vaporization of the wire or foil might be expected to increase the current-carrying burden on the vaporized sample material to a far greater extent than inefficient vaporization of a film.

Although the intensities of the emission lines examined decrease as the gas pressure is reduced, the continuum background intensity decreases to a greater extent under the same conditions. Table III lists the line-to-background ratios for explosions at five pressures in both Ar and air. These values are based on average intensities from five explosions at the indicated conditions. For every pair listed, the ratio is greater in dry air than in Ar. In most cases, the air values are a factor of two to three greater than the Ar values. There appears to be no significant difference between film and sample species or between neutral-atom and ion lines in Table III.

When pressures are compared, it is observed that line-to-background ratios increase with decreasing pressure in both gases with maximum values usually occurring at 100 or at 500 Torr. Analyte lines show relatively little change in line-to-background ratios in Ar in the range from 700 to 500 Torr. In air, however, a two- to threefold increase is observed as the pressure is reduced to 500 Torr. The maximum observed ratios at 100 or 50 Torr typically are about a factor of three greater than at 700 Torr in both gases and for both film and

Table V. Discharge Parameters for Energy Studies

charging voltage, kV	capacitance, μF	energy, J	peak current, kA	ringing frequency, kHz
2.0	22.5	45	4.0	15.5
3.0	22.5	101	6.1	15.5
4.0	22.5	180	7.9	15.5
5.0	22.5	281	10.0	15.5
5.8	22.5	378	11.8	15.5
5.0	7.5	94	5.8	26.0
5.0	15	188	8.3	18.9
5.0	22.5	281	10.0	15.5
5.0	30	375	11.5	13.4

analyte species. Qualitatively similar results were reported for line-to-background ratios in Ar with exploding-foil excitation (*3*).

Table IV lists relative standard deviations for the line intensities in Table III. For the 20 pairs of values for the four analyte species, only in three cases are the dry air values greater than the corresponding Ar values. This greater precision coupled with the consistently higher line-to-background ratios strongly suggests the use of dry air for further analytical studies. When the five pressures are compared, a trend toward larger relative standard deviations at lower pressure is observed in both gases. None of the six values listed for dry air at 300 Torr exceed ±10%. These values are significantly better than those previously reported for exploding-foil excitation, where relative standard deviations in the ±15 to ±30% range were obtained for analyte line intensities without an internal reference technique (*2*).

Discharge Energy. The capacitive discharge circuit used here is an underdamped tank and thus produces a damped, sinusoidal current waveform. Time and spacially resolved spectra of exploding Al films (*17*) have indicated that most of the analytically useful radiation as well as continuum background is produced during the first current halfcycle and in the discharge current channel volume within 5 mm of the substrate surface. Thus, the current density during this first half-cycle should be important in controlling the radiative properties of exploding thin films. Since peak current density should bear some continuous relationship to peak current, manipulation of the latter through changes in either circuit capacitance or charging voltage should be illustrative.

The peak current i_p in the first current half-cycle approximately is given by $i_p \simeq (2E/L)^{1/2}$, where i_p is in A, the discharge energy E in J, and the circuit inductance L in H. The discharge energy increases linearly with capacitance and as the square of the charging voltage. Increasing capacitance increases the time from film vaporization to peak current and thus may result in reduced analyte and film material in the current channel zone at the time of peak current. Increasing charging voltage should decrease the time for dielectric breakdown of the gas or metal vapor relative to the start of the discharge as well as affecting the nature of current conduction processes in the plasma (*14*).

Table V lists the discharge parameters for two sets of experiments, one in which the discharge voltage is varied at a constant capacitance of 22.5 μF and the other in which the capacitance is varied at a constant charging voltage of 5 kV. Peak current was measured with a shorting bar in place of the thin film.

Figure 6 shows plots of background, Al(I), and Al(II) line intensities as functions of discharge energy at constant capacitance for five pressures in dry air. In this and in all subsequent figures, broken lines indicate explosions conducted at 500 and 300 Torr. The continuum background decreases steadily with decreasing energy at all pressures, but the extent of the decrease is greater at the higher pressures.

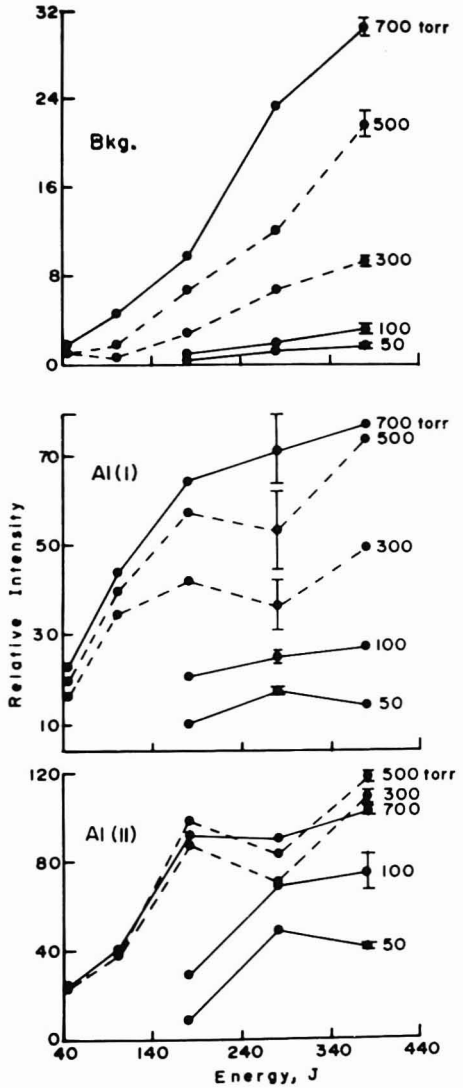


Figure 6. Plots of relative intensity of continuum background, the Al(I) line and the Al(II) line as functions of energy for 400-Å Al films exploded in air at 22.5 μF

The plots for Al(I) show a pronounced minimum at 281 J for the 500- and 300-Torr explosions. The intensities then increase somewhat at 180 J followed by a rapid decrease at still lower energies. The trends are quite different at 100 and 50 Torr. Here, no minimum is observed at 281 J and, in fact, there is indication of a maximum at this energy for the 50-Torr explosions. At energies less than 180 J, this line was undetected at the two lowest pressures. This change in energy dependence between 300 and 100 Torr is even more pro-

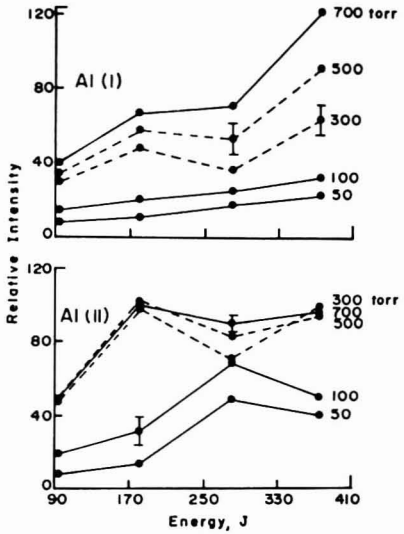


Figure 7. Plots of relative intensity of the Al(I) and Al(II) lines as functions of energy for 400-Å Al films exploded in air at 5 kV

nounced for the Al(II) line. It is interesting to note that for both Al(I) and Al(II), the 700-Torr plots in the energy range from 101 to 281 J are qualitatively similar to the 100-Torr plots at higher energy. This also applies to the 500-Torr (low energy) and 50-Torr (high energy) plots.

These trends suggest two different explosion mechanisms, one at high pressure and energies greater than 281 J and the other over the entire energy range at low pressure as well as at lower energies for the higher pressure explosions. Corroborating evidence for a change in explosion mechanism when the pressure is reduced from 300 to 100 Torr is provided in Figure 7 which shows plots of Al(I) and Al(II) intensity as a function of energy at constant charging voltage. A very pronounced minimum is observed at 281 J for both species at pressures of 300 Torr and above. Maxima are observed at this energy for the Al(II) line at pressures of 100 and 50 Torr. The Al(I) line intensity varies almost linearly with energy over the entire range at pressures of 100 and 50 Torr. Again it is observed that the Al(II) plots at low pressure show qualitatively similar trends to the lower energy portions (less than 281 J) of the Al(II) plots at pressures of 300 Torr and greater.

Decreasing either discharge energy or gas pressure should result in a decrease in current density in the discharge current channel. Decreasing energy results in a corresponding decrease in peak current and thus should decrease current density. Decreasing pressure results in reduced inertial confinement and thus more rapid expansion of the current channel (*18*). At high pressure and high energy, the plasma current density may be sufficient to result in a significant magnetohydrodynamic pinch (*19*). This would further increase current density with a corresponding increase in continuum background as well as line radiation from the film. At lower energy and lower pressure, where current density is insufficient to obtain a significant pinch, the plasma may operate in a more diffuse mode, where current density decreases rapidly with decreasing pressure and energy. While this explanation is highly speculative, it may provide a framework for further study.

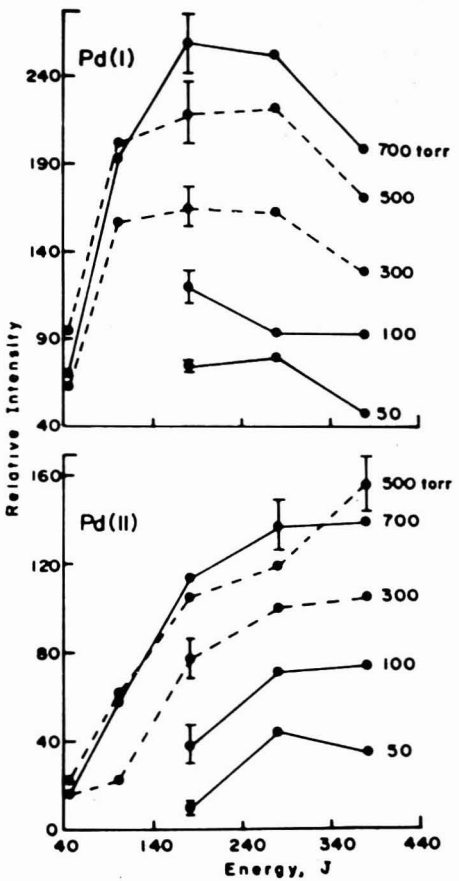


Figure 8. Plots of relative intensity of the Pd(I) and Pd(II) lines as function of energy for 400-Å Al films exploded in air at 22.5 μF

Figure 8 shows plots of Pd(I) and Pd(II) line intensities as functions of discharge energy at constant capacitance. The trends observed here are very different from those for the Al film species.

The minima observed for Al(I) and Al(II) at 281 J for the higher pressure explosions are completely absent. The Pd(I) line intensities show broad maxima at about 180 J for pressures of 300 Torr and greater. The intensities then drop very rapidly at lower energies. The Pd(II) intensities generally show a rather gradual decrease with decreasing energy at high energy and a more precipitous decrease at lower energy. Very similar results were obtained for Mn(I) and Mn(II) lines with two notable exceptions. First, the maxima observed at 180 J for the Pd(I) line at higher pressure is more pronounced for Mn(I). Second, the plots for Mn(II) showed minima at 281 J at the higher pressures and were qualitatively similar to the corresponding Al(II) plots. The constant voltage plots for the four analyte species also were similar to their Al analogues.

From an analytical viewpoint, emission line-to-background ratios appear to be quite dependent on discharge energy or

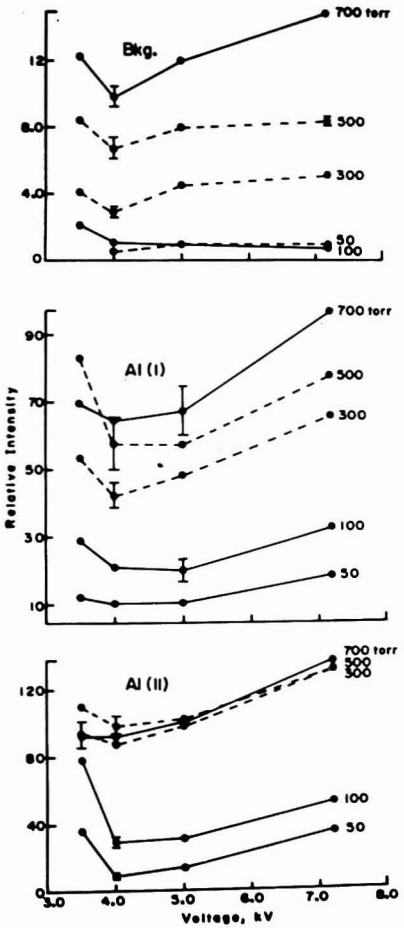


Figure 9. Plots of relative intensity of continuum background, the Al(I) line and the Al(II) line as functions of charging voltage for 400-Å Al films exploded in air with an energy of 180 J

peak current. Increasing the energy above about 180 J results in a rapid increase in continuum background intensity as well as a significant decrease in neutral-atom line intensities from the analyte species. Below 180 J, analyte line intensities fall off with decreasing energy more rapidly than the background intensity. Thus, about 180 J results in the most favorable line-to-background ratios for analyte species.

Voltage–Capacitance Combination. In the final part of this parametric study, the discharge energy was held constant at 180 J and the voltage–capacitance combination varied. Here, the peak current is constant at about 7.9 kA, but the time of peak current relative to sample vaporization increases with increasing capacitance.

Figure 9 shows plots for continuum background, Al(I) and Al(II). At all pressures, a minimum is observed at 4 kV and 22.5 μF. The intensities increase gradually at higher voltages and more rapidly at the lower voltage. It is noteworthy that the plots for Al(II) are relatively pressure independent at pressures of 300 Torr and greater. Not only do the intensities fall off drastically at lower pressure but also, the intensity increase at 3.46 kV relative to 4.0 kV is greater at the two lower pressures. Again, this suggests a change in explosion mechanism as the pressure is reduced below 300 Torr. While the indication of a mechanism change is less obvious for the Al(I) plots, a change in current conduction processes might be expected to affect Al(II) more than Al(I) since the former species may be a principal carrier of the discharge current.

The general trend toward lower intensity at higher capacitance (lower voltage) may reflect an increasing tendency for the escape of metal vapor from the current channel region prior to peak current. The reason for the increase in intensity at 3.46 kV, however, is unclear.

The response of Pd(II) intensity to voltage–capacitance combination is very similar to that of Al(I), particularly at pressures of 300 Torr and greater. The intensities are relatively independent of voltage–capacitance combination at 50 and 100 Torr. The other three analytical species, however, respond very differently and show maxima at or near 4 kV for all pressures. The intensities drop off gradually at higher voltages and more rapidly at the lower voltage. While the reasons for these trends are not clear, they are analytically significant, since three of the four analyte species investigated showed maximum intensity at 4 kV for nearly all pressures and the continuum background intensity indicated minimum values at this voltage.

CONCLUSIONS

Over the range of values studied, each parameter resulted in changes in analyte line-to-background ratios by typically a factor of 3 to 5. Their combined effects, however, reflect an increase of 1 to 2 decades in these ratios and should obtain concomitant improvements in signal-to-noise ratios and powers of detection.

The response of all measured line intensities and continuum intensity to the parameters discussed here is much smaller with exploding films relative to wires and foils. The plots shown in this report all employed a linear intensity scale with intensity changes seldom greater than one decade for a given spectral element. For analogous studies with wires (*14*) and foils (*3*) covering similar parameter ranges, intensity changes often spanned 3 to 4 decades and required a log intensity scale. Complete film vaporization over a wider range of parameter values together with the much smaller metal vapor mass may provide some explanation for the smaller range of intensity values. This is analytically significant, since small, uncontrollable changes in operating conditions are much less significant with thin-film excitation. This should result in greater analysis precision.

The data in Figures 1 and 2 suggest that film thickness or mass control is important since, for the range of thickness values studied, a 1% change in film thickness typically results in about a 1% change in line intensities from both film material and analyte species.

The response of the Al line intensities to the various parameters often differs from the response of the analyte species line intensities. This suggests that the Al film material may not be useful as an internal reference. However, the results reported here suggest that internal referencing may be counterproductive with photographic detection since photometric error rather than explosion reproducibility may be the limiting factor in determining analytical precision.

The explanations provided for the observed intensity trends are in many cases very speculative. Since exploding conductor plasmas are very heterogeneous in both space and time (*14,18*), temporally and spacially resolved intensity measurements will be required to obtain a more definitive description of exploding thin-film plasmas.

LITERATURE CITED

(1) J. A. Holcombe and R. D. Sacks, *Spectrochim., Acta, Part B*, **28**, 451 (1973).
(2) C. S. Ling and R. D. Sacks, *Anal. Chem.*, **47**, 2074 (1975).
(3) C. S. Cling and R. D. Sacks, *Anal. Chem.*, **48**, 1500 (1976).
(4) D. V. Duchane and R. D. Sacks, *Anal. Chem.*, preceding paper in this issue.
(5) "Exploding Wires", W. G. Chace, and H. K. Moore, Ed., Plenum, New York, N.Y., Vol 1, 1959.
(6) Ref. 5, Vol. 2, 1962.
(7) Ref. 5, Vol. 3, 1964.
(8) Ref. 5, Vol. 4, 1968.
(9) J. A. Holcombe, D. W. Brinkman, and R. D. Sacks, *Anal. Chem.*, **47**, 441 (1975).
(10) F. A. Cotton and G. Wilkinson, "Advanced Inorganic Chemistry", Interscience, New York, N.Y., 1972, p 852.
(11) Ref. 10, pp 990–1000.
(12) O. Kubaschewski and B. E. Hopkins, "Oxidation of Metals and Alloys", Academic Press, London, 1962, pp 102, 103, and 230.
(13) R. D. Sacks, "Shock Tubes, Exploding Conductors and Flashlamps", in "Analytical Uses of Plasmas", R. M. Barnes, Ed., Wiley-Interscience, New York, N.Y., in press.
(14) R. D. Sacks and J. A. Holcombe, *Appl. Spectrosc.*, **28**, 518 (1974).
(15) U. R. Evans, "Metallic Corrosion, Passivity and Protection", E. Arnold & Co., London, 1946.
(16) S. Greenfield, *Metron 3*, 224 (1971).
(17) D. V. Duchane, "The Application of Exploding Thin Films to Trace Metals Analyses", Ph.D. dissertation, University of Michigan, Ann Arbor, Mich., 1978.
(18) P. Thomas and R. D. Sacks, *Anal. Chem.*, **50**, 1084 (1978).
(19) L. A. Arzimovich, "Elementary Plasma Physics", Blaisdell, New York, N.Y., 1965.

RECEIVED for review June 13, 1978. Accepted August 7, 1978. Work supported by the National Science Foundation through grant number CHE76-11646 A01.

Atomic Emission Determination of Selected Trace Elements in Micro Samples with Exploding Thin-Film Excitation

D. V. Duchane[1] and R. D. Sacks*

Department of Chemistry, University of Michigan, Ann Arbor, Michigan 48109

The highly luminous metal-vapor plasma obtained from the electrical explosion of 400-Å thick, 13-μg Al thin films has been used as a free-atom generator and excitation source for the analysis of selected trace elements in aqueous media. Ten-microliter samples of metal salts are applied to the film surface. The film strips are exploded in 300 Torr dry air with a 4-kV, 180-J capacitive discharge. Analytical curves and reproducibility data are presented for Mn, Sn, Cd, Pb, and Pd, both with and without an internal reference technique. The relative standard deviations for these elements at the 100-ng level are 5, 11, 8, 9, and 5%, respectively. Detection limits, usually in the low to sub-ng range, are presented for 14 elements. Concomitant effects are found to be relatively minor if the total solute content is less than about 0.01 M.

When furnace techniques are used for the volatilization of micro solid or solution residue samples, the relatively low rate of furnace heating results in reducing analyte free atom number densities (*1*) as well as significant concomitant effects (*2*). Since noncapacitive power sources generally are used for furnace heating, the heating rate is limited by laboratory wiring as well as the heat capacity of the relatively massive furnace. Peak power dissipation in the furnace is usually no more than a few kW.

If a high-voltage capacitive discharge power source is used to heat a thin metal film of low mass and heat capacity, explosive vaporization of the film and a sample deposited on its surface probably is complete in about 1 μs. When an Al film of 1.3×10^{-4} mm^2 cross sectional area is vaporized by a 4-kV, 22.5-μF discharge, a current of 3.7 kA is measured 1 μs after the start of the discharge. If the film material still exists as a metallic conductor at this time, it would carry a current density of over 10^7 A/mm^2 and dissipate over 10 MW, assuming room temperature resistance. This probably is conservative.

If the film is exploded from a polymeric substrate such as polyethylene, complete scavenging of the film and sample is observed (*3*). Since a fresh film is used each time, memory effects and furnace deterioration problems are obviated. Since only a few micrograms of high-purity metal are vaporized from a hydrocarbon substrate, the analytical blank is minimal for most elements.

If dielectric breakdown of the gas surrounding the film occurs during or after film vaporization, a high current density plasma is formed which excites and to some extent ionizes the analyte vapor. Since the plasma is in close proximity to the substrate surface, ablation may augment film and sample atomization.

This report considers exploding thin films for volatilization and excitation of trace elements in micro-volume solution samples. Companion reports consider thin film preparation and control (*3*) and the effects of various parameters on exploding thin-film excitation (*4*).

EXPERIMENTAL

Apparatus. The capacitive discharge circuit used for the explosive vaporization of thin films has been described (*3*). The thin-film production apparatus and ancillary hardware also are considered. All spectra were recorded on Kodak SA1 photographic plates. Emulsion processing and calibration have been discussed (*5*). A 1.0-m Czerny-Turner spectrograph (Jarrell-Ash model 78-460) with a first-order reciprocal linear dispersion of about 0.8 nm/mm and using a 35-μm entrance slit was used throughout this study. Entrance slit illumination is the same as in Reference 4.

Procedures. Aluminum films prepared by vacuum deposition on high-density polyethylene substrates were used exclusively. Film preparation and control is described in Reference 3. Each film had a tensile bar shape with a 0.95-cm^2 region on each end for electrical contact and a 1.9 cm × 0.32 cm center region on which a 10-μL aqueous solution sample was placed as five small, evenly

[1] Present address, Los Alamos Scientific Laboratory, P.O. Box 1663, Los Alamos, N.M. 87544.

0003-2700/78/0350-1765$01.00/0 © 1978 American Chemical Society

Table I. Thin-Film Specifications and Explosion Conditions

thin-film specifications	
film thickness, A	400
surface area exploded, cm²	1.2
film mass exploded, μg	13
film material	aluminum
mean film resistance, Ω	5.9
substrate material	high density polyethylene
explosion conditions	
discharge energy, J	180
discharge voltage, kV	4
circuit capacitance, μf	22.5
ringing frequency, kHz	15.5
chamber gas composition	dry air
chamber gas pressure, Torr[a]	300

[a] Exception, all work with Sn done at 700 Torr.

spaced drops. The solvent was completely evaporated with a heat lamp. Prior to each experiment, the excitation chamber was evacuated to less than 1 Torr and then filled to operating pressure.

Sample Preparation and Explosion Conditions. Sample stock solutions (1000 ppm) were prepared from reagent grade materials. Volumetric dilutions were prepared daily. Sample solutions were applied to the films with a 10-μL disposable-tip syringe. Table I summarizes the thin-film specifications and explosion conditions. The bases for selection of parameter values are discussed in Reference 4.

RESULTS AND DISCUSSION

Relatively intense neutral-atom and ion lines were detected for nearly all elements tested. As was the case with exploding wire (6) and foil (7) excitation, the spectra are more spark-like than arc-like in general features. While numerous lines from neutral-atom, singly-ionized and doubly-ionized Al were present, significant line interference problems were infrequent even on a multielement basis. Cyanogen band spectra were observed in the 360 nm to 390 nm range, but their intensity over background was much lower than that usually observed with graphite-electrode dc arc excitation in air.

Analytical Curves. Curves were prepared for Mn, Sn, Cd, Pb, and Pd. The curves were determined on a single-element basis. These elements were chosen because of their wide range of thermodynamic properties. Each point on these curves represents the average intensity or intensity ratio from five determinations at the indicated concentration. All spectra for a given element and concentration were recorded on a single photographic plate to minimize photographic processing error.

Since exploding thin-film excitation is based on a transient, nonrepetitive event, conventional noise reduction devices such as lock-in amplifiers cannot be used. Thus, an internal reference technique was evaluated as a means for compensating for certain problems such as positional instability of the plasma. Table II summarizes pertinent date for the analyte and internal reference species. In all cases, attempts were made at matching the analyte and reference species in terms of both thermodynamic properties and excitation potentials of the lines used.

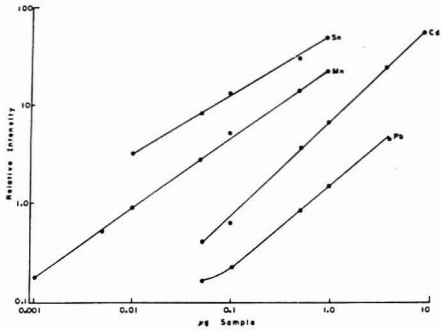


Figure 1. Analytical curves for Mn, Sn, Cd, and Pb without internal referencing

Holcombe and Sacks (6) and Ling and Sacks (7) evaluated the use of a convenient emission line from the exploding conductor material as a built-in internal reference for exploding wire and exploding foil excitation, respectively. This procedure also was evaluated here using a convenient line from the Al thin film matrix.

Figure 1 shows a composite of analytical curves for all elements except Pd. In general, these curves are linear over at least two to three decades of concentration. Analogous curves for exploding foil excitation (7) frequently showed a negative deviation with sample mass greater than about 1 μg. It is interesting that the Cd curve is linear at least up to 10 μg. This is only slightly less than the 13-μg film mass. The curvature at the low sample mass end of the Pb curve is caused by a spectral interference of unknown origin. These curves have slightly different slopes, all of which are less than unity. This may be the result of a nonlinear atomization or excitation process or a change in the emulsion contrast. Exploding foils were used as a radiation source for the calibration procedure. Since both the intensity and temporal variation of radiation from foils and films are quite different, reciprocity failure is suspected.

Analytical curves using an added internal reference have slightly different slopes and considerably more point scatter than the corresponding curves in Figure 1. This is in strong contrast with exploding foil excitation (7) where point scatter was considerably reduced with internal referencing. It was also observed that the analytical curve for Sn with an added internal reference has some curvature at low sample mass. Very similar analytical curves were obtained using the Al film material as an internal reference. The point scatter was about the same as with an added internal reference.

Pd is treated as a special case since, at high concentrations, the solutions were sufficiently acidic to cause noticeable deterioration of the Al films. Test solutions of Pd were prepared by dissolving the metal in 10 N HNO_3. After di-

Table II. Data for Analyte and Internal Reference Materials

analyte species	int. ref. species	concn of int. ref., ppm	boiling pt., K		emission line measured, nm		excitation potential, eV	
			anal.	ref.	anal.	ref.	anal.	ref.
Mn(II)	Ni(II)	10	2420	3000	294.9	254.6	5.35	6.70
Sn(I)	Pb(I)	10	2540	2000	286.3	287.3	4.31	5.61
Cd(I)	Zn(I)	50	1040	1180	340.3	334.5	7.37	7.75
Pb(I)	Tl(I)	50	2000	1730	283.3	276.8	4.36	4.46
Pd(I)	V(I)	10	4250	3730	340.4	318.5	4.44	3.94

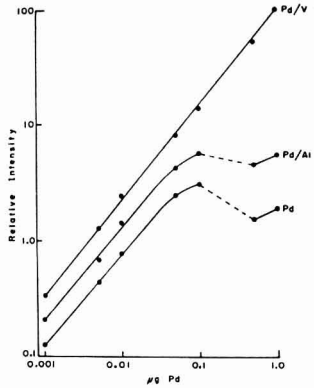


Figure 2. Analytical curves for Pd without an internal reference, with ratioing to a line from the Al film, and with ratioing to a line from the V added internal reference

lution, the 1.0-ppm solution (10 ng per aliquot) was 0.01 N in HNO_3, while the 50-ppm solution (500 ng per aliquot) was 0.5 N in HNO_3. The high acidity of this latter solution caused visible holes in the film at the locations of the sample spots. In addition, the resistance along the film length increased by a factor of two or more. At Pd concentrations greater than 100 ppm, the acidity was so high that rapid attack of the film surface ensued, resulting in complete loss of film continuity, thus rendering subsequent explosion of the film impossible.

Figure 2 shows analytical curves for Pd without an internal reference, with ratioing to an Al film line, and with ratioing to a line from the V added internal reference. Without ratioing, the curve is linear up to about 0.05 μg Pd. A discontinuity occurs at Pd mass greater than 0.1 μg with a decrease in intensity for larger sample mass. This is hardly surprising since the film was completely dissolved at the locations of the sample spots. The discontinuity is less pronounced but still significant when the Al film material is used as an internal reference. This indicates a decrease in film vaporization efficiency for the larger Pd samples. With the V internal reference, the curve is linear over three full decades of concentration.

This indicates that even under very unfavorable circumstances, reliable analytical data can be obtained with an added internal reference. In general, however, with regard to analytical curve linearity, there appears to be no compelling reason to use an internal reference unless the film matrix is severely attacked by the sample solution.

Powers of Detection. Detection limits were determined for the 14 elements in Table III. These values are defined as the minimum amount of the element required to produce a line intensity equal to three times the intensity equivalent of the root-mean-square noise on the microdensitometer trace in a nearby wavelength region of continuum background.

To obtain reliable extrapolated detection limits, the SAI photographic plates were prefogged with a Kodak Wrattan series OA filter to obtain an absorbance sufficient to ensure operation on the linear region of the emulsion calibration curve.

Absolute detection limits generally are in the low to sub-ng range. The relative detection limits in Table III are based on 10-μL aliquots. Decreasing concentrational detection limits by using larger sample volume is considerably easier with films than with foils because of the larger film surface area.

These detection limits were obtained on a simultaneous,

Table III. Exploding Thin-Film Detection Limits

element	line measured, nm	detection limit, ppm[a]	detection limit, ng
Ag(I)	328.0	0.0087	0.087
As(I)	278.0	0.69	6.9
Bi(I)	302.5	2.1	21
Cd(I)	346.6	1.3	13
Co(I)	345.4	0.11	1.1
Hg(I)	253.7	0.75	7.5
Li(I)	323.3	3.0	30
Mn(II)	294.9	0.0076	0.076
Ni(I)	341.5	0.037	0.37
Pb(I)	283.3	0.96	9.6
Pd(I)	340.4	0.033	0.33
Sn(I)	317.5	0.27	2.7
Tl(I)	351.9	1.0	10
V(II)	327.6	0.027	0.27

[a] Based on 10-μL sample size.

multielement basis using a single set of operating conditions. Element-specific parameter manipulation could lead to lower detection limits for some of these elements. The higher quantum efficiency of photoelectric detection also might provide greater powers of detection than the rather low optical speed emulsion used here.

The detection limits shown in Table III are comparable to the better of the two sets of detection limits reported by Ling and Sacks (7) using exploding Al foil excitation. However, these foil excitation values were obtained in 50-Torr Ar, which is experimentally more difficult than the 300-Torr air used in the thin-film work as well as being a rather less favorable gas and pressure regarding analytical precision with either foil or thin-film excitation. These multielement detection limits typically are one to two orders of magnitude better than reported single-element values using flame atomic absorption and one to two orders of magnitude poorer than typical values using flameless atomic absorption (2).

Reproducibility of Exploding Thin-Film Excitation. The reproducibility of the film preparation techniques has been discussed (3). The reproducibility of the sample introduction techniques was previously evaluated in conjunction with exploding foil excitation (7). The relative standard deviation of the dried sample residue mass was found to be ±1.4%.

The overall method reproducibility was determined for the replicate determinations used in obtaining the data for the analytical curves in Figures 1 and 2. Table IV summarizes the relative standard deviations for the 0.1-μg data points. For the unratioed emission line intensities, values generally are in the ±5–10% range. Only for Pd is the reproducibility significantly poorer than this. These values are similar to those reported for flameless atomic absorption (2).

In the case of Pd, ratioing to the V internal reference line reduces the relative standard deviation from ±18 to ±5%, thus making it comparable to the other values. In no other instance does ratioing to either a line of an added internal reference or to one from the Al film material result in improved reproducibility. In fact, ratioing often results in larger relative standard deviations. This is particularly true for data obtained by ratioing to an Al line.

The larger relative standard deviations for the unratioed Pd line probably originate from deterioration of the film by the acidic sample medium. It should be noted that the discontinuity in the Pd analytical curve occurred with sample mass just greater than the 0.1-μg value for which the relative standard deviation was computed. It is also interesting that ratioing the Pd line to an Al line resulted in little improvement in the shape of the analytical curve. On the other hand,

Table IV. Relative Standard Deviations of 0.1-μg Data Points from Analytical Curves

analyte element	reference element	rel. std. dev., %		
		no ref.	added ref.	Al ref.
Cd	Zn	8	18	14
Mn	Ni	5	8	9
Pb	Tl	9	10	17
Pd	V	18	5	14
Sn	Pb	11	15	29

ratioing the Pd line to a line from the added internal reference not only significantly reduced the relative standard deviation but also eliminated the discontinuity in the analytical curve.

In work with Al foil excitation using sample introduction techniques essentially the same as those utilized in this work, Ling and Sacks (7) reported relative standard deviations for unratioed emission line intensities in the range of ±15–30%. Also they reported that an added internal reference reduced these values to the ±5–10% range; although, like the results reported here, ratioing to a line from the Al matrix resulted in poorer reproducibility relative to the unratioed values. Thus, films appear to be superior to foils from the standpoint of analytical reproducibility. The greater relative variance using an added internal reference suggests that a significant fraction of the total variance with thin film excitation, unlike foil excitation, is a result of photometric error from the emulsion. This further suggests that analytical reproducibility may be significantly improved using photoelectric detection.

Concomitant Effects. Previous studies with exploding wires (6) and foils (7) have indicated that compound form and the presence of relatively high concentrations of concomitant species have relatively little effect on analyte line intensities. This is probably the result of rapid total sample vaporization along with high energy density in the plasma. Fractional volatilization, which is troublesome with furnace volatilization techniques as well as with arc excitation, should not be significant when sample vaporization is complete in about 1 μs. This time is short with respect to both analyte vapor loss by diffusion and the duration of radiation from analyte species in the plasma. In this respect, the smaller film mass with its attendant shorter vaporization time together with experimental indication of more complete film and sample vaporization (3, 4) may render thin-film excitation freer of concomitant effects than wire or foil excitation.

The very high energy density during the first current half-cycle, when most of the analytically useful radiation occurs, should minimize compound formation in the plasma. For example, band spectra from the second positive N_2 system and from CN, when carbon electrodes are used in the film cassette, are detected only during the very early stages of the discharge before analytical radiation is detected. On the other hand, the much smaller mass of the film material relative to wires or foils may result in more significant changes in excitation environment in the presence of variable concentrations of concomitant species. That is, the total sample mass will not be insignificant with respect to the film mass at high sample loadings.

In the preliminary studies reported here, the analyte was present at fixed concentration, and the concomitant concentration was varied from zero to 10^3 times the analyte concentration. In every case, an attempt was made to utilize as the concomitant a species often associated with the analyte in practical situations.

The results are summarized in Table V. In the case of the acidic Pd samples, addition of relatively high concentrations of the chloride salt increased deterioration of the film. In the presence of 1000 ppm Ni as $NiCl_2$, the film was so degraded by the sample that it could not be exploded. For the other elements examined, significant concomitant effects were observed only when the concomitant element was present at the 40-μg level. Only substrates from those samples showed significant residues of unvaporized material at the spots where the sample had been placed. Thus, for these high total mass samples, the decrease in emission intensities may be due primarily to overloading the film and consequent incomplete vaporization of the sample. It should be noted that 40 μg of concomitant element represents a mass more than three times the mass of the Al film material.

Table V. Effect of Concomitant Species on Analyte Line Intensities

analyte element and concn	concomitant species	concomitant concn, ppm	relative analyte line intensity
Tl	Zn	0	57.8
		50	59.7
5 ppm	($ZnCl_2$)	500	56.3
		4000	21.6
Pb	Zn	0	30.5
		50	34.7
5 ppm	($ZnCl_2$)	500	35.7
		4000	19.3
Pd	Ni	0	62.4
		10	64.3
1 ppm	($NiCl_2$)	100	57.7
		1000	film attacked by acid
Mn	Fe	0	48.7
		50	53.3
5 ppm	($Fe(SO_4)_2$)	500	43.8
		4000	12.9
Ni	Fe	0	46.2
		50	51.3
5 ppm	($Fe(SO_4)_2$)	500	49.3
		4000	21.0

It would appear that concomitant effects may pose a problem in special situations. Certainly, when the concomitant material results in destruction of the film, results will be affected. In addition, the micro nature of this technique is emphasized by the overloading apparent in cases where relatively large samples have been used. Other than these instances, concomitants do not appear to be a serious problem for the conditions tested with exploding thin-film excitation. Further studies in this area clearly are warranted, however.

CONCLUSIONS

Line interference problems from the film material cannot be completely eliminated, but variation of film material can minimize the compromises which might emerge in a specific multielement determination. Recent studies in $Ar–O_2$ gas mixtures have shown that CN line interferences can be eliminated by using an N_2-free atmosphere with no significant loss in precision or sensitivity.

Since the maximum sample size appears to be in the 4- to 40-μg range (neglecting counterions), solutions with a total solute content greater than about 0.01 M might pose problems with a 10-μL sample. The parameters which control maximum sample size are as yet unknown. Film thickness and support gas pressure, however, are prime suspects (3, 4).

While exploding thin-film vaporization and excitation appear to offer some analytically attractive features for multielement analyses of micro solution samples, photoelectric detection will be required to verify the linearity and the slope of the analytical curves as well as the speculation of greater analytical precision. These studies are in progress.

LITERATURE CITED

(1) D. J. Johnson, B. L. Sharp, T. S. West, and R. M. Dagnall, *Anal. Chem.*, **47**, 1234 (1975).
(2) A. Syty, *Crit. Rev. Anal. Chem.*, **4**, 155 (1974).

(3) D. V. Duchane and R. D. Sacks, *Anal. Chem.*, accompanying paper in this issue.
(4) R. D. Sacks and D. V. Duchane, *Anal. Chem.*, preceding paper in this issue.
(5) J. A. Holcombe, D. W. Brinkman, and R. D. Sacks, *Anal. Chem.*, **47**, 441 (1975).
(6) J. A. Holcombe and R. D. Sacks, *Spectrochim. Acta, Part B*, **28**, 451 (1973).
(7) C. S. Ling and R. D. Sacks, *Anal. Chem.*, **47**, 2074 (1975).

RECEIVED for review June 13, 1978. Accepted August 7, 1978. Work supported by the National Science Foundation through grant number CHE76-11646 AO1.

Nebulizer for Analysis of High Salt Content Samples with Inductively Coupled Plasma Emission Spectrometry

Ronald F. Suddendorf and Kenneth W. Boyer*

Division of Chemistry and Physics, U.S. Food and Drug Administration, Washington, D.C. 20204

A new mechanically simple nebulizer is described for analysis of high salt content samples with the inductively coupled plasma (ICP). Because of its design, the nebulizer is capable of continuous operation without clogging, and thus is free from drift commonly associated with capillary bore pneumatic nebulizers. Detection limits are found to be equal to those obtained with a conventional pneumatic nebulizer. In addition, the nebulizer possesses rapid cleanout and convenient sample changing capability.

The current trend toward multielement analysis has been accelerated by the availability of the inductively coupled plasma (ICP). However, most analytical procedures currently employing the ICP require that the sample be made available in the form of a solution for introduction by a nebulizer into the ICP as a finely dispersed aerosol. One of the major problems of the ICP has been the absence of a totally satisfactory nebulizing device, especially for solutions that have a high salt content.

Sample introduction devices for direct analysis of solutions with the inductively coupled argon plasma (ICP) must meet two general requirements. First, the nebulizer must conveniently produce a stable generation of aerosol and, second, the aerosol must be produced with an argon flow rate compatible with the ICP. The argon may serve as both the aerosol generating force and the carrier gas for the aerosol, as occurs with conventional pneumatic nebulizers, or it may serve as the carrier gas only, as with ultrasonic nebulizers. In either case, its flow rate must be approximately 1 L/min to be compatible with most commercially available ICPs.

Because of the restraint placed on the argon flow rate, nebulizers commonly used in atomic absorption or flame emission with a higher flow rate of aspirating gas will not operate at optimum efficiency and thus will not produce a sufficient quantity of aerosol to be of value with the ICP. For this reason, several new nebulizer designs have appeared which are capable of efficient aerosol production at low gas flow rates.

Two of the most popular types currently in use are the crossflow (*1*) and concentric glass nebulizers (*2*). Both devices rely on capillary tubes in their design to generate aerosol using low flow rates of argon gas. Although these nebulizers are capable of efficient aerosol generation, it is possible for the capillary tubes to become partially or completely clogged, especially when analyzing high salt content samples. Thus, they require frequent cleaning to restore the original rate of aerosol generation or necessitate restandardization of the ICP.

Several designs based on ultrasonic nebulization have been reported for use with the ICP (*3–7*). One of the advantages of ultrasonic nebulizers is the absence of restricted capillary tubes for sample introduction. As a result, instability due to clogging is eliminated. However, a disadvantage is the inconvenient and time consuming sample changing procedure along with the requirement of electronics to drive the piezoelectric transducer. A more recent design (*8*) has improved the sample changing procedure with ultrasonic nebulizers.

Fritted disk nebulizers (*9*) are also being investigated as sample introduction devices for the ICP. Like ultrasonic nebulizers, the fritted disk nebulizer does not require the solution to pass through restricted capillary tubes for aerosol generation. At the present time, relatively little data are available documenting the use of this nebulizer with the ICP.

Application of the Babington nebulizer for analysis of high salt content samples by flame atomic absorption analysis has been reported (*10*). The nebulizer was designed for atomic absorption and for that purpose operates at a gas flow of 9 to 12 L/min, far in excess of the 1 L/min flow rate suitable for use with the ICP. However, the nebulizer possibly could be redesigned with a smaller orifice to reduce the total gas flow, making it more compatible with the ICP.

This paper describes the design and operation of a mechanically simple nebulizer suitable for analysis of high salt content samples with the ICP. Data are reported for analysis of high salt content samples showing improved precision over that obtained with a conventional crossflow nebulizer. Included are data showing detection limits and freedom from memory effects.

EXPERIMENTAL

Inductively Coupled Plasma. The ICP used in this work was a Jarrell-Ash model 975 Plasma Atom Comp (Jarrell-Ash Co., 590 Lincoln St., Waltham, Mass. 02154) direct reading spectrometric system with dynamic background correction, capable of the simultaneous determination of 25 elements. Data handling was accomplished with the aid of a PDP-8 minicomputer. Forward power to the plasma was maintained at 1100 W with reflected power less than 2 W. Argon flow through the nebulizers was 1 L/min.

Nebulizers. Two different nebulizers were used in this work. One was a commercially available crossflow nebulizer (Jarrell-Ash Co., 590 Lincoln St., Waltham, Mass. 02154) similar in design to that reported in the literature (*1*).

The nebulizer described here consists of a goldplated stainless steel base 5 cm long and 8 mm wide (Figure 1) in which a "V"-shaped groove has been cut. A small hole (0.23-mm diameter), which serves as a gas exit port, is drilled half way from the top of the base perpendicular to the center of the "V"-shaped groove.

This article not subject to U.S. Copyright. Published 1978 by the American Chemical Society

Table I. Data Comparing Precision of Analysis between the Jarrell-Ash Crossflow and the "V" Nebulizer

analysis of high salt content samples,[a,b] μg/g

	NBS bovine liver, 3.0 g/100 mL			cattle manure high fiber, 3.69 g/100 mL		Denver sewage sludge, 0.99 g/100 mL	
	"V" nebulizer	Jarrell-Ash crossflow	NBS	"V" nebulizer	Jarrell-Ash crossflow	"V" nebulizer	Jarrell-Ash crossflow
Al	[c]	[c]	[d]	3381 (3.3)	2817 (12.0)	8899 (2.2)	8765 (8.5)
Ca	114 (1.8)	118 (7.3)	(123)[e]	18060 (5.5)	20864 (8.7)	46745 (3.4)	41200 (5.1)
Cu	182 (3.4)	168 (4.6)	193 ± 10	19.2 (3.7)	15.7 (12.8)	691 (2.8)	691 (9.3)
Cr	[c]	[c]	[d]	[c]	[c]	487 (4.1)	461 (11.6)
Fe	241 (3.2)	268 (9.5)	270 ± 20	4325 (4.3)	4857 (9.0)	12992 (2.5)	11631 (5.6)
Mn	9.7 (3.5)	11.2 (12.2)	10.3 ± 1	141 (4.9)	173 (7.9)	205 (3.1)	186 (4.6)
Mg	555 (3.8)	712 (13.8)	(605)[e]	3634 (5.1)	4269 (7.0)	3251 (3.2)	2962 (4.2)
Pb	[c]	[c]	0.34 ± 0.08	[c]	[c]	754 (2.7)	700 (4.0)
P	10009 (2.6)	9891 (4.7)	[d]	3923 (4.3)	4377 (7.8)	13074 (2.5)	11951 (5.4)
Zn	130 (4.0)	157 (12.9)	130 ± 10	1507 (4.4)	1337 (4.2)	106 (7.6)	115 (8.5)

[a] Mean of 12 analyses of each sample. [b] Percent relative standard deviation given in parentheses. [c] Below quantitation limit. [d] No value given. [e] Uncertified value.

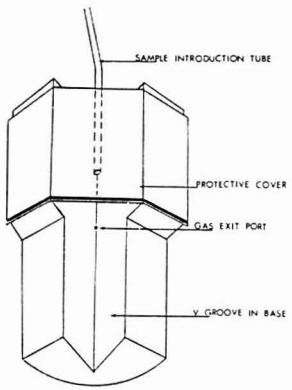


Figure 1. Construction of nebulizer base. Aerosol is produced when the liquid stream flowing down the V groove is ruptured by gas coming from the gas exit port

The walls from the top of the gas exit port to the top of the base are 2 mm high; below the exit port they are 1 mm high. Making the walls of the groove shorter from the gas exit port to the bottom of the base prevents aerosol droplets from settling on the walls and again flowing over the gas exit port, causing pulsations to occur in the production of aerosol. A Teflon-lined stainless steel sample introduction tube is centered in and touches the "V"-shaped groove near the top of the base. The sample introduction tube and base are covered by a gold plated aluminum protective cover which extends from just above the gas exit port to the top of the base. The protective cover serves to prevent aerosol droplets from settling on the base or sample introduction tube and again flowing over the gas exit port. Such an occurrence would produce pulsations in the rate of aerosol production.

The nebulizer is mounted in a Plexiglas housing as shown in Figure 2. An impactor rod mount and adjustment, fabricated from gold plated aluminum, is used to position a glass impactor rod in front of the gas exit port. An "O" ring in the nebulizer housing press fits around the outside wall of the spray chamber, forming a leaktight seal.

Operation of the nebulizer consists of pumping a liquid with a peristaltic pump (Gilson Minipuls 2, Gilson Medical Electronics, P.O. Box 27, 3000 West Beltline Highway, Middleton, Wis. 53562) through the sample introduction tube onto the "V"-shaped groove. The "V" groove forces the liquid, under the influence of gravity, to flow in a stream over the gas exit port. Breakup of the liquid stream by the exiting gas results in the formation of a dense and fine aerosol. Larger drops formed by this process are forced against the impactor rod and are further broken up. The gas used to generate the aerosol also serves as the carrier gas to deliver the aerosol to the plasma.

RESULTS AND DISCUSSION

Efficiencies of the two nebulizers were calculated by aspirating a known amount of water through each nebulizer with the spray chamber attached. The drain-off liquid was collected and measured, and the efficiency of the nebulizer calculated. For the "V" nebulizer with a sample uptake rate of 5 mL/min, the efficiency was found to be 5%; the efficiency of the crossflow nebulizer was 10% with a sample uptake rate of 1.5 mL/min. Although the efficiency of the "V" nebulizer is less than that of the crossflow nebulizer, the higher sample uptake rate of the "V" nebulizer results in more aerosol being produced. The 5 mL/min uptake rate is not unreasonable since most atomic absorption nebulizers operate with sample uptake rates in this range.

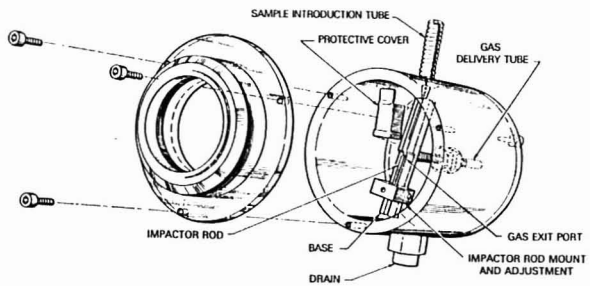


Figure 2. Complete nebulizer assembly

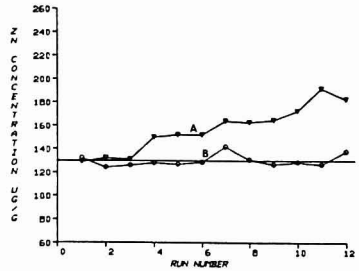


Figure 3. Variation of calculated Zn concentration in NBS Bovine Liver for twelve consecutive analyses of the same sample solution. (A) Cross flow nebulizer. (B) "V" nebulizer

Table I compares the precision of analyses obtained with the "V" nebulizer and crossflow nebulizer for some high salt content samples. For each sample matrix, the percent relative standard deviation is lower with the "V" nebulizer by a factor of from two to three times that found with the crossflow nebulizer. Improved precision with the "V" nebulizer is a result of its freedom from partial or complete clogging of the sample introduction tube.

Figure 3 shows the variation in calculated concentration of zinc in NBS bovine liver when the same sample is analyzed 12 consecutive times with each nebulizer. Total time for the analyses was 36 min. It is apparent that the first three analyses with both nebulizers are essentially equivalent, each value for zinc being within 5% of the 130 μg/g value given by NBS. However, after the sample has been run for the third time, the calculated zinc concentration using the crossflow nebulizer begins to drift upward. This upward drift continues until, after the sample has been run 11 times, the calculated concentration of zinc is 192 μg/g, over 48% above the 129 μg/g calculated when the sample was first run. At the same time the calculated concentration of zinc using the "V" nebulizer remains within 5% of the original 130 μg/g calculated on the first analysis. Only the seventh analysis shows any significant deviation from the certified value and it is still within the confidence limits supplied by NBS.

Table II is a tabulation of detection limits found for both nebulizers. A detection limit was defined as the concentration required to produce a signal twice the standard deviation of the background. All detection limits were determined with the element of interest in distilled deionized water. In operation, although the "V" nebulizer produces a signal which is noisier than that obtained with the crossflow nebulizer, the nebulizer introduces more sample to the plasma, which results in a larger signal and detection limits comparable to those obtained with the crossflow nebulizer. Reducing the noise through better sample introduction to the nebulizer base should result in improved detection limits for the "V" nebulizer.

Because of the design characteristics of the "V" nebulizer, sample solution comes in contact with a large surface area of the nebulizer base. Consequently, memory effects might be expected to occur with this nebulizer. To investigate this, a blank solution was analyzed followed by the constant nebulization for 15 min of a solution containing 10 μg/mL of 10 selected elements. At the end of 15 min, the blank solution was run for 90 s and then again analyzed. The elemental concentration of the blank found before and after running the 10 μg/mL test solution can be found in Table III. It is apparent that a 90-s cleanout time is adequate to return the blank reading to its original value and that no memory effect exists under these conditions.

Table II. Comparison of Detection Limits for the Jarrell-Ash Crossflow Nebulizer and the "V" Nebulizer (All Detection Limits in μg/mL)

	λ (A)	"V" nebulizer	Jarrell-Ash crossflow nebulizer
Al	3082	0.1	0.05
B	2497	0.006	0.007
Be	3130	0.01	0.004
Ca	3933	0.001	0.001
Cd	2265	0.01	0.01
Co	2388	0.01	0.02
Cr	3578	0.004	0.002
Cu	3247	0.01	0.02
Fe	2599	0.03	0.05
Ge	2651	0.09	0.1
Mg	2795	0.01	0.04
Mn	2576	0.001	0.006
Mo	2038	0.3	0.2
Ni	3414	0.008	0.007
P	2149	0.4	0.3
Pb	2203	0.1	0.1
Sb	2068	0.04	0.02
Se	1960	0.07	0.03
Sn	1899	0.03	0.03
Te	2142	0.1	0.03
Ti	3349	0.005	0.003
Tl	3519	0.3	0.07
V	3093	0.09	0.05
Zn	2061	0.04	0.05

Table III. Blank Reading (μg/mL) before and after Running a 10 μg/mL Solution of Each Element for 15 Minutes, Showing the Absence of Any Memory Effect at These Levels with the "V" Nebulizer

	before	after
Al	0.1	0.1
Ca	0.13	0.14
Co	0.00	0.02
Cr	0.00	0.00
Cu	0.00	0.01
Fe	0.00	0.00
Mg	0.00	0.00
Mn	0.00	0.00
Ni	0.00	0.00
Zn	0.00	0.00

An additional advantage of the "V" nebulizer is the simplicity of adjustments needed to obtain optimum performance. Whereas exact positioning of capillary tubes is required with the crossflow nebulizer, the only requirement of the sample introduction tube with the "V" nebulizer is that it must lie in the groove of the nebulizer base. A small misalignment of the sample tube will not affect performance, as the solution is forced to flow over the gas exit port in the same fashion each time by the "V"-shaped groove in the nebulizer base.

LITERATURE CITED

(1) R. N. Kniseley, H. Amenson, C. C. Butler, and V. A. Fassel, *Appl. Spectrosc.*, **28**, 285 (1974).
(2) J. E. Meinhard Associates Catalogue 1976, P.O. Box 9, Tustin, Calif. 92680.
(3) R. H. Wendt and V. A. Fassel, *Anal. Chem.*, **37**, 920 (1965).
(4) H. C. Hoare and R. A. Mostyn, *Anal. Chem.*, **39**, 1153 (1967).
(5) V. A. Fassel and G. W. Dickinson, *Anal. Chem.*, **40**, 247 (1968).
(6) J. M. Mermet and J. P. Robin, *Anal. Chem.*, **40**, 1918 (1968).
(7) G. W. Dickinson and V. A. Fassel, *Anal. Chem.*, **41**, 1021 (1969).
(8) K. W. Olsen, W. J. Haas, Jr., and V. A. Fassel, *Anal. Chem.*, **49**, 632 (1977).
(9) C. T. Apel, T. M. Bieniewski, L. E. Cox, and D. W. Steinhaus, *ICP Inf. Newsl.*, **3**, 1 (1977).
(10) R. C. Fry and M. B. Denton, *Anal. Chem.*, **49**, 1413 (1977).

RECEIVED for review March 13, 1978. Accepted August 18, 1978. Paper presented at the Pittsburgh Conference on Analytical Chemistry and Applied Spectroscopy, Cleveland, Ohio, February 27–March 3, 1978.

Intensified Diode Array Detector for Molecular Fluorescence and Chemiluminescence Measurements

Mary Andrieu Ryan, Robert J. Miller, and J. D. Ingle, Jr.*

Department of Chemistry, Oregon State University, Corvallis, Oregon 97331

An intensified diode array is used in a rapid scan spectrometer configuration to record fluorescence and chemiluminescence spectra from 197 to 823 nm. For steady-state quinine sulfate measurements, a linear calibration curve from a detection limit of 0.2 up to 100 ppb was obtained. The slow oxidation of thiamine to fluorescent thiochrome is monitored by taking complete fluorescence emission spectra during the course of the reaction. The initial rate extracted from the spectral data is proportional to the thiamine concentration from a detection limit of about 10^{-7} up to 10^{-5} M. The potential spectral interferences from vitamins A and B_2 are also studied. Sequential chemiluminescence spectra are taken during the course of reactions involving lucigenin and pyrogallol in basic peroxide solutions. Spectra are compared with and without metal activation and to fluorescence spectra of the reaction products.

The great potential of multichannel, array, or TV type detectors such as vidicons (V) and diode arrays (DA) for spectrometric measurements has been discussed in recent reviews (*1–10*) and demonstrated in numerous research papers. When placed at the focal plane of a monochromator, the intensity of up to 1024 separate wavelength regions can be simultaneously monitored. One primary disadvantage of these basic detectors is that the lowest light levels measurable above detector-readout noise are much higher than with a photomulitplier tube (PMT). For many spectrometric applications, an intensifier must be placed in front of the basic detector (e.g. silicon intensified target vidicon (SIT), intensified SIT (ISIT), or intensified diode array (IDA) to improve detection at low light levels.

In atomic spectrometry (see (*9–11*) and references cited in these papers and (*12–16*)), these detectors have been exploited primarily to carry out multielement analysis. Because glass fiber optics are used in many intensifiers, the response below 300 nm where many atomic transitions lie is poor even with a scintillator (*14*). In atomic absorption spectrometry where light levels are reasonably high, much success has been achieved (*15–18*). For atomic emission or fluorescence spectrometry, where light levels are much lower, Winefordner and co-workers (*11, 19*) have concluded that multichannel detectors will find more limited use because of seriously degraded detection limits. However, in many cases where analyte concentrations are well above conventional detection limits, simultaneous quantitative analysis with multichannel detectors by atomic emission has been demonstrated to be quite feasible (*13, 14, 20, 21*). In atomic work, multichannel detectors have also been employed for profiling (*22, 23*), correlation (*24*), time resolved studies (*25*), spectral stripping (*26*), and internal standard compensation (*27*).

In molecular spectrometry, these detectors are not used as much for multicomponent analysis because molecular bands are much broader than atomic lines. However, Christian and co-workers (*28*) and Pardue, Milano, and co-workers (*29, 30*) have shown that multicomponent fluorescence and absorbance analysis, respectively, is feasible for a few components in certain cases. Multicomponent kinetics-based analysis with absorbance monitoring has also been demonstrated (*31*). In molecular absorbance applications (*32–35*) often non-intensified multichannel detectors can be employed. However, for photoluminescence work (*28, 36–41*) where light levels are much lower, an intensified multichannel (usually a SIT) has been used.

In molecular work, these detectors are often employed as one means to construct a rapid scan spectrometer to view transient species such as from a HPLC or GC (*11, 32, 33, 38, 39*), or in kinetics experiments (*31, 34–46*). For kinetics experiments in solution with absorbance monitoring, the disappearance of reactants, appearance and disappearance of intermediates, and appearance of products can be monitored, simultaneously by the changes in the absorbance spectrum (*31, 35*). In addition, kinetic parameters such as rate constants can be calculated. The only application of multichannel detectors for monitoring kinetics with fluorescence has been presented by Kohen and Kohen and co-workers (*36*). They employed a SIT for monitoring kinetics in living cells and for topographical or multisite fluorescence.

This report is concerned with the application of an IDA to molecular fluorescence and chemiluminescence measurements. Although the IDA (with different types of intensifiers) has been used in astronomy applications (*42–48*), there are no reports of the application of IDAs to chemical measurements. There are also no previous reports of the application of any type of multichannel detector to kinetics-based measurements in solution involving fluorescence monitoring or chemiluminescence measurements.

More specifically the steady-state fluorescence from quinine sulfate is measured and the detection limits obtained with the IDA and with a conventional photomultiplier (PMT) configuration are compared to indicate the relative sensitivity of the IDA detector. Reasons for the superior performance of the PMT configuration are given. Next, the use of the IDA as a diagnostic and quantitative tool for monitoring kinetic changes with fluorescence monitoring is discussed. For this purpose, spectra are obtained during the course of the reaction involving the oxidation of thiamine (vitamin B_1) to the fluorescent product thiochrome. The measured rate extracted from the IDA data is proportional to the initial thiamine concentration. The IDA is also used as a diagnostic tool to determine the potential interference from vitamins A and B_2 which also fluoresce. Finally, the applicability of the IDA for chemiluminescence measurements is demonstrated with time resolved spectra taken during the course of the chemiluminescence reactions of lucigenin and pyrogallol with Co(II) in basic peroxide solutions.

EXPERIMENTAL

A Tracor Northern TN-1710-21 DARSS intensified diode array system was used for all measurements. It consists of an intensified 512-element cooled diode array (TN-1223-21), a f/3 holographic grating spectrograph (TN-1150), and a microcomputer based signal analyzer (TN-1710). The signal analyzer includes an optical spectrometer module (TN-1710-21) with a sample and hold

0003-2700/78/0350-1772$01.00/0 © 1978 American Chemical Society

amplifier and 12-bit ADC, a high voltage controller for the intensifier (TN-1710-17), and a CRT display screen. Operating and display conditions controlled by the signal analyzer and used in this work include: integration time for the signal (variable from 5 ms to 60 s), background subtraction, signal averaging via adding the results of n scans in the same 512-work memory block, automatic acquisition, storage, and subsequent display of successive scans in separate 512-work blocks of memory, readout of the intensity information from a specific diode or group of diodes. Spectra displayed on the CRT were saved by taking photographs.

The diode array consists of 512 adjacent detectors (50 μm wide by 0.45 mm high) to yield a total active detector width of 25.6 mm. The linear reciprocal dispersion of the spectrograph is 24.4 nm/mm and the simultaneous wavelength coverage is from about 197 to 823 nm. With a 50-μm wide entrance slit, each diode theoretically intercepts a 1.22-nm wavelength range. Because of aberrations from the monochromator and the line pair resolution of the microchannel plate intensifier, the actual resolution is specified to be about 4 nm. For all measurements, a 250-μm wide slit was employed which yields a resolution of about 6.3 nm. The maximum integration time is limited by the time required for the dark current to cause saturation of the diode detector. The diode array was cooled to about 5 °C and the maximum integration time was about 40 s. For most measurements, an intensifier gain setting of 6 to 10 was employed which corresponds to a photon gain of about 10^4.

For fluorescence measurements, the entrance slit of the spectrograph was directly mounted to the emission port on the sample module of a previously described molecular fluorescence spectrometer (*49*) designed for kinetics-based measurements. Hence the spectrograph plus diode array detector replaced the previously used $f/4.7$ emission monochromator or emission filter plus 1P28 photomultiplier tube (PMT). A one-inch diameter $f/3$ lense was placed 3 in. from the spectrograph entrance slit on the emission optical rail to focus an image of the face of the fluorescence cell onto the spectrograph entrance slit and fill the grating with radiation.

For chemiluminescence measurements, the entrance slit of the spectrograph was directly interfaced to the emission port on the sample module of a previously described chemiluminescence photometer (*50*). The entrance slit was approximately 1.7 cm from the front wall of the chemiluminescence sample cell such that the spectrograph defined the solid angle of collection of the chemiluminescence radiation. Previously (*50*) a 1P28 PMT was mounted directed toward the emission port and no wavelength descrimination was employed.

All solutions were prepared with deionized distilled water (Millipore Milli-Q system). All glassware was cleaned and quinine sulfate solutions were prepared as previously described (*49*). For fluorescence kinetics-based measurements, vitamin B_1 (MC & B), vitamins B_2 and A (ICN Pharmaceuticals, Inc.), reagent grade $HgCl_2$ (Baker), and analytical reagent Na_2HPO_4 (Mallinckrodt) were used. For chemiluminescence measurements, lucigenin (K and K Laboratories), analytical reagent pyrogallol (Mallinckrodt), analytical reagent $Co(NO_3)_2{\cdot}6H_2O$ (Mallinckrodt), analytical reagent KOH (Mallinckrodt), analytical reagent $NaHCO_3$ (Mallinckrodt), and analytical reagent H_2O_2 (Mallinckrodt) were employed. A 0.575-g multivitamin and mineral pill (Bi-Mart) was crushed, dissolved, and filtered and then diluted to 1 L with water. The solution was then adjusted to pH 4 with HCl. It nominally contains 2.5 mg of vitamins B_1 and B_2.

RESULTS AND DISCUSSION

Steady-State Fluorescence Measurements of Quinine Sulfate. Measurements of quinine sulfate (QS) fluorescence were made since QS is commonly used as a standard to evaluate the sensitivity and detection limit capabilities of molecular fluorescence spectrometers. All measurements were made as previously described with PMT detection (*49*) with excitation at 365 nm from a 200-W Xe-Hg arc lamp and a 17-nm excitation spectral bandpass. Complete spectra from 197 to 823 nm were obtained for solutions ranging from 0.1 ppb to 100 ppb QS and for the blank (0.05 M H_2SO_4) with signal integration times from 1 to 32 s. Repetitive integrations were made on the blank solution to evaluate the noise for detection limit calculations and for QS solutions to evaluate the signal-to-noise ratio (S/N) in the fluorescence signal. The signal from the diode at the peak of the QS fluorescence (460 nm), the sum of the signals from 6 diodes centered at the fluorescence peak (about a 7.5-nm wavelength range), and the sum of the signals from 80 diodes (covering from 425 to 525 nm) were simultaneously recorded for each integration. the last sum covers a wavelength range equal to about 50% of the basewidth of the QS fluorescence peak and was chosen to exclude the Raman peak of water.

The best detection limit was obtained with an integration time of 8 s and summation of the signals from the 6 adjacent diodes centered at the peak wavelength of fluorescence. A linear calibration curve was obtained from the detection limit of 0.2 up to 100 ppb QS. A blank signal approximately equal to the dark current signal was observed. At higher QS concentrations, signal shot noise was limiting and the noise was proportional to the square root of the analyte signal.

With the same fluorescence spectrometer with an emission filter and PMT detector, a detection of QS of about 0.001 ppb was obtained with an 8-s integration time (*49*, *51*). Clearly the IDA can be used to measure ultratrace concentrations of fluorescent species; however, the detection limits will be considerably worse than obtainable with a high quality conventional spectrofluorometer.

A lower detection limit or S/N at low concentrations is expected (*11*) with multichannel detector for a few reasons. First, the amplifier–readout rms noise for a multichannel detector is typically 1000–5000 e's whereas for a PMT with a high quality current-to-voltage converter the same noise would typically be 10 e's or less when referenced to the photocathode and usually negligible compared to other noise sources. This disadvantage can be mostly offset if the intensifier gain is high enough so that one photoelectron from the photocathode of the intensifier results in a number of electron-hole pairs generated at the detector element which is greater than the amplifier-readout noise (assuming the quantum efficiency of the PMT and intensifier plus scintillator are the same).

Finally, the size of the detector element in the diode array is much smaller, 0.05 × 0.45 mm in this case, than the area of the photocathode of a PMT or the area of the exit slit of the emission monochromator. Thus, the absolute photon flux seen by a given diode is much less than seen by a PMT in a conventional configuration. Because of the smaller detector size, the effective number of incident photons seen by a single diode was measured to be approximately 10^3 less than seen by the PMT with the conventional emission monochromator configuration. Of course, the signals from n diodes can be averaged together but the amplifier-readout noise will increase as the $\sqrt{n}$ if the diodes are independent discrete detectors.

The advantages of the multichannel detector are better illustrated in the fluorescence spectrum of 100 ppb QS from 197 to 823 nm shown in Figure 1. This and all figures presented are tracings from the original photographs where care was taken to reproduce all noise superimposed on the spectra. This complete spectrum was taken in 1 s with the signal at all wavelengths and averaged the same amount of time. A scan rate of 50 nm/min is employed with the conventional emission monochromator PMT configuration (*51*) so that the same spectrum takes normally about 13 min to acquire. The S/N's of the spectra are comparable with both detector systems. The detector is sufficiently sensitive that the Raman peak from water is clearly obvious in the spectrum of QS at 10 ppb and below. Hence, the IDA is useful for obtaining spectra of steady state fluorescence signals in much less time (a factor of 100 to 1000) than normally possible for analyte concentrations yielding fluorescence signals much

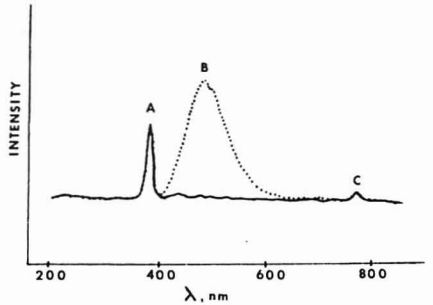


Figure 1. Fluorescence spectra for 1-s integration period. 100 ppb QS in 0.05 M H_2SO_4 (...) and 0.05 M H_2SO_4 (–). (A) First-order Rayleigh scattering peak (365 nm). (B) QS fluorescence peak (maximum at 460 nm). (C) Second-order Rayleigh scattering peak (730 nm)

greater than the blank signal. This provides a substantial time savings in surveying the fluorescence characteristics of a number of molecules (analyte or potential interfering substances) which can be used to choose optimum emission wavelengths for fixed wavelength measurements with a normal PMT configuration to prevent overlap from scattering, background fluorescence, or fluorescence from interfering substances.

Kinetics-Based Measurements of Thiamine. The QS measurements illustrate that the IDA allows spectral information to be obtained rapidly. In this case, the time savings is a convenience but it is not essential. However the rapid scan capability is essential for measurements of transient species or where the concentration of the monitored species changes with time such as in kinetics and chemiluminescence experiments or for monitoring of effluent from a chromatographic column.

The use of the IDA as both a diagnostic and quantitative tool for monitoring kinetics involving fluorescent species is illustrated below by studies of the oxidation of thiamine (vitamin B_1) to thiochrome with Hg^{2+} (*54, 55*). The standard assay for thiamine is an equilibrium-based procedure in which the thiamine in a sample is quantitatively converted to the fluorescent product thiochrome by potassium ferricyanide. Usually extensive separation procedures are required to isolate the thiamine from other fluorescent species in vitamin preparations, blood, urine, wheat, etc. (*52–57*). For such a situation, kinetics-based analysis can be advantageous (*49, 58, 59*) both in terms of time, since this reaction is kinetically slow, and in terms of specificity since the fluorescence of species not involved in the reaction does not contribute to the measured rate.

Initial studies have shown that for a mixture of 1 mL each of a 0.2 M pH 12.2 phosphate buffer, 500 ppm Hg^{2+}, and thiamine containing solution that the reaction takes about 60 min to reach within 5% of equilibrium and the initial rate measured over 32 s is directly proportional to the thiamine concentration from a detection limit of 7×10^{-9} up to 5×10^{-5} M. These studies were carried out with excitation at 365 nm and with the conventional emission monochromator PMT configuration viewing the emission at 444 nm.

Figure 2 is a time sequence in which a complete fluorescence spectrum was obtained in 2.5 s at about 5 s, 1 min, 2 min, and 3 min after initiation of the reaction for a 1×10^{-6} M solution of thiamine. The growth of the fluorescence peak due to the formation of thiochrome is clearly shown.

Time sequence spectra such as in Figure 2 were obtained for different initial thiamine concentrations. The initial rate was calculated from the difference in the summed signal for

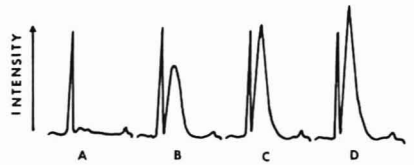


Figure 2. Successive fluorescence spectra of thiamine reaction mixture from 197 to 823 nm. Conditions: 1×10^{-6} M thiamine; 2.5-s integration time; (A) 5 s; (B) 1 min; (C) 2 min; (D) 3 min

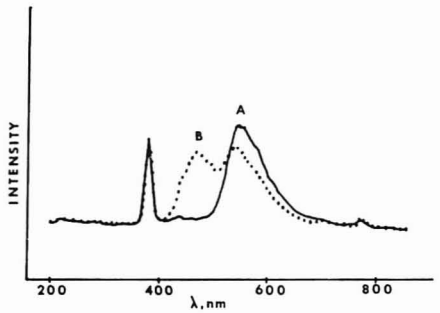


Figure 3. Superimposed fluorescence spectra of reaction mixture with thiamine and riboflavin. Conditions: 5×10^{-7} M thiamine; 5×10^{-6} M riboflavin; 2.5-s integration time; (A) 5 s; (B) 5 min

a 1-s integration from the 35 diodes centered at the peak (about 44 nm) measured at two times spaced 30 s apart. A linear calibration curve was obtained from an approximate detection limit of 1×10^{-7} up to 1×10^{-5} M thiamine. Thus, the IDA can be employed to obtain quantitative rate information at relatively low concentrations. As for the steady state QS measurements, a much lower detection limit can be obtained with the conventional fixed wavelength PMT system but the sensitivity of the IDA system is quite adequate for many samples such as thiamine in vitamin pill preparations.

The IDA is also a powerful tool for quick evaluation of spectral interferences and for quantitative multicomponent analysis. Figure 3 shows two complete superimposed fluorescence spectra of a reaction mixture of 5×10^{-7} M thiamine and 5×10^{-6} M riboflavin (vitamin B_2) with Hg^{2+} and the phosphate buffer with a 2.5-s integration time. Spectrum A was taken right after initiation of the reaction and is predominately due to the inherent fluorescence of riboflavin. Spectrum B was taken after 5 min and shows the somewhat overlapped fluorescence peaks of both thiochrome and riboflavin. Very quickly one experiment shows that if measurements are made at the peak wavelength of thiochrome, there will be little interference from riboflavin. Note that the peak position of the riboflavin shifts to lower wavelengths because of the overlap and that the peak intensity due to riboflavin decreases. Other work showed that a slow photodecomposition of riboflavin occurred at high pH without mercury, and at acid pH, Hg^{2+} caused a similar decrease in fluorescence. The rate of decrease of fluorescence increased to the magnitude seen in Figure 3 when UV light, high pH, and Hg^{2+} were all present. Since the scattering peak at 365 nm does not change in intensity, the decrease is not due to the inner filter effect or absorption of a significant amount of the excitation radiation by the thiochrome produced.

Figure 4 shows time sequence spectra of a reaction mixture where the analyte solution is from an actual multivitamin pill. All four spectra were taken with a 1-s integration and within

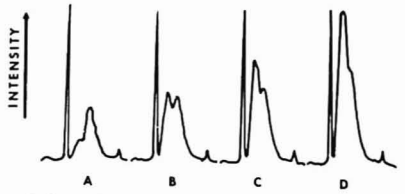


Figure 4. Successive fluorescence spectra from multivitamin pill analysis over 197 to 823 nm. Conditions: 1-s integration time spaced approximately equally apart over 30 s

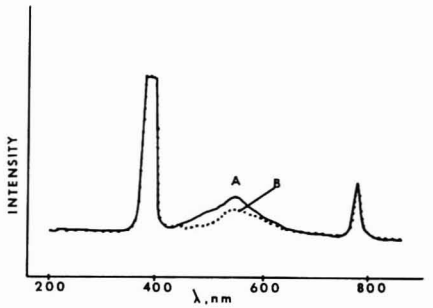


Figure 5. Superimposed fluorescence spectra of vitamin A in reaction mixture. Conditions: 5900 IU/L of vitamin A; 1-s integration time; (A) 5 s; (B) 10 min

30 s of the initiation of the reaction. The growth and final dominance of the thiochrome peak (A) is clear. The figure also indicates that riboflavin (peak B) is the main spectral interference for this particular analysis.

Figures 3 and 4 also illustrate the potential for simultaneous quantitative analysis of thiamine and riboflavin. The riboflavin could be determined by the fluorescence signal at 510 nm from a spectrum taken immediately after initiation of the reaction while the thiamine could be determined by the change in fluorescence signal over 30 s measured at 444 nm. Normally B_2 is determined at acidic pH's where the fluorescence intensity is greater and the maximum emission is at 530 nm.

Figure 5 shows the emission spectrum of 5900 IU/L of vitamin A in the thiamine reaction mixture right after mixing (A) and after about 10 min (B). Clearly there is some chemical or photo-decomposition of vitamin A and it also appears that the shape of the spectrum has changed with time.

In Figure 6, the emission spectrum of a mixture of thiamine and vitamin A is shown immediately after mixing (A) and after about 4 minutes (B). Here both the growth of the thiochrome peak and decrease in the vitamin A peak are obvious. Also there is spectral overlap of the vitamin A fluorescence at the peak wavelength of thiochrome emission. Hence, even for a kinetics-based determination of thiamine, there is a potential interference from vitamin A since its signal also changes with time. However, by monitoring the intensity of the vitamin A fluorescence initially, the magnitude of the interference can be estimated or perhaps compensated for.

Chemiluminescence Measurements. The rapid scan capability of the IDA polychromator system is well suited for obtaining spectra in solution chemiluminescence (CL) measurements with discrete sampling since the Cl peak may last only a few seconds. Normally no wavelength discrimination is employed since the spectrum is the same with or without the analyte species and only the intensity changes with concentration of the analyte. CL signals are normally

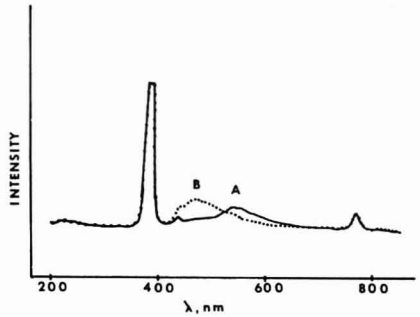


Figure 6. Superimposed fluorescence spectra of thiamine and vitamin A in reaction mixture. Conditions: 2.5-s integration time; (A) 5 s; (b) 4 min

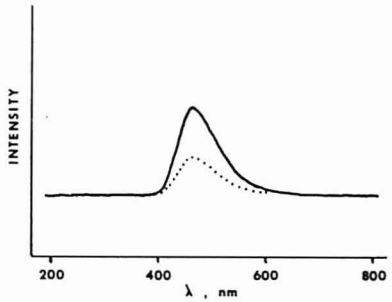


Figure 7. Superimposed chemiluminescence spectra in lucigenin reaction mixture for reagent blank (...) and 100 ppb Co(II) (–). Conditions: 10-s integration time; 6×10^{-5} M Lc, 1 M KOH, 0.4% H_2O_2

weak and the addition of a monochromator and the substitution of a detector less sensitive and smaller in active area than a PMT results in S/N problems and may account for the fact that CL spectra obtained with a multichannel detector have not been previously reported.

For CL measurements, multichannel detectors will be more useful as a diagnostic tool rather than a quantitative tool. Spectral information is a useful aid for (i) choosing PMT photocathodes for maximum sensitivity at the wavelengths of CL emission but not to choose optimum filters or monochromator parameters as for fluorescence measurements where wavelength selection is required, (ii) understanding spectral absorption interferences by non-analyte species or nonlinearity in calibration curves due to self-absorption since these effects would cause distortion of spectral shapes, and (iii) obtaining fundamental information about reaction mechanisms (e.g., CL spectra are commonly compared with the fluorescence spectra of products as evidence that the chemiluminescent species is the excited state of the product rather than an intermediate (*60*)).

We have studied in detail the CL reaction of lucigenin (LC) with H_2O_2 in strong basic solutions and the enhancement of the CL by various metal ions (*61*). This reaction is very sensitive to Co(II) and a detection limit of 0.02 ppb has been achieved. Figure 7 shows the superimposed CL spectrum of a reagent blank run and a run with the addition of 100 ppb Co(II). The spectra were obtained using a 10-s integration time initiated just prior to the start of the reaction by injection of the KOH solution. The figure shows that the CL spectrum can be obtained with a good S/N and that the CL spectrum



Figure 8. Consecutive lucigenin chemiluminescence spectra from 197 to 823 nm. Conditions: 5-s integration time, 10 ppb Co(II); other conditions same as for reagent blank in Figure 7

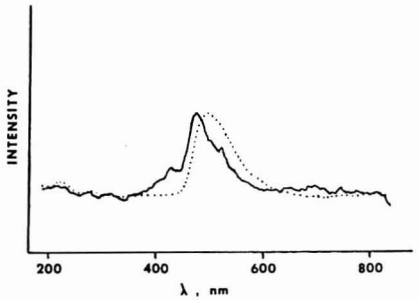


Figure 9. Superimposed spectra of pyrogallol chemiluminescence (–) and reaction mixture fluorescence (...). Conditions: fluorescence reaction mixture, 10 mM Pg, 0.4% H_2O_2, 0.1 M $NaHCO_3$ (pH 9.9), 10 ppb Co(II), 15-s integration time; CL reaction mixture, same as for fluorescence except 30 ppm Co(II), and 2 mM Pg; sum of twenty 5-s integrations

is the same with or without the metal activator as previously thought but not experimentally confirmed.

Figure 8 shows a time sequence of spectra taken, using the same cell conditions as for Figure 7, with consequent 5-s integration periods during one 10 ppb Co(II) run. This particular CL reaction is rather long lived and can be seen to reach its maximum intensity between 5 and 10 s from initiation and then slowly decrease in intensity. The detection limit was estimated to be about 2 ppb for Co(II) which again is adequate for some samples but about 2 orders of magnitude worse than achievable with PMT detection and no wavelength discrimination. The CL peak maximum of 472 nm agrees well with the literature value of 475 nm (*60*).

We have also been studying the enhancement of the CL signal by metal ions for the pyrogallol (Pg) + H_2O_2 system in an alkaline medium. Figure 9 shows the superimposed CL and fluorescence (FL) spectrum of the Pg + H_2O_2 + Co(II) system. The FL spectrum was obtained approximately 5 min after initiation of the reaction using the IDA and fluorescence instrument used for the studies mentioned above on thiamine and QS. The figure shows that the CL occurs at 466 nm and that the FL of a similar reaction mixture after 5 min contains a single peak at 482 nm. The results suggest that the fluorescence of the chemiluminescent species is below detectability and that the FL spectrum is due to either a longer lived intermediate that does not CL or one of the end products from the Pg + H_2O_2 + Co(II) + $NaHCO_3$ reaction. It should be noted that neither Pg or purpurogalline (*62*), the main end product of the reaction, alone exhibits a FL signal. Two CL peaks for the Pg + H_2O_2 + KOH CL system are reported in the literature (*63*). Melvzova and Vassilev suggest that the two peaks located at 470 nm and 640 nm are due to the CL of singlet oxygen dimers (*64*). However, they also reported that the 640-nm peak is "always an order of magnitude higher"

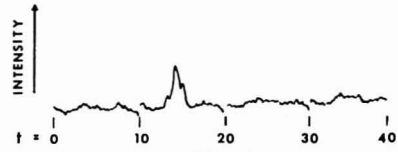


Figure 10. Consecutive pyrogallol chemiluminescence spectra from 197 to 823 nm for 1000 ppm Mn(II). Conditions: 10 mM Pg, 0.4% H_2O_2, 0.1 M $NaHCO_3$ (pH 9.9); sum of five 10-s integration times

and precedes the 470-nm peak. A time sequence determination for the Pg + H_2O_2 + Co(II) system indicated that only one peak appeared and it was within the first 5 s from initiation. The scan range of Figure 9 is 197 to 823 nm and no evidence of a peak at 640 nm is indicated.

The CL peak intensity of the reagent blank for the Pg + H_2O_2 system, measured with a PMT is about four orders of magnitude less than the peak intensity of the LC-CL reaction and was not detected with the IDA. Thus S/N problems were encountered for this system and the CL spectrum in Figure 9 is still noisey even though it is the sum of 20 runs with a 5-s integration time for each run. Hence for this particular CL system, the IDA would not be useful for quantitative analysis.

Figure 10 shows a time sequence study of the Pg + H_2O_2 + Mn(II) CL system using 1000 ppm Mn(II). This is the only case we have seen in our laboratory or the literature where the CL is delayed from the initiation of the reaction. At this concentration of Mn(II), the CL signal consists of one peak that occurs between 10 and 20 s from the time of reaction initiation. At lower concentrations of Mn(II) the CL signal consists of two peaks, one immediately after initiation similar to that of Co(II) and the other peak occurs between 30 s and 7 min from the time of reaction initiation where the exact delay depends on the Mn(II) concentration. This presents the interesting possibility of simultaneous analysis of Co(II) and Mn(II). Simultaneous analysis would also be possible with the IDA if two CL reagents were used, each specific to one metal, but where the CL peak wavelengths were sufficiently separated. Figure 10 also shows that the CL species for the Mn(II) system is the same as for the Co(II) system since the peak wavelengths are the same.

CONCLUSIONS

The IDA has been shown to be a very useful diagnostic and quantitative tool for low light level steady-state and kinetics-based luminescence measurements. For analytical fluorescence measurements, it is particularly helpful for initial studies of chemical systems to quickly determine optimum measurement wavelengths and possible spectral overlap problems from potential interfering species. The rapid scan capability of the IDA is essential for obtaining spectral information in kinetics studies. Once the analysis wavelength and spectral bandpass are chosen, a choice must be made between the multichannel detector and conventional PMT detection. To achieve the lowest possbile detection limits, the PMT system should be used. However, for many situations (e.g., thiamine in vitamin pills), the IDA is sufficiently sensitive to use for quantititive measurements. Use of the IDA in these situations is advantageous because both quantitative and spectral information are provided simultaneously. Thus spectral interference problems in real samples can be quickly identified whereas they may go undetected with conventional fixed-wavelength PMT detection. Also simultaneous equilibrium-based, kinetics-based, or equilibrium- and kinetics-based measurements can be implemented with the IDA.

For chemiluminescence measurements, the IDA and other intensified multichannel detectors will be most useful for

initial characterization of new chemical systems and for fundamental mechanistic studies. Its use for quantitative chemiluminescence measurements is more limited because of the very low levels usually measured. This is not totally due to the limitations of the IDA but also to the fact that analytical chemiluminescence measurements are normally made without any wavelength discrimination in order to maximize the amount of luminescence detected.

ACKNOWLEDGMENT

We thank Tracor Northern for loaning us the TN-1710 signal analyzer.

LITERATURE CITED

(1) R. E. Santini, M. H. Milano, and H. L. Pardue, *Anal. Chem.*, **45**, 915A (1973).
(2) G. Horlick and E. G. Codding, *Anal. Chem.*, **45**, 1490 (1973).
(3) Y. Talmi, *Am. Lab.*, March, 79 (1978).
(4) G. Horlick, *Appl. Spectrosc.*, **30**, 113 (1976).
(5) D. E. Osten, *Ind. Res.*, **82**, October (1975).
(6) J. A. Hass, L. J. Perko, and D. E. Osten, *Ind. Res.*, May (1977).
(7) Y. Talmi, *Anal. Chem.*, **47**, 658A (1975).
(8) Y. Talmi, *Anal. Chem.*, **47**, 699A (1975).
(9) K. W. Busch and G. H. Morrison, *Anal. Chem.*, **45**, 712A (1973).
(10) J. D. Winefordner, J. J. Fitzgerald, and N. Omenetto, *Appl. Spectrosc.*, **29**, 369 (1975).
(11) R. P. Cooney, G. D. Boutilier, and J. D. Winefordner, *Anal. Chem.*, **49**, 1048 (1977).
(12) D. F. Brost, B. Malloy, and K. W. Bush, *Anal. Chem.*, **49**, 2280 (1977).
(13) H. L. Felkel, Jr., and H. L. Pardue, Anal. Chem., **50**, 602 (1978).
(14) N. G. Howell and G. H. Morrison, *Anal. Chem.*, **49**, 106 (1977).
(15) H. L. Felkel, Jr., and H. L. Pardue, *Anal. Chem.*, **49**, 1112 (1977).
(16) F. S. Chaung, D. F. S. Natusch, and K. R. O'Keefe, *Anal. Chem.*, **50**, 525 (1978).
(17) G. Horlick and E. G. Codding, *Appl. Spectrosc.*, **29**, 167 (1975).
(18) K. M. Aldous, D. G. Mitchell, and K. W. Jackson, *Anal. Chem.*, **47**, 1034 (1975).
(19) T. L. Chester, H. Haraguchi, D. O. Knapp, J. D. Messman, and J. D. Winefordner, *Appl. Spectrosc.*, **30**, 410 (1976).
(20) T. E. Cook, M. J. Milano, and H. L. Pardue, *Clin. Chem.*, (*Winston-Salem, N.C.*), **20**, 1422 (1974).
(21) E. G. Codding and G. Horlick, *Spectrosc. Lett.*, **7**, 33 (1974).
(22) T. E. Edmonds and G. Horlick, *Appl. Spectrosc.*, **31**, 536 (1977).
(23) M. Franklin, C. Baber, and S. R. Koirtyohann, *Spectrochim. Acta, Part B*, **31**, 589 (1976).
(24) K. R. Betty and G. Horlick, *Appl. Spectrosc.*, **32**, 31 (1978).
(25) G. Horlick, E. G. Codding, and S. T. Leung, *Appl. Spectrosc.*, **29**, 48 (1975).
(26) K. W. Busch, N. G. Howell, and G. H. Morrison, *Anal. Chem.*, **46**, 2074 (1974).
(27) N. G. Howell, J. D. Ganjei, and G. H. Morrison, *Anal. Chem.*, **48**, 319 (1976).
(28) D. W. Johnson, J. B. Callis, and G. D. Christian, *Anal. Chem.*, **49**, 747A (1977).
(29) A. E. McDowell, R. S. Harner, and H. L. Pardue, *Clin. Chem. Winston-Salem, N.C.*, **22**, 1862 (1976).
(30) M. J. Milano and K. Y. Kim, *Anal. Chem.*, **49**, 555 (1977).
(31) G. M. Ridder and D. W. Margerum, *Anal. Chem.*, **49**, 2090, 2098 (1977).
(32) A. E. McDowell and H. L. Pardue, *Anal. Chem.*, **49**, 1171 (1977).
(33) R. E. Dessy, W. D. Reynolds, W. G. Nunn, C. A. Titus, and G. F. Moler, *Clin. Chem.* (*Winston-Salem, N.C.*), **22**, 1472 (1976).
(34) D. A. Yates and T. Kuwana, *Anal. Chem.*, **48**, 510 (1976).
(35) T. A. Nieman, F. J. Holler, and C. G. Enke, *Anal. Chem.*, **48**, 899 (1976).
(36) E. Kohen, C. Kohen, J. M. Salmon, *Mikrochim. Acta*, **1976 II**, 195 (1976).
(37) J. P. Fillard, M. deMurcia, J. Gasiot, and S. Chor, *J. Phys. E.*, **8**, 993 (1975).
(38) J. R. Jadamec, W. A. Saner, and Y. Talmi, *Anal. Chem.*, **49**, 1316 (1977).
(39) R. P. Cooney, T. Vo-Dinh, and J. D. Winefordner, *Anal. Chim. Acta*, **89**, 9 (1977).
(40) R. P. Cooney, T. Vo-Dinh, G. Walden, and J. D. Winefordner, *Anal. Chem.*, **49**, 939 (1977).
(41) H. Steinhart and J. Sandmann, *Anal. Chem.*, **49**, 950 (1977).
(42) A. L. Broadfoot and B. R. Sandel, *Appl. Opt.*, **16**, 1533 (1977).
(43) S. S. Vogt, R. G. Tull, and P. Kelton, *Appl. Opt.*, **17**, 574 (1978).
(44) B. R. Sandell and A. L. Broadfoot, *Appl. Opt.*, **15**, 3111 (1976).
(45) J. F. McNall, *Imaging in Astronomy*, p FB8-1, June 18–21, 1975.
(46) J. F. McNall and K. H. Nordsieck, "An Intensified Self-Scanned Array Detector System that is Photon Noise Limited", preprint, University of Wisconsin, Madison, Wis.
(47) S. B. Mende and F. H. Chaffee, *Appl. Opt.*, **16**, 2698 (1977).
(48) R. G. Tull, J. P. Choisser, and E. H. Snow, *Appl. Opt.*, **14**, 1182 (1975).
(49) R. L. Wilson and J. D. Ingle, Jr., *Anal. Chem.*, **49**, 1060 (1977).
(50) S. D. Hoyt and J. D. Ingle, Jr., *Anal. Chim. Acta*, **87**, 163 (1976).
(51) R. L. Wilson and J. D. Ingle, Jr., *Anal. Chem.*, **48**, 1641 (1976).
(52) E. E. Edwin, R. Jackman, and N. Hebert, *Analyst* (*London*), **100**, 689 (1975).
(53) W. I. M. Holman, *J. Biochem.*, **38**, 388 (1944).
(54) R. Strohecker and H. M. Henning, "Vitamin Assay—Tested Methods", Verlag Chemie, Germany, 1966.
(55) "Methods of Vitamin Assay", Assoc. of Vitamin Chemists, Inc., Interscience, New York, 1966.
(56) G. Rindi and V. Perri, *Int. Z. Vitaminforsch*, **32**, 398 (1962).
(57) "Official Methods of Analysis of the Association of Official Analytical Chemists", William Horwitz, Ed., AOAC, Washington, D.C., 1970.
(58) R. L. Wilson and J. D. Ingle, Jr., *Anal. Chem.*, **49**, 1066 (1977).
(59) R. L. Wilson and J. D. Ingle, Jr., *Anal. Chim. Acta*, **92**, 417 (1977).
(60) J. R. Totter, *Photochem. Photobiol.*, **3**, 231 (1964).
(61) Larry A. Montano, Master's Thesis, Oregon State University, Corvallis, Ore., 1978.
(62) J. Slawinsk, *Photochem. Photobiol.*, **13**, 489 (1971).
(63) E. J. Bowen and R. A. Lloyd, *Proc. Chem. Soc.*, October, 305 (1963).
(64) G. B. Melvzova and R. F. Vassil'ev, *Mol. Photochem.*, **2**, 251 (1970).

RECEIVED for review July 12, 1978. Accepted August 18, 1978. Acknowledgement is made to the NSF (grant CHE-76-16711) for partial support of this research and one of us (M.A.R.) gratefully acknowledges an NSF graduate fellowship.

Quantitative Measurement of Ethylene Incorporation into Propylene Copolymers by Carbon-13 Nuclear Magnetic Resonance and Infrared Spectrometry

John R. Paxson* and James C. Randall

Phillips Petroleum Company, Research and Development, Bartlesville, Oklahoma 74004

Carbon-13 NMR has been used successfully to characterize a series of ethylene–propylene copolymers for weight per cent ethylene. Once characterized, this copolymer series served as calibration standards for development of a faster infrared method. An excellent correlation was obtained between the techniques. These copolymers contained >95% propylene, with the ethylene units present as isolated entities between two head-to-tail propylene units.

Carbon-13 nuclear magnetic resonance has proved to be an excellent technique for analyses of sequence distributions and comonomer contents in ethylene–propylene, E-P, copolymers (*1–5*). These analyses are particularly straightforward if one of the monomer units is present at a level of 95% or greater because the other monomer will occur primarily as an isolated unit. The branching content has been examined previously for ethylene–propylene copolymers containing predominantly ethylene (*6*); however, corresponding quantitative measurements have not been reported for the ethylene content in copolymers containing predominantly propylene. Accessible, accurate, and reasonably fast routine analytical methods are needed for process control and development. Infrared (IR) spectrometry is probably the most extensively applied spectral technique for such applications (*7, 8*). It is conceivable that

0003-2700/78/0350-1777$01.00/0 © 1978 American Chemical Society

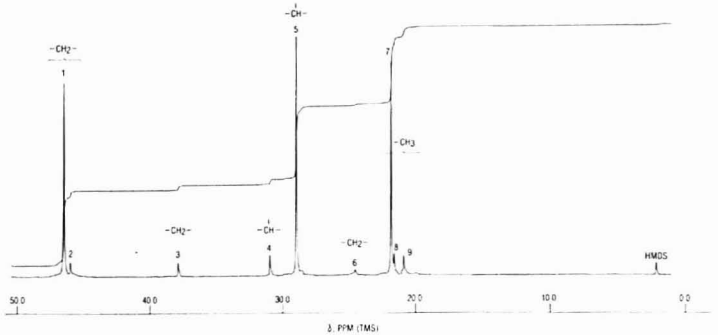


Figure 1. A ^{13}C NMR spectrum at 25.2 MHz and 125 °C of a 97/3 propylene–ethylene copolymer in 1,2,4-trichlorobenzene and perdeuterobenzene. The internal standard is hexamethyldisiloxane, HMDS

most IR bands used for determining copolymer compositions are sensitive to sequences of both monomers. Thus, IR methods for compositional analysis can be calibrated if: (a) known standards of similar constitution to the copolymers being analyzed are available and (b) assignments and behavior of the calibration bands are well established; preferably the absorptivities of these bands should be relatively independent of the position of monomer units in the chain. Thus, quantitative infrared analysis of copolymers depends primarily on the standards employed whose composition can be determined directly and reliably. In this study, ^{13}C NMR is used to provide such reference standards for the less time-consuming infrared measurements. Because it is relatively inexpensive and easy to operate, IR equipment is more feasible than ^{13}C NMR for quality or process control in commercial applications. This study shows that an excellent correlation, which can be used for quantitative analysis, is obtained between ^{13}C NMR and IR results on a series of E-P copolymers containing greater than 95 wt% propylene.

EXPERIMENTAL

The copolymers examined in this study were prepared by a method described previously (*9*). The ethylene contents varied from 1 to 3 wt%.

Nuclear Magnetic Resonance Measurements. NMR spectra were measured from polymer samples dissolved in a mixture of 1,2,4-trichlorobenzene and perdeuterobenzene at concentrations between 10–15 wt%. Sufficient perdeuterobenzene was added to maintain a lock signal on a Varian XL-100-15 NMR spectrometer at a temperature of 125 °C. The spectrometer system was equipped with Varian's FT-100 pulsed NMR-Fourier transform system and a disk accessory. The ^{13}C NMR spectra were obtained utilizing the following conditions for the pulse sequences:

pulse angle	90°	transients accumulated	2000-5000
pulse delay	8.5 s	spectral width	5000 Hz
acquisition time	1.5 s	no signal enhancement used	

A pulse interval of 10 s is sufficient to satisfy the spin-lattice relaxation time, T_1, of the methyl group, which is the slowest relaxing nucleus with a T_1 of 2 s at 125 °C (*10, 11*). The number of transients accumulated depended upon the ethylene content and, in each case, accumulations were allowed to continue until a satisfactory signal-to-noise ratio was achieved. As shown by a typical example in Figure 1, each ^{13}C NMR spectrum was recorded with proton noise-decoupling to remove unwanted ^{13}C–^{1}H scalar couplings. No corrections were made for differential nuclear Overhauser effects (NOE) since constant NOEs were assumed (*12, 13*) in agreement with previous workers (*1–4*). Constant NOEs for all major resonances in low ethylene content ethylene–propylene copolymers have been reported recently (*14*).

Infrared Measurements. Infrared spectra were obtained on molded films of a nominal 1-mm thickness. Approximately 0.52 g of sample was placed between 31.8-mm diameter aluminum foil disks on a 1-mm brass spacer of 19.0-mm i.d. and 31.8-mm o.d. resting in a Buehler 20-2112 specimen mold. The temperature of the assembled mold was maintained to 175 °C by a standard thermocouple temperature controller. After the sample was pressed to 6000 psig (40.34 megapascals) in a Buehler 1315 AB specimen mold and cooled to 35 °C under pressure, the film was removed and mounted in a holder. Five measurements with a Starrett Model 230-M micrometer were averaged to provide a film thickness for the ethylene calculations. Since small variations in thickness introduce substantial errors in final calculations, the film was discarded if the readings varied by more than 0.05 mm and another sample was molded.

Infrared spectra were obtained on a Digilab Model 15 Fourier Transform system at four wavenumber resolution in double beam operation. An adequate signal-to-noise ratio resulted from 1000 scans. Standard double precision Digilab/Data General computer software was used to present data properly scale expanded in absorbance form. The absorbance of the 732 cm^{-1} infrared band, attributed to $\gamma_r (CH_2)_3$ (*7*) was recorded. Comparable transmission spectra were obtained on a typical plant instrument, the Perkin-Elmer 257.

RESULTS AND DISCUSSION

Since the infrared method depends upon the availability of reference copolymer and ^{13}C NMR is used for the purpose of providing well-characterized copolymers, the ^{13}C NMR method will be discussed first. Ethylene–propylene copolymers have been the subject of extensive ^{13}C NMR investigations (for example, see references 3, 4, and 5) and complete spectral assignments are available. Thus, these copolymers containing predominantly propylene should be readily characterized by the ^{13}C NMR technique.

The ^{13}C NMR spectrum of an ethylene–propylene copolymer, containing approximately 97% propylene in primarily isotactic sequences, is shown in Figure 1. The major resonances are numbered consecutively from low to high field. Chemical shift data and assignments, according to Ray, Johnson, and Knox (*4*) in a study of related E-P copolymers, are listed in Table I. Greek letters are used to distinguish the various methylene carbons and designate the location of the nearest methine carbons as suggested by Carman (*1*). Reference chemical shift data from the study of Ray et al., a predominantly isotactic polypropylene and an ethylene–propylene copolymer containing 97% ethylene, are also listed in Table I. The latter two polymers establish a base for comparing the various chemical shift data and lend support to the assignments of Ray, Johnson, and Knox. (Chemical

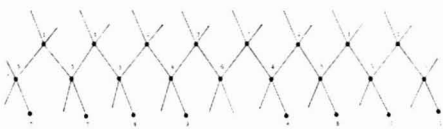
Table I. Observed and Reference ^{13}C NMR Chemical Shifts in ppm for Ethylene–Propylene Copolymers and Reference Polypropylenes as Measured with Respect to an Internal TMS Standard

line	carbon	3/97 E/P[a]	E/P [Ray et al. (4)]	97/3[a] E/P	sequence assignment	reference crystalline (12)	PP amorphous (12)
1	$\alpha\alpha$-CH_2	46.4	46.3		PPPP	46.5	47.0–47.5 r 46.5 m
2	$\alpha\alpha$-CH_2	46.0	45.8		PPPE		
3	$\alpha\gamma$-CH_2	37.8	37.8		PPEP		
4	CH	30.9	30.7		PPE		
5	CH	28.8	28.7		PPP	28.5	28.8 mmmm 28.6 mmmr 28.5 rmmr 28.4 mr+rr
6	$\beta\beta$-CH_2	24.5	24.4		PPEPP		
7	CH_3	21.8	21.6		PPPPP	21.8	21.3–21.8 mm 20.6–21.0 mr 19.9–20.3 rr
8	CH_3	21.6	21.4		PPPPE		
9	CH_3	20.9	20.7		PPPEP		
	CH_3		19.8	19.8	EPE		
	CH		33.1	33.1	EPE		
	α-CH_2			37.4	EPE		
	β-CH_2			27.3	EPE		
	$-(CH_2)_n-$		29.8	29.8	EEE		

[a] As measured in this laboratory.

shift measurements are known to vary a few tenths of a ppm between laboratories.)

From the chemical shift assignments, it can be established that the E-P copolymers examined in this study contain principally isolated ethylene linkages. The nine resonances shown in Figure 1 can be easily attributed to isolated ethylene linkages (*4*) as shown below:



With the structure of these E-P copolymers firmly established, the ^{13}C NMR relative intensities can be used to determine the ethylene–propylene content and thereby establish reference copolymers for the faster infrared method. One advantage of the ^{13}C NMR approach is that the ethylene content can be measured independently from more than one region of the ^{13}C NMR spectrum. Conceivably, six different resonances could be used to establish the ethylene content while the weight per cent propylene can be measured in three ways. These relationships are given below:

$$(P) = k(I_7 + I_8 + I_9) \quad (1)$$

$$(P) = k(I_4 + I_5) \quad (2)$$

$$(P) = k(I_1 + I_2 + (1/2)I_3) \quad (3)$$

$$(E) = kI_6 \quad (4)$$

$$(E) = (1/2)kI_3 \quad (5)$$

$$(E) = (1/2)kI_4 \quad (6)$$

$$(E) = (1/2)kI_2 \quad (7)$$

$$(E) = (1/2)kI_8 = (1/2)kI_9 \quad (8)$$

The quantitative relationships given by Equations 1 and 8 are from methyl resonances only, Equations 3, 4, 5, and 7 utilize methylene resonances only, and Equations 2 and 6 are developed from methine resonances only. (Note that k is the NMR proportionality constant that includes all of the variables in an NMR analysis that become fixed when a specific set of experimental conditions is selected. Such factors include the number of molecules in the vicinity of the receiver coil, instrumental response, and recorded attenuation. It is unnecessary to evaluate k because every resonance has the same value for k. I_x is the intensity of the peak x.) Although the ethylene and propylene measurements are certainly overdetermined through the use of Equations 1 through 8, the accuracies of the various ways that (E) and (P) can be measured are not the same. For example, there is considerable overlap between peaks 1 and 2 and also among peaks 7, 8, and 9. The second point of concern is tacticity. The methyl, methine, and methylene carbon resonances of polypropylene display different degrees of sensitivity toward configurational differences (*15*). As shown in Table I, resonances from propylene units in configurational sequences other than isotactic may overlap with corresponding resonances from isotactic propylene units associated with the isolated ethylene linkage. This overlap could be a factor in an analysis of both the methylene resonances, 1 and 2, and the methyl resonances 7, 8, and 9. As a consequence, the methine resonances, 4 and 5, should be the best suited for quantitative measurements because the methine carbon resonance is the least sensitive toward configurational differences (*15*) and also the least affected by overlap from neighboring resonances. Otherwise, the accuracy of the ^{13}C NMR method for (E), (P) may be related to the ethylene content. As the ethylene content drops to a level comparable to the various resonances from atactic

Table II. Carbon-13 NMR Intensity Data for 3/97 and 1/99 Ethylene-Propylene Copolymers

	relative areas		peak heights	
line	3/97	1/99	1/99	3/97
1	155.0	186.5	1217	202
2	18.0	14.0	40	17
3	14.0	7.0	40	17
4	17.0	6.5	52	23
5	169.0	195.0	1447	245
6	6.0	2.0	18	8
7	{176.0	{176.0	1477	220
8			74	25
9	21.0	16.5	57	22

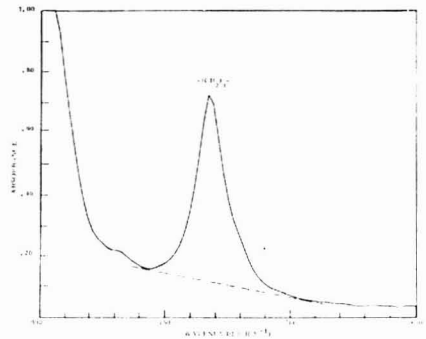


Figure 2. An infrared spectrum of a low ethylene content ethylene–propylene copolymer. The 732 wavenumber band indicates random ethylene monomer units. A typical base line is illustrated

polypropylene sequences, the calculated ethylene content could be considerably different from the true value. This point is illustrated in Table II where intensity data are listed for resonances 1 through 9 for two ethylene–propylene copolymers with 3/97 and 1/99 comonomer distribution, respectively. The peak intensities for resonances 2, 8, and 9, which should be identical, are enhanced to different extents by configurational overlap in the 1/99 ethylene/propylene copolymer sample. The best quantitative results, therefore, are obtained by using methine resonances 4 and 5 to determine the comonomer composition. Similar results are obtained whether one uses peak heights or peak areas as shown below:

	weight per cent ethylene	
sample	by peak heights	by peak areas
3/97 (E)/(P)	2.8	3.0
1/97 (E)/(P)	1.1	1.1

The composition of the remaining ethylene–propylene copolymers were determined by peak heights using the methine resonances only. In no instance was there any evidence for an inclusion of consecutive ethylene units. Thus, composition data from ^{13}C NMR could now be used to establish an infrared method based on a correlation with the 732 wavenumber band which is attributed to the rocking mode, γ_r, of the methylene trimer, $-(CH_2)_3-$, between tertiary carbon atoms (*16*). Figure 2 shows the infrared spectral region and baseline used for the measurement of the random ethylene monomer unit content in these polymers. Typical calibration curves were based on data obtained in single application of the infrared technique. Peak height measurements were made on the 732 cm^{-1} band, which, once again, is characteristic of an ethylene unit isolated between two head-to-tail propylene units. To set 95% confidence limits on the ethylene concentration, we used a procedure (*17*) to calculate upper and lower calibration curves that can be set on a daily constructed calibration line in much the same way as confidence bands are set on regression lines. However, the upper and lower calibration curves differ from confidence bands in that they apply back to the independent variable (the ethylene concentration) used in determining the calibration curve. Using this procedure, an ethylene concentration can be predicted, given an observed peak height, and a confidence interval can be set on this predicted value for which a probability statement applies. Table III shows the results of such a process on calibration data obtained in a single application of the infrared method. Identical precision was obtained for data sets from both the FTS-15 and PE-257.

Table III. Precision of Determination of Ethylene in Ethylene-Propylene Copolymers from Infrared Analysis

ethylene level[a]	95% confidence level
1.1	0.90-1.29
1.4	1.21-1.58
1.6	1.42-1.78
2.0	1.83-2.17
2.1	1.93-2.27
2.3	2.13-2.48
2.5	2.33-2.68
2.7	2.52-2.89
2.8	2.62-2.99

[a] From ^{13}C NMR, weight per cent.

The final equation relating the infrared absorbance to the ethylene content is:

$$Y = 2.465X + 0.451 \quad (9)$$

where Y is the infrared absorbance at 732 wavenumbers divided by the film thickness in centimeters and X is the wt% ethylene. The standard errors are 0.110 for the intercept and 0.051 for the slope.

In conclusion, it is apparent from the data in Table III that the infrared absorbance at 732 cm^{-1} is sufficiently sensitive to the ethylene incorporation to determine the wt% ethylene to within 0.1–0.2% at the 95% confidence level. Of course, this uncertainty in part reflects the uncertainty in the ^{13}C NMR measurements; however, it is gratifying that, collectively, the measurements can be made within the indicated limits at the 95% confidence level. From the ^{13}C NMR data, it can be concluded that the propylene units occur in predominantly isotactic, head-to-tail sequences and that the ethylene units are incorporated as isolated units only. Thus, this structural prerequisite is a requirement for application of this method because it has not been tested on copolymers containing propylene configurational irregularities or ethylene sequences two units and longer. This method does illustrate the feasibility, however, in combining infrared and ^{13}C NMR data to develop quantitative, analytical methods for polymer structural analysis.

ACKNOWLEDGMENT

The authors express their appreciation to J. P. Butler and F. T. White for the infrared measurements and to F. L. Tilley for the NMR measurements. Appreciation is also expressed to the Phillips Petroleum Company for permission to publish this work.

LITERATURE CITED

(1) C. J. Carman and C. E. Wilkes, *Rubber Chem. Technol.*, **44**, 781 (1971).
(2) C. E. Wilkes, C. J. Carman, and R. A. Harrington, *J. Polym. Sci.*, **43**, 237 (1973).
(3) C. J. Carman, R. A. Harrington, and C. E. Wilkes, *Macromolecules*, **10**, 536 (1977).
(4) G. J. Ray, P. E. Johnson, and J. R. Knox, *Macromolecules*, **10**, 773 (1977).
(5) J. C. Randall, *Macromolecules*, **11**, 33 (1978).
(6) J. C. Randall, *J. Polym. Sci., Polym. Phys. Ed.*, **11**, 275 (1973).
(7) H. V. Drushel, *Crit. Rev. Anal. Chem.*, **1**, 161-192 (1970).
(8) C. Tosi and F. Ciampelli, *Adv. Polym. Sci.*, **12**, 88-130 (1973) and references therein.
(9) R. J. Perry, U.S. Patent 3 736 307, issued May 29, 1973.
(10) D. E. Axelson, L. Mandelkern, and G. C. Levy, *Macromolecules*, **10**, 557 (1977).
(11) J. C. Randall, *J. Polym. Sci., Polym. Phys. Ed.*, **14**, 1693 (1976).
(12) J. Schaefer and D. F. S. Natusch, *Macromolecules*, **5**, 416 (1972).
(13) Y. Inoue, A. Nishioka, and R. Chûjô, *J. Polym. Sci., Polym. Phys. Ed.*, **11**, 2234 (1973).
(14) J. M. Sanders and R. A. Komoroski, *Macromolecules*, **10**, 1214 (1977).
(15) J. C. Randall, "Polymer Sequence Determination", Academic Press, New York, 1977, Chap. 1.
(16) C. Tosi, *Spectrochim. Acta, Part A*, **24**, 2157 (1968).
(17) H. Scheffe, "A Statistical Method Calibration", University of California, Berkeley, paper presented at Gordon Research Conference on Statistics, July 10, 1972.

RECEIVED for review March 30, 1978. Accepted August 16, 1978.

Electron Capture Negative Ion Chemical Ionization Mass Spectrometry

Donald F. Hunt* and Frank W. Crow

Department of Chemistry, University of Virginia, Charlottesville, Virginia 22901

In this paper we discuss the analytical potential of electron capture negative ion chemical ionization mass spectrometry, provide data which define the lowest level of sample detection achieved with our present instrument configuration, and furnish experimental details on the operation of a negative ion chemical ionization quadrupole mass spectrometer. Detection of dopamine, amphetamine, and Δ^9-tetrahydrocannabinol derivatives at the attomole (10^{-18}) level by conventional GC-MS selected ion monitoring methodology is reported.

In an earlier paper we described new methodology, pulsed positive ion-negative ion CI (PPINICI) (*1*), which facilitates simultaneous recording of positive and negative ion CI spectra on a quadrupole mass spectrometer. Also discussed were unique analytical applications of several negative ion chemical ionization (NICI) reagent gases and the capability of NICI to provide conformation of sample molecular weight, structural information complementary to that obtained in the positive ion mode of operation, and sample ion currents 100 to 1000 times greater than that available from positive ion methodology. It was also suggested that electron capture NICI would facilitate detection and quantitation of many organics at the 10^{-12}–10^{-13} g level and therefore would find widespread use as a technique for the quantitation of trace level mixture components by combined GC-MS.

In this paper we discuss the analytical potential of electron capture NICI in greater detail, provide data which define the lowest level of sample detection achieved using electron capture NICI with our present instrument configuration, and furnish additional experimental details on the operation of a NICI quadrupole mass spectrometer.

Papers describing unusual negative ion–molecule isotope exchange reactions (*2*), the utility of OH^- as a CI reagent ion (*3*), electron capture NICI methodology for detecting metal chelates (*4*), and the first biological assay using the GC-MS electron capture NICI technique (*5*) have appeared recently. A review of negative ion CIMS (*6*) and a paper reporting negative ion studies under atmospheric pressure ionization conditions have also been published (*7*).

EXPERIMENTAL

General. All spectra were recorded on a Finnigan model 3300 quadrupole mass spectrometer (Finnigan Corp., Sunnyvale, Calif.), equipped with a standard CI source. Primary ionization of the CI reagent gas was accomplished using a 100-eV beam of electrons generated from a heated rhenium filament. Reagent gas and sample pressures were maintained at 0.6–0.8 Torr and $<10^{-3}$ Torr, respectively. Source temperatures were in the range of 100–150 °C unless otherwise specified. Sample introduction was accomplished by means of a Finnigan model 9500 gas chromatograph interfaced to the CI source via a heated glass capillary flow restrictor $^6/_{1000}$ inch in diameter. Methane (99.9%) was purchased from Matheson Gas Products, Inc., East Rutherford, N.J., and passed through a Hydro-Purge gas filter (Applied Science Laboratories, Inc., State College, Pa.) before use as both the GC carrier gas and CI reagent gas. For the determination of detection limits reported in Table II, a 1-μL volume of sample dissolved in a suitable solvent was injected onto a 5-ft by $^1/_4$-inch o.d., silylated, and conditioned glass column packed with either OV-1 (3%) or OV-17 (3%) on 60/80 Gas Chrom Q. The reported detection limit values refer to total amount of sample injected on column.

Solutions containing the proper concentration of sample were prepared by consecutive dilution of stock solutions. In all cases, solvent "blanks" injected immediately prior to sample injections produced a base-line signal. The origin of most "ghost" peaks observed on injection of solvent blanks was found to be absorption of sample onto the GC septum. This problem was alleviated by changing the septum frequently and by avoiding injection of samples larger than 10 pg onto the column.

Chemicals and Derivatives. Silylating agents and DMF were purchased from Pierce Chemical Co., Rockford, Ill.

All fluorinated reagents were obtained from PCR, Inc., Gainesville, Fla. Dopamine was purchased from Sigma Chemical Corporation, St. Louis, Mo.

Synthesis of the Pentafluorobenzylimine-Trimethylsilyl Derivative of Dopamine (1). Preparation of 1 was accomplished by modifying the procedure of Lhuguenot and Maume (*8*). Dopamine hydrochloride 1 mg, (5.3 mmol), dimethylformamide (0.5 mL) and pentafluorobenzaldehyde (10 μL) were placed in a capped Pierce Reacti-vial and heated at 85 °C for 5 min. *N,O*-Bis(trimethylsilyl)acetamide (100 μL) was added to the vial and the reaction mixture was allowed to stand at room temperature for 15 min, and then extracted with 1 mL of high purity hexane (Burdick and Jackson Laboratories, Muskegon, Mich.). The hexane extract was used to prepare stock solution for GC analysis. GC conditions were: column (3% OV-17) temperature, 200 °C; injector and transfer line temperatures, 225 °C.

Synthesis of the Pentafluorobenzoyl Derivative of Δ^9-Tetrahydrocannabinol (2). Δ^9-Tetrahydrocannabinol (1 mg, 3.2 μmol), pentafluorobenzoyl chloride (2.8 mg, 12 μmol) and several drops of triethylamine were placed in 0.2 mL of methylene chloride. After standing for several minutes, the reaction mixture was placed on a silica gel microcolumn in a disposable pipet and eluted with methylene chloride. Compound **2**, 1.6 mg, was obtained as a yellow oil. Stock solutions for GC-MS analysis were prepared by dissolving this oil in 100 mL of methanol. GC conditions were: column (3% OV-17) temperature, 230 °C; injector temperature, 250 °C; and transfer line temperature, 200 °C.

Synthesis of the Pentafluorobenzoyl Derivative of Amphetamine (3). Amphetamine (171 mg, 1 mmol), pentafluorobenzoyl chloride (230 mg, 1 mmol), and several drops of triethylamine were placed in 10 mL of methylene chloride and the resulting mixture was stirred at room temperature for 15 min (*9*). Evaporation of solvent under a stream of nitrogen afforded crude product which was purified by either preparative TLC or microcolumn chromatography in a disposable pipet using silica gel as the absorbent and methylene chloride as the eluant. Isolated yields of **3** were typically 25%. Stock solutions for GC analysis were prepared by dissolving 1 mg of **3** in 100 mL of ethyl acetate. GC conditions were: column (3% OV-1) temperature, 230 °C; injector and transfer line temperature, 260 °C.

Synthesis of the Tetrafluorophthaloyl Derivative of Amphetamine (4). Amphetamine hydrochloride (342 mg, 2 mmol), tetrafluorophthalic anhydride (440 mg, 2 mmol), triethylamine (300 μL, 2.1 mmol) and 8 mL of toluene were heated under reflux while water was removed from the reaction via a Dean-Stark trap (*10*). After 3 h, the reaction mixture was filtered and the resulting precipitate was triturated with acetonitrile.

0003-2700/78/0350-1781$01.00/0 © 1978 American Chemical Society

Evaporation of the acetonitrile gave a yellow oil which was purified by microcolumn chromatography on silica gel in a disposable pipet using 1/1 methylene chloride/hexane as the eluant. White crystalline **4** (40 mg) (mp 142–143 °C) was obtained on evaporation of the solvent. Stock solutions for GC-MS analysis were prepared by dissolving 1 mg of **4** in 100 mL of ethyl acetate. GC conditions were: column (3% OV-1) temperature, 230 °C; injector temperature, 275 °C; and transfer line temperature, 280 °C.

Negative Ion Detection System. Methodology for recording positive and negative ion CI mass spectra simultaneously on a Finnigan quadrupole mass spectrometer has been described in an earlier publication (*1*). The technique is employed here to determine the ratio of the ion currents, N/P, carried by the most abundant negative and positive ions derived from the sample. It is important to note that this measurement must be carried out on a small quantity of sample to avoid saturation of the negative ion signal. In our present instrumentation, we find that for efficient electron capture agents the increase in negative ion current as a function of sample concentration can become nonlinear when the sample size exceeds ca. 10 ng. Saturation of the negative ion signal can occur for sample quantities as low as 100 ng. In contrast saturation of the positive ion current requires microgram quantities of sample.

Detection of negative ions from femtogram size samples is accomplished using the newly developed conversion dynode (CD) electron multiplier developed by George Stafford of Finnigan Corporation, Sunnyvale, Calif. (*11*). In this device, negative ions are accelerated into a metallic surface held at a high positive potential (+2500 V) and placed several millimeters away from the face of a Galileo Model #4770 continuous dynode electron multiplier (Galileo Electrooptics Corporation, Sturbridge, Mass.). Positively charged sample and/or metal ions generated as a result of negative ion impact on the conversion dynode are then collected on the first dynode (−2000 V) of the nearby conventional positive ion electron multiplier. In the conversion dynode mode of operation, noise on both the positive and negative ion signals is equal and 10 times less than that observed on the negative ion signal from our earlier detection system. Measurements indicate that the gain on the continuous dynode multiplier increases from 2 to 5×10^5 over the range from 100 to 600 amu.

Experiments to determine the lowest level of sample detectable by electron capture negative ion CIMS were conducted with the spectrometer operating in the selected ion monitoring mode. Measurements were made with a Finnigan Programmable Multiple Ion Monitor (PROMIM) and Rikadenki recorder (Soltec Corporation, Sunnyvale, Calif.). Maximum signal intensity and S/N ratio were obtained by optimizing the electron beam energy, filament emission, and ion source and lens potentials. Resolution was adjusted to give a 50% valley between peaks.

DISCUSSION AND RESULTS

Bombardment of methane at 1 Torr with 100 eV electrons generates CH_5^+ and $C_2H_5^+$ ions in high abundance (*12*). As indicated in Equations 1–3,

$$2CH_4 + 2e \rightarrow CH_4^{+}\cdot + CH_3^+ + H\cdot + 2e^* + 2e \quad (1)$$

$$CH_4^{+}\cdot + CH_4 \rightarrow CH_5^+ + CH_3 \quad (2)$$

$$CH_3^+ + CH_4 \rightarrow C_2H_5^+ + H_2 \quad (3)$$

formation of each positive reagent ion is accompanied by the production of a low energy electron. Each ionizing event removes about 30 eV from the bombarding electron (*13*) and the energy of the incident electron beam is further reduced by additional nonionizing collisions with neutral methane molecules (*14*). Thus, operation of a mass spectrometer under methane CI conditions should afford a mixture of both positive reagent ions and a population of electrons with near thermal energies.

Gas phase positive and negative ion molecule reactions which proceed at the diffusion controlled limit exhibit rate constants near 1×10^{-9} cm^3 s^{-1} (*15*). In contrast the rate constant for formation of a negative ion by resonance electron capture can be as high as 4×10^{-7} cm^3 s^{-1} (*16*) or ca. 400 times greater than that for an ion molecule reaction. Accordingly, if sample molecules are converted to stable positive and negative ions on every encounter with CH_5^+ and thermal electrons, respectively, the negative sample ion current should exceed the positive ion sample current by a factor of ca. 400. Ionization by resonance electron capture methodology should therefore facilitate detection and quantitation of many organic molecules at levels 2 orders of magnitude lower than that accessible by positive ion EI or CI methodology. At present, quantitation of many organics can be accomplished at the low picogram level using GC-MS in combination with the selected ion monitoring (SIM) technque. Operation of the mass spectrometer under CI conditions in the negative ion mode should extend the sensitivity of the GC-MS SIM techniques to the low femtogram (10^{-15} g) or attomole (10^{-18} mol) level.

For the detection of organic samples at the femtogram level, it is necessary that the sample form a molecular anion on nearly every encounter with a thermal electron.

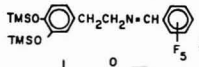
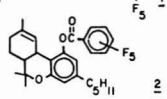
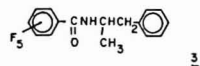
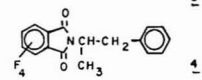
Many organic samples capture low energy electrons and undergo dissociative electron capture to produce low mass fragments (*17–20*). Very few molecules capture thermal electrons and form either stable molecular ions or high mass fragment ions with anything near unit efficiency. Despite this fact, ionization by resonance electron capture will undoubtedly become the method of choice for quantitating many trace level mixture components by combined gas chromatography–mass spectrometry. Most organic samples have to be derivatized to increase their volatility and to facilitate passage through the gas chromatograph. Realization of the enhanced sensitivity inherent to the resonance electron capture technique can be achieved by employing derivatives which facilitate high efficiency electron capture to produce stable sample anions.

To illustrate the analytical potential of the above methodology, we report positive and negative ion CI mass spectra as well as negative ion detection limits for several derivatives of phenols and amines under GC-MS conditions. As shown in Table I, the silylated Schiff base derivative formed from pentafluorobenzaldehyde and dopamine affords a negative ion CI mass spectra in which the molecular anion carries 95% of the negative ion sample current. At low sample concentration in the ion source, the current carried by this ion exceeds that of the most abundant positive ion by two orders of magnitude (N/P = 102). The tetrafluorophthaloyl derivative of amphetamine and the perfluorobenzoyl derivatives of amphetamine and Δ^9-tetrahydrocannabinol behave in a similar manner and afford electron capture negative ion spectra in which the molecular anion or an $M^{-}\cdot$–HF ion carries most of the sample ion current. In each case the ratio of negative sample ion current to positive sample ion current exceeds 10^2.

Previously we reported that the N/P ratio obtained at low levels of perfluorobenzoyl amphetamine also held at the detection limit; 500 pg (S/N = 4/1) in the positive ion mode and 5 pg (SN = 4/1) in the negative ion mode (*1*). The negative ion detection limits reported in Table II were obtained using the newly developed conversion dynode electron multiplier (*11*). In this system, the noise on both the positive and negative ion signal is equal and a factor of 10 less than that observed on our earlier negative ion detector (*1*). By improving the S/N ratio, we now find that the limit of detection is between 10–25 fg (20–50 attomol) for each of the four compounds, **1–4**. Tracings of the actual data recorded in the SIM mode for the dopamine derivative **1** are shown in Figure 1.

It is important to note that the enhanced sensitivity reported above is achieved by simply switching the sample ionization mode from positive ion CI to electron capture NICI. All other instrumental parameters remain unchanged. We wish also to emphasize the significance of the N/P ratio

Table I. Methane PPINICI Mass Spectra[a]

compound	MW	% total negative sample ion current N/P[b]	M⁻·	(M-HF)⁻·	other m/e (%)	% total positive sample ion current (M + 1)⁺	other m/e (%)
 1	475	102	95.0	---	385 (1.4),[e] 167 (3.7)[f]	56.7	504 (4.6),[c] 460 (35.4) 267 (3.3)
 2	508	328	90.1	---	167 (9.9)[f]	48.6	537 (14.3),[c] 296 (7.1),[g] 195 (11.4),[h] 135 (18.6)
 3	329	100	---	83.3	289 (11.3),[i] 212 (2.7), 198 (2.7)	45.4	370 (1.1),[d] 358 (7.0),[c] 238 (30.4),[j] 118 (16.2)
 4	337	678	100	---	---	34.7	378 (0.8),[d] 366 (2.8),[c] 246 (30.2),[j] 245 (25.0), 147 (6.7)

[a] Ion source temperature, 100 °C; ion source pressure, 600 μ. [b] Ratio of the most abundant negative and positive sample ions at low sample concentration. [c,d] Ions resulting from the attachment of $C_2H_5^+$ and $C_3H_5^+$, respectively, to the sample. [e] $(M - (CH_3)_3SiF)^{-}$·. [f] $C_6F_5^-$. [g] $(M + 1 - C_6F_5COOH)^+$. [h] $C_6F_5CO^+$. [i] $(M - 2HF)^{-}$·. [j] $(M + 1 - C_6H_5(CH_3)^+$.

Table II. Lowest Levels of Detection Achieved Using Electron Capture Negative Ion CIMS

compound	sample quantity injected onto GC column	S/N[a]
1[b]	25 fg[c] (53 attomol)[d]	4
2[b]	10 fg (20 attomol)	1
3[b]	10 fg (30 attomol)	4
4[b]	10 fg (30 attomol)	12

[a] Signal to noise ratio. [b] Structures corresponding to these numbers appear in Table I. [c] 1 fg = 10^{-15} g. [d] 1 attomol = 10^{-18} mol.

obtained at low sample concentration. This ratio is a direct measure of the ionization efficiency in the positive ion and negative ion mode of operation and should remain constant when determined on different spectrometers. Thus, if the lowest level of detection in the positive ion mode is known on a given instrument, the N/P ratio reported here can be employed to calculate the lowest level of detection achievable on the same equipment using EC-NICI methodology. In contrast, absolute lowest levels of detection reported under either positive ion CI or EC-NICI conditions are dependent on many experimental parameters other than ionization efficiency and therefore can be expected to vary from laboratory to laboratory.

In addition to providing enhanced sample ion current, the use of EC-NICI for quantitation of organics may also result in significantly reduced background noise and a lower probability that a sample ion at a particular m/e ratio will be obscured by the presence of a fragment ion derived from a high molecular weight contaminent unresolved from the sample by the GC conditions employed in the analysis. We pointed out earlier that most organic molecules do not suffer efficient ionization on interaction with thermal electrons in the gas phase. Through proper choice of derivatizing agents, it is possible to selectively enhance the ion current derived from the analyte without increasing the ion current due to other molecules in the sample mixture. Although this aspect of the EC-NICI method may be important in many quantitation studies, it must also be mentioned that trace quantities of impurities with high electron affinities (i.e., molecules containing halogen) can seriously deplete the population of electrons in the ion source available for sample ionization. A

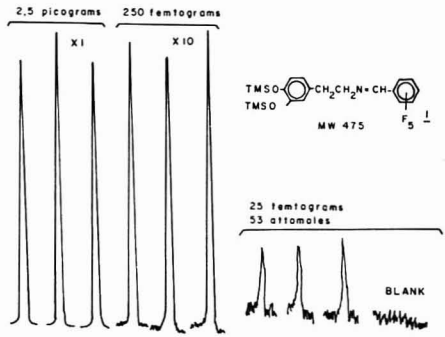


Figure 1. Response obtained by monitoring the M⁻· ion (m/e 475) of the dopamine derivative under GC-MS conditions with the instrument operating in the SIM mode. Signals correspond to three successive injections of 2.5 pg, 250 fg, and 25 fg samples, respectively

sharp drop in sample sensitivity results. For this reason, halocarbons are undesirable solvents for use in electron capture GC-NICIMS studies.

Comparison of EC-GC and EC-NICIMS. Since the mechanism of sample ionization is the same under both EC-GC and EC-NICI conditions, it is perhaps appropriate to comment on the analytical potential of the two techniques. Detection of organics under EC-GC conditions is accomplished by passing the sample through a chamber containing a population of thermal electrons and by monitoring the electron current passing through two electrodes placed within the chamber (*14*). A decrease in the standing current occurs when sample molecules capture electrons and are converted to negative ions which in turn suffer neutralization by the three-body recombination of positive and negative ions mediated by the carrier gas. The theoretical detection limit of the EC-GC detector is estimated to be 330 attomol (10^{-18}) (*14*). Because the EC-NICI technique measures negative ion abundance rather than variations in the standing electron current, it is expected that the mass spectrometric technique will be at least 10–100 times more sensitive than present EC-GC detectors. The experimental EC-NICI detection limits

reported in this paper already exceed the above theoretical limits of the EC-GC detector by a factor of 10. Information concerning sample molecular weight and structure furnished by the mass spectrometer further enhance the value of the EC-NICI technique. Of course, if the dominant sample ionization mechanism is dissociative electron capture to produce small anions such as Cl^-, no advantage is gained by employing the more expensive EC-NICI methodology.

ACKNOWLEDGMENT

The authors thank M. Story and G. C. Stafford of Finnigan Corporation for many helpful discussions during the course of this research.

LITERATURE CITED

(1) D. F. Hunt, G. C. Stafford, Jr., F. W. Crow, and J. W. Russell, *Anal. Chem.*, **48**, 2098 (1976).
(2) J. H. Stewart, R. H. Shapiro, C. H. DePuy, and V. M. Bierbaum, *J. Am. Chem. Soc.*, **99**, 7650 (1977).
(3) A. L. C. Smit and F. H. Field, *J. Am. Chem. Soc.*, **99**, 6471 (1977).
(4) S. R. Prescott, J. E. Campana, and T. E. Risby, *Anal. Chem.*, **49**, 1501 (1977).
(5) A. J. Lewy and S. P. Markey, *Science*, **201**, 741 (1978).
(6) K. R. Jennings, "Mass Spectrometry", Vol. 4, R. A. W. Johnstone, Ed., The Chemical Society, Burlington House, London, 1977, Chapter 9.
(7) E. C. Horning, D. I. Carroll, I. Dzidic, S.-N. Lin, R. N. Stillwell, and J.-P. Thenot, *J. Chromatogr.*, **142**, 481 (1977).
(8) J. C. Lhuguenot and B. F. Maume, *J. Chromatogr. Sci.*, **12**, 411 (1974).
(9) G. R. Wilkinson, *Anal. Lett.*, **3**, 289 (1970).
(10) A. K. Bose, F. Greer, and C. C. Prince, *J. Org. Chem.*, **23**, 1335 (1958).
(11) G. C. Stafford, Jr., Patent Pending.
(12) F. H. Field, "MTP International Review of Science, Physical Chemistry, Series One", Vol. 5, A. Maccoll, Ed., Butterworth, London, 1972, pp 133–165.
(13) C. E. Klotz, "Fundamental Processes in Radiation Chemistry", P. Ausloos, Ed., John Wiley and Sons, New York, 1968, p 40.
(14) E. D. Pellizzari, *J. Chromatogr.*, **98**, 324 (1974).
(15) S. G. Lias and P. Ausloos, "Ion Molecule Reactions", American Chemical Society, Washington, D.C., 1975, Chapter 4.
(16) L. G. Christophorou, *Chem. Rev.*, **76**, 409 (1976).
(17) L. G. Christophorou, "Atomic and Molecular Radiation Physics", Wiley Interscience, New York, 1971, Chapter 6.
(18) J. H. Bowie and B. D. Williams, "MTP International Review of Science, Physical Chemistry, Series Two", Vol. 5, A. Maccoll, Ed., Butterworth, London, 1975, pp 89–127.
(19) J. G. Dillard, *Chem. Rev.*, **73**, 589 (1973).
(20) M. von Ardenne, K. Steinfelder, and R. Tümmler, "Electronenanalagerungs—Massenspektrographie Organischer Substanzen", Springer-Verlag, New York, 1971.

RECEIVED for review March 17, 1978. Accepted August 18, 1978. This research was supported by the U. S. Army Research Office (DAAG29-76-G-0326).

Plasma Chromatography of Benzene with Mass Identified Mobility Spectra

S. H. Kim, K. R. Betty, and F. W. Karasek*

Guelph–Waterloo Centre for Graduate Work in Chemistry, Department of Chemistry, University of Waterloo, Waterloo, Ontario N2L 3G1

The reduced mobility value (K_o) of the molecular or quasi-molecular ion clusters of benzene increases as temperature increases from 2.22 $cm^2/V \cdot s$ at 50 °C to 2.32 $cm^2/V \cdot s$ at 207 °C. This increase of K_o appears to be due to the decrease of the ionic mass to that of the M^+ or MH^+ ion of benzene as the temperature increases above 200 °C. Identity of the ions associated with the two or three product-ion mobility peaks is assigned by PC/MS to M^+, MH^+, MNO^+, and an equilibrium mixture of ion clusters of the $[(M)(H_2O)_n(N_2)_m]H^+$ species. Above 200 °C, each peak in the ion mobility spectrum contains only a single component that can be assigned to a single product ion. The types of ion–molecule reactions occurring at atmospheric pressure appear to be proton transfer, charge transfer, electrophilic NO addition to form MNO^+, and ion clustering with neutral molecules of N_2 or H_2O.

Plasma chromatography (PC) allows detection and identification of picogram levels of organic gas or liquid phase samples from the characteristic product ions resulting from both positive and negative ion–molecule reactions occurring at atmospheric pressure (*1*). The ionic species present can be observed and identified by plasma chromatography coupled with mass spectrometry (PC/MS) (*2–8*).

The reactions observed in plasma chromatography are similar to those of chemical ionization mass spectrometry (CIMS) using CH_4 or NO/N_2 as reactant gases (*9, 10*), and almost identical with those of atmospheric ionization mass spectrometry (APIMS) (*11*). Understanding of the ion–molecule reaction mechanisms is necessary in order to interpret PC spectra. Several types of positive ion–molecule reactions can occur and be observed in PC. Proton transfer typically occurs for most polar organic compounds by reaction of the sample molecule, M, with reactant ions $(H_2O)_nH^+$ or $(H_2O)_nNH_4^+$ (n = 0, 1, 2, 3, ...) to produce MH^+ ions. The path of this reaction depends upon the relative proton affinities and the relative concentration ratio between the sample and the protonated reactant ion. Hydride ion (H^-) abstraction is observed for the alkanes yielding the $(M-H)^+$ ion as the most intense ion. Formation of $(M-H)^+$ results because hydride ion abstraction by NO^+ is only slightly exo- or endothermic. Charge transfer reactions are governed energetically by the ionization potential (IP) or appearance potential (AP) difference between the individual compounds and reactant gases. Clustering reactions with NO^+ can occur to form MNO^+. Clustering with the major reactant ion $(H_2O)_nH^+$ occurs with polar compounds like alcohols to form $M(H_2O)_nH^+$ as product ions. Clustering with N_2 has also been observed in recent PC/MS studies (*6*). The neutral molecules of N_2 attach to the reactant ions $(H_2O)_nNH_4^+$, $(H_2O)_nNO^+$, and $(H_2O)_nH^+$ to form $(H_2O)_n(N_2)_mNH_4^+$, $(H_2O)_n(N_2)_mNO^+$, and $(H_2O)_n(N_2)_mH^+$ (n, m = 0, 1, 2, ...). Some low molecular weight compounds containing nucleophilic groups also appear to undergo clustering with N_2 molecules (*12*).

In this paper, we report the temperature effect on the ion mobilities of the product ions of benzene, and the various types of ion–molecule reactions observed using data obtained from PC/MS.

EXPERIMENTAL

Total ion mobility spectra, mass spectra, and mass identified mobility spectra were obtained using a Phemto-Chem MMS 160 ion mobility spectrometer coupled with a mass spectrometer

0003-2700/78/0350-1784$01.00/0 © 1978 American Chemical Society

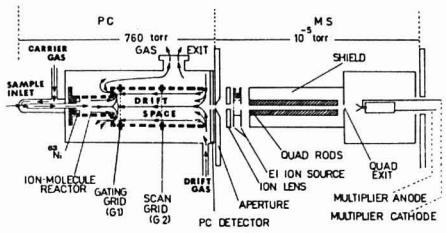


Figure 1. Schematic diagram of Phemto-Chem MMS-160 PC/MS combined system

(PC/MS) (PCP Inc., 2155 Indian Rd., West Palm Beach, Fla. 33409). The instrument consists of a plasma chromatograph interfaced with a quadrupole mass spectrometer as shown in Figure 1. The ion mobility spectrometer used in the Phemto-Chem MMS-160 has a drift space consisting of a 5-cm section between grids G_1 and G_2, and another $5 + x$ cm section between grid G_2 and the collector of the mass spectrometer. The distance x arises from the sample orifice system of the PC/MS interfaced instrument, and was calculated to be 1.61 cm. The total drift length is therefore 11.61 cm.

The mass spectral data were obtained by holding both grids G_1 and G_2 open, allowing all the ions formed in the plasma chromatograph to drift down through the tube and into the quadrupole mass spectrometer. A mass spectrum of the ions present was then obtained. Total ion mobility spectra were obtained by gating grid G_1 with grid G_2 held continuously open, and monitoring the drift times of the ions with the total ion monitor of the mass spectrometer. Finally, mass identified ion mobility spectra were obtained by operating the PC with the grid gating procedure described above, but with the mass spectrometer tuned to a specific m/e value.

To obtain an accurate ion drift velocity, two sets of ion mobility spectra were recorded by gating G_1 and G_2, respectively. The drift time difference between the two ion peaks recorded corresponds to the drift time required for the 5.0-cm drift length. All the data from the Phemto-Chem MMS-160 were obtained by signal averaging a number of 20-ms scans with a Nicolet signal averaging computer. All the spectra data used were subjected to multiple 3-point curve smoothing operations.

The operating parameters unless indicated otherwise in the figure captions were as follows: N_2 drift gas flow rate, 500 mL/min, N_2 carrier gas flow rate, 100 mL/min; gate width, 0.2 ms; electric field gradient, 214–247 V/cm; pressure, 762–764 Torr. Both carrier and drift gas inlets and the sample injection port were held 5–10 °C lower than the reaction section temperatures indicated in the figure captions. Samples were introduced by injection of the head space vapor obtained by inserting a microsyringe needle through the sealed aluminum foil over the reagent bottle top. Sample volumes were 0.2 ~ 0.3 μL for the PC and 5 ~ 15 μL for the PC/MS, respectively. Nitric oxide was added into the carrier gas stream using a 1-μL syringe. Benzene was obtained from MCB Co., Norwood, Ohio, and nitric oxide (98.5%, lecture bottle) was obtained from Matheson of Canada, Ltd., Whitby, Ontario. Both carrier and drift gas were Linde high purity N_2, 99.996%.

Reduced mobility data of the reactant ionic species and benzene throughout the temperature range investigated in this study were obtained with a Beta VI plasma chromatograph (*1*). The instrument was baked at 240 °C for three days with a high flow rate of carrier gas before each set of experiments. The temperature was allowed to stabilize for 1 h after reaching the set temperature before sample introduction. Three or four different measurements were made at each indicated temperature and the average was adopted. The temperature for an observation was reached both by cooling down from high temperature and by heating up from a lower temperature.

Operating conditions for the Beta VI PC instrument were as follows: N_2 carrier gas, 65 mL/min; drift gas, 350 mL/min; electric field gradient, 179–214 V/cm; gate widths, 0.2 ms; pressure, 726–734 Torr. Both carrier and drift gas were Linde high purity N_2, 99.996%.

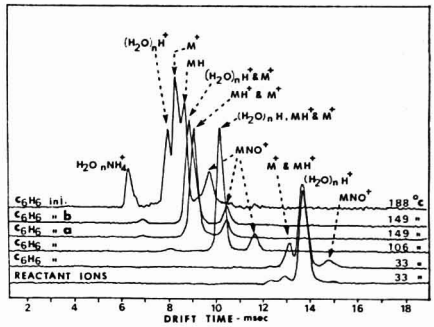


Figure 2. Ion mobility spectra of benzene at 33, 106, 149, and 188 °C (top). At 149 °C, trace (a) of the top figure shows the product ion spectrum of benzene immediately after injection and trace (b) shows product ion spectrum taken 2 min after injection

RESULTS AND DISCUSSION

Ion Mobility Behavior. The experimental reduced ion mobility K_o is calculated using Equation 1:

$$K_o = \frac{d}{tE} \times \frac{273}{T} \times \frac{P}{760}\ \text{cm}^2/\text{V·s} \qquad (1)$$

where d = drift length (cm), t = drift time (s), E = electric field gradient (V/cm), T = temperature (K), and P = pressure (Torr).

Although reduced mobility of single ions theoretically should be relatively insensitive to temperature (*13*), the reduced mobilities of reactant ions and low molecular weight ions (<100 amu) have been observed to increase as temperature increases (*12*). Benzene exhibits this type of behavior. The mobility spectrum of benzene shows two distinctive ion peaks: the most intense ion peak near the $(H_2O)_nH^+$ ion peak and with a K_o of 2.20–2.32 cm²/V·s and another of lower intensity with a K_o of 2.00–2.07 cm²/V·s which we have identified as MNO^+.

Figure 2 shows the changes in the ion mobility spectra of benzene with temperature. All ion identities were confirmed by PC/MS. At 33 °C, the ions M^+ and MH^+ with a K_o of 2.17–2.72 cm²/V·s have higher reduced mobility than $(H_2O)_nH^+$ ion with K_o of 2.12 cm²/V·s. At 106 °C, the M^+ and MH^+ and $(H_2O)_nH^+$ give overlapping peaks. At 149 °C, with a high sample concentration, M^+ and MH^+ at a K_o of 2.24–2.29 cm²/V·s remain overlapped as shown in trace (a) of Figure 2. As the concentration of the reactant ion $(H_2O)_nH^+$ recovers from depletion by reaction with the sample, the major peak shifts toward smaller drift time (higher mobility) with peak broadening. A temperature of 149 °C or higher allows separation of this ion mobility peak into two or three ions as traced in (b) of Figure 2. At 188 °C the two product ions M^+ and MH^+, and $(H_2O)_nH^+$ are clearly separated with K_o = 2.31 cm²/V·s for M^+, 2.27 cm²/V·s for MH^+ and 2.35 cm²/V·s for $(H_2O)_nH^+$ as shown in the top trace of Figure 2.

Figure 3 shows observed reduced mobilities of M^+, MH^+, and MNO^+ in the temperature range of 30 to 210 °C, together with the $(H_2O)_nH^+$ ion mobility. Mobilities were observed by PC and ion identities confirmed by PC/MS. The vertical range of the dotted line in the curve of Figure 3 indicates that even at a fixed temperature, these ions show a measurable variation of ion mobility in the range of ±0.03 cm²/V·s, depending on the measurement time.

Figure 4 shows the mass spectral scans obtained with both PC gates held open at 50, 93, and 207 °C. Several ions are observed at each of the temperatures used. Table I shows the

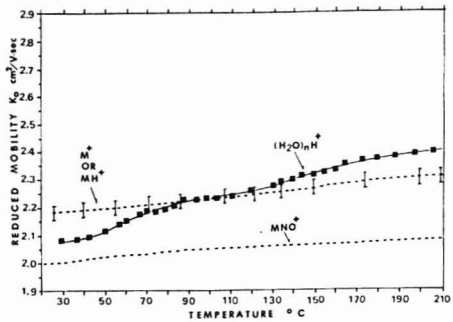


Figure 3. Observed mobilities vs. temperature for the product ions of benzene and $(H_2O)_nH^+$ reactant ions

Table I. PC/MS Spectral Data for Benzene

m/e	postulated ionic formula	rel. intensity	K_o (cm²/V·s)
	at 207 °C		
78	$(C_6H_6)^+$	31.3	2.32
79	$(C_6H_6)H^+$	100.0	2.27
108	$(C_6H_6)NO^+$	0.1	2.07
	at 93 °C		
51	unknown	12.3	2.20
69	unknown	60.4	2.23
78	$(C_6H_6)^+$	100.0	2.25
79	$(C_6H_6)H^+$	30.2	2.23
92	unknown	37.7	2.23
97	$[(C_6H_6)(H_2O)]H^+$	15.1	2.23
106	$[(C_6H_6)(N_2)]^+$	0.8	2.23?
107	$[(C_6H_6)(N_2)]H^+$	0.8	2.23?
108	$(C_6H_6)NO^+$	1.0	2.04
	at 50 °C		
78	$(C_6H_6)^+$	100.0	2.22
92	unknown	26.1	2.22
106	$[(C_6H_6)(N_2)]^+$	5.9	2.22
107	$[(C_6H_6)(N_2)]H^+$	5.8	2.22?
108	$(C_6H_6)NO^+$	8.0	2.00
120	$[(C_6H_6)(N_2)]N^+$	24.0	2.22?
125	$[(C_6H_6)(H_2O)(N_2)]H^+$	2.2	2.22?
134	$[(C_6H_6)(N_2)_2]^+$	4.2	2.22?

identities, relative ion intensities, and reduced mobilities for the ionic species observed. At 50 °C, two distinctive product ion peaks ($M^+ + MH^+$) and MNO^+, were observed. The ionic species identified by PC/MS have the same mobility, K_o = 2.22 cm²/V·s with the exception of MNO^+ with K_o = 2.00 cm²/V·s. The ion mobility peak at K_o = 2.22 cm²/V·s thus appears to be a mixture of ions composed of the molecular ion and several ion–molecule clusters. If the benzene molecules involved in each ionic species undergo rapid chemical exchange and the exchange rate is faster than 10^3 times/s, the resolution of these ions by PC is no longer possible. The average mass of the unresolved ion mobility peak is about 102 amu based on the intensity ratios found by the mass spectral data.

At 93 °C, a single MNO^+ ion of m/e 108 produces the ion-mobility peak at K_o = 2.04 cm²/V·s, while ions of m/e 51, 69, 78, 79, 92. 97, 106, and 107 are responsible for the ion mobility peak of K_o = 2.23–2.25 cm²/V·s. The average mass of the latter complex is 92 amu. The ions with m/e from 78 to 107 are similar to the ion–neutral molecule clusters that appear in the spectrum at 50 °C.

At 207 °C, ion–molecule clusters with N_2 or H_2O are no longer observable. Under these conditions, three ion mobility peaks are observed which correspond to three individual ions at unit mass resolution: M^+ at m/e 78, MH^+ at m/e 79, and MNO^+ at m/e 108.

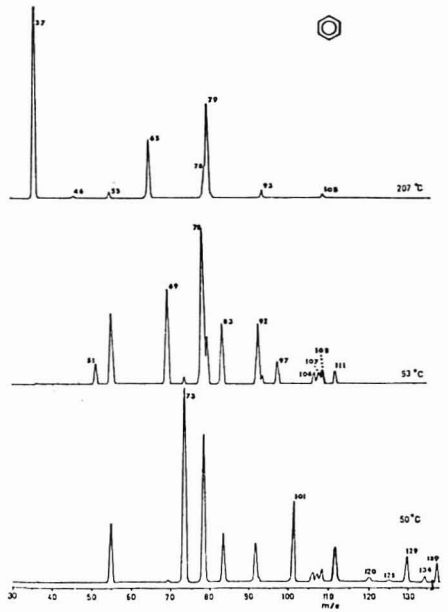


Figure 4. PC/MS mass scans for benzene with both PC gates open. Data obtained at 50, 93, and 207 °C, respectively

These data allow us to describe the temperature dependence of benzene in terms of ionic mass and size. The most complete theoretical ion mobility equation is the Mason–Schamp equation (*14*) shown in Equation 2:

$$K_o = \frac{3e}{16N}\left(\frac{1}{m}+\frac{1}{M}\right)^{1/2}\left(\frac{2\pi}{kT}\right)^{1/2}\left(\frac{1}{\pi r_m^{\,2}\Omega^{(1,1)*}}\right) \quad (2)$$

where e is electronic charge (esu), N is gas density (g/cm³), m is mass of the ion, M is the mass of the neutral gas, k is the Boltzmann constant, r_m is a measure of the closest approach of the ion and neutral molecule during binary collisions, and $\Omega^{(1,1)*}$ is the collision integral for the first approximation. Mason and Schamp tabulated $\Omega^{(1,1)*}$ values against T^* as a dimensionless temperature for values of up to the value γ = 0.50, where γ is the parameter for the relative strength of the 10^{-6} term in the 12–6–4 ion–molecule interaction potential equation (*14, 15*). Equation 2 shows that the direct dependence of the mobility of an ion upon molecular weight is via the reduced mass term $(1/m + 1/M)^{1/2}$ and the dependence upon the ionic size is expressed by the term $\pi r_m^{\,2}\,\Omega^{(1,1)*}$ in the denominator.

The combined factors of the mass increase and the accompanied size increase can be used to partially explain the temperature dependence of reduced mobility. If the mass of an ion, m, decreases because of reduced clustering, then the reduced mass term $(1/m + 1/M)^{1/2}$ in Equation 2 increases, causing a corresponding increase in K_o. Further, a smaller ionic radius associated with the decreasing mass would make the term for the collision cross-section, $\pi r_m^{\,2}\Omega^{(1,1)*}$, in Equation 2 smaller and again cause mobility to increase.

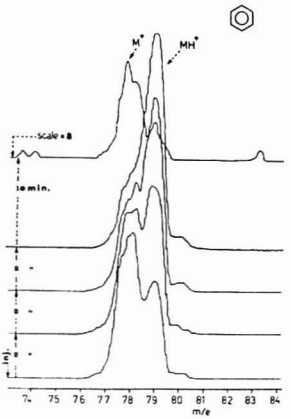


Figure 5. PC/MS mass spectra of benzene from 73–84 amu as a function of time

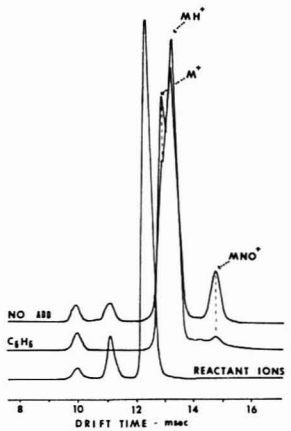


Figure 6. Ion mobility spectra of reactant ions and benzene at 207 °C. See text for discussion

Ion–Molecule Reactions. Benzene exhibits the major types of ion–molecule reactions in PC, including charge transfer, proton transfer, clustering with NO^+, and clustering with N_2 or H_2O molecules. MNO^+ does not appear to exhibit strong ion clustering with neutral molecules.

The concentration dependence of the PC of benzene is shown in the PC/MS data of Figure 5. At the high sample concentrations predominating 2 min after injection, the major species observed is M^+. After 4 min, the sample concentration in the ion–molecule reaction section decreases and reactant ion concentration gradually returns. This causes an increase in the observed concentration of MH^+ and a decrease in the intensity of M^+. The predominance of MH^+ increases until 8 min after injection. However, after 10 min, the relative intensities of M^+ and MH^+ alternate. This alternation may be responsible for the 0.03 $cm^2/V{\cdot}s$ variation of K_0 mentioned above.

The probable mechanism for formation of these ions can be explained by utilizing the established mechanism for formation of the terminal reactant ion $(H_2O)_nH^+$ in PC with a ^{63}Ni ionization source (*16*).

$$N_2 \xrightarrow{\beta^-} N_2^+ + 2e \quad (3)$$

$$N_2^+ + 2N_2 \rightarrow N_4^+ + N_2 \quad (4)$$

$$N_4^+ + H_2O \rightarrow H_2O^+ + 2N_2 \quad (5)$$

$$H_2O^+ + H_2O \rightarrow H_3O^+ + OH \quad (6)$$

$$H_3O^+ + H_2O + N_2 \rightleftarrows (H_2O)_2H^+ + N_2 \quad (7)$$

$$(H_2O)_{n-1}H^+ + H_2O + N_2 \rightleftarrows (H_2O)_nH^+ + N_2 \quad (8)$$

Reaction 3 represents the original ionization of the N_2 carrier gas by a β particle emitted by a ^{63}Ni source. Reaction 4 represents formation of N_4^+ by clustering of N_2^+ with N_2 (*16*). The IP of N_2 is 15.5 eV and the IP of H_2O is 12.9 eV (*17*). When benzene vapor (IP = 9.52 eV (18)) is introduced into the ionization source, it will compete with reactions 5 and 6:

$$N_4^+ + M \rightarrow M^+ + 2N_2 \quad (9)$$

$$H_2O^+ + M \rightarrow M^+ + H_2O \quad (10)$$

Thus, benzene initially undergoes charge transfer reactions to form M^+ ion with m/e 78 as shown in the first spectrum of Figure 5.

The results of injecting NO gas into the carrier gas flow are shown in Figure 6. The MNO^+ ion peak is increased as the concentration of NO^+ increases (*18*). This is due to the electrophilic addition of NO^+:

$$M + (H_2O)_nNO^+ \rightarrow MNO^+ + nH_2O \quad (11)$$

Four minutes after injection, the intensity of MH^+ ion (m/e = 79) increases and the M^+ ion intensity decreases. A possible explanation is that as the concentration of $(H_2O)_nH^+$ returns toward the original concentration, the proton transfer reaction to benzene dominates over the charge transfer reaction. This hypothesis is supported by the fact that the proton affinity (PA) of benzene is 14.5 kcal greater than that of H_2O (*19*). Therefore reaction 12 will occur to produce MH^+ ion:

$$M + (H_2O)_nH^+ \rightarrow MH^+ + nH_2O \quad (12)$$

Ten minutes after injection, the intensity of M^+ again increases above that of MH^+. This clearly indicates that the mechanisms given earlier are insufficient to completely explain the complex phenomena occurring in PC, and that further work is necessary to elucidate reaction mechanisms.

Benzene also appears to undergo a clustering reaction with neutral molecules of N_2 and H_2O to form clustered ions of the $M(N_2)_m(H_2O)_nH^+$ type (n, m = 0, 1, 2, ...):

$$M + xN_2 + (H_2O)_yH^+ \rightarrow [M(N_2)_m(H_2O)_n]H^+ + (x - m)N_2 + (y - n)H_2O \quad (13)$$

The type of binding existing in such ion–molecule clusters is not yet established. The energy involved in such clustering reactions is believed to be less than that for hydrogen bonding (*20*). The reactant ion $(H_2O)_nNH_4^+$ ion does not appear to undergo ion–molecule reactions with benzene, as is shown by the unchanged intensity of the ion peak shown in Figure 2.

At lower temperatures, an ion of m/e 92 was observed. Although this mass corresponds to that of $(C_6H_6)N^+$, it is difficult to postulate feasible reaction steps to account for its formation. It could be explained as the M^+ of a toluene trace impurity present.

The formation of ion–molecule clusters between benzene and neutral H_2O or N_2 molecules is responsible for the unusual temperature dependence in the PC of benzene. Ion mobility spectra obtained at lower temperatures are not representative of the true mobility of the benzene molecule or quasimolecular

ion. To obtain well resolved reference ion mobility data, a temperature of 180 to 220 °C should be utilized.

The MNO^+ ion observed in the plasma chromatography of benzene contains only a single m/e ion at any temperature and appears to be very stable. This ion may therefore be used as a characteristic product ion for benzene identification, particularly at low temperatures. Increased sensitivity may be achieved by the addition of NO to the carrier gas.

LITERATURE CITED

(1) F. W. Karasek, *Anal. Chem.*, **46**, 710A (1974).
(2) M. J. Cohen and F. W. Karasek, *J. Chromatogr. Sci.*, **8**, 330 (1970).
(3) F. W. Karasek, M. J. Cohen, and D. I. Carroll, *J. Chromatogr. Sci.*, **9**, 390 (1971).
(4) D. I. Carroll, I. Dzidic, R. N. Stillwell, and E. C. Horning, *Anal. Chem.*, **47**, 1956 (1975).
(5) F. W. Karasek, H. H. Hill, Jr., and S. H. Kim, *J. Chromatogr.*, **117**, 327 (1976).
(6) F. W. Karasek, S. H. Kim, and H. H. Hill, Jr., *Anal. Chem.*, **48**, 1133 (1976).
(7) T. W. Carr, *Anal. Chem.*, **49**, 828 (1977).
(8) T. W. Carr, *J. Chromatogr. Sci.*, **15**, 85 (1977).
(9) D. F. Hunt and T. M. Harvey, *Anal. Chem.*, **47**, 1965 (1975).
(10) D. F. Hunt and T. M. Harvey, *Anal. Chem.*, **47**, 2136 (1975).
(11) E. C. Horning, M. G. Horning, D. I. Carroll, I. Dzidic, and R. N. Stillwell, *Anal. Chem.*, **45**, 936 (1973).
(12) S. H. Kim, Ph.D. Thesis, Department of Chemistry, University of Waterloo, Waterloo, Ontario, 1977.
(13) E. W. McDaniel, V. Cermak, A. Dalgarno, E. E. Ferguson, and L. Friedman, "Ion-Molecule Reactions", Wiley-Interscience, New York, N.Y., 1970, p 66.
(14) E. A. Mason and H. W. Schamp, Jr., *Ann. Phys.*, **4**, 233 (1958).
(15) H. E. Revercomb and W. E. Mason, *Anal. Chem.*, **47**, 970 (1975).
(16) A. Good, D. A. Durden, and P. Kebarle, *J. Chem. Phys.*, **52**, 212 (1970).
(17) F. H. Field and J. L. Franklin, "Electron Impact Phenomena and the Properties of Gaseous Ions", Academic Press, New York, N.Y., 1970, pp 243–482.
(18) F. W. Karasek and D. W. Denney, *Anal. Chem.*, **46**, 633 (1974).
(19) P. Kebarle, R. Yamdagni, K. Hiraoka, and T. B. McMahome, *Int. J. Mass Spectrom. Ion Phys.*, **19**, 71 (1977).
(20) A. Good, *Chem. Rev.*, **75**, 561 (1974).

RECEIVED for review May 9, 1978. Accepted August 2, 1978.

Solvent Extraction–Spectrophotometric Determination of Boron with 2,4-Dinitro-1,8-naphthalenediol and Brilliant Green

Kiyoaki Kuwada, Shoji Motomizu, and Kyoji Tôei*

Department of Chemistry, Faculty of Science, Okayama University, Tsushima-naka, Okayama-shi, Japan

The highly sensitive and selective spectrophotometric method for boron was newly developed. Boric acid aqueous solution was evaporated to dryness in the presence of sodium acetate and mannitol, and boron reacted with 2,4-dinitro-1,8-naphthalenediol (DNNDO) in acetic acid medium to form a complex anion, which was extracted into toluene with brilliant green. The excess of brilliant green co-extracted into toluene was removed by washing the organic phase with 2 M hydrochloric acid. By measuring the absorbance of brilliant green in toluene at 637 nm, boron was determined. The calibration curve in toluene was linear in the range from 0 to 1×10^{-5} M of boron, and the molar absorptivity was 10.3×10^4 L mol^{-1} cm^{-1}. The absorbance of the reagent blank was 0.020 ± 0.002, and the reproducibility was very good. By the recommended procedure, about 0.5 ppb of boron in an aqueous solution can be determined. This method was applied for the determination of boron in natural waters.

The analytical chemistry of boron is very important in the fields of nuclear-reactor materials, industrial metallurgy materials, pharmacy, and agriculture. Furthermore, boron is one of a few common elements whose spectrophotometric determination must be developed. Several spectrophotometric methods for boron were reported up to date. Of these, the methods using the extraction of tetrafluoroborate with methylene blue (*1–3*) and the curcumin (*4–10*) are very sensitive and have been used for the determination of micro amounts of boron. In the former, though the reaction can be carried out in an aqueous solution, the hydrofluoric acid is necessary and a long time is consumed for the complete formation of tetrafluoroborate. Besides, the absorbance of the reagent blank is relatively large. The latter is probably the most sensitive of the reagents reported up to date and has often been used for the determination of boron since 1903 (*11*). In general, the methods using curcumin are very troublesome, involve many practical difficulties, and often require many precautions, though many improvements have been made. For such reasons, the sensitive, selective, and moreover simple method for determining micro amounts of boron is now expected to be developed.

The studies of the solvent extraction of the ion pairs formed between complex anions and large cations are very important in analytical chemistry. Of these extractions, the one with a cationic dye possessing a large molar absorptivity can be applied to the spectrophotometric determination of metals. Such a method possesses the possibility for development of a highly sensitive and selective method, in which the chelate reagent takes charge of the high selectivity and the cationic dye takes charge of the high sensitivity. The authors reported such extraction systems for the determination of neodymium with 5,7-dinitrooxine and Rhodamine B (*12*), iron with 4-chloro-2-nitrosophenol and Rhodamine B (*13–15*), and arsenic with 4-nitrocatechol and brilliant green (*16*).

In this paper, the authors report the very useful method for boron, in which boron reacts with 2,4-dinitro-1,8-naphthalenediol in acetic acid medium to form a complex anion, and subsequently this anion is extracted into toluene with brilliant green and the absorbance of the brilliant green in toluene is measured. The proposed method is very sensitive, selective, reproducible, and not troublesome, and the absorbance of the reagent blank is very small.

EXPERIMENTAL

Apparatus. The absorptiometric measurements were made on a Hitachi-Perkin-Elmer model 139 spectrophotometer and a Hitachi EPS-3T recording spectrophotometer in a glass cell of 10-mm path length. An Iwaki, Model V-S Type KM, shaker was

0003-2700/78/0350-1788$01.00/0 © 1978 American Chemical Society

used to shake the separatory funnel.

Reagents. *1,8-Naphthalenediol.* This was synthesized according to literature (*17, 18*). A mixture of 4 g of 1-naphthol-8-sulfonic acid sodium salt (Tokyo Kasei Co.), 18 g of potassium hydroxide, and 8 mL of water was fused slowly, with vigorous stirring, to 200–230 °C in a zirconium crucible. After fusion and cooling, the mixture was dissolved in 100 mL of 13% hydrochloric acid solution, and a few milliliters of concentrated hydrochloric acid was added to it, and it was diluted with water to 300 mL. After being boiled and filtered hot, it was cooled. The product precipitated was recrystallized from a mixture of benzene and ligroin (mp 143–145 °C, lit. (*17*) mp 140 °C).

2,4-Dinitro-1,8-naphthalenediol. This was synthesized according to the literature (*19*). To 4 g of 1,8-naphthalenediol, 10 mL of acetic anhydride and about 0.5 mL of pyridine were added. After warming on the water-bath for 10 min, water was added and the excess of acetic anhydride was hydrolyzed. The product precipitated (1,8-diacetoxynaphthalene) was recrystallized from acetic anhydride (crystalline: mp 152–154 °C). Six grams of the diacetoxynaphthalene recrystallized was slowly added to 30 mL of concentrated nitric acid, kept at 25–30 °C. The product was washed with water, dried on the steam-bath, and recrystallized from acetic acid (crystalline: mp 200 °C). A solution of 4 g of potassium hydroxide in 100 mL of methyl alcohol was boiled with 2 g of 2,4-dinitro-1-hydroxy-8-acetoxynaphthalene for 1 h. The alcohol was driven off and the dark red product was dissolved in boiling water and excess of hydrochloric acid was added. The product precipitated was recrystallized from dilute hydrochloric acid (crystalline: mp 180–182 °C, lit. (*19*): 180–182 °C).

2,4-Dinitro-1,8-naphthalenediol (DNNDO) Acetic Acid Solution. Recrystallized DNNDO, 0.064 g, was dissolved in glacial acetic acid to give a 100-mL of solution (2.5×10^{-3} M). This solution was used for at least 10 days.

Cationic Dye Solution. Cationic dye was dissolved in deionized water to give a 1×10^{-3} M solution.

Standard Boron Solution. Boric acid (H_3BO_3), 0.618 g, was dissolved in deionized water to give a 100-mL solution (1.000×10^{-2} M). This solution was stocked in a polyethylene bottle and used after accurate dilution.

Sodium Acetate Solution. Sodium acetate ($CH_3COONa{\cdot}3H_2O$), 0.136 g, was dissolved in deionized water or glacial acetic acid to give a 100-mL solution (1×10^{-2} M). This solution was stocked in a polyethylene bottle.

Mannitol Solution. Mannitol, 0.016 g, was dissolved in deionized water to give a 100-mL solution (1×10^{-3} M). This solution was stocked in a polyethylene bottle.

Commercially available acetic acid contains less than 0.5% of water and was used without further purification.

All reagents used were of analytical-reagent grade.

Procedure. From the results examined in this work, the following procedure is most recommended as the standard procedure.

Standard Procedure. Transfer the sample solution containing boron up to 0.5 μg into a porcelain or platinum evaporating dish, and add 1 mL each of mannitol (1×10^{-3} M) and sodium acetate (1×10^{-2} M) solutions and, if necessary, adjust the pH with sodium hydroxide or hydrochloric acid to 3–11. Evaporate to dryness on the water-bath. Add 3 mL of glacial acetic acid and 1.5 mL of DNNDO acetic acid solution (2.5×10^{-3} M) and allow it to stand for more than 1 h. Transfer this acetic acid solution into a separatory funnel, wash the dish with water, and pour into the separatory funnel. Add 1 mL of 1 N sodium hydroxide solution and dilute it to about 30 mL with water (the pH is adjusted to 2.5 to 3.5). Add 0.5 mL of a brilliant green solution (1×10^{-3} M) and 5 mL of toluene. After shaking it for 10 min, discard the aqueous phase. Add 10 mL of 2 N hydrochloric acid solution and shake for 10 min. Measure the absorbance in toluene at 637 nm in a glass cell of 10-mm path length.

Pre-experiments. Reaction of Boric Acid with Some Reagents. In general, boric acid reacts with anthraquinones possessing hydroxyl group in the peri position (*20, 21*), aliphatic 1,3-diols (*22*), and catechols (*23*) to form six- or five-membered rings. Boric acid also reacts with chromotropic acid (1,8-dihydroxynaphthalene-3,6-disulfonic acid) (*24–26*) in aqueous solution at pH 3–5. 1,8-Dihydroxynaphthalene and DNNDO, though these are very similar to chromotropic acid, did not react with boric acid in aqueous solution at room temperature or even at higher temperature. When the mixture of boric acid and DNNDO solutions was evaporated to dryness at pH 3.5 to 4.5 (initial pH), the boron complex was formed and extracted into toluene with brilliant green. The absorbance of the reagent blank, however, was large and what is worse, the reproducibility was very low. This is because the reagent and the complex formed are unstable at the higher temperature. The other nine reagents such as 1,8-dihydroxynaphthalene, 2,6-dihydroxybenzoic acid, 5-nitrosalicylic acid, 3,5-dinitrocatechol, 4,5-dichlorocatechol, 3,5-dinitrosalicylic acid, 5-chlorosalicylic acid, saligenine, and pyrocatechol were examined at room and higher temperature. Of these reagents, 2,6-dihydroxybenzoic acid reacted with boric acid at room temperature and the ion-pair was extracted into toluene, and the reproducibility was the highest of the reagents examined. The molar absorptivity was smaller than that expected and was 4.3×10^4 L mol^{-1} cm^{-1} and the absorbance of the reagent blank was relatively large (about 0.3) with malachite green. Even when the mixture of boric acid and 2,6-dihydroxybenzoic acid was evaporated to dryness and the complex formed was extracted into toluene with malachite green, the molar absorptivity was about 8×10^4 L mol^{-1} cm^{-1}.

It was found that boric acid reacted with DNNDO in glacial acetic acid and less than 2% (v/v) of water did not interfere with the complex formation, and the salt such as sodium acetate was necessary to complete the reaction with DNNDO. Thus, boric acid aqueous solution (1×10^{-3} M) was diluted with glacial acetic acid to give a 1×10^{-5} M or less solution. To 3 mL of this boric acid–acetic acid solution, 1.5 mL of DNNDO acetic acid solution and 1 mL of sodium acetate acetic acid solution (10^{-2} M) were added. After standing for 1 h, the boron complex was extracted into toluene according to the standard procedure. The calibration curve was linear at the range of $0–1 \times 10^{-5}$ M boric acid and the molar absorptivity calculated from the slope was 10.6×10^4 L mol^{-1} cm^{-1}. When the sodium acetate was not added, about 80% of the boron was reacted with DNNDO. Of the other nine reagents, 1,8-dihydroxynaphthalene reacts with boric acid. In this reagent, however, the reproducibility was very low because a substance insoluble both in aqueous and organic phase was produced on extraction. For these reasons, the complex formation of boric acid with DNNDO was carried out in an acetic acid medium in the presence of a salt such as acetate.

RESULTS AND DISCUSSION

Contamination from Water, Reagents, and Vessels. Contamination from water was examined by using five kinds of waters: (1) type 2 water was treated with anion-exchange resin (Dowex 21K(SBR-P), -OH type), by passing through a glass column (20 cm in length and 2 cm in diameter), (2) water deionized with ordinary apparatus and distilled with distilling apparatus of Pyrex glass commercially available, (3) water deionized and distilled with distilling apparatus of copper, (4) type 5 was treated with anion-exchange resin, and (5) deionized water. The contamination from these waters was checked according to the standard procedure. Water type 2 showed relatively large absorbance increase as the sample taken increased. When 0, 10, and 30 mL of water 2 were used, the absorbances were 0.020, 0.068, and 0.142, respectively. When 10 and 30 mL of water 3 were used, the absorbances were 0.027 and 0.036, respectively, and when 10 and 30 mL of water 4 were used, the absorbances were 0.034 and 0.039, respectively, and when 10 and 30 mL of water 5 were used, the absorbances were 0.036 and 0.040, respectively. When 10 and 40 mL of water 1 were used, the absorbances were 0.020 and 0.026, respectively: that is, the absorbance is the smallest of the five. From these results, water which is deionized, distilled, and treated with anion-exchange resin is the best of all, and must be used when the calibration curve is prepared.

Contamination from vessels of glass and of polyethylene was examined. In the same kinds of vessel which are made of the same material and by the same manufacturer, the solutions which pHs are various from 6.5 to 11.5 were transferred and a 5-mL portion of the solution was pipetted

into a platinum dish and the contamination was checked according to the standard procedure. The contamination from glass vessels was very large and the more alkaline the solution was and the longer the solution stayed in the vessel, the larger the contamination was. For example, when the aqueous solutions of pH 8.5 and 11.5 remained in a new volumetric flask for three days, the absorbance increases were 0.028 and 1.423, respectively. Contamination from the polyethylene bottle was very small even when the solution was strongly alkaline. For example, even when the solution of pH 11.5 remained in a new 100-mL polyethylene bottle for 13 days, the absorbance increase was 0.010. Contamination from the evaporating vessel was examined on evaporating to dryness. As evaporating vessels, porcelain and platinum dishes, glass beakers (Pyrex and standard glass beakers, 50 mL), Teflon beakers (50 mL), zirconium crucible (50 mL) and nickel crucible (50 mL) were checked. Deionized water, 10 mL, was transferred into each vessel and contamination from the evaporating vessels was examined according to the standard procedure. As a result of the examination, it was concluded that platinum and porcelain dishes showed the smallest absorbance, their dispersion was very small, and there was no difference between porcelain and platinum dishes: that is, the absorbance was 0.020 ± 0.002 (five determinations). Teflon beakers and zirconium crucibles also showed small absorbances (0.024 ± 0.004 and 0.028, respectively). The former, however, is not recommended because of more time consumed for evaporation and it is more expensive than porcelain dishes. Other vessels (glass beakers and nickel crucibles) showed large absorbances and, what is worse, the reproducibility was very bad. For these reasons, the porcelain dish is the most useful of the vessels examined, because it is very cheap and has large thermal conduction. In this work, the authors used the porcelain dish with diameter and volume of about 80 mm and 80 mL, respectively. Though the porcelain dish is very useful, never use it when the solution is very alkaline: the absorbance was too large to be measured when about 0.1 N sodium hydroxide solution was evaporated to dryness in a new porcelain dish.

Contamination from reagents used in this procedure seems to be very small: that is, the absorbance of the reagent blank is 0.02 to 0.03 and only small parts of the absorbance of the reagent blank seem to be caused by reagents. In this work, the reagents were used without purification.

Evaporation of the Sample Solution to Dryness. In the curcumin method (*10*), evaporation is carried out in the presence of sodium hydroxide, and the reaction with curcumin is carried out in the mixture of acetic acid and sulfuric acid. The authors also examined evaporation in the presence of sodium hydroxide in place of mannitol and sodium acetate in platinum dishes, and the boron was reacted in the mixture of acetic and sulfuric acids with DNNDO. Though the reaction of boron with DNNDO proceeded almost to completion, the amounts of sulfuric acid must be controlled very severely according to the amounts of sodium hydroxide used and, what is worse, the reproducibility was bad. Thus, another method for prevention of volatilization of boron was examined. In general, boron does not volatize more in the alkaline solution than in the neutral or acidic solutions, and boric acid reacts in the aqueous solution easily with mannitol. So, the effects of mannitol and alkalies which are not so strong as sodium hydroxide were examined. When, in the absence of mannitol and sodium acetate, 10 mL of boric acid aqueous solution (boron: 0.324 μg) was evaporated to dryness, only about 8% boron remained in the dish. When in the presence of 1 mL of mannitol (10^{-3} M) 10 mL of the solution was evaporated, 88% boron remained in the dish, and when in the presence of 1 mL of sodium acetate (10^{-2} M) 10 mL of solution was evaporated, 90% of the boron remained in the dish. When in the presence of 1 mL of mannitol and sodium acetate, 10 mL of the solution was evaporated, the loss of boron was very small and constant. As a result of this examination, both mannitol and sodium acetate must be added to the sample solution before evaporation. It must be noted that sodium acetate is necessary not only to prevent the boron from volatilization, but also to complete the reaction with DNNDO.

The effect of alkaline substances as well as neutral and acidic substances (Na_2CO_3, $NaHCO_3$, KH_2PO_4, Na_2HPO_4, NaCl, $NaHSO_4$, Na_2SO_4, NH_4Cl) was examined. Of these salts, the salts of weak acids such as carbonate and phosphate are very effective, and when 1 mL of 10^{-2} M solution of CH_3COONa, Na_2CO_3, $NaHCO_3$, and Na_2HPO_4 was used, the absorbances obtained according to the standard procedure (boron: 0.324 μg) were 0.638, 0.629, 0.629, and 0.638, respectively, and the absorbances of the reagent blank were 0.016 to 0.020. Unexpectedly, the salts of strong acids such as chloride and sulfate are also effective, though their effect is smaller than acetate: that is, when 1 mL of 10^{-2} M solution of NaCl, $NaHSO_4$, Na_2SO_4, and NH_4Cl were used in place of sodium acetate, the absorbances obtained according to the standard procedure (boron: 0.324 μg) were 0.506, 0.272, 0.588, and 0.547, respectively.

When only the amounts of sodium acetate were varied in the standard procedure, the largest and most constant absorbances were obtained in the range of 0.2 to 6.0 mL of sodium acetate (1×10^{-2} M) added to 10 mL of sample solution. In the case of disodium hydrogen phosphate, the optimal amounts added to 10 mL of sample solution were 0.2 to 1.0 mL of 1×10^{-2} M solution.

The effect of pH on the evaporation of the sample solution was examined for sodium acetate and disodium hydrogen phosphate. The pHs were adjusted with hydrochloric acid and sodium hydroxide solutions after adding 1 mL of sodium acetate (1×10^{-2} M) or 0.6 mL of disodium hydrogen phosphate (1×10^{-2} M) to 10 mL of sample solution. The optimal pH regions both in acetate and phosphate were very wide and were pH 3 to 12 and 4 to 10, respectively. Phosphate reacts easily with metal ions such as iron and alkaline earth metal ions to give a complex or precipitate. In fact, calcium ions which amount was one hundred-fold of boron interfered with the boron determination. In these results, acetate is the most useful in the practical analysis and the most effective of all salts examined.

The effect of the amounts of mannitol was examined by varying only the amounts of mannitol added in the standard procedure. When 0.6 to 2.0 mL of mannitol solution (1×10^{-3} M) was added to 10 mL of sample solution, the absorbances obtained were maximum and constant. When mannitol solution below 0.6 mL or above 2.0 mL was added, the absorbances decreased gradually.

The effect of the volume of sample solution was examined by varying the volume from 5 to 45 mL according to the standard procedure. But no effect of the volume was observed.

The volatilization of boron in evaporation was examined in detail. Fifteen milliliters of boric acid solution were transferred into a porcelain dish. When the sample solution was evaporated and concentrated to 10, 5, 3, and 1 mL, 1 mL of mannitol solution and 1 mL of sodium acetate solution were added to the concentrated sample solution, and again the solution was heated and evaporated to dryness. It was found that volatilization of boron did not occur until the volume reached about 5 mL.

Reaction of Boron with DNNDO in Acetic Acid Medium. Boron reacts with DNNDO in acetic acid medium even in the presence of mannitol. Mannitol is very effective not only in prevention of loss of boron on evaporation, but

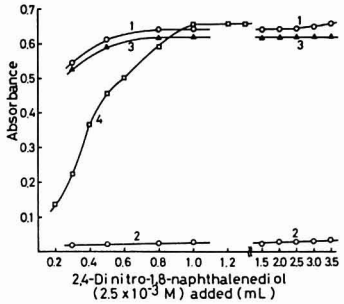


Figure 1. Effect of DNNDO on the complex formation in acetic acid medium. Boron(III): 0.324 μg. (1), (2), and (3): in the presence of mannitol, (4): in the absence of mannitol, (1) and (4): sample (ref: toluene), (2): reagent blank (ref: toluene), (3): net (ref: reagent blank)

Table I. Molar Absorptivities (ε) of Ion Pairs Extracted into Toluene

cationic dye	washing solution, HCl, N	λ_{max}	ε(× 10^4 L mol^{-1} cm^{-1})
malachite green	2.0	636	9.5
brilliant green	2.0	637	10.3
crystal violet	1.5	605	9.5
Rhodamine B	4.0	569	9.5
Rhodamine 6G	5.0	536	8.3

also in the formation of the boron complex with DNNDO as shown in Figure 1, which was obtained by mixing the boron, sodium acetate, and DNNDO acetic acid solutions in the absence of mannitol, and by evaporating the sample solution in the presence of mannitol and sodium acetate and reacting with DNNDO. In the presence of mannitol, the amounts of DNNDO necessary to complete the reaction were smaller than the amounts in the absence of mannitol. This is probably because mannitol is an auxiliary complexing agent and helps the formation of the boron–DNNDO complex.

The effect of time on the complex formation in acetic acid medium was examined. The constant and maximum absorbance was obtained 50 min after adding DNNDO solution at 20 °C, and the complex formed was stable at least one day. When the solution was heated on the water bath for only 5 min, the complex formation was almost completed. The absorbances, however, varied a little widely. This is probably because a part of DNNDO or complex will decompose. In this work, the mixture stood for more than 60 min at room temperature.

The effect of amounts of total glacial acetic acid on the formation of the boron complex was examined by varying the volume from 1 to 6 mL. The constant and maximum absorbance was obtained in a volume above 3 mL.

Extraction of Boron–DNNDO Complex with Cationic Dye and Washing the Organic Phase. Four kinds of cationic dye as well as brilliant green were examined. As shown in Table I, brilliant green shows the largest molar absorptivity of the five. Brilliant green shows the maximum and constant absorbance at the amounts from 0.1 mL to 1 mL of 1×10^{-3} M aqueous solution. The optimal pH region in the extraction was 1 to 4, but the emulsion sometimes forms in shaking near pH 2. Therefore, the extraction was carried out at pH 2.5–3.5.

Washing the organic phase after extracting the ion pair and discarding the aqueous phase is necessary to remove the large excess of dye co-extracted into toluene. This removal was

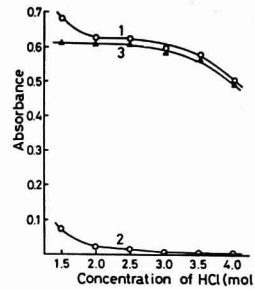


Figure 2. Effect of acid concentration on the back-washing. Boron(III): 0.324 μg. (1): sample (ref: toluene), (2): reagent blank (ref: toluene), (3): net (ref: reagent blank)

Table II. Effect of Co-existing Ions[d]

ion	added, mg[a]	added as	absorbance[b]
none			0.638
Na^+	11[c]	NaCl	0.638
K^+	2[c]	KCl	0.638
Ca^{2+}	2×10^{-1}	$CaCl_2$	0.638
Mg^{2+}	1.2×10^{-1}	$MgCl_2$	0.629
Ba^{2+}	6.8×10^{-1}	$BaCl_2$	0.635
Cu^{2+}	3.2×10^{-2} [c]	$CuSO_4$	0.638
Zn^{2+}	1.6×10^{-1} [c]	$ZnSO_4$	0.638
Cd^{2+}	5.6×10^{-2} [c]	$Cd(NO_3)_2$	0.648
Mn^{2+}	2.7×10^{-2} [c]	$MnCl_2$	0.648
Co^{2+}	2.9×10^{-2} [c]	$Co(NO_3)_2$	0.642
Ni^{2+}	2.9×10^{-2} [c]	$Ni(NO_3)_2$	0.638
Pb^{2+}	1×10^{-1} [c]	$PbCl_2$	0.648
Hg^{2+}	1×10^{-1} [c]	$HgCl_2$	0.648
Fe^{3+}	8.4×10^{-2}	$Fe(NO_3)_3$	0.635
Al^{3+}	1.4×10^{-2}	$Al(NO_3)_3$	0.642
As(III)	3.8×10^{-2} [c]	As_2O_3	0.635
As(V)	3.8×10^{-2} [c]	Na_2HAsO_4	0.635
Sb^{3+}	6.1×10^{-2} [c]	$SbCl_3$	0.633
Cl^-	18[c]	NaCl	0.638
Br^-	4[c]	NaBr	0.652
I^-	6.3×10^{-2}	KI	0.646
F^-	4×10^{-3}	KF	0.623
NO_3^-	3.1×10^{-2} [c]	$NaNO_3$	0.638
SO_4^{2-}	4.8[c]	Na_2SO_4	0.638
PO_4^{3-}	1.1[c]	Na_2HPO_4	0.642
SiO_3^{2-}	1.9×10^{-1} [c]	Na_2SiO_3	0.638

[a] Maximum tolerance concentration. [b] Reference: toluene. [c] Maximum tested. [d] Boron: 0.324 μg. Total initial volume of aqueous solution: 12 mL.

carried out effectively by washing the organic phase with hydrochloric acid solution as shown in Figure 2. The optimal concentration of the hydrochloric acid is 2 to 2.5 N, at which the reagent blank is very small and constant and the absorbance of the complex is maximum and constant.

Both in extraction and washing, shaking for 5 min was enough to complete the extraction and removal. The ion pair extracted into toluene was very stable and the absorbance of the organic phase did not vary for at least 4 days.

Absorption Spectra and Calibration Curve. The absorption spectra of the ion pair formed between boron complex and brilliant green in toluene obtained by the standard procedure are shown in Figure 3. The maximum absorbance of the ion pair is at 637 nm, where the absorbance of the reagent blank is very small. The calibration curve obtained by the standard procedure was linear in the range from 0 to 0.5 μg of boron and the molar absorptivity calculated from the slope of the curve was 10.3×10^4 L mol^{-1} cm^{-1}. The curve obtained by using the boric acid–acetic acid solution without evaporation also was linear and the molar absorptivity was

Table III. Determination of Boron in River and Seawater and Recovery of Boron

		recovery test				
sample[a]	boron, ppb	boron in sample soln. taken, ng	boron added, ng	found, ng	recovery, ng	boron added, %
River water[b]	8.7	87	216	289	202	95.4
River water[c]	11.6	116	216	327	211	98.5
River water[d]	8.8	88	216	305	217	100.3
River water[e]	10.2	102	216	317	215	99.7
Seawater[f]	4300	215	108	325	110	100.6
Seawater[g]	4400	220	108	324	104	98.8

[a] 10 mL of river water was taken and seawater was diluted to one hundred-fold, and 5 mL of the diluted sea water was taken. [b] Asahi River, Okayama Prefecture, Japan. [c] Asahi River. Samples *b* and *c* were sampled at different places. [d] Takahashi River, Okayama Prefecture. [e] Yoshii River, Okayama Prefecture. [f] Seashore at Tanohama, Ehime Prefecture, Japan. [g] Seashore at Uno, Okayama Prefecture.

Table IV. Comparison of Some Spectrophotometric Methods

method	wavelength, nm	ϵ($\times 10^4$ L mol^{-1} cm^{-1})	absorbance of reagent blank	absorbance[a] (per 0.1 μg B)	lit.
chromotropic acid (extraction)	351	1.4	0.098	0.026	(*26*)
BF_4^-–methylene blue (extraction)	660	8.3	0.124	0.077	(*3*)
curcumin–oxalic acid (in ethanol soln)	550	9.6	0.040	0.044	(*9*)
curcumin (extraction)	555	17.0	0.750	0.157	(*10*)
curcumin (in ethanol soln)	550	16.2	0.060	0.059	(*7*)
this method	637	10.3	0.020	0.187	

[a] These were calculated from absorbance data obtained by each method.

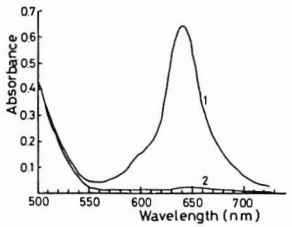


Figure 3. Absorption spectra in toluene. Boron(III): 0.324 μg. (1): sample (ref: toluene), (2): reagent blank (ref: toluene)

10.6×10^4 L mol^{-1} cm^{-1}, which is a little larger than that obtained by the standard procedure.

Effect of Co-existing Ions. The effect of co-existing ions was examined by the standard procedure and the results obtained are shown in Table II, from which it can be seen that alkali and alkaline earth metals, and transition metals, arsenic, and antimony do not interfere with the determination of boron even at the amounts of one thousand-fold, and one hundred-fold of boron, respectively. Of the common anions, fluoride ion at amounts more than tenfold of boron gives rise to negative errors because fluoride reacts with boron to form tetrafluoroborate.

Application to the Determination of Boron in Natural Waters. The amounts of co-existing ions generally existing in river and seawaters are much smaller than those listed in Table II.

Ten milliliters of river water, and 5 mL of seawater which was diluted with water to one hundred-fold were transferred into a porcelain dish and the boron was determined by the standard procedure. The results obtained are shown in Table III. The recovery tests of the boron were also carried out by adding known amounts of boron (as the boric acid) and determining the boron according to the standard procedure. The results are also shown in Table III. The recoveries of boron are good and are 95.4 to 100.6%.

CONCLUSION

In Table IV, this new method is compared with other methods, particularly in point of actual sensitivity calculated from the absorbance data obtained according to the procedure. Of these, the method proposed in this work shows the largest absorbance per 0.1 μg of boron. This new method seems to be much more useful and general in a practical analysis for boron than other spectrophotometric methods reported up to date in the following advantages: (1) high sensitivity and high selectivity for boron, (2) relatively more simple and less time-consuming procedure, (3) procedure using common apparatus and vessels, especially evaporation of the sample solution is carried out in the cheap porcelain dish, (4) good reproducibility of determination of boron, and (5) very small absorbance of the reagent blank.

LITERATURE CITED

(1) L. Ducret, *Anal. Chim. Acta*, **17**, 213 (1957).
(2) L. Pasztor and J. D. Bode, *Anal. Chem.*, **32**, 277 (1960).
(3) S. Utsumi, S. Ito, and A. Isozaki, *Nippon Kagaku Zasshi*, **86**, 921 (1965).
(4) J. A. Naftel, *Ind. Eng. Chem., Anal. Ed.*, **11**, 407 (1939).
(5) L. Silverman and K. Trego, *Anal. Chem.*, **25**, 1264 (1953).
(6) G. S. Spicer and J. D. H. Strickland, *Anal. Chim. Acta*, **18**, 231 (1958).
(7) M. R. Hayes and J. Metcalfe, *Analyst (London)*, **87**, 956 (1962).
(8) L. R. Uppström, *Anal. Chim. Acta*, **43**, 475 (1968).
(9) M. Miyamoto, *Bunseki Kagaku*, **11**, 635 (1962).
(10) H. Gotô, Y. Kakita, and K. Takada, *Bunseki Kagaku*, **18**, 52 (1969).
(11) C. E. Cassal and H. Gerrans, *Chem. News*, **87**, 27 (1903).
(12) K. Tôei and K. Nakato, *Nippon Kagaku Zasshi*, **92**, 731 (1971).
(13) T. Korenaga, S. Motomizu, and K. Tôei, *Anal. Chim. Acta*, **65**, 335 (1973).
(14) T. Korenaga, S. Motomizu, and K. Tôei, *Talanta*, **21**, 645 (1974).
(15) K. Tôei, S. Motomizu, and T. Korenaga, *Analyst (London)*, **101**, 974 (1976).
(16) K. Kuwada, S. Motomizu, and K. Tôei, *Bunseki Kagaku*, **26**, 609 (1977).
(17) H. Erdmann, *Ann.*, **247**, 356 (1888).
(18) A. P. Lurie, G. H. Brown, J. R. Thirtle, and A. Weissberger, *J. Am. Chem. Soc.*, **83**, 5015 (1961).
(19) F. Calvet and M. C. Carnero, *J. Chem. Soc.*, **1936**, 556.
(20) I. M. Korenman, *Zh. Anal. Khim.*, **2**, 135 (1947).
(21) K. Emi, K. Tôei, and K. Harada, *Nippon Kagaku Zasshi*, **78**, 1299 (1957).
(22) B. Egneus and L. Uppström, *Anal. Chim. Acta*, **66**, 211 (1973).
(23) E. J. Hakoila, J. J. Kankare, and T. Skarp, *Anal. Chem.*, **44**, 1857 (1972).
(24) D. F. Kuemmel and M. G. Mellon, *Anal. Chem.*, **29**, 378 (1957).
(25) J. Lapid, S. Farhi, and Y. Koresh, *Anal. Lett.*, **9**, 355 (1976).
(26) T. Korenaga, S. Motomizu, and K. Tôei, *Analyst (London)*, **103**, 745 (1978).

RECEIVED for review June 14, 1978. Accepted August 7, 1978.

Spectrophotometric Determination of Trace Sulfate in Water

Purnendu K. Dasgupta, Lionel G. Hanley Jr., and Philip W. West*

Environmental Sciences Institute, Chemistry Department, Louisiana State University, Baton Rouge, Louisiana 70803

Determination of trace levels of sulfate in water samples is described. The method relies upon the formation of insoluble 2-perimidinylammonium sulfate, $(PDA)_2SO_4$, by reaction of the sulfate ion with 2-perimidinylammonium bromide on a glass fiber substrate. The excess bromide is removed by frontal elution chromatography with methanol and the remaining organic amine, bound as the sulfate salt, is converted to highly colored 2-amino-4,6,9-trinitroperimidine by treatment with concentrated nitric acid. The colored compound may be monitored in acidic solution at 420 nm or in basic solution at 550 nm. No pretreatment is required and for a 100-μL aliquot the sensitivity is 1 ppm and the working range is 2–500 ppm sulfate. There are no known cationic interferences and, among anions likely to be present, only oxalate and phosphate interfere.

The determination of sulfate ion at trace levels is one of the most widely studied problems in analytical chemistry. A detailed account of the two centuries of scientific investigation devoted to this end is now available (*1*). Stephen (*2*) introduced 2-aminoperimidine (in the form of the hydrochloride salt) as a sulfate precipitant. 2-Perimidinylammonium sulfate, $(PDA)_2SO_4$, is second only to barium sulfate in insolubility (20 mg/L at 18 °C). An automated version of Stephen's nephelometric method has since been developed (*3*) and, in an alternative approach, after filtering off the organic sulfate, remaining excess of accurately added precipitant has been determined by UV absorptiometry (*4*, *5*). Work done in this laboratory (*6*), however, revealed that the data obtained by this method for most field samples are substantially higher than those obtained by the gravimetric barium sulfate procedure which is the accepted reference method (*7*) or a standard turbidimetric barium sulfate method (*8*). The high results are caused by simultaneous precipitation of other anions, notably bicarbonate.

Maddalone et al. (*9*) discovered that pyrolysis of the precipitated $(PDA)_2SO_4$ results in the quantitative formation of SO_2 which could then be determined by the West–Gaeke method or by means of the flame photometric detector. This principle was adopted and optimized by Thoma et al. (*6*) for aqueous sulfate determinations. Based on a new reaction, we report here a new spectrophotometric procedure that is fast, sensitive, requires no sample pretreatment, and does not involve pyrolysis.

EXPERIMENTAL

Reagents. 2-Perimidinylammonium bromide (1%). The reagent was synthesized and purified according to Dasgupta et al. (*10*). One hundred milligrams of this reagent were dissolved in 10 mL of warm methanol and stored in a dark bottle. Addition of a small amount (~1 mg) of *tert*-butyl hydroxy toluene (BHT) lengthened the shelf life of the reagent to several months.

All other reagents used were of analytical reagent grade.

The preparation of standard sulfate solutions and standard solutions of other anions has been described (*6*).

Apparatus. A Beckman DB spectrophotometer with a 1-cm path length cell was used. Gelman spectrograde A glass fiber filters were cut in 18 mm × 72 mm wide strips. Fifty such strips were cleaned in a batch by boiling them for 4 h in a mixture of 50% ethanol, 20% HCl, and 30% water (v/v). The solvent was then decanted and the strips washed thrice with 50-mL portions of ethanol and twice with 50-mL portions of acetone and then oven-dried at 80 °C. Teflon-tipped stainless steel forceps were used throughout to handle these strips.

Procedure. A precleaned glass fiber strip was placed on a Teflon block having a 13-mm diameter annular opening. The bottom of the strip was ~20 mm from the center of the aperture (a guide mark was inscribed on the block to facilitate positioning, see Figure 1) and covered with another identical block to hold it in place. Fifty μL (one drop) of the PDA-Br solution was added from a Pasteur pipet to the strip at the center of the aperture followed by the sample aliquot. Another 50 μL of PDA-Br solution was next added to the same spot. The strip was then removed and dried (~3 min) in a stream of filtered cold air.

Methanol was placed in a 250-mL tall form Griffin beaker, to a depth not exceeding 5 mm. Up to five strips were then lowered in the solvent and allowed to remain in the beaker for a period of 10 to 15 min during which time the methanol moved up the strip thus removing the unreacted PDA-Br.

The strips were removed from the beaker, placed on the Teflon block, and the injection spot was cut away with a stainless steel filter cutter. The sample circle was then placed in a funnel resting on a 10-mL volumetric flask. Methanol was allowed to evaporate from the circle until it was just moist. Six drops (~300 μL) of concentrated nitric acid were added from a Pasteur pipet to the circle, distributing it as evenly as possible. The material on the filter was then allowed to react for approximately 1 min.

Measurement was carried out according to either one of the following procedures.

Measurement in Acidic Solution. The colored product on the circle was washed into the flask with 2 mL concd HNO_3 from an automatic pipet. One mL was added at a time, slowly, to facilitate the removal of all the colored material. The solution was then made up to the mark with distilled deionized water, mixed thoroughly, and filtered through glass wool into the measuring cuvette. The filtration step was necessary to remove fibrous material that unavoidably resulted from the substrate. Absorbance was measured at 420 nm against water as reference and the amount of sulfate was calculated from the calibration plot.

Measurement in Basic Solution. The colored product was washed into the flask with 1 mL of acetone using the technique described above. Two mL of 4 N NaOH was next added and the solution made up to the mark with distilled deionized water. The solution was filtered into the cuvette and the absorbance was measured at 550 nm.

RESULTS AND DISCUSSIONS

Sulfate ion was liberated and 2-amino-4,6,9-trinitroperimidine was formed when nitric acid reacted with $(PDA)_2SO_4$ under the conditions described (Figure 2). Details of structural determination of this and related compounds will be published elsewhere (*11*). Calibration plots for both acidic and basic solutions were perfectly linear within the range studied (0–50 μg sulfate) and therefore are not shown. The absorbance obtained in acidic solution is 0.021 absorbance unit/μg sulfate put on the filter, while measurement in basic solution increased the sensitivity by 30% to 0.028 absorbance unit/μg sulfate put on the filter. All data were obtained in sets of five and representative standard deviations are shown in Table I. The limit of detection, normally defined to be 2.5 times the standard deviation of the blank, is hard to define in this case because the absorbance of the blank was uniformly

0003-2700/78/0350-1793$01.00/0 © 1978 American Chemical Society

Table I. Precision of the Aqueous Sulfate Determination Method

amount of sulfate on filter, μg	measurement in acid: mean absorbance	acid: range	acid: % standard deviation	measurement in base: mean absorbance	base: range	base: % standard deviation
0.56	0.011	0.010	14.8	0.015	0.011	11.8
1.39	0.029	0.013	8.3	0.038	0.018	8.4
3.46	0.070	0.019	4.6	0.097	0.027	4.4
8.67	0.182	0.048	4.3	0.243	0.044	2.8
10.0	0.211	0.030	2.4	0.280	0.052	3.1
21.7	0.457	0.104	3.9	0.610	0.141	4.0
54.2	1.14	0.210	4.1	1.53	0.350	4.1

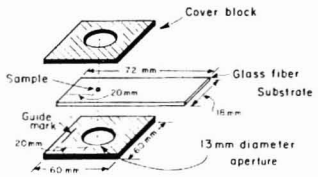


Figure 1. Positioning the substrate for sample injection

and reproducibly 0.000 (Procedure carried out with distilled water instead of sample solution). One-tenth of a microgram sulfate corresponding to ~0.002 absorbance unit may be taken as the detection limit, this being the smallest scale increment in the spectrophotometer used.

Glass fiber filters are water repellent and aqueous solutions tend to bead on it. To transfer an aqueous solution effectively to such a substrate, the substrate must first be moistened with a water-miscible solvent that has a surface tension low enough to wet the substrate. Methanol was a suitable solvent for this purpose. If the original spot of methanolic PDA-Br put on the filter became dry by the time transfer of the sample solution was attempted, the spot was remoistened with another 50-μL drop of methanol. However, this was done only if necessary, because it was advantageous to keep the diameter of the injection spot as small as possible.

Two separate sets of calibration plots were constructed to study the effect of the sample volume. One set was constructed by varying the amount (1–100 μL) of a 200 ppm sulfate solution placed on the substrate and in the other set 100 μL of sulfate solutions of varying concentration was used. There was no discernible difference in the data obtained.

Transfer of solutions up to 25 μL in volume was rapid and convenient. Aliquots exceeding 25 μL were slow in transfer but the process could be facilitated somewhat by adding another drop of PDA-Br at some halfway point during the transfer. Sample aliquots should be kept within 25 μL to reduce analysis time, unless higher sensitivity is necessary. Reproducibility was improved, especially with amounts below 1 μg, by allowing the spot to dry as completely as possible before chromatographing, thus apparently allowing the $(PDA)_2SO_4$ to form and nucleate completely. With very small amounts of sulfate, proper precleaning of the substrate (and keeping it free from contamination) is an absolute necessity

Table II. Extent of Interference on Aqueous Sulfate Determination (100-μL 100 ppm sulfate injection, methanol elution)

interfering ion	concentration (times that of sulfate) 1:1	1:10	1:100	1:1000
F^-	–	none	none	[a]
Cl^-	–	none	none	none
Br^-	–	–	none	none
I^-	–	–	–	none
$HCOO^-$	none	none	50–100%[c]	–
$C_2O_4^{2-}$	133%	v.h.[b]	v.h.	–
CH_3COO^-	none	none	16.5%	–
$H_2PO_4^-$	33%	v.h.	v.h.	–
HCO_3^-	11%	v.h.	v.h.	–
NO_3^-	none	none	v.h.	–

[a] Not sufficiently soluble. [b] v.h. = very high, >500%. [c] Irreproducible.

Table III. Threshold Concentrations at Which Interference First Appears (100-μL injection, methanol elution)

interfering ion	threshold concentration
Cl^-, Br^-, I^-, F^-	saturated sodium/potassium salt solutions do not interfere
$HCOO^-$	>1000 ppm
$C_2O_4^{2-}$	interferes at all levels studied, down to 10 ppm
CH_3COO^-	>5000 ppm
$H_2PO_4^-$	>25 ppm
HCO_3^-	>100 ppm
NO_3^-	>1000 ppm

since, according to manufacturer's specifications, the sulfate content of this substrate may range up to 2 μg/cm² (*12*).

Ethanol cannot be substituted as a solvent for methanol because it undergoes a rapid explosive reaction with concentrated nitric acid via the formation of ethyl nitrate. Methanol was not found to undergo any visible reaction under the experimental conditions. Acetone is the best solvent to remove the colored product from the filter. While acetone is known to undergo an acid or base catalyzed aldol condensation leading to yellowish products, no appreciable change in color was noted after keeping 1:1 mixtures of acetone with concd HNO_3 and NaOH, respectively, for several hours.

Similar to water, nitric acid does not penetrate the glass fiber substrate. The substrate must be moist with a suitable

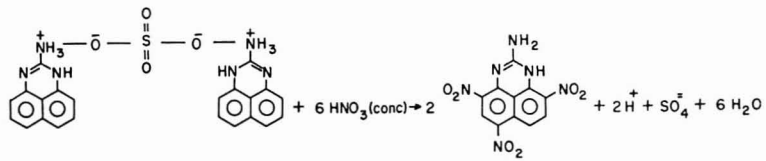


Figure 2. 2-Perimidinylammonium sulfate–nitric acid reaction

Table IV. Comparison of Analytical Results Obtained by Different Methods (ppm sulfate)

sample	pH	$(PDA)_2SO_4$ pyrolytic method	$BaSO_4$ gravimetric	$BaSO_4$ turbidimetric	barium chloranilate	$(PDA)_2SO_4$ nephelometric	this work
Baton Rouge, La.	8.67	10.4 ± 0.5	9.8	10.4 ± 0.3	6.96 ± 0.19	43.2 ± 7.3	10.8 ± 0.8
Garnavillo, Ia.	7.86	11.3 ± 1.9	12.6	13.6 ± 0.2	13.24 ± 1.04	71.0 ± 2.4	12.8 ± 1.0
Kenner, La.	9.61	54.9 ± 1.9	52.8	54.4 ± 0.8	46.8 ± 0.84	61.2 ± 0.3	53.0 ± 1.9
Natchitoches, La.	7.32	48.4 ± 0.5	43.6	45.2 ± 0.4	41.20 ± 0.99	42.0 ± 1.0	46.0 ± 1.1
Diamondhead, Miss.	8.67	8.2 ± 0.3	9.1	9.5 ± 0.1	7.60 ± 0.40	19.8 ± 0.5	9.1 ± 2.2

solvent to ensure proper distribution of solutions into the filter. If the circle became dry before acid treatment, it could be remoistened with methanol/acetone. Excessive amounts of solvent should be avoided because overdilution of the acid results in a longer reaction time and precision also decreases, presumably because of introduction of undesired products through side reactions (*11*).

With sulfate levels over 10 μg, it was not possible to remove every trace of color developed from the substrate. However, the amount remaining was not sufficient to significantly affect the results. In regard to measurement in acidic or alkaline medium, there is no significant superiority of one approach over the other. While measurement in basic solution enhances the sensitivity slightly, measurement in acidic solution is slightly faster. If the latter method is chosen, the nitric acid used must be free from oxides of nitrogen, which absorb strongly in the same region. The colored product is yellow in strong acid and purple in strong base and does not exhibit a great extent of pH-dependence at either extreme of the pH scale and therefore no adjustment of pH is necessary.

Interferences. Interference studies were carried out in detail only with selected anions, initial experiments indicated no cationic interference, as may be expected from the chemical basis of the method. Interference studies were carried out to determine (a) the percentage interference (in terms of increased absorbance from calibration value without interferant) imposed by the interfering ion on 10 μg sulfate (100 μL, 100 ppm) where the former was present in amounts 1000, 100, 10, and 1 times the amount of sulfate; (b) the interfering threshold, i.e., the smallest concentration of an interferant ion which produces the first detectable tinge of color in the substrate when the procedure is carried out with a 100-μL aliquot of the interferant ion solution in the absence of sulfate.

The results of the study (all determinations were carried out in sets of five) are shown in Tables II and III. If the mean of the results were within 5% of the mean calibration value without interferant, extent of interference is reported as none. From the tables, it can readily be ascertained that the method can be regarded as relatively interference free, at least as far as application to actual water samples is concerned. The only significant interferences were due to oxalate, phosphate, and bicarbonate. (Studies with carbonate could not be carried out because highly alkaline solutions such as sodium carbonate react with PDA salts liberating the free amine, the free amine is rapidly air oxidized to tarry products. For the same reason, the method was inapplicable to samples with pH >9 without pretreatment.)

Studies were carried out with an eluting solvent of 1% monochloracetic acid in methanol to investigate if the extent of interference could be reduced. The precision of the data was poorer than obtained with pure methanol. The standard deviation was acceptable (<10%) at levels over 10 μg but severely deteriorated at lower levels. Between 5 and 10 μg, the standard deviation was between 10 and 20% but unacceptable at levels of 1 μg and below. It is questionable whether any actual situation would justify the use of this solvent rather than methanol to obtain more reliable results. Solvent systems containing varying amounts of hydrochloric acid, trichloroacetic acid, dichloroacetic acid, and higher concentrations of monochloroacetic acid were tried as eluting solvent but resulted in poor precision and loss in sensitivity. Buffered systems containing phthalate, citrate, or borate were also unsuccessful as eluting solvents; these ions themselves interfere at high concentrations.

Results of analyses of actual field samples are shown in Table IV along with the uncertainties for a 95% confidence limit ($\pm 2\sigma$). The data show that the results obtained by the present method correlate well with the standard methods (barium sulfate gravimetry and turbidimetry), as well as the $(PDA)_2SO_4$ pyrolytic method and within reasonable degree to the barium chloranilate method. Stephen's $(PDA)_2SO_4$ nephelometric procedure produced values far higher than those obtained by other methods.

Results that are almost as reliable as the standard methods may be obtained by the present method at a fraction of the time used for other procedures. The current method takes about half an hour for a single determination and an hour for 10 simultaneous determinations.

LITERATURE CITED

(1) P. K. Dasgupta, "Specific Determination of Airborne Sulfates and Sulfuric Acid", Ph.D. Dissertation, Louisiana State University, Baton Rouge, La., December 1977.
(2) W. I. Stephen, *Anal. Chim. Acta*, **50**, 413 (1970).
(3) B. Audouze and G. Bonometti, *Inf. Quim. Anal.*, **107**, 223 (1972).
(4) P. A. Jones and W. I. Stephen, *Anal. Chim. Acta*, **64**, 85 (1973).
(5) D. T. Burns, J. S. Coy, W. P. Haynes and D. M. Kent, *Mikrochim. Acta*, 245 (1974).
(6) L. M. Thoma and P. W. West, *Envir. Lett.*, in press.
(7) M. J. Taras et al., Ed., "Standard Methods for the Examination of Water and Wastewater", 13th ed., American Public Health Association, New York, 1971, Part 156.
(8) "1975 Annual Book of ASTM Standards, Part 31, Water", American Society for Testing and Materials, Philadelphia, Pa., 1975; Designation D 516-68 (1974).
(9) R. F. Maddalone, G. L. McClure, and P. W. West, *Anal. Chem.*, **47**, 316 (1975).
(10) P. K. Dasgupta, G. L. Lundquist, K. D. Reiszner, and P. W. West, *Anal. Chim. Acta*, **94**, 205 (1977).
(11) P. K. Dasgupta, A. Nayak, G. R. Newkome, and P. W. West, submitted for publication in *Anal. Chem.*
(12) C. Gelman and J. C. Marshall, *Am. Ind. Hyg. Assoc. J.*, **36**, 512 (1975).

RECEIVED for review June 26, 1978. Accepted August 18, 1978.

AC-Coupled Inverse Raman Spectrometry

Michael D. Morris,* David J. Wallan, G. Patrick Ritz, and Jeanne P. Haushalter

Department of Chemistry, University of Michigan, Ann Arbor, Michigan 48109

Inverse Raman spectra are observed using a CW laser as ω_1 and a pulsed dye laser as ω_2. The detector electronics are ac-coupled, allowing amplification of the pulsed component generated on the CW laser beam by the Raman process. The present system allows detection of an absorption as small as 0.005%. Coherent Raman spectra generated by this technique are not distorted by a nonresonant background process and are obtained with better signal-to-noise ratio than CARS spectra. The major experimental problem is thermal blooming modulation of the CW laser signal caused by the pulsed laser. High resolution spectra of benzene are presented and spectra of aqueous nitrate solutions are presented and compared to CARS spectra. System modifications to decrease thermal blooming problems and to lower detection limits are discussed.

The problem of sample fluorescence has long plagued Raman spectrometrists and has limited the analytical applications of Raman spectrometry. Although many ad hoc techniques have been developed for removal of fluorescent impurities from samples, none have proved wholly satisfactory and none allow examination of molecules which are themselves fluorescent.

Recently, coherent anti-Stokes Raman spectrometry (CARS) has emerged as a powerful technique for examination of fluorescent materials (*1, 2*) such as laser dyes (*3*) and flavins (*4*) and for the examination of nonfluorescent materials in fluorescent matrices.

However, CARS suffers from well-known drawbacks (*5, 6*). First, the Raman emission is always accompanied by a coherent nonresonant background emission which is out of phase with the Raman signal. The nonresonant signal adds coherently to the Raman signal and the resulting observed signal may not resemble an ordinary Raman spectrum.

In addition to distorting spectra, the nonresonant emission sets a high detection limit on CARS. At some point, CARS signals disappear into the noise of the nonresonant background. The problem is particularly severe in aqueous solution, since the background emission of water is about ten times greater than that of benzene and certain other organic solvents (*7*). There have been no really systematic studies made of CARS detection limits, but they are probably 10–100 times higher than those obtainable with normal Raman spectrometry (*6*) under comparable conditions. Thus, while CARS overcomes the problems of sample fluorescence, the technique may have limited prospects for trace analysis.

Because of the clear advantages and the limitations of CARS, there has been an extensive effort to develop other coherent Raman techniques which do not suffer from nonresonant background problems. Levenson and co-workers have advocated the use of the Raman-induced Kerr effect (RIKES) to circumvent the background problem (*8–10*). They measure the birefringence change induced in a sample by the interaction of two laser beams separated in frequency by a Raman active vibrational frequency. A major experimental problem with RIKES is the need for linearly polarized light with an extinction ratio of 10^5 or greater. RIKES depends on the cancellation of two components of the third-order susceptibility of the sample. While this cancellation appears to be good under normal Raman conditions, it has not been demonstrated under resonance Raman conditions.

The Inverse Raman Effect. An alternative approach to background-free coherent Raman spectrometry is the use of the inverse Raman effect. The term inverse Raman effect refers to the absorption in a sample from a laser beam at frequency ω_1 induced by interaction with another laser beam of lower frequency ω_2. The absorption occurs when $\omega_1 - \omega_2$ is equal to the frequency of a Raman-active vibration of the sample. Alternatively, one can measure the increase in intensity induced in beam ω_2 under these conditions. This induced increase is called Raman gain.

The inverse Raman effect was first observed by Jones and Stoicheff in 1964 (*11*). In that classic paper it was pointed out that inverse Raman spectrometry could be used for acquisition of Raman spectra of fluorescent samples. However, the limitations of existing technology prevented widespread use of this technique. Yeung (*12*) significantly improved inverse Raman spectrometric instrumentation by substituting a dye laser for the incoherent probe sources previously used by workers in this field. He also reformulated inverse Raman theory and cleared up inconsistencies in earlier theoretical treatments.

Yeung has shown that the induced absorption is given by Equation 1.

$$P_1(l) = P_1(0) \exp\left[-\frac{P_2}{{n_2}^2} \times \frac{^{10^7}\omega_1}{2hc^2\Delta\omega\ {\omega_2}^4} \times \left(\frac{d\sigma}{d\Omega}\right) \times Nl \right] \quad (1)$$

where $P_1(0)$ is the power density (W/cm^2) in the laser beam at frequency ω_1 (cm^{-1}) incident on the sample, $P_1(l)$ is the power density as a function of beam interaction length, l (cm), P_2 is the power density of the laser beam at frequency ω_2, $\Delta\omega$ is the bandwidth of the Raman-active vibration (cm^{-1}), n_2 is the refractive index of the sample at ω_2, $(d\sigma/d\Omega)$ is the Raman cross-section (cm^2/steradian-molecule, N is the concentration of the sample (molecules/cm^3), h is Planck's constant and c is the speed of light. For the inverse Raman effect, $\omega_1 > \omega_2$. A similar expression describes Raman gain at ω_2.

The basic experimental problem of inverse Raman spectrometry is that it is difficult to obtain an induced absorption of more than a few percent even using very high peak power lasers such as ruby or neodymium-YAG. Thus, conventional inverse Raman measurements have shown even higher detection limits than CARS and the technique has remained fairly obscure.

Recently, Owyoung and co-workers (*13–15*) have described a modified inverse Raman and Raman gain experiment in which one laser beam is modulated and lock-in detection is used to extract the induced component on the other laser beam. By this technique, which they call CW stimulated Raman spectrometry, they are able to measure much smaller absorptions or gains than is possible by the classical methods. They have reported measurements of Raman gains as low as 10^{-7} and calculate an ultimate limit of about 4×10^{-9} (*13*). Similar limits could be obtained for absorption measurements. However, since Owyoung has used CW lasers, the induced

0003-2700/78/0350-1796$01.00/0 © 1978 American Chemical Society

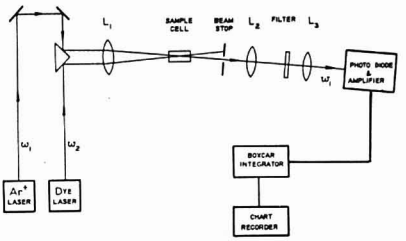


Figure 1. Apparatus for ac-coupled inverse Raman spectrometry. L_1, L_2, 200-nm f/1 achromats; L_3, 100-mm f/1 achromat; filter; 488.0-nm interference filter, 1-nm bandwidth

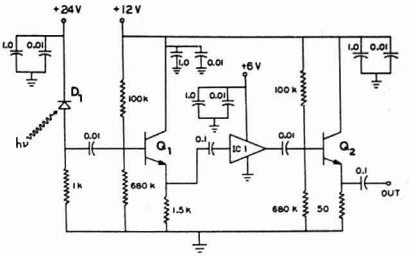


Figure 2. Detector and amplifier. D_1; H-P 5082-2407; Q_1 and Q_2, 2N5109; IC-1 SL-1550C. 1-μF capacitors are Ta-electrolytic; all others are ceramic disks. +12 V, +6 V derived from +24 V by 78L series 3-terminal regulators (not shown)

absorption or gain is limited by the low (less than 1 watt) peak power of those lasers.

From Equation 1, it is clear that increasing power P_2 should greatly improve the detection limits of inverse Raman spectrometry. Indeed, the need for high power is the reason why most inverse Raman work has employed a ruby or neodymium-YAG laser to generate ω_2.

By using a CW laser to generate ω_1 and a high peak power pulsed dye laser to generate ω_2, it is possible to obtain fairly high Raman induced absorptions or, by interchanging the functions of the lasers, fairly high Raman gains. The induced absorption or gain will have exactly the same time dependence as the pulsed laser. Therefore, by using ac-coupled electronics in the detector system, it is possible to measure only the absorption or gain component on the CW beam, down to 1 part in 10^5 or smaller. The induced absorption or gain will generally be much less than 1%, and, therefore, directly proportional to concentration. This hybrid technique, which we call ac-coupled inverse Raman spectrometry (or Raman gain spectrometry) offers experimental simplicity, good detection limits, and freedom from the problems of nonresonant background.

AC-coupled Raman gain measurements were made by Owyoung and Peercy (*16*) in the course of an investigation of nonlinear susceptibility of benzene with a Jamin interferometer. They reported Raman gain measurements for the benzene 992 cm^{-1} band obtained by point-by-point measurements, using the second harmonic of a YAG laser (532 nm) and a manually-tuned CW dye laser.

It is clear that ac-coupled inverse Raman spectrometry can be carried out with any pulsed laser/CW-laser pair with the proper (optical) frequency relationship. Use of a high peak power pulsed dye laser has certain advantages. First, high peak powers simplify signal acquisition since they generate relatively deep modulations of the CW beam. Second, such lasers are commercially available, reliable, and are tunable over a wide range of wavelengths.

Raman gain and inverse Raman measurements give equivalent information. Because inverse Raman measurements are made at the highest frequency incident on the sample, they provide spectral as well as spatial rejection of fluorescence. For that reason, we have made our measurements in the induced absorption rather than the induced gain mode.

EXPERIMENTAL

The experimental apparatus is diagrammed in Figure 1. The CW laser was a Lexel Model 85-1 operated at 488.0 nm and fitted with an intra-cavity etalon for single longitudinal mode operation. The pulsed dye laser was a Molectron DL-200 with motor-driven grating. Dye laser power was limited to 3–5 kW by operating the nitrogen laser at a low discharge voltage and by an aperture in the dye laser beam. The CW laser power was controlled at 25–50 mW at the laser head.

All lenses used were achromatic cemented doublets and aluminum mirrors were used in the beam steering optics. Conventional spectrophotometer cells were used as sample cells.

The beam alignment system was similar to that for CARS (*17*). A small crossing angle (1°–1.5°) was used in these experiments. Although crossing the beams reduces the interaction length, it allows separation of the pulsed and CW beams without the need for monochromation beyond that provided by an argon laser spike filter.

The detector and ac-coupled amplifier are shown as Figure 2. The photodiode (Hewlett-Packard, 5082-4207) has an area of 0.008 cm^2. The transistors used as impedance converters were chosen for low noise figure and good high frequency response. The amplifier (Plessey Semiconductor SL 1550 C) is an integrated circuit video amplifier and is a low noise gain block requiring no external components for operation. The overall gain of the circuit is about 32 db. The primary power source is two small 12-volt storage batteries (Globe-Union 1215) connected in series. Batteries are used to avoid the problem of adequate filtering and shielding of a line-operated power supply.

The photodiode and amplifier components were mounted on a double-sided printed circuit board so that a good ground plane was available The circuit board was mounted in a commercial RFI-shielded box (Compac 6210-5120-2-1). The batteries were enclosed in a locally constructed brass box, since commercial RFI-shielded boxes of suitable dimensions were not readily available. These precautions were necessary to elminate interference from the burst of RF noise which accompanies each laser firing.

The output of the photodiode amplifier was fed to a Princeton Applied Research gated integrator (Model 162, with Model 164 plug-in). The aperture duration of the gated integrator was set for about 50 ns, while its time constant was 1 μs. According to the manufacturer, these conditions give a signal/noise ratio improvement of approximately 6 when the device is operated in the exponential averaging mode. The output of the gated integrator system was recorded on a conventional strip chart recorder.

For these experiments, ACS reagent grade benzene and sodium nitrate were employed. Distilled water was used to prepare sodium nitrate solution. All solutions were filtered through 0.1-μm pore diameter membrane filters before introduction into the sample cell.

RESULTS AND DISCUSSION

AC-coupled inverse Raman spectra of benzene are shown in Figure 3. Under the conditions of this experiment, the resolution is limited by the bandwidth of the dye laser, about 0.02 nm (0.8 cm^{-1}). We observe the strong ring breathing mode at 992 cm^{-1} and the four nearby weaker bands commonly seen in high resolution benzene Raman spectra (*18*). These bands are more clearly resolved here than in CW stimulated Raman spectra. Because we cannot calibrate our dye laser with sufficient accuracy to make absolute frequency assignments, we have *assumed* a frequency of 991.5 cm^{-1} for the benzene

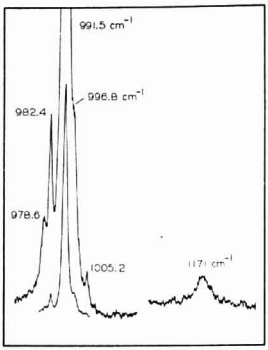


Figure 3. AC-coupled inverse Raman spectra of benzene. Inset is 992 cm^{-1} region at 10X attenuation

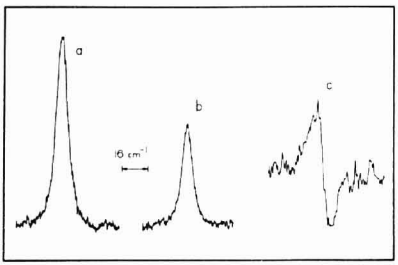


Figure 4. AC-coupled inverse Raman and CARS spectra of aqueous sodium nitrate solutions. (a) inverse Raman 1 M; (b) inverse Raman, 0.5 M; (c) CARS, 0.5 M

ring-breathing mode and have measured all other band positions relative to this one.

Figure 3 also shows the 1171 cm^{-1} CH deformation band of benzene. This band is about 40 times less intense than the 992 cm^{-1} band. It is difficult to observe this band above the nonresonant background in CARS spectra, but in these experiments the band is clearly visible.

Figure 4 shows the 1050 cm^{-1} symmetric stretching vibration of aqueous sodium nitrate solutions at 1 M and 0.5 M. For comparison, a CARS spectrum of 0.5 M sodium nitrate is shown. These data demonstrate two important properties of ac-coupled inverse Raman spectrometry. First, as shown in the figure, the band intensity varies *linearly* with nitrate concentration. By contrast, CARS intensities have a square law dependence at high concentrations and a linear dependence at low concentrations. Second, there is no evidence of a nonresonant signal here. The spectra are identical to conventional Raman spectra of this band. By contrast, the CARS spectra are severely distorted by background emission at 0.5 M.

Figure 4 also demonstrates the superior signal/noise ratio of ac-coupled inverse Raman spectrometry. The CARS spectrum was taken with a dual-channel gated integration system (*19*), with digital signal averaging of 36 laser pulses and digital ratioing of signal and reference channels. The inverse Raman spectrum was taken with a fully-analog system whose manufacturer urges that digital storage and averaging be used when the pulse repetition rate is as low as in these measurements. Moreover, no reference channel is employed here to compensate for dye laser output fluctuations. Even under these adverse conditions, the inverse Raman spectra show better signal/noise ratios at 0.5 M than CARS spectrum taken under more nearly optimum experimental conditions.

We have found it necessary to use an intra-cavity etalon on the argon ion laser. In the absence of the etalon, the laser oscillates on many longitudinal modes simultaneously. These modes are separated by 188 MHz in this laser, which has a short cavity. Consequently, with no etalon, a 188-MHz oscillation is always observed at the detector and can obscure the Raman signal. The etalon completely suppresses multimode oscillation and removes this beat frequency.

The major experimental problem with ac-coupled inverse Raman spectrometry is that thermal blooming (*20*) modulation always accompanies the process, because a pulsed laser is employed. Thermal blooming modulation is observed as a long pulse (typically about 50 ns) which occurs slightly after the laser pulse. The effect is caused by the defocusing of the CW beam by the transient thermal expansion and subsequent cooling induced by the pulsed laser beam. This causes the beam to slightly overflow the detector and results in a spurious signal.

We have minimized the effects of thermal blooming by collimating the argon laser with lens L_2 prior to presenting it to the detector focusing lens, L_3. This operation decreases the convergence angle of the beam and thus decreases the change in the area of the beam caused by the defocusing.

Resonance enhanced inverse Raman spectra have been obtained (*21*, *22*). We have attempted to observe the ac-coupled resonance inverse Raman spectrum of cyanocobalamin using the argon ion 488.0 nm line and scanning the dye laser through a region 1500 cm^{-1} to the green. Under these conditions, the cyanocobalamin 1504 cm^{-1} band should have an intensity approximately equal to that of 0.2 M nitrate (*23*). However, the thermal blooming signal is so large it completely obscures the Raman signal.

There are several approaches to the circumvention of the thermal blooming problem in ac-coupled inverse Raman spectrometry. First, one can use a large area pin photodiode or vacuum photodiode so that beam expansion beyond the active area of the device is negligible. The major experimental problems are high junction capacitances of the pin diodes and the high bias voltages of both devices. The large bias voltage required makes battery operation impractical and introduces the problem of adequate RFI shielding of line-operated power supplies. Alternatively, one can diffuse the light by inserting a ground glass plate in front of the detector, effectively integrating the beam. A small f/number lens can be used to focus the diffused beam into the detector. However, diffusion of the beam results in loss of the detector of about 90% of the incident light, requiring either additional amplifier gain or a photosensor with internal gain, such as an avalanche photodiode or a low gain photomultiplier tube. These approaches are under investigation and will be the subject of a later report.

At present the detection limits of our ac-coupled inverse Raman system are set by noise in the photodiode–amplifier system. The rms noise voltage is about 10 mV. Since the amplifier has a gain of 40, this corresponds to a primary photocurrent of about 250 nA. Under typical operating conditions, the dc current in the photodiode is about 2 to 5 mA. Thus, our detector system is currently limited to measurement of induced absorption of 5×10^{-5} or greater. We must emphasize that this detector system is only a first design. Transistors and video amplifiers with lower noise figures than those used here are available and can be used to improve system performance. Moreover, cooling the entire system to ca. −20 °C is quite feasible and would reduce system noise at least 20 db. In addition, digital storage and averaging of the boxcar integrator output would improve the performance of

that device, while use of a reference channel monitoring the dye laser fluctuations would further improve system performance. With these modifications to our apparatus, measurement of induced absorption of 10^{-7} or less is very feasible. Under these conditions, the detection limits of ac-coupled inverse Raman spectrometry should be equal to or better than those obtainable by spontaneous Raman spectrometry.

ACKNOWLEDGMENT

The authors thank Nestor Clough, Lexel Corporation, for the loan of the argon ion laser used in these experiments.

LITERATURE CITED

(1) P. R. Regnier and J. P. E. Taran, *Appl. Phys. Lett.*, **23**, 240 (1973).
(2) R. F. Begley, A. B. Harvey, and R. L. Byer, *Appl. Phys. Lett.*, **25**, 387 (1974).
(3) L. A. Carriera and L. P. Goss, 32nd Symposium on Molecular Spectroscopy, Ohio State University, Columbus, Ohio, June 1977, paper WE-8.
(4) P. K. Dutta, J. R. Nestor, and T. G. Spiro, *Proc. Natl. Acad. Sci.*, **74**, 4146 (1977).
(5) W. M. Tolles, J. W. Nibler, J. R. McDonald, and A. B. Harvey, *Appl. Spectrosc.*, **31**, 253 (1977).
(6) M. J. Levenson, *Phys. Today*, **30** (5), 44 (1977).
(7) J. Nestor, T. G. Spiro, and G. Klaumin, *Proc. Natl. Acad. Sci.*, **73**, 3328 (1976).
(8) D. Heiman, R. W. Hellwarth, M. D. Levenson, and G. Martin, *Phys. Rev. Lett.*, **36**, 189 (1976).
(9) M. D. Levenson and J. J. Song, *J. Opt. Soc. Am.*, **66**, 641 (1976).
(10) G. L. Eesley, M. D. Levenson, and W. M. Tolles, IEEE *J. Quantum Electron.*, **14**, 45 (1978).
(11) W. J. Jones and B. P. Stoicheff, *Phys. Rev. Lett.*, **13**, 657 (1964).
(12) E. S. Yeung, *J. Mol. Spectrosc.*, **53**, 379 (1974).
(13) A. Owyoung, *Opt. Commun.*, **22**, 323 (1977).
(14) A. Owyoung and E. D. Jones, *Opt. Lett.*, **1**, 152 (1977).
(15) A. Owyoung, IEEE *J. Quantum Electron.*, **14**, 192 (1978).
(16) A. Owyoung and P. S. Peercy, *J. Appl. Phys.*, **48**, 674 (1977).
(17) D. J. Wallan, G. P. Ritz, and M. D. Morris, *Appl. Spectrosc.*, **31**, 475 (1977).
(18) A. Langseth and R. C. Lord, *J. Chem. Phys.*, **6**, 203 (1938).
(19) G. P. Ritz, D. J. Wallan, and M. D. Morris, *Appl. Spectrosc.*, in press.
(20) J. H. Whinnery, *Acc. Chem. Res.*, **7**, 225 (1974).
(21) S. H. Lin, E. S. Reid, and C. J. Tredwell, *Chem. Phys. Lett.*, **24**, 389 (1974).
(22) W. Werncke, A. Lau, M. Pfeiffer, H.-J. Weigmann, G. Hunsalz, and K. Lenz, *Opt. Commun.*, **16**, 128 (1976).
(23) C.-W. Tsai and M. D. Morris, *Anal. Chim. Acta*, **76**, 193 (1975).

RECEIVED for review May 11, 1978. Accepted August 17, 1978. Work supported in part by National Institutes of Health grant GM-22604.

Computer-Controlled Dual Wavelength Spectrophotometer

K. L. Ratzlaff[1]

School of Chemical Sciences, University of Illinois, Urbana, Illinois 61801

F. S. Chuang, D. F. S. Natusch, and K. R. O'Keefe*

Department of Chemistry, Colorado State University, Fort Collins, Colorado 80523

The construction and evaluation of a computer-controlled dual wavelength spectrometer for use in making UV-visible molecular absorption measurements is described. An electromechanical modulator is used to step the grating of a Czerny-Turner configuration monochromator to either of two positions at a maximum rate of 2 Hz. A wavelength modulation precision of better than $\pm 2.5 \times 10^{-4}$ nm is achieved. The spectrophotometer is evaluated in terms of instrumental precision, linearity, and accuracy in typical measurement configurations and several applications of the instrument are described.

The measurement of electronic energy transitions in molecules in solution has found widespread application in chemistry with the major limitation of electronic transition (UV-visible) spectrometry being related to sample characteristics. Dual-beam-in-time or dual-beam-in-space and time spectrophotometers generally rely for their accuracy on the ability of the experimenter to prepare a reference solution that closely approximates the sample matrix. This ability is often quite limited when dealing with samples that are strongly scattering or that contain appreciable amounts of interferents that absorb in the wavelength region of interest.

The technique of Dual Wavelength Spectrophotometry (DWS) represents a fundamental departure from conventional ratio spectrophotometry in this regard. Rather than ratioing transmitted light intensities at one wavelength for separate sample and reference cells, DWS uses light of two different wavelengths which passes through a single sample cell. Operationally, the advantage of DWS derives from the fact that both beams experience the same sample environment. The implications of this characteristic have been considered in previous papers (*1*, *2*).

The technique was first suggested and subsequently developed by Britton Chance for the determination of reaction rates in biological media (*3–9*); however, it was 1969 before the utility of DWS for equilibrium methods of chemical analysis was realized; at that time, commercial DWS instruments became available (*10–12*) and applications were presented for analyses in the presence of spectral interferents (*10–22*).

In the past, DWS instrumentation has been directed toward beam-modulated approaches with high modulation rates. In these techniques, the source illuminates two independent wavelength isolation devices (monochromators or filters) and the phase-separated outputs of these devices illuminate the sample. Another possible approach to DWS involves wavelength modulation of a single monochromator. This is the method often used in derivative spectrometers.

Regardless of the type of wavelength selection used, a dual wavelength spectrophotometer that is to be useful for a range of applications must incorporate a variety of features. These include the following.

(1) The spectrophotometer must measure transmitted intensities at two separate wavelengths either simultaneously or alternately. If the latter, the modulation rate should be significantly faster than the half-time of the fastest reaction

[1] Present address, Department of Chemistry, Northern Illinois University, DeKalb, Ill. 60115.

0003-2700/78/0350-1799$01.00/0 © 1978 American Chemical Society

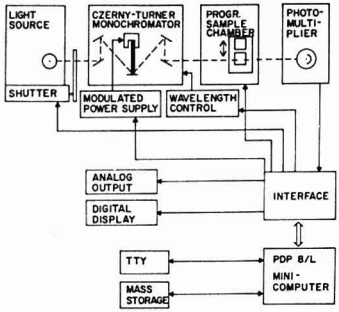


Figure 1. Block diagram of dual wavelength spectrophotometric system

to be studied. In addition, the modulation frequency should be in a favorable signal-to-noise ratio (S/N) region for the source, detector, and associated electronics. That is, the modulation frequency should be higher than the frequency components of instrument drift, but low enough to "average out" high frequency noise.

(2) The wavelength step should be precisely adjustable over a wide range to allow a variety of applications and it should be possible to scan the wavelength in a conventional manner to allow "derivative" spectroscopy with a variable wavelength step size.

(3) In order to maximize the signal-to-noise ratio, a large proportion of the measurement interval should be spent in actual spectral measurement as opposed to mechanically performing the modulation.

(4) The instrument should be capable of conventional single wavelength spectrophotometry as well as DWS.

(5) The instrument should provide high source intensity since in turbid samples much of the incident radiant energy is lost through scattering resulting in a reduced S/N.

Wavelength-modulated instruments for molecular absorption have been employed only for derivative spectroscopy where the modulation amplitude need not be large, typically about 1 nm. The following methods of direct wavelength modulation have been employed primarily for derivative spectroscopy: (i) rotating the entrance mirror (*23*); (ii) vibrating the exit mirror (*24*); (iii) vibrating the Littrow mirror of a Littrow monochromator (*25*); (iv) "wobbling" (vibrating) the exit slit (*26*); (v) using a dual exit slit (*27, 28*); (vi) rotationally oscillating a quartz plate in the optical path (*29–32*); (vii) moving a refractor plate in and out of the beam at an angle (*33*); (viii) slewing the grating drive motor between two positions (*34*); and (ix) rotating an interference filter (*35*).

With the exception of method (viii) all of these methods suffer from major disadvantages; thus they are limited to small wavelength excursions and/or they exhibit a nonlinear relationship between wavelength change and the amplitude of mechanical movement. The applicability of method (viii) above is limited by the rate at which the grating can be moved using a drive motor.

In order to reduce or eliminate these problems while achieving the goals stated earlier, a new method of wavelength modulation has been developed and integrated into an automated, computer-controlled dual-wavelength spectrophotometer for use in the UV-visible region of the spectrum. This spectrophotometer has been applied to a variety of analytical problems with excellent results.

INSTRUMENTATION

A block diagram of the DWS instrument is shown in Figure 1. The optical system is constructed using modules from the EU

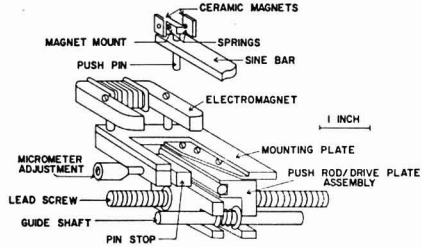


Figure 2. Modulator assembly for dual wavelength operation

700 spectrometer series (GCA/McPherson Instruments, Acton, Mass.) modified as described. The light source for measurement in the near UV-visible region of the spectrum is a tungsten halogen lamp (type 500Q, Sylvania Inc., Danvers, Mass.) powered directly from the output of a harmonic neutralized constant voltage transformer (type CVS, Sola Electric Corp., Elk Grove Village, Ill.). The imprecision of photometric measurements due to the approximately 2% ripple in the source output caused by operating the lamp from an ac power supply and using an asynchronous measurement system varies from a maximum of about 0.1% for a 40-ms measurement time to a maximum of about 0.004% for a 1-s measurement time as calculated from the integral of a 60-Hz sine wave over these periods. These values can be reduced so that they make insignificant contributions to overall system imprecision by using measurement times which are exact multiples of the ripple period or by using a dc power supply. The source module also incorporates an externally controlled electromechanical shutter to facilitate computer-controlled dark current measurements.

The wavelength modulated monochromator is a modified 0.35-m Czerny-Turner monochromator (EU-700, GCA/McPherson). The sine bar drive of the commercial monochromator is adapted for wavelength modulation by the addition of an electromagnetic assembly which is mounted on the lead screw follower as shown in Figure 2. In the conventional drive, the sine bar push pin is held firmly against the lead-screw driven push rod by means of a spring. In the modified drive, the retaining spring is removed and the sine bar is free to move between limits set by the push rod and by a second pin stop that is mounted on the disk plate assembly. The position of the pin stop is adjusted by means of a micrometer head mounted on the mounting plate. The sine bar is moved between the two positions by action of magnetic attraction/repulsion. Two ceramic magnets (Edmund Scientific, Barrington, N.J.) are mounted on the sine bar in such a manner that they repel each other. The magnets are within the field of an electromagnet which when activated attracts one ceramic magnet and repels the other, thereby forcing the push pin against either the push rod or pin stop, depending upon the polarity of the dc voltage applied to the winding of the electromagnet. The electromagnet is powered by a computer-controlled bipolar power supply capable of supplying up to ±20 V at ±2 A.

The position of the two stops determines the grating angles for the two states of the monochromator and, hence, determines the wavelengths of light that illuminate the sample cell. Because the push rod stop is not changed with respect to the conventional monochromator design, the wavelength selected in this position is as read out from the monochromator wavelength indicator. The wavelength displacement that occurs when the push pin is driven against the adjustable pin stop can be calculated from the design parameters of the monochromator, and is 76 nm wavelength displacement per centimeter of mechanical displacement when used with the standard 1180 line per mm grating. Because of design limitations, a maximum travel of 1.8 cm is available, resulting in a maximum wavelength modulation of 137 nm. Using a micrometer graduated in 0.0001-inch increments, a wavelength setability of 0.02 nm is available.

The maximum modulation rate that can be achieved with this design is determined by the time required for the sine bar to move

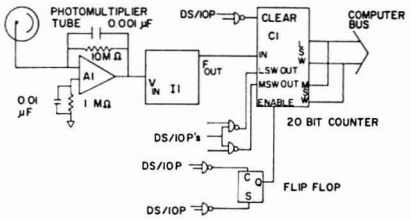


Figure 3. Transducer and signal processing circuitry. DS/IOP signals are sequencing signals from the computer. MSW and LSW are the most significant and least significant parts of the 20-bit count

to its new position when the polarity of the power supply changes and the time required for the sine bar to stabilize in the new position. With the design reported here, the travel time varies from 50–100 ms, depending upon the distance moved, and the settling time is about 50 ms as determined from observation of the photomultiplier tube output during modulation. The worst case modulation frequency is thus about 2 Hz assuming equal amounts of time are spent in movement and making a measurement.

The addition of the wavelength modulator in no measurable way adversely affects the basic optical or mechanical characteristics of the monochromator. For example, the monochromator can be scanned exactly as with the conventional device if the electromagnet is energized to keep the pin stop against the push rod, or the wavelength can be modulated while scanning to obtain a "derivative" spectrum. Because of the 2-Hz maximum modulation rate, scanning to obtain derivative spectra must be quite slow.

The programmable sample chamber used in this work is an EU-721-11 module (GCA/McPherson). This module allows either of two conventional spectrometer cells to be positioned in the optical path under external control, and provides feedback signals to the controller indicating when either cell is in the optical path.

The detector is a 1P28A photomultiplier tube housed in an EU-701-30 module (GCA/McPherson) which incorporates a regulated high voltage power supply.

The control element in the automated dual wavelength spectrometer is a PDP 8/L minicomputer with 8K words of core memory (Digital Equipment Corp., Maynard, Mass.), a dual drive floppy disk mass storage device (Sykes Datatronics Inc., Rochester, N.Y.), and input/output devices including a CRT display, line printer, Teletype, and plotter. In addition, a custom built interface provides control and data transmission between the spectrometer and the controller. Programming is done either in PAL III, an assembly level language, or OS/8 FORTRAN IV, both of which are supplied by Digital Equipment Corp.

SIGNAL PROCESSING

It can be shown (*1*) that the dual wavelength readout, ΔA, is related to radiant power as

$$\Delta A = -\log \frac{P_1}{P_2} + \log \frac{P_{o_1}}{P_{o_2}} = \log \frac{P_{o_1}}{P_1} - \log \frac{P_{o_2}}{P_2} \qquad (1)$$

where P_1 and P_2 are transmitted radiant powers and P_{o_1} and P_{o_2} are incident radiant powers at λ_1 and λ_2, respectively. A block diagram of the circuitry used to transduce the radiant powers to proportional electric signals, digitize the resulting signals, and present the resulting numbers to the computer is shown in Figure 3. In the configuration used in this work, amplifier A1 was a FET input operational amplifier (NE536, Signetics, Corp., Sunnyvale, Calif.), I1 was a high precision voltage-to-frequency converter (Model 4705/01, Teledyne Philbrick, Dedham, Mass.), and C1 was made up of five tristate counters (8554, National Semiconductor Corp., Santa Clara, Calif.).

The number transferred to the computer by the circuit of Figure 3 is a count accumulated by the counter, C1, and is the sum of a term related to the radiant power illuminating the PM tube and terms that result from offsets in the analog electronics. If a measurement is made with no light illuminating the PM tube, a dark measurement, C_D, is obtained. Measurements subsequently made for the same interval at λ_1 and λ_2 yield results C_{λ_1} and C_{λ_2} that can be substituted in Equation 1, viz.,

$$\Delta A = -\log \frac{C_{\lambda_1} - C_D}{C_{\lambda_2} - C_D} + \log \frac{C_{o,}\lambda_1 - C_D}{C_{o,}\lambda_2 - C_D} \qquad (2)$$

where $C_{o,}\lambda_1$ and $C_{o,}\lambda_2$ are the counts obtained with a "blank" solution in the optical path. Equation 2 is the basic equation that defines the dual wavelength measurement in the system described in the present work. Operationally, C_D is measured with the source shutter closed, $C_{o,}\lambda_1$ and $C_{o,}\lambda_2$ are measured at λ_1 and λ_2 with a blank solution in the cell and the right-hand term of the right-hand side of Equation 2 is calculated. Subsequent measurements of C_{λ_1} and C_{λ_2} for any solution placed in the optical path of the spectrometer allow the calculation of ΔA for that sample.

PERFORMANCE AND RESULTS

Modulator Precision. Modulation noise in wavelength modulated instruments has been considered previously (*1*) and it was shown that the uncertainty in the wavelength, σ_w, gives rise to a variance in the measured value of ΔA, σ_A^2:

$$\sigma_A^2 = ((\sigma_w M_1 \epsilon_1 bc)^2 + (\sigma_w M_2 \epsilon_2 bc)^2)^{1/2} \qquad (3)$$

In this expression, ϵ_1 and ϵ_2 are the absorptivities and M_1 and M_2 are the slopes (A nm^{-1}) at the two wavelengths, respectively.

For this experiment, a peak of $PrCl_3$ in 2 M HCl at 444 nm was used. This peak has a width at half-height of about 4 nm and a peak absorptivity of about 9.25 molar^{-1} cm^{-1}. If λ_1 and λ_2 are located at wavelengths above and below the peak so that $\epsilon_1 = \epsilon_2$ ($\Delta A = 0.0$) and so that both M_1 and M_2 are large, a good case for worst case modulation performance in molecular spectrometry results. The slits were opened to 400 μm so that although photometric accuracy was lost (*2*), the precision was not photon limited. The apparent slopes, determined from a conventional dual cell measurement, were plus and minus 1.15 A nm^{-1}. Since $\epsilon_1 bc = \epsilon_2 bc = 1.05$, σ_A should be 8.0×10^{-3} for $\sigma_w = 5 \times 10^{-3}$ nm.

The observed standard deviations for three sets of 35 measurements were 0.40×10^{-3}, 0.49×10^{-3}, and 0.41×10^{-3}. To obtain an indication of whether or not those values were modulation noise limited, the modulator was over-ridden so that the transmittance at a single wavelength was ratioed against itself; this removes the modulation noise contribution to the variance. A standard deviation of 0.41×10^{-3} was obtained indicating that σ_w was less than 2.5×10^{-4} nm.

Photometric Linearity. Photometric linearity of the instrument was estimated by measuring ΔA as a function of concentration for a series of dilutions of an appropriate standard. Basic chromate is an often used absorbance standard and was selected for this study. A series of K_2CrO_4 solutions were made up in 0.05 M KOH with nominal absorbances up to about 1.1 at 373 nm. Dual wavelength measurements were made at 373 and 393 nm and a flow cell was used to reduce sample cell positioning errors. These results were compared with measurements made in a conventional absorbance mode. The results of these measurements are shown in Table I.

The excellent linearity and low intercept for the measurements made in a conventional absorbance mode (column labeled A (373 nm)) are consistent with results obtained in other work (*36*) with similar equipment and indicate the utility of the spectrometer in this mode. Measurements in the dual wavelength mode result in a smaller intercept but slightly worse linearity than the conventional absorbance mode. The lower intercept probably results from reduction in systematic errors such as sample presentation and source drift, while the poorer correlation coefficient is due both to the smaller net absorbance range for the dual wavelength measurements and to poorer measurement precision. This conclusion is sup-

Table I. Potassium Chromate Calibration Curves

relative concn	A (373 nm)	ΔA (373, 393 nm)
0	0.0006	0.0008
5	0.0563	0.0277
10	0.1115	0.0565
20	0.2261	0.1148
40	0.4523	0.2302
50	0.5640	0.2870
70	0.7917	0.4023
100	1.1238	0.5697
intercept	0.00061	0.00015
slope	0.01258	0.00573
correlation coefficient	0.999990	0.999977
std error of estimate of concn on A or ΔA	0.15	0.21

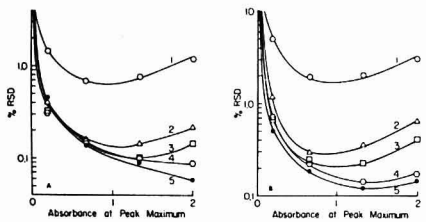


Figure 4. Instrument precision at various values of photon flux. Relative photon flux: Curve 1, 1; Curve 2, 8; Curve 3, 32; Curve 4, 73; Curve 5, 120. (A) Base absorptivity 40% of maximum absorptivity. (B) Base absorptivity 22% of maximum absorptivity

ported by comparison of the standard errors of estimate when concentration is regressed against A or ΔA. The slightly poorer standard error in the dual wavelength mode indicates that, under favorable measurement conditions, dual beam measurements are capable of higher precision than dual wavelength measurements, a condition predicted by earlier theoretical treatments (*1*, *2*).

Photometric Precision. The photometric precision of the dual wavelength spectrometer was evaluated over a wide range of photon flux, both to attempt to determine the major noise sources inherent in dual wavelength measurements and to define the ultimate precision expected with this instrument in different measurement situations.

The photometric precision of the system was evaluated by making ΔA measurements on a series of $PrCl_3$ solutions made up in 2 M HCl and having nominal peak absorbances at 444 nm of 0–2.0 A. Measurements of ΔA were made with one wavelength set to the peak absorbance wavelength and the other wavelength selected such that the absorptivity was 40% or 22% of the peak value. The photon flux was varied by changing the slit width of the monochromator. Slit widths from 50 to 1000 μm were used to give a range of photon flux that varied from a relative value of 1 to 120, with the maximum photon flux producing a photocurrent of about 1 μA.

The results of these experiments are shown in Figure 4. The plot labeled a is that for the 40% peak absorptivity case and b is the 22% absorptivity case. The percent relative standard deviation (RSD) for 30 measurements on a solution with the peak absorbance shown on the abscissa is plotted in each case. The curves labeled 1–5 in each plot are for relative photon fluxes of 1, 8, 32, 73, and 120, respectively. Previous work (*1*) has shown that error will be minimized at about 0.5, 0.9, and infinity for the "constant", "square root", and "proportional" error, respectively. In both plots, curve 1

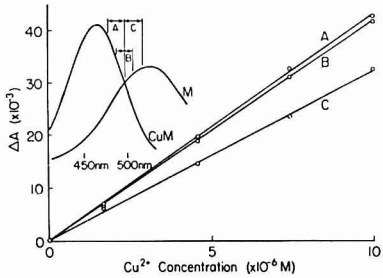


Figure 5. Spectra and analytical curves for copper–murexide system

experiences a minimum at about 0.9, apparently due to "square root" error, suggesting photon-limited precision. However, a combination of "constant" and "proportional" errors could also produce that effect. Measurement at higher photon flux does not support this contention, however, and the precision remains photon limited until the flux-independent "proportional" error due to source flicker is approached at larger slit widths.

Applications. *Conventional DWS.* One of the classic applications of DWS is the measurement of absorbing species that are in equilibrium with each other in solution. An example of this is the measurement of copper concentration in solution by complexation with murexide (ammonium purpurate). In this case the spectra of the indicator (M) and the complex (CuM) have overlapping spectra as shown in the inset of Figure 5, so the determination of the CuM is difficult using dual-beam spectrophotometry. The murexide system is especially useful for monitoring the amount of metal ion present in a variety of biochemical systems (*37*).

The spectrometer was evaluated for conventional DWS by measuring Cu(II) concentrations as the CuM species. Several solutions were prepared with various Cu(II) concentrations and constant total murexide concentration and dual wavelength measurements were made with various wavelength pairs as shown in the inset of Figure 5. In all cases the difference between the two wavelengths was 20 nm. The ΔA values presented are referenced to a solution containing the same total murexide concentration as the samples to give the zero intercept. The slopes of the three analytical curves are different, as expected, and all are linear over the concentration range studied. Correlation coefficients of the three lines are 0.997, 0.999, and 0.996 for A, B, and C, respectively, indicating good linearity even with a large, wavelength varying background absorbance.

Analysis of Turbid Solutions. A second application for which the spectrophotometer was evaluated was the determination of a molecular absorbing species in the presence of solution turbidity. For this purpose, a series of K_2CrO_4 solutions was prepared as before with absorbances at 373 nm up to a nominal value of 0.9. Absorbance was measured at 373 nm and the results are plotted as curve A in Figures 6a and 6b. A second series of solutions contained the same K_2CrO_4 concentrations, but a scattering material (a calcium caseinate suspension) was added so that the apparent absorbance due to turbidity was about 1.6. These solutions were intentionally prepared so the turbidity varied by ±10%, resulting in the absorbance scatter shown in Figure 6b. The results of these measurements are illustrated in curve B of Figures 6a and 6b.

When no turbidity is present (curve A in Figures 6a and 6b), good linearity is demonstrated for either conventional or dual wavelength measurements. However, when turbidity is

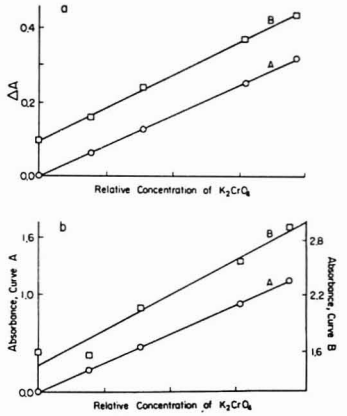


Figure 6. Analytical curves for K_2CrO_4 in the presence of turbidty. Curves (A) without and Curves (B) with turbidity. (a) Dual wavelength, (b) Single wavelength

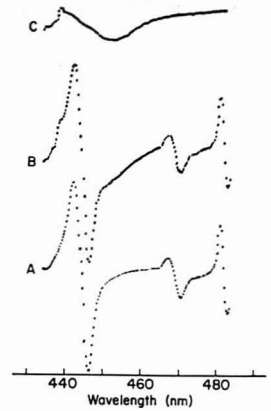


Figure 8. Effect of baseline on derivative spectrum. Curves A and B are derivative spectra of $PrCl_3$ in HCl with and without baseline correction. Curve C is the baseline

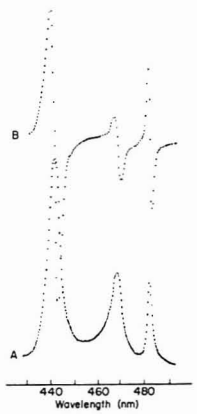


Figure 7. Spectrum and derivative spectrum of $PrCl_3$ with $\Delta\lambda = 0.3$ nm. (A) Spectrum. (B) Derivative Spectrum.

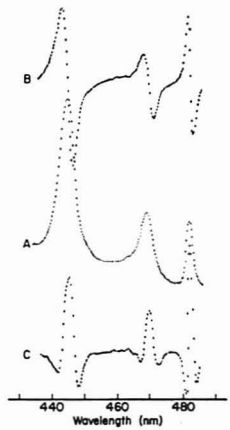


Figure 9. Differentiation by digital computation. First- (B) and second- (C) order derivatives of $PrCl_3$ spectrum (A)

present (curve B), two effects on the analytical curves are noticed. First, an intercept is introduced in the dual wavelength case due to the wavelength dependence of the turbidity, but the intercept is much smaller than for the direct absorbance measurement. Secondly, the sensitivity to variations in turbidity is greatly reduced by use of dual wavelength as shown by the low scatter of the points on curve B of Figure 6a as compared to curve B of Figure 6b.

Derivative Spectroscopy. Another application for which dual wavelength spectrometers find wide application is "derivative" spectroscopy, although the output obtained if one modulates the wavelength while simultaneously scanning is not a true derivative spectrum. The DWS spectrometer described herein was evaluated in two modes for derivative spectroscopy: a modulated/scanning mode and a numerical mode.

Figure 7 shows the spectrum of $PrCl_3$ in 2 M HCl from 425 to 485 nm (Figure 7A) and also the output of the spectrometer in the dual wavelength mode for a wavelength modulation of 0.3 nm at each wavelength (Figure 7B). The latter plot is a dual wavelength "derivative" spectrum ($\Delta A/\Delta\lambda$ vs. λ).

The method used in this case to correct the spectrum for variations in source intensity is to move the sample in and out of the optical path at each wavelength and to determine the intensity ratio for the pair of wavelengths (Equation 2). Previous instruments have employed cams (*38*) or used a series of potentiometers (*39*, *40*) to adjust the baseline. The alternative in a digital instrument would be to store the baseline if sufficient memory were available and the source sufficiently stable.

In Figure 8, the effect of failure to compensate for source variations with respect to wavelength is shown. The corrected (Figure 8A) and uncorrected (Figure 8B) first derivative spectra are shown with the uncorrected baseline (first derivative of the source, Figure 8C).

An alternative method of obtaining the derivative spectrum is the use of numerical differentiation, for example, by the method of Savitzky and Golay (*41*, *42*). Curve A of Figure 9 is a spectrum of 2 M $PrCl_3$ in a solution containing colloidal

silica. The effect of the silica is to add turbidity and to cause the baseline to decrease monotonically at longer wavelengths; however, this monotonic variation has a negligible effect on the derivative. The first derivative, curve B, was produced by digital differentiation as was curve C, the second derivative. Note the similarity of the curve obtained by this technique with that obtained using the modulation/scanning approach.

In comparing the dual wavelength and digital methods, the digital method is often more convenient and probably is equally precise and accurate when on-line digital processing is available. It is certainly faster since, in a dual wavelength system, every value for sample and reference is effectively measured twice as first λ_1 and then λ_2 past the point. This is true no matter which of the baseline correction methods is used. Second, using digital differentiation, the higher order derivatives are immediately available if required.

LITERATURE CITED

(1) K. L. Ratzlaff and D. F. S. Natusch, *Anal. Chem.*, **49**, 2170 (1977).
(2) K. L. Ratzlaff and D. F. S. Natusch, submitted for publication in *Anal. Chem.*
(3) B. Chance, *Rev. Sci. Instrum.*, **13**, 158 (1942).
(4) B. Chance, *Rev. Sci. Instrum.*, **22**, 634 (1951).
(5) B. Chance, *Science*, **120**, 767 (1954).
(6) B. Chance, D. Mayer, N. Graham, and V. Legallais, *Rev. Sci. Instrum.*, **41**, 111 (1970).
(7) B. Chance, D. Mayer, and V. Legallais, *Anal. Biochem.*, **42**, 494 (1971).
(8) B. Chance, V. Legallais, J. Sorge, and N. Graham, *Anal. Biochem.*, **66**, 498 (1975).
(9) B. Chance, N. Graham, J. Sorge, and V. Legallais, *Rev. Sci. Instrum.*, **43**, 62 (1972).
(10) S. Shibata, M. Furukawa, and K. Goto, *Anal. Chim. Acta*, **46**, 271 (1969).
(11) T. J. Porro, *Anal. Chem.*, **44** (4), 93A (1972).
(12) R. L. Sellers, G. W. Lowry, and R. W. Kane, *Am. Lab.*, March 1973.
(13) S. Shibata, M. Furukawa, and K. Goto, *Anal. Chim. Acta*, **53**, 369 (1971).
(14) S. Shibata, M. Furukawa, and Y. Ishiguro, *Anal. Chim. Acta*, **62**, 305 (1972).
(15) S. Shibata, M. Furukawa, and Y. Ishiguro, *Anal. Chim. Acta*, **65**, 49 (1973).
(16) S. M. Gerchakov, *Spectrosc. Lett.*, **4**, 403 (1971).
(17) S. Shibata, M. Furukawa, and T. Honkawa, *Anal. Chim. Acta*, **78**, 487 (1975).
(18) T. Ohnishi and S. Ebashi, *J. Biochem. (Tokyo)*, **55**, 599 (1964).
(19) R. Rikmenspoel, *Rev. Sci. Instrum.*, **36**, 497 (1965).
(20) R. J. De Sa and Q. H. Gibson, *Rev. Sci. Instrum.*, **37**, 900 (1966).
(21) B. Hess, H. Kleinhans, and H. Schlutter, *Hoppe-Seyler's Z. Physiol. Chem.*, **351**, 515 (1970).
(22) J. Rapp and G. Hind, *Anal. Biochem.*, **60**, 479 (1974).
(23) M. Bryant, University of Illinois, Urbana, Ill., personal communication, 1974.
(24) G. Bonfiglioli and P. Brovetto, *Appl. Opt.*, **3**, 1417 (1964).
(25) V. Hammond and W. Price, *J. Opt. Soc. Am.*, **43**, 924 (1953).
(26) R. Hager, *Anal. Chem.*, **45**, 1131A (1973).
(27) J. Kirkpatrick, Ph.D. Thesis, University of Illinois, Urbana, Ill., 1969.
(28) J. Defreese and H. Malmstadt, submitted for publication in *Anal. Chem.*
(29) R. Elser and J. Winefordner, *Anal. Chem.*, **44**, 698 (1972).
(30) I. McWilliams, *Anal. Chem.*, **41**, 674 (1969).
(31) D. Brinkman and R. Sacks, *Anal. Chem.*, **47**, 1723 (1975).
(32) R. Spillman and H. Malmstadt, *Anal. Chem.*, **48**, 303 (1976).
(33) E. C. Stanley, Ph.D. Thesis, University of Illinois, Urbana, Ill., 1972.
(34) T. O'Haver, G. Green, and B. Keppler, *Chem. Instrum.*, **4**, 197 (1973).
(35) R. J. Sydor and G. M. Hieftje, *Anal. Chem.*, **48**, 535 (1976).
(36) K. R. O'Keefe and H. V. Malmstadt, *Anal. Chem.*, **47**, 707 (1975).
(37) L. Mila and B. Chance, *Biochemistry*, **7**, 4059 (1968).
(38) R. Woodriff and D. Schrader, *Appl. Spectrosc.*, **27**, 181 (1973).
(39) *Aminco Laboratory News*, **29** (3), 2 (1973).
(40) Perkin-Elmer Corporation, UV/FL Produce Department Technical Memo No. 1 (1970).
(41) A. Savitzky and M. Golay, *Anal. Chem.*, **36**, 1627 (1964).
(42) J. Steinier, Y. Termonia, and J. Deltour, *Anal. Chem.*, **44**, 1906 (1972).

RECEIVED for review December 22, 1977. Accepted August 3, 1978.

Resolution and Instrument Line Shape Effects on Spectral Compensation with Fourier Transform Infrared Spectrometers

Robert J. Anderson

Department of Chemistry, Ithaca College, Ithaca, New York 14850

Peter R. Griffiths*

Department of Chemistry, Ohio University, Athens, Ohio 45701

The effect of limited instrument resolution on spectral subtraction experiments performed using Fourier transform infrared spectrometers is examined from a theoretical standpoint and the predicted results are tested experimentally. For weak absorption bands, boxcar truncation is found to yield better compensation than triangular apodization. For strong bands, whose peak absorbance is greater than one, there are certain conditions under which boxcar truncation leads to better compensation and others where triangular apodization is preferable. The results are discussed in terms of removing strong solvent bands from solution spectra, compensating atmospheric absorption bands, and measuring the effects of intermolecular interactions. The effect of a triangular slit function on subtraction experiments performed using spectra measured with grating monochromators and the possibility of using other apodization functions to improve the results on Fourier spectrometers are also discussed.

One of the many advantages of having a digital data system as an integral component of an infrared spectrophotometer is the ease with which bands due to a single component can be subtracted from a spectrum having absorption features due to more than one component. A typical procedure for compensating bands due to a component, A, in the spectrum of a mixture involves separately measuring transmittance spectra (usually against an air reference) of the mixture and of a pure sample of A under the same instrumental conditions. The spectra are digitized, converted to a linear absorbance format, and stored. The absorbance spectrum of A is then multiplied by an appropriate factor and the scaled spectrum of A is subtracted from the absorbance spectrum of the mixture. The resultant spectrum should then correspond to that which would be measured if A were not present in the mixture. For N-component mixtures, the spectrum of each pure component can theoretically be obtained provided that N samples are available in which the relative concentrations of the components are varied (*1*). Koenig (*2*) has given several interesting examples of the application of the scaled absorbance subtraction routine to problems in macromolecular chemistry, and procedures of this type are now routinely applied by most users of mid-infrared Fourier transform spectrometers.

The validity of the scaled absorbance subtraction technique depends on two fundamental assumptions. First, the shape

0003-2700/78/0350-1804$01.00/0 © 1978 American Chemical Society

of an absorption band must not change when the optical depth (the product of pathlength and concentration) of the sample changes. That is, increasing the pathlength or concentration of a sample should simply multiply the absorbance at all frequencies by a constant factor. Second, the absorbance of a mixture must be the sum of the absorbances of the components. Simply put, the requirement for good compensation is that the Beer–Lambert law be followed, and it must be followed not just by the true spectra of the samples but by the spectra as actually measured since these are the spectra one manipulates.

There are two basic reasons why the Beer–Lambert law fails. First, there are real deviations from the law which are due to structural changes in the sample, e.g., intermolecular associations, which occur when conditions such as concentration are changed. These effects can prevent accurate compensation, and can be of interest in themselves, but are not really errors in the measurement process. The second cause of deviations is instrumental error, and in infrared spectrometry a principal source of error is limited instrument resolution. The purpose of this paper is to report the effects of instrument resolution and instrument line shape function (ILS) on spectral subtraction and to discuss quantitatively the instrumental conditions necessary for good spectral compensation using FT-IR spectrometers.

In a recent publication (*3*) we showed how the apparent peak absorbance, A^a_{peak}, of bands with a Lorentzian (Cauchy) profile depends not only on the true peak absorbance, A^t_{peak}, but also on the ILS and the ratio of the spectral resolution to the width of the band. Results were given in terms of a resolution parameter, ρ, which is the ratio of the instrument resolution, R (defined for FT-IR spectra as the reciprocal of the maximum retardation of the interferometer for that measurement), to the full width at half-height of the absorption band. The ILS is determined by the way in which the interferogram is apodized. For triangular apodization the ILS is a function of the form $\sin^2 x/x^2$ (or $\mathrm{sinc}^2 x$) and R represents the distance in frequency units between the measurement frequency, ν_i, and the frequency at which the ILS first assumes a zero value. For unapodized interferograms (boxcar truncation), the ILS is of the form $\sin x/x$ (or $\mathrm{sinc}\ x$) and R is the distance between ν_i and the second zero of the ILS, so that it bounds the first positive and negative lobes of the ILS.

Except for strong bands, the dependence of A^a_{peak} on A^t_{peak} and ρ for a band measured by an FT-IR spectrometer using triangular apodization is similar to the dependence noted previously (*4*, *5*) for spectra measured using grating spectrometers with a triangular ILS function. In both types of spectra, A^a_{peak} is always less than A^t_{peak} to an extent that depends both on A^t_{peak} and ρ. For weak absorption bands, A^a_{peak} approximates A^t_{peak} if $\rho \leq 0.2$ (cf. the Ramsay (*5*) criterion for grating spectrometers).

If FT-IR spectra are computed from *unapodized* interferograms, A^a_{peak} can be greater than A^t_{peak} for strong lines, and under certain circumstances the apparent transmittance of bands can even become negative. For weak bands measured using boxcar truncation, the value of A^a_{peak} is usually very close to that of A^t_{peak} if $\rho \leq 1$. For such bands the photometric accuracy which can be achieved using a Michelson interferometer at a certain retardation if the interferograms are unapodized is as good as that from triangularly apodized interferograms measured with ten times the retardation (*3*).

Though these studies indicated that improved photometric accuracy can often be obtained if interferograms are not triangularly apodized, it is not immediately apparent whether that approach leads to better compensation. As stated above, the basic requirement for good compensation is not photometric accuracy but merely that the Beer–Lambert law be obeyed, and this is possible as long as A^a_{peak} is proportional to A^t_{peak}, even if the two are not equal. In our previous work (*3*), plots of $\log (A^a_{peak})$ vs. $\log (A^t_{peak})$ were presented for both unapodized and triangularly apodized interferograms. In both cases for small values of A^t_{peak} the plots were linear with a slope of one indicating that A^a_{peak} is proportional to A^t_{peak} and accurate compensation is possible. For larger values of A^t_{peak}, the slopes in both cases differed from one showing that complete compensation is impossible.

In view of these findings and recognizing that compensation experiments are performed using the whole band and not just the peak absorption frequencies, we have carried out a series of computer-simulated compensation experiments to study the effects of resolution and ILS on spectral compensation in FT-IR. We have focused on the problem of eliminating from a spectrum a single Lorentzian peak obtained at one optical depth by using scaled absorbance subtraction with the same peak obtained at a greater optical depth. This corresponds to the common problem of eliminating a solvent peak from a solution spectrum using the spectrum of the pure solvent for compensation. Here the optical depth of the solvent in the solution is less than in the pure compound because some solvent has been displaced by solute.

The procedure for the simulated experiments was as follows. First the true peak absorbance of the reference spectrum was specified along with the value of ρ and whether or not apodization was to be used. The apparent band shape which would actually be measured, spectrum 1, was then computed using the method described below. A second true peak absorbance, smaller than the first, was then specified and the apparent spectrum for the sample, spectrum 2, was computed. Spectrum 1 was then scaled by appropriate factors and subtracted from spectrum 2 and the results were plotted.

If there are no real deviations from the Beer–Lambert law, the true absorbance of the jth sample at frequency, ν, is given by:

$$A^t_\nu(j) = a_\nu \cdot b(j) \cdot c(j) \tag{1}$$

where a_ν is the absorptivity at frequency ν, $b(j)$ is the pathlength for the jth sample, and $c(j)$ is the concentration for the jth sample. Where Beer's law is obeyed experimentally, the apparent absorbance at ν is given by:

$$A^a_\nu(j) = f_\nu \cdot A^t_\nu(j) \tag{2}$$

where f_ν is not necessarily equal to unity but is independent of A^t_ν. Under these conditions, for spectra measured at two different optical thicknesses, $j = 1$ and 2:

$$\frac{A^a_\nu(2)}{A^a_\nu(1)} = \frac{A^t_\nu(2)}{A^t_\nu(1)} = \frac{b(2)c(2)}{b(1)c(1)} \tag{3}$$

Since the right side of Equation 3 is clearly frequency independent, for experiments carried out under these conditions, $A^a_\nu(2) - kA^a_\nu(1) = 0$ for all frequencies when $k = A^t_{peak}(2)/A^t_{peak}(1)$ and perfect compensation is possible. When f_ν is not independent of A^t_ν, as a result of limited resolution for example, perfect compensation is impossible.

In practice the value of $A^t_{peak}(2)/A^t_{peak}(1)$ is rarely known and an adjustable scaling factor, k, is used whose value is changed until $A^a_\nu(2) - kA^a_\nu(1)$ is as small as possible at all frequencies. In our simulations, three different values of k were used:

$$k_1 = A^t_{peak}(2)/A^t_{peak}(1) \tag{i}$$

$$k_2 = A^a_{peak}(2)/A^a_{peak}(1) \tag{ii}$$

$$k_3 = \int A^a_\nu(2)\mathrm{d}\nu \Big/ \int A^a_\nu(1)\mathrm{d}\nu \tag{iii}$$

Table I. Peak Absorptivities and Half-Widths of the Principal Benzonitrile Bands between 2500 and 1400 cm^{-1}

ν_o, cm^{-1}	a_{peak} cm^2 mol^{-1}	2γ, cm^{-1}
2231	9.8×10^4	7.4
1980	0.26×10^4	9.0
1949	0.44×10^4	10.4
1912	0.26×10^4	10.0
1892	0.52×10^4	10.0
1810	0.44×10^4	9.4
1764	0.29×10^4	12.0
1680	0.36×10^4	11.6
1601	0.12×10^4	5.0
1583	0.53×10^4	5.4
1492	11.3×10^4	2.7
1448	12.5×10^4	2.2

The first factor gives perfect compensation if the Beer–Lambert law is followed experimentally, the second always gives perfect compensation at the peak of the band, and the third makes the integrated absorbance of the compensated band zero. The results of the simulations are presented below followed by experimental tests of the conclusions.

CALCULATIONS

The procedure used for the calculations is similar to that described earlier (*3*) and will only be outlined here. The apparent transmittance of a sample as determined by a spectrometer measuring at frequency, ν_i is given by:

$$T^a(\nu_i) = \int_0^\infty \sigma(\nu - \nu_i)\exp(-K(\nu)l)d\nu \Big/ \int_0^\infty \sigma(\nu - \nu_i)d\nu \quad (4)$$

where σ is the ILS, $K(\nu)$ is the absorption coefficient, and l is the pathlength. For a Lorentzian shaped band:

$$K(\nu)l = \frac{\ln(10)A^t_{peak}\gamma^2}{(\nu - \nu_o)^2 + \gamma^2} \quad (5)$$

where γ is the half-width at half-height of the band, and ν_o is the frequency of maximum absorption. Defining $y = (\nu - \nu_i)/R$ and $\delta = (\nu_i - \nu_o)/R$ and introducing the definition of ρ gives:

$$T^a(\delta) = \int_{-\infty}^{\infty} \sigma(y)\exp(-\ln(10)A^t_{peak}/[1 + 4\rho^2(y + \delta)^2])dy \quad (6)$$

For boxcar truncation, $\sigma(y) = 2\sin(2\pi y)/(2\pi y)$ and for triangular apodization, $\sigma(y) = \sin^2(\pi y)/(\pi y)^2$. The integration in Equation 6 is performed numerically on a computer for a series of values for δ, thereby generating the apparent band shape to be expected for specified values of A^t_{peak} and ρ. The results of such calculations and those of the simulated compensations were plotted on a digital plotter.

EXPERIMENTAL

Solution spectra were measured using a Digilab FTS-14 Fourier transform infrared spectrometer with the solutions held in amalgamated sealed cells. As in our previous study (*3*), a solution of benzonitrile in carbon tetrachloride was used because it was known that the C≡N stretching band in the spectrum of benzonitrile (at 2231 cm^{-1}) is well separated from other bands, has very close to a Lorentzian shape, and absorbs at a frequency where the solvent is very clear. Two other less isolated bands in the spectrum of benzonitrile, at 1492 and 1448 cm^{-1}, were also found to be very useful in this study, since they are of approximately the same peak absorptivity as the 2231 cm^{-1} band but are considerably narrower. In addition several other much weaker, but still reasonably well isolated, bands in the spectrum between 1500 and 2000 cm^{-1} were also investigated. The full width at half-height and peak absorptivity for each band are given in Table I.

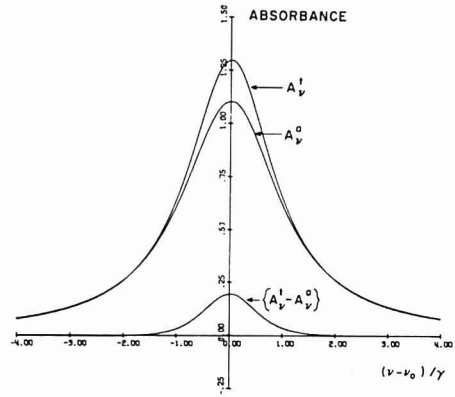


Figure 1. Apparent absorbance spectrum, A^a_ν, of a Lorentzian band with $A^t_{peak} = 1.30$, calculated using a $sinc^2$ x ILS with $\rho = 0.2$; the true absorbance spectrum, A^t_ν and $(A^t_\nu - A^a_\nu)$ are shown for comparison

Prior to each measurement, the pathlength of the empty cell was determined by counting fringes. The thicker cell ($b(1) = 152.6$ μm) was then filled with CCl_4 and interferograms of the solvent (front beam) and an air reference (back beam) were measured in double-precision (32 bits per datum) at several different nominal resolutions and stored in the memory of the data system of the spectrometer. The cell was then emptied, dried, and refilled with the solution, and interferograms of the solution and a corresponding air reference were then measured under the same conditions as the solvent measurements. The same procedure was followed for measurements in the thinner cell, for which $b(2) = 95.5$ μm. For each resolution and cell thickness, the absorbance spectrum of the solute, A^a_ν, was obtained by first calculating the transmittance spectra of the solution and solvent, converting each to a linear absorbance format and subtracting the solvent spectrum from the solution spectrum. By using this procedure, long-term variations in atmospheric water absorption could best be compensated.

Spectra were calculated using both boxcar truncation and triangular apodization. Resolution settings intermediate between the nominal values on our instrument (0.5, 1, 2, 4, and 8 cm^{-1}) could be obtained by suitably adjusting the breakpoints of a trapezoidal apodization function. All interferograms giving nominal resolution values numerically greater than or equal to 2 cm^{-1} were zero-filled so that at least eight output points per resolution element were calculated (*6*).

By changing the cell pathlength and not the sample concentration, any effects due to intermolecular interactions were limited, and an accurate value for k_1 could be calculated from the ratio of the two pathlengths. For our cells, $k_1 = b(2)/b(1) = 0.626$.

COMPUTED RESULTS

Triangular Apodization. An illustration of the way in which a Lorentzian band is distorted by limited instrument resolution is presented in Figure 1. The curve A^t_ν is the true band shape with a peak absorbance, $A^t_{peak} = 1.3$. The curve A^a_ν illustrates how this band would appear if measured with a ρ value of 0.2. Note that although the Ramsay criterion is met, A^a_{peak} is only about 85% of A^t_{peak}.

The result of attempting a spectral compensation experiment when the reference peak absorbance, $A^t_{peak}(1)$, is 1.3 and the sample peak absorbance, $A^t_{peak}(2)$, is 1.1 and $\rho = 0.2$ is shown in Figure 2. Ideally the reference spectrum should be scaled by the factor $k_1 = 1.1/1.3 = 0.8462$ but as is seen from curve A, this produces incomplete compensation since the apparent peak absorbance of the sample is actually 0.8672 $= k_2$ times that of the reference. Curve B shows how the use of k_2 as a scaling factor produces exact compensation at the

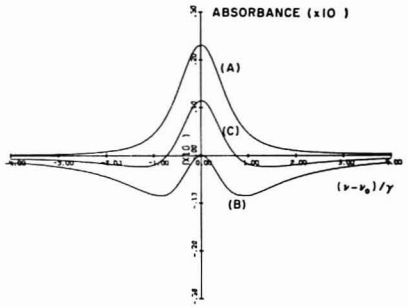


Figure 2. Difference spectra, $|A^a_\nu(2) - kA^a_\nu(1)|$, for $A^t_{peak}(1) = 1.30$ and $A^t_{peak}(2) = 1.10$, calculated using a sinc^2 x ILS with $\rho = 0.2$. Spectrum A is for $k = k_1$, spectrum B is for $k = k_2$, and spectrum C is for $k = k_3$

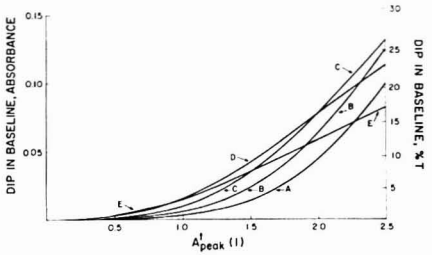


Figure 3. Magnitude of the dip in the baseline due to uncompensated absorbance calculated for various values of ρ as a function of $A^t_{peak}(1)$ for $k_1 = 0.85$, assuming a sinc^2 x ILS. (A) $\rho = 0.05$, (B) $\rho = 0.1$, (C) $\rho = 0.2$, (D) $\rho = 0.5$, (E) $\rho = 1.0$

peak but too much compensation elsewhere. Curve C is the result using $k_3 = 0.8567$, and although the integrated absorbance of the band is zero, complete compensation is not achieved and is in fact impossible.

When compensation experiments are performed in practice using a sinc^2 ILS, it is probable that the optimum scaling factor chosen on a trial and error basis will lie between k_1 and k_2 and be closest to k_3. If quantitative information is to be derived from the value of the empirical scaling factor, it will be in error by approximately $100(k_3 - k_1)/k_1$ percent but by no more than $100(k_2 - k_1)/k_1$ percent. For the above example the former quantity is 1.24% and the latter 2.48%.

Figure 3 shows, in both absorbance and % T units, the magnitude of the dip in the baseline (100% T line) due to uncompensated absorbance which will result when $k_1 = 0.85$ if the scaling factor k_1 is used. The dip when using k_3 or an empirical scaling factor will be smaller than this by a factor of 2 to 3. It is seen that the dip increases rapidly as A^t_{peak} becomes large and somewhat less rapidly with ρ. (The apparently anomalous result that curve E for $\rho = 1$ lies below curves for smaller ρ values over much of the range is due mainly to the fact that a large value of ρ significantly lowers the apparent peak heights of the bands. If A^a_{peak} had been used for the abscissa, this anomalous behavior would disappear.) The dip is generally larger for smaller values of k_1, and for $0.8 < k_1 < 1.0$ the magnitude of the dip for weak bands is approximately proportional to $(1 - k_1)$.

In order to quantify the limitations on spectral compensation experiments imposed by limited resolution, we have determined the maximum values of $A^t_{peak}(2)$ which will produce less than a 1% T dip in the baseline when using k_1

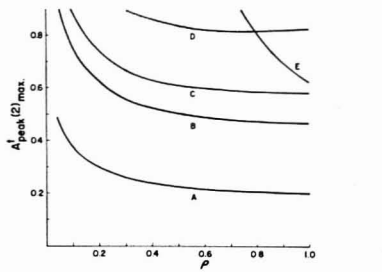


Figure 4. Maximum value of $A^t_{peak}(2)$ producing a 1% dip in the baseline calculated as a function of ρ for several different values of k_1, assuming a sinc^2 x ILS. (A) $k_1 = 0.50$, (B) $k_1 = 0.85$, (C) $k_1 = 0.90$, (D) $k_1 = 0.95$; curve E gives the corresponding plot for $k_1 = 0.85$ for a sinc x ILS

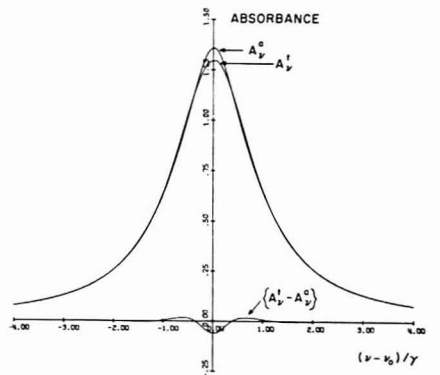


Figure 5. Apparent absorbance spectrum, A^a_ν, of a Lorentzian band with $A^t_{peak} = 1.30$, calculated using a sinc x ILS with $\rho = 1.0$; the true absorbance spectra, A^t_ν, and $(A^t_\nu - A^a_\nu)$ are shown for comparison

for a scaling factor for various values of k_1 and ρ and these results are presented in Figure 4. With triangular apodization for each value of k_1, the maximum allowed value of $A^t_{peak}(2)$ decreases rapidly until ρ reaches about 0.3 and then levels off. Thus for a true peak absorbance ratio of 0.9, any band with a true peak absorbance less than 0.58 can be compensated with any practical value of ρ, but if $A^t_{peak}(2)$ is twice this value, no practical resolution may permit compensation to the specified accuracy. A careful control over pathlength and concentration in compensation experiments is therefore necessary.

Boxcar Truncation. When spectra are computed from triangularly apodized interferograms, A^a_{peak} is always less than A^t_{peak}; however for spectra computed from unapodized interferograms, A^a_{peak} may be greater or less than A^t_{peak}. For weaker bands measured with $\rho > 1.0$, A^a_{peak} is always less than A^t_{peak}; but if $\rho < 1.0$, A^a_{peak} is often larger than A^t_{peak} and for strong lines the apparent transmittance of the band can fall below zero and become negative. In this case A^a_{peak} cannot be computed, and absorbance subtraction procedures are precluded.

For weak bands ($A^t_{peak}(1) < 1.0$), better compensation can be achieved for spectra measured with a sinc ILS and $\rho = 1.0$ than for the same spectra measured with a sinc^2 ILS and $\rho = 0.2$. Even for fairly strong bands ($1 \leq A^t_{peak}(1) \leq 1.5$) our calculations suggest that the compensation for spectra measured from unapodized interferograms and $\rho = 1.0$ should

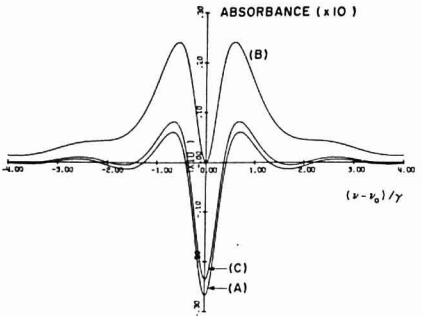


Figure 6. Difference spectra, $|A^a_x(2) - kA^a_x(1)|$, for $A^t_{peak}(1) = 1.30$ and $A^t_{peak}(2) = 1.10$, calculated using a sinc x ILS with $\rho = 1.0$. Spectrum A is for $k = k_1$, spectrum B is for $k = k_2$, and spectrum C is for $k = k_3$

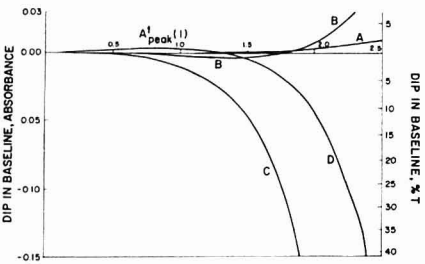


Figure 7. Magnitude of the dip in the baseline due to uncompensated absorbance calculated for various values of ρ as a function of $A^t_{peak}(1)$ for $k_1 = 0.85$, assuming a sinc x ILS. (A) $\rho = 0.5$, (B) $\rho = 0.7$, (C) $\rho = 1.0$, (D) $\rho = 3.0$

be about as good as that achieved for spectra measured from triangularly apodized interferograms and $\rho = 0.2$ if k_1 is not very different from unity. This can be seen by comparing the spectra shown in Figures 5 and 6 calculated for $A^t_{peak}(1) = 1.3$, $A^t_{peak}(2) = 1.1$, $\rho = 1.0$, and a sinc ILS with those shown in Figures 1 and 2 for the identical bands calculated with $\rho = 0.2$ and a sinc^2 ILS. (Note with the sinc ILS that k_1 produces overcompensation at the peak and that results with k_1 and k_3 are comparable.) Compensation experiments with $\rho \sim 1.0$ and a sinc ILS cannot be performed if A^t_{peak} is much greater than about 1.5 since A^a_{peak} increases rapidly beyond this value and T^a_{peak} becomes negative as A^t_{peak} exceeds 2.2.

The dip in the baseline produced with k_1 and boxcar truncation is shown in Figure 7. Negative values for the dip imply overcompensation. The dip with k_3 would be about the same. A comparison with Figure 3 suggests that far better compensation at the peak should be achieved with boxcar truncation than with triangular apodization for bands with $A^t_{peak}(1) < 1.0$.

The results in Figures 3 and 7 may be somewhat biased in favor of the sinc ILS, since the values for $A^a_{peak}(1)$ were scaled by k_1 and not by k_3 which is probably a closer approximation to the factor by which spectra are scaled in practice. Whereas results would be little changed for a sinc ILS if k_3 were used, the use of k_3 rather than k_1 would improve results for a sinc^2 ILS (by about a factor of two).

EXPERIMENTAL RESULTS

Triangular Apodization. For the cells being used in this study, $k_1 = b(2)/b(1) = A^t_{peak}(2)/A^t_{peak}(1) = 0.626$. Since this value is significantly different from unity, we would expect to find appreciable resolution errors in the measured difference spectra if $A^t_{peak}(1) > 1$ for both boxcar truncation and triangular apodization, but good compensation if $A^t_{peak}(1) < 0.5$. To check these predictions made from our calculations, a 0.916 M solution of benzonitrile in CCl_4 was used. For this solution in the thicker cell, A^t_{peak} for the three strongest bands is approximately 1.5, while the peak absorbance for the weak bands between 2000 and 1500 cm^{-1} is less than 0.20 (see Figure 5 of Reference 3).

Difference spectra were plotted for three resolution values (2, 4, and 8 cm^{-1}) using scaling factors of $0.626 + 0.04\,n$, where $n = -1, 0, 1, 2, 3$, and 4. The results for triangularly apodized interferograms are shown in Figure 8. The scaling factor giving the best compensation, k_{opt}, was found to be dependent on A^t_{peak} and 2γ for each band as expected. Although it cannot be easily seen from this figure, optimum compensation for weak bands was found with $k_{opt} \sim 0.67$ for each resolution, giving a quantitative error, $100(k_{opt} - k_1)/k_1$, of 7%. A somewhat larger scaling factor was required to minimize the features in the difference spectra due to the three strong bands. The relatively broad band at 2231 cm^{-1} was best compensated with $k_{opt} = 0.66$ for 2 cm^{-1} resolution, $k_{opt} = 0.685$ for 4 cm^{-1}, and $k_{opt} = 0.71$ for 8 cm^{-1} resolution. As expected, the two sharp bands at 1492 and 1448 cm^{-1} required even greater scaling factors of 0.70, 0.72, and 0.74 for 2, 4, and 8 cm^{-1} resolution, respectively, for optimum compensation. It was never possible to minimize the features in the difference spectra caused by the strong bands and the weak bands simultaneously. It was found that the magnitude of the largest features in a difference spectrum calculated using the value of k giving the best *overall* compensation for both strong and weak bands was slightly smaller for the measurements made at 8 cm^{-1} resolution. Once again this is due mainly to the decreased peak heights observed with large ρ values (cf.

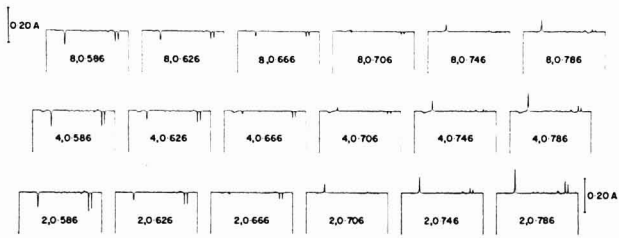


Figure 8. Difference spectra, $|kA^a_x(1) - A^a_x(2)|$, for a 0.916 M solution of benzonitrile in CCl_4 using cells with $b(1) = 152.6$ μm and $b(2) = 95.5$ μm, measured at resolutions of 2 cm^{-1} (lower row), 4 cm^{-1} (middle row), and 8 cm^{-1} (upper row), computed with triangular apodization, and plotted between 2500 cm^{-1} and 1300 cm^{-1} using scaling factors of $k = k_1 + 0.04n$, where $k_1 = 0.626$ and $n = -1, 0, 1, 2, 3$, and 4

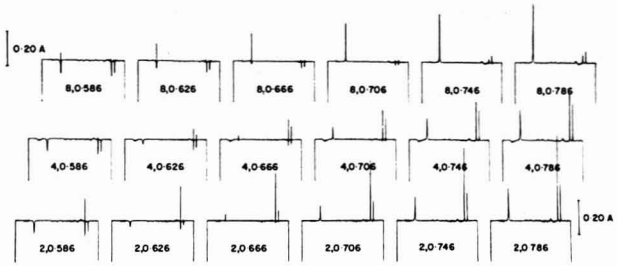


Figure 9. Difference spectra, $|kA^a_\nu(1) - A^a_\nu(2)|$, computed from the same set of interferograms and plotted with the same parameters as the spectra in Figure 9, but without apodization; the difference in the behavior of the two sharp bands at 1492 and 1448 cm^{-1} for 2-cm^{-1} resolution is particularly significant

discussion of Figure 3). If the width of the bands had been much greater than the values shown in Table I, better compensation would have been found for the measurements made at higher resolution. If quantitative data are desired from the value of k_{opt} required to give the best compensation, it can be said as a general rule that the greater is ρ or $A^t_{peak}(1)$, the greater is the quantitative error.

Boxcar Truncation. Difference spectra were then computed from the same interferograms used to compute the data shown in Figure 8, but without apodizing the interferograms. These spectra, which are shown in Figure 9, somewhat surprisingly indicate that the weak bands are again best compensated with a scaling factor of 0.67, and show that the behavior of the strong bands on spectral subtraction is quite different when the interferograms are not apodized. The shape of the difference feature for each band is strongly dependent on the value of ρ. For example, the strong but relatively broad band at 2231 cm^{-1} is fairly well compensated with $k = k_1$ if $\rho \leq 0.5$. However at 8 cm^{-1} resolution ($\rho \sim 1$) the compensation is never very good, and a fairly large feature is seen in the difference spectrum no matter what scaling factor is applied. From the sharper bands at 1492 and 1448 cm^{-1} measured at 2 cm^{-1} resolution, it is seen that for $\rho \sim 1$ the magnitude of the features in the difference spectra can depend on very small differences in ρ. For example, with $k = 0.626$, the slightly narrower band at 1448 cm^{-1} ($2\gamma = 2.2$ cm^{-1}) appears quite well compensated, but the broader band at 1492 cm^{-1} ($2\gamma = 2.7$ cm^{-1}) is poorly compensated.

Our calculations had led us to expect that for spectra computed without apodization, rather poor compensation could be expected for larger values of A^t_{peak} when $\rho \sim 1$. The experimental results suggest that this is true sometimes, but not always. If experimental values of A^a_{peak} are plotted against ρ, the explanation for this effect becomes apparent. A typical plot is shown in Figure 10, where it can be seen that for $\rho < 1.5$, A^a_{peak} is actually a very rapidly varying function of ρ. The greater A^t_{peak}, the greater is the amplitude of the oscillations in the region where $\rho \sim 1$. As A^t_{peak} approaches 2, the variation can become so large that the apparent transmittance becomes negative for certain values of ρ. If $A^t_{peak} < 1$, the variation is quite small and $A^a_{peak} \sim A^t_{peak}$ for $\rho < 1$. Similarly if $\rho < 0.2$, A^a_{peak} is approximately equal to A^t_{peak}. In either case excellent compensation is achieved, and the quantitative error is small.

For the strong bands in the spectra of our samples ($0.80 < A^t_{peak} < 1.75$) the maxima and minima of such plots appear to fall at approximately the same values of ρ. Thus if ρ happens to take a value such that $A^a_{peak} \sim A^t_{peak}$, good compensation will result, as illustrated by line A in Figure 10. However if ρ is such that A^a_{peak} is at a maximum or minimum on the curve (see line B in Figure 10), very poor compensation

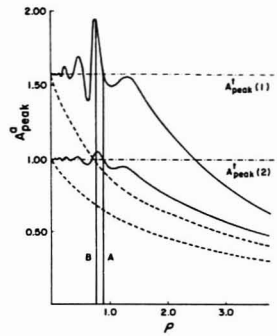


Figure 10. Experimental variation of A^a_{peak} with ρ for the 1492 cm^{-1} band of a 0.916 M solution of benzonitrile measured in cells with $b(1) = 152.6$ μm and $b(2) = 95.5$ μm, both unapodized (—) and apodized (---); the values of $A^t_{peak}(1)$ and $A^t_{peak}(2)$ are included for comparison. Line A is for $\rho = 0.90$, for which $A^a_{peak} \sim A^t_{peak}$ for both samples, i.e., $k_2 \sim k_1$; line B is for $\rho = 0.74$, and $A^a_{peak} \neq A^t_{peak}$ for either sample, and $k_2 \sim 0.54$

can result. This behavior explains why the band at 1448 cm^{-1} measured at 2 cm^{-1} resolution is well compensated, since $\rho = 0.90$ (line A in Figure 10). On the other hand, the band at 1492 cm^{-1} is poorly compensated, since $\rho = 0.74$ (line B in Figure 10).

It should be emphasized that the rapid oscillation in A^a_{peak} with ρ observed experimentally near $\rho = 1$ is not predicted by our calculations, and we have no satisfactory explanation for the effect. Apparently these oscillations in the plot of experimental values of A^a_{peak} vs. ρ near $\rho = 1$ were not observed in our earlier report (Reference 3, Curve A of Figure 6) since data had only been taken for the 2231 cm^{-1} benzonitrile band measured at the nominal resolution settings of 0.5, 1, 2, 4, 8, and 16 cm^{-1} so that only one data point was obtained near the critical region near $\rho = 1$. No intermediate values had been investigated, and a smooth curve was drawn through the observed values of A^a_{peak}. Further investigations into this effect are being made, and at this stage we are inclined to believe the computed results are probably more accurate than the experimental data, but the cause of the experimental error has not yet been determined.

For spectra measured without apodization at lower resolution than 2 cm^{-1}, the quantitative error for all three strong bands is less than it was when the interferograms were triangularly apodized, although the magnitude of the residual feature in the difference spectrum is usually greater. When $\rho > 2$, the side-lobes generated by the sinc x ILS are also very

apparent in the difference spectrum.

DISCUSSION

The results described above are of importance for several applications in which scaled absorbance subtraction techniques have been used. These include solvent compensation for the accurate measurement of solute spectra, elimination of features due to atmospheric components such as H_2O and CO_2, and studies of intermolecular interactions.

Solvent Compensation. For the measurement of solute spectra, absorption features due to the solvent can be removed from the spectrum either by placing in the reference beam a cell containing an optical thickness of pure solvent exactly equal to that in the sample beam, or by using scaled absorbance subtraction routines. It is not easy experimentally to adjust the pathlength of a variable pathlength cell to better than 0.5 μm in order to compensate for all absorption bands, so that digital methods, using the same cell to hold the solution and solvent reference, are commonly applied by users of FT-IR spectrometers. (It should be noted that this technique eliminates vignetting errors and minimizes wedging and reflectivity errors.) If good solvent compensation is required, the cell pathlength must be short enough that no band "blacks out" in the spectral range of interest, but sufficiently long that solute absorption is appreciable at reasonably low concentration (to minimize the effect of intermolecular interactions).

To illustrate what is involved for this type of measurement, consider the measurement of the spectra of aqueous solutes in the fingerprint region of the spectrum. Using the shortest sealed CaF_2 cell, we have been able to obtain commercially (measured pathlength = 19.1 μm), the peak absorbance of the strongest solvent band, the H–O–H bending mode at 1640 cm^{-1}, is 2.20 and 2γ for this band is 94 cm^{-1}. To obtain a high signal-to-noise ratio (SNR) in the solvent compensated spectrum around 1640 cm^{-1}, we performed all measurements at 8 cm^{-1} resolution, so that ρ for the 1640 cm^{-1} band is 0.085.

Under these conditions, our calculations and experiments suggest that better compensation should be found for spectra computed without apodization than if triangular apodization is applied. However, in the former case $A^a_{peak} = 2.21$ ($T^a_{peak} = 0.62\%$) and in the latter case $A^a_{peak} = 1.83$ ($T^a_{peak} = 1.48\%$). For equal numbers of scans, the noise level of a spectrum computed without apodization is $\sqrt{2}$ times higher than that of a spectrum computed with triangular apodization (7). Therefore the SNR at 1640 cm^{-1} will be $(2)^{1/2}(1.48/0.62) = 3.4$ times greater for the spectrum computed after triangular apodization than for the one computed without apodization. Obviously, a decision between photometric accuracy and high SNR must be made by the spectroscopist.

Similar considerations apply to the measurement of the spectra of solutes in nonaqueous solvents for which the absorption bands are usually much narrower than the rather broad water band discussed above. To avoid the effect of resolution errors for measurements where a large degree of scaling is required, it is necessary to keep the pathlength as short as possible so that the peak absorbance for all bands which are being subtracted is less than about 1.0. Otherwise all information in the region of strong bands should be disregarded.

Compensation of Atmospheric Absorption. Most infrared spectroscopists occasionally have the need to remove the effect of atmospheric absorption features (especially those due to water vapor) from ratio-recorded spectra measured using an incompletely purged or unpurged spectrometer. Absorption lines in the vibration–rotation spectrum of water vapor are so narrow (even when broadened by air) that ρ is usually much greater than one. Even for lines which appear to be of only moderate intensity when measured at, e.g., 4 cm^{-1} resolution, A^t_{peak} may be greater than 10 or even 100. When

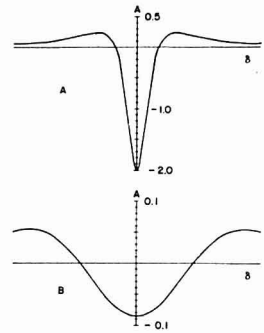


Figure 11. A simulated experiment for the investigation of self-broadening coefficients, in the absence of (A), and in the presence of (B), resolution errors. (A) $A^t_A(2) - 2A^t_A(1)$, for $A^t_{peak}(1) = A^t_{peak}(2) = 2.0$, and $\gamma(2) = 2\gamma(1)$. (B) $A^a_A(2) - 2A^a_A(1)$, for $A^t_{peak}(1) = A^t_{peak}(2) = 2.0$, $\gamma(2) = 2\gamma(1)$, and $\rho(1) = 2\rho(2) = 4.0$, assuming a sinc^2 x ILS

such lines are measured using triangular apodization, A^a_{peak} is proportional to $(A^t_{peak})^{1/2}$ (3). Therefore, Beer's law is not obeyed and scaled absorbance subtraction techniques cannot be used to completely eliminate these lines from spectra. If boxcar truncation is used for the computation of the spectra, the apparent transmittance can sometimes become negative, and the application of scaled absorbance subtraction routines is impossible. This effect has been illustrated previously for the atmospheric CO_2 band at 2347 cm^{-1} (see Figure 3 of Reference 3).

Studies of Intermolecular Interactions. It has been suggested that absorbance subtraction is a convenient way of studying real deviations from Beer's law in solution or pressure broadening effects in gases (8). Though this may be true, the effects of limited resolution must be considered.

For the solution experiment one would typically measure the absorbance spectrum at one concentration and then double the solute concentration and measure the spectrum again. The first spectrum would be scaled by a factor of two and subtracted from the second. In the absence of deviations from Beer's law, exact cancellation would result and any peaks observed in the difference spectrum, therefore, reflect deviations. Such deviations, however, may not be real, since the procedure corresponds to compensation using the scale factor k_1, and because the ratio of peak heights is far from 1, the effects illustrated in curve A of Figure 2 may be significant.

For the pressure broadening experiment one would measure the spectrum of a gas at two different pressures and absorbance subtract using the ratio of pressures as a scaling factor. When the pressure of a pure gas is doubled, the width of a vibration–rotation line doubles (halving the value of ρ), and the true peak height remains constant. (Typical conditions where linewidths are determined by pressure broadening are assumed.) The result for an experiment in which this happens is illustrated in Figure 11. A true peak absorbance of 2.0 was assumed for the band, ρ values of 4.0 and 2.0 for spectra 1 and 2, and triangular apodization. The upper curve represents what would be observed in the absence of instrumental errors and the lower curve what would actually be observed. It can be seen that, although there is a real effect, the observation of it is obscured by limited resolution, and any attempt to measure the amount of pressure broadening, for example by measuring the distance between zero ordinates, which ignores this factor would produce a serious error.

Frequency Shifts. The preceding discussions have focused on the way in which instrumental resolution affects peak

heights. If the bands are symmetrical, these will be the only effects. It should be recognized, however, that if the bands are unsymmetrical, limited resolution can also cause shifts in the apparent peak frequencies. This can cause additional problems with absorbance subtraction.

Spectral Subtraction with Grating Monochromators. Now that digital data systems have been developed for infrared grating spectrophotometers, spectral subtraction experiments can also be performed on this type of instrument. The results of calculations to find the effect of ρ on A^a_{peak} for a triangular slit function (*3*) are very similar to the results of calculations for a sinc^2 ILS at all values of ρ if $A^a_{peak} < 1$. For strong bands measured with a sinc^2 ILS, A^a_{peak} is proportional to $(A^t_{peak})^n$, where $n < 1$. If ρ is large, $n = 1/2$, but for small ρ, n can become even smaller. For a triangular slit function, the square root relationship ($n = 1/2$) is observed for large ρ, but the larger errors for small ρ are not found. Therefore, if a monochromator has a triangular ILS, subtraction experiments for strong bands should be able to be performed more effectively (but still not perfectly) with a monochromator than with a Fourier spectrometer and triangular apodization.

On the other hand the effect of stray light is generally much greater for a monochromator than for a rapid-scanning Fourier spectrometer. If stray light represents an appreciable proportion of the transmitted energy, the Lambert–Beer law is not followed, and subtraction experiments will not be successful. (With stray light, the ILS is no longer triangular.) In practical experiments we have shown that good subtractions are only achieved when $A^t_{peak} < 1$, and in this case the effect of stray light will be small. Therefore difference spectra measured using a grating monochromator and a Fourier spectrometer with triangular apodization will be very similar in practice.

Other Apodization Functions. No ILS will cause A^a_{peak} to be proportional to A^t_{peak} over a wide range of A^t_{peak} and ρ. However since a sinc x ILS can cause A^a_{peak} to be greater than A^t_{peak} for strong bands, while a sinc^2 x ILS always causes A^a_{peak} to be less than A^t_{peak}, it would appear that an apodization function somewhere between boxcar and triangular might be optimum for subtraction experiments involving strong bands. Such a function might be a trapezoid with the third break point about half way along the interferogram, but the amplitude of the side-lobes of the ILS for this function is still quite large. Other functions which might weight the data array more strongly near zero retardation than the triangular apodization function but which do not have the discontinuity of the trapezoidal function may well have the desired effect. Such a function might be the commonly used Hamming function (*9*); however, in view of the fact that recent studies (*10*) have shown that neither the triangular nor the Hamming function produces the optimum combination of resolution and side-lobe suppression, the optimum function is more likely to be either one of the trigonometric functions described by Filler (*11*) or the polynomial algebraic functions described by Norton and Beer (*10*). One of us (P.R.G.) is now starting to investigate the relative utility of these apodization functions for spectral subtraction experiments.

Other Measurement Errors. Even in the absence of resolution errors, absorbance subtraction experiments may only be performed accurately using homogeneous samples (such as solutions, gases and, to a lesser extent, KBr disks) held in cells of uniform pathlength. Useful experiments have been carried out using cast films of polymers (*2*), but the pathlength of these films may be expected to vary slightly across the sample. Solid samples prepared as mineral oil mulls are not homogeneous, and subtraction experiments would not be expected to work well for this type of sample. Imperfect subtractions can also be caused by wedge effects of cells, vignetting, and front surface reflections. However, in carefully controlled experiments, each of these effects is usually far smaller than the effect of resolution errors, and should be negligible.

LITERATURE CITED

(1) T. Hirschfeld, *Anal. Chem.*, **48**, 721 (1976).
(2) J. L. Koenig, *Appl. Spectrosc.*, **29**, 293 (1975).
(3) R. J. Anderson and P. R. Griffiths, *Anal. Chem.*, **47**, 2339 (1975).
(4) J. R. Neilsen, V. Thornton, and E. B. Dale, *Rev. Mod. Phys.*, **16**, 307 (1944).
(5) D. A. Ramsay, *J. Am. Chem. Soc.*, **74**, 72 (1952).
(6) P. R. Griffiths, *Appl. Spectrosc.*, **29**, 11 (1975).
(7) P. R. Griffiths, *Anal. Chem.*, **44**, 1909 (1972).
(8) T. Hirschfeld and K. Kizer, *Appl. Spectrosc.*, **29**, 345 (1975).
(9) R. B. Blackman and J. W. Tukey, "The Measurement of Power Spectra", Dover, New York, N.Y., 1959, p 98.
(10) R. H. Norton and R. Beer, *J. Opt. Soc. Am.*, **66**, 259 (1976).
(11) A. H. Filler, *J. Opt. Soc. Am.*, **54**, 762 (1964).

RECEIVED for review August 11, 1977. Accepted August 1, 1978. The authors gratefully acknowledge the financial support provided by the National Science Foundation. This work was presented in part at the 1977 International Conference on Fourier Transform Infrared Spectroscopy, Columbia, S.C., June 23, 1977.

Speed of Analysis in Open Tubular Columns Gas Chromatography

Georges Guiochon

Laboratoire Chimie Analytique Physique, Route de Saclay, 91128 Palaiseau Cedex, France

The optimization of capillary columns is discussed, and a number of practical rules are given. It is shown that small diameter open tubular columns offer large possibilities of improving current performances. The analysis time is proportional to column diameter, while the detection limits are practically constant, although the sample size has to decrease in proportion to d_c^2. The necessary inlet pressure, although higher than usual, is easy to achieve. For easy separations, packed columns offer more reasonable experimental conditions. Although their performances can also be improved by the use of small particles, they cannot compete with open tubular columns in terms of analysis time. Small diameter capillary columns ($d_c < 0.1$ mm) demand specially designed equipment, contributing little to band broadening, but offer the possibility to achieve the separation of very closely related compounds.

The past year has seen a rebirth of capillary columns in gas chromatography. The interest in their use is rapidly increasing and a variety of new techniques of preparation have been published. The use of glass capillaries is favored, with a consequence, which has been perceived by only one group yet (*1*), the possibility to select the inner diameter most suited to any given analysis. Glass drawing machines are very flexible, and it is easy, using any of the recommended processes, to prepare a column of any length and diameter.

The use of columns of large inner diameter, with a porous layer of an inert support of Chromosorb (2), Silanox (*3*), or graphitized Carbon black (*4*) or without such a layer (*5*), has already been recommended as a means to increase the sample size and thus to decrease the detection limits in GC or in GC-MS. Certainly caution is strongly advised in that matter, as the detection limits are functions of many parameters and the effect of column diameter on efficiency, gas flow-rate, etc. may reduce the actual effect much below what is expected.

It does not seem yet to have been realized how the analysis time is directly related to the column diameter and how the actual performances of equipment can be considerably improved by using small diameter columns. The present paper discusses the theoretical background of the problem. Some experimental results will be given in a forthcoming paper. We discuss first the parameters which determine the analysis time and the way to reduce it, then the effect on detection limits, and the requirements regarding equipment whose contribution to peak broadening should not be too large.

THEORETICAL

Preliminary. The analysis time increases rapidly with difficulty of separation. As we show later, it increases more rapidly that the necessary plate number N. This number is related to the thermodynamics data by:

$$N = 16R^2\left(\frac{\alpha}{\alpha-1}\right)^2\left(\frac{1+k'}{k'}\right)^2 \qquad (1)$$

where R is the resolution requested between two peaks, α the relative retention of the corresponding compounds, and k' the column capacity factor of the second peak. This equation is used below, and we just want to point out here how much N increases rapidly with decreasing $\alpha - 1$. Table I gives some examples.

Table I. Relative Retention, Retention Free Energies, and Column Efficiency

α	$\Delta(\Delta G)^a$ (cal/mol)	N^b	N^c
1.2	146	1 020	1 420
1.15	112	1 670	2 310
1.10	76	3 440	4 760
1.05	39	12 500	17 350
1.03	24	33 500	46 400
1.02	16	74 000	102 000
1.015	12	130 000	180 000
1.01	8.0	290 000	400 000
1.005	4.0	1 150 000	1 590 000

[a] $\Delta(\Delta G) = \Delta G_2 - \Delta G_1$; $T = 400$ K (127 °C). [b] $k' = 3$, $R = 1$. [c] $k' = 1.76$. $R = 1$(The choice of $k' = 1.76$ is justified below in the discussion of Figure 1).

Now α is related (*6*) to the difference between the Gibbs free energies ΔG_1, ΔG_2, associated with the passage of one mole of solute from the stationary to the mobile phase:

$$\Delta(\Delta G) = \Delta G_2 - \Delta G_1 = RT \ln \alpha \qquad (2)$$

or in practice:

$$\Delta(\Delta G) = RT(\alpha - 1) \qquad (3)$$

Table I shows that for difficult separations $\Delta(\Delta G)$ is in the range of a few tens calories per mole or less, which is not much considering that both ΔG_1 and ΔG_2 are in the order of 10 to 30 kcal/mol or about 10^3 times larger.

It is reasonable to think that changing the nature of the stationary phase will affect ΔG_1 and ΔG_2 in a slightly different way and modify largely their difference. This is indeed the basic reason why analysts are using so many different stationary phases and why, in spite of various suggestions to the opposite, the situation is not going to change much with the development of capillary columns: increasing the range of column efficiency practically available by one order of magnitude decreases by a mere factor of 4 the difference in free energies of retention between two compounds which can be resolved (cf. Table I).

Practically all chromatographic separations have to be made in the efficiency range of 10^3–10^6. For easier separation, no optimization is really interesting. The analysis is so fast any way. More difficult separations are almost impossible. This corresponds to a small range of 40 in $\Delta(\Delta G)$, or $\alpha - 1$, which shows how limited is the field of optimization: in many cases it is better to change the stationary phases as analysts have found experimentally.

There are cases, however, when it is just impossible, either because all available phases have been tried unsuccessfully or because the mixture is complex enough and interferences between some compounds on one phase are replaced by interferences between other compounds on another phase.

0003-2700/78/0350-1812$01.00/0 © 1978 American Chemical Society

Any time it is important to reduce the analysis time, the kinetic theory of chromatography can give useful clues.

Flow Velocity through the Column. The integrated Poiseuille law relates the outlet column flow velocity, u_o, to the column length, L, and to the outlet and inlet pressures, P_i and P_o, respectively:

$$u_o = \frac{B_o}{2\eta L P_o}(P_i^2 - P_o^2) \tag{4}$$

where η is the gas velocity and B_o the column permeability, which for an empty tube is:

$$B_o = \frac{d_c^2}{32} \tag{5}$$

while for a packed column it is about (7):

$$\frac{d_p^2}{1000} \tag{5a}$$

Because of the compressibility of gases, the gas velocity varies largely along the column. The average velocity, $\bar{u}$, is given by:

$$\bar{u} = \frac{L}{t_m} = j u_o \tag{6}$$

with:

$$j = \frac{3}{2}\frac{p^2 - 1}{p^3 - 1}, \quad p = \frac{P_i}{P_o} \tag{7}$$

t_m is the transit time of an inert tracer, or the retention time of a nonretained compound.

As we are interested in difficult and rapid analysis, we can assume in most cases that the inlet pressure is large compared to the outlet pressure so Equations 4, 6, and 7 become respectively:

$$u_o = \frac{B_o P_i^2}{2\eta L P_o} \tag{8}$$

$$j = \frac{3P_o}{2P_i} \tag{9}$$

$$\bar{u} = \frac{3B_o}{4\eta L} P_i \tag{10}$$

Equation 10 can be compared to the similar equation written for liquid flow:

$$\bar{u} = \frac{B_o \Delta P}{\eta L} \tag{11}$$

For the same inlet and outlet pressures, the average flow rate at large pressure drop is only $^3/_4$ as large with a gas than with a liquid of the same viscosity.

Plate Height and Gas Velocity. For a capillary column, the plate height is given by the Golay (8, 9) equation:

$$H = \frac{B}{u_o} + C_G u_o + C_L \bar{u} \tag{12}$$

with:

$$B = 2D_G \tag{13}$$

$$C_G = \frac{1 + 6k' + 11k'^2}{(1 + k')^2}\frac{d_c^2}{96 D_G} \tag{14}$$

$$C_L = \frac{k'}{6(1 + k')^2}\frac{d_f^2}{D_L} \tag{15}$$

In practice it is possible to prepare columns with C_L coefficients less than 2–3 times the value calculated from Equation 15, using for d_f, the average film thickness, the ratio $V_L/\pi d_c L$ of the volume of liquid phase coated on the column wall to the wall surface. In such a case, C_L is negligible compared to C_G. It has been observed that with capillary columns, even with relatively large phase ratio, the resistance to mass transfer in the liquid phase is negligible (9). A similar relationship holds for packed columns prepared with low coating ratios.

In these cases we may write:

$$H = \frac{B}{u_o} + C_G u_o \tag{16}$$

or using the reduced plate height and velocity:

$$h = H/d_p \quad (\text{or } H/d_c) \tag{17}$$

$$\nu = \frac{u d_p}{D_G} \quad \left(\text{or } \frac{u d_c}{D_G}\right) \tag{18}$$

In the following we use ν_o for the reduced velocity corresponding to u_o.

$$h = \frac{2\gamma}{\nu} + C\nu \tag{19}$$

with $\gamma = 1$ for an open tubular column and C is easily derived from Equation 14. The packing term ($A\nu^{0.33}$) conventional in the plate height equation of a packed column is neglected here.

The Minimum Pressure. This concept has been suggested by Giddings (10) who has shown that for each analysis, characterized by a chromatographic system, hence a number of plates to achieve, and a column type (including column diameter for an open tubular column), there is a minimum pressure. If the equipment does not permit work at this pressure, the analysis is impossible. The analysis is possible at higher pressures; the higher the pressure, the faster the analysis.

It results from the definition of the plate number and plate height that:

$$L = NH \tag{20}$$

Combination of Equations 8 and 20 gives:

$$u_o = \frac{B_o P_i^2}{2\eta P_o N H} \tag{21}$$

For a given chromatographic system and sample, N is given by Equation 1, B_o and P_o depend on the column characteristics. Only P_i and H can be adjusted. But as shown by Equation 16, H is a function of u_o. Eliminating H between Equations 16 and 21 and solving for u_o gives:

$$\mu_o = \sqrt{\frac{1}{C_G}\left[\frac{B_o P_i^2}{2\eta P_o N} - B\right]} \tag{22}$$

which is meaningful only if:

$$P_i \geq P_i^* \tag{23}$$

with:

$$P_i^* = \sqrt{\frac{2\eta P_o N B}{B_o}} \tag{24}$$

Before discussing the value of this characteristic pressure, we want to stress its importance. No analysis is possible if

the inlet pressure is not at least equal to P_i^*.

The optimum flow-rate and the minimum plate height are easily derived from Equation 16.

$$H_{min} = 2\sqrt{BC} \tag{25}$$

$$u_{opt} = \sqrt{\frac{B}{C}} \tag{26}$$

Introduction of these values in Equation 21 gives:

$$P_{i,opt} = \sqrt{\frac{4\eta P_o N B}{B_o}} = P_i^* \sqrt{2} \tag{27}$$

The analysis time is given by:

$$t_R = \frac{L}{\bar{u}}(1 + k') \tag{28}$$

or

$$t_R = \frac{NH}{ju_o}(1 + k') \tag{29}$$

Combination of Equations 21 and 22 gives:

$$\frac{H}{u_o} = \frac{B_o P_i^2}{2\eta P_o N u_o^2} = \frac{B_o P_i^2 C_G}{2\eta P_o N\left[\frac{B_o P_i^2}{2\eta P_o N} - B\right]} \tag{30}$$

or, using Equation 24:

$$\frac{H}{u_o} = \frac{C_G P_i^2}{P_i^2 - P_i^{*2}} \tag{31}$$

Combination of Equations 9, 29, and 31 gives:

$$t_R = \frac{2N}{3}(1 + k')\frac{C_G P_i^3}{P_o(P_i^2 - P_i^{*2})} \tag{32}$$

It is easy to show by differentiation of Equation 32 that t_R is minimum for:

$$P_i = P_i^* \sqrt{3} \tag{33}$$

The variation of t_R is slow around the minimum. The pressure dependent term, $P_i^3/(P_i^2 - P_i^{*2})$ is 2.60 P_i^* for $P_i = P_i^*\sqrt{3}$ and 2.83 P_i^* for $P_i = P_i^*\sqrt{2}$.

In conclusion the column should be operated around 1.5 times the minimum pressure for optimum performance. Then:

$$t_R = 1.8N(1 + k')\frac{C_G P_i^*}{P_o} \tag{34}$$

As results obviously from Equations 27, 33, and 34 the minimum pressure P_i^* is an important parameter. Table II gives some results. Only values of P_i^* larger than 3 are given. Otherwise the assumption that $P_i >> P_o$ would not be valid.

It is important to observe that the values are much larger with packed columns than with capillary columns, because of the larger permeability of the latter. Finally, the values obtained even for very large plate numbers are not very difficult to achieve. Indeed gas chromatography has been carried out in many instances with inlet pressure larger than 20 atm.

The minimum pressure is independent of the outlet pressure, since B is proportional to D_G (Equation 13) and the product $P_o D_G$ constant in a large pressure range. Thus the three factors which determine the minimum pressure are the plate number, the column permeability, and the nature of the carrier gas.

Table II. Minimum Pressure for Various Separations

	argon	helium	hydrogen	nitrogen
Capillary columns[a]				
$N = 10^5$				
d_c = 50	-	3.5	3.0	-
100	-	-	-	-
$N = 10^6$				
d_c = 50	5.4	11.1	9.6	5.2
100	-	5.5	4.8	-
250	-	2.2	-	-
Packed columns[b]				
$N = 10^4$				
d_p = 50	2.7	5.5	4.8	2.6
80	-	3.6	3.1	-
$N = 10^5$				
d_p = 50	8.5	17.65	15	8.5
125	3.4	7	7	3.3
$N = 10^6$				
d_p = 80	17.2	35	31	17
200	7	14.5	12	7

[a] $D_G = 0.2$ with hydrogen. $P_o = 10^6$ (1 atm). $P_i = (8/d_c)(2\eta D_G P_o N)^{1/2}$. [b] $D_G = 0.2$ with hydrogen. $P_o = 10^6$, $\gamma = 0.8$. $P_i = (20/d_p)(10\eta D_G \gamma P_o N)^{1/2}$. Diameters are in μm. No data are given for low pressures.

The first parameter is a function of the analysis to be made and cannot be changed much. The minimum pressure is proportional to the reverse of the column diameter. We show in the following section, however, that the smaller the column diameter, the faster the analysis. This is already apparent in Equation 34. This leads to the use of rather large pressures. The nature of the carrier gas determines the product ηD_G. Thus hydrogen in preferred to helium (cf. Table III and below).

Optimization of analytical conditions cannot be really achieved after the minimum pressure, although this is a very important parameter. N, C_G, and P_i^* are all functions of more basic parameters and the optimization had better be carried out on the explicit equation.

The Minimum Analysis Time. Combination of Equations 1, 5, 13, 14, 24, 34, gives:

$$t_R = 9.6R^3\left(\frac{\alpha}{\alpha - 1}\right)^3 \frac{(1 + k')^2(1 + 6k' + 11k'^2)}{k'^3} d_c\sqrt{\frac{2\eta}{P_o D_G}} \tag{35}$$

This equation is the same as the one obtained previously in the case of packed columns, replacing B and C by the values these coefficients have for capillary columns (*10*).

It shows that a good resolution factor R is very costly in term of analysis time: it takes 3.4 times longer to achieve a resolution of 1.5 than a resolution of unity. Similarly the analysis time is proportional to the reverse of $(\alpha - 1)^3$ which is a very heavy dependence. In fact, as already shown (*10*), the analysis time is proportional to $N^{3/2}$: an analysis requiring 10^6 plates will be 32 000 times longer than one needing 10^3 plates only. Time is the limiting factor to achieve very difficult separations.

Differentiation of t_R with respect to k' permits the calculation of the optimum value of k': 1.76, a value in close agreement with the one derived earlier through a different approach (Ref. 11, p 1027). The analysis time is smaller than with $k' = 3$, although the plate number is about a third larger as well as the column length (cf. Table I). If we calculate the analysis time by mere combination of Equations 1 and 28 and neglect the influence of k' on H and $\bar{u}$, we find an optimum value of k' equal to 2. As H decreases rapidly with increasing

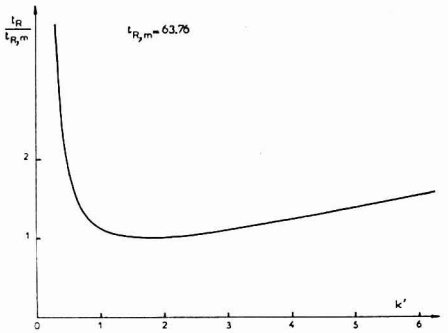


Figure 1. Variation of retention time with the column capacity factor for the second component of the pair of compounds to separate (cf. Equation 35). The minimum is at $k' = 1.76$ for which the k'-dependent factor in Equation 35 is worth 63.76

Table III. Speed Characteristic of Carrier Gas[a]

gas	$\eta \times \sqrt{M}$ ($\mu P \times g^{1/2}$)
argon	1138
carbon dioxide	995
helium	440
hydrogen	90
nitrogen	741

[a] Product of viscosity by square root of molecular weight.

k' in this range, it is normal that the correct optimum is somewhat smaller.

As shown on Figure 1, however, the analysis time does not vary rapidly around the optimum. While k' is between 1.1 and 3, the analysis time is smaller than 1.1 times the minimum and this variation may be neglected. Note, however, that the column length necessary to separate the two compounds decreases with increasing k'. If k' is adjusted by changing the temperature of the column for example, assuming that N does not change with temperature, the analysis time is proportinal to $1 + k'$, the resolution is larger than 1.0 at k' values above 1.76 and smaller for lower k' values, if α is independent of the temperature.

As a first approximation, the diffusion coefficient is proportional to the square root of the reverse of the molecular weight of the carrier gas. Table III gives the value of $\eta\sqrt{M}$ of the most conventional carrier gases and shows that hydrogen is considerably better than all other gases (*12*). It also gives the lowest critical pressure.

Finally Equation 35 shows that the analysis time is proportional to the column diameter and, thus, that the use of 65-μm i.d. columns, which is quite feasible, permits a 4-fold reduction of the analysis time compared to the conventional 0.25-mm i.d. columns.

The analysis times corresponding to the optimum values of the parameters (hydrogen carrier gas, $k' = 1.76$) are given in Table IV for a pair of compounds with various relative retention (same as for Table I) and for columns with 65-μm and 0.25-mm i.d. The values obtained are remarkably small: an analysis requesting about 1.5 million plates is achieved in about 1 h in the optimum conditions with a 0.25-mm i.d. column. Note that it would take 5 h with helium carrier gas. Even taking into account the fact that practical columns are not as efficient as theory predicts, it remains that performances much better than currently obtained could be achieved

Table IV. Retention Times[a] and Length of Capillary Columns Which Can Separate a Pair of Compounds of Given α

	d_c = 65 μm		d_c = 0.25 mm	
α	t_R (s)	L (m)	t_R (s)	L (m)
1.2	26×10^{-3}	0.07	0.1	0.27
1.15	53×10^{-3}	0.11	0.21	0.44
1.10	160×10^{-3}	0.23	0.6	0.90
1.05	1.1	0.85	4.3	3.26
1.03	4.8	2.26	18.6	8.7
1.02	15.7	5.0	61	19.2
1.015	37	8.8	142	34
1.01	122	19.6	473	76
1.005	966	78	3750	299

[a] $t_R = 0.0184(\alpha/(\alpha - 1))^3 d_c$ (d_c, cm; t_R, s). $L = 0.75 \times N d_c = 29.5(\alpha/(\alpha - 1))^2 d_c$.

if long columns can be prepared.

The column length is calculated from Equation 20. Combination of Equations 16, 22, 24, and 33 shows that:

$$H = \left(\sqrt{2} + \frac{1}{\sqrt{2}}\right)\sqrt{BC} = 2.12\sqrt{BC} \qquad (36)$$

$$L = 0.53\frac{Nd_c}{1 + k'}\sqrt{\frac{1 + 6k' + 11k'^2}{3}} \qquad (37)$$

or:

$$L = 8.5R^2\left(\frac{\alpha}{\alpha - 1}\right)^2 \frac{1 + k'}{k'^2}\sqrt{\frac{1 + 6k' + 11k'^2}{3}}\, d_c \qquad (38)$$

The values of L are given in Table IV. Except for the most difficult separation calculated, there is no serious problem to foresee in the preparation of the column.

There are two last problems to discuss: first, we are interested in the analysis of complex mixtures, not usually in the separation of a pair of compounds. Second, we need a more phenomenological approach to optimization to be able to deal with the real columns used in practical applications.

Multicomponent Analysis. The most difficult pair to separate is usually somewhere in the chromatogram, preceded by compounds not too difficult to separate, although as k' decreases the separation power of the column drops sharply, and followed by much more retained compounds.

The column must generate enough plates to separate the critical pair of compounds while giving the minimum retention time for the last component of the mixture (*13*). If k_2' and k_3' are the column capacity factors for the second component of the pair and for the last component of the mixture respectively, let n be:

$$n = \frac{k_3'}{k_2'} = \frac{k_3'}{k'} \qquad (39)$$

The analysis time is then:

$$t_R = \frac{L}{u}(1 + nk') \qquad (40)$$

The column length and the gas velocity are determined by the condition that the pair 1,2 be separated, so N is given by Equation 1, H/u_o by Equation 31 and t_R by Equation 35 modified as shown in Equation 40:

$$t_R = 9.6R_3\left(\frac{\alpha}{\alpha - 1}\right)^3 \frac{(1 + nk')(1 + k')(1 + 6k' + 11k'^2)}{k'^6} d_c\sqrt{\frac{2\eta}{P_o D_G}} \qquad (41)$$

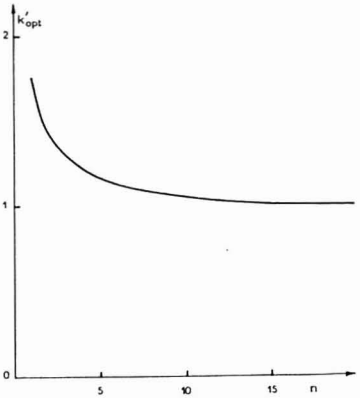


Figure 2. Variation of the optimum value of k' (minimum analysis time) for the second component of the most difficult pair of compounds to resolve in a mixture with the relative retention of the last component of the mixture to the second compound of the pair

Table V. Analysis Time of a Complex Mixture[a]

n	$k'_{opt,2}$	$t_{R,2}$ (s)	$t_{R,n}$ (s)[b]
1	1.76	473	473
1.5	1.55	476	620 (624)
2	1.43	480	763 (775)
3	1.30	489	1042 (1076
4	1.22	497	1317 (1378)
6	1.13	509	1860 (1980)
8	1.08	517	2400 (2600)
10	1.05	523	2935 (3200)
13	1.02	530	3740 (4100)
20	0.99	537	5610 (6200)

[a] $\alpha_{1,2} = 1.01$; column $d_c = 0.25$ mm. [b] In parentheses, analysis time if k' is kept to 1.76 for the second compound.

The conclusions are the same except as regards the optimum value of k'. Differentiation of t_R in respect to k' gives the equation:

$$-3 - (2n + 14)k' - (7n + 17)k'^2 + 11nk'^4 = 0 \quad (42)$$

The optimum value of k' is a function of n, decreasing with increasing value of n. The variation of k'_{opt} with n is given on Figure 2. Obviously for $n = 1$, $k' = 1.76$.

For the sake of comparison, Table V gives the analysis time of a mixture of 3 compounds, with a pair of compounds with $\alpha_{1,2} = 1.01$ and a third compound with increasing values of $\alpha_{2,3}$ from 1 to 20. Obviously the analysis time increases markedly, but so does the number of compounds which can be eluted and resolved, the complexity of the mixture which can be analyzed. The data in the last column of Table V compares the minimum analysis time achieved by optimizing the column capacity factor, and the time obtained by merely keeping the same k' for the most difficult pair of compounds to resolve and waiting. For complex mixtures with a large range of retention times, the reduction can be 10% which is not too rewarding.

The separation of the compounds eluted before the critical pair of compounds is achieved only if their relative retention is large enough. This can be a problem with pair of compounds having a large α value but eluted soon after the unretained tracer, and this is why the analysis of complex mixtures has often to be made in temperature programming.

Table VI. Separation Power of a Capillary Column

k'	$1/(\alpha - 1)$
∞	100 (arbitrary unit)
1.76	80
0.70	60
0.50	50
0.33	40
0.22	30
0.13	20
0.06	10

As the efficiency of capillary columns decreases steadily with increasing k', it is interesting to calculate the variations of the relative retention of a pair of compounds separated by a resolution 1 as a function of k'. For packed columns it is given with a fairly good approximation by solving Equation 1 for α. For a capillary column, we have to take into account the variation of the plate height with k' at constant u_o. As the column length is constant:

$$L = N(k_2')H(k_2') = N(k')H(k') \quad (43)$$

where k_2' is the column capacity factor for the second compound of the pair. $N(k_2')$ is given by Equation 1 with $k' = 1.76$, assuming the analysis has been optimized. $H(k_2')$ is given by Equation 36 (with $k_2' = 1.76$). Combinations of Equations 22 and 33 show that:

$$u_o = \sqrt{\frac{2B_2}{C(k_2')}} \quad (44)$$

Hence:

$$H(k') = B\sqrt{\frac{C(k_2')}{2B_2}} + C(k')\sqrt{\frac{2B_2}{C(k_2')}} \quad (45)$$

We assume in the following that D_G is the same for all compounds, hence $B = B_2$. Hence:

$$H(k') = \sqrt{BC(k_2')}\left(\frac{1}{\sqrt{2}} + \frac{C(k')}{C(k_2')}\sqrt{2}\right) \quad (46)$$

Equation 43 can thus be rewritten:

$$N(k') = 16R^2\left(\frac{\alpha}{\alpha - 1}\right)^2 \frac{(k'+1)^2}{k'^2} = \frac{2.12N}{0.707 + 0.236\,\dfrac{1 + 6k' + 11k'^2}{(1 + k')^2}} \quad (47)$$

Equation 47 can easily be solved for α. It gives as a function of the column capacity factor for the second compound, the relative retention of a pair of compounds which can be resolved with a resolution unity by a column which has N theoretical plates for the compound with $k' = 1.76$.

Figure 3 shows a plot of $\alpha - 1$ vs. k' for the columns (cf. Table I) which give a resolution 1 for the pair of compounds with α between 1.005 and 1.05 and $k_2' = 1.76$. This figure shows that the separation power of a capillary column drops much more slowly than usually believed. From the numerical data used to draw Figure 3 we can calculate (cf. Table VI) the loss of separation power, using $1/(\alpha - 1)$ for the pair of compounds separated with a resolution 1 as a measure of the separation power. The corresponding value of $\Delta(\Delta G)$ would perhaps be a more meaningful measure, but it is somewhat too foreign to the analyst problems. Excellent results are obtained for k' larger than 0.4.

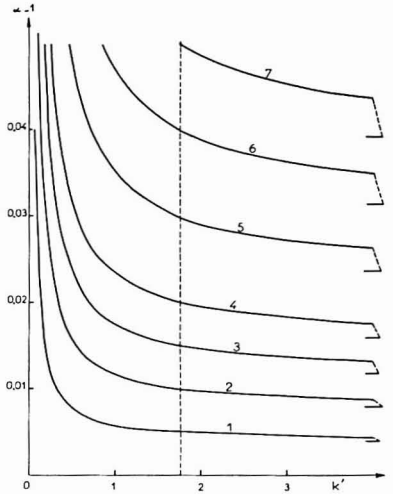


Figure 3. Variation of the relative retention of a pair of compounds separated with a resolution unity, as a function of the column capacity factor of the second component of the pair. The segment at right gives the asymptote of each curve. The different columns correspond to those described in Tables I and V. The values of α for $k' = 1.76$ are respectively (1) 1.005, (2) 1.010, (3) 1.015, (4) 1.020, (5) 1.030, (6) 1.040, (7) 1.050

Optimization for Real Columns. Practical columns often have an efficiency which is somewhat lower than the one predicted from the Golay equation (cf. Equations 12 to 15), although the efficiency is often between 0.5 and 0.8 times the predicted maximum. Lower values tend to be obtained for polar compounds, but various treatments are available to prepare good columns even for these compounds (*14*).

In this case, we cannot rely any more on a theoretical equation for predictions and we have to use a phenomenological approach. We can safely predict however, that the optimum value of k' is between 1.7 and 3.0 (*11*, *15*). As regards the effects of column diameter we can proceed as follows.

Knox (*16*) has shown that the plate height of a chromatographic column can be written:

$$h = A\nu^{0.33} + \frac{B}{\nu} + C\nu \qquad (48)$$

the reduced plate height and velocity being given by Equations 17 and 18, respectively. A is a characteristic of the quality of the column packing and is zero for capillary columns. To be exact and reconcile Equations 12 and 48, we should add a second term to account for the mass-transfer in the stationary phase, a term function of j and ν. As our approach is empirical, we shall not do it. However we cannot completely ignore this phenomenon. Depending whether the resistance to mass-transfer in the stationary phase is important or not, we have to keep constant the average flow velocity or the outlet flow velocity (*15*). Although I am of the opinion that the very efficient columns used in difficult problems where optimization is really useful are lightly loaded and consequently have low resistance to mass-transfer in the liquid phase, the two series of equation are given.

We observe that, in practice, packed columns have a maximum efficiency at a value of the reduced velocity slightly below 2, the reduced plate height being somewhat below 3. As columns are used at a velocity larger than the optimum,

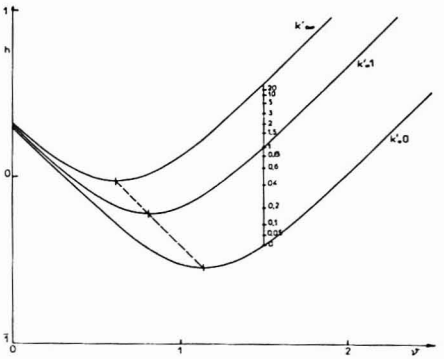


Figure 4. Variation of plate height of a capillary column as a function of velocity. The resistance to mass-transfer in the liquid phase is neglected. Reduced plate height $h = H/d_c$, vs. reduced velocity, $\nu = ud_c/D_G$. The numbers on the vertical scale are the values of k'. (cf. Equation 14). The dotted line is the locus of the minima of the h vs. ν curves

we shall consider that for a packed column $h_m = 3$, $\nu_o = 2$.

For a capillary column, Equation 48 is written:

$$h = \frac{2}{\nu} + \frac{1 + 6k' + 11k'^2}{96(1 + k')^2}\,\nu \qquad (49)$$

Plots of h vs. ν are given on Figure 4 for various values of k'. The optimum value of ν is between 5 and 14 while the minimum value of h is between 0.3 and 1. Indeed values of h lower than 1 for retained peaks have been published (*17*). We have selected conservative values of 1.5 and 5 for h and ν, respectively. It will thus be possible to achieve performances better than predicted below.

The approach used here is similar to the one we have already applied to the optimization of liquid chromatography (*18*). The column length is:

$$L = NH = Nd_c h \qquad (50)$$

where d_c is for the column diameter or the particle diameter.

If we keep constant the average flow rate to maintain constant the plate height, we derive from Equation 10:

$$P_i = \frac{4\eta L\bar{u}}{3B_o} = \frac{128}{3}\eta D_G\, h\bar{\nu}\,\frac{N}{d_c^2} \qquad (51)$$

and from Equation 28:

$$t_R = \frac{L}{\bar{u}}(1 + k') = \frac{h(1 + k')}{\bar{\nu}D_G}\,Nd_c^2 \qquad (52)$$

The equations corresponding to the numerical application discussed later are given in Table VII.

If we keep constant the outlet flow velocity to achieve a constant reduced plate height while changing column length and diameter, we can derive the inlet pressure from Equation 8:

$$P_i = \sqrt{\frac{2\eta LP_o u_o}{B_o}} = \frac{8}{d_c}\sqrt{\eta NhP_o\nu_o D_G} \qquad (53)$$

The retention time is obtained by a combination of Equations 10 and 28:

$$t_R = \frac{4\eta L^2(1 + k')}{3B_o P_i} = \frac{16(1 + k')}{3}\left[\frac{2\eta N^3 h^3 d_c^2}{P_o\nu_o D_G}\right]^{1/2} \qquad (54)$$

Similar equations (cf. Table VII) are obtained for packed

Table VII. Equations for the Optimization of Practical Columns[a]

A. Capillary columns,[b] $L = 1.5\,Nd_c$

$\nu_o = C^{te}$	$\bar{\nu} = C^{te}$
$P_i = 93N^{1/2}d_c^{-1} = 76\,L^{1/2}d_c^{-3/2}$	$P_i = 5.76 \times 10^{-3}\,Nd_c^{-2} = 3.84 \times 10^{-3}\,Ld_c^{-3}$
$t_R = 3.94 \times 10^{-4}\,N^{3/2}\,d_c$	$t_r = 4.5Nd_c^2$

B. Packed columns,[c] $L = 3Nd_c$

$\nu_o = C^{te}$	$\bar{\nu} = C^{te}$
$P_i = 465N^{1/2}d_p^{-1} = 268\,L^{1/2}d_p^{-3/2}$	$P_i = 0.144\,Nd_p^{-2} = 0.048\,Ld_p^{-3}$
$t_R = 1.31 \times 10^{-2}N^{3/2}d_p$	$t_R = 30\,Nd_p^2$

[a] Hydrogen $\eta = 9 \times 10^{-5}P$, $D_G = 0.2$ cm²/s, $P_o = 10^5$ (1 atm). [b] $h = 1.5$, $\nu = 5$, $k' = 2$. [c] $h = 3$, $\nu = 2$, $k' = 3$.

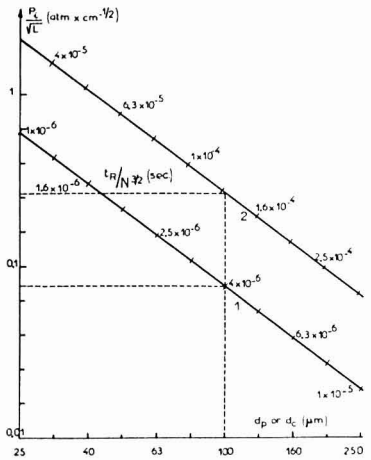


Figure 5. Optimization of real columns operated at constant outlet reduced velocity (to keep h constant). P_i = inlet pressure, L, column length; t_R, retention time; N, plate number. (cf. Table VII). $P_i/\sqrt{L}$ vs. column diameter; d_c (capillary columns) or particle diameter, d_p (packed column). (1) Capillary columns, (2) packed columns. The dotted lines correspond to the examples discussed in the text

columns. The differences are the permeability (cf. Equation 5) and the numerical values of h and ν.

If we plot log $P_i/\sqrt{L}$ vs. log d_c (cf. Figure 5) in the case when ν_o is kept constant, we obtain a straight line with slope of −1.5. Along this line, the ratio of the retention time to $N^{3/2}$ increases in proportion to d_c. A similar plot is obtained for packed columns (cf. Figure 5). In the conditions selected for the numerical application, which are quite typical, the packed column is 33 times slower than the capillary column of same diameter. The best current packed column ($d_p \simeq 100$ μm) is still 12 times slower than the conventional capillary column ($d_c = 0.25$ mm). Thus capillary and packed columns operate in a quite different range of performances.

For example, if we wish to perform an analysis requiring 6000 plates and we want to do it in 60 seconds, a column packed with 100-μm particles will do, the column length will be 1.80 m and the inlet pressure 3.5 atm. But we would need a capillary column of about 3-mm i.d. 27 m long, not very practical. A conventional 225 cm long, 0.25-mm i.d. capillary column gives 6000 plates in 4.7 seconds, which is not practical

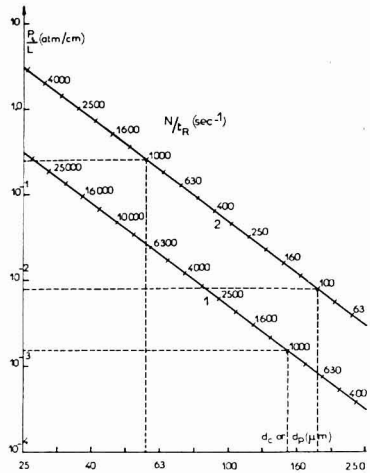


Figure 6. Optimization of real columns operated at constant average flow velocity (to keep h constant). Pressure gradient (P_i/L) vs. diameter. (1) Capillary columns, (2) packed columns. The dotted lines correspond to the examples discussed in the text

either: equipment problems are too difficult to solve. To achieve 60 000 plates in 60 seconds is possible on the other hand with a 100-μm i.d. capillary column, 9 m long with an inlet pressure of 2.4 atm. This would require an impossible packed column, using 3-μm particles, 54 cm long, with an inlet pressure of 380 atm! This example also illustrates how an increase of performances by a factor of 10 (60 000 plates per minute instead of 6000) transforms an easy problem into a very difficult one. The range of performances which are practically possible is thus very narrow. In other words, it is difficult for the expert analyst to do much better than the beginner, which may, in part, explain why the theory of chromatography enjoys a limited interest.

Although the use of charts like Figure 5 is easy to calculate approximately the characteristics of columns necessary to achieve certain kind of performances, it should be emphasized that in the case when ν_o is maintained constant, which is the most important, P_i and t_R are not linear functions of the plate number or column length. This is why we have used $t_R/N^{3/2}$ and not the reverse as the concept of number of plates per unit time is not valid. It is more difficult to generate a few more plates when a large number is necessary than when they are few.

A similar plot can be obtained in the other case, when $\bar{\nu}$ is kept constant (cf. Figure 6). This time, since P_i is proportional to L and N and t_R is proportional to N as in liquid chromatography (*18*), we show a plot of P_i/L vs. d_c and we give the number of plates per unit time as a function of the diameter.

To discuss the same example as above, the generation of 6000 plates in 60 seconds, we can use a 3.2-m long column packed with 180-μm particles (instead of 100 μm) and the pressure drop will be 2.6 atm. The capillary column will have 475-μm i.d., 4.25 m long, and a very small pressure drop. To achieve 60 000 plates in one minute we can use a 10-m long column packed with 57-μm particles, the pressure drop being 256 atm, or a capillary column 150-μm i.d., 13.5 m long with a 2-atm pressure drop.

It might seem tempting to decide that it is better to keep constant the average velocity, which seems to offer slightly

Table VIII. Characteristics of Very Efficient Columns

plate number	t_R (s)	d_c (μm)	P_i (atm)	L (m)
$N = 1.6 \times 10^4$	1.000	12.5	164	30
	2.000	25	47	60
	3.600	50	23	120
	5.000	65	19	156
	7.200	90	13	214
	20.200	250	5	600
	(5 h, 37 min)			
$N = 4 \times 10^5$	500	50	11.5	30
	1.000	100	6	60
	2.000	200	3	120
	3.600	360	2	215

better analytical conditions. It should be stressed, however, that we have no choice. The reduced plate height has to be kept constant if we want to be able to make comparison between columns. There are two extreme cases, discussed here, when this is obtained by keeping constant either the average or outlet velocity, which corresponds, respectively, to experimental conditions where resistance to mass transfer in either the liquid or the gas phase is controlling peak broadening. It is obvious that in many cases intermediary situations will occur, or that, because of the effect of pressure, with a given capillary column or packing material, resistance to mass transfer in the liquid phase may dominate for short columns while resistance to mass transfer in the gas phase prevails for long columns. This together with the experimental problems associated with the preparation of columns of widely different length with internal diameter or particle size covering a large range, means that theory cannot give precise answers but merely point out trends and give useful guidelines.

Finally it is necessary to mention that comparison and optimization of capillary columns assumes that the column capacity factor is kept constant. As:

$$k' = K \frac{V_L}{V_G} = 4K \frac{d_f}{d_c} \tag{55}$$

This means that the average film thickness is varied in proportion to the column diameter. Although it has been shown that the liquid phase is not a continuous film but a dispersion of droplets, so that changing d_f results in changing either the size or the density of these droplets per unit surface area of the column wall, it is not certain that a given preparation procedure can supply good columns giving constant k' in a large range of diameters. This problem, together with other experimental problems, is currently under investigation.

One of the major conclusions is that the more difficult a separation problem is, the more interesting it is to use small diameter columns. There are however pressure limitations. Table VIII gives some characteristics of columns able to give 1.6 million plates ($k' = 2$) in a reasonable time. Comparison with the data in Table IV shows the performances are less good but still fairly acceptable. The analysis time is about 5 times longer. This is because the less efficient column has to be longer and the elution time increases faster at that column length. Furthermore the columns were used at the velocity giving the fastest analysis while they are used merely here at the velocity giving maximum efficiency. The search for the optimum ν (minimum of h^3/ν_o) would offer a faster analysis.

The advantage of using narrow bore columns to achieve difficult separations is thus obvious. There are two more problems to discuss: the smaller the column diameter, the smaller the sample size (this drawback does not occur with packed columns, since particle diameter and column diameter are independent). How does that affect the detection limits? Last, what are the requirements regarding the equipment, in terms of injection time, detector response time, and dead volume?

Detection Limits. The detection limit (*19*) results from the importance of the detector response and the signal noise. When we reduce the column diameter while keeping constant the column capacity factor, we have to reduce the sample size in proportion to the cross-section area. We want to compare the detector signal obtained for a given component of a mixture analyzed on different columns offering the same efficiency.

The maximum concentration (g/cm^3) of the compound in the carrier gas, at column outlet, is given by the following equation which is valid provided the peak be gaussian.

$$C = \frac{m\sqrt{N}}{V_R\sqrt{2\pi}} \tag{56}$$

where m is the sample size.

The retention volume is proportional to column length so we can write:

$$V_R = (1 + k')V_G = (1 + k')A_G L \tag{57}$$

where A_G is the average cross-section area of the gas phase. Combining with Equation 50, we have:

$$C = \frac{m}{(1 + k')A_G} \frac{1}{\sqrt{2\pi N h d_c}} \tag{58}$$

The first factor of the rhs of Equation 58 is kept constant and, because this column is shorter, the concentration at the end of the smaller diameter column is the larger. The concentration is proportional to the reverse of the column diameter since the reduced efficiency is supposed to be the same for all columns. The effect on the detector signal depends on the nature of the detector. There are three kinds of detectors:

(1) Concentration-sensitive detectors, like the thermal conductivity detector or the electron capture detector, give a signal, y, proportional to the concentration:

$$y = SC = S \frac{m}{(1 + k')A_G} \frac{1}{\sqrt{2\pi N h d_c}} \tag{59}$$

Provided the detector cell volume be sufficiently small (cf. following section) the signal increases with decreasing column diameter. The column flow-rate decreases in proportion to d_c^2, the detector noise, which usually is about constant up to a certain flow rate and then increases, will thus not change appreciably. Consequently the detection limit increases in proportion to d_c, i.e., the sensitivity improves when the diameter of the column decreases (*19*).

(2) Concentration-sensitive detector with a scavenger gas. Because it is difficult to build a detector with a very small cell volume, larger detector cells are sometimes used with an additional flow of scavenger gas to sweep the cell and reduce the residence time, which is the important parameter. This flow rate, F_s, being kept constant and supposed to be large compared to the column flow rate, $F_c = \pi d_c^2 u_o/4$, the response is proportional to the concentration of solute in the cell, i.e.:

$$y = SC_d = SC \frac{F_c}{F_s} = S \frac{m}{(1 + k')A_G} \frac{1}{F_s} \frac{\pi d_c u_o}{4\sqrt{2\pi N h}} \tag{60}$$

But u_o is given by Equation 18 since to achieve the same plate number we keep h and u_o constant, so we have:

$$y = S \frac{m}{(1 + k')A_G} \frac{1}{F_s} \frac{\pi D_G \nu_o}{4\sqrt{2\pi N h}} \tag{61}$$

The response and the detection limits are now independent of the column diameter, since provided the columns are operated close to optimum conditions when the diameter is

Table IX. Zone Width at the Outlet of Capillary Columns

N	t_R (s)	k'	d_c, (μm)	F_c[a] (cm³/s)	ω_t (s)[c]	ω_v (μL)[d]
			I. Zone width according to Equation 16			
46 400	19	1.76	250	0.031	0.35	11
	76	10	-	-	1.4	43
102 000	61	1.76	250	0.031	0.76	23
	243	10	-	-	3.0	93
180 000	142	1.76	250	0.031	1.3	40
	566	10	-	-	5.3	164
400 000	473	1.76	250	0.031	3.0	93
	1 885	10	-	-	12	370
	122	1.76	65	8.2×10^{-3}	0.8	6
	486	10	-	-	3.1	25
1 600 000	3 750	1.76	250	0.031	12.	370
	14 950	10	-	-	47	1.460
	966	1.76	65	8.2×10^{-3}	3.0	25
	3 850	10	-	-	12	100
			II. Zone width for real columns at $\nu = 5$ [b]			
400 000	1 000	2	100	8×10^{-3}	6.3	50
	3 700	10	-	-	23	180
	2 000	2	200	16×10^{-3}	12.6	200
	7 400	10	-	-	47	750
1 600 000	3 600	2	50	4×10^{-3}	11	43
	13 200	10	-	-	42	165
	7 200	2	90	7×10^{-3}	23	165
	26 400	10	-	-	83	600
	20 200	2	250	20×10^{-3}	64	1 250
	74 100	10	-	-	234	4 600

[a] $F_c = (\pi d^2/4)u_o = (\pi d^2/4)(2B/C)^{1/2}$, $C = C(1.76)$, cf Equation 14. [b] $F_c = (\pi d^2/4)u_o = (\pi d D_G \nu)/4$. [c] ω_t = Base peak width in time units. [d] ω_v = Base peak width in volume units.

decreased, the reduced dilution (smaller H, larger u_o) compensates for the smaller flow-rate.

(3) Mass-flow sensitive detectors, like the flame ionization detector and to a certain degree the mass spectrometer (when it is used in fragmentography, i.e., recording the current intensity on one or several masses), give a signal proportional to the mass-flow rate of solute:

$$y = S\frac{dm}{dt} = SCF_c \tag{62}$$

since h and ν_o are kept constant, the result is similar to the previous one:

$$y = S\frac{m}{(1+k')A_G}\frac{1}{\sqrt{2\pi N}}\frac{\pi D_G \nu_o}{4h} \tag{63}$$

The sample size per unit column cross-section area being kept constant, the detection limit is unchanged, independent of column diameter, provided S is kept constant. This may require an adjustment as for the FID for example, S is a function of the flow rate of an inert gas.

In summary when using capillary columns, the detection limit is not affected markedly by a decrease in column diameter, provided the column efficiency (N) is kept constant. If the efficiency is increased in the process, the dilution increases the detection limits increases in proportion to $\sqrt{N}$ (i.e., the sensitivity decreases). Sensitivity problems, trace analysis, are no objections to the use of small diameter capillary columns. With packed columns, the sample size and the column cross-section area, A_G, remain constant, thus Equation 59 is also valid, the detection limit of concentration sensitive detectors increases with d_p. However the flow rate is now:

$$F_c = A_G u_o = A_G D_G \frac{\nu_o}{d_p} \tag{64}$$

and the response of a mass-flow sensitive detector is proportional to $1/d_p^2$. The detection limits are then proportional to the square of the particle diameter, which is a strong incentive to the use of fine particles, as long as the corresponding high inlet pressure is accessible and the large flow rate does not interfere with proper detector operation.

As made obvious by the previous discussion, the real problem encountered in practical applications together with column preparation is the one of having equipment which does not destroy the column work, because its response time and dead volumes are too large.

Equipment Specifications. The first fact to understand is how narrow are the zones eluted out of efficient capillary columns. Some data are given in Table IX, corresponding to the same columns discussed previously. Both time and volume zone width are given. It has been shown by Schmauch (*20*) that the time or volume zone width contributed by the detector should be less than 1/20 the zone width, in order to prevent noticeable degradation of column performance.

In order to permit the determination of correct equipment specifications we give on Figure 7 the variation of the zone width with increasing k' in the same conditions as those selected for Figure 3. The efficiency of the corresponding columns for $k' = 1.76$ is given in Table I. The zone width is given by:

$$\frac{t_R}{\omega_t} = \frac{V_R}{\omega_V} = \frac{\sqrt{N}}{4} \tag{65}$$

The zone widths are extremely small, and vary quasi-linearly with k'. The response time of the detector has to be in the 0.1–0.5 s range depending on the performances, but for rapid, relatively easy separations, response times in the 10–50 ms range might prove necessary. This is relatively easy to achieve with computer coupling or with UV recorders if the detector amplifier or electronic transducer is fast enough which is now the case of several kinds of equipments commercially available, but might prove difficult to achieve with standard digital integrators, while conventional recorders are difficult to operate below 0.5-s response time.

Equipment for gas chromatography with capillary columns should have at least a 10 times smaller response time than

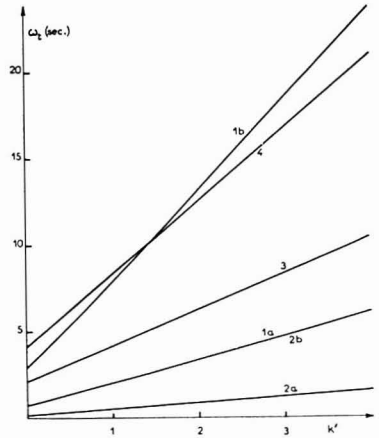


Figure 7. Zone width in time unit, as a function of the column capacity factor (cf. Tables I, VIII, IX). (1) $N = 1.6 \times 10^6$ plates. (a) $d_c = 65$ μm, $t_m = 350$ s. (b) $d_c = 250$ μm, $t_m = 1360$ s. (2) $N = 4 \times 10^5$ plates. (a) $d_c = 65$ μm, $t_m = 44$ s. (b) $d_c = 250$ μm, $t_m = 171$ s. Lines 1a and 2b are practically identical. (3) $N = 4 \times 10^5$ plates. $d_c = 100$ μm, $t_m = 333$ s. (4) $N = 4 \times 10^5$ plates, $d_c = 200$ μm, $t_m = 666$ s

conventional equipment. The handling of chromatographic data is difficult. On the one hand, most recorders are too slow and give distorted peak profiles, especially at the beginning of the chromatograms and in temperature programming. On the other hand, the very large amount of information generated by efficient columns makes difficult the use of other systems. There is probably a need for a delayed recorder, using an intermediate memory storage as buffer between the detector and the recorder. There is certainly a need for specific software to handle the information generated by high efficiency open tubular columns.

The acceptable dead volume is another stringent requirement. Carefully designed sampling systems and detector connections are more necessary than ever. The fluid logic injection devices (*21*, *22*) are attractive in spite of the huge amounts of gas and sample which are necessary to operate them. All these problems have solutions since 65-μm i.d., 1-m long capillary columns have been operated with performances which compare well to those predicted by theory (*22*, *23*). In that work, the major equipment contribution to peak broadening was the FID amplifier time constant, 7 ms (*23*).

CONCLUSION

Difficult analytical problems, especially those related to the composition of complex mixtures, could be solved more easily by using narrow bore capillary columns, which are relatively easy to prepare from drawn glass tubes. The sensitivity is practically unchanged, but some equipment problems remain to be solved. In fact, they determine the lowest inner diameter which can be used. The practical limit seems now to be around 65 μm, a fourfold decrease in the last 20 years. It so happens that the narrow capillary columns used by Desty in his pioneering work in high speed gas chromatography were in the 50–65 μm range (*24*).

ACKNOWLEDGMENT

Thanks are due to the Washington Chromatography Discussion Group and its program committee for their invitation to give a seminar on optimization in gas chromatography and for fruitful discussions.

LITERATURE CITED

(1) J. Simon and L. Szepesy, *J. Chromatogr.*, **119**, 495 (1976).
(2) I. Halasz, C. Horvath, *Anal. Chem.*, **35**, 499 (1963).
(3) A. L. German and E. C. Horning, *J. Chromatogr. Sci.*, **11**, 76 (1973).
(4) C. Vidal-Madjar, S. Bekassy, M. F. Gonnord, P. Arpino, and G. Guiochon, *Anal. Chem.*, **49**, 768 (1977).
(5) L. S. Ettre, E. W. Cieplinski, and W. Averill, *J. Gas Chromatogr.*, **1** (2), 7 (1963).
(6) B. Karger, *Anal. Chem.*, **39** (8), 24A (1967).
(7) I. Halasz, H. Schmidt, and P. Vogtel, *J. Chromatogr.*, **126**, 19 (1976).
(8) M. J. E. Golay, "Gas Chromatography 1958", D. H. Desty, Ed., Butterworth, London, 1958, p 36–55.
(9) L. S. Ettre, "Open tubular columns in gas chromatography", Plenum Press, New York, N.Y., 1965.
(10) G. Guiochon, *Adv. Chromatogr.*, **8**, 179 (1969).
(11) G. Guiochon, *Anal. Chem.*, **38**, 1020 (1966).
(12) G. Schomburg, R. Dielmann, H. Husmann, and F. Weeke, *J. Chromatogr.*, **122**, 55 (1976).
(13) J. H. Purnell and C. P. Quinn, "Gas Chromatography 1960", R. P. W. Scott, Ed., Butterworth, London, 1960.
(14) K. Grob and G. Grob, *J. Chromatogr.*, **125**, 471 (1976).
(15) E. Grushka and G. Guiochon, *J. Chromatogr. Sci.*, **10**, 649 (1972).
(16) J. H. Knox and M. Saleem, *J. Chromatogr. Sci.*, **7**, 614 (1969).
(17) F. I. Onuska and M. E. Comba, *J. Chromatogr.*, **126**, 133 (1976).
(18) M. Martin, C. Eon, and G. Guiochon, *J. Chromatogr.*, **99**, 357 (1974) and **108**, 229 (1975).
(19) B. Karger, M. Martin, and G. Guiochon, *Anal. Chem.*, **46**, 1640 (1974).
(20) L. J. Schmauch, *Anal. Chem.*, **31**, 225 (1959).
(21) R. L. Wade and S. P. Cram, *Anal. Chem.*, **44**, 131 (1972).
(22) G. Gaspar, P. Arpino, and G. Guiochon, *J. Chromatogr. Sci.*, **15**, 256 (1977).
(23) G. Gaspar, R. Annino, C. Vidal Madjar, and G. Guiochon, *Anal. Chem.*, in press.
(24) D. M. Desty, *Adv. Chromatogr.*, **1**, 199 (1965).

RECEIVED for review December 19, 1977. Accepted August 4, 1978.

Determination of Nitrogen Compound Distribution in Petroleum by Gas Chromatography with a Thermionic Detector

D. Kendall Albert

Standard Oil Company (Indiana), Amoco Research Center, Naperville, Illinois 60540

A selective thermionic nitrogen detector was used in combination with a flame-ionization detector for the gas chromatographic determination of nitrogen compound distribution in light catalytic cycle oil and light vacuum gas oil. Distribution of the dominant nitrogen compound types—pyridines, quinolines, indoles, and carbazoles—was determined by compound type and carbon number in the cycle oil and by boiling point in the vacuum gas oil. Accuracy and precision of the method were judged from analysis of reference blends, comparison to nitrogen distribution obtained by gas chromatography with a microcoulometric detector for a cycle oil, and comparison to distribution obtained from elemental nitrogen analyses of distillation fractions of a light vacuum gas oil. With reference blends, accuracy approached precision—about 3% relative. For gas oils, accuracy was generally about 7 to 8% relative. The analyses particularly demonstrate the feasibility of employing the thermionic detector to determine nitrogen compound distribution by boiling point.

Nitrogen compounds in petroleum adversely affect many important catalytic processes and product stability. For example, they cause catalyst poisoning and are involved with gum and color formation in products. To overcome these effects, sensitive and accurate analytical methods are needed to determine the distribution and the different types of nitrogen compounds, e.g., pyridines, quinolines, indoles, and carbazoles.

Gas chromatography with a selective nitrogen detector is a sensitive, rapid, and accurate analytical approach to the analysis of nitrogen compounds in petroleum, and the advantages of this technique over slower, complex fractionation methods have been discussed (*1*, *2*).

There are four major types of nitrogen-selective detectors: thermionic or alkali flame, microcoulometric, electrolytic conductivity, and the chemiluminescent detector. The thermionic detector is a flame-ionization detector that is modified with some means for vaporizing a suitably volatile alkali metal, such as sodium, potassium, or rubidium, so that the vapors are present in the flame. The resulting flame shows an enhanced response to halogen, phosphorous, and nitrogen organic compounds. With proper choice of alkali metal and experimental conditions, the detector can be made specific for the different elements. The other detectors employ some means of chemical conversion of organo-nitrogen compounds to a detectable species. With the microcoulometric and electrolytic conductivity detectors, nitrogen compounds undergo hydrogenolysis to form ammonia. With the chemiluminescent detector, chemically-bound nitrogen is converted to metastable nitrogen dioxide (NO_2^*) which produces a photoemission. All of these detectors have been described in detail and are well documented in the literature, e.g., (*3–7*).

Of these detectors, the microcoulometric (*1*, *8*) and electrolytic conductivity (*2*, *9*) detectors have been the most widely used in gas chromatographic analyses of petroleum. An application of the newer chemiluminescent detector to gas chromatographic analysis of fossil fuels was recently reported (*10*). The thermionic detector has been used relatively little in petroleum analyses, although it has advantages over the electrochemical detectors of higher sensitivity, faster response, and simpler apparatus. Because of these advantages, the thermionic detector would seem to be the most attractive detector for petroleum analysis, and in this paper our studies to determine this applicability are described.

Historically, the major drawback of the thermionic detector has been its instability (*3*, *11*). As a result, it has not been generally as suitable as the electrochemical detectors for routine quantitative work (*2*). This instability has been generally attributed to aging of the alkali metal source and to the method employed to generate the thermionic emissions. In earlier detector designs, the hydrogen flame was employed for both combusting the sample and heating the alkali metal source. The thermionic emission or detector sensitivity could not be controlled independently of the flame. However, in newer detector designs that are now available, e.g., (*12–16*), the instability problem has been minimized and made controllable by employing more thermally stable alkali metal sources, such as rubidium silicate, and providing an electrical heating source so that the level of thermionic emission can be precisely controlled. These newer detector designs are receiving increasing attention in the analysis of many complex materials.

Most reported applications have been in nonpetroleum areas; for example, analysis of nitrogen-containing drugs (*17*, *18*) and amino acids (*19*) in biological fluids. Applications to petroleum have been mainly qualitative, such as obtaining nitrogen compound profiles or "fingerprint" chromatograms of petroleum fractions. Such applications have been reported for oil spills (*20*), engine oils (*21*), and distillate fuels (*6*). This method has also been used to follow changes in nitrogen distribution upon hydrotreating of shale naphthas (*22*).

This paper extends previous work by evaluating the quantitative performance of the thermionic detector for analyses of nitrogen compound distributions in gas oils. The work includes a study of detector response characteristics, analyses of reference blends, comparison of nitrogen distribution analyses of a light catalytic cycle oil with that obtained by microcoulometry, and a comparison of distribution analyses of a light vacuum gas oil with that obtained from elemental nitrogen analysis of distillation fractions.

EXPERIMENTAL

Materials. Reference nitrogen compounds were obtained from commercial sources except for two compounds, 2,3,5,7-tetramethylcarbazole and 1,2,4,6,7-pentamethylcarbazole, which were synthesized (*23*). Hydrocarbons were Phillips pure grade. Other reagents were reagent grade. Solutions were prepared with isooctane or acetone solvents.

Petroleum fractions included a hydrocracked recycle oil, a light catalytic cycle oil, and a light vacuum gas oil. The boiling ranges, nitrogen, and sulfur contents are shown in Table I.

Apparatus. The gas chromatograph was a Perkin-Elmer Model 3920 equipped with a nitrogen phosphorus detector (NPD) and a flame-ionization detector (FID). The detectors were operated in parallel with a dual-pen 1-mV recorder. Data reduction

0003-2700/78/0350-1822$01.00/0 © 1978 American Chemical Society

Table I. Petroleum Fractions Employed in Study

	hydro-cracked recycle oil	light catalytic cycle oil	light vacuum gas oil
boiling range, °C	200-345	200-325	245-455
nitrogen, ppm	5	240	390
sulfur, wt%	0.0155	0.31	0.38

Table II. Chromatographic Operating Conditions

column flow rate	60 cm³/min, helium
effluent split[a]	29 cm³/min to NPD
	31 cm³/min to FID
NPD	hydrogen, 4.0 cm³/min
	air, 100 cm³/min
	bead voltage, adjusted as required
FID	hydrogen, 35 cm³/min
	air, 350 cm³/min
temperatures	injector (glass liner), 275 to 300 °C
	manifold (detectors), 350 °C
	column, (see text)

[a] Achieved with two Perkin-Elmer B_1 capillary restrictors.

was accomplished with an on-line computer.

A polar and three nonpolar packed columns were employed. The polar column was 6 ft of $^1/_4$-inch o.d., 2-mm i.d., glass tubing packed with 10% Carbowax 20M on 80–100 mesh Gas Chrom Q. The nonpolar columns contained 20% polyethylene (mol wt 12000) on 80–100 mesh, non-acid washed Chromosorb W, which was pretreated with 3% potassium carbonate. The columns were prepared from 8 ft × $^1/_8$ inch o.d., 2-mm i.d., stainless steel tubing and 6 ft and 3 ft lengths of $^1/_4$ inch o.d., 2-mm i.d., glass tubing. Polyethylene was chosen as the high temperature liquid phase because nitrogen background from column bleed was less than that obtained with conventional silicone liquid phases (*8*). Life of the polyethylene columns was equivalent to that of SE-30 columns.

Operating Conditions. The gas chromatographic operating conditions are summarized in Table II. The column flow rate and effluent split ratio were maintained at the values shown for all columns.

A hydrogen flow rate of 4.0 cm³/min was optimum for maximum sensitivity without sacrificing selectivity. Incremental adjustments were made, as appropriate, in the bead current to compensate for loss in sensitivity due to aging of the bead. The dependence of the detector performance on the intrarelationships between the flow rates of the carrier gas, hydrogen, and air and the bead heating current have been described in detail (*24*).

Various isothermal and temperature programmed column temperatures were employed depending on the boiling range of the sample and the separations desired. Isothermal column temperatures are indicated in the text. For temperature programmed runs, the sample was charged to the column at 80 °C and after 4 min programming was initiated at a rate of 4 °C/min and was continued to a maximum of 250 °C for the polar column and 310 °C for the nonpolar columns. Elution was continued, if needed, at the maximum temperature until completion of the chromatogram.

Procedures. At the beginning of each day of operation, the chromatographic system was "conditioned" by heating the column to an elevated temperature, e.g., 200 °C, and while at that temperature charging at least two successive 1-μL injections of a solution containing 1000 ppm N, as 2,4,6-trimethylpyridine (TMP), in isooctane. Subsequently, the column temperature was re-equilibrated as required for calibration and analysis.

In general, the NPD bead voltage was such that the system background or bead current was no greater than 30 picoamperes (pA) (*24*). With well-conditioned columns, the bead current was generally of the order of 5 pA or less. The electrometer range setting was 10 for both detectors.

Calibration of the chromatographic system was made with a reference solution containing 95 ppm of TMP, which corresponded to 11 ppm N, and 10000 ppm of 1,2,3,4-tetramethylbenzene (TMB), which corresponded to 8950 ppm C. The composition of this solution was chosen to represent a reasonable test for both sensitivity and selectivity. As criteria for acceptable system performance, an NPD sensitivity—expressed as the NPD/FID area response ratio for TMP—of at least 8 and a nitrogen-to-carbon selectivity of at least 8000 was maintained. Selectivity (S) was calculated as follows.

$$S = \frac{A_1 \times g_2}{g_1 \times A_2}$$

where A_1 = NPD area response to TMP, A_2 = NPD area response to TMB, g_1 = grams of nitrogen, as TMP, charged to the NPD, and g_2 = grams of carbon, as TMB, charged to the NPD. Calibration was made (following conditioning of the column) at an isothermal column temperature generally in a range of 100–125 °C with a sample size of 1 μL. The sensitivity and selectivity of the NPD are further discussed in the subsequent section.

For distribution analysis of petroleum fractions, sample sizes were generally 1 μL. Distributions were calculated by normalizing the total area of the chromatogram to 100% or the total nitrogen content of the sample. For fractions with low concentration levels of nitrogen, e.g., 5 ppm N, as for the hydrocracked oil, distribution analyses were not feasible because of the inability to distinguish nitrogen compounds at sub-ppm nitrogen concentration levels from hydrocarbon background response. [Such distributions could be expedited, however, by concentrating the nitrogen compounds by liquid chromatography, e.g., (*1*), prior to gas chromatographic analysis.]

The methodology employed for the microcoulometric distribution analyses has been reported (*1*).

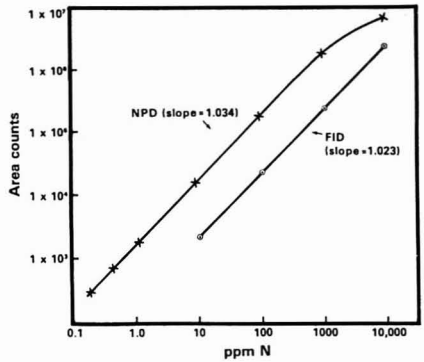


Figure 1. Linearity of NPD and FID. Polyethylene column, 8 ft stainless steel; column temperature, 110 °C. Sample: 1.0 μL; 2,4,6-trimethylpyridine in isooctane

RESULTS AND DISCUSSION

Detector Response Characteristics. Detector response characteristics that were determined were linearity, lower limit of detection, selectivity, and response factors. The FID was used qualitatively to help interpret peak identifications in NPD chromatograms and quantitatively to help judge the performance of the chromatographic system. Therefore, response characteristics of the FID were also determined.

Satisfactory operation of the dual detectors was indicated by a linear response for each detector, as shown in Figure 1. This shows a log–log plot of detector response vs. concentration of nitrogen in ppm. The slopes were calculated from a linear regression fit of the log–log data, and they agree within experimental error with a slope of unity for a linear response. The NPD response was linear from a lower detection limit of about 0.2 ppm N to 1000 ppm. The FID response was linear to at least 10000 ppm N. Tailing of the solvent peak into the

Table III. Lower Limit of Detection for 2,4,6-Trimethylpyridine (TMP)

	LLD = g/s for 2:1 signal/noise ratio	
	stainless steel column[a]	glass column[b]
NPD	4.12×10^{-12} (TMP)	1.73×10^{-12} (TMP)
	4.75×10^{-13} (N)	2.00×10^{-13} (N)
FID	3.55×10^{-11} (TMP)	7.96×10^{-12} (TMP)

[a] 8 ft, polyethylene packing, column temperature 125 °C. [b] 6 ft, polyethylene packing, column temperature 125 °C.

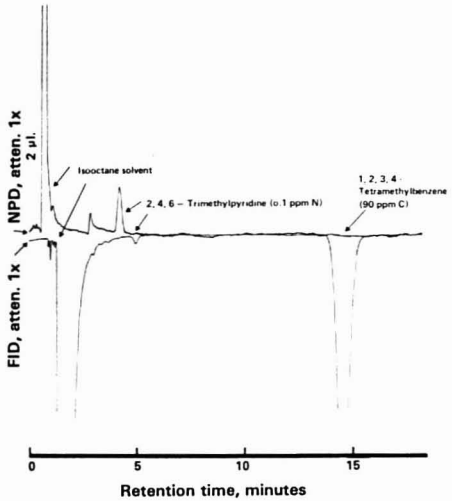


Figure 2. Illustrative chromatogram of NPD sensitivity and selectivity. Polyethylene column, 6-ft glass; column temperature, 125 °C

TMP peak prevented a better lower detection limit, which was 10 ppm N, for the FID.

Separations were satisfactory with either stainless steel or glass columns, but better sensitivity was obtained with the glass columns. This is illustrated in Table III, which compares lower limits of detection for both detectors on a stainless steel and a glass column. For the NPD, the glass column was more favorable by a factor of 2.4; for the FID, the glass column was better by a factor of 4.5. In comparing the sensitivities of the detectors for each column, the lower limit of detection for the NPD was better than that of the FID by factors of 8.6 and 4.6 for the stainless steel and glass columns, respectively. The NPD sensitivity is of the same order of magnitude that has been reported for this detector for other types of nitrogen-containing compounds (*13*).

The sensitivity and selectivity of the NPD are illustrated in Figure 2, which shows a chromatogram that was obtained with a glass column for a blend of TMP and TMB, representing approximately 0.1 ppm N and 90 ppm C, respectively (a 100:1 dilution of the calibration standard). Although the C to N ratio was 900 to 1, the NPD response to the TMB was not measurable. On the other hand, the NPD response to the TMP was about nine times greater than that of the FID.

Analyses of the undiluted calibration blend with 11 ppm N and 8950 ppm C for which the NPD hydrocarbon response was measurable, showed the nitrogen selectivity was generally in the range of 8000 to 11 000 on a g N/g C basis. This compares with reported values of 5000 to 7500 (*12*, *13*).

Table IV. Effect of Alkylsubstituents on Detector Response

compound	NPD	FID
pyridine	1.000	1.000
2-methylpyridine	1.167	0.9971
4-methylpyridine	1.006	0.9902
3-ethylpyridine	1.020	0.9549
4-*tert*-butylpyridine	0.9160	0.9347
2,6-dimethylpyridine	1.235	0.9522
2,4,6-trimethylpyridine	1.202	0.9530
quinoline	1.000	1.000
2-methylquinoline	1.301	1.036
6-methylquinoline	1.015	0.9873
2,6-dimethylquinoline	1.266	1.014
2,4-dimethylquinoline	1.296	1.033
indole	1.000	1.000
3-methylindole	1.020	0.9544
2,3-dimethylindole	1.090	0.9493
2,5-dimethylindole	1.117	0.9971
1,2-dimethylindole	0.7408	0.9318
carbazole	1.000	1.000
1,2,3,4-tetrahydrocarbazole	0.9566	0.9818
6-methyl-1,2,3,4-tetrahydrocarbazole	0.9520	0.9626
N-ethylcarbazole	0.7924	0.9010
2,3,5,7-tetramethylcarbazole	1.156	not det.
1,2,4,6,7-pentamethylcarbazole	1.179	not det.

For petroleum analyses it is also important that the detector have good nitrogen selectivity relative to sulfur. Benzothiophenes, for example, are a major sulfur compound type in petroleum. Analysis of a blend containing 120 ppm N as 2,4,6-trimethylpyridine and 250 ppm S as benzothiophene, in acetone, showed a nitrogen to sulfur selectivity of 2100 on a g N/g S basis. Little comparative information is available, although the N/S selectivity has been indicated to be of the same order of magnitude as the N/C selectivity (*12*). However, in our experience, the N/S selectivity is of an order of magnitude of 10^3, as compared with an order of magnitude of 10^4 for the N/C selectivity. Although lower, the N/S selectivity is still satisfactory.

The NPD also responds to phosphorus when it is operated in the nitrogen mode. However, the phosphorus content of petroleum appears to be low enough that the NPD response to phosphorus can be assumed to be negligible. For example, in the oils used in this study, analysis by X-ray fluorescence showed less than 5 ppm phosphorus. Gas chromatographic analyses with the NPD operated in the phosphorus mode showed no measurable phosphorus. The lower limit of detection was 0.1 ppm P as determined with tricresylphosphate in dodecane.

The response of the NPD is approximately proportional to the nitrogen content of a compound, but the response is also dependent on the compound structure. The detector mechanism is not completely understood, but it is based on the formation of cyano radicals (·C≡N:) in a cool flame zone (*12*). In general, those compounds having structures that would be expected to be favorable for this reaction would be expected to give the larger response.

The effect of alkylsubstituents on detector response is shown in Table IV. The responses are relative to 1.00 for the parent compound of each class. The NPD factors are the ratios of weight percent of nitrogen that was blended divided by the corresponding peak area percent. The FID factors are ratios of weight percent of compounds that were blended, divided by the corresponding peak area percent. Analyses were made with a polyethylene column (8-ft stainless steel) with temperature programming.

The data indicate that for most of the compounds the alkyl substituents affect the FID response by no more than 6% relative; whereas, for the NPD, the effect is more widespread,

Table V. Relative Responses of NPD and FID to Different Types of Nitrogen Compounds

compound[a]	blended weight ratio		relative area response ratio		relative response factor, weight/area	
	nitrogen	carbon	NPD	FID	NPD	FID
pyridine	1.278	0.7988	1.617	0.7122	0.7904	1.122
2,6-dimethylpyridine	0.9494	0.8308	1.120	0.8450	0.8477	0.9832
4-methylpyridine	1.076	0.8082	1.564	0.7534	0.6880	1.073
2,4,6-trimethylpyridine	0.8720	0.8759	1.109	0.9438	0.7863	0.9281
4-*tert*-butylpyridine	0.7551	0.8515	1.145	0.8995	0.6595	0.9466
quinoline	1.008	1.133	1.101	1.037	0.9155	1.093
2-methylquinoline	0.9857	1.235	1.054	1.252	0.9352	0.9864
6-methylquinoline	0.7314	0.9154	0.8450	0.8880	0.8656	1.031
2,6-dimethylquinoline	0.6445	0.8853	0.6985	0.9255	0.9227	0.9566
2,4-dimethylquinoline	0.9146	1.257	0.9732	1.318	0.9398	0.9537
indole	1.000	1.000	1.000	1.000	1.000	1.000
3-methylindole	1.017	1.145	0.9628	1.184	1.056	0.9671
2,3-dimethylindole	0.7061	0.8815	0.6260	0.8730	1.128	1.010
N-ethylcarbazole	0.5466	0.9567	0.5942	0.9525	0.9199	1.004
N-methylcarbazole	0.6129	0.9981	0.6596	0.9257	0.9292	1.078
5,6-benzoquinoline	0.7819	1.272	0.8492	1.284	0.9207	0.9907
1,2,3,4-tetrahydrocarbazole	0.6224	0.9360	0.5204	0.9078	1.196	1.031
6-methyl-1,2,3,4-tetrahydrocarbazole	0.5481	0.8928	0.4831	0.8889	1.135	1.004
carbazole	0.7472	1.120	0.6621	1.072	1.128	1.045

[a] Listed in order of elution from the Carbowax 20M glass column (see text).

Table VI. NPD Analysis of Blend of Nitrogen Compounds in a Hydrocracked Gas Oil

compound	ppm N blended	ppm N determined						
		1	2	3	4	av	std dev	error
4-*tert*-butylpyridine	22.0	21.6	21.4	20.9	21.1	21.3	0.31	−0.7
quinoline	32.5	33.4	33.9	32.9	33.1	33.3	0.43	0.8
6-methylquinoline	28.1	28.8	29.2	28.6	28.9	28.9	0.25	0.8
2,4-dimethylquinoline	25.9	26.5	26.8	26.5	26.4	26.6	0.17	0.7
indole	29.1	28.1	27.8	27.5	27.4	27.7	0.32	−1.4
3-methylindole	28.0	28.8	28.7	28.5	28.7	28.7	0.13	0.7
2,3-dimethylindole	24.2	24.2	23.7	23.3	23.0	23.6	0.52	−0.6
N-methylcarbazole	18.7	22.3	22.3	21.8	22.0	22.1	0.24	3.4
carbazole	21.6	21.4	21.7	20.9	21.4	21.4	0.33	−0.2

e.g., as high as 30% relative for the alkylquinolines. Notable are the relatively low factors for 1,2-dimethylindole and *N*-ethylcarbazole. In both of these compounds, an alkyl group is bonded to the nitrogen atom, which is especially favorable for the formation of cyano radicals. These compounds also produced the largest deviations in the FID response. In general, the compound structure is more favorable for the formation of cyano radicals as the response factor decreases.

As a further comparison of differences in response among the different classes of nitrogen compounds, a blend of several compounds representing pyridines, quinolines, indoles, and carbazoles was chromatographed with temperature programming on the Carbowax column, and response factors relative to 1.00 for indole were calculated for both the NPD and FID, Table V. The area response ratios for each detector are compared with the corresponding ratios of nitrogen and carbon that were blended and then a weight-to-area ratio or response factor was calculated. It will be noted that the FID response follows the carbon content much closer than does the NPD response with the nitrogen content. The data are summarized in Figure 3, which shows the range of factors for each class of compounds vs. the boiling range that was covered for each class. The data show significant response differences among the different types with the largest differences for the pyridines. Quinolines, indoles, and carbazoles are the dominant types in the oils used in this study.

Blend of Nitrogen Compounds in Hydrocracked Oil. To determine the reliability of the NPD in component analysis of a petroleum fraction, a blend of nitrogen compounds in a hydrocracked oil was analyzed on the Carbowax column with temperature programming. An illustrative chromatogram is shown in Figure 4, which shows both the NPD and FID responses. The prominent peaks in the FID trace are *n*-paraffins, which are present in an approximate carbon number range of C_{11} to C_{30}. The NPD trace shows the blended nitrogen compounds, which were added at a concentration level corresponding to 20 to 30 ppm N each. The absence of significant peaks between those of the blended compounds illustrates the selectivity of the detector and shows the absence of other nitrogen compounds.

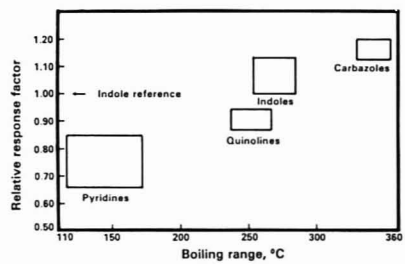


Figure 3. Comparison of NPD responses for different types of nitrogen compounds

The first component, 2,4,6-trimethylpyridine (TMP), is an internal standard. Four consecutive analyses were made with the detector bead voltage at the same setting for all runs. Peak areas were corrected with response factors (Table V). A reference run on the unspiked oil showed that the area count of the background for each of the nitrogen compound peaks

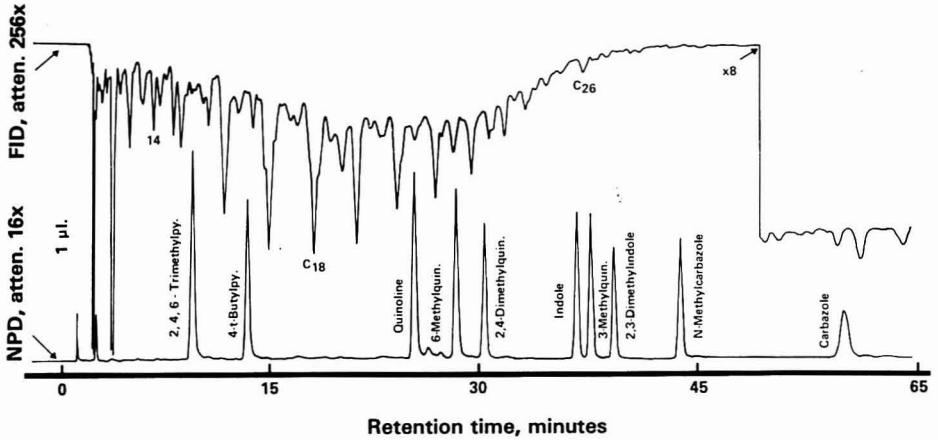


Figure 4. Chromatogram of blend of nitrogen compounds in hydrocracked gas oil

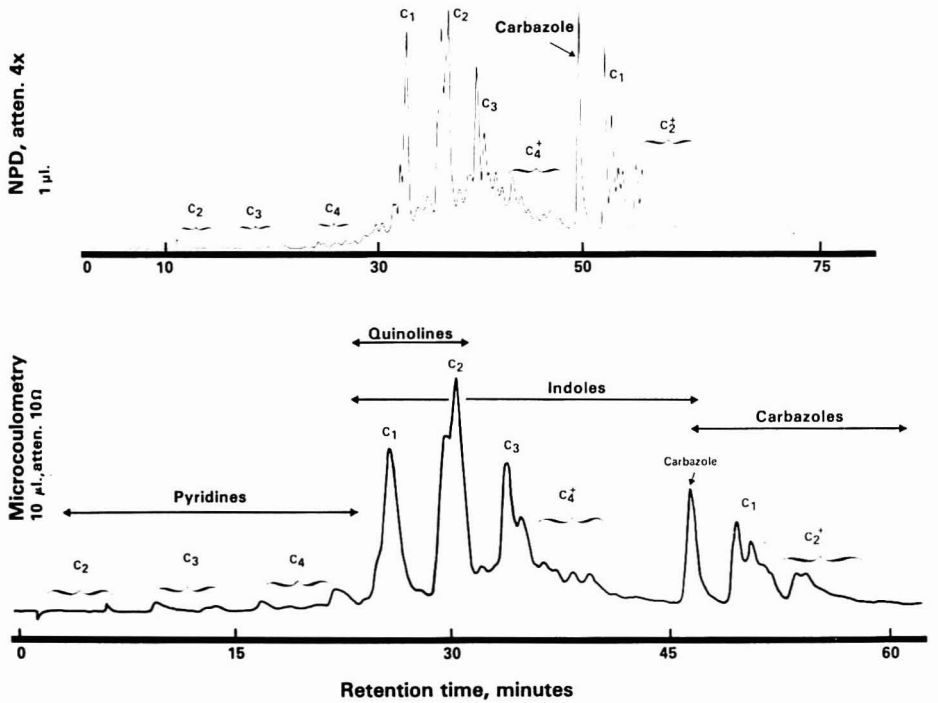


Figure 5. Comparison of NPD and microcoulometric chromatograms of LCCO

was less than 0.1% of the total counts for the nitrogen compound.

Results are shown in Table VI. The overall standard deviation was 0.3 ppm with an overall error of approximately ±1 ppm. The largest error was for the *N*-methylcarbazole, although the precision was good. The data indicate that with an internal standard technique and response factors, good accuracy and precision can be obtained with the NPD.

Light Catalytic Cycle Oil. Reliability of the NPD in determining the nitrogen compound distribution in a light

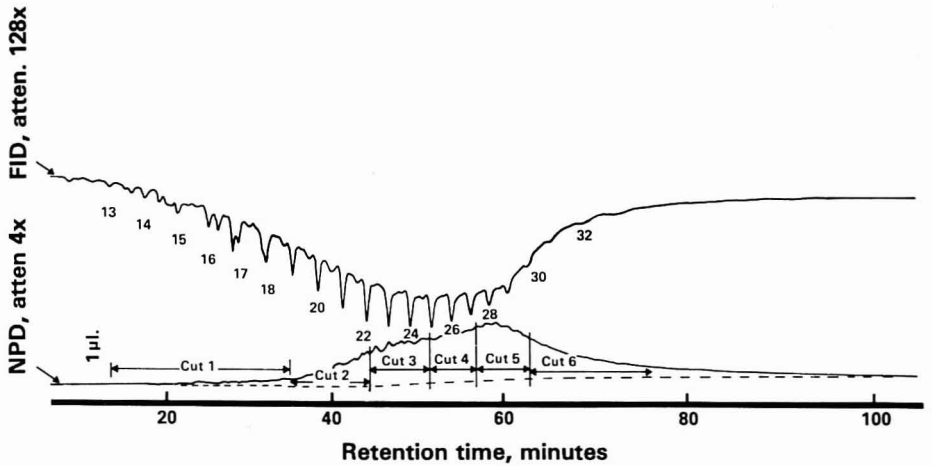


Figure 6. Chromatogram of a light vacuum gas oil

catalytic cycle oil (LCCO) was judged by comparing the distribution with that obtained with a GC/microcoulometric method (*1*). Comparison of the chromatograms is shown in Figure 5. The NPD chromatogram was obtained on an 8 ft × $^1/_8$ inch o.d. stainless steel polyethylene column with temperature programming. To simplify the comparison, the FID trace was omitted. The microcoulometric chromatogram was obtained on the same type of column and with temperature programming, but the column was 20 ft × $^1/_4$ inch o.d. stainless steel tubing. A larger capacity column was used with the microcoulometric method because of the relatively large sample size (10 µL vs. 1 µL for the NPD). With the GC/microcoulometric method, relatively large sample sizes of the order of 10 to 20 µL were generally required to provide a suitable signal-to-noise ratio (*1*).

The carbon number ranges of the major nitrogen compound types are indicated (Figure 5) with the carbon numbers referring to the number of carbon atoms in the alkyl substituents. Identifications were established in previous work and were based on a combination of chromatographic and spectroscopic methods (*1*). The basic compounds, which account for 9.6% of the total nitrogen in the oil as determined by titration (*25*), overlap in boiling range with the indoles. Good separation is obtained between the indoles and carbazoles with only trace amounts of C_4^+ indoles overlapping with carbazole. The NPD chromatogram shows the same overall distribution as in the microcoulometric chromatogram; however, more detailed separations are evident with the NPD as a result of more efficient separations. The higher sensitivity and faster response of the NPD enable smaller samples to be used with more efficient columns, which enhances component analyses.

A comparison of the area percent distributions is shown in Table VII. Because of limited component separations and a lack of appropriate reference compounds, it was not feasible to correct the NPD detector response. Consequently, the NPD areas are compared directly with the microcoulometric areas, which are proportional to the nitrogen content. The standard deviations are based on four runs for each method with each run made on different days.

The overall precision of the NPD analyses is slightly better than that of the microcoulometric analyses with an average relative standard deviation of about 4% for the NPD and 6% for the microcoulometric methods. The distribution analyses are in reasonable agreement with an overall difference of about 7%, relative.

Table VII. Comparison of NPD and Microcoulometric GC Distributions of LCCO

	NPD, area %		microcoulometric area %	
compound type	av	rel % std dev	av	rel % std dev
C_4^- pyridines	3.59	6.6	3.36	15.7
C_4^+ pyridines + indole + quinoline	1.82	5.3	2.02	17.1
C_1 indoles + quinolines	14.4	5.3	15.9	2.5
C_2 indoles + quinolines	23.2	3.4	24.7	5.0
C_3 indoles	19.9	3.1	19.3	6.6
C_4^+ indoles	11.0	4.9	12.1	4.8
total indoles + basic	73.9	1.1	77.4	2.6
carbazole	7.44	3.9	6.16	8.4
C_1 carbazoles	11.6	4.0	10.7	2.2
C_2^+ carbazoles	7.09	7.1	5.71	5.2
total carbazoles	26.1	3.0	22.6	2.3

Although the basic compounds and indoles are not separated, the sum of the two classes obtained by either method is in general agreement with that obtained by chemical methods. Analysis for indoles by a spectrophotometric method (*26*) showed 68.6% of the total nitrogen was present as pyrrolyic nitrogen. This value plus the 9.6% for basic nitrogen gives a total of 78.2%, which compares with 73.9% and 77.4% obtained by the NPD and microcoulometric methods, respectively.

The comparative results indicate that for general distribution analyses by carbon number the NPD can be used with reasonable accuracy without response factor corrections. With a complex array of many unresolved components, as shown in the distribution analysis, the net effect of differences in individual component responses appears to be sufficiently small to disregard if accuracy better than 7–8% relative is not needed.

Light Vacuum Gas Oil. The nitrogen compound distribution in virgin gas oil is much more complex than in cycle oil. The major types—quinolines, benzoquinolines, carbazoles, and benzocarbazoles—are not separated because of the

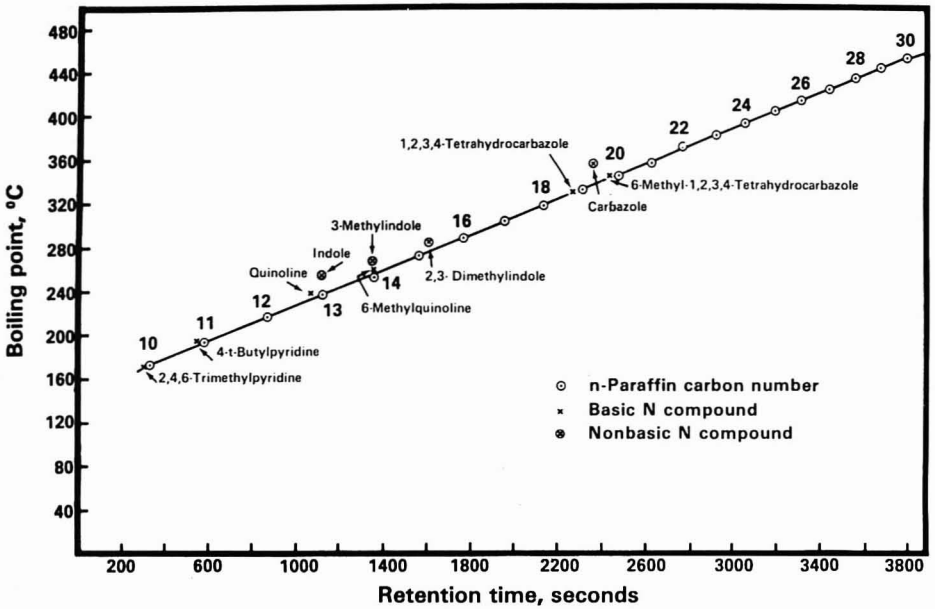


Figure 7. Boiling point calibration curve

Table VIII. Comparison of Nitrogen Distribution in a Light Vacuum Gas Oil by GC and Elemental Analyses

cut	cut points, °F	percent of total N in cut[a]	GC, area %				
			1	2	3	av	std dev
1	423-590	1.86	2.19	2.02	2.87	2.33	0.37
2	590-710	14.5	11.1	13.0	12.6	12.2	0.82
3	710-767	17.5	15.0	17.8	17.1	16.5	1.20
4	767-810	16.8	15.2	16.8	16.9	16.2	0.82
5	810-855	19.6	19.0	20.7	20.0	20.0	0.71
6	855-925	29.7	37.5	29.7	30.5	32.8	3.53

[a] From elemental analyses; total N = 390 ppm.

predominance of highly substituted compounds in each class (*1*). Because of lack of separations, a chromatogram of the nitrogen distribution results in a continuous profile with very little definition of components. This is illustrated in Figure 6, which shows the dual FID and NPD chromatograms of a light vacuum gas oil. The chromatograms were obtained on a polyethylene column (3 ft, glass) with temperature programming. The prominent peaks that are numbered on the FID trace are *n*-paraffins, which cover a carbon number range of about C_{11} to C_{33}. The NPD chromatogram shows nitrogen compounds are distributed across most of the boiling range of the sample with the distribution skewed toward the upper boiling range.

Since the determination of nitrogen distribution by compound type and carbon number was not feasible by direct analysis, it was of interest to determine the feasibility of relating the area to the amount of nitrogen compounds eluted in a given boiling range. Such a relationship depends on the elution of nitrogen compounds in a precise boiling point order. To determine this, blends of *n*-paraffins and nitrogen compounds were chromatographed under the same experimental conditions as used for the light vacuum gas oil. The true boiling point or atmospheric boiling point was then plotted vs. the retention time for each compound, as shown in Figure 7. The results show a linear relationship with the nitrogen compounds being eluted very closely to the temperatures defined by the *n*-paraffin boiling point curve. Higher boiling reference nitrogen compounds with known boiling points were not available to establish reference points in the upper region of the calibration curve. It is assumed that the relationship can be extrapolated over the linear range. Interestingly, the basic compounds are in closer agreement with the *n*-paraffin curve than are the nonbasic compounds—indoles and carbazole. The tetrahydrocarbazoles, which are basic compounds, lie essentially on the curve. The nonbasic compounds are eluted about 8 °C earlier than that predicted by the *n*-paraffin boiling point curve. This behavior is not unusual and is similar to observations that have been made for aromatic compounds in the ASTM standard method, D2887, for the determination of boiling range distributions of petroleum fractions by gas chromatography (*27*) or the so-called "simulated distillation" method. In that method, aromatic compounds, particularly polycyclics, are generally eluted earlier than predicted by the *n*-paraffin curve.

To test the boiling point distribution analysis, six distillation cuts of the oil were each analyzed for total nitrogen by the

Kjeldahl method. The distribution of nitrogen was calculated and then compared with the area % distribution of nitrogen as determined by GC analysis of the total sample. The chromatogram was divided into zones (Figure 6) that corresponded to the boiling points at which the cuts were taken. The distillation was carried out at reduced pressure, about 10 mm, and the column overhead temperature at which each cut was taken was converted to atmospheric boiling point. From the boiling point–retention time calibration curve, the retention time corresponding to each cut point temperature was determined. The area of each zone was planimetered and the areas were normalized to 100%. A base-line or system background correction, as indicated by the broken line in the chromatogram, was determined by making a blank run under the same experimental conditions that were used for the sample.

A summary of the comparative analyses is given in Table VIII. The cut point temperatures, the calculated distributions from the elemental analyses, and the GC analyses from three consecutive runs (all at the same bead voltage) are shown for each cut. The overall standard deviation of the GC analyses is about 8% relative. The overall relative percent difference between the two analyses is also about 8%. Considering the various sources for experimental error, the agreement between the two distributions is reasonably good and indicates that the GC method has potential for development as a "simulated distillation" method for nitrogen compounds.

CONCLUSIONS

In conclusion, this work has shown that (1) with response factors and an internal standard technique, the thermionic detector or NPD can be used for accurate component analyses of petroleum without prior separations; (2) the NPD is applicable to the determination of nitrogen compound distributions in petroleum and results compare favorably with those obtained by microcoulometry or elemental analyses of fractions; and (3) nitrogen compound distribution by boiling point is feasible with the NPD-FID system. Further development of this technique is being done in our laboratory.

ACKNOWLEDGMENT

I am grateful to R. B. Armstrong of Amoco Oil Company who provided the light vacuum gas oil distillation fractions and to J. J. Miskovich of Standard Oil Company (Indiana) who assisted with the experimental work.

LITERATURE CITED

(1) D. K. Albert, *Anal. Chem.*, **39**, 1113 (1967).
(2) E. R. Adlard and P. H. D. Matthews, "Selective Nitrogen Detectors for the Determination of Organonitrogen Compounds Separated by Gas Chromatography", in Recent Anal. Dev. Pet. Ind., (Proc. Inst. Pet. Symp.), D. R. Hodges, Ed., John Wiley & Sons, New York, 1974, p 59.
(3) D. J. David, "Gas Chromatographic Detectors", John Wiley & Sons, New York, 1974, pp 114, 194.
(4) M. Krejci and M. Dressler, *Chromatogr. Rev.*, **13**, 1 (1970).
(5) D. F. S. Natusch and T. M. Thorpe, *Anal. Chem.*, **45**, 1184A (1973).
(6) R. Pigliucci, W. Averill, J. E. Purcell, and L. S. Ettre, *Chromatographia*, **8**, 165 (1975).
(7) H. V. Drushel, *Anal. Chem.*, **49**, 932 (1977).
(8) R. L. Martin, *Anal. Chem.*, **38**, 1209 (1966).
(9) J. C. Escaller, M. Caude, C. Bollet, and R. Rosset, *Analusis*, 395 (1977).
(10) H. V. Drushel, "Nitrogen Compounds in Fossil Fuels by Gas Chromatography with a Chemiluminescent Detector", presented before the Analytical Division, 175th National Meeting, American Chemical Society, March 12–17, 1978, Anaheim, Calif.
(11) T. A. Gough and K. Sugden, *J. Chromatogr.*, **86**, 65 (1973).
(12) B. Kolb and J. Bischoff, *J. Chromatogr. Sci.*, **12**, 625 (1974).
(13) M. J. Hartigan, J. E. Purcell, M. Novotny, M. L. McConnell, and M. L. Lee, *J. Chromatogr.*, **99**, 339 (1974).
(14) C. A. Burgett, D. H. Smith, and H. B. Bente, *J. Chromatogr.*, **134**, 57 (1977).
(15) P. L. Patterson, R. Howe, V. Hornung, and C. H. Hartman, "Selective Nitrogen and Phosphorus Detection with Electrically Heated Alkali Beads", presented at the Pittsburgh Conference on Analytical Chemistry and Applied Spectroscopy, February 27–March 3, 1978, Cleveland, Ohio.
(16) R. C. Hall and P. W. Thiede, "Extended Capability for the Detection of Nitrogen and Phosphorous Compounds", presented at the Pittsburgh Conference on Analytical Chemistry and Applied Spectroscopy, February 27–March 3, 1978, Cleveland, Ohio.
(17) D. N. Bailey and P. I. Jatlow, *Clin. Chem. (Winston-Salem, N.C.)*, **22**, 777 (1976).
(18) J. K. Baker, *Anal. Chem.*, **49**, 906 (1977).
(19) R. F. Admas, F. L. Vandemark, and G. J. Schmidt, *J. Chromatogr. Sci.*, **15**, 63 (1977).
(20) G. A. Flanigan and G. M. Frame, *Res./Dev.*, **28**, (9), 28 (1977).
(21) M. L. Lee, K. D. Bartle, and M. V. Novotny, *Anal. Chem.*, **47**, 540 (1975).
(22) C. E. Kennard, S. M. Sonchik, and M. P. T. Bradley, "Detailed Analysis of Shale Oil Using Specific Detectors", presented before the Analytical Division 174th National Meeting, American Chemical Society, August 28–September 2, 1977, Chicago, Ill.
(23) I. Puskas, E. K. Fields, and E. M. Banas, *Div. Pet. Chem., Am. Chem. Soc., Prepr.*, **17** (1), B56, (1972).
(24) J. A. Lubkowitz, J. L. Glajch, B. P. Semonian, and L. B. Rogers, *J. Chromatogr.*, **133**, 37 (1977).
(25) American Society for Testing and Materials, "1977 Annual Book of ASTM Standards", Part 24, p 830, Method D2896-73 (1977).
(26) M. A. Muhs and F. T. Weiss, *Anal. Chem.*, **30**, 259 (1958).
(27) American Society for Testing and Materials, "1977 Annual Book of ASTM Standards", Part 24, p 770, Method D2887-73.

RECEIVED for review June 13, 1978. Accepted August 17, 1978. Presented before the Division of Analytical Chemistry, 175th National Meeting, American Chemical Society, Anaheim, Calif., March 12–17, 1978.

Cubic Spline Interpolation for the Calculation of Retention Indices in Temperature-Programmed Gas–Liquid Chromatography

Wolfgang A. Halang,* Rolph Langlais, and Ernst Kugler

Coca-Cola GmbH, Research & Development Department, Kaninenbergstr. 66, 4300 Essen 1, West Germany

A method is described for the calculation of retention indices based on nonlinear calibration data in temperature-programmed gas–liquid chromatography. It is the method of choice when the indices serve as input for statistical analyses and identification procedures. A comparison of this technique with the polygonal technique is discussed. For easier implementation of the calculation procedure into existing gas–liquid chromatography computer programs, a detailed description of the spline interpolation procedure is given.

Temperature-programmed gas–liquid chromatography (GLC) is extensively used in our laboratories for the analysis of essential oils and other mixtures of volatile oils and substances. The methods applied for the collection, processing, and evaluation of our GLC data have been described earlier (*1–3*). All GLC retention data are converted into Kovàts indices for further handling and reference. Hence, the indices need to be calculated as accurately as possible.

This paper describes the method we employ, which has been

0003-2700/78/0350-1829$01.00/0 © 1978 American Chemical Society

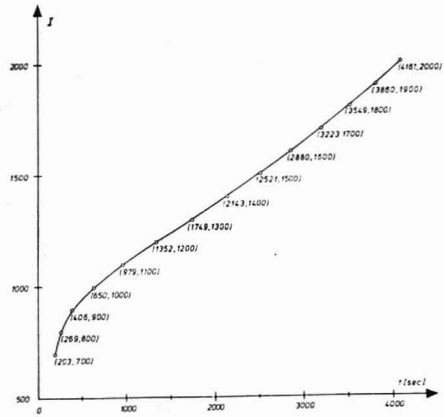


Figure 1. Kovàts indices vs. retention time in seconds for the calibration mixture of *n*-alkanes (C_7–C_{20}) and natural cubic spline interpolating the data points

used satisfactorily since 1974.

The retention times of the higher members of a homologous series correlate almost linearly with their numbers of carbon atoms as long as a linear temperature program of the correct slope is applied (*4*). If a number of restrictive assumptions are made, this can be derived theoretically, but as experiments show "the departure from linearity is reproducible and real" (*4*).

It is commonly known among those skilled in the art, that the temperature programs of commercial instruments may deviate considerably from linearity. These deviations, which are most pronounced at the beginning and at the end of the program, are due among other causes to changes in ambient temperature. The dependence of carrier gas flow upon temperature further enhances the nonlinearity of the retention times of a homologous series. This is illustrated by determining the retention times of the homologous series of *n*-alkanes (C_7–C_{20}) under our standard conditions, namely 50–200 °C at 2 °C min^{-1}.

Figure 1 shows the correlation between Kovàts indices and retention time in seconds.

Any linear approximation of this data set is obviously inappropriate because of large errors. A simple method yielding an acceptable calibration curve connects the data points by a polygon. A smooth function going through the given data set should, however, lead to more precise results.

Of the methods most commonly used for generating smooth curves, the cubic spline interpolation was considered to be the most suitable. Cubic splines are functions composed of third-order polynomials pieced together in the data points. The fact that they are twice differentiable in these junction points represents their essential property; consequently, adjacent polynomials have a common tangent in any data point.

Furthermore, the cubic splines offer the following advantages: smoothness, no introduction of extraneous oscillations, easily computable, good fit to nonlinear as well as to linear data sets. In Figure 1 a spline function is displayed interpolating the experimental data points.

CALCULATION OF RETENTION INDICES BY NATURAL CUBIC SPLINE INTERPOLATION

Since 1946 the theory of "spline functions" was rapidly developed to a powerful and versatile tool in numerical analysis. More than a thousand papers dealing with this area of research have appeared. Spline functions distinguish themselves by remarkable properties. For further details we refer to two books (*5*, *6*) covering the most important aspects of the subject. In this section we shall present only the topics necessary to apply natural cubic spline interpolation to the calculation of retention indices.

Construction of Interpolating Natural Cubic Splines. Given a set of data points $\{(x_i,y_i)|i = 1, ..., n\}$ with $x_1 < x_2 < ... < x_n$ and $n \geq 2$, there exists a unique function s with the following properties: (1) $s(x_i) = y_i$, $i = 1, ..., n$; (2) s is twice differentiable for all real x; (3) s reduces to a polynomial of degree three in each of the subintervals $[x_i,x_{i+1}]$, $i = 1, ..., n - 1$; (4) outside of $[x_1,x_n]$ s reduces to polynomials of degree one, i.e., to straight lines.

The function s is called an interpolating natural cubic spline. Since s minimizes the integral

$$\int_{x_1}^{x_n} \left[\frac{d^2}{dx^2} f(x) \right]^2 dx$$

among all functions f interpolating the given data set, the spline s is the smoothest of these functions and reduces to a polynomial of degree one, if the data points lie on a straight line.

Considering properties 2 and 3, we see that there must be a representation of s in the form

$$(P)\ s(x) = a_i + b_i(x - x_i) + c_i(x - x_i)^2 + d_i(x - x_i)^3$$

where $x_i \leq x \leq x_{i+1}$ and $i = 1, ..., n - 1$, with the parameters a_i, b_i, c_i, and d_i, i.e., s coincides in each partial interval with a cubic polynomial. Since the polynomial segments are twice differentiably pieced together, the coefficients cannot all be independent from each other. We shall now state the relations between the parameters facilitating the numerical construction of a spline when a set of interpolation data is given.

Algorithm. The parameters of the natural cubic spline s in the representation (P) interpolating the data $\{(x_i,y_i)|i = 1, ..., n\}$, may be computed according to the following scheme and the indicated sequence using the auxiliary variables h_o and h_i, v_i, and w_i, $i = 1, ..., n$.

$$a_i = y_i,\ i = 1, ..., n. \tag{A-1}$$

$$h_i = x_{i+1} - x_i,\ i = 1, ..., n - 1;\ h_o = h_1;\ h_n = h_{n-1}. \tag{A-2}$$

$$v_1 = 2h_1;\ v_i = 2(h_i + h_{i-1}),\ i = 2, ..., n - 1;\ v_n = 2h_{n-1}.$$

$$w_1 = 3(a_2 - a_1);\ w_n = 3(a_n - a_{n-1});\ w_i = 3\left[\frac{h_{i-1}}{h_i}(a_{i+1} - a_i) + \frac{h_i}{h_{i-1}}(a_i - a_{i-1}) \right],\ i = 2, ..., n-1.$$

$$v_i = v_i - \frac{h_i}{v_{i-1}} \cdot h_{i-2},\ w_i = w_i - \frac{h_i}{v_{i-1}} \cdot w_{i-1},\ i = 2, ..., n. \tag{A-3}$$

$$b_n = \frac{w_n}{v_n};\ b_i = \frac{w_i - h_{i-1} \cdot b_{i+1}}{v_i},\ i = n - 1, ..., 1. \tag{A-4}$$

$$c_1 = c_n = 0;\ c_i = 3\frac{a_{i+1} - a_i}{h_i^2} - \frac{2b_i + b_{i+1}}{h_i},\ i = 2, ..., n - 1. \tag{A-5}$$

$$d_i = \frac{c_{i+1} - c_i}{3h_i},\ i = 1, ..., n - 1. \tag{A-6}$$

We outline the proof of this algorithm.

Table I. Retention Data of the *n*-Alkane Standards C_7-C_{18} and of 15 Peaks of a Cold Pressed Lemon Oil Chromatographed 17 Times

peak no.	compound	retention time, s		retention indices calculated by the spline method		retention indices calculated by the polygon method	
		mean	σ_t	mean	σ_S	mean	σ_P
1	heptane	217.4	3.98				
2	octane	282.7	9.97				
3	nonane	417.5	21.19				
4	α-pinene	542.6	27.88	955.3	0.73	952.1	0.50
5	decane	657.5	34.68				
6	β-pinene	702.8	35.13	1015.8	0.76	1013.5	0.54
7	myrcene	803.8	40.84	1047.6	0.48	1043.5	0.57
8	α-phellandrene	875.2	42.65	1068.1	0.69	1064.8	0.70
9	undecane	993.5	46.35				
10	γ-terpinene	1066.1	47.65	1119.2	0.41	1118.9	0.38
11	terpinolene	1164.2	50.16	1145.0	0.53	1144.3	0.48
12	dodecane	1378.5	53.63				
13	linalool	1741.5	58.55	1289.3	0.62	1289.3	0.64
14	tridecane	1785.2	57.17				
15	decanal	1802.9	58.59	1304.3	0.73	1304.4	0.75
16	neral	2121.4	60.40	1383.4	0.96	1383.7	0.96
17	tetradecane	2187.1	58.35				
18	geranial	2270.5	60.55	1421.3	0.88	1421.6	0.89
19	terpinyl acetate	2432.0	60.05	1463.0	0.92	1463.4	0.91
20	neryl acetate	2500.7	60.19	1480.9	0.82	1481.2	0.81
21	pentadecane	2573.1	58.38				
22	geranyl acetate	2595.4	60.16	1505.9	0.83	1506.0	0.84
23	?	2783.0	60.14	1556.1	1.00	1556.6	0.97
24	β-bisabolene	2843.4	59.58	1572.5	0.56	1572.9	0.53
25	hexadecane	2943.8	58.36				
26	heptadecane	3298.5	58.48				
27	octadecane	3635.7	59.18				

The step A-1 immediately follows from the interpolation conditions $y_i = s(x_i) = a_i$, $i = 1, ..., n$. The continuity and differentiability requirements provide at each mesh point x_i the three equations

$$a_{i+1} = a_i + b_i h_i + c_i h_i^2 + d_i h_i^3 \quad \text{(i)}$$

$$b_{i+1} = b_i + 2c_i h_i + 3d_i h_i^2 \quad \text{(ii)}$$

$$2c_{i+1} = 2c_i + 6d_i h_i \quad \text{(iii)}$$

where Equation iii furnishes Equation A-6, at once. Eliminating the parameter d_i in Equations i and ii and solving for c_i gives the Equations A-5. Condition 4 is equivalent with $c_1 = c_n = 0$. The parameters b_i are determined from the linear system

$$2h_1 b_1 + h_1 b_2 = 3(a_2 - a_1)$$

$$h_i b_{i-1} + 2(h_i + h_{i-1}) b_i + h_{i-1} b_{i+1} = 3\left[\frac{h_{i-1}}{h_i}(a_{i+1} - a_i) + \frac{h_i}{h_{i-1}}(a_i - a_{i-1})\right], \quad i = 2, ..., n-1;$$

$$h_{n-1} b_{n-1} + 2h_{n-1} b_n = 3(a_n - a_{n-1})$$

whose coefficient matrix is strictly diagonally dominant establishing the unique solvability of the algebraic system. Its first equation follows from Equation A-5 for $i = 1$ after insertion of $c_1 = 0$ and its last row is set up analogously. We eliminate in Equation ii the parameters c_i and d_i by using the relations A-5 and A-6 and, after elementary transformations, we obtain the remaining equations of the linear system. Application of the Gaussian elimination method finally leads to the steps A-2, A-3, and A-4 of the algorithm.

Calculation of Retention Indices. Let $n \geq 2$ peaks with the retention times $x_1 < x_2 < ... < x_n$ of a chromatogram with known Kovàts indices a_i, $i = 1, ..., n$, be given. Note that for the mathematical procedure they do not necessarily have to belong to a homologous series. The calculation of the retention indices of the other peaks of the chromatogram starts with applying the above stated algorithm to the given data set. Then, we compute the retention index s of an arbitrary peak with the retention time t according to

$$s = \begin{cases} a_1 + b_1(t - x_1) & \text{for } t \leq x_1 \\ a_i + b_i(t - x_i) + c_i(t - x_i)^2 + d_i(t - x_i)^3 \\ \quad \text{for } x_1 \leq t \leq x_n \text{ and } x_i \leq t \leq x_{i+1} \text{ with} \\ \quad 1 \leq i \leq n - 1 \\ a_n + b_n(t - x_n) & \text{for } t \geq x_n \end{cases}$$

FORTRAN PROCEDURES

Program listings of the subroutines mentioned below are available from the authors upon request. The spline parameters b_i, $i = 1, ..., n$, and c_i, d_i, $i = 1, ..., n-1$, are calculated by the subroutine COEFF requiring as input data the number of data points n ($n \geq 3$) and the retention times $x_1 < x_2 < ... < x_n$ of the *n*-alkanes. The main program has to provide the corresponding retention indices as array a. This seems superfluous when *n*-alkanes are applied, but it allows the calculation of retention indices by means of an arbitrarily selected set of calibration compounds not belonging to a homologous series. Note that the arrays b, c, and d may share their storage locations with the auxiliary vectors **v**, **w**, and **h**, respectively. After COEFF has been called, the procedures SPLINE and CUBIC can be applied. They need the number n and the arrays x, a, b, c, d as input parameters. The function SPLINE computes the Kovàts index of a single peak with retention time t whereas CUBIC provides the retention indices s_j, $j = 1, ..., m$, for each of the m peaks with the retention times $t_1 \leq t_2 \leq ... \leq t_m$.

EXPERIMENTAL AND RESULTS

In order to compare the results obtained by polygonal and by spline interpolation with each other, a cold pressed lemon oil was subjected to multiple chromatography, an arbitrarily

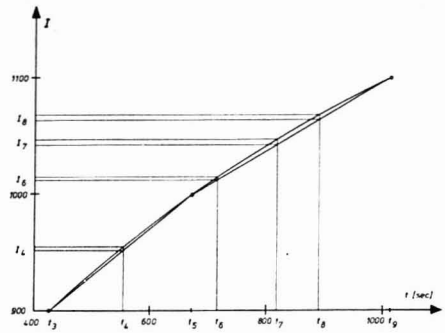


Figure 2. Calculation of retention indices by spline and linear interpolation. The figure shows the respective calibration curves for the interval between nonane and undecane. The retention times are taken from Table I

Table II. Sums of Squared Second Divided Differences of Each Three Consecutive Retention Indices Calculated by the Spline and the Polygon Method. The Given Values Are Multiplied by 10^7

chromatogram no.	Σ_s	Σ_p
1	0.758	1.006
2	0.996	1.321
3	1.286	1.617
4	0.852	0.976
5	1.956	2.432
6	1.382	1.878
7	1.253	1.659
8	0.772	0.954
9	0.737	1.015
10	0.592	0.761
11	1.042	1.271
12	1.013	1.350
13	0.759	0.906
14	0.753	0.969
15	0.622	0.771
16	0.721	0.991
17	1.036	1.361

chosen 17 times. Prior to the analysis, the *n*-alkane standard mixture (C_7–C_{18}) was added to the oil. The retention indices of all peaks were computed by using both methods. The principle of either calculation is demonstrated in Figure 2. Experimental details are given in (*1*). For the alkane standards and 15 other peaks selected according to size and retention time, the means and standard deviations of their retention times are listed in Table I. Furthermore, the table contains for each of the nonstandard peaks the means and standard deviations of the retention indices computed by both methods.

Comparing columns σ_P and σ_S we observe that there is no significant difference in contrast to the corresponding mean values. This shows that both methods produce comparable methodological errors but lead to significantly different results in the regions where the calibration data show a nonlinear behavior.

According to the chromatographic theory, there are (almost) linear relationships between the retention times of homologous series' higher members and their numbers of carbon atoms, providing that linear temperature programs are applied. The retention indices of the other compounds are defined on the basis of these linear relationships. In order to determine which of the two considered techniques yields results more consistent with this definition, a further evaluation was carried out. For each chromatogram and either method, the sums of squared second divided differences

$$\Sigma_M = \sum_{i=2}^{14} \left[\frac{\dfrac{r_{i+1}^{(M)} - r_i^{(M)}}{t_{i+1} - t_i} - \dfrac{r_i^{(M)} - r_{i-1}^{(M)}}{t_i - t_{i-1}}}{t_{i+1} - t_{i-1}} \right]^2$$

where M = S, P, were calculated, where t_i designates the retention time of a nonstandard peak and $r_i^{(S)}$, $r_i^{(P)}$ its retention index computed by the spline and the polygon method, respectively, for $i = 1, \ldots, 15$. The results are listed in Table II and show that the values obtained by spline interpolation are 1.15 to 1.38 times smaller than the corresponding values calculated with the polygon technique. Retention indices obtained by spline interpolation show a "more linear" behavior, since the sum of squared second divided differences vanishes for a set of points lying on a straight line.

LITERATURE CITED

(1) E. Kugler, R. Langlais, W. Halang, and M. Hufschmidt, *Chromatographia*, **8**, 468–473 (1975).
(2) E. Kugler, W. Halang, R. Schlenkermann, H. Webel, and R. Langlais, *Chromatographia*, **10**, 438–443 (1977).
(3) R. Langlais, M. Lauster, G. Lohre, and E. Kugler, Optimisation of Sensory Attributes through Quality Assurance, in "Sensory Properties of Foods", G. G. Birch, J. G. Brennan, and K. J. Parker, Ed., Applied Science Publishers Ltd., London, 1977, pp 213–224.
(4) J. C. Giddings, *J. Chromatogr.*, **4**, 11–20 (1960).
(5) J. H. Ahlberg, E. N. Nilson, and J. L. Walsh, "The Theory of Splines and Their Applications", Academic Press, New York and London, 1967, Chapters II and III.
(6) K. Böhmer, "Spline-Funktionen", B. G. Teubner, Stuttgart, 1974, Chapters 1, 2, 6, and 7.

RECEIVED for review April 5, 1978. Accepted July 17, 1978.

Comparison of Thin-Layer and Column Chromatography for Separation of Sedimentary Hydrocarbons

Juanita N. Gearing* and Patrick J. Gearing

Marine Ecosystems Research Laboratory, Graduate School of Oceanography, University of Rhode Island, Kingston, Rhode Island 02881

Thomas F. Lytle and Julia S. Lytle

Gulf Coast Research Laboratory, P.O. Drawer AG, Ocean Springs, Mississippi 39564

Several thin-layer (TLC) and column chromatographic (CC) methods were compared for efficiency and precision of separation of standard mixtures into hydrocarbon classes. TLC with activated silica gel G and CC with 2:1 (v/v) activity grade I silica gel-alumina gave similar and excellent separation of aliphatic from aromatic hydrocarbons. Extracts of 12 replicate sediment samples from Narragansett Bay, R.I., separated by these two methods gave $\bar{x} \pm s$ values (μg hydrocarbons per g dry weight of sediment) of 111.5 ± 26.2 (TLC) and 116.9 ± 14.4 (CC) for the aliphatic hydrocarbon fraction, and 29.9 ± 9.7 (TLC) and 31.3 ± 8.6 (CC) for the aromatic hydrocarbon fraction. The results suggest that the two techniques may be used interchangeably for purification of sedimentary hydrocarbon extracts. Interlaboratory precision for sediment samples from the same area is equal to that reported for artificial calibration samples.

With the great increase in worldwide transportation of petroleum and petroleum products (refined oil, solvent, and plastics to name only a few), concern has grown over the extent and effect of accidental spills and other inputs to the marine environment. It has become necessary to increase not only the number but also the accuracy and replicability of measurements of hydrocarbons in the environment. It is now critical that many laboratories be able to carry out these complex measurements on an almost routine basis. Because of the chemical variety of extracts from environmental samples and because of the experimental difficulties involved in analyzing a number of different sample types, it may never be possible or advisable to set a standard method for hydrocarbon analyses. Thus, the characteristics and replicability of the different methods used must be firmly established so that results from different laboratories may be compared.

Much of this work is now being done. It has been centered upon the extraction techniques since incomplete extraction can affect not only the quantitative but also the qualitative results. Relative efficiencies have been determined for extraction of hardshell clams (*1*) and for surface sediments (*2*). Examination of results on intercalibration samples (tuna meal and cod liver oil) analyzed in several laboratories (*3*) points out the importance of the extraction procedure. Relative standard deviations less than 20% have been reported for homogenized sediments analyzed by three laboratories (*4*). However, such close agreement is not always the case. Hilpert et al. (*5*) gave the precision of total sedimentary hydrocarbon determinations between eight laboratories. Relative standard deviations were 114 and 122% for two different samples, while intralaboratory results on the same samples had relative standard deviations of 25% (12 samples) and 30% (9 samples). It should be noted that these results were obtained on actual homogenized sediments with very low hydrocarbon concentrations.

One aspect of the methods currently in use which has not received much attention is the purification and separation into "aliphatic" and "aromatic" hydrocarbon fractions by solid–liquid chromatography. Many different chromatographic columns, plates, and elution schemes have been used to separate the vast number of compounds in petroleum into general classes (*5, 6*). In 1961, Synder (*7*) demonstrated the applicability of both silica gel and alumina to petroleum hydrocarbons. Since then, columns of alumina overlying silica gel have been favored. Variability occurs in the proportions of the two materials, in their mesh size, in their state of activation, and in the eluents. Column chromatography (CC) with ratios of silica gel to alumina (v/v) of 4:1 (*3*), 3:1 (*5*), 2:1 (*8*), 3:2 (*9*), and 1:1 (*3*) has been done. Elution with varying proportions of pentane, hexane, heptane, petroleum ether, benzene, toluene, methylene chloride, and carbon tetrachloride has been used. Work with thin-layer chromatography (TLC) has often been carried out on plates coated with silica gel and developed with hexane or petroleum ether (*3, 10–12*). It has been routinely assumed that these many schemes can be used interchangeably without affecting the precision or accuracy of the measurement. Such assumptions are dangerous when not supported by published experimental evidence.

This paper reports results of separation of standard hydrocarbon mixtures by TLC and by CC using several of the more widely applied chromatographic conditions. We have also examined the relative efficiency of the two techniques in separating aliphatic and aromatic fractions from each other and from more polar compounds in extracts of an actual marine sediment.

EXPERIMENTAL

All solvents used were distilled in glass to remove any hydrocarbon contaminants. Standards included a mixture of *n*-alkanes (with 16, 17, 18, 24, 28 and 32 carbon atoms), the isoprenoid pristane (2,6,10,14-tetramethylpentadecane), two monounsaturated paraffins (n-$C_{16:1}$ and n-$C_{18:1}$), 3-methylnonadecane, and a number of aromatics (1,2,4,5-tetramethylbenzene, naphthalene, 2,3,6-trimethylnaphthalene, phenanthrene, and anthracene). The standards were purchased from Aldrich Chemical Company, Analabs, and Applied Science Laboratories.

Column chromatography used silica gel (Woelm) and neutral alumina (Woelm). Both reagents were activated by heating overnight at 200 °C. Deactivation was by thorough mixing with the appropriate volume of extracted tap water. All columns had an adsorbent to sample weight ratio greater than 100 and were prewashed with two column volumes of hexane before the sample was charged.

Thin-layer chromatography was carried out using the technique described by Quinn and Wade (*11*). Plates were coated with a 0.37-mm layer of silica gel G Type 60 (Analabs) containing no organic binder, activated at 110 °C for 12 h and then precleaned with CH_2Cl_2:CH_3OH (80:20, v/v). After spotting, samples were eluted by hexane with 1% NH_4OH added to aid in visualization of bands. A mixture of 3-methylnonadecane and phenanthrene standards was eluted on the same plate to act as a guide in removing the hydrocarbon fractions of the sample. Bands were

0003-2700/78/0350-1833$01.00/0 © 1978 American Chemical Society

Table I. Fractionation of Standards by Column Chromatography

		μg recovered from column (silica gel:alumina)							
		3:2, 5% deactivated		4:1, activated		2:1, activated			
	μg charged	hexane (3 vols)	benzene (3 vols)	hexane (2 vols)	benzene (2 vols)	hexane 1st vol.	hexane 2nd vol.	hexane 3rd vol.	benzene (1 vol.)
n-alkanes	5075	2535	175	2630	20	3640	55	0	0
isoprenoids	710	460	39	495	0	605	0	0	0
unsaturates	1050	380	53	1030	5.5	660	145	0	0
aromatics	2900	945	74	1010	90	0	0	24	2365

Table II. Fractionation of Standards by TLC and CC (percent recovery, two runs)

	TLC, activated silica gel				CC, 2:1 (v/v) silica gel:alumina (activated)			
	aliphatic band		aromatic band		hexane (2 vols)		benzene (2 vols)	
3-methylnonadecane	46	53	1	2	32	20	0	0
1,2,4,5-tetramethylbenzene	0	0	6	31	0	0	24	27
naphthalene	0	0	3	17	0	0	26	19
2,3,6-trimethylnaphthalene	0	0	50	67	0	0	57	80
phenanthrene	0	0	54	69	0	0	58	84

visualized by spraying the plate with bromothymol blue and viewing under UV light.

A sediment extraction procedure similar to that of Boehm and Quinn (*12*) was followed. Twelve aliquots were taken from a wet, homogenized silty clay from central Narragansett Bay (71°22'N, 41°35'W) which had been put through a 0.82-mm sieve to remove large organisms and shells. After addition of 3-methylnonadecane plus phenanthrene internal standards, each aliquot was refluxed for 4 h in equal portions of methanolic KOH (1 N) and benzene, with 5% pre-extracted water added. The nonsaponifiable fraction was extracted with three separate portions of benzene, taken to 5 mL on a rotary evaporator, and treated with activated copper to remove elemental sulfur. Six aliquot extracts were then separated on columns consisting of 2:1 (v/v) silica gel under alumina (both activity grade I) and eluted with two column volumes of hexane (aliphatic fraction) followed by two column volumes of benzene (aromatic fraction). The other six extracts were separated into two fractions by TLC in the procedure described above.

The same procedure, using TLC, was carried out on 25 samples of sediment from the tanks at the Marine Ecosystems Research Laboratory, Rhode Island. These tanks were originally filled with sediment from the same location as the homogenate described in the preceding paragraph.

Analysis of hydrocarbons was by gas chromatography with a Perkin-Elmer model 3920B or 990 chromatograph equipped with dual flame ionization detectors and dual 2 m × 3.2 mm stainless steel columns packed with 4% FFAP on 80/100 mesh Gaschrom Z. Temperature programming was from 90 to 230 °C at 8 °C min^{-1} with a 4-min initial hold and final hold until Kovats Index 3200 was reached.

RESULTS AND DISCUSSION

Comparison of Standards on Various Columns. Table I shows the separations achieved with a known hydrocarbon mixture put through three columns containing differing proportions of silica gel to alumina. The mixture contained all the standards listed previously except 3-methylnonadecane and phenanthrene. In comparing the composition of the eluates from the three columns, it can be seen that the 3:2 (v/v), 5% deactivated column and the 4:1 (v/v), activity grade I columns with the elution schemes described were ineffective in separating the hydrocarbon classes. All of the standards eluted predominantly with the hexane in both columns. The column made up of 2:1 (v/v) silica gel to alumina (both activity grade I) was most effective of those examined. Two column volumes of hexane removed virtually all of the aliphatic hydrocarbons while leaving the aromatics on the column. Aromatics began to be eluted by the third column volume of hexane and were removed completely when the elution solvent was changed to benzene for the fourth column volume. It was concluded that excellent separation of aliphatic from aromatic hydrocarbons could be obtained by use of such a column and elution with two volumes of hexane (aliphatic fraction) followed by two volumes of benzene (aromatic fraction).

This comparison of the three column chromatography schemes was designed primarily to test the efficiency of the procedure routinely used in our laboratory. The results do not imply that the many schemes used in other laboratories may not be just as efficient, but that any procedure used should be experimentally validated. In particular, it should be noted that vastly different separations may be obtained by the use of silica gel and alumina of different mesh ranges.

Comparison of Standards Separation by TLC and CC. A mixture of one aliphatic and four aromatic hydrocarbons (see Table II) was prepared. Two aliquots were separated by the column conditions shown to be effective in the last section, and two by TLC. All four runs gave nearly identical separations. Because of evaporative losses of the lower molecular weight aromatics, the final proportions in the aromatic fractions differed slightly from the standard mixture. There was, however, virtually no overlap of aliphatics with aromatics in either method.

This indicates that TLC and CC may be used interchangeably, resulting in increased flexibility and thus efficiency in hydrocarbon analysis, for each method has certain definite advantages. With TLC, standards may be run routinely on the same plate as the samples, providing a check on each separation. It is particularly good with small samples, several of which may be developed on the same plate. However, samples must be reduced to a very small volume for spotting on a TLC plate, increasing the risk of loss of the more volatile compounds by evaporation (see Table II, where some loss of tetramethylbenzene and naphthalene was observed during TLC). Moreover TLC involves greater exposure of the hydrocarbons to sunlight, increasing the risk of photo-oxidation.

Column chromatography may be faster than TLC but, as previously noted, great care must be taken to standardize a chromatography scheme and to periodically test its efficiency since standards cannot be run with each sample. The greater ratio of solvent to hydrocarbons in CC lessens the danger of evaporative loss.

Comparison of Sediment Replicates by TLC and by CC. The separation of standard hydrocarbon mixtures tested the precision of the methods on a simple sample. These mixtures contained ten or fewer compounds. Environmental

Table III. Fractionation of Twelve Replicate Sediment Extracts by TLC and CC (concentrations, μg/g)

	aliphatic fraction		aromatic fraction		total hydrocarbons	
	TLC	CC	TLC	CC	TLC	CC
	106	112	44.7	17.2	151	130
	114	118	25.1	24.4	139	142
	90.1	91.4	20.7	38.9	111	130
	79.3	130	20.8	34.5	100	164
	127	131	37.5	34.6	165	165
	152	119	30.5	38.0	183	157
mean	111.5	116.9	29.9	31.3	141.4	148.2
std. dev.	26.2	14.4	9.7	8.6	31.6	16.4
rel. std. dev.	23.5%	12.3%	32.4%	27.5%	22.3%	11.1%
t statistic (tabulated value at 99% confidence)					3.7 (10.97)	
variance ratio, F (tabulated value at 99% confidence)					0.49 (4.03)	

Table IV. Total Hydrocarbon Concentrations in Sediments from Adjacent Areas of Narragansett Bay[a]

date	no. of samples	ref.	laboratory[b]	range, μg/g	mean, μg/g	std. dev.	rel. std. dev., %
1973	3	(4)	3	130–160	147	15.3	10.4
1976	6	(16)	1, 2	141–185	157	16.8	10.7
Aug. 1976	6	(16)	2, 3	144–210	185	27.6	14.9
Aug. 1976	12	this work	1	100–183	145	24.3	16.8
Sept. 1976	25	this work	1	45.1–186	140	34.2	24.4
1977	8	(17)	2	130–168	144	13.9	9.7

[a] All sediments except those in this work are from 71° 22'N and 41° 35'W. [b] Laboratories are (1) this laboratory, (2) T. Wade and J. Quinn, University of Rhode Island, and (3) J. Farrington, Woods Hole Oceanographic Institute.

samples may contain hundreds or even thousands of compounds, including not only n-alkanes, isoprenoids, and fused-ring aromatics such as in the standard mixtures, but a vast array of less readily identifiable compounds such as alicyclic hydrocarbons. Such complex samples are needed to test the separation efficiencies of the methods under actual conditions.

Table III gives hydrocarbon concentrations and standard deviations, based on gas chromatography, of 12 aliquots (six extracts separated by TLC and six by CC) of the homogenized sediment. The variance ratio (F) was calculated and when compared with the tabulated values at the 99% level ($\alpha = 0.01$) showed that the standard deviations of values from the two different methods are statistically indistinguishable. Thus, although the values suggest that column chromatography may be slightly more reproducible, the greater precision is not statistically significant. The equality of variances allows a simple t test to be performed, which showed that the two means are also equal at the 99% level.

The hydrocarbons in central Narragansett Bay surface sediments give complex chromatograms with compounds eluting from Kovats Index 1400 to 3200+. Peaks of C_{25} cycloalkenes and odd carbon number n-alkanes from n-C_{25} to n-C_{31} are superimposed on a large, unresolved complex mixture (UCM). The source of the C_{25} alkenes, also found in Buzzard's Bay and Gulf of Maine (13), Scotian Shelf (14), and Gulf of Mexico shelf sediments (8), is presently unknown. The heavy n-alkanes are thought to originate from terrestrial plant waxes (14, 15). The UCM contains naphthenic, naphthenoaromatic, and aromatic hydrocarbons, which strongly suggest an anthropogenic source for that component (13, 14). This assemblage of hydrocarbons from disparate sources provides a good test for the separating efficiency of thin-layer and column chromatography. Examination of the gas chromatograms of fractions separated by the two methods showed no discernible qualitative differences in the patterns.

Precision and Accuracy of Sediment Analyses. The accuracy of the results of the 12 sediment analyses was tested relative to published data by other investigators on sediments from the same area of Narragansett Bay, as well as to additional determinations in our own laboratory. These data are summarized in Table IV. A one-sided F test of variance coupled with a t test on the means indicated that neither the means nor the standard deviations were statistically different when comparing the 12 determinations reported in Table III with either the 21 determinations by other laboratories ($F_{1,31} = 1.80$, $t_{31} = 1.335$) or with all the other observations (21 from other laboratories and 25 from our laboratory) ($F_{1,58} = 0.184$, $t_{58} = 0.095$). The one-sided F test of variance was also applied to the data as grouped by laboratories. The variance between laboratories was not statistically greater than the variance within laboratories ($F = 1.234$; the tabulated value for $F_{2,34}$ is 5.29 at the 99% confidence level). Thus the results obtained by both column chromatography and thin-layer chromatography are accurate (assuming that the mean of 48 analyses is accurate) as well as precise within normal experimental levels.

Moreover, the results indicate the interlaboratory reproducibility which can be obtained. The methods of analysis used by the three laboratories were very similar, but the sediments were collected and analyzed by a least 5 people over 5 years in 3 laboratories. The relative standard deviations (≤25%) compare favorably with intralaboratory variances. Farrington and Tripp (18) reported relative standard errors of ≤37% for western North Atlantic surface sediment with hydrocarbon concentrations from 113 to 150 μg/g. Hilpert et al. (5) reported intralaboratory relative standard deviations of 25 and 30% on sediments in the 0.5 to 1 μg/g range, but interlaboratory ranges (8 laboratories) of up to two orders of magnitude for the same homogenized sediments. The low concentrations of these Alaskan sediments make the analysis for total hydrocarbons much more difficult. However, where hydrocarbon concentrations are greater and similar methods are used, much better interlaboratory precision is achievable.

ACKNOWLEDGMENT

The authors thank Harry McCarty for laboratory assistance.

LITERATURE CITED

(1) J. W. Farrington and G. C. Medeiros, "Proceedings, 1975 Conference on Prevention and Control of Oil Pollution", American Petroleum Institute, Washington, D.C., 1975, p 115.
(2) J. W. Farrington and B. W. Tripp, *Mar. Chem. Coastal Environ.*, **18** (ACS Symp. Serv.), 267 (1975).

(3) J. W. Farrington, J. M. Teal, G. C. Medeiros, K. A. Burns, E. A. Robinson, J. G. Quinn, and T. L. Wade, *Anal. Chem.*, **48**, 1711 (1976).
(4) T. L. Wade and J. G. Quinn, submitted for publication in *Environ. Pollut.*
(5) L. R. Hilpert, W. E. May, S. A. Wise, S. N. Chesler, and H. S. Hertz, *Anal. Chem.*, **50**, 458 (1978).
(6) R. C. Clark, Jr. and D. W. Brown, in "Effects of Petroleum on Arctic and Subarctic Marine Environments and Organisms", D. C. Malins, Ed., Academic Press, New York, N.Y., 1977, pp 1–90.
(7) L. R. Snyder, *Anal. Chem.*, **33**, 1527 (1961).
(8) P. Gearing, J. N. Gearing, T. F. Lytle, and J. S. Lytle, *Geochim. Cosmochim. Acta*, **40**, 1005 (1976).
(9) R. S. Clark and J. S. Finley, "Proceedings of the 1973 Joint Conference on Prevention and Control of Oil Spills", American Petroleum Institute, Washington, D.C., 1973, p 161.
(10) L. Hunter, *Environ. Sci. Technol.*, **9**, 241 (1975).
(11) J. G. Quinn and T. L. Wade, Marine Memorandum Series No. 33, University of Rhode Island, Kingston, R.I., 1974, 8 pp.
(12) P. D. Boehm and J. G. Quinn, *Estuarine Coastal Mar. Sci.*, **6**, 471 (1978).
(13) J. W. Farrington, N. M. Frew, P. M. Gschwend, and B. W. Tripp, *Estuarine Coastal Mar. Sci.*, in press.
(14) P. D. Keizer, J. Dale, and D. C. Gordon, Jr., *Geochim. Cosmochim. Acta*, **42**, 165 (1978).
(15) J. W. Farrington and P. A. Meyers, in "Environmental Chemistry", Vol. 1, G. Eglinton, Ed., The Chemical Society, Burlington House, London, 1975.
(16) J. W. Farrington and J. G. Quinn, *Estuarine Coastal Mar. Sci.*, **1**, 71 (1973).
(17) T. L. Wade, University of Rhode Island, Kingston, R.I., personal communication, 1978.
(18) J. W. Farrington and B. W. Tripp, *Geochim. Cosmochim. Acta*, **41**, 1627 (1977).

RECEIVED for review June 23, 1978. Accepted August 14, 1978. Work supported by Grant R803902020 of the Environmental Protection Agency.

Determination of Volatile Halogenated Hydrocarbons in Water with XAD-4 Resin

Lars Renberg

Special Analytical Laboratory, National Swedish Environment Protection Board, Wallenberg Laboratory, University of Stockholm, S-106 91 Stockholm

The determination of trihalomethanes, chloroethenes, and dichloroethane in water was carried out by adsorption on an XAD-4 polystyrene resin, followed by elution with ethanol. The method results in an extract concentrated enough for both chemical determination and small scale biological tests. By using two series-connected columns, the degree of adsorption was studied and the chloroethenes were found to be more strongly adsorbed than the haloalkanes. The recovery was found to be 60–95% of the substances studied.

The presence of volatile halogenated hydrocarbons such as trihalomethanes and chloroethenes in water has been established in water samples from several sources. The trihalomethanes have been shown to be formed during the chlorination process, used in water treatment plants, and the average levels of chloroform, bromodichloromethane, and chlorodibromomethane in drinking water samples from 80 cities in the U.S.A. were found to be 21, 6, and 1.2 μg/L, respectively (*1*). Also the incoming water to a water treatment plant has been shown to contain several halogenated compounds such as the commonly used solvents 1,2-dichloroethane, trichloroethene, and tetrachloroethene (*2*). The main interest in these types of compounds is focused on possible toxic effects, particularly carcinogenicity. Using bacterial systems, bromodichloromethane, chlorodibromomethane, trichloroethene, and 1,2-dichloroethane have been shown to possess mutagenic properties (*3, 4*).

The need for determination of volatile hydrocarbons in water samples has resulted in several methods such as solvent extraction (*5, 6*), gas stripping (*7*), head space (*8*), and direct injection techniques (*9*).

In this paper, a method is described which involves the adsorption of volatile halogenated hydrocarbons on an Amberlite XAD-4 resin followed by elution with ethanol. The use of XAD-2 or XAD-4 resins for the determination of less volatile substances has been described earlier (*10–12*), and adsorption of haloforms on acetylated XAD-2, followed by elution with pyridine (*13*), and on non-acetylated XAD-2 (*14*) has also been reported. Recently, the use of XAD-resins for the determination of total organic halogen content in water has been described (*15*).

The advantages of using the XAD-4 technique are several. The method is simple and allows sampling in situ, thus avoiding changes of water sample composition between time of sampling and time of analysis. The procedure involves a concentration step which makes it possible to reach desired detection limits, as these limits may vary with applications. It also allows the collection of samples large enough for both chemical determination and small scale biological tests such as the Ames' bacterial system for mutagenicity determination (*16*).

EXPERIMENTAL

Materials. Amberlite XAD-4 (Rohm and Haas Company), acetone (pesticide grade), methanol and ethanol (spectroscopic grade) were used. The purity of the methanol and ethanol was checked by the gas chromatographic system described below.

Polymeric Resin Cleanup. Amberlite XAD-4 was placed in a column with a glass filter. Five bed volumes of acetone were passed through the column with a flow rate about 0.1 bed volume/min. Then water was passed upflow through the column at a rate sufficient to expand the bed by about 50% to remove the smallest particles. The resin was then extracted by means of a Soxhlet apparatus with methanol for at least 6 h, then replaced into the column and eluted with 20 bed volumes of purified water and finally stored under purified water. The purity of the resin was checked in a blank procedure.

Purified Water. Deionized water was distilled through an all glass apparatus. The first 10% of the distillate was discarded and the 10–50% portion was passed through a column containing 10 mL XAD-4 at a flow rate of about 30 mL/min. If the resin was taken directly from the Soxhlet extraction and thus containing methanol, the first 200 mL of the eluate was discarded.

Adsorption and Desorption Steps. Two glass columns, 15 × 1.1 (i.d.) cm, with Teflon stopcocks, were each filled with 5 mL of XAD-4. Purified water was added to the top of the columns and the beds were stirred to release air bubbles. The columns were connected in a series and the water sample was allowed to pass through the columns at a flow rate of 30 mL/min.

The columns were allowed to run dry and disconnected. To each column, ethanol (3 mL) was added, the beds were stirred, and the resins were allowed to swell for at least 20 min. The beds were stirred once more to release air bubbles and the columns

0003-2700/78/0350-1836$01.00/0 © 1978 American Chemical Society

Table I. Results of Recovery Experiments from Five Spiked Samples

substance	amount of spiked substance, μg/250 μL	recoveries[a] mean value (%) ± rel std dev	ratio a_2/a_1[b] ± std dev
chloroform	2.9	85 ± 4.1	0.27 ± 0.03
bromodichloromethane	0.63	86 ± 9.6	0.22 ± 0.08
chlorodibromomethane	1.3	91 ± 6.7	0.12 ± 0.03
1,2-dichloroethane	120	95 ± 9.0	0.44 ± 0.09
trichloroethene	2.5	74 ± 3.6	0.07 ± 0.03
tetrachloroethene	1.4	60 ± 4.5	0.06 ± 0.02

[a] Sum of the amounts found in the two series-connected columns ($a_1 + a_2$). [b] Ratio of the amounts found in the second and the first column, respectively.

were eluted separately with ethanol (flow rate 1 mL/min) until 20 mL of eluate were collected. The eluates were then analyzed by gas chromatography.

Recovery Experiments. Purified water (250 mL) was transferred to a 250-mL separatory funnel and 250 μL of an ethanol solution containing chloroform, bromodichloromethane, chlorodibromomethane, 1,2-dichloroethane, and tri- and tetrachloroethene was added. The funnel was shaken and the spiked water allowed to pass the columns. The flow was stopped when the level just reached the top of the upper bed. In order to rinse the glass walls from substances adsorbed, additional water (3 × 250 mL) was passed through the funnel columns and the columns were eluted as described. The separatory funnel was shaken with ethanol (25 mL) for the determination of substances adsorbed on the glass walls. Five spiked and two blank samples were analyzed.

Gas Chromatographic System. A Varian 3700 gas chromatograph equipped with an electron capture detector was used. Injector and detector temperatures were 250 °C. The ethanol extracts were injected into a 170 × 0.18 (i.d.) cm glass column, packed with Chromosorb 101 80/100 mesh which was kept at 145 °C. Alternatively, ethanol extract (1 mL) was shaken with purified water (5 mL) and hexane or pentane (1 mL). The organic phase was, after centrifugation, injected into a 50-m OV-17 capillary column at a split ratio of 1:10. After injection, the column was held 5 min at 80 °C, then programmed at a rate of 2 °C/min until 120 °C was reached.

RESULTS AND DISCUSSIONS

Among several possible adsorbents, XAD-4 was judged to be the most suitable. Pilot experiments showed that the substances tested were less strongly adsorbed on the polyacrylic ester resin XAD-7. As the average pore diameters for XAD-4 and XAD-2 (50 and 90 Å) were both sufficiently large for the substances tested, the XAD-4 resin was also preferred when compared to the chemically similar XAD-2, because of a larger surface area (750 and 330 m^2/g, respectively).

The results of recovery experiments for different volatile organohalogens are summarized in Table I. Recovery experiments have also been made with spiked drinking water with similar results. It should be pointed out that the flow rates used here for both the adsorption and the desorption step (360 bed vol/h and 12 bed vol/h, respectively) are much higher than those recommended by the manufacturer (4–16 bed vol/h and 1–4 bed vol/h, respectively) (*17*). Such high flow rates speed up the time of analyses while still maintaining high recoveries.

The method described, however, is intended to be used not only for the volatile organohalogens tested in this paper, but also for other unpolar substances, which can be found in different types of waters (including wastewater). The main reason for choosing an enrichment method, instead of the above referred techniques (*5–9*), is the fact that the present

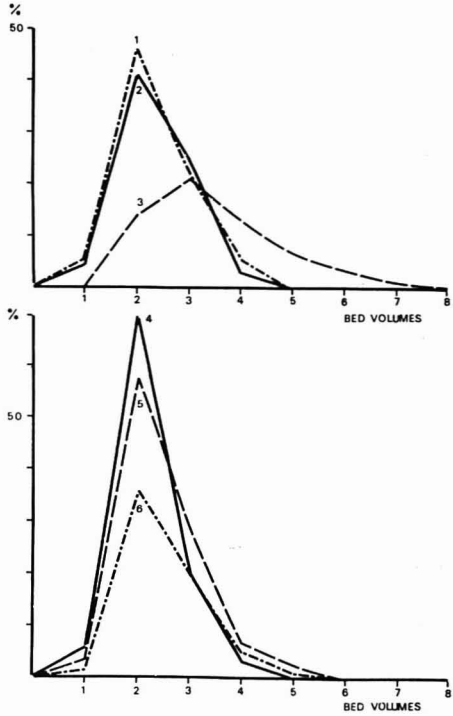


Figure 1. Elution curves of some volatile halogenated hydrocarbons (5 mL XAD-4 column). (1) Chloroform, (2) 1,2-dichloroethane, (3) tetrachloroethene, (4) bromodichloromethane, (5) chlorodibromomethane, (6) trichloroethene

method results in an extract, sufficiently concentrated to be used both for chemical determination, e.g., gas chromatography/mass spectrometry, and also in biological tests. Consequently, the solvent used for the elution of the adsorbent should, besides a good eluting ability, also possess a low toxicity, which restricts the choice of solvent to, for instance, acetone or ethanol. The latter solvent was chosen because of the difficulties in obtaining sufficiently pure acetone compared to ethanol.

If desired, the unpolar components in the ethanol extract can be transferred into a hexane solution, by adding water to the ethanol extract, followed by extraction with hexane.

Activated carbon was excluded as a possible adsorbent, because of the high toxicity of eluting solvents, commonly used for activated carbon, e.g., benzene, toluene, or carbon disulfide.

To study the adsorption character of substances described here, as well as other compounds, two columns were connected in a series and after the passage of the water sample the columns were eluted separately. The recovery of the substances of the second column, compared to those of the first one, will indicate the leakage of substances which is dependent on, e.g., water flow rate and polarity of the substances.

The ratio (a_2/a_1) of the amounts found in the second (a_2) and the first columns (a_1), respectively, will predict the degree of adsorption, which can be regarded as a measurement of the lipophilicity of the substances studied. The values of the ratios found in the recovery experiments, shown in Table I, indicate

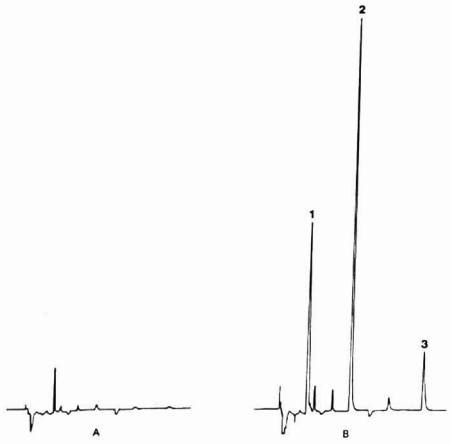


Figure 2. Gas chromatogram of water extracts from a water treatment plant (OV-17 capillary column). (A) Incoming water, (B) outgoing water. (1) Chloroform, 5.0 μg/L; (2) bromodichloromethane, 2.5 μg/L; (3) chlorodibromomethane, 0.54 μg/L

tetrachloroethene and 1,2-dichloroethane as the most and the least lipophilic of the substances tested. As long as the desorption step is carried out quantitatively, an approximation of the original concentration can be calculated, using the values from the two individual columns as the first two terms in an infinite geometrical series, giving a finite sum (s) as long as $a_2/a_1 < 1$ according to the formula

$$s = a_1^2/(a_1 - a_2)$$

Thus, using Table I, the calculated true values for, e.g., chloroform and chlorodibromomethane are both 92%. However, for tri- and tetrachloroethene, the values are still 74 and 60%, respectively, in spite of their low a_2/a_1 values, which indicates that these compounds are strongly adsorbed, but not so easily desorbed. The elution profiles (see Figure 1) show that this is especially pronounced for tetrachloroethene. It seems that this strong adsorption, compared to, e.g., the trihalomethane, is not only dependent on the unpolar character of the chloroethenes, but may also depend on interference of the π-electrons with the polystyrene matrix. The recoveries of the chloroethenes are increased if either a larger elution volume or shorter columns are used. However, the technique described is a compromise between relatively small elution volumes and satisfactory recoveries for compounds with quite different water solubilities.

The method has been applied to incoming and outgoing water from a water treatment plant (see Figure 2) and on wastewater from a poly(vinyl chloride) plant for the determination of trihalomethanes and 1,2-dichloroethane. Furthermore, the ethanol extract of wastewater from poly(vinyl chloride) production was found to possess mutagenic properties, using the Ames' bacterial system (M. Möller and L. Renberg, unpublished work).

ACKNOWLEDGMENT

The author is indepted to Karin Sund-Nygård for skillful technical assistance and to the staff of the laboratory for valuable discussions.

LITERATURE CITED

(1) J. M. Symons, T. A. Bellar, J. K. Carswell, J. DeMarco, K. L. Kropp, G. G. Robeck, D. R. Seeger, C. J. Slocum, B. L. Smith and A. A. Stevents, *J. Am. Water Works Assoc.* **67**, 634 (1975).
(2) B. J. Dowty, D. R. Carlisle, and J. L. Laseter, *Environ. Sci. Technol.*, **9**, 762 (1975).
(3) U. Rannug and C. Ramel, *J. Tox. Environ. Health*, **2**, 1019 (1977).
(4) V. F. Simmons, K. Kauhanen, and R. G. Tardiff in "Progress in Genetic Toxicology", D. Scott, B. A. Bridges, and F. H. Sobels, Eds., Elsevier/North Holland Biomedical Press, **2**, 249 (1977).
(5) J. P. Mieure, *J. Am. Water Works Assoc.*, **69**, 60 (1977).
(6) J. J. Rickard and G. A. Junk, *J. Am. Water Works Assoc.*, **69**, 62 (1977).
(7) K. Grob and G. Grob, *J. Chromatogr.*, **90**, 303 (1974).
(8) K. L. E. Kaiser and B. G. Oliver, *Anal. Chem.*, **48**, 2207 (1976).
(9) A. A. Nicholson, O. Meresz, and B. Lemytk, *Anal. Chem.*, **49**, 814 (1977).
(10) P. R. Musty and G. Nickless, *J. Chromatogr.*, **89**, 185 (1974).
(11) G. A. Junk, J. J. Rickard, M. D. Grieser, D. Witiak, J. L. Witiak, M. D. Arguello, R. Vick, H. J. Svec, V. S. Fritz, and G. V. Calder, *J. Chromatogr.*, **99**, 745 (1974).
(12) J. A. Coburn, I. A. Valdmanis, and A. S. Y. Chau, *J. Assoc. Off. Anal. Chem.*, **60**, 224 (1977).
(13) L. D. Kissinger and J. S. Fritz, *J. Am. Water Works Assoc.*, **68**, 435 (1976).
(14) G. A. Junk, D. C. Chriswell, R. C. Chiang, L. D. Kissinger, J. J. Rickard, J.S. Fritz, and H. J. Svec, *Fresenius Z. Anal. Chem.*, **282**, 331 (1976).
(15) W. H. Glaze, G. R. Peyton, and R. Rawley, *Environ. Sci. Technol.*, **11**, 685 (1977).
(16) B. N. Ames, W. E. Dunston, E. Yamasaki, and F. D. Lee, *Proc. Natl. Acad. Sci. USA*, **70**, 2281 (1973).
(17) Rohm and Haas Company, Amberlite XAD-4, Technical Bulletin (1974).

RECEIVED for review March 27, 1978. Accepted July 31, 1978. Work supported by the Research Committee at the National Swedish Environment Protection Board.

Solid Sorbent for Sampling Acrolein in Air

Avram Gold,* C. E. Dubé, and R. B. Perni

Department of Environment Health Sciences, Harvard School of Public Health, 665 Huntington Avenue, Boston, Massachusetts 02115

Activated 13X molecular sieves were found to be an excellent solid sorbent for sampling acrolein in air, providing quantitative trapping and recovery and stability of stored samples. Although water vapor decreases acrolein breakthrough times, a sample volume of 8 L/g sieve sorbent is permissible at 100% relative humidity, allowing determination of acrolein at sub-ppm levels even under such unfavorable conditions. The dynamic adsorption isotherm of acrolein on 13X sieves was determined and found to be adequately described by a Langmuir curve. Statistical Moments Theory was applied to breakthrough data to estimate breakthrough times of acrolein over a range of concentrations. Field trials indicate that 13X sieves would also be suitable for sampling other low molecular weight aldehydes, short chain alcohols, and volatile ketones.

To date, the available methods for air sampling of low molecular weight, water soluble aldehydes involve the use of liquid absorbing solutions (*1, 2*). These aldehydes, especially acrolein, are of increasing interest in industrial hygiene and environmental analysis, and a solid sorbent would be highly desirable for convenience in making field measurements.

Molecular sieves have been employed as a gas chromatographic medium for volatile hydrocarbons (*3–5*). Reports on the adsorptive properties of sieves with regard to a number of polar and nonpolar organic compounds (*6–8*) and widespread industrial use of sieves for gas purification (*9, 10*) suggest the possible utility of molecular sieves for air sampling. The adsorption and breakthrough characteristics of aldehyde vapors on sieves have not been reported; therefore this investigation was undertaken to determine the suitability of activated molecular sieves as a sorbent for acrolein vapor. Large pore size in the sieves was desirable to ensure rapid mass transfer and efficient adsorption of acrolein; therefore 13X molecular sieves were selected as sorbent for the study.

Activated 13X sieves were found to be an excellent sampling medium for acrolein, providing quantitative trapping and recovery and stability for storage of adsorbed samples. Although water vapor decreases acrolein breakthrough times, 1 g of sieves has sufficient capacity to allow adequate sampling volumes for determination of sub-ppm concentrations even at 100% relative humidity. Field trials indicate that the 13X sieves should also prove suitable for sampling formaldehyde, acetaldehyde, methanol, ethanol, and acetone.

EXPERIMENTAL

Reagents. Acrolein (Eastman) was freshly distilled before use. Standards were made up by addition of appropriate amounts of liquid acrolein to distilled water.

Linde 13X molecular sieves, 12–30 mesh, were activated by slow heating under vacuum to 400 °C and maintaining that temperature overnight. The sieves were packed into 8 mm i.d. × 6 cm Pyrex sampling tubes and held in place by glass wool plugs. The tubes were capped by serum stoppers.

Analysis. Sieves were desorbed by slow addition to distilled water (2 mL/g sieves) in polyethylene stoppered glass vials chilled in ice. Desorbate, liquid standards, and gas mixtures were analyzed for acrolein by gas chromatography (GC) using a flame ionization detector. Blank runs on activated sieves desorbed with distilled water showed no peaks at lowest attenuation settings. A stainless steel column 11 ft × $^1/_8$ inch packed with Tenax GC was operated at 85 °C with a nitrogen carrier flow of 20 mL/min.

Recovery Experiments. Measured volumes of air containing acrolein vapor in known concentration were added to sampling tubes by syringe. The tubes were desorbed and the desorbate was analyzed.

Breakthrough and Dynamic Adsorption. The apparatus shown in Figure 1 was capable of providing constant concentrations of acrolein for periods of 3–4 h over the range of concentrations indicated in Table I. Nitrogen flow rate through the acrolein reservoir was ~20mL/min and dilution air (0, 30, 100%, relative humidity) was adjusted to provide the desired acrolein input concentration c_i.

Breakthrough was followed by periodic monitoring of carrier gas downstream from the sieves.

Points on the dynamic adsorption isotherm were established by (i) gravimetric and/or desorption analysis for determination of sieve capacity and calculation of input concentration c_i by Equation 2 with the breakthrough time of $c_i/2$ or (ii) GC determination of c_i and calculation of capacity by Equation 2 with the appropriate breakthrough time of $c_i/2$. Combinations of these procedures were simultaneously applied to some experiments as indicated in Table I.

Saturation Capacity by Static Adsorption. Sieves (0.5 to 1 g) were weighed into a small container fabricated from stainless steel screen which was suspended in a closed vessel over pure liquid acrolein at 23 °C. Acrolein uptake was measured by weight gain and/or analysis of desorbate.

RESULTS AND DISCUSSION

Essentially quantitative recovery was achieved with both high and low loadings of acrolein on sieves. Recovery for 11 runs with nominal loadings of 3–8 μg acrolein/g of sieves was 97 ± 11%, while for higher loadings of 60–200 μg/g, recovery was 90 ± 7% for six runs. Sampling tubes loaded with acrolein were analyzed at intervals over four weeks with no observable loss of aldehyde when stored at 0 °C. The quantitative recovery of acrolein is noteworthy since this compound is reactive and irreversible adsorption (*8*) or transformation (*11–13*) of reactive compounds has been observed on sieves even at low temperatures.

The performance of sieves as a trap for acrolein at relatively high concentrations in dry air was evaluated by breakthrough experiments. Breakthrough curves (Figure 2) show to a good approximation the sigmoid form of the normal probability distribution and each curve can be adequately reproduced from a breakthrough time t_{c/c_i} (concentration c < input concentration c_i) and standard deviation σ. The experimental breakthrough curves, tabulated in terms of $t_{0.5}$, σ, and relative standard deviation $\sigma^* = \sigma/t_{0.5}$ are presented in Table I along with experimentally determined sieve capacities and corresponding c_i.

Within experimental uncertainty, the values of σ^* (~0.20) are independent of concentration. The conformity of the breakthrough curves to the normal probability distribution and the invariance of σ^* suggest that the behavior of acrolein on 13X sieves can be described by Statistical Moments Theory (SMT) (*14–16*) despite the nonlinearity of the adsorption isotherm (Figure 3). When mass transfer is controlled by intraparticle diffusion, σ^* may be approximated by the ratio

0003-2700/78/0350-1839$01.00/0 © 1978 American Chemical Society

Table I. Breakthrough Data for Acrolein and Water on 13X Sieves

c_i, mg/L			acrolein A, mg/g					
gravimetric	desorption	GC	gravimetric	desorption	GC	$\sigma^* = \sigma/t_{0.5}$	$t_{0.5}$, min	F, L/min
		0.903[a]			76[a]	0.18	84	1.1
	1.66[a]	2.45		121[a]	178	0.18	69	1.1
		1.96[a]			147[a]	0.15	67	1.1
2.79[a]	2.73	2.25	169[a]	166	136	0.21	54	1.1
		3.08[a]			127[a]	0.24	39	1.1
	3.22[a]	3.68		148[a]	170	0.20	46	1.1
3.53[a]	3.39	3.52	179[a]	171	179	0.21	43	1.1
	4.68[a]	5.55		151[a]	178	0.21	31	1.1
4.81[a]		5.11	166[a]		176	0.19	32	1.1
5.08[a]		4.24	174[a]		146	0.39	33	1.1
6.31[a]	6.94	6.42	179[a]	197	182	0.21	25	1.1
			water					
21.3			260			0.18	22	1.1
6.6			230			0.29	18.3	2.0

[a] Data used in least squares fit to Langmuir isotherm. Accuracy of results was assumed to be gravimetry > desorption > GC.

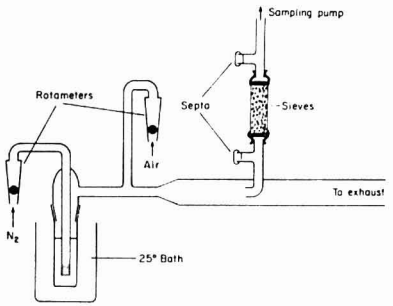


Figure 1. Dynamic dilution apparatus

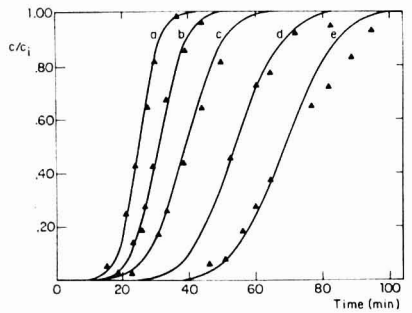


Figure 2. Representative breakthrough experiments for the following input concentrations compared to the normal probability distributions (solid curves) generated from values of $t_{0.5}$ and corresponding standard deviations in Table I: (a) 6.31 mg/L, (b) 4.68 mg/L, (c) 3.08 mg/L, (d) 2.79 mg/L, (e) 1.66 mg/L

of the central statistical moment M_2 and the ordinary moment M_1 (16):

$$\frac{\sqrt{M_2}}{M_1} \sim \sqrt{\frac{2}{15}}\left(\frac{R^2U}{HD_i}\right)^{1/2} \qquad (1)$$

where R = radius of adsorbent particles, U = linear velocity of carrier, H = bed length, and D_i = diffusion coefficient.

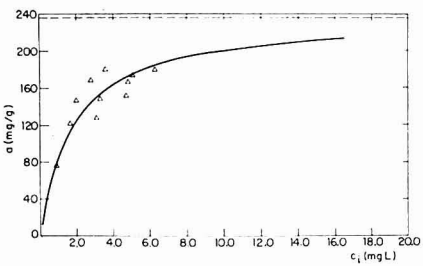


Figure 3. Dynamic adsorption isotherm of acrolein at 21 °C

Table II. Breakthrough Times of 5% of Acrolein Input Concentration in Dry Air

c_i, mg/L	$t_{0.05}$, min
4.57	20
2.29	43
0.229	72
0.023	82
0.0023	82
0.0002	82

Substitution into Equation 1 of the values for the parameters used in the experimental work (R = 0.06 cm, U = 30 cm/s, H = 4 cm, and $D_i \sim 0.1$ cm^2/s) yields a value of 0.19 for σ^*, in agreement with the values in Table I and confirming the validity of SMT in interpreting the acrolein breakthrough data. From SMT, the breakthrough curve at any point on the isotherm may be constructed from $t_{0.5}$ which is calculated by Equation 2 and the standard deviation σ (= $\sigma^* \cdot t_{0.5}$).

$$t_{0.5} = \frac{a}{c_i}\cdot\frac{W}{F} \qquad (2)$$

where a = sieve capacity (mg/g), c_i = input concentration (mg/L), W = weight of sieves (g), and F = flow rate (L/min).

Table II shows breakthrough times $t_{0.05}$ at a sampling rate of 1 L/min with various c_i for 1 g of 13X sorbent, indicating that in dry air, large sampling volumes are permissible.

Capacities and corresponding concentrations from Table I show a good fit by least squares to a Langmuir isotherm in the linear form $(1/a) = m(1/c_i) + (1/a_{sat})$; coefficient of correlation 0.94, standard error of estimate 19%. The isotherm replotted in conventional form is shown in Figure 3. The value

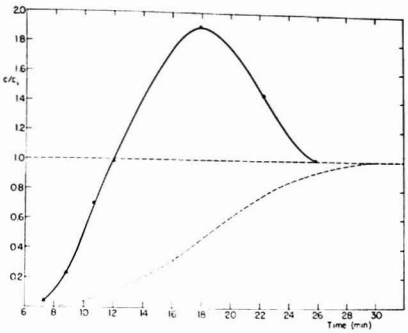


Figure 4. Acrolein breakthrough, 100% relative humidity

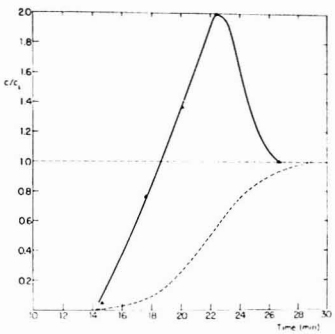


Figure 5. Acrolein breakthrough, 30% relative humidity

of 236 mg/g calculated for saturation capacity a_{sat} agrees well with the value of 226 mg/g obtained by static adsorption experiments.

Figures 4 and 5 show the effect of water vapor on the breakthrough of 1500 ppm acrolein in air at relative humidities of 30% and 100%, respectively. The ratio of breakthrough concentration to input concentration (c/c_i) plotted vs. time is superimposed on the calculated breakthrough curve of water. The water curves were generated for the required conditions from experimentally determined relative standard deviations, and $t_{0.5}$ values estimated from Equation 2 applied to experimental water breakthrough curves (Table I). Figures 4 and 5 indicate that acrolein is displaced by the water front and emerges from the sieve bed in much the same form as an elution GC peak, with a concentration maximum occurring at approximately $t_{0.5}$ of water and a variance similar to that of the water curve. Recalculating the curves for a flow rate of 1 L/min yields breakthrough time $t_{0.05}$ of 8 and 20 min per gram of sieves for 100% and 30% relative humidities, respectively. Since 2 μg acrolein/g of sieves can be detected readily by desorption and GC analysis, the 8-L sample volume at 25 °C and 100% relative humidity permits detection of 0.11 ppm acrolein/g of sorbent. With larger allowable sample

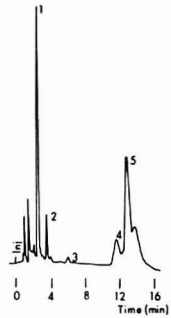


Figure 6. Gas chromatogram of a 2.5-L field sample collected over 12 min at a sampling rate of 208 mL/min. The following concentrations were calculated on the basis of a comparison of peak heights with those of standard solutions: (1) methanol, 110 ppm; (2) acetaldehyde, 9.7 ppm; (3) ethanol, 3.3 ppm; (4) acrolein, 16 ppm; (5) acetone, 66 ppm

volumes at lower relative humidities, sensitivity increases correspondingly.

Sampling tubes containing 2 g activated sieves were included in a sampling package for combustion gases. The chromatogram in Figure 6 is typical of samples collected at residential fires. Formaldehyde did not elute from the Tenax GC column and consequently does not appear in the chromatogram in Figure 6. Formaldehyde and acrolein have been verified (but not quantitated) by colorimetric methods (*1*, *2*) while the identities of the remaining compounds were nonrigorously established by comparison of retention times and spiking experiments.

ACKNOWLEDGMENT

The authors thank O. Grubner for helpful discussions.

LITERATURE CITED

(1) "NIOSH Manual of Analytical Methods," 2nd ed., U.S. Department of Health, Education, and Welfare, Public Health Service, Center for Disease Control, NIOSH, Cincinnati, Ohio, Publication #77-157-A. P and CAM 118, 125.
(2) Intersociety Committee, "Methods of Air Sampling and Analysis," American Public Health Association, Washington, D.C., 1972, pp 187, 194, 199.
(3) C. F. Nightingale and J. M. Walker, *Anal. Chem.*, **34**, 1435 (1962).
(4) W. M. Graven, *Anal. Chem.*, **31**, 1197 (1959).
(5) A. Amano and M. Uchiyama, *J. Phys. Chem.*, **67**, 1242 (1963).
(6) R. M. Barrer, F. W. Butitude, and J. W. Sutherland, *Trans. Faraday Soc.*, **53**, 1111 (1957).
(7) R. M. Barrer and J. W. Sutherland, *Proc. R. Soc. London, Ser. A*, **237**, 439 (1956).
(8) R. M. Barrer and P. J. Reucroft, *Proc. R. Soc. London, Ser. A*, **258**, 431 (1960).
(9) H. Lee, *Adv. Chem. Ser.*, **121**, 311 (1973).
(10) R. A. Anderson, "Mol Sieves II", *ACS Symp. Ser.*, **40**, 637 (1977).
(11) P. B. Venuto and P. S. Landis, *Adv. Catal.*, **18**, 259 (1968).
(12) M. L. Poutsma, "Zeolite Chem. and Catalysis", *ACS Monogr.* **171**, 529 (1976).
(13) R. M. Barrer and D. W. Brook, *Trans. Faraday Soc.*, **49**, 940 (1953).
(14) O. Grubner, A. Zikanova, and M. Ralek, *J. Chromatogr.*, **28**, 209 (1967).
(15) O. Grubner, *Adv. Chromatogr.*, **6**, 173 (1968).
(16) O. Grubner and D. Underhill, *Sep. Sci.*, **5**, 555 (1970).

RECEIVED for review June 22, 1978. Accepted August 8, 1978. Supported by NIOSH Grant 5 RO1 OH 00369-05, National Fire Protection and Control Administration Contract NFPCA 7X 008, and the Society of Plastics Industries.

Comparison of Porous Copolymers and Related Adsorbents for the Stripping of Low Molecular Weight Compounds from a Flowing Air Stream

Robert Sydor and Donald J. Pietrzyk*

Chemistry Department, The University of Iowa, Iowa City, Iowa 52242

Retention of low molecular weight organic compounds varying widely in polarity was determined on commercially available porous copolymers (XAD-2, XAD-4, XAD-7, Tenax GC, Porapak P, and Porapak Q), silica gel, alumina, and activated carbon. The sorbent was packed into a collection tube and air, doped with the model compound, passed through it at a known, controlled concentration and flow rate. Breakthrough was followed by a flame ionization detector (FID). The sorbent capacity was calculated from the weight change of the tube and breakthrough data. Overall capacity increased in the order Tenax GC ≈ XAD-1 < Porapak P ≪ XAD-2 < Porapak Q < XAD-7 < XAD-4. Thermal stripping was used to remove the model compounds and desorption was monitored by the FID and by the weight change of the tube. These studies were compared to sorption–desorption data obtained by a batch equilibrium method. Adsorption isotherms and the effects of particle size, column length, flow rate, column reuse, coelution of water, and the coelution of organic compounds were determined.

In atmospheric sampling, a preconcentration step is often necessary to raise the concentration of the pollutants above the sensitivity level of the detecting apparatus. One common technique used for preconcentration is to draw the air sample through a column containing an adsorbent which retains the pollutants.

Several commercially available porous organic polymers have been used as adsorbents in air sampling (*1–14*) and headspace analysis (*15–17*). In general, these are inert polymers and have permitted easy elution of retained compounds. Some polymers were selected solely on their temperature stability while disregarding their physical properties in various environments. Others were selected after the determination of capacity factors or breakthrough volumes for a series of model compounds (*1, 2, 6, 8–14*). In these experimental approaches, which represent efforts at a systematic study of the properties of the adsorbents, it was assumed that equilibrium was established and linear isotherms were followed. However, these conditions may not be present under actual atmospheric sampling conditions. Furthermore, in capacity factor measurements, the model compound is introduced as a small highly concentrated plug rather than continuously in a diluted state as present in actual atmospheric sampling.

In this study we have adopted an approach, which more closely resembles atmospheric sampling, to systematically characterize the organic polymers used in these kinds of studies. The capacity is expressed directly in terms of weight uptake of the model compound after its removal from a flowing air stream. The air stream contains the compound at a dilute, known, constant concentration. The variables which influence the retention and several different inorganic and organic copolymeric adsorbents, including Tenax GC and the Amberlite XAD copolymers, are systematically studied.

EXPERIMENTAL

Adsorbents. The adsorbents used in this study are listed in Table I. All are commercially available except XAD-9 and -12 which were obtained as experimental copolymers.

In general, the adsorbents were available only in a large particle size. Size reduction was achieved by grinding in a Waring Blender using an EtOH–H_2O slurry. The slurry was sieved using U.S. Standard series sieves collecting the 50–80 mesh (295 to 175 μm) and 80–100 mesh (175 to 147 μm) fractions. Each fraction was cleaned by extraction in a Soxhlet extractor with EtOH for at least a week. The adsorbent was air dried and vacuum dried (40 °C at 5–7 mm) and stored in glass bottles.

The nonpolymeric adsorbents were reduced in size either by direct sieving (alumina and silica gel) or by sieving after grinding in a mortar and pestle (carbons). The solvent extraction clean-up procedure was not used with these adsorbents, however, they were activated at 300 °C in air for 24 h and packed into the columns immediately after cooling.

Apparatus. Stripping columns were made from stainless steel tubing (10 cm × 0.62 cm o.d.) which were equipped with Swagelok fittings. These were soaked in $CHCl_3$, washed with soap and water, rinsed with water, ethanol, and finally baked at 300 °C for at least 12 h, and stored in a desiccator until packed. A silanized glass wool plug was inserted at one end and the adsorbent dry-packed into the tube (about 0.2 to 0.6 g was used depending on the adsorbent). The other end was plugged with silanized glass wool. All packed columns were preconditioned at 200 °C for 24 h in flowing He at 50 mL/min (XAD-9 and XAD-12 were heated at 150 °C). After cooling, the He flow was stopped and the columns were sealed at both ends with Swagelok plugs.

The apparatus utilized for the weight uptake studies is shown in Figure 1. Dry air passes through a two-stage regulator and a trap filled with 5Å molecular sieves and activated carbon to remove trace water vapor or organic contaminants. The stream is split by a Nupro cross-pattern fine metering valve with 500 mL/min flowing through the reference path and 1000 mL/min flowing through the sampling path. Sho-Rate Model 150 rotometer flow meters were used for the flow measurements. The model organic compound contained in a gas tight syringe is introduced into the sample chamber at a known, continuous, reproducible rate using a Sage Insts. syringe pump. As the sample vaporizes from the syringe tip, it is swept into the flowing air stream. Concentration of the compound is altered by changing either the syringe size or syringe drive speed. Usually 0.06 mL/h was used. This corresponds to 600 to 1500 ppm of the compound in the air; the actual concentration depends on the density of the model compound, and is within the linear portion of the adsorption isotherm. The air stream containing the sample passes through the stripping tube at a linear velocity of 93 cm/s. After this, the flow is divided again by a Swagelok Tee connector. A Nupro Model SA needle valve provides sufficient back pressure to split the flow into two 500 mL/min segments, one of which is exhausted and the other enters a 2-way Whitey Co. switching valve. The 500 mL/min reference air flow enters the other switching valve inlet. One of the two outlets of the switching valve always provides the air supply for the flame of the FID (flame ionization detector in a Hewlett-Packard Model 5750 gas chromatograph). Consequently, a constant flow of 500 mL/min is always maintained into the FID. The detector responds either to the reference flow

0003-2700/78/0350-1842$01.00/0 © 1978 American Chemical Society

Table I. Sorbents Investigated

sorbent	chemical structure	surface area, m^2/g	pore size, A	source
Tenax GC	diphenyl-phenylene oxide	18.6 (*20*)	720 (*20*)	Applied Science Laboratories
Porapak P	styrene-ethylvinyl-benzene-divinyl-benzene	50-100 (*18*)		Waters Associates
Porapak Q	ethylvinylbenzene-divinylbenzene	550-650 (*18, 19*)	75 (*19*)	Waters Associates
XAD-1	styrene-divinylbenzene	100 (*21*)	205 (*21*)	Rohm and Haas
XAD-2	styrene-divinylbenzene	300 (*21*)	90 (*19*)	Rohm and Haas
XAD-4	styrene-divinylbenzene	849 (*21*)	50 (*21*)	Rohm and Haas
XAD-7	acrylic ester	445 (*21*)	82 (*21*)	Rohm and Haas
XAD-8	acrylic ester	212 (*21*)	160 (*21*)	Rohm and Haas
XAD-9	sulfoxide	70	370	Rohm and Haas (Experimental)
XAD-12	very polar N, O group	20	1300	Rohm and Haas (Experimental)
alumina	F20			Alcoa Chemicals
silica gel	#62			Grace
Darco	activated carbon			
MCB	activated coconut carbon			Matheson Coleman & Bell
PCB	activated coconut carbon	1150-1250		Pittsburgh Activated Carbon
BPL	activated coconut carbon	1050-1150		Pittsburgh Activated Carbon

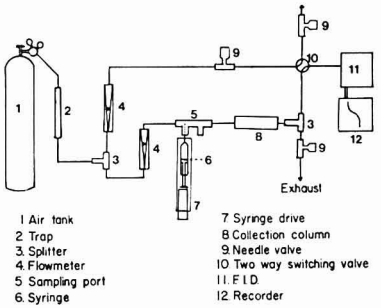


Figure 1. Apparatus for weight uptake studies

or the effluent from the column, depending on the switching valve setting.

Weight Uptake Studies. An empty column was first mounted in the apparatus. All flow rates were adjusted and the syringe containing the model compound was mounted in the syringe pump and turned on. The apparatus, still using the empty column, was equilibrated for at least 1 h under the sample-air flow. The two-way valve can be turned so that only purified air enters the detector in order to establish a zero concentration baseline. Or, it can be turned so that the equilibrated air-sample mixture flows through the FID detector, thus, establishing the maximum detector response for the mixture. After equilibration and establishment of the baseline, a carefully packed and weighed stripping tube was placed in the apparatus.

Since the system operates at constant pressure and back pressures vary for the different columns, flow rates will vary. This is compensated for by placement of a needle valve on the exhaust side of the two-way switching valve which was adjusted to provide the same back pressure as the stripping column. A flowmeter was attached after the needle valve to measure the flow in both positions of the two-way valve and ensure that the flow rate (500 mL/min) is the same in both the reference and sampling stream. After adjustment and equilibration, the two-way valve is positioned so that the sampling stream enters the FID. Upon breakthrough, as indicated by the recorded detector response reaching the maximum value found previously for the sample-air mixture, the stripping tube is carefully removed and weighed.

Capacity Factor Measurements. Capacity factors for several model compounds and adsorbents were determined by a column procedure. The gas flow through the apparatus was rerouted so that the outlet from the switching valve entered the carrier gas inlet. The stripping column was placed in the GC oven in the usual way. Samples of the model compounds were introduced through the sample injection port (100 °C) by syringe. The retention volumes were determined and used to calculate the capacity factors.

Table II. Batch Equilibrium Studies for the Retention of Organic Vapors

adsorbent	g benzene/g adsorbent	g heptane/g adsorbent	g chloroform/g adsorbent
XAD-2	0.128	0.095	0.215
XAD-4	0.237		
XAD-7	0.177		
coconut carbon	0.291	0.249	0.539

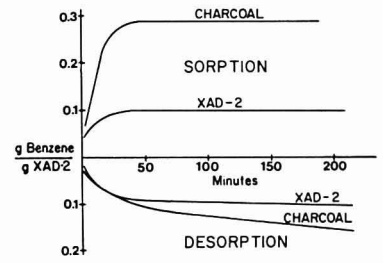


Figure 2. Comparison of sorption-desorption of benzene vapor on XAD-2 and charcoal

RESULTS AND DISCUSSION

Preliminary Studies. Initially, several sorbents were selected and their ability to sorb organic vapor was compared by a batch procedure. In these experiments, the clean, dried sorbent was placed in a closed system that had been equilibrated with organic vapor. The weight of the sorbent was recorded as a function of time. The sorbents and organic vapors used and a summary of the results are listed in Table II.

Several important properties were demonstrated with these preliminary batch experiments. First, the amount of organic vapor taken up for a given vapor varied with the sorbent used. Similarly, for a fixed sorbent, the several vapors were taken up at different amounts. In general, charcoal had the greatest uptake while all the sorbents studied showed a greater preference for the nonpolar organic vapors over the polar ones.

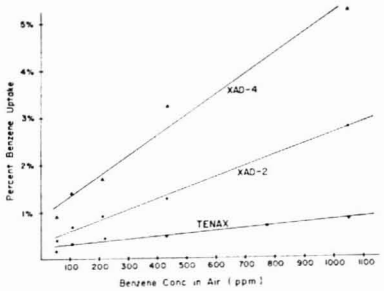


Figure 3. Adsorption isotherm for benzene

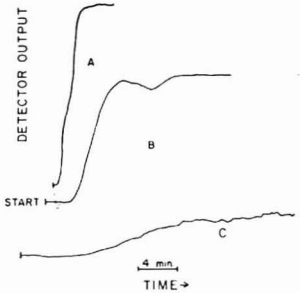


Figure 4. Benzene breakthrough profile for Tenax GC. (A) Air stream benzene concentration of 8200 ppm. (B) Air stream benzene concentration of 430 ppm. (C) Air stream benzene concentration of 50 ppm

A third observation is demonstrated in Figure 2 where the rate of vapor sorption is compared to the rate of vapor desorption for the XAD-2 copolymer and charcoal. In these experiments, the rate of sorption was determined in the closed system as previously described. After reaching the vapor sorption equilibrium state, the sorbent was subjected to an atmosphere free of the sorbed vapor and its weight loss was recorded as a function of time. Of the sorbents studied by the batch procedure, only the charcoal showed a significant difference in the desorption rate relative to the sorption rate, suggesting a kinetic difference in the two processes.

This batch method has several disadvantages. First, the levels of organic vapor equilibrated with the sorbents were much larger than would ever be experienced in atmospheric sampling. And second, this sampling system, not being a flowing one as would be used in actual atmospheric sampling, cannot be readily used to evaluate several parameters that are faced in atmospheric sampling. For these reasons, a flowing–stripping system was designed in order to compare the different sorbents.

Weight Uptake Studies. The experimental system designed to closely resemble atmospheric sampling is shown in Figure 1. With this apparatus, it is possible to prepare an air sample containing a fixed, known amount of organic vapor and pass it at a controlled rate through a carefully prepared column of sorbent. By monitoring the effluent from the column, the breakthrough can be detected. Thus, the weight of vapor sorbed within the column is determined from the weight difference of the column before and after breakthrough. The data are expressed as weight uptake by dividing the weight difference by the weight of sorbent in the column.

A series of preliminary experiments were done in order to establish the limitations of the components in the apparatus in Figure 1 and to establish the experimental procedure. The precision of the procedure was examined by using benzene and five supports: XAD-2, XAD-4, XAD-7, Porapak P, and Tenax GC. Three individual columns were packed with each of these supports and carried through the procedure as outlined using benzene vapor. The relative standard deviation for the three runs was found to be 3.8% for XAD-2, 8.5% for XAD-4, 3.1% for XAD-7, 6.2% for Porapak P, and 23.8% for Tenax GC. The poor precision for the Tenax GC was not obvious but may be the result of capacity changes due to reuse as described in a latter section.

Adsorption Isotherms. The percent uptake of benzene was measured for XAD-2, XAD-4, and Tenax GC at several different benzene concentrations in an air flow of 500 mL/min. (This was experimentally accomplished by changing either the speed of the syringe drive pump or the syringe size.) Figure 3 illustrates these adsorption isotherms for the three sorbents where percent uptake of benzene is plotted vs. benzene concentration in the air stream. The experimental points were an average of at least two independent runs for each sorbent over a benzene concentration range of 50 to 1000 ppm. (Concentrations below 50 ppm were not studied because of the excessively long time before breakthrough with XAD-4 and the difficulty of determining the small weight change for the Tenax GC collection tubes.) A linear least squares fit of these experimental points yielded correlation coefficients of 0.965, 0.997, and 0.986 for the Tenax GC, XAD-2, and XAD-4, respectively. From these values, a high linear correlation exists for XAD-2 and XAD-4 and a lower one for Tenax GC.

Typical breakthrough curves found for Tenax GC are shown in Figure 4. The recordings show the flame ionization detector output vs. time for 8200 ppm (A), 430 ppm (B), and 50 ppm (C) for benzene. Note the gradual transition in tracing C during the breakthrough period which is characteristic of a linear isotherm with the formation of a monolayer of sorbed benzene on the surface of the resin. At the two higher benzene concentrations, the breakthrough transition is more pronounced and it tends to be irregular before reaching an equilibrium value. At these concentrations, the bulk of the benzene is initially moving faster than the equilibrium concentration. For the highest concentration of benzene, there is a fluctuation at approximately the 50% breakthrough level. This may result from either the formation of a second benzene layer on top of the first or the filling of the relatively small pores in the Tenax to form pools of liquid rather than by an adsorption process. In either case, at this high concentration, the adsorption isotherm is no longer linear. A comparison can be made between those results for the Tenax GC to those obtained with the XAD-2 or XAD-4. For the latter two sorbents, the breakthrough profiles are well-defined S-shaped curves at all concentrations and do not have the irregularities as found in Figure 4A and 4B for Tenax. The slopes of the rising portion of the breakthrough profiles for the XAD copolymers are less than that found for the Tenax at each benzene concentration. Also, the time period between the start of the collection and breakthrough, generally, is 8 to 15 times longer for the XAD-2 and XAD-4, respectively.

Effect of Support. The results found for the uptake of several organic vapors on the sorbents (listed in Table I) are shown in Table III. It was assumed that all other sorbents had adsorption isotherms similar to those in Figure 3.

Consider the six nonpolar sorbents listed in Table I. As seen by the data in Table III, Tenax GC, which is widely used in atmospheric sampling, demonstrated the least percent uptake of all sorbents studied. A slightly higher capacity was found for Porapak P, a styrene–ethylvinylbenzene–divinylbenzene copolymer. XAD-1, -2, and -4 are polystyrene–divinylbenzene copolymers and the latter two showed signifi-

Table III. Percent Uptake for the Retention of Several Organic Model Compounds on a Series of Sorbents

	percent uptake															
model compound	Tenax GC	XAD-1	XAD-2	XAD-4	Porapak P	Porapak Q	XAD-7	XAD-8	XAD-9	XAD-12	silica gel	alumina	MCB Darco	carbon	PCB	BPL
heptane	0.31		2.1	5.6	0.66		2.1				1.0			26.4	27.4	21.0
benzene	0.53	0.36	1.8	2.9	0.28		1.8	1.0	0.82	0.28	NR	0.82			24.7	16.5
carbon tetrachloride	0.18		2.4	6.0	0.75		1.6						11.5	42.6	50.2	36.3
trichloroethylene	1.2		2.9	8.6	1.38		4.2									
acetone	0.09		0.19	0.60	0.04		0.75		0.095	0.031			4.6	9.6	10.7	6.7
methyl ethyl ketone	0.32	0.33	0.90	2.6	0.32	1.5	2.1	1.2	1.0		4.3	5.07				
methyl propyl ketone	0.86	0.60	2.3	6.3	0.95	3.1	4.5	2.6	1.8							
methyl cellosolve	0.70	0.87	2.1	7.6	0.74	3.5	5.2	3.1	3.9							
tetrahydrofuran	0.41	0.22	0.96	2.3		1.1	1.7	0.75	0.92							
butyl amine	0.43	0.29	1.4	4.4		2.14	3.1	1.2	2.6		6.9	5.7				
ethanol	NR		0.023	0.40		0.18	0.9	0.50	0.70	NR	13.1	1.2	5.2	8.7	7.9	1.28
propanol	0.43	0.18	0.75	2.6		1.2	2.9	1.3	1.5							
dimethylformamide	1.62		4.8	8.7			7.6									

cantly larger capacities than the Porapak P. This difference is due to the greater surface area and smaller pore size for the XAD copolymers in comparison to Porapak P (see Table I.) Porapak Q, which is an ethylvinylbenzene–divinylbenzene copolymer has capacities intermediate to the XAD-2 and XAD-4 copolymer; its surface area and pore size are also intermediate. Although there is a slight difference in the structure of the monomers used in preparing Porapak P and Q and XAD-1, -2, and 4, the principal contributing factor to the difference in capacities appears to be the result of the significant variation in surface areas (and pore size) for the sorbents. The low capacity for Tenax GC is probably due to its small surface area; however, a direct comparison to the Porapak and XAD copolymers is not possible since the Tenax GC is significantly different in structure.

The influence of polymeric structure on capacity is illustrated by comparing the weight uptake data in Table III found for the nonpolar sorbents to those data found for the polar sorbents. For example, the range of surface areas for the XAD-7, -8, -9, and -12 are similar to the range for XAD-1, -2, and -4; however, weight uptake of the solvent vapor is different for the two series of copolymers. The former more polar series of sorbents shows a preference for the polar organic vapors while the latter nonpolar series shows a preference for the nonpolar organic vapors. Although the polymeric structures of the polar XAD series are different, the one with the largest surface area (XAD-7) (smallest pore size) has the greatest capacity not only for the polar vapors but also for the nonpolar vapors (A direct comparison in Table III is possible for XAD-7 and -8 since they are similar copolymers) even though it is the least polar of the group. Not only was the capacity significantly greater than that of the more polar XAD-9 and -12 for polar vapors, but it was similar to that found for the XAD-2. Of all the organic polymers studied, XAD-4 had the highest capacity for each of the organic vapors examined.

A very polar organic polymer that was studied briefly was Dowex 50-X8, which is a sulfonated polystyrene–divinylbenzene copolymer. The ion exchanger was in the H-form and ethanol and benzene were examined as the model compounds. The ion exchanger was dried under a vacuum of 5 mm at 80 °C, which produced dehydrated, unswollen ion-exchange beads. No measurable uptake was found for these conditions.

Several nonpolymeric sorbents, which are characterized by large surface areas (see Table I), were studied with the anticipation that they would show high retention for both the polar and nonpolar model compounds. These results are shown in Table III. The nonpolar carbon adsorbents exhibited the largest uptake of all sorbents studied, particularly for the nonpolar organic vapors. It appears from this brief study that the polar nonpolymeric sorbents (alumina and silica gel) have low uptakes for the nonpolar vapors and moderately large uptakes for the polar vapors. As indicated previously, these sorbents suffer from a slow desorption process even when using thermal elution. At least an hour of heating at 200 °C with a He flow rate of 50 mL/min was required to remove the sorbed model compounds. Also, the greater chemical activity of these sorbents may cause decomposition or rearrangement of the retained compounds at the elevated temperature.

Type of Organic Vapor. Attempts to correlate the weight uptake data in Table III to several types of solvent parameters did not prove to be successful. In general, the more nonpolar the vapor, the greater the uptake on the nonpolar support while the reverse was observed for the polar supports. Although not examined in detail, it appears that an increase in the hydrophobic character of the vapor increases the uptake on both the polar and nonpolar adsorbents. For example, compare the data in Table III for the three ketones and for the two alcohols.

Effect of Stripping Column Length. The retention of the model compound may result from a physical trapping within the porous structure of the adsorbent or via an adsorption process. In the latter case, a distribution is formed between the model compound in the air stream and the adsorbent bead. At a fixed flow rate, the air stream must pass through a column of a certain length before the distribution is established. Consequently, as the linear velocity of the air flow varies, the length of travel through the column must change in order for the distribution to be established. With shorter columns, the distribution will not be established and premature breakthrough would be observed. The effect of this parameter was investigated by determining the weight uptake of organic vapor as a function of column length.

Tenax GC was selected as the adsorbent to study this variable because it had exhibited the lowest capacity. Thus, a nonequilibrium condition, if it existed, would be more readily indicated. Several columns differing in length were packed with the Tenax GC. The stripping was undertaken at a fixed flow rate of 1000 mL/min and introducing methyl ethyl ketone as the model compound into the air flow at a concentration of 620 ppm.

Initially, the percent uptake per gram of resin for the ketone increased linearly as the length of the Tenax GC column increased (4 to 8 in.). Beyond this length, the percent uptake reached a constant value even though the column length was increased. These results indicate that an equilibrium distribution is in operation between the airflow and the adsorbent beads. Below a column length of 8 in. and at a flow rate of 1000 mL/min, the Tenax GC column was found to be not operating in an equilibrium condition.

Effect of Particle Size on Vapor Uptake. A study was undertaken to determine the effect of the particle size of

Table IV. Effect of Concomitant Elution of Water and Methyl Ethyl Ketone on Several Organic Model Compounds

injected model compound	capacity factor/g of sorbent								
	individual elution			coelution of H_2O			coelution of MEK[a]		
	XAD-2	XAD-4	XAD-7	XAD-2	XAD-4	XAD-7	XAD-2	XAD-4	XAD-7
H_2O	6.5	9.5	62	5.8	4.3	57	3.9	15	44
EtOH	86	270	700	73	200	1000	60	220	620
acetone	220	710	900	190	590	980	140	390	410
CCl_4	1700	5300	1300	1400	3800	1400	1100	3100	800
MEK[a]	1400	4000	2000	1100	4100	4000	570	2000	56
benzene	3000	7300	2400	1600	7700	2900	1600	5900	2900

[a] Methyl ethyl ketone.

adsorbent on the weight uptake. XAD-2 and methyl ethyl ketone were used as the adsorbent and model compound, respectively. Four individual cuts from crushed XAD-2 particles were collected by a sieving technique and packed into 4-in. tubes. These were 50 (295 μm) to 80 mesh, 80–100 mesh, 120–150 mesh, and 150–200 (74 μm) mesh. An airflow of 1000 mL/min and a ketone concentration of 620 ppm were used. For the small particles, air pressure at the regulator had to be increased by 10 psig.

No significant change in capacity was observed when comparing the results found for the four particle sizes. In practice, the larger size packing (50 to 80 mesh) is preferred because of the convenience that it offers. Within this size range, all adsorbents are generally commercially available, column pressure drops are small, and columns are easily packed.

Effect of Flow Rate. A 4-in. column packed with 80 to 100 mesh XAD-2 was used to establish the effect of flow rate on capacity with methyl ethyl ketone at 620 ppm. An equilibrium condition was assumed to be present under these experimental conditions.

Weight uptake measurements were made at flow rates varying from 100 mL/min (9.3 cm/s) to 1000 mL/min (93 cm/s). No significant difference in weight uptake was found over the flow rate range studied suggesting that the uptake is independent of flow rate in this range.

Concomitant Elution. All the experiments cited to this point were carried out with samples prepared by introducing a single organic compound into a purified air flow. In practice, atmospheric samples will contain many different compounds, including water, and it is possible that they will mutually affect each other's degree of retention.

In order to study this effect, the apparatus in Figure 1 was modified so that a second model compound can be introduced into the air stream at a known controllable concentration. Initially, experiments were carried out in which two syringe drives were used. Although weight changes in the adsorption tubes were noted, the change was very small and it was not easily ascertained as to which or how the two components in the air sample lead to the weight change.

A more successful technique to establish this effect was one in which air was used as a carrier gas and one component was continuously introduced into it at a constant, known concentration by the syringe drive. To introduce the second component, the apparatus in Figure 1 was modified by rerouting the outlet of the two-way switching valve directly into the GC carrier gas stream. The collection column was placed in the GC oven and the outlet of the column was connected to the air inlet of the flame for the FID. The second model compound was then introduced by syringe in the sample port in the usual way. (The sample port was maintained at 100 °C to ensure instantaneous vaporization.)

Using this experimental setup, capacity factors can be measured for individual compounds in the presence of a continuous flow of a second compound in the air stream. These experiments were performed using stripping columns of XAD-2, XAD-4, and XAD-7 and several model compounds as one component and either water or methyl ethyl ketone as the second component. Water was chosen since actual atmospheric samples would contain water as a major component while methyl ethyl ketone was chosen to represent a major organic contaminant.

The first set of experiments was with water as the continuous background component. Each of the organic compounds listed in Table IV was injected at three temperatures over a range of 50 to 80 °C. The retention volumes for the model compounds were determined from triplicate injections of each and a log plot of retention volume vs. temperature was made. This yielded a straight line. Using linear regression analysis, the retention volume at room temperature was determined for each model compound and used to calculate its capacity factor. These data are listed in Table IV along with capacity factor data in the absence of background water. The regression coefficient was +0.996 for all organic compounds studied.

In the presence of the water vapor, a decrease in capacity was found for the nonpolar polymers. For example, XAD-2 and XAD-4 had an average decrease of 24% and 12.5%, respectively. The polar XAD-7 had an average increase of 23% in capacity. Even with the increase in capacity of the XAD-7 and decrease for the XAD-4, the XAD-4 still provides the highest overall capacity.

The capacity factors were determined for the model compounds in the presence of methyl ethyl ketone using the same procedure. (See Table IV for the data.) Under these conditions, the capacity factors decreased on all three copolymers. For example, the decrease was 38% for XAD-2, 32% for XAD-4, and 23% for XAD-7. Although XAD-7 exhibited the smallest change in capacity factor, XAD-4 was still found to be about 80% higher in capacity.

Repeated Use Study. Tenax GC has been reported to have a tendency to degrade when sampling atmospheric samples at elevated temperatures or during thermal elution (7, 22). Other organic polymers used as sorbents may also undergo thermal decomposition either during sampling or thermal elution. Because of these potential effects and the magnitude of the relative standard deviation found in our studies, particularly for Tenax GC, a study was undertaken to determine the weight uptake for the column as a function of repeated used by employing a known, controlled stripping and desorbing procedure. Tenax GC, XAD-4, and XAD-7 with methyl ethyl ketone at a concentration of 620 ppm in air at a flow rate of 1000 mL/min were used. After breakthrough, the weight increase was determined, the column removed, and it was thermally eluted at 200 °C for 5 min in a He flow of 50 mL/min. Following cooling, the procedure was repeated.

The data for these repeated use studies are shown in a Figure 5 where the percent uptake is plotted vs. run number. As the number of uses increases, the capacity appears to gradually rise. This change, which is not clearly understood,

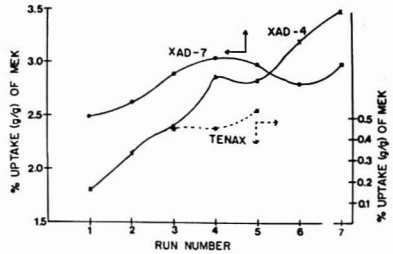


Figure 5. Effect of reusing a column on weight uptake of methyl ethyl ketone

may be the result of polymer decomposition, the opening of polymer pores through heating, or other reasons; these results are being investigated further.

Summary. This investigation shows that a vast capacity difference exists between the sorbents studied, several of which are routinely used in atmospheric and head space sampling. Also, the capacity is quite different for the numerous model compounds investigated. For the nonpolar organic copolymers, the weight uptake increases with increasing molecular weight and decreasing polarity of the model compound. The overall order of increasing weight uptake is Tenax GC $\approx$ XAD-1 < Porapak P $\ll$ XAD-2 < Porapak O < XAD-7 < XAD-4. Although XAD-4 exhibited the largest overall capacity, the use of XAD-7 should be considered and studied further under real sampling conditions because of its apparent favorable coelution behavior.

Greater uptake of the polar model compounds was found for the polar copolymers in comparison to the nonpolar copolymers. However, capacities were low and the copolymers, in general, were lacking in thermal stability. The inorganic adsorbents studied had modest weight uptakes except for the carbon adsorbents which exhibited the largest uptakes of all sorbents studied. The disadvantage of the carbon type sorbents appears to be the poor kinetics of desorption when employing thermal elution.

It should be noted that the experiments described here were designed and performed in order to achieve an equilibrium condition. In a true sampling situation, this may not always be accomplished. Consequently, this should be taken into consideration when applying these data to real atmospheric or head space sampling.

LITERATURE CITED

(1) W. Bertsch, R. C. Chang, and A. Zlatkis, *J. Chromatogr. Sci.*, **12**, 175 (1974).
(2) L. D. Bulter and M. F. Burke, *J. Chromatogr. Sci.*, **14**, 117 (1976).
(3) L. Collier, *Environ. Sci. Technol.*, **6**, 930 (1972).
(4) J. DeGreef, M. DeProft, and F. DeWinter, *Anal. Chem.*, **48**, 38 (1976).
(5) A. Dravnicks, R. K. Krotoszynski, J. Whitfield, A. O'Donnell, and T. Burgwald, *Environ. Sci. Technol.*, **5**, 1220 (1971).
(6) J. Janak, J. Ruzickova, and J. Novak, *J. Chromatogr.*, **99**, 689 (1974).
(7) P. W. Jones, P. E. Strup, R. D. Giammar, and T. B. Stanford, *Environ. Sci. Technol.*, **10**, 806 (1976).
(8) J. P. Mieure and M. W. Dietrich, *J. Chromatogr. Sci.*, **11**, 559 (1973).
(9) J. S. Parsons and S. Mitzner, *Environ. Sci. Technol.*, **9**, 1053 (1975).
(10) E. D. Pellizzari, J. E. Bunch, R. E. Berkley, and J. McRae, *Anal. Lett.*, **9**, 45 (1976).
(11) E. D. Pellizzari, J. E. Bunch, B. H. Carpenter, and E. Sawicki, *Environ. Sci. Technol.*, **9**, 522 (1975).
(12) J. W. Russell, *Environ. Sci. Technol.*, **9**, 1175 (1975).
(13) B. Versino, M. DeGroot, and F. Geiss, *Chromatographia*, **7**, 302 (1974).
(14) A. Zlatkis, A. Lichtenstein, and A. Tishbee, *Chromatographia*, **6**, 67 (1973).
(15) M. Novotny, M. L. Lee, and K. D. Bartle, *Chromatographia*, **7**, 333 (1974).
(16) W. E. May, S. N. Chesler, S. P. Cram, B. H. Gump, H. S. Hertz, D. P. Enagonio, and S. M. Dyszel, *J. Chromatogr., Sci.*, **13**, 535 (1975).
(17) K. E. Murray, *J. Chromatogr.*, **135**, 49 (1977).
(18) M. F. Burke, and D. G. Ackerman, *Anal. Chem.*, **43**, 573 (1971).
(19) J. F. Johnson and E. M. Barrall, *J. Chromatogr.*, **31**, 547 (1967).
(20) K. Sakodynski, L. Panina, and N. Klinskaya, *Chromatographia*, **7**, 339 (1974).
(21) J. Paleos, *J. Colloid Interface Sci.*, **31**, 7 (1969).
(22) M. B. Neher and P. W. Jones, *Anal. Chem.*, **49**, 512 (1977).

RECEIVED for review February 6, 1978. Accepted July 31, 1978. This investigation was supported by Grant Number CA 18555, awarded by the National Cancer Institute, DHEW. Part of this work was presented at the 174th American Chemical Society Meeting, Chicago, Ill., Aug. 28, 1977, and at the Fourth Annual Federation of Analytical Chemistry and Sepctroscopy Societies Meeting, Detroit, Mich., Nov. 11, 1977.

Determination of Sub-nanogram per Gram Quantities of Light Hydrocarbons (C_2–C_9) in Rock Samples by Hydrogen Stripping in the Flow System of a Capillary Gas Chromatograph

Rainer G. Schaefer,* Bernd Weiner, and Detlev Leythaeuser

Kernforschungsanlage Jülich GmbH, Programmgruppe für Erdöl und Organische Geochemie, Postfach 1913, D-5170 Jülich 1, Federal Republic of Germany

A method has been developed for measurement of sub-nanogram per gram quantities of light hydrocarbons (molecular range C_2 to C_9) in rock samples. The method combines both extraction of hydrocarbons from the rock and subsequent capillary gas chromatography into a single-step procedure carried out in a closed gas-flow system. The stripping gas (hydrogen) acts also as the carrier gas in the capillary column. Splitless sample introduction ensures high sensitivity. The lowest detectable quantity is about 10^{-11} g butane, representing 0.01 ppb for the maximum weight of 1 g. A backflush technique removes higher boiling components during the analysis. Total analysis time is about 50 min. The method is applied for geochemical analysis of the light hydrocarbons in rock and fluid samples from oil and gas exploration wells.

Light hydrocarbons (molecular range $<C_{10}$) are trace components of most sedimentary rocks. Information about their origin, migration, and concentration in oil and natural gas deposits in the subsurface is of prime importance when searching for new hydrocarbon accumulations. Most previous studies utilized gas chromatography (GC) for analysis of these light hydrocarbons. However, a great variety of techniques have been developed to extract these compounds from the rock sample prior to GC analysis. The simplest method is the analysis of the headspace gas (*1*) accumulated at room temperature in the sample container bearing the water covered rock sample. Heating of the container to just below 100 °C and simultaneous high-speed grinding of the rock sample increases the yield of the hydrocarbons accumulating in the headspace (*2, 3*). Other extraction procedures mobilize the compounds continuously from the rock, collecting them in a cold trap. Mobilization can be carried out by combined heating and grinding either under reduced pressure (*4*) or with the aid of an auxiliary gas (*5–7*). Durand and Espitalie (*5*) also applied freon extraction on rock samples, but, because of the boiling point of the solvent, this method has applications only in a higher molecular range ($>C_6$). Finally, Le Tran (*8*) isolated occluded light hydrocarbons from carbonate rocks by acid digestion of the mineral matrix.

Most of these light hydrocarbon extraction procedures have analytical restrictions which seriously limit their application for routine work in petroleum geochemistry, e.g., large sample size requirements of 10–100 g (*2, 3, 5*), compositional fractionation effects due to partitioning between phases (headspace analysis), restricted over-all sensitivity with respect to sample size (1 ppb per weight (*7*) or 5 ppt in 100 g of rock (*3*), respectively), or excessive time requirements (2-h extraction time (*7*)).

Most of these problems are overcome by the new method described in this paper. It represents an innovation to the extent that it combines both removal of light hydrocarbons (molecular range C_2 to C_9) from the rock sample at ambient temperature and their capillary GC analysis into a single-step rapid procedure. This is achieved by a flow system designed in such a manner that hydrogen functions both as carrier gas for the GC capillary and as auxiliary gas stripping the light hydrocarbons from the rock sample. In this way the analysis can be carried out on a microscale and the effects of fractionation during extraction and transfer procedures are minimized.

The concept of our method stems from the so-called thermovaporization technique of Jonathan et al. (*9*) designed to cover the molecular range C_6 to C_{15}. Their method combines the extraction of small-size rock samples (ca. 200 mg) at elevated temperatures followed by splitless capillary GC analysis in a gas-flow system utilizing helium both as stripping and carrier gas. However, Jonathan et al. take no precautions which might prevent the introduction of pore water into the column, a factor which severely reduces the efficiency of the chromatographic separation. Compounds are identified throughout the chromatogram only by retention times and not by Kovats indices as in the method described below for the C_2 to C_8 molecular range. Furthermore Jonathan's procedure does not include a backflush control, and the cold trap is installed in the GC oven, both features not being favorable with respect to the time required and the accuracy of the analysis of C_2 to C_9 hydrocarbons.

EXPERIMENTAL

Sample Preparation. Rock samples for light hydrocarbon analysis should be stored in sealed containers, e.g., gas-tight tin cans. Additionally, storage at deep freeze temperatures to reduce evaporation losses is recommended.

Samples containing drilling mud are first washed thoroughly with cold water. Excessive water is then removed with filter paper before sample introduction. Sample preparation consists of crushing the sediment in a steel mortar and sieving followed by introduction of the 0.6- to 2-mm particle fraction into a glass extraction tube. The weight of the rock sample analyzed varies between 0.2 and 1 g according to density and expected light hydrocarbon yield. The glass extraction tube is prepared in the following way (Figure 1). The upstream end of the tube is closed with a plug of glass wool. At the downstream end of the tube, a second plug of glass wool and a small amount of dry $CaCl_2$ (about 4-cm length) prevent the entry of both water and dust particles into the GC capillary during subsequent hydrogen stripping. During sample preparation, extreme caution is essential in order to avoid contamination. To this end all glassware is pretreated with chromic acid while glass wool and $CaCl_2$ are heated to 400 °C for 2 h before storage in glass stoppered bottles. Prior to introducing the rock particles, flushing the glass tube plus $CaCl_2$ with pure oxygen at 500 °C for about 5 min further reduces the hydrocarbon blank values for the whole procedure.

Care should be taken that the sample preparation sequence is accomplished in a short and reproducible time. On the other hand, as shown later in a sample aging experiment, evaporation losses of hydrocarbons (except methane) at this stage are minor, compared to those occurring during sample collection and storage. For this reason, in our technique methane is omitted from quantitative analysis.

Hydrogen Stripping and Gas Chromatographic Analysis. The analytical apparatus, shown schematically in Figure 2, consists

0003-2700/78/0350-1848$01.00/0 © 1978 American Chemical Society

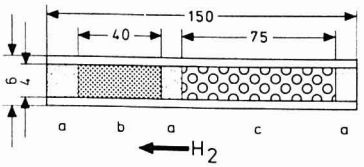


Figure 1. Preparation of glass tube for hydrogen stripping of light hydrocarbons from rock samples. Dimensions are given in mm. (a) glass wool, (b) $CaCl_2$, (c) rock sample (particle size between 0.6 and 2.0 mm)

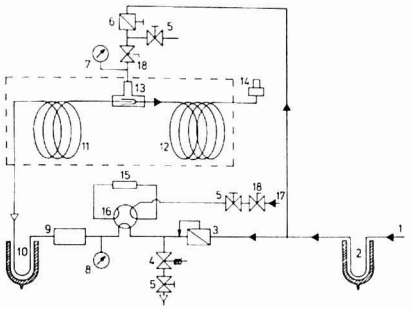


Figure 2. Modified capillary gas chromatographic system for light hydrocarbon analysis of rock samples by hydrogen stripping. (1) hydrogen inlet, (2) hydrogen purification trap, (3) flow controller, (4) solenoid valve, (5) needle valve, (6) pressure regulator, (7, 8) pressure gauges, (9) sample tube; (10) cold trap, (11, 12) capillary column, (13) T-union, (14) flame ionization detector, (15) gas loop, (16) six-port valve, (17) inlet for external standard, (18) valve. -▶-: direction of gas flow. -▷- reversed flow during backflush

of a capillary gas chromatograph which has been substantially modified. Modifications are made to the sample inlet and the carrier gas supply, and include the installation of a backflush system. In detail, the injection port unit has been removed completely. Instead, the front length (ca. 25 cm) of the capillary column, bent into a U-shape, extends outside the GC oven, itself serving as a cold trap when immersed in liquid nitrogen (No. 10 in Figure 2). For the light hydrocarbon extraction step, the glass tube containing the sample (No. 9 in Figure 2) is placed between the cold trap and carrier gas supply. The sample is stripped by passing a measured volume of hydrogen through the tube. Because of its low viscosity, hydrogen is preferred as stripping and carrier gas. However, to reduce the hydrocarbon blank values of the whole procedure to about detection limit, pure-grade hydrogen (99.999%) has to be further purified by passage through a charcoal filled liquid nitrogen cold trap (No. 2 in Figure 2). For the same reason, the flow rate of the hydrogen is controlled by an all-metal precision flow controller (Siemens). Since the gas flow is always held at a known rate, the volume of the stripping gas is deduced directly from the flushing time which in our routine procedure is 10 min. Generally, hydrogen stripping is carried out at room temperature. Since only a fraction of the light hydrocarbons present in the rock is recovered by this method, it is essential that measurements be made under constant conditions with respect to temperature, gas flow, and volume.

The development of the backflush technique employed here is based on Deans' method of column switching (*10*). For the backflush system the capillary column is cut into two lengths (ca. 1:2 ratio). The carrier gas flow is reversed in the initial length after the last desired compound has passed through; separation continues in the second part. In order to prevent peak-broadening by diffusion in the T-shaped capillary connection (No. 13 in Figure 2), a minimum dead volume design modified after Schomburg et al. (*11*, *12*) is used. A reamed out $^1/_{16}$-inch Swagelok T-union has been used for this purpose. Backflush is started by opening

Table I. Conditions for Hydrogen Stripping and Gas Chromatographic Analysis

extraction	
stripping gas	hydrogen
flow	10 mL·min^{-1}
stripping time	10 min
temperature	ambient (22 °C)
sample weight	<1 g
sample particle size	0.6 to 2 mm
GC analysis	
column	
type	SCOT column (stainless steel)
phase	Squalane
length	45 m
diameter (i.d.)	0.5 mm
carrier gas	hydrogen
flows through column	
first part (15-m length)	10 mL·min^{-1}
second part (30-m length)	12.5 mL·min^{-1}
reversed flow	10 mL·min^{-1}
temperatures	
column (programmed)	60 °C for 23 min; 4 °C per min to 110 °C; hold 1 min
detector	110 °C
external standard	butane in hydrogen (50 vpm)

to atmosphere the solenoid valve (No. 4 in Figure 2) between sample tube and flow controller. Thereby the flow in the initial part of the capillary is reversed. The pressure to maintain the gas flow for the continuation of the analysis is supplied at the T-union by an auxiliary pressure regulator (No. 6 in Figure 2). In order to purge the T-union dead-volume during GC separation, the pressure regulator (No. 6 in Figure 2) has to be carefully adjusted to contribute a small additional flow through the by-pass. A precision pressure gauge (No. 7 in Figure 2) is essential to guarantee reproducible retention times.

Upon completion of the hydrogen stripping, the sample tube is replaced with an empty glass tube. Once a stable baseline is obtained (ca. 5 min), gas chromatographic analysis is started by removing the liquid nitrogen cold trap. This step initiates the transport of the trapped components onto the capillary according to their volatilities. No splitting is used with sample introduction. Subsequent GC separation is performed isothermally for the greater part of the analysis (i.e., up to octane). Details of hydrogen stripping and GC separation conditions are summarized in Table I. As steel capillary columns were found to give excellent separation of the peaks of interest in the C_2 to C_9 range, development with possibly more efficient glass capillary columns has not been attempted.

Compound Identification and Quantitative Analysis. The GC detector output is linked to a dedicated chromatography data system (Datachrom II, Instem Ltd., England) run on a PDP 11/10 computer (Digital Equipment Corp.). This on-line system outputs partially processed data (peak areas and retention times) on punched tape for off-line re-calculations of retention data and concentrations using a FORTRAN program system. Components eluted under isothermal conditions are identified by their Kovats retention indices. Although the initial part of the GC separation is run non-isothermally (warming of sample cold trap), its effect on precision of retention indices is of minor importance. In the range butane to octane (pentane and heptane serving as reference peaks), a standard deviation generally within ±0.5 index unit is obtained. However, below butane, retention indices are less precise due to nonreproducible trap heating, but in any case they do not exceed ±3 index units if calculation is based on propane and butane as reference compounds. Compound identification has been obtained by comparison with literature data of both Kovats indices and their corresponding temperature coefficients (*13*).

After elution of octane, temperature programming is initiated and compound names are assigned on the basis of retention times. Nevertheless, for the definite identification of hydrocarbons in

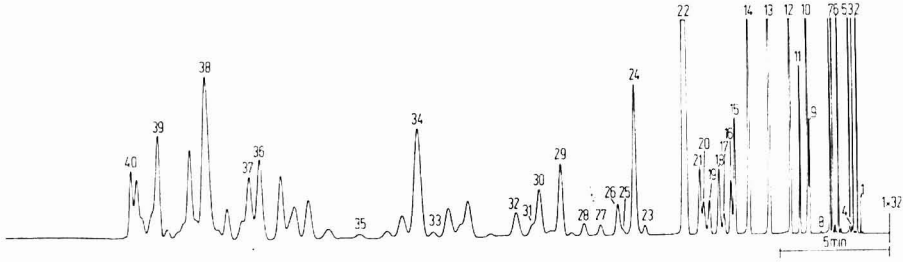


Figure 3. Typical light hydrocarbon distribution obtained by the hydrogen stripping of a sandy shale core sample (1190-m depth, Lower Cretaceous, NW Germany). For assignment of peaks see Table II

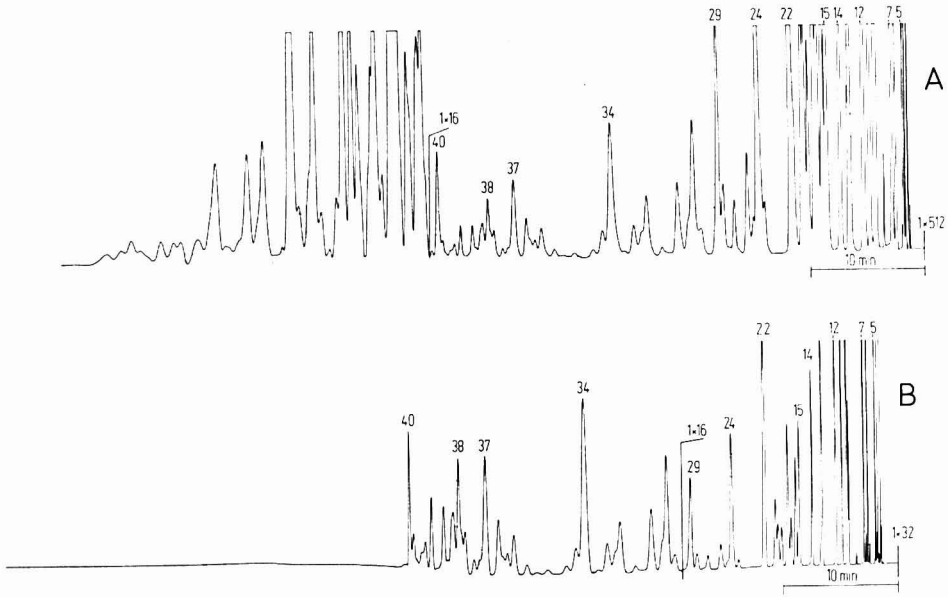


Figure 4. Effect of backflush on analysis time. Chromatogram A without backflush, Chromatogram B with backflush. Selected hydrocarbons, identified by numbers, are listed in Table II

this range, isothermal analysis has also been applied. Peak areas are calculated with the aid of an external standard, e.g., butane in hydrogen, which is introduced into the GC flow system via a six-port valve (No. 16 in Figure 2) at least once a day. Interpretation of geochemical data requires the normalization of hydrocarbon yields to rock sample weight or its organic carbon content. For purpose of comparison between different samples, the volume of stripping gas is held constant. Hence, quantitative results are given in units such as ng (10^{-9} g) hydrocarbon per g of rock and per volume of stripping gas.

RESULTS AND DISCUSSION

Analytical Applications. An example of a chromatogram showing the light hydrocarbon distribution of a rock sample (Lower Cretaceous, sandy shale, 0.53% organic carbon content) from an exploration well is depicted in Figure 3. Forty compounds identified so far are listed in Table II. According to our experience, distribution of light hydrocarbons in rock samples generally shows little variation in type and number of the main constituents. Therefore, routine compound identification as described above is sufficiently reliable. However, the total yields and compound ratios vary considerably and form the basis for the geochemical interpretation.

Efficiency of Backflush System. The efficiency of the backflush system is demonstrated by comparison of chromatograms shown in Figure 4. In this case a crude oil instead of a rock sample has been selected for the analytical procedure (Modification for oil analysis is discussed in a later section). To obtain the upper chromatogram (without backflush), 75 min are required to allow elution of several high-retention components above nonane which are of no interest in the context of our study. In the lower chromatogram, the same sample has been run with the backflush system in operation. Reversed flow through the initial length of the capillary (see Figure 2) is initiated at 23 min after the start of the analysis by opening valve No. 4. There is no visible baseline deviation

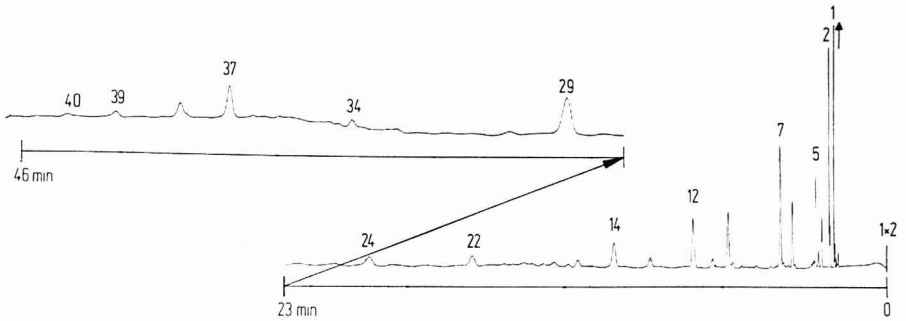


Figure 5. Hydrogen stripping method applied to a low hydrocarbon-yield rock sample. Concentrations of selected compounds (numbered according to Table II) are listed in Table III

as a result of flow switching. An advantage of this type of backflush system is the time saved (31 min in this case) by initiating reversed-flow not after but during the GC separation. Hence, the apparatus is ready for the next analysis after the last peak of interest is detected and the oven cooled to its starting temperature.

Reproducibility. The over-all reproducibility of the analytical procedure is calculated on the basis of two rock samples, each of which has been subdivided in five parallel samples. A sample lean in light hydrocarbons (ca. 40 ppb yield) and a relatively rich sample (ca. 3000 ppb yield) have been chosen for estimation of reproducibility. The richer sample showed the greater standard deviation of hydrocarbon yield (±21%) than the low concentration sample (±11%). This might be due to higher sensitivity of richer samples to, for example, evaporation losses during the preparation procedure. However, compound ratios which are the basis of further geochemical interpretation, are measured generally with a higher precision. For these ratios, as expected, the precision increases with increasing light hydrocarbon content because of higher accuracy of gas chromatographic results. The standard deviation for the majority of hydrocarbon ratios calculated is below 10%, e.g., hexane/methylcyclopentane 0.8%, 2-methylpentane/3-methylpentane 1.7%, 2-methylbutane/pentane 4.2%, cyclohexane/methylcyclopentane 1.6%, toluene/heptane 11.8%.

It should be pointed out that light hydrocarbon quantities in rock samples from exploration wells may vary by several orders of magnitude with depth or rock type. Hence, the error of this analytical procedure can, in general, be neglected in geochemical data interpretation. However, as a result of the errors introduced during the collection and transportation of the rock samples, results of geochemical significance are best obtained by analyzing and establishing trends within a sample *series* from, for example, an oil exploration well (see below, requirements for sample quality).

Lowest Detectable Quantities. In order to demonstrate the application of the hydrogen stripping method near the detection limit, the chromatogram of a core sample of suspected very low light hydrocarbon content from a Deep Sea Drilling Project Site (DSDP/IPOD Leg 47b, Site 398, off N. Africa, core No. 116-3) is depicted in Figure 5. From this example and other measurements, estimated values for the lowest detectable quantities over the total molecular range have been calculated. Assuming a sample weight of 1 g, which is the maximum sample size, lowest detectable quantities for selected compounds are tabulated in Table III. For practical purposes, the detection limit has been defined with respect to a minimum peak height represented by the half-height of the nonane peak in Figure 5. Since there is no possibility of hydrocarbon loss after introducing the sample into the stripping gas flow, sensitivity is only a function of FID and amplifier noise, and peak width, i.e., normal gas chromatographic detection limitations. Hence, even in the C_9 molecular range, amounts of less than 1 ng/g of rock can easily be detected by our procedure.

Table II. C_1 to C_9 Hydrocarbons Identified in a Sandy Shale Core Sample (1190 m Depth, Lower Cretaceous, N.W. Germany) by Capillary Gas Chromatography (see Figure 3)

reference no.	compound
1	ethane
2	propane
3	methylpropane
4	2,2-dimethylpropane
5	butane
6	methylbutane
7	pentane
8	2,2-dimethylbutane
9	cyclopentane
10	2-methylpentane
11	3-methylpentane
12	hexane
13	methylcyclopentane + 2,2-dimethylpentane
14	benzene
15	cyclohexane
16	2-methylhexane
17	2,3-dimethylpentane
18	3-methylhexane
19	1,*cis*-3-dimethylcyclopentane
20	1,*trans*-3-dimethylcyclopentane
21	1,*trans*-2-dimethylcyclopentane
22	heptane
23	1,*cis*-2-dimethylcyclopentane
24	methylcyclohexane
25	2,5-dimethylhexane
26	ethylcyclopentane
27	1,*trans*-2,*cis*-4-trimethylcyclopentane
28	1,*trans*-2,*cis*-3-trimethylcyclopentane
29	toluene
30	2-methylheptane
31	4-methylheptane
32	3-ethylhexane
33	cycloheptane
34	octane
35	isopropylcyclopentane
36	ethylcyclohexane
37	ethylbenzene
38	*p*-xylene + *m*-xylene
39	*o*-xylene
40	nonane

Table III. Lowest Detectable Hydrocarbon Quantities as a Function of Molecular Size and Type Based on the Measurement of a Low Hydrocarbon-Yield Rock Sample (Cretaceous Shale, see Figure 5). 1 pg = 10^{-12} g

compound	reference no.	quantity, pg	lowest detectable quantity, pg·g^{-1}
ethane	1	592	5
propane	2	835	8
butane	5	547	11
pentane	7	1486	24
hexane	12	1069	42
benzene	14	764	59
heptane	22	458	86
methylcyclohexane	24	677	131
toluene	29	2955	152
octane	34	388	97
ethylbenzene	37	774	93
o-xylene	39	351	105
nonane	40	274	137

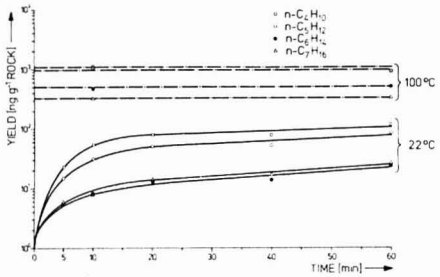


Figure 6. Hydrocarbon yield as a function of hydrogen stripping time at ambient temperature in comparison to the total yield obtained by stripping at 100 °C

Stripping Efficiency as a Function of Time and Temperature. For routine application of our analytical method, the light hydrocarbons are stripped from the rock sample at room temperature. This limitation means that a sizeable portion of the total light hydrocarbons present in the rock is not removed, even if extended stripping times are applied. On the other hand, stripping at room temperature requires less effort for the whole process. High temperature stripping according to Jonathan et al. (*9*) creates several problems by which the process is unnecessarily complicated, e.g., large amounts of pore water to be eliminated prior to GC analysis, splitting required to avoid column overloading and to enable isothermal GC analysis, higher carrier gas flow affecting the efficiency of the cold trap. Furthermore, according to our experience, hydrogen stripping at room temperature preferentially mobilizes the light hydrocarbons dissolved in the pore water of the rock.

To examine the influence of time and temperature on the hydrocarbon yield and composition, a rock sample was subdivided into five portions. Each of these was stripped for a different time at constant hydrogen flow. The results are given in Figure 6 which shows the amounts of selected hydrocarbons as a function of the volume of stripping gas. Furthermore, two of these samples (stripped for 10 and 60 min) have been heated later up to 100 °C and simultaneously stripped of residual light hydrocarbon content. The total amounts obtained in this way are in good agreement with each other and are represented by horizontal lines in the diagram.

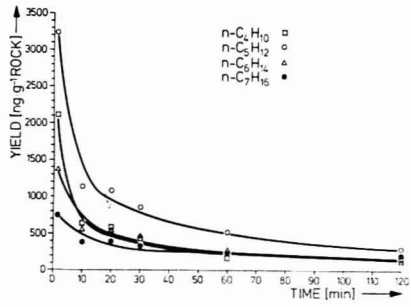


Figure 7. Hydrocarbon yield as a function of sample aging. Abscissa equals time of exposure of rock sample to atmosphere prior to hydrogen stripping

Obviously, even by a stripping gas volume of 600 mL, the amount of hydrocarbons recovered at room temperature is only a small fraction ($^1/_{10}$ and $^1/_{20}$ for ethane and hexane, respectively) of the hydrocarbons present in the rock.

Since hydrocarbon yields show an exponential relationship with respect to stripping time, samples should be compared on the basis of equal volumes of stripping gas. To calculate the total light hydrocarbon content present in a rock sample requires the determination of a recovery factor by heating a representative sample as described above. In a recent paper, Kolb and Pospisil (*14*) suggested a mathematical method to recalculate the total concentration of volatiles in solid materials using the exponential function of the recovery obtained by stepwise gas extraction.

Requirements for Sample Quality. For comparison of quantitative results, special precautions should be taken during sampling, e.g., at the well site and during sample transit and storage. It is suspected that variations in sampling method or storage may result in severe inaccuracies with respect to quantity and/or molecular distribution pattern of the detected light hydrocarbons. To clarify this point, an artificial sample aging experiment was undertaken. In detail, a portion of a freshly crushed sample was measured immediately. The remainder was stored in a water-saturated atmosphere at room temperature, during which time the hydrocarbons were able to diffuse from the rock sample. After certain times (10, 20, 30, 60, 120 min), small portions of the sample were submitted to the hydrogen stripping procedure. The results of this experiment are shown in Figure 7 for selected hydrocarbons. By far the highest yields were obtained from the fresh sample (1.5-min preparation time). After 10 min, already a drastic loss in hydrocarbon content occurs, especially for the lighter species (56% loss for butane, 33% loss for heptane). After 2 h, the concentration of butane had dropped to about 8% of the initial value, whereas 24% of heptane could still be recovered. Both decrease of hydrocarbon yield and deviations of the molecular distribution as a function of sample aging time must be taken into account for geochemical data interpretation. For example, the compound ratio hexane/methylcyclopentane increases in this experiment perhaps because of their difference in diffusibility, from 1.3 (initial value) to 1.6 (after 2 h).

Comparison between Hydrogen Stripping and Blender Headspace Techniques. For comparison of the hydrogen stripping procedure with other already established methods, a blender headspace technique similar to the method applied by Hunt (*2, 3*) had been selected. In detail, a rock sample (Paleocene Fm., argillaceous shale, 11.9% organic carbon content) covered with hot water (95 °C) has been crushed in

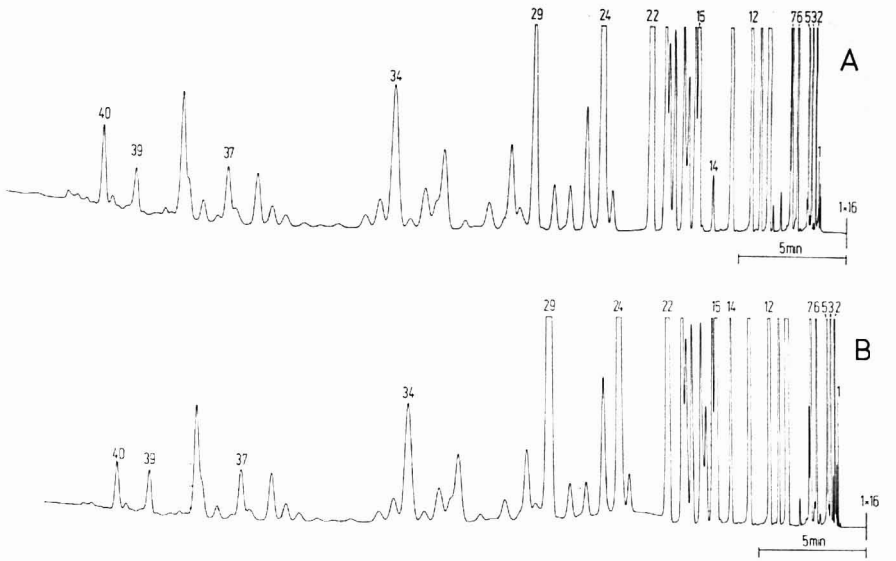


Figure 8. Comparison of gas chromatograms obtained by different light hydrocarbon extraction techniques: (A) Blender headspace technique, (B) hydrogen stripping method. Yields of selected compounds (numbered according to Table II) are listed in Table IV

an 1-quart volume blender. From the headspace gas (73 mL), a 250-μL volume was removed with a syringe and injected directly into the gas chromatograph. Another representative split of the same rock sample has been analyzed by our hydrogen stripping procedure. Results of this comparison are shown in Figure 8. With respect to overall hydrocarbon distribution, chromatograms from both techniques are similar. However, pronounced differences are observed for yields of selected compounds (Table IV). Concerning heptane, almost equal recovery of about 300 ng was obtained with both procedures. However, the recovery of the low-molecular weight aromatic hydrocarbons is selectively reduced in the blender headspace technique: recovery of benzene is only approximately 20% and toluene 38% of the amounts obtained by hydrogen stripping. This effect can be explained by fractionation due to partitioning between water and vapor phases in the blender. The same argument explains the decreased recovery rate of light gases in the headspace, e.g., butane reduced to 68% and propane to 35% of the value obtained by hydrogen stripping. However, ethane shows reversed behavior.

In summary, the hydrogen stripping technique shows less fractionation effects over the molecular range C_2 to C_8, especially for aromatic compounds and the C_3 to C_5 hydrocarbons.

Finally, in the case of the above experiment, the hydrocarbon yield per weight of rock seems to be more favorable for the hydrogen stripping technique: only 330 mg of rock were necessary for the analysis, whereas the blender headspace experiment required 62 g of rock material. However, Hunt applies an additional concentration step (a complete displacement of the headspace by an auxiliary gas, combined with trapping of the removed hydrocarbons and quantitative transfer to a gas chromatograph). This increases the yield by a factor of 73 mL/0.25 mL = 292 in this example. Hence, total yield of hydrocarbons (C_2 to C_9 range; see Table III) per unit rock weight would be very similar: 26 μg/g recovery in the blender headspace experiment, 21 μg/g by hydrogen stripping.

Table IV. Comparison of Hydrocarbon Yields Obtained by Hydrogen Stripping vs. Blender Headspace Technique (Core Sample, Paleocene Shale, W. Greenland, see Figure 8). 1 ng = 10^{-9} g

compound	reference no.	H_2-stripping method quantity, ng	blender-headspace technique quantity, ng
ethane	1	3	4
propane	2	176	61
methylpropane	3	381	247
butane	5	867	591
methylbutane	6	590	497
pentane	7	1135	953
hexane	12	618	501
benzene	14	50	10
cyclohexane	15	250	198
heptane	22	320	347
methylcyclohexane	24	284	267
toluene	29	302	115
octane	34	90	107
ethylbenzene	37	29	33
o-xylene	39	22	24
nonane	40	21	33
total amount of hydrocarbons detected between ethane and nonane		6898	5561
weight of rock sample analyzed		0.33 g	62 g

An additional advantage of the hydrogen stripping procedure concerns the fact that very small amounts of rock samples are required. Therefore, by this technique, selected parts of a rock sample can be analyzed selectively, e.g., hand-picked lithologies from a mixture of drill cuttings.

Analysis of Crude Oil Samples by Hydrogen Stripping. As an example of light hydrocarbon analysis of fluids, a crude oil sample has been introduced into the sample tube. The chromatographic result is shown in Figure 4 and discussed with respect to demonstration of backflush efficiency. In order not to overload the capillary, only trace amounts of hydrocarbons should enter the column. This can be achieved by applying short stripping times (ca. 1 min) on a very small amount of crude oil, e.g., a quantity which has been drawn into a very thin glass capillary (generally <0.1 mg).

The main advantage of this type of crude oil characterization is the absence of any pretreatment before the stripping procedure; hence, one droplet of oil is sufficient for an analysis. Furthermore, thermal degradation of sensitive compounds in the heated injection ports used in normal gas chromatographs is avoided.

CONCLUSIONS

The hydrogen stripping combined with capillary GC in a single-step procedure represents an attractive alternative as compared to other light hydrocarbon analytical techniques used so far in the field of organic geochemistry. However, great caution should be exercised when comparing hydrocarbon concentrations obtained from different analytical methods.

In this paper, emphasis has been placed on the description of the analytical procedure of the hydrogen stripping technique as well as on a discussion of its limitations. Examples for the application of this technique in geochemical studies are given in a recent paper by Leythaeuser et al. (*15*). For this purpose, both light hydrocarbon yield and molecular distribution patterns are considered in order to characterize organic matter in sedimentary rocks.

Finally, it is emphasized that this method can also be applied to other problems of similar kind, i.e., determination of volatile trace components in solid or liquid matrices.

ACKNOWLEDGMENT

The authors express thanks to B. Geisler for contributing the FORTRAN program system required for off-line data processing. Assistance with the experimental work by F. Schlosser and B. Beckers is gratefully appreciated, as well as intense support in preparing the English version of this manuscript by C. Cornford.

LITERATURE CITED

(1) H. Hachenberg and A. P. Schmidt, "Gas Chromatographic Headspace Analysis", Heyden & Son, London–New York–Rheine, 1977.
(2) J. M. Hunt, *Adv. Org. Geochem.*, **1973**, 593.
(3) J. M. Hunt, *Nature (London)*, **254**, 411 (1975).
(4) R. Gedenk, *Erdöl Kohle, Erdgas, Petrochem.*, **19**, 720 (1966).
(5) B. Durand and J. Espitalie, *Adv. Org. Geochem.*, **1971**, 455.
(6) K. Le Tran, *Bull. Cent. Rech. Pau*, **9**, 223 (1975).
(7) G. T. Philippi, *Geochim. Cosmochim. Acta*, **39**, 1353 (1975).
(8) K. Le Tran, *Adv. Org. Geochem.*, **1971**, 717.
(9) D. Jonathan, G. L'Hote, and J. Du Rouchet, *Rev. Inst. Fr. Pet.*, **30**, 65 (1975).
(10) D. R. Deans, *Chromatographia*, **1**, 18 (1968).
(11) G. Schomburg, H. Husmann, and F. Weeke, *J. Chromatogr.*, **112**, 205 (1975).
(12) G. Schomburg, R. Dielmann, H. Husmann, and F. Weeke, *J. Chromatogr.*, **122**, 55 (1976).
(13) R. A. Hively and R. E. Hinton, *J. Gas Chromatogr.*, **6**, 203 (1968).
(14) B. Kolb and P. Pospisil, *Chromatographia*, **10**, 705 (1977).
(15) D. Leythaeuser, R. G. Schaefer, and B. Weiner, *Chem. Geol.*, in press.

RECEIVED for review March 13, 1978. Accepted July 28, 1978. Financial support by the German Federal Ministry for Research and Technology (B.M.F.T.) Grant No. ET 3070 B is gratefully acknowledged.

Scanning Laser Mass Spectrometer Milliprobe

R. J. Conzemius* and H. J. Svec

Ames Laboratory—USDOE and Department of Chemistry, Iowa State University, Ames, Iowa 50011

Focused laser beam excitation of solids to produce ions in the ion source of a mass spectrometer is shown to have powerful milliprobe capabilities. This is achieved through proper choices of laser power, laser beam control, ion source parameters, and type of mass spectrometer. Experiments show that elemental sensitivities are relatively uniform, ion intensities can be quantified through the use of standards, and close correlations can be made of ion signals to position of laser excitation on the specimen.

Lasers have been shown to be useful for characterizing solids especially in milliprobe applications (*1*, *2*). This application of the laser has been more successful in optical emission spectrography than in mass spectrometry (*3*). There are several reasons for the slower development of the mass spectrometric laser ion source for solids. Early work (*4*) utilized high laser pulse energies creating large ion current pulses (≫1 μA) and causing severe space charge aberrations. Other early studies (*5*, *6*) reported widely differing elemental ion selectivities due to small differences in ionization potential or to selective volatilization. These difficulties can be attributed to the use of low power densities (<10^8 W cm^{-2}) obtained in continuous wave or normal pulse mode laser operation. When Q-switching was used to increase power density, relatively low laser pulse repetition rates (<100 Hz) required long observation times during spectral integration techniques thus limiting certain mass spectrometric applications (*7–9*). Finally, early mass spectrometric applications employed instruments such as time-of-flight (*6*, *10*), quadrupole (*11*), and single focusing magnetic sectors (*12*) which are all limited in ion energy bandwidth acceptance and in mass resolution. Many of these applications were used to characterize chemical structure or to study mechanisms of ion formation. In these cases, lower laser power densities and rapid mass spectral scanning are beneficial (*2*, *6*, *10*, *13*). Analytical features such as relating elemental ion signals to concentration and to location in the solid sample were not stressed.

Recent work has shown that uniform elemental sensitivities are attained through the use of higher power densities (i.e.

0003-2700/78/0350-1854$01.00/0 © 1978 American Chemical Society

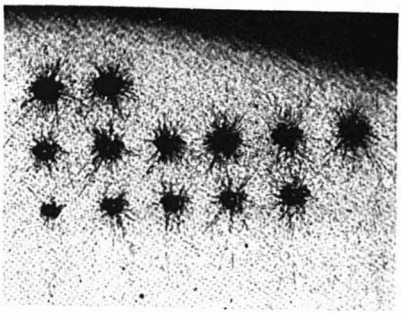


Figure 1. Demonstration of growth in spot size with increased laser power and number of laser shots-per-site (Mag. = 150X)

$\geq 10^9$ W cm^{-2}) (*7, 8, 14*). These higher power densities, easily attained by focused Q-switched laser pulses, produce ions with greater energy spreads and lower molecular ion intensities. Double focusing mass spectrometers, especially those of the Mattauch–Herzog ion optical design, can accommodate well to higher energy spreads and can also provide for simultaneous ion detection of a large mass range (e.g., M to 36 M). However this application has been slowed somewhat because of the limited availability of such mass spectrometers and also because of the limited range of features available in applied laser systems.

The laser ion source–mass spectrometer system described here has several new and unique features which significantly expand its capability to a highly desirable and workable system. The energy-per-laser pulse is only about 1 mJ, thus yielding microplasmas more amenable to ion acceleration and focusing. The power density is about 10^9 W cm^{-2}, high enough to provide uniform elemental sensitivities. The laser repetition rate is variable over a range two to three orders of magnitude greater than previous systems.

Much more versatile control for selecting the laser spot is provided through the use of optical scanners. Thus rapid electronic control of the laser beam position is allowed as well as site selection by sample manipulation.

EXPERIMENTAL

Apparatus. *Laser.* The laser system is a Holobeam Laser Inc., subsidiary of Control Laser Inc., model 255QT with changeable mode selector. The system is operated in the single-transverse-mode TEM_{00} and is Q-switched with an acousto-optic Q-switch with external control of repetition rate from 1 Hz to 24 kHz. The total energy and the temporal distribution of the laser pulse are dependent upon the lamp (optical pump) excitation current. The pulse repetition rate is nominally chosen to provide ~200-ns pulses with an energy of 1 mJ. This results in an instantaneous power output of approximately 5000 W. With a focused spot 15 μm in diameter, a power density of approximately 2×10^9 W cm^{-2} is attained. An illustration of spot size and typical erosion for a low alloy steel is shown in Figure 1 for various exciting lamp currents and also for multiple pulses at the same focused spot. In the lower row of craters, the laser excitation current was increased from 15 to 19 A in 1-A increments starting at the left. In the upper two rows, the number of laser shots-per-site was increased from 1 to 8 starting at the left of the center row. Significant growth in the crater dimensions are visible especially in the upper row where 7 and 8 laser shots-per-site were made.

Specimen viewing is in line with the laser optics and provided with a trinocular optical system consisting of binocular and television viewing at 100X magnification. The focused laser spot coincides with a cross-hair indicator in the viewing system. Focus adjustment (z axis) is made with a manual adjustment range of 2 cm. Both the x and y axes are provided with electrically

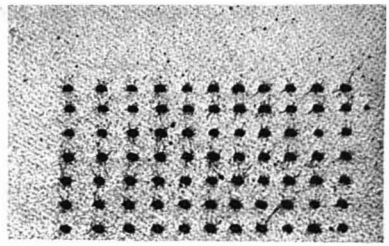


Figure 2. 7 × 11 array of laser eroded sites with a single laser shot-per-site (Mag. = 75X). Site control via external voltage to x-y galvoscanners

controlled laser beam directors (galvoscanners) over a range of ±2 mm at the focal plane with a resolution and repeatability of less than 12 μm. An electrical drive signal controls the galvoscanner deflection which sets the viewing area (and focused laser spot) to a particular site or scans each axis independently at frequencies up to 600 Hz. Figure 2 shows a matrix of eroded sites in a low alloy steel sample by single laser shots with site control via the galvoscanners. A heavy duty x-y stage on the optics head provides for manual adjustment of the viewed spot over a 5 cm by 5 cm area with a resolution of 12 μm. An electronic circuit constructed in the Ames Laboratory provides control of the laser such as start, stop, repetition rate, and total number of laser shots desired. For the work described here, the repetition rate was adjusted from 1 to 1000 Hz. All other circuitry associated with powering and controlling the laser was provided by the manufacturer.

Ion Source. A schematic view of the laser ion source is given in Figure 3. The laser beam enters the vacuum chamber through a 7.5-cm diameter, 0.32-cm thick borosilicate glass (Corning 7740) window and is deflected onto the sample with a 2.5 by 2.5 cm 60° equilateral prism. The distance between the prism and the sample is approximately 4.6 cm. The surface of the sample is set normal to the laser beam principally to provide better viewing of the sample. Emitted ions are taken off at 60° to the surface and travel within a 1.9-cm diameter closed tube to a 95% transparent grid which is 0.5 cm in diameter. The sample tube and grid are held at the ion accelerating voltage of 24 kV. The positive ion cathode ray tube lens was specially designed (*15*) to transport the ion beam efficiently from the grid to the object slit of the spectrograph. Ion beam adjusting lenses are also provided along the y and z axes just before the object slit although only the lower z plate was found to require an adjusting voltage of ~100 V to maximize the ion signal at the ion beam monitor located in the field free region between the electrostatic and magnetic analyzer of the spectrograph. The sample is mounted on the end of a rod insulated for 24 kV and manipulated through a vacuum bellows by digital motors which drive the 3 axes independently. Movement resolution is 1 μm and the range of movements is ±5 mm along the x and z axes and 6 cm along the y axis. The ion source vacuum chamber was designed specially to bolt directly onto an original rf spark ion source chamber and is evacuated with a 500 Ls^{-1} turbomolecular pump which maintains a vacuum of $\sim 10^{-8}$ Torr. Pump down from 1 atm to the 10^{-7} Torr region where experiments can begin requires about 20 min.

Mass Spectrograph. The spectrograph is a model Graf II-2 constructed by Nuclide Corp. Spectrograph parameters are given in Table I. The instrument is equipped with both electrical and photoplate ion detection. Photoplate detection was used for all but one of the experiments described here.

Sample Materials. Three cartridge brass samples, NBS C1100, C1101, and C1102, and two low alloy steel samples, NBS 461 and 463 were used in the work. Four additional sample materials were prepared in the Ames Laboratory: Pure silicon bar, 6 cm long and 3 × 3 mm^2; thorium rod, 2.5-mm diameter, containing a concentration gradient of cobalt along the rod axis; pure tantalum rod, 2.5-mm diameter, welded to a 2.5-mm diameter tantalum rod containing 10 ppmw silicon; and a welded tantalum–thorium junction with rods of 2.5-mm diameter. A rock specimen con-

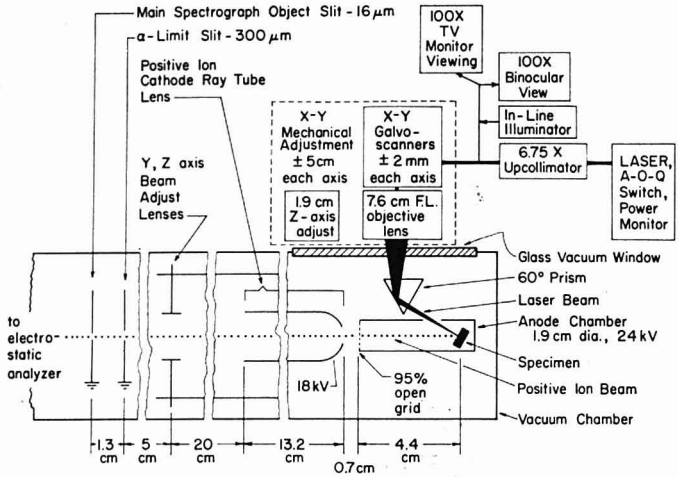


Figure 3. Schematic view of laser ion source

Table I. Spectrograph and Photoplate Parameters

main object slit	13 μm
α limit slit	300 μm
maximum allowed α (half angle of angular divergence)	0.011 radians
maximum allowed β (fractional energy spread transmitted to magnetic field) for α = 0	0.006
maximum allowed β for α = 0.01	0.012
accelerating voltage	24 kV
electrostatic analyzer	radius 15 cm cylindrical, sector 53° 2', voltage ±1350
magnetic analyzer	radius 5 to 30 cm, sector 90°, field 12 kG
ion detector	Ilford Q2 Photoplate, mass range M to 36 M
photoplate developing	MK9 with bleach according to Cavard (*16*)
emulsion calibration	Franzen and Schuy (*17*)
photoplate data recording	semiautomatic (*18*)
vacuum:	ion source 10^{-6} Torr
	analyzers 10^{-8} Torr
	photoplate prepumping chamber 10^{-7} Torr

taining feldspar, quartz, and muscovite mica obtained from the Earth Science Department, Iowa State University, Ames, Iowa, was also examined.

Procedure. An advantage of the laser ion source lies in its straightforward implementation. The sample is manipulated to a selected site onto the optic axis of the spectrograph. Then the laser is adjusted into viewing focus at the site and sample excitation is initiated. However after 5 to 10 laser shots at the same site, refocusing is necessary because erosion lowers the surface below the focal plane. The laser may be rastered along one or both the x and y axes which permits the excitation to continue for long periods without refocusing. Adjustment of rastering range and frequency is performed prior to turning the laser on by adjusting the lateral range desired. Each axis is adjusted independently, and then the frequencies are increased as desired but usually with one axis at a low frequency and the other at a high frequency so as to obtain a rectangularly eroded site. The laser repetition rate and the number of laser shots desired are set by thumbwheel switches on the control circuit. The start button initiates the laser shots and the laser produced plasma is viewed on the television monitor. For long exposures where significant sample erosion occurs some refocusing of the laser is performed either by raising the sample or adjusting the laser. Evidence of focus at the specimen surface is easily monitored by the relative brightness of the excitation as well as by the relative ion beam intensity.

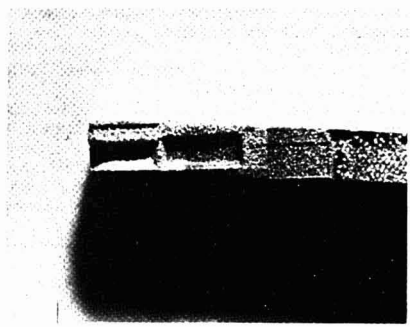


Figure 4. Rectangularly eroded sites into the side of NBS Brass Sample C1102. The bar is 1 mm wide

Sample preparation is simple since sample roughness is not a deterrent to laser excitation. However optical viewing, important for milliprobe applications, is improved with relatively flat reflective surfaces.

Three experiments, characterization of bulk impurities, milliprobe application to concentration profiles, and excitation of a geological specimen, will be described to illustrate the applicability of the system.

Characterization of Bulk Impurities. Three cartridge brass and two low alloy steel standards were analyzed by exciting areas via rastering of approximately 1 mm^2 to provide photoplate exposures ranging from 10^{-13} to 10^{-8} C of ion charge. The longest exposure required 10^6 laser shots which, at a repetition rate of 10^3 Hz, required 17 min. A picture of such a series of analyzed sites is shown in Figure 4 where the different erosions are due to movement of the sample to new areas for the different ex-



Figure 5. Picture of tantalum (lower half) and thorium (upper half) weld interface. Magnification = 100X

posures. The resulting mass spectra for the C1100 brass and the 461 low alloy steel were used as standards to which the C1101 and C1102 brass and 463 steel samples were compared, respectively, for computation of impurity levels.

Milliprobe Application. Three experiments were performed to demonstrate this capability. The first involved the analysis of a welded tantalum–thorium junction. Twelve sites were analyzed in steps of 48 μm across the junction. The spectra were recorded photographically with one exposure per site. Each exposure consisted of 100 laser shots made while the laser was being rastered along the axis parallel to the weld interface. A picture of the sample showing the 12 sites is shown in Figure 5. The weld interface is located above the fifth eroded site as indicated on the figure and may also be seen as the straight horizontal line [the weld junction] extending right and left beyond the erosions and between the two differently textured metals. An exposure of approximately 10^{-11} C was collected for each of the 12 sites.

In the second experiment, the system was used to measure the concentration profile of cobalt over a 6-mm range in a thorium sample which had previously been analyzed by spark source mass spectrometry. Again the spectra were measured with photographic ion detection.

The third experiment was performed utilizing electrical ion detection in measuring the concentration profile of silicon across the welded junction of a pure tantalum rod and a tantalum rod previously doped with 10 ppmw silicon. The silicon concentration was measured while the laser was being rastered along a 1-mm line parallel to the weld junction similar to the first experiment shown in Figure 5. In this case the $^{28}Si^{+1}$ ion signal was being monitored with a 20-stage electron multiplier whose output was amplified with a vibrating reed electrometer. The ratio of the $^{28}Si^{+1}$ ion signal to the total ion beam monitor signal was measured (*19*) three times for each site. Each measurement required ~30 s. After each set of three measurements, the sample was moved 25 μm and the determination repeated. A total of 21 sites were analyzed over a total range of 500 μm with 250 μm on each side of the weld junction. Such profiles are useful in studying chemical diffusion and thermo- and electrotransport.

A silicon matrix is also of current interest in similar studies and although a reference material was not available, concentration profiles in silicon samples have been analyzed similarly to the thorium and tantalum samples. The resulting mass spectra are similar to those from other matrices with the exception of the appearance of higher Si_N molecular ion intensities. The observed relative intensities of these ions are given in Table II. These relative intensities indicate considerable fractionation of molecular ions which predominated at lower power densities (*20*).

Geological Specimen. A very general characterization of a rock was made by scanning in a manner similar to the scan across the Ta-Th weld junction. However, in this case, 1000 laser shots were used at each site with a repetition rate of 300 Hz and each site produced ~10^{-10} C of exposure. Each site was rastered within a 0.2 by 0.5 mm rectangular area. For this particular rock, the feldspar eroded at least 10X faster than the mica although the ion currents were similar.

Table II. Relative Intensities of Molecular Ion Signals from Silicon

Si_1	100.
Si_2	21.
Si_3	6.0
Si_4	5.8
Si_5	1.7
Si_6	3.6
Si_7	0.7

Table III. Reduction in Ion Current from Ion Source to Ion Detector

position along ion path	coulombs per laser shot	reduction factor
sample chamber	~10^{-7}	-
at object slit	~10^{-9}	10^{-2}
at ion beam monitor	~10^{-12}	10^{-3}
at detector	~10^{-13}	10^{-1}
approximate collection efficiency =		10^{-6}

RESULTS AND DISCUSSION

Collection efficiency is of primary importance in any mass spectrometric development. Table III gives nominal values of ion charge as collected per-laser-shot at various apertures along the ion optical path of the spectrograph. Actual ion currents vary for different sample configurations and laser beam parameters as well as for different materials but the relative reduction in ion signal at the various apertures remains relatively constant. The reductions noted in Table III are generally predictable based upon solid angle acceptance of apertures along the ion optical path. Interpretation of these laser-created ion signals is easier than for ions created with the rf spark since multiply charged ions account for only a few percent (<5%) of the total laser-created ion beam whereas this percentage is much higher (30–40%) for the rf spark.

Mass resolution and abundance sensitivity were slightly higher than that obtained with the rf spark for the Graf II ion optic system. Figure 6 shows a strip chart recording of a photographic plate produced from a brass sample for an exposure of 10^{-8} C. The scan is in the mass spectral region of the major ion signals due to copper and zinc. The mass resolution is approximately 2000 and the sensitivity is indicated by the signal-to-noise level adjacent to these lines. The ion signal at m/z = 59 of 0.7 ppma is not greatly affected by fogging from the most intense ion signals in the spectrum located between m/z 63 and 70.

Bulk Analysis. Table IV gives the results for the bulk analysis of the NBS cartridge brass samples. Column 1 identifies the elements sought and columns 2, 3, and 5 are the levels reported by NBS for the three brass samples. Columns 4 and 6 give the experimentally determined levels using the laser probe. The agreement is considered to be semiquantitatively valid and the use of internal references such as iron to improve the instrument response function would not improve the agreement significantly. This is apparently due to the capability of the instrument to measure the matrix lines as accurately as the trace level impurities. The relative elemental sensitivity coefficients (RSC), determined with the C1100 brass sample, are given at the far right of the table. The narrow range indicates that differences in elemental sensitivities, observed to be high when lower power densities are used, are quite low here. RSC values for copper and zinc

Table IV. Measurement of Trace Level Elements in NBS Brass Samples (values in percent weight)

element	C1100 reported	C1101 reported	C1101 computed[a]	C1102 reported	C1102 computed[a]	RSC[b]
Be	0.001_5	0.0005_5	0.0003_8	0.0000_3	0.00002_5	0.96
Al	0.008	0.0006	0.00008	0.0007	0.0004	1.16
Si	(0.010)	(0.005)	(0.006_4)	(0.002)	(0.002_4)	0.81
P	0.010	0.002_0	0.0029	0.004_8	0.0036	0.67
Mn	0.003	0.005_5	0.006	0.004_4	0.004	1.22
Fe	0.072	0.037	0.043	0.011	0.013	≡1.00
Ni	0.052	0.013	0.015	0.005	0.0067	0.83
As	0.019	0.009	0.011	0.004	0.0052	0.74
Ag	0.019	0.003	0.0061	0.0010	0.00088	0.48
Cd	0.013	0.005_5	0.0069	0.004_4	0.0040	0.54
Sn	0.055	0.016	0.016	0.020	0.0049	0.36
Sb	0.018	0.012	0.018	0.005	0.0044	0.28
Pb	0.106	0.05	0.036	0.020	0.016	0.47

[a] Computed values = (observed signal for "unknown"/observed signal for C1100) × reported value for C1100. [b] RSC = (observed signal in C1100/reported value in C1100)(reported value for iron in C1100/observed signal for iron in C1100).

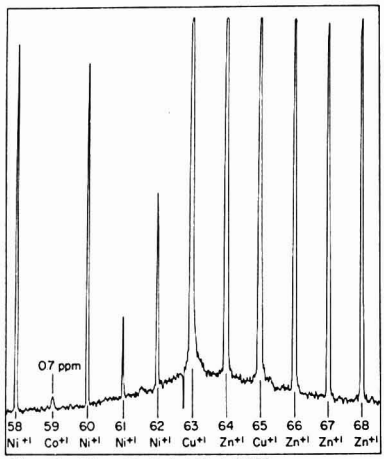


Figure 6. Scan of photoplate recorded spectrum of brass sample

were measured at 0.58 and 0.62, respectively. The closeness of the RSCs for these two elements indicates that *ions* produced were not significantly fractionated because of difference in vapor pressures, melting points, or local phase alterations (*21*).

Table V gives the data obtained for the NBS low alloy steel samples. Again the agreement indicates at least semiquantitative usefulness. Some elemental fractionation may be emerging in these data by the observation of very low RSCs for B, P, and As and somewhat high RSCs for V and Cr.

Milliprobe Scanning. Figure 7 is a plot of the ion signals for tantalum and thorium as experimentally excited in stepped sites as indicated in Figure 5. The thorium ion signal is seen to rise from a relative value of less than ~1000 to ~450 000 as the excitation moves from one side of the weld junction to the other. The tantalum signal drops by about 100X at the first site past the junction and then by ~3X at the next two sites before leveling off. This tailing off of the tantalum signal is probably due to transfer of tantalum to the thorium surface by molten liquid or by recondensation of vapor when the pure tantalum was being excited. This level of "memory" is not considered to be serious and could perhaps be reduced if necessary by pre-excitation of the sites prior to taking

Table V. Measurement of Trace Level Elements in NBS Iron Samples (values in percent weight)

element	NBS #461, reported	NBS #463 reported	NBS #463 computed[a]	RSC[b]
B	0.000_2	0.0012	0.001	0.13
P	0.053	0.031	0.038	0.046
Si	0.047	0.41	0.31	0.29
V	0.024	0.10	0.080	7.6
Cr	0.13	0.26	0.21	4.8
Mn	0.36	1.15	1.00	1.1
Co	0.26	0.01_1	0.014	1.43
Ni	1.73	0.39	0.44	0.91
Cu	0.34	0.47	0.40	1.1
As[c]	0.028	0.10	0.047	0.024
Mo	0.30	0.12	0.10	1.84
Sn	0.022	0.013	0.022	0.54
Ta	0.002	0.15	0.13	0.54
W	0.012	0.10_3	0.12	0.32

[a] Computed value = (observed signal for "unknown"/observed signal for 461) × reported value for 461. [b] RSC = (observed signal for 461/reported value for 461)-(reported value for iron in 461/observed signal for iron in 461). [c] As observed previously to be inhomogeneous.

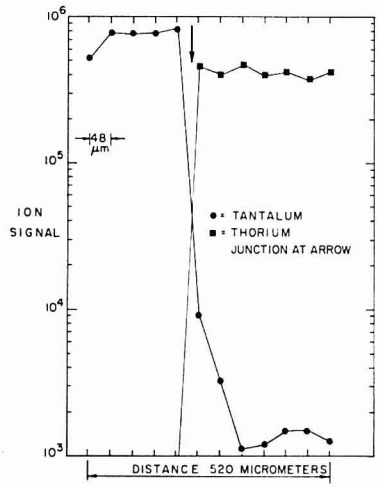


Figure 7. Scan of tantalum–thorium weld junction

Table VI. Comparison of Recent Laser Ion Sources Adapted to Double Focusing Mass Spectrographs

			Bykowskii et al.	Bingham and Salter	this work
laser	Q-switch Type		unknown	Pockel's cell	Acoustooptic
	energy/pulse	mJ	20	10	1
	maximum repetition rate	Hz	100	50	10 000
ion signal	emitted from sample	C/pulse	10^{-5}	1.6×10^{-5}	10^{-7}
		C/J	5×10^{-3}	1.6×10^{-3}	10^{-4}
	collected at image of spec.	C/pulse	5×10^{-13}	10^{-12}	10^{-13}
		C/J	2.5×10^{-11}	10^{-10}	10^{-10}
mass spectrograph	object slit width	μm	50	10	15
	transmission efficiency		5×10^{-8}	6×10^{-8}	10^{-6}
	mass resolution		2100	3000	2 000
	time required for collection of 10^{-7} C	s	2000	2000	100

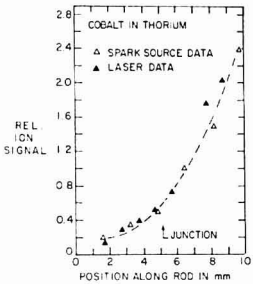


Figure 8. Comparison of laser data with spark source data

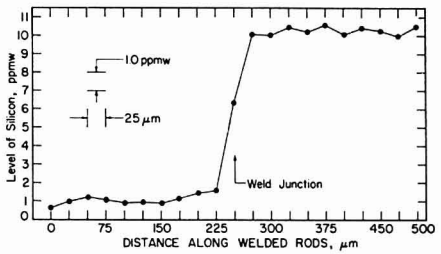


Figure 9. Scan of diffusion couple containing 1 and 10 ppm silicon in tantalum

analytical data. Although not shown here, ion signals were recorded simultaneously at the 20 to 5000 ppma level for carbon, oxygen, nitrogen, sodium, and carbon monoxide. Relatively smooth profiles were obtained indicating interesting concentration variations across the weld junction.

Figure 8 shows a comparison of data measured by the rf spark ion source and by the laser ion source for a concentration gradient of cobalt in thorium. The cobalt was present at approximately 150 ppmw and the data shows that the laser ion source can follow the gradient as well as the rf spark ion source.

Figure 9 shows the results of measuring silicon in 25-μm steps across the junction from pure tantalum to tantalum containing 10 ppmw. The ten determinations (average of three measurements at each site) to the left of the junction average 1.1 ± 0.6 RSD. The reading at the weld junction is 6.3, apparently being due to excitation occurring partially in both the pure and in the doped tantalum. The determination made 25 μm past the junction is shown to rise to the 10 ppmw level. The average of the ten determinations to the right of the junction is 10 ± 0.4 RSD.

Geological Sample. Results typical of those obtained from rock samples are shown in Figure 10 for phosphorus, fluorine, and titanium in a rock containing feldspar and muscovite mica. The concentrations of titanium and fluorine are high in the mica whereas the phosphorus is low. No titanium is observed in the pure feldspar. Although not shown, similar profiles were also established simultaneously for all elements (except rare gases) between atomic numbers 2 and 30 as well as for rubidium. Electronic detection of these ion signals and subsequent correlation of the ion signals to the site of excitation would provide a powerful tool for earth scientists.

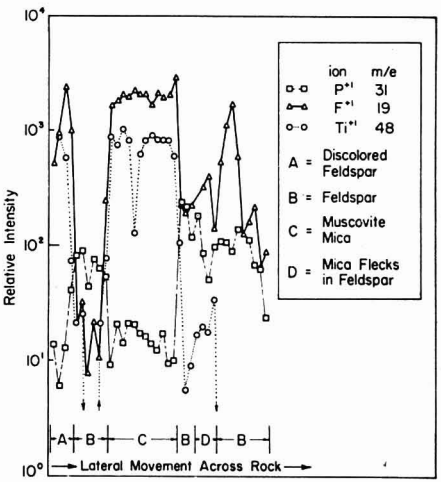


Figure 10. Example of scan of elemental signals at sites along a rock sample

CONCLUSION

A brief comparison will be made of this work to other similar laser ion source–mass spectrometer developments. Table VI gives a general comparison of some salient features of three such instrumental developments. The data given are only approximations since many of the parameters are quite difficult to measure and intercompare between laboratories. The comparisons given are for systems that use Q-switched lasers with double focusing mass spectrographs of the Mattauch–Herzog ion optical design. The laser beam wave length used in these comparisons was 1.06 μm from the Nd doped YAG laser although other lasers have also been tried. The 1.06-μm wavelength has been found to give good coupling of laser power to a large variety of substances although shorter

wavelengths have been found to be advantageous at least for some applications (*22, 23*). As may be noted in the table, the energy per pulse is lowest for this work but it is the authors' observation that this laser parameter should be kept low to minimize space charge effects. The much higher laser repetition rate for this system is a distinct advantage when time considerations are important, such as integration of ion signals from a large number of laser pulses for work at high sensitivity. Figures-of-merit might be considered to be the ion signals measured at the ion source and at the image of the spectrograph. The three systems shown in Table VI are similar with the two instruments using higher energy-per-laser-pulse yielding the higher signals emitted from the sample. However this work shows as high or higher signals received at the image per joule of laser energy. Improvements are noted in this development in transmission efficiency and in the time necessary to deliver a given ion charge to the image of the spectrograph.

Concentration and absolute sensitivity can be estimated from basic parameters. Figures 1 and 2 indicate crater diameters of $\sim 25\ \mu m$. The depths of the craters in Figure 2 average $3.2\ \mu m$. These craters are shaped approximately as segments of spheres which permits calculation of an approximate crater volume of $3 \times 10^{-9}\ cm^3$. For the low alloy steel, this erosion from a single laser shot is 2×10^{-8} g. At the image of the spectrometer, 10^{-15} C will be assumed necessary to detect a line by photoplate detection and 10^{-18} C by electrical detection. Since 10^{-13} C is collected per single laser shot, the total system has a calculated average absolute sensitivity of 2×10^{-10} g for photoplate detection and 2×10^{-13} g for electrical detection. If 10^6 laser shots are used and 10^{-7} C are collected, then the concentration sensitivity is 10^{-8} and 10^{-11} for photoplate and electrical detection, respectively. These sensitivities are considered reasonable although the 10^{-11} figure may be limited by spectral background or other noise-contributing factors.

The relatively uniform elemental sensitivities observed here confirm earlier observations (*7, 8, 14*). These uniform sensitivities will permit the laser ion source to perform semiquantitative surveys without standards as is practiced successfully with the rf spark ion source. Further experiments will indicate whether the laser ion source can be used similarly for direct semiquantitative analysis of semiconductor, nonconductor, inorganic, organic, biological, or geological specimens.

Limitations in this system should also be pointed out. As mentioned earlier, some advantages may be found at shorter laser wavelengths. Recent work (*7, 8, 22*) has indicated that laser pulses shorter than used here may also have some advantages. Further investigation is needed to establish the effects that laser pulse length has on analytical usefulness of ion signals. The laser power density used here is only slightly greater than $10^9\ W\ cm^{-2}$. This may be considered to be marginal, but again the optimum level for power density is not well established.

Other laser ion source developments have utilized different mass analyzing systems with success (*24*). However, it appears that the high power densities necessary to provide uniform and reproducible elemental sensitivities will require double focusing mass spectrometers if reasonably high mass resolution is desired. A notable development of a true laser mass spectrometer microprobe (*23*) is based upon time-of-flight techniques and achieves $1\text{-}\mu m$ spatial resolution. Thin biological specimens are sampled and an absolute sensitivity of 10^{-20} g for Li has been observed.

This development began with the notion of using a miniature dc arc (*25*), initiated by the laser excitation, as a means of extending the analytical usefulness of the laser ion source. However direct laser excitation was technically so much easier than control of a miniature dc arc that initial efforts were concentrated on direct laser excitation. Work with the dc arc will again be studied since it has radically different mass spectral characteristics, some of which are desirable in special analytical situations.

ACKNOWLEDGMENT

The authors thank John Duncanson for advice on directing the laser beam to the solid and Clarence Ness for aiding in the experimental measurements.

LITERATURE CITED

(1) "Microprobe Analysis", C. A. Anderson, Ed., John Wiley and Sons, New York, N.Y., 1973, Chapters 12–15.
(2) B. E. Knox, in "Trace Analysis by Mass Spectrometry", A. J. Ahearn, Ed., Acedemic Press, London, 1972, Chapter 14, pp 423–444.
(3) H. Moenke and L. Moenke-Blankenburg, "Laser Micro-Spectrochemical Analysis", Crane, Russak, and Co., Inc., New York, N.Y., 1973, 261 pp; translated from "Einfuhrung in die Laser-Mikro-Emissionsspectralanalyse", 2. Auflage. Akademische Verlagsgesellschaft Geest and Portig K.-G., Leipzig, 1968.
(4) R. E. Honig and J. R. Woolston, *Appl. Phys. Lett.*, **2**, 138 (1963).
(5) V. Mossotti et al., XV Colloquium Spectroscopicum Internationale, Madrid, Spain, May 1969, "Laser-Assisted Spark Source Mass Spectrographic Trace Analysis of Semiconducting and Nonconducting Materials".
(6) E. Beahm, Thesis, The Pennsylvania State University, University Park, Pa., 1973, "An Investigation of the Laser Source Mass Spectrometer".
(7) R. A. Bingham and P. L. Salter, *Anal. Chem.*, **48**, 1735 (1976).
(8) Y. A. Bykovskii et al., *J. Anal. Chem. USSR*, **31**, 1528 (1976); Original Russian Article, *Zh. Anal. Khim.*, **31**, 2092 (1976).
(9) R. H. Scott et al., *Nature (London)*, **232**, 623 (1971).
(10) V. S. Ban, Thesis, The Pennsylvania State University, University Park, Pa., 1969, "Mass Spectrometric Studies of Laser-Induced Vaporization of Solids".
(11) J. F. Friichtenicht et al., *Rev. Sci. Instrum.*, **47**, 1489 (1976).
(12) J. L. Dumas, Thesis, Universite de Grenoble, Grenoble, France, 1970; "Etude de la Photoionisation des Cibles Metalliques en Vue D'Application a la Spectrometrie de Mass".
(13) K. A. Lincoln and M. A. Covington, *Int. J. Mass Spectrom. Ion Phys.*, **16**, 191 (1975).
(14) J. F. Eloy, *Int. J. Mass Spectrom. Ion Phys.*, **6**, 101 (1971).
(15) D. W. Epstein, *Proc. Inst. Radio Eng.*, **24**, 1095 (1936).
(16) A. Cavard, *Adv. Mass Spectrom.*, **4**, 419 (1968).
(17) J. Franzen and K. D. Schuy, *Z. Naturforsch. A*, **21**, 1479 (1966).
(18) R. J. Conzemius and H. J. Svec, *Talanta*, **20**, 477 (1973).
(19) R. J. Conzemius and H. J. Svec, *Talanta*, **16**, 365 (1969).
(20) B. E. Knox, *Adv. Mass Spectrom.*, **4**, 491 (1968).
(21) J. M. Baldwin, *Appl. Spectrosc.*, **24**, 429 (1970).
(22) G. Brochard and J. F. Eloy, presented at the Twenty-fifth Annual Conference on Mass Spectrometry, Washington, D.C., 1977.
(23) F. Hillenkamp et al., in "Microprobe Analysis as Applied to Cells and Tissues", T. Hall, P. Echlin, and R. Kaufmann, Ed., Academic Press, London, 1974, pp 1–14.
(24) R. J. Conzemius and J. Capellen, to be published.
(25) R. J. Conzemius and H. J. Svec, presented at the Twenty-fourth Annual Conference on Mass J. Spectrometry, San Diego, Calif., 1976.

RECEIVED for review June 7, 1978. Accepted July 28, 1978. Work supported by the U.S. Department of Energy, Office of Basic Energy Sciences, Chemical Sciences Division.

Digital Image Processing in Ion Microscope Analysis: Study of Crystal Structure Effects in Secondary Ion Mass Spectrometry

J. D. Fassett and G. H. Morrison*

Department of Chemistry, Cornell University, Ithaca, New York 14853

Methodology is developed to make multielement, multifeature measurements from secondary ion images by digital image processing. Microfeatures within the image field are identified by thresholding or edge detection. Related images are registered such that ion intensity measurements can be made from comparative regions. Correlations are displayed by the construction of ion ratio images. The methodology is applied to the analysis of polycrystalline iron. The effect of fundamental instrument parameters on the production of intensity contrast from the crystal grain structure is investigated.

Secondary Ion Mass Spectrometry is an extremely powerful analytical technique because of its high elemental sensitivity, its micrometer sampling scale, and its ability to provide compositional morphological information from solid samples (*1*). The ion microscope is a secondary ion mass spectrometer of specialized design (*2*) that is capable of imaging the secondary ions of a particular mass emitted from a region of the surface of a specimen of less than 0.05 mm^2 with one-micrometer point-to-point resolution. Photographic recording of the image results in a spatial analysis of a surface region of a specimen for a single element. A series of ion images spanning differing ion species results in a compositional spatial analysis of the surface of the sample. The power of ion microscopy rests in its ability to simultaneously collect chemical information from a field of a solid sample which may contain a number of component microstructures. The identities and composition of microstructures can be ascertained in an ion microscopic analysis as well as the relationships between microstructures within the image field.

An ion microscopic analysis produces a large amount of multidimensional information, both spatial and elemental. This large amount of information can be only qualitatively assimilated by visual interpretation. Quantitative evaluation of ion images requires the ability to quantitatively evaluate each image picture element and to combine and reduce the sum of image information to its basic components. By means of a microphotodensitometry and digital image processing system that has been previously described (*3*), such quantitative evaluations are now possible.

Digital image processing is now routinely used in satellite reconnaissance, light microscopy, electron microscopy, astronomy, as well as many other fields that produce large amounts of photographic information (*4–6*). In chemistry, digital image processing has been successfully applied to electron density mapping in X-ray crystal structure determinations (*7*). Another recently reported example describes the production and manipulation of images produced by a video fluorimeter where the images display the "excitation–emission matrix" fluorescence spectra of multicomponent samples produced at different excitation energies (*8*). Digital image processing shares many of the characteristics of pattern recogition (*9*), which has been applied to a large number of multivariant problems in analytical chemistry (*10, 11*). The four elements of pattern recognition: display, preprocessing, supervised learning, and unsupervised learning are all contained in image processing methods. Digital image analysis, per se, has yet to be applied to compositional morphological information that is produced by ion microscopy or that can be produced by the related scanning techniques of X-ray microprobe, Auger microprobe, and ion microprobe. Methodology is described in this study that utilizes image processing techniques to handle the chemical information contained within ion micrographs.

Processing methodology in image analysis as developed and applied in other fields is, in general, not directly applicable to the analysis of compositional morphology. A primary concern of image processing with the "quality" of an image where quality is subjectively defined and includes a priori information about the image is only of peripheral interest here. The primary concern with the image processing of the spatial compositional information in ion micrographs is the correlation of structure and composition. Thus, the image analysis methodology is more concerned with the identification of microfeatures within the image field and the absolute measurements of ion intensities of the microfeatures.

As an exemplary demonstration of the image analysis methodology that has been developed, a specific problem is studied: the effect of crystal structure in secondary ion microanalysis. Crystalline effects in ion sputtering have been observed for some time (*12–14*) with ion sputtering also being aptly described as ion etching. Qualitatively, ion images of polycrystalline samples have shown significant intensity contrast between grains (*15, 16*). Studies of single crystals have demonstrated that this contrast effect is due to the relative orientation of a crystal face to the ion beam (*16–19*). Both secondary ionization yield and sputtering yield are dependent upon the relative orientation of a crystal grain. This effect has obvious adverse ramifications for achieving quantitative analysis of polycrystalline material. The amelioration of the effect has been reported by the surface flooding of the sample with oxygen during sputtering (*15–20*).

Ion microscopic imaging of a polycrystalline sample allows the simultaneous observation of differently oriented grains and the effect of experimental conditions on the secondary ion emission from these grains. In this study the experimental conditions varied were relative sample orientation, surface flooding of the sample by oxygen during the analysis, primary ion gas species, and primary ion gas polarity.

Previous studies of crystal effects have been of Cu (*13, 16*), Cr (*20*), Al (*16, 17, 19*), Ge and InSb (*21*), a Cr–Ni alloy (*13*), and a Pt–Rh–W alloy (*22*). This study was made with high purity 5–9 s Fe.

EXPERIMENTAL

Instrumental. A CAMECA IMS-300 Ion Microscope of a design originally developed by Castaing and Slodzian (*2*) and previously described in the literature (*1*) was utilized. The primary ion beam was O_2^+, Ar^+, or O^- with primary ion energy of 5.5, 5.5, and 14.5 keV, respectively. The primary ion current was less than 1.0 μA rastered over a 300 μm × 300 μm area. The instrument vacuum was typically 10^{-7} Torr.

0003-2700/78/0350-1861$01.00/0 © 1978 American Chemical Society

The ion microscope has a field of view of 250 μm or less with a spatial point-to-point resolution of about 1 μm. The image spatial information is simultaneously produced, energy and mass filtered, and simultaneously recorded. Detection is achieved by conversion of the secondary ion image to an equivalent secondary electron image which is recorded on electron-sensitive 35-mm film. This film is normally processed.

Digital Image Processing. The digital imaging system and computer software and hardware have been described previously (*3*). Ion images produced are digitized using a Photomation Mark II scanning microphotodensitometer into 256 × 256 point density arrays. These digital images in optical density space are converted into ion intensity space by the determination of the characteristic curve of the film. All image processing was done on a PDP-11/20 computer and involved manipulations of the 65 536 data points within each image file.

Experimental Procedure. The procedure applied in each experiment was similar. A specific area of the specimen was imaged. The area was randomly chosen and differed from experiment to experiment. The sample was presputtered to remove the immediate surface and polishing artifacts. A series of images was taken, typically spanning several masses of interest, for the experimental parameter varied. In each case the experiment was completed by the imaging of the specimen under the original conditions. Since ion sputtering is a dynamic destructive process, this step ensured the continuity between the initial and final states of the specimen.

RESULTS AND DISCUSSION

Multifeature Measurements. The correlation of structure and composition requires the identification of structures within the image field in order that measurements of ion intensity can be made for those features. Structure, or the presence of microfeatures within the image field, may be determined compositionally from ion microscopy alone, or by alternative microscopic techniques that highlight this structure. Ion microscopy can initiate form and function analyses by the identification of compositional structure or ion microscopy can provide compositional analysis of known structures.

The ability to differentiate a feature prior to ion image analysis represents an example of supervised learning. A feature which is defined by its form and possible function can be specifically ion microscopically analyzed. The identification of the feature or features in the ion micrograph is supervised by the presumptive knowledge about the specimen. The ion images can be correlated with light microscopic or other microscopic images.

The alternative type of feature analysis of ion images is representative of unsupervised learning. Here the features are defined in the ion microscope analysis by the intensity contrast in a single ion micrograph, or by the combination of information from several ion micrographs of a single field region of the specimen. The analysis is nonpresumptive and decisions concerning the form and function of the features can only be made a posteriori the ion microscopic feature analysis. The advantage of the ion microscope relative to the ion microprobe is this ability to make a posteriori analyses through ion imaging since presumptive knowledge in the positioning of the probe is requisite in any probe analysis. A previous study on the characterization of the heterogeneity of microstandards (*15*) illustrates an important application of this type in imaging analysis.

A typical ion microscopic analysis consists of a series of related images from the same area of the surface of the specimen. The identification of the features within the image area field is the first step in the analysis and is done with only the ion images or with the ion images and supplementary information about the region of the sample. A feature map characteristic of the image series is constructed where the feature map is an artificial image in which the features are differentiated and arbitrarily labeled. The characterization

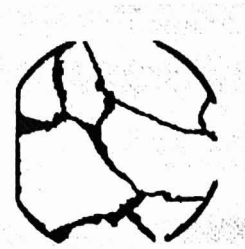


Figure 1. Edge map for image series depicted in Figure 2

of the features in each ion image is accomplished by the registration of the feature map with each image and the analysis of corresponding regions.

The method of construction of the feature map and identification of the features is dependent upon the nature of the field-feature interaction. Intensity, shape, size, and contiguity are all programmable characteristics which may be used to identify and define features. The most trivial case of feature analysis consists of a simple background-foreground thresholding decision, where features are dispersed within a homogeneous background phase. The identification of inclusions within steel is readily accomplished by this method (*23*). The delineation of the ion image within the digital image file is also simply accomplished by this method.

A more complex method is required for homogeneous features that do not have a constant background. The differentiation of the crystal grains, the features of interest in the analysis of polycrystalline iron, is an example of this case. The crystal grains can be bounded by grains of lesser, greater, or equal intensity. The method developed to differentiate the grains, identified the grain boundary regions, or edge regions, which surrounded each grain. The grain boundary regions are characterized both as regions of changing intensity between two grains and as regions of topographical enhancements. The features were identified as the contiguous regions defined by the determined grain boundaries.

The determination of the grain boundaries is accomplished by the application of a particular image analysis edge detection routine (*24*) on one of the images in the series. Edge detection is a well studied problem in image processing (*25*) and the routine used is but one example. The method involves the convolution of an image with a series of compass gradient masks which perform a two-dimensional discrete differentiation of the image. For each point within the image, the direction (within the eight compass directions) and magnitude of maximum change are determined. A point is defined as an edge point if it satisfies both gradient thresholding and connectivity criteria. The connectivity criterion limits edge points to those with at least two neighboring, directionally related edge points. The thresholding criterion requires a minimum magnitude gradient to be surpassed for a point to be defined as an edge point. The gradient threshold is established by the experimenter who strives to produce the most proper edge point image. The result of edge detection is the construction of a bit map which defined each point in the original image as an edge point or not.

In this particular study, the image used to produce the edge map was chosen as the one with the most obvious contrast. The digital image was smoothed prior to edge processing by two-dimensional box-car averaging. The edge map produced was also smoothed by the rejection of noncontiguous edge regions. Figure 1 illustrates the edge map produced for the

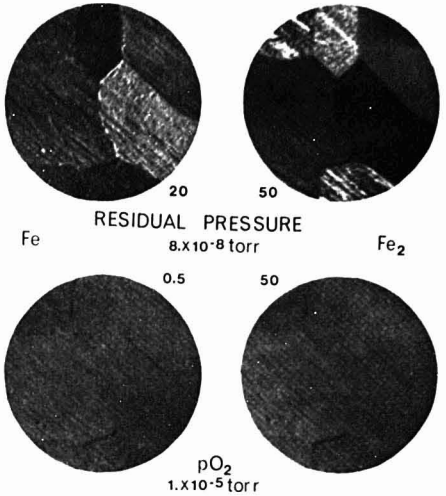


Figure 2. Effect of leaking oxygen into sputtering chamber on $^{56}Fe^+$ and $^{112}[Fe_2]^+$ ion images. Pressures represent no leak and maximum practical leak conditions. Times of exposure are denoted in seconds

image series displayed in Figure 2.

The actual feature map is constructed from the edge map by the identification and labeling of the contiguous non-edge regions. If the grain boundary regions were identified as the feature of interest, the edge map would suffice as the feature map.

Registration. The comparison of the ion images with the feature map or with each other requires registration or correlation of the image fields. There are three aspects of the registration problem: (1) registration of images taken of the same area of the sample, (2) registration of images taken after movement or reorientation of the sample, and (3) registration of images of the same area of the sample taken at different magnifications. All three registration problems were encountered in this study.

The registration of images taken of the same area of the sample is required because the images can be expected to be slightly translationally offset relative to each other within the image file because of the manual positioning of the microphotodensitometer during acquisition. This offset is calculated by the determination of the centers of the circular ion images within the square image files. These centers define coincident points for the images.

If the sample is moved, the centers of the ion image fields within the square image files will not define coincident points. Coincident regions between images can be rotationally offset as well as translationally offset within the circular image field. One experiment done in this study investigated the effect of orientation of a polycrystalline region of the iron specimen relative to the primary beam. To compare these images before and after rotation required the determination of both the rotational and translational offset.

The rotational and translational offsets can be analytically determined by applying the cross-correlation function to similar images (*3, 26*). Accurate determination of offsets can be accomplished by cross-correlating multiple subsections of one image with subsections of the other image. Each cross-correlation is an iterative routine that converges to the region with the best correlation. Convergence requires that

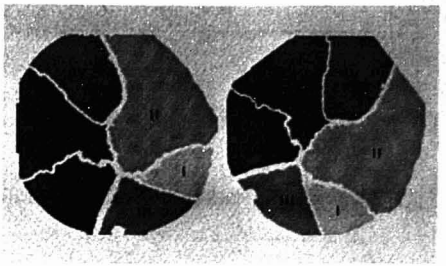


Figure 3. Feature maps for image series in Figure 4: unrotated and rotated files. Density is scaled lightest to darkest for features which are arbitrarily labeled 1 to 6

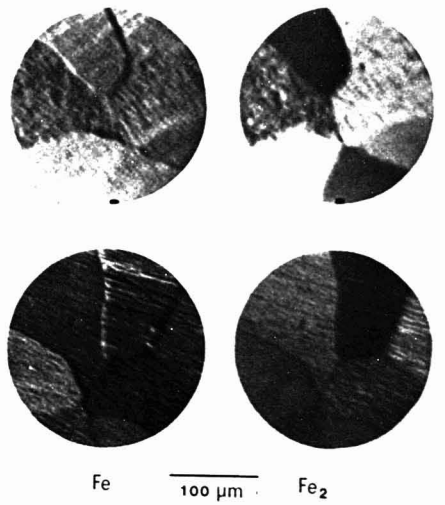


Figure 4. $^{56}Fe^+$ and $^{112}[Fe_2]^+$ ion images at two orientations: top is orientation I, bottom is orientation II. Times of exposure: $^{56}Fe^+$, 20 s; $^{112}[Fe_2]^+$, 50 s

the initial estimate for the offset of the two regions be within a minimum distance of the actual offset. The result of each cross-correlation is two coordinate pairs: the coordinate pair of the best matching subsection in one image and the coordinate pair of the reference subsection of the second image being matched. Determination of the translational and rotational vectors to orient the two images can be done by an iterative least-squares routine utilizing the coordinate pairs of the multiple cross-correlations.

In actual practice, this method of determining the rotational and translational offsets is extremely time consuming and requires a relatively accurate initial input of the offsets. Thus, for the experimental images in this study, the offsets were determined by the overlaying of transparencies of contour maps of the related images and measurement with protractor and ruler.

Once the rotational and translational offsets are known, registration is achieved by transposing one image data file relative to the other data file by the proper rotational offset, creating a rotated image file. This step is necessary because of the structure of the image data file as records, each con-

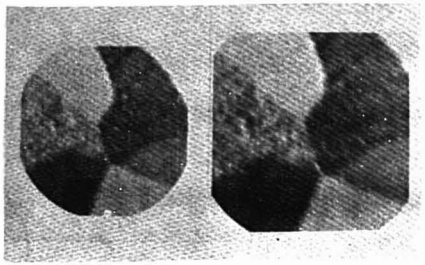


Figure 5. Image data file demagnified (0.85X) and magnified (1.15X): file sizes 256 × 256; negative contrast. Original image data file is of the $^{112}[Fe_2]^+$ image in Figure 4. The digitized image data are scaled from an ion intensity of 0.5 (darkest output) to an ion intensity of 0.1 (lightest output)

taining a line of data. Translational offset does not require this step because the offset can be made without crossing record line boundaries. Figure 3 illustrates the effect of rotation on the feature map file or the image series of Figure 4.

The third type of registration problem results from a change in magnification in the microscopy of an area of the sample. In a typical ion image analysis, the microscopic conditions are not changed and this problem does not occur. However, if correlation is desired with light or electron micrographs, such a registration problem will be bound to occur. In this study, the microscopic conditions were changed in one ion imaging experiment which resulted in a change of magnification for a particular region of the sample. A region of the polycrystalline iron was imaged using both positive and negative primary ion beam while collecting positive secondary ions. For the CAMECA instrument, a change in magnification results from the switch in polarity of the primary ions.

Magnification of an image file is accomplished by eliminating edge points and expanding the information in the remaining points. Thus, one picture element is expanded into M^2 picture elements, where M is the magnification factor. The amount of information lost from the original image file is $(1 - 1/M^2)$. Demagnification of an image file is accomplished by contracting the information in the original file and adding background edge points. Potential information is lost in the contraction process by the loss of point-to-point resolution. Figure 5 illustrates the result of magnification and demagnification of the Fe_2^+ image in Figure 4.

Feature Analysis. Once a feature is identified, relevant descriptors of that feature are calculable. The most important descriptor in ion image analysis is average feature intensity and this descriptor is calculated by the determination of the integrated intensity and integrated area for the feature. There exist other descriptors of features that are potentially useful in certain analyses, such as shape and form descriptors, gradient descriptors, and noise or texture descriptors. These descriptors, once software defined, can be calculated in a feature analysis.

A second aspect of feature analysis is field analysis which explores the interrelationships between features in the image field. Automatic image analysis is both a commercially and scientifically established field that has developed its own mathematical and statistical measures for evaluating microstructures in microscopic fields (*27, 28*). These measures are also derivable from ion micrographs with the inclusion of the appropriate software procedures.

Image Ratioing. The visual display of correlation or noncorrelation between similar images is possible by the creation of artificial ratio images where each data point in one



Figure 6. Ratioed image data files, different ion images of the same sample area: (left) $^{72}[FeO]^+/^{56}Fe^+$, scaled from 0.03 (darkest output) to 0.01 (lightest output); (right) $^{112}[Fe_2]^+/^{56}Fe^+$ scaled from 0.5 (darkest output) to 0.1 (lightest output). $^{56}Fe^+$ and $^{112}[Fe_2]^+$ images are pictured in Figure 4; $^{72}[FeO]^+$ image is also in this series

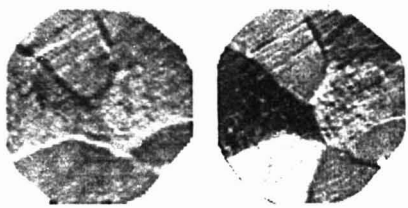


Figure 7. Ratioed image data files, same ion image at two different orientations: (left) $^{56}Fe^+/^{56}Fe^+$; (right) $^{112}[Fe_2]^+/^{112}[Fe_2]^+$. Images are pictured in Figure 4; ratioed images are of orientation II divided by orientation I, scaled from 1.5 (darkest output) to 0.5 (lightest output)

image is ratioed to a corresponding data point in a second image. If the two images have strong correlation, the amount of displayed contrast will be reduced; for noncorrelation, the amount of contrast will be increased. Contrast caused by topographical enhancements can be markedly reduced in the ratioing of correlated ion micrographs. Illustrative examples are shown of the polycrystalline iron experiments in Figures 6 and 7.

The display output of digital image files, whether primary data files or artificially constructed data files, is by means of an electrostatic plotter (Model 900A, Versatec) programmed to display half-tone images, 256 × 256 in 16 gray levels, or 128 × 128 in 64 gray levels. This display mode allows the immediate display of the results and immediate feedback for the optimization of any image processing routine.

POLYCRYSTALLINE IRON IMAGING

Elemental Correlations. A series of ion images was taken which spanned the major secondary positive ion species produced from a particular area of the surface of the iron specimen at two orientations relative to a positive oxygen primary beam. This experiment investigated the effect of both ion species and orientation on the ion intensity contrast produced from the randomly oriented crystal grains in the field of view. The images of $^{56}Fe^+$ and $^{112}[Fe_2]^+$ at the two different orientations are pictured in Figure 4. The feature map derived for this series of images is in Figure 3 and Table I summarizes the results of the feature analysis.

The correlation of molecular ion species' images with the elemental iron ion image indicates that correlation exists between $^{56}Fe^+$ and $^{72}[FeO]^+$ images and between $^{112}[Fe_2]^+$ and

Table I. Feature Mass Analysis

feature mass	exp. (s)	orientation	intensities I	II	III	IV	V	VI
^{16}O	300	I	0.68	0.52	0.82	0.39	0.67	0.85
^{56}Fe	20	I	94.	78.	120.	96.	78.	130.
		II	105.	86.	118.	96.	96.	147.
$^{72}[FeO]$	200	I	1.8	1.8	2.1	1.7	1.7	2.6
		II	1.6	1.6	1.8	1.7	1.7	1.8
$^{112}[Fe_2]$	50	I	30.	34.	21.	14.	21.	47.
		II	24.	29.	19.	14.	33.	27.
$^{128}[Fe_2O]$	50	I	17.	16.	15.	9.0	12.	26.
		II	9.9	12.	9.3	7.7	15.	12.

Characteristic curve: $Dc = 0.896 + 1.033\ (t \cdot I/100)$. $I(Fe_{av}) = 1.00$.

$^{128}[Fe_2O]^+$ but there is anomalous noncorrelation between monomer and dimer iron images. This anomalous behavior is contrary to published results for aluminum and copper sputtered with an Ar^+ primary beam where atomic and diatomic species correlate closely (*16*). If the ion intensities of the iron image are examined in light of the qualitative sputtering yield information available from topography in the image, it is seen that the ion intensity is inversely related to sputtering yield. This result is in agreement with the analyses of Bernheim and Slodzian (*29*) who maintain that the ionization yields under oxygen bombardment depend mainly on the chemical effect induced by the oxygen concentration built up in the sample by the implantation of the bombarding ions. Since the higher is the sputtering yield, the lower is the implanted oxygen concentration, and the lower is the ion intensity. Thus, the anomalous lack of correlation between $^{56}Fe^+$ and $^{112}[Fe_2]^+$ images is explainable by the differences in ionization mechanisms: Fe^+ emission is controlled by the chemical effect, Fe_2^+ emission is not. The variations in the measured Fe_2^+ intensities are closely related to the variations in sputtering yields. Visual display of ratioing the $^{72}[FeO]^+$ and $^{112}[Fe_2]^+$ images to the $^{56}Fe^+$ image, examples of correlation and noncorrelation, respectively, is illustrated in Figure 6.

The second part of the experiment investigating the effect of rotating the sample and thus reorienting the randomly oriented grains relative to the primary beam caused little effect on the relative contrast on the $^{56}Fe^+$ image. However, the $^{112}[Fe_2]^+$ image at one orientation did not correlate with the $^{112}[Fe_2]^+$ image at the second orientation. Visual display of the results of this orientation change is illustrated by $^{56}Fe^+$ and $^{112}[Fe_2]^+$ ratioed images in Figure 7.

Oxygen Flooding. Oxygen flooding has been shown to reduce or eliminate the contrast produced by crystalline samples (*15–20*). It has been hypothesized that the oxygen produces an amorphous compound on the surface while sputtering is taking place (*17*). To investigate the effect of oxygen flooding on the relative contrast in a polycrystalline specimen, a series of images of $^{56}Fe^+$ and $^{112}[Fe_2]^+$ was taken at different partial pressures of oxygen leaked into the sputtering chamber. Representative images obtained at a residual pressure in the sputtering chamber 8×10^{-8} Torr, and at 1×10^{-5} Torr of oxygen in the sputtering chamber are illustrated in Figure 2.

The relative effect of differing oxygen pressures on two representative crystal grains is graphically presented in Figure 8. Qualitatively the variation of secondary ion intensities for both $^{56}Fe^+$ and $^{112}[Fe_2]^+$ is in good agreement with the results of MacDonald and Martin (*20*) and Benninghoven and Muller (*30*) who studied Cr. The reduction in contrast is more rapid for the $^{56}Fe^+$ signal relative to the $^{112}[Fe_2]^+$ signal, again indicative of the importance of the chemical effect on Fe^+ ionization. The reduction and homogenization of the Fe_2^+

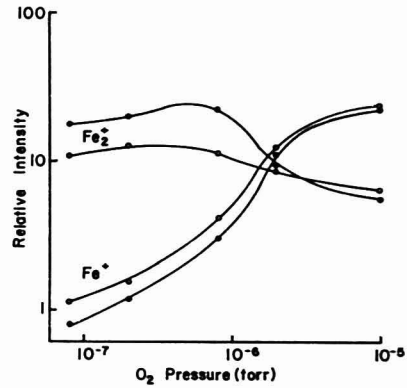


Figure 8. Effect of leaking oxygen into sputtering chamber on the measured intensities from two of the crystal grains in the image field of Figure 2. Partial display of information extracted from the image series by digital image processing. Grains are located at 12 o'clock (●) and 9 o'clock (○). Actual ratio of intensity scales for $^{56}Fe^+$ to $^{112}[Fe_2]^+$ is 100 to 1

intensities presumably parallels the reduction and homogenization of the sputtering yields from the different grains (*17*).

Other Experiments. Experiments were also done investigating the polycrystalline contrast produced by a positive argon primary beam, with and without the oxygen leak, and investigating the relative effect primary ion beam polarity has on the analysis. With argon bombardment, the Fe^+ and Fe_2^+ intensities were well correlated, in agreement with the previous discussion and the results of Bernheim (*16*). The effect of the oxygen leak was qualitatively similar to the effect of the oxygen leak with an oxygen primary beam, although less severe at similar pressures.

Changing the polarity of the primary ion beam results in a change in the angle of incidence and energy of the primary ion beam at the surface of the specimen (positive primary-positive secondary: 72° and 4.5 keV; negative primary-positive secondary: 36° and 14.5 keV). For the CAMECA instrument, the predominant nature of the primary oxygen beam also changes from the dimer ion in the positive mode to the monomer ion in the negative mode. Bernheim has investigated the effect of changing the angle of incidence and energy of a primary argon ion beam without changing the polarity and observed large modifications in the contrast (*16*). This observation was verified in this experiment. The polycrystalline contrast produced in the negative primary-positive secondary ion images was less severe than in the positive primary-positive

secondary ion images. The relative contrast of the images produced in the two modes showed poor correlation, as expected.

CONCLUSIONS

The application of digital image analysis to the specific problem of the effect of crystal structure in secondary ion microanalysis is presented in this study. Although this problem has been approached before, ion microscopy provides a unique dimension in its elucidation and interpretation. The simultaneous analysis of a field of microfeatures by means of image processing allows the important comparison of relative effects of experimental conditions on secondary ion yields. Since the goal of ion microscopy is the chemical analysis of unknown microstructures, the elucidation and eventual control of experimental parameters and their effect on image fields are prerequisite.

The methodology developed in this study to handle ion images is primarily concerned with identification of features and the quantitative manipulation of related microscopic images. The broader role of digital image processing in the combination and display of information from related images was of secondary concern. The production of artificial or amended images is potentially extremely valuable in summarizing image information and displaying elemental interrelationships. The potential correction of image ion intensities by calibrating localized image field sputtering conditions through the use of matrix species ion images is also promising, having been successfully applied in microprobe analysis (*31*).

The general applicability of digital image analysis of morphological compositional information to other imaging techniques as well as to the wide range of structure-composition problems in biology, geology, and metallurgy is obvious. Features such as grain boundaries, inclusions, interfaces, mineral phases, and biological structures such as cell walls or organelles are all candidates for feature analysis. Investigations are presently underway in several of these areas.

LITERATURE CITED

(1) G. H. Morrison and G. Slodzian, *Anal. Chem.*, **47**, 932A (1975).
(2) R. Castaing and G. Slodzian, *J. Microsc. (Paris)*, **1**, 395 (1962).
(3) J. D. Fassett, J. R. Roth, and G. H. Morrison, *Anal. Chem.*, **49**, 2322 (1977).
(4) N. M. Short, P. D. Lowman, Jr., S. C. Freden, and W. A. Finch, Jr., "Mission to Earth: Landsat Views the World", NASA, Washington, D.C., 1976.
(5) R. C. Gonzalez and P. Wintz, "Digital Image Processing", Addison-Wesley, Reading, Mass., 1977.
(6) A. Rosenfeld, Ed., "Digital Picture Analysis", Springer-Verlag, New York, N.Y., 1976.
(7) N. Xuong and S. T. Freer, *Acta. Crystallogr., Sect. B*, **27**, 2380, (1971).
(8) B. W. Johnson, J. B. Callis, and G. D. Christian, *Anal. Chem.*, **49**, 747A (1977).
(9) R. O. Duda and P. E. Hart, "Pattern Classification and Scene Analysis", Wiley-Interscience, New York, N.Y., 1973.
(10) B. R. Kowalsky, *Anal. Chem.*, **47**, 1152A (1975).
(11) P. S. Schoenfeld and J. R. DeVoe, *Anal. Chem.*, **48**, 403R (1976).
(12) G. D. Magnusson and C. E. Carlston, *J. Appl. Phys.*, **34**, 3267 (1963).
(13) J. M. Fluit, P. K. Roll, and J. Kistemaker, *J. Appl. Phys.*, **34**, 690 (1963).
(14) D. Onderdelinden, *Appl. Phys. Lett.*, **8**, 189 (1966).
(15) G. J. Scilla and G. H. Morrison, *Anal. Chem.*, **49**, 1529 (1977).
(16) M. Bernheim, *Radiat. Eff.*, **18**, 231 (1973).
(17) M. Bernheim, G. Slodzian, *Int. J. Mass Spectrom. Ion Physics*, **12**, 93 (1973).
(18) M. Bernheim and G. Slodzian, *Surf. Sci.*, **40**, 169 (1973).
(19) P. J. Martin and R. J. MacDonald, *Radiat. Eff.*, **32**, 177 (1977).
(20) R. J. MacDonald and P. J. Martin, *Surf. Sci.*, **67**, 237 (1977).
(21) E. Zwangobani and R. J. MacDonald, *Radiat. Eff.*, **20**, 81 (1973).
(22) W. H. Christie, D. H. Smith, R. E. Eby, and J. A. Carter, *Am. Lab.*, **10**, 19 (1978).
(23) D. M. Drummer, J. D. Fassett, and G. H. Morrison, *Anal. Chim. Acta*, in press.
(24) G. S. Robinson, *Comp. Graph. Image Proc.*, **6**, 492 (1977).
(25) L. S. Davis, *Comp. Graph. Image Proc.*, **4**, 248 (1975).
(26) K. B. Welles, Ph.D. Thesis, Cornell University, Ithaca, N.Y., 1976.
(27) S. Nazaré and G. Ondracek, *Microscope*, **22**, 39 (1974).
(28) E. E. Underwood, *Microscope*, **22**, 69 (1974).
(29) M. Bernheim and G. Slodzian, *Int. J. Mass Spectrom. Ion Phys.*, **20**, 295 (1976).
(30) A. Benninghoven and A. Muller, *Surf. Sci.*, **39**, 416 (1975).
(31) J. D. Ganjei, D. P. Leta, and G. H. Morrison, *Anal. Chem.*, **50**, 285 (1978).

RECEIVED for review May 16, 1978. Accepted August 14, 1978. Financial support provided by the National Science Foundation under Grant No. CHE77-04405 and through the Cornell Materials Science Center, and the National Institutes of Health under Grant No. GM24314-01.

Spark Source Mass Spectrometric Procedure Employing Stable Isotopes to Study the Uptake of Copper by Fish from Seawater and Food

B. R. Harvey

MAFF, Fisheries Radiobiological Laboratory, Hamilton Dock, Lowestoft NR32 1DA, U.K.

Because of the lack of suitable radioisotopes, the use of electromagnetically enriched stable isotopes as a means of studying the uptake of copper by fish (plaice) has been investigated. ^{65}Cu (99.81% enriched) was chosen for the tracer, while the other stable isotope ^{63}Cu (99.88% enriched) was used as a standard spike in the spark source mass spectrometric analysis. An attractive feature of this method is that both the natural copper content of the fish organs and the concentration of added tracer are determined on the same sample by making two measurements of isotopic ratio—one before and one after the addition of the standard spike. The sensitivity of the analysis is such that all but the very smallest organs of a 30-g (wet) plaice (e.g., heart, kidney, spleen) may be analyzed individually for both natural copper and the absorbed tracer. A low processing blank was achieved by the use of quartz apparatus and clean room conditions.

Our knowledge of the fate of many elements during the metabolic processes of living organisms has been greatly enhanced in recent years as a result of the ready availability of suitable radioactive tracers (*1*). There are, however, some important gaps in this study where suitable radioisotopes do not exist or are prohibitively expensive to manufacture. One such element is copper which is toxicologically important for many species of fish; unfortunately the readily available ^{64}Cu ($t_{1/2}$ = 12.8 h) decays too rapidly for convenient use, while ^{67}Cu ($t_{1/2}$ = 61.6 h) is less readily available, rather expensive, and still too short-lived for lengthy experiments.

Both stable isotopes of copper are however available in a highly enriched state (>99.8%, for example from AERE, Harwell, England) and these isotopes constitute ideal tracers in many ways, being readily available at low cost as well as being free from radiation hazards of any kind. In order to

0003-2700/78/0350-1866$01.00/0 © 1978 American Chemical Society

make use of such stable isotopes, a comparatively expensive analytical instrument, capable of providing the isotopic analysis, is required and this may present problems if access to a mass spectrometer designed specifically for isotopic ratios is not available. The present work shows how the procedure can be arranged so that a spark source mass spectrometer (SSMS) may be used to provide the necessary isotopic ratio measurements. Leipziger (2) demonstrated the possibility of using SSMS for isotope dilution analysis by determining copper in a nickel oxide matrix while Bingham and Vossen (3) demonstrated the use of the modern equivalent of the instrument used by Leipziger (Associated Electrical Industries MS702R) to measure the isotopic abundances of neodymium in a 1-μg sample of Nd_2O_3. This instrument has electrical detection equipment which greatly facilitates isotopic ratio measurements. More recently Jaworski and Morrison (4) have demonstrated the potential of solid state isotope dilution SSMS using graphite spiked with suitable stable isotopes to provide the internal standards for the solid source. This procedure appeared to offer adequate sensitivity and precision for the proposed copper uptake experiments, and preliminary experiments confirmed this view.

One important advantage of the stable isotope technique for elements such as copper, having more than one stable isotope (a long-lived radioactive isotope may also be used), is that the concentration of the element occurring naturally in the organism may be determined simultaneously with the added tracer on the same portion of sample. This is achieved by a double ratio measurement technique; one isotope (^{65}Cu in the present case) is used as the tracer for the uptake experiment while the other (^{63}Cu in the present case) is used as internal standard (hereafter called the standard spike) for the mass spectrometric analysis. The naturally-occurring isotopic abundance of the two copper isotopes occurring in the fish tissues must be known, and then two ratio measurements are made on copper extracted from the experimental samples: one before and one after the addition of a known amount of the standard spike. From the three ratios and a knowledge of the amount of spike added, it is possible to calculate both the amount of naturally-occurring copper present and the excess ^{65}Cu (which is a measure of the tracer taken up by the fish during the experiment).

The basic sensitivity of the technique is high making it possible to determine the copper content of many individual body organs from a 30-g (wet) plaice. However, the copper must first be separated from the biological matrix and the high sensitivity can only be utilized if contamination during processing is strictly controlled. In the present work, use has been made of low temperature ashing (LTA), quartz apparatus, and clean room conditions to reduce the processing blank down to about 10 ng per sample. This was sufficiently low to enable all but the very smallest organs to be studied individually. In the case of these small organs, e.g., spleen, heart, kidney, bulking from about four fish provided sufficient copper for satisfactory measurements.

EXPERIMENTAL

The analytical procedures were developed for studying the uptake of copper by plaice (*Pleuronectes platessa*) of about 30-g wet weight. Uptake of ^{65}Cu from water was investigated for periods in excess of two months in one set of experiments and uptake from food was studied by feeding the fish with gelatine pellets containing ^{65}Cu in other experiments. The detailed results and biological significance of these experiments will be reported elsewhere (5).

Extraction of Cu from Seawater Samples. In the experiments to study the uptake of copper from water, the plaice were kept in 1500-L polythene tanks of seawater to which had been added ^{65}Cu as simple cupric ions. The natural level of copper in the seawater was about 2 $\mu g\ L^{-1}$ to which was added about 8 $\mu g\ L^{-1}$ of ^{65}Cu. The water was changed at approximately 3-day intervals and analysis for both natural and tracer copper was carried out at the beginning and end of each batch although very little loss of copper was observed in the 3-day period.

Samples of the seawater, 500 mL, were acidified to pH 2 ± 0.2 by adding about 1 mL redistilled 6 M HCl. The samples were filtered through 0.45-μm membrane filters to prevent the formation of emulsions with the organic extractant, and the copper was then extracted as a primary dithizonate by mixing the sample vigorously with 10 mL of a 30 $\mu g\ mL^{-1}$ solution of dithizone in chloroform for 15 min. This extraction was carried out in a 1-L separating funnel fitted with a glass and Teflon stirrer and a Teflon tap. After running off the chloroform layer, a further 5 mL of the dithizone solution was added and the extraction repeated. The two extracts were then combined in a 100-mL separating funnel and washed with 2 × 2 mL distilled water to remove traces of salt. The copper was then back-extracted into aqueous solution by shaking with 5 mL 6 M HCl; this was finally washed with 2 mL chloroform to remove the last traces of dithizone.

In order to carry out the isotopic ratio analysis on the MS702R, the sample had to be converted into the form of electrically-conducting electrodes and this was achieved by evaporating the acid back-extract on to high purity graphite of very small particle size (Ultra Carbon IM USP). This graphite was found to display an extremely low background count at the mass lines required for the copper analysis. The 5 mL of acid extract was therefore evaporated onto 0.4 g of the graphite and subsequently mixed with the aid of a little redistilled methanol as a lubricant to ensure the best possible homogenization before preparing the first pair of electrodes. The portion of graphite remaining after preparing the first pair of electrodes was then weighed (0.2 g approximately) and, after spiking with a known amount of ^{63}Cu, the mixing process with methanol was repeated. Drying at 110 °C was carried out as before, and finally the second pair of electrodes was made. Then the isotopic ratio for each pair of electrodes was determined (see below under Mass Spectometric Analysis).

Extraction of Copper from Biological Materials. The low concentration of Cu found in most fish organs precluded the use of direct analysis even on the ash residue. Thus it was decided to extract Cu as a primary dithizonate in a manner similar to that used for water samples. The principal differences between the extraction for biological tissue and that for water samples lay in the relative amounts of Cu available for analysis; with organs weighing as little as 30 mg wet, the processing blank becomes very significant and great care was necessary to avoid contaminating the sample during the analysis.

As the fish were dissected, the organs (or representative part thereof in the case of muscle, skin, etc.) were transferred directly to a previously cleaned and weighed quartz boat (100 × 20 × 10 mm). Cleaning procedures are discussed under Processing Blank. After weighing to obtain the wet weight of the sample, moisture was removed by vacuum freeze drying (Edwards High Vacuum model 30 P1T). The quartz boats containing the dried sample were then transferred to a low temperature asher (Tracerlab LTA 600) to destroy the organic matrix prior to the extraction stage. Problems arising from the buildup of static electrical charges on the boats during the ashing process were overcome by using a peizo-electric pistol (Zerostat) to neutralize the charge when the boats were removed from the asher.

To each boat was then added 3 mL of 0.5 M HCl which had been redistilled and stored in quartz vessels plus 3 drops (about 0.2 mL) of 30% hydrogen peroxide (analytical grade). The mixture was warmed on a ceramic-topped hot-plate to dissolve out the Cu and then transferred quantitatively to a 100-mL quartz separating funnel (fitted with a Teflon tap) with the aid of high purity distilled water. After adjusting the volume to 35 mL, 1 mL of 0.5 M ascorbic acid was added to destroy the residual peroxide and the solution (now at pH 1.5–1.8) was extracted with 5 mL of 15 $\mu g\ mL^{-1}$ dithizone in carbon tetrachloride. This solvent was chosen for the biological samples because of the more favorable partition coefficient of the Cu-dithizonate between carbon tetrachloride and water; this helped to reduce the quantities of reagents used and, hence, the blank.

At first the Cu was back-extracted from the carbon tetrachloride into 2 mL 6 M hydrochloric acid prior to evaporating onto

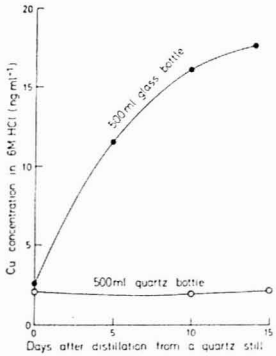


Figure 1. The difference between quartz and borosilicate glass

graphite, but it was subsequently found that the presence of the organic compounds did not produce interfering lines in the mass spectrum. The back-extraction was therefore discontinued for biological samples with a resultant improvement in the blank reading; the dithizone extract was evaporated directly onto 40 mg of graphite, 10 mg being used to form the tip of each electrode. Spiking with the standard ^{63}Cu solution was carried out as for the water samples using half the sample as before.

Processing Blank. When working at sub-microgram levels, the success of an analytical procedure of this type is heavily dependent on the establishment of a low and constant blank. Copper is an almost universal contaminant at such levels and the strictest precautions are necessary to eliminate unwanted input of the metal from apparatus chemicals and the laboratory atmosphere.

Particulate contamination from atmospheric dust was virtually eliminated by carrying out all the chemical processing in a "Microflow" environmental work station. Samples processed in this way showed steady blanks on the mass spectrometer whereas blanks processed using the same reagents and apparatus in an ordinary laboratory atmosphere showed erratic high readings, suggesting the entrainment of dust particles into the graphite matrix during processing.

Probably the major source of copper contamination came from container walls. Despite vigorous acid cleaning, it was found that borosilicate glass continued to release copper into the sample even after months of continual use. Plastic containers, though better in this respect, are unsuitable for use in the LTA and for separating funnels, so quartz was investigated. After an initial cleaning by alternately soaking for 24 h in 6 M HCl followed by treatment with dithizone/CCl_4 several times, quartz was found to be suitable for use in all the apparatus, yielding almost no copper into the sample even after prolonged contact. The difference between quartz and borosilicate glass is well illustrated in Figure 1. HCl (6M) was distilled from an all quartz distillation unit and collected into (a) a 500-mL clear glass bottle of a type used for proprietary brands of high quality HCl, (b) a 500-mL quartz flask. Both containers were capped with a polythene film and samples were withdrawn at intervals for analysis. It can be seen that levels of Cu in the quartz flask remained constant while those in the glass bottle increased with time. This experiment was repeated several times with the same result. Glass separating funnels were found to contribute Cu to the blank in a decreasing fashion over several weeks of constant usage in the extraction process; quartz separating funnels were found to clean up much more quickly and more thoroughly and were therefore preferred for this work.

Reagents were cleaned by distillation from quartz where possible. Distilled water was produced by a deionized feed, all quartz still and the dithizone was purified by dissolving in ammoniacal solution followed by reprecipitation with acid and drying in a vacuum desiccator.

Table I. Cu Levels in Various Materials and Reagents

material	copper concn, ng g^{-1} or ng mL^{-1}
graphite (ultra carbon IMUSP)	25
6 M HCl, quartz distilled	2
distilled water	0.1
methanol (redistilled)	0.1
dithizone solution in CCl_4 (15 μg mL^{-1})	0.2
polythene film ("Clingfilm")	100
absorbent paper tissues ("Kleenex")	630

Table I gives details of the Cu levels found in the reagents used and some of the other materials employed during processing.

Mass Spectrometric Analysis. Isotopic ratio determinations were carried out using an MS702R spark source mass spectrometer with electrical detection in the peak switching mode (Kratos Associated Electrical Industries). Integrated readings for each of the two peaks were recorded alternately using a Fluke 8300A digital volt-meter. Ten measurements corresponding to a monitor/integrator reading of 0.03 nanocoulomb were obtained for each peak giving a convenient periodicity to the measurements and a total time of about 10–15 min for the assessment of each sample.

Electrodes held in spring-loaded, tantalum holders (for rapid assembly) were loaded into the source at 5 mm from the No. 1 slit, and aligned on the ion axis using a simple optical alignment jig. A spark gap monitor (6) was used to hold the gap between the electrodes constant during sparking; once set up, this device can be used to bring each new pair of electrodes together and subsequently hold the required gap without re-setting for long periods of time, thus simplifying both the setting-up and the operation of the instrument.

The enriched stable isotopes were obtained as copper metal, each being supplied with a certificate of batch analysis. Standard solutions of each of the two separate isotopes were prepared by dissolving weighed quantities of the metal in nitric acid and making up to standard volume in 0.2 M HNO_3. Working dilutions were then prepared regularly from the stock solutions (approximately 200 μg mL^{-1}).

The analytical performance of the mass spectrometer was determined by preparing a range of artificial mixtures of the two isotopes mixed with the graphite powder. In addition to this, samples were prepared containing analytical grade $CuCl_2 \cdot 2H_2O$; the abundance of the two isotopes in commercially processed copper is substantially constant (7) and this material therefore provided a useful reference. Electrodes were also prepared from the pure graphite (Ultra Carbon IM-USP) to establish whether the graphite would cause any bias to the readings and if so at what level. The results of this study are given in Table II. The concentration of total copper in each of the mixtures with graphite was approximately 100 μg g^{-1} and each determination represents about 15 min total sparking, each peak being integrated for about 30 s at a time. The precision with which the ratio can be determined by this procedure is in all cases (except the graphite blank) better than ±5% 1σ. The instrument appears to favor the lighter isotope and for the calculations a mean instrumental bias factor was taken as the mean of all the experimental measurements. It could be argued that the bias obtained from the natural copper measurements would have been more accurate but it was felt that this could not be justified even though there does appear to be a shift in the bias from one end of the range to the other for the artificial mixtures. In the absence of another mass spectrometer for comparative analysis, this trend is thought to be due to slight inaccuracies in the isotopic standards which show up as a trend when mixed together in a sequence such as this.

Three separate isotopic ratio measurements are required in order to establish both the level of natural copper occurring in the fish tissue and the amount of ^{65}Cu taken up during the experiments (Figure 2). As expected, the isotopic composition of copper extracted from fish tissue was not significantly different

Table II. Isotopic Ratio Measurement on Standard Mixtures of ^{63}Cu and ^{65}Cu in Graphite

	sample composition (atomic)						
determination no.	$\frac{^{63}Cu}{^{65}Cu} \approx \frac{4}{1}$	$\frac{^{63}Cu}{^{65}Cu} \approx \frac{2.5}{1}$	$\frac{^{63}Cu}{^{65}Cu} \approx \frac{1}{1}$	$\frac{^{63}Cu}{^{65}Cu} \approx \frac{1}{2.5}$	$\frac{^{63}Cu}{^{65}Cu} \approx \frac{1}{4}$	natural copper	graphite blank
1	4.0942	2.4063	1.0156	0.4624	0.2838	2.2981	2.2240
2	3.8484	2.4206	1.0591	0.4010	0.2555	2.3507	2.6511
3	3.8456	2.4204	1.0167	0.4307	0.2721	2.3408	2.1343
4	3.9112	2.3957	1.0230	0.4450	0.2871	2.2290	2.5731
5	3.7952	2.5286	1.0301	0.4390	0.2757	2.2440	2.5485
6	3.8147	2.4579	1.0163	0.4141	0.2736	2.2689	2.5862
7	3.9609	2.4245	1.0386	0.4176	0.2638	2.4304	2.4289
8	3.8775	2.4710	1.0007	0.4386	0.2655	2.2566	2.0091
mean ratio $\frac{^{63}Cu}{^{65}Cu}$	3.8935	2.4406	1.0250	0.4311	0.2721	2.3023	2.3944
± 1σ	0.0968	0.0435	0.0177	0.0195	0.0105	0.0679	0.2404
std dev, %	2.49	1.78	1.73	4.52	3.86	2.95	10.04
theoretical ratio $\frac{^{63}Cu}{^{65}Cu}$ (atomic)	3.8417	2.4017	0.9846	0.4041	0.2517	2.2440	unknown
bias factor, $\frac{\text{measured ratio}}{\text{theoretical ratio}}$	1.0135	1.0162	1.0410	1.0668	1.0810	1.0260	-

mean instrumental bias 1.0407.

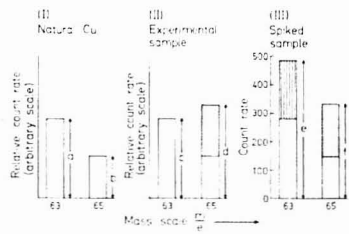


Figure 2. (I) The natural abundances (A_N) of the two isotopes of Cu in nature are $A_{N63} = a/(a + b)$ and $A_{N65} = b/(a + b)$. (II) The relative peak intensities of the two Cu isotopes in the experimental sample. (III) ^{63}Cu spike of the experimental sample has been added

from that found in the commercially prepared $CuCl_2{\cdot}2H_2O$, thus the isotopic composition of the naturally-occurring copper was known. Each sample was then divided into two parts at the graphite stage. The unspiked portion (first pair of electrodes) was measured to give a figure for the isotopic ratio as found in the experimental sample, and the second portion of each sample to which had been added a known amount of the ^{63}Cu spike (second pair of electrodes) was measured to give the third isotopic ratio and to quantify the result.

RESULTS AND DISCUSSION

Because both tracer and spike were so highly enriched, the calculation may be simplified by assuming that both isotopes are in fact pure (^{63}Cu 99.88% enriched and ^{65}Cu 99.81% enriched).

From Figure 2 (I), the natural abundances (A_N) of the two isotopes of Cu in nature are given by $A_{N63} = a/(a + b)$ and $A_{N65} = b/(a + b)$ where a and b are the relative peak intensities determined for ^{63}Cu and ^{65}Cu in uncontaminated fish flesh (after allowing for instrumental bias).

From Figure 2 (II) we have that the relative peak intensities of the two Cu isotopes in the experimental sample are c and d.

Further, in the experimental sample to which an additional known amount of ^{63}Cu (spike) has been added (Figure 2 (III)),

Table III. Quality of Data Obtained by the Method

processing blank		analysis of mixed standard containing 210 ng natural Cu plus 150 ng ^{65}Cu		
sample no. (1)	ng Cu (2)	sample no. (3)	natural Cu found, ng (4)	excess ^{65}Cu found, ng (5)
1	12.6	1	195	139
2	9.7	2	184	126
3	9.4	3	186	143
4	9.8	4	172	115
5	9.7	5	197	132
6	8.8	6	157	112
7	11.4	7	206	141
8	8.9	8	213	148
9	8.7	9	173	123
10	9.7	10	186	128
11	9.7			
12	6.8			
mean	9.6	mean	187	131
std dev, %	±14.8	std dev, %	±9.0	±9.2
(16)		(16)		
		mean recovery, %	89.0	87.3

the peak intensities are e and f respectively. Thus in the spiked sample the peak intensity due to ^{63}Cu contributed by the sample is fc/d. So the peak intensity due to the ^{63}Cu spike is $e - (fc/d)$. Now if the amount of ^{63}Cu standard added to the spiked sample is W μg, and K_1 is the ratio of the natural atomic weight of Cu divided by the atomic weight of the spike, then the amount of natural Cu (A_{NCu}) in the spiked portion of the sample is

$$A_{NCu} = \frac{K_1 W}{e - \left(\frac{fc}{d}\right)} \times \frac{fc}{d} \times \frac{1}{A_{N63}}\ \mu g \qquad (1)$$

Also since the peak intensity due to natural ^{65}Cu in the spiked sample is $(fc/d)(A_{N65}/A_{N63})$, then the peak intensity due to

Table IV. Cu Content and Accumulation of ^{65}Cu Tracer in a 30-g (wet) plaice (*Pleuronectes platessa*)

organ	wet weight, g (A)	percentage of body weight (B)	total natural Cu in organ, μg (C)	concn of natural Cu in organ, μg g^{-1} (wet) (D)	^{65}Cu accumulated in organ after 2-month exposure at 8 μg L^{-1} (E)
blood cells	0.15	0.5	0.04 ± 0.004	0.27 ± 0.03	0.03 ± 0.003
blood serum	0.3	1.0	0.17 ± 0.02	0.57 ± 0.06	0.14 ± 0.01
heart	0.02	0.06	0.06 ± 0.006	3.0 ± 0.3	0.15 ± 0.02
spleen	0.01	0.04	0.03 ± 0.003	3.0 ± 0.3	0.13 ± 0.01
liver	0.5	1.7	0.85 ± 0.09	1.7 ± 0.2	1.0 ± 0.1
kidney	0.12	0.4	0.08 ± 0.008	0.67 ± 0.07	0.14 ± 0.01
gut	0.3	1.0	0.33 ± 0.03	1.1 ± 0.1	0.25 ± 0.03
stomach	0.15	0.5	0.12 ± 0.01	0.80 ± 0.08	0.28 ± 0.03
gill filaments	0.2	0.6	0.12 ± 0.01	0.60 ± 0.06	0.33 ± 0.03
skin	2.2	7.2	1.4 ± 0.1	0.64 ± 0.06	0.06 ± 0.006
muscle	17.5	58.3	3.9 ± 0.4	0.22 ± 0.02	0.02 ± 0.002
bone	4.0	13.2	6.4 ± 0.6	1.6 ± 0.2	0.20 ± 0.02

the ^{65}Cu tracer in the spiked sample is $f - ((fc/d)(A_{N65}/A_{N63}))$, and hence the amount of ^{65}Cu tracer in the spiked sample

$$A_{T65} = \left[\frac{K_2 W}{e - \left(\frac{fc}{d}\right)}\right] \times \left[f - \left(\frac{fc}{d} \times \frac{A_{N65}}{A_{N63}}\right)\right] \mu g \quad (2)$$

where K_2 is the ratio of the atomic weight of the tracer to that of the spike.

Using isotopes of high enrichment, it is possible to quantify both the natural copper and the amount of ^{65}Cu tracer absorbed by the fish tissue during the experiment with a fair degree of accuracy. A simpler single magnetic sector mass spectrometer with thermal ionization source would undoubtedly have accomplished this project with greater precision, but mass spectrometers are expensive instruments and the most suitable type is not necessarily available. One of the aims of this paper therefore was to demonstrate the way in which an instrument such as the SSMS, not usually looked upon as giving a high degree of precision, can be used to explore the application of enriched stable isotopes for experimental studies such as this.

Correction for the processing blank, which incidentally must be assumed to be of natural isotopic composition, is made at Equation 1 in the calculations. As with all work of this kind, the establishment of a low and constant blank is vital; for an element such as copper, this is not easy but it can be achieved. Our working blank for the biological samples was about 10 ng (see Table III). It was decided therefore to maintain a separation process aimed at obtaining an approximately constant amount of copper (100–500 ng) for a measurement. Table IV illustrates the type of data obtained in a typical experiment and it can be seen that the amount of copper available for analysis varied appreciably from one type of tissue to another (column C). Thus, as far as possible, the size of sample taken for analysis was adjusted by sub-sampling (muscle, bone, skin, etc) or by bulking organs from more than one fish (heart, spleen, kidney, etc.). In this way, a constant amount (200 ng) of ^{63}Cu standard could be added to all samples, thus greatly simplifying the procedure at that stage.

Perhaps the major drawback to the technique as applied in this study concerns the uncertainty of recovery of copper throughout the processing. A direct result of trying to extract data simultaneously for natural copper in the fish and for the ^{65}Cu tracer is that the standard spike of ^{63}Cu cannot be used to follow the complete process. This would, of course, have been possible for an element with three or more usable isotopes and the inherent advantages of a true isotope dilution method would have been obtained. The overall uncertainties of the method were therefore assessed on standard samples and from these a mean recovery figure was calculated. Table III illustrates the type of data obtained both for the processing blank (column 2) and for standard samples containing 210 ng of natural copper to which had been added 150 ng of additional ^{65}Cu. The results were calculated as described earlier and are expressed in terms of copper of natural isotopic composition plus the excess ^{65}Cu.

LITERATURE CITED

(1) R. J. Pentreath, in "Design of Radiotracer Experiments in Marine Biological Systems", *Tech. Rep. Series I.A.E.A.*, **167** 137–170 (1975).
(2) F. D. Leipziger, *Anal. Chem.*, **37**, 171–172 (1965).
(3) R. A. Bingham, and P. G. T. Vossen, *Int. J. Mass Spectrom. Ion Phys.*, **14**, 259–266 (1974).
(4) J. F. Jaworski and G. H. Morrison, *Anal. Chem.*, **47**, 1173–1175 (1975).
(5) R. J. Pentreath and B. R. Harvey, in preparation.
(6) C. W. Magee and W. W. Harrison, *Anal. Chem.*, **45**, 852–856 (1973).
(7) W. R. Shields, S. S. Goldich, E. L. Garner, and T. J. Murphy, *J. Geophys. Res.*, **70**, 479–491 (1965).

RECEIVED for review November 16, 1977. Accepted July 31, 1978.

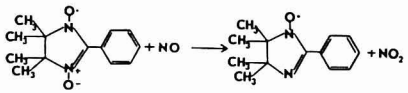
Mass Transfer Effects in a Nitric Oxide Dosimeter

J. S. Nadeau, M. E. Treen, and D. G. B. Boocock*

Department of Chemical Engineering and Applied Chemistry, University of Toronto, Toronto, Ontario, Canada M5S 1A4

Mass transfer studies have resulted in the selection of a membrane for a nitric oxide passive dosimeter. The mass transfer rate of nitric oxide to a free radical reagent on silica gel increases nonlinearly when wind velocity is raised from stagnant conditions to 7 m/s. When a reinforced poly(methylvinylsiloxane) membrane with a thickness of 0.05 mm is attached to the front of the plate, a constant mass transfer rate occurs at all wind velocities in the range studied. Reagent surface loading on the plate is best controlled by changes in reagent solution concentration rather than by use of multispotting procedures. Blank readings may be decreased significantly by pretreatment of the plate preparation room with small ozone concentrations.

We recently reported a reagent which when supported on thin-layer silica gel plates formed the basis of a nitric oxide passive dosimeter (*1*). This reagent, a nitronylnitroxide free radical 1 reacts with nitric oxide to produce an iminonitroxide free radical 2 as shown in Equation 1.



[1] [2]

The reagent is applied to the plate in chloroform solution and after exposure, the product is separated by thin-layer chromatography, extracted with a measured volume of *p*-dioxane and quantified by electron spin resonance. We report here on the selection of a membrane to buffer mass transfer effects caused by wind. This involved the study of the mass transfer of nitric oxide in membrane-covered and membrane-free plates. We also report on techniques which may be used to reduce blank readings.

The reaction of nitric oxide with the reagent 1 on the plate is mass transfer controlled (*1*). It is therefore essential that the transport rate of nitric oxide to the reagent be independent of wind velocity. Therefore the boundary layer over the plate must not be part of the limiting resistance. It is usual to deliberately introduce a limiting resistance into a passive dosimeter. This resistance may be a membrane as in West's vinyl chloride (*2*) and sulfur dioxide (*3*) dosimeters, or it may be some kind of air gap as in the general dosimeter described by Tompkins and Goldsmith (*4*) and the tubular type of nitrogen dioxide dosimeter described by Palmes (*5*). The geometry of our collection/reaction surface indicated that a membrane would be the simplest and most convenient resistance layer.

Analogy between Dosimeters and Electrical Metering. The term "limiting resistance" is used when discussing both mass transfer and electrical circuits. The analogy of a dosimeter to an electrical measuring circuit is very useful, particularly to those who may not be familiar with mass transfer concepts. Figure 1 shows an electrical circuit which is analogous to the nitric oxide dosimeter containing a membrane. R_b, R_m, R_s, and R_c are resistances equivalent to the mass transfer resistances of the boundary layer, membrane, silica gel, and reagent–nitric oxide reaction, respectively. R_b in the dosimeter would generally decrease as wind velocity increases. R_s in the dosimeter would be made up of resistances due to molecular diffusion, Knudsen diffusion, and surface diffusion in the silica gel. R_c may become limiting if the reagent surface loading falls below a certain value for a particular nitric oxide concentration. The reaction of nitric oxide with the reagent would then be chemically controlled. This would be equivalent to changing the response of the meter in the electrical circuit and would obviously be undesirable. Finally, the EMF of the electrical circuit is analogous to the nitric oxide concentration difference across the dosimeter. This may be taken as the ambient nitric oxide concentration in most cases. The boundary layer, in the absence of a membrane or air gap, is usually the limiting and variable resistance. The membrane or air gap added to the dosimeter should therefore have a significantly larger resistance and this will result in a decrease in sensitivity of the device.

The Membrane. Reiszner and West (*3*) have studied the permeation of sulfur dioxide in various membranes and concluded that permeation rates are high in silicone membranes and are not greatly affected by changes in temperature. We had access to membranes which have been specially made for evaluation as artificial lung material (Sci-Med Inc. 13070 County Rd. 6, Minneapolis, Minn., 55441). These membranes are not listed in the manufacturer's catalogue but are available on request. After some preliminary studies, we chose a type 2A membrane which is silica-filled poly(methylvinylsiloxane) reinforced with a polyester knit. The membrane is available in two forms and we used the one in which the knots of the reinforcing material are placed upwards in the pouring process and thus appear on the rough side of the membrane. The overall material thickness is 0.17 mm (0.007 in.) but the actual membrane thickness is 0.050 mm (0.0020 in.). We used the membrane with the rough side facing the plate. We have studied the mass transfer of nitric oxide to membrane-covered plates and membrane-free plates in a simple wind tunnel using ambient air.

Reagent Application Procedure. We have also studied the flexibility in the method of applying reagent to the plates. In our initial studies, plates were spotted with single 10-μL portions of a 6.28×10^{-2} M solution of the reagent in chloroform (*1*). We first investigated the effect of changing the concentration of the reagent in the spotting solution. Six different concentrations ranging from 0.81×10^{-2} M to 6.28×10^{-2} M were used. Plates were exposed to 0.38 ppm nitric oxide in nitrogen for 1 h in a 1000-L chamber (*1*). The plate response was directly proportional to the reagent solution concentration. This relationship is due to changes in spot area and not to a change in surface loading of reagent. Earlier studies showed that the reaction of nitric oxide and reagent is mass transfer controlled. Figure 2, which displays the results of multispotting procedures (see below), shows that, as expected, there is a limit to the spot size which can be obtained using 10-μL portions of spotting solution. It appears, from

0003-2700/78/0350-1871$01.00/0 © 1978 American Chemical Society

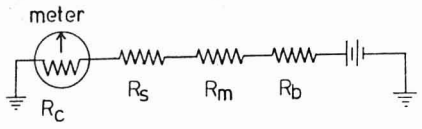


Figure 1. Electrical circuit analogous to nitric oxide dosimeter

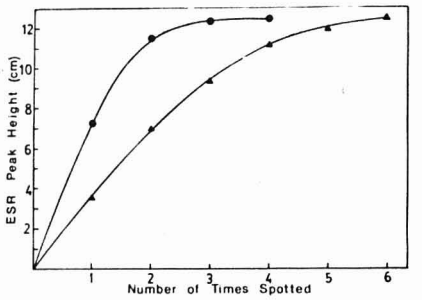


Figure 2. Plate response as a function of the number of 10-μL superimposed spots of reagent solution. Upper points 6.28×10^{-2} M, lower points 3.14×10^{-2} M

a consideration of the two data points representing single spots, that for a reagent concentration of 10.84×10^{-2} M, the spot would be close to this limiting size.

In a second investigation, the effect of using multiple superimposed spots was studied. The chloroform from a 10-μL spot was allowed to evaporate before applying a second spot at the identical position on the plate. Successive spots could be applied in the same way. Two reagent concentrations, 6.28×10^{-2} and 3.14×10^{-2} M were used. Plates, carrying up to six superimposed spots, were exposed to 0.38 ppm nitric oxide in nitrogen for 1 h. The plate responses are shown in Figure 2. Curves have been drawn only to show the trend in results. The same maximum response is reached using both spotting solutions and this occurs with six successive spottings of the weaker solution and three successive spottings of the stronger solution. This again demonstrates that the reagent eventually reaches the same outer limit that the chloroform reaches before it evaporates. The increase in spot area with successive spottings was observed visually. It was also noticed that the annulus of reagent at the periphery of the spot became wider and darker as successive spots were applied, thus indicating that most of the reagent was located at the edge of the spot.

The results of these two studies indicate that when the reagent is applied in spot form, then the spot size and reagent surface loading are best controlled by changes in the reagent solution concentration and the volume of reagent applied, and not by use of superimposed spots.

Blank Readings. The lower limits of detection for the method are strongly determined by the magnitude of blank readings. The iminonitroxide blank is produced by two processes. First, product 2 can be formed from the reagent by nitric oxide or strong light prior to its application to the plate and, secondly, product can be formed during plate handling and preparation. This latter effect is important when measuring typical ambient concentrations of nitric oxide over very short periods such as 1 h. In our wind tunnel studies (see below), blanks were initially as high as 80% of the sample plate readings. One obvious method for reducing blanks caused by product in the reagent, would involve a thin-layer separation prior to plate exposure. We studied this possibility using a single spot of reagent, 6.28×10^{-2} M, on a plate which was slightly longer than usual. The reagent spot spreads during elution and increases in area by 36% after 30 min. The area then remains constant for at least the next 30-min period of elution. The increase in area was measured from the response of the eluted plates. For the second separation, made after plate exposure, elution was carried out in the opposite direction, that part of the plate carrying the product blank having been cut off at an appropriate distance from the reagent spot. We did not employ the above procedure because, in our wind tunnel studies, the major source of the blank was plate preparation. We therefore removed nitric oxide from our plate preparation room with ozone by turning on a 6-in. pencil-type UV lamp for 10 min. The lamp was switched off and 10 min later the plates were prepared. In this way, blanks were reduced to 8% and less in the wind tunnel studies. Ozone dosage should be carefully designed for the plate preparation area to avoid any hazard to personnel.

EXPERIMENTAL

Plate Preparation. The silica gel plates used were Eastman Kodak 6061 type containing a poly(vinyl alcohol) binder. Although these have now been replaced by the manufacturer with type 13179 which contain a poly(acrylic acid) binder, we continued to use them so that we could relate our results to our previous work (*1*). The plate size has now been reduced to 5 × 2 cm thus allowing 40 of them to be cut from a 20 × 20 cm sheet. The plates were preconditioned by drying them for at least 0.5 h at a temperature of 80 °C. The temperature is limited by the thermal stability of the polyester backing. Twenty minutes prior to plate preparation, a six-inch pencil-type ultraviolet lamp (Pen-Ray SCT 1) was switched on in the preparation room (dimensions, 3 m × 4 m × 3 m high) for 10 min. Sample plates and plates for blanks were spotted alternately as described previously (*1*) and covered with the type 2A membrane so that the rough side of the membrane faced the plate. Commercially available invisible tape (0.75 inch wide) was immediately fastened on the membrane over the spot area. This is a convenient method of reducing the plate response to zero. Plate storage has been described previously (*1*).

Wind Tunnel Studies. The wind tunnel consisted of metal ductwork with a square cross section and 30-cm sides. Ambient air was drawn from outside the building, around a 90° turn, through vertical baffles, and along a 6-m linear section. A rigid polyester door was installed at the midpoint of the linear section. At the exhaust, a Dehli single inlet exhauster fan was driven by a constant speed Delco AC motor (1725 rpm). The air velocity was varied by adjusting a flap at the tunnel entrance. Immediately prior to measurement, prepared plates were introduced through the door and taped face up on the lower surface of the tunnel. The adhesive tape was removed from the face of the membrane-covered plates. The membrane was removed completely in the case of membrane-free plates. The temperature of the air was measured 15 cm downstream. Air velocity was measured 2 cm above the tunnel floor using a pitot tube and a Wilk–Lambrecht slant manometer. Nitric oxide and nitrogen dioxide time-weighted average concentrations were measured as described previously (*1*). The tunnel inlet was located on a second floor facing an East–West street in Toronto. On a weekday this street typically carried 1000 vehicles per hour in a daytime nonrush-hour period (10:00 a.m.–11:00 a.m.). Plate exposures were made for either 1 or 2 h. For 1-h exposures, parallel nitric oxide sampling was performed over the first and last 20 min. For 2-h exposures, sampling was carried out in the initial and final 50 min. The ambient nitric oxide concentrations varied between 0.02 and 0.12 ppm. For air velocities of zero, plates were exposed in a 1000-L chamber under natural convective conditions.

After exposure, the plates were developed in a 2:1 by volume mixture of *n*-pentane and diethyl ether. This elution mixture differed from that described previously (*1*) in that the carbon tetrachloride component was replaced by more *n*-pentane. It was found that the presence of carbon tetrachloride can cause the radicals to undergo reversible salt formation on the plates. This is presumably caused by the trace amounts of hydrochloric acid which can form in carbon tetrachloride containing small amounts of water. After development, the product radical 2 was extracted

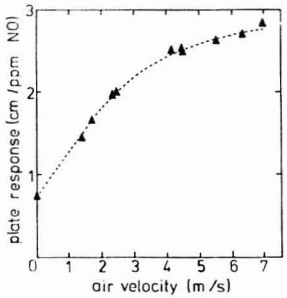


Figure 3. Response for membrane-free plate as a function of air velocity

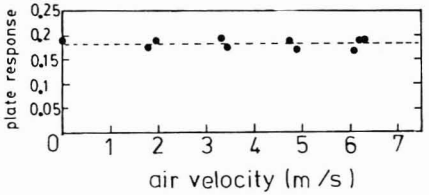


Figure 4. Response (cm/ppm NO) for membrane-covered plate as a function of air velocity

from the silica gel with dioxane and spectra were obtained using a Varian-E4 spectrometer as described previously (*1*). All results were expressed as a plate response in the form

$$\text{plate response} = \frac{1}{c \cdot t}\left(\frac{H_s}{G_s} - \frac{H_b}{G_b}\right)$$

where c is the concentration of nitric oxide in ppm, t is the time in hours, H_s and H_b are the ESR peak heights in cm of the product extracted from the sample and blank plates, respectively, and G_s and G_b are the respective receiver gains of the instrument.

RESULTS AND DISCUSSION

Plate responses for membrane-free and membrane-covered plates, plotted as a function of air velocity, are shown in Figures 3 and 4, respectively. It should be noted that the response scale in Figure 4 has been expanded compared to that in Figure 3. Simple boundary layer theory predicts that when the boundary layer has the limiting resistance, then for laminar flow the plate response should be proportional to the square root of the wind velocity, v, and for turbulent flow the response should vary as $(v)^{0.8}$. These relationships should hold until the plate resistance becomes part of the limiting resistance. The plates may be considered as being infinitely long when taped to the bottom of the wind tunnel and thus the flow should be turbulent in most of the velocity range studied. The results shown in Figure 3 are not inconsistent with the above theory, especially if there is a small laminar-flow region between the first two data points. However, there is one serious inconsistency in the data shown in Figures 3 and 4. It can be seen that introduction of the membrane reduced the plate response only 75% under natural convective conditions. Using the previous analogy this would be equivalent to R_m being equal to $3R_b$. This observation, together with steepness of the response curve in Figure 3, indicated that the membrane should not be capable of completely buffering wind effects, whereas Figure 4 demonstrates that the membrane is very effective. One reasonable explanation for this anomaly is that at least part of the limiting resistance in the membrane-free plate is within the silica gel layer, even under natural convective conditions. In fact, earlier studies showed a mass transfer rate in natural convective conditions which was concentration dependent above about 0.5 ppm nitric oxide, and this was attributed to diffusional processes on the silica gel (*1*). It is suggested that the airflow over the membrane-free plates penetrates the silica gel layer and increases the mass transfer coefficient in it. In the absence of such an effect, the curve in Figure 3 would be much less steep. The membrane would prevent the penetration and this, together with the extra resistance provided by the membrane, would account for its effectiveness.

The introduction of the membrane eliminates the nonlinear portion of the calibration curve in the range 0.5–1.00 ppm nitric oxide. This is expected because, at 1.0 ppm nitric oxide, the theoretical concentration above the silica gel is 0.25 ppm and at this concentration the diffusion coefficient of nitric oxide on the silica gel is still in the linear region. Even in a nitric oxide concentration of 4.0 ppm, for which the theoretical concentration above the silica gel is 1.0 ppm, the plate response should exceed the linear value by only 7.5%. More resistive membranes would be used for measurement of higher nitric oxide concentrations because in the present system a membrane-free plate can tolerate only 0.7 ppm nitric oxide for eight hours before the plate response changes. In this situation, diffusional effects on the silica gel would become negligible. However, the concentration dependent diffusional effects could be a problem if the reagent were employed as a colorimetric reagent, supported on silica gel in a flow-through tube-type dosimeter. The above results may also have relevance to dosimeters using activated charcoal. In particular, the results emphasize that the evaluation of membranes and air gaps as limiting resistances for dosimeters which contain solid adsorbents, should include air flow conditions, especially if the maximum sensitivity is required for the dosimeter.

With the membrane in place, the dosimeter is 450 μm thick but in some applications a light shield may be required.

Present Studies. The device is currently being tested with the new plates. A carbon-14 labeled reagent is also being studied so that the product radical may be measured by liquid scintillation counting, a procedure which we believe will be more convenient than electron spin resonance.

LITERATURE CITED

(1) J. S. Nadeau and D. G. B. Boocock, *Anal. Chem.*, **49**, 1672 (1977).
(2) L. H. Nelms, K. D. Reiszner, and P. W. West, *Anal. Chem.*, **49**, 994 (1977).
(3) K. D. Reiszner and P. W. West, *Environ. Sci. Technol.*, **7**, 526 (1973).
(4) F. C. Tompkins and R. L. Goldsmith, "A new personnel dosimeter for the monitoring of industrial pollutants", paper presented at the AIH conference, Atlanta, Ga., May 1976.
(5) E. D. Palmes, A. F. Gunnison, J. DiMattio, and C. Tomczyk, *Am. Ind. Hyg. Assoc. J.*, **37**, 570 (1976).

RECEIVED for review May 3, 1978. Accepted August 7, 1978. Work supported by Grants from the National Research Council of Canada and a scholarship from the McAllister Foundation of the University of Toronto.

Enzyme-Bound Thermistor as an Enthalpimetric Sensor

Canh Tran-Minh* and Didier Vallin

Ecole Nationale Supérieure des Mines de Saint-Etienne, 158, cours Fauriel - 42023 Saint-Etienne Cédex, France

The construction of a new type of immobilized enzyme sensor for the determination of chemical species is described. The sensitive part of a thermistor is coated with an artificial enzyme membrane obtained by the cross-linking of the enzyme together with an inert protein, using glutaraldehyde as a bifunctional reagent. The enthalpy change during the enzymatic reaction induces a production or absorption of calories which can be taken as a reaction product and depends then upon the reaction parameters (K_m, V_m, [S]). This type of enzyme-bound thermistor is used for the determination of hydrogen peroxide, glucose, and urea. The pH and temperature dependence of the hydrolysis of urea by urease given by this sensor are compared to the results previously obtained by other methods.

During the past years, extensive research has been conducted on the construction and the use of new types of matrix-bound enzyme systems (*1–3*). A large number of those studies have been concerned with the construction of enzyme electrodes for the determination of organic and biological compounds (urea, uric acid, aminoacids, etc.). In that type of sensor, an enzymatically active membrane is bound to a specific electrode such as a gas electrode: O_2, CO_2 (*4–7*), or a monovalent cation electrode: H^+, NH_4^+ (*7–11*). The electrode is sensitive either to the substrate or to the product of the reaction.

Although this type of sensor offers many advantages, it depends essentially on the basic electrode, the detection of which is often restricted to a single chemical species whatever the immobilized enzyme may be. The specificity of the electrode (O_2, CO_2, H^+, NH_4^+) implies that the enzymatic reaction gives rise to species detectable by the sensitive part of the electrode.

In the present work, we describe the construction of an enzymatic sensor using the detection of an entity belonging to all the enzymatic reactions: the enthalpy change of the reaction. Several authors have applied microcalorimetry to the determination of many chemical and biochemical species (*12–14*). However, this technique demands an expensive and cumbersome apparatus. From the principle of microcalorimetry, some authors have constructed measuring cells with thermistors, using a flow system, to measure the temperature change of the substrate solution once it passed through a bed of immobilized enzyme (*15–18*). These cells allowed the determination of several substrates, but they need a large quantity of enzyme, and their response time is still long.

Our aim is to construct a new type of enzymatic sensor which could be applied to all the enzymatic reactions provided that their enthalpy change is not equal to zero and large enough to be detected by the thermistors. We use two thermistors, both are coated with crosslinked proteins on their sensitive parts. The first one—the measuring thermistor—is covered with a mixture of albumin and enzyme crosslinked together by a bifunctional reagent: glutaraldehyde. The second one coated only with albumin is used as a reference. For measurements, both thermistors are dipped into a stirred solution of substrate. The differential device eliminates the effect of temperature fluctuations induced by the thermostat.

During the exothermic reaction, one part of the calories produced inside the enzyme active layer diffuses toward the solution, and the other toward the thermistor. In order to favor the second way of exhausting calories, we surrounded the measuring thermistor with a glass jacket. This one decreases the liquid flow velocities (forced convection) along the active membrane, and then reduces the amount of calories lost by diffusion toward the solution. It also allows sufficient supply of the substrate for the enzymatic reaction. The same technique has been applied to the reference thermistor to have a symmetrical device (Figure 1). Both thermistors are parts of a Wheatstone bridge. Electric zero is established by using a solution without substrate. As soon as the substrate is introduced into the solution, the temperature changes because of absorption or production of calories. It induces a variation in the measuring thermistor resistance which unbalances the Wheatstone bridge. An electrical signal is sent to an amplifier and then to a recorder. For a given concentration of substrate, a steady state of temperature can be achieved quickly all over the active layer. This type of sensor has been used for the determination of hydrogen peroxide, glucose, and urea, with a response time lower than 10 s (Figures 2–4). For a given enzyme membrane and a given substrate concentration, the precision on the repeatability of the sensor response is approximately 3%.

EXPERIMENTAL

Apparatus. Thermistors provided by Feenwall Electronics were used. The main characteristics are: R_0^{25}, resistance at 25 °C: 2000 Ω and α, percent resistance change per °C at 25 °C: −3.9.

Thermistors were connected to a Wheatstone bridge (temperatur-Messgerät from Knauer).

As the fluctuations of temperature inside the active membrane occur in a small range, a linear variation of R_0 with temperature can be assumed.

Reagents. Enzymes are provided by Sigma. Enzyme activities are given by Sigma.

Urease. Powder from Jack beans, type IX, 5.1 Sigma units/mg. One unit of urease activity is the amount of enzyme that will liberate 1 mg of ammonia nitrogen from urea in 5 min at pH 7 at 30 °C.

Glucose Oxidase. From *Aspergillus niger*, type II, 18.9 Sigma units/mg, catalase impurity 2% by weight (800 Sigma units/mg).

One unit of glucose oxidase activity is the amount of enzyme that will oxidize 1.0 μmol of β-D-glucose to D-gluconic acid and H_2O_2 per minute at pH 5.1 at 35 °C.

Catalase. From bovine liver 15 000 Sigma units/mg. One Sigma unit will decompose 1 μmol of H_2O_2 per minute at pH 7.0 at 25 °C, while H_2O_2 concentration falls from 10.3 to 9.2 μmol per mL of reaction mixture.

Procedure. The enzyme was dissolved in 200 μL of 17.5% human albumin solution. Then 20 μL of 25% glutaraldehyde solution was added. The solution was stirred for 30 s. A drop of this solution (≃20 mg) was deposited on the sensitive part of the thermistor and left for crosslinking at 25 °C during approximately 15 min. Then a glass jacket could be fitted if necessary. Before use in biological media, the sensor must be rinsed for a few hours with a phosphate buffer solution (P_i) at pH 7.0, and then with a glycine solution, in order to elute or neutralize the excess of bifunctional agent. All measurements

0003-2700/78/0350-1874$01.00/0 © 1978 American Chemical Society

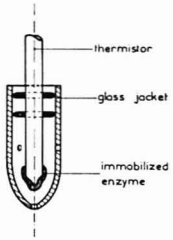


Figure 1. Enzyme-bound thermistor

were carried out in phosphate buffer solutions (0.1 M) and in thermostated cells.

RESULTS

The response of the above-mentioned sensor has been studied with catalase, glucose oxidase, and urease.

Enzyme Thermistor Using Immobilized Catalase. The enzymatic reaction is:

$$H_2O_2 \rightarrow H_2O + \tfrac{1}{2}O_2 + \Delta H$$

The enthalpy change of this reaction is: $\Delta H = -23.44$ kcal/mol^{-1}. The enzymatic membrane was obtained by dissolving 5 mg of catalase according to the above-described procedure. The amount of catalase immobilized on the sensitive part of the thermistor was approximately 10 000 Sigma units. Because of this amount of catalase, it was not necessary to use the glass jacket. For much greater amounts of catalase, the temperature increase inside the active layer is large enough to give a partial and irreversible destruction of enzyme activity (*19*, *20*).

The assays were performed in buffer solution (P_i, 0.1 M, pH 7.0) in thermostated cells (25.0 ± 0.1 °C) for various concentrations of hydrogen peroxide between 10^{-2} M and 7×10^{-1} M. The steady-state response curve of the sensor as a function of substrate concentration is shown on Figure 2. For concentrations ranging from 10^{-2} M to 5×10^{-1} M, the sensor response is proportional to the substrate concentration. For higher concentrations ($>5 \times 10^{-1}$ M) the response curve tends towards a plateau corresponding to the maximum rate of the enzymatic reaction. The precision of the sensor response is approximately 5% when hydrogen peroxide concentration is lower than 10^{-2} M and 3% for higher substrate concentration.

Enzyme Thermistor Using Immobilized Glucose Oxidase (GOD). The glucose oxidase used for these assays contains catalase impurity (800 Sigma units/mg). Then the catalyzed reaction implies two consecutive steps.

$$H_2O + \beta\text{-D-glucose} + O_2 \xrightarrow{\text{GOD}} H_2O_2 + \text{D-gluconic acid} + \Delta H_1 \quad \text{(I)}$$

$$H_2O_2 \xrightarrow{\text{catalase}} {}^1/_2O_2 + H_2O + \Delta H_2 \quad \text{(II)}$$

These reactions can also be simplified as follows:

$$\beta\text{-D-glucose} + O_2 \xrightarrow[\text{catalase}]{\text{GOD}} \text{D-gluconic acid} + {}^1/_2O_2 + \Delta H_3 \quad \text{(III)}$$

The total enthalpy change ΔH_3 of the reaction III is the sum of the two enthalpy changes referring to both steps. The production of 1 mol of D-gluconic acid from 1 mol of β-D-glucose requires 0.5 mol of oxygen. Consequently, the oxidation rate of β-D-glucose is a function of the oxygen concentration (*7*). If ΔH_3 is taken as a product of the reaction, the rate of the reaction can be written:

$$\frac{\partial \Delta H_3}{\partial t} = K[O_2]^{\alpha}\,[\text{glucose}]^{\beta}$$

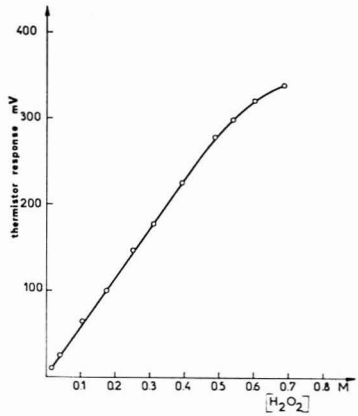


Figure 2. Response of the catalase-bound thermistor to various hydrogen peroxide concentrations

For the determination of β-D-glucose, the proportionality between the reaction rate and the glucose concentration requires $[O_2]$ = constant. However, the enzymatic reaction involves a consumption of both β-D-glucose and oxygen, and then a decrease of oxygen concentration. This concentration could be kept approximately constant at the gas saturation concentration, provided that the production of oxygen is continuous. As glucose oxidase contains catalase impurity, the addition of H_2O_2 into the buffer solution gives rise to an evolution of oxygen inside the active layer up to its saturation concentration for a given temperature and a given atmospheric pressure. The excess of oxygen is removed from the solution as a gas. Under this condition, the oxidation rate is only a function of glucose concentration specially for high substrate concentrations when increasing H_2O_2 quantities are necessary to keep $[O_2]$ = constant. The assays were performed in phosphate buffer (P_i, 0.1 M, pH 5.50) at 25.0 °C. For this study, the glass jacket is required. The enzyme membrane is obtained by dissolving 20 mg of glucose oxidase according to the above-described procedure. The amounts of glucose oxidase and catalase on the thermistor are approximately 60 and 2200 Sigma units, respectively. Measurements were performed with various concentrations of β-D-glucose and H_2O_2. The response curves of the sensor to β-D-glucose concentrations for various concentrations of hydrogen peroxide (10^{-3} M, 2×10^{-3} M, 3×10^{-3} M, 4×10^{-3} M, 6×10^{-3} M) are shown on Figure 3. The hydrogen peroxide is added in the buffer solution before any introduction of β-D-glucose. The slight production of calories from the catalytic decomposition of added H_2O_2 gives rise to a small electric signal which is taken as reference (sensor response → 0 when [glucose] → 0).

For a given concentration of hydrogen peroxide, the sensor response is linear for low β-D-glucose concentrations (Figure 3). For higher substrate concentrations, the response curve tends toward a plateau corresponding to a maximum reaction rate. For a given β-D-glucose concentration the sensor response and then the reaction rate is a function of the hydrogen peroxide concentration. This agrees with the predicted kinetic concerning the consumption of oxygen during the enzymatic

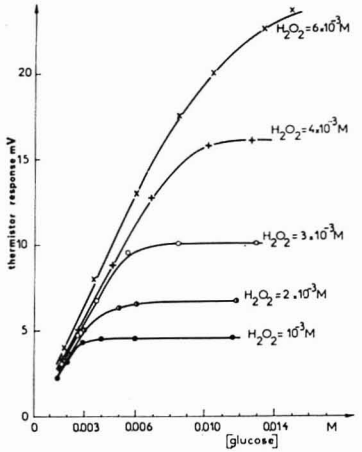


Figure 3. Response of the glucose oxidase-bound thermistor to β-D-glucose concentrations for various hydrogen peroxide concentrations

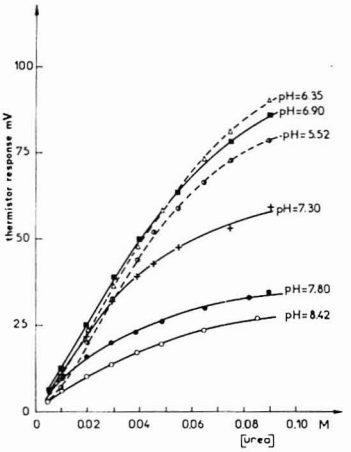


Figure 5. Response of the urease-bound thermistor to urea concentrations for various pH's of the buffer solution

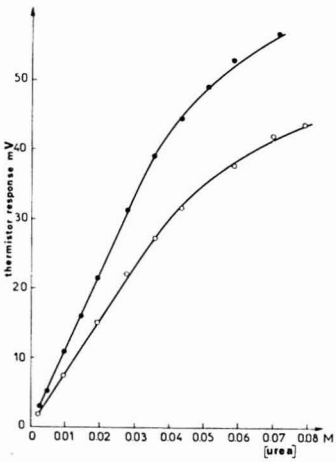


Figure 4. Response of the urease-bound thermistor to various urea concentrations for 10 Sigma units (O) and 20 Sigma units (●) of immobilized enzyme on the thermistor

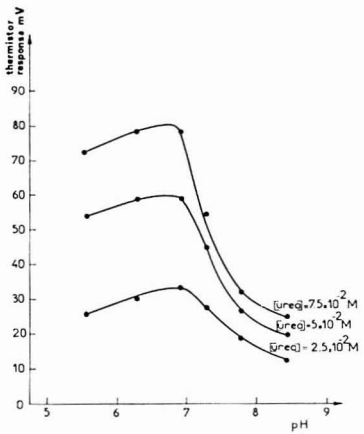


Figure 6. Effect of buffer solution pH on the response of the urease-bound thermistor for various urea concentrations

oxidation of β-D-glucose. The experiments were carried out with an approximate precision of 5% for [glucose] $< 3 \times 10^{-3}$ M, and 2% for [glucose] $> 5 \times 10^{-3}$ M.

Enzyme Thermistor Using Immobilized Urease. The enzymatic reaction is:

$$O=C\begin{matrix}NH_2\\NH_2\end{matrix} + H_2O \rightarrow CO_2 + 2NH_3 + \Delta H$$

where $\Delta H = -13.17$ kcal mol^{-1}.

Considering the enzymatic membrane activity, the use of the glass jacket is required. With this device, the response curve of the sensor to various urea concentrations has been obtained. The enzymatic reaction is pH and temperature dependent, so the influence of these two parameters on the catalytic decomposition of urea can also be determined by means of the sensor. Figure 4 shows the response curve of the sensor to various urea concentrations for 20 Sigma units and 10 Sigma units of immobilized enzyme on the thermistor. The experiments were carried out with an approximate precision of 5% for [urea] $< 5 \times 10^{-3}$ M, and 2% for higher substrate concentration. These curves are quite similar to those previously obtained with an urease-coated glass electrode (7). The response time is below 10 s with buffer solutions containing urea as well as with plasma samples.

Figure 5 shows the sensor response to urea concentrations for various pH values of the buffer solution. The response curves are quite normal, except for pH 6.35 and pH 5.52. In these two cases, the response curves have a sigmoid shape that can be explained by an autocatalytic effect of the reaction. As the decomposition of urea increases the pH inside the active

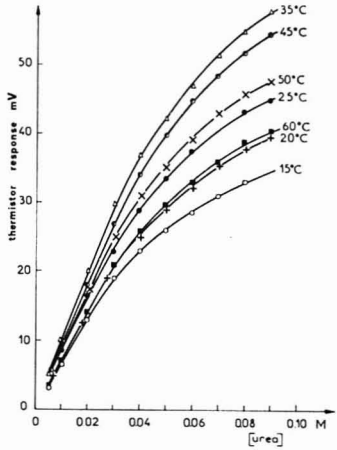


Figure 7. Response of the urease-bound thermistor to urea concentrations for various temperatures of the buffer solution

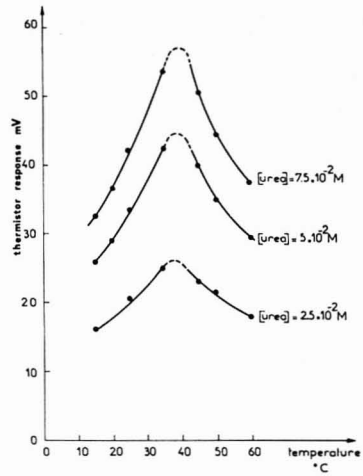


Figure 8. Effect of temperature on the response of the urease-bound thermistor, for various urea concentrations

layer, the activity of the enzyme increases (Figure 6) and so does the reaction rate. This phenomenon can also be found with allosteric enzymes. For higher pH values, as the enzymatic reaction proceeds, there is an increase of the pH inside the active layer which induces a decrease of the urease activity and then a decrease of the reaction rate. No sigmoid curves were then obtained in this range of pH.

From the previous curves, Figure 6 reports the effect of pH on the sensor response for various urea concentrations (2.5×10^{-2} M, 5.0×10^{-2} M, 7.5×10^{-2} M). The sensor response tends toward a maximum value when the pH of the buffer solution is 6.75. Below and above this value, the sensor response and then the reaction rate decreases. These results agree with those already known concerning enzyme kinetics.

Figure 7 represents the sensor response to urea concentrations for various temperatures of the buffer solution (P_i 0.1 M, pH 6.80). The sensor response increases with temperature when ranging from 15 to 35 °C, and then decreases for higher temperatures.

From the previous curves, Figure 8 reports the effect of temperature on the sensor response for various urea concentrations (2.5×10^{-2} M, 5.0×10^{-2} M, 7.5×10^{-2} M). This response and then the reaction rate tend toward a maximum value at approximately 38 °C. Below this value, the increase in sensor response with temperature can be explained by the variation of the kinetic parameters according to the Arrhenius law (*20*). Above 38 °C, the sensitivity of the enzyme thermistor decreases as the enzyme itself is affected by an irreversible denaturation of its active sites (*20*).

DISCUSSION

In the simplest case where the enzyme irreversibly transforms one substrate into one product, the reaction rate can be written:

$$E + S \underset{k_{-1}}{\overset{k_{+1}}{\rightleftarrows}} ES \xrightarrow{k_2} E + P$$

where E is the free enzyme, S the substrate, P the product, and ES the enzyme/substrate complex.

The reaction rate can be written (*21*, *22*)

$$v = \frac{d[P]}{dt} = -\frac{d[S]}{dt} = V_m \frac{[S]}{K_m + [S]}$$

where V_m is the maximum reaction rate and K_m the Michaelis constant.

Inside the active layer, concentrations of S and P are controlled by diffusion coupled with the enzyme reaction. This effect can be illustrated by the following equations:

$$\frac{\partial[S]}{\partial t} - D_S \frac{\partial^2[S]}{\partial x^2} + V_m \frac{[S]}{K_m + [S]} = 0 \quad (1)$$

$$\frac{\partial[P]}{\partial t} - D_P \frac{\partial^2[P]}{\partial x^2} - V_m \frac{[S]}{K_m + [S]} = 0 \quad (2)$$

where t is the time of the reaction, D_S and D_P effective diffusion coefficients of S and P inside the active layer, and x the distance of each point of the membrane to the external surface of this membrane.

The enzymatic reaction gives rise to an enthalpy change ΔH which induces an increase ($\Delta H < 0$) or a decrease ($\Delta H > 0$) of temperature per unit of time:

$$\frac{\partial\theta}{\partial t} = \frac{\Delta H}{\rho C} \times V_m \frac{[S]}{K_m + [S]} \quad (3)$$

where C is the thermal capacity and ρ the specific gravity of the layer.

The change in temperature inside the active layer induces a heat transfer controlled by the equation:

$$\frac{\partial\theta}{\partial t} = \frac{\lambda}{\rho C} \frac{\partial^2\theta}{\partial^2 x^2} \quad (4)$$

where λ is the specific heat conductivity.

The temperature change inside the active layer is then given by the sum of the diffusion term in Equation 4 and the reaction term in Equation 3:

$$\frac{\partial\theta}{\partial t} = \frac{\lambda}{\rho C} \frac{\partial^2\theta}{\partial x^2} + \frac{\Delta H}{\rho C} V_m \frac{[S]}{K_m + [S]} \quad (5)$$

At the steady state, we have $\partial\theta/\partial t = 0$, so we can write:

$$\frac{\partial^2\theta}{\partial x^2} + \frac{\Delta H}{\lambda} V_m \frac{[S]}{K_m + [S]} = 0 \quad (6)$$

Equation 6 shows the relationship between the temperature inside the active layer and the reaction rate, and then with the substrate concentration. When $[S]/K_m \rightarrow 0$, $v = (V_m [S])/(K_m + [S]) \rightarrow (V_m/K_m)[S]$ (first-order kinetics for S). The increase of the temperature at the interface active layer/thermistor becomes proportional to the substrate concentration. When $K_m/[S] \rightarrow 0$, $v \rightarrow V_m$ (zero-order kinetics for S), the reaction rate V_m becomes proportional to the number of active sites of bound enzyme. The response curve of the sensor tends toward a plateau.

This type of curve is obtained with the catalase-bound thermistor (Figure 2), with the urease-bound thermistor (Figure 5) and with the glucose oxidase-bound thermistor (Figure 3), although in this latter case, the presence of oxygen as a cosubstrate changes the enzyme kinetic. For these enzyme-bound thermistors, lifetimes of two or three weeks were obtained, without any detectable change in the response curves.

CONCLUSION

A new type of immobilized enzyme sensor can be obtained by coating the sensitive part of a thermistor with an enzymatic membrane. The immobilization of the enzyme and an inert protein by the use of glutaraldehyde gives chemical covalent bonds which result in a good stabilization of the enzyme molecules. The temperature change inside the active layer resulting from a production ($\Delta H < 0$) or an absorption ($\Delta H > 0$) of calories during the reaction can be explained in terms of an equation which includes both diffusion and chemical reaction. When the substrate concentration is lower than the K_m of the immobilized enzyme, the enzyme-bound thermistor gives a linear response and may then act as a sensor. When the production of calories during the enzymatic reaction is small, the use of a glass jacket around the thermistor decreases the calories lost by diffusion toward the external solution and then increases the sensor response for a given substrate concentration. In the case of urease and glucose oxidase-bound thermistors, only a very small electric signal could be obtained without this glass jacket, even for large substrate concentrations.

The use of thermistors with a higher α (percent resistance change per °C) and an improvement of the sensor technology should allow the detection of lower substrate concentrations with low enzyme activities, and the use of enzymatic reactions with lower enthalpy changes (L-amino acid oxidase, acetylcholinesterase, etc...). Miniaturization of such enzyme-bound thermistors may allow them to be used in vivo in the future, since very small thermistors are easily constructed and the assays carried out with plasma give similar results.

ACKNOWLEDGMENT

We express our appreciation to J. Fraisse and Melle Croze from Centre de Transfusion Sanguine de Saint-Etienne for providing calibrated plasma samples.

LITERATURE CITED

(1) O. R. Zaborsky, "Immobilized Enzymes", CRC Press, Cleveland, Ohio, 1973.
(2) M. Salmona, C. Saronio, and S. Garattini, "Insolubilized Enzymes", Raven Press, New York, N.Y., 1974.
(3) R. A. Messing, "Immobilized Enzymes for Industrial Reactors", Academic Press, New York, N.Y., 1975.
(4) G. P. Hicks and S. K. Updike, *Anal. Chem.*, **38**, 726 (1966).
(5) S. J. Updike and G. P. Hicks, *Nature (London)*, **214**, 936 (1967).
(6) S. J. Updike and G. P. Hicks, *Science*, **270**, 158 (1967).
(7) C. Tran Minh and G. Broun, *Anal. Chem.*, **47**, 1359 (1975).
(8) G. G. Guilbault and J. G. Montalvo, *J. Am. Chem. Soc.*, **92**, 2533 (1970).
(9) G. G. Guilbault and J. G. Montalvo, *Anal. Lett.*, **2**, 289 (1969).
(10) G. G. Guilbault, R. K. Smith, and J. G. Montalvo, *Anal. Chem.*, **41**, 600 (1969).
(11) G. G. Guilbault and E. Hrabankova, *Anal. Chem.*, **42**, 1779 (1970).
(12) A. Johansson, B. Mattiasson, and K. Mosbach, *Methods Enzymol.*, **44**, 659 (1976).
(13) A. Johansson, *Protides Biol. Fluids, Proc. Colloq.*, **20**, 567 (1973).
(14) A. Johansson, J. Lundberg, B. Mattiasson, and K. Mosbach, *Biochim. Biophys. Acta*, **304**, 217 (1973).
(15) B. Danielsson and K. Mosbach, *Methods Enzymol.*, **45**, 666 (1976).
(16) B. Danielsson, K. Gadd, B. Mattiasson, and K. Mosbach, *Anal. Lett.*, **9**, 987 (1976).
(17) B. Mattiasson, B. Danielsson, and K. Mosbach, *Anal. Lett.*, **9**, 217 (1976).
(18) B. Mattiasson, *FEBS Lett.*, **77**, 107 (1977).
(19) V. Bilhou-Bougnol, Thesis, Saint-Etienne, 6 C.I. (1976).
(20) I. H. Segel, "Enzyme Kinetics", John Wiley and Sons, New York, N.Y., 926 (1975).
(21) C. Tran-Minh and G. Broun, *C. R. Hebd. Seances Acad. Sci., Ser. D.*, **276**, 2215 (1973).
(22) D. Thomas, G. Broun, and E. Selegny, *Biochimie*, **54**, 229 (1972).

RECEIVED for review March 20, 1978. Accepted June 15, 1978.

Indirect Coulometric Titrations of Complex IV in Intact Mitochondria and Submitochondrial Particles

Robert Szentirmay[1] and Theodore Kuwana*

Department of Chemistry, The Ohio State University, Columbus, Ohio 43210

The complex IV region of intact mitochondria or submitochondrial particles was studied using electrogenerated viologen radical cation for reductant and molecular O_2 as oxidant by the indirect coulometric titration method (ICT). Double-wavelength modulation specrophotometry was employed to circumvent the problems of solution turbidity and low redox component concentrations. The redox potentials for components evaluated using ICT were in good agreement with previous reports. It was also demonstrated that redox information could be obtained using ICT generation of reductant or oxidant in the presence of mediators for acquisition of potentiometric data. Best fit potential data from Minnaert plots gave values of redox potentials for cytochrome *c* oxidase which were in good agreement with those obtained from purified materials.

At our present level of understanding of the respiratory chain, it is well established that any study directed toward elucidating energy transduction processes must be carried out utilizing intact membrane particles (*1*). The more intact the sample is, the more efficient the energy utilization process. In order to prepare submitochondrial fractions with the capabilities of ATP generation, special preparation procedures must be followed (*2*). The critical role of membrane topography and vectorially directed chemical reactions has again been re-emphasized in a series of recent reviews concerning oxidative phosphorylation and photophosporylation (*1*). In addition, cytochrome oxidase manifests in the intact system a number of properties which are not observed in the isolated preparations. The highest oxygen turnover rates have been reported in the intact system (*3*). In the intact membrane, evidence has suggested that the enzyme exists in an asymmetric transmembrane orientation. Heme a_3 has been identified reacting with oxygen on the matrix side of the inner membrane, while heme *a* is found with cytochrome *c* in the inner membrane space (*4*). Rapid oxidation of oxidase and the *c* cytochromes is accomplished in the intact mitochondria by synchronous proton releases (*1*). The apparent mid-point potential for heme a_3 or heme *a*, or both has a significant dependence on the phosphate potential and pH only in the intact system (*5*). In addition, effects of ATP on both the spectroscopic and ligation properties of heme a_3 have been reported (*3*).

Unfortunately in working with the intact systems, a number of experimental difficulties arise. Because of the high turbidity of the samples and the low relative cytochrome concentrations, the concentrations of cytochromes *c* and oxidase in mitochondrial and submitochondrial preparations for visible spectroscopic studies are typically only 1 to 3 μM. This results in a considerable sacrifice of experimental precision for these studies. In addition, one must contend with the possible interference and complications arising from the additional membrane components and exogenous species present in the preparations. Variations also occur in the activities and properties of different preparations. Most importantly for the purposes of redox studies, it is often difficult to poise the respiratory enzymes at well defined redox states because of continuous reduction of the respiratory chain by substrates naturally found in the preparations. It is also difficult to assess whether true equilibrium is ever achieved in such complex multiphase systems.

This portion of our research was undertaken to investigate whether the Indirect Coulometric Titration, ICT, method could be utilized to study intact membrane systems. No such investigation had been made previously. However, a number of reports have shown the feasibility of coupling intact membrane systems to electrochemical methods utilizing mediators (*6–11*). In particular, the extensive work of D. L. Wilson and P. L. Dutton (*12, 13*) has shown the reality of obtaining valuable potentiometric information on the respiratory components utilizing a judiciously chosen set of redox mediators to couple the platinum-sensing electrode to the enzymes. In this way, a well recognized and important thermodynamic picture of the respiratory components has evolved (*12, 13*). Our first objective in this research was to test the ICT method to find out whether quantitative redox information could be obtained on the complex IV region of the chain. Then we wanted to compare this information to data obtained by different methods. Our second objective was to test whether the ICT method could be coupled to the potentiometric technique. The experimental versatility, ease of application, and accuracy of the technique, as previously found in our laboratory with purified enzymes, suggested that the ICT method might be an extremely powerful technique for biochemists in studying the redox and kinetic properties of intact biological systems as well.

EXPERIMENTAL

Intact washed Nagarse beef heart mitochondria (HBHM) were a gift of G. P. Brierly of the Department of Physiology of The Ohio State University. HBHM suspensions, 44 mg/mL and 25 mg/mL, were stored in 0.25 M sucrose, 0.01 M Tris at pH 7.4, frozen at −10 °C and were thawed only immediately prior to use. Mediator and enzyme solutions were prepared fresh just prior to use for each experiment. Electron Transport Particles (ETP) were prepared from HBHM according to the following procedures.

HBHM (25 mg/mL) was sonicated in two 30-s bursts in 30-mL batches at high power. The samples were then centrifuged for 30 min at 12 000 rpm using an SS 34 Sorvall. The supernatant was then decanted and centrifuged at 40 000 rpm for 30 min. Pellets from the second centrifugation were resuspended in Tris–pH 8 buffer to original volume and homogenized using a Teflon homogenizer. ETP samples prepared in this fashion were found to be relatively unstable for quantitative redox titrations. The cytochromes were completely autoreduced by residual substrates in approximately 90 min. ETP samples, prepared according to the initial procedure, were then resonicated for two 30-s bursts, again centrifuged at 40 000 rpm for 30 min, and then the pellets redissolved to original volume. This procedure was repeated once more so that all samples were sonicated at least

[1] Present address, Shell Development Co., P.O. Box 1380, Houston, Texas 77001.

0003-2700/78/0350-1879$01.00/0 © 1978 American Chemical Society

three times and resuspended three times. ETP particles redissolved in this fashion were found to be stable for redox titration for periods of 4 to 6 h after initial thawing before the onset of slow autoreduction. All preparative procedures were performed in ice baths at 0 °C. Samples were stored frozen at −10 °C. Once autoreduction set in, the stability of the samples could not be recovered by freezing and reuse.

One cell for potentiometric work was constructed similarly to that described previously (*14*), except that a 1.25-cm diameter cavity was bored out as the working cell cavity and a platinum flag (1 cm × 1 cm) was incorporated for potentiometric measurements. A second cell of larger volume (9.45 mL) was constructed of similar design for quantitative titrations. All valves and windows were epoxied into position. Sample and mediator preparations and procedures including solution deoxygenation were identical to those described previously (*14*, *15*). All experiments were performed in phosphate buffer pH 7.0 and μ = 0.15 at 50-mM sucrose levels.

Spectroscopic and electronic equipment used were the same as described previously (*14–16*). The sample cell was moved near the PMT housing approximately 1 cm from the PMT front surface. For all experiments, no reference sample was used. Baseline corrections to spectra were made utilizing the NOVA 800 minicomputer on a real-time basis. After an initial spectrum of the fully oxidized respiratory chain was acquired into computer memory, all subsequent spectra were plotted as baseline corrected by the computer utilizing the Fortran program TITREP1 (*17*, *18*). Thus, difference spectra were plotted out directly during the course of the experiment. All raw data, however, was stored on disc memory for future analysis and comparison.

RESULTS AND DISCUSSION

Attempts to poise and quantitatively reduce and oxidize the cytochromes of intact mitochondria without potentiometric redox buffers proved unsuccessful. Utilizing electrogenerated methyl viologen radical cation, $MV^{+\cdot}$, and O_2 as mediator titrants (*19*), the ICT method could readily be applied for reducing and oxidizing the cytochromes to appropriate redox levels including complete oxidation. The order of reduction and oxidation was exactly that expected on the basis of the thermodynamic $E^{o\prime}$ values of the components. That is, optical components were reduced in the order cyto $a_3 \rightarrow a, c, c_1 \rightarrow b_T, b_K \rightarrow$ excess $MV^{+\cdot}$. Reduction of the entire respiratory chain by endogenous substrates occurred in 10 to 30 min, depending on how long the sample was maintained under anaerobic conditions. The longer the experimental sample was analyzed, the faster autoreduction occurred, even in the presence of 8 μg/mg protein of Antimycin or Rotenone.

Stability to autoreduction was considerably improved in the presence of potentiometric redox buffers. Spectra and correlations, as shown previously (*16*), could be obtained for approximately the first 2 or 3 h after rendering the solution anaerobic. The autoreduction rates for the samples depended on the potential and at potentials approximating the $E^{o\prime}$ (±60 mV) of the *potentiometric mediators*, rates were approximately −1 mV per 1 to 10 min for 50 to 100 μM mediator concentrations. In addition, a slow hysteresis was consistently observed for titrations where the *b* cytochromes were being titrated. Equilibrium appeared to require 10 to 30 min before the redox levels of the *c* and *b* cytochromes reached a steady state.

The potentiometric data obtained in the experiment discussed above are shown in Figure 1. These data essentially agree with the results of Dutton, Wilson, and Lee (*6*) for the complex IV region, except that the *a* and *c* cytochromes appear to be 15 to 30 mV higher in potential. The curvature in the potentiometric data at lower potentials (150–250 mV) may be the result of these hysteresis effects or poor mediation to the *b* cytochromes which are imbedded within the mitochondrial membrane (*4*). A computer simulation drawn through the cytochrome oxidase data represents the best fit (±10 mV) as determined by visual inspection of simulation

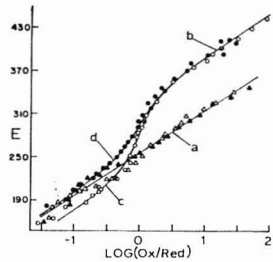


Figure 1. The oxidation (O, △) and reduction (●, ▲) potential dependence of the 605–620 nm (O, ●) and 551–540 nm (△, ▲) absorbance changes of intact mitochondria suspended at 2.2 mg/mL protein at pH 7.0 in phosphate buffer with 50 mM sucrose. Potentiometric mediators added were hydroquinone (80 μM), duroquinone (50 μM), $Fe(CN)_6^{3-}$ (100 μM), PMS (40 μM), CoQ_1 (50 μM). MV = 1.2 mM. Solid lines are for computer simulations for (a) cyto *c*, n = 1.0, $E^{o\prime}$ = 255 mV; (b) heme a_H, n = 1.0, $E^{o\prime}$ = 350 mV (50/50 model); (c) low potential heme, n = 1.0, $E^{o\prime}$ = 215 mV; (d) low heme, n = 1.0, $E^{o\prime}$ = 240 mV. Oxidation was with electrogenerated oxygen

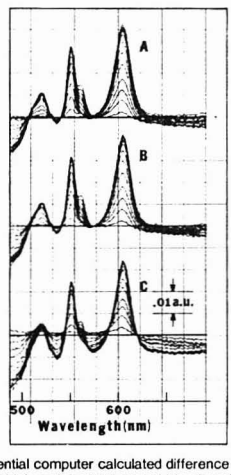


Figure 2. Sequential computer calculated difference spectra obtained for submitochondrial particles (1.0 mg/mL) in phosphate buffer at pH 7.0 in 50 mM sucrose. Spectra were taken during the course of an ICT reduction with BV^+ (1.0 mM). (A) reference λ = 540 nm; (B) reference λ = 562 nm; (C) reference λ = 620 nm

curves. Both curves d and c merge in the high potential region and fit the simulated curve labeled as curve b in this region. The 50/50 percent absorbance model for the two hemes was assumed. Again, this agrees with the observations of D. F. Wilson (*6*, *12*, *13*).

Submitochondrial particles sonicated and centrifuged only once at a high rate (40000) showed an approximately threefold improvement in redox stability. When samples were carried through the sonication and washing procedure three times, a considerably high degree of stability was achieved. Redox states for the complex IV region of the chain could be set and poised for as long as 15 min with no noticeable spectral change (±0.001 au). In addition, if excess O_2 was generated in the cell, it had to be reduced quantitatively by $MV^{+\cdot}$ or benzylviologen radical, $BV^{+\cdot}$ before reduction of oxidase could be initiated. A sample of the type of difference spectra that could be obtained during a reductive titration is shown in

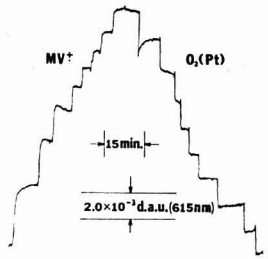


Figure 3. Single wavelength monitor of the cytochrome oxidase peak during the course of an ICT reduction with $MV^{+}\cdot$ (1.0 mM) and subsequent oxidation with electrogenerated O_2. Derivative spectroscopy (dau = derivative absorbance unit) with a 10-nm peak to peak sine wave modulation was used (*16*). Submitochondrial particles were at 1.0 mg/mL protein concentration

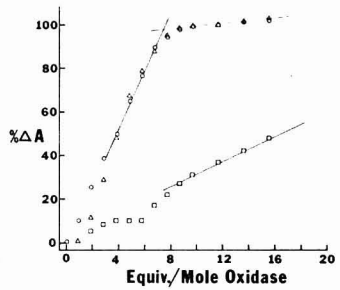


Figure 4. $\Delta A-q$ plots for quantitative ICT reduction of submitochondrial particles (1.0 mg/mL) with $MV^{+}\cdot$ (1.5 mM). (O) 605–620 nm, 100% ΔA = 0.033 au; (Δ) 551–540 nm, 100% ΔA = 0.032 au; (□) 562–575 nm, 100% ΔA = 0.028 au. A 9.44-mL cell with 1.25-cm path length was used

Figure 2, where part A shows the original spectra obtained utilizing 540 nm as the reference wavelength. These spectra were used to quantitate the $c + c_1$ components (552–540 nm). The computer was utilized to replot the data, as shown in Figure 2, parts B and C, with respect to the wavelengths of 575 nm and 620 nm, respectively. These data plots allowed for the quantitiation of the b (562 nm) and oxidase (605 nm) components with respect to their individual isosbestics.

Figure 3 shows the absorbance changes observed for the cytochrome oxidase α peak during the course of a titration. The derivative spectroscopic approach was used for this monitoring, since the high frequency modulation (500 Hz) allowed for continuous monitoring while stirring. In this case, a calibration run indicated that a change of 0.0010 au in the derivative spectrum (10 nm peak-to-peak sine wave modulation) at the α band corresponded to 0.0014 au in the dual wavelength mode. In these cases, titration through the b cytochrome region resulted again in a redox hysteresis similar to that described above.

In Figures 4 and 5 are plotted the absorbance vs. charge data for cytochromes aa_3, $c + c_1$, and $b_T + b_K$ obtained during the course of reduction with $MV^{+}\cdot$ and oxidation with O_2. The charge axis was normalized to equivalents per mole oxidase, where the oxidase concentration was calculated using a $\Delta\epsilon$ of 24 mM for the enzyme at 605–620 nm. Ideally, for complex IV, the extrapolated end point should have required approximately 5 equivalents, since the oxidase (~1.1 μM) and c cytochromes (~1.2 μM) were found approximately

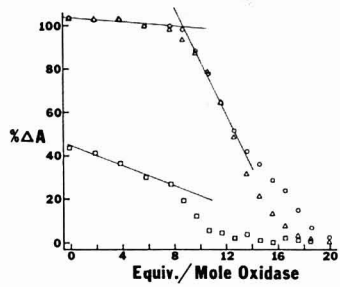


Figure 5. $\Delta A-q$ plots for the quantitative ICT oxidation of the solution described in Figure 4 using electrogenerated O_2 as the oxidant

equivalent in concentration. The order of reduction and oxidation of the cytochromes appeared to be reversible and in agreement with their accepted $E^{\circ\prime}$ values (a_3 = 0.380 V, a = 0.210, $c + c_1$ = 0.225, b = 0.040). The titration slopes on reoxidation were reversible (+10%) to that obtained on reduction, except for a lag in the oxidation of the last 20 to 40% of oxidase, which usually required excess oxygen for complete oxidation. Similar results for oxidations were obtained when using ferrocene methyl trimethylammonium perchlorate as the oxidizing mediator titrant. However, in these cases, 10 to 30% of the oxidase could not be reoxidized with the mediator titrant, but could be readily oxidized using O_2. This result suggests that possibly a portion of the oxidase was shielded by membrane and not accessible to the ferricinium dication.

For six reductions, the average extrapolated end point for the complex IV portion of the titration was 7.3 ± 0.4 equiv/mol oxidase. This value included a 5% correction for background charging currents. Part of the excess reducing charge necessary for the reduction of the c and oxidase portion of the chain can be accounted for by the optically invisible "Rieske" iron sulfur protein found in complex III (~1 equiv, $E^{\circ\prime}$ = 0.285 V) (*7, 8*). The reduction of 5 to 10% of the b cytochrome band at 562 nm during the course of complex IV reduction was found to be qualitatively reproducible. This did not appear to be reversible, as shown in Figure 5, and may thus represent the trapping of high potential b components during reduction with $MV^{+}\cdot$. Similar observation was also made during titrations of intact mitochondria. The rest of the reducing charge was utilized to titrate invisible high potential components, endogenous species, or species which cannot come to thermodynamic equilibrium with the respiratory chain. For example, this might include unsaturated membrane lipids that can be reduced by $MV^{+}\cdot$. In order to test these hypotheses, the experiments would have to be repeated utilizing a less potent reducing agent or using a normal substrate for the respiratory chain.

In these titrations, as with intact mitochondria, equilibrium between cytochromes c and oxidase was achieved very rapidly (<2 min, as shown in Figure 3). However, once the b components were reduced, reoxidation required 10 to 30 min, depending on the extent of reduction of the b cytochromes. Only by waiting for the necessary time could reversible behavior be obtained for complex IV oxidation. In these titrations, as with intact particles, no loss in total absorbance change was observed upon repeated redox cycling.

The type of Minnaert plots obtained for redox titrations similar to those shown in Figures 4 and 5 is shown in Figure 6. The comparative data between cytochromes c and oxidase are reversible and reproducible, but skewed from the expected behavior of heme a_3 which should have a potential of 0.36 V.

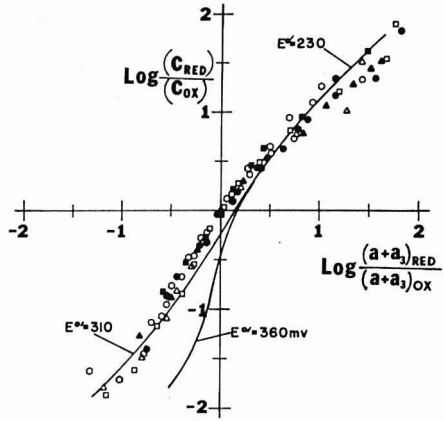


Figure 6. Minnaert plot for the quantitative ICT titrations of submitochondrial particles under the conditions described in Figures 4 and 5. (●, ▲, ■, ■) reductions; (○, △, □, □) corresponding oxidations. The data represent two separate experimental samples

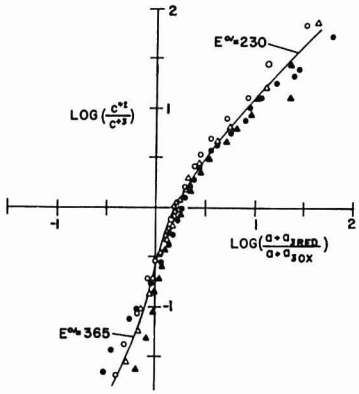


Figure 7. Minnaert plot for cytochrome *c* and oxidase of submitochondrial particles (1.0 mg/mL) obtained during ICT titrations with MV and O_2 in the presence of redox mediators. (●, ▲) reductions; (○, △) corresponding oxidations. Mediators added were $Fe(CN)_6^{3-}$ (100 μM), diaminodurene or hydroquinone (50 μM), PMS (70 μM), duroquinone (40 μM), CoQ_0 or CoQ_1 (40 μM). $E^{o\prime}$ for cytochrome *c* was assumed = 255 mV for the simulations

In this figure, $E^{o\prime}$ for cytochrome *c* was assumed to be 0.255 V. Heme a_3 appears to have a potential of only 60 mV higher than cytochrome *c* and heme *a* a potential 25 mV lower. However, if it is assumed that 20% of the oxidase was not oxidized by O_2 under the experimental conditions, an excellent correlation between the data and the simulation for a 0.36 V high potential component can be obtained, along with a better fit for a low potential component at 0.23 V. The results suggest that even with excess oxygen (4–8 oxidase equiv) in the system, it may be difficult to poise complex IV at high redox potentials.

Minnaert plots obtained during the course of the same type of ICT redox titrations, but in the presence of potentiometric redox mediators, are shown in Figure 7. It should be noted

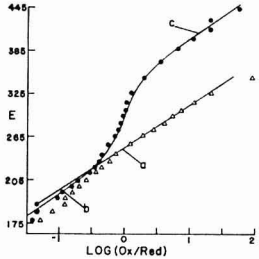


Figure 8. The potential dependence of 605–620nm (●) and 551–540 nm (△) absorbance changes of submitochondrial particles during reduction with MV^+·. Experimental solution conditions are the same as in Figure 7. Computer simulations are for (a) $n = 1.0$, $E^{o\prime} = 252$ mV; (b) low potential heme (50/50 model), $n = 1.0$, $E^{o\prime} = 225$ mV; (c) high potential heme, $n = 1.0$, $E^{o\prime} = 365$ mV

that these mediators were not present in the experiments whose results were shown in Figure 2–5. These results are more in line with the type of data anticipated for cytochromes *c* and oxidase. The potentiometric data for one of the titrations of Figure 7 are plotted in Figure 8. The best fit for the potentiometric data for cytochrome oxidase is for potentials of 0.225 V and 0.365 V using a 50/50 percent model for the two heme absorbances. These potentials are in good agreement with those results obtained for intact mitochondria and with the results obtained previously (*6*).

CONCLUSIONS

The experiments described herein clearly demonstrate that the ICT method can be readily applied to the intact membrane bound systems. Potentiometric data comparable to those obtained by other methods can also be conveniently obtained. The problems of hysteresis and redox mediation that may periodically occur appear to be inherent to the complex nature of the respiratory chain and not to the ICT approach.

To achieve rapid equilibration in these membrane systems, judicious choice of redox mediators (*12*, *21*) is required.

With the evaluation of mediators and mediator titrants, as discussed in reference 19, a wide range of compounds is available for attacking the problems posed herein. Kula et al. have recently applied the ICT approach for the anaerobic titration of the cytochromes in membrane vesicles of *Paracoccus denitrificans*. They, too, were able to reversibly redox cycle the system through reductive and oxidative titrations with no loss in absorbance change or evidence of denaturation (*20*). They found no problem in achieving rapid equilibration in the presence of potentiometric mediators.

It has also been demonstrated that submitochondrial ETP particles can be prepared with sufficient stability for quantitative work. The differences observed for heme a_3 with and without redox mediators may reflect a true difference in thermodynamic characteristics. On the other hand, the experimental results may suggest that even under "poised" conditions a considerable oxygen tension might be required for the complete oxidation of the heme a_3 component in the intact system (*22*). The problem of the incomplete oxidation of heme a_3 requires further investigation. The possibility that endogenous reductants are present and are reducing oxidase has been suggested previously (*23*).

The ICT method, as applied, is essentially the same as that previously utilized for the study of purified enzyme systems. Only the addition of improved spectroscopic techniques and of an experimental awareness of the complex chemistry involved was required. The ease in the application of ICT for adjustment of redox level of components provides a powerful

tool for biochemists to perform quantitative, potentiometric, or characterization studies of known and unknown intact biological systems. In addition, the technique allows for control of redox levels by applications of charge injections *continuously* or *incrementally* at nanoequivalent quantities. The technique can readily be interfaced with other physical methods to study such systems. In particular, it should be most advantageous in combination with those where the cell is not readily manipulated or requires remote operation. In many newer techniques, the low signal level may require signal averaging for extended periods of time. ICT control of such systems would be most advantageous because of its ease in repetitive operation.

Hendler et al. (*9*) have recently automated an electrochemical method to intact systems. They have pointed out the advantages of using electrochemistry with computer control for obtaining potentiometric information. Unfortunately, their "current" pulse method has some serious limitations which could lead to erroneous and detrimental results. That is, unless a sufficiently large amount of *known* depolarizer (could be a mediator) is present in the solution to control the potential during the current pulses, the potential would increase (e.g., for an oxidation) to where the faradaic reaction may involve undesirable components. The preferred method of coulometry such as in ICT, is by controlling the *applied potential* of the working electrode (vs. a reference electrode) to a *known, constant value* where the electrolysis current is carried by a known depolarizer, e.g., mediator titrant. The problems of electrode potential memory and "instability" at the working electrode and the incomplete optical absorbance changes for certain components in Hendler's work (*9*) could have been due to the "uncontrolled" electrolysis conditions. These problems are accentuated when the current density is relatively high and the solution does not contain readily electrolyzable, faradaic reactants, such as mediators. The advantages of computer automation, as described by Hendler (*9*), can also be applied to the ICT method, as conducted in our laboratory for several years (*16, 17, 24*). It cannot be overemphasized to those planning to use electrochemical methods to change redox levels of biocomponents that *potential control* of the working electrode is the preferred method with a faradaic reactant determining the current level.

ACKNOWLEDGMENT

We hereby acknowledge the kind assistance of John S. Rieske in the preparation of the mitochondrial particles.

LITERATURE CITED

(1) E. C. Slater, *Ann. Rev. Biochem.*, **46**, 1015–1025 (1977).
(2) R. W. Estabrook, and M. E. Pullman, *Methods Enzymol*, **10**, (1967).
(3) P. Nicholls, and B. Chance, in "Molecular Mechanism of Oxygen Activation", O. Hayaishi, Ed., Academic Press, New York, N.Y., 1974, p 479.
(4) J. W. Depierre, and L. Ernster, *Ann. Rev. Biochem.*, **46**, 201–262 (1977).
(5) B. G. Malmstrom, *Q. Rev. Biophys.*, **6**, 389 (1973).
(6) P. L. Dutton, D. F. Wilson, and C. P. Lee, *Biochemistry*, **9**, 5077 (1970).
(7) M. Erecinska, and D. F. Wilson, *Arch. Biochem., Biophys.*, **174**, 143–157 (1976).
(8) M. Erecinska, D. F. Wilson, and Y. Miyata, *Arch. Biochem. Biophys.*, **177**, 133–143 (1976).
(9) R. W. Hendler, D. Songco, and T. R. Clem, *Anal. Chem.*, **49**, 1908–1913 (1977).
(10) J. J. Eiler, J. E. Goyan, L. D. Tuck, and C. C. Collins, *J. Am. Pharm., Assoc.*, **47**, 497 (1958).
(11) B. Ke, F. M. Hawkridge, and S. Sahu, *Proc. Natl. Acad. Sci. USA*, **73**, 2211 (1976).
(12) D. F. Wilson, P. L. Dutton, M. Wagner, in "Current Topics in Bioenergetics", D. R. Sanadi, Ed., Vol. 5, Academic Press, New York, N.Y., 1973.
(13) D. F. Wilson, P. L. Dutton, M. Erecinska, J. G. Lindsay, and N. Sato, *Acc. Chem. Res.*, **5**, 234 (1972).
(14) F. M. Hawkridge and T. Kuwana, *Anal. Chem.*, **45**, 1021 (1973).
(15) J. L. Anderson, T. Kuwana, and C. R. Hartzell, *Biochemistry*, **15**, 3847 (1976).
(16) R. Szentirmay, and T. Kuwana, *Anal. Chem.*, **49**, 1348 (1977).
(17) D. Yates, R. Szentirmay, and T. Kuwana, manuscript submitted for publication.
(18) R. Szentirmay, Ph.D. Thesis, The Ohio State University, Columbus, Ohio, 1978.
(19) R. Szentirmay, P. Yeh, and T. Kuwana, "Electrochemical Studies of Biological Systems", D. T. Sawyer, Ed., *ACS Symp. Ser.*, **38**, 143 (1977).
(20) T. Kula, R. Szentirmay, E. Stellwagon, and T. Kuwana, presented at the Annual Meeting American Chemical Society for Microbiology (1978).
(21) P. L. Dutton, and D. F. Wilson, *Biochim. Biophys. Acta*, **346**, 165–212 (1974).
(22) B. Chance, R. Oshino, T. Sugano, and N. Oshino, *Biochim. Biophys. Acta*, **368**, 298 (1974).
(23) D. Wilson, and Y. Miyata, *Biochim. Biophys. Acta*, **461**, 218–230 (1977).
(24) D. Yates, Ph.D. Thesis, The Ohio State University, Columbus, Ohio, 1976.

RECEIVED for review May 23, 1978. Accepted July 27, 1978. Work supported by funds from U.S. PHS Grant GM 19181. Portions of the instrumentation utilized in this work were provided by NSF Grant CHE76-81591.

Reexamination of Potentiometric Studies of the Oxidation of *o*-Tolidine

M. A. Ditzler and W. F. Gutknecht*

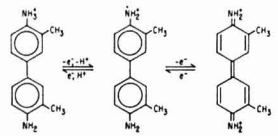
Department of Chemistry, Duke University, Durham, North Carolina 27706

Several studies have shown that optimizing conditions for the formation of the intensely-colored intermediate observed during the oxidation of *o*-tolidine leads to a reduction in the ESR signal normally associated with this oxidation process. This observation is in conflict with an earlier theory based on potentiometric data, that is, that the intensely-colored intermediates observed during the oxidation of this and similar compounds (i.e., benzidine analogues) are radical-cations. Here the earlier data are reevaluated and new potentiometric data are presented. It is shown that these data are consistent with a dimeric intermediate, which is in agreement with the ESR results.

o-Tolidine and related compounds such as benzidine and *o*-dianisidine (i.e., [1,1′-biphenyl]-4,4′-diamines) have been widely used in analytical chemistry. They have recently been used as model compounds in spectroelectrochemical studies (*1, 2*), as indicators in trace element detection schemes (*3, 4*), in the production of ion-selective electrodes (*5*), and for chemically modifying electrode surfaces (*6*). Their analytical utility is due, in part, to the fact that these compounds can be reversibly oxidized to give intensely colored products. If the oxidation is carried out in a weakly acidic solution, two products are observed. One product is at a maximum concentration after one equivalent of an oxidizing agent has been added, while a second product reaches a maximum concentration after two equivalents of the oxidizing agent have been added. A survey of the literature shows that there is a disagreement over the identity of the first of these products.

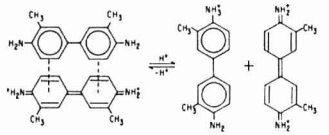
0003-2700/78/0350-1883$01.00/0 © 1978 American Chemical Society

Oldfield and Bockris have made potentiometric studies of *o*-tolidine and related compounds and concluded that the first oxidation product is a semiquinone radical-cation and the final product is a quinonediimine (*7*) (Equation 1).



(1)

Recently this conclusion was supported by further potentiometric studies by Ghimicescu and Dima (*8*). However it has been shown for *o*-tolidine that, if the concentration of the intermediate species is optimized by adjusting the pH, the ESR signals disappear (*9, 10*). This observation led to dilution studies by these same workers which suggest that the observed intermediate is dimeric. Furthermore, the presence of a strong, broad absorption band at 630 nm suggests that the dimer is a charge transfer complex, which is proposed to exist in equilibrium with the reduced and oxidized forms of *o*-tolidine as shown in Equation 2 (*9*).



(2)

This apparent contradiction (radical-cation *vs.* dimer) has not been explained. In an attempt to clarify this matter, previously reported data and arguments have been reexamined; in addition, new potentiometric data have been collected via the oxidation of *o*-tolidine by bromine. In the following discussion we show that the potentiometric data previously used to support the existence of a radical-cation intermediate are also consistent with the existence of a dimeric intermediate, e.g., a 1:1 complex of the type shown in Equation 2.

EXPERIMENTAL

Materials. *o*-Tolidine (Eastman) solutions were prepared in spectral grade acetone (Fisher). The buffer solutions were prepared from acetic acid (B & A reagent grade) and sodium acetate (Fisher ACS certified) so as to have a pH of 3.5 and a concentration of 0.5 M in acetate ion. Aqueous bromine (Fisher reagent grade) solutions were made 1.0 M in KBr (Merck, reagent grade) to lower the Br_2 volatility. As_2O_3 (Mallinckrodt, reagent grade) solutions were prepared for use as primary standards. A spiraled platinum wire and a saturated calomel electrode served as the electrodes. Potentials were measured with a Beckman SS-3 pH meter.

Procedures. Bromine solutions were standardized by addition of excess KI (MCB, reagent grade) followed by titration of the resulting iodine with As_2O_3 (*11*). *o*-Tolidine solutions were diluted with sufficient buffer to make solutions that were 90% aqueous–10% acetone. Portions of these solutions, 100 mL, were titrated with bromine solutions that were of appropriate concentration to give only a 1% volume change. Titrant was added in quantities which allowed at least 10 potential measurements before the end point. Since the oxidized form of *o*-tolidine is unstable in weakly acid solutions (*9, 10*), care was taken to ensure that all titrations were performed uniformly and rapidly (about 2 min per sample).

RESULTS AND DISCUSSION

In the potentiometric studies there were four arguments presented in favor of the intermediate being a semiquinone radical-cation rather than a dimer.

1. The titration curve obtained when *o*-tolidine is titrated with aqueous bromine is symmetric. It was argued that this indicates that a dimeric intermediate is unlikely (*7*).

2. The index potentials (difference in potential at one-half and either one-fourth or three-fourths completion of the titration) observed in the titrations of *o*-tolidine with aqueous bromine at 25 °C are greater than 14.1 mV. It was reported than an index potential greater than 14.1 mV (the theoretical value for a two-electron oxidation) establishes the presence of a semiquinone radical-cation intermediate (*7*).

3. A graph of the potentiometric titration of 5×10^{-3} M *o*-tolidine with $S_2O_8^{2-}$ shows two vertical regions. The first corresponds to the addition of sufficient $S_2O_8^{2-}$ to remove one electron per *o*-tolidine molecule and the second corresponds to removal of two electrons per molecule. This, it was argued, supports the existence of a stable radical-cation (*8*).

4. It was reported that the shapes of the titration curves obtained when *o*-tolidine is titrated with aqueous bromine are independent of the initial concentration used, that is, they are superimposable. If the intermediate is a dimer, the curves would not be superimposable (*7*).

It can be shown that the first three observations actually are not inconsistent with the existence of a 1:1 complex (i.e., the dimer shown in Equation 2). We have made measurements similar to those which served as the basis for the fourth observation and found results that agree with those expected for a 1:1 complex, in conflict with those reported in the earlier study. An examination of the four arguments follows.

1. A potentiometric titration curve is symmetric about the midpoint if the following condition is met:

$$E_{(1/2p)} - E_{(1/2p-q)} = E_{(1/2p+q)} - E_{(1/2p)} \tag{3}$$

where E is the measured potential and the subscripts on E represent the moles of sample titrated. Here p represents the moles of sample initially present and q is any number from zero to $1/2p$. This condition can be shown to hold for the case when a 1:1 complex is present during the titration. That is, since this type of complex ties up equal quantities of both the oxidized and reduced species, $E_{(1/2p)}$ would be equal to E^0 and thus Equation 3 can be rewritten as

$$E^0 - E_{(1/2p-q)} = E_{(1/2p+q)} - E^0 \tag{4}$$

This same property allows us to express $E_{(1/2p-q)}$ and $E_{(1/2p+q)}$ as

$$E_{(1/2p-q)} = E^0 + \frac{0.059}{n} \log \left(\frac{\frac{1}{2}p - q - w}{\frac{1}{2}p + q - w} \right) \tag{5}$$

$$E_{(1/2p+q)} = E^0 + \frac{0.059}{n} \log \left(\frac{\frac{1}{2}p + q - m}{\frac{1}{2}p - q - m} \right) \tag{6}$$

where w and m are, respectively, the moles of complex present after $(1/2p - q)$ and $(1/2p + q)$ moles of sample have been titrated. If we substitute these expressions into Equation 4 and simplify, we get

$$\frac{\frac{1}{2}p + q - w}{\frac{1}{2}p - q - w} = \frac{\frac{1}{2}p + q - m}{\frac{1}{2}p - q - m} \tag{7}$$

From inspection it is obvious that this equality holds for all possible values of p and q (the requirement for symmetry) when $w = m$, that is, when the moles of complex present at $(1/2p - q)$ and $(1/2p + q)$ are equal. It can be shown that $w = m$ by examining K_{eq} expressions. Using the conditions present at $(1/2p - q)$ and $(1/2p + q)$ and assuming the

equilibrium in Equation 2 holds, K_{eq} for formation of the complex can be written as either

$$K_{eq} = \frac{(w)(H^+)}{\left(\frac{1}{2}p - q - w\right)\left(\frac{1}{2}p + q - w\right)} \text{ or } K_{eq} = \frac{(m)(H^+)}{\left(\frac{1}{2}p + q - m\right)\left(\frac{1}{2}p - q - m\right)}$$

These expressions are written in terms of moles rather than concentrations since the volume terms cancel. Setting the two K_{eq} expressions equal, cross multiplying, and collecting terms gives

$$(w - m)\left[\left(\frac{1}{2}p - q\right)\left(\frac{1}{2}p + q\right) - wm\right] = 0 \quad (8)$$

Equation 8 implies that either $w = m$ or $(1/2p - q)(1/2p + q) = wm$. However, the second possibility is not physically significant. This becomes apparent when it is realized that the moles of both species involved in complexation, w and m, must both be less than $(1/2p - q)$ since K_{eq} (complex formation) $< \infty$. Since w, m, and p represent moles of a species present they must be nonnegative; therefore, if $(1/2p - q)(1/2p + q) = wm$, $(1/2p + q)$ must be less than $(1/2p - q)$, which would imply that q is negative. However, this is not possible since the preceding argument is based on the earlier definition that $0 < q < 1/2p$. An analogous argument based on $0 < q < -1/2p$ would lead to the contradiction that q be positive. Therefore, w and m must be equal. This implies that Equation 7 holds and thus the potentiometric titration curves would be symmetric even if the 1:1 complex is reversibly formed during the titration. Thus, the observed symmetry is not inconsistent with the formation of a 1:1 complex as has been reported (7).

2. If the 1:1 complex forms, the index potential for *o*-tolidine can be expressed as

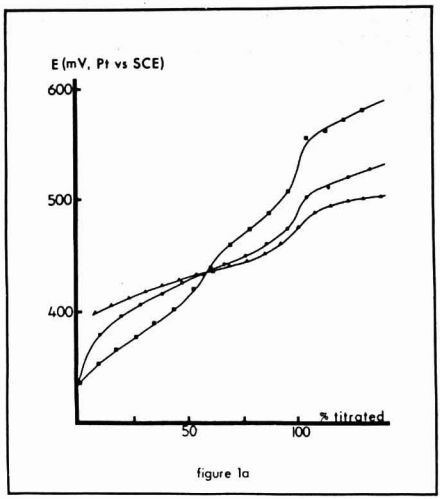
$$E_{(index)} = E_{(3/4p)} - E_{(1/2p)} = E^0 + 0.0295 \log\left(\frac{\frac{3}{4}p - y}{\frac{1}{4}p - y}\right) - E_{(1/2p)} \quad (9)$$

where again, E is the measured potential and the subscripts on E represent the moles of the *o*-tolidine that have been titrated; here y represents the moles of the complex present. Since, as was explained earlier, $E_{(1/2p)} = E^0$ even with the complex present, Equation 9 can be simplified to

$$E_{(index)} = 0.0295 \log\left(\frac{\frac{3}{4}p - y}{\frac{1}{4}p - y}\right)$$

If the amount of complex present (y) is greater than zero, but less than $1/4p$ (as it must be), the term in the parentheses would be greater than three, and hence $E_{(index)}$ would be greater than 14.1 mV. Thus the observation that the index potential for *o*-tolidine is greater than 14.1 mV at 25 °C does not establish the presence of semiquinone radical-cation as has been reported (7).

3. Some years past Michaelis and Schubert carried out theoretical studies of the redox titrations of analogous systems (12). In one case they assumed that reactant and product formed a 1:1 complex; for this case they subsequently predicted that if the mathematical product of K'_{eq} (the apparent formation constant for the complex) and the initial reactant concentration was greater than four, an additional vertical region would appear in the titration curve at the point where one half of the reactant had undergone a two-electron oxidation. Phenomenologically this vertical region corresponds first to a rapid decrease in "free" reactant as it is both oxidized and complexed by product, and subsequently, a rapid increase in "free" product as no "free" (uncomplexed) reactant remains to complex with product. The midpoint of this region corresponds then to the concentration of the complex being at a maximum. A value for K'_{eq} of 1.03×10^5 (pH 4) has been



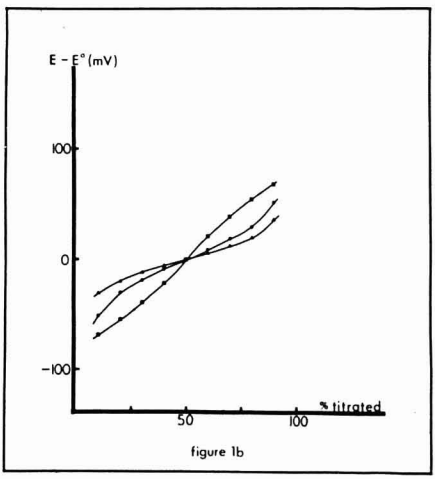


Figure 1. A comparison of experimental (1a) and calculated (1b) potentiometric titration curves for the oxidation of *o*-tolidine with Br_2. Curves shown for 10^{-3} M (■), 10^{-4} M (●), 10^{-5} M (▲) *o*-tolidine at pH 3.5. Titrant concentrations were such that volume changes were negligible. Calculated potentials were based on a K_{eq} of 11 for the formation of a 1:1 complex between the oxidized and reduced forms of *o*-tolidine.

reported for the *o*-tolidine system (*9*). Thus it would be predicted that a titration curve of an *o*-tolidine sample at pH 4 with an initial concentration greater than 3.88×10^{-5} M would contain the additional vertical region. So too, the observation that the titration of a 5×10^{-3} M *o*-tolidine solution produces two vertical regions does not necessarily indicate that there is a free semiquinone radical-cation formed, as has been suggested (*8*).

4. We have carried out potentiometric titrations of 10^{-3}, 10^{-4}, and 10^{-5} M solutions of *o*-tolidine with aqueous bromine using Pt and SCE electrodes. Plots of the potentials measured during the titrations are shown in Figure 1a. As in the earlier study, the titrant concentrations were such that volume changes were insignificant. It is apparent that our results do not agree with those reported earlier in which the titration curves were found to be superimposable regardless of the initial concentration of the *o*-tolidine (*7*). The pH of the solutions used in the earlier study was not reported, but from the midpoint potentials of the titrations shown and a graph of pH vs. the midpoint potentials presented in the earlier study, it is apparent that the pH was less than 2.0. This may explain the discrepancy since the intermediate species is either absent or present only in low concentrations at such a low pH (*9, 10*). The solutions represented in Figure 1a were buffered at a pH of 3.5, which is within the range over which the intermediate form is observed (*10*).

Figure 1b shows the *theoretical* titration curves for aqueous *o*-tolidine solutions of analogous concentrations and pH, assuming the 1:1 complex is formed according to the reverse of Equation 2 and using a previously reported K_{eq} of 11 (the absolute formation constant) (*9*). In preparing the theoretical curves, it was assumed that the solubility of the complex is not exceeded. In reality this is not the case for the 10^{-3} M solution (*7*), so a 10% acetone–90% water solvent was used in all cases to ensure complete solubility throughout. The difference between the theoretical and experimental curves due to this difference in solvents should be small since it has been reported that the concentration of the intermediate species is only slightly affected by switching from water to a water–acetone solvent (*7*). The difference between the expected point of intersection of all curves at 50% (where $E = E^0$, even with complex present) and the experimental 58% is probably due to the fact that the oxidized form of *o*-tolidine gradually decomposes under the experimental conditions used (*9, 10*). This would cause the oxidized and reduced forms of *o*-tolidine to be of equal concentrations later in the titration; hence, the potentials would be independent of the initial concentrations at a later point, and thus the titration curves should intersect at a later point. The curves are not superimposable after 100% oxidation as might be expected since the oxidizing solutions contained different bromine to bromide ratios. Taking these points into consideration, it is apparent that the change in shapes of the curves resulting from a variation of the initial *o*-tolidine concentration corresponds closely to that predicted on the basis of the 1:1 complex forming.

In conclusion, we have shown that the results of the potentiometric and ESR studies of the colored intermediate observed during the oxidation of *o*-tolidine are not inconsistent. Of the four potentiometric measurements that appeared to be inconsistent with the ESR data, three have been shown to actually be consistent with the ESR data, and the fourth measurement becomes consistent when repeated at a higher pH.

LITERATURE CITED

(1) T. P. DeAngelis, R. W. Hurst, A. M. Yacynych, H. B. Mark, Jr., W. R. Heineman, and J. S. Mattson, *Anal. Chem.*, **49**, 1395–1398 (1977).
(2) V. E. Norvell and G. Mamantov, *Anal. Chem.*, **49**, 1470–1472 (1977).
(3) C. Ghimicescu, M. Stan, and B. Dragomir, *Talanta*, **20**, 246–247 (1973).
(4) J. Malý and H. Fadrus, *Analyst (London)*, **99**, 128–136 (1974).
(5) M. Sharp, *Anal. Chim. Acta.*, **61**, 99–114 (1972).
(6) J. F. Evans and T. Kuwana, *Anal. Chem.*, **49**, 1632–1635 (1977).
(7) L. F. Oldfield and J. O'M. Bockris, *J. Phys. Colloid Chem.*, **55**, 1255–1274 (1951).
(8) C. Ghimicescu and F. Dima, *Talanta*, **23**, 67–69 (1976).
(9) T. Kuwana and J. W. Strojek, *Discuss. Faraday Soc.*, **45**, 134–144 (1968).
(10) J. D. Johnson and R. Øverby, *Anal. Chem.*, **41**, 1744–1750 (1969).
(11) A. I. Vogel, "Quantitative Inorganic Analysis", 3rd ed., Longmans, Green & Co. Ltd., London, 1961, p 355.
(12) L. Michaelis and M. P. Schubert, *Chem. Rev.*, **22**, 437–470 (1938).

RECEIVED for review May 22, 1978. Accepted August 28, 1978. One of us (M.D.) was supported by an ACS Analytical Division Fellowship sponsored by the Society for Analytical Chemists of Pittsburgh.

Adsorption and Polymeric Film Formation at Mercury Electrodes by Solutions of Lead(II) and Chelating Ligands Containing a Thioether Group

Bruce A. Parkinson and Fred C. Anson*

Arthur Amos Noyes Laboratory, California Institute of Technology, Pasadena, California 91125

The adsorption on mercury of the complexes of several chelating carboxylate ligands bearing thioether groups with Pb(II) and some other d^{10} metal cations is examined. The extraordinarily large adsorption observed with a number of complexes is attributed to the formation of new phases on the mercury electrode surface. The structure of the adsorbed films may resemble the polymeric crystals formed by several metal salts of the same ligands.

As part of continuing studies of the surface and coordination chemistry attending the adsorption of metal cations on mercury electrodes in the presence of adsorption-inducing ligands (*1*), we have examined the ability of a series of carboxylic ligands containing thioether groups to induce the adsorption of lead(II) and some other d^{10} metal cations. The idea was to exploit the expected propensity of the sulfur atom in the thioether group to adsorb on the mercury surface while the carboxylate arms of the ligand chelated the metal cation. Somewhat to our surprise we found that the presence of the thioether group does not result in particularly strong adsorption of the ligands. However, the complexes of such ligands with heavy metal cations, especially lead, are strongly attracted to mercury surfaces. The observed behavior is novel

0003-2700/78/0350-1886$01.00/0 © 1978 American Chemical Society

in that neither the ligand nor the metal cation exhibit strong spontaneous adsorption when present alone. In this report, the combination of surface and coordination chemistry that is responsible for the observed behavior is discussed. It might be termed "metal-activated-ligand-induced adsorption".

The dependence of the adsorption on the ligand concentration and the electrode potential show many similarities with behavior that has been described by Murray and co-workers (*2–5*) for the halide-induced adsorption of lead(II) and thallium(I) from solutions in which the limit of the metal halide solubility is approached (but not attained). "Crystalline bilayers" can be obtained in such cases in which the total quantity of metal cation present on the electrode surface exceeds (by about twofold) that calculated for a close-packed monolayer (*3*). Several of the thioether ligands utilized in these studies induce the adsorption of comparably large quantities of Pb(II) in the form of what appears to be a new phase on the electrode surface. The formation, properties, and possible structures of these adsorbed films are described in what follows.

EXPERIMENTAL

Reagents. The thioether ligands examined in this study are listed in Table I. They were obtained commercially in the form of the parent acid: 2,2′-thiodiacetic, 3,3′-thiodipropionic (Matheson, Coleman and Bell); thiodisuccinic, methylenebisthioacetic, and thioacetosuccinic (Evans Chemetics); ethylthioacetic and diglycollic (Aldrich). The acids were converted to sodium salts and recrystallized repeatedly from water–ethanol until no odor could be detected from the solids. As a final test for the absence of traces of mercaptans, cyclic voltammograms were recorded in 0.1 M solutions of each ligand with a hanging mercury drop electrode which was exposed to the solution for 30 to 60 s. Insufficiently purified samples frequently produced current peaks or sharp spikes so that a smooth, featureless background current between +200 and −600 mV was a requirement for each solution of ligand before it was utilized in adsorption experiments.

Metal cations were obtained from reagent grade nitrate salts. Oxygen was removed from solutions with prepurified argon or nitrogen that had been passed through a vanadium(II) solution. Triply distilled mercury (Bethlehem Instrument Co.) and water were employed.

Apparatus and Procedure. A conventional hanging mercury drop electrode (Brinkmann Instruments Co.), a two-compartment cell, and a sodium chloride-saturated calomel electrode were employed. The quantity of each complex adsorbed was determined by double potential step chronocoulometry (*6*) with a PDP 11/40 minicomputer and an associated electrochemical instrument based on conventional utilization of operational amplifiers. Data acquisition rates and electrode equilibration times were adjusted to achieve adsorption equilibrium. With solutions of Pb(II) the measured adsorption values were independent (±10%) of the equilibration time for times from ca. 10 to 100 s in unstirred solutions. However, with several complexes of Cd(II) the measured adsorption remained time-dependent at all equilibration times from 5 to 60 s. The few values given for Cd(II) adsorption in Figure 1 were obtained after the electrode was exposed to the solution for 5 s. They were reproducible but are not equilibrium values.

At the high coverages obtained with Pb(II) complexes, the concentration of adsorbed Pb(II) did not reach its final equilibrium value until late in the reverse potential step. The resulting small errors in the value of the charge consumed by the electrical double layer (*7*) were neglected in evaluating the much larger quantities of adsorbed reactant from the intercepts of the chronocoulometric charge–time plots.

The double layer capacitance and cell resistance were obtained from ac impedance measurements with an applied ac voltage of 5-mV amplitude and 10^3 Hz. The ac signal was imposed via a Princeton Applied Research Model 173 potentiostat and the in-phase and quadrature ac responses were obtained with an Ithaco Model 391-A Lock-in-Amplifier and a Fluke Model 2000A Digital Voltammeter.

RESULTS AND DISCUSSION

Adsorption of Ligands. Data on the adsorption of simple carboxylate anions on mercury are relatively sparse (*8–10*). Pospisil and Kuta (*9*), who examined the adsorption of maleic and succinic acids and the corresponding monoanions, concluded that the netural acids behave similarly to other uncharged organic adsorbates in that their adsorption is maximal near the point of zero charge. The acid anions, on the other hand, resemble simple inorganic anions in showing steadily increasing adsorption as the charge on the mercury surface becomes more positive.

Quantitative data on the adsorption of thioethers or of molecules bearing both carboxylate and thioether groups have not been reported. We examined the adsorption of several ligands qualitatively by measuring the change in the electronic charge density on the electrode produced by the addition of the ligand to solutions of NaF or $NaClO_4$ (0.3 M) adjusted to pH values between 6 and 7 where the ligands were anionic. For example, at potentials between −100 and −800 mV, the presence of 0.05 M thiodiacetate produced small, positive increases in the charge density similar to those observed with the hydrogenmaleate anion (*9*). The increase in charge density is much smaller at potentials negative of −800 mV, presumably because anion adsorption becomes insignificant at sufficiently negative surfaces. At potentials positive of −100 mV, larger increases in charge density are produced by the presence of thiodiacetate anions and it seems likely that the sulfur atom of the thioether may begin to participate in the adsorption at the most positive potentials. Polarograms of solutions containing 1 to 2 mM thiodiacetate anions show no well-defined anodic wave corresponding to the formation of a Hg(II)–ligand complex. This is not surprising if the formation constant for the Hg(II) complex is comparable to the known values for Pb(II), Cd(II), and Zn(II), ca. 10^3 M^{-1}.

All of the ligands listed in Table I produced charge–potential curves that were qualitatively similar to that of thiodiacetate. That is, none of the ligand anions appears to be adsorbed on mercury as strongly as, for example, iodide, thiocyanate, or bisulfide.

Adsorption of Pb(II)–Ligand Complexes. Despite the relatively weak interaction between the free ligands and mercury electrodes, the Pb(II) complexes of all of the ligands in Table I show extraordinarily large adsorption. With TAS and TDS as ligands, as much as 8×10^{-10} mol cm^{-2} of Pb(II) is attached to the electrode surface. The adsorption can be eliminated by lowering the pH below 2 where the Pb(II)–ligand complexes are unstable. Figure 1 summarizes some representative data for four of the ligands. The other ligands in Table I behaved similarly except for thiodisuccinate which deviated somewhat from the common pattern shown in Figure 1. (The complete data set is available in reference 11).

There are several remarkable features in the behavior shown in Figure 1. The Pb(II) complexes of the ligands all exhibit an adsorption which is rather insensitive to the electrode potential over a significant range with a shallow minimum usually appearing between +50 and −50 mV. However, outside of this central potential range, the adsorption increases both at more negative and more positive potentials. In many cases, plots of adsorption vs. potential exhibit a common intersection point on the positive side near +200 mV. A similar common intersection point also appears to result on the negative side if the plots are extrapolated to potentials beyond that at which the reduction of Pb(II) commences. These common intersection points may signal the formation of particularly stable configurations of the adsorbed films toward which solutions of all compositions converge. However, the significantly larger value of the adsorption at the intersection point on the negative side indicates that two different stable forms (or

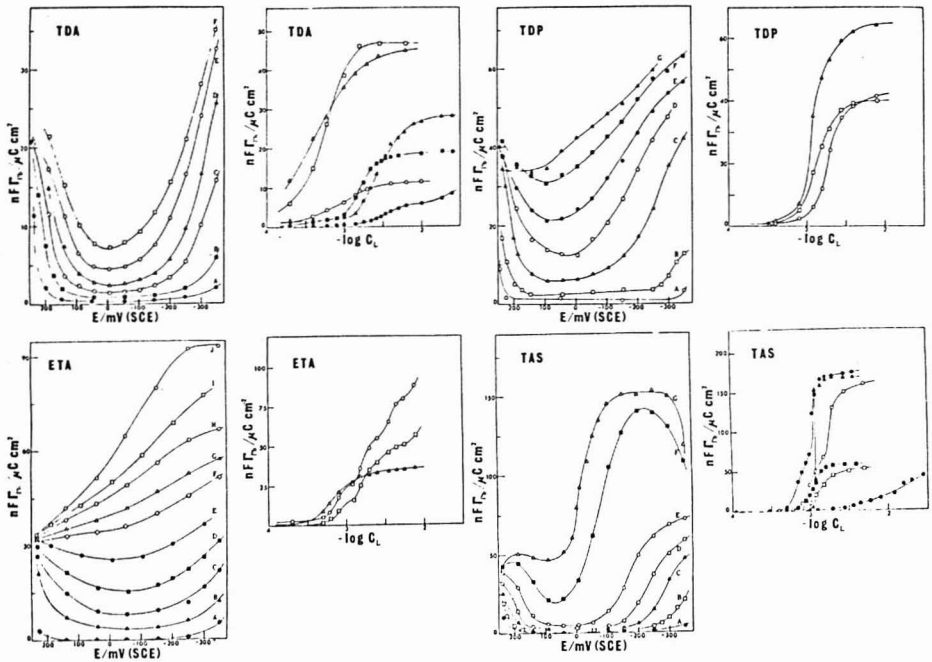


Figure 1. Representative adsorption behavior of Pb(II) complexes of four ligands. The first plot in each pair gives the potential-dependence and the second plot the ligand concentration dependence of the adsorption. Unless otherwise noted all measurements were made with 0.5 mM Pb(II) in 1 M $NaClO_4$. Other experimental parameters: For TDA: first plot: concn. of TDA: (A) 0.8, (B) 1.4, (C) 2.2, (D) 3.0, (E) 6.0, (F) 18.4 mM. Second plot: potential vs. SCE: (■) +200 mV; (●) 0 mV; (▲) −300 mV. Supporting electrolyte 0.1 M $NaClO_4$: (○) +200 mV; (△) 0 mV; (□) −300 mV. For TDP: first plot: concn of TDP: (A) 0.4, (B) 0.8, (C) 1.2, (D) 1.6, (E) 2.0, (F) 2.8, (G) 4.0 mM. Second plot: potential vs. SCE: (□) +200 mV; (○) 0 mV; (△) −300 mV. For ETA: first plot: [Pb(II)] = 1.0 mM; concn of ETA: (A) 0.2, (B) 0.6, (C) 0.8, (D) 1.2, (E) 1.5, (F) 2.0, (G) 2.5, (H) 3.5, (I) 5.5, (J) 7.5 mM. Second plot: potential vs. SCE: (△) +200 mV; (□) 0 mV; (○) −300 mV. For TAS: first plot: concn of TAS: (A) 0.6, (B) 0.8, (C) 1.0, (D) 1.2, (E) 1.5, (F) 2.0, (G) 2.8 mM. Second plot: potential vs. SCE: (□) +200 mV; (○) −300 mV; [Pb(II)] = 1 mM: (■) +200 mV; (▲) 0 mV; (●) −300 mV. Lowest lying curve: 1 mM Cd(II) (no Pb(II)) at −300 mV

compositions) of the films are involved.

Equally noteworthy is the narrow range of ligand concentrations within which the adsorption of Pb(II) rises from low to very high values that are much less sensitive to further increases in the ligand concentration. The sudden increase in adsorption occurs in the range of ligand concentrations where the fraction of Pb(II) that is complexed undergoes its most rapid increase. However, the adsorption increases much more abruptly than does this fraction. The behavior resembles a phase transition rather than a smooth change in speciation. It is reminiscent of the behavior reported by Murray and co-workers (*3-5*), Armstrong et al. (*12*), and Sluyters and co-workers (*13*) in which unusually large and abruptly changing adsorptions were interpreted as arising from the formation of a new phase on the electrode surface.

The solubilities of the lead salts of most of the ligands listed in Table I have not been measured but precipitates do result with several of the ligands if the concentrations of Pb(II) and ligand are increased to values somewhat larger than were employed in the adsorption measurements. For example, the solubility of Pb(II) in a millimolar solution of TDA is only ca. 1.4 mM (*14*). It seemed reasonable, therefore, to examine the possibility that a new surface phase is formed under the conditions corresponding to the sudden increases in adsorption shown in Figure 1. Murray and co-workers were able to correlate abrupt changes in the adsorption of Pb(II) and Tl(I) from halide solutions with a reasonably constant ("surface solubility") product of the bulk concentrations of the anion and metal cation (*3-5*). No similar correlation was observed with the ligands investigated in this study.

Characteristic properties of phase formation on electrode surfaces have been described by Armstrong and Barr (*15*). They include a sudden decrease in the effective differential double layer capacitance to values well below the background capacitance as well as increases in the apparent cell resistance. Figure 2 shows how the double layer capacitance and cell resistance are affected by the adsorption of Pb(II) solution containing the ligand TAS. Throughout the potential range (−100 to −350 mV) where the adsorption is large, the capacitance is depressed and the cell resistance is enhanced compared with their values in the supporting electrolyte alone. As the adsorption decreases rapidly between −100 and 50 mV the capacitance increases and the resistance falls. (The steep rise in capacitance at more positive potentials is probably associated with anodic depolarization of the mercury electrode.) At potentials more negative than −400 mV, where any adsorbed film containing Pb(II) is destroyed by the reduction of Pb(II) to Pb(Hg), the capacitance increases again to within 10% of the background value.

This behavior matches closely that to be expected when initial adsorption gives way to the formation of an insulating phase on the electrode surface (*15*).

Table I. Ligands Examined

ligand	abbreviation	formula	log of formation constants for Pb(II) complexes (*20*)
ethylthioacetate	ETA	$CH_3CH_2S(CH_2CO_2^-)(CH_2CO_2^-)$	3.7 2.9
thiodiacetate	TDA	$S(CH_2CO_2^-)(CH_2CO_2^-)$	3.6
thiodipropionate	TDP	$S(CH_2CH_2CO_2^-)(CH_2CH_2CO_2^-)$	2.7
methylenebisthioacetate	MBTA	$CH(SCH_2CO_2^-)(SCH_2CO_2^-)(CH_2CO_2^-)$	3.7
thioacetatosuccinate	TAS	$S(CHCO_2^-)(CH_2CO_2^-)(CH_2CO_2^-)(CHCO_2^-)$	...
thiodisuccinate	TDS	$S(CHCO_2^-)(CHCO_2^-)(CH_2CO_2^-)$	...

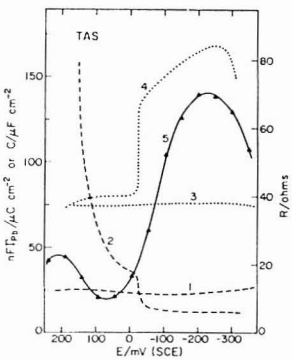


Figure 2. Effect of adsorption on differential capacitance and apparent cell resistance. 1 M $NaClO_4$ supporting electrolyte: Differential capacitance (curve 1, left ordinate) and cell resistance (curve 3, right ordinate). 1 M $NaClO_4$ + 0.5 mM Pb(II) + 2 mM TAS: Quantity of adsorbed Pb(II) (curve 5, left ordinate), differential capacitance (curve 2, left ordinate) and cell resistance (curve 4, right ordinate)

Effect of Adsorption on the Electronic Charge Density of the Electrode. Under conditions where the quantity of Pb(II) adsorbed is well below the approximate value calculated for a close-packed monolayer, the change in electronic charge density produced by the adsorption is in fair agreement with that predicted thermodynamically on the basis of the Gibbs adsorption equation. Thus, the potential dependence of the adsorption, $(\partial n\Gamma/\partial E)_\mu$, can be used to calculate the effect of adsorption on the electronic charge density, $(nF/2.3RT)(\partial q^m/\partial \log C)_E$. ($\mu$ is the chemical potential of the adsorbing species, approximated as $2.3RT$ times the logarithm of its concentration, and q^m is the electronic charge density.) As an example, 30 $\mu C\ cm^{-2}$ of Pb(II) is adsorbed at −175 mV from a solution containing 1.0 mM Pb(II) and 4.0 mM TDA. The corresponding values of $(\Delta(n\Gamma/\Delta E)_\mu$ and $(nF/2.3RT)(\Delta q^m/\Delta \log C)_E$ are ca. 0.16 and 0.18 $\mu C\ cm^{-2}\ mV^{-1}$, respectively. By contrast, under conditions where much sharper potential dependences of the adsorption prevail, the apparent values of these two differential coefficients are no longer in approximate accord. For example, the adsorption of Pb(II) at −200 mV from a 4 mM solution of TDS increases from 5 to 73 $\mu C\ cm^{-2}$, and the electronic charge on the electrode is decreased by 3 $\mu C\ cm^{-2}$ when the concentration of Pb(II) is increased from 0.2 to 0.4 mM. The value of $(nF/2.3RT)(\Delta_q{}^m/\Delta \log C)_E$ is, thus, 0.33 $\mu C\ cm^{-2}\ mV^{-1}$. However, the corresponding value of $(\Delta(n\Gamma)/\Delta E)_\mu$ is only ca. 0.07 $\mu C\ cm^{-2}\ mV^{-1}$. The clear implication is that the Gibbs adsorption equation is not applicable in the second case, presumably because the adsorbed film effectively insulates the electrode surface from the solution phase so that its electronic charge does not remain in thermodynamic equilibrium with the solution. This interpretation is consistent with the very large quantity of Pb(II) that is present on the surface when it appears to become insulated from the solution.

It is also noteworthy that under these conditions the quantity of Pb(II) present in the adsorbed film shows very little dependence on the electrode potential but remains a strong function of the concentration of Pb(II) in the bulk of the solution. Therefore, the high plateaus in the plots of adsorption vs. potential do not necessarily represent saturated surface layers. Instead, they may signal the presence of a compact surface layer containing sites which are effectively insulated from the electric field emanating from the charged electrode surface, but where adsorption of additional Pb(II) may be induced by increasing its bulk concentration.

Very similar behavior has been reported (*13*) for the thick films that form spontaneously on mercury electrodes in 1 M KCl solutions in the presence of sufficiently high concentrations of Pb(II). In (more dilute) bromide and iodide electrolytes, limiting coverages of adsorbed Pb(II) are obtained that are independent of both the electrode potential and the bulk concentration of Pb(II) (*4*). Apparently true saturation of the surface layer is achieved in these latter electrolytes.

Composition and Structure of the Surface Films. We were unable to devise a successful method for assaying the ligand content of the surface films. The relatively weak interaction of the free ligands with Hg^{2+} means that no well-defined anodic waves were present which might have been utilized to measure the quantity of ligand present on the surface. Furthermore, the lack of equilibrium between the electrode surface and the solution phase in the presence of the densely packed films prevented the use of conventional thermodynamic methods for relating changes in interfacial tension to the superficial excesses of ligand (or metal cations).

However, despite the lack of full analytical data on the composition of the surface films, some speculation on its possible structure may be warranted on the basis of recent crystal structures that have been determined for the acid form of TDA (*16*), its cadmium(II) salt (*17*), and several additional carboxylate amino acid salts of cadmium(II) (*18–21*). (No crystal structures for the corresponding lead derivatives are available, perhaps because of the greater difficulties in locating the positions of lighter atoms in the presence of an atom with as high an X-ray scattering cross section as lead.) All of the substances mentioned crystallize from aqueous solutions to give polymeric structures containing layers which are held together by hydrogen-bonded water molecules or bridging

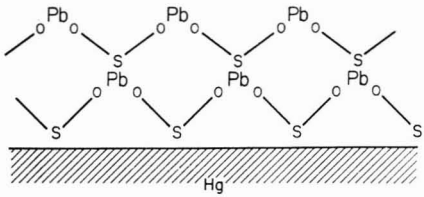


Figure 3. Possible schematic structure for the adsorbed layer

carboxylate ligands. It seems reasonable that the same substances might form layered structures on the surface of liquid mercury to which they are spontaneously attracted. A structure something like the highly simplified version shown in Figure 3 suggests itself. The atom that binds the array to the electrode seems most likely to be sulfur despite the weak adsorption of the free ligand because the complex of Pb(II) with oxydiacetate anions, $O(CH_2CO_2)_2^{2-}$, is much less strongly adsorbed than that with thiodiacetate. Molecular models suggest that upon chelation with Pb(II) the sulfur atom in the TDA molecule suffers few steric impediments toward binding to mercury atoms in the electrode surface. The interaction between Pb(II) and the sulfur atom in its complex with TDA is not particularly strong because the formation constant for the analogous, sulfur-free Pb(II)–oxydiacetate complex is over six times larger (*22*). Nevertheless, some Pb(II)–sulfur interaction seems likely because a charge-transfer band appears in the UV spectrum of the TDA complex (*14*). Furthermore, the Zn(II) complexes of TDA and TDS, while more stable than the Pb(II) complexes (*22*), are not adsorbed on mercury. Thus, in addition to whatever steric advantages the sulfur atom enjoys because of the formation of a metal–ligand complex its propensity for binding to the mercury surface is apparently also altered by interaction with the metal cation in the complex.

The structure shown in Figure 3 is only one of a variety of possible structures which can be constructed from molecular models. One virtue of the structure shown is that it can accommodate the observation that the adsorption remains dependent on the concentration of Pb(II) under conditions where it has become independent of potential. The Pb(II) sites in the upper-most layer may be only partially occupied by lead cations at lower bulk concentrations of Pb(II) while the primary, anchoring layer is fully metallated and insensitive to changes in potential. In addition, an upper-most layer which exhibits cation exchange behavior at the carboxylate groups would account for the observation that the adsorption of Pb(II) from solutions of TDA increases substantially when the concentration of the sodium perchlorate supporting electrolyte is decreased from 1 to 0.1 M (Figure 1). It is difficult to imagine an alternative explanation for this strong ionic strength dependence of the amount of Pb(II) incorporated into the adsorbed film.

If the crystal structure of the C(II)–TDA hydrate (*17*) is used to estimate the quantity of a divalent metal cation that might be accommodated in a close-packed monolayer, a value of ca. 90 $\mu C\ cm^{-2}$ is obtained. This is greater than the measured values of Pb(II) adsorbed in TDA solutions under any conditions. However, values as large as 150 $\mu C\ cm^{-2}$ were obtained with larger ligands such as TAS and TDS. These higher values may reflect the binding of more than one Pb(II) by these multidentate ligands although the presence of multilayered films is not excluded.

Adsorption of Other Metals. Inasmuch as the ability of the ligands studied to produce the strong adsorption of Pb(II)–complexes depends upon the presence of a thioether group in each ligand, it might seem reasonable to expect that every metal cation which forms complexes with the ligands would be comparably adsorbed. In fact, this is not the case. Not all of the ligands in Table I were tested with every metal cation studied but general trends became apparent from experiments with representative ligands.

(i) The relative adsorbabilities of the metals tested is Pb(II) > Cd(II) > Tl(I) > Zn(II). No adsorption of Zn(II)-complexes was detected with any of the ligands investigated.

(ii) The adsorption of Cd(II) does not attain equilibrium as rapidly as that of Pb(II). Substantial adsorption is obtained but under no conditions does it match the extraordinarily large surface concentrations obtained with Pb(II).

(iii) With most of the ligands Zn(II) forms stronger complexes than Cd(II) but none of the Zn(II)-complexes were adsorbed detectably.

(iv) Tl(I) forms rather weak complexes with the ligands tested and their adsorption is detectable but weak.

The variation in the adsorbability of the structurally similar metal complexes of the same ligand seems likely to be the reflection of two influential factors: the extent of metal–sulfur interaction in a complex and its solubility or tendency to form polymeric solids. The solubility of the metal salts of TDA increase in the same order as their adsorption decreases: Pb < Cd < Zn. In addition, Zn(II) shows less tendency to form polymeric sheets in its salts with ligands such as *S*-methylcysteinate than does Cd(II) (and, presumably, Pb(II)) (*21*).

The need to invoke differences in metal–sulfur interaction in the complexes stems from comparisons of relative adsorptions at low surface coverages where stabilizing interactions among adsorbed molecules of the complex are minimized and no new surface phase is formed. The large and persistent differences in the relative adsorbability of the Pb(II), Cd(II), Tl(I), and Zn(II) complexes under these conditions require an explanation that is specific to the metal involved. The degree of electronic interaction between each metal and the thioether sulfur atom seems the most likely candidate for the needed variable parameter.

CONCLUSIONS

The thioether carboxylate ligands examined in this study displayed a surprising variety in the adsorption of their metal complexes despite the basic similarities in their structures. The thioether group in these ligands shows little tendency toward adsorption on mercury without participation by coordinated metal cations and there are large differences in adsorbability among the cation complexes tested. Thus, the thioether carboxylates do not provide a general means for anchoring metal ions to mercury electrode surfaces.

Extremely large quantities of the Pb(II) complexes of several of the ligands can be adsorbed in the form of a multilayered phase on the mercury surface. This phenomenon appears to correlate with the intrinsic solubility of the Pb(II)–ligand salt but large adsorption can be obtained from solutions which are not close to saturation with respect to the formation of bulk phases.

The potential dependence of the adsorption matches that of many neutral organic adsorbates which suggests that the lower dielectric constant of the aqueous layer at the electrode surface may play an important role in controlling the adsorption.

ACKNOWLEDGMENT

Helpful discussions with Pamela Peerce are acknowledged with pleasure.

LITERATURE CITED

(1) F. C. Anson, *Acct. Chem. Res.*, **8**, 400 (1975) and references cited therein.
(2) R. W. Murray and D. J. Gross, *Anal. Chem.*, **38**, 392 (1966).
(3) C. M. Elliott and R. W. Murray, *J. Am. Chem. Soc.*, **96**, 3321 (1974).

(4) H. B. Herman, R. L. McNeely, P. Surana, C. M. Elliott, and R. W. Murray, *Anal. Chem.*, **46**, 1258 (1974).
(5) C. M. Elliott and R. W. Murray, *Anal. Chem.*, **48**, 259 (1976).
(6) F. C. Anson, *Anal. Chem.*, **38**, 54 (1966).
(7) C. M. Elliott and R. W. Murray, *Anal. Chem.*, **47**, 908 (1975).
(8) E. Blomgren, J. O'M Bockris, and C. Jesch, *J. Phys. Chem.*, **65**, 2000 (1961).
(9) L. Pospisil and J. Kuta, *Collect. Czech. Chem. Commun.*, **34**, 3047 (1969).
(10) B. Damaskin, A. Frumkin, and A. Chizhov, *J. Electroanal. Chem.*, **28**, 93 (1970).
(11) B. A. Parkinson, Ph.D. Thesis, California Institute of Technology, Pasadena, Calif., 1978.
(12) R. D. Armstrong, W. P. Race, and H. R. Thirsk, *J. Electroanal. Chem.*, **23**, 351 (1969).
(13) M. Sluyters-Rehbach, J. Breukel, K. A. Gijsbersen, C. A. Wiznhorst, and J. H. Sluyters, *J. Electroanal. Chem.*, **38**, 17 (1972).
(14) A. Napoli and P. L. Cignini, *J. Inorg. Nucl. Chem.*, **38**, 2013 (1976).
(15) R. D. Armstrong and E. Barr, *J. Electroanal. Chem.*, **20**, 173 (1969).
(16) S. Paul, *Acta Crystallogr.*, **23**, 491 (1967).
(17) S. H. Whitlow, *Acta Crystallogr., Sect. B*, **31**, 2531 (1975).
(18) W. Harrison and J. Trotter, *J. Chem. Soc., Dalton Trans.*, 956 (1972); 1923 (1974).
(19) M. L. Post and J. Trotter, *Acta Crystallogr. Sect. B*, **30**, 1880 (1974).
(20) P. J. Flook, H. C. Freeman, C. J. Moore, and M. L. Scudder, *J. Chem. Soc., Chem. Commun.*, 753 (1973).
(21) P. DeMeester and D. J. Hodgson, *J. Am. Chem. Soc.*, **99**, 6884 (1977).
(22) L. G. Sillen and A. E. Martell, "Stability Constants", The Chemical Society, London, 1964.

RECEIVED for review May 8, 1978. Accepted July 20, 1978. This work, Contribution No. 5783, was supported by a grant from the National Science Foundation.

Determination of Thiols by Conductometric Titration with Mercury(II) Chloride in Water and in *N*,*N*-Dimethylformamide

L. M. Doane and J. T. Stock*

Department of Chemistry, University of Connecticut, Storrs, Connecticut 06268

A conductometric device that allows simultaneous ac bridge balance, without regard to capacitance effects, and generation of a signal proportional to solution conductance has been constructed and used to determine solution conductance in titrations of thiols with mercury(II) chloride. Quantitative data for determination of submillimolar solutions of 1-propanethiol, 2-propanethiol, and 2-methyl-2-propanethiol in water and in DMF were obtained with an accuracy and precision of ±1%. Determinations of aqueous cysteine solutions gave similar results. Chloride, bromide, iodide, or thiocyanate up to concentrations of 1 mM did not generally interfere in the aqueous titrations. Similar titrations in DMF were unsuccessful. The accurate titration of thioglycolic acid in aqueous solution required the presence of bromide, iodide, or thiocyanate ion. With 3-mercaptopropanoic acid, accurate titration was successful with added thiocyanate, but not in the presence of bromide or iodide.

Apart from recent work with high-frequency signals (*1*, *2*), conductometric thiol titrimetry with precipitating or complexing reagents has received little attention. Although high-frequency methods permit measurements without solution electrolysis or electrode deactivation effects, the titration curves are rarely linear (*3*). A great advantage of conventional low-frequency conductometry is the ease and precision of end-point location.

Mercury(II) chloride and silver nitrate have found wide use in thiol titrimetry, since the mercaptides formed have very large formation constants, e.g., for cysteine, $\log K_{f[Hg(RS)_2]} = 43.5$ (*4*); $\log K_{sp[AgRS]}$ = ca. −20 (*5*). The results obtained in the conductometric titration of thiols with silver nitrate were not very satisfactory (*6*) and similar titrations with mercury(II) salts have not been attempted. The present work shows that mercury(II) chloride is an effective titrant in thiol conductometry both in aqueous and in DMF solution. The use of DMF minimizes electrode deactivation effects because mercaptide precipitation is prevented.

One of the problems in the conventional Wheatstone bridge conductance methods is obtaining a sharp "null". One approach is to use a switching circuit that is insensitive to phase shifts (*7*, *8*). The present authors have modified this circuit to eliminate losses due to transistor bias and have added an analog circuit to give fast conductance readouts. Because the two outputs are independent, they can be used simultaneously.

EXPERIMENTAL

Reagents. *N*,*N*-Dimethylformamide (DMF) was used as received from Eastman Kodak Co. L-(+)-Cysteine (J. T. Baker Chemical Co.) was dried over P_2O_5. All thiols were obtained from the Aldrich Chemical Co. D,L-Penicillamine was used as received. 1-Propanethiol, 2-propanethiol, and 2-methyl-2-propanethiol were distilled under nitrogen. Thioglycolic acid and 3-mercaptopropanoic acid were distilled under reduced pressure. The thiols were stored under nitrogen.

Standard Solutions. Fresh standard 0.1 M thiol solutions were prepared daily. To avoid volatilization and oxidation of the liquid thiols, the following procedure was used. A volumetric flask having a Teflon stopper with a small center hole was flushed with nitrogen. The hole was then closed with a short plug of stainless steel rod and the flask was weighed. The appropriate amount of liquid thiol was then introduced by a syringe. The stopper was then plugged and unplugged to establish vapor pressure equilibrium, and the flask plus thiol weighed. To minimize loss of thiol, dilutions of the stock solutions were made by use of a syringe. With the exception of cysteine and D,L-penicillamine, which were diluted with outgassed water, 95% ethanol was used as diluent.

Aqueous mercury(II) chloride solution was standardized with potassium iodide (*9*). The standard solution in DMF was prepared by the direct weighing of mercury(II) chloride that had been assayed with potassium iodide (*9*).

Two-milliliter microburets (Roger Gilmont Instruments, Inc.) were used to deliver the thiol solutions and the titrant.

Instrumental. A circuit diagram of the conductometric device is shown in Figure 1. The device was assembled largely from dual operational amplifiers (National Semiconductor LM 1458 N) and standard electronic components (*10*). In the simplified block diagram in Figure 2, the signal from the bridge at point B is inverted by A3 and then fed into a precision limiter, which simulates ideal diode behavior (*11*). A similar limiter accepts the signal from point C. Positive half-cycles are thus removed from

0003-2700/78/0350-1891$01.00/0 © 1978 American Chemical Society

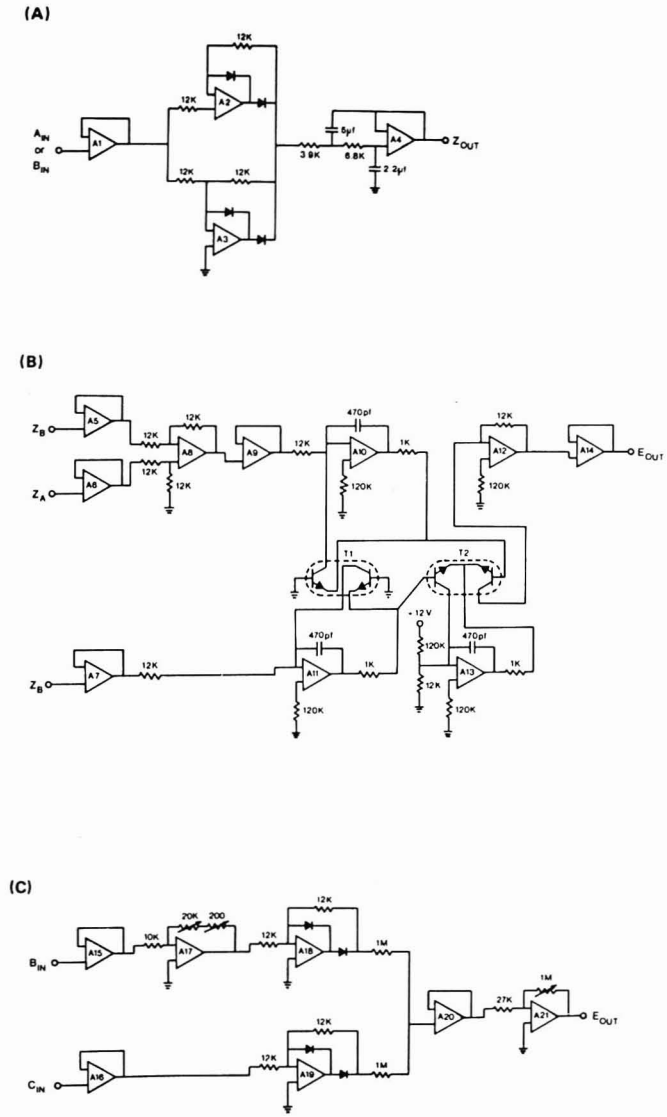


Figure 1. Circuit diagrams of (A) rectifier and filter, (B) difference/analog divider, and (C) bridge balance circuit. Operational amplifiers A1–A21: National LM 1458 N. Match transistor pair T1–T2: National LM 394. Diodes 1N914

each signal. The two resultants are added by A4 and this combination signal is applied to the "vertical" input of an oscilloscope with a horizontal scan rate of 100 kHz. Two overlapping rasters appear. The bridge is balanced by changing R_3 (Figure 2) until the bright-lit tops of the rasters coincide. Any capacitance changes merely shift the half-cycle across the screen, leaving the amplitudes essentially unaffected.

The analog signal is obtained from E_2, the voltage at point B, and E, the voltage applied to the other electrode at A. Provided that essentially no current is drawn from B, the output at A14 (Figure 1B) is directly proportional to solution conductance. Phasing problems were removed by rectifying and smoothing both E_2 and E (*10*). The analog output is well suited to following fast conductance changes, e.g., driving a strip chart recorder in kinetic experiments. However, the bridge balance output was used exclusively in the titrations. This output gave an additional significant figure beyond the read-out of the available digital voltmeter attached to the analog output.

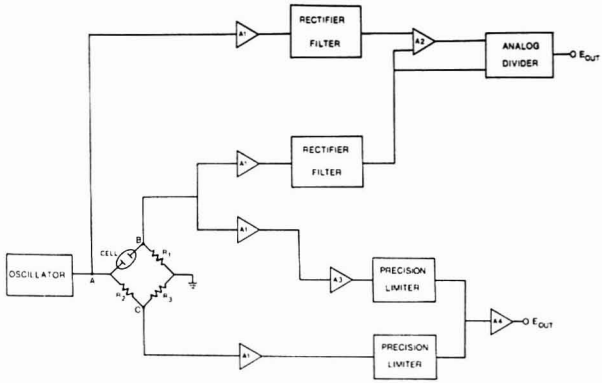


Figure 2. Block diagram of conductometric device. Amplifiers: A1, buffer; A2, difference amplifier; A3, inverter; and A4, signal amplifier

Table I. Results of Thiol Titrations in Aqueous Solution

compound	end point molar ratio, Hg:RSH	concn range, mM	accuracy and rel std dev, %	runs	ions tolerated
1-propanethiol	1:2	0.1–1.0	−0.36 ± 0.92	22	Cl^-
2-propanethiol	1:2	0.1–1.0	+0.16 ± 0.61	16	Cl^-, Br^-, SCN^-
2-methyl-2-propanethiol	1:2	0.3–1.0	+0.79 ± 0.97	15	Cl^-, Br^-, I^-, SCN^-
cysteine	1:2	0.3–1.0	+0.32 ± 0.53	13	Cl^-, Br^-, I^-, SCN^-
D, L-penicillamine	1:1	0.3–0.7	+0.03 ± 0.20	7	
	1:2	1.0	+0.15 ± 0.25	3	
thioglycolic acid	1:1	0.3–0.7	−8.28 ± 0.77	4	
	1:2	0.3–1.0	+1.05 ± 0.98	6	I^-
	1:2	0.3–1.0	+0.48 ± 0.45	6	Br^-
	1:2	0.3–1.0	+0.45 ± 0.33	6	SCN^-
3-mercaptopropanoic acid	1:2	0.3–1.0	+0.75 ± 0.73	9	SCN^-

Procedure. Fifty milliliters of diluent were put in the titration cell, which was then mounted in a small waterbath maintained at ±0.1 degree of ambient temperature (23–25 °C). The cell contents were stirred magnetically and sparged with nitrogen. The gas was cut off when the cell contents attained constant temperature. Standard thiol solution was then added to the cell and the titration was started immediately. The wire electrodes (*8*) were continually checked during the course of the titration to determine if a precipitate was adhering to the electrodes, since an accumulation reduced the solution conductance below its correct value.

RESULTS AND DISCUSSION

Titrations in Aqueous Solution. A typical titration curve has the form shown at A in Figure 3. Since thiols are very weak electrolytes [$pK_a > 8$] (*12*), the initial conductance is low. The highly mobile hydrogen ion produced according to:

$$HgCl_2 + 2RSH \rightleftharpoons Hg(RS)_2 + 2H^+ + 2Cl^- \quad (1)$$

should cause an immediate rise in conductance. Inexplicably, however, rapid rise in conductance did not occur until approximately 0.5 equivalents of titrant had been added, as shown at B in Figure 3. In most cases, little or no curvature was detectable in the region of the end point. As expected, the excess-titrant line is essentially horizontal.

When the titration of thiols at concentrations less than 0.1 mM was attempted, curves such as C in Figure 2 were obtained, so that precise end-point location was impossible. At such low concentrations, the conductance was not stable at and beyond the end point.

The results in Table I show that 1-propanethiol, 2-propanethiol, 2-methyl-2-propanethiol, and cysteine can be titrated with precision and accuracy to better than ±1%.

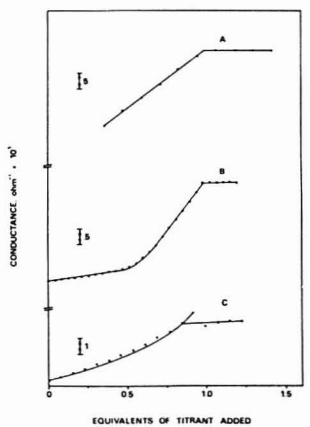


Figure 3. Titration curves of 1-propanethiol with $HgCl_2$ in water. Concentration of 1-propanethiol is (A) 0.3 mM, (B) 0.1 mM, and (C) 0.5 mM

Cysteine and 2-methyl-2-propanethiol can be titrated with no loss of accuracy in the presence of up to 1 mM chloride, bromide, iodide, or thiocyanate ion, despite the fact that these anions form very stable compounds with mercury(II). However, iodide must not be present when 2-propanethiol is to be titrated, and only chloride did not interfere with ti-

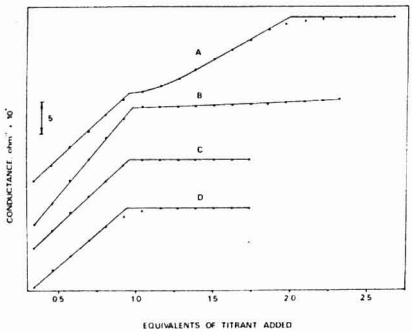


Figure 4. Titration curves of 0.3 mM D,L-penicillamine with $HgCl_2$ in water and in the presence of 1.0 mM (A) KCl, (B) KSCN, (C) KBr, and (D) KI

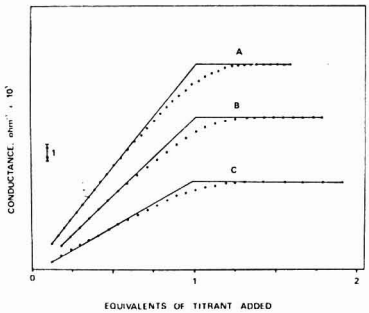


Figure 5. Titration curves of 1-propanethiol with $HgCl_2$ in DMF. Concentration of 1-propanethiol is (A) 1.0 mM, (B) 0.7 mM, and (C) 0.3 mM

trations of 1-propanethiol. Foreign electrolyte concentrations greater than approximately 1.0 mM gave large background conductances, with corresponding loss of precision and accuracy.

Negative errors of at least 1% occurred when the thiol concentrations were above approximately 1 mM. Even the titration of cysteine, in which no precipitation occurs, showed this effect.

D,L-Penicillamine and the two mercapto carboxylic acids gave titration curves of the form shown at A in Figure 4. The first end point corresponds to a mercury/thiol molar ratio of 1:2 and the second to a ratio of 1:1. However, the first end point is generally unusable. Only in the titration of D,L-penicillamine at a concentration of 1.0 mM (Table I) could the first end point be effectively used. The addition of chloride ion had little effect, but the addition of bromide, iodide, or thiocyanate suppressed the second end point (Figure 4, curves B, C, and D). Titrations of D,L-penicillamine in the presence of these anions were low by greater than 2%.

Attempts to titrate thioglycolic acid or 3-mercaptopropanoic acid without added electrolytes were unsuccessful because of erratic conductance data. The addition of bromide, iodide, or thiocyanate ion permitted the accurate titration of thioglycolic acid. Only in the presence of thiocyanate were the results of 3-mercaptopropanoic acid accurate. The added electrolytes suppressed the second end point, so that titrations performed in the presence of these electrolytes were based on the 1:2 combining ratio (Figure 4, curves B, C, and D).

Equation 1 indicates a 1:2 combining ratio. Presumably, the continued addition of titrant can bring about the reaction indicated by Equation 2

$$HgCl_2 + Hg(RS)_2 \rightleftharpoons 2HgRS^+ + 2Cl^- \qquad (2)$$

For this reaction to occur, the 1:2 mercaptide from which the thiol anion is abstracted must be less stable than similar mercaptides formed by cysteine and the aliphatic thiols. The products of Equation 2 are written as ions to explain the steady increase in conductivity past the first end point.

The suppression of the second end point by thiocyanate ion and some of the halide ions implies that the mercaptide interacts with the excess of these ions, as indicated by Equation 3, where X^- is bromide, iodide, or thiocyanate ion.

$$HgCl_2 + Hg(RS)_2 \xrightleftharpoons{2X^-} 2HgRSX + 2Cl^- \qquad (3)$$

This reaction has little effect on the conductance, because X^- and chloride ion have similar ionic conductances.

Titrations in DMF. Although mercaptide precipitation did not occur in DMF, inaccurate results were found at thiol concentrations greater than 1.0 mM. Some titrations that are possible in water failed when the medium was changed to DMF.

Table II. Results of Thiol Titrations in DMF Solution

compound	end point molar ratio, Hg:RSH	concn range, mM	accuracy and rel std dev, %	runs
1-propanethiol	3:2	0.3–1.0	−0.10 ± 0.47	9
2-propanethiol	3:2	0.3–1.0	−0.36 ± 0.45	9
2-methyl-2-propanethiol	3:2	0.3–1.0	+0.92 ± 1.06	10
cysteine	1:1	0.3–1.0	−12.40 ± 3.45	9
	2:1	0.3–1.0	−8.55 ± 1.64	9
D,L-penicillamine	1:1	0.3–0.7	−2.73 ± 2.04	6
	2:1	0.3–0.7	−0.32 ± 0.55	6
thioglycolic	3:2	0.3–1.0	+0.53 ± 2.24	9
3-mercapto-propanoic acid	3:2	0.3–1.0	+8.63 ± 0.92	9

In DMF, the mercury/thiol stoichiometry of the aliphatic thiols was found to be 3:2. Figure 5 shows typical aliphatic thiol titration curves. The linearity of the pre-equivalence line from the beginning of the titration is noticeable, but so is the curvature in the region of the end point. In fact, if enough readings are not obtained prior to the half-titrated point, accurate extrapolation to the end point is impossible.

Results obtained in DMF media, summarized in Table II, show that aliphatic thiols can be titrated with precision and accuracy of ±1%. It is probable that DMF influences the form of these titration curves, since the titration curves of cysteine and D,L-penicillamine differ radically when the medium is changed from water to DMF. Titrations of cysteine and D,L-penicillamine exhibited three end points as shown in Figure 6. This is in sharp contrast to the behavior in aqueous solution. The first end point is concentration dependent and is useless. In the case of cysteine, neither of the other end points gave accurate results. However, the third end point, in which the mercury/thiol stoichiometry is 2:1, could be used to determine D,L-penicillamine with errors less than 1%. Titration curves of thioglycolic acid and 3-mercaptopropanoic acid were similar to those of the aliphatic thiols and involved a 3:2 mercury/thiol stoichiometry. Since the end point of thioglycolic acid was concentration dependent (indicated by its large standard deviation) and that of 3-mercaptopropanoic acid had a large (although precise) error in accuracy, standardizing the titrant against the thiol at a thiol con-

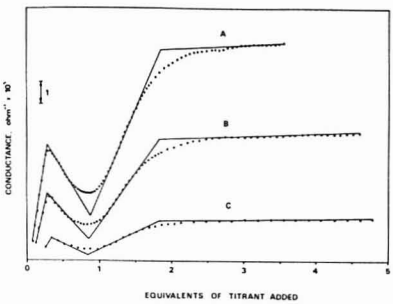
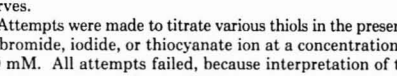


Figure 6. Titration curves of cysteine with $HgCl_2$ in DMF. Concentration of cysteine is (A) 1.0 mM, (B) 0.7 mM, and (C) 0.3 mM

centration close to that in the sample is recommended to obtain accuracies within 1%.

The titrations of cysteine and D,L-penicillamine in DMF undoubtedly were affected by the amino group, since titration curves of 3-mercaptopropanoic acid (I) [a compound similar to cysteine (II), but with the amino group absent]



had the form and stoichiometry of the aliphatic thiol titration curves.

Attempts were made to titrate various thiols in the presence of bromide, iodide, or thiocyanate ion at a concentration of 1.0 mM. All attempts failed, because interpretation of the titration curves was impossible.

Stricks and Kolthoff (*4*) examined the interaction of cysteine and mercury(II) chloride in aqueous solution and suggested that Reaction 1 is followed by Reaction 4

$$2HgCl_2 + Hg(RS)_2 \rightarrow Hg(RS)_2 \cdot 2HgCl_2 \qquad (4)$$

This implies 3:2 stoichiometry. These workers stated that an excess of mercury(II) chloride was required to obtain the addition compound. If the 3:2 stoichiometry in our work implies the formation of the same addition compound, this compound must be considerably more stable in DMF than in aqueous solution, since it had to be formed during the titration, i.e., without excess of mercury(II) chloride. Only Reaction 1 contributes to the solution conductance. If Reaction 4 occurs after the thiol has been consumed by Reaction 1, the solution conductance would not change and the mercury/thiol molar ratio would appear to be 1:2. Only when Reaction 4 occurs simultaneously with Reaction 1 can a 3:2 stoichiometry be indicated by the end point. Thus, the addition compound actually appeared to form in an excess of thiol in DMF. However, it also seemed apparent that there was some unknown role that DMF was playing in forming this apparent addition compound.

LITERATURE CITED

(1) L. Serrano Berges and T. Fernandez Perez, *An. Real Soc. Espan. Fis. Quim., Ser. B.*, **62**, 807–820 (1966).
(2) F. Oehme, *Erdol Kohle*, **13**, 394–396 (1960).
(3) H. Willard, L. Merritt, and J. Dean, "Instrumental Methods of Analysis", 5th ed., D. Van Nostrand, New York, N.Y., 1974, Chapter 26.
(4) W. Stricks and I. M. Kolthoff, *J. Am. Chem. Soc.*, **75**, 5673–5681 (1953).
(5) R. Cecil and J. R. McPhee, *Adv. Protein Chem.*, **14**, 262 (1959).
(6) W. Scheele and C. Gensch, *Kautsch. Gummi*, **6**, 147–157 (1953).
(7) M. Michaelis, *Pract. Electronics (London)*, **5**, 587–593 (1969).
(8) J. T. Stock, *J. Chem. Educ.*, **52**, A165–A168 (1975).
(9) W. Scott, "Standard Methods of Chemical Analysis", 5th ed., D. Van Nostrand, New York, N.Y., 1944, p 580.
(10) L. M. Doane, Ph.D. Thesis, University of Connecticut, Storrs, Conn., 1977.
(11) H. Malmstadt, C. Enke, and S. Crouch, "Electronic Measurements for Scientists", W. A. Benjamin, Reading, Mass., 1974, p 436.
(12) S. Patai, "The Chemistry of the Thiol Group", Interscience Publishers, New York, N.Y., 1974, pp 398–400.

RECEIVED for review April 26, 1978. Accepted August 4, 1978.

Voltammetric Behavior of the (Pt)H_2O,CO_2/H_2,CO_3^{2-} System in Molten Alkali Nitrates

Elio Desimoni, Francesco Palmisano, Luigia Sabbatini, and Pier Giorgio Zambonin*

Cattedra di Chimica Analitica della Università di Bari, Via Amendola 173, 70126 Bari, Italy

An electrochemical investigation was performed on the H_2O,CO_2/H_2,CO_3^{2-} system in the (Na-K)NO_3 equimolar melt at 513 K by RDE and peak voltammetry and DME polarography. Solutions containing CO_3^{2-}, $CO_3^{2-} + H_2$, $CO_2 + H_2O$, and $CO_3^{2-} + H_2 + CO_2 + H_2O$ were investigated. The reported experimental results represent a quite complete qualitative description of the mentioned system for which a reversible or quasi-reversible voltammetric behavior can be hypothesized. The possibility to employ the reaction $H_2 + CO_3^{2-} = H_2O + CO_2 + 2e$ for the analytical detection of hydrogen and carbon dioxide in the given solvent is briefly discussed.

A systematic investigation on hydrogen systems in the (Na-K)NO_3 equimolar mixture was recently initiated in our laboratory in the course of a wide study on gaseous systems in fused salts. Solubility (*1*), potentiometric (*2*), and voltammetric (*3, 4*) data were already published together with the results of a kinetic investigation (*5*) on the slow reaction of hydrogen with the solvent anions

$$H_2 + NO_3^- = H_2O + NO_2^- \qquad (1)$$

A brief review of preliminary results on all these topics is contained in reference 6.

Interesting results, showing an unusual behavior in the field of hydrogen electrooxidation were obtained in the course of rotating disk electrode (RDE) voltammetric investigations (*3, 4*) performed on the (Pt)$H_2O/H_2,OH^-$ and (Au)$H_2O/H_2,OH^-$ systems in the (Na-K)NO_3 equimolar melt. The mechanistic model proposed (*3, 4*) to explain the experimental results involves the chemical consumption of the electroactive species (H_2) catalyzed by electrochemically produced radicals ($OH^\bullet$) in the diffusion layer. The direct involvement of the electrode

0003-2700/78/0350-1895$01.00/0 © 1978 American Chemical Society

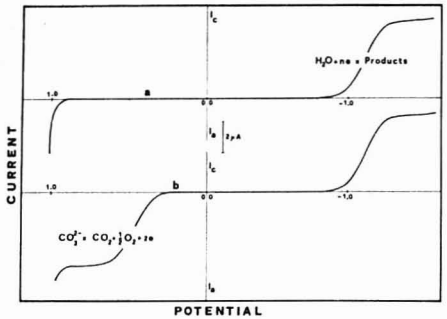


Figure 1. Base voltammograms recorded in a pure melt maintained under flux of partially wet nitrogen, by using a Pt-RDE (i.d. = 1 mm) rotated at 600 rpm. $T = 513$ K. Potential values referred to the Ag/Ag^+ (0.07 mol kg^{-1}) reference half-cell. Curve a: $[CO_3^{2-}] = 0.0$ mol kg^{-1}; curve b: $[CO_3^{2-}] = 7.0 \cdot 10^{-4}$ mol kg^{-1}

surface was excluded. Further hydrogen systems were investigated which could, in theory, be interesting for fuel cell utilization. This paper reports on the voltammetric behavior of the $H_2O,CO_2/H_2,CO_3^{2-}$ system on Pt-RDE in the (Na-K)NO_3 equimolar melt at the temperature of 513 K.

EXPERIMENTAL

Most of the information about chemicals and methodology as well as about the cell, the voltammetric setup, and the thermostatic system were previously described (*3, 6*). Increasing carbonate concentrations were obtained by adding to the melt small drops of hydroxide-free solid solutions of Na_2CO_3 in the (Na-K)NO_3 equimolar mixture. The water partial pressure of the flowing gases (hydrogen, nitrogen, and carbon dioxide of UPP grade) was varied by means of water saturators and traps of "Molecular sieves 5A" maintained at different temperatures. The actual water concentrations was controlled by RDE voltammetry (*7*).

The traces of nitrite ions always present in a "pure" melt (*8, 9*) were eliminated to avoid overlapping of nitrite and carbonate electrooxidation waves: this was done by direct injection into the melt of concentrated nitric acid which thermally decomposes (*10*) giving origin to nitrogen dioxide in the solution. The disappearance of the nitrite wave, due to the reaction (*11*)

$$NO_2^- + NO_2 = NO_3^- + NO \uparrow \qquad (2)$$

was controlled voltammetrically, as well as the absence of OH^- traces.

All the RDE voltammograms were recorded at 513 K on a platinum electrode (i.d. = 1 mm; rotation speed 600 rpm unless otherwise specified). The same electrode was used to perform cyclic voltammetry experiments.

Some polarographic measurements were performed by substituting the Pt RDE with a capillary of suitable length (40 cm) connected, via a Tygon tubing, to a traditional mercury reservoir. A cold trap (dry ice + acetone) was connected to the outlet of the cell to avoid the escape of mercury vapors.

All the potentials are referred to the Ag/Ag^+ (0.07 mol kg^{-1}) reference half-cell.

RESULTS AND DISCUSSION

Pure Melt + Nitrogen (or Hydrogen). The base curve recorded in a nitrite-free, hydroxide-free melt maintained under flux of slightly wet nitrogen is reported in Figure 1, curve a. Only the reduction wave of water (*7*) is detectable in the solvent electroactivity range. In agreement with previous results (*3, 4*), no wave appeared which could be ascribed to an electrode process involving hydrogen when hydrogen was fluxed through the melt in the absence of proton-acceptor species (like OH^- and CO_3^{2-}).

The same result was obtained by using the DME.

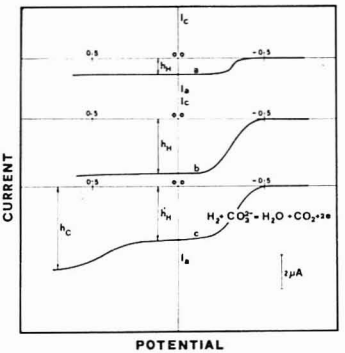


Figure 2. "Hydrogen waves" recorded in a melt maintained under bubbling of partially wet hydrogen ($p_{H_2} \simeq 1$ atm) in the presence of variable $[CO_3^{2-}]$ under the same experimental conditions as Figure 1. Curve a: $[CO_3^{2-}] = 1.4 \times 10^{-4}$ mol kg^{-1}; curve b: $[CO_3^{2-}] = 4.8 \times 10^{-4}$ mol kg^{-1}; curve c: $[CO_3^{2-}] = 7.5 \times 10^{-4}$ mol kg^{-1}

Pure Melt + Carbonate + Nitrogen. If CO_3^{2-} ions are added to the melt maintained under flux of wet nitrogen, voltammogram b of Figure 1 is obtained in which the anodic wave of carbonate electrooxidation is present due (*12*) to the process

$$CO_3^{2-} = CO_2 + {}^1/_2O_2 + 2e \qquad (3)$$

This irreversible (*12*) wave appears approximately in the same potential region of the nitrite wave ($E_{1/2(NO_2/NO_2^-)} = +0.48$ V).

No carbonate wave was recorded at a dropping mercury electrode under the given experimental conditions; then carbonate ions cannot be electrooxidized on mercury in the solvent electroactivity range.

Pure Melt + Carbonate + Hydrogen. A completely different result is obtained if hydrogen is bubbled in a carbonate-containing melt. A set of current–potential profiles obtained in the presence of variable carbonate concentrations under flux of hydrogen (partial pressure ~1 atm) is reported in Figure 2. As can be seen, a new anodic wave appears which can be likely attributed to the process

$$H_2 + CO_3^{2-} = H_2O + CO_2 + 2e \qquad (4)$$

previously observed in other media such as molten carbonates (see for example references 13–15).

Voltammograms a and b in Figure 2 do not show any carbonate wave owing to the carbonate-consuming character of reaction 4. In the presence of hydrogen, the carbonate wave has to appear for carbonate concentrations higher than

$$[CO_3^{2-}] = \left(\frac{D_{H_2}}{D_{CO_3^{2-}}}\right)^{2/3} [H_2] \qquad (5)$$

where D_{H_2} and $D_{CO_3^{2-}}$ are the diffusion coefficients of the relevant species and $[H_2]$ is the equilibrium concentration of hydrogen (*1*) under a partial pressure of 1 atm. Equation 5 states, in fact, the conditions under which the anodic limiting current h_H (curve b in Figure 2) is controlled by the diffusion of both H_2 and CO_3^{2-}. Therefore, in the presence of carbonate concentrations higher than the value given by Equation 5, the current relevant to process 4 reaches a quite constant value, h'_H, while the carbonate excess is electrooxidized according to Equation 3 (see voltammogram c in Figure 2).

It should be pointed out that in the course of these voltammetric experiments, surface poisoning phenomena were often observed which were ascribed to the adsorption (*12*) of

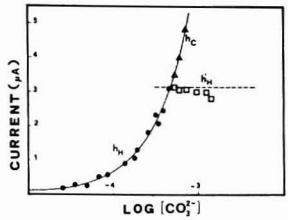


Figure 3. Plot of the currents h_H, h'_H and h_C in Figure 2 vs. log $[CO_3^{2-}]$ for a series of voltammograms obtained under 1 atm of hydrogen at various $[CO_3^{2-}]$; (●) values of h_H; (□) values of h'_H; (△) values of h_C. The continuous curve represents the carbonate calibration curve obtained in a separate experiment in the absence of hydrogen while the dashed line represents the limiting hydrogen current as calculated from known solubility and diffusion coefficient data (*1*, *3*)

species involved in the electrode reactions. These effects produced a more or less marked distortion in the shape of the relevant voltammetric waves related, in particular, to the time of use of the microelectrode. The experimental data here reported are relevant to voltammetric experiments performed under optimum conditions, i.e., minimum carbonate ion excess and RDE surface cleaned before each experiment. Under these conditions the half-wave potential relevant to process 4, read for a series of curves recorded at various carbonate concentrations (up to 4.8×10^{-4} mol kg^{-1}) at 513 K, was $E_{1/2} = -0.32 \pm 0.10$ V. As a matter of fact, the limiting current values h_H obtained under these conditions were unaffected by "adsorption effects" and proved diffusion controlled on the basis of their adherence to the Levich equation

$$i_L = 0.62\, nFAD^{2/3}\, \nu^{-1/6}\, \omega^{1/2}\, C \qquad (6)$$

where the symbols have their usual meaning in electrochemistry. Straight lines were in fact obtained by plotting the limiting h_H currents vs. the square root of the electrode rotation speed (least square analysis correlation coefficient $r = 0.998$).

Figure 3 gives, as a function of log $[CO_3^{2-}]$, the currents h_H, h'_H and h_C of Figure 2 obtained for a series of experimental voltammograms recorded at different $[CO_3^{2-}]$ in a hydrogen saturated melt. Since the continuous curve in this figure represents the calibration curve of carbonate ions obtained in a separate experiment (under flux of nitrogen) one can conclude that the currents h_H and h_C are controlled by the diffusion of carbonate ions while h'_H is limited by the diffusion of hydrogen. This last evidence is in accordance with the experimental linear dependence between h'_H and $[H_2]$ (correlation coefficient $r = 0.997$).

Finally it can be noted that the dashed line reported in Figure 3 was calculated on the basis of the solubility (*1*) of hydrogen and its diffusion coefficient estimated in the course of previous study (*3*) on the $(Pt)H_2O/H_2,OH^-$ system under similar experimental conditions. This suggests a general accordance between data obtained in the presence of two different proton acceptor species, i.e., hydroxide and carbonate ions. The only difference consists in the fact that no current minimum (*3*) of the "hydrogen current" was obtained on using carbonate in place of hydroxide so that no autocatalytic mechanism (*3*) exists in the present case which can consume the electroactive species (H_2) in the diffusion layer.

From an analytical point of view this means that the limiting current value h'_H can be used for determining the hydrogen content in the melt. At present this method represents the only tool for the analytical detection of hydrogen in molten nitrates.

Finally it can be reported that no hydrogen wave was obtained on DME under the described conditions, thus indicating that the hydrogen electrooxidation on mercury lies outside of the solvent electroactivity range.

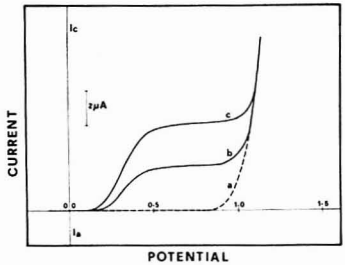


Figure 4. Current–potential profiles obtained in a melt equilibrated with CO_2–N_2–H_2O mixtures; curve a: $p_{H_2O} = 15$ Torr and $p_{N_2} = 745$ Torr; curve b: $p_{CO_2} = p_{N_2} = 372$ Torr and $p_{H_2O} = 15$ Torr; curve c: $p_{CO_2} = 745$ Torr and $p_{H_2O} = 15$ Torr

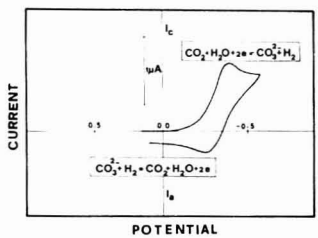


Figure 5. Peak voltammogram obtained in the same experimental conditions as curve c in Figure 4 at a scan speed of 50 mV/s

Pure Melt + Carbon Dioxide + Water. The base curve obtained in a carbonate-free melt under flux of nitrogen previously equilibrated with water (water partial pressure 15 Torr) is reported in Figure 4, curve a. On substituting nitrogen with CO_2, a new cathodic wave appears whose half-wave potential was found to be again $E_{1/2} = -0.32 \pm 0.01$ V at 513 K: see curves b and c in Figure 4. This is in agreement with the overall electrode process

$$CO_2 + H_2O + 2e = CO_3^{2-} + H_2 \qquad (7)$$

different from the one observed (*12*) in melts saturated with dry CO_2

$$CO_2 + NO_3^- + 2e = CO_3^{2-} + NO_2^- \qquad (8)$$

which occurs at more negative potentials ($(E_{1/2})_8 = -0.52$ V at 510 K).

The limiting current relevant to reaction 7 is controlled, under the present experimental conditions (electrodic excess of water) by the actual concentration of CO_2 in the melt (see Figure 4); it shows a good reproducibility (on freshly polished electrodes) and proved diffusion controlled as stated by the linear dependence (correlation coefficient $r = 0.998$) of the plot limiting current vs. $\omega^{1/2}$. By using the Levich equation a diffusion coefficient equal to 1.8×10^{-5} cm^2 s^{-1}, at 513 K, was calculated for CO_2 which is in good agreement with the datum (1.9×10^{-5} cm^2 s^{-1} at 510 K) previously (*12*) obtained on the basis of the voltammograms relevant to reaction 8.

A qualitative support to reaction 7 was also obtained by peak voltammetry experiments. Figure 5 reports a typical peak voltammogram obtained at a standing platinum electrode in a melt maintained under flux of wet carbon dioxide (i.e., same experimental conditions of curve c in Figure 4). As can be seen, the cathodic and anodic peak currents (relevant

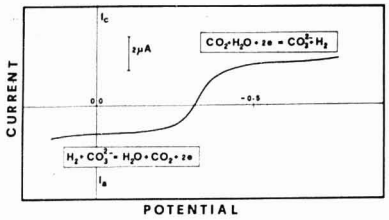


Figure 6. Cathanodic profile relevant to process 4 recorded in a melt containing $[CO_3^{2-}] = 2.7 \times 10^{-4}$ mol kg^{-1} and maintained under flux of a mixture of CO_2, H_2, and H_2O: $p_{CO_2} = p_{H_2} = 372$ Torr and $p_{H_2O} = 15$ Torr

respectively to reactions 7 and 4) have similar values. The cathodic peak currents (better resolved than the anodic ones) were linearly related to the square root of the scan rate while the peak potentials remained practically constant for moderate scan rate variations (up to 200–500 mV/s).

Pure Melt + Carbonate + Water + Carbon Dioxide + Hydrogen. As expected on the basis of the experimental results described in the previous paragraphs, a cathanodic profile was obtained when a mixture of wet hydrogen and CO_2 was fluxed in a carbonate containing melt: see Figure 6.

LITERATURE CITED

(1) E. Desimoni, F. Paniccia, and P. G. Zambonin, *J. Chem. Soc. Faraday Trans. 1*, **69**, 2014 (1973).
(2) E. Desimoni, F. Paniccia, L. Sabbatini, and P. G. Zambonin, *J. Appl. Electrochem.*, **6**, 445 (1976).
(3) E. Desimoni, F. Palmisano, and P. G. Zambonin, *J. Electroanal. Chem.*, **84**, 323 (1977).
(4) E. Desimoni, B. Morelli, F. Palmisano, and P. G. Zambonin, *Ann. Chim.*, **67**, 451 (1977).
(5) E. Desimoni, F. Paniccia, and P. G. Zambonin, *J. Phys. Chem.*, **81**, 1985 (1977).
(6) E. Desimoni, F. Paniccia, L. Sabbatini, and P. G. Zambonin, "Proceedings of the 149th International Symposium Molten Salts," J. P. Pemsler, Ed., The Electrochemical Society Princeton, N.J., 1976.
(7) P. G. Zambonin, V. L. Cardetta, and G. Signorile, *J. Electroanal. Chem.*, **28**, 237 (1970).
(8) H. S. Swafford and P. G. McCormick, *Anal. Chem.*, **37**, 970 (1965).
(9) P. G. Zambonin, *Anal. Chem.*, **41**, 868 (1969).
(10) H. S. Johnston, L. Foering, Yu Shang Tao, and G. H. Messerly, *J. Am. Chem. Soc.*, **73**, 2319 (1951).
(11) G. G. Bombi, R. Freddi, and M. Fiorani, *Ann. Chim.*, **57**, 759 (1966).
(12) P. G. Zambonin, *Anal. Chem.*, **44**, 763 (1972).
(13) G. H. J. Broers and M. Shenke, "Fuel Cells", Vol. 2, G. J. Young, Ed., Reinhold, New York, N.Y., 1963, p 6.
(14) A. D. S. Tantram, A. C. C. Tseung, and B. S. Harris, "Hydrocarbon Fuel Cell Technology", B. S. Baker, Ed., Academic Press, New York, N.Y., 1965, p 187.
(15) W. M. Vogel and C. D. Iacovangelo, *J. Electrochem. Soc.*, **124**, 1305 (1977).

RECEIVED for review March 30, 1978. Accepted July 25, 1978. Work carried out with the financial assistance of the Italian National Research Council (C.N.R. ROME).

Determination of Microgram Amounts of Tellurium in Steels by Atomic Absorption Spectrometry

Michael Bedrossian

The Armco Inc., Research & Technology, Middletown, Ohio 45043

A solvent extraction procedure has been developed for the determination of tellurium in all types of steel. After dissolution, the sample is extracted with trioctylphosphine oxide–methyl isobutyl ketone. The extract is then nebulized directly into the atomic absorption burner flame. This method requires 25 minutes and can determine as low as 2 parts per million level tellurium.

Since certain properties of iron and steel critically depend on the presence of trace amounts of tellurium, it is desirable to have a reliable analytical method for determining tellurium in steel below 100 ppm. The accurate determination of less than 50 ppm of tellurium is time consuming by classical methods (*1–5*), and difficult by direct instrumental techniques (*6, 7*). Concentration techniques are required to compensate for low sensitivities.

Solvent extraction techniques, which have been used successfully to separate tellurium from many types of sample matrix (*8–10*) have been combined with both photometric and gravimetric measurements to determine tellurium. The above procedures require a preliminary separation of tellurium in order to remove interfering elements and they lack sensitivity. Atomic absorption methods have been used in several procedures for tellurium in steel (*11–14*). These methods are either insensitive, suffer from interference, or require elaborate separations.

This present atomic absorption procedure is applicable to a wide variety of steels. The high sensitivity allows the determination of 0.0002% tellurium.

EXPERIMENTAL

Apparatus. A Perkin-Elmer Model 503 Atomic Absorption Spectrophotometer, equipped with an air–acetylene, three-slot burner head and Perkin-Elmer tellurium hollow cathode lamp was used.

Reagents. All chemicals used were ACS certified reagent grade quality. Standard tellurium of 100 μg/mL was prepared from the pure metal. Working solution of 25 μg/mL was prepared monthly by appropriate dilution of the stock solution in 10% HCl acid. Iodide reagent solution (30%) was prepared by dissolving 30 g of KI and 10 g of ascorbic acid in water containing 10 mL of HCl. This solution was prepared daily. Trioctylphosphine oxide–methyl isobutyl ketone (TOPO-MIBK) solution (5%) was prepared by dissolving 12.5 g of TOPO in MIBK in a 250-mL volumetric flask.

Procedure. The desired sample size (0.1 to 2.0 g) was dissolved in 25 mL of HCl (1 + 1) and 5 drops of HF. After dissolution, 7 mL of H_2O_2 (30%) were added dropwise; then the solution was digested over medium heat and cooled. Sufficient ascorbic acid (8 g) was added to change the dark yellow color to light yellow; then 15 mL of the iodide reagent were added and the sample solution was transferred to a 100-mL volumetric flask which had been marked at the 50-mL level. The volume was adjusted to 50 mL and 10.0 mL of the 5% TOPO-MIBK reagent were added. The extraction was made by shaking the solution for 1 min. Deionized water was added to raise the TOPO-MIBK layer to the top of the flask.

0003-2700/78/0350-1898$01.00/0 © 1978 American Chemical Society

Table I. Effect of Hydrogen Peroxide on the Recovery of Tellurium

sample	grade (stainless)	% Te present	% Te recovered with H_2O_2	% Te recovered without H_2O_2
A80	type 18-8	0.0068	0.0066	0.0059
A81	type 18-8	0.0189	0.0190	0.0176
A82	type 18-8	0.105	0.105	0.0977

Standard calibration solutions were prepared from the working solution (25 μg/mL) by extracting 0.00, 25.00, 50.00, 75.00, and 100.00 μg of tellurium using the above procedure.

The TOPO-MIBK extract was nebulized directly into the burner flame. The absorbance readings were made at the optimum instrumental settings, and the concentration of tellurium in the test solution was determined.

RESULTS AND DISCUSSION

Generally, most samples are dissolved in hydrochloric acid, hydrofluoric acid, and hydrogen peroxide, and extracted from a 5% (v/v) hydrochloric acid solution. Hydrogen peroxide oxidizes Te(II) to Te(IV) for quantitative extraction. When Armco standards 80, 81, and 82 were analyzed using no hydrogen peroxide, lower tellurium values were obtained as shown in Table I.

The dissolution of certain types of steels may require the use of a combination of acids. If hydrochloric and nitric acids are used, it is important that any nitric present be removed; otherwise, the organic phase becomes dark and viscous, and low tellurium values are obtained. Formic acid completely decomposes the nitrate ion. The excess of formic acid is removed by evaporation with hydrochloric acid.

The extraction of tellurium as TeI_4 complex with TOPO-MIBK is quantitative since phosphine oxides are more efficient metal extractants than ethers, alcohols, and ketones. As a result, the extraction need not be controlled as closely as does extraction with MIBK alone. Complete complexation of tellurium can be achieved by the addition of 0.6–7.5 g KI per 50 mL of solution. Small variations in the volume of the aqueous phase are not important. However, large variations will affect the final volume of the organic phase because of the solubility of the MIBK in the aqueous phase. A study was made on the effect of hydrochloric acid concentration on the MIBK extraction. Little or no effect was noted if the normality of hydrochloric acid is between 1.2 and 4.8. Above 4.8 N hydrochloric acid, the solubility of MIBK in the aqueous layer increased. Precise control of the equilibration time is not required because the extraction can be completed in a few seconds. The extracts are stable for several days.

Occasionally, with some samples, an emulsion is formed in the organic phase due to partially hydrolyzed silicon. This emulsion can be broken by the addition of a few drops of hydrofluoric acid during extraction.

Although antimony, bismuth, lead, and tin are quantitatively extracted (*15*), these elements are normally present at microgram levels and, therefore, do not interfere. Zinc is also partially extracted; however, it is not generally present in steels. Copper, if present, is extracted along with tellurium. It was found that 0.2 mg of tellurium can be determined in the presence of as much as 75 mg of copper without interference. Any level of copper greater than 100 mg gives a precipitate of copper(I) iodide and low results are obtained. Iron(III) must not be present in the sample solution when the extraction is performed, since it will also be extracted and the organic phase will be dark and viscous. Therefore, prior to the extraction, ascorbic acid is added to reduce iron(III) to iron(II). Various amounts of ascorbic acid in excess of the amount necessary to reduce the iron (up to 12 g) did not interfere with the extraction.

Table II. Analyses of Armco Standards, SRM Standards, and Standard Reference Materials with Tellurium Added

sample	grade	% Te present	% Te recovered
A80	type 18-8	0.0068	0.0064
A81	type 18-8	0.0189	0.0187
A82	type 18-8	0.105	0.103
SRM 1261	low alloy	0.0006	0.00057
SRM 1262	low alloy	0.0011	0.0011
SRM 1263	low alloy	0.0009	0.00083
SRM 1264	low alloy	0.00018	0.00014
SRM 1175	cast iron	0.009	0.009
SRM 365	carbon	0.0013	0.0013
SRM 25b	silicon	0.0050	0.0049

Table III. Comparison of Methods

sample	grade	% Te atomic absorption, TOPO-MIBK	% Te photometric
A80	type 18-8	0.0065	0.0068
A81	type 18-8	0.0191	0.0189
A82	type 18-8	0.103	0.105

The proposed TOPO-MIBK extractant is a useful solvent for several reasons. The extraction of tellurium is essentially complete, while less than 1% of aluminum, calcium, chromium, cobalt, iron(II), magnesium, manganese, molybdenum, nickel, niobium, titanium, vanadium, and zirconium is extracted. It was confirmed that the 1% extracted causes no appreciable interference. All the results indicate that tellurium can be determined by this method without interference, except from large amounts of copper and zinc. Results obtained on Armco standards, SRM standards, and standard reference materials with tellurium added are given in Table II.

A comparison between the TOPO-MIBK–atomic absorption procedure and the tellurium diethyldithiocarbamate–photometric procedure (*16*) for three steel samples is presented in Table III.

LITERATURE CITED

(1) T. Kuroha and S. Shibuya, *Bunseki Kagaku*, **21**, 1197–1201 (1972); *Chem. Abstr.*, **77**, 172321m (1972).
(2) G. Filep and G. Balogh, *Banyasz. Kohasz. Lapok, Kohasz*, **107** (2), 75–76 (1974); *Chem. Abstr.*, **81**, 3287g (1974).
(3) H. Goto and Y. Kakita, *Jpn. Anal.*, **3**, 299–304 (1954).
(4) S. Kaneschi and C. Gallazzi, *Anal. Chim. Acta*, **54**, 461–467 (1971).
(5) E. Y. Zel'tser and N. N. Kuznetsova, *Tr. Vses. Nauchno-Issled. Inst. Elektromekh.*, **35**, 167–171 (1971); *Chem. Abstr.*, **77**, 69741Z (1972).
(6) M. Ito and K. Yanagihara, *Bunseki Kagaku*, **22**, 10–16 (1973); *Chem. Abstr.*, **79**, 26848p (1973).
(7) L. S. Kopanskaya and A. T. Russu, *Ostsillograficheskaya Peremennotokovaya Polyarogr.*, 109–118 (1971); *Chem Abstr.*, **77**, 121813r (1972).
(8) Y. Uzumasa, K. Hayashi, and S. Ito, *Bull. Chem. Soc. Jpn.*, **36**, 301–306 (1963); *Chem. Abstr.*, **58**, 13130h (1963).
(9) H. Goto, Y. Kakita, and T. Furukawa, *Nippon Kakagu Zasshi*, **79**, 1513–1520 (1958).
(10) N. Iordanov, and Iv. Khavezov, *Fresenius' Z. Anal. Chem.*, **248** (5–6), 296–298 (1969); *Chem. Abstr.*, **72**, 74353a (1970).
(11) W. D. Cobb, W. W. Foster, and T. S. Harrison, *Analyst (London)*, **101** (1198), 39–43 (1976).
(12) W. B. Barnett and J. D. Kerker, *At. Absorpt. Newsl.*, **13** (3), 56–60 (1974).
(13) G. G. Welcher, O. H. Kriege, and J. Y. Marks, *Anal. Chem.*, **46**, 1227–1231 (1974).
(14) M. V. Marčec, K. Kinson, and C. B. Belcher, *Anal. Chim. Acta*, **41**, 447–451 (1968).
(15) K. E. Burke, *Analyst (London)*, **97**, 19–28 (1972).
(16) Snell & Snell, Colorimetric Methods of Analysis, IIA, 678, 683 (1959).

RECEIVED for review March 10, 1978. Accepted August 16, 1978.

Background Correction and Related Problems in the Determination of Chromium in Urine by Graphite Furnace Atomic Absorption Spectrometry

Barbara E. Guthrie,[1] Wayne R. Wolf,* and Claude Veillon

Nutrition Institute, U.S. Department of Agriculture, SEA, Beltsville, Md. 20705

Factors influencing the determination of Cr in urine by furnace atomic absorption spectrometry were investigated. Tests showed that the conventional deuterium background corrector was inadequate and that the apparent concentration of chromium in urine was highly dependent on the amount of background present during atomization. In light of these findings, current literature values for Cr in urine analyzed by use of graphite furnace AAS should be reconsidered.

Chromium is an essential trace element for man and deficiencies have occurred in human subjects (*1, 2*). Biologically active Cr is required for the normal action of insulin. Determination of urinary Cr excretion has been proposed as a means for assessing the Cr nutritional status of humans (*1*).

Published values for Cr in human urine measured by furnace atomic absorption spectrophotometry range from 3–33 ppb (*3–7*). The question of whether there are different forms of Cr present in urine is unresolved. "Volatile" (*3, 4*) or "difficult-to-analyze" (*5*) forms of Cr have been hypothesized. Apparently these forms are not detected if urine is injected directly into a carbon furnace; but are detected if urine is first gently charred and ashed under conditions such as those found in a low temperature asher.

We now describe the types of problems encountered when attempting to determine Cr in urine. The effects of sample volume, charring conditions, type and mode of inert gas flow and of individual graphite tubes on background, and the apparent Cr content of urine are discussed. We concluded that a deuterium background corrector is inadequate for the correction of nonatomic absorbance during the determination of Cr in urine.

EXPERIMENTAL

Instrumentation. A Perkin-Elmer 603 Atomic Absorption Spectrophotometer (AAS) equipped with an HGA 2100 graphite furnace, a deuterium (D_2) arc background corrector, and a Model 56 recorder were used.

On the 603 AAS, the signal was set for concentration and the mode on continuous. The D_2 background corrector was on and aligned. The Cr wavelength of 357.9 nm was used. The integration time was 0.5 s and the slit width was 0.4 nm.

In the initial parts of the study, we used a 10-fold scale expansion with 30-μL sample injections, nonpyrolytic tubes, and N_2 as the purge gas in the interrupt mode. Furnace conditions were as follows: drying, 120 °C for 30 s (ramped); char, 1300 °C for 30 s; and atomize, 2600 °C for 9 s. These conditions, however, gave highly variable results over a 10-week period so we reexamined the analytical conditions as described in the Results and Discussion section.

Samples. We prepared two stock urines. One was from two 24-h urine samples from two healthy adults, a male and female, each aged 30 years. The second stock was from seven 24-h urine samples collected by healthy male adults aged 20–40 years. Immediately after collection, the urines were mixed thoroughly, divided into aliquots, and frozen. Aliquots were thawed immediately prior to sample preparation.

Because of the unresolved question of volatile Cr in urine, all samples were gently pretreated prior to injection into the graphite furnace. Samples of 500 μL in Coors porcelain crucibles were dried for 6 h in a vacuum oven, then treated for 3 h in a low temperature asher (Trapelo 505, LFE Coporation) set at 1 mm O_2 pressure and 400-W power. After samples cooled, 100 μL 50% H_2O_2 (Fisher Scientific Co.) was added as an ashing aid. The samples were dried again for 2 h in the vacuum oven and then treated in the low temperature asher for an additional 3 h. The white ash remaining was dissolved in 500 μL 1M HCl (National Bureau of Standards, sub-boiling distillation preparation).

The sample response was compared to that of inorganic Cr as potassium chromate (Fisher Scientific Co.). Working standards in the range of 0.5–5.0 ng/mL were prepared daily in a 1 M HCl solution.

RESULTS AND DISCUSSION

In the initial part of the study, the same stock urine sample showed three phases in peak shapes for Cr. Typical recorder tracings are shown in Figure 1. For the first 6 weeks of this study, there were characteristically two peaks for Cr in urine; the first peak was larger than the second. This was followed by a 2-week period with only one peak. Then there were two peaks again for another 2 weeks until three peaks, often of most irregular shapes, appeared. The three-peak phase corresponded exactly with the use of a new batch of graphite tubes.

The two-peak phase was by far the most common but we did not know which represented Cr, or whether both or neither represented Cr.

Figure 2 shows a comparison of peaks from urine measured with Cr and D_2 lamps (peak A) vs. Ni and D_2 lamps (peak B). The Ni wavelength of 357.6 nm was used as a nearby nonabsorbing line for Cr. If the D_2 or Ni or Cr lamp were used alone, peak C was virtually identical, and showed the presence of massive nonatomic absorbance. Inspection suggested that the first peak might be due to background alone, and that the second peak might be for Cr. However, in Figure 3 are examples of spiked and unspiked urine samples. The unspiked urine initially showed two peaks. The spiked sample could show an increase in both peaks (peaks A and B) but sometimes the spiked sample would show only one peak (peaks C and D). That observation suggested that when two peaks were present, both represented Cr.

The mode of purge gas did not influence the number of peaks for urine Cr, but did influence peak shape. The normal mode resulted in irregular peaks and a 2- to 3-fold loss in sensitivity compared to the interrupt mode. This loss is shown in Figure 4 for a 2 ng/mL Cr standard.

We then began to reinvestigate charring conditions and recorded background for each sample. Scale expansion was changed from 10X to 20X.

Our observations indicated that the apparent Cr concentration in urine depends on the amount of background. This dependence is illustrated in Figure 5. Peak A was the re-

[1] Current address, Nutrition Department, University of Otago, Dunedin, New Zealand.

This article not subject to U.S. Copyright. Published 1978 by the American Chemical Society

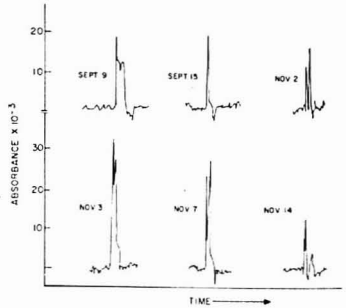


Figure 1. Examples of peak shapes on different days for Cr in urine

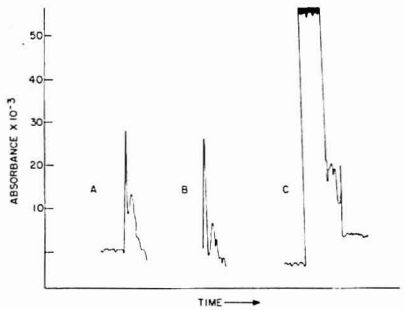


Figure 2. Use of nearby nonabsorbing line technique. (A) Cr and D_2 lamps, (B) Ni and D_2 lamps, (C) Cr or Ni cr D_2 lamp alone

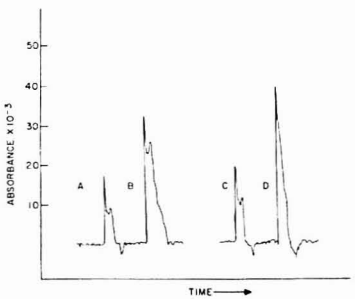


Figure 3. Examples of spiked and unspiked urine samples on different days. (A) Unspiked urine, day 1; (B) spiked urine, day 1; (C) unspiked urine, day 2; (D) spiked urine, day 2

sponse with a char temperature of 1100 °C for 90 s; background was 0.20 absorbance (abs.) unit and the apparent Cr concentration in urine was 3.8 ng/mL. Peak B was the response with a char temperature of 1200 °C for 90 s; background was 0.12 abs. unit, and the apparent Cr concentration in urine was 2.2 ng/mL. Peak C was the response with a char of 1300 °C for 90 s; background was 0.05 abs. unit, and the apparent Cr content in urine was 1.0 ng/mL. The response was a single peak only with a char temperature of 1300 °C. At 1100 °C and 1200 °C the responses were two peaks.

The volume of sample injected was also critical as shown in Table I. As the volume increased, so did the background and the apparent Cr concentration in urine.

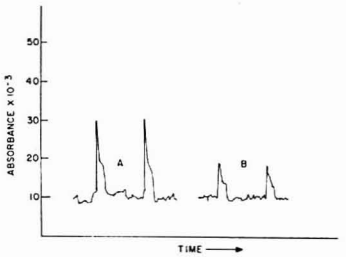


Figure 4. Effect of the purge gas mode on a 2 ng/mL Cr standard. (A) N_2 on interrupt mode; (B) N_2 on normal mode

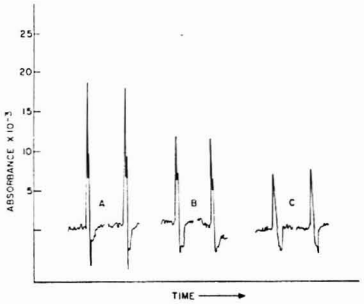


Figure 5. Effect of char temperature on urine Cr peak. (A) Char, 1100 °C, (B) char, 1200 °C, (C) char, 1300 °C

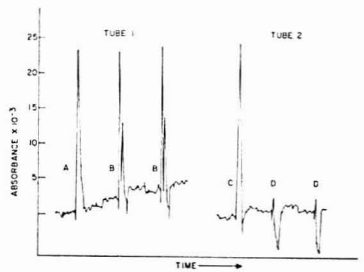


Figure 6. Effect of graphite tubes from different batches on the response of a 4 ng/mL Cr standard (A and C) and a urine sample (B and D)

Table I. Effect of Sample Volume on Background and the Apparent Cr Concentration in Urine

sample volume, μL	background, abs. unit	apparent Cr content of urine, ng/mL
20	0.01	0.32
30	0.04	0.56
40	0.10	0.95
50	0.16	1.19

Apparently there should be only one peak for Cr in urine, but when the nonatomic absorbance was greater than the background corrector could cope with, two peaks were seen. Optimal conditions now seemed to involve the use of 20 μL samples and a char at 1300 °C for 90 s. However, another factor, the individual graphite tubes, had a major effect on background. With different graphite tubes from the same

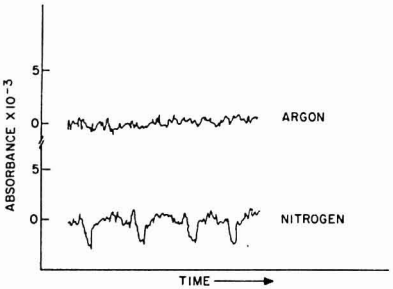


Figure 7. Effect of purge gas on the base line during 4 firings of an empty furnace

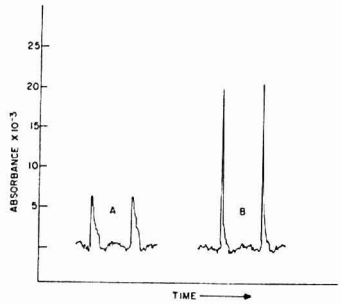


Figure 8. Effect of pyrolytic vs. nonpyrolytic graphite tubes on a 1 ng/mL Cr standard. (A) Nonpyrolytic tubes; (B) pyrolytic tubes

batch, background varied in the order of 0.03 to 0.05 abs. unit for the same urine sample. Figure 6 illustrates the magnitude of these differences with graphite tubes from different batches. With tube 1, background was 0.32 abs. unit, and the response was two peaks and apparent Cr content in urine was 6.3 ng/mL. With tube 2 from a different batch, background was 0.05 abs. unit, and response was one peak and apparent Cr content in urine was 0.5 ng/mL. The same urine sample was injected into each tube and analytical parameters were identical for each. The 4 ng/mL Cr standard (peaks A and C) gave virtually identical responses in each tube. Figure 6 shows two new problems particularly in peak D, lack of sensitivity and marked negative peaks after the peak for Cr.

Figure 7 represents four firings of an empty furnace; the negative peaks apparently were due to cyanogen absorption and seemed to be eliminated with argon as the purge gas. Figure 8 demonstrates that sensitivity increased about threefold with pyrolytically coated graphite tubes. So argon plus pyrolytic tubes apparently offered the solution to both of the above problems. With pyrolytic tubes, however, no char conditions could be found that would give only one peak for Cr in urine. This problem seemed to be related to the relatively high background produced in the pyrolytic compared to the nonpyrolytic tubes. Also with pyrolytic tubes the apparent Cr content in urine exceeded 2 ng Cr/mL.

Figure 9 shows that the apparent Cr concentration in urine was dependent on the level of background present. The correlation coefficient was 0.94.

At the Cr wavelength of 357.9 nm, the intensity of the D_2 lamp is very low. Over the first 4 months of operation, we

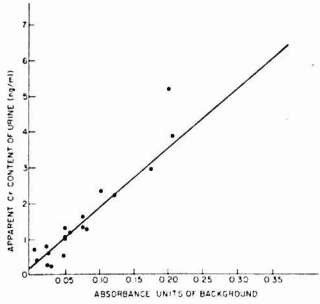


Figure 9. Correlation between background and apparent Cr concentration

had three new D_2 lamps. As the D_2 lamp aged, the intensities of the Cr and D_2 lamps could not be matched. The D_2 system approached effectiveness with a background of less than 0.05 abs. unit, but that level of background required the right graphite tube. Selection of the right tube was more by chance than good management.

The results presented in this paper demonstrate the inadequacy of a conventional D_2 background correction system for determinations of Cr in a high solid matrix at the 1 ng/mL level. Clearly an alternative system allowing for adequate background correction is needed at the 357.9-nm wavelength. The alternatives appear to include the polarized Zeeman effect (*8*); a continuum source wavelength modulated, echelle AA system (CEWM-AA) (*9*, *10*); or the modification of existing D_2 systems by substituting for the D_2 lamp a continuum source with greater intensity at the Cr wavelength.

We have carried out preliminary studies with a CEWM-AA (*11*) and have found it to be satisfactory for the determination of Cr in urine. In these studies the concentration of Cr in human urine was found to be less than 1 ng/mL, which corresponds to the values reported in this paper when the background was less than 0.05 abs unit.

The problems we encountered with the D_2 background correction system may partially explain the divergence of published values for Cr in urine.

LITERATURE CITED

(1) W. Mertz, *Physiol. Rev.*, **49**, 163 (1969).
(2) K. N. Jeejeebhoy, R. C. Chu, E. B. Marliss, G. R. Greenberg, and A. Bruce-Robertson, *Am. J. Clin. Nutr.*, **30**, 531 (1977).
(3) R. T. Ross, J. G. Gonzalez, and D. A. Segar, *Anal. Chim. Acta*, **63**, 205 (1973).
(4) W. K. Canfield and R. J. Doisy, in "The Biomedical Role of Trace Elements in Aging", J. M. Hsu et al., Ed., Eckerd College Gerontology Center, Fla., 1976, p 119.
(5) W. R. Wolf, *Fed. Proc.*, **34**, 927 (1975).
(6) C. T. Gurson, G. Saner, W. Mertz, W. R. Wolf, and S. Sokucu, *Nutr. Rep. Int.*, **12**, 9 (1975).
(7) S. Punsar, W. Wolf, W. Mertz, and M. J. Karvonen, *Ann. Clin. Res.*, **9**, 79 (1977).
(8) H. Koizumi, K. Yasuda, and M. Katayama, *Anal. Chem.*, **49**, 1106 (1977).
(9) A. T. Zander, T. C. O'Haver, and P. N. Keliher, *Anal. Chem.*, **48**, 1166 (1976).
(10) J. M. Harnly and T. C. O'Haver, *Anal. Chem.*, **49**, 2187 (1977).
(11) B. E. Guthrie, W. R. Wolf, C. Veillon, and W. Mertz, in "Trace Substances in Environmental Health-XII", D. D. Hemphill, Ed., University of Missouri, Columbia, Mo., in press.

RECEIVED for review July 5, 1978. Accepted August 25, 1978. Barbara E. Guthrie was supported by a U.S. Public Health Service International Research Fellowship No. 1F05 TW 02529-01. Presented at the MARM 12th Meeting ACS, Hunt Valley, Md., March 1978.

Oscillating Slit Mechanism for the Determination of Hydrogen Isotope Ratios in a Microwave Induced Plasma

Frederick P. Schwarz,* Walter Braun, and Stanley P. Wasik

National Bureau of Standards, Washington, D.C. 20234

A low pressure microwave discharge through deuterated and hydrogenated hydrocarbon mixtures eluting from a gas chromatograph results in fragmentation of the hydrocarbons and generation of intense atomic hydrogen emission at 6562.8 Å and atomic deuterium emission at 6561.0 Å. By replacing the exit slit mechanism of the monochromator viewing the emissions with an oscillating slit mechanism (OSM), the hydrogen emission is measured alternately with the deuterium emission. The operation of the OSM is based on oscillating mechanically the exit slit aperture twice across the hydrogen line and once across the deuterium line during one cycle of oscillation. Two lock-in amplifiers resolve the modulated emissions into a hydrogen and a deuterium signal. The ratio of the two signals is a linear function of the atomic hydrogen isotope ratio in the isotope hydrocarbon mixtures over one order of magnitude.

Quantitative measurements of hydrogen to deuterium isotope ratios are important in water pollution analysis. The amount of a pollutant in a water sample can be determined by adding a known amount of the perdeuterated analogue to the water sample and measuring the hydrogen to deuterium isotope ratio. The concentration of the pollutant is determined by multiplying the known concentration of the perdeuterated analogue by the isotope ratio. Mass spectrometry and gas–liquid chromatography (GLC) are currently employed in measuring the hydrogen isotope ratio (*1*). Mass spectrometric analysis is limited by expense and GLC analysis by possible overlap of the separated isotope peaks with other hydrocarbon peaks and poor separation of the isotope peaks.

An alternative method of determining hydrogen isotope ratios based on spectroscopic analysis of the atomic hydrogen and deuterium emissions generated in a radio frequency discharge through flowing gas mixtures was fist reported by Broida and Morgan (*2*). They found that the isotope ratio in hydrogen, deuterium, and air mixtures could be accurately determined under carefully controlled flow conditions. Later Luippold and Beauchamp spectroscopically determined hydrogen isotope ratios in isotopically mixed hydrocarbons eluting from a GLC (*3*). They analyzed the CH and CD emissions generated in a low pressure microwave discharge through the flowing elutants. Recently, Schwarz analyzed the hydrogen and deuterium atomic emissions generated in a low pressure microwave discharge through isotopically mixed octane vapors eluting from a GLC and found the emission ratio to be proportional to the hydrogen isotope ratio (*4*). This method was found to be quantitative over at least one order of magnitude and showed promise of being applicable to other hydrogen isotope mixtures.

In this report, we describe and evaluate in more detail the method of determining hydrogen isotope ratios based on measuring the deuterium and hydrogen atomic emissions generated in a microwave discharge through hydrocarbons eluting from a GLC. This investigation was facilitated by a novel instrumental modification of the monochromator viewing the emissions. By replacing the monochromator exit slit mechanism with an oscillating slit mechanism (OSM), the hydrogen emission at 6562.8 Å was measured alternately with the deuterium emission at 6561.0 Å. The OSM modulated the hydrogen emission at twice the frequency of the deuterium emission. Two lock-in amplifiers resolved the modulated emissions into a deuterium signal and a hydrogen signal of an isotopically diluted elutant. The analytical range and response were investigated for different classes of hydrocarbons and partially deuterated hydrocarbons. Application of the method to isotope dilution analysis of a water sample was also investigated.

EXPERIMENTAL

The microwave plasma detection apparatus was a modified version of one described previously (*4*). This modification consisted of replacing the exit slit mechanism of the detection monochromator by an oscillating slit mechanism (OSM) to measure alternately the hydrogen emission at 6562.8 Å and the deuterium emission at 6561.0 Å. The operation of the OSM is shown schematically in Figure 1. A 1 cm × 0.1 cm vane (Bulova Watch Co.) with a 0.5 cm × 0.03 cm opening was driven by a mechanical resonanting circuit to oscillate at 200 Hz (ν in Figure 1) with a spectral sweep of 3.4 Å. (The monochromator dispersion is 16.7 Å/min and the vane oscillated with an amplitude of ±0.01 cm). At rest the vane holder was positioned so that the vane opening transmitted light at the wavelength reading of the monochromator dial. During one cycle of oscillation and with the monochromator set at 6562.8 Å, the vane opening crossed the hydrogen line (6562.8 Å) twice and the deuterium line (6561.0 Å) once, thereby modulating the hydrogen signal at 2 ν and the deuterium signal at 1 ν. The photomultiplier output was fed into two lock-in amplifiers operated in the external reference mode with the reference signal supplied by the mechanical resonanting circuit. One lock-in amplifier was referenced at 2 ν to monitor the hydrogen emission and the other at 1 ν to monitor the deuterium emission. Prior to the experiment, the vane opening was conveniently centered on the background hydrogen emission line by turning the wavelength dial of the monochromator until the 1-ν signal registered zero and the 2-ν signal was maximized. The entrance slit of the monochromator was set at 0.03 cm. For direct measurements of the emissions, the OSM was turned off and the photomultiplier output was connected to a picoammeter.

The microwave plasma was maintained at the optimum sensitivity conditions of 0.5 to 1.0% O_2 concentration in helium carrier gas and at a pressure of 5 Torr (*4*). The stainless steel GLC columns were 3 m × 3 mm containing 3% Dexsil 300 on 80/100 chromosorb WAW and 8 m × 3 mm containing Squalane on 80/100 chromosorb WAW. The helium carrier gas had a stated purity of 99.999% and was used without further purification.

The hydrocarbon solutions were made up by weight on a microgram electrobalance and injected into the GLC by a 10-μL syringe. The naphthalene–benzene–water sample was prepared by mixing aliquots of saturated aqueous solutions of benzene and naphthalene. The saturated water solutions were prepared by stirring an excess of the solute in distilled water for at least 24 h.

The hydrocarbon vapor mixtures in 760 Torr helium were prepared on a separate gas handling system and contained in 1-L stainless steel cylinders. Samples of 10 μL of the mixtures were injected into the GLC by a gas sampling valve.

The butylbenzene and 1-methylnaphthalene were 99 mol% pure. The octane, isooctane, cyclohexane, toluene, cyclohexene,

This article not subject to U.S. Copyright. Published 1978 by the American Chemical Society

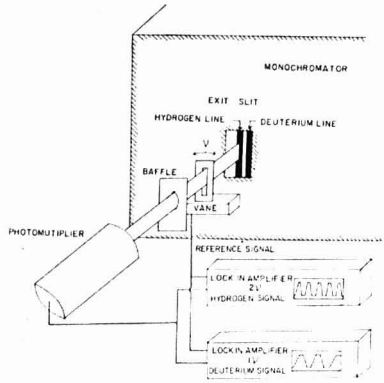


Figure 1. Schematic diagram of operation of the OSM

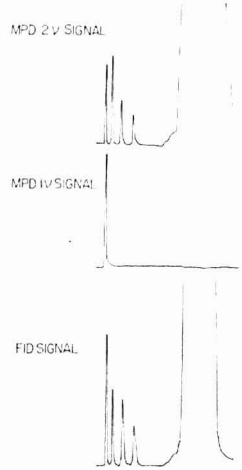


Figure 2. OSM hydrogen (2 ν) and deuterium (1 ν) and FID chromatograms of a 0.2-μL injected sample of 0.33 wt % each of benzene, butylbenzene, naphthalene, methylnaphthalene, and 0.10 wt % perdeuterated benzene in hexadecane. The Dexsil column was operated at 165 °C

benzene, and naphthalene and their perdeuterated isomers were all 99 mol% pure. The partially deuterated toluene-αd_3, benzene-d_1, butane-1,1,1-d_3, and ethylene-1,1-d_2 were also 99 mol% pure.

RESULTS AND DISCUSSION

In Figure 2 are shown OSM hydrogen (2 ν) and deuterium (1 ν) chromatograms of a 0.2-μL injected sample of 0.33 wt% each of benzene, butylbenzene, naphthalene, methylnaphthalene, and 0.10 wt% perdeuterated benzene in hexadecane. Despite the high hexadecane concentration, 1000X greater than the C_6D_6 concentration, the hexadecane peak is absent in the OSM deuterium (1 ν) chromatogram. The OSM chromatograms are similar in peak shape and resolution to the FID chromatogram of the sample in Figure 2. As verified by earlier results, the FID-to-OSM hydrogen peak height ratio is proportional to the C/H composition ratio for each solute.

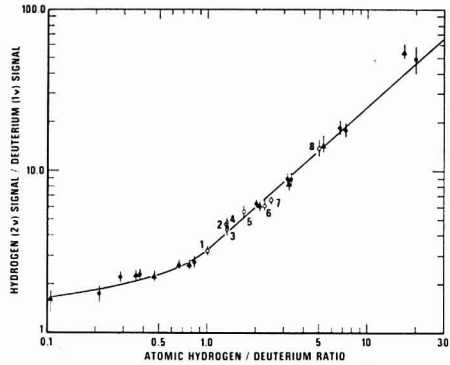


Figure 3. OSM hydrogen-to-deuterium peak height ratios as a function of the hydrogen to deuterium atom ratio, H/D. C_6H_{18}/C_6D_{18} vapor in helium mixtures (▲) and in $C_{10}H_8/C_{10}D_8$ in hexadecane solutions (●). 0.01 mL samples in 760 Torr helium of 1 Torr C_6H_{18} and from 0.6 to 0.06 Torr of C_6D_{18} (above H/D = 1) and of 1 Torr C_6D_{18} and from 0.8 to 0.1 Torr of C_6H_{18} (below H/D = 1). 0.2-μL samples in hexadecane of 0.40 wt % $C_{10}H_8$ and from 0.3 to 0.02 wt % of $C_{10}D_8$ (above H/D = 1) and of 0.40 wt % $C_{10}D_8$ and from 0.32 to 0.08 wt % $C_{10}H_8$ (below H/D = 1). The circle points are (1) ethylene-1,1-d_2, (2) 8(7) isooctane/isooctane-d_{18}, (3) cyclohexane/cyclohexene-d_{10}, (4) toluene/toluene-d_8, (5) toluene-αd_3, (6) butane-1,1,1-d_3, and (8) benzene-d_1. For the octane ratios, the dexsil column was operated at 130 °C and for the other perdeuterated/hydrogen ratios, the dexsil column was operated at 165 °C. For the partially deuterated ratios, the squalene column was operated at room temperature

(The FID peak height includes both the perdeuterated and protonated benzene (*4*)).

In Figure 3 are plotted the OSM hydrogen isotope signal ratios as a function of the atomic hydrogen to deuterium ratio (H/D) in protonated and perdeuterated hydrocarbon mixtures and in partially deuterated hydrocarbons. The total concentrations of the injected samples were below the microwave plasma saturation level in all cases (*4*). At the saturation level, the large concentration of the elutant resulted in an unstable plasma and reduction of the hydrogen and deuterium emission intensities. The vapor mixtures of octane in helium and solutions of naphthalene in hexadecane were sampled to determine the measurement range of the OSM signal ratios. The calibration curve covers a linear range of more than one order of magnitude. A least squares fit of the data points to a linear equation yields a slope of 2.81 ± 0.26 and a OSM signal ratio intercept of 0.67 ± 0.38. This range is a practical working range for most hydrogen isotope dilution measurements. The upper limit of the curve was fixed by two constraints, the microwave plasma saturation level and the signal-to-noise ratio of the deuterium signal. Since the noise in the deuterium signal consisted of photomultiplier and electronic noise, improvement of the deuterium signal-to-noise ratio at the upper limit could have been obtained through larger deuterium concentrations but the total deuterium and hydrogen concentration would have been above the saturation level.

Reduction of the error in the OSM ratios in Figure 3 could be achieved through reduction of the OSM duty cycle. The duty cycle is the ratio of the period of oscillation to the emission observation time during one cycle. For deuterium, the duty cycle was 0.2 mm/0.03 mm (the amplitude of the vane oscillation/the opening of the vane) = 6.7 and for hydrogen 3.4 since the hydrogen emission was observed twice during one cycle of observation. For example, an increase in the vane opening would reduce the duty cycle. When the OSM was turned off and the photomultiplier connected to

Table I. Naphthalene H/D Ratios of Benzene and Naphthalene in Organic Solvent Extracts Following Treatment by Various Analytical Procedures

treatment	FID benzene concn rel. units	FID naphthalene/-benzene ratios	naphthalene OSM ratio
1 mL extract	1258	1.5	4.3 ± 0.3
extract after standing 24 h	792	2.1	4.3 ± 0.3
extract aerated for 5 min	350	4.8	4.3 ± 0.3
0.05 mL fresh organic solvent extract from $AgNO_3$ extract	302	1.4	4.6 ± 0.3

the picoammeter which is analogous to reducing the duty cycle of the OSM, the deuterium signal-to-noise ratio improved by at least a factor of 3.

At the lower limit of the curve, i.e., where the hydrogen concentration = 0, a hydrogen (2 ν) peak was observed simultaneously upon the elution of perdeuterated octane or naphthalene through the microwave plasma. A hydrogen peak was also observed for the perdeuterated analogues of cyclohexane, cyclohexene, isooctane, toluene, and benzene. However, a corresponding deuterium peak was not observed upon the elution of the protonated hydrocarbon through the microwave plasma. The intercept in the least squares fit of the data points resulted from the constant contribution (the deuterium concentration was kept constant below H/D = 1) of this hydrogen (2 ν) peak to the hydrocarbon hydrogen (2 ν) peak.

In Figure 3, the OSM signal ratios fall on the same calibration curve for all of the isotope mixtures and for the partially deuterated hydrocarbons. The toluene/toluene-d_8, the isooctane/isooctane-d_{18} and the cyclohexene/cyclohexene-d_{10} mixtures were made up by weight on the tenths of the weight % level in hexadecane so that the 0.5-μL injected sample was below the microwave plasma saturation level. The OSM measurements on the partially deuterated species, toluene-αd_3, benzene-d_1,butane-1,1,1-d_3, and ethylene-1,1-d_2, were performed on a 10^{-2}-mL injected sample of a mixture of 1 Torr each of the partially deuterated hydrocarbon vapor in 760 Torr of helium. The independence of the calibration curve from elutant structure suggests either complete or constant fragmentation of the perdeuterated and partially deuterated hydrocarbons in the microwave helium plasma. Similar results were reported for the protonated hydrocarbons (*4*). The calibration curve in Figure 3 can thus be prepared from structurally known partially deuterated hydrocarbons, thereby avoiding the necessity of preparing accurately calibrated isotope mixtures.

A typical application of isotope dilution analysis by the OSM was performed on a water sample containing approximately 20 ppm naphthalene and 18 ppm benzene. Approximately 15 mg of perdeuterated naphthalene was added to a 1-L portion of the sample. The 1-L portion was then extracted with 1 mL of an organic solvent, a typical method for concentrating contaminants in water (*1*). The extract was treated by additional operations of the type that normally would be performed in water pollution analysis. Effects of excessive handling of the extract were simulated by letting the extract stand for 24 h and by bubbling air through the sample. A 0.5-mL aliquot of the extract was extracted with 10 mL saturated $AgNO_3$ solution and the 10 mL $AgNO_3$ extract was reextracted with 0.5 mL of a fresh organic solvent. The $AgNO_3$ extraction is analogous to the case where the contaminant is distributed between the bulk solution and the surfaces of the sediment and container. The results of these operations are presented in Table I along with the split flow FID integrated areas for benzene and naphthalene. In all the operations, the OSM-determined naphthalene hydrogen isotope ratios remain constant within the experimental error of 8%. On the calibration curve in Figure 3, this ratio yields a H/D ratio of 1.33 which is equal to the naphthalene/naphthalene-d_8 ratio in the isotopically diluted protion of the water sample.

The principal advantage of the isotope dilution method is the constancy of the isotope ratio in the sample during the concentration of the sample by traditional analytical methods. From the standpoint of cost and simplicity, the OSM isotope ratio determinations are preferable to mass spectrometric isotope ratio determinations. Furthermore, some of the hydrocarbons would be difficult to analyze by mass spectrometric techniques because of complex fragmentation patterns. The OSM isotope ratio determinations are, however, independent of the fragmentation kinetics of the hydrocarbon in the plasma and the hydrocarbon structure. This independence permits the calibration of the isotope ratio measurement curve by known partially deuterated hydrocarbons, thereby eliminating the necessity of weighing known mixtures of the isotopes. From the standpoint of resolution of the isotopes, the OSM method is preferable to the GLC method which does not provide complete separation of the isotopes (*1*). Furthermore, the GLC isotope peaks may overlap other hydrocarbon peaks in the chromatogram.

One disadvantage of the OSM method is the poor S/N of the isotope ratio measurements which results in an inaccuracy in the isotope ratio measurements of almost 10% and restricts the measurement range to almost one order of magitude. However, the S/N can be improved by reducing the duty cycle of the OSM, which would also extend the measurement range to at least two orders of magnitude.

ACKNOWLEDGMENT

The authors wish to acknowledge the help of Brenton L. Baugher in the design and fabrication of the OSM.

LITERATURE CITED

(1) S. P. Wasik and W. Tsang, *Anal. Chem.*, **42**, 1649 (1970).
(2) H. P. Broida and J. H. Morgan, *Anal. Chem.*, **24**, 799 (1952).
(3) D. A. Luippold and J. L. Beauchamp, *Anal. Chem.*, **42**, 1374 (1970).
(4) F. P. Schwarz, *Anal. Chem.*, **50**, 1006 (1978).

RECEIVED for review March 24, 1978. Accepted August 23, 1978. This work has been supported by the Office of Air and Water Measurement at the National Bureau of Standards, Washington, D.C. Certain commercial equipment, instruments and materials are identified in this paper in order to adequately specify the experimental procedure. In no case does such identification imply recommendation or endorsement by the National Bureau of Standards, nor does it imply that the material, instruments, or equipment identified is necessarily the best available for the purpose.

Diffuse Reflectance Measurements by Infrared Fourier Transform Spectrometry

Michael P. Fuller and Peter R. Griffiths*

Department of Chemistry, Ohio University, Athens, Ohio 45701

An optical system for diffuse reflectance infrared spectrometry is described. The device uses an on-axis ellipsoidal collecting mirror and a commercial Fourier transform spectrometer. Almost any type of powdered sample can be studied and the feasibility of good quantitative analysis is discussed. Submicrogram detection limits are found for samples dispersed in KCl and for materials chromatographically separated directly on TLC plates. Results indicating the possibility of studying heterogeneous reactions of gases with powdered solids are shown.

The popularity of infrared spectrometry can in large part be attributed to its versatility, since samples may be readily studied as gases and liquids and, somewhat less readily, as solids. Two types of solid samples may be distinguished. Polymers may be prepared as free-standing or cast films and their spectra measured using conventional transmission or attenuated total reflection techniques. Powdered solids require preparation as solutions in a suitable solvent, as KBr disks, or as mineral oil mulls, and measurement of the spectra of powders without sample preparation is generally thought of as being rather difficult. Two possible techniques have been discussed in the past for measuring the infrared spectra of powdered samples without prior preparation, namely emission and diffuse reflection spectrometry. Infrared emission spectrometry is fraught with experimental hazards, in particular the effect of temperature gradients on the spectra and sample decomposition on heating. To date no good quantitative measurements have been obtained by infrared emission spectrometry for powdered samples. Diffuse reflectance infrared spectrometry has been largely ignored in the past by analytical spectroscopists, since it has generally been considered that the intensity of radiation reflected from powders is too low to enable spectra to be measured at medium resolution (2–4 cm^{-1}) and high signal-to-noise ratio (SNR).

Diffuse reflectance spectrometry has been widely used for the measurement of the ultraviolet–visible spectra of powders and turbid liquids, and a number of books on this subject have been written (*1–5*). The technique has been applied to clinical measurements (*6*), pharmaceutical quality control (*7*), heat transfer studies (*8*), and in food science (*9–11*). The most commonly used device for collecting diffusely reflected UV-visible, and even near infrared, radiation from a sample is an integrating sphere whose interior is coated with a diffusing, nonabsorbing powder, such as MgO or $BaSO_4$. The sample and detector are usually held at the surface of the sphere, and the measured spectrum is, to a good approximation, independent of the spatial distribution of the reflected light and the relative position of the sample and the detector.

The use of an integrating sphere for mid infrared diffuse reflectance spectrometry presents several problems. Firstly, the devices are intrinsically inefficient, and infrared detectors are several orders of magnitude less sensitive than photomultiplier tubes, so that the SNR of measured spectra would be expected to be low. Secondly, it is not easy to prepare suitable coatings for the interior of spheres designed for mid infrared spectrometry with equivalent performance to that of MgO or $BaSO_4$ in the UV-visible region. As a result, reports of vibrational spectrometry using diffuse reflectance techniques are sparse, and most of the published work in this field is more concerned with the acquisition of accurate engineering data, and describes the optimization of sample illumination, scattered radiation collection, and focusing methods rather than chemical or analytical spectrometry.

Previous devices which have been employed in the measurement of mid infrared diffuse reflectance spectra have included the Coblentz hemisphere (*12*), the Gier–Dunkle cavity (*13*), hemispherical (*14*), hemiellipsoidal (*15*) and ellipsoidal (*16–18*) collecting mirrors, in addition to integrating spheres (*19, 20*). Of these devices, the hemiellipsoidal and ellipsoidal reflectometers are probably the most efficient in terms of collecting and transmitting diffusely reflected radiation to the detector. The feasibility of applying these mirrors in conjunction with prism monochromators to chemical spectroscopy (*15*) and catalysis (*16*) has been demonstrated. Recently a special-purpose Fourier transform infrared (FT-IR) spectrometer has been interfaced to an integrating sphere for diffuse reflectance measurements (*20*), but the sphere is so inefficient that, in spite of the high performance of the spectrometer, spectra at adequate resolution and SNR required rather long measurement times.

In this report we describe results obtained when a fairly efficient ellipsoidal collecting mirror is interfaced to a commercial rapid-scanning FT-IR spectrometer. We demonstrate that diffuse reflectance infrared Fourier transform (DRIFT) spectra of a variety of powdered samples can be measured rapidly at medium resolution and high SNR. These spectra provide useful analytical information, and suggest that many types of previously intractable samples can be studied using this technique.

INSTRUMENTAL

The optical configuration of the diffuse reflectometer used in this work is shown in Figure 1. The beam from a modified Nernst glower source (Perkin-Elmer Corp., Norwalk, Conn.) is collimated using a 7.5-cm focal length, 45° off-axis paraboloidal mirror (Special Optics Corp., Little Falls, N.J.) and passed through a Model 296 Michelson interferometer (Digilab, Inc., Cambridge, Mass.). The collimated exit beam is then reflected by two plane mirrors to a 3.7-cm focal length, 90° off-axis paraboloidal mirror (Special Optics Corp.) which focuses the beam onto the powdered sample held in a small cup at one focus of an ellipsoidal mirror. This mirror (Special Optics Corp.) is the ellipsoid of revolution about the x axis of the ellipse:

$$\frac{x^2}{(992)^2} + \frac{y^2}{(386)^2} = 1 \qquad (1)$$

A small hole centered on the major axis is drilled to allow the beam from the paraboloid to pass onto the sample. Because of this geometry, any specularly reflected radiation from the sample returns through the hole, but the diffuse component is collected by the ellipsoid and focused at the other principal focus of the ellipsoid. In principle a detector could be held at this focus, but in practice the magnification is so great that we use a second

0003-2700/78/0350-1906$01.00/0 © 1978 American Chemical Society

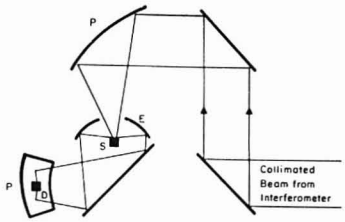


Figure 1. Optical diagram of the diffuse reflectometer. Radiation from the interferometer is focused on the sample, S, by the off-axis paraboloid, P, and the diffusely reflected radiation is collected by the ellipsoid, E, and then focused onto the detector, D. (Note that the detector is not coplanar with the other optics)

3.7-cm focal length, 90° off-axis paraboloid which focuses the beam to a diameter of approximately 2 mm.

Both a triglycine sulfate (TGS) and a mercury cadmium telluride (MCT) detector were used for the diffuse reflectance measurements. We favored the use of the MCT detector for most measurements since the time required to achieve an acceptable SNR (less than 0.1% noise) could be reduced below 5 min. The detector is a short range (λ_{max} = 12 μm), high sensitivity device (Texas Instruments, Dallas, Texas) and generally necessitated that the output beam from the interferometer had to be attenuated by a wire mesh screen to avoid digitization noise. If a state-of-the-art interferometer was used with a new TGS detector, we believe that a TGS detector could be used for all the measurements described in this paper.

Particle size classification was achieved using a Sonic Sifter (ATM Corp, Milwaukee, Wis.) with appropriately sized sieves, after grinding the samples manually or in a Wig-L-Bug (Crescent Dental Manufacturing Co., Chicago, Ill.). Powdered samples were transferred to a 4-mm diameter cup without compression, and were levelled using a spatula.

QUANTITATIVE MEASUREMENTS

A general theory for diffuse reflectance at scattering layers within powdered samples has been developed by Kubelka and Munk (*21*, *22*). This theory relates sample concentration and scattered radiation intensity much in the same manner as the Bouger–Beer law of transmittance spectrometry. For an "infinitely thick" layer, the Kubelka–Munk equation may be written as:

$$f(R_\infty) = \frac{(1 - R_\infty)^2}{2R_\infty} = \frac{k}{s} \qquad (2)$$

where R_∞ is the absolute reflectance of the layer, s is a scattering coefficient, and k is the molar absorption coefficient.

In practice a perfect diffuse reflection standard has not been found and R_∞ in Equation 2 may be replaced by R_∞', where

$$R_\infty' = \frac{R_\infty' \text{ (sample)}}{R_\infty' \text{ (standard)}} \qquad (3)$$

R_∞' (sample) represents the single-beam reflectance spectrum of the sample and R_∞' (standard) is the single-beam reflectance spectrum of a selected nonabsorbing standard exhibiting high diffuse reflectance throughout the wavelength regions being studied. We investigated the diffuse reflectance of powdered gold, germanium, and several alkali halides and found that finely ground KCl (Harshaw Chemical Company, Crystal and Electronic Products Dept., Solon, Ohio) has the fewest interferences and the highest overall reflectance. The reflectance of KCl was found to vary with particle size, as shown in Figure 2, with the highest reflectance at high wavenumber being found for the smallest average particle size. We selected KCl with a particle size less than 10 μm as the reflectance standard for this work. However it is interesting to note the small drop

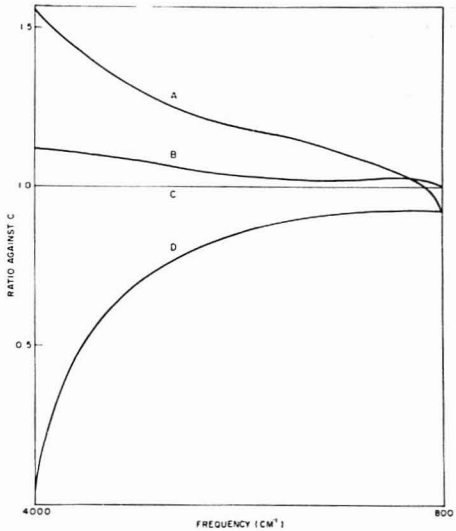


Figure 2. Reflectance spectra of powdered KCl for different particle sizes, $\bar{d}$, vs. reflectance of KCl sized between 75 and 90 μm. (A) $\bar{d}$ < 10 μm, (B) 10 < $\bar{d}$ < 75 μm, (C) 75 < $\bar{d}$ < 90 μm, and (D) $\bar{d}$ > 90 μm

in reflectance around 1000 cm^{-1}. This effect presumably occurs when the wavelength of the radiation is approximately equal to the diameter of the particles. For brevity we refer to all subsequent spectra as R_∞ or $f(R_\infty)$ in common with previous investigators, whereas strictly they should be referred to as R_∞' and $f(R_\infty')$, respectively.

The Kubelka–Munk theory predicts a linear relationship between the molar absorption coefficient, k, and the peak value of $f(R_\infty)$ for each band, provided s remains constant. Since s is dependent on particle size and range, these parameters should be made as consistent as possible if quantitative data are needed. It has been shown (*23*) that for dilute samples in low absorbing or nonabsorbing matrices:

$$k = 2.303\epsilon c \qquad (4)$$

where ϵ is the molar absorptivity and c is the molar concentration. Therefore:

$$f(R_\infty) = \frac{(1 - R_\infty)^2}{2R_\infty} = \frac{c}{k'} \qquad (5)$$

where $k' = s/2.303\epsilon$. Thus diffuse reflectance spectra of samples dispersed in finely powdered KBr or KCl might be expected to be quite similar to the absorbance spectra of the same samples prepared as a KBr disk. That this is the case is shown in Figures 3 and 4 for cholic acid and carbazole, respectively.

It is well known that the spectra of samples prepared as KBr disks can vary depending on the way in which the sample is prepared. Figure 3B was obtained from a disk made by adding about 5 mg of cholic acid of less than 10-μm particle size to about 300 mg of KBr and pressing the disk directly. The absorbance spectrum of this sample is almost identical to the Kubelka–Munk spectrum of neat cholic acid, and both spectra show band splittings due to the crystallinity of the sample. The spectrum shown in Figure 3C was obtained from about 1 mg of cholic acid which was *ground* with about 300

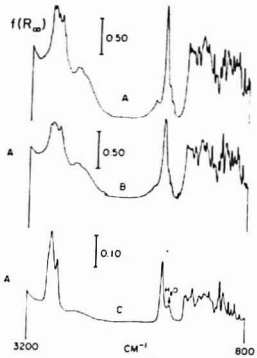


Figure 3. (A) Kubelka–Munk spectrum of neat cholic acid vs. a KCl reference. (B) Linear absorbance spectrum of a KBr disk of cholic acid prepared by adding 5 mg of cholic acid (particle size less than 10 μm) to 100 mg of KBr, and pressing the disk directly. (C) Linear absorbance spectrum of a KBr disk prepared by grinding 1 mg of cholic acid with 100 mg of KBr in a Wig-L-Bug, with subsequent pressing

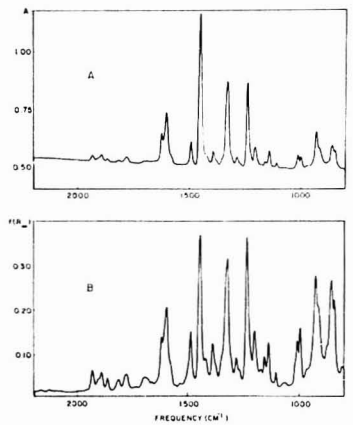


Figure 4. (A) Linear absorbance spectrum of a KBr disk of carbazole. (B) Kubelka–Munk diffuse reflectance spectrum of 5% carbazole in KCl vs. a KCl reference

mg of KBr, after which the disk was pressed. No band splittings are observed in this spectrum, and the relative intensities of the bands are somewhat different from those of the other two spectra.

The carbazole spectra shown in Figure 4 are more typical of results found for most organic compounds, and few, if any, crystal splittings are observed. Minor differences between the absorbance spectra of the KBr disks of most organics and their diffuse reflectance spectra may be attributed to the effect of particle size and deviations from the Kubelka–Munk equation, which is only expected to hold for moderately absorbing species at controlled particle size. A typical "Kubelka–Munk law" plot is shown in Figure 5, and deviations from linearity at high sample concentration are indeed observed. It is also noteworthy that Christiansen filter effects (*24*) are completely absent from diffuse reflectance spectra.

The effect of particle size on the diffuse reflectance spectra of pure compounds is illustrated in Figure 6. It can be seen that the bandwidths and relative intensities change con-

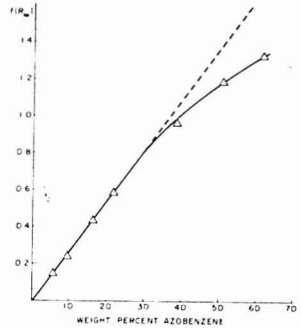


Figure 5. Variation of $f(R_\infty)$ with weight percent azobenzene in KCl for the 1960 cm^{-1} band of azobenzene

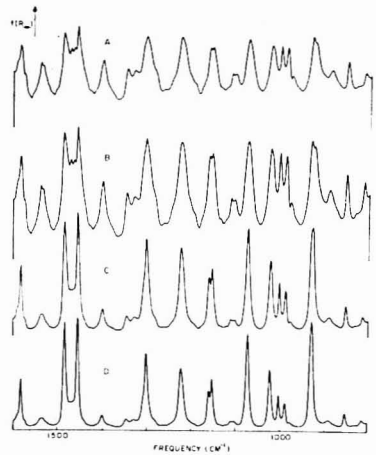


Figure 6. Effect of particle size on the diffuse reflectance spectrum, plotted as $f(R_\infty)$, of neat azobenzene vs. a KCl reference. (A) $\bar{d} >$ 90 μm, (B) 75 $< \bar{d} <$ 90 μm, (C) 10 $< \bar{d} <$ 75 μm, and (D) $\bar{d} <$ 10 μm

siderably with particle size. The bandwidths decrease substantially as the particle diameter is reduced. It is interesting to note that the intensity of certain bands appears to change more dramatically with particle size than others. This effect is particularly noticeable for the azobenzene bands at 1540 and 1405 cm^{-1} shown in Figure 6.

In view of the tremendous importance of scaled absorbance subtraction procedures in the study of mixtures by computerized infrared spectrophotometers (*25–27*), we were curious as to the feasibility of the analogous procedure, "Kubelka–Munk subtractions", for diffuse reflectance spectra. In general, we found that spectral subtraction is possible provided that $f(R_\infty)$ for both components is low, but that accurate subtraction over the complete spectrum for mixtures which were not diluted with KCl was not possible. In spite of this observation, we believe that diffuse reflectance difference measurements may be extremely important for detecting and quantitating small differences between powdered mixtures. As an example, the result of subtracting the $f(R_\infty)$ spectrum of a 2.9% mixture of magnesium stearate in lactose from a 5.1% mixture is shown in Figure 7. All the positive-going bands are due to magnesium stearate while the negative-going bands may be as-

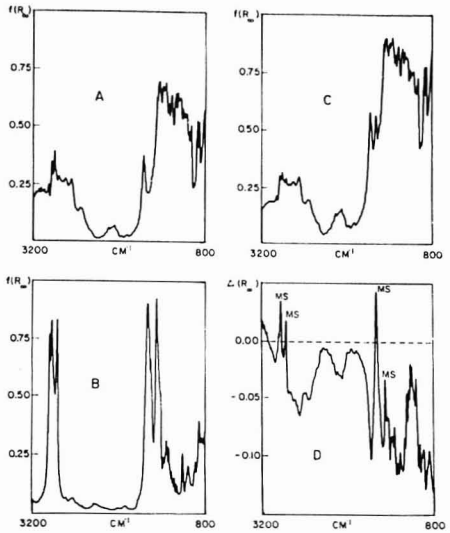


Figure 7. (A) Diffuse reflectance spectrum of pure lactose. (B) Diffuse reflectance spectrum of pure magnesium stearate. (C) Spectrum of 5.1% magnesium stearate and 94.9% lactose. (D) Difference spectrum of the $f(R_\infty)$ spectra of 5.1% magnesium stearate and 2.9% magnesium stearate in lactose. Positive-going bands due to magnesium stearate are marked MS

signed to lactose. These two materials happen to be commonly used excipients for pharmaceutical tablets, and we believe that diffuse reflectance difference spectrometry may prove to be a very useful technique for quality assurance and content uniformity determinations of pharmaceutical products, presumably after the careful construction of working curves. Further investigations into this area are now being performed in this laboratory and will be reported at a later date.

QUALITATIVE ANALYSIS

The first and most obvious application of qualitative analysis by DRIFT spectrometry is the rapid identification of powders without sample preparation. As mentioned above, not only is sample preparation time very short but the amount of sample required to produce a strong spectrum is also quite small; 100 μg of most samples is all that is required to give a strong spectrum, and bands from less than 200 ng of moderately absorbing compounds can usually be observed, as shown in Figure 8. For selected strong absorbers we have been able to observe bands from as little as 2 ng of sample dispersed in KCl. The depth of the KCl matrix required to yield samples of "infinite thickness", i.e., where further increasing the thickness causes no change in the spectrum, appears to be less than 5 mm. However, the difference in band intensity between samples of, for example, 2 mm and 5 mm depth is not very great. The depth of the samples whose spectra are shown in Figure 8 was approximately 0.5 mm, since the greatest contribution to $f(R_\infty)$ originates in the first few layers of sample. It is surprizing to find such low detection limits using a technique which has been so little used in the past because of its supposedly poor SNR.

The nature of the matrix affects detection limits for microsampling by DRIFT spectrometry, but strong bands of adsorbed compounds can be seen even for strongly absorbing matrices such as silica gel. This observation suggested the possibility of measuring the spectra of species separated by

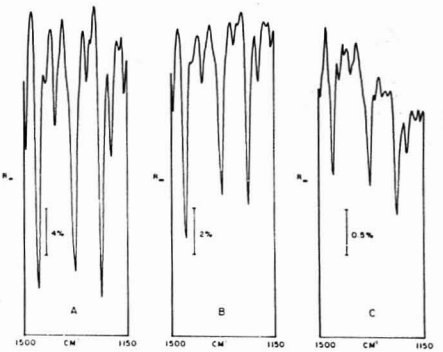


Figure 8. Microsampling by diffuse reflectance: spectra of (A) 12 μg, (B) 1.2 μg, and (C) 180 ng of carbazole dispersed in KCl vs. a KCl reference

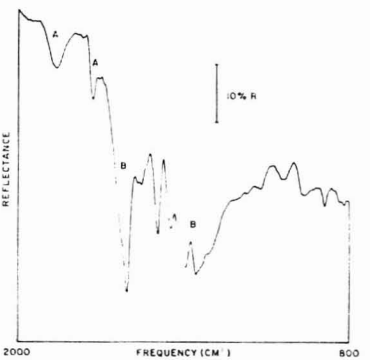


Figure 9. In situ spectrum of 1.2 μg of methylene blue on an aluminum-backed silica gel TLC plate. Bands marked A are due to the uncompensated adsorbent alone, bands marked B are due to both the adsorbent and sample, and all other bands are due to the sample

thin-layer chromatography (TLC-IR) without sample preparation. The most common method currently used for TLC-IR involves extracting the spots using a polar solvent, evaporating down the extract, and measuring the spectrum by microtransmittance or ATR techniques. An in situ method for TLC-IR has been suggested (*28–30*), but requires the preparation of the TLC plate on an infrared transmitting plate, such as silver chloride. We have measured TLC-IR spectra of samples separated on commercially available aluminum-foil-backed silica gel TLC plates after punching out the spots with a standard 6-mm diameter file punch and holding each spot at the sample focus of the DRIFT spectrometer. Although this system is by no means optimized for TLC-IR measurements and accurate compensation for the strong SiO_2 bands has not yet been achieved, the spectrum of 1.2 μg of methylene blue dye on a silica gel TLC plate shown in Figure 9 indicates the feasibility of TLC-IR by diffuse reflectance, even in the region of strong absorption bands of the adsorbent.

These results suggest that DRIFT measurements may be very useful for following reactions of adsorbed species on catalyst surfaces without having to follow the currently accepted practice of compressing the catalyst into a thin self-supporting disk. With such a system, the kinetics of

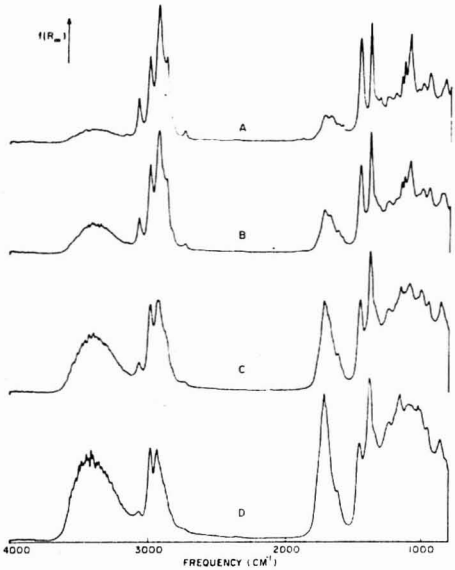


Figure 10. Diffuse reflectance spectra of a sample of powdered poly(dimethylfulvene) as a function of time; (A) 15 min, (B) 70 min, (C) 255 min, and (D) 1285 min after sample preparation

heterogeneous reactions may be more realistically studied than with more conventional techniques. The use of DRIFT spectrometry for studying the kinetics of reactions is illustrated in Figure 10 for a powdered sample of a rather unstable polymer, poly(dimethylfulvene). This compound reacts with air and, at least in the latter stages of the reaction, the oxidation rate appears to be diffusion controlled. Although the time interval between the spectra shown in Figure 10 is relatively long, useful spectra could readily be measured at intervals of approximately 1 min.

The number of potential applications for diffuse reflectance spectrometry appears to be enormous. We believe that this technique will provide analytical chemists and applied spectroscopists with an important tool for studying previously intractable samples.

LITERATURE CITED

(1) A. C. Hardy, "Handbook of Colorimetry", M.I.T. Press, Cambridge, Mass., 1936.
(2) D. B. Judd and G. Wyszecki, "Color in Business, Science and Industry", 2nd ed., John Wiley and Sons, New York, 1963.
(3) F. W. Billmeyer, Jr., and M. Saltzman, "Principles of Color Technology", John Wiley and Sons, New York, 1966.
(4) G. Kortum, "Reflectance Spectroscopy", Springer-Verlag, New York, 1969.
(5) R. W. Frei and J. D. MacNeil, "Diffuse Reflectance Spectroscopy in Environmental Problem-Solving", CRC Press, Cleveland, Ohio, 1973.
(6) F. A. Rodrigo, *Am. Heart J.*, **45**, 809 (1953).
(7) C. W. McKeehan and J. E. Christian, *Am. Heart J.*, **46**, 631 (1957).
(8) E. V. Ashburn and R. G. Waldon, *J. Pharm. Sci.*, **46**, 442 (1956).
(9) N. B. Guerrant, *J. Agric. Food. Chem.*, **5**, 207 (1957).
(10) D. W. Kent-Jones and W. Martin, *Analyst (London)*, **75**, 127 (1950).
(11) K. Yamaguchi, S. Fujii, T. Tobatata, and S. J. Kato, *J. Pharm. Soc. Jpn.*, **74**, 1322 (1954).
(12) W. W. Coblentz, *Natl. Bur. Stand. (U.S.). Bull*, **9**, 283 (1913).
(13) J. T. Gier, R. V. Dunkle, and J. T. Bevans, *J. Opt. Soc. Am.*, **44**, 558 (1954).
(14) J. V. White, *J. Opt. Soc. Am.*, **54**, 1332 (1964).
(15) B. E. Wood, J. G. Pipes, A. M. Smith, and J. A. Roux, *Appl. Opt.*, **15**, 940 (1976).
(16) G. Kortüm and H. Delfs, *Spectrochim. Acta*, **20**, 405 (1964).
(17) W. R. Blevin and W. J. Brown, *J. Sci. Instrum.*, **42**, 385 (1965).
(18) S. T. Dunn, J. C. Richmond, and J. A. Wiebelt, *J. Res. Natl. Bur. Stand., Sect. C*, **70**, 75 (1966).
(19) S. T. Dunn, "Flux Averaging Devices for the Infrared", *Natl. Bur. Stand. (U.S.) Tech. Note*, **No. 279** (1965).
(20) R. R. Willey, *Appl. Spectrosc.*, **30**, 593 (1976).
(21) P. Kubelka and F. Munk, *Z. Tech. Phys.*, **12**, 593 (1931).
(22) P. Kubelka, *J. Opt. Soc. Am.*, **38**, 448 (1948).
(23) P. Kortum, W. Braun, and G. Herzog, *Angew. Chem., Int. Ed. Engl.*, **2**, 333 (1963).
(24) G. Duyckaerts, *Analyst (London)*, **84**, 201 (1959).
(25) J. L. Koenig, *Appl. Spectrosc.*, **29**, 293 (1975).
(26) M. K. Antoon, J. H. Koenig, and J. L. Koenig, *Appl. Spectrosc.*, **31**, 518 (1977).
(27) R. W. Hannah, S. C. Pattacini, J. G. Grasselli, and S. E. Mocadlo, *Appl. Spectrosc.*, **32**, 69 (1978).
(28) C. J. Percival and P. R. Griffiths, *Anal. Chem.*, **47**, 154 (1975).
(29) M. M. Gomez-Taylor, D. Kuehl, and P. R. Griffiths, *Appl. Spectrosc.*, **30**, 447 (1976).
(30) M. M. Gomez-Taylor and P. R. Griffiths, *Appl. Spectrosc.*, **31**, 528 (1977).

RECEIVED for review May 22, 1978. Accepted August 24, 1978. Work supported by Merrell-National Laboratories, Division of Richardson-Merrell, Inc., Exxon Research and Engineering Corporation, and the Environmental Protection Agency.

Separation of Alkylphenols by Normal-Phase and Reversed-Phase High-Performance Liquid Chromatography

J. F. Schabron and R. J. Hurtubise*

Department of Chemistry, University of Wyoming, Laramie, Wyoming 82071

H. F. Silver

Mineral Engineering Department, University of Wyoming, Laramie, Wyoming 82071

Empirical correlation factors were developed which relate log k' values for alkylphenols, the naphthols, and two phenylphenols to structural features. Both normal-phase and reversed-phase chromatographic systems were studied. The stationary phases employed in the normal-phase work were μ-Bondapak CN, μ-Bondapak NH_2, and μ-Porasil. The structural features which affect retention in the normal-phase chromatographic systems are the number of ortho substituents, the number of aliphatic carbons, and the number of aromatic rings. The stationary phases employed in the reversed-phase work were μ-Bondapak C_{18} and μ-Bondapak CN. The structural features which affect retention in the reversed-phase chromatographic systems are the number of aliphatic carbons and the number of aromatic double bonds. On μ-Bondapak C_{18}, the presence or absence of a nonaromatic ring is of added importance.

The isolation of phenols is important in the study of coal liquefaction processes (*1*), in industrial and in environmental pollution work (*2*), and in other areas (*3–5*). The separation of phenols by high-performance liquid chromatography (HPLC) has been studied by a few workers. Kirkland (*6*) separated phenol and six alkylphenols on a polymeric ether bonded-phase packing. Karger et al. (*7*) separated phenol, 4-isopropylphenol, and 2,6-di-*tert*-butyl-4-methylphenol on surface etched glass beads coated with β,β'-oxydipropionitrile. The separation of phenols on reversed-phase HPLC systems has been reported by Karch et al. (*8*) and by Wolkoff and Larose (*9*). Husain et al. (*10*) explored the separation of 13 isomeric alkylphenols on microparticulate silica gel columns. They found the HPLC method to be superior to gas–liquid chromatography (GLC). Liquid–liquid chromatographic systems consisting of long-chain aliphatic amines on 4–7 μm solid supports with aqueous acid solution mobile phases for the separation of acidic compounds have been studied (*11*, *12*). Several variables affecting the separation process were explored. Callmer et al. (*13*) studied structural effects on the separation of 33 alkyl-substituted phenols on microparticulate nitrile and octadecylsilane bonded phases. They pointed out that one disadvantage of using GLC for the separation of alkylphenols was that the structural information in GLC chromatograms is not straightforward because of the simultaneous influence of vapor pressure and polar interactions. Structure–retention relationships were studied on both nitrile and octadecylsilane HPLC stationary phases (*13*). The separations on the nitrile phases were divided into three groups depending on the number of ortho substituents. For each group, log k' decreased linearly with increasing aliphatic carbon number. The log k' values on the octadecylsilane stationary phase increased linearly with aliphatic carbon number regardless of the position of substitution (*13*). Although Bark and Graham (*14–17*) had studied extensively structure–retention relationships of alkylphenols in both normal-phase and reversed-phase thin-layer chromatographic (TLC) systems, Callmer et al. (*13*) were the first to study the separation of phenols by HPLC in this manner.

In the present work, the retention behavior of phenol, several alkylphenols, the naphthols, and two phenylphenols was studied in three normal-phase and two reversed-phase HPLC systems. The stationary phases employed in the normal-phase work were μ-Bondapak CN, μ-Bondapak NH_2, and μ-Porasil. The stationary phases employed in the reversed-phase work were μ-Bondapak C_{18} and μ-Bondapak CN. Empirical correlation factors were developed which relate log k' values to structural features of the phenols studied in both the normal-phase and reversed-phase systems.

EXPERIMENTAL

High-Performance Liquid Chromatograph. The liquid chromatograph used was a Waters model ALC/GPC 244 equipped with a model 6000-A pump, a U6K injector, a free standing ultraviolet detector set at 254 nm, and a 10-mV strip chart recorder.

Columns. The columns used were all 3.9 mm i.d. × 30 cm columns prepacked and obtained from Waters Associates, Milford, Mass. The columns were μ-Porasil packed with 10-μm porous silica, μ-Bondapak C_{18}, μ-Bondapak CN, and μ-Bondapak NH_2. The last three columns consisted of octadecyl groups, propylnitrile groups, and propylamine groups, respectively, chemically bonded to Waters μ-Porasil (*18*).

Reagents. HPLC grade methanol and HPLC grade *n*-heptane were obtained from Fisher Scientific, St. Louis, Mo. These solvents were prefiltered through 0.2-μm filters. Distilled water was filtered through a Millipore type G-S 0.22-μm filter. Chloroform was J. T. Baker AR grade and for the HPLC work was filtered through a Millipore type F-H 0.5-μm filter. Isopropyl alcohol was Mallinckrodt spectro grade and was not filtered. Ethanol was reagent grade absolute ethanol from U.S. Industrial Chemicals, New York, N.Y. The phenol standards were obtained from commercially available sources and were purified when necessary.

Chromatographic Systems Studied.

1. Normal-phase, μ-Bondapak CN with a *n*-heptane mobile phase at 2 mL/min.
2. Normal-phase, μ-Bondapak NH_2 with a *n*-heptane:isopropyl alcohol (99:1) mobile phase at 2 mL/min.
3. Normal-phase, μ-Porasil with a *n*-heptane:chloroform (90:10) mobile phase at 2 mL/min.
4. Reversed-phase, μ-Bondapak C_{18} with a methanol:water (65:35) mobile phase at 1 mL/min.
5. Reversed-phase, μ-Bondapak CN with a methanol:water (50:50) mobile phase at 1 mL/min.

Phenol Standards. Solutions of 3–12 mg/mL of the phenol standards were prepared in both ethanol and chloroform. The retention volumes of the phenol standards were determined by injecting 2–4 μL of the standard solutions onto the chromatographic systems listed above. Two sets of solutions were used, one set with chloroform and the other set with ethanol. Two sets were used because it was found that distorted or split peaks resulted if some standards were injected onto system 4 in chloroform solution, or onto systems 1 and 3 in ethanol solution. For example, 2,6-dimethylphenol gave a split peak when injected onto system 4 in a chloroform solution, but a single peak when injected in an ethanol solution. Split peaks were observed for

0003-2700/78/0350-1911$01.00/0 © 1978 American Chemical Society

Table I. Log k' Values for the Standards Chromatographed

compound	1	2	3	4	5
non-ortho substituted	(μ-CN)	(μ-NH_2)	(μ-Porasil)	(μ-C_{18})	(μ-CN)
phenol	1.10	1.07	1.23	−0.74	−0.56
m-cresol	1.02	0.99	1.19	−0.40	−0.37
p-cresol	1.02	0.98	1.20	−0.40	−0.37
3,4-dimethylphenol	0.98	0.94	1.19	−0.20	−0.22
3,5-dimethylphenol	0.94	0.91	1.17	−0.16	−0.22
3-ethylphenol	1.01	0.94	1.17	−0.16	−0.22
4-ethylphenol	1.01	0.97	1.20	−0.14	−0.22
3-isopropylphenol	0.96	0.91	1.15	0.050	−0.087
4-isopropylphenol	1.00	0.95	1.19	0.073	−0.12
4-*n*-pentylphenol	0.98	0.92	1.18	0.59	- - -
3,5-diisopropylphenol	0.87	0.73	1.08	0.57	0.22
3,5-di-*tert*-butylphenol	0.82	0.65	1.04	0.83	0.38
5-indanol	0.98	0.93	1.20	−0.056	−0.14
5,6,7,8-tetrahydro-2-naphthol	0.98	0.93	1.19	0.13	0.050
2-naphthol	1.35	1.27	1.31	−0.14	0.061
4-phenylphenol	1.37	1.25	1.34	0.15	0.22
mono-ortho substituted					
o-cresol	0.81	0.80	0.92	−0.37	−0.31
2,3-dimethylphenol	0.78	0.73	0.86	−0.16	−0.20
2,4-dimethylphenol	0.73	0.70	0.87	−0.12	−0.20
2,5-dimethylphenol	0.71	0.68	0.85	−0.10	−0.20
2,3,5-trimethylphenol	0.68	0.62	0.81	0.084	−0.056
2-ethylphenol	0.79	0.72	0.81	−0.10	−0.16
2-isopropylphenol	0.75	0.68	0.75	0.094	−0.056
2,4-di-*tert*-butylphenol	0.59	0.40	0.38	0.99	0.54
2,5-di-*tert*-butylphenol	0.49	0.16	0.13	1.02	0.62
5,6,7,8-tetrahydro-1-naphthol	0.75	0.72	0.85	0.16	0.084
1-naphthol	1.26	1.11	1.07	−0.056	0.14
2-phenylphenol	0.43	0.72	0.39	0.15	0.17
di-ortho substituted					
2,6-dimethylphenol	0.24	0.23	0.37	−0.16	−0.20
2,3,6-trimethylphenol	0.22	0.15	0.31	0.061	−0.056
2,4,6-trimethylphenol	0.19	0.17	0.41	0.11	−0.087
2,3,5,6-tetramethylphenol	0.14	0.050	0.27	0.21	0.038
2,6-di-*sec*-butylphenol	−0.26	−0.56	−0.44	0.93	0.49
2,6-di-*tert*-butylphenol	N[a]	N	N	1.08	0.57
2,6-di-*tert*-butyl-4-methylphenol	N	N	N	1.25	0.66

[a] N = not retained.

3,5-diisopropylphenol, 3,5-di-*tert*-butylphenol, and 2,4- and 2,5-di-*tert*-butylphenol when they were injected onto system 1 in ethanol solutions, but single peaks were observed when they were injected in chloroform solutions. Peak splitting was observed for phenol when it was injected onto system 3 in ethanol solution, but a single peak was observed when it was injected in chloroform solution. This was not studied further, but similar peak splitting phenomena were observed by Tseng and Rogers (*19*) and Snyder (*20*). The chloroform solutions were used for injection onto the normal-phase systems, and the ethanol solutions were used for injection onto the reversed-phase systems. The capacity factor, k', was calculated by $k' = (V_R - V_m)/V_m$, where V_R (mL) is the measured retention volume and V_m (mL) is the column void volume. The value of V_m was determined to be 3.3 mL for the systems studied and was obtained by eluting methanol in the reversed-phase systems and toluene in the normal-phase systems. The method of least squares was employed for the lines in Figures 1–3.

RESULTS AND DISCUSSION

Normal-Phase Retention. The log k' values for the standards chromatographed in systems 1–3 were determined and are listed in Table I. The log k' values for the phenol standards chromatographed by Callmer et al. (*13*) on Cyano Sil-X-I with a *n*-heptane:isopropyl alcohol (99.5:0.5) mobile phase were considered also. This chromatographic system is labeled system 6. An attempt was made to correlate empirically the log k' values from these chromatographic systems with the structural features of the standards chromatographed.

Most of the standards chromatographed were alkylphenols. The naphthols and 2- and 4-phenylphenol were also studied. For each chromatographic system, the structural effects on log k' were assumed to be additive. Initially, each aliphatic carbon, regardless of type, was assigned arbitrarily a value of 1, and a plot of log k' vs. aliphatic carbon number (C_n) was made. The log k' vs. C_n plot for the alkylphenols chromatographed on the μ-Bondapak CN column (chromatographic system 1) is presented in Figure 1. The points grouped around three lines, as in chromatographic systems 2 and 3, depending on the number of alkyl ortho substituents. This type of behavior was also observed by Callmer et al. (*13*). By observing the relative positions of the three lines in Figure 1, it appeared possible to merge the lines into one continuous line by making several assumptions. The presence of one substituent ortho to the hydroxyl group was assumed to exhibit a constant additive effect on retention, and the presence of a second ortho substituent was assumed to exhibit a constant additive effect on retention. The magnitude of these effects was not necessarily the same. Also, these constant effects were considered to be independent of the size of the group or groups ortho to the hydroxyl group. To merge line 2 into line 1, a value of 8 aliphatic carbons was added to C_n for each point in line 2 as shown in Figure 1. The new "C_n" value for *o*-cresol, for example, with a log k' value of 0.81 is 9, which puts the point for *o*-cresol near the point for 3,5-di-*tert*-butylphenol, with a log k' value of 0.82 and a C_n value

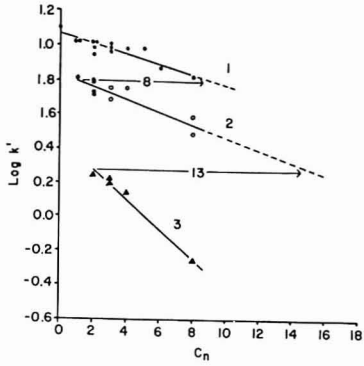


Figure 1. Log k' vs. C_n for the alkylphenol standards in chromatographic system 1. Non ortho-substituted (●), mono-ortho substituted (O), di-ortho substituted (▲)

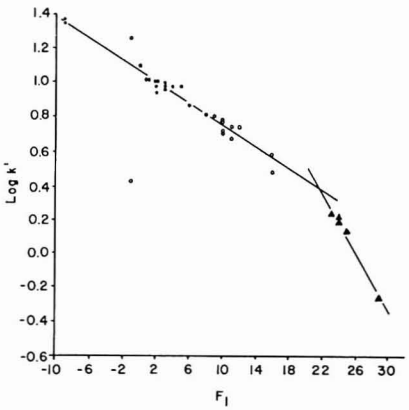


Figure 2. Log k' vs. F_1 for the standards in chromatographic system 1. Non-ortho substituted (●), mono-ortho substituted (O), di-ortho substituted (▲)

of 8. Line 3 was shifted to the right in a similar manner by adding 8 + 13 or 21, to the value of C_n for each point in line 3 (Figure 1). The merged lines for chromatographic system 1 are shown in Figure 2. The lines for the other normal-phase chromatographic systems were merged in a similar manner. It was also assumed that the presence of a second aromatic ring exhibits a constant increase in retention for a given chromatographic system. For example, with chromatographic systems 1–3, 2-naphthol and 2-phenylphenol have similar log k' values which are larger than the log k' value for phenol (Table I). With the assumptions above, the data in Table I and Reference 13, and the results from Figure 1, an empirical correlation factor, F_i, for the compounds in chromatographic systems 1–3 and 6 was developed and is defined by Equation 1. This equation was obtained by making the several assumptions discussed previously and presently we have no strong theoretical justification for it.

$$F_i = A_i + B_i + n \cdot C_i - D_i \quad (1)$$

where F_i = correlation factor for chromatographic system i, A_i = effect of one ortho substituent on log k', B_i = effect of a second ortho substituent on log k', n = the number of aliphatic carbons, C_i = 1 for each aliphatic carbon, and D_i = effect of a second aromatic ring.

Table II. Values of the Constants in Equation 1

system	A_i	B_i	C_i	D_i
1	8.0	13	1.0	9.0
2	5.0	6.0	1.0	3.0
3	12	4.0	1.0	3.0
6	5.0	4.0	1.0	–

With the correlation factor in this form, F_i for phenol is zero for all the chromatographic systems. The values of A_i, B_i, C_i, and D_i for chromatographic systems 1, 2, 3, and 6 are listed in Table II. The values of the terms A_i and B_i were determined graphically as described above for chromatographic system 1 (Figure 1). The value of the term C_i is 1 for each aliphatic carbon for all the chromatographic systems. The values of the D_i terms for chromatographic systems 1–3 were obtained by using the log k' values of 2-naphthol and 4-phenylphenol and reading the values of F_i from the X-axis of the correlation graphs (Figure 2). For these compounds, A_i, B_i, and n are all zero, so $F_i = -D_i$. The calculated values of F_1, F_2, and F_3 for the standards are listed in Table III. The log k' vs. F_i plot for chromatographic system 1 is presented in Figure 2 and is typical of the chromatographic systems investigated. It was apparent that for each chromatographic system instead of one correlation line, two lines appeared. For chromatographic systems 1 and 2, the two lines intersected near the data points corresponding to 2,6-dimethylphenol and 2,4-di-*tert*-butylphenol, respectively. The points of intersection of the correlation lines for chromatographic systems 3 and 6 occurred near the data points for 2,3,5-trimethylphenol and 2,5-dimethylphenol, respectively. It is at these points of intersection that the assumptions of the presence of one or two ortho substituents results in an additive effect, and that this effect is independent of the size of the ortho group or groups, appear to break down. For example, in chromatographic system 1, the slope of line 2 in Figure 1 is about the same as the slope of line 1, and thus the points for lines 1 and 2 can be combined to give a single line (Figure 2). The slope of line 3 in Figure 1 is steeper and line 3 cannot be merged with the line resulting from combining lines 1 and 2 (Figure 2). Beyond the point at which the slope changes with increasing values of F_i, the presence of one or two ortho groups and the size of the ortho groups cause a decrease in retention greater than that predicted by the merged lines 1 and 2 (Figure 2). For the μ-Bondapak CN stationary phase (chromatographic system 1), the slope of the correlation line does not change for non-ortho and mono-ortho substituted phenols (Figure 2). For the μ-Bondapak NH_2 stationary phase (chromatographic system 2), the slope of the correlation line did not change for non-ortho and mono-ortho substituted phenols with the exception of the data point for 2,5-di-*tert*-butylphenol. For the μ-Porasil and Cyano Sil-X-I (*13*) stationary phases, (chromatographic systems 3 and 6), the correlation lines had unchanging slopes only for non-ortho substituted phenols, and mono-ortho substituted phenols with $C_n < 3$. In the calculation of F_1, F_2, and F_3 for 1-naphthol, the term for an additional aromatic ring, D_i, and the term for a single ortho substituent, A_i, were included (Table III). The term A_i was included since one point of ring fusion is ortho to the hydroxyl group. Both A_i and D_i were also included in the calculation of F_1, F_2, and F_3 for 2-phenylphenol (Table III). The points for 1-naphthol lay near the correlation lines for chromatographic systems 2 and 3, and above the correlation line for chromatographic system 1 (Figure 2). The points for 2-phenylphenol, however, lay significantly below the lines in each case. This is probably due to the nonplanar configuration of the two rings of 2-phenylphenol, preventing interaction of both rings and the hydroxyl group with the

Table III. Values of F_i for the Standards Chromatographed

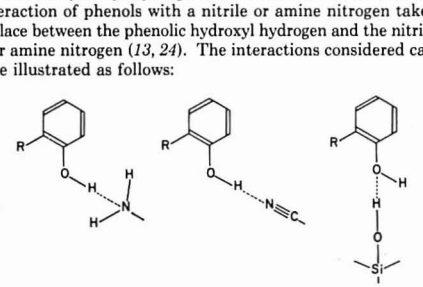
compound	F_1	F_2	F_3	F_4	F_5
non-ortho substituted					
phenol	0.0	0.0	0.0	3.0	6.0
m-cresol	1.0	1.0	1.0	4.0	7.0
p-cresol	1.0	1.0	1.0	4.0	7.0
3,4-dimethylphenol	2.0	2.0	2.0	5.0	8.0
3,5-dimethylphenol	2.0	2.0	2.0	5.0	8.0
3-ethylphenol	2.0	2.0	2.0	5.0	8.0
4-ethylphenol	2.0	2.0	2.0	5.0	8.0
3-isopropylphenol	3.0	3.0	3.0	6.0	9.0
4-isopropylphenol	3.0	3.0	3.0	6.0	9.0
4-*n*-pentylphenol	5.0	5.0	5.0	8.0	11.0
3,5-diisopropylphenol	6.0	6.0	6.0	9.0	12.0
3,5-di-*tert*-butylphenol	8.0	8.0	8.0	11.0	14.0
5-indanol	3.0	3.0	3.0	5.5	9.0
5,6,7,8-tetrahydro-2-naphthol	4.0	4.0	4.0	6.5	10.0
2-naphthol	−9.0	−3.0	−3.0	5.0	10.0
4-phenylphenol	−9.0	−3.0	−3.0	6.0	12.0
mono-ortho substituted					
o-cresol	9.0	6.0	13	4.0	7.0
2,3-dimethylphenol	10	7.0	14	5.0	8.0
2,4-dimethylphenol	10	7.0	14	5.0	8.0
2,5-dimethylphenol	10	7.0	14	5.0	8.0
2,3,5-trimethylphenol	11	8.0	15	6.0	9.0
2-ethylphenol	10	7.0	14	5.0	8.0
2-isopropylphenol	11	8.0	15	6.0	9.0
2,4-di-*tert*-butylphenol	16	13	20	11.0	14.0
2,5-di-*tert*-butylphenol	16	13	20	11.0	14.0
5,6,7,8-tetrahydro-1-naphthol	12	9.0	16	6.5	10.0
1-naphthol	−1.0	2.0	9.0	5.0	10.0
2-phenylphenol	−1.0	2.0	9.0	6.0	12.0
di-ortho substituted					
2,6-dimethylphenol	23	13	18	5.0	8.0
2,3,6-trimethylphenol	24	14	19	6.0	9.0
2,4,6-trimethylphenol	24	14	19	6.0	9.0
2,3,5,6-tetramethylphenol	25	15	20	7.0	10.0
2,6-di-*sec*-butylphenol	29	19	24	11.0	14.0
2,6-di-*tert*-butylphenol	29	19	24	11.0	14.0
2,6-di-*tert*-butyl-4-methylphenol	30	20	25	12.0	15.0

Table IV. Values of the Terms in Table II Divided by A_i Values (see text)

system	A_i'	B_i'	C_i'	D_i'
1	1.0	1.6	0.12	1.1
2	1.0	1.2	0.20	0.60
3	1.0	0.33	0.08	0.25
6	1.0	0.80	0.20	--

stationary phase at the same time.

To compare the effects of a second ortho substituent relative to a single ortho substituent, the terms used in calculating the correlation factors in Equation 1 (Table II) were recalculated relative to the effect of one ortho substituent (Table IV). The values of the new terms, A_i', B_i', C_i' and D_i', were calculated from the data in Table II by dividing the values of the terms for a given chromatographic system by the value of A_i for that system. For example, the values of B_i' are 1.6 for μ-Bondapak CN (chromatographic system 1) and 1.2 for μ-Bondapak NH_2 (chromatographic system 2). The values of B_i' for μ-Porasil (chromatographic system 3) and Cyano-Sil-X-I (chromatographic system 6) are 0.33 and 0.80, respectively. The effects of a second ortho substituent relative to the effects of a single ortho substituent, which are indicated by the values of B_i', are similar in magnitude for chromatographic systems 1 and 2. The effects of a second ortho substituent are smaller for chromatographic systems 3 and 6. Values of B_i' greater than 1 imply that the effect of two ortho groups on decreasing retention is greater than the effect of one ortho group. Values of B_i' less than 1 imply that the effect of a single ortho group on decreasing retention is greater than the effect of a second ortho group. The observed results for chromatographic systems 1–3 can be explained in terms of the nature of the stationary phases and the type of hydrogen bonding taking place between the stationary phase and the phenolic hydroxyl group of a sample molecule. The hydrogen bonding interactions occurring between the phenolic hydroxyl group and the silica silanol group was discussed by Callmer et al. (*13*) and Snyder (*20*). The major interaction takes place between the silanol hydrogen and the phenolic oxygen. In general, the strength of a hydrogen bond increases with the acidity of the donor hydrogen and the basicity of the acceptor (*21*). The dissociation constants of silanol hydrogens are about 10^{-6} to 10^{-8} (*22*), and the dissociation constants of most phenolic hydroxyl hydrogens are about 10^{-10} (*23*). The interaction of phenols with a nitrile or amine nitrogen takes place between the phenolic hydroxyl hydrogen and the nitrile or amine nitrogen (*13, 24*). The interactions considered can be illustrated as follows:



From the above illustration and the work of Callmer et al. (*13*), it is apparent by geometric considerations that the hydrogen bond with the silanol hydrogen is subject to greater disruption by a single bulky ortho group R than the hydrogen bond between a phenolic hydroxyl hydrogen and a nitrile or amine nitrogen. The latter type of hydrogen bond is subject to greater disruption by two ortho groups than one. The values of 1.6 and 1.2 for B_1' and B_2', respectively, support the previous conclusion for the μ-Bondapak CN and μ-Bondapak NH_2 chromatographic systems. The value of 0.33 for B_3' for the μ-Porasil chromatographic system supports the conclusion that a single ortho group causes more disruption of hydrogen bond with a silanol hydrogen than does the presence of a second ortho group. The hydrogen bonding considerations predict that B_6' should be greater than 1 for the Cyano Sil-X-I chromatographic system. The value of 0.80 for B_6', however, suggests that a single ortho group has a greater effect on decreasing retention than do two ortho groups. This apparently violates the above hydrogen bonding concepts. What can be considered, however, is the extent to which the presence of residual silanol groups affects the retention of the phenols chromatographed with chromatographic system 6 (*13*). The residual silanol groups on μ-Bondapak CN and μ-Bondapak NH_2 in the normal phase modes have been shown not to be readily accessible (*18*). A contribution to the adsorption of phenols on Cyano Sil-X-I in the normal phase mode (chromatographic system 6) was, however, noted by Callmer et al. (*13*). The value of 0.80 for B_6' supports the conclusion that surface silanol groups contribute substantially to the chromatographic behavior of phenols in chromatographic system 6.

The different values of C_i' and D_i' listed in Table IV illustrate differences in selectivity between the various chromatographic systems for aliphatic carbon substituents and a second aromatic ring, respectively. An explanation for these differences in selectivity is not presented here as they are due probably to various polar and nonpolar interactions between the stationary phase, the sample molecule, and the mobile phase. The mobile phases employed for the systems studied were not identical, and a study into the effects of different mobile phases on the values of the terms in Tables II and IV was not undertaken. The values of C_i' of 0.12, 0.20, and 0.08 for chromatographic systems 1–3, respectively, are not identical, and thus show some small differences in selectivity toward the presence of alkyl substituents. The values of D_i' of 1.1, 0.60, and 0.25 for chromatographic systems 1–3, respectively, show that a phenolic compound with more than one aromatic ring will be retained relatively longer in chromatographic system 1 than in chromatographic systems 2 and 3, and longer in chromatographic system 2 than in chromatographic system 3.

The correlation factors, F_i, can be used to predict the approximate retention volumes of known standards or sought-after compounds. Use of the correlation factor would provide an important tool in the separation of phenols in complex samples. Speculation as to the types of structural features of the phenolic compounds present in chromatographic peaks could be made. The values of the terms such as those listed in Tables II and IV can be used in studying a particular normal-phase system for the presence of a significant amount of residual silanol groups and relative selectivities between systems toward aliphatic carbon substituents and additional aromatic rings. By using the correlation factor, more insight into the mechanism of retention in a given system can be obtained, and the optimum system for a given application can be chosen. In the development and application of the correlation factors, the effects of the mobile phase were not considered. Additional work in this area is required to gain more insight into the mechanism of retention of phenols in these and similar chromatographic systems.

Reversed-Phase Retention. The log k' values for the standards in chromatographic systems 4 and 5 were determined and are listed in Table I. Empirical correlation factors relating log k' to structural features of the phenol standards were developed for these chromatographic systems. The structural features which were found to affect retention significantly in chromatographic systems 4 and 5 were the number of aliphatic carbons and the number of aromatic double bonds. There were no nonaromatic double bonds present in the standards studied, so these were not considered. The presence of a nonaromatic ring was found to affect retention in chromatographic system 4 but not in chromatographic system 5. A log k' vs C_n plot was made by Callmer et al. (*13*) for alkylphenols chromatographed on a μ-Bondapak C_{18} column with an ethanol:water (60:40) mobile phase. A linear relationship resulted. By including a term for the presence of aromatic double bonds in the correlation factors developed by us for chromatographic systems 4 and 5, such a plot can be extended to include larger phenolic compounds such as the naphthols and hydroxylated polycyclic ring systems. The position of alkyl substitution does not affect significantly the retention of alkylphenols chromatographed on reversed-phase chromatographic systems (*13*). Correlation factors for such chromatographic systems therefore require no terms to account for ortho substitution.

For chromatographic system 4, an aromatic double bond was found to be equivalent to one aliphatic carbon in affecting the retention of phenols. For example, the log k' values for 2-naphthol and 3,5-dimethylphenol in chromatographic system 4 are −0.14 and −0.16, respectively (Table I). There are 5 aromatic double bonds in 2-naphthol, and 3 aromatic double bonds plus 2 aliphatic carbons in 3,5-dimethylphenol. A tertiary aliphatic carbon was found to affect retention in a manner similar to a primary aliphatic carbon. For example, the log k' values of 0.094 and 0.084 for 2-isopropylphenol and 2,3,5-trimethylphenol, respectively (Table I), are very similar. The log k' value of −0.10 for 2,5-dimethylphenol (Table I) is not similar to the log k' value of 0.084 for 2-isopropylphenol. There are three primary aliphatic carbons in 2,3,5-trimethylphenol, two primary and one tertiary aliphatic carbons in 2-isopropylphenol, and just two primary aliphatic carbons in 2,5-dimethylphenol. This effect on retention by tertiary aliphatic carbons was a somewhat surprising observation, since tertiary aliphatic carbons present in alkyl substituents on aromatic hydrocarbons were found to have no affect on retention in the same chromatographic system (*25*). The correlation factor F_4 is defined as: F_4 = the number of aromatic double bonds + the number of aliphatic carbons − 0.5 for a nonaromatic ring. The calculated values of F_4 for the phenols chromatographed are listed in Table III. A plot of log k' vs. F_4 is presented in Figure 3. The correction of −0.5 for a nonaromatic ring was necessary because the presence of a nonaromatic ring resulted in less retention than would be predicted by a plot of log k' vs. a correlation factor which did not include the correction of −0.5. Such a correction was also applied by us to a correlation factor developed for aromatic and hydroaromatic hydrocarbons in the same chromatographic system (*25*). From examination of Figure 3, it is apparent that the correlation factor is applicable for the phenol standards in this chromatographic system. 2,6-Di-*tert*-butyl-4-methylphenol has a value of 12 for F_4 if the two quaternary aliphatic carbons are included in the calculation of F_4 (Table III). The point for this compound lies near the correlation line. Thus, both tertiary and quaternary aliphatic carbons must be included in the calculation of the

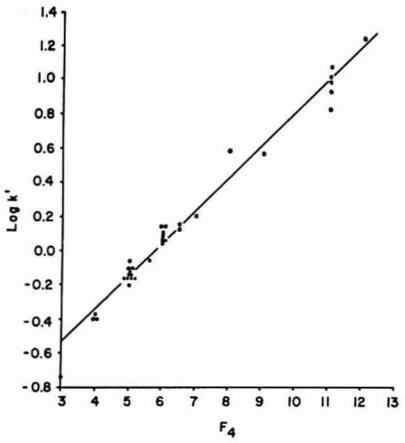


Figure 3. Log k' vs. F_4 for the standards in chromatographic system 4

correlation factor for alkylphenols in this chromatographic system.

A log k' vs. % water plot was made for some of the standards chromatographed on μ-Bondapak C_{18} with methanol:water mobile phase mixtures of 80:20, 65:35, and 50:50. The results showed that as the amount of water in the mobile phase is increased from 20% to 50%, the log k' values of each standard increases in an approximately linear fashion. Such a plot is typical of reversed-phase systems (8). The differences between log k' values of the standards remained approximately constant for the different mobile phase compositions. A correlation graph as in Figure 3 obtained with a methanol:water (65:35) mobile phase could be applied to a methanol:water (50:50) mobile phase by adding a constant value to all the log k' values for the methanol:water (65:35) mobile phase. For example, the log k' for 2-isopropylphenol in methanol:water (50:50) is 0.66. The log k' for 2-isopropylphenol in methanol:water (65:35) is 0.094. The difference is 0.57. If this constant is added to the log k' of -0.40 for *m*-cresol in methanol:water (65:35), the resultant value of 0.17 is near the observed value of 0.15 in methanol:water (50:50). Thus, the entire correlation curve (Figure 3) shifts upward by a value of approximately 0.57 on the log k' axis.

For chromatographic system 5, the effect of an aromatic double bond on increasing retention was found to be equivalent to the effect of two aliphatic carbons. For example, the log k' values of 2-naphthol and 2,3,5,6-tetramethylphenol in chromatographic system 5 are 0.061 and 0.038, respectively (Table I), indicating the retention of these compounds is similar. There are five aromatic double bonds in 2-naphthol, and three aromatic double bonds and four aliphatic carbons in 2,3,5,6-tetramethylphenol. The correlation factor F_5 is defined as: $F_5 = 2 \times$ the number of aromatic double bonds + the number of aliphatic carbons. A correction of -0.5 for a nonaromatic ring is not required in the calculation of F_5. For example, the log k' values for 2,3,5,6-tetramethylphenol and 5,6,7,8-tetrahydro-2-naphthol are 0.038 and 0.050, respectively, showing the retention of these compounds is similar. The values of F_5 for the standards are listed in Table III. A plot of log k' vs. F_5 showed that the correlation factor is applicable for the phenol standards in this chromatographic system. A log k' vs. % water plot was made for some of the standards chromatographed on μ-Bondapak CN with methanol:water mobile phase mixtures of 50:50, 30:70, and 10:90. The results showed an approximate linear increase in log k' with % water similar to that observed on μ-Bondapak C_{18}. Tailing peaks were observed for the standards chromatographed on μ-Bondapak CN with methanol:water (30:70) and (10:90) with log k' values greater than about 0.5. No tailing peaks were observed for any of the standards chromatographed with a methanol:water (50:50) mobile phase. Except for the differences in selectivity for aromatic double bonds observed between chromatographic systems 4 and 5, it appears that chromatographic system 5 is generally not as useful as chromatographic system 4 for the separation of phenols. The greater effect of an aromatic double bond on increasing the retention of phenols on μ-Bondapak CN could possibly be studied with other types of compounds such as polycyclic aromatic hydrocarbons. Compounds differing in the number of aromatic double bonds which are not completely separated on μ-Bondapak C_{18} might be separated readily on μ-Bondapak CN.

The greater effect of an aromatic double bond on retention in chromatographic system 5 could be caused by polar interactions between the propylnitrile groups of the μ-Bondapak CN stationary phase and the phenols. Such polar interactions are not possible between the octadecyl groups of the μ-Bondapak C_{18} stationary phase and the phenols. The polar interactions, or perhaps the limited solubility of the phenol standards in the water-rich mobile phases which were used with the μ-Bondapak CN column, may be responsible for the observed tailing. Scott and Kucera (26) have studied the wetting limits of several reversed-phase stationary phases as a function of the amount of water in mixed mobile phases. If the water in the mobile phase exceeds the wetting limit of the stationary phase, column efficiency is severely reduced (26). Further studies on these effects on μ-Bondapak CN and μ-Bondapak C_{18} were not undertaken. Other solvent mixtures with water, such as tetrahydrofuran, acetonitrile, or ethanol were not studied. If such mobile phases are to be used, the validity of the correlation factors must be substantiated.

Since V_R values may vary slightly on two similar columns obtained from the same manufacturer or on the same column over a period of time, the correlation lines should be established for each column used and checked occasionally by injecting phenol standards. The effects of structural features on the relative retention of isomeric phenols with identical correlation factor values for a given normal-phase or reversed-phase chromatographic system were not considered in the present work. As with the normal-phase correlation factors, the reversed-phase correlation factors can be useful in predicting the approximate retention volumes of known standards or sought-after compounds, and predicting several possible structures for an unknown. For example, the log k' value of 3-isopropylphenol in chromatographic system 4 is predicted to be 0.05 from Figure 3 and a calculated F_4 value of 6.0. The actual value of log k' is in fact 0.05 (Table I).

A General Separation Scheme. The correlation factors developed for both the normal-phase and reversed-phase chromatographic systems can be useful in devising a general separation scheme for complex mixtures of phenols. The normal-phase separations on μ-Bondapak CN, μ-Bondapak NH_2, and μ-Porasil occur mainly by the number of ortho substituents, as discussed previously. The R_f values reported by Dietz et al. (27) for several alkylphenols on silica gel TLC plates eluted with benzene show a similar effect. By analogy, these results indicate that the separation of phenols from complex samples such as coal liquids on silica gel open columns should provide two or more phenol-rich fractions separated from complex samples according to the number of ortho substituents. This is presently under investigation. Once

these fractions are obtained, they could be separated further by normal-phase chromatography on μ-Bondapak-CN (chromatographic system 1) or μ-Bondapak-NH_2 (chromatographic system 2). At this stage, phenolic compounds with more than one aromatic ring could be separated from phenol and alkylphenols. Fractions could then be collected, and injected onto a reversed-phase column such as μ-Bondapak C_{18} (chromatographic system 4). The separation on chromatographic system 4 is mainly by aliphatic carbon number, assuming the same number of aromatic double bonds for the compounds to be separated. By using the correlation factors in these latter two separation steps and information as to the number of ortho substituents obtained from the first separation step, several possible structures can be assigned to an isolated phenolic compound. By combining chromatographic systems, at least a partial separation of several isomeric phenols with the same number of ortho substituents and aliphatic carbon number should be possible. The concepts developed in this work are presently being used for the separation of phenols from coal liquefaction solvents.

LITERATURE CITED

(1) Mobil, R. & D Corp., EPRI Project RP 410-1 (1976).
(2) R. Amos, *Talanta*, **20**, 1231 (1973).
(3) V. Das Gupta, *J. Pharm. Sci.*, **65**, 1706 (1976).
(4) A. F. Cunningham and D. E. Hillman, *J. Chromatogr.*, **148**, 528 (1978).
(5) A. N. Crabtree and A. E. J. McGill, *Mikrochim. Acta*, **1**, 85 (1967).
(6) J. J. Kirkland, *J. Chromatogr. Sci.*, **9**, 206 (1971).
(7) B. L. Karger, K. Conroe, and H. Engelhardt, *J. Chromatogr. Sci.*, **8**, 242 (1970).
(8) K. Karch, I. Sebestian, I. Halász, and H. Engelhardt, *J. Chromatogr.*, **122**, 171 (1976).
(9) A. W. Wolkoff and R. H. Larose, *J. Chromatogr.*, **99**, 731 (1974).
(10) S. Husain, P. Kunzelmann, and H. Schildknecht, *J. Chromatogr.*, **137**, 53 (1977).
(11) J. C. Kraak and J. F. K. Huber, *J. Chromatogr.*, **102**, 333 (1974).
(12) C. P. Terweij-Groen and J. C. Kraak, *J. Chromatogr.*, **138**, 245 (1977).
(13) K. Callmer, L.-E. Edholm, and B. E. F. Smith, *J. Chromatogr.*, **136**, 45, (1977).
(14) L. S. Bark and J. T. Graham, *J. Chromatogr.*, **23**, 120 (1966).
(15) L. S. Bark and J. T. Graham, *J. Chromatogr.*, **23**, 417 (1966).
(16) L. S. Bark and J. T. Graham, *J. Chromatogr.*, **27**, 116 (1967).
(17) L. S. Bark and J. T. Graham, *Talanta*, **13**, 1281 (1966).
(18) R. V. Vivilecchia, R. L. Cotter, R. J. Limpert, N. Z. Thimot, and J. N. Little, *J. Chromatogr.*, **99**, 407 (1974).
(19) P. K. C. Tseng and L. B. Rogers, 29th Pittsburgh Conference Abstr. on Analytical Chemistry and Applied Spectroscopy, Cleveland, Ohio, Feb. 27–Mar. 3, 1978, No. 197.
(20) L. R. Snyder, "Principles of Adsorption Chromatography", Marcel Dekker, New York, N.Y., 1968.
(21) J. March, "Advanced Organic Chemistry: Reactions, Mechanisms, and Structure", 2nd ed., McGraw-Hill Book Company, New York, N.Y., 1977.
(22) H. W. Kohlschütter and K. Unger, "Thin Layer Chromatography, A Laboratory Handbook", E. Stahl, Ed. Springer-Verlag, New York, N.Y., 1969.
(23) R. T. Morrison, and R. N. Boyd, "Organic Chemistry", 2nd ed., Allyn and Bacon, Boston, Mass., 1966.
(24) R. S. Drago and B. B. Wayland, *J. Am. Chem. Soc.*, **87**, 3571 (1965).
(25) J. F. Schabron, R. J. Hurtubise, and H. F. Silver, *Anal. Chem.*, **49** 2253 (1977).
(26) R. P. W. Scott and P. Kucera, *J. Chromatogr.*, **142**, 213 (1977).
(27) F. Dietz, J. Traud, P. Koppe, and Ch. Rübelt, *Chromatographia*, **9**, 380 (1976).

RECEIVED for review July 27, 1978. Accepted September 5, 1978. Financial support was provided by Department of Energy, Washington, D.C., Contract No. EX-76-S-01-2367.

Polarographic Behavior of Benzylpenicillenic Acid

Mohammed Jemal[1] and Adelbert M. Knevel*

Department of Medicinal Chemistry and Pharmacognosy, School of Pharmacy and Pharmacal Sciences, Purdue University, West Lafayette, Indiana 47907

The direct current and differential pulse polarographic behavior of benzylpenicillenic acid based on the sulfhydryl group has been investigated in 0.056 M citrate buffer of pH 6.45. Benzylpenicillenic acid gives a single wave at low concentrations and two waves at high concentrations. The single wave is adsorption-controlled and the double wave is diffusion-controlled. Triton X-100 shifts the first wave to a more positive value. It also increases the peak current and the increase varies from 2-fold to 14-fold, depending on the concentration of benzylpenicillenic acid. The i_d/C value is independent of concentration and presence of Triton X-100 whereas the i_p/C value changes with concentration and in the presence of Triton X-100. Constant i_p/C is obtained for concentrations below 1.0×10^{-5} M in the presence of Triton X-100 at 0.004% and above. The i_p/C value calculated from the i_d/C value was higher or lower than the experimental i_p/C value depending on the absence or presence of Triton X-100, respectively.

Benzylpencillenic acid (BPA) has been reported to be the prominent acylating agent in the formation of antigenic determinants in penicillin allergy (*1*). Since BPA is a degradation product produced in parenteral solutions of benzylpenicillin (BPN) under normal conditions of storage (*1*), parenterally administered solutions of BPN serve as a potential source of BPA for pencillin allergy in the body.

Analysis of BPA is based on its UV absorbance at 322 nm (*2, 3*). The chief drawback to this method of analysis is that other substances related to BPA also absorb at this wavelength. Depending upon the absence or presence of oxygen and concentrations of buffer, BPA may be converted to such products as benzylpenicillenic acid disulfide (and possibly sulfinic and sulfonic acids) and benzylpenicilloylpenicillenic acid (*3*). These substances all absorb radiant energy at 322 nm and, hence, interfere with the UV analytical method for BPA.

We have shown in a previous study (*4*) that differential pulse (DP) polarography is capable of resolving the sulfhydryl containing compounds, benzylpenicillenic acid and penicillamine, known degradation products of BPN. Hence it was decided to study the polarographic behavior of BPA based on the electrochemical reactivity of the sulfhydryl group. With the exception of one reference (*5*) which attributes the presence of catalytic waves in Brdicka solutions containing BPN to the sulfhydryl group of BPA formed as a degradation product of BPN, no study has been reported in the literature on the polarographic behavior of BPA on this functional group.

This paper describes the systematic study of the DP polarographic behavior of BPA in 0.056 M citrate buffer at pH 6.45 based on the electrochemical reactivity of the sulfhydryl

[1] Present address, Squibb Institute for Medical Research, New Brunswick, N.J. 08903.

0003-2700/78/0350-1917$01.00/0 © 1978 American Chemical Society

group. Direct current (dc) polarographic studies were conducted in an attempt to explain the interesting effects observed when various surfactants were added to solutions of BPA. The results reported in this paper serve as a basis for the assay of BPA in the presence of BPN, its degradation products, and derivatives of BPA which absorb at 322 nm.

EXPERIMENTAL

Apparatus. A Polarographic Analyzer Model 174A in conjunction with a Model 174/70 Drop Timer was used (Princeton Applied Research Corporation, Princeton, N.J.) along with the PAR Model 9300 and 9301 top and bottom polarographic cell. A three-electrode system was employed with platinum wire serving as the counter (auxiliary) electrode, calomel electrode model 3-712 (Coleman Instruments, Oak Brook, Ill.) as the reference electrode and dropping mercury as the working electrode. The capillary had the following characteristics. In 0.056 M citrate buffer of pH 6.45 (with 5% ethanol) at open circuit, the mercury flow rate was 2.57 mg/s and the natural drop time was 3.0 s at h_{uncorr} of 78.6 cm. Except when the effect of mercury pressure on wave height was studied, h_{uncorr} at 78.6 cm was used. Unless otherwise indicated, a drop time of 2 s and a pulse amplitude of 25 mV were employed in the DP mode and a natural drop time was used in the dc mode. The scan rate was 2 mV for both DP and dc studies.

Materials. BPA was obtained commercially from Sigma Chemical Company, St. Louis, Mo. Since this substance is unstable even in solid form, it was necessary to estimate its purity using the technique as reported (*6*). Scintillation grade Triton X-100 was obtained from Eastman Kodak Co. Benzylpenicilloic acid was prepared from BPN according to a literature procedure (*7*). Other chemicals were obtained commercially and used as purchased.

Selection of Buffer. A 0.056 M citrate buffer of pH 6.45 (containing 14.03 mg of trisodium citrate and 0.47 mg of citric acid per mL) was used in this study because it is one of the buffers in which Benzylpenicillin U.S.P. is stored. Also this system was selected because it provides maximum stability of both BPN and BPA in solution (*8*, *9*). The buffer concentration was found to be dilute enough not to cause the dimerization of BPA to such products as benzylpenicilloylpenicillenic acid (*3*).

Procedure. All experiments were carried out at 22 °C ± 1. Since BPA is unstable in aqueous media (*3*, *8*), all stock solutions of this compound were prepared in absolute ethanol. Polarographic solutions were prepared as follows. A volume of absolute ethanol which gave a final concentration of 5% upon dilution, was introduced into a 10-mL volumetric flask. A pre-determined amount of BPA stock solution was then added followed by the buffer (containing a surfactant when required) to bring the volume to the 10-mL mark. The solution was then shaken and immediately transferred to the polarographic cell, where pre-purified nitrogen was bubbled through it. When bubbling was started, about 100 s had elapsed since the time mixing began. Bubbling was continued for about 200 s and then the nitrogen flow was directed so it formed a blanket over the solution. Recording was started when the solution was exactly 400 s old. The initial potential for all recordings was −0.8 V and the potential scan rate was 2 mV/s. It was essential to maintain uniform timing, and initial potential and scan rate settings so that the age of all analytical solutions at their peak potential (for DP polarography) or at their plateau (for dc polarography) was the same. In this way the relation between concentration and polarographic output could be compared.

The concentrations of BPA reported here are for time zero, unless otherwise stated. When desired, the ratio between initial concentration and the concentration at a given time was determined using UV absorbance. The absorbance at time zero for an aqueous solution was taken to be equal to the absorbance in absolute ethanol.

RESULTS AND DISCUSSION

To determine if the concentration of BPA affected the rate of degradation, absorbance-vs.-time scans of different concentrations were run for a period of over 1 h in pH 6.45 citrate buffer. The ratio of the absorbance at $t = 0$ and $t = x$ after solution preparation was found to be independent of concentration. Hence, the relationship between the initial concentration of BPA in the polarographic solution and the concentration at the time the polarographic signal is measured remained linear.

Table I. Wave Height vs. Concentration of Benzylpenicillenic Acid Giving Single and Double Waves

concn, M	no. of waves	wave height,[a] μA
0.96×10^{-5}	1	0.023
1.91×10^{-5}	1	0.048
3.82×10^{-5}	1	0.098
5.73×10^{-5}	1	0.150
7.64×10^{-5}	2	0.200
9.55×10^{-5}	2	0.254
13.37×10^{-5}	2	0.346
17.19×10^{-5}	2	0.438
19.1×10^{-5}	2	0.486
63.0×10^{-5}	2	1.62
126×10^{-5}	2	2.85

[a] For concentrations giving two waves, wave height is the total wave height as measured from the residual current to the plateau of the second wave.

Direct Current Polarographic Behavior. *Concentration Effects.* BPA exhibited a well-defined wave with a half-wave potential of −0.54 V at low concentrations. This wave height increased up to a concentration of 7.0×10^{-5} M. At this point, a second wave with a half-wave potential of −0.34 V began to appear. When the concentration was further increased, the height of the second wave steadily increased and the height of the first wave remained practically the same. Table I lists concentrations of BPA giving a single wave and double wave along with respective wave heights. As can be seen from Table I, there was a direct relationship between concentration and wave height.

Diffusion and Adsorption Control. To determine whether the wave heights are limited by diffusion, adsorption, kinetic, or catalytic phenomena, the effect of mercury pressure on the heights of the first and double wave was studied. First, a concentration of BPA (3.90×10^{-5} M) known to give only one wave, was investigated at different pressures of mercury. The wave height varied in direct proportion to $h_{corr}^{1/2}$ indicating that the limiting current of the single wave was diffusion controlled. A concentration of BPA (1.22×10^{-4} M) known to give two waves at all pressures of mercury investigated, was then studied. The limiting current of the first wave exhibited the behavior of an adsorption controlled wave as shown by the direct proportion relationship of the wave height to h_{corr}. On the other hand, the limiting height of the double wave was found to vary in direct proportion to $h_{corr}^{1/2}$ indicating that the total limiting current was diffusion controlled.

A 7.13×10^{-5} M BPA solution gave two waves at h_{corr} of 31.85 cm but only one wave at h_{corr} of 91.75 cm confirming the fact that the height of the first wave of a double wave increases at a larger rate than the total wave when mercury pressure is increased.

Diffusion Coefficient. The diffusion coefficient was calculated using the Ilkovic equation. A solution concentration which gave a double wave was employed and the total wave height was measured at −0.2 V. Because of degradation of BPA during the polarographic procedure, the concentration used in the Ilkovic equation was 82.7% of the concentration at $t = 0$. The diffusion coefficient determined in this manner was found to be 5.32×10^{-6} cm^2/s.

Electrocapillary Curves. Electrocapillary curves in 0.056 M citrate buffer of pH 6.45 with 5% ethanol, the buffer with 5% ethanol and 0.008% Triton X-100, and the buffer with 5% ethanol and 1.50×10^{-4} M BPA are shown in Figure 1. A comparison of curves a and c shows that the 1.50×10^{-4} M

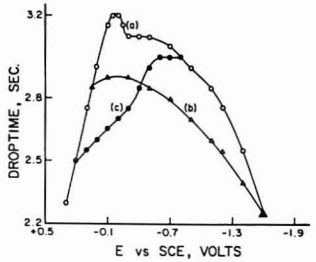


Figure 1. Electrocapillary curves. (a) Citrate buffer of pH 6.45 with 5% ethanol. (b) a plus 0.008% Triton X-100. (c) a plus 1.5×10^{-4} M benzylpenicillenic acid

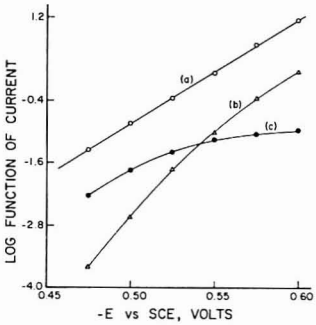


Figure 2. Log plot analysis for 6.50×10^{-5} M benzylpenicillenic acid. (a) log $(i_d - i)/i$ vs. E. (b) log $(i_d - i)^2/i$ vs. E. (c) log $(i_d - i)$ vs. E

BPA solution markedly decreases the drop times indicating that the interfacial tension between the mercury drop and the solution has been lowered. The decrease of drop times is seen in the potential range between −0.7 V and +0.2 V. The course of drop time depression indicates that there is adsorption (or film formation) on the electrode surface starting at the potential where BPA does not undergo electrode reaction and that the adsorption continues in the potential region where all of the BPA has been converted to its product (note that a 1.50×10^{-4} M BPA solution gives a double wave which starts at −0.6 V and reaches its second plateau at −0.2 V). Curve b shows that Triton X-100 in the medium is adsorbed over a long range of potential including the region where BPA or its product is adsorbed.

Log Plot Analysis. Direct current polarograms exhibiting only single waves were analyzed. The log plots for a 6.50×10^{-5} M solution are shown in Figure 2. The results show that the electrode reaction is of the type RSH + Hg ⇄ RSHg + $H^+ + e$ (*10, 11*). The slope of plot a is 0.05 V, which is smaller than the theoretically expected value of 0.059 V at 22 °C. The smaller slope value is probably due to complications of adsorption. The reliability of plot a is evidenced by the fact that the half-wave potential obtained from the plot is equal to that obtained from the polarogram. Another indication of the reliability of the plot is seen when comparing the slope of the plot with the value of $E_{3/4} - E_{1/4}$ obtained from the polarogram. The measured value of $E_{3/4} - E_{1/4}$ was 0.046 V, as compared to its calculated value of 0.048 V.

Effects of Surfactants. First, the effect of different concentrations of Triton X-100 (0.002–0.020%) on a given concentration of BPA in citrate buffer of pH 6.45 was studied. For a concentration of BPA which gave a single wave, the half-wave potential was shifted to a more positive value by the presence of Triton X-100. As the concentration of Triton X-100 was increased, the half-wave potential continued to shift accordingly. At a concentration of 0.008%, the half-wave potential reached a value of −0.39 V where it remained constant even though the Triton X-100 concentrations were further increased. On the other hand, the wave height was not affected. For a concentration which gave two waves, the half-wave potential of the second wave was not shifted at all, whereas the first wave was shifted in the manner of the single wave described above. Thus, as the Triton X-100 concentration was increased, the two waves came closer together until at sufficiently high concentrations the two waves merged for all practical purposes.

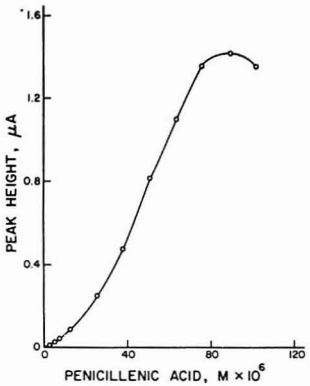


Figure 3. Variation of height of the first peak of benzylpenicillenic acid with concentration. At 1.10×10^{-4} M, the second peak is apparent although it is not seen as a distinct peak

The effects of gelatin and camphor were also studied. Gelatin generally exhibited an effect similar to that of Triton X-100. However, none of the concentrations of gelatin investigated (0.005–0.050%) moved the wave to the same extent as that of Triton X-100. Whereas gelatin at concentrations of 0.025% and above caused a maximum shift of 0.08 V in the wave of BPA solution (6.39×10^{-5} M), a saturated solution of camphor caused a shift of only 0.02 V. The height of the wave was not affected in either case.

Differential Pulse Polarographic Behavior. *Concentration Effects.* As in the case of dc polarography, low concentrations of BPA exhibited a single peak whereas high concentrations showed two peaks. Once the second peak started to appear, the first peak remained at practically the same height. The peak potential of the first peak changed only slightly with change in concentration (e.g., −0.51 V at 2.54×10^{-6} M). Until the appearance of the second peak, the height of the first peak increased with concentration. As shown in Figure 3, the relationship between concentration and peak height did not show a proportionality. The ratio of i_p/C continued to increase with concentration up to the point where the second wave was about to appear.

It was believed that some of the impurities found in the commercial products of BPA used in this study caused the variation of i_p/C with concentration. One such impurity, benzylpenicilloic acid (BPO), is known not to give a DP peak in the potential region of BPA; but it was thought that it might affect the height of the BPA peak indirectly. When mixtures of BPA and BPO of different proportions were investigated, there was little or no change in the heights of the BPA peaks due to presence of BPO. Hence, BPO did not cause the

variation of the ratio i_p/C. Another substance in the BPA product that was suspected as causing variation of i_p/C was an impurity of protein origin. Ordinary BPN preparations are known to contain high molecular weight compounds, proteins, and sulfur-containing polymers (*12*). Since the BPA product used was prepared from BPN, it was possible that it contained some of the impurities. Since the concentration of the impurities in the polarographic solutions would change in proportion to the volume of the BPA stock solution taken, the polarograms of the different concentrations of BPA would be affected by different concentrations of the impurities. If a given concentration of BPA is followed with time, this in effect gives different concentrations of BPA but with the same concentration of impurity. Accordingly the peak height of a BPA solution at selected ages of the solution was compared with the UV absorbance at 322 nm of an identical solution. The ratio of peak height to absorbance was found to decrease with the age of solution which was in agreement with the decreases of i_p/C with decrease in concentration. Thus it was concluded that the inconstancy of the i_p/C ratio was not caused by an impurity in the BPA preparation.

In an attempt to find a medium in which a proportionality exists between concentration and peak height, the following buffer systems were investigated: tetraethylammonium phosphate (pH 6.0), sodium potassium phosphate (pH 6.80), acetate (pH 5.18), borate (pH 8.0), and McIlvaine buffer (pH 6.65). BPA in all buffers investigated, behaved in the same manner as in citrate buffer of pH 6.45 in that the ratio i_p/C increased with concentration.

It is not clear why i_p/C should increase with concentration whereas i_d/C remains unchanged. Literature survey shows that in the few studies reported most of the sulfhydryl compounds show a linear relationship between concentration and peak height (*13, 14*). It is conceivable that i_p/C could change with concentration if a change in concentration is accompanied by a change in reversibility. However, it was found that the $E_{3/4} - E_{1/4}$ values for concentrations covering the range in which i_p/C increased were found to be the same (46 mV).

Effects of Surfactants. First the effect of Triton X-100 (0.002–0.020%) on BPA in pH 6.45 citrate buffer which give single peaks was studied. The peak potential was shifted to a more positive value with increase in Triton X-100 through 0.008% after which there was little change. For example, for a 3.74×10^{-6} M solution the shift in the presence of 0.008% Triton X-100 was from –0.52 V to –0.40 V. A very interesting and analytically useful effect of Triton X-100 was that the peak height increased significantly. The peak height increased as the concentration of Triton X-100 was increased through 0.004% after which it showed little or no change when concentrations as high as 0.020% were used.

The effect of Triton X-100 on solutions (e.g., 2.54×10^{-4} M) which gave two peaks was also studied. In the absence of Triton X-100, the two peaks were well resolved, but as Triton X-100 was added the resolution between the two peaks became poorer. This was because the first peak was shifted toward the second peak while the latter remained unaffected. None of the concentrations of Triton X-100 included in this study caused a complete merger of the two peaks, and only a slight effect was observed on the peak heights.

The effects of gelatin and a saturated solution of camphor were also studied to determine if the effects observed with Triton X-100, particularly the increase in peak height, were also obtained with other surfactants. Gelatin (0.005–0.050%) in pH 6.45 citrate buffer exhibited qualitatively a similar effect both on peak potential and peak height. For example, the peak potential of a 3.74×10^{-6} M solution moved from –0.52 V to –0.46 V as gelatin concentration was increased through

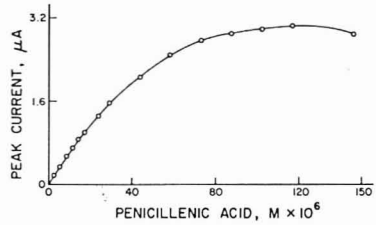


Figure 4. Height of the first peak of benzylpenicillenic acid vs. concentration in the presence of 0.004% Triton X-100

0.035% after which there was no change. The peak height increased with gelatin concentration until 0.025% and then remained unaffected as gelatin concentrations were increased. The peak height obtained with 0.025% gelatin was about half the peak height obtained with 0.008% Triton X-100 (0.120 μA as compared to 0.228 μA). The peak in the presence of Triton X-100 was sharper than that obtained in the presence of gelatin for the same concentration of BPA and experimental conditions. To investigate the effects of camphor, a saturated solution of camphor in citrate buffer of pH 6.45 was used. The peak potential of a 3.74×10^{-6} M solution was shifted to a more positive value by only 0.01 V. Height of the peak was increased but it was only about $^1/_3$ the height obtained in the presence of 0.008% Triton X-100 and the peak was not as sharp as in the presence of Triton X-100.

Because of the larger peak height and narrower peak width, Triton X-100 would be the surfactant of choice as an analytical aid for the analysis of BPA.

It is not clear why Triton X-100 brings about an increase in peak height. When $E_{3/4} - E_{1/4}$ values in the absence and presence of Triton X-100 were compared, the value obtained in the presence of Triton X-100 was higher; e.g. for a 2.17×10^{-5} M solution, it was 46 mV without Triton X-100 but 61 mV with 0.004% Triton X-100. According to these results, the electrode reaction became less reversible in the presence of Triton X-100 and, therefore, the peak height was expected to decrease. This, however did not occur.

The use of surfactants with DP polarography is not common. In the few cases where Triton X-100 was used, it caused depression of peak currents (*15, 16*). In a recent report on the effects of surfactants in DP polarography, Jacobsen and Lindseth (*17*) mention that the cationic surfactant decylamine increased DP peak current of folic acid by 50% whereas Triton X-100 completely inhibited the electrode reaction. They suggest that the cationic surfactant makes the electron transfer more reversible.

Concentration Effects in Presence of Triton X-100. Relationships between peak height and concentration of BPA in the presence of Triton X-100 at concentrations of 0.002%, 0.004%, 0.006%, 0.008%, 0.010%, 0.012%, 0.014%, 0.016%, and 0.020% were investigated. In the 0.002% Triton X-100 solution, i_p/C increased with an increase in the BPA concentration. The relationship between concentration and peak height in BPA solution containing 0.004% Triton X-100 is shown in Figure 4, and this is typical of Triton X-100 at concentrations ranging through 0.020%. A linear relationship in the concentration region below the 1.0×10^{-5} M level was obtained.

A comparison of Figures 3 and 4 shows that in the concentration region where i_p/C is decreasing with concentration in the presence of Triton X-100 (0.004% and above), i_p/C is increasing with concentration in the absence of Triton X-100. This indicates that the ratio of peak height in the presence of Triton X-100 to that in the absence of Triton X-100 is not

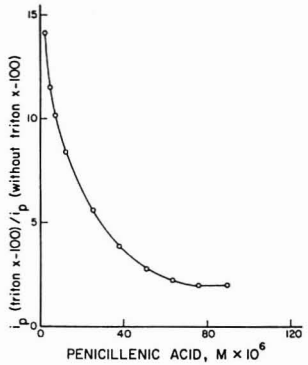


Figure 5. Variation of the ratio of peak current in the presence of 0.004% Triton X-100 to peak current in the absence of Triton X-100 with concentration of benzylpenicillenic acid

constant but decreases with concentration of BPA. A plot of such a ratio vs. concentration is shown in Figure 5. The increase in peak height due to the presence of Triton X-100 varies from 14-fold for a 2.5×10^{-6} M solution to 2-fold for a 9.0×10^{-5} M solution.

Comparison of Experimental and Theoretical Values of Peak Current. Since i_p/C values did not remain constant, it was necessary in reporting these values to give the concentrations of BPA and state whether or not Triton X-100 was or was not used in the determinations. This was not necessary when reporting i_d/C values, because they remained constant for all concentrations of BPA in the absence or presence of Triton X-100. Noting that i_p/C varies from about 4 to 18 μA/mM in the absence of Triton X-100 and from 61 to 26 μA/mM in the presence of Triton X-100, it was of interest to compare the experimental values of i_p/C with the theoretically expected (*15*, *18*) values. The i_d/C value obtained under the same conditions (e.g., same drop time of 2 s) as the i_p/C values was 2.45 μA/mM.

The calculated i_p/C value is 2.47 μA/mM which is much lower than the experimental values. Much of the difference is due to instrumentation. In the polarographic analyzer PAR model 174A, the differential pulse mode has a tenfold gain in the output not present in the other modes. The peak currents reported here are the values as read from the instrument. To obtain the "true" values, they must be divided by 10. Therefore, the "true" experimental i_p/C varied from 0.4 to 1.8 in the absence of Triton X-100 and from 6.1 to 2.6 in the presence of Triton X-100. Thus the experimentally obtained i_p/C in the absence of Triton X-100 is lower than the calculated i_p/C at all concentrations of BPA, but the converse is true in the presence of Triton X-100. While there has been a report where the experimental i_p is lower than calculated i_p due to irreversibility and instrumental artifacts (*15*), we have not come across a case where experimental i_p is higher than calculated i_p.

Selection of the Optimum Concentration of Triton X-100 for Quantitative Analysis of BPA. It was noticed, when using a high sensitivity and a large pulse amplitude, that there was a small inflection just before the start of the main peak for BPA solutions containing Triton X-100. The source of the inflection was investigated to determine whether it was due to Triton X-100, BPA or one of its impurities, or ethanol. By studying the effect on the inflection of change of concentration of the suspected source while keeping the concentration of the others the same, it was concluded that the inflection was due to the Triton X-100. When solutions of different concentrations of Triton X-100 containing no BPA were examined, a small peak at about −0.6 V was seen. The size of the peak decreased as the concentration was increased from 0.002% through 0.008% and then increased slightly as the concentration was further increased. In the presence of BPA, the peak due to Triton X-100 became a shoulder preceding the BPA peak and appeared larger. The resolution between the Triton X-100 peak and the BPA peak improved as the concentration of Triton X-100 was increased from 0.002% through 0.008% but there was no improvement above 0.008%. Therefore, the medium containing 0.008% Triton X-100 seemed to be the optimum concentration for BPA analysis at low concentrations. In this medium, a direct relationship between concentration and peak height was observed from 1.0×10^{-5} M down to 4.0×10^{-7} M after which measurement of the peak was difficult.

CONCLUSION

The finding that Triton X-100 causes a dramatic increase in peak current is quite interesting because previous studies (*15–17*) of other compounds showed that this surfactant caused a decrease. The increase in peak current of BPA was shown not to be due to a change in reversibility. Experimental values of i_p/C in the presence of Triton X-100 were found to be higher than theoretical values calculated using the method reported by Parry and Osteryoung (*18*). To our knowledge, this is the first example of its kind to be reported in the literature.

The relationship between peak current and concentration seems to be quite unique in that the ratio of i_p/C increases with concentration in the absence of Triton X-100 but remains either constant or decreases (depending on the concentration region) with increased concentration in the presence of Triton X-100.

Although some of the results observed in this study could not be readily explained, Triton X-100 was shown to be a useful analytical aid in the analysis of benzylpenicillenic acid using DP polarography. The applications of DP polarography for the simultaneous analysis of benzylpenicillenic acid and penicillamine in parenteral benzylpenicillin preparations is planned for future work.

LITERATURE CITED

(1) M. A. Schwartz, *J. Pharm. Sci.*, **58**, 643 (1969).
(2) B. B. Levine, *Arch. Biochem. Biophys.*, **93**, 50 (1961).
(3) K. H. Dudley, T. C. Butler, and D. Johnson, *J. Pharmacol. Exp. Ther.*, **179**, 505 (1971).
(4) M. Jemal, S. L. Hem, and A. M. Knevel, *J. Pharm. Sci.*, **67**, 302-305 (1978).
(5) N. Narasimhachai, G. R. Rao, and K. S. V. Santhanam, *Curr. Sci.*, **34**, 309 (1965).
(6) M. Jemal and A. M. Kneval, *Anal. Chim. Acta*, **96**, 143–151 (1978).
(7) M. A. Schwartz and J. J. Delduce, *J. Pharm. Sci.*, **58**, 1137 (1969).
(8) J. L. Longridge and D. Timms, *J. Chem. Soc. B*, 852 (1971).
(9) P. Finholt, G. Jürgensen, and H. Kristiansen, *J. Pharm. Sci.*, **54**, 387 (1965).
(10) I. M. Kolthoff and C. Barnum, *J. Am. Chem. Soc.*, **62**, 3061 (1940).
(11) W. Stricks and I. M. Kolthoff, *J. Am. Chem. Soc.*, **74**, 4646 (1952).
(12) G. T. Stewart, *Lancet*, 1, 1177 (1967).
(13) D. R. Canterford and A. S. Buchanan, *J. Electroanal. Chem.*, **44**, 291 (1973).
(14) F. Peter and R. Rosset, *Anal. Chim. Acta*, **79**, 47 (1975).
(15) D. J. Myers and J. Osteryoung, *Anal. Chem.*, **45**, 267 (1973).
(16) K. Hasebe and J. Osteryoung, *Anal. Chem.*, **47**, 2412 (1975).
(17) E. Jacobsen and H. Lindseth, *Anal. Chim. Acta*, **86**, 123 (1976).
(18) E. P. Parry and R. A. Osteryoung, *Anal. Chem.*, **37**, 1634 (1965).

RECEIVED for review May 10, 1977. Resubmitted May 15, 1978. Accepted August 24, 1978. Supported in part by the General Research Support Grant 5S01RR05586-07 and the African-American Institute.

Buffers for the Physiological pH Range: Thermodynamic Constants of 3-(*N*-Morpholino)propanesulfonic Acid from 5 to 50 °C

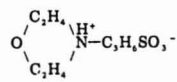
Munessar Sankar[1] and Roger G. Bates*

Department of Chemistry, University of Florida, Gainesville, Florida 32611

The pK_2 values for the dissociation of the NH^+ charge center of the ampholyte 3-(*N*-morpholino)propanesulfonic acid (MOPS) have been determined at 10 temperatures from 5 to 50 °C by measurements of the emf of cells without liquid junction, utilizing hydrogen electrodes and silver–silver bromide electrodes. The pK_2 was found to be 7.184 at 25 °C, confirming the expectation that the NH^+ group in the substituted propanesulfonic acid is weaker than that in the corresponding ethanesulfonic acid previously studied. Enthalpy and entropy values for the dissociation process were derived from the temperature coefficient of pK_2, and MOPS was shown to be useful for pH control in the region close to that of blood serum.

The buffer substances recommended by Good (*1*) have proved useful for pH measurement and control in the physiological region of pH 7 to 9. These compounds, primarily protonated amines or *N*-substituted amino acids, are compatible with many media of biochemical importance. An inconsistency earlier observed between the pH of certain of these buffers in saline media of ionic strength (*I*) equal to 0.16 and the NBS standard pH scale has recently been attributed to abnormal liquid-junction potentials (*2*).

Four substituted aminoethanesulfonic acids, designated MES, BES, TES, and HEPES, were the subject of an earlier communication (*3*). [**N.B.** A hydrogen atom has been omitted from the nitrogen atom in the formula for TES given on p 1293 of reference 3.] The pK_2 values of BES, TES, and HEPES at 37 °C fall in the useful range 7 to 7.5 (near the pH of blood serum), but that of MES, 2-(*N*-morpholino)-ethanesulfonic acid, is near 6.15. Since morpholinium ion itself has a pK_a near 8.2 at 37 °C (*4*), it is clear that substitution of $-(CH_2)_nSO_3^-$ on the nitrogen atom of morpholine increases the acidity of the NH^+ group. This enhancement should fall off as n becomes greater, thus providing a means of tailoring a buffer substance with pK_2 in the desired range. The ampholyte 3-(*N*-morpholino)propanesulfonic acid, known as MOPS,



would be expected to have a pK_2 value somewhat higher than that of MES. The thermodynamic constants for the second dissociation of MOPS have now been determined at intervals of 5 °C from 5 to 50 °C, and the pK_2 has indeed been found to be 7.184 at 25 °C and 7.041 at 37 °C. The pH of a MOPS solution (buffer ratio 1:1) in a saline medium of $I = 0.16$ has been determined at 25 and 37 °C.

[1] On leave from the University of Durban-Westville, South Africa, 1977–78.

EXPERIMENTAL

MOPS, purchased from the Sigma Chemical Co., was recrystallized twice from 80 wt % redistilled ethanol. It was dried under vacuum for 4 h at 80 °C and stored over Drierite. The purified compound was assayed by titration with a carbonate-free solution of NaOH; the results obtained for two samples were 100.05 and 99.97%. Reagent-grade NaBr was crystallized twice from conductivity water. It was heated slowly to 140 °C in vacuum and maintained at this temperature for 5 h. The salt was stored over Drierite. Reagent-grade HBr solution was purified by distillation. Two stock solutions were prepared by weight methods from MOPS, NaBr, and standard NaOH solution in such amounts that the molalities of MOPS, NaMOPS, and NaBr were equal in each. Additional solutions for the cell measurements were prepared by adding weighed amounts of CO_2-free water. Other details of the emf techniques have been described elsewhere (*3*).

RESULTS

The values of the emf (E) of the cell

$$\mathrm{Pt;H_2(g,\ 1\ atm)|MOPS}(m),\ \mathrm{NaMOPS}(m),\ \mathrm{NaBr}(m)|\mathrm{AgBr;Ag} \quad \text{(A)}$$

where m is molality, from 5 to 50 °C are summarized in Table I. The standard emf ($E°$) of the cell was determined by measuring the emf (E_S) of the cell

$$\mathrm{Pt;H_2(g,\ 1\ atm)|HBr}(m = 0.01)|\mathrm{AgBr;Ag}$$

by the equation

$$E° = E_S - 4k + 2k \log \gamma_{\pm}(\mathrm{HBr}) \qquad (1)$$

In Equation 1, k is written for $(RT \ln 10)/F$ (*5*), and $\gamma_{\pm}$(HBr) is the mean ionic molal activity coefficient of HBr, molality 0.01 mol kg^{-1}. Values of the latter at 0, 25, and 50 °C were taken from the work of Hetzer et al. (*6*), and values at the other temperatures were interpolated. The values of $E°$ given at the foot of Table I are the means derived from the emf (E_S) of 12 cells at each of the 10 temperatures.

The pH of the buffer solutions of MOPS and its sodium salt is so close to neutrality that hydrolysis is negligible, even in the most dilute buffers included in this study. Furthermore, the molalities of MOPS, NaMOPS, and NaBr were equal, and hence an apparent pK_2, designated pK_2', is defined by

$$pK_2' \equiv pK_2 - \log \frac{\gamma_M \gamma_{Br}}{\gamma_{M^-}} = \frac{E - E°}{k} + \log m \qquad (2)$$

where γ_M and γ_{M^-} represent the activity coefficients of the ampholyte MOPS and its anion, respectively. As in the earlier study (*3*), pK_2' was found to vary linearly with ionic strength (I), and the limit (pK_2) at $I = 0$ was readily found by linear regression analysis:

$$pK_2' = pK_2 + \alpha I \qquad (3)$$

The values of pK_2 and α are summarized in Table II, together

0003-2700/78/0350-1922$01.00/0 © 1978 American Chemical Society

Table I. Electromotive Force (E) and Standard Emf ($E°$), in Volts from 5 to 50 °C, of the Cell: Pt;H_2(g, 1 atm)|MOPS(m), NaMOPS(m), NaBr(m)|AgBr;Ag

m	5 °C	10 °C	15 °C	20 °C	25 °C	30 °C	35 °C	40 °C	45 °C	50 °C
0.004880	0.61844	0.62245	0.62624	0.62985	0.63328	0.63652	0.63961	0.64250	0.64522	0.64779
0.007331	0.60891	0.61278	0.61633	0.61974	0.62296	0.62600	0.62887	0.63157	0.63410	0.63649
0.009786	0.60224	0.60594	0.60941	0.61271	0.61580	0.61870	0.62146	0.62404	0.62645	0.62872
0.012251	0.59702	0.60066	0.60397	0.60715	0.61015	0.61296	0.61559	0.61807	0.62037	0.62253
0.014721	0.59292	0.59642	0.59971	0.60281	0.60571	0.60842	0.61099	0.61339	0.61562	0.61768
0.019679	0.58627	0.58970	0.59280	0.59576	0.59855	0.60114	0.60356	0.60583	0.60791	0.60986
0.02467	0.58131	0.58457	0.58762	0.59049	0.59313	0.59561	0.59794	0.60010	0.60209	0.60392
0.02962	0.57723	0.58046	0.58336	0.58613	0.58868	0.59109	0.59332	0.59538	0.59727	0.59904
0.03472	0.57390	0.57699	0.57987	0.58257	0.58508	0.58741	0.58958	0.59157	0.59341	0.59509
0.03979	0.57091	0.57399	0.57675	0.57937	0.58182	0.58409	0.58618	0.58811	0.58987	0.59149
0.04488	0.56844	0.57142	0.57417	0.57673	0.57912	0.58133	0.58339	0.58526	0.58698	0.58853
0.05000	0.56613	0.56909	0.57173	0.57423	0.57659	0.57876	0.58074	0.58256	0.58422	0.58574
$E°$:	0.07986	0.07795	0.07587	0.07362	0.07122	0.06869	0.06605	0.06324	0.06030	0.05725

Table II. pK_2 Values for MOPS from 5 to 50 °C. Constants of Equation 3.

t/°C	pK_2	α	$\sigma(pK_2)^a$
5	7.442	0.699	0.0007
10	7.376	0.671	0.0006
15	7.310	0.640	0.0007
20	7.247	0.611	0.0007
25	7.184	0.589	0.0006
30	7.123	0.569	0.0005
35	7.064	0.547	0.0005
40	7.006	0.526	0.0005
45	6.949	0.509	0.0006
50	6.893	0.491	0.0005

[a] Standard deviation of the intercept.

with the standard deviation of the intercept, $\sigma(pK_2)$.

DISCUSSION

The values of pK_2 at the 10 temperatures fitted extremely well an equation of the form suggested by Harned and Robinson (7):

$$pK_2 = \frac{749.430}{T} + 5.8233 - 0.0038661T \qquad (4)$$

where T is the thermodynamic temperature (t °C + 273.15). The standard deviation for regression was only 0.0002. The standard thermodynamic quantities for the process

$$\text{MOPS} \rightleftharpoons \text{H}^+ + \text{MOPS}^- \qquad (5)$$

at T = 298.15K, calculated from the constants of Equation 4, are as follows: $\Delta G°$, 9801 cal mol^{-1}; $\Delta H°$, 5000 cal mol^{-1}, and $\Delta S°$, −16.10 cal K^{-1} mol^{-1}, while $\Delta C_p°$ is estimated to be 10.5 cal K^{-1} mol^{-1}. The standard deviations in these quantities can be estimated from the standard deviation of pK_2 (0.0006) by the method described by Please (8). They are as follows: $\sigma(\Delta G°)$ = 0.4 cal mol^{-1}; $\sigma(\Delta H°)$ = 6 cal mol^{-1}; $\sigma(\Delta S°)$ = 0.02 cal K^{-1} mol^{-1}; and $\sigma(\Delta C_p°)$ = 1 cal K^{-1} mol^{-1}.

It is evident from a comparison of the thermodynamic constants for the dissociation of MOPS (*N*-morpholinopropanesulfonic acid) with those of MES (*N*-morpholinoethanesulfonic acid) that lengthening of the chain has, as expected, decreased the acidity of the NH^+ group. At the same time, the enthalpy of dissociation has increased from 3.5 to 5.0 kcal mol^{-1}, yet the change in $\Delta S°$ (from −17.0 to −16.1 cal K^{-1} mol^{-1}) is small and no change in $\Delta C_p°$ is apparent.

The usefulness of MES and related ampholytes for pH control in the physiological region has been pointed out by Good (1). It rests in part on the fact that these substances do not, in general, form stable complexes with metal ions and other compounds common to biological media. In addition, they may provide suitable secondary reference solutions at I = 0.16 for the standardization of pH measuring equipment close to the pH of blood and plasma (2). It was therefore considered worthwhile to ascertain whether the pH of MOPS buffer solutions (I = 0.16) is consistent with the pH(S) based, like the NBS primary standards, on the emf of cells without liquid junction.

Our earlier work (2) has shown that inconsistencies are most likely to arise from failure to match the ionic strength of the buffers being compared. It was suggested that a suitable reference solution for pH measurements in isotonic saline and media of similar composition is a phosphate/NaCl solution of I = 0.16 having the composition (in molality units); KH_2PO_4, 0.005217; Na_2HPO_4, 0.018258; NaCl, 0.1. The pH(S) of this reference solution was shown to be 7.323 at 25 °C and 7.297 at 37 °C. A buffer solution with the composition: MOPS, 0.04 molal; NaMOPS, 0.04 molal; NaCl, 0.12 molal, was prepared. The emf of cell (B)

$$\text{Pt;H}_2\text{(g, 1 atm)|MOPS/NaCl soln|AgCl;Ag} \qquad \text{(B)}$$

was measured at 25 and 37 °C and values of pH(S) calculated at these two temperatures (5). In addition, the pH of the MOPS/NaCl solution was determined in a cell with liquid junction,

$$\text{Hg;Hg}_2\text{Cl}_2\text{,3.5 M KCl||Buffer soln|H}_2\text{(g, 1 atm);Pt} \qquad \text{(C)}$$

standardized with the phosphate/NaCl reference solution.

The results of these measurements of cells B and C are summarized in Table III. The pH of the MOPS/NaCl solution based on a cell with liquid junction is the same as the assigned pH(S) at 25 °C but differs by 0.005 at 37 °C. Although the difference at 37 °C is larger than those for buffers of MES and TES under similar circumstances (2), it is evident that MOPS buffers may prove to be useful secondary pH standards in the range of physiological interest.

Table III. Comparison of pH(S) from Cell B with pH from Cell C at 25 and 37 °C

t, °C	E_B[a]	$E_B°$	pH(S)	E_C(std.)[b]	E_C	pH
25	0.70628	0.22255	7.128	−0.67989	−0.66837	7.128
37	0.70847	0.21453	6.976	−0.69068	−0.67125	6.981

[a] Emf for both cells in volts. [b] Cell standardized with phosphate/NaCl solution having the following composition (in molalities): KH_2PO_4, 0.005217; Na_2HPO_4, 0.018258; NaCl, 0.1.

LITERATURE CITED

(1) N. E. Good, G. D. Winget, W. Winter, T. N. Connolly, S. Izawa, and R. M. M. Singh, *Biochemistry*, **5**, 467 (1966).
(2) R. G. Bates, C. A. Vega, and D. R. White, Jr., *Anal. Chem.*, **50**, 1295 (1978).
(3) C. A. Vega and R. G. Bates, *Anal. Chem.*, **48**, 1293 (1976).
(4) H. B. Hetzer, R. G. Bates, and R. A. Robinson, *J. Phys. Chem.*, **70**, 2869 (1966).
(5) R. G. Bates, "Determination of pH", 2nd ed., Wiley, New York, N.Y., 1973, Chap. 4 and appendix, table 1.
(6) H. B. Hetzer, R. A. Robinson, and R. G. Bates, *J. Phys. Chem.*, **66**, 1423 (1962).
(7) H. S. Harned and R. A. Robinson, *Trans. Faraday Soc.*, **36**, 973 (1940).
(8) N. W. Please, *Biochem. J.*, **56**, 196 (1954).

RECEIVED for review July 21, 1978. Accepted August 14, 1978. Work supported in part by the National Science Foundation under Grant CHE76 24556. M.S. thanks the following organizations in the Republic of South Africa for financial assistance: the C.S.I.R., Ernest Oppenheimer Memorial Trust, and Sentrachem Ltd.

Instrumental Approach to Potentiometric Stripping Analysis of Some Heavy Metals

Daniel Jagner

Department of Analytical Chemistry, University of Gothenburg, Fack, S-402 20 Göteborg, Sweden

The method is based on the potentiostatic reduction and amalgamation of analytes and the subsequent registration of the potential–time curve when the reduced metals are reoxidized by means of mercury(II) ions. Potentiostatic reduction is achieved by means of a simple battery-operated potentiostat, equipped with a timer/switcher unit facilitating semiautomatic analysis. The time–potential curves are registered by means of a pH-meter and/or an *x–t* recorder. Analytical procedures for bismuth, cadmium, thallium, lead, copper, and zinc ions in different media are reported. The relative precision is approximately 0.06.

The increasing need for trace metal analysis, in particular for the determination of lead and cadmium, is well documented. Consequently, there is also a need for simple analytical instrumentation suitable for this purpose. The hitherto simplest instrumental approach to trace metal analysis is that of ion-selective electrodes, a general purpose pH meter being the main instrumentation. Unfortunately ion-selective electrodes are not selective and sensitive enough for metal analysis in the concentration range below 10^{-6} M (*1*), which is that of most interest. The majority of the most important trace metals do, however, dissolve readily in mercury. This has been utilized in a large number of analytical procedures based on anodic stripping voltammetry (*2*). Advanced instrumentation, e.g., for differential pulse anodic stripping voltammetry, has been designed for this purpose (*3*). Such dedicated instrumentation is, however, normally expensive since it does not consist of equipment usually available in the chemical laboratory.

This paper describes an instrumental technique, which combines the simplicity of the ion-selective electrode instrumentation with the selectivity and sensitivity of anodic stripping voltammetry.

PRINCIPLE

If a working electrode, consisting of material insoluble in mercury and with a high hydrogen overvoltage, is held potentiostatically at a sufficiently reductive potential in a deaerated sample containing Hg(II) ions and mercury soluble metal ions M(n) the reactions

$$\mathrm{Hg(II)} + 2e^- \rightarrow \mathrm{Hg(l)}$$

$$\mathrm{M}(n) + ne^- \rightarrow \mathrm{M(Hg)}$$

will occur simultaneously. If the hydrodynamic conditions at the working electrode surface are kept constant, e.g., by rotating the electrode or by stirring the sample, the rate of reduction of M(n) ions will be constant until a significant fraction of these ions has been reduced. By keeping the electrode surface small the decrease in M(n) concentration will occur only very slowly.

If, at unchanged hydrodynamic conditions, the potentiostatic circuitry is disconnected and at the same time the working and the reference electrodes remain connected to a high input impedance voltmeter (e.g., a pH meter) the potential changes due to the reactions

$$\mathrm{M(Hg)} + \frac{n}{2}\mathrm{Hg(II)} \rightarrow \mathrm{M}(n) + \frac{n}{2}\mathrm{Hg(l)}$$

can be observed. The experimental curve thus registered, potential vs. time, consists of a normal redox titration curve superimposed on a capacitance background. If the background contribution is accounted for, the time elapse between two consecutive equivalence points will be proportional to the amount of the particular metal in the mercury phase. Analogous to anodic stripping voltammetry, the amount of amalgamated metal is proportional to the concentration of metal ions M(n) in the sample and to the time of pre-electrolysis (plating). Consequently, the potential–time curve can be made the basis for quantitative analysis, either by the use of a calibration plot, an internal standard, or by using a standard addition procedure.

The principle of potentiometric stripping analysis has been described previously by the author in connection with more complicated instrumentation (*4*, *5*).

EXPERIMENTAL

Instrumentation. The only instrumentation required for potentiometric stripping analysis is a potentistatic circuitry and a pH meter, the latter being used both for the adjustment of an adequate plating potential and for the registration of the stripping curves. In all experiments, the same potentiostat was used but three different ways of registering the potentiometric stripping analysis curves were investigated. In the first method, which is

0003-2700/78/0350-1924$01.00/0 © 1978 American Chemical Society

Table I. Optimum Experimental Conditions for the Determination of Six Different Ions by Potentiometric Stripping Analysis

element	optimum pH range	optimum plating potential, E vs. SCE, V	scanning potential, $E_{1/2}$ vs. SCE, V	remarks
Bi(III)	0–0.5	−0.8–−1.0	−0.15	HCl suitable medium.
Cu(II)	0–3	−0.7–−0.95	−0.25	Zn(II) interference possible when plating below −0.95 V. Acidity with HCl.
Pb(II)	0–3	−0.8–−1.2	−0.50	Hydrogen evolution may commence at −1.3 V when pH <2. Acidity with HCl.
Tl(III), Tl(I)	0–3	−0.9–−1.2	0.65	Hydrogen evolution may commence at −1.3 V when pH <2. Acidity with HCl.
Cd(II)	0–3	−1.0–−1.2	−0.65	Hydrogen evolution may commence at −1.3 V when pH <2. Acidity with HCl.
Zn(II)	2–6	−1.30–−1.4	−1.05	Cu interference eliminated by addition of Ga(III) in pH range 5–6.

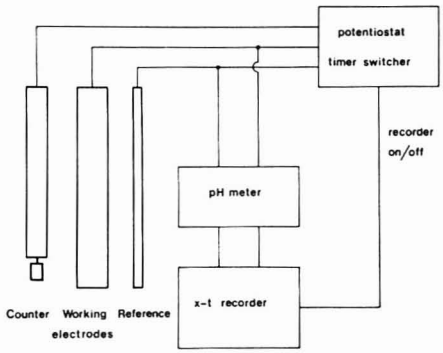


Figure 1. Block scheme of the instrumentation used. In most experiments, the pH meter was replaced by a high input impedance recorder amplifier

illustrated schematically in Figure 1, a digital pH meter (Radiometer pHM 64) connected to a low input impedance (x–t recorder) (Radiometer, REC 61 Servograph, amplifier REA 112) was used for the registration. In the second setup, the recorder in Figure 1 was omitted and the stripping curves were registered by visual observation of the potential jumps occurring at the equivalence points. The time elapse between two consecutive equivalence points was registered on a stop-watch. This setup could be used only for samples with relatively high concentrations of the metals determined,or after long plating times. In the third approach, the pH meter in Figure 1 was replaced by a high input impedance operational amplifier on the recorder (Radiometer, REA 105 pH unit). This setup was used in most of the experiments described below.

The battery operated three-electrode potentiostat was fitted with a timer/switcher unit (Radiometer, Research model) operated by the same 9-V battery source. The time unit was a 3.2 MHz quartz crystal. By means of the timer/switcher unit the plating time could be pre-chosen as 1, 2, 4, 8, ..., 512 min. Just before the termination of the plating period, the timer/switcher unit started the paper feed of the recorder and stopped it after a pre-chosen fraction of the plating time. This fraction could be pre-chosen as $^1/_4$, $^1/_8$, ..., $^1/_{128}$, the larger fractions being used for samples with high metal concentrations and vice versa. The timer/switcher unit could be operated in the repetitive mode, the plating and potentiometric stripping cycle thus being repeated automatically. The plating sequence could be terminated manually at any time by means of a reset function.

Electrodes. A platinum foil (Radiometer P 101) was used as counter and a saturated calomel electrode (Radiometer K 4040) as reference electrode. The working electrode was a Teflon fitted glassy carbon electrode (Radiometer F 3500) with a total surface of approximately 7 mm^2. The outer diameter of the Teflon rod was 8 mm and no glue of any kind was used in the working electrode.

Electrochemical Cell. The electrochemical cells were glass vessels (Radiometer V 532/3) with volumes between 8 and 150 mL. The vessels were fitted into a gas-tight titration assembly (Radiometer TTA 60) modified so that all packings were of Teflon and no metal parts were in contact with the sample. The three electrodes were screwed into the lid of the vessel. The sample was agitated mechanically at constant rate by a three-edged Teflon stirrer. Inert gas could be passed either through the sample or just above the sample surface.

Chemicals. All chemicals were of analytical grade, except sodium acetate, sodium chloride, and the mineral acids which were of Suprapur grade (Merck). The mercury(II) solution used for the formation of the thin-film electrode and for the oxidation of amalgamated metals contained only neglible amounts of other metals.

Preparation and Regeneration of the Working Electrode Surface. The final preparation step of the working electrode included polishing with 3-μm diamond paste. When in constant use, the working electrode was repolished manually for 1–2 min several times each day using the polishing kit. After polishing, the glassy carbon surface was washed carefully with acetone to remove the diamond paste solvent and fingerprints. Re-polishing was essential after exposure of the working electrode to oxidizing chemicals or to large amounts of surface-active agents for a long period of time.

When not in use, the working electrode was stored in ethanol. For storing periods of more than two days, the electrode was stored dry.

Pre-Coating of a Mercury Film. During analysis, the working electrode must be covered with a mercury film which is thick enough to dissolve all the mercury soluble metals which are reduced during plating. The working electrode must therefore be pre-coated with mercury before the commencement of the analysis. This was achieved by holding the working electrode at −0.5 V vs. SCE for 10–30 s in a non-deaerated sample containing 0.1 M hydrochloric acid and 25 mg/L of mercury(II). By pushing the reset function, a stripping curve was registered and a steady base line established. The plating potential was then changed to −0.60 V and the plating/stripping cycle repeated. This procedure was repeated at −0.70, −0.80, and −0.90 V. Finally at −0.90 V, a plating period of 2 min was initiated and immediately after stripping the working electrode was washed with distilled water. If the working electrode is allowed to stand in the pre-coating solution for a longer period of time, calomel will finally be formed on the electrode surface according to the reaction

$$Hg(l) + Hg(II) + 2\ Cl^- \rightarrow Hg_2Cl_2(s)$$

This will result in a decreased sensitivity, particularily for copper. Pre-coating was performed in a titration vessel under stirring. Once coated, the electrode could be used for a number of analyses if stored in distilled water in contact with air. Re-coating of the mercury film was normally performed a few times each week. Mercury coating can also be performed in situ in the sample according to the procedure above. This is recommended if the analyte concentrations are below 100 μg/L.

Table II. Experimental Conditions for the Registration of the Potentiometric Stripping Curves Shown in Figure 2

metal ion	metal concn, M	[Hg(II)], M	ionic medium	plating potential, E vs. SCE	plating time, min
Bi(III)	10^{-6}	2×10^{-5}	1 M HCl	−0.9	2
Cu(II)	10^{-6}	2×10^{-5}	0.05 M HCl, 0.5 M NaCl	−0.9	4
Pb(II)	10^{-6}	2×10^{-5}	0.05 M HCl, 0.5 M NaCl	−1.1	4
Tl(I), Tl(III)	10^{-6}	2×10^{-5}	0.05 M HCl, 0.5 M NaCl	−1.1	2
Cd(II)	10^{-6}	2×10^{-5}	0.05 M HCl, 0.5 M NaCl	−1.1	4
Zn(II)	10^{-6}	2×10^{-5}	0.01 M HCl, 0.5 M NaCl	−1.3	4

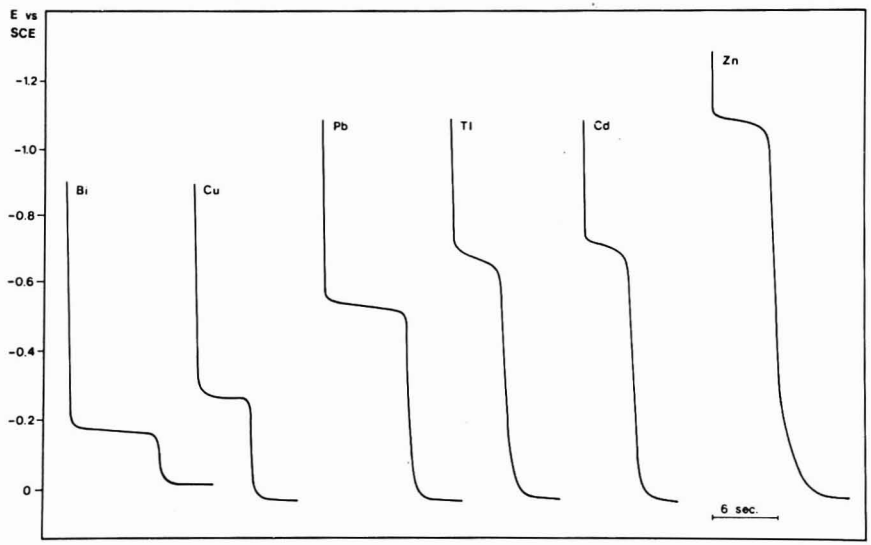


Figure 2. Potentiometric stripping curves obtained for six different elements under the experimental conditions specified in Table II

Recommended Analaytical Procedure. Mercury(II) is added to a sample of known volume until the final concentration is between 1 and 5 mg/L. If necessary, the sample pH is adjusted to the optimum pH range shown in Table I. The stirrer is started and a stream of pure nitrogen is allowed to pass through the sample for 15 min, after which the nitrogen stream is passed above the sample surface. In routine analysis of many samples it is preferable to deaerate separately in order to save time.

After deaeration, a plating/stripping cycle comprising a plating time of 2 min and a stripping time of 0.25 min is performed at the appropriate plating potential (cf. Table I). Suitable plating and stripping times to be used in the subsequent analysis can then be estimated from the stripping curve thus registered. The working potential should be chosen as negative as possible to obtain maximum sensitivity and precision. Small bubbles of hydrogen, which are sometimes formed at the interface between the glassy carbon rod and the surrounding Teflon can usually be neglected since they do not interfere with the analysis. If substantial amounts of hydrogen bubbles are formed at the electrode surface, the electrode surface must be re-polished. If diamond paste is not sufficient, emery paper could be used prior to diamond paste.

Depending on the analytical problem, the analytical procedure is performed either by means of standard addition, or by using an internal standard or calibration plots. The last method is preferable in routine analysis of samples of approximately the same composition. Standard addition is recommended in samples of unknown composition. Care should be taken during analysis so that the mercury-coated working electrode is not exposed to the mercury(II)-containing sample for longer period of times without the potentiostat operating. If not kept at a reductive potential (i.e., below 0.0 V vs. SCE), formation of calomel on the working electrode surface will commence.

RESULTS AND DISCUSSION

Metals Analyzed. To illustrate which metals are most conveniently analyzed by potentiometric stripping analysis, six different 40-mL solutions, with the compositions specified in Table II, were exposed to the plating potentials indicated in Table II for the times specified. The resulting stripping curves are shown in Figure 2.

As seen from Figure 2, ions which can be analyzed by anodic stripping voltammetry can also be analyzed by potentiometric stripping analysis. Furthermore, as expected, the potentials at the half-titration points on the stripping curves correspond closely to the potentials at the stripping peaks in anodic stripping voltammetry. As is also seen from Figure 2, the sensitivity for all the metals is of the same order of magnitude.

Evaluation of Potentiometric Stripping. The magnitude of the background contribution to the potentiometric stripping curve can be determined by exposing the working electrode to the plating potential for a few seconds and then registering the stripping curve. A typical background contribution is shown as curve I of Figure 3. This background curve has been registered in a sample of the same composition as the Pb(II) sample specified in Table II. The form of the background curve is to some extent dependent on the response rate of the recorder pen.

Curves II and III of Figure 3, which were obtained under the same experimental conditions as the Pb curve in Figure 2 (cf. Table II), illustrate two ways of eliminating the

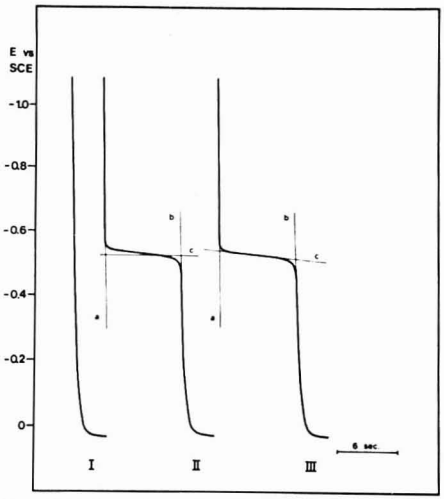


Figure 3. Background curve (I) and two different ways of evaluating potentiometric stripping curves (II and III). All curves have been registered in a 10^{-6} M Pb(II) sample containing 4 mg/L of Hg(II), 0.05 M HCl, and 0.5 M NaCl

background contribution. In curve II, the lines a and b are drawn parallel to the stripping curve just before and after a titration plateau. Line c is drawn parallel to the time axis to intersect the stripping curve at the potential of the half-titration point. The time distance between the intersections of line c with lines a and b is then taken as the analytical signal. In curve III, line c is replaced by line c', drawn parallel to the slope of the potentiometric stripping curve on the titration plateau. Again, the time distance between the intersection of c' with a and b comprises the analytical signal. The results obtained by the two different methods normally come very close to each other. As in chronopotentiometry, the evaluation method shown in curve III yields, however, the most accurate results.

Signal Dependence on Plating Time and Hg(II) Concentration. The potentiometric stripping signals should increase linearly with the plating time. This was verified using the Tl solution and the plating potential indicated in Table II.

The dependence of the potentiometric stripping signal on the Hg(II) concentration has been investigated previously (*5*). According to this investigation, the analytical signal decreases linearly with the Hg(II) concentration in the concentration range 1–20 mg/L. For mercury(II) concentrations below 0.5 mg/L, traces of oxygen contribute significantly to the oxidation rate causing deviation from linearity. It was also shown (*5*) that high concentrations of hydrogen ions could contribute to the oxidation rate for zinc.

Decrease in Mercury(II) Concentration during Plating. During plating, mercury(II) ions are reduced continuously at the working electrode. In contrast to the amalgamated metals to be analyzed, mercury is not re-oxidized during stripping. Consequently there is a continuous decrease in Hg(II) concentration in the sample solution. Obviously this decrease is more rapid if large electrode surfaces or small sample volumes are used. If significant, the decrease in Hg(II) concentration will result in a continuous increase in the analytical signal if the plating/stripping cycle is repeated in a particular sample. This decrease will have an analytical significance if the method of standard addition is used to evaluate the trace metal concentrations. If internal standards of calibration plots are used, the decrease is of neglible importance.

Table III. Relative Decrease (%) in Mercury(II) Concentration for Different Sample Volumes and Plating Times

sample volume, mL	plating time, min			
	1	16	64	1024
10	<2%	<2%	3%	<50%
50	<2%	<2%	<2%	15%
200	<2%	<2%	<2%	<2%

To elucidate the rate of decrease in mercury(II) concentration, 40 mL of a deaerated 0.1 M HCl solution containing 2 μg/L of mercury(II) was plated at −0.65 V vs. SCE and the plating current was registered. The mercury(II) concentration was then increased in three steps each equal to 2 mg/L. The increase in current was registered on a micro-amperemeter. This increase was used to calculate the relative decrease in mercury(II) concentration during plating. The results for a number of different sample volumes and plating times are shown in Table III. It is seen that the decrease in mercury(II) is of little practical importance.

Precision. To estimate the precision obtained by repetitive plating/stripping in the same solution, a 40-mL 0.1 M hydrochloric acid sample containing 25 μg/L of cadmium(II), lead(II), and copper(II) and 2 mg/L of mercury(II) was deaerated in a nitrogen stream. Ten repetitive plating/stripping cycles were then performed at a plating potential of −1.10 V vs. SCE for a plating time of 8 min. The relative standard deviation obtained was less than 0.06 for all three elements investigated.

The same experiment was repeated at a plating potential of −0.85 V. The relative standard deviations for lead and copper were unaffected but the precision for cadmium decreased slightly. Obviously the plating potential should be chosen as low as possible to obtain optimum precision.

Detection Limit. The detection limit in potentiometric stripping analysis depends on the plating time, the mercury(II) concentration, and, to some extent, on the speed of the recorder. Consequently it is not possible to uniquely define a detection limit for each element. Obviously the maximum possible plating time sets the ultimate detection limit.

To ascertain the maximum practical plating time, 80 mL of a 0.1 M hydrochloric acid solution containing 1 mg/L of mercury(II) was divided into two equal subsamples. To one of the samples 0.2 μg/L of cadmium(II), 0.5 μg/L of lead(II), and 1 μg/L of copper(II) were added. In two subsequent experiments, the samples were plated for 16 h at −0.85 V vs. SCE. The potentiometric stripping curves were of the same form as those obtained for shorter plating times. This indicated that very long plating times can be employed. The increase in potentiometric stripping signals obtained in the spiked samples indicated background values of 0.06, 0.25, 0.25 μg/L of cadmium, lead, and copper, respectively.

Accuracy. The accuracy of potentiometric stripping analysis was investigated by means of calibration plots, standard addition analysis, and by comparison with a combined solvent extraction atomic absorption method (*6*).

Linear calibration plots were obtained for all the elements indicated in Figure 2 in the concentration range 1–100 μg/L. At lower concentrations, calibration plots are less reliable since the contamination contribution is difficult to estimate. This is particularly true for lead and copper.

Standard addition analysis was performed on a sample containing 0.05 M hydrochloric acid, 0.5 M sodium chloride, and 1 mg/L of mercury(II). The sample was plated for 128

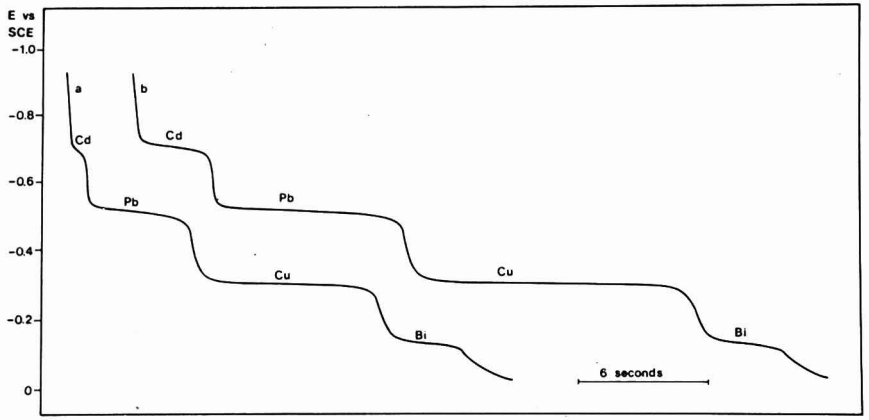


Figure 4. Potentiometric stripping curves obtained in a sample containing 0.05 M HCl, 0.5 M NaCl, and 1 mg/L of Hg(II) before and after (curve b) the addition of 0.5 μg/L of Cd(II), Pb(II), and Cu(II)

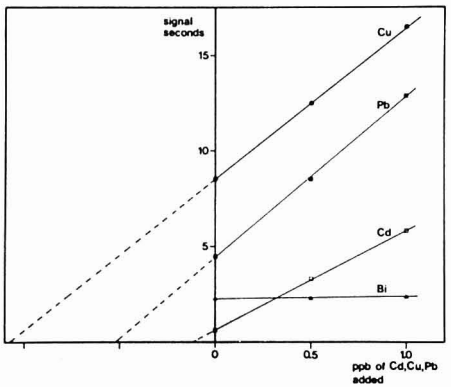


Figure 5. Standard addition analysis of a sample containing 0.05 M HCl, 0.5 M NaCl, and 1 mg/L of Hg(II). No standard addition of bismuth was made

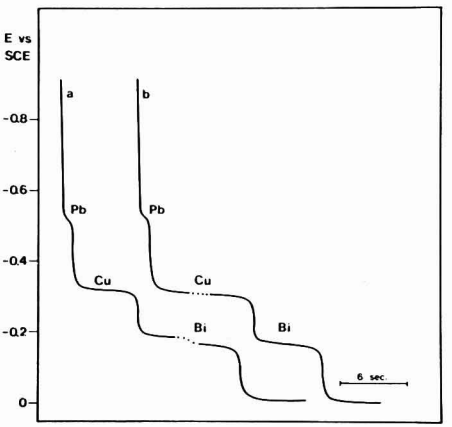


Figure 6. Potentiometric stripping curves registered in a 1 M HCl solution containing 2 mg/L of Hg(II). In curve a, the Bi(III) concentration was 100 μg/L and Cu(II) was 10 μg/L. In curve b, Bi(III) was 10 μg/L and Cu(II) was 100 μg/L. Signals from lead impurities are indicated in the two curves

minutes at −0.95 V prior to the registration of the potentiometric stripping curve which is shown as curve a of Figure 4. The potentiometric stripping curve, registered under the same experimental conditions, after the standard addition of 0.5 μg/L of cadmium, copper and lead is also shown in Figure 4 (curve b). The linear relationship between the increase in potentiometric stripping signal and the concentration after two standard addition aliquots is shown in Figure 5. The bismuth signal shown in Figure 4, which is not very well developed, because of the low concentration of hydrochloric acid, originates as a contamination from previous bismuth experiments. Bismuth was not added during the standard additions and, as seen from Figure 5, the bismuth signal did not increase during the three plating/stripping cycles.

Comparison between potentiometric stripping analysis and solvent extraction/AAS was carried out for three different samples. The results are summarized in Table III. Sample I was a cold tap water sample acidified to pH 2 with hydrochloric acid prior to analysis. Sample II was composed of mussels from the Swedish west coast which had been digested in boiling nitric acid for 1 h prior to potentiometric stripping analysis or solvent extraction. Sample III was Baltic seawater acidified to pH 1 with nitric acid during sampling. The mercury(II) concentration in all samples was adjusted to 2 mg/L and the plating time was either 16 or 32 min at −0.95 V. Both analytical procedures exploited the method of standard addition for quantification.

Interferences. Potentiometric stripping analysis is subject to two kinds of interference. One is the overlapping of the stripping signals due to similar redox potentials of the elements stripped. The other is the formation of intermetallic compounds in the mercury thin-film. According to Figure 2, stripping overlap is most likely to occur between copper and bismuth and between the thallium and cadmium. To investigate the copper–bismuth overlap, two samples, each containing 1 M hydrochloric acid and 2 mg/L of mercury(II), were prepared. To one of the samples 100 μg/L of Cu(II) and 10 μg/L of Bi(III) were added while 10 μg/L of Cu(II) and 100 μg/L of Bi(III) were added to the other. After deaeration,

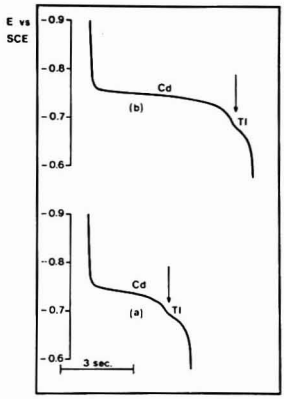


Figure 7. Potentiometric stripping curves registered in a 0.1 M HAc, 0.1 M NaAc sample containing 2 mg/L of Hg(II). In curve a, the Cd(II) and Tl(III) concentrations were each 50 μg/L while in curve b, the Cd(II) concentration had been increased to 100 μg/L

Table IV. Comparison of the Results Obtained by Potentiometric Stripping Analysis and by Combined Solvent Extraction-AAS on Three Different Samples

	potentiometric stripping analysis			solvent extraction + AAS		
sample	Cd	Pb	Cu	Cd	Pb	Cu
cold tap water, μg/L	0.08	0.90	3.1	0.11	0.76	3.6
mussels, μg/g wet weight	-	1.0	-	-	1.2	-
seawater μg/L	0.25	0.65	2.2	0.23	0.42	2.2

the samples were plated for 32 min at −0.90 V vs. SCE and the curves registered are shown in Figure 6. The stripping signal obtained from lead impurities is also visible.

The potentiometric stripping overlap between thallium and cadmium is illustrated in Figure 7. Curve a was obtained in a 0.1 M acetic acid–0.1 M sodium acetate buffer containing 50 μg/L of cadmium(II) and thallium(III) and 2 mg/L of mercury(II) after plating for 4 min at −0.90 V. Curve b was registered under the same experimental conditions except that the cadmium(II) concentration had been increased to 100 μg/L.

The most common intermetallic compound formed in the mercury phase is that between copper and zinc. In samples containing both these elements, zinc will interfere with copper and vice versa. The zinc interference with the analysis of copper can be eliminated by employing a plating potential above −0.95 V so that zinc ions are not reduced. The copper interference with the analysis of zinc can be eliminated by the addition of excess gallium(III), since the gallium–copper intermetallic compound has a higher stability constant than the corresponding zinc–copper compound. This is illustrated in Figure 8 in which a seawater sample (for composition, see Table IV), buffered with 0.05 M acetic acid–0.05 M sodium acetate has been analyzed at −1.25 V before and after the addition of 200 μg/L of gallium(III).

CONCLUSIONS

All elements which have hitherto been analyzed by anodic stripping procedures can also be analyzed by potentiometric stripping analysis. Consequently, although potentiometric stripping analysis introduces a new instrumental approach, a large number of possible analytical procedures have already been devised (e.g., reference (2)). The only modification needed is the addition of a small amount of mercury(II) ions.

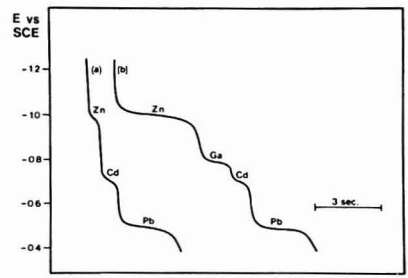


Figure 8. Effect of the addition of Ga(III) on the zinc signal in a seawater sample. Curve a was registered before and curve b after the addition of 200 μg/L of Ga(III)

One of the major advantages of potentiometric stripping analysis is the simple instrumentation required. The most expensive parts, the pH meter and/or the recorder, are standard laboratory equipment and are therefore usually already available. Since the principle of potentiometric stripping analysis does not involve the necessity for generation of potential ramps or the measurement of small currents, the potentiostat can be made very simple. More important, the measurement of potential is much simpler and reliable than the measurement of small currents.

Potentiometric stripping analysis gives a good precision, primarily because the same transport mechanism is exploited in the plating/reduction phase as in the stripping/oxidation phase. Consequently, potentiometric stripping analysis is little affected by small bubbles of gas formed on the electrode surface or by the presence of surface active agents.

Potentiometric stripping analysis is likely to give accurate results. The major reason for this is that only very few chemicals have to be added to the sample. The manipulation of the sample can also be kept at a minimum.

The detection limits in potentiometric stripping analysis are very low. Because of the limited risk for sample contamination the method ought to be well suited for the determination of low background values in, e.g., body fluids, natural waters, and beverages. In some applications, potentiometric stripping analysis is rather time-consuming. This is particularly true for samples with extremely low concentrations of analytes. However, to obtain accurate results in such samples, extreme care must be exercised. This is in itself time-consuming and although plating times of more than 1 h have to be used in potentiometric stripping analysis, this still represents only a minor fraction of the total time needed to obtain an accurate result. Moreover, when a timer/switcher controller is used, there is no need for operator control so that the analysis can be carried out unattended.

LITERATURE CITED

(1) J. Koryta, *Anal. Chim. Acta*, **61**, 329 (1972).
(2) F. Vydra, E. Julaková, and K. Stulík, "Electrochemical Stripping Analysis", Ellis Horwood Ltd, Chichester, 1976.
(3) J. B. Flato, *Anal. Chim. Acta*, **44**, 75A (1972).
(4) D. Jagner and A. Graneli, *Anal. Chim. Acta*, **83**, 19 (1976).
(5) D. Jagner and K. Årén, *Anal. Chim. Acta*, **100**, 375 (1978).
(6) L. G. Danielsson, B. Magnusson and S. Westerlund, *Anal. Chim. Acta*, **98**, 47 (1978).

RECEIVED for review March 9, 1978. Accepted August 25, 1978.

Capacitive Integration to Produce High Precision Isotope Ratio Measurements on Methyl Chloride and Methyl Bromide Samples

John F. Willey and James W. Taylor*

Department of Chemistry, University of Wisconsin, Madison, Wisconsin, 53706

A capacitive integration circuit for the measurement of ion current ratios in an isotope ratio mass spectrometer is described. Sources of error and their effect on measurement precision are discussed. Results from the isotopic analysis of methyl chloride and of methyl bromide gases are presented. The relative standard deviation of measured ratios for methyl chloride was 13 parts in 10^6 while that for methyl bromide was 7 parts in 10^6.

The measurement of heavy atom kinetic isotope effects (KIE) is used to elucidate reaction mechanisms (*1*, *2*) and to probe transition state structures (*3*, *4*). The precise measurement of isotope ratios, which are used to calculate KIE, is generally performed via isotope ratio mass spectrometry using a dual inlet, dual collector instrument specifically designed for this purpose (*5*).

Because the magnitude of the KIE is proportional to the relative mass difference of the isotopes involved, the determination of meaningful KIE values for increasingly heavier elements requires a corresponding increase in the precision with which isotope ratios may be measured. For example, chlorine leaving group KIE have a maximum value of approximately 1.01, and the instrumental precision with which chlorine isotope ratios have routinely been measured in our laboratories is 7 parts in 10^5. Bromine, an element of significant mechanistic interest, should have a maximum leaving group effect of about 1.0033. Thus it would be desirable to increase the routine measurement precision to at least 2 parts in 10^5. It is primarily for this reason that we undertook to study the sources of error in isotope ratio measurements with the aim of increasing the measurement precision.

Most modern isotope ratio instruments are based on the original design of Nier (*6*) with the modifications of McKinney et al. (*7*). In these instruments, the larger of the two ion beam currents is converted to a voltage using an operational amplifier with a large (typically 10^{11} Ω) feedback resistor and this voltage is fed to a Kelvin–Varley voltage divider. The output of the voltage divider is fed through a second large resistor to produce a current which is nulled against the smaller ion beam current using the variation in the voltage divider to approach the null condition. A second operational amplifier is used to sense accurately the approach to null, and differences smaller than the least significant digit on the voltage divider are interpolated by recording the output of the second amplifier on a strip chart recorder and measuring the residual off null signal from the chart tracings.

The factors limiting the precision of this type of circuitry are the inherent noise of the large value resistors, the large voltage and temperature coefficients for these resistors, and the ability of the operator to draw reproducibly the "best" straight line through the recorder tracings and measure the off null signal.

An alternate means of determining the ratio of the ion beam currents is a capacitive integration system described by Jackson and Young (*8*). In this system, the two ion beam currents are integrated and the output of the two integrators is inverted to obtain positive voltages which are ratioed using a $5^1/_2$ digit digital voltmeter (DVM). This system has several advantages over the conventional circuitry including (a) improved precision due to the elimination of the high value resistors and averaging of ion beam fluctuations, (b) elimination of the need for manually drawing a "best" line through a noisy recorder trace to measure the off null residuals, and (c) the availability of data in a digital form for automatic printing or computer processing.

A circuit similar to that of Jackson and Young has been constructed which avoids the use of voltage inverters. This paper discusses the various sources of error in this type of circuit and the selection of circuit components to minimize these errors. Results of measurements on methyl chloride and methyl bromide gases are presented and discussed. These gases were selected for analysis because a procedure exists for the quantitative conversion of chloride ion into methyl chloride gas (*5*), and work in these laboratories has shown that a similar conversion of bromide ion to methyl bromide is possible (*9*).

EXPERIMENTAL

The capacitive integration circuit is shown schematically in Figure 1. The amplifiers are Teledyne Philbrick model 1702-01 (Teledyne Philbrick Co., Dedham, Mass.). These units have a specified bias current of 5×10^{-15} A (max) with a temperature coefficient of 2×10^{-15} A/°C. The output noise in the 0.016 to 1.6 Hz frequency range is 10 μV p-p. The amplifiers are mounted in Teflon insulated sockets (Teledyne Philbrick model 6123).

The capacitors are hermetically sealed Teflon dielectric capacitors (Series D51D, Component Research Co., Santa Monica, Calif.). Teflon capacitors were chosen because of their high insulation resistance, low dielectric adsorption coefficient, and low temperature coefficient. They are rated for 200 V and have a specified minimum insulation resistance of 10^{13} Ω.

The reed relays were a custom order item (Coto-Coil Co., Inc., Providence, R.I., engineering number E-8246) and consist of a Hamlin model MRH-15 Form A relay (Hamlin, Inc., Lake Mills, Wis.) wound for 12 V dc operation and fitted with complete electrostatic shielding. They are operated at 8 V dc and are fitted with 1N48 diodes across the coils to suppress transients when the coils are de-energized. A 1000-Ω resistor is placed in series with each relay to limit the discharge rate of the capacitors and avoid dielectric strain.

The manual switches were constructed as single pole, single throw switches with beryllium copper contacts which are isolated on Teflon standoffs. These switches were patterned after the zero check switch of a Keithley Model 602 solid state electrometer (Keithley Instruments, Inc., Cleveland, Ohio). The switch shafts are sealed with O-rings so that the circuit boxes can be desiccated. The open contact resistance of these switches was measured to be greater than 10^{14} Ω.

The operating sequence is controlled by a cam actuated, motor driven timer (Model 540, Cramer Division, Conrac Corporation, Old Saybrook, Conn.) with six single pole, double throw switches. The total cycle time may be selected as 90, 135, or 180 s by changing the gear ratio. Each of the controlled events (e.g., reed relay opening/closing, DVM data hold, gas valve switching, etc.) may be individually adjusted by the proper positioning of the cams

0003-2700/78/0350-1930$01.00/0 © 1978 American Chemical Society

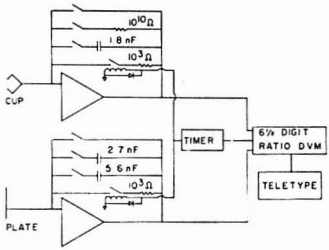


Figure 1. Schematic of capacitive integration circuit

on the timer shaft. Typically a 135-s cycle is used with a 60-s integration time. A typical operating sequence is as follows.

(1) The reed relays are opened and integration begins.

(2) After a delay to allow the plate circuit integrator to reach a voltage greater than 5 V (the minimum reference voltage required by the DVM), the hold mode on the DVM is released and the ratio of the integrator outputs is displayed.

(3) Sixty seconds after the start of integration, the hold mode of the DVM is actuated and the final ratio value is transmitted to the Teletype.

(4) The reed relays are closed, thus discharging the capacitors.

(5) The gas valve assembly is switched such that the gas from the other half of the dual inlet system is fed into the mass spectrometer source. The instrument is allowed to stabilize with this new gas for 75 s.

(6) The cycle is repeated.

The digital voltmeter is a Julie Model DM 1010PM (Julie Research Laboratories, Inc., New York, N.Y.). This is a $6^1/_2$ digit unit which operates on the principle of an auto-balancing reed switched Kelvin–Varley voltage divider. It has an accuracy in the ratio mode of better than 1 part in 10^6, and thus will not be the limiting factor in the overall measurement precision. It is capable of ratioing negative voltages directly so inverters can be avoided.

The output of the DVM is interfaced to a Comdata Modified ASR33 Teletype (ComData Corp., Skokie, Ill.).

The mass spectrometer used for these studies was a Nuclide Model 6-60 RMS (Nuclide Corporation, State College, Pa.). It has been modified by the addition of an externally adjustable source slit assembly. This assembly consists of two fixed slits of 0.30-mm width with the second slit located 9 mm behind the first slit. Each of the slits may be independently translated by means of micrometers with bellows sealed feedthroughs.

For the analysis of methyl chloride gases, the mass spectrometer is operated at an accelerating potential of 4.0 kV and the source filament is regulated to maintain a constant source trap current of 200 μA. The source slits are centered. The sample and standard pressures are adjusted such that the ion beam currents for the m/z 52 ions ($CH_3{}^{37}Cl$) are between 1.99000×10^{-10} and 2.00000×10^{-10} A and are matched to within 3×10^{-13} A. This requires a sample inlet pressure of approximately 12 Torr. The cup circuit and plate circuit capacitors are 0.0018 μF (1.8 nF) and 0.0056 μF (5.6 nF), respectively.

For the analysis of methyl bromide samples, an accelerating potential of 3.8 kV is used and the source trap current is regulated at 200 μA. The slits are narrowed by moving the front slit 0.18 mm toward the center of curvature of the ion path and the rear slit 0.01 mm away from the center of curvature. The sample and standard pressures are adjusted such that the ion beam currents for the m/z 96 ions ($CH_3{}^{81}Br$) are between 2.49000×10^{-10} and 2.50000×10^{-10} A and are matched to within 3×10^{-13} A. This requires an inlet pressure of approximately 7 Torr. The cup circuit and plate circuit capacitors are 0.0018 μF (1.8 nF) and 0.0027 μF (2.7 nF), respectively.

Upon the initial introduction of either methyl chloride or methyl bromide gas to the instrument, it is observed that the intensity of the ion beam currents drifts steadily downward. The rate of drift decreases with time and it has been found necessary to allow a 2-h stabilization period before any ratio measurements are made.

RESULTS AND DISCUSSION

In isotope ratio work, it is the *relative difference* between the measured ratios for the standard and sample gases which is used in determining the isotopic composition of the unknown gas. This relative difference may be calculated using Equation 1.

$$\text{relative difference} = \frac{R_s - R_u}{R_s} = 1 - \frac{R_u}{R_s} \qquad (1)$$

where R_u is the measured ion current ratio for the unknown gas, and R_s is the measured ion current ratio for the standard gas.

Instrumental Factors Affecting Precision. In the capacitive integration circuit, the precision of the relative difference is limited by variations in the amplifier bias currents, leakage currents, switching transients, and amplifier input voltage noise (flicker). The theoretical limit to the precision arises from statistical variations in the ion beam intensity. The influence of each of these factors on circuit design and performance will be discussed separately. In this context the errors considered here are only those associated with the electronic processing of the detector responses. Other factors such as peak overlap, valve leakage, and background pressure will also affect the measurement results and have been discussed in detail by Deines (*10*) and by Mook and Grootes (*11*).

Bias Currents. The operational amplifier bias currents are integrated along with the currents from the detectors and will thus constitute a source of error. The output of the integrator may be expressed as

$$V_o = \frac{-1}{C}\int_0^t (I_i + I_b)dt = \frac{-t}{C}(I_i + I_b) \qquad (2)$$

where I_i is the ion beam current, I_b is the amplifier bias current, t is the integration time (in seconds), and C is the capacitance (in farads). From typical values for the ratios and ion currents and by using the manufacturer's specification of $\pm 5 \times 10^{-15}$ A for the bias current, it can be shown that the bias currents contribute equally to the integrations for both the sample and standard gases and, thus, introduce no error at the part-per-million level provided the bias currents remain the same during the period in which the ratios for both the standard and sample gases are measured.

Leakage Currents. The transfer of charge to or from the input of the operational amplifier via any path other than from the detector or the active feedback component will give rise to an error signal. To minimize these currents, all elements were insulated with Teflon and components of the feedback loop were selected to provide maximum insulation resistance. In addition, the circuit was thoroughly degreased after assembly. Further, because surface conduction across insulators increases with high relative humidity, the circuit box was sealed and desiccated with Drierite (calcium sulfate).

Switching Transients. Switching transients may occur as the reed relays open to initiate the integration cycle. The reed relays were constructed with electrostatic shielding to minimize this but, when initially tested, shifts in the integrator output upon reed opening of up to 2.5 mV were observed using a Biomation Model 802 Transient Recorder. Reduction of the coil voltage from 12 V to 8 V and the addition of diode coil suppression reduced these shifts to below the limits of detectability (estimated to be 0.05 mV).

Amplifier Voltage Noise. Fluctuations in the input offset voltage (input voltage noise) will cause corresponding fluctuations in the output voltage. The specified input noise for the Teledyne Philbrick model 1702-01 amplifier in the low frequency range (0.016 to 1.6 Hz) is 10 μV peak to peak. The measured ratio value would be most affected if the error in

the output of one amplifier were +5 μV and that of the other amplifier were −5 μV at the time when the final ratio value was recorded. If, at the end of the next integration period, the offset voltage values were reversed (−5 μV and +5 μV), then the maximum error in the relative difference value between these two ratios would be observed. Under these conditions, and assuming typical current and voltage values for methyl bromide samples, the value calculated for the relative difference would be in error by 0.000002.

Statistical Variation in Ion Beam Intensity. The ultimate limit to the measurement precision is the statistical variation of the ion beams. The random distribution in time of the ions gives rise to fluctuations in the instantaneous currents. The uncertainty in the measurement of the ion beam current is related to the number of ions collected (N) according to Equation 3 (*12*).

$$\sigma_N = \sqrt{N} \tag{3}$$

The integrator voltage is related to N by Equation 4

$$V = \frac{Q_e}{C} N \tag{4}$$

where Q_e is the charge per ion (1.6×10^{-19} C per ion for singly charged ions) and C is the capacitance in farads. Thus, by propagation of errors (*13*), the relative error in the integrator voltage is

$$\frac{\sigma_v}{V} = \left[\left[\frac{1}{V}\frac{\delta V}{\delta N}\right]^2 \sigma_N{}^2\right]^{1/2} = \frac{Q_e}{VC}\sqrt{N} = \frac{1}{\sqrt{N}} \tag{5}$$

Similarly, because the measured ratio is the ratio of the two integrator voltages, the relative uncertainty in the ratio is given by

$$\begin{aligned}\frac{\sigma_R}{R} &= \left[\left(\frac{1}{R}\frac{\delta R}{V_1}\right)^2 \sigma_{V_1}{}^2 + \left(\frac{1}{R}\frac{\delta R}{\delta V_2}\right)^2 \sigma_{V_2}{}^2\right]^{1/2} \\ &= \left[\frac{1}{R^2 V_2{}^2}\frac{V_1{}^2}{N_1} + \frac{V_1{}^2}{R^2 V_2{}^4}\frac{V_2{}^2}{N_2}\right]^{1/2} \\ &= \left(\frac{1}{N_1} + \frac{1}{N_2}\right)^{1/2}\end{aligned} \tag{6}$$

Under normal operating conditions for methyl bromide, the output voltages at the end of the integration cycle are approximately 9.3 V and 9.7 V for the cup and plate circuits, respectively. From Equation 4, the values of N_1 and N_2 are calculated to be 1.0×10^{11} and 1.6×10^{11}. The statistical limit to the relative uncertainty in the measured ratio values calculated from Equation 6 is then 4.0 parts in 10^6. The uncertainty in the relative difference values (which are calculated from the ratio of these ratios) would then be about 5.5×10^{-6}.

Statistical Treatment of Data. The measured ratios for one sample and standard of methyl bromide are listed in Table I. It can be seen that the ratios for both the standard and sample drift downward during the course of the measurements. This is typical of the results although occasional data sets show an upward drift or a reversal. The drift for both, however, is always in the same direction. The origin of this drift is unknown but is believed to be related to the drift in ion currents. The presence of this drift complicates somewhat the procedure for calculating the relative difference between the sample and standard ratios. In the absence of a technique for random switching, it is possible to correct for this drift mathematically by fitting all of the ratios for both the standard and sample to a quadratic line using a least squares fit with a dummy shift variable (*14*). In this method, the data are fit

Table I. Measured Ratios for a Sample of Methyl Bromide

entry	standard ratios	sample ratios
1	0.956 889	0.955 813
2	0.956 660	0.955 802
3	0.956 882	0.955 795
4	0.956 881	0.955 783
5	0.956 870	0.955 768
6	0.956 859	0.955 756
7	0.956 850	0.955 743
8	0.956 827	0.955 729
9	0.956 805	0.955 713
10	0.956 795	0.955 705
11	0.956 790	0.955 693
12	0.956 771	

to a line described by Equation 7 where x is the order (time) variable

$$y = ax^2 + bx + c + dz \tag{7}$$

such that $x = 1$ for the first measured ratio, $x = 2$ for the second measured ratio, etc. The dummy shift variable, z, is assigned a value of 1 for each standard ratio and 0 for each sample ratio. The values of y used for the fit are $y_i = R_i/R_s$, where R_s is the average of all of the ratios measured for the standard gas. The effect of this fitting process is that the ratios for both the standard and sample gas are fit to a single line by selecting the value of d which shifts the standard ratios to fit with the sample ratios. The resulting value for d is the average relative difference between the sample and standard ratios.

This type of regression analysis is possible using the Minitab II statistical package developed at Pennsylvania State University, Department of Statistics. Using this program provides not only the value of d but the standard deviation of y about the regresson line, the standard deviation of d, and a table of the standardized residuals. (The standardized residual is the residual, y observed − y predicted, divided by the estimated standard deviation.) Also a "scatter plot" of standardized residuals vs. x and a histogram of the standardized residuals is provided as a convenient visual check for systematic errors and outliers.

Outliers, ratios which are widely deviant from the least squares line, are occasionally observed. Entry 2 of column 1 in Table I is an example of one such point. The most common source of these is believed to be irreproducible valve seating in the glass ball valves which are used to select which of the two gases in the dual inlet system is introduced into the mass spectrometer. To determine when a data point is sufficiently deviant to be discarded, a Dixon Test (*15*) is applied to the standardized residuals at the 0.05 level of significance. The frequency of occurrence of outliers is about 2%, that is, 15 outliers were found in a total of about 900 data points representing 45 analyses on methyl bromide.

Methyl Chloride. Four samples of methyl chloride which had previously been analyzed on this instrument using conventional null detecting circuitry were analyzed using the capacitive integration circuitry. The results are listed in Table II. A plot of the relative difference values determined via capacitive integration vs. those determined via null detection had a linear least squares slope of 1.05 (standard deviation = 0.06) and a correlation coefficient of 0.996. These results indicate that the relative differences obtained from both circuits are equivalent. The average standard error for the null detecting circuit was 3.02×10^{-5} while that for the capacitive integration circuit was 5.25×10^{-6}. This represents an improvement in precision of better than a factor of 5.

Methyl Bromide. Forty-five samples of methyl bromide have been analyzed. The average standard deviation of y

Table II. Results for Methyl Chloride Samples Analyzed via Null Detecting and Capacitive Integration Circuitry

Sample[c]	calculated relative difference values[a] (and standard errors)[b] 1	2	3	4
null detecting	0.010 261 (0.000 034)	0.009 972 (0.000 031)	0.009 655 (0.000 030)	0.008 758 (0.000 026)
capacitive integration	0.010 179 (0.000 005)	0.009 926 (0.000 005)	0.009 720 (0.000 005)	0.008 770 (0.000 006)

[a] The reported relative differences were calculated using the least squares regression, with shift variable, as described in the discussion of Equation 4. [b] The standard error values are the standard deviations of the calculated shift variable. All data sets contained 10 to 12 ratio measurements for each of the two gases (sample and standard). [c] These samples represent various fractions of reaction so the actual measured ratios are not expected to be the same for each sample.

Table III. Results of Day to Day Precision Study on Methyl Bromide

	relative differences (and standard errors) sample 1	sample 2	sample 3
day 1	0.001 149 (0.000 003)	0.001 157 (0.000 003)	0.001 153 (0.000 003)
day 2	0.001 149 (0.000 003)	0.001 136 (0.000 003)	0.001 147 (0.000 003)
day 3	0.001 137 (0.000 002)	0.001 154 (0.000 003)	0.001 149 (0.000 004)

about the regression line (from Equation 7) was 7.6×10^{-6}. This corresponds to a relative standard deviation of the measured ratios of 8 parts in 10^6. The average standard deviation of the shift variable was 3.4×10^{-6}. Comparison of these results with those obtained for methyl chloride indicates that the experimental precision is better for the data obtained on methyl bromide. The errors reflected in these data are a combination of the errors inherent in the electronics, the statistical fluctuations in the ion beam intensities, and the errors introduced by other instrumental factors such as peak overlap and background pressure. Since the error inherent in the electronics should be the same regardless of the nature of the ions which make up the ion beam current, and the contribution from ion beam fluctuations is nearly the same (3.7 parts in 10^6 for methyl chloride vs. 4.0 parts in 10^6 for methyl bromide), it seems probable that the difference in the precision observed for the two gases arises from instrumental factors relating to the mass spectrometer itself. This is especially likely in light of the fact that a great deal of effort was expended in maximizing the instrumental performance for methyl bromide while the methyl chloride data were obtained with the instrument operated under the same conditions normally used with the null detecting circuitry.

To test the day to day repeatability, three identical bromide samples were converted to methyl bromide and were run on each of three days. The results are presented in Table III. A one-way analysis of variance with the data grouped according to day run was carried out using the procedures described by Wetherill (*16*). The calculated F value to test the null hypothesis that the groups all have the same mean was 1.36. The F (2, 6) value at 5% from the F-table (*17*) is 5.14. Thus there was no significant difference between the values obtained on the different days.

The standard deviation of the nine values in Table III was 7.2×10^{-6}. This is larger than the average of the standard deviation of the shift variables of the 45 analyses cited above (3.4×10^6). This indicates that there is a run to run variation which is larger than the variation within a single run. The largest single factor contributing to this variation is believed to be the matching of the sample and standard gas pressures prior to the run and the amount of pressure mismatch which develops during the time that the ratios are being measured (45 min for 20 ratios). The effects of pressure mismatch have been studied by Mook and Grootes (*11*) with the conclusion that changes in ion beam broadening caused by ion molecule collisions are a major contribution to this effect.

CONCLUSIONS

The ability of capacitive integration to increase the precision with which relative isotope ratios may be determined has been demonstrated for methyl chloride and methyl bromide. In addition to increased precision, the use of capacitive integration also has the advantages that the data are available in a digital form for automatic printing or computer analysis, and the need for manually drawing the "best" line through a noisy recorder trace and making measurements from these tracings is eliminated.

ACKNOWLEDGMENT

The authors express their appreciation to Paul Bender and Ted DiFiore for their aid with the isotope-ratio instrument and to Ted Weigt for his circuit design and aid in the interfacing to the teletype.

LITERATURE CITED

(1) A. Fry in "Isotope Effects in Chemical Reactions", C. J. Collins and N. S. Bowman, Ed., Van-Nostrand Reinhold, New York, N.Y., 1970.
(2) D. G. Graczyk and J. W. Taylor, *J. Am. Chem. Soc.*, **96**, 3255 (1974).
(3) R. C. Williams and J. W. Taylor, *J. Am. Chem. Soc.*, **96**, 3721 (1974).
(4) R. L. Julian and J. W. Taylor, *J. Am. Chem. Soc.*, **98**, 5238 (1976).
(5) J. W. Taylor and E. P. Grimsrud, *Anal. Chem.*, **41**, 805 (1969).
(6) A. O. Nier, *Rev. Sci. Instrum.*, **18**, 398 (1947).
(7) C. R. McKinney, J. M. McCrea, S. Epstein, H. A. Allen, and H. C. Urey, *Rev. Sci. Instrum.*, **21**, 724 (1950).
(8) M. C. Jackson and W. A. Young, *Rev. Sci. Instrum.*, **44**, 32 (1973).
(9) J. F. Willey and J. W. Taylor, Department of Chemistry, University of Wisconsin, Madison, Wis., unpublished work, 1977.
(10) P. Deines, *Int. J. Mass Spectrom. Ion Phys.*, **4**, 283 (1970).
(11) W. G. Mook and P. M. Grootes, *Int. J. Mass Spectrom. Ion Phys.*, **12**, 273 (1973).
(12) W. J. Dixon and F. J. Massey, Jr., "Introduction to Statistical Analysis", 3rd ed., McGraw-Hill, New York, N.Y., 1969, p 248.
(13) H. D. Young, "Statistical Treatment of Data", McGraw-Hill, New York, N.Y., 1962, p 96–101.
(14) N. R. Draper and H. Smith, "Applied Regression Analysis", John Wiley & Sons, New York, N.Y., 1966, p 134–137.
(15) W. J. Dixon, *Biometrics*, **9**, 74 (1953).
(16) G. B. Wetherill, "Elementary Statistical Methods", Chapman and Hall, London, 1972, p 270–271.
(17) Ref. 12, p 470.

RECEIVED for review June 5, 1978. Accepted July 24, 1978. The authors gratefully acknowledge the support of the National Science Foundation (Grant MPS 75-21059). Purchase of the mass spectrometer and digital voltmeter was made possible through funds from the Wisconsin Alumni Research Foundation and from the Chemistry Department. Portions of the work were presented at the American Society for Mass Spectrometry Meeting in Houston, Texas, May 1975.

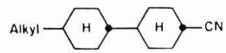
CORRESPONDENCE

High-Resolution Nuclear Magnetic Resonance Spectrometry in Thermotropic Nematic Liquid Crystals with Negative Diamagnetic Anisotropy

Sir: It has hardly been possible to keep pace with the number of papers appearing on the subject of high-resolution NMR spectrometry in liquid crystals since the fundamental studies by Saupe and Englert (*1*, *2*). Investigations in this field have been carried out mainly in thermotropic nematic liquid crystals which had without exception a positive diamagnetic anisotropy $\Delta X = X_{\parallel} - X_{\perp}$, $X_{\parallel}$ and $X_{\perp}$ being the diamagnetic susceptibility parallel and perpendicular to the preferred direction of the long axis (director) of the liquid crystal molecules. Since every system aligns itself with the axis of its greatest susceptibility in the direction of the field, "diamagnetic positive" liquid crystals orient themselves with their director always parallel to a magnetic field (Figure 1a).

In NMR measurements, it is a common technique to rapidly spin the sample tube oriented perpendicular to the magnetic field, in order to average out residual inhomogenities in the sample and thus to improve resolution. Since direction-dependent properties of molecules are investigated by NMR in liquid crystals, a constant orientation of the dissolved molecules in the magnetic field is necessary. Therefore it has not been possible to use spinning techniques in nematic solvents, since spinning would destroy this orientation, unless the liquid crystal is oriented perpendicular to the magnetic field by an additional electric field, or the sample tube is aligned in the direction of the field as in superconducting magnets. NMR signals in a nematic solvent therefore generally manifest half-height width much larger than in isotropic solutions with sample spinning. Corresponding nonspinning spectra are consequently characterized by a comparatively low detection sensitivity (small signal/noise ratio) and resolution.

The purely alicyclic *trans,trans*-4-alkyl-4′-cyanocyclohexylcyclohexanes (I)



I

recently described by R. Eidenschink et al. (*3*) represent a new class of liquid crystals which, in contrast to previous concepts on conditions which influence liquid crystal properties, manifest stable and broad mesophases (see Table I). Maier and Saupe (*4–6*) who postulate clearing points to be proportional to molecular anisotropy of polarizability, molecules of type I should be expected to exhibit no enantiotropic nematic properties or, at the most, very low clearing points. According to their molecular structure, these liquid crystals have no UV absorption above 200 nm, and thus are interesting anisotropic solvents for UV and fluorescence spectroscopy (*7*). In addition to a positive dielectric anisotropy $\Delta\epsilon = \epsilon_{\parallel} - \epsilon_{\perp}$ between +3 and +4, they possess a negative diamagnetic anisotropy (*8*) of approximately $\Delta X = -2 \times 10^{-8}$ [cm^3 g^{-1}] with $X_{\perp} = -7.4 \times 10^{-7}$ [cm^3 g^{-1}] (*9*). They are thus the first known class of thermotropic-nematic liquid crystals with this property, since no reference has hitherto been made to nematic substances with negative anisotropy of susceptibility except for a paper by E. Sackmann et al. (*10*) on nematic systems of compensated cholesteric liquid crystals.

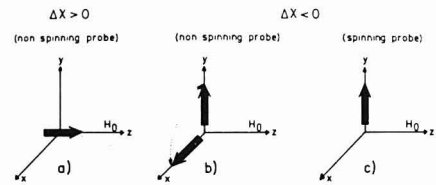


Figure 1. Orientation of the director in a nematic liquid crystal aligned by a magnetic field for molecules with positive diamagnetic anisotropy (a) and with negative diamagnetic anisotropy in a non-ordered (b) and ordered (c) state

Table I. Physical Data of *trans,trans*-4-Alkyl-(bicyclohexyl)-4′-carbonitriles I[a]

R =		C_3H_7–	C_5H_{11}–	C_7H_{15}–	ZLI-1167
Mp	[°C]	58	62	71	8
Clp	[°C]	80	85	83	83
S_1–S_G	[°C]	(18)			
S_G–S_H	[°C]	(44)	(39)		
S_H–N	[°C]	(57)	(50)		
S –N	[°C]				32
ΔH	[kcal/Mol]	6,4	6,7	8,1	

[a] ZLI-1167 is a ternary eutectic of propyl-, pentyl- and heptylbicyclohexylcarbonitrile I. S_x and N are abbreviations for smectic and nematic transitions. Monotropic transitions are in parentheses.

Because of their negative diamagnetic anisotropy, liquid crystalline bicyclohexane molecules should align themselves in a plane perpendicular to a magnetic field, initially without a preferred orientation of their longitudinal axis in between this plane (Figure 1b). In a sample tube which is spun normal to the magnetic field, those molecules not oriented in the spinning axis must experience a torque, tending to align all of them homogeneously in the long axis of the tube, and thus forming a uniaxial nematic liquid crystal with the director field oriented in the rotation axis (Figure 1c). Since dissolved molecules are aligned uniformly with the liquid crystal matrix, they no longer experience a change in orientation with respect to the magnetic field by sample spinning. Therefore liquid

0003-2700/78/0350-1934$01.00/0 © 1978 American Chemical Society

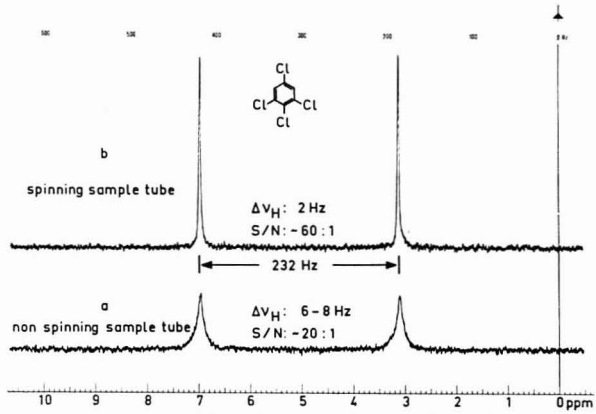


Figure 2. ^{1}H NMR spectrum of a 0.5 M solution of 1,2,3,5-tetrachlorobenzene in the nematic solvent ZLI-1167 at room temperature measured with nonspinning sample tube (lower curve) and spinning sample tube (upper curve)

crystals of type I should permit the common spinning technique in NMR and hence enable an improved resolution comparable to that of measurements in isotropic solutions.

EXPERIMENTAL

Measurements were performed with a Varian NMR spectrometer EM-360 at room temperature. Commercial sample tubes (Wilmad Glass Co.) were used with 5.0-mm o.d., 4.2-mm i.d., and 190-mm length. The nematic solvent was ZLI-1167 (product of E. Merck, Darmstadt, and EM Laboratories, Elmsford N.Y.). This solvent is a ternary eutectic of the three "diamagnetic negative" propyl-, pentyl-, and heptylbicyclohexylcarbonitriles, which is liquid crystalline between +8 and +83 °C. The commercially available 1,2,3,5-tetrachlorobenzene (Schuchard, Munich) was purified by recrystallization and dissolved in ZLI-1167 at 80 °C, i.e., above the clearing point of the nematic solution, in order to achieve a homogeneous sample.

RESULTS AND DISCUSSION

Figure 2 illustrates the ^{1}H NMR spectrum of a 0.5 M nematic solution of 1,2,3,5-tetrachlorobenzene using a nonspinning sample tube (lower curve). It is characterized by a half-height width of 6–8 Hz, which concurs with that published by G. Englert and A. Saupe in 1964 (2). When the sample tube is spun at a speed greater than 20 Hz (all other instrumental parameters remained unchanged), a dramatic change takes place (see upper curve).

Resolution and signal-to-noise ratio are increased by a factor of 3, whereas splitting remains unchanged. Despite the high concentration of dissolved substance, a spectrum is obtained with a half-height width of the signals of 2 Hz, i.e., a resolution common in isotropic solvents. Simultaneously, the probe, cloudy before rotating, has become transparent without any light scattering over the total sample volume, indicating a high-ordered liquid crystal with $S_\parallel$ near +1 and $S_\perp$ near −0.5, $S_\parallel$ and $S_\perp$ being the order parameter in the rotation axis and in magnetic field direction, respectively. When spinning is stopped, the original low resolutions and small signal-to-noise ratio again is to be observed, whereas the optical appearance of the probe remains unchanged even for hours and also outside the magnet gap of the spectrometer. By changing from "dynamic" to "static" drive mode, improvement and deterioration of resolution can be reproduced. Thus the observed improvement cannot be related to molecular ordering phenomena but has to be explained as an effect of averaging out magnetic field inhomogeneities in a probe, in which magnetic field and spinning procedure have transformed the nematic solution into a uniaxial liquid crystal, the director of which oriented orthogonal to the field and in the axis of rotation. Only in such a nematic system, spinning does not affect the orientation of molecules under investigation and makes possible a reduction of inhomogeneities by sample spinning. Measurements on benzene have shown that, with appropriate experimental skill, a resolution even better than 1.0 Hz can be achieved in this new type of nematic solvents (*11*).

Although the nematic solvent ZLI-1167 has a relative small negative diamagnetic anisotropy, nonetheless the specific behavior, theoretically expected from such a type of liquid crystals, can be observed experimentally and utilized already in a magnetic field of 14 000 Gauss as demonstrated. Thus, bicyclohexanes of type I represent a new class of anisotropic solvents, which open up in conventional magnets a high resolution NMR spectrometry in nematic liquid crystals previously possible only in isotropic solvents.

LITERATURE CITED

(1) A. Saupe and G. Englert, *Phys. Rev. Lett.*, **11**, 462 (1963).
(2) G. Englert and A. Saupe, *Z. Naturforsch A*, **19**, 172 (1964).
(3) R. Eidenschink, D. Erdmann, J. Krause, and L. Pohl, *Angew. Chem.*, **90** (2), 133 (1978).
(4) W. Maier and A. Saupe, *Z. Naturforsch. A*, **13**, 564 (1958).
(5) W. Maier and A. Saupe, *Z. Naturforsch. A*, **14**, 882 (1959).
(6) W. Maier and A. Saupe, *Z. Naturforsch. A*, **15**, 287 (1960).
(7) H. Wedel and W. Haase, *Chem. Phys. Lett.*, **55** (1), 96 (1978).
(8) L. Pohl, R. Eidenschink, J. Krause, and G. Weber, *Phys. Lett. A*, **65** (2), 169 (1978).
(9) H. Schad, G. Baur, and G. Meier, presented at the Seventh International Liquid Crystal Conference, Bordeaux, France, July 1978.
(10) E. Sackmann, E. Meiboom, and L. C. Snyder, *J. Am. Chem. Soc.*, **89**, 5981 (1967).
(11) P. Diehl, Universität Basel, Switzerland, private communication, 1978.

Ludwig Pohl*
Rudolf Eidenschink

E. Merck
Darmstadt, Germany

RECEIVED for review January 16, 1978. Accepted August 16, 1978.

Thermal Effects upon Spatial Mode Structure of a Linear Flashlamp-Pumped Dye Laser

Sir: The ability of a double beam spectrometer to compensate for changes in pulse energy of a pulsed dye laser has been found to be influenced by the reproducibility of the spatial mode structure of the laser beam from one pulse to the next (*1*). Reproducible cross section intensity patterns are important because the two beams of a double beam system usually do not respond with the same relative sensitivities to all corresponding cross-sectional regions of the two beams. This might be due, for instance, to detectors that have nonuniform responses across their surfaces, or to randomly located imperfections in the optical components through which the two beams pass. A pulse to pulse shift in the most intense region of the beam, for example, from the right hand side to the left hand side of the beam, could cause a significant change in the ratio of the signals produced by the two beams, even though the pulse energy did not change.

We have studied the influence of the temperature difference between the cooling water and dye solution upon the spatial mode structure and energy reproducibility of a flashlamp pumped dye laser beam, used in a double beam atomic absorption and fluorescence spectrometer (*1*, *2*). The laser was a CMX-4 (Chromatix, Sunnyvale, Calif.) with a birefrigent filter for coarse wavelength selection and a Fabry–Perot etalon for fine wavelength selection. The dye tube and a linear flashlamp are located, respectively, at the two foci of an ellipsoidal reflector. The flashlamp is cooled by dry nitrogen which passes through a tube coaxial with the flashlamp.

Cooling water flows throughout the ellipsoidal reflector cavity and is therefore in direct contact with the dye tube. The laser cavity has a plane front mirror and a slightly concave rear mirror. The dye was 1.1×10^{-4} M R640 (Exciton Chemical Co., Inc., Dayton, Ohio) in a solvent containing equal volumes of water and methanol.

Because the cooling water in our laboratory was frequently above the maximum of 20 °C specified by the manufacturer, the cooling system of the laser was modified to include a refrigerated water bath. Consequently, the measurements discussed below were not made for the regular cooling system supplied with the laser. The temperature of the dye was controlled independently of the laser cooling water, and the temperatures of the dye and water were stable to within 0.1 °C for each set of measurements.

The spatial mode structure of a horizontal section of the laser beam was obtained by directing the 3-mm diameter laser beam through a 0.5-mm horizontal slit to a 500-channel, one-dimensional vidicon (Princeton Applied Research Corp., Princeton, N.J.). Beam attenuators were used to prevent saturation of the vidicon. Total laser energy and the response of each of the 500 vidicon channels were transferred to a computer for 20 successive laser pulses and then stored on tape for later analysis. The laser pulse rate was 1 Hz, and was synchronized with the sweep of the vidicon. The reproducibility of the mode structure at each dye temperature was observed by superimposing on an X-Y recorder the intensity vs. channel number plots for all 20 laser pulses. Examples for three different temperature differences are shown in Figure 1. Plots for each separate shot were also obtained.

It was apparent from the superimposed plots that the mode structure within the horizontal sample of the beam was most reproducible when the dye temperature was from 0.5 °C cooler than the ellipsoidal cavity water to 2.0 °C warmer. Reproducibilities within the most intense, and therefore most influential, regions of the sampled section of the beam were studied. For this temperature range, the intensities within each of the most intense spatial regions deviated by only 10 to 20% from the mean value for the 20 shots in a data set. This was also the temperature range where the relative standard deviation of the energy of the laser pulses was the best, 4–5%.

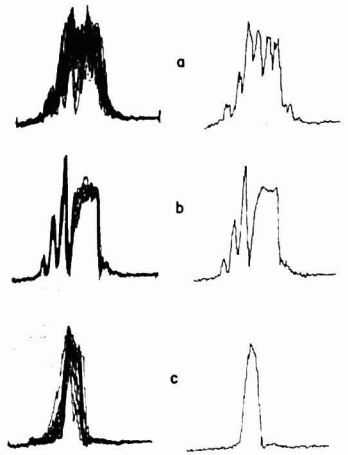


Figure 1. Mode structure pattern (intensity vs. position) along a 0.5-mm slice of the flashlamp pumped laser beam. Typical pattern for a single shot (right) and 20 superimposed patterns from successive laser pulses (left). (a) Dye 3.3 °C cooler than water, (b) dye 0.3 °C cooler than water, and (c) dye 3.6 °C warmer than water

Outside of the best temperature range, from a dye temperature 1.0 °C cooler to 4.9 °C cooler and from a dye temperature 3.0 °C warmer to 5.8 °C warmer than the cavity water, the mode structure varied dramatically from pulse to pulse. The intensities within narrow parts of the most intense regions typically varied by factors of 2 to 6 from one pulse to the next. The standard deviation of the total energy of the entire beam from pulse to pulse was worse in these temperature ranges, becoming as poor as 50% when the dye was 5.8 °C warmer than the water.

These effects seem to be due to the influence of thermal focusing which is caused by a gradient in temperature from the outside of the dye to the center of the dye when the water flowing around the dye cell is at a different temperature than the dye. The temperature gradient is accompanied by a gradient in refractive index, which causes the dye to act like a lens (*3*). When the dye is cool in the center, the thermal lens is convergent. Adding a convergent lens to the laser cavity degrades spatial selectivity and increases the divergence of the laser beam, producing a wider beam as shown in Figure 1a. Random optical fluctuations in the cavity may then allow the development of intense rays in random directions, causing dramatic changes in the intensity distribution pattern across the beam.

When the dye is warmer in the center than around its circumference, the thermal lens is divergent, and the cavity increases its spatial selectivity by becoming more like the

0003-2700/78/0350-1936$01.00/0 © 1978 American Chemical Society

parallel plane mirror configuration. The parallel plane configuration boarders on being an unstable cavity resonator, and random optical fluctuations in the cavity can readily reduce the development of lasing in random areas of the beam by causing the rays to scatter or quickly walk out of the cavity. The more selective cavity produces a narrower beam, Figure 1c, but the effects of random optical fluctuations become more critical causing larger shot-to-shot energy fluctuations.

The dye temperature region corresponding to the generation of the most reproducible mode structure apparently produces a compromise cavity configuration that does not let random optical fluctuations generate too many widely divergent rays, when the thermal lens is too convergent on the one hand, or cause too many random cavity losses when the divergent thermal lens produces a less stable configuration on the other hand. In any case, we have found that careful control of the temperature difference between the dye and the water in the ellipsoidal cavity is necessary to obtain reproducible mode structure. Temperature difference control and knowledge about other experimental conditions that influence the noise level of a laser double beam spectrometer system (2), have helped to produce a reliable system for analytical measurements.

ACKNOWLEDGMENT

The authors wish to express appreciation to Princeton Applied Research Corp. for their loan of the vidicon system.

LITERATURE CITED

(1) J. W. Hosch and E. H. Piepmeier, *Appl. Spectrosc.*, Sept./Oct. (1978).
(2) J. W. Hosch and E. H. Piepmeier, *Appl. Spectrosc.*, Sept./Oct. (1978).
(3) J. M. Drake and R. I. Morse, *Opt. Commun.*, **12**, 132 (1974).

[1] Present address, Los Alamos Scientific Laboratory, P.O. Box 1663, Los Alamos, N.M. 87545.

John R. FitzPatrick[1]
Edward H. Piepmeier*

Department of Chemistry
Oregon State University
Corvallis, Oregon 97331

RECEIVED for review May 4, 1978. Accepted August 14, 1978. This research program was supported by National Science Foundation Grant Number CHE73-05031.

Exchange of Comments on Interferometric Concentration Determination of Dextran after Gel Chromatography

Sir: Hagel (*1*) has described a method to determine the dextran concentration in solution from the relation between its concentration and refractive index. He measures a signal from a Multiref 901 (2) that is presumably proportional to the retardation difference between a dextran solution cell and a reference cell. The signal reading is calibrated against the values of dextran concentration obtained by the anthrone method (*3*).

The method of measuring the refractive index using the principle outlined in the theory presented by Hagel is capable of accurately measuring a small difference in retardations, i.e., less than one wavelength, between the sample and reference cells. Therefore, it is a very good method for determining a small refractive index such as that of a gas. Likewise, it is suitable for the detection of very small concentration differences between solutions.

However this method is not capable of determining the order of the retardation differences. If one dextran solution produces a retardation difference of a fraction of one wavelength and another produces an equal retardation plus a number of whole wavelengths, the Multiref 901 reads the same signal. Therefore, the retardation difference between the sample and reference cells, and hence the refractive index of the sample, cannot be unambiguously determined unless the order is known. Hagel did not offer a solution to resolve this ambiguity. This note is written to point out that erratic results may be obtained unless this matter is resolved, and also to offer the solution.

Fortunately there are ways to determine the order of retardation difference. The use of a compensator with white light can determine the order and may resolve this problem.

The number of orders contained in the retardation difference can also be determined by measuring the retardation at two wavelengths that are slightly different (*4*). The magnitudes of the measured retardation difference can be used to calculate the number of orders.

Suppose that the number of orders contained in a retardation difference is n, the additional fraction of retardation is Δ_1 when using light with wavelength λ_1, and Δ_2 for light with wavelength λ_2. The path difference of the light between the sample and reference cells is the same for the two wavelengths, provided that the wavelengths are close enough to neglect the effect of dispersion. Therefore,

$$(n + \Delta_1)\lambda_1 = (n + \Delta_2)\lambda_2 \quad (1)$$

From this it can be shown that

$$n = \frac{(\Delta_1 - \Delta_2)\lambda_2}{\lambda_2 - \lambda_1} - \Delta_1 \quad (2)$$

Thus, the retardation difference can be readily determined as $(n + \Delta)\lambda$.

LITERATURE CITED

(1) Lars Hagel, *Anal. Chem.*, **50**, 569 (1978).
(2) "Multiref 901, Instruction Manual", Optilab AB, Box 138, S-162 12 Vallingby 1, Sweden.
(3) J. R. Burt, *Anal. Biochem.*, **9**, 293 (1964).
(4) F. El-Hosseiny, *J. Opt. Soc. Am.*, **65**, 1279 (1975).

F. El-Hosseiny*
R. D. Gilbert

Fiber Sciences Department
Weyerhaeuser Company
3400 - 13th Avenue SW
Seattle, Washington 98134

RECEIVED for review May 19, 1978. Accepted August 7, 1978.

0003-2700/78/0350-1937$01.00/0 © 1978 American Chemical Society

Sir: The comments from El-Hosseiny and Gilbert on my paper "Interferometric Concentration Determination of Dextran after Gel Chromatography" (*1*) are in some respects not correct. I am compelled to correct some of their statements.

(1) The signal reading is not calibrated against the anthrone method. The instrument, Multiref 901, is calibrated directly into RIU for full scale (e.g., $\Delta n = 100 \times 10^{-6}$, 50×10^{-6}, etc. for full scale). The conversion from chart reading to concentration is thus performed on the basis of a pre-known value of the specific refractive index increment of the solute. The analysis using the anthrone method was in (*1*) used as a measure of the accuracy of the interferometric method.

(2) The method is, for certain, capable of determining the order of the retardation difference between the continuous flowing sample and reference solutions. The description of the interferometric method was mainly devoted to the determination of small concentrations of solute (e.g., less than 700 μg/mL dextran) in column effluents, since this is an analysis of utmost interest. However, as readily seen from the presented theory of the instrumental principle (*1*), higher concentrations of the solute can be determined also.

The sinusoidal signal from the instrument will cause a cyclical pattern of the signal when the refractive index difference between the sample and reference cells exceeds the measuring range of the instrument ($\Delta n \sim 273 \times 10^{-6}$ on the Calibration range, see Equation 1 (*1*)).

Thus, for two solutes with refractive indices producing a retardation difference of $\Delta\varphi_1$ and $\Delta\varphi_2$, respectively, where $\Delta\varphi_2 = \Delta\varphi_1 + m \times 360$ degrees and $\Delta\varphi_1 \leq 66$ degrees, the recorder pen will for solute 2 move up and down to produce m fringes, read a "peak height" equivalent to that of solute 1, and finally produce a fall of the curve also consisting of m fringes before reaching the baseline.

This type of signal has been presented earlier for a LC detector based upon the interferometric principle (*2*). It is thus obvious that the interpretation of the recorder signal is unambiguous and, furthermore, the order of the retardation difference is readily determined from the number of fringes produced by the recorder pen (provided that the response time of the system is sufficiently low). This approach is far more convenient than that suggested by El-Hosseiny and Gilbert, which includes the measurements of the retardation at two different wavelengths, which is so far not possible with the Multiref 901.

LITERATURE CITED

(1) L. Hagel, *Anal. Chem.*, **50**, 569 (1978).
(2) M. Bakken and V. I. Stenberg, *J. Chromatogr. Sci.*, **9**, 603 (1971).

Lars Hagel

Pharmacia Fine Chemicals AB
Box 175
S-751 04 Uppsala, Sweden

RECEIVED for review June 12, 1978. Accepted August 7, 1978.

AIDS FOR ANALYTICAL CHEMISTS

Programmable-Gain or Auto-Gain Amplifier

K. R. O'Keefe

Department of Chemistry, Colorado State University, Fort Collins, Colorado 80523

It is frequently desirable in the chemical laboratory to provide variable gain output from instrumentation that has a large working range. Examples of such instrumentation include fluorometers, gas and liquid chromatographs, polarographs, pulse polarographs and related voltammetric instruments, and plasma emission spectrometers. The outputs from these instruments can vary by up to 5 orders of magnitude over their useful working range (*1*). In many cases, gain or attenuation controls are provided on the instrumentation and/or on associated readouts, such as strip-chart recorders; however, these manual controls are not generally useful for automatic data processing or data logging. Automatic gain control circuits have been described in the literature (2), but have often been complicated, expensive, and/or slow in addition to providing only attenuation of large signals. This report describes a fast, accurate, inexpensive programmable-gain amplifier that is useful with automatic data acquisition systems. This device has been used in our laboratories on a dc plasma emission spectrometer, a gas chromatograph, and a pulse polarograph with excellent results. Operation in either programmable-gain or autoranging mode is possible.

INSTRUMENTATION

A schematic diagram of the basic programmable gain amplifier is shown in Figure 1. The operation of the amplifier can be best understood by considering the input–output characteristics of operational amplifier A1 (Model 3308/12C, Burr Brown Corporation, Tucson, Ariz.). The output voltage of this device, V_{out}, can be related to the inputs by the expression:

$$V_{out} = A(V_+ - V_-) + \left(\frac{V_+ + V_-}{2}\right) \Big/ R_{CM} \qquad (1)$$

where A is the open loop gain of the amplifier, V_+ and V_- are the input voltages at the noninverting and inverting inputs of the amplifier, respectively, and R_{CM} is the common-mode rejection ratio of the amplifier (*3*). The input voltage, V_+, in the configuration shown is the input voltage to the programmable gain amplifier, and V_- is a voltage determined by the digital-to-analog converter (DAC) and amplifier (A2, Model 3308/12C, Burr Brown Corp.) in the feedback loop of A1. The output current, i_o, of the DAC used in this work (Model IC8BC, Datel Systems, Canton, Mass.) is determined by the output voltage of A1 which supplies the DAC reference current through R1 and by the scale factor inputs to the DAC (symbolized in Figure 1 by inputs of the form 2^n) and can be represented by the relationship:

$$i_o = \frac{N}{256}(V_{out}/R1) \qquad (2)$$

where N is the decimal representation of the scale factor input to the DAC. The output voltage of A2, which is V_- of A1, is thus (with $R2 = R1$):

$$V_- = N \cdot V_{out}/256 \qquad (3)$$

0003-2700/78/0350-1938$01.00/0 © 1978 American Chemical Society

Table I. PROM Settings, Gain, and Voltage Ranges for +1.25 to +10.00 V Output from Autoranging Amplifier

PROM address	PROM contents	gain	input voltage range, V
0	255	1.0039	1.2451 - 9.961
1	32	8	0.15625 - 1.25
2	4	64	0.01953 - 0.15625
3	1	256	0.00488 - 0.03906

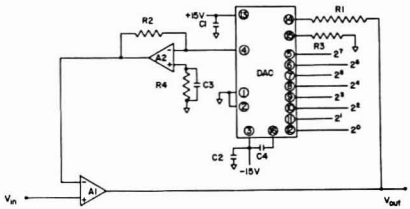


Figure 1. Schematic diagram of programmable-gain amplifier

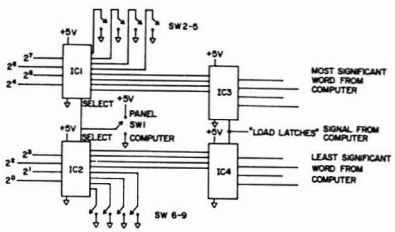


Figure 2. Control input schematic diagram

Equation 3 can be substituted in Equation 1 and, recognizing that the second term in the right hand side of Equation 1 is usually very small with respect to the first term for modern operational amplifiers, the output voltage is expressed as:

$$V_{out} = \left[\frac{256 \cdot A}{256 + A \cdot N}\right] V_{in} \qquad (4)$$

or, if $A \sim 10^6$, which is true for the amplifiers used in this work,

$$V_{out} \cong \frac{256}{N} \cdot V_{in} \qquad (5)$$

Thus, by putting the multiplying DAC in the feedback loop of A1, the circuit shown exploits the programmable less-than-one gain of the DAC to allow gains in the range of 1.0039 (N = 255) to 256 (N = 1). If a multiplying DAC with a larger range of input scale factors is used, a larger gain is available. For example, a 10-bit DAC allows gains of 1.0010 to 1024 and a 16-bit DAC allows gains of 1.00002 to 65,636.

The configuration of Figure 1 is used directly as a programmable gain amplifier with scale factor inputs selected either by means of switches or by the control element, which is usually a computer or microprocessor-based data acquisition system. The control configuration used is shown in Figure 2. In this circuit SW1 selects panel switch or computer gain setting by multiplexing the two sets of control lines to the DAC scale factor inputs through IC1 and IC2 (both SN74157). When the gain is controlled by the computer, an appropriate 8-bit output word is latched upon computer command into IC3 and IC4 (both SN74LS174) and this word controls the gain of the amplifier. Operation in the panel control mode allows setting the gain by manually setting panel switches (SW2-9).

The amplifier can be used in an auto-gain configuration as well as in the programmable-gain configuration described above. The auto-gain configuration is shown in Figure 3. In this circuit, operational amplifiers A3 and A4 (Model 3308/12C, Burr Brown Corp.) are used as voltage comparators, comparing the output voltage from the auto-gain amplifier with reference voltages set by the potentiometers associated with the two amplifiers. Typical reference voltages are +10.00 V and +1.25 V, and the auto-gain circuit adjusts the programmable gain to keep the voltage output within this range. If, for example, the output of the programmable-gain amplifier goes above +10.00 V, the output of A3 changes from about +13.5 to about -13.5 turning Q1 (2N3393) off. Q1 acts as a level converter that converts the comparator output to a TTL compatible signal. The output of Q1 is inverted and gated to the up/down counter, U/D1, by means of a gating circuit described by Defreese, Woodruff, and Malmstadt (4) that is intended to ensure that the counter is not triggered spuriously. The high logic level produced when Q1 turns off is inverted and is clocked into FF1 at the next high-to-low transition of the 100-kHz clock input. The low logic datum at D is toggled onto

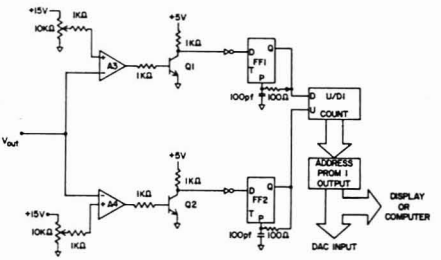


Figure 3. Schematic diagram of control for auto-gain mode of operation

the Q output of FF1 on the subsequent low-to-high transition of the clock. The 100-pf capacitor connected to the preset input of FF1 then begins to discharge through the 100-Ω resistor and, after about 20 ns, the Q output of FF1 is reset to a high logic level. This 20-ns low logic level pulse appears at the "count down" input of U/D1. The output of the counter thus decreases by 1 selecting a new programmable read-only memory (PROM 1) address whose contents are output. These contents are the input to the gain select of the DAC of the programmable-gain amplifier and are available for display or input to a computer so the gain of the amplifier can be determined. For example, if the gain of the amplifier is 64 as the voltage output approaches +10.00 V, corresponding to an input voltage of 0.15625 V, the PROM contents at the address selected by U/D1 would be 4 (N = 4) as can be verified by inspection of Equation 5. When the voltage increases above +10.00 V, the PROM address decreases by 1 as described above and the contents of the new address are output to the gain control inputs of the DAC. To reduce the output to 1.25 V, the contents of this new location should be 32 (N = 32). This value of N reduces the gain of the amplifier to 8, and hence reduces the output voltage to +1.25 V for an input voltage of 0.15625 V. The circuit operates similarly if the output voltage decreases below +1.25 V. Table I shows the contents of PROM locations and voltage range available for the conditions selected. Note that for this configuration a 2-bit up-down counter and a 4 × 8 PROM is adequate. Tighter voltage limits or higher maximum gain requires a longer counter and a larger PROM.

PERFORMANCE OF THE CIRCUIT

Performance characteristics of the programmable-gain amplifier that affect its utility for instrumental applications include input-output linearity, gain predictability, and response time. These characteristics were evaluated for the system described here and were found to be generally as

Table II. Linearity of the Programmable-Gain Amplifier of Figure 1

input voltage, V	output voltage, V	predicted output voltage, V[a]	error, %
	$N = 255$		
10.000	9.949	9.997	−0.5
8.820	8.858	8.841	+0.2
7.890	7.953	7.930	+0.3
7.132	7.215	7.187	+0.4
5.998	6.084	6.076	+0.1
4.273	4.400	4.386	+0.3
3.322	3.447	3.454	−0.2
2.711	2.853	2.855	−0.1
1.999	2.121	2.158	−1.7
1.421	1.618	1.591	+1.7
0.727	1.358	0.911	+33.7
0.488	1.088	0.677	+37.8
0.246	0.510	0.440	+13.7
0.136	0.051	0.332	−551.0
	$N = 8$		
0.2500	8.200	8.222	−0.3
0.2000	6.647	6.621	+0.4
0.1500	5.033	5.021	+0.2
0.1250	4.211	4.221	−0.2
0.1000	3.422	3.420	+0.1
0.0750	2.611	2.620	−0.3
0.0500	1.823	1.820	+0.2
0.0300	1.177	1.180	−0.3
0.0200	0.864	.860	+0.5
0.0100	0.471	.540	−14.6

[a] Predicted from regression expression $V_{out} = 0.9797 V_{in} + 0.199$ V for $N = 255$ and $V_{out} = 32.01 V_{in} + 0.219$ V for $N = 8$.

expected, based upon the specifications of the devices used in the actual circuit.

The linearity of the programmable-gain amplifier of Figure 1 was measured at several different values of N and was generally excellent for output voltages greater than about 1 V. Typical results for two values of N are presented in Table II. The values of gain from the regression expressions from Table I agree well with the theoretical values of 1.003 and 32.000 (errors −2.4 and +0.03%, respectively, for $N = 255$ and $N = 8$). To achieve low offset voltages, amplifier A1 must be very carefully adjusted for zero offset voltage. Alternatively, an offset circuit can be added to the output of A2 of Figure 1. It is important to keep the voltage output of A2 positive at all times as a negative excursion will cause the circuit to become unstable and latch-up. It is also important to work in the range of output voltages from +1.5 to +10.00 V. This is largely due to the DAC specifications which ensure good linearity for input reference currents of only 0.4 to 4.2 mA (5). Within these limitations, a linearity of about ±0.3% can be achieved.

Gain predictability was evaluated by measuring the gain of the circuit of Figure 1 as a function of input scale factor N. These results are summarized in Table III. The regression equation relating voltage gain to input scale factor is very close

Table III. Gain Predictability of the Programmable-Gain Amplifier of Figure 1

V_{out}, V[a]	N	$1/N$ (× 100)	predicted V_{out}, V[b]	error, %
1.414	255	0.392	0.969	+31.5
1.974	127	0.787	1.983	−0.5
2.280	111	0.901	2.275	+0.2
2.911	87	1.149	2.912	0
3.207	79	1.266	3.212	−0.2
4.044	63	1.587	4.036	+0.2
5.433	47	2.128	5.424	+0.2
6.550	39	2.564	6.543	+0.1
8.230	31	3.226	8.242	−0.1
11.11	23	4.348	11.121	−0.1

[a] Input voltage, 1.000 V. [b] Based upon regression expression $V_{out} = [256.6/N]\ V_{in} - 0.037$ V.

to the predicted expression (Equation 5). The gain factor differs from the predicted value by about 0.2% and the offset (−37 mV) is well within the range expected from the specifications of the devices used.

Response time of the programmable-gain amplifier was determined in both the programmed and auto-gain modes of operation. The 3-db point of the circuit of Figure 1 was determined by increasing the frequency of a 1.00-V peak-to-peak input sine wave until the output voltage dropped to 2.86 V peak-to-peak with $N = 63$. The 3-db point was estimated to be 215 kHz. This value varies by about ±20% as the gain is varied over the range 1 to 100. The settling time was estimated by observing the output waveform (V_{out}) on an oscilloscope when a 1- to 2-V square wave with a rise time of about 20 ns was V_{in}. The settling time was observed to be about 3 μs. About the same settling time was observed when the input voltage was fixed at 1 V and the gain was stepped from 2.02 to 2.95 by changing N from 127 to 87. This is expected since the DAC exhibits faster response than the OA's used in this work. The circuit response of the auto-gain circuit is identical to that of the programmable gain circuit when the gain does not change. When the input voltage goes outside the preset limits of the auto-gain amplifier, the circuit output requires about 15 μs to settle to its new value. Again, this is partially determined by the slew rate of the OA's used in this work, although there is an additional fixed 5–10 μs delay due to the clocked nature of the auto-gain circuit.

The circuit described thus has excellent characteristics in terms of response speed, linearity, gain predictability, and range. Any of these characteristics can be extended by selection of different components, e.g., faster OA's, a higher resolution DAC, etc.

LITERATURE CITED

(1) H. H. Willard, L. L. Merritt, Jr., and J. A. Dean, "Instrumental Methods of Analysis," 5th ed., D. Van Nostrand and Co., New York, N.Y., 1974.
(2) S. R. Pareles, *Anal. Chem.*, **46**, 464 (1974).
(3) J. G. Graeme, G. E. Tobey, and L. P. Huelsman, "Operational Amplifiers," McGraw-Hill Book Co., New York, N.Y., 1971.
(4) James D. Defreese, Terry A. Woodruff, and H. V. Malmstadt, *Anal. Chem.*, **46**, 1471 (1974).
(5) Data Sheet DICAJ1 0702, Datel Systems, Inc., Canton, Mass., 1977.

RECEIVED for review April 10, 1978. Accepted July 11, 1978.

Highly Regulated Power Supply for Hydrogen or Deuterium Arc Lamps Used in Ultraviolet Spectrometry

Ronald D. Edstrom

Department of Biochemistry, The Medical School, University of Minnesota, Minneapolis, Minnesota 55455

In designing detectors for spectrophotometric and fluorometric devices, it became apparent that the power supplies for incandescent and arc lamps generally provided with the older single beam spectrophotometer were not adequate for highly critical work. We are therefore constructing individual circuit modules to provide power for the tungsten and hydrogen lamp sources of a spectrophotometer. The tungsten lamp power supply described in an earlier report provided a constant voltage for a highly stable visible spectrum light output (*1*). In this paper we describe the design and construction of a regulated constant current source and ignition circuit for use with the standard deuterium or hydrogen lamps. The gas discharge tubes used in these instruments consist of a heavy tungsten filament surrounded by a metal tube which, with the filament, serves as the cathode; a few millimeters away is the anode and the light emitting arc is formed between the two electrodes. The lamps depend on thermionic emission from the filament to form and maintain the arc. Initially, arc formation also requires a brief, high potential pulse (several hundred volts) between the electrodes. Once the arc has formed, the interelectrode potential is normally between 75–100 V at the usual current (0.3 A). The supply described here provides the three necessary sources of power to the lamp: (1) low voltage high current (2.5 V, 4 A) ac for the filament, (2) high voltage pulse (800 V for 0.2 ms) for ignition, and (3) the constant current source for sustaining the gas discharge (300 mA at up to 100 V).

CIRCUIT DESCRIPTION AND CONSTRUCTION DETAILS

The hydrogen lamp power supply (Figure 1) will be considered as the three separate functional components described above. The filament is energized by a 2.5-V, 10-A transformer. Originally it had been thought that the filament voltage might need to be regulated either by a constant voltage-harmonic transformer or after rectification by a low voltage dc regulator. In fact, relatively large changes in the filament voltage have little effect on the light output with this supply. A rather high current capacity filament transformer was used to provide a lower operating temperature and thus increased reliability. The center tap of the transformer provided a convenient place to connect the filament to the cathode current sink (transistor Q_3).

The ignition voltage pulse is provided by the relaxation oscillator consisting of unijunction transistor Q_2, resistors R_1 and R_2, and capacitor C_2. The values of R_1 and C_2 together with the high intrinsic standoff ratio of the specified unijunction transistor provide a pulse through the primary of T_4 every 5–10 s. The primary to secondary turns ratio of T_4 increases the amplitude of that pulse to 800 V. The positive component of the pulse passes through D_6 to the anode. The silicon diode (D_6) isolates the secondary of T_4 from the anode supply. As soon as the lamp conducts, transistor Q_1 is turned on by the positive voltage developed across R_{10}. This shuts off the unijunction oscillator and keeps it off while the lamp is on. Transformer T_4 was chosen because it is designed for high voltage across the secondary. It is not certain that other transformers with similar turns ratios would be able to withstand the 800-V pulse. When the supply ignites a hydrogen or deuterium lamp, the output of the high impedance pulse transformer does not rise above the ignition voltage, usually below 350 V. If for any reason the current through the lamp is interrupted, the circuit will automatically reignite the lamp.

The anode current is provided by transformer T_1 (120 V), bridge rectifier (D_{1-4}), choke L_1, and C_1. Pilot lamp (P_{L2}) is mounted on the front panel and is lighted when the discharge lamp is conducting. The pilot lamp bulb chosen is rated at 0.35 A and acts as a fuse in case of a short circuit in the arc lamp housing or wiring. Diode D_5 isolates the anode supply from the ignition pulse source. The use of the filter choke (L) provides a 175-V output prior to ignition. When the lamp begins to conduct, the voltage drops to 105 V. This provides a high voltage at the time of ignition to ensure a reliable start and then the lowered output voltage reduces dissipation in the series pass transistor Q_3. Neon lamp P_{L3}, together with resistor R_3, provides protection of transistor Q_3 against high voltage transients, especially the ignition pulse. The neon lamp fires at 80–90 V and thus prevents the voltage on the collector of Q_3 from rising substantially above that level for short-lived transients.

Regulation of the arc current through the lamp is provided by a constant current sink which senses changes in current by comparing the voltage across resistor R_{10} with a reference voltage provided by diode D_9 and resistor R_5 (*2*). The operational amplifier IC_2 compares the two potentials and, as appropriate, provides more or less drive current to pass transistor Q_3. This negative feedback loop with a gain of about 10^5 ensures a constant potential across R_{10} (3 V) and thus a constant current through the discharge lamp which is in series with it. The major contribution to the small current variations with time are due to temperature induced changes in the offset voltage of the integrated circuit amplifier, the resistors, and reference diode D_9. For that reason it is essential that resistors R_4, R_5, R_6, R_7, R_9, and R_{10} have low temperature coefficients (less than 100 ppm/°C) and that diode D_9 be a temperature compensated reference diode rather than a simple zener diode. Transformer T_3, diodes D_7 and D_8, capacitor C_3, and voltage regulator IC_1 provide a constant voltage source (+15 V) for operation of the relaxation oscillator, reference diode, and operational amplifier. The last is specified to be an RCA CA3140 integrated circuit which, unlike most operational amplifiers, requires only one power supply (*3*). Better stability might be obtained with an operational amplifier having a lower offset voltage temperature coefficient, but that would require the addition of a −15-V supply.

The power supply was assembled using standard construction practices and enclosed in a 6 × 10 × 7 inch aluminum box. The components shown within the dotted line on the schematic diagram were mounted on a 3 × 5 inch printed circuit board (the printed circuit board layout pattern is available from the author on request). The components could as well have been assembled on a piece of Vectorboard or similar substrate. In that case, special attention should be given to short lead lengths to avoid instability in the feedback loop. All ground leads were brought to one point on the cabinet. Transistor Q_3 was mounted on the specified circuit board heat sink with a thin film of silicone grease to improve heat conduction. Transformers T_1 and T_2, as specified, have the same spacing of their mounting holes and were stacked to provide for a more compact assembly.

Four screen-covered $^3/_4$-in. holes were placed at each end of the cabinet for ventilation. The circuit board was positioned to allow R_5 to be adjusted through one of them. Jacks were provided on the back of the cabinet to allow easy measurement of the voltage across R_{10}. The cathode and anode leads for the gas discharge lamp were brought to a female socket on the back of the supply which mates with the socket on the cable from the spectrophotometer lamp housing.

Prior to attaching the supply to the lamp with which it is to be used, a 100–300 Ω 50-W resistor should be inserted between the anode output and one of the cathode sink terminals. The supply can be adjusted with R_5 to give 3 V across R_{10} indicating

0003-2700/78/0350-1941$01.00/0 © 1978 American Chemical Society

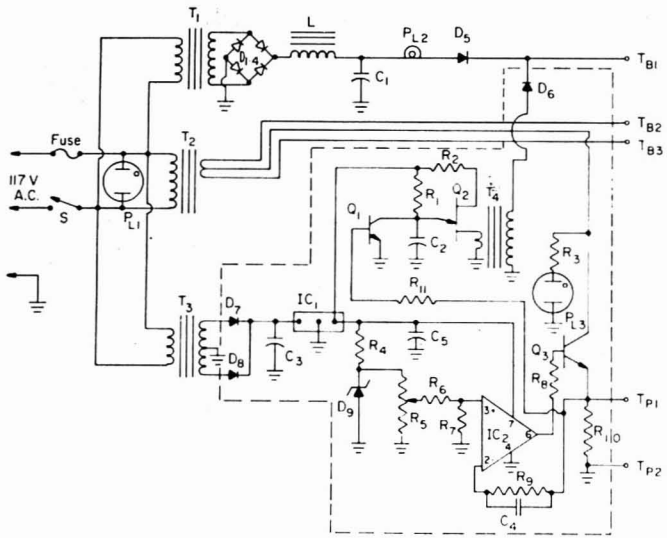


Figure 1. Schematic diagram of hydrogen lamp power supply. Component list: Q_1, 2N6175 transistor; Q_2, 2N4871 transistor; Q_3, MJ410 transistor (Motorola); D_1 through D_8, 1N4007 rectifier diodes; D_9, 1N938B temperature compensated reference diode (9 V); IC_1, μA7815, +15-V regulator (Fairchild); IC_2 CA3140T operational amplifier (RCA); C_1, 200-μF, 250-V electrolytic capacitor; C_2, 47-μF, 25-V electrolytic capacitor; C_3, 100-μF, 50-V electrolytic capacitor; C_4 and C_5, 0.047-μF, 100-V Mylar capacitor. R_1, 47-kΩ, 1/2-W carbon resistor; R_2, 100-Ω, 1/2-W carbon resistor; R_3 and R_{11} 27-kΩ, 1/2-W carbon resistor; R_4, 825-Ω, 1/2-W metal film resistor; R_5, 10-kΩ Cermet 10-turn trim potentiometer; R_6 and R_7, 17.8-kΩ, 1/2-W metal film resistor; R_8, 680-Ω, 1/2-W carbon resistor; R_9, 2.3-kΩ, 1/2-W metal film resistor; R_{10}, 10-Ω, 5-W wire wound resistor; T_1, 120-V, 0.5-A transformer (Signal Transformer Co., N.Y., Model 241-7-120); T_2, 2.5-V 10-A transformer (Triad F-3X); T_3, 28-V, C.T., 0.08-A transformer (Signal 241-3-28); T_4, blocking oscillator transformer (Triad TY-202X); L, 0.8-H, 375-mA, 25-Ω inductor (Stancor C2328); P_{L1}, neon pilot lamp assembly for 117 V; P_{L2}, 3.2-V, 0.35-A bulb (General Electric No. 45); P_{L3}, Neon Lamp (NE-2H) Fuse; 2-A, 250-V

a current of 300 mA. A 117-V, 60-W incandescent light bulb should serve well for such a dummy load. Final adjustment in current can be made after the supply has been in operation with the hydrogen or deuterium lamp. The lamp anode connected to T_{B1} and the filament leads to T_{B2} and T_{B3}.

OPERATING CHARACTERISTICS

The supply has been in use for 13 months with four different deuterium lamps. Three of them were ignited by the first pulse after the 7-s warmup. The fourth ignited prior to the pulse by the 175-V output of the anode supply under no load conditions. The current stability of the supply was assessed by using power resistors as dummy loads. The resistance ranged from 100 to 275 Ω. Current was monitored by measuring the voltage drop across a 0.6-Ω thermostated resistor with a four digit voltmeter. Beginning 10 s after the supply was turned on, the current changed less than 1% over a 3-h period. After a 10-min warmup of the supply, changes in all cases were less than 0.1% over 3 h. The change in current as a function of change in load resistance was determined to be 0.013 mA/Ω. Additionally, the stability of the supply was determined as a function of changes in light output with time. The supply was attached to the deuterium lamp of a Beckman DU spectrophotometer. The standard Beckman supplied photomultiplier tube and associated electronics were used as a detector. Measurements were made at both 260 and 205 nm in separate experiments. With the monochromater exit slit set at 0.02 mm for 260 nm and 0.4 mm for 205 nm, the sensitivity of the photomultiplier was adjusted to give an apparent absorbance of 0.200 with no sample in the light path. The deuterium lamp and all electronics except the supply under test were operated 2 h by means of an independent power source in order to stabilize both the detector system and any thermally-induced mechanical changes in the lamp housing and focus system. Measurements of the apparent absorbance were made over a 3-h period beginning 30 s after the supply under test was turned on. At 260 nm, the apparent absorbance at all times was 0.200 ± 0.003. After 10 min, the total short-term drift was less than 0.001 during any 20-min interval. For the 205-nm wavelength, the maximum deviation from an absorbance of 0.200 was ±0.005 with a short-term drift of 0.003/20 min. Starting with a cold lamp and housing, about 30 min were required to achieve similar stability in the apparent absorbance. The drift during that period was probably due to the mechanical changes in the lamp and its housing. Changes in the nominal 117-V ac line voltage between 110 and 130 V caused a variation of less than ±0.002 absorbance unit; from 95 to 140 V input, the changes were ±0.004. Since the filament voltage on the arc lamp is unregulated, it changes in proportion to the input voltage; the highly regulated anode current must prevent the changes in light output which would otherwise occur with such large differences in filament temperature. The power supply described here seems to be close to reaching the limit of useful stability with lamp supplies for ordinary single beam, general use laboratory spectrophotometers. Heat induced mechanical changes in the optical system and drift in the detector become important in trying to increase the stability. Obviously the use of double beam or other self-compensating spectrophotometers is to be recommended when greater freedom from drift is needed. Total costs of materials, if purchased in 1977 in unit quantities, would be $80 including a coat of epoxy paint on the cabinet. The supply has been in use for a year without problem. As with the previously published design for the tungsten lamp supply, it is very important to use high quality, conservatively

rated components to increase the operating time before breakdown (*1*).

LITERATURE CITED

(1) R. D. Edstrom, *Anal. Biochem.*, **80**, 612 (1977).
(2) M. J. Salvati, *Electronics*, **49**, 107 (1976).
(3) RCA, Solid State Division, Box 3200, Somerville, N.J. 08876, CA3140 Data File No. 957 (1976).

RECEIVED for review April 11, 1978. Accepted June 26, 1978. Supported in part by a grant from the USPHS National Cancer Institute CA 14351.

Carboxylate Anions from Fatty Acids by Esterification with *p*-Nitrobenzyl Bromide for Analysis of Fatty Acid Mixtures by Negative Ion Mass Spectrometry

Yukio Hirata and Tsugio Takeuchi

School of Materials Science, Toyohashi University of Technology, Toyohashi 440, Japan

Kozo Matsumoto*

Department of Synthetic Chemistry, Faculty of Engineering, Nagoya University, Nagoya 464, Japan

In the analysis of fatty acids, often the problem is with the separation, since they usually exist as complex mixtures in natural products such as fat or lipids. Although it is relatively straightforward to separate fatty acid mixtures composed of homologues by GC or LC, the complete separation of fatty acids from natural products is sometimes very difficult, because they contain various types of fatty acids with or without double bonds.

Negative ion mass spectrometry, which usually yields simple spectra highly characteristic of the types of compounds, has been applied to the analysis of alcohols and aldehyde mixtures (*1*), and mercaptans (2).

This report describes the qualitative analysis of fatty acid mixtures by negative ion mass spectrometry. The negative ion mass spectra of fatty acid *p*-nitrobenzyl esters yield carboxylate anions as the base peak, and molecular anions and other fragments become negligibly small. By this derivatization, more than several hundreds times enhancement is achieved on the carboxylate anions.

EXPERIMENTAL

Reagents. 18-Crown-6(1,4,7,11,13,16-hexaoxycyclooctadecane) was purchased from Nippon Soda Company, Japan. *p*-Nitrobenzyl bromide and phenacylbromide were purchased from Tokyo Kasei Industries, Japan, and recrystallized from methanol/water solutions. The stock benzene solutions of *p*-nitrobenzyl bromide (22 mg/mL) and phenacylbromide (20 mg/mL) were prepared, where the molar ratio of alkylating reagent/crown ether was adjusted to 20:1, respectively.

Alkylating Procedure. Alkylation was performed according to the method by Durst et al. (*3*). A fatty acid sample (ca. 0.5 mM) was dissolved in 2 mL methanol and neutralized to a phenolphthalein end point by a KOH/methanol solution (0.5 N). After the solution was evacuated to remove the solvent by rotary pump, 5 mL of the alkylating solution was added and the suspending solution was refluxed for 30 min to complete the reaction. The resulting solution was used for mass spectrometric measurement.

An oil sample about 80 mg(0.4–0.3 mM of total fatty acids) was dissolved in 4 mL of the KOH/methanol solution. After cooling, the solution was neutralized to a phenolphthalein end point by a HCl/methanol solution (0.5 N). The following procedures are the same as mentioned above.

Apparatus. JMS-01SG double focusing mass spectrometer from JEOLCO was used in the negative ion mode under the following conditions: ionizing energy of 150 eV, ionizing current of 200 μA, accelerating voltage of 6 kV, ion source temperature of 130–200 °C and ion source pressure of 10^{-5} Torr. All mass spectra were obtained using a direct inlet probe.

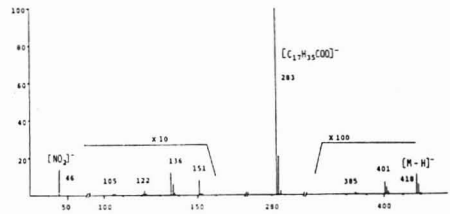


Figure 1. Negative ion mass spectrum of *p*-nitrobenzyl stearate

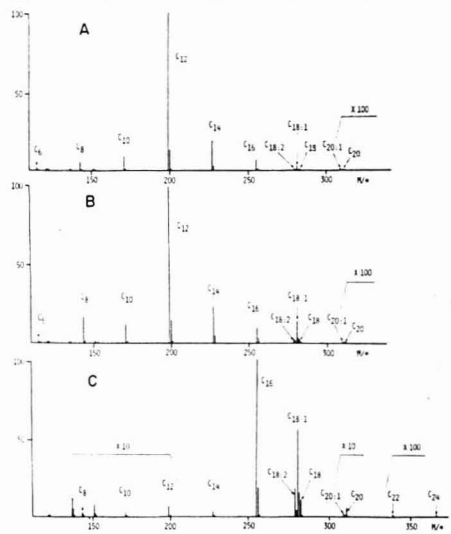


Figure 2. Negative ion mass spectra of *p*-nitrobenzyl esters of fatty acids from (A) coconut oil, (B) palmseed oil, and (C) palm oil

RESULTS AND DISCUSSION

Figure 1 shows the negative ion mass spectrum of *p*-nitrobenzyl stearate. The other *p*-nitrobenzyl esters show basically the same type of spectra. The peak of $[RCOO]^-$,

0003-2700/78/0350-1943$01.00/0 © 1978 American Chemical Society

which is always the base peak, compiles more than 95% of the total ion abundance on the spectrum. The ions of $[RCOO-H]^-$ and $[RCOO-2H]^-$ are less than 0.1% of the peak of $[RCOO]^-$.

Phenacyl esters of fatty acids and free acids also yield carboxylate anions. The order of the intensities of $[RCOO]^-$ from these compounds was as follows: free acid ≪ phenacyl ester < *p*-nitrobenzyl ester. By the derivatization of free acids into the *p*-nitrobenzyl esters, the intensity of $[RCOO]^-$ was enhanced by more than several hundreds times, and fatty acid could be detected in nanogram quantity.

Therefore, *p*-nitrobenzyl ester was adopted for the analysis of fatty acid mixtures from natural oils. They contain many fatty acids with or without double bonds, but fortunately the determination of molecular weight of individual components is sometimes sufficient for the qualitative analysis.

Figure 2 shows the negative ion mass spectra of *p*-nitrobenzyl esters of fatty acids from coconut oil, palmseed oil, and palm oil. As the spectra are composed only of the series of carboxylate anions, it is easy to identify individual components even if they are minor components less than 0.1% of the most abundant one. In addition, traces of odd-carbon-number fatty acids were observed; C_{11}(0.06%), C_{13}(0.04%), and C_{15}(0.02%) for palmseed oil. Here, 1 μL of the sample solution containing about 80 nM of total fatty acids was injected into the sample tube. Therefore, 0.1% of the base peak corresponds to the quantity less than 80 pM (about 20 ng). This method could be applicable to the quantitative analysis of fatty acid mixtures.

ACKNOWLEDGMENT

The authors are greatful to S. Tsuge of Nagoya University for helpful discussions and suggestions, and to Fuji Seiyu Co. Ltd., Japan for oil samples.

LITERATURE CITED

(1) P. C. Rankin, *Lipids*, **5**, 825 (1970).
(2) H. Knof, R. Large, and G. Albert, *Anal. Chem.*, **48**, 2124 (1976).
(3) H. D. Durst, M. Milano, E. J. Kikta, Jr., S. A. Connelly, and Eli Grushka, *Anal. Chem.*, **47**, 1797 (1975).

RECEIVED for review January 30, 1978. Accepted August 14, 1978. Work supported by a grant from Ministry of Education.

Rapid Transferring Device for Immiscible Liquids

Harvey A. Schwertner

Deparment of Pathology, The University of Texas Health Science Center at San Antonio, 7703 Floyd Curl Drive, San Antonio, Texas 78284

A device is described which allows the rapid transfer of extraction solvents from culture tubes or conical centrifuge tubes. It is especially useful for transferring liquids from an upper phase and has several advantages over manual pipetting methods for transferring solvents and methods employing the use of separatory funnels. Serum, plasma, and other fluids can also be effectively transferred after separation from the formed elements or particulate material. The transfer of liquid is activated by air flow and controlled manually with a finger-operated flow control. The delivery tube is constructed of non-adhesive, solvent resistant, transparent, and light weight Teflon tubing which accommodates a wide range of tube sizes and volumes. Constant volumes of the upper phase of immiscible liquids can be transferred rapidly with little or no sample carry-over.

EXPERIMENTAL

Description. The phase transfer device consists of a 12-inch Teflon delivery tube, a two-hole rubber stopper, a T-connector, and Tygon and latex tubing. The Teflon delivery tube has an i.d., wall thickness, and o.d. of 0.062, 0.030, and 0.122 inches, respectively (Catalogue No. 6406-62, Cole-Palmer Instrument Co., Chicago, Ill. 60648). Two holes are drilled into a rubber stopper, size 00, to support the delivery tube and the T-connector (Nalge 6151, $^3/_{16}$ in. o.d.). An airline made of Tygon R-3603 tubing, 3.2 mm i.d. × 1.6 mm wall thickness, (Catalogue No. 14-169-10, Fisher Scientific, Pittsburgh, Pa. 15219) is attached to one end of the T-connector. To the other end of the T-connector is placed a small strip of latex tubing to facilitate easy finger-operated flow control. A photograph of the phase transfer device is shown in Figure 1.

RESULTS AND DISCUSSION

The phase transfer device described here has many advantages over other methods for routine phase transfer and is especially suited for the transfer of liquids from an upper phase. Such transfers are faster and more efficient than those achieved manually with a pipet. A constant volume is delivered. There is insignificant carry-over since the delivery tube is made of non-adhesive material. The clear delivery tube also permits visualization of carry-over and completeness of transfer. If there is concern with carry-over, the tube can be rapidly washed between sample transfers with a suitable solvent or solution. The device is constructed of flexible light weight material and can be conveniently carried in the lab coat pocket. The Teflon delivery tube is preferred over stainless steel tubing because of its non-adhesive properties, transparency, light weight, and low cost. Teflon is also considered more chemically inert than polypropylene tubing. Glass tubing could meet the need if it were not for liquid adhesion and the fragility of glass.

The delivery tube of the device can be easily adjusted to the varying volumes and tube sizes encountered in the laboratory. The adjustment is made by pulling the Teflon tubing in either direction through the rubber stopper until the desired length is obtained. In our laboratory, the solvent transfer device is most frequently used for transferring about 10 mL of extraction solvent from 16-mm i.d. culture tubes or conical centrifuge tubes. With this size tube, the delivery tube is adjusted to recover all but 0.5 mL of the supernatant phase. The remaining supernatant phase is not recovered so as to prevent the possibility of carry-over of the aqueous phase. The transfer device, as described, permits easy transfer of volumes ranging from 3–50 mL, however, if smaller volumes (0.5–2.0 mL) are to be transferred, one should use the smaller 0.031-inch i.d. tubing. For tubes with tops greater than 1 cm in diameter, a larger size rubber stopper may be needed.

Many procedures for drug extraction employ culture tubes or conical centrifuge tubes rather than separatory funnels. A new "Separatube" is also available and is a plastic separatory funnel of centrifuge tube size (Quantimetrix, Culver City, Calif. 90230). It, thus, possesses many of the advantages of both tubes and separatory funnels. There are several advantages for using tubes rather than separatory funnels. Tubes allow the simultaneous extraction of a large number of samples. The bench-space requirement is minimal since test tube racks substitute for separatory funnel supports. Considerable time can be saved when emulsions are broken by centrifugation and in not having to assemble and disassemble a large number

0003-2700/78/0350-1944$01.00/0 © 1978 American Chemical Society

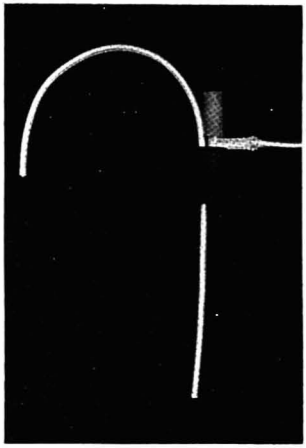


Figure 1. Photograph of the phase transfer device

of separatory funnels. For such tube extractions, the phase transfer device provides a simple solution to a routine transfer problem, especially if the organic phase solvent is less dense than that of the aqueous phase. If the extraction solvent is more dense, there can be some contamination with the aqueous material as the delivery tube is lowered through the aqueous layer. Under such conditions, it may be desirable to discard the first fraction of the solvent since it would contain some of the aqueous material. Alternatively, one may eliminate contamination of the delivery tube by momentarily introducing air flow through the tube or a slight positive pressure.

The majority of solvents used for extraction are less dense than water and thus would pose no problem. The exceptions are the halogenated solvents such as carbon tetrachloride, chloroform, and ethylene dichloride. Carbon tetrachloride is not recommended for laboratory use because of its potential health hazard; however, chloroform is widely used. Based on the procedures published in Sunshine's "Methodology for Analytical Toxicology" (*1*) and Curry's "Poison Detection in Human Organs" (*2*), chloroform, either alone or in combination with other solvents, is used in 34% of the toxicological procedures; ethyl ether, 20.1%; hexane, 9.6%; benzene, 7.2%; toluene, 6.4%; ethylene dichloride and ethyl acetate, 3.2%. If these data, based on 124 methods, are representative of the analytical methods as a whole, the majority (≥60%) of solvents used for drug analysis are less dense than water and, thus, could be transferred with the device without contamination from the aqueous layer. In instances where it is desirable to retain chloroform as a major component of the extraction solvent, the transfer problem associated with the use of chloroform can be overcome simply by adding sufficient amounts of hexane (or ethyl ether) to the chloroform to effect phase inversion (*3*).

An informative and comprehensive review covering many aspects of sample extraction has been written recently by Reid (*4*). In the review, it is noted that it is still common practice to remove a portion of one phase manually with the aid of a bulb-controlled pipet. It is also pointed out that phase-separating filter-paper can be helpful, although it may introduce contaminants such as tin. The phase transfer device described here should represent an improvement over many pipetting methods of phase transfer and should be useful not only for drug analysis but for other analytical procedures employing small scale partition systems.

LITERATURE CITED

(1) I. Sunshine, "Methodology for Analytical Toxicology", CRC Press, Cleveland, Ohio, 1975.
(2) A. Curry, "Poison Detection in Human Organs", Charles C Thomas Publisher, Springfield, Ill. 1976.
(3) H. A. Schwertner, J. E. Wallace, and K. Blum, *Clin. Chem. (Winston-Salem, N.C.)*, **24**, 360 (1978).
(4) E. Reid, *Analyst (London)*, **101**, 1 (1976).

RECEIVED for review May 30, 1978. Accepted August 7, 1978.

Automatic Gravimetric Titration System

Roger Guevremont[1] and Byron Kratochvil*

Department of Chemistry, University of Alberta, Edmonton, Alberta T6G 2G2, Canada

Gravimetric titrations, in which solutions are prepared on a weight basis and the weight rather than the volume of titrant delivered is measured, have not attained widespread popularity owing to the slowness of the many weighing operations that have been required. Titrations in which the amount of reagent added is measured by weight rather than volume have a number of advantages, however (*1*).

The major disadvantage, slowness of weighing, has been alleviated with the development of top-loading balances. New electromechanical systems no longer use the beam and knife-edge principle; these designs, coupled with digital electronics, allow convenient interfacing of the weighing operation with microprocessor or minicomputer systems.

The use of automated weighing to measure samples for analysis has been described by Renoe, O'Keefe, and Malmstadt (*2*), but this method has not been used to measure titrants. Most commercial automatic titrators use a titrant delivery system based on a motor-driven syringe. The volume of solution delivered is obtained in terms of the movement of the syringe plunger; a precision on the order of a few tenths of a percent is possible with the best of these systems. We describe here an automatic titrator in which the weight of titrant delivered is measured and recorded automatically. Titrant delivery may be controlled manually or by minicomputer, allowing conventional titrations to a visual end point, or completely automated potentiometric titrations under minicomputer control. Precision on the order of a few hundredths of a percent is attainable, the principal uncertainty arising in the potential sensing system used to locate the end point.

Two arrangements for the automatic delivery operation in a gravimetric titration were studied. In the first, the titrant is contained in a bottle, and the delivery tube is closed with a pinch clamp. Titrant is delivered by means of a mechanical arm which contacts the clamp during the delivery period only,

[1] Present address, Atlantic Regional Laboratory, National Research Council, Halifax, Nova Scotia, Canada.

0003-2700/78/0350-1945$01.00/0 © 1978 American Chemical Society

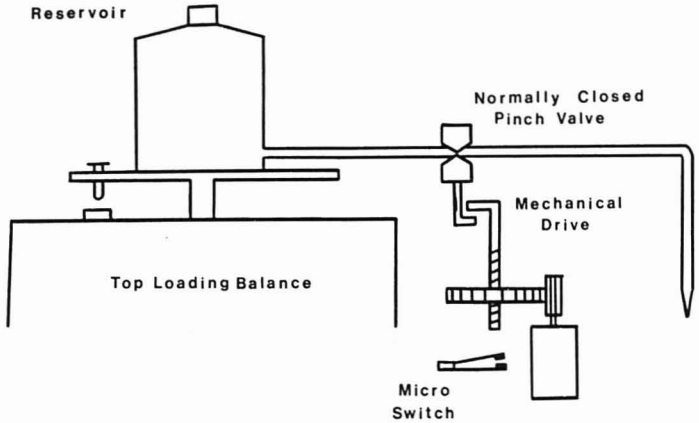


Figure 1. Schematic diagram of the automatic gravimetric delivery system based on a mechanical couple

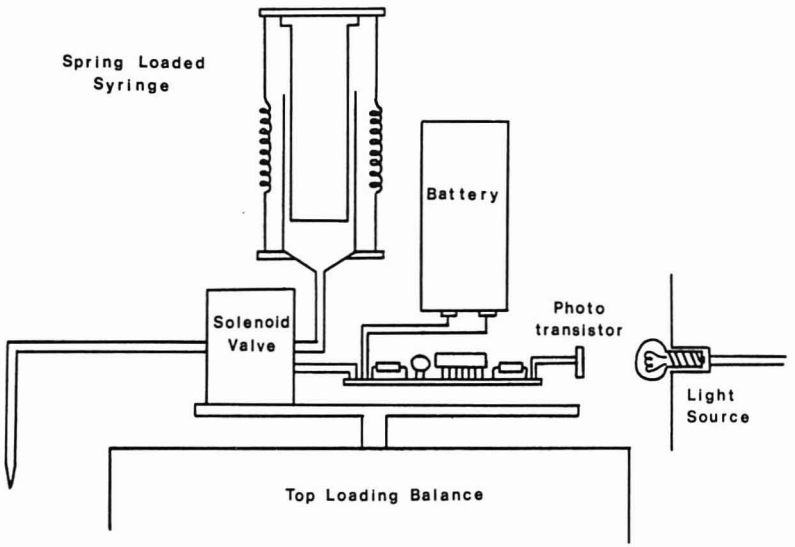


Figure 2. Schematic diagram of the automatic gravimetric delivery system based on an optical couple

and not during the weighing operations. In the second, the titrant is contained in a spring-loaded syringe, and delivery is controlled by a battery-powered solenoid valve through an optically-coupled trigger. The precision and reliability of the systems were evaluated by a series of potentiometric acid–base titrations.

EXPERIMENTAL

Instrumentation. *The Gravimetric Delivery System.* The mechanical couple design of the weight titrator is shown in Figure 1. It is composed of a titrant reservoir and delivery tubes, a normally-closed pinch valve, and a mechanical unit to open and close the valve. The reservoir is a polyethylene bottle connected to the delivery tip by Teflon tubing except in the valve, where a short section of pliable thin-walled silicone tubing was found more satisfactory. A lever arm driven by a small electric motor opens the valve to deliver titrant. A micro switch is positioned to stop the motor when the valve reaches the open position. The motor is run in reverse to close the valve and disengage the lever arm from the delivery unit. The gravimetric delivery system is enclosed in a Plexiglas housing to prevent air currents from affecting balance readings.

The optical couple delivery system is shown in Figures 2 and 3. The titrant is delivered from a spring-loaded 10-mL Hamilton Gas-Tight syringe with a Luer-type fitting through Teflon or polyethylene tubing to a solenoid valve. From the valve, the titrant passes to a delivery tip, the end of which is drawn to a small diameter so that the titrant is delivered under pressure as a fine jet. This eliminates the problem of evaporation from a hanging drop, which may be serious with volatile solvents and small titration volumes. The delivery tip is positioned above the solution

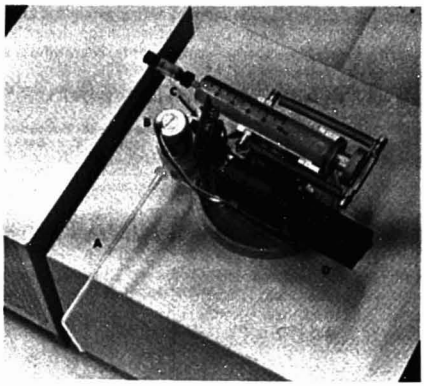


Figure 3. Photograph of titration unit on electronic top-loading balance. (A) Delivery tube of polyethylene inside glass tubing, (B) solenoid valve for control of titrant delivery, (C) circuit board with phototransistor (top center of board) for switching valve on and off from external light source, (D) battery for valve operation

level in the titration vessel; immersion in the solution causes errors in weight on the order of 10 mg or more owing to surface tension effects. A General Valve Corporation 2-way 12-V dc, Iso-Latch miniature solenoid valve controlled the solution flow. The valve latches open with a single 12-V, 700-mA, 150-ms pulse, and close with an equivalent pulse of reversed polarity. The power is supplied from ten Eveready B225T, 1.25-V nickel–cadmium batteries. Signals for opening and closing the valve are sent through an optical couple consisting of a tungsten lamp source and a phototransistor detector. The lamp can be controlled manually or with TTL compatible signals from a computer.

A Sartorius Model 3015 electronic top-loading balance (rated capacity 160 g, sensitivity 0.001 g) was used. Because the titrator assembly weighed on the order of 330 g, the pan and lead tare weights were removed from the balance and replaced with a light weight aluminum support frame. The digital output of the balance was interfaced to a PDP 11/10 (Digital Equipment Corporation) minicomputer through a multiplexer.

Application of the Gravimetric Delivery System to Potentiometric Titrations. Potential measurements were made with a Fisher Accumet Model 520 pH Meter and a glass–silver–silver chloride electrode pair. The meter and electrodes were calibrated against buffer solutions prepared according to NBS specifications.

A PDP 11/10 minicomputer was used to control the gravimetric buret and to collect the weight and indicating electrode potential data. Titrations were carried out under control of a program designed to: (a) sample the binary coded decimal (BCD) outputs of the electronic balance and the digital pH meter through a multiplexer, (b) calculate the approximate quantity of titrant to be delivered for the next data point, (c) control the delivery of titrant through the gravimetric buret, (d) calculate and store the weight of delivered solution along with the potentiometric data, and (e) calculate the titration results. The logic step (b) is based on the effect of the previous delivery on the indicating electrode potential. If the potential change is less than a predetermined minimum value, such as 5 mV, the delivery time, and thus the size of the next increment, is doubled. Within other selected ranges of potential change, the quantity of titrant delivered remains the same as for the previous increment, or is reduced or increased by factors of two to five. The limits of these ranges are selected on the basis of the sharpness of the expected end point and the number of data points desired. A flow chart of the program is shown in Figure 4.

Materials. All solutions were prepared with boiled distilled water which was cooled in a glove box under nitrogen. Carbonate-free sodium hydroxide was prepared by dilution of saturated NaOH solution (AnalaR analytical reagent NaOH, BDH Chemicals, Toronto, Ontario). Potassium hydrogen phthalate

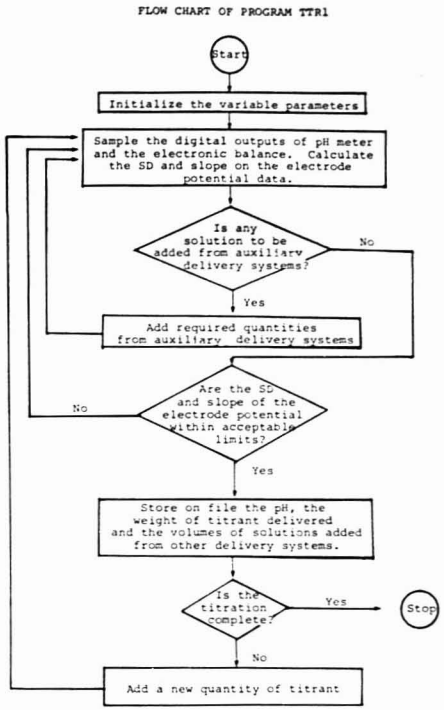


Figure 4. Flow chart of program TTR1

(Primary standard, J. T. Baker Chemical Co., Phillipsburg, N.J.) was dried 1 h at 120 °C before sample preparation. Nitric acid stock solutions were prepared by dilution of concentrated acid (J. T. Baker Chemical Co.). Individual samples for titration were weighed by difference in a syringe.

RESULTS AND DISCUSSION

Using the mechanical couple gravimetric buret, the relative standard deviation for a set of six titrations of approximately 0.5 g KHP each with NaOH was 0.06%, or about 4 mg in the 6 to 7 g of titrant that were required. The relative standard deviation decreased to 0.04% or about 1 mg in 3 g of titrant for a set of 8 titrations of 5 to 8 g of nitric acid. Similar titrations performed with the optical couple gravimetric delivery system gave standard deviations (in terms of weight of titrant) of 0.06% for 9 titrations of KHP with 0.4 M NaOH, and 0.018% for 9 titrations of nitric acid with about 3 M NaOH. The results indicate that the two designs of titrators are equivalent in accuracy and precision. The limit of sensitivity of the balance used in this work, 1 mg, establishes the limit of precision for titrations in which end point detection is not a significant source of error, as in strong acid–strong base titrations.

A delay was introduced between delivery of titrant and measurement of potentials to allow time for mixing and electrode equilibration. Electrode potential data were then collected for 6 s, and the average, standard deviation, and rate of electrode drift calculated. If the standard deviation or drift exceeded preset levels, the 6-s measurement period was repeated. The length of the delay period, and the criteria for electrode equilibria, can be varied as necessary. The me-

chanical couple titrator required about 30 min to collect 35 to 40 equilibrium pH data points suitable for equivalence point determination; the optical couple system required about 20 min. Most of the time was spent in waiting for pH values to come to equilibrium.

Computer control of the titration system allows rapid response to sharp equivalence points. Of approximately 35 data points collected in each titration of nitric acid with sodium hydroxide, 12 were within ±0.4 g of the equivalence point (total titrant delivery, 10 g). This allows precise determination of end points where the potential change is slight. The apparatus therefore should be applicable to a variety of titration systems, including complexation, oxidation reduction, and precipitation as well as acid base reactions.

ACKNOWLEDGMENT

The assistance of Hubert Priebe in the design and construction of the syringe holder and spring assembly, and of Mark Ingram and Frank Dreissigacker in the design and construction of the electronic components, is gratefully acknowledged.

LITERATURE CITED

(1) W. E. Harris and B. Kratochvil, "Chemical Separations and Measurements, Background and Procedures for Modern Analysis", W. B. Saunders, Philadelphia, Pa., 1974, p 160.
(2) B. W. Renoe, K. R. O'Keefe, and H. V. Malmstadt, *Anal. Chem.*, **48**, 661 (1976).

RECEIVED for review May 2, 1978. Accepted August 24, 1978. Research supported in part by the National Research Council of Canada and the University of Alberta. Financial support to R. G. by a National Research Council of Canada Scholarship is gratefully acknowledged.

Trace Determination of Subnanogram Amounts of Acrylonitrile in Complex Matrices by Gas Chromatography with a Nitrogen-Selective Detector

R. S. Marano,* S. P. Levine, and T. M. Harvey

Ford Motor Company, Technical Services Department, Engineering & Research, Scientific Research Staff—Research, Dearborn, Michigan 48121

The determination of acrylonitrile (ACN) in a variety of matrices has received attention in recent months because of its extensive industrial usage and its purported carcinogenic properties (*1–3*). The commonly used techniques for trace analysis of ACN depend on gas chromatographic (GC) separation followed by flame ionization detection (FID) (*4*). Since the FID has poor specificity, it may be difficult to detect low levels of ACN in the presence of other organic species. For this reason, long GC analysis times or confirmation of peak identity by GC–mass spectrometry (MS) is required.

A previously reported technique (*5*) utilizing a GC equipped with a nitrogen–phosphorus detector (NPD) (*6*) has been developed further in this laboratory. This technique offers significant advantages in terms of sensitivity and specificity of analysis. It has been applied to the determination of trace levels of ACN in simulated air, water, and paint samples in order to illustrate the utility of this method.

EXPERIMENTAL

Apparatus and Operating Conditions. Hewlett-Packard Model 5710 and 5840 gas chromatographs were used. Each was equipped with a nitrogen-specific detector (Model 18789A Dual N-P FID). Two separate chromatographic conditions were used. Acetone solutions were analyzed on a 1.8 m × 2 mm i.d. glass column (on-column injection) packed with 10% SP-1000 on 80/100 mesh Supelcoport. The column was operated at 80 °C with a helium flow of 30 cm^3/min and an injection port temperature of 80 °C (analysis A). Aqueous solutions were analyzed on a 1.2 m × 2 mm i.d. glass column (on-column injection) packed with 60/80 mesh Chromosorb 102. This column was operated at 150 °C with a helium flow of 45 cm^3/min and an injection port temperature of 100 °C (analysis B). In both cases, the NPD was operated at 300 °C under standard operating conditions of 2 to 3 cm^3/min hydrogen, 50 cm^3/min air, and 16 to 18 volts. Confirmation of acrylonitrile peaks was carried out on a combined Perkin-Elmer 910 GC/VG Micromass MM-16 mass spectrometer/Finnigan (INCOS) 2000 data system. Chromatographic analysis A (above) was utilized for GC/MS studies, with the MS operating under standard electron impact conditions.

Samples and Analysis. Simulated air samples were taken by drawing air containing ACN or ACN plus various organic vapors through charcoal tubes (SKC lot 106, 100 mg + 50 mg back section) at a rate of 50–200 cm^3/min for up to 100 min. Tubes were capped and refrigerated until analyzed. Water samples were prepared by adding ACN to tap water. A simulated paint system was prepared by adding ACN to a sample of enamel paint. All solvents and ACN were reagent grade. In all cases, blanks were run to ensure the lack of interferences.

Each charcoal tube was scored at the front end of the tube and broken. The glass wool and 100-mg portion of charcoal were transferred to a 1-mL vial (Reactivial, Pierce Chemical Co.), 0.5 mL of acetone was added, and the vial immediately sealed. The urethane foam separating the two sections of charcoal was discarded and the back section was desorbed in the same manner. The samples were desorbed (SKC Charcoal Developer) at room temperature for 30 min before analysis. Analyses were performed by injecting 1–2 μL of the acetone solution into the GC using a gas-tight syringe.

For the simulated paint analysis, a 0.5-mL portion of an enamel paint that had previously been spiked with ACN was added to a 50-mL volumetric flask and water was added to volume. After vigorous mixing (Thermolyne MaxiMix), 2 μL of the aqueous phase was injected into the GC for analysis.

Stock solutions of ACN were made for 4 μg/μL in acetone, 40 μg/μL in hexane, and 4 μg/μL in water. By successive dilution with the same solvent, appropriate standards were generated.

Sealed vials containing charcoal and acrylonitrile were prepared at three levels of ACN. This was done by injecting the vials with 2.5 μL of standards containing 0.8 μg/μL, 8 μg/μL, and 40 μg/μL of ACN in hexane. The charcoal was allowed to adsorb the standard for 24 h at room temperature after which time the vials were desorbed with 0.5 mL acetone. This simulated three sets of charcoal tubes which had adsorbed ACN at nominal levels of 2, 20, and 100 μg. The desorption efficiency was determined by comparing the levels of ACN in these vials to that in vials prepared by injecting the standards into sealed vials containing *only* 0.5 mL of acetone.

RESULTS AND DISCUSSION

The sampling of ambient air for organic vapors using charcoal tubes is a well known technique (*7*). In fact, a National Institute for Occupational Safety and Health (NIOSH) procedure has been validated for the collection and

0003-2700/78/0350-1948$01.00/0 © 1978 American Chemical Society

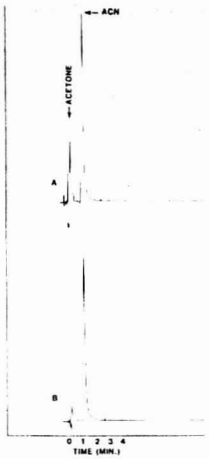


Figure 1. Chromatograms resulting from 1-μL acetone injections on SP-1000 column: (A) 8 ng/μL standard, (B) extract from tube #5. Analysis A

analysis of ACN in air (*4*). By using the NPD in place of a FID, the sensitivity of the NIOSH method is improved while the possibility of interferences from other organics is greatly reduced.

An initial experiment was performed to assess the freedom from interference and the linearity of the method under simulated industrial use conditions. Air containing trace levels of ACN and a complex mixture of organic solvent vapors was drawn through seven charcoal tubes as previously described. The total ACN found on the tubes was in the range between 0.34 and 60.8 μg of ACN per tube. In each case >90% of the ACN was found on the front section of the tube. The precision of three replicate determinations for each tube was approximately 1% of the mean. ACN standards in acetone demonstrated linear detector response over the 0.8 to 500 ng/μL range, which is essentially equivalent to tubes containing 0.4 to 250 μg of ACN. In all cases, acetone sample extracts were analyzed along with standards of approximately the same concentration using GC analysis condition A (SP1000 column). Figure 1 gives typical chromatograms resulting from 1-μL injections of tube #5 (from the group of seven) and an 8 ng/μL standard. In this case, the charcoal tube extract is shown to contain 4.1 ± 0.2 μg of ACN.

Tube #1 was analyzed by this technique and the analysis was confirmed by GC/MS. This is illustrated in Figure 2. The GC-NPD analysis yielded a result of 60.8 ± 0.7 μg ACN on tube #1 while the GC/MS analysis yielded a result of 61.5 μg ACN. One can appreciate the selectivity of the NPD from the examination of Figure 2. The potential interferences with the ACN analysis by high concentrations of organic solvent vapors is evidenced in the computer-reconstructed gas chromatogram from the GC/MS analysis. The ion current attributable to major ACN ions (*m/e* 53 $CH_2{=}CHCN^{+\cdot}$, m/e 26 $C_2H_2^{+\cdot}$) is less than 0.1% of the total ion current. Nevertheless analyses by GC/MS and GC-NPD were in good agreement. It was observed that the GC-NPD analyses could be repeated every 3 to 4 min because of the highly specific response of the detector.

The results of recovery studies are given in Table I. These levels of ACN were chosen so as to correspond to levels expected to be found on actual sample tubes. The desorption step of the analysis appears to represent the limiting step in

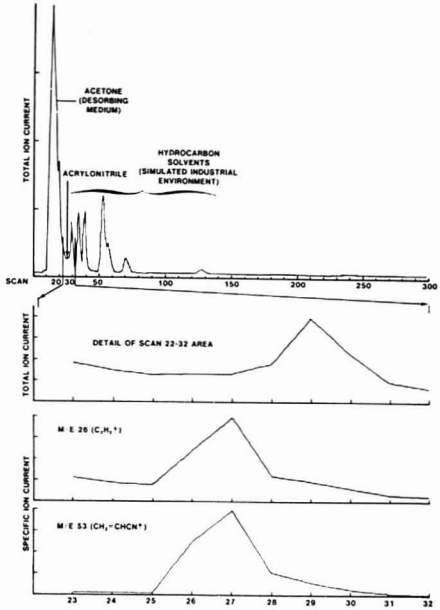


Figure 2. Ion current chromatograms illustrating high level of hydrocarbon background relative to acrylonitrile in tube #1

Table I. Recovery of Acrylonitrile from Charcoal

acrylonitrile, μg		desorption	rel std
added	found	efficiency, %	dev, %[a]
2	1.41	70.4	6.8
20	13.6	68.1	3.5
100	82.0	82.0	5.5
		av 73.5	5.3

[a] Four determinations.

terms of precision and accuracy. Recovery values obtained using acetone appear to be in the same range as those obtained by McCammon using methanol desorption (*4*). The values thus obtained may then be corrected by considering the desorption efficiency of the method used.

Preliminary results (Figure 3) were obtained for the determination of water spiked with ACN by direct aqueous injection into GC-NPD using chromatographic analysis condition B (Chromosorb 102). These conditions were also used for the analysis of the water extract of enamel paint spiked with ACN. Both tap water and the paint were spiked with ACN to give concentrations of 5–10 ng/μL. The paint was extracted with water at a volume ratio of 100:1 (water/paint). The detection limit was comparable to that quoted for acetone injections (10 pg/μL) and appears to offer significant improvement over that obtained in previous work (*5*), yet in background matrices which are more complex. This was achieved by optimizing chromatographic conditions and detector operating parameters.

A test was also run to analyze a methanol solution of ACN (analysis condition B, Chromosorb 102). The chromatogram appears identical to those shown in Figure 3. This permits the use of either acetone or methanol (*4*) elution of ACN on the charcoal tubes.



Figure 3. Chromatograms resulting from 2-μL water injections on Chromosorb 102 column: (A) 8.8 ng/μL standard, (B) extract from spiked enamel paint

The NPD will yield a positive or negative response to the solvent depending on the bias voltage and the cleanliness of the crystal (*8*), thus necessitating the separation of the solvent from the ACN. This is accomplished using an SP1000 column for acetone and a Chromosorb 102 column for methanol or water. Neither carbon disulfide nor nitrogen-containing solvents can be used because of the extreme response and slow recovery of the detector to these solvents.

The application of this technique to direct analysis of air samples without preconcentration on a charcoal tube should present no difficulty (although these tests have not yet been performed in this laboratory). A 1.0-mL gas sample injection of air containing 1.0 ppm of ACN will contain 2.3 ng of ACN. Since the detection limit of ACN is 10 pg per injection, direct air analysis should be applicable at concentrations as low as 10 ppb ACN in air.

ACKNOWLEDGMENT

The authors thank Michael D. Kelly for his technical assistance and suggestions.

LITERATURE CITED

(1) R. J. Steichen, *Anal. Chem.*, **48**, 1398 (1976).
(2) M. E. Hall and J. W. Stevens, Jr., *Anal. Chem.*, **49**, 2277 (1977).
(3) J. F. Finklea, *Am. Ind. Hyg. Assoc. J.*, **38**, 417 (1977).
(4) NIOSH method and data report No. S-156 supplied by C. S. McCammon; National Institute for Occupational Safety and Health, Cincinnati, Ohio, March 1978.
(5) C. A. Burgett, "The Gas Chromatographic Determination of Residual Acrylonitrile Monomer", Hewlett-Packard Note ANGC8-76 (1976).
(6) C. W. Rice, U.S. Patent 2,550,498 (April 24, 1951).
(7) "NIOSH Manual of Analytical Methods", HEW Publication No. (NIOSH) 75-121, U.S. Government Printing Office, Washington, D.C. 1974, P & CAM 127 (1975).
(8) H. B. Bente, "Evaluating and Optimizing the Performance of the Nitrogen-Phosphorus Detector", Hewlett-Packard Note 5950-3535 (February, 1977).

RECEIVED for review June 8, 1978. Accepted July 6, 1978.

Pepperbush Powder, a New Standard Reference Material

Kensaku Okamoto,* Yuko Yamamoto, and Kelichiro Fuwa

National Institute for Environmental Studies, P.O. Yatabe, Ibaraki, 300-21, Japan

The importance of standard reference materials for metal analysis has been recently well-recognized by scientists in many fields. The authors, in a cooperative study with NBS research groups, have performed some research for new biological reference materials, and the work includes the preparation of Japanese Tea Leaves (*1*) and "wet" Shark Meat samples (*2*).

Pepperbush tree is known to accumulate Zn, Mn, Co, Ni, and Cd in the leaves (*3*); thus the elemental composition of pepperbush leaves is significantly different from that of other botanical reference materials such as Kale Powder (*4*), Orchard Leaves (*5*), Tomato Leaves (*6*), Spinach (*7*), and Pine Needles (*8*). We have, therefore, prepared pepperbush powder as a new biological standard reference material.

EXPERIMENTAL

Sampling and Drying. The leaves of pepperbush (*Clethra barbinervis*), collected in September 1975, at Mikouchi in the Ashio district and free from stems, were washed with deionized water and dried in an air oven at 80 °C overnight. About 30 kg of the dry leaves were used in this work.

Grinding and Sieving. The dry leaves (about 700 g) were ground for about 1 h in a ball-mill (95% Al_2O_3, 7 L) which had been previously ground well with the leaves to minimize contamination with metals. The pulverized samples were placed on a set of sieves; a 50-mesh (297 μm) nylon sieve (top), a 80-mesh (177 μm) nylon sieve (middle), and a reservoir made of vinyl chloride (bottom), and vibrated mechanically for 15 min.

Table I. Homogeneity of Pepperbush Samples

	μg/g dry wt		
	Zn	Fe	Mn
maximum value	345	172	2110
minimum value	325	161	2020
average	337	166	2090
rel std dev, %	1.5	2.2	1.0

Mixing. The powder which passed through a 80-mesh sieve was divided into two parts with a riffle sampler (JIS No. 2) made of vinyl chloride. The powder was piled up in two layers and again divided by passing through the riffle sampler. Pepperbush samples were homogenized by repeating this procedure ten times.

Metal Determinations for Assessment of Homogeneity. Samples were dry-ashed as follows: One gram of pepperbush powder (dried at 105 °C to constant weight) was ashed in a platinum crucible at 450 °C overnight, dissolved in 2 mL of 6 M HCl and made up to 100 mL with doubly-distilled water. Samples were also wet-digested with nitric acid and hydrogen peroxide as described previously (*3*). Zn, Fe, Mn, and Mg were determined by atomic absorption spectrometry using an air–acetylene flame. Co, Cd, Pb, and Cu were determined by atomic absorption

0003-2700/78/0350-1950$01.00/0 © 1978 American Chemical Society

Table II. Elemental Composition of Pepperbush Powder and Comparison with Other Botanical Reference Materials

	Pepperbush NIES No. 1, μg/g dry wt	Orchard Leaves (5), NBS 1571	Tomato Leaves (6), NBS 1573	Spinach (7), NBS 1570	Pine Needles (8), NBS 1575
K	1.57 (%)	1.47 (%)	4.46 (%)	3.56 (%)	0.37 (%)
Ca	1.45 (%)	2.09 (%)	3.00 (%)	1.35 (%)	0.41 (%)
Mg	4090	6200	(7000)		
Fe	172	300	690	550	200
Mn	2050	91	238	165	675
Co	(21)[a]	(0.2)	(0.6)	(1.5)	(0.1)
Pb	(8)[a]	45	6.3	1.2	10.8
Cd	(8)[a]	0.11	(3)	(1.5)	(<0.5)
Cu	11	12	11	12	3.0
Zn	328	25	62	50	

[a] Approximate value.

spectrometry using a heated graphite atomizer. K and Ca were determined by flame emission spectrometry.

Large-Scale Preparation. Seven lots (total 14.4 kg) of the pepperbush powder (below 80 mesh) were mixed in the riffle sampler (ten times) and the powder was randomly packaged in 1150 glass bottles (about 14 g each). To check homogeneity of the pepperbush powder, 38 samples were taken from every 30 bottles, dry-ashed, and analyzed.

RESULTS AND DISCUSSION

Homogeneity of Pepperbush Samples. A preliminary study indicated that pepperbush powder below 80 mesh was most suitable (50–80 mesh and above 50 mesh were also considered) and that mixing the powder with a riffle sampler achieved good homogeneity.

Table I shows the relative standard deviations of Zn, Fe, and Mn contents in 38 samples were 1.5, 2.2, and 1.0%, respectively. When standard solutions of Zn, Fe, and Mn at the same concentrations as the samples were measured ten times under similar conditions, the relative standard deviations were 1.4, 2.7, and 1.0%, respectively. Variations of the metal contents of the pepperbush samples were almost the same as the corresponding results for the standard solutions, indicating that the prepared pepperbush powder is homogeneous and practically useful as a standard reference material.

Elemental Composition of Pepperbush and Comparison with Other Botanical Samples. Table II shows the elemental composition of the pepperbush powder (these values have not been certified yet) and compares the elemental contents with those of other botanical reference materials. Six samples (1 g each) were taken from each bottle selected randomly, dried at 105 °C to constant weight, wet-digested with nitric acid and hydrogen peroxide, and analyzed by atomic absorption and flame emission spectrometry. The most typical characteristic of pepperbush is the high concentrations of Mn, Co, Cd, and Zn. Pepperbush powder is, therefore, particularly suitable for measurement of plant materials which contain high levels of such metals. The pepperbush sample would also serve to check analytical methods for Co and Cd in plant materials where the levels of Co and Cd are usually very low.

LITERATURE CITED

(1) K. Fuwa, K. Notsu, K. Tsunoda, H. Kato, Y. Yamamoto, K. Okamoto, Y. Dokiya, and S. Toda, *Bull. Chem. Soc. Jpn.*, **51**, 1078 (1978).
(2) Y. Dokiya, M. Taguchi, S. Toda, and K. Fuwa, *Anal. Chem.*, **50**, 533 (1978).
(3) K. Okamoto, Y. Yamamoto, and K. Fuwa, *Agric. Biol. Chem.*, **42**, 663 (1978).
(4) H. J. M. Bowen, *Analyst (London)*, **92**, 124 (1967).
(5) Certificate for Orchard Leaves, U.S. Department of Commerce, National Bureau of Standards, Washington, D.C., 1971.
(6) Certificate for Tomato Leaves, U.S. Department of Commerce, National Bureau of Standards, Washington, D.C., 1976.
(7) Certificate for Spinach, U.S. Department of Commerce, National Bureau of Standards, Washington, D.C., 1976.
(8) Certificate for Pine Needles, U.S. Department of Commerce, National Bureau of Standards, Washington, D.C., 1976.

RECEIVED for review June 19, 1978. Accepted July 26, 1978. This work is supported partially by Japan–U.S. Cooperative Project between JSPS and NSF No. 6R023.

Metal Dendrites for Lithium Cationization in Mass Spectrometry

Tim L. Youngless, Maurice M. Bursey,* and Carl E. Rechsteiner, Jr.[1]

William Rand Kenan, Jr.-Laboratories of Chemistry, The University of North Carolina, Chapel Hill, North Carolina 27514

The recent development of lithium ion attachment, or cationization, as a method of ionizing molecules for mass spectral analysis has been pursued in several laboratories (*1–5*). Other alkali ions have also been used (*5, 6*). The technique has been applied both to volatile (*2, 3*) and to involatile substances (*4, 5*) and shows considerable promise for involatile compounds for which field desorption fails (*4, 5*). The cationization technique is applicable to quantitative analysis (*7*) and there have been inorganic applications (*8*). The chemistry of ions prepared in this way has been studied using collisional activation (*9*) and ion cyclotron resonance (*10*), and the results are in keeping with behavior anticipated from coordination of Li^+ with unshared pairs in the molecules studied.

It has been noted that carbon microneedles have no great merit in promoting lithium ion attachment. Indeed, they frequently decrease the efficiency of ionization sample molecules (*2, 5*). An advantage of metal emitters is their greater capacity for loading sample than carbon microneedles (*11*). It is now also known that activated metal emitters are particularly useful for salts and for other samples with ionization efficiencies below 11 eV (*12, 13*); the mechanism of ion desorption from salt layers is based upon ion conduction, and one consideration in evaluating the energetics of such desorptions is the energetics of the electron transition at the support/salt phase boundary (*14*). Examining activated metal emitters for their effect in lithium cationization seemed reasonable because of these previous observations.

Over a period of a year we have used metal dendrites, first described as an alternative to carbon dendrites for use in field desorption mass spectrometry (*15*), to increase the efficiency of lithium cationization of a range of organic compounds with different functional groups. The enhancement was found to vary somewhat with the type of functional group, but the increase in intensity of the cationized molecule MLi^+ is generally close to an order of magnitude. Signals for the

[1] Present address, Arthur D. Little, Inc., Acorn Park, Cambridge, Mass. 02140

0003-2700/78/0350-1951$01.00/0 © 1978 American Chemical Society

ketones and aldehydes we examined increased the least, but at least by a factor of two, and other compound classes by more. Benzonitrile was increased the most. Individual experiments gave a wide variation in the increase factor, from 2 to about 10, even though no experimental parameters were changed. The bare-wire sensitivity for volatile nitriles, alcohols, ketones, and aldehydes admitted without a gas inlet jet into the source is 1×10^{-4} C/kg or less; ionization on a dendrite-covered wire of the same samples introduced in the same way gives a sensitivity of at least 2×10^{-4} C/kg up to 1×10^{-3} C/kg. This implies routine analysis at the high end of the range of sensitivities quoted for other Li^+ attachment and field desorption studies (*16*, *17*). The possibility that wires slightly roughened by the deposition of only small amounts of metal would prove more effective than fully grown dendrites was investigated and found not to be the case; from these the efficiency of cationization was less than, or only as much as, the efficiency of cationization from wires with dendrites grown in the usual fashion (*18*). In our experience it was easier to grow uniform dendrites than to uniformly roughen a wire slightly with metal deposits. For most of the recent work cobalt dendrites (*18*, *19*) were used because of their generally superior performance to nickel in field desorption.

Using a duPont 21-492 B mass spectrometer with cobalt emitters and a cathode/anode potential of 10.5 kV with 3-mm separation, it is possible to obtain substantial Li^+ currents from salts such as LiCl with no heating current for a period of at least 2 h with a source temperature of 50 °C. These currents are sufficient to produce cationization of organic molecules in large enough quantities to yield good spectra. Experience has been that the emission of Li^+ currents from Li salts adsorbed on unheated *bare* wires is rather low and not sustained for more than a few minutes; furthermore, the intensity of the singal is erratic (*2*, *14*). The intensity, the duration, and the stability of the signal from Li salts on a bare wire are improved to satisfactory levels by heating the wire, with good results at the above 100 °C. However, the product yield for the ion–molecule reaction between Li^+ and the neutral decreases with increasing temperature. Presumably the improved cross section for this cationization reaction at lower temperatures balances the lower yield of Li^+ ions (*2*). We have not observed any substantial loss of stability of the Li^+ current from unheated *cobalt* emitters. Heating the emitters with currents of up to 45 mA did not produce changes of more than 50% in the intensity of cationized molecules MLi^+. Although there were both increases and decreases for molecules with different functional groups, at the maximum heating currents used there was usually a reduction in the intensity of the cationized molecule MLi^+ from the intensity at no heating current.

Preparing cobalt dendrites on wires used for field desorption and lithium cationization mass spectrometry is so trivial and rapid that the modest gain in sensitivity and reduction in harshness of the operating conditions are worth the extra step. While sensitivities at the nanogram level for qualitative and at least the microgram level for quantitative studies are possible for experienced operators (*7*), those new to the technique may wish to add this simple step to their procedures to improve signal intensity.

LITERATURE CITED

(1) F. W. Röllgen and H.-R. Schulten, *Org. Mass Spectrom.*, **10**, 660 (1975).
(2) U. Giessmann and F. W. Röllgen, *Org. Mass Spectrom.*, **11**, 1094 (1976).
(3) F. Borchers, U. Giessman, and F. W. Röllgen, *Org. Mass Spectrom.*, **12**, 539 (1977).
(4) H. J. Veith, *Angew. Chem., Int. Ed. Engl.*, **15**, 696 (1975).
(5) H. J. Veith, *Tetrahedron*, **33**, 2825 (1977).
(6) J. C. Prome and G. Puzo, *Org. Mass Spectrom.*, **12**, 28 (1977).
(7) W. D. Lehmann and H.-R. Schulten, *Angew. Chem., Int. Ed. Engl.*, **16**, 184 (1977).
(8) H.-R. Schulten and F. W. Röllgen, *Angew. Chem., Int. Ed. Engl.*, **14**, 561 (1975).
(9) F. W. Röllgen, F. Borchers, U. Giessmann, and K. Levsen, *Org. Mass Spectrom.*, **12**, 541 (1977).
(10) R. L. Woodin and J. L. Beauchamp, *J. Am. Chem. Soc.*, **100**, 501 (1978).
(11) M. M. Bursey, C. E. Rechsteiner, Jr., T. L. Youngless, D. F. Fraley, M. C. Sammons, and J. R. Hass, *Adv. Mass Spectrom.*, **7**, 932 (1978).
(12) F. W. Röllgen, U. Giessmann, H. J. Heinen, and S. J. Reddy, *Int. J. Mass Spectrom. Ion Phys.*, **24**, 235 (1977).
(13) S. J. Reddy, F. W. Röllgen, A. Mass, and H. D. Beckey, *Int. J. Mass Spectrom. Ion Phys.*, **25**, 147 (1977).
(14) F. W. Röllgen, U. Giessmann, and H. J. Heinen, *Z. Naturforsch. A*, **31**, 1729 (1976).
(15) R. M. Wightman, D. M. Hinton, M. C. Sammons, and M. M. Bursey, *Int. J. Mass Spectrom. Ion Phys.*, **17**, 208 (1975).
(16) F. W. Röllgen and H. R. Schulten, *Z. Naturforsch. A*, **30**, 1685 (1975).
(17) H. R. Schulten, *Cancer Treat. Rep.*, **60**, 501 (1976).
(18) C. E. Rechsteiner, Jr., D. E. Mathis, M. M. Bursey, and R. P. Buck, *Biomed. Mass. Spectrom.*, **4**, 52 (1977).
(19) M. M. Bursey, C. E. Rechsteiner, Jr., M. C. Sammons, D. M. Hinton, T. S. Colpitts, and K. M. Tvaronas, *J. Phys. E*, **9**, 145 (1976).

RECEIVED for review July 5, 1978. Accepted August 21, 1978. Work supported by the National Science Foundation (CHE 74-12390).

Author Index

Albert, D. K. 1822
Anderson, R. J. 1804
Anson, F. C. 1886

Bates, R. G. 1922
Bedrossian, M. 1898
Bertels, P. C. 1730
Betty, K. R. 1784
Boocock, D. G. B. 1871
Boyer, K. W. 1769
Braun, W. 1903
Bursey, M. M. 1951

Chakrabarti, C. L. 1730
Chuang, F. S. 1799
Conzemius, R. J. 1854
Crow, F. W. 1781

Dasgupta, P. K. 1793
Desimoni, E. 1895
Ditzler, M. A. 1883
Doane, L. M. 1891
Dubé, C. E. 1839
Duchane, D. V. 1752, 1757, 1765

Edstrom, R. D. 1941
Eidenschink, R. 1934
El-Hosseiny, F. 1937

Fassett, J. D. 1861
FitzPatrick, J. R. 1936
Fuller, M. P. 1906
Fuwa, K. 1950

Gearing, J. N. 1833
Gearing, P. J. 1833
Gilbert, R. D. 1937
Gold, A. 1839
Gregoire, D. C. 1730
Griffiths, P. R. 1804, 1906
Guevremont, R. 1945
Guiochon, G. 1812
Guthrie, B. E. 1900
Gutknecht, W. F. 1883

Hagel, L. 1937
Halang, W. A. 1829
Hanley, L. G., Jr. 1793
Harvey, B. R. 1866
Harvey, T. M. 1948
Haushalter, J. P. 1796
Hirata, Y. 1943
Hunt, D. F. 1781
Hurtubise, R. J. 1911

Ingle, J. D., Jr. 1737, 1745, 1772

Jagner, D. 1924
Jemal, M. 1917

Karasek, F. W. 1784
Kim, S. H. 1784
Knevel, A. M. 1917
Kratochvil, B. 1945
Kugler, E. 1829
Kuwada, K. 1788
Kuwana, T. 1879

Langlais, R. 1829
Levine, S. P. 1948
Leythaeuser, D. 1848
Lytle, J. S. 1833
Lytle, T. F. 1833

Marano, R. S. 1948
Matsumoto, K. 1943
Miller, R. J. 1772
Morris, M. D. 1796
Morrison, G. H. 1861
Motomizu, S. 1788

Nadeau, J. S. 1871
Natusch, D. F. S. 1799

Okamoto, K. 1950
O'Keefe, K. R. 1799, 1938

Palmisano, F. 1895
Parkinson, B. A. 1886
Paxson, J. R. 1777
Perni, R. B. 1839
Piepmeier, E. H. 1936
Pietrzyk, D. J. 1842
Pohl, L. 1934

Randall, J. C. 1777
Ratzlaff, K. L. 1799
Rechsteiner, C. E., Jr. 1951
Renberg, L. 1836
Ritz, G. P. 1796
Ryan, M. A. 1772

Sabbatini, L. 1895
Sacks, R. D. 1752, 1757, 1765
Salin, E. D. 1737, 1745
Sankar, M. 1922
Schabron, J. F. 1911
Schaefer, R. G. 1848
Schwarz, F. P. 1903
Schwertner, H. A. 1944
Silver, H. F. 1911
Stock, J. T. 1891
Suddendorf, R. F. 1769
Svec, H. J. 1854
Sydor, R. 1842
Szentirmay, R. 1879

Takeuchi, T. 1943
Taylor, J. W. 1930
Tôei, K. 1788
Tran-Minh, C. 1874
Treen, M. E. 1871

Vallin, D. 1874
Veillon, C. 1900

Wallan, D. J. 1796
Wasik, S. P. 1903
Weiner, B. 1848
West, P. W. 1793
Willey, J. F. 1930
Wolf, W. R. 1900

Yamamoto, Y. 1950
Youngless, T. L. 1951

Zambonin, P. G. 1895

Future Articles

Stability Constants of Calcium and Lanthanide Ions with Murexide
K. S. Balaji, S. D. Kumar, and P. Gupta-Bhaya

Quantitative Ion Probe Analysis of Glasses by Empirical Calibration Methods
J. D. Ganjei and G. H. Morrison

Instrumental Approach to Potentiometric Stripping Analysis of Some Heavy Metals
D. Jagner

Effects of Operating Variables on Peak Shape in Gel Permeation Chromatography
J. L. Glajch, D. C. Warren, M. A. Kaiser, and L. B. Rogers

Microcomputer-Controlled Monochromator Accessory Module for Dual Wavelength Spectrochemical Procedures
J. D. Defreese, K. M. Walczak, and H. V. Malmstadt

Mobility Behavior and Composition of Hydrated Positive Reactant Ions in Plasma Chromatography with Nitrogen Carrier Gas
S. H. Kim, K. R. Betty, and F. W. Karasek

Plasma Chromatography of Alkyl Amines
F. W. Karasek, S. H. Kim, and S. Rokushika

Fluorimetric Determination of Pyridine after Hydroxylation with the Hamilton Hydroxylation System
M. P. Wong and K. A. Connors

Trace Arsenic Determination by Volatilization and X-ray Photoelectron Spectroscopy
M. B. Carvalho and D. M. Hercules

Determination of Technetium by Graphite Furnace Atomic Absorption Spectrometry
J. H. Kaye and N. E. Ballou

Effect of Thermal Lag and Measurement Precision in Differential Scanning Calorimetry: Enzyme-Substrate Reactions by the Method of Orthogonal Collocation
L. F. Whiting and P. W. Carr



Want the only dispenser with a Teflon®-coated plunger?

Ask for the 'Teflon Dispenser.'

Why does a Brinkmann Dispensette seem to work more smoothly than other bottle-top dispensers?

The secret is its Teflon-coated plunger.

Dispensers with glass or polypropylene plastic plungers ofte 'freeze' or 'stick' when used with alkaline reagents. On a Dispen sette, the Teflon coating on the plunger insures smooth operat with any reactive chemical (except HF), even with concentrate acids and bases.

Of course, it takes more than a smoothly-working plunger to make a dependable dispenser. Instead of external glass tubing that could break or chip, Dispensettes are equipped with flexible Teflon filling and discharge tubes that can easily be cut to any desired length. Simply pull them off and a Dispensette is ready for autoclaving at 120°C without further disassembly.

Dispensette offers a wide selection of models for fast, accurate dispensing of volumes from 0.1 to 50ml, with better than ±1.0% accuracy and ±0.1% reproducibility. There is hardly a standard size screw-neck reagent bottle, can or container (even STJ 24/40 and 29/42 glassware) which a Dispensette will not fit, either directly or with optional screw-in adapters.

Some Dispensette design features have been copied by other dispensers, but none has its smooth, foolproof operation. That's because only Dispensette has a Teflon-coated plunger. Write for literature: Brinkmann Instruments, Inc., Cantiague Rd., Westbury, N.Y. 11590. In Canada: Brinkmann Instruments (Canada), Ltd.

Brinkmann Dispensette®

Available from: Ace Scientific
Beckman Instruments, Science Essentials Operation
Bio-Rad Laboratories/Cole-Parmer Instrument Co.
Curtin Matheson Scientific/Fisher Scientific
General Scientific/Markson Scientific/Preiser Scient
Sargent Welch/Scientific Products/SGA Scientific
Arthur H. Thomas/VWR Scientific/Wilkens-Anderson

Dispensette® is a registered trademark of R. Brand Co.
Teflon® is a Du Pont trademark.

CIRCLE 23 ON READER SERVICE CARD